

1N-35  
72792  
344P.

# Summary Report of Mission Acceleration Measurements for STS-73

Launched October 20, 1995

Melissa J.B. Rogers  
*Tal-Cut Company*  
*Beachwood, Ohio*

and

Richard DeLombard  
*Lewis Research Center*  
*Cleveland, Ohio*

July 1996



National Aeronautics and  
Space Administration



**SUMMARY REPORT OF MISSION ACCELERATION  
MEASUREMENTS FOR STS-73**

**Launched October 20, 1995**

Authors:

Melissa J. B. Rogers

*Tal-Cut Company*

*Beachwood, Ohio*

and

Richard DeLombard

*Lewis Research Center*

*Cleveland, Ohio*

### Abstract

The microgravity environment of the Space Shuttle Columbia was measured during the STS-73 mission using accelerometers from five different instruments: the Orbital Acceleration Research Experiment, the Space Acceleration Measurement System, the Three-dimensional Microgravity Accelerometer, the Microgravity Measuring Device, and Suppression of Transient Accelerations by Levitation Evaluation System. The quasi-steady environment was also calculated in near real-time during the mission by the Microgravity Analysis Workstation. The Orbital Acceleration Research Experiment provided investigators with real-time quasi-steady acceleration measurements. The Space Acceleration Measurement System recorded higher frequency data on-board for post-mission analysis. The Three-dimensional Microgravity Accelerometer provided some real-time data downlink and also recorded data for post-mission analysis. The Microgravity Measuring Device was used by the crew to increase their awareness of the effects their activities have on the microgravity environment. The Suppression of Transient Accelerations By Levitation Evaluation active vibration isolation system demonstrated the feasibility of this type of disturbance attenuation on the Orbiter. The Microgravity Analysis Workstation quasi-steady environment calculation and comparison of this calculation with Orbital Acceleration Research Experiment data was used to assess how appropriate a planned attitude was expected to be for one Crystal Growth Facility experiment sample.

The microgravity environment related to several different Orbiter, crew, and experiment operations is presented and interpreted in this report. Data for a crew quiet period is presented as a basis for comparison with other activities. This data example includes the effects of vernier reaction control system jet firings for Orbiter attitude control. Plots showing this component of the Orbiter background acceleration environment are compared to examples of data when no thrusters were firing, when the primary reaction control system jets were used for attitude control, and when single vernier jets were fired for test purposes. In general, vernier jets, when used for attitude control, cause accelerations in the  $3 \times 10^{-4}$  g to  $7 \times 10^{-4}$  g range. Primary jets used in this manner cause accelerations in the 0.01 to 0.025 g range.

Other significant disturbance sources and their associated acceleration signal characteristics were water dump operations with  $Y_b$  axis acceleration deviations of about  $1 \times 10^{-6}$  g; payload bay door opening motion with  $Y_o$  and  $Z_o$  axis accelerations of frequency 0.4 Hz; and probable Glovebox fan operations with notable frequency components at 20, 38, 43, 48, and 53 Hz.

The STS-73 microgravity environment is comparable to the environments measured on earlier microgravity science missions. The data from STS-73 show the usual influence of thruster firings and crew motion (transient events) and of crew exercise and Orbiter systems and experiment operations (oscillatory events). Orbiter structural modes and crew exercise frequencies are typically the same among Orbiters, missions, and crew members. The main differences among missions are the specific frequencies of equipment vibrations.



## Table of Contents

Abstract.....	i
Table of Contents.....	ii
List of Tables.....	iii
List of Figures.....	iv
Abbreviations and Acronyms.....	v
Acknowledgments.....	vi
1. Introduction and Purpose.....	1
2. Mission Overview.....	1
3. Accelerometer Systems and Related Studies.....	2
3.1 Orbital Acceleration Research Experiment.....	2
3.2 Space Acceleration Measurement System.....	3
3.3 Three-dimensional Microgravity Accelerometer.....	4
3.4 Microgravity Measuring Device.....	4
3.5 Suppression of Transient Accelerations by Levitation Evaluation.....	4
3.6 Microgravity Analysis Workstation .....	5
4. SAMS and OARE Data Analysis.....	6
4.1 Time Domain Analysis.....	7
4.2 Frequency Domain Analysis.....	8
5. Columbia Microgravity Environment - STS-73.....	9
5.1 Crew Activity - Reference Plots.....	9
5.2 Orbiter Attitude.....	10
5.3 Attitude Control.....	10
5.4 Payload Bay Door Motion.....	11
5.5 Glovebox Fan Operations.....	12
5.6 Water Dump Operations.....	12
6. Summary.....	13
7. References.....	14
APPENDIX A ACCESSING ACCELERATION DATA VIA THE INTERNET.....	A1
APPENDIX B SAMS TIME HISTORIES.....	B1
APPENDIX C SAMS COLOR SPECTROGRAMS.....	C1
APPENDIX D USER COMMENTS SHEET.....	D1

**List of Tables**

Table 1. USML-2 Experiments and Facilities.....	16
Table 2. STS-73 Payloads.....	17
Table 3. STS-73 Developmental Test Objectives.....	17
Table 4. STS-73 Detailed Supplementary Objectives.....	18
Table 5. STS-73 Crew.....	18
Table 6. STS-73 OARE Head Location and Orientation.....	19
Table 7. STS-73 SAMS Head Location and Orientation.....	20
Table 8. USML-2 AS-Flown Timeline.....	21
Table 9. Number of VRCS firings for certain attitudes on STS-73.....	26



## List of Figures

Figure 1. OARE instrument location on STS-73.....	27
Figure 2a. Approximate location of SAMS and 3DMA sensors on STS-73, Spacelab Center aisle.....	28
Figure 2b. Approximate location of SAMS and 3DMA sensors on STS-73, Spacelab starboard side.....	29
Figure 2c. Approximate location of SAMS and 3DMA sensors on STS-73, Spacelab port side.....	30
Figure 3. STABLE Physical Layout.....	31
Figure 4. Base and Isolated Acceleration Time History.....	31
Figure 5. Trimmean filter OARE data for entire STS-73 mission.....	32
Figure 6. SAMS TSH A data for crew quiet period.....	33
Figure 7. USML-2 Major Attitudes.....	34
Figure 8. Trimmean filter OARE data for period when Columbia was in the modified nominal USML-2 attitude.....	35
Figure 9. Trimmean filter OARE data for period when Columbia was in the CGF attitude in support of one CGF experiment.....	36
Figure 10. Trimmean filter OARE data for period when Columbia was in the .....	37
Figure 11. Trimmean filter OARE data for period when Columbia was in the solar inertial attitude for tire warming.....	38
Figure 12. SAMS TSH A data for free drift period.....	39
Figure 13. SAMS TSH A data for VRCS R5R jet test firing.....	40
Figure 14. SAMS TSH A data for VRCS R5D jet test firing.....	41
Figure 15. SAMS TSH B data vector magnitude for five hour period.....	42
Figure 16. SAMS TSH A data for PRCS jet firing as Orbiter comes out of free drift.....	43
Figure 17. SAMS TSH A data during payload bay door opening motion.....	44
Figure 18. SAMS TSH C data recorded during Glovebox fan operations.....	45
Figure 19. SAMS TSH C vector magnitude color spectrogram for Glovebox fan turn off times.....	46
Figure 20. Trimmean filter OARE data showing the effects of two water dump operations.....	47

## Abbreviations and Acronyms

3DMA	Three-dimensional Microgravity Accelerometer
accel <sub>avg</sub>	root-sum-square of averaged triaxial data
accel <sub>RMS</sub>	root-sum-square of RMS of triaxial data
CGF	Crystal Growth Furnace
DSO	Detailed Supplementary Objective
DTO	Development Test Objective
EDT	Eastern Daylight Time
EST	Eastern Savings Time
GFFC	Geophysical Fluid Flow Cell experiment
GG	gravity gradient
GMT	Greenwich Mean Time (day/hour:minute:second)
HRM	high rate multiplexer
JSC	NASA Johnson Space Center
k	number of time series intervals used in analysis
LeRC	NASA Lewis Research Center
M	number of points in time series interval used in analysis
MAWS	Microgravity Analysis Workstation
MDA	McDonnell Douglas Aerospace
MET	mission elapsed time (day/hour:minute:second)
MMD	Microgravity Measuring Device
MSAD	Microgravity Science and Applications Division
MSFC	NASA Marshall Space Flight Center
OARE	Orbital Acceleration Research Experiment
PGSC	Payload General Support Computer
PIMS	Principal Investigator Microgravity Services
POCC	Payload Operations Control Center
PRCS	primary reaction control system
PSD	power spectral density
RMS	root mean square
SAMS	Space Acceleration Measurement System
STDCE	Surface Tension Driven Convection Experiment
STABLE	Suppression of Transient Accelerations By Levitation Evaluation
TBE	Teledyne Brown Engineering
TSH	triaxial sensor heads
USML-1	first United States Microgravity Laboratory
USML-2	second United States Microgravity Laboratory
VRCS	vernier reaction control system
X <sub>o</sub> , Y <sub>o</sub> , Z <sub>o</sub>	Orbiter structural coordinate system axes
X <sub>b</sub> , Y <sub>b</sub> , Z <sub>b</sub>	Orbiter body coordinate system axes



### **Acknowledgments**

Nissim Lugasy and Kimberly Destro-Sidik, respectively, prepared computer software for real-time and off-line processing of OARE data during the USML-2 mission. Roshanak Hakimzadeh, PIMS Project Scientist, and the rest of the PIMS team provided acceleration environment interpretation during the mission and in preparation for this report. Ken Hrovat, Milton Moskowitz, and Kevin McPherson provided SAMS and OARE data analysis for this report. Tim Reckart was responsible for the layout of this report; Christine Frederick provided editorial support.

Larry French, Teledyne Brown Engineering, Huntsville, Alabama, provided information about the Microgravity Analysis Workstation. Samantha MacDonald, Johnson Space Center, provided information about the Microgravity Measuring Device. Robert Boucher, McDonnell Douglas Aerospace, provided information about the Suppression of Transient Accelerations by Levitation Evaluation demonstration. Pat Tamburro, ADF, provided information about the Space Acceleration Measurement System.



## 1. Introduction and Purpose

Microgravity science experiments are conducted on the NASA Space Shuttle Orbiters to take advantage of the reduced gravity environment resulting from the continuous free fall state of low earth orbit. Accelerometer systems are flown on the Orbiters to record the microgravity environment which is composed of quasi-steady accelerations and vibrations of the Orbiter, equipment, and local structures. The second United States Microgravity Laboratory (USML-2) payload flew on the Orbiter Columbia on mission STS-73 from 20 October to 5 November 1995. The USML-2 payload on STS-73 was dedicated to microgravity experiments. Two accelerometer systems managed by the NASA Lewis Research Center (LeRC) flew to support these experiments: the Orbital Acceleration Research Experiment (OARE) and the Space Acceleration Measurement System (SAMS). These accelerometers are sponsored by the Microgravity Science and Applications Division (MSAD) of the NASA Office of Life and Microgravity Sciences and Applications. In addition, the Three-dimensional Microgravity Accelerometer (3DMA), designed and sponsored by the University of Alabama in Huntsville, collected acceleration data as part of USML-2. The Microgravity Measuring Device (MMD) developed by JSC was used in the Orbiter middeck to record vibration levels associated with crew activity. The Suppression of Transient Accelerations By Levitation Evaluation (STABLE), managed by the NASA Marshall Space Flight Center (MSFC), demonstrated vibration isolation technology in the Spacelab. The Microgravity Analysis Workstation (MAWS), developed by Teledyne Brown Engineering (TBE), was used to calculate the quasi-steady environment of the Orbiter.

The Principal Investigator Microgravity Services (PIMS) project at the NASA Lewis Research Center supports principal investigators of microgravity experiments as they evaluate the effects of varying acceleration levels on their experiments. This report is provided by PIMS to furnish interested experiment investigators with a guide to evaluating the acceleration environment during STS-73 and as a means of identifying areas which require further study. To achieve this, various pieces of information are presented. Section 2 of this report provides an overview of the STS-73 mission, the payloads, and the experiments manifested on the payloads. Section 3 describes the accelerometer systems flown on STS-73 and the means by which they recorded data and provided data to the user. Section 4 discusses specific analysis techniques applied to the accelerometer data. Section 5 discusses the microgravity environment of Columbia during STS-73 in relation to various activities which occurred during the mission. Appendix A describes how OARE and SAMS data can be accessed through the internet. Appendices B and C provide plots of SAMS data as an overview of the microgravity environment during the entire mission. Appendix D contains a user comment sheet. Users are encouraged to complete this form and return it to the authors.

## 2. Mission Overview

At 09:53:00 a.m. EDT on 20 October 1995 the Space Shuttle Columbia launched on the STS-73 mission from NASA Kennedy Space Center. Landing was at Kennedy Space Center on



5 November at 06:45:00 a.m. EST. In terms of other time conventions used in this report, launch was at Greenwich Mean Time (GMT) 293/13:53 or mission elapsed time (MET) 000/00:00 and landing was at GMT 309/11:45 or MET 15/21:52. Both GMT and MET are recorded in day/hour:minute:second format. The primary objective of the STS-73 mission was to perform the science experiments that constituted the USML-2 payload. USML-2 was a cooperative effort of the U.S. government, universities, and industry to push back the frontiers of science and technology in microgravity. The USML-2 experiments cover a variety of scientific disciplines including biotechnology, combustion science, fluid physics, and materials science. USML-2 experiments and facilities are listed in Table 1; as indicated, some facilities have multiple experiments and principal investigators. Other payloads on STS-73 are listed in Table 2. Twelve development test objectives (DTO) and fourteen detailed supplementary objectives (DSO) were accomplished on STS-73; they are listed in Tables 3 and 4. The seven member crew worked two twelve hour shifts on STS-73 so USML-2 experiments could be performed and monitored around the clock. The crew members are listed in Table 5.

### **3. Accelerometer Systems and Related Studies**

Four accelerometer systems measured the microgravity and vibration environment of the Orbiter Columbia during the STS-73 mission: the Orbital Acceleration Research Experiment, the Space Acceleration Measurement System, the Three-dimensional Microgravity Accelerometer, and the Microgravity Measuring Device. Two other investigations involving the Orbiter microgravity environment were performed as part of USML-2: a vibration isolation platform, the Suppression of Transient Accelerations By Levitation Evaluation, and the real-time calculation of the quasi-steady environment of Columbia by the Microgravity Analysis Workstation.

#### **3.1. Orbital Acceleration Research Experiment**

The OARE was designed to measure quasi-steady accelerations from below  $1 \times 10^{-8}$  g up to  $2.5 \times 10^{-3}$  g. The OARE consists of an electrostatically suspended proof mass sensor, an in-flight calibration subsystem, and a microprocessor which is used for in-flight experiment control, processing, and storage of flight data [1-5]. In support of USML-2 experiments, the sensor output acceleration signal was filtered with a Bessel filter with a cut-off frequency of 1 Hz. The output signal was digitized at 10 samples per second and was processed and digitally filtered with an adaptive trimmean filter prior to electronic storage. Simultaneously, the unprocessed data were recorded on the Orbiter payload tape recorder and routed to the Spacelab High Rate Multiplexer (HRM). Using the HRM interface, the unprocessed OARE data were downlinked from the Orbiter to the PIMS computers in the MSFC Payload Operations Control Center (POCC). The PIMS computers processed the OARE data and displayed data for the PIs using the POCC video matrix and the World Wide Web.

The OARE was mounted to the floor of Columbia's cargo bay on a keel bridge, close to the Orbiter center of gravity. The location and orientation of the sensors with respect to the Orbiter structural coordinate system are given in Table 6 and Fig. 1. In this report, the OARE data are presented in terms of the Orbiter body coordinate system. The OARE data sign con-



vention is such that when there is a forward thrust of the Orbiter (such as during an OMS firing), it is recorded as a negative  $X_b$  acceleration. We refer to this convention as being consistent with a frame of reference fixed to the Orbiter. The subscript b represents the Orbiter body coordinate system. OARE data are available from MET 000/00:10 to 015/21:03. Appendix A describes how these data can be accessed using the internet.

### 3.2. Space Acceleration Measurement System

The SAMS was developed to measure the low-gravity environment of Orbiters in support of MSAD-sponsored science payloads. STS-73 was the thirteenth flight of a SAMS unit on an Orbiter. The SAMS unit consisted of three remote triaxial sensor heads, connecting cables, and a controlling data acquisition unit with a digital data recording system using optical disks with 200 megabytes of storage capacity per side. On STS-73, SAMS was located in the Spacelab module in support of USML-2 experiments. The signals from the three triaxial sensor heads were filtered by low-pass filters with cutoff frequencies of 5 (TSH A), 2.5 (TSH B), and 25 Hertz (TSH C). These signals were then sampled at 25, 12.5, and 125 samples per second, respectively, and the data were recorded on optical disks. In this report, the SAMS data are presented in terms of the Orbiter structural coordinate system. The SAMS data sign convention is such that when there is a forward thrust of the Orbiter (such as during an OMS firing) it is recorded as a negative  $X_o$  acceleration. We refer to this convention as an inertial frame of reference fixed to a point in space. The orientations and locations of the SAMS heads, with respect to the Orbiter structural coordinate system, are given in Table 7 and Fig. 2. More detailed descriptions of the SAMS accelerometers are available in the literature [6-12].

For STS-73, 2.5 gigabytes of SAMS data are available between MET 000/06:48:37 and 015/12:19:23. Appendix A describes how these data can be accessed using the internet. SAMS data recorded on STS-73 are also available on CD-ROM from the PIMS project at LeRC.

During analysis, PIMS found that the data from the SAMS TSH C appear to be lower in magnitude by a factor of approximately ten compared with the levels measured by a similar sensor on STS-50 (USML-1). There is also a factor of approximately ten difference when comparing the levels of acceleration contained in the STS-73 TSH C data (in the frequency regime of less than 5 Hz) to the STS-73 TSH A data. The STS-73 TSH A and B data compare well with the STS-50 data.

The PIMS group believes that the TSH C data magnitudes from the STS-73 mission were somehow compromised. Common frequency components appear as expected at Orbiter structural modes and at the Ku band antenna dither frequency and, therefore, the general trends and indications of mission activities appear to be accurate. Because TSH C had the highest cutoff frequency of the SAMS TSHs on this mission, it was decided to prepare this report using TSH C data for some specific plots and for the color spectrograms in Appendix C. Numeric values should not be used while interpreting these data.



### 3.3 Three-dimensional Microgravity Accelerometer

The 3DMA was developed by the Consortium for Materials Development in Space at the University of Alabama in Huntsville to measure the quasi-steady and vibratory environment of the Orbiters. The 3DMA, located in the Spacelab module, consisted of three remote triaxial sensors and three single axis invertible accelerometers located in the central unit. See Figure 2 for approximate sensor locations. Data were recorded in the central unit for post-mission analysis. Most of the high-frequency data were telemetered to the ground in near real-time for analysis and display in the POCC. For more information about 3DMA and data from USML-2, contact the developers, Table 2.

### 3.4. Microgravity Measuring Device

The MMD is a triaxial accelerometer with a nominal measurement resolution of  $1.1 \times 10^{-7}$  g from 0 to 100 Hz and a range of  $\pm 6 \times 10^{-4}$  g. The MMD was originally designed to measure the microgravity environment of the Wake Shield Facility but has since been utilized for measurements in the Orbiter middeck. On STS-73, the MMD was flown as DTO-913. The USML-2 Mission Scientist requested that the MMD be used to provide USML-2 PIs with acceleration measurements in the middeck. An Orbiter Payload and General Support Computer (PGSC) was used for MMD data recording and real-time display. A software upgrade, for compatibility with a PGSC-486 with color display capability, improved the crew interface from the previous flight on STS-65 by increasing the amount of data collected per minute and providing a real-time frequency domain display. The on-board display allowed the crew to monitor the effects of their daily activities on the Orbiter acceleration environment. By increasing their awareness of the levels of these vibrations the crew modified their operations to successfully reduce the vibrations produced during their activities and exercise periods. For more information about MMD, contact JSC.

### 3.5 Suppression of Transient Accelerations By Levitation Evaluation

The STABLE isolation system was developed by McDonnell Douglas Aerospace (MDA) and MSFC. Its flight on STS-73 was the first flight of an active microgravity vibration isolation system on the Orbiter. The STABLE isolator can prevent unwanted disturbances from reaching critical scientific and commercial payloads and can provide environments in the  $10^{-6}$  g range. The STABLE system provides component-level isolation. The concept of isolating only the vibration-sensitive portion of a payload may minimize the number and size of utility umbilicals. In multi-experiment racks, it also protects individual experiments regardless of disturbances produced by nearby experiments. Component-level isolation eliminates the potential for disturbances due to unintentional crew contact with the rack or its enclosure.

The STABLE hardware, in the configuration successfully flown on STS-73, is shown in Figure 3. It was contained within a single middeck locker container and located in the Spacelab module rack 10, Fig 2. In addition to providing a microgravity environment to the on-board



fluids demonstration unit CHUCK, STABLE transferred power, data, and video signals to the platform by flexible umbilical cables. For more information on STABLE, contact the developers, Table 2.

STABLE isolates by floating a platform on electromagnetic actuators that apply forces to counteract those that are transmitted through umbilicals or that originate within the experiment itself. Accelerations caused by these disturbing forces are measured by accelerometers on the platform, and these signals are used by a high bandwidth feedback controller to command the counteracting actuator forces. In addition to the acceleration controller, there is a very low bandwidth position loop that tends to keep the platform centered. Signals from three, two-axis optical sensors measure the position of the platform with respect to the base and are used to maintain centering. The centering function compensates for the extremely low-frequency disturbances.

The STABLE flight demonstration included measurements of the isolated payload's acceleration and position, base acceleration, actuator currents, accelerometer temperature, and control system gain settings for system performance evaluation [17]. STABLE was designed for autonomous operations with minimal crew attention and little or no feedback concerning operation or data gathering. The accelerometer sensor signals were passed through a 130 Hz filter. The data acquisition system sampled and recorded data from all accelerometers at a rate of 250 samples per second. A longer sampling period, 10 samples per second, was used for slowly varying quantities such as accelerometer temperature. Three accelerometers were located on the frame of the STABLE locker box to provide a reference signal for the determination of isolation performance. Six accelerometers were located on the floating platform. During the flight, the crew provided various force inputs to the Orbiter by pushing off the wall, typing on a computer console, closing a locker door, and doing exercises. Orbiter thrusters were fired every few minutes during the mission for normal Orbiter attitude control. Other events such as water dumps and payload bay door operations were also captured in the STABLE data. STABLE was not able to access the Orbiter time reference system; instead, approximate mission time was recorded by a crew member during the change of each STABLE hard disk drive. Thus, these events can be only approximately located in the data.

The simplest performance demonstration is an acceleration time history plot, Fig. 4. The vibration levels aboard STABLE's isolated platform are nearly insignificant compared to the ambient vibration levels measured. The base acceleration trace shows instantaneous accelerations as high as  $3 \times 10^{-3}$  g, while the isolated platform acceleration is more than 30 times less throughout the displayed data. Additional analyses show that STABLE's isolation system performed well across a wide frequency spectrum.

### 3.6 Microgravity Analysis Workstation

The Microgravity Analysis Workstation was conceived at the MSFC and developed by TBE to support USML-2. The primary objectives were to provide real-time quasi-steady



microgravity environment information to sensitive experiments and to provide guidance in how to optimize the quasi-steady acceleration environment. MAWS consisted of a PC-based system configured to acquire real-time Orbiter dynamics data and use the data to calculate the combined levels of the aerodynamic drag, gravity gradient, and Eulerian components of the Orbiter quasi-steady acceleration environment. The calculation algorithms were extracted from a TBE six degree of freedom model.

MAWS successfully acquired and processed data for the entire mission. The MAWS analytically derived microgravity environment information agreed well with the OARE-measured quasi-steady acceleration environment data. This was true in both local vertical/local horizontal and inertial attitudes. Notable differences between the two data sets were due to Orbiter venting operations that are not modelled by MAWS and due to OARE instrument drift. Regular OARE calibration operations consistently corrected for this drift and returned the data sets to within  $5 \times 10^{-8}$  g differences. One other consistent difference between MAWS results and OARE data is a fifteen minute period oscillation that was seen by OARE in the  $X_b$  axis data and was not indicated by MAWS. The cause of this oscillation is still under investigation.

On MET day 013, MAWS ran a series of parametric simulations to determine the optimal attitude for the CGF experiment. Based on the MAWS team's recommendations to the CGF and mission management teams, the Orbiter attitude for this CGF experiment run was modified. This attitude change permitted the CGF experiment to experience the most desirable acceleration environment, as predicted by MAWS.

#### 4. SAMS and OARE Data Analysis

The data recorded by SAMS on STS-73 were processed to correct for pre-mission bias calibration offsets and to compensate for temperature and gain related errors of bias, scale factor, and axis misalignment. The resulting units of acceleration are g's where  $1 \text{ g} = 9.8 \text{ m/s}^2$ . The data were orthogonally transformed from the three SAMS TSH coordinate systems to the Orbiter structural coordinate system ( $X_o, Y_o, Z_o$ ). The OARE data recorded during STS-73 and presented here have been compensated for temperature, bias, and scale factors. This processing is described in reference [5].

After this initial data correction phase, additional data analyses were applied to the SAMS and OARE data to characterize the acceleration environment of the mission. Because of the inherent differences between OARE (frequency range  $10^{-5}$  Hz to 1 Hz, sampling rate 10 samples per second) and SAMS (frequency range 0.01 Hz to 25 Hz, sampling rate 12.5 to 125 samples per second) data, some data analysis techniques are more applicable to data from one system than the other. The particular processing technique used also depends on the type of information desired.



#### 4.1 Time Domain Analysis

The time domain analysis techniques used in this report are acceleration versus time, interval average acceleration versus time and interval root mean square (RMS) acceleration versus time. For OARE time domain analysis, plots of trimmean acceleration versus time are provided. The notation for all the data analysis discussed here is defined in the Abbreviations and Acronyms list.

Acceleration versus Time: These are plots of the acceleration in units of g versus time. Among the time domain plots displayed in this report, this one yields the most precise accounting of the variation of acceleration magnitude as a function of time.

Interval Average Acceleration versus Time: A plot of this quantity in units of g versus time gives an indication of net accelerations which last for a number of seconds equal to or greater than the interval parameter. Shorter duration, high amplitude accelerations can also be detected with this type of plot, however, the exact timing and magnitude of specific acceleration events cannot be extracted. The interval average acceleration for generic x-axis data is defined as

$$x_{avg_k} = \frac{1}{M} \sum_{i=1}^M x_{(k-1)M+i}.$$

Corresponding expressions for y- and z-axis data can be combined to form the interval average acceleration vector magnitude as follows:

$$accel_{avg_k} = \sqrt{x_{avg_k}^2 + y_{avg_k}^2 + z_{avg_k}^2}.$$

Interval Root Mean Square Acceleration versus Time: A plot of this quantity in units of gRMS versus time gives a measure of the oscillatory content in the acceleration data. If it is assumed that the net acceleration over the interval number of seconds is negligible, then this quantity will give a indication of the energy in the signal due to purely oscillatory acceleration sources. The interval RMS acceleration for generic x-axis data is defined as

$$x_{RMS_k} = \sqrt{\frac{1}{M} \sum_{i=1}^M (x_{(k-1)M+i})^2}.$$

Corresponding expressions for y- and z-axis data can be combined to form the interval RMS acceleration vector magnitude as follows:



$$\text{accel}_{\text{RMS}_k} = \sqrt{x_{\text{RMS}_k}^2 + y_{\text{RMS}_k}^2 + z_{\text{RMS}_k}^2}.$$

Trimmean Acceleration versus Time: The trimmean filter is applied to OARE data to reject transient, higher magnitude accelerations from analysis that is concerned with the quasi-steady accelerations experienced at the sensor location. This filtering procedure ranks the collected data in order of increasing magnitude, measures the deviation of the distribution from a normal distribution, and deletes (trims) an adaptively determined amount of the data. The mean of the remaining data is calculated and this value is assigned to the central time of the interval analyzed [5]. For this report the trimmean filter was applied to fifty seconds of OARE data every twenty-five seconds.

## 4.2 Frequency Domain Analysis

Transformation of data to the frequency domain is typically done to gain more insight about the environment and to identify potential acceleration sources. The SAMS frequency domain analysis and displays used in this report are acceleration power spectral density versus frequency and acceleration power spectral density versus frequency versus time (spectrogram). Frequency domain analysis of OARE data is not often performed because of the relative lack of pertinent frequency information in the range of interest.

Power Spectral Density versus Frequency: Spectral analysis is performed on time series data to identify the relative magnitudes of sinusoidal signals that compose the series. The basis of this computation is the Fourier transform which indicates the magnitude of each frequency (sinusoid) present in the time history signal. The PIMS team uses the power spectral density (PSD) as the basis of its frequency domain analysis. The PSD is computed directly from the Fourier transform of a time series so that Parseval's Theorem is satisfied: the RMS of a time signal is equal to the square root of the integral of the PSD across the frequency band represented by the original signal. The PSD is reported in units of  $\text{g}^2/\text{Hz}$ .

Spectral averaging is often used to produce PSDs that represent the average spectral content of a time period of interest. The PSD of  $k$  successive intervals is calculated and the  $k$  resulting spectral series are averaged together on a point by point basis. This averaging technique is often referred to as Welch's Averaged Periodogram Method.

Power Spectral Density versus Frequency versus Time (Spectrogram): Spectrograms provide a roadmap of how acceleration signals vary with respect to both time and frequency. As such, they are particularly useful in identifying when certain activities begin and end. To produce a spectrogram, PSDs are computed for successive intervals of time. The PSDs are oriented vertically on a page such that frequency increases from bottom to top. PSDs from successive time slices are aligned horizontally across the page such that time increases from left to right. Each time-frequency bin is imaged as a color corresponding to the logarithm of the PSD magnitude at that time and frequency.



## 5. Columbia Microgravity Environment – STS-73

The microgravity environment measured by an accelerometer system on the Orbiter has many components. The quasi-steady microgravity environment is related to orbital phenomena such as aerodynamic drag and rotational motion and to gravity gradient effects based on the distance from the Orbiter center of gravity. In addition to these quasi-steady accelerations, all ongoing operations of crew life support systems and activities and operations of the Orbiter, crew, carrier, and experiments tend to have transient and vibratory components that contribute to the background acceleration environment.

In this report we are concerned with the identification of activities that cause acceleration levels above the background acceleration environment. The remainder of this section discusses the environment recorded during crew quiet times, during different attitude control situations and Orbiter configurations, during payload bay door motion, during Glovebox fan operations, during water dump operations, and while the Orbiter was positioned in different attitudes. The Appendices provide an overview of the microgravity and vibration environment during the STS-73 mission. Appendix B shows time history plots of SAMS TSH C (25 Hz filter cutoff) data. Appendix C provides a frequency domain representation of the SAMS TSH C data.

### 5.1. Crew Activity – Reference Plots

The seven member crew of STS-73 worked on a dual shift schedule. Because of this schedule, the variation in the microgravity environment between the crew sleep and awake periods that is seen in data from single shift missions is not as apparent in STS-73 OARE or SAMS data [11]. Fig. 5 shows OARE data for the extent of the STS-73 mission. Note that the quasi-steady environment represented by these data is relatively constant throughout the mission. Daily cycles in the acceleration levels may be seen in the  $X_b$  axis, especially for the first 250 hours of the mission. These are due to the daily mission activities of experiment operation and crew cycles. Waste water dumps can be seen in the  $Y_b$  axis data as periodic, short (about one hour) negative displacements. Waste water dump operations are discussed in more detail later as are variations due to attitude changes.

Fig. 6 shows an example of the vibration environment of the Spacelab module as recorded by SAMS during a period when the working crew voiced down that they were being quiet. Such calls by the crew were made as part of the OARE calibration procedure. The data plots in column a) of Fig. 6 are twenty minute time histories of the three axes of SAMS TSH A data starting at approximately MET 005/07:09. The data plots in column b) of Fig. 6 show PSD representations of the column a) data. These plots represent the microgravity and vibration environment in the Spacelab during STS-73 that resulted, in part, from various equipment and life support systems that were operational at the time. Therefore, Fig. 6 can be used as a basis of comparison for other activities discussed in this report.



## 5.2 Orbiter Attitude

Orbiter attitudes for missions are typically defined well in advance of launch. Several factors drive the determination of attitude, for example Orbiter thermal conditions, maximizing continuous communications, and experiment operations requirements. The original attitude timeline for the STS-73 mission included a nominal USML-2 gravity gradient (GG) attitude and specific attitudes designed for the GFFC and CGF experiments. Not long before the launch of the STS-73 mission, the desirability of certain Orbiter attitudes was reassessed. This assessment was related to the predicted number of debris collisions with the leading face of the Orbiter and the effect of such hits on crew safety. Two changes were made to the USML-2 attitude timeline as a result of this assessment. The CGF Attitude was disallowed for the more than 150 hours needed for the Marshall Space Flight Center crystal growth experiment sample. The nominal attitude for the USML-2 microgravity time was modified during the mission as indicated in Table 8. This modification was indirectly related to the debris impact concerns.

To help limit the number of debris hits in the cargo bay (specifically on the radiators), the port cargo bay door was kept partially closed during the mission. The nominal USML-2 attitude had been designed so that the combined Orbiter/payload center of gravity would be in a predicted location. The altered payload bay door configuration moved the center of gravity location enough that one thruster jet did not need to fire as often as originally predicted in order to maintain the attitude. As a result, this jet experienced low temperatures during the early part of the mission, and the nominal USML-2 attitude was adjusted so that the jet maintained an acceptable temperature. The major STS-73 attitudes are shown pictorially in Fig. 7.

The acceleration environment differences related to the different attitudes are not particularly apparent in the whole mission OARE data plot, Fig. 5. Figures 8-11 show the quasi-steady acceleration levels recorded by OARE when the Orbiter was in the nominal GG USML-2 attitude, the CGF attitude, the GFFC attitude, and a Solar inertial attitude used for thermal conditioning. Thermal conditioning attitudes are used to warm up or cool off various systems or structures on the Orbiter. Surfaces and structures on the Orbiter can become very cold if they are not heated by some external source, such as heat from the sun or heat radiated from the earth. During USML-2, the Orbiter's tires (stowed in the belly) became too cold, resulting in lower tire pressure. The thermal analysis flight controllers at Johnson Space Center (JSC) designed an attitude to point the Orbiter belly at the sun to increase the temperature of the tires. A solar inertial attitude was used, which means that the Orbiter maintained constant orientation relative to the position of the sun. The effects on the microgravity environment can be seen in Fig. 11. The cyclical variations in the acceleration levels (as compared with Figs. 8-10) are typical of such an attitude.

## 5.3 Attitude Control

The frequency of thruster firings is one factor that microgravity experimenters like to control when they are submitting mission requirements. Acceleration levels caused by thruster



firings are also of concern to investigators. Orbiter attitudes for microgravity payloads are therefore often designed to minimize the number of firings of the vernier reaction control system (VRCS) jets used for attitude control. The number of thruster firings per hour was analyzed for the three main attitudes flown during USML-2 experiment operations, Table 9. The VRCS average rates of firing were derived from data from 4.5 hour time periods. Missing data were replaced with a no firing indicator and if more than one jet fired at a time, this was counted as a single firing event. Also included in Table 9 are data for two times when the solar inertial attitude was maintained using the primary reaction control system (PRCS) jets.

The loss of one VRCS jet results in the loss of the entire vernier mode. So, when a failure of a VRCS jet is evident, the system automatically shuts off, putting the Orbiter into a free drift situation. An intermittent power supply failure during STS-73 caused the aft, starboard jets to fail several times. This resulted in several free drift periods during the mission. Fig. 12 is a six-panel SAMS TSH A data plot of one of these free drift periods. Note that the main difference between this time period and that shown in Fig. 6 is the presence of VRCS firings in Fig. 6. The time histories of Figs. 6 and 12 are plotted on different scales.

During one of the power supply failure periods, specific tests were performed to evaluate the problem. Figures 13 and 14 show SAMS data from when the R5R and R5D jets fired, respectively. These figures are good examples of what effect individual VRCS firings have on the acceleration environment. Note that the PSDs lack detail because of the small amount of data analyzed.

Figure 15 provides additional insight into the microgravity environment caused by VRCS and PRCS jet firings. This plot is the vector magnitude of the three axes of SAMS TSH B data collected over five hours when the Orbiter was cycling among VRCS attitude control, PRCS attitude control, and free drift. PRCS and VRCS jet firing events are indicated across the top of the plot. The acceleration magnitude difference between PRCS and VRCS activity is obvious. Acceleration magnitudes related to a single PRCS jet firing used in this manner are in the 0.01 to 0.025 g range, compared to VRCS jet acceleration magnitudes of about  $3 \times 10^{-4}$  to  $7 \times 10^{-4}$  g. Figure 16 is a snapshot of one series of the PRCS jet firings for comparison with previous reference (crew quiet) and VRCS test firing figures.

#### 5.4 Payload Bay Door Motion

The port payload bay door had to be fully opened once during the mission so that a Spacelab condensate dump could be performed. Condensate dumps are performed using a vent on the module's forward end cone ( $X_0 = 905$  in,  $Y_0 = -2$  in,  $Z_0 = 455.4$  in) to release excess water accumulated in the Spacelab. The nozzle is angled up 29 degrees above the horizontal plane of the Orbiter. The condensate dump occurred at MET 005/00:19. The dump duration was two minutes. The port payload bay door began to open for the dump at about 004/23:49 and motion to return the door to its partial closed position began at about 005/00:26. Figure 17 shows SAMS TSH A data collected during the door opening operations. The impact of the door motion is seen



most clearly on the  $Y_0$  and  $Z_0$  axes. The  $\sim 0.4$  Hz frequency of the acceleration has previously been identified as a payload bay door mode [13,14]. No obvious acceleration signature that could be attributed to the payload bay door partial closing could be identified in the SAMS data.

### 5.5 Glovebox Fan Operations

The STDCE investigators noticed several perturbations in their experiment during USML-2 that prompted them to suspect that vibratory components of the microgravity environment may have been the cause. Coordination among STDCE, 3DMA, PIMS, GFFC, the Mission Scientist team, the Glovebox engineering team, the JSC Flight Activities Officer, and the crew led to the identification of several operations as possible sources for the deleterious vibrations. In the course of these investigations, two fans in the Glovebox were turned off in succession so that STDCE could evaluate the fans' effects on the experiment. At about 001/22:37, the Glovebox cooling fan was turned off. Thirty seconds later the Glovebox air circulation fan was turned off. The 3DMA downlink data were used in real-time to observe how the fans affected the microgravity environment.

Fig. 18 shows SAMS TSH C data (sensor head located on the Glovebox facility) for the time period when the two fans were shut off. A slight decrease in acceleration levels can be seen in the time history data about 2.5 minutes into the time history plot. Note that the PSDs are displayed out to the highest frequency possible to show the frequency components at approximately 38, 43, 48, and 53 Hz which may be related to the fans. Fig. 19 provides a better picture of the effects of these two Glovebox fans. The SAMS TSH C color spectrogram shows that there are frequency components at 20, 38, 43, 48, and 53 Hz. Those at 20, 38, and 48 Hz stop at time 001/22:37 and those at 53 and, possibly, 43 Hz stop at time 001/22:38:30. This seems to correlate with the turn off times of the Glovebox fans. The PIMS group has requested more information from the Glovebox engineering team at MSFC so that they can better characterize the effects the Glovebox had on the acceleration environment during USML-2.

### 5.6 Water Dump Operations

The Orbiter Food, Water, and Waste Management Subsystem provides storage and dumping capabilities for potable and waste water [15]. Supply and waste water dumps are performed using nozzles on the port side of the Orbiter. Water dumps from these nozzles are expected to cause a steady acceleration of about  $4 \times 10^{-7}$  g in the  $Y_b$ -axis [16]. About sixteen water dumps can be clearly seen in the Fig. 5 plot of OARE data for the entire mission. These dumps each lasted for about one hour and the apparent acceleration in the  $Y_b$ -axis is on the order of  $-1 \times 10^{-6}$  g. Two larger excursions in the OARE data at about MET 90 hours and 190 hours were caused by simultaneous waste and supply water dump operations. The OARE data plot in Fig. 20 represents the acceleration environment for a twenty-four hour period during STS-73. Two water dump operations are obvious in this plot.



## 6. Summary

The microgravity environment of the Space Shuttle Columbia was measured during the STS-73 mission using accelerometers from five different instruments: OARE, SAMS, 3DMA, MMD, and STABLE. An estimate of the quasi-steady environment was also calculated in near real-time during the mission by MAWS. The OARE provided investigators with real-time quasi-steady acceleration measurements. SAMS recorded higher frequency data on-board for post-mission analysis. 3DMA provided some real-time data downlink and also recorded data for post-mission analysis. MMD was used by the crew to increase their awareness of the effects their activities have on the microgravity environment. The STABLE active vibration isolation system demonstrated the feasibility of this type of disturbance attenuation on the Orbiter. The MAWS quasi-steady environment calculation and comparison of this calculation with OARE data was used to assess how appropriate the planned CGF attitude was for one CGF experiment run.

The standard data analysis techniques used to process SAMS and OARE data are discussed. Using a combination of these techniques, the microgravity environment related to several different Orbiter, crew, and experiment operations is presented and interpreted. SAMS data for a crew quiet period is presented as a basis for comparison with other activities. This example of SAMS data includes the effects of VRCS jet firings for Orbiter attitude control. Plots showing this component of the Orbiter background acceleration environment are compared to examples of SAMS data when no thrusters were firing, when the PRCS jets were used for attitude control, and when single VRCS jets were fired for test purposes. In general, VRCS jets, when used for attitude control cause accelerations in the  $3 \times 10^{-4}$  g to  $7 \times 10^{-4}$  g range. PRCS jets used in this manner cause accelerations in the 0.01 to 0.025 g range.

Other significant disturbance sources and their associated acceleration signal characteristics were water dump operations with  $Y_b$  axis acceleration deviations of about  $1 \times 10^{-6}$  g; payload bay door opening motion with  $Y_o$  and  $Z_o$  axis accelerations of frequency 0.4 Hz; and probably Glovebox fan operations with notable frequency components at 20, 38, 43, 48, and 53 Hz.

The STS-73 microgravity environment represented by SAMS and OARE data is comparable to the environments measured by the instruments on earlier microgravity science missions. The OARE data compared well with MAWS predictions of the quasi-steady environment and, therefore, must be accurately representing this regime of the environment. OARE measures actual accelerations, so the effects of venting operations such as water dumps and flash evaporator system activities can be seen in this data set. The SAMS data from STS-73 show the usual influence of thruster firings and crew motion (transient events) and of crew exercise and Orbiter systems and experiment operations (oscillatory events). Orbiter structural modes and crew exercise frequencies are typically the same among Orbiters, missions, and crew members. The main differences among missions are the specific frequencies of equipment oscillations. Better coordination between PIMS and experiment and Orbiter systems designers and engineers is needed to help identify the sources of all distinct characteristics of the Orbiter microgravity environment.



## 7. References

- [1] Blanchard, R. C., M. K. Hendrix, J. C. Fox, D. J. Thomas, and J. Y. Nicholson, Orbital Acceleration Research Experiment. *J. Spacecraft and Rockets*, Vol. 24, No. 6, (1987) 504 - 511.
- [2] Blanchard, R. C., J. Y. Nicholson, and J. R. Ritter, STS-40 Orbital Acceleration Research Experiment Flight Results During a Typical Sleep Period. NASA Technical Memorandum 104209, January 1992.
- [3] Blanchard, R. C., J. Y. Nicholson, J. R. Ritter, Preliminary OARE Absolute Acceleration Measurements on STS-50. NASA Technical Memorandum 107724, February 1993.
- [4] Blanchard, R. C., J. Y. Nicholson, J. R. Ritter, and K. T. Larman, OARE Flight Maneuvers and Calibration Measurements on STS-58. NASA Technical Memorandum 109093, April 1994.
- [5] Canopus Systems, Inc., OARE Technical Report #147, STS-73 (USML-2) Final Report. CSI-9601, February 1996.
- [6] DeLombard, R., B. D. Finley, Space Acceleration Measurement System description and operations on the First Spacelab Life Sciences Mission. NASA Technical Memorandum 105301, November 1991.
- [7] DeLombard, R., B. D. Finley, and C. R. Baugher, Development of and flight results from the Space Acceleration Measurement System (SAMS). NASA Technical Memorandum 105652, January 1992.
- [8] Baugher, C. R., G. L. Martin, and R. DeLombard, Low-frequency vibration environment for five shuttle missions, NASA Technical Memorandum 106059, March 1993.
- [9] Rogers, M. J. B., C. R. Baugher, R. C. Blanchard, R. DeLombard, W. W. Durgin, D. H. Matthiesen, W. Neupert, and P. Roussel, A Comparison of low-gravity measurements onboard Columbia during STS-40. *Microgravity Science and Technology VI/3* (1993) 207 - 216.
- [10] Finley, B. D., C. Grodsinsky, and R. DeLombard, Summary report of mission acceleration measurements for SPACEHAB-01, STS-57. NASA Technical Memorandum 106514, March 1994.
- [11] Rogers, M. J. B., and R. DeLombard, Summary report of mission acceleration measurements for STS-62. NASA Technical Memorandum 106773, November 1994.



- [12] Rogers, M. J. B., and R. DeLombard, Summary report of mission acceleration measurements for STS-65. NASA Technical Memorandum 106871, March 1995.
- [13] Cooke, C., M. Koenig, J. Lepanto, G. Levine, J. Miller, D. Sargent, and R. Schlundt, SDI Space Shuttle Based Experiments for Acquisition, Tracking, and Pointing-Definition of Space Shuttle Operational Environment, The Charles Stark Draper Laboratory, Cambridge, Massachusetts, R-1868, 1986.
- [14] Rogers, M. J. B. and J. I. D. Alexander, Data Analysis for Spacelab Missions. Microgravity Science and Technology V/1 (1992) 43-49.
- [15] Shuttle Operational Data Book, Volume 1, JSC-08934, Rev. E, Johnson Space Center, Houston, TX, January 1988.
- [16] Rogers, M. J. B., B. P. Matisak, and J. I. D. Alexander, Venting Force Contributions-Quasi-steady Acceleration on STS-50. Microgravity Science and Technology VII/4 (1995) 293-298.
- [17] Results of the STABLE Microgravity Vibration Isolation Flight Experiment, AAS 96-071, Donald Edberg\*, Robert Boucher\*, David Schenck\* , Gerald Nurre† , Mark Whorton†, Young Kim†, and Dean Alhorn†, AAS 96-071, presented at the 19th AAS Guidance, Navigation, and Control Conference, Breckinridge CO, February 1996.

Identification and Mitigation of Low-Frequency Vibrations on Space Station, Robert Boucher, AIAA 96-1205, presented at the AIAA Dynamics Specialists Conference, Salt Lake City UT, April 1996.

\* McDonnell Douglas Aerospace

† National Aeronautics and Space Administration, Marshall Space Flight Center

**Table 1.** USML-2 Experiments and Facilities

<i>Experiments and Facilities</i>	<i>Location</i>	<i>Contact</i>	<i>Affiliation</i>
Astroculture Facility and Experiment (ASC), <i>15 experiments</i>	Middeck	Raymond J.Bula	Wisconsin Center for Space Automation & Robotics Madison, WI
Advanced Protein Crystallization Facility (APCF), <i>15 experiments</i>	Spacelab Rack 10	Gottfried Wagner	University of Giessen Giessen, Germany
Crystal Growth Furnace (CGF), <i>4 experiments</i>	Spacelab Rack 9	Martin Volz	NASA Marshall Space Flight Center, Huntsville, AL
Surface Tension Driven Convection Experiment (STDCE)	Spacelab Rack 3	Simon Ostrach	Case Western Reserve University Cleveland, OH
Zeolite Crystal Growth (ZCG)	Middeck	Albert Sacco, Jr.	Worcester Polytechnic Institute Worcester, MA
Single-Locker Protein Crystal Growth - Two Methods (SPCG)	Middeck	Daniel Carter	NASA Marshall Space Flight Center, Huntsville, AL
Commercial Protein Crystal Growth (CPCG)	Middeck	Larry DeLucas	Center for Macromolecular Crystallography Birmingham, AL
Space Acceleration Measurement System (SAMS)	Spacelab - Center Aisle Rack 3, Rack 9 Rack 12	Ron Sicker	NASA Lewis Research Center Cleveland, OH
Drop Physics Module (DPM), <i>2 experiments</i>	Spacelab Rack 8	Arvid Croonquist	NASA Jet Propulsion Laboratory, Pasadena, Ca
Geophysical Fluid Flow Cell Experiment (GFFC)	Spacelab Rack 5	Fred Leslie	University of Colorado Boulder, CO
Glovebox (GBX), <i>7 experiments</i>	Spacelab Rack 12	Donald A. Reiss	NASA Marshall Space Flight Center, Huntsville, AL
Commercial Generic Bioprocessing Apparatus (CGBA)	Middeck	Louis Stodieck	Center for Bioserve Space Technologies University of Colorado Boulder, CO



**Table 2.** STS-73 Payloads

<i><b>Payloads</b></i>	<i><b>Location</b></i>	<i><b>Contact</b></i>	<i><b>Affiliation</b></i>
USML-2	Cargo Bay	Marcus Vlasse	NASA Marshall Space Flight Center, Huntsville, AL
Orbital Acceleration Research Experiment	Keel Bridge	William Wagar	NASA Lewis Research Center Cleveland, OH
Three-dimensional Microgravity Accelerometer	Spacelab Center Aisle	Jan Bijvoet	University of Alabama in Huntsville, Huntsville, AL
Suppression of Transient Accelerations By Levitation Evaluation	Spacelab Rack 10	Gerald Nurre	NASA Marshall Space Flight Center, Huntsville, AL

**Table 3.** STS-73 Developmental Test Objectives

DTO 301D	Ascent Structural Capability Evaluation
DTO 307D	Entry Structural Capability
DTO 312	ET TPS Performance
DTO 319D	Shuttle/Payload Low Frequency Environment
DTO 414	APU Shutdown Test
DTO 623	Cabin Air Monitoring
DTO 655	Foot Restraint Evaluation
DTO 667	Portable In-Flight Landing Operations Trainer
DTO 679	Ku-Band Communications Adapter Demonstration
DTO 805	Crosswind Landing Performance
DTO 913	Microgravity Measuring Device Evaluation
DTO 1121	Ground-to-Air TV Demonstration

**Table 4.** STS-73 Detailed Supplementary Objectives

DSO 487	Immunological Assessment of Crew Members
DSO 491	Characterization of Microbial Transfer Among the Crew
DSO 603C	Orthostatic Function During Entry, Landing and Egress
DSO 604	Visual Vestibular Integration as a Function of Adaptation
DSO 605	Postural Equilibrium Control During Landing/Egress
DSO 611	Air Monitoring Instrument Evaluation and Atmosphere Test
DSO 621	In-Flight Use of Florinef to Improve Orthostatic Intolerance
DSO 624	Pre and Postflight of Cardiorespiratory Response to Exercise
DSO 626	Cardiovascular and Cerebrovascular Response Before and After Flight
DSO 802	Educational Activities
DSO 901	Documentary Television
DSO 902	Documentary Motion Picture Photography
DSO 903	Documentary Still Photography
DSO 904	Assessment of Human Factors

**Table 5.** STS-73 Crew

<i>Crewmember</i>	<i>Position</i>	<i>Team</i>
Kenneth D. Bowersox	Commander	Red Team
Kent V. Rominger	Pilot	Red Team
Catherine G. Coleman	Mission Specialist 1	Blue Team
Michael E. Lopez-Alegria	Mission Specialist 2	Blue Team
Kathryn C. Thornton	USML-2 Payload Commander	Red Team
Fred W. Leslie	Payload Specialist 1	Blue Team
Albert Sacco, Jr.	Payload Specialist 2	Red Team
David H. Matthiesen	Alternate Payload Specialist	
Glynn Holt	Alternate Payload Specialist	



**Table 6.** STS-73 OARE Head Location and Orientation

<b>OARE Sensor</b>		Sample Rate: 10 samples/second
Location: Orbiter Cargo Bay Keel Bridge		Frequency: 0 to 1 Hz
<b>ORIENTATION</b>		<b>LOCATION</b>
<b>Orbiter Structural Axis</b>	<b>Sensor Axis</b>	<b>Structural Axis</b>
$X_o$	$-X_{OARE}$	$X_o = 1153.3$ in
$Y_o$	$Z_{OARE}$	$Y_o = -1.3$ in
$Z_o$	$Y_{OARE}$	$Z_o = 317.8$ in

**Table 7.** STS-73 SAMS Head Location and Orientation

<b>Unit C TSH A</b>		Sample Rate: 25 samples/second
Serial no.: 821-3		
Location: Spacelab - behind STDCE in Rack 3		Frequency: 0 to 5 Hz
<b>ORIENTATION</b>		<b>LOCATION</b>
<b>Orbiter Structural Axis</b>	<b>Sensor Axis</b>	<b>Structural Axis</b>
X <sub>o</sub>	+Y <sub>H</sub>	X <sub>o</sub> = 992.29 in
Y <sub>o</sub>	+X <sub>H</sub>	Y <sub>o</sub> = -63.37 in
Z <sub>o</sub>	-Z <sub>H</sub>	Z <sub>o</sub> = 401.3 in

<b>Unit C TSH B</b>		Sample Rate: 12.5 samples/second
Serial no.: 821-5		
Location: Spacelab - below CGF in Rack 9		Frequency: 0 to 2.5 Hz
<b>ORIENTATION</b>		<b>LOCATION</b>
<b>Orbiter Structural Axis</b>	<b>Sensor Axis</b>	<b>Structural Axis</b>
X <sub>o</sub>	+Y <sub>H</sub>	X <sub>o</sub> = 1086.47 in
Y <sub>o</sub>	-0.2079X <sub>H</sub> + 0.9781Z <sub>H</sub>	Y <sub>o</sub> = -51.25 in
Z <sub>o</sub>	0.9781X <sub>H</sub> - 0.2079Z <sub>H</sub>	Z <sub>o</sub> = 358.35 in

<b>Unit C TSH C</b>		Sample Rate: 125 samples/second
Serial no.: 821-15		
Location: Spacelab - under GBX in Rack 12		Frequency: 0 to 25 Hz
<b>ORIENTATION</b>		<b>LOCATION</b>
<b>Orbiter Structural Axis</b>	<b>Sensor Axis</b>	<b>Structural Axis</b>
X <sub>o</sub>	+Y <sub>H</sub>	X <sub>o</sub> = 1118.57 in
Y <sub>o</sub>	+Z <sub>H</sub>	Y <sub>o</sub> = 36.94 in
Z <sub>o</sub>	+X <sub>H</sub>	Z <sub>o</sub> = 396.65 in

**Table 8.** USML-2 As-Flown Timeline

	<i>MET Time</i>	<i>Ref Att / Remarks</i>	<i>Event</i>
1	000/00 = 26:52		OMSA-2 BURN ATT
2	000/01 = 12:00	LVLH R = 0.00 P = 180.00 Y = 270.00	-ZLV -YVV
3	000/02:45:00	LVLH R = 0.00 P = 348.00 Y = 0.00	TRIM BURN ATT
4	000/03:01:10	INRTL R = 123.80 HOLD P = 247.48 Y = 297.44	-X RCS BURN TIG: 0/03:01 = 40
5	000/03:04:00	LVLH R = 0.00 P = 348.00 Y = 0.00	TRIM BURN ATT
6	000/03:07:00	STARS -Y: 97 -Z: 57	IMU ALIGN STAR PAIR AT
7	000/03:48:00	STAR: 23 BETELGEUSE	-X HUD CAL
8	000/04:45:00	LVLH R = 287.01 P = 90.58 Y = 358.09	BIAS -XLV -YVV
9	000/11:15:00		B4 DB Collapse
10	000/13:29:00	LVLH R = 285.85 P = 96.24 Y = 358.68	Bias -XLV -YVV FSL Jet Warmer Original Bias
11	001/03:01:00	LVLH R = 288.88 P = 94.41 Y = 359.26	Bias -XLV -YVV Optimize F5L Bias Test Att
12	001/08:00:00	LVLH R = 270.00 P = 95.00 Y = 355.00	-XLV -YVV 1st F5L Bias GFFC



**Table 8.** USML-2 As-Flown Timeline (continued)

13	001/11:24:00	LVLH R = 280.99 P = 91.98 Y = 0.38	FREE DRIFT
14	001/11:40:00	LVLH R = 270.00 P = 95.00 Y = 355.00	-XLV -YVV Return to att GFFC
15	001/14:10:00	LVLH R = 285.98 P = 96.24 Y = 356.88	Bias -XLV -YVV
16	004/23:30:00	LVLH R = 270.00 P = 85.00 Y = 355.00	-XLV -YVV GFFC
17	005/08:30:00	LVLH R = 288.98 P = 96.24 Y = 356.58	BIAS -XLV -YVV
18	007/04:11:52	LVLH R = 289.80 P = 92.10 Y = 355.20	FREE DRIFT R5R, R5D Fail Off
19	007/04:24:00	LVLH R = 293.21 P = 90.29 Y = 358.82	FREE DRIFT
20	007/04:34:00	LVLH R = 298.80 P = 91.01 Y = 1.70	FREE DRIFT
21	007/04:42:48	LVLH R = 303.55 P = 93.03 Y = 1.41	FREE DRIFT
22	007/04:48:47	LVLH R = 306.94 P = 95.88 Y = 358.17	FREE DRIFT
23	007/04:58:44	LVLH R = 301.90 P = 96.40 Y = 357.80	FREE DRIFT HOT FIRE R5D 7/05:01:25

**Table 8.** USML-2 As-Flown Timeline (continued)

24	007/05:05:36	LVLH R = 293.30 P = 98.70 Y = 0.30	FREE DRIFT HOT FIRE R5R 7/05:05:38
25	007/05:11:00	LVLH R = 286.96 P = 96.24 Y = 356.88	BIAS -XLV -YVV Return to ATT
26	007/15:00:00	LVLH R = 270.00 P = 95.00 Y = 355.00	-XLV -YVV GFFC
27	007/23:30:00	LVLH R = 286.98 P = 96.24 Y = 356.68	BIAS -XLV -YVV
28	008/14:30:00	INRTL R = 93.74 P = 160.25 Y = 58.60	+ZSI MLG TC 1st period
29	008/22:34:00	LVLH R = 286.96 P = 98.24 Y = 368.88	BIAS -XLV -YVV
30	010/15:11:00	INRTL R = 56.93 P = 302.80 Y = 310.82	+ZSI MLG TC 2nd period
31	011/04:57:00	LVLH R = 286.96 P = 96.24 Y = 356.68	BIAS-XLV -YVV
32	012/13:30:00	INRTL R = 75.54 P = 324.49 Y = 306.42	+ZSI MLG TC 3rd period
33	013/00:45:10	LVLH R = 180.40 P = 263.40 Y = 303.30	FREE DRIFT R5D & R5R FAIL
34	013/00:51:17		Return to + ZSI 3rd Period



**Table 8.** USML-2 As-Flown Timeline (continued)

35	013/06:22:00	LVLH R = 286.95 P = 96.24 Y = 356.68	BIAS -XLV - YVV
36	013/07:00:00	LVLH R = 288.74 P = 92.23 Y = 343.88	FREE DRIFT
37	013/07:16:00	LVLH R = 301.17 P = 92.04 Y = 8.23	FREE DRIFT
38	013/07:37:00	LVLH R = 286.96 P = 98.24 Y = 358.68	BIAS -XLV - YVV Return to Att
39	013/09:30:00	LVLH R = 181.00 P = 90.00 Y = 0.00	-XLV - ZVV CGF
40	013/18:21:00	LVLH R = 288.96 P = 96.24 Y = 356.68	BIAS -XLV - YVV
41	013/21:59:00	INRTL R = 36.14 P = 253.53 Y = 357.18	+ ZSI MLG TC 4th period
42	014/21:06:00		SAMS INIT ATT
43	014/21:30:00	INRTL R = 54.00 P = 287.00 Y = 27.00	SAMS PITCH
44	014/21:40:00	INRTL R = 3.58 HOLD P = 192.95 Y = 301.65	Pitch Complete 500 Degrees
45	014/21:42:00	INRTL R = 3.88 P = 192.95 Y = 301.65	SAMS ROLL
46	014/21:49:00	INRTL R = 63.58 HOLD P = 192.95 Y = 301.65	ROLL COMPLETE 420 DEGREES

**Table 8.** USML-2 As-Flown Timeline (continued)

47	014/21:51:00	INRTL R = 63.58 P = 192.95 Y = 301.85	SAMS YAW
48	014/21:58:00	INRTL R = 28.82 HOLD P = 140.23 Y = 347.09	YAW COMPLETE 420 DEGREES
49	014/22:00:00	INRTL R = 28.82 HOLD P = 140.23 Y = 347.09	SAMS FREE DRIFT
50	014/22:09:00	LVLH R = 0.00 P = 90.00 Y = 270.00	-YLV + ZVV
51	015/16:11:00	STARS -Y:37 -Z:18 COAS:18	IMU ALIGN & -Z COAS CAL
52	015/16:47:00	INRTL R = 47.65 P = 337.06 Y = 34.73	-XSI
53	015/17:55:00	STARS -Y:38 -Z:13	D/O IMU ALIGN
54	015/18:09:00	STARS -Y:21 -Z:49	D/O IMU VERIF
55	015/18:20:00		D/O THERMAL & COMM ATT
56	015/20:35:00	OOP SOUTH	D/O BURN TO KSC TIG: 15/20:53
57	015/20:58:00		EI-25 INERTIAL At TIG + 5
58	015/21:18:00	LVLH R = 0.00 P = 40.00 Y = 0.00	EI-5 LVLH At TIG +25



**Table 9.** Number of VRCS firings for certain attitudes on STS-73

<i>Attitude</i>	<i>MET Start</i>	<i>VRCS Firings Per Minute</i>	<i>VRCS Firings Per Hour</i>
+ZSI	010/15:30	$\geq 1.2$	$\geq 72.7$
+ZSI PRCS attitude control	014/09:50—014/10:50	$\geq 0.65$	$\geq 39.0$
+ZSI PRCS attitude control	014/07:50—014/08:50	$\geq 0.53$	$\geq 32.1$
CGF	013/09:40	$\geq 0.38$	$\geq 22.7$
GFFC	007/15:02	$\geq 0.33$	$\geq 20.0$
GG	008/23:00	$\geq 0.28$	$\geq 16.7$

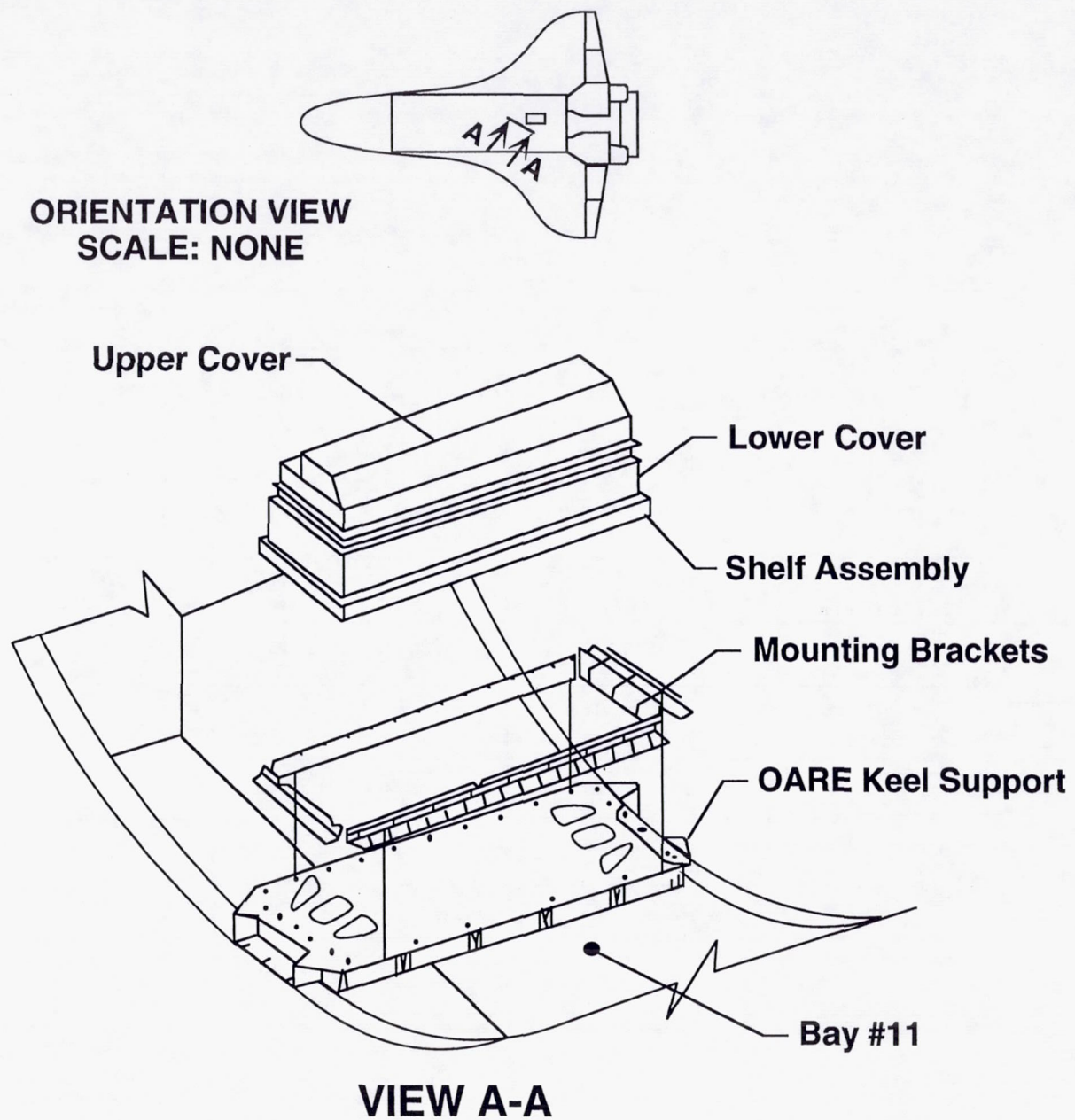


**Figure 1.** OARE instrument location on STS-73



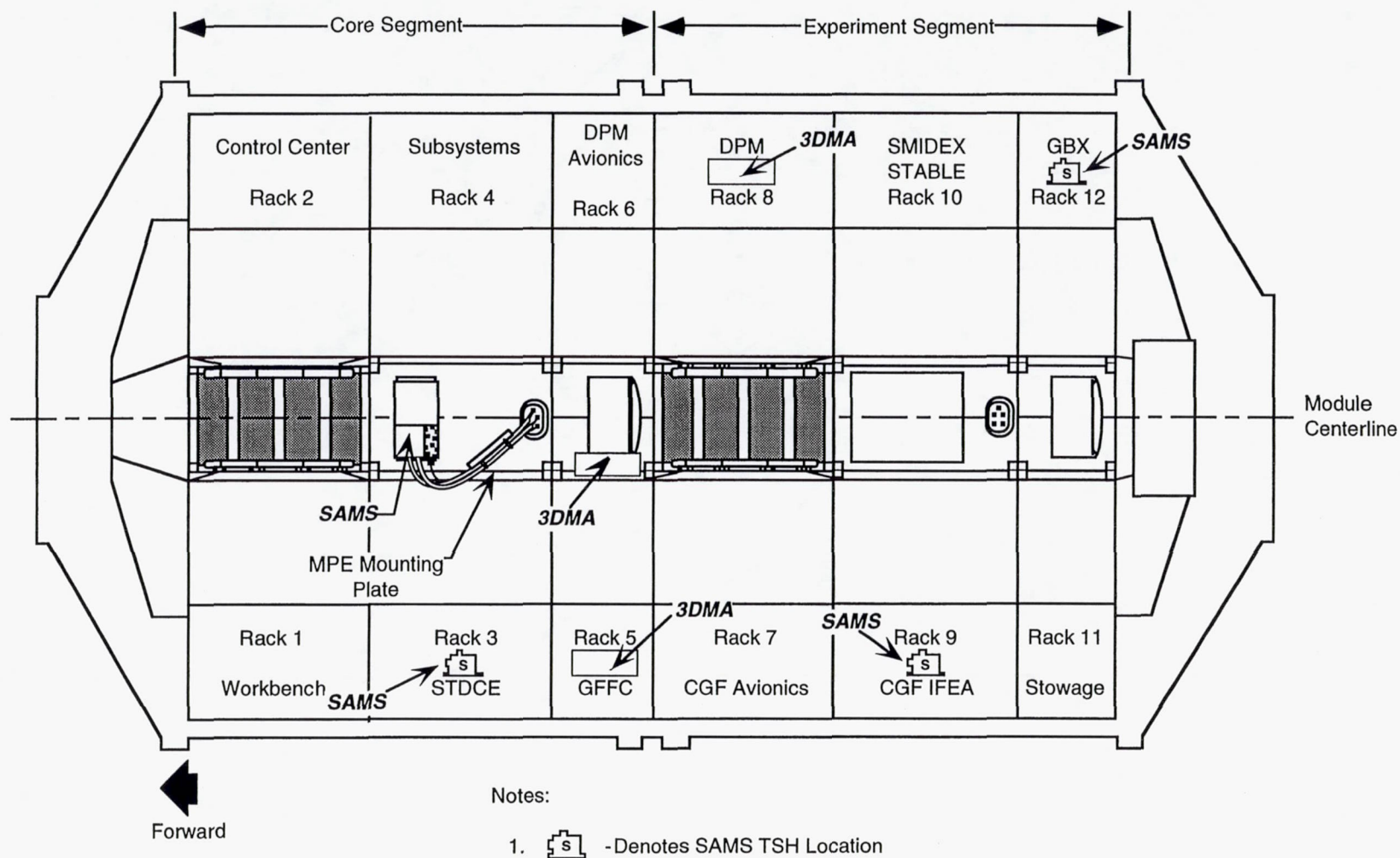
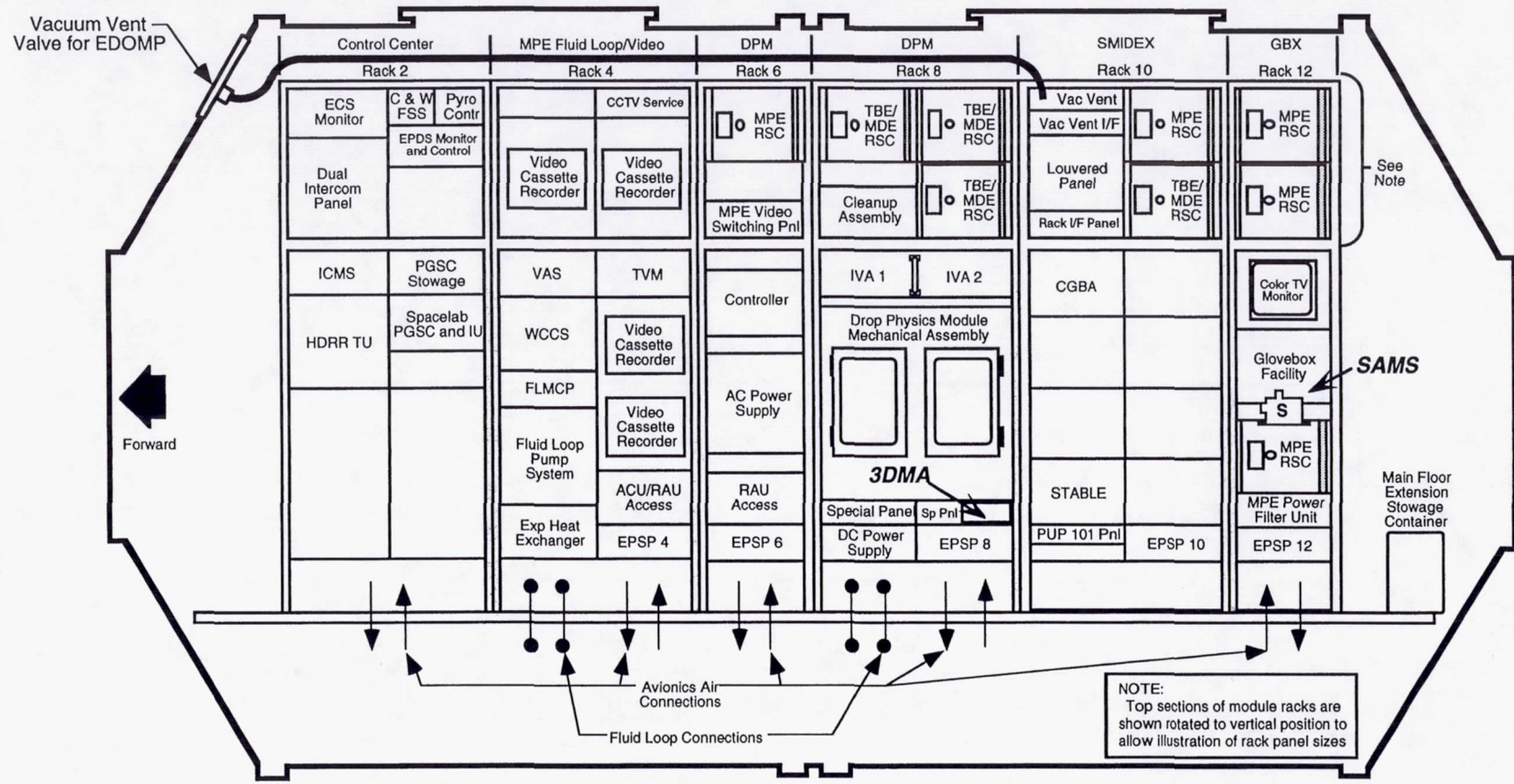


**Figure 2a.** Approximate location of SAMS and 3DMA sensors on STS-73, Spacelab Center aisle.

29

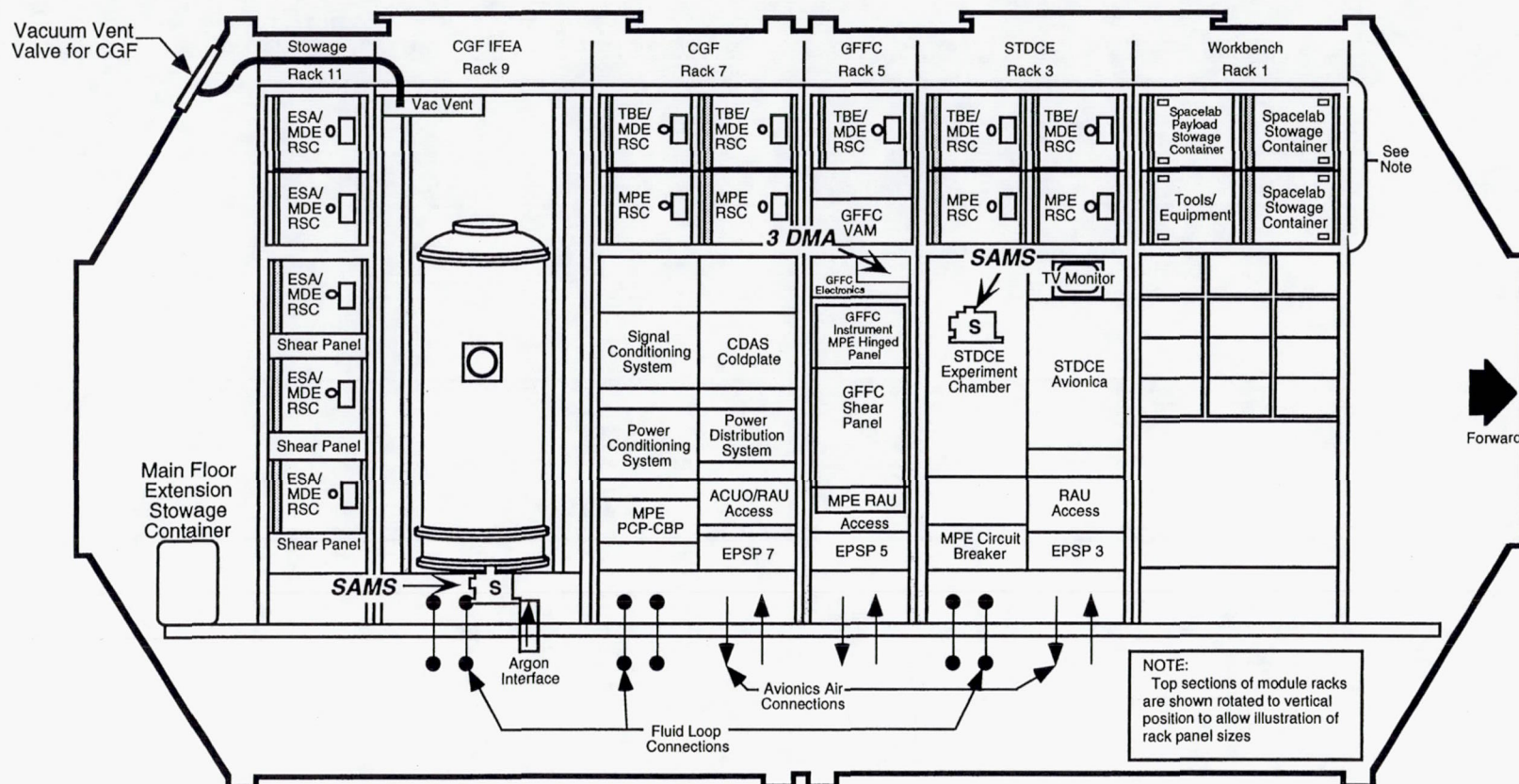


USML-2 MODULE CONFIGURATION, STARBOARD SIDE

Figure 2b. Approximate location of SAMS and 3DMA sensors on STS-73, Spacelab starboard side.



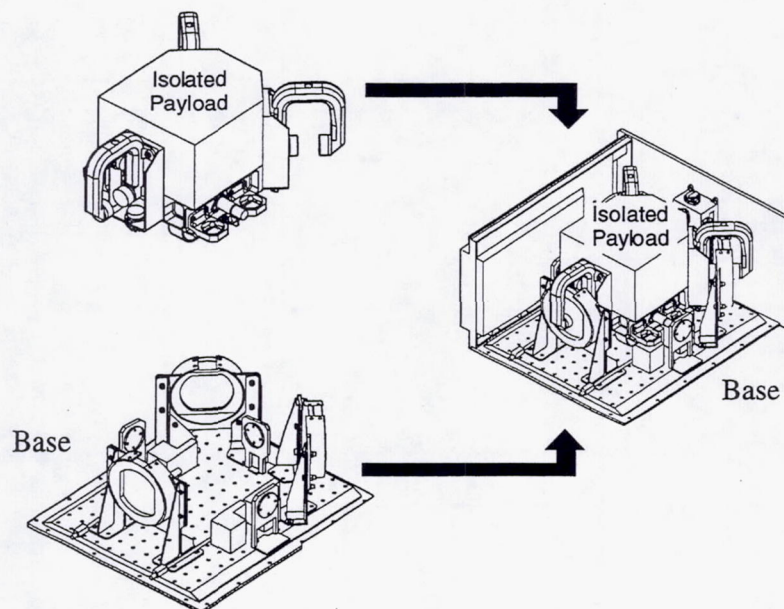
30



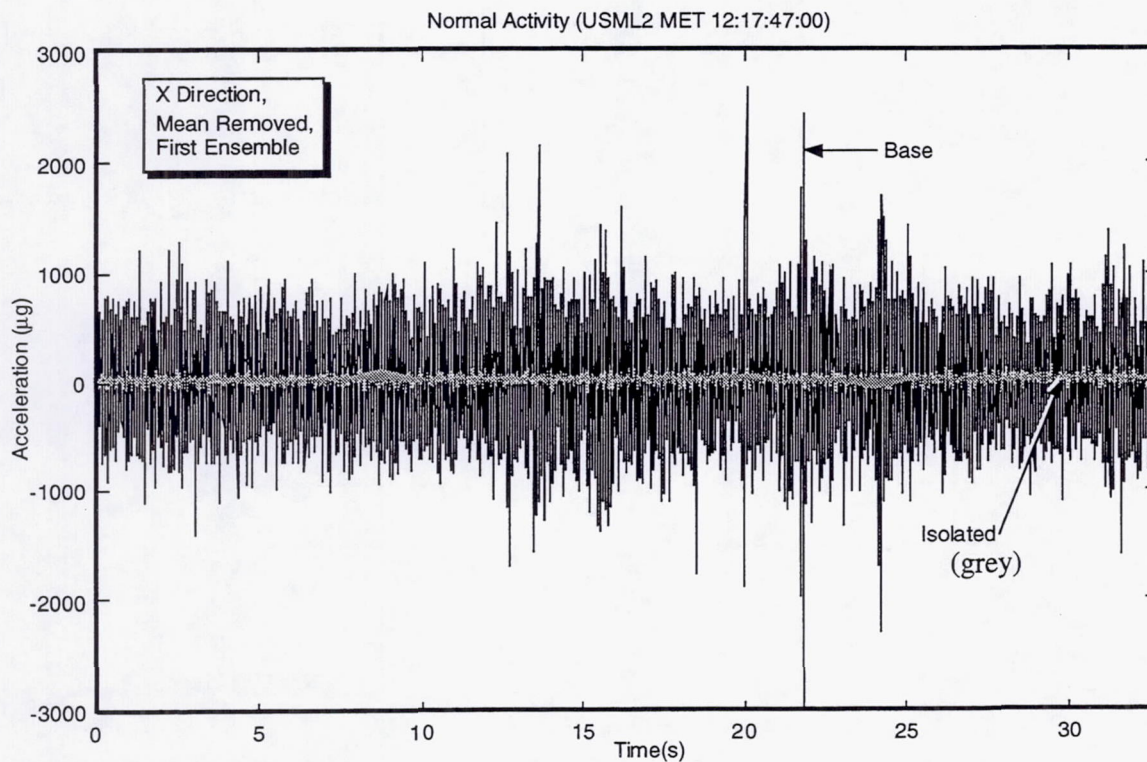
### USML-2 MODULE CONFIGURATION, PORT SIDE

Figure 2c. Approximate location of SAMS and 3DMA sensors on STS-73, Spacelab port side.

01546REU6.2

**Figure 3.** STABLE Physical Layout

01465REU6.3

**Figure 4.** Base and Isolated Acceleration Time History



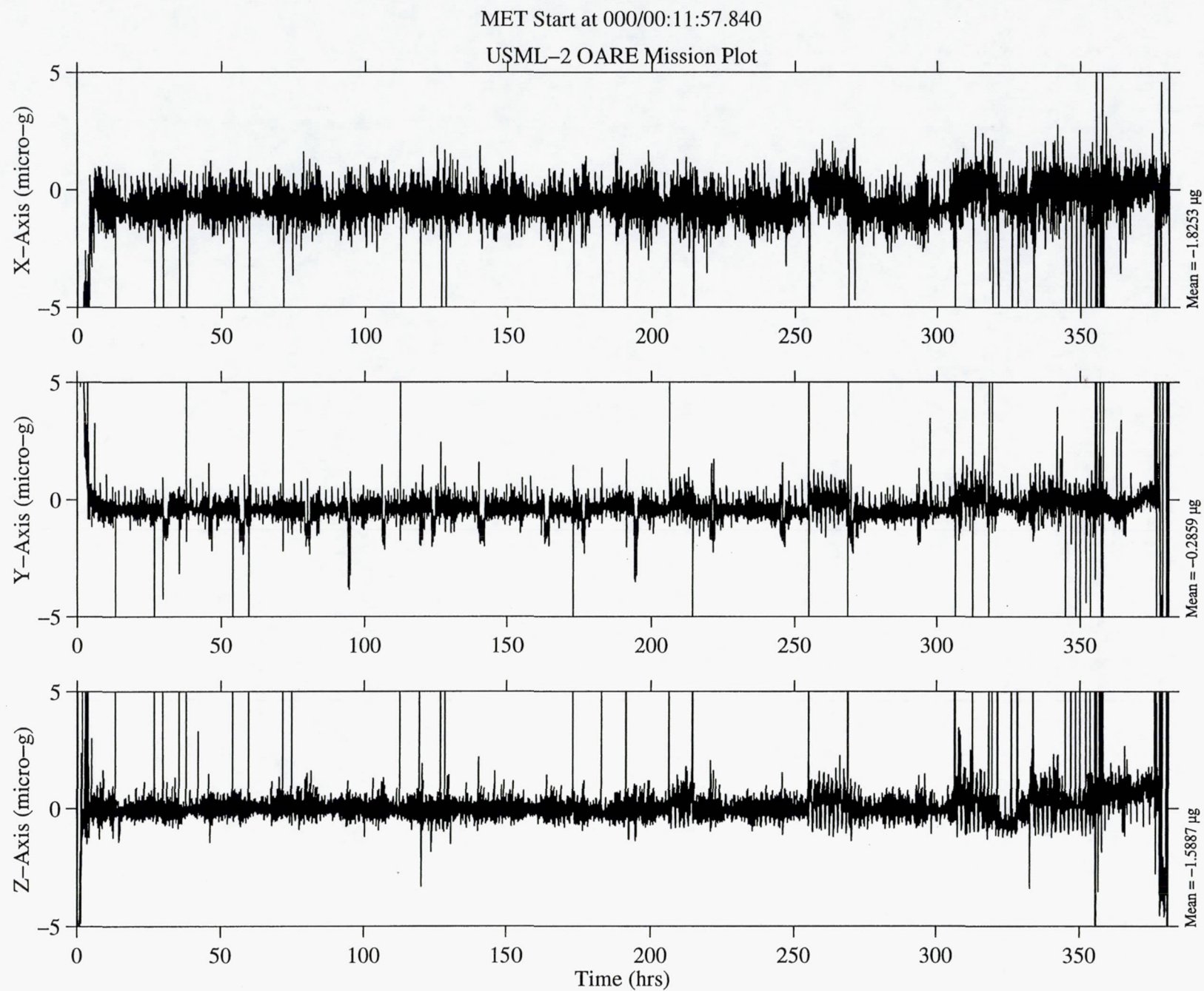


**Figure 5.** Trimmean filter OARE data for entire STS-73 mission.

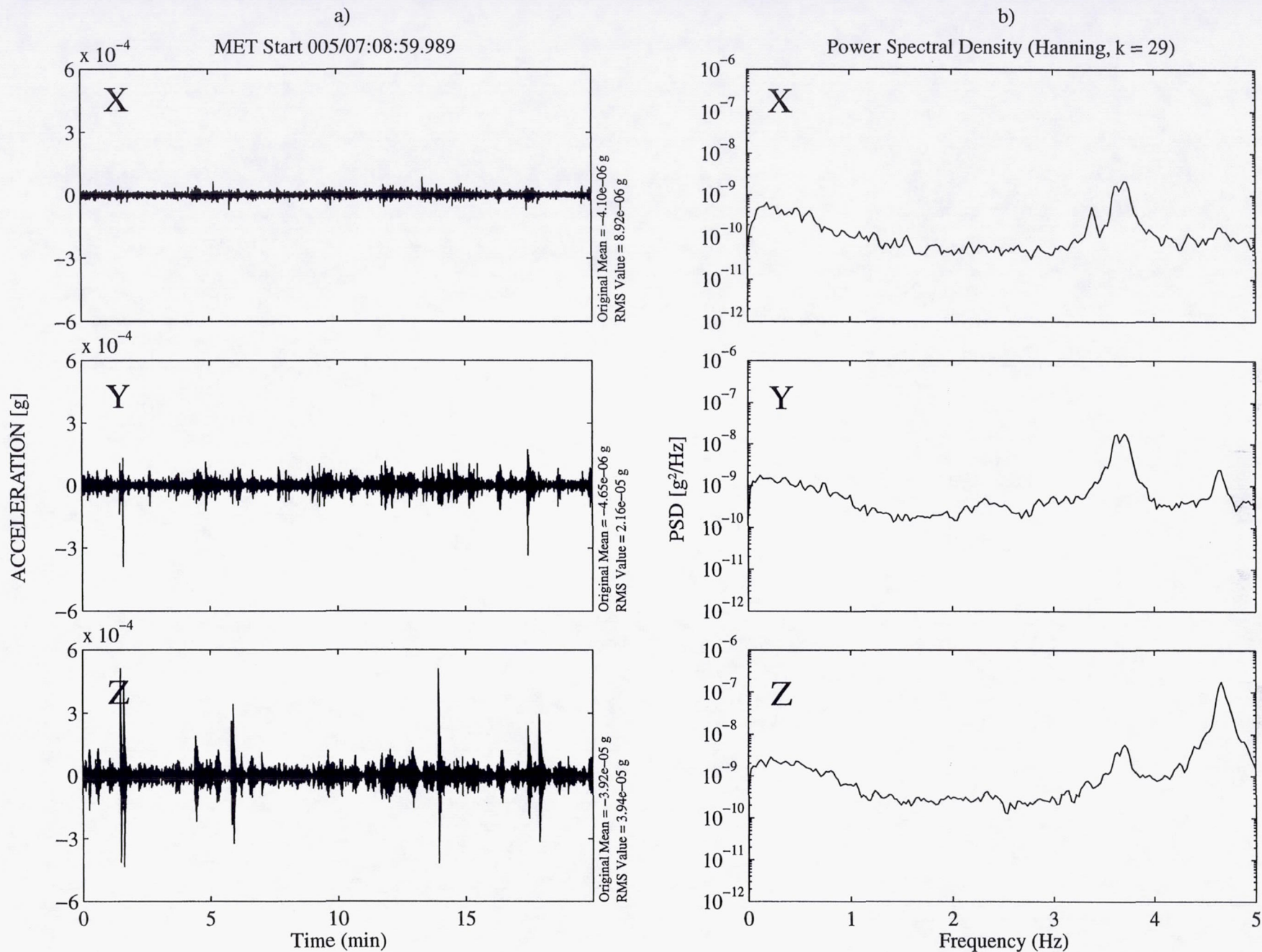


Figure 6. SAMS TSH A data for crew quiet period. a) Time history, b) PSD.



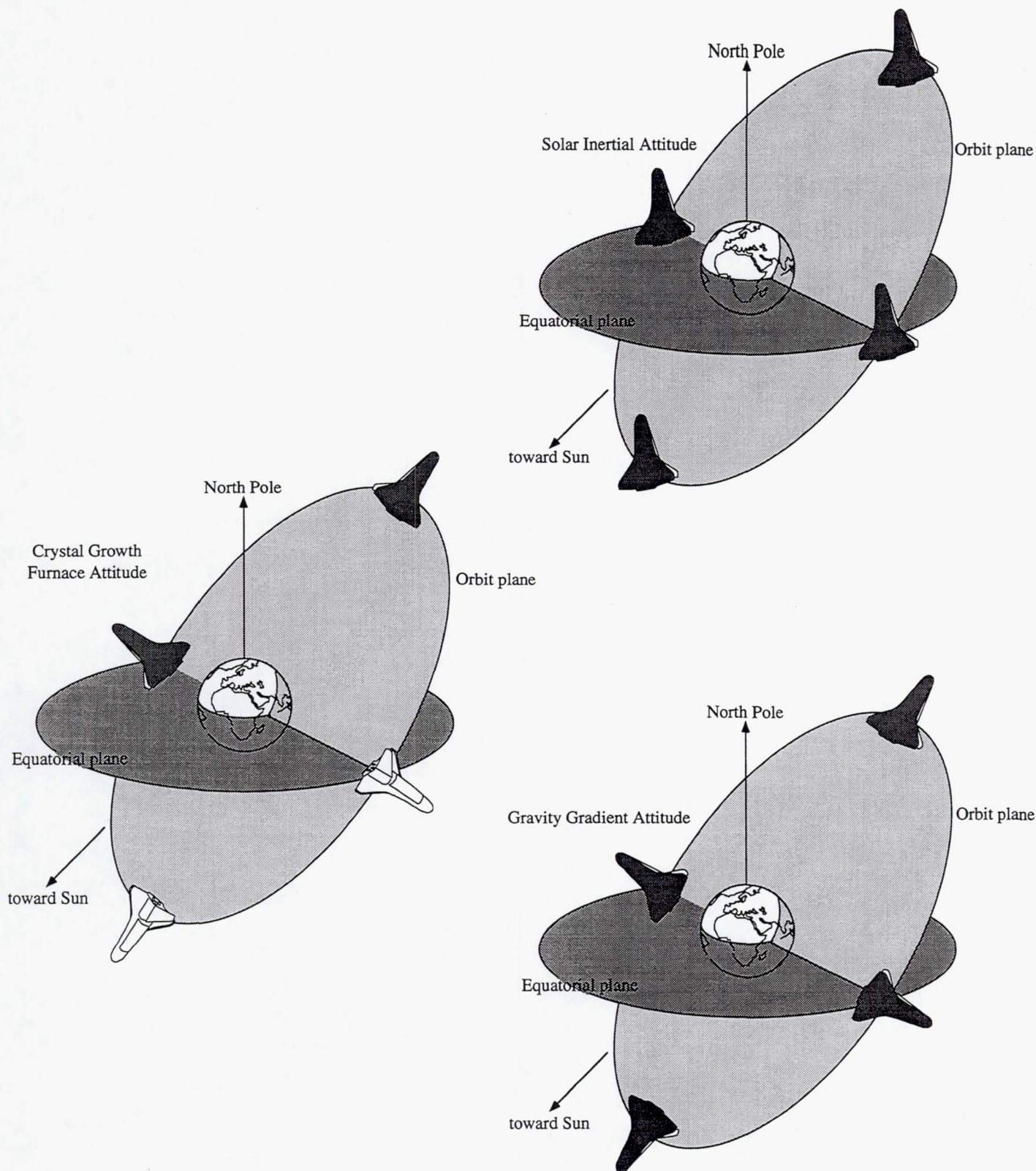
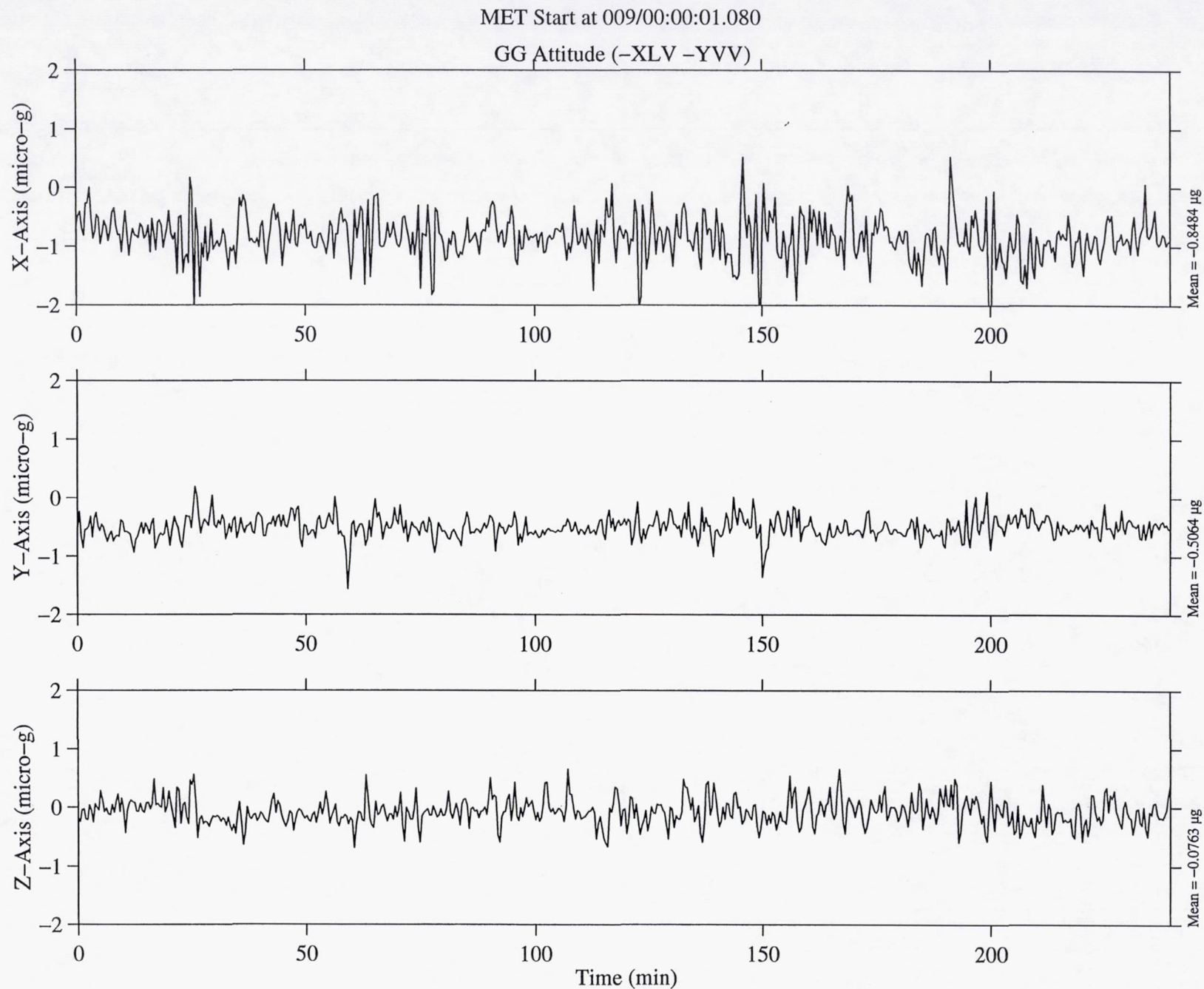
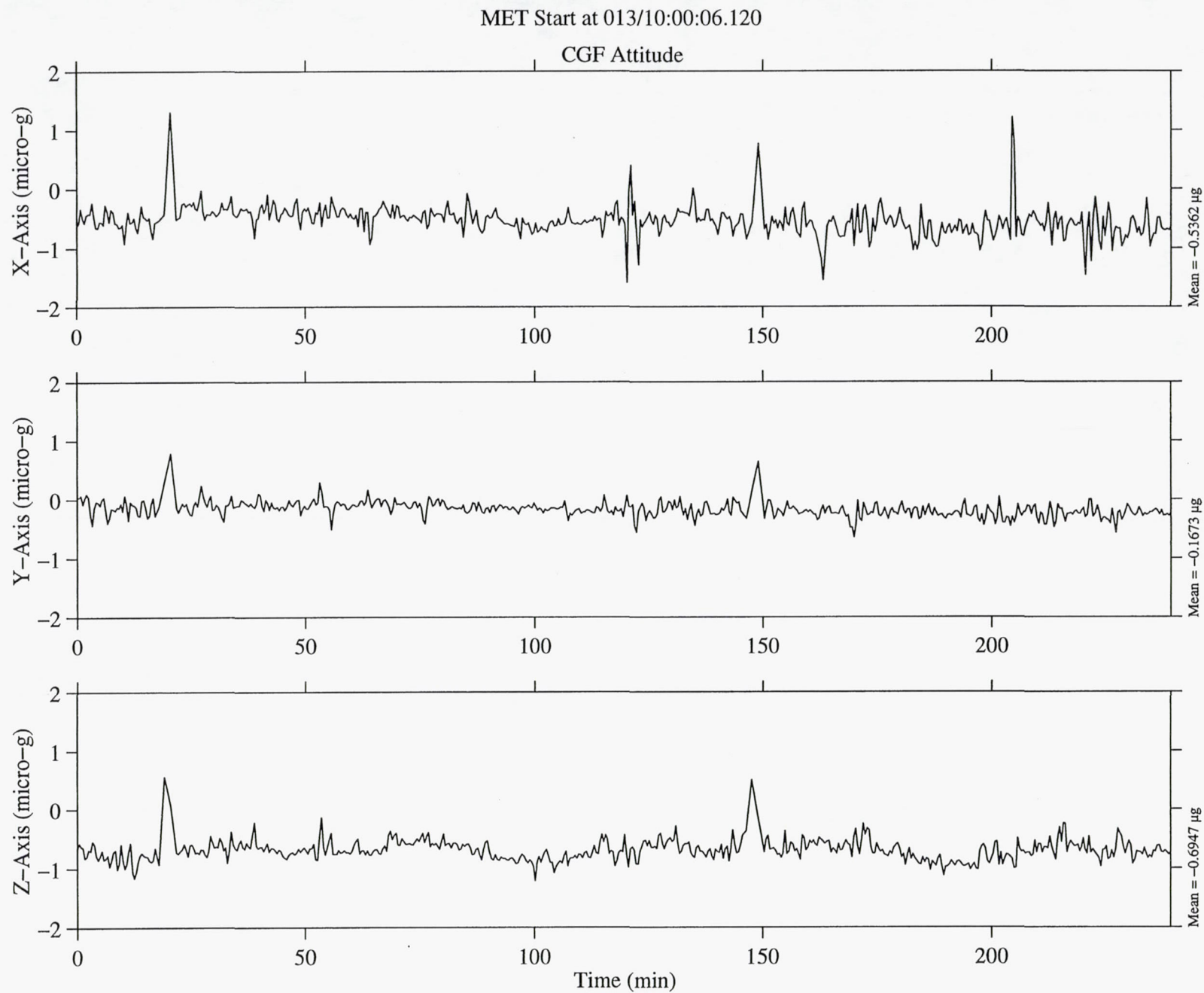


Figure 7. USML-2 Major Attitudes



**Figure 8.** Trimmean filter OARE data for period when Columbia was in the modified nominal USML-2 attitude.





**Figure 9.** Trimmean filter OARE data for period when Columbia was in the CGF attitude in support of one CGF experiment.

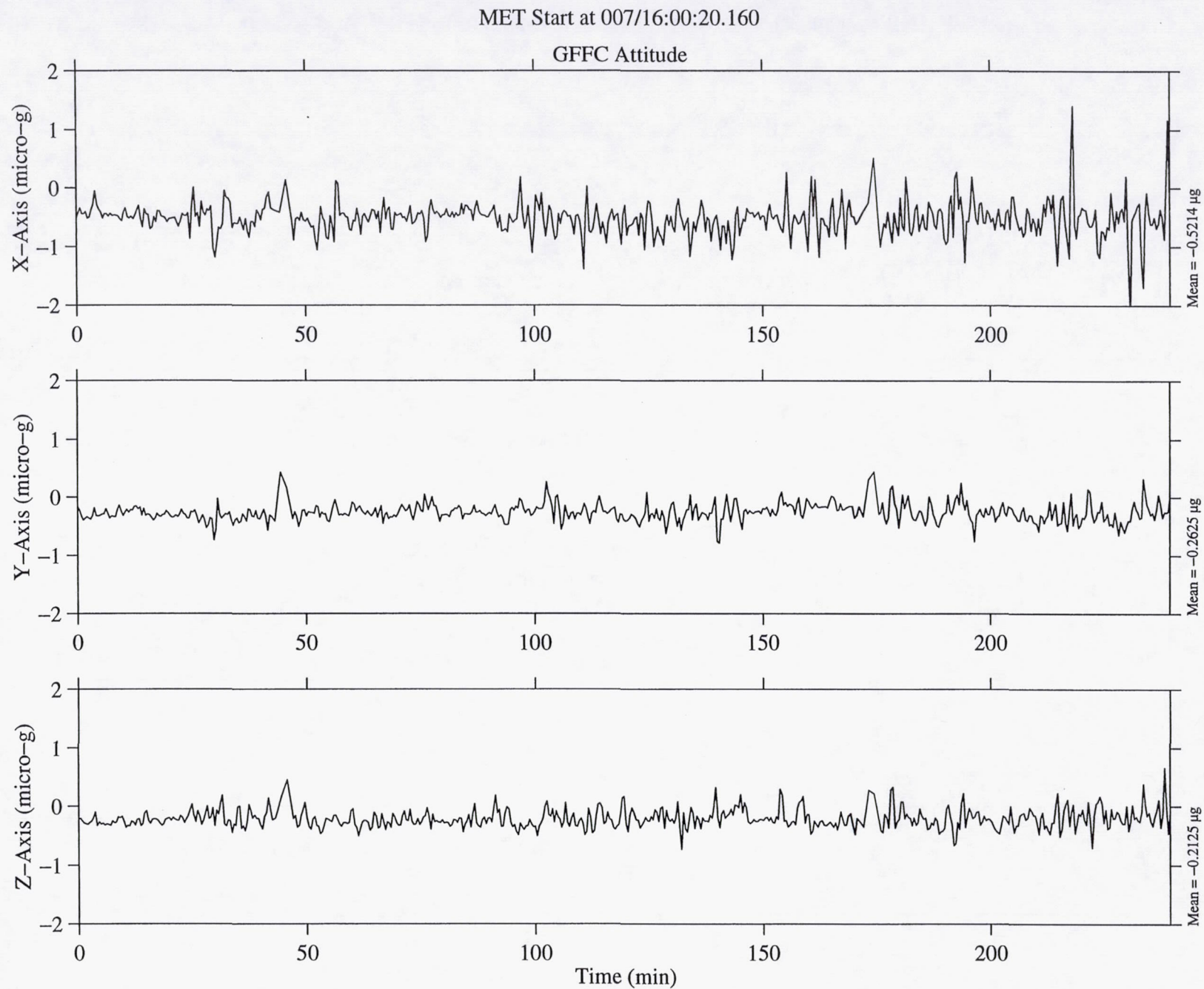


**Figure 10.** Trimmean filter OARE data for period when Columbia was in the GFFC attitude.



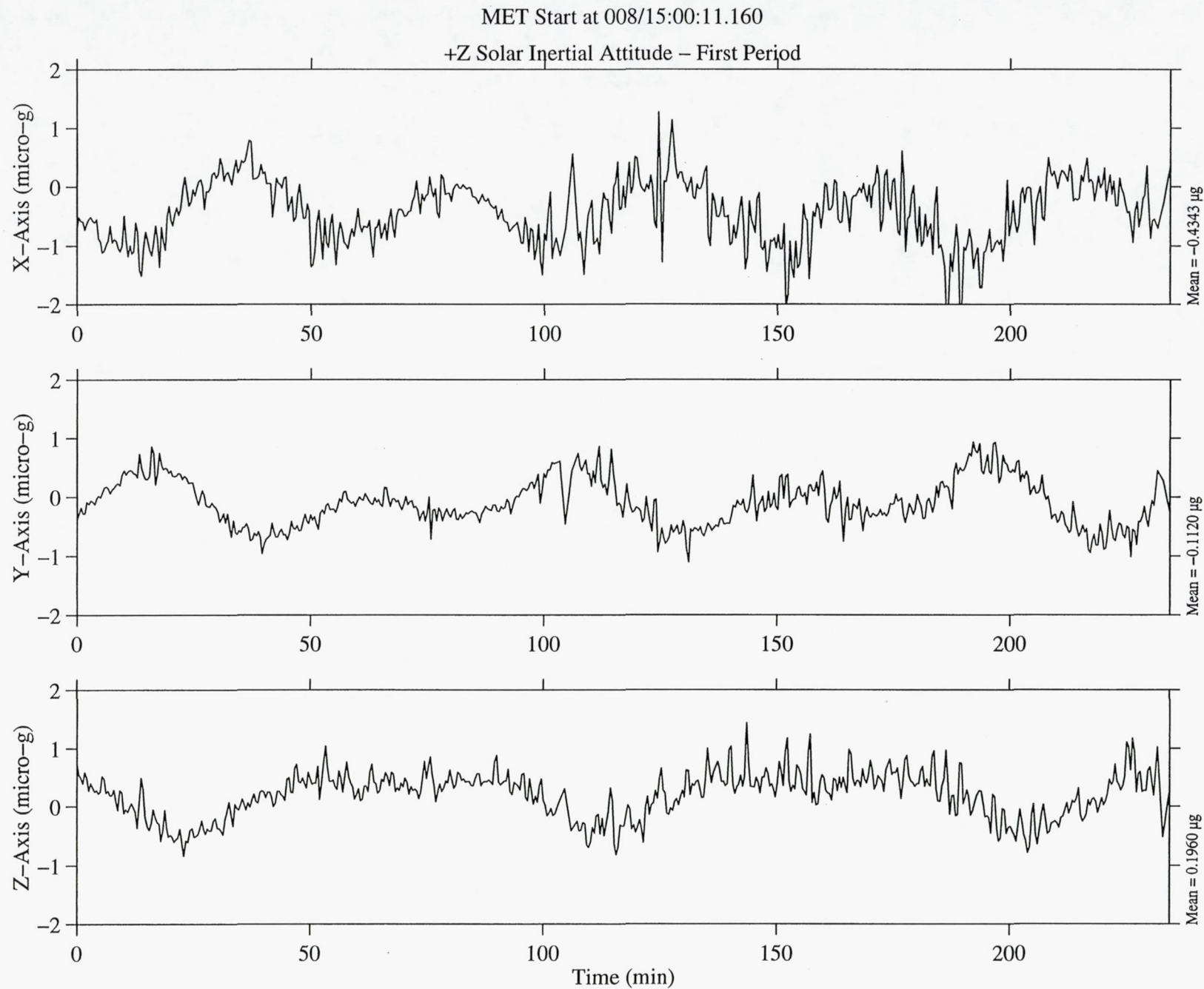


Figure 11. Trimmean filter OARE data for period when Columbia was in the solar inertial attitude for tire warming.

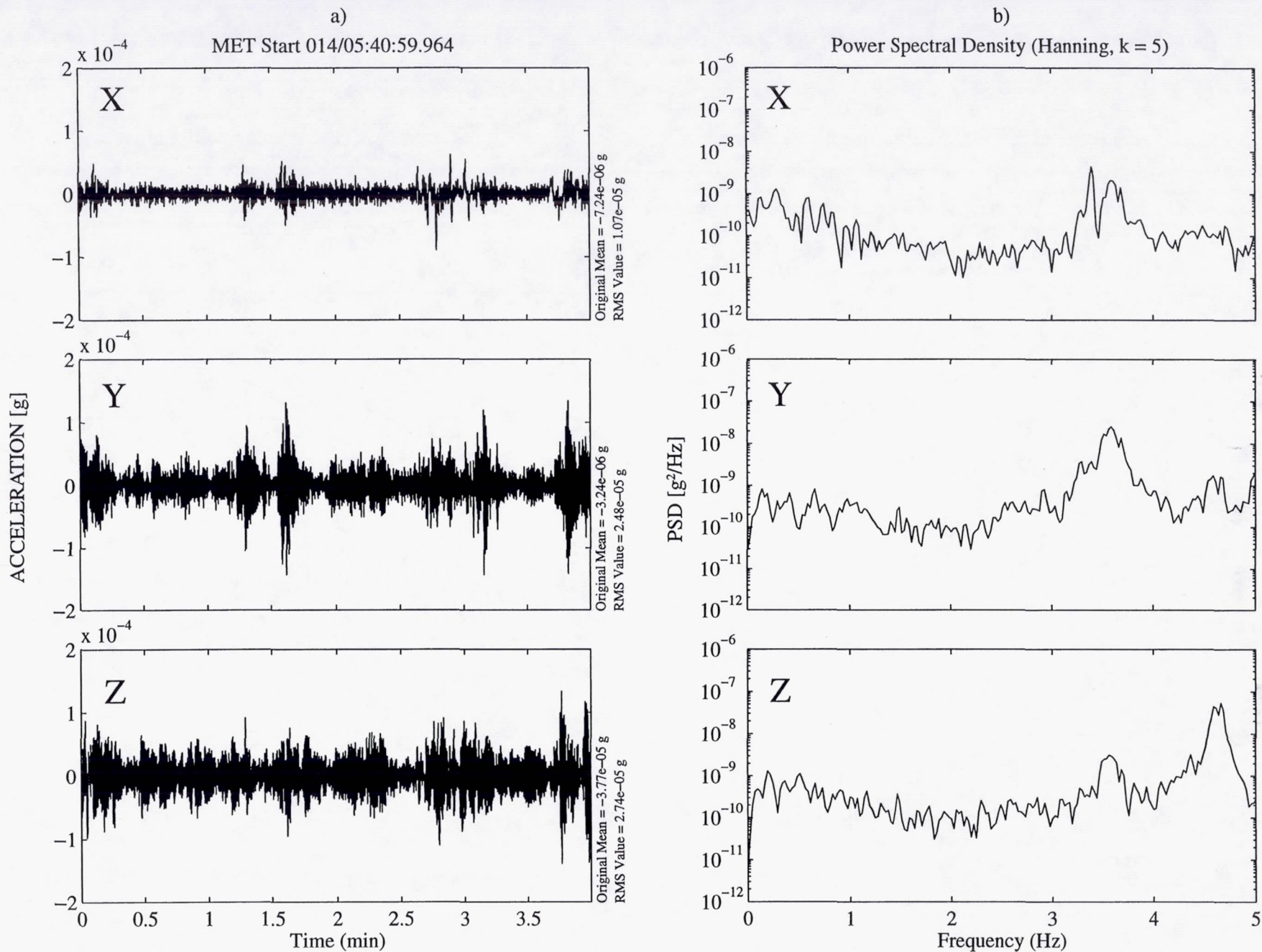
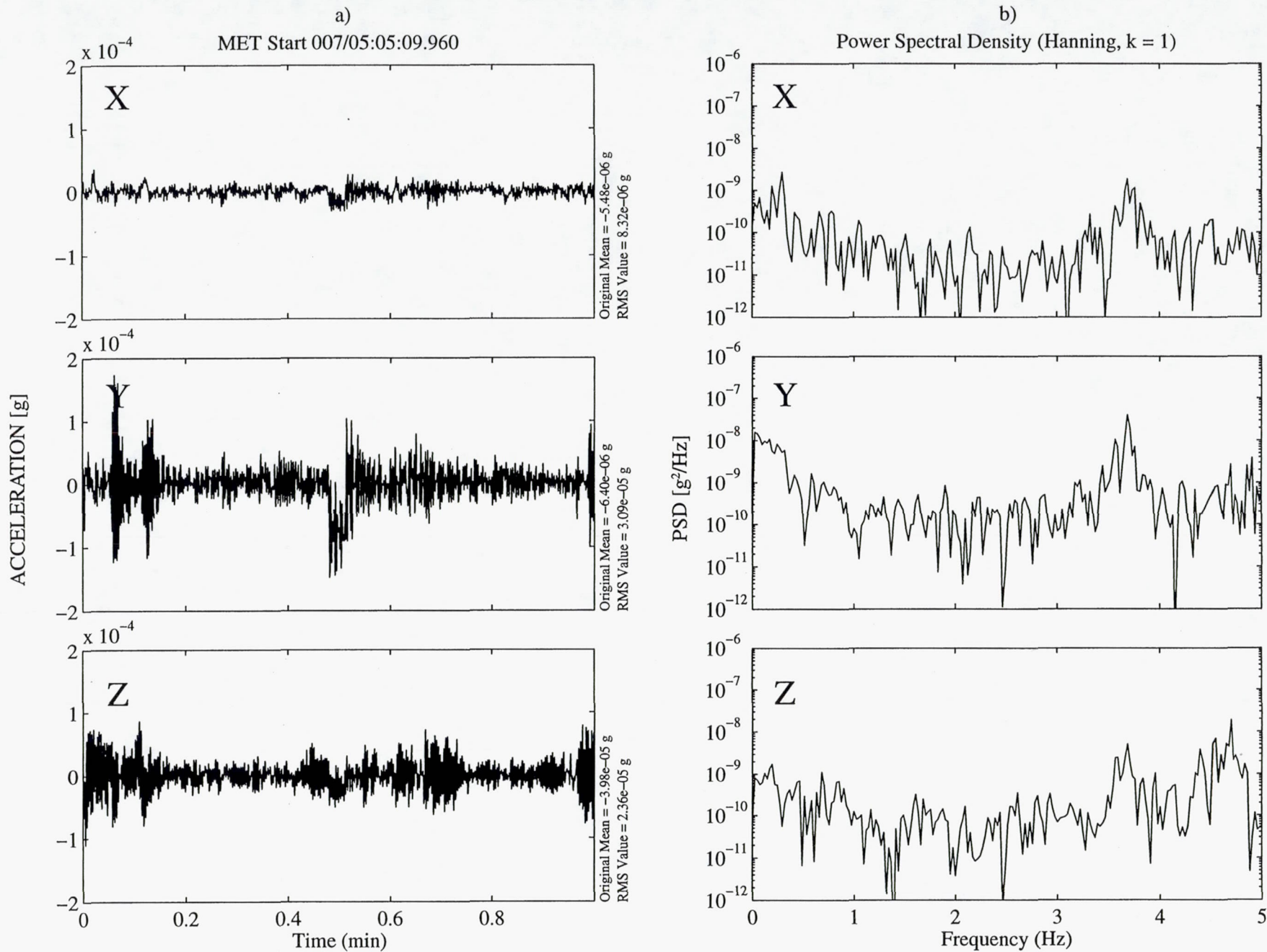


Figure 12. SAMS TSH A data for free drift period. a) Time history, b) PSD.





**Figure 13.** SAMS TSH A data for VRCS R5R jet test firing. Note main disturbance is in Orbiter Y-axis direction. a) Time history, b) PSD.

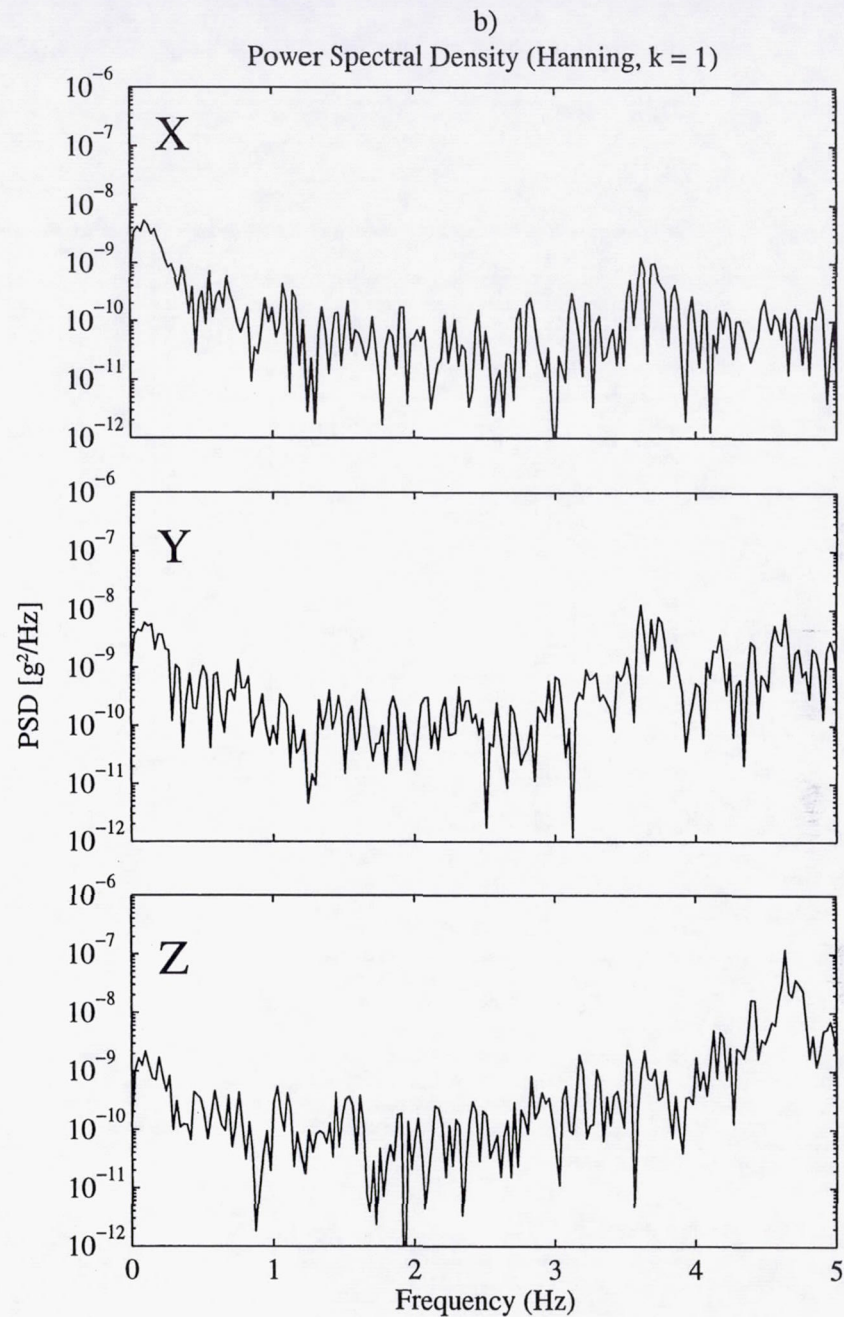
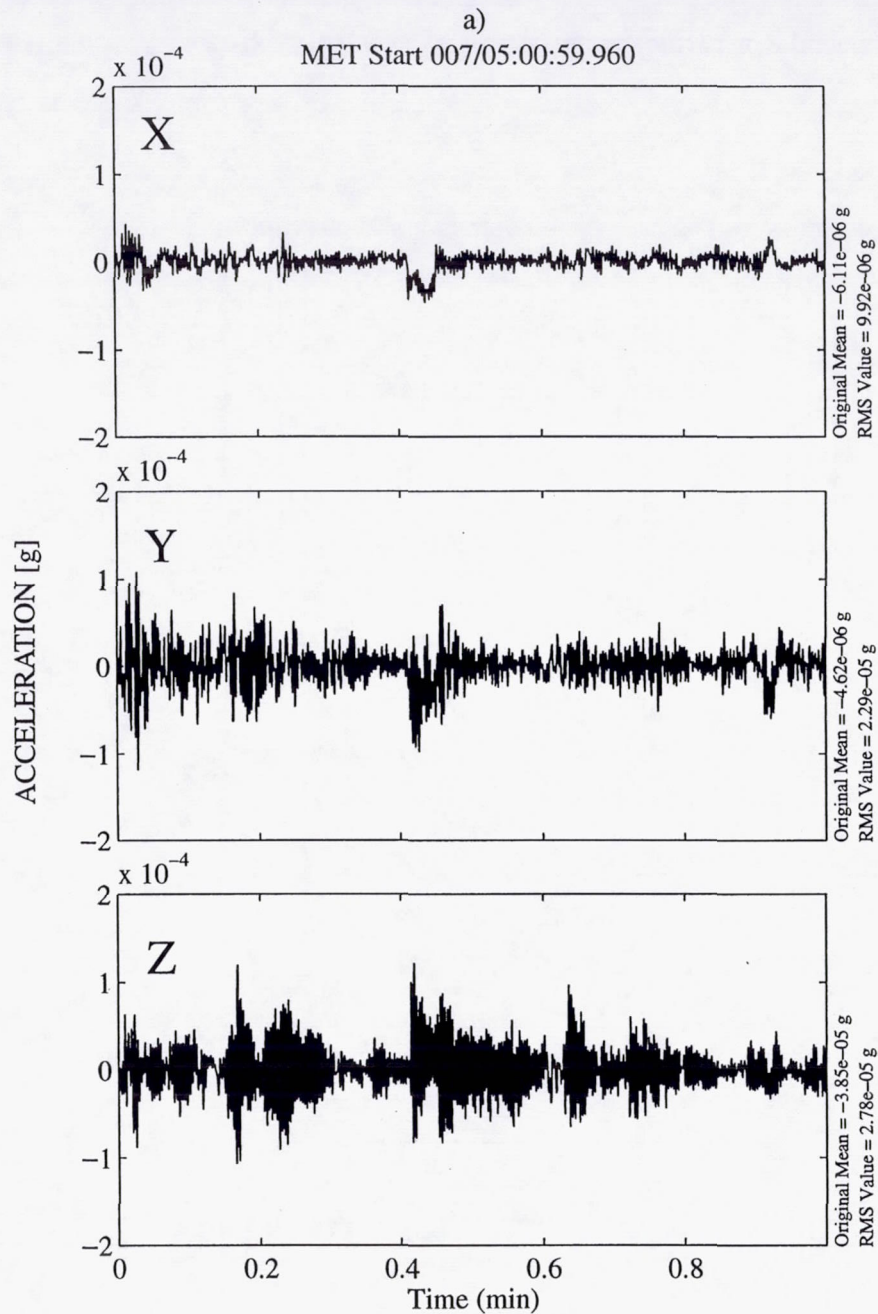
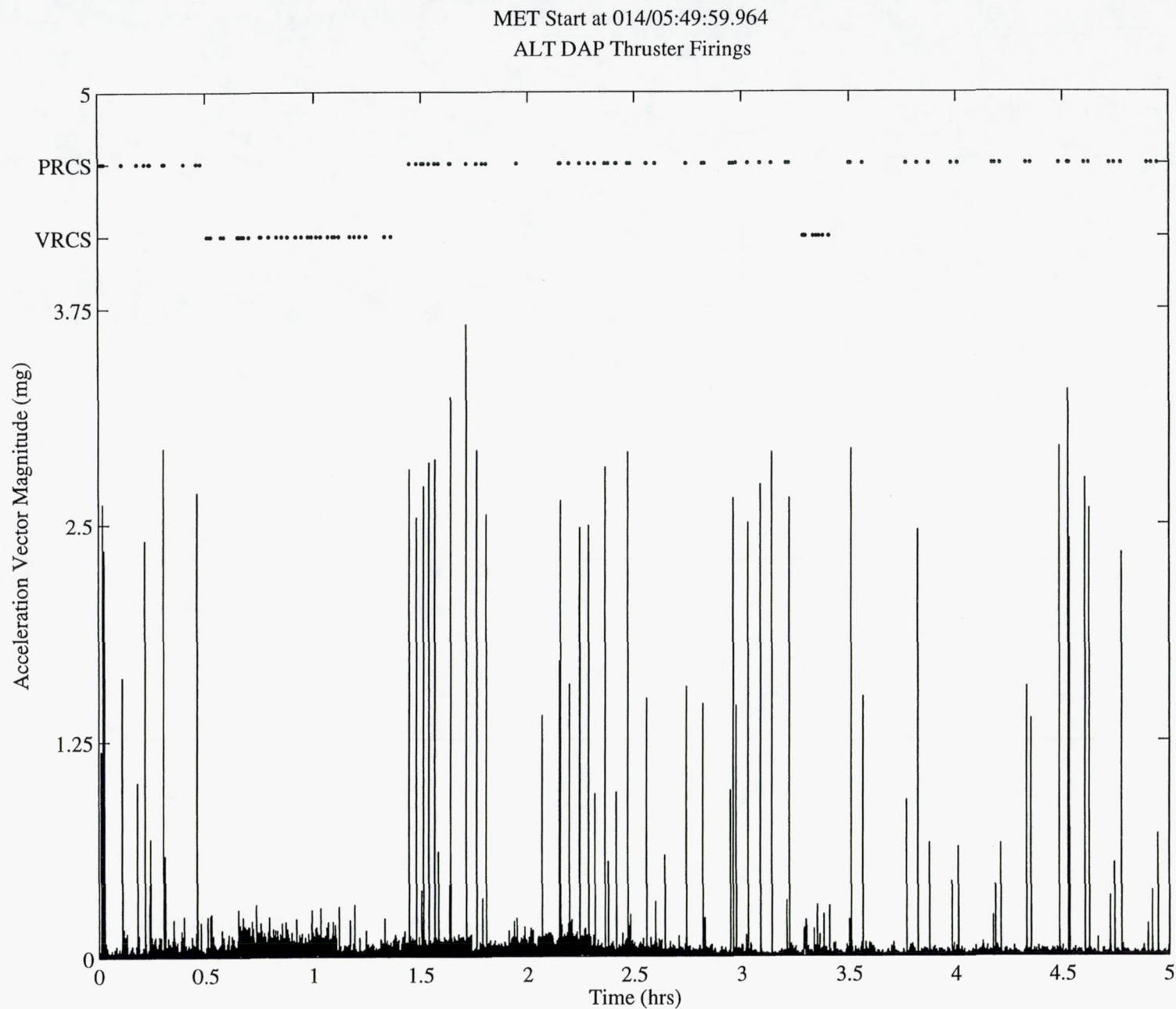
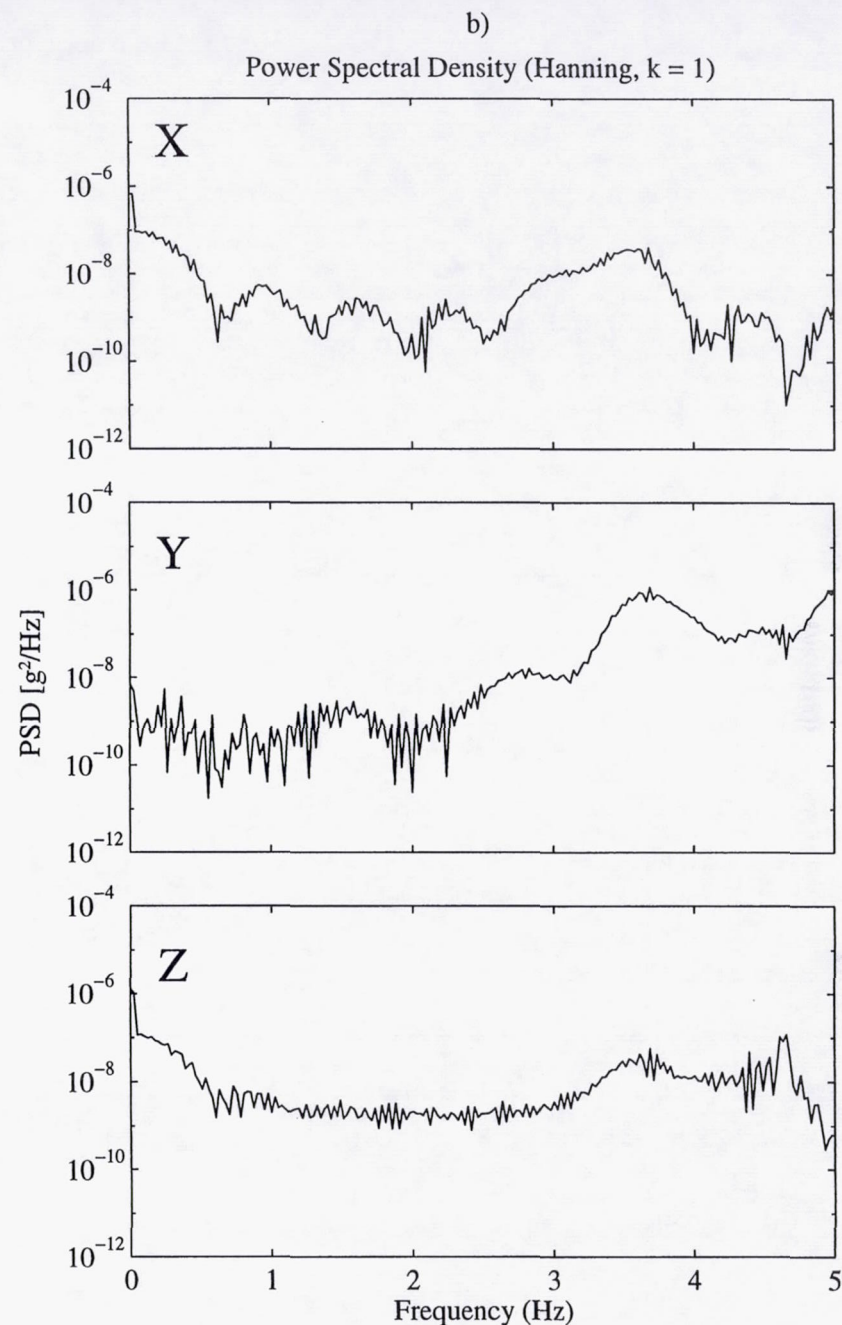
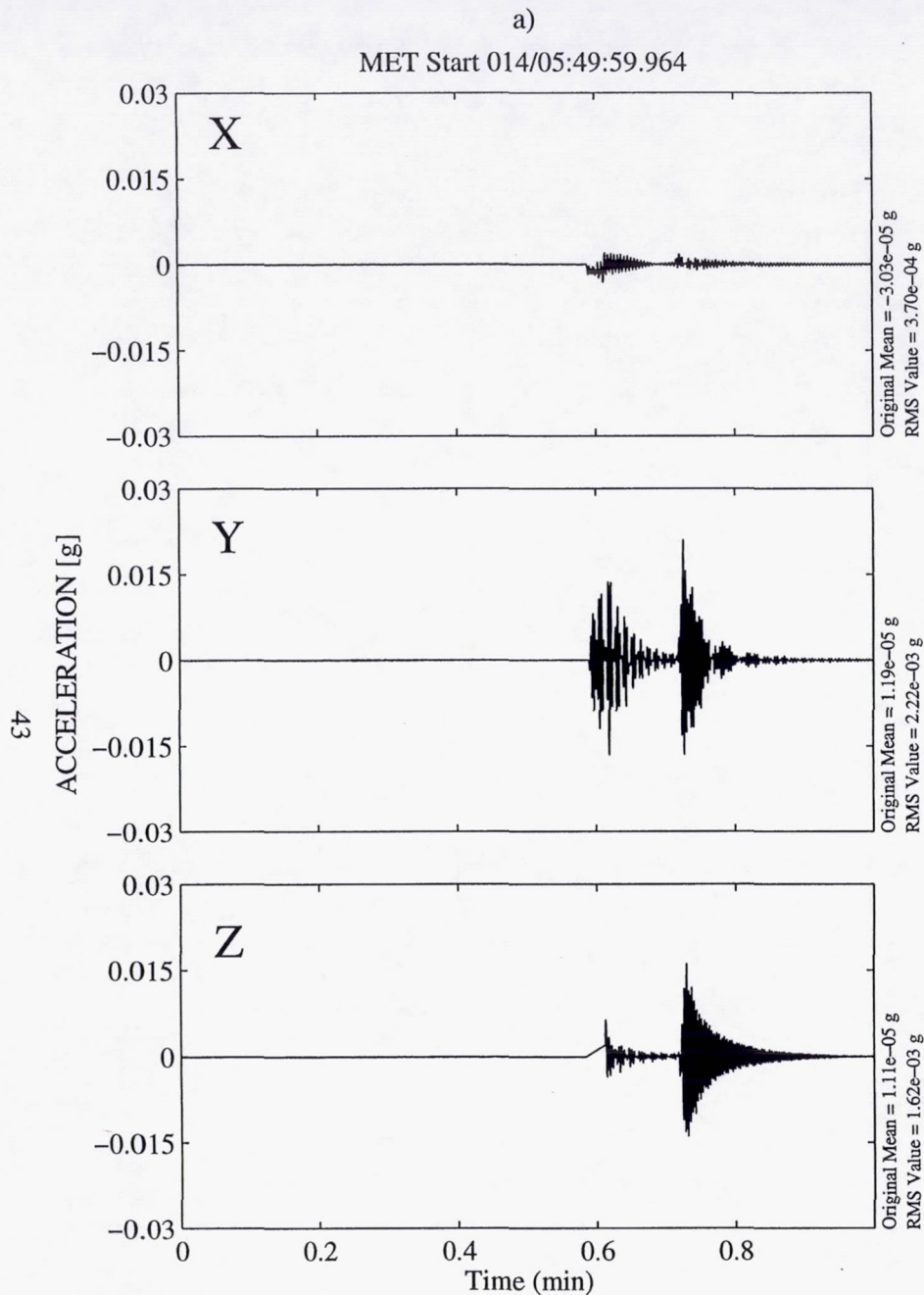


Figure 14. SAMS TSH A data for VRCS R5D jet test firing. a) Time history, a) PSD.





**Figure 15.** SAMS TSH B data vector magnitude for five hour period. PRCS and VRCS jet firings are indicated across top of plot.



**Figure 16.** SAMS TSH A data for PRCS jet firings as Orbiter comes out of free drift. a) Time history, b) PSD.



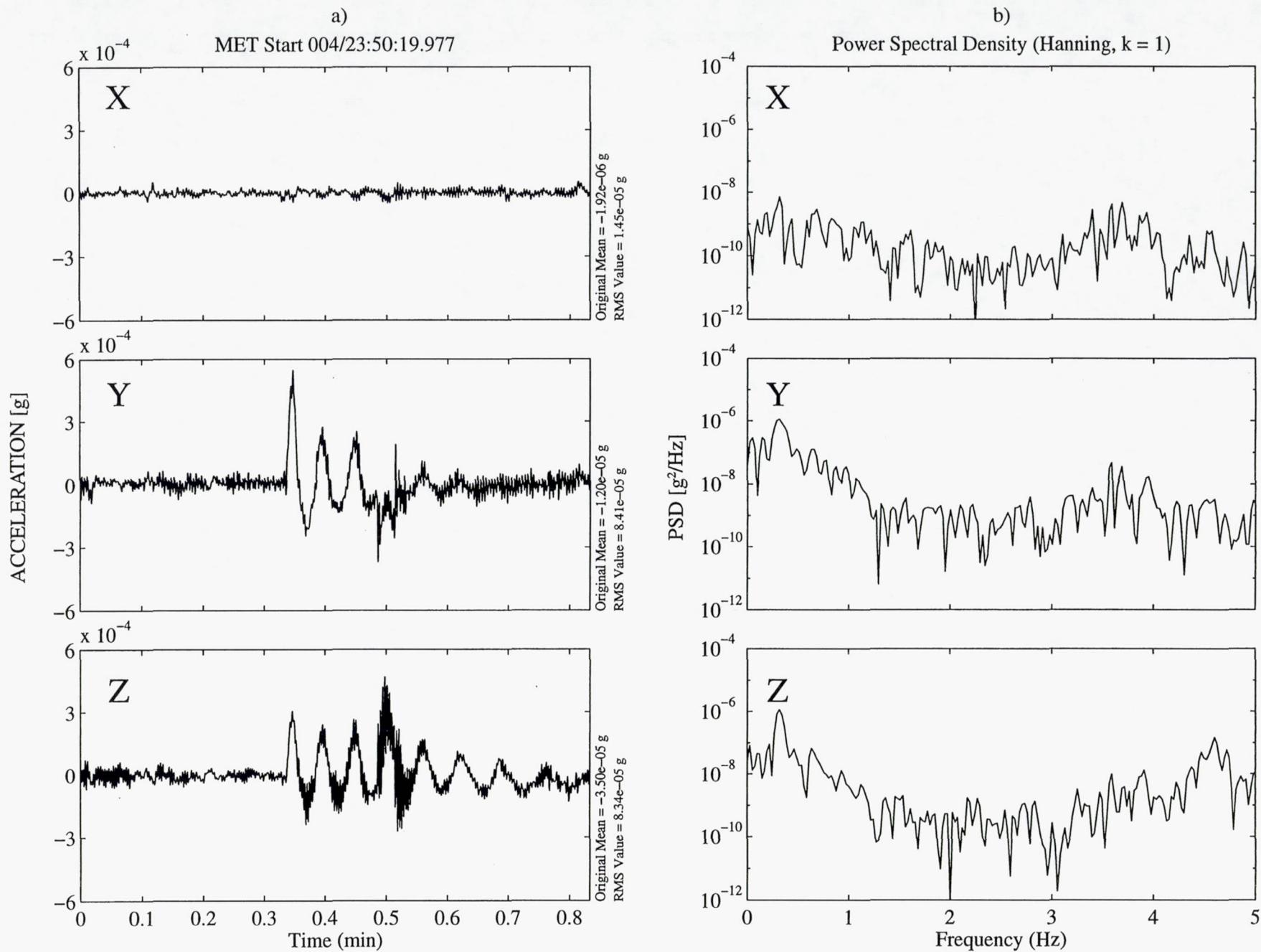
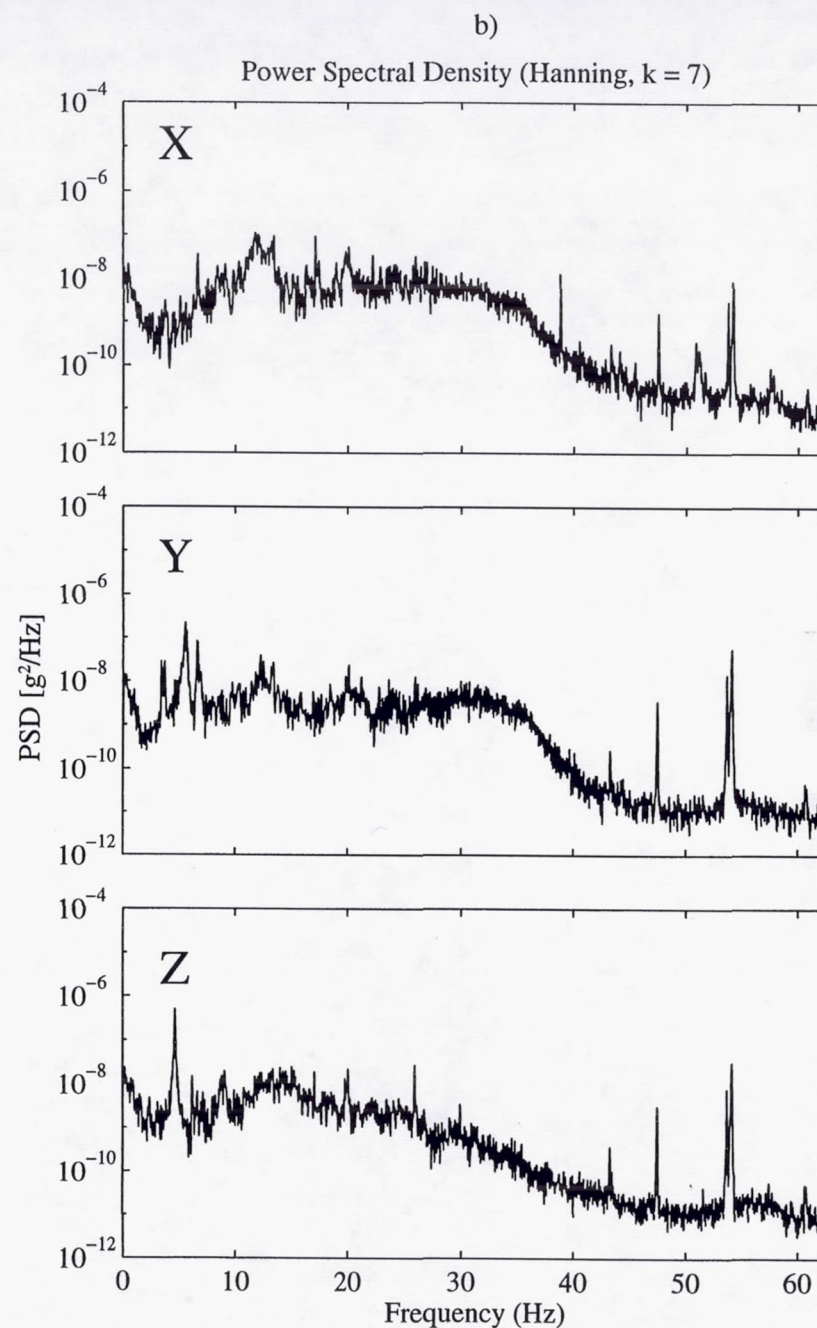
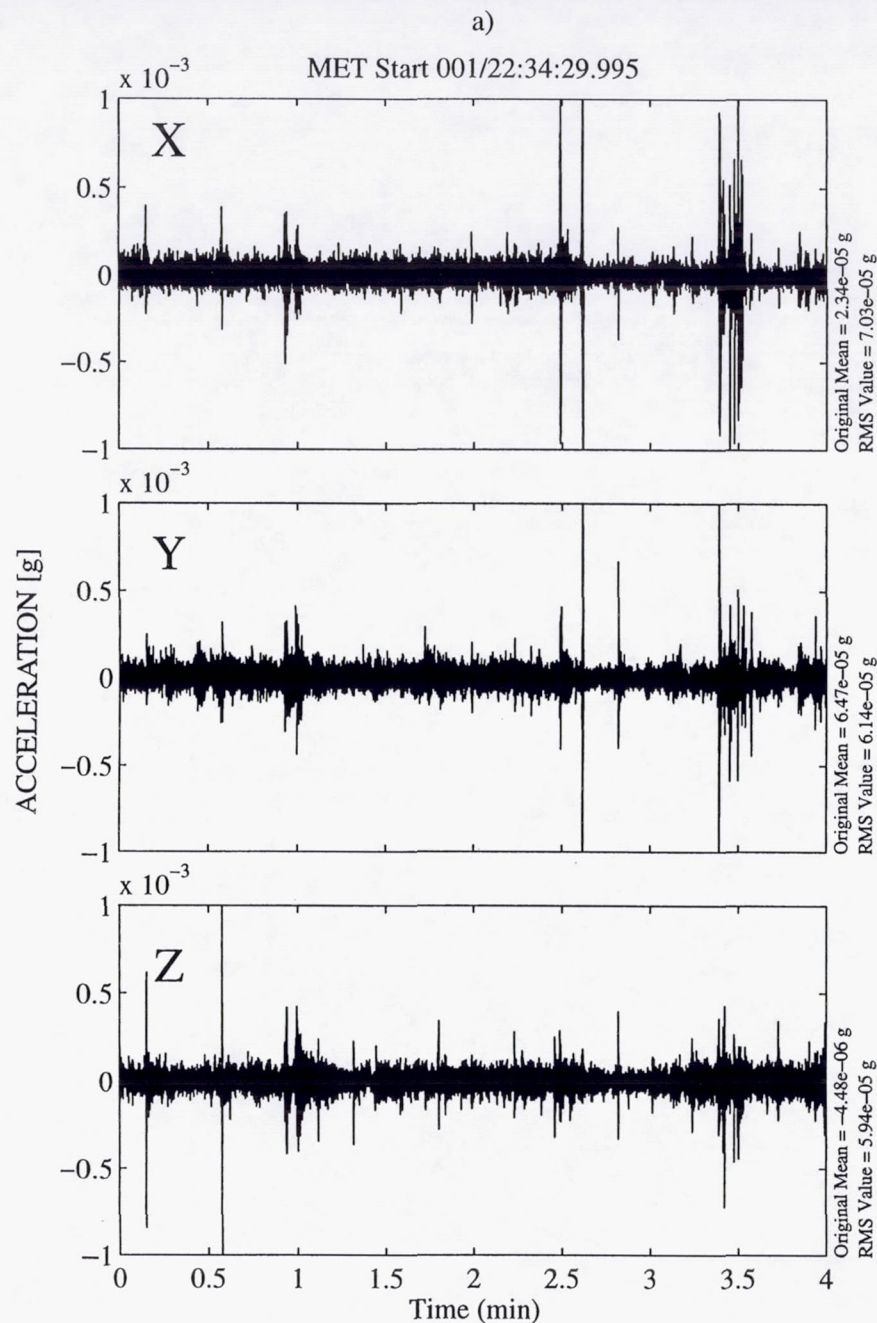


Figure 17. SAMS TSH A data during payload bay door opening motion. a) Time history, b) PSD.



**Figure 18.** SAMS TSH C data recorded during Glovebox fan operations. a) Time history, b) PSD.



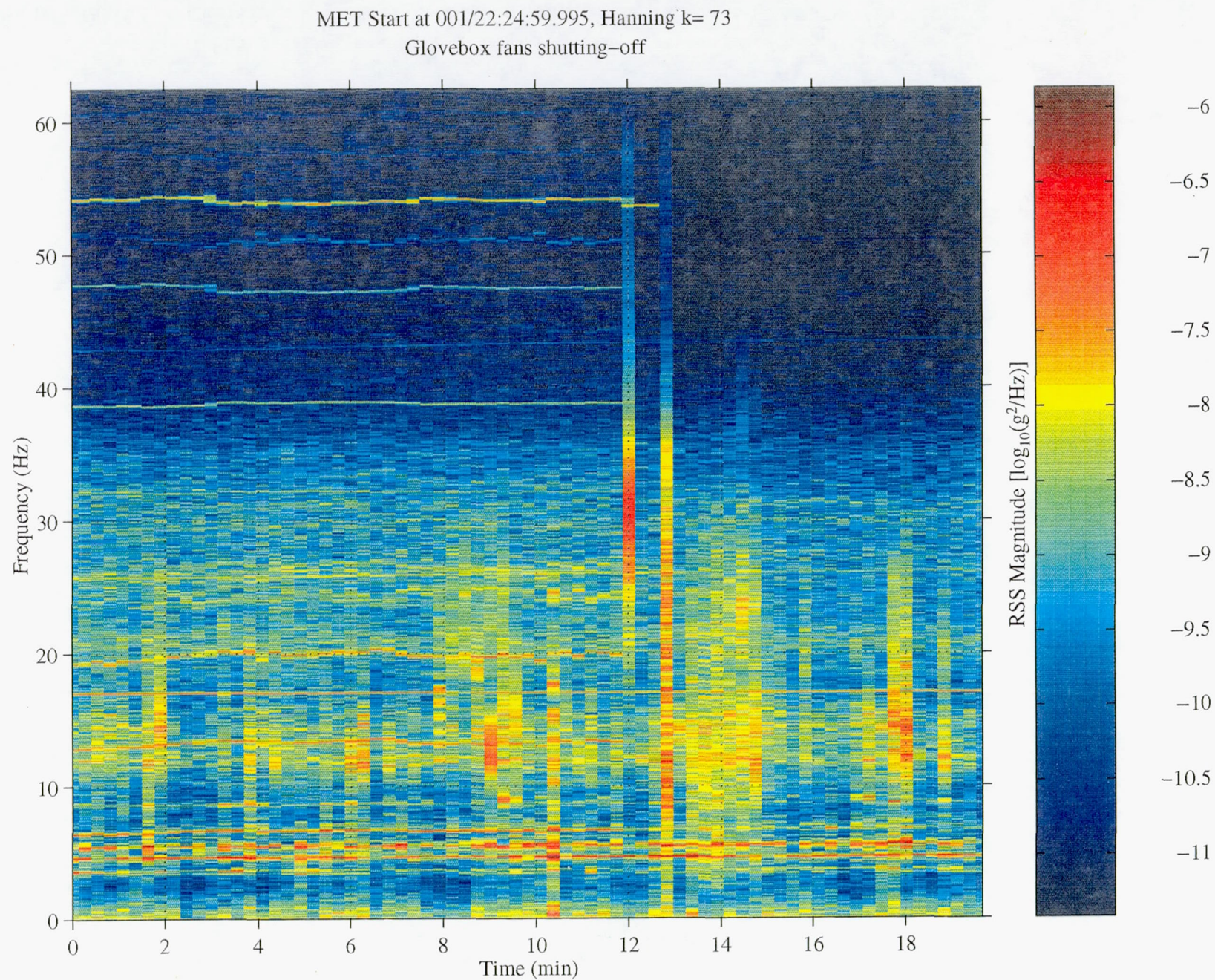
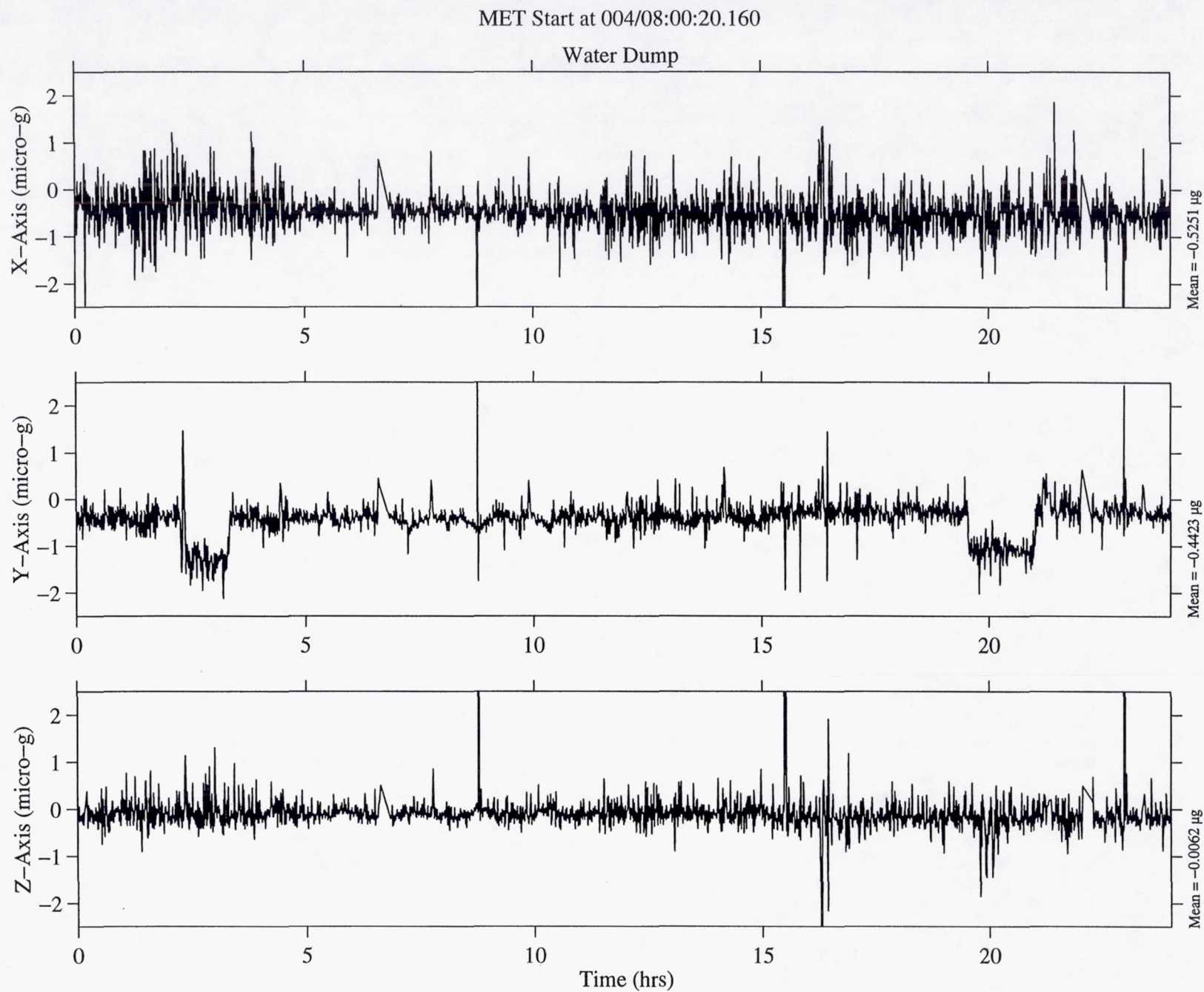


Figure 19. SAMS TSH C vector magnitude color spectrogram for Glovebox fan turn off times.





**Figure 20.** Trimmean filter OARE data showing the effects of two water dump operations.

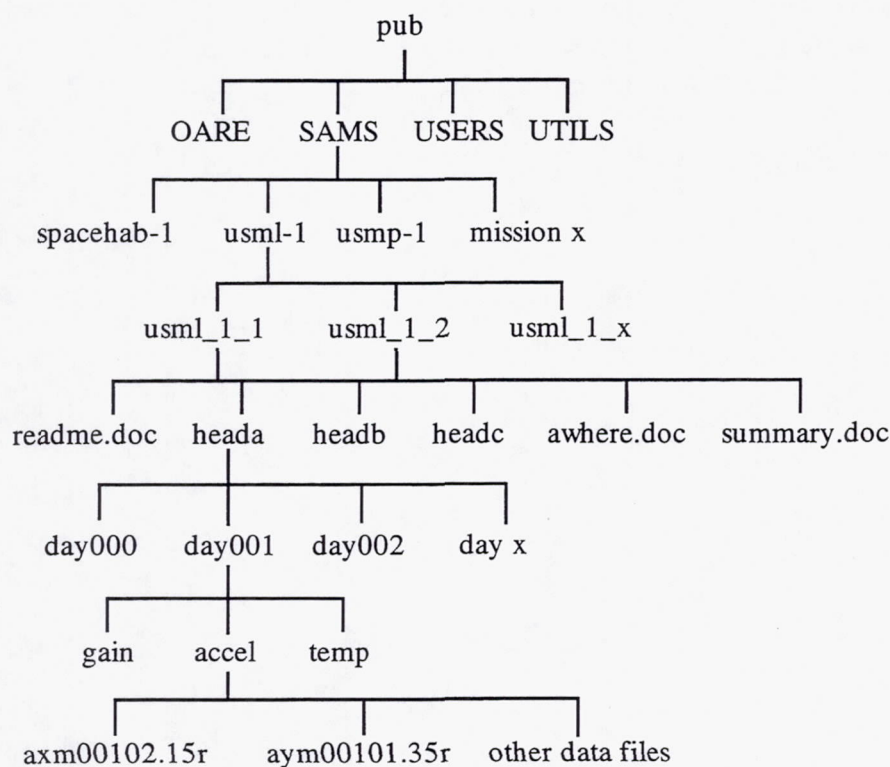


## Appendix A Accessing Acceleration Data via the Internet

SAMS and OARE data are available over the internet from the NASA LeRC file server [beech.lerc.nasa.gov](http://beech.lerc.nasa.gov). SAMS data are also available on CD-ROM format. The SAMS data files are formatted the same on both the file server and on CD.

Files of SAMS data are organized in a tree-like structure. Data acquired from a mission are categorized based upon sensor head, mission day, and type of data. Data files are stored at the lowest level in the tree and the file name reflects the contents of the file. For example, the file named axm00102.15r contains data for sensor head A, the X-axis, the time base was Mission Elapsed Time, day 001, hour 02, 1 of 5 files for that hour, and it contains reduced data. The file readme.doc provides a comprehensive description and guide to the data.

The OARE TMF data are organized into three files, one each for the X-, Y-, and Z-axes. The applicable OARE data are found in the mission directories.



SAMS Data File Structure

Also available from the file server are some data access tools for different computer platforms.

The NASA LeRC file server `beech.lerc.nasa.gov` can be accessed via anonymous file transfer protocol (ftp), as follows:

- a) Establish ftp connection to the beech file server.
- b) Login: anonymous
- c) Password: guest
- d) Change the directory to: pub
- e) List the files and directories in the pub directory. There are four directories at this level: OARE, SAMS, UTILS, and USERS.
- f) Change to the directory of choice.
- g) Change the directory to the mission of interest, for example: `usml-2`
- h) List files and directories for the specific mission chosen in previous step.
- i) Use the data file structure to find the files of interest.
- j) Enable binary transfer mode: `bin`.
- k) Transfer the data files of interest.

If you encounter difficulty in accessing the data using the file server, please send an electronic mail message to the internet address below. Please describe the nature of the difficulty and a description of the hardware and software you are using to access the file server.

`pims@lerc.nasa.gov`



## Appendix B SAMS Time Histories

The Principal Investigator Microgravity Services (PIMS) group has further processed SAMS data from STS-73, USML-2, Head C to produce the plots shown here. Two time history representations of the data are provided: ten second average and ten second root mean square (RMS) plots. These calculations are presented in two hour plots, with the corresponding average and RMS plots on one page. The ten-second interval average plots give an indication of net accelerations which last for a period of 10 seconds or more. Shorter duration, high amplitude accelerations may be seen with this type of plot, however their exact timing and magnitude cannot be extracted. The ten-second interval RMS plots give a measure of the oscillatory content in the acceleration data. Plots of this type may be used to identify times when oscillatory and/or transient deviations from the background acceleration levels occurred.

These average and RMS plots differ from similar plots produced in PIMS mission summary reports prior to January 1996. Previous plots tended to show an artificial spike when a gain change occurred within the SAMS unit. This artifact has been suppressed using gain change compensation routines.

### Interval Average and Root Mean Square Calculations

These data were collected at 125 samples per second, and a 25 Hz low pass filter was applied to the data by the SAMS unit prior to digitization.

Prior to the production of the interval average and RMS plots, the data were demeaned. This was accomplished by demeaning individual sections with a nominal length of 60 minutes. The average plots were produced by calculating the average of ten second intervals of data for each axis.

This operation is described as: 
$$x_{avg_k} = \frac{1}{M} \sum_{i=1}^M x_{(k-1)M+i},$$

where x represents the x, y, or z axis data, M is the number of points analyzed in an interval, and k refers to the kth interval analyzed.

The resulting data streams ( $x_{avg}$ ,  $y_{avg}$ ,  $z_{avg}$ ) are then combined by a vector-magnitude operation.

This computation is expressed mathematically as: 
$$accel_{avg_k} = \sqrt{x_{avg_k}^2 + y_{avg_k}^2 + z_{avg_k}^2}.$$

The RMS plots were produced by taking the root-mean-square of ten second intervals of data for each axis and forming a vector magnitude of the resulting data streams.

The interval RMS operation is expressed mathematically as: 
$$x_{RMS_k} = \sqrt{\frac{1}{M} \sum_{i=1}^M (x_{(k-1)M+i})^2}.$$

The same definitions apply for x, M, and k as in the interval average computation. The resulting data streams are combined by a vector-magnitude operation.

**THIS PAGE INTENTIONALLY LEFT BLANK.**



B-3

Figure 1a: USML-2, Head C (fc=25 Hz), Ten Second Interval Average

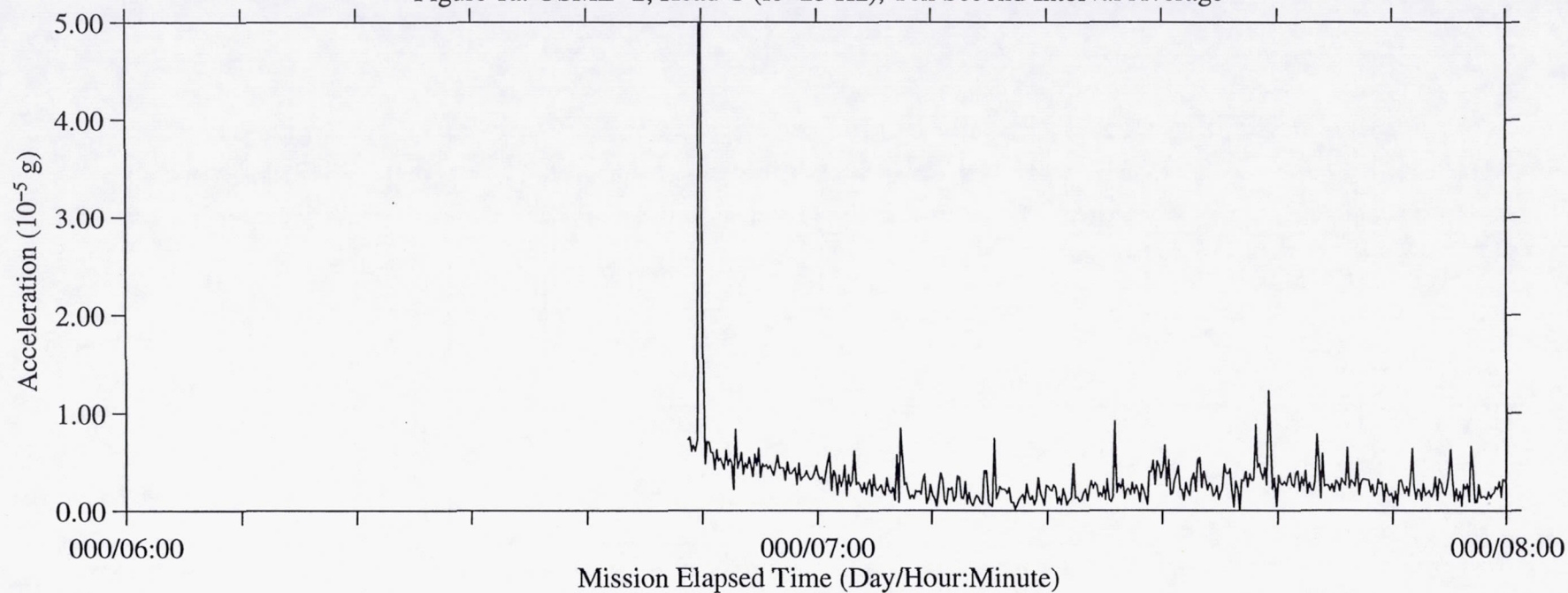


Figure 1b: USML-2, Head C (fc=25 Hz), Ten Second Interval RMS

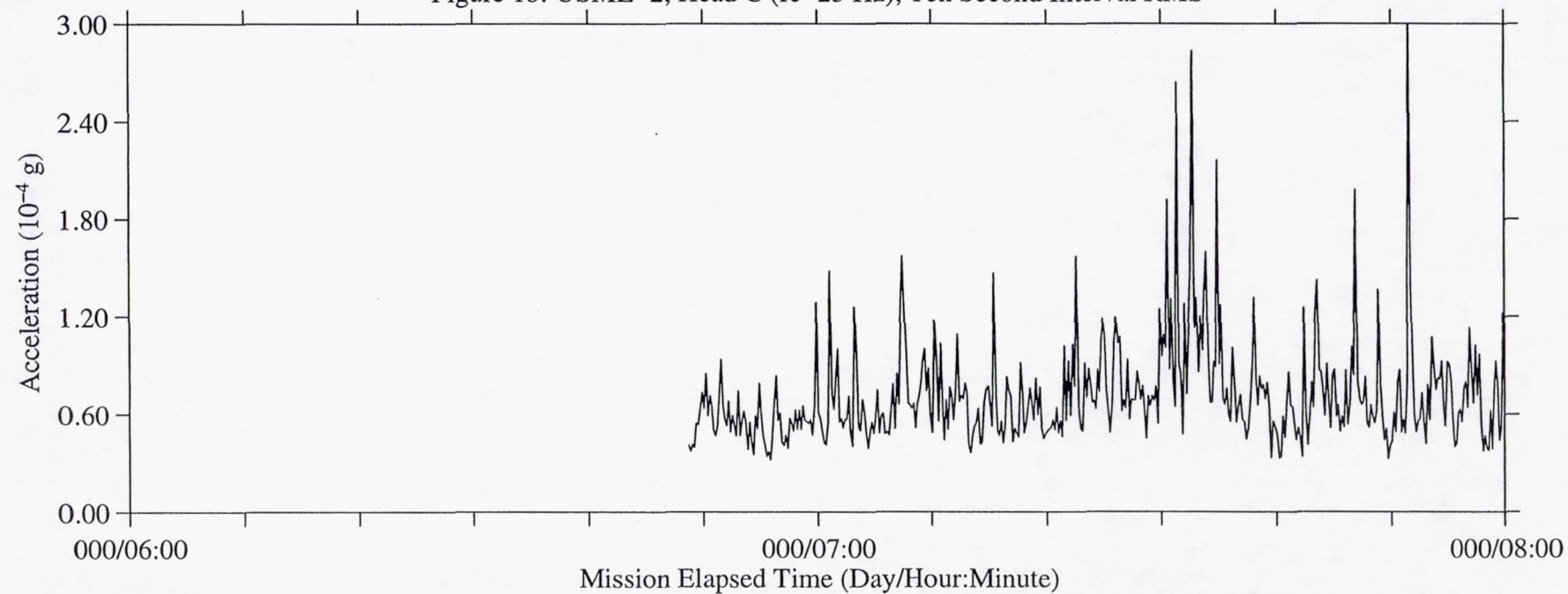


Figure 2a: USML-2, Head C (fc=25 Hz), Ten Second Interval Average

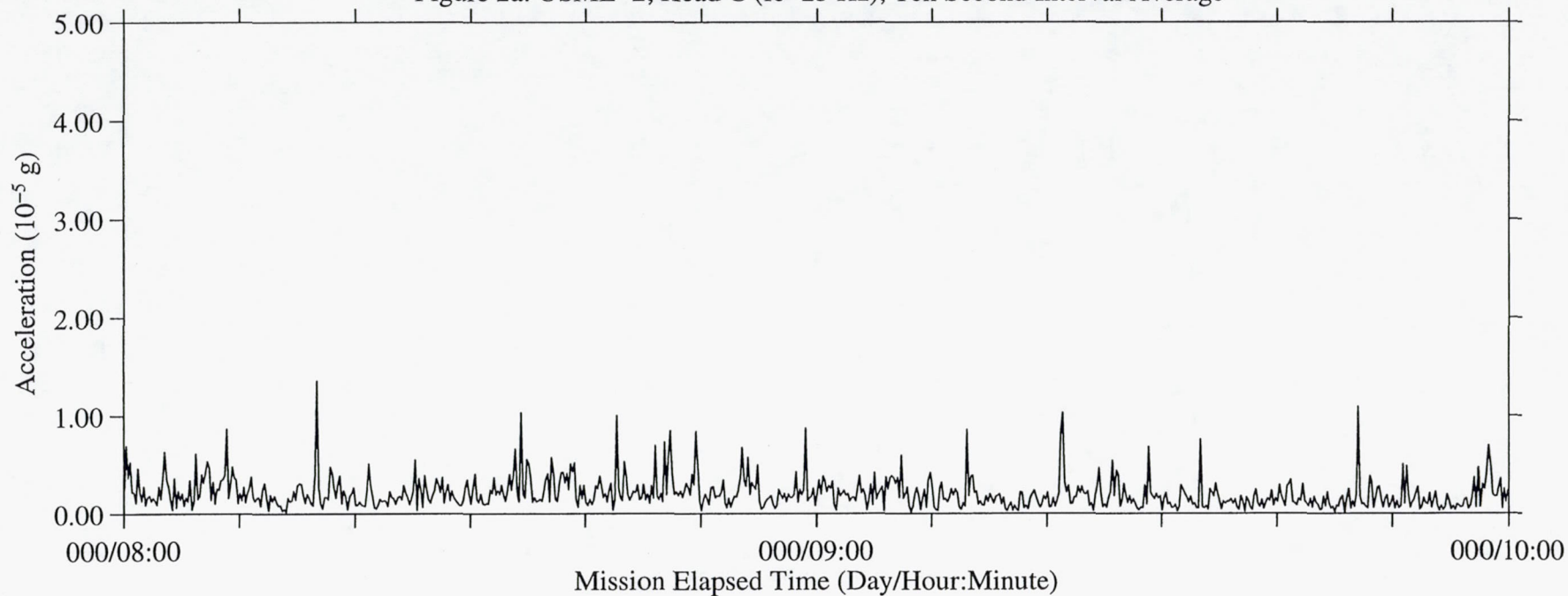
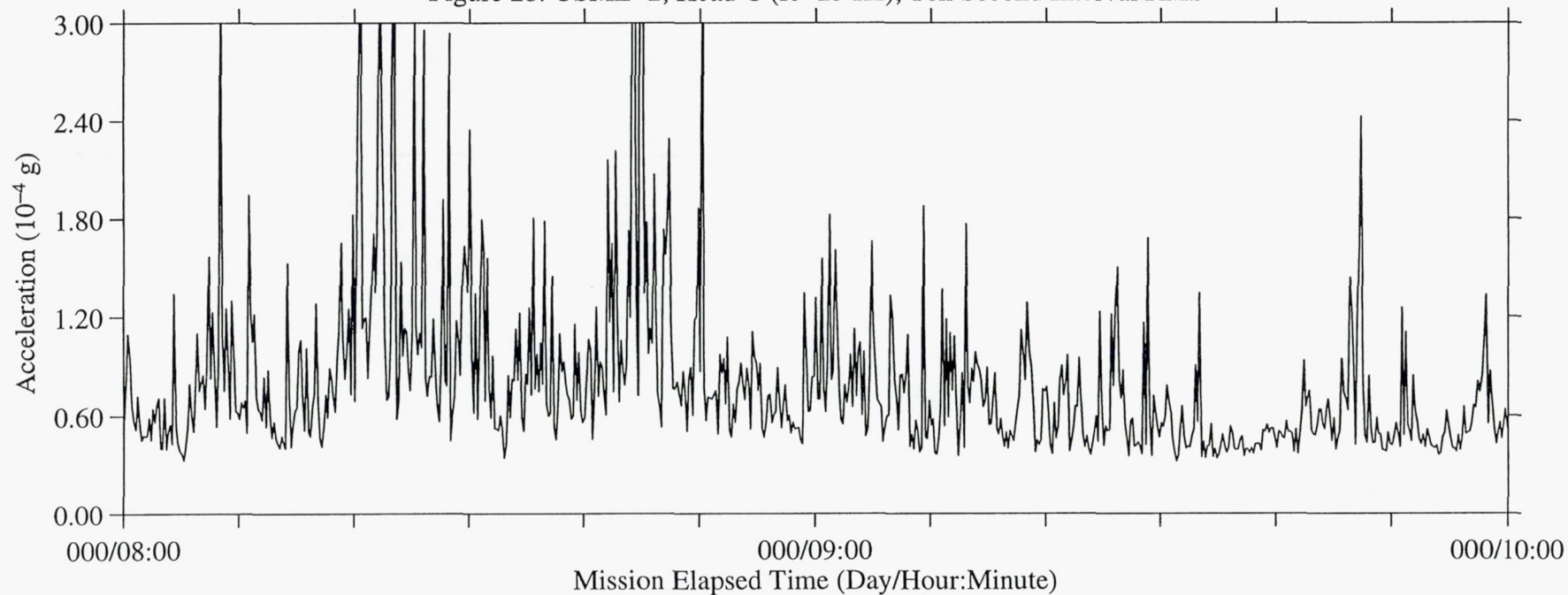


Figure 2b: USML-2, Head C (fc=25 Hz), Ten Second Interval RMS





B-5

Figure 3a: USML-2, Head C (fc=25 Hz), Ten Second Interval Average

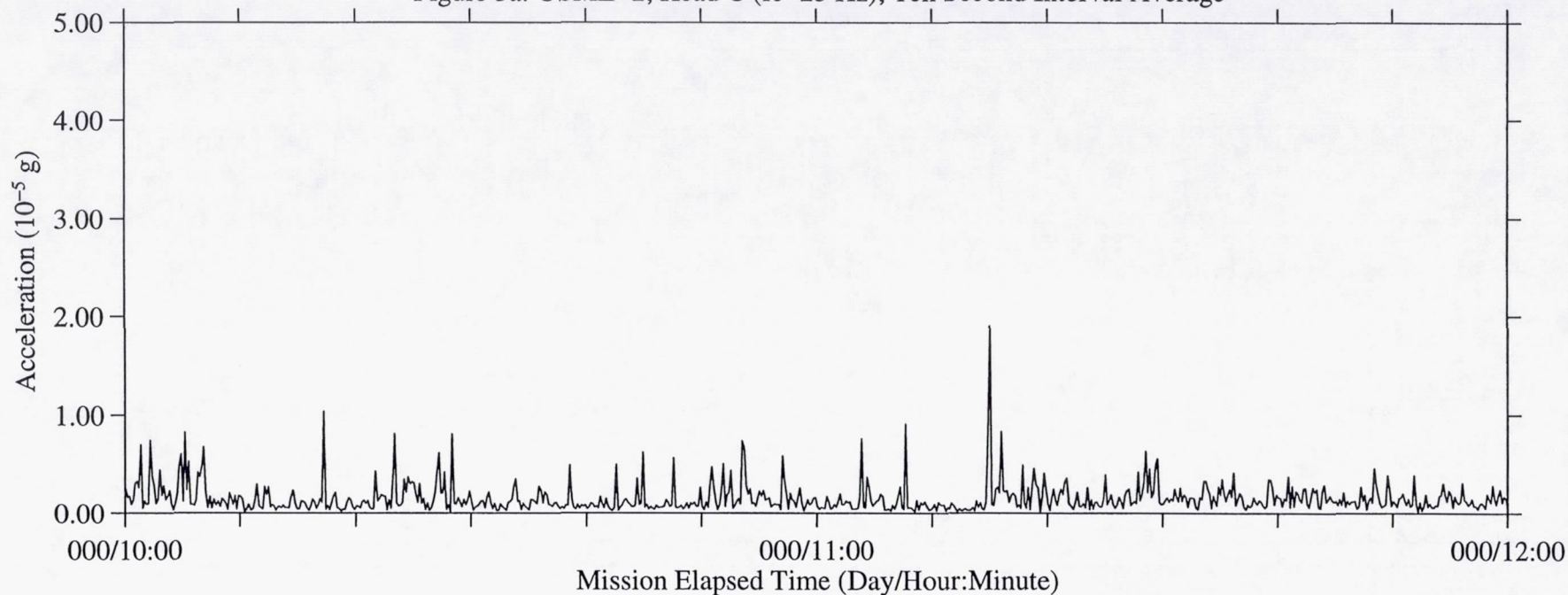


Figure 3b: USML-2, Head C (fc=25 Hz), Ten Second Interval RMS

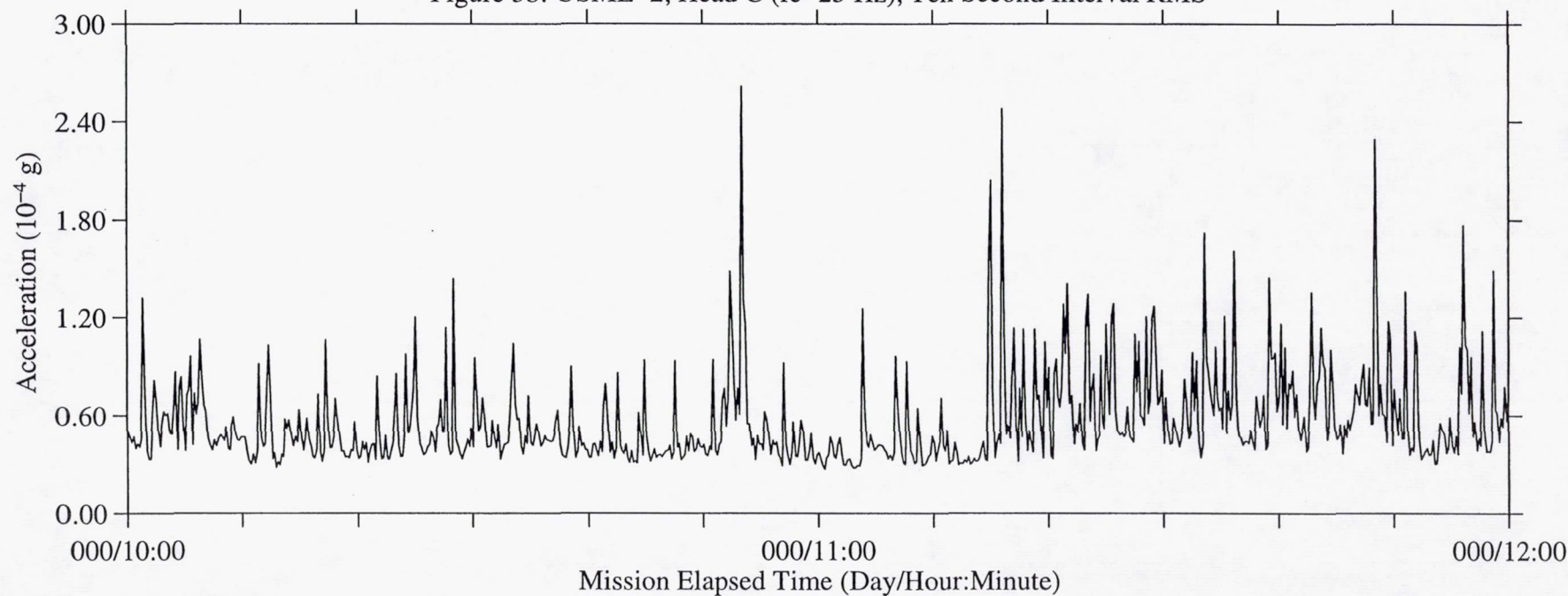


Figure 4a: USML-2, Head C (fc=25 Hz), Ten Second Interval Average

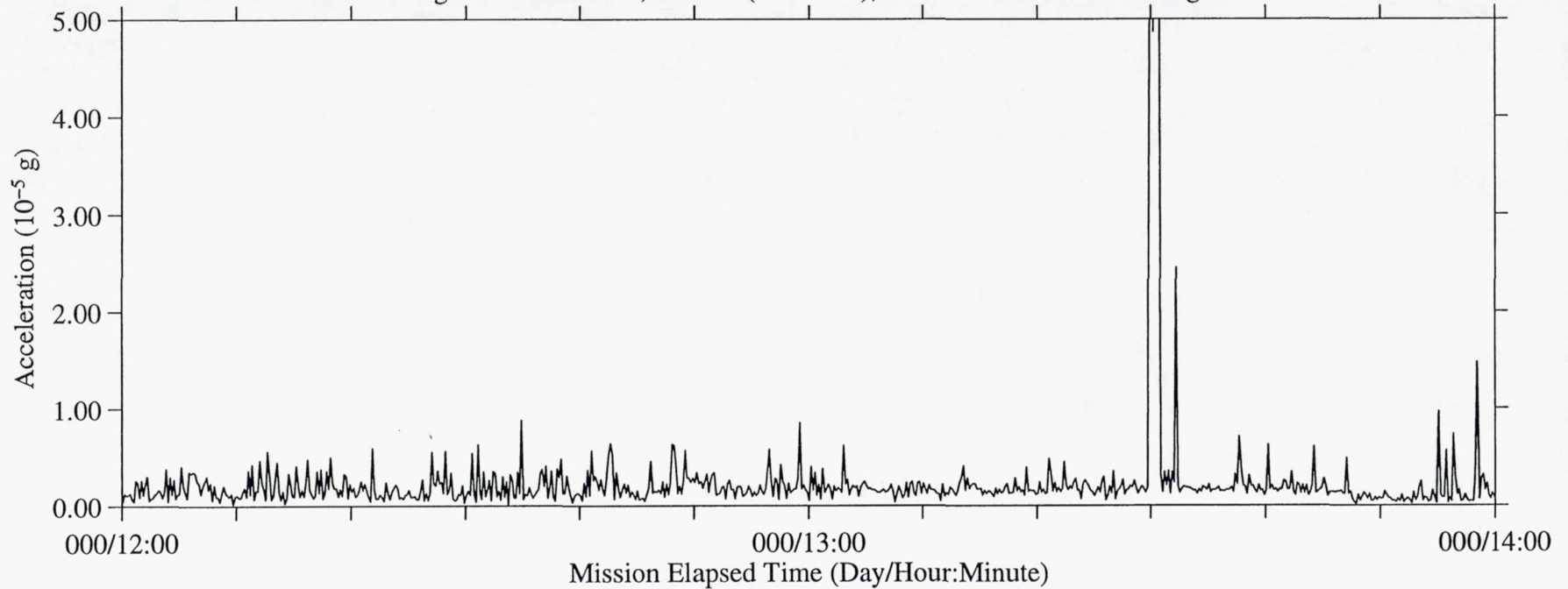


Figure 4b: USML-2, Head C (fc=25 Hz), Ten Second Interval RMS

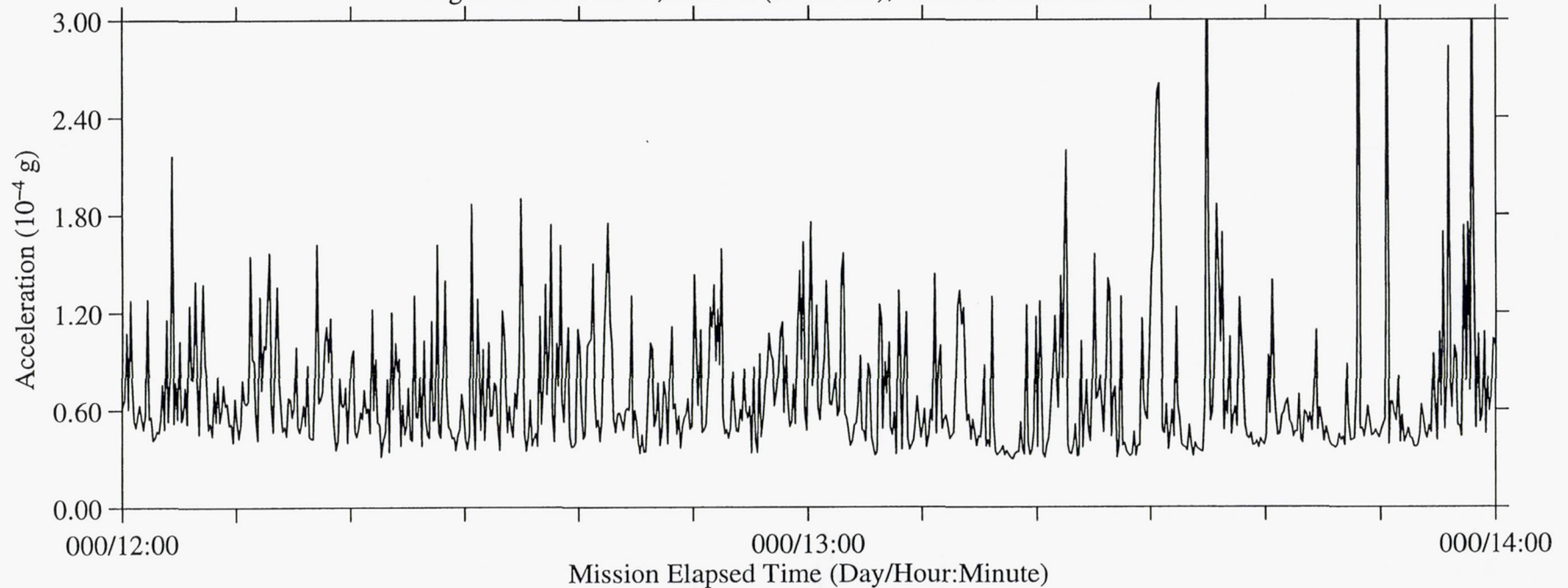




Figure 5a: USML-2, Head C (fc=25 Hz), Ten Second Interval Average

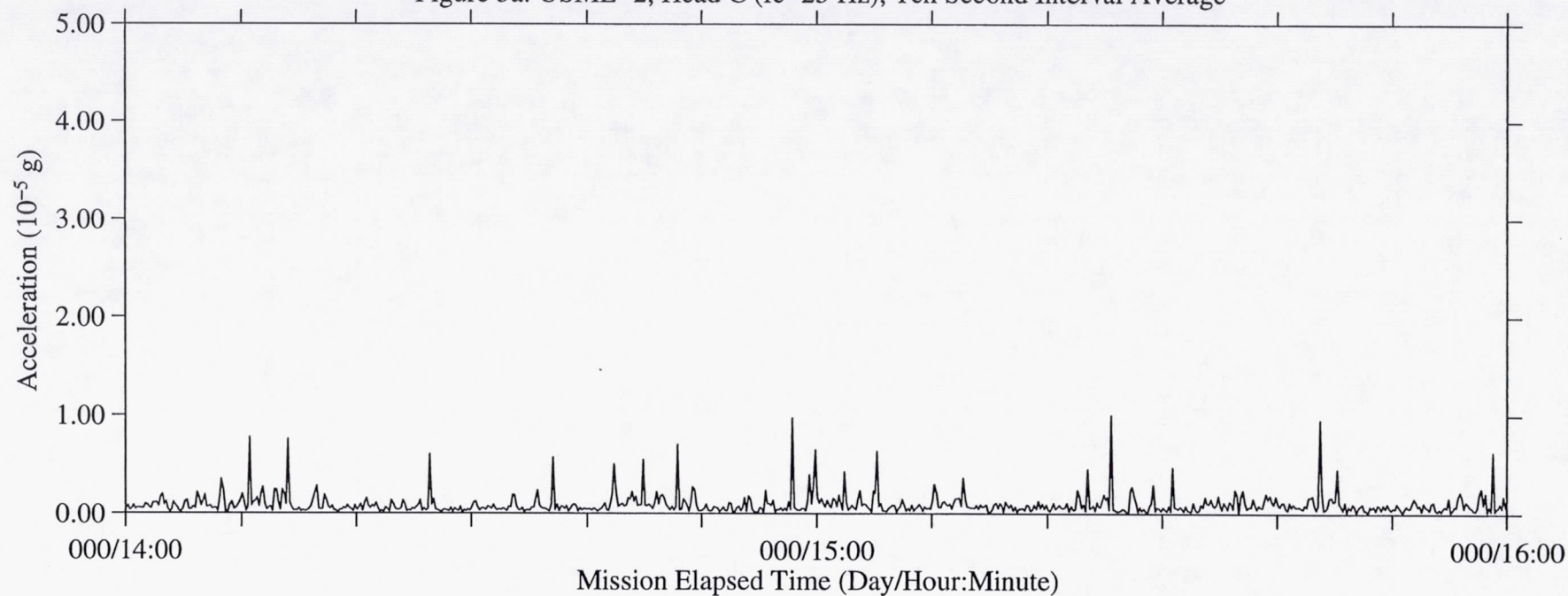


Figure 5b: USML-2, Head C (fc=25 Hz), Ten Second Interval RMS

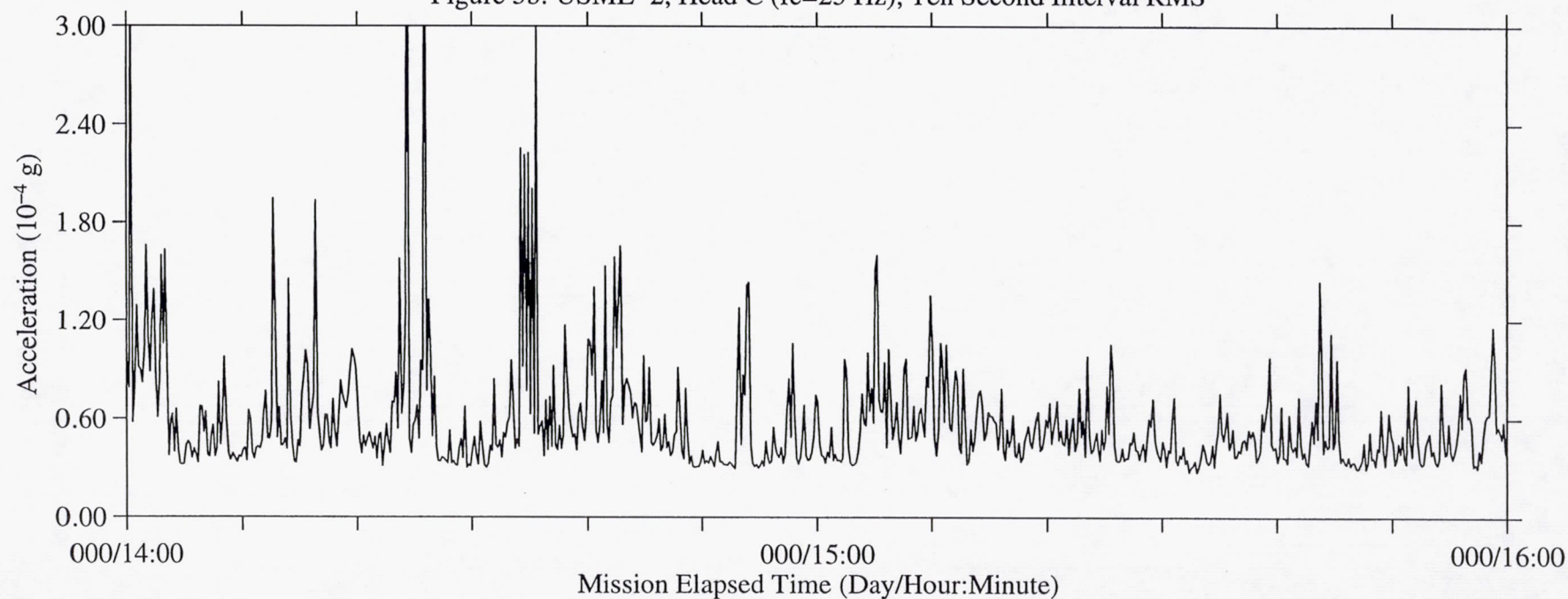


Figure 6a: USML-2, Head C (fc=25 Hz), Ten Second Interval Average

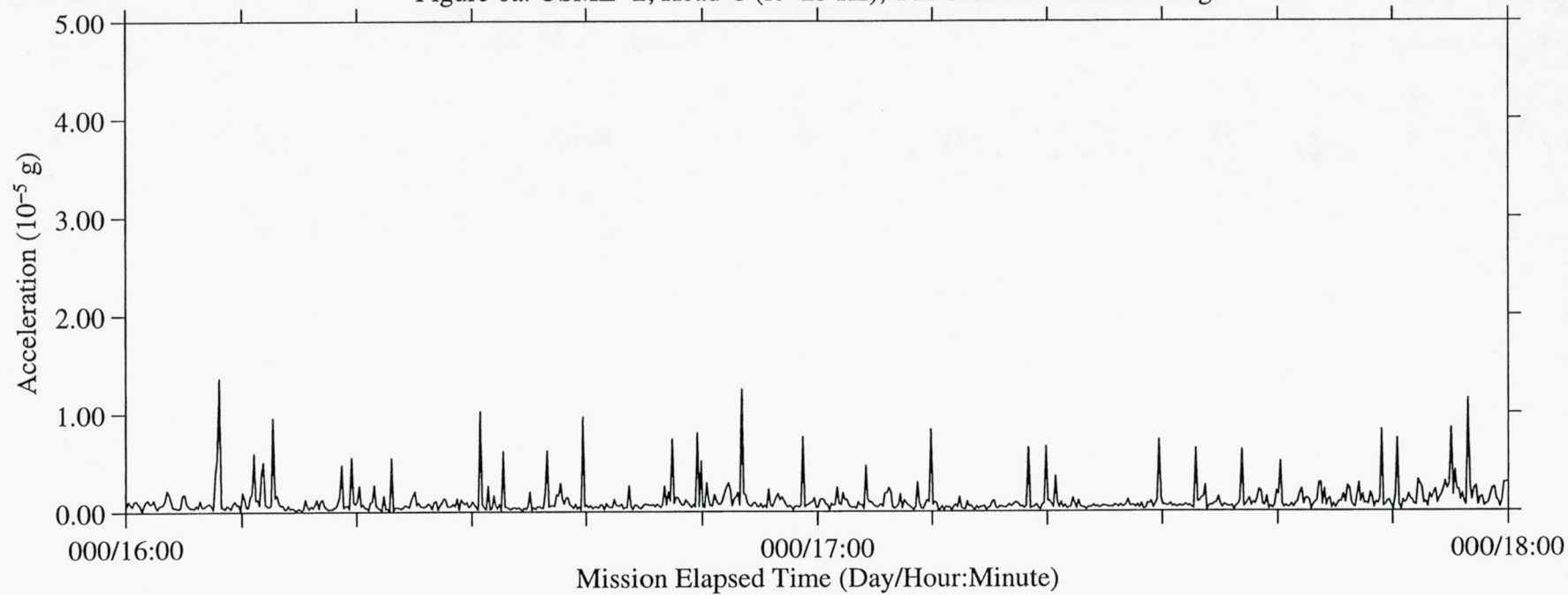
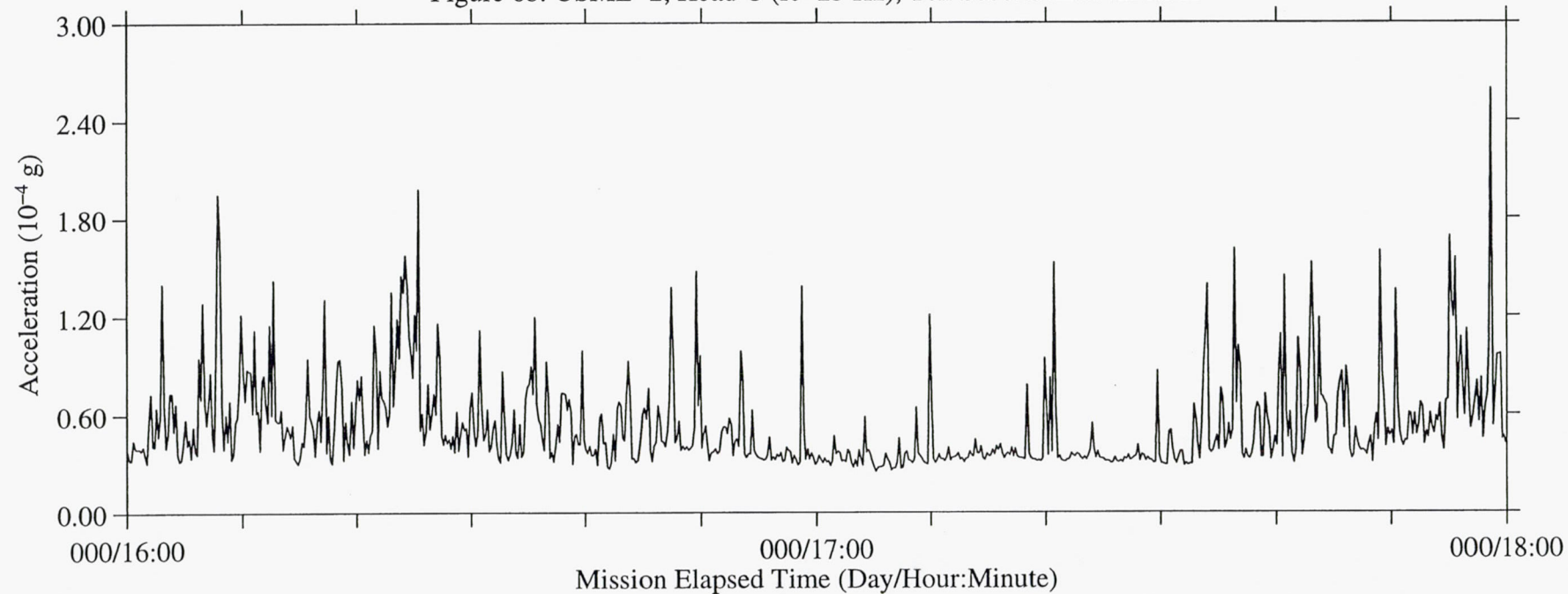


Figure 6b: USML-2, Head C (fc=25 Hz), Ten Second Interval RMS





6-8

Figure 7a: USML-2, Head C (fc=25 Hz), Ten Second Interval Average

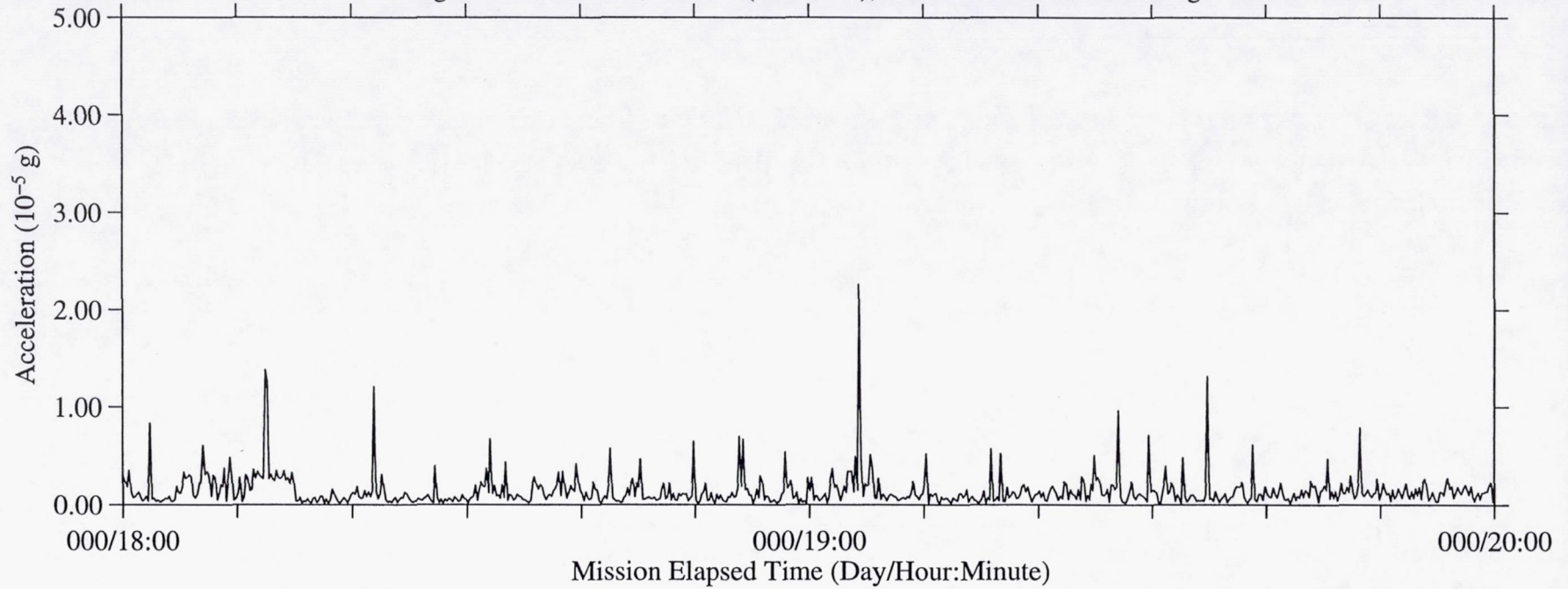


Figure 7b: USML-2, Head C (fc=25 Hz), Ten Second Interval RMS

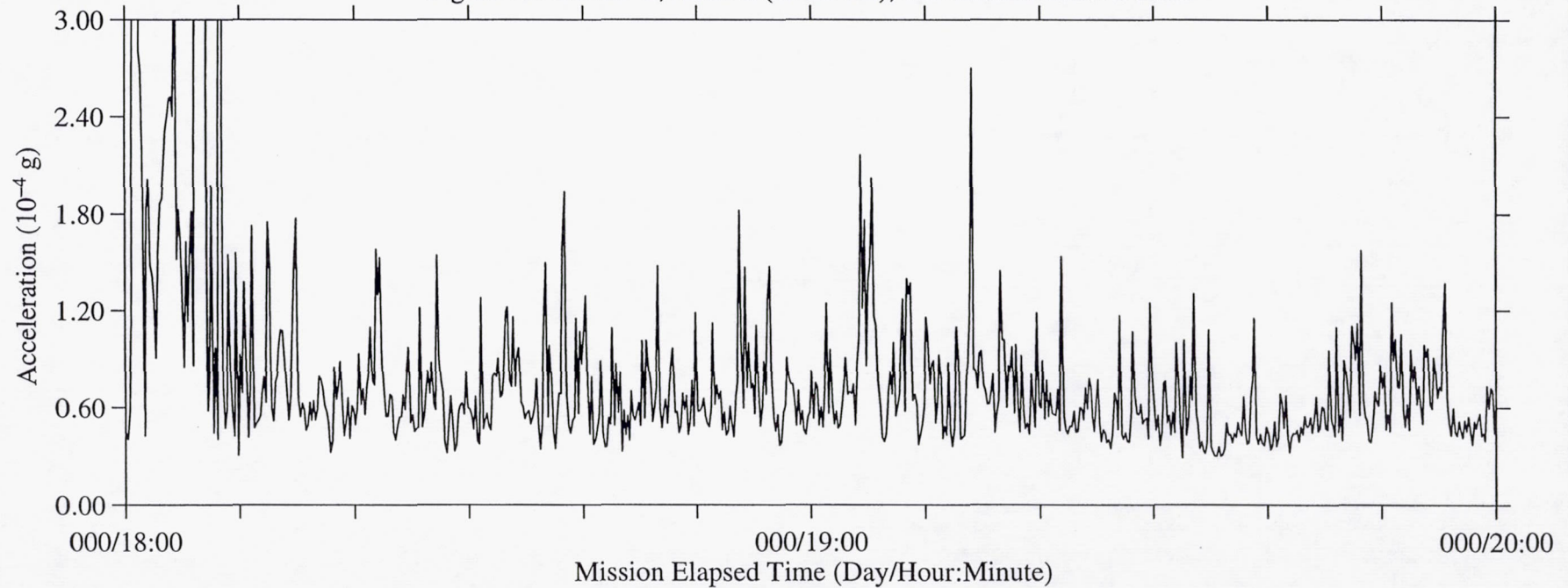


Figure 8a: USML-2, Head C (fc=25 Hz), Ten Second Interval Average

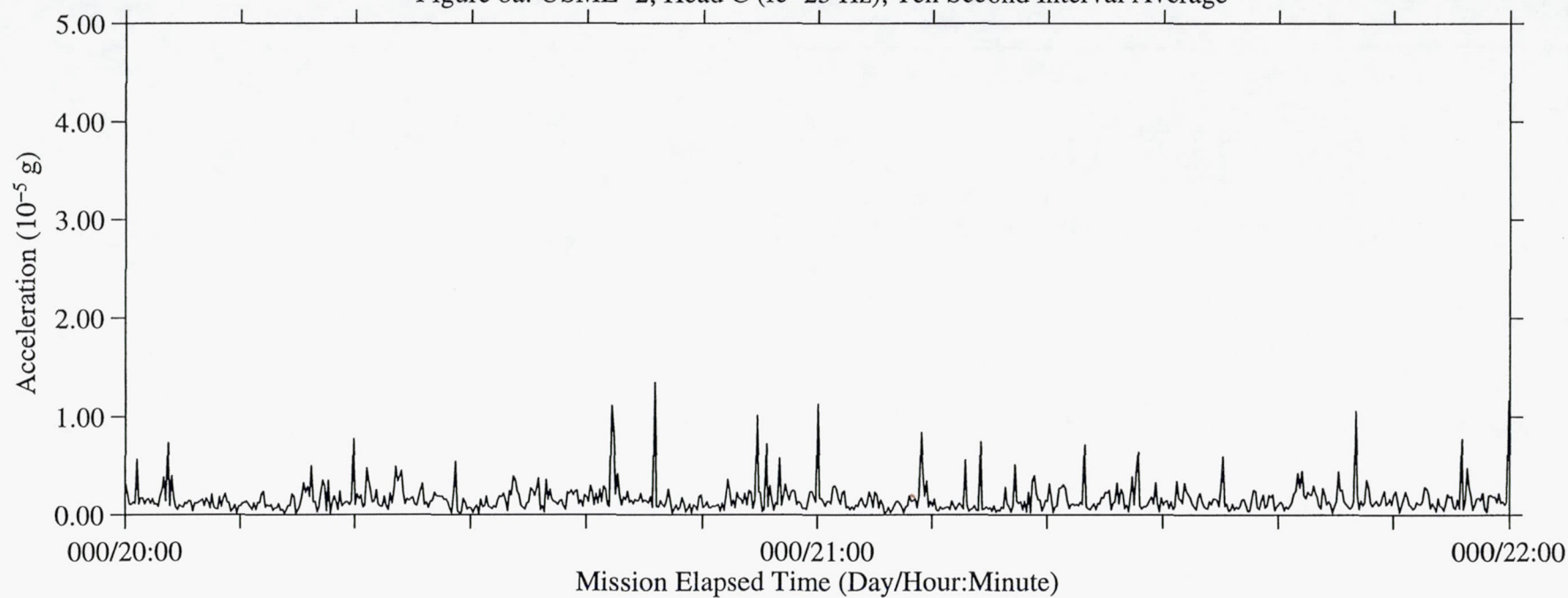
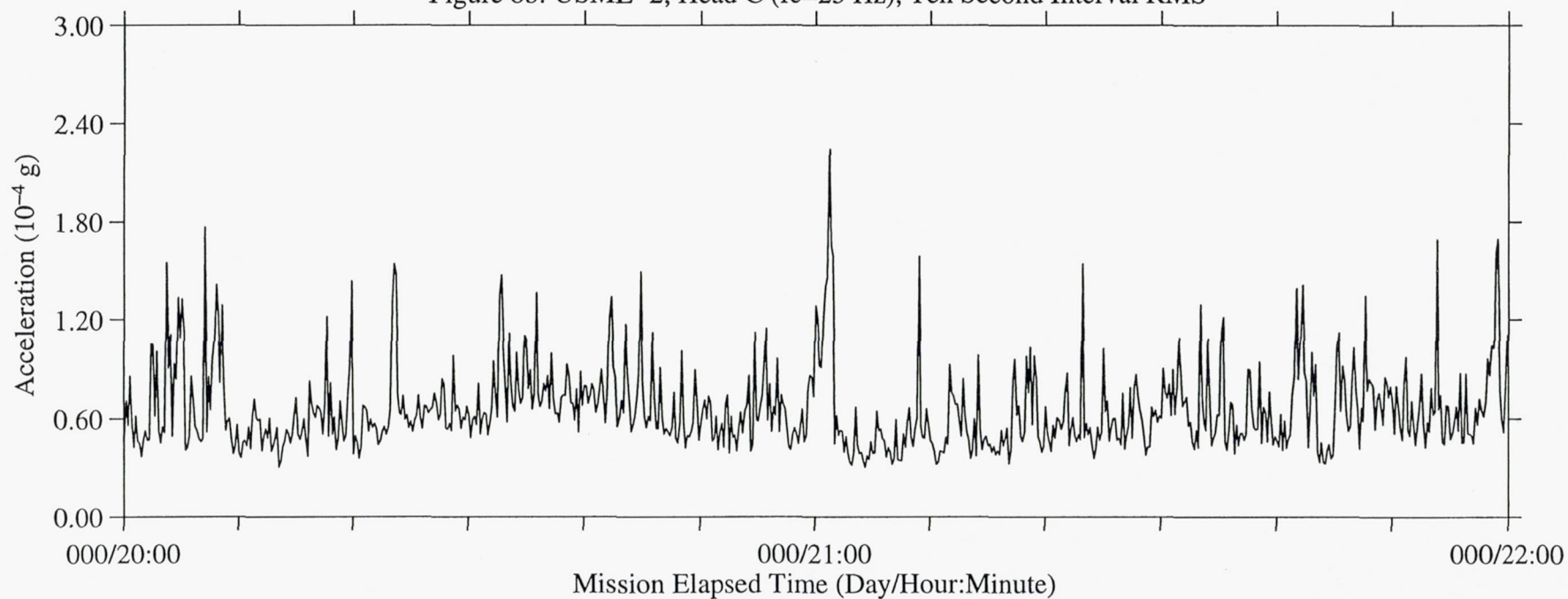


Figure 8b: USML-2, Head C (fc=25 Hz), Ten Second Interval RMS





B-11

Figure 9a: USML-2, Head C (fc=25 Hz), Ten Second Interval Average

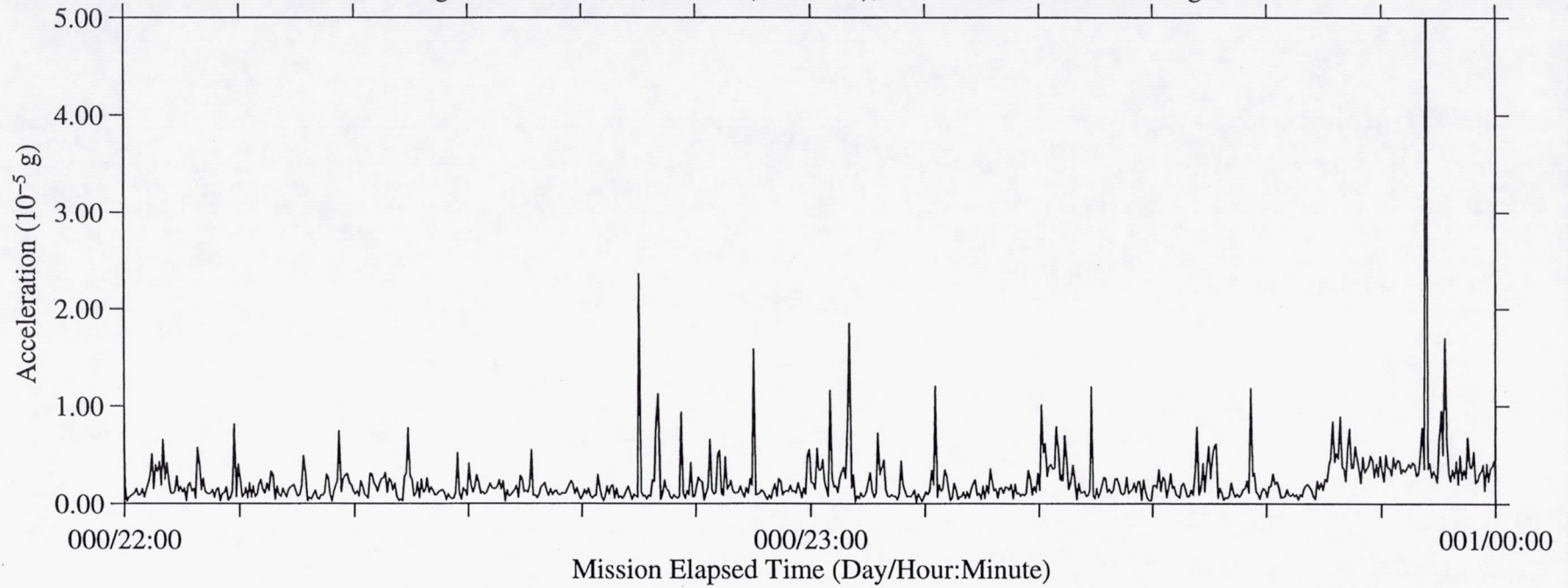


Figure 9b: USML-2, Head C (fc=25 Hz), Ten Second Interval RMS

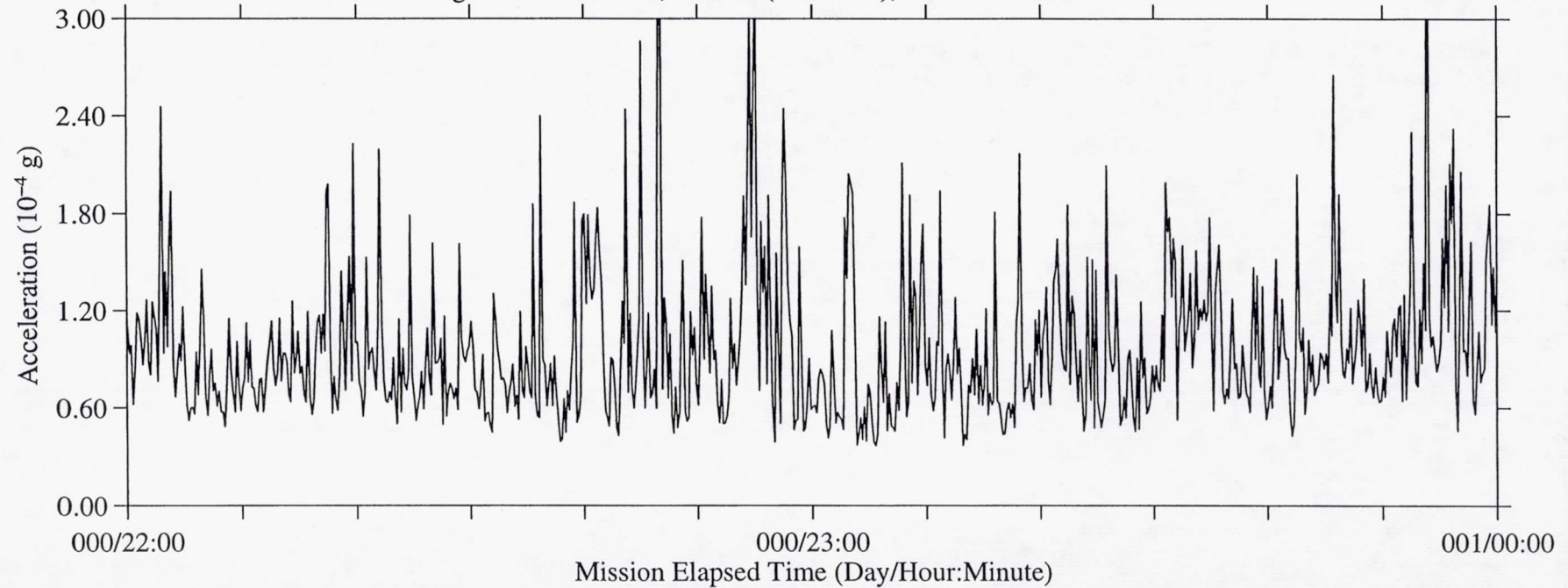


Figure 10a: USML-2, Head C (fc=25 Hz), Ten Second Interval Average

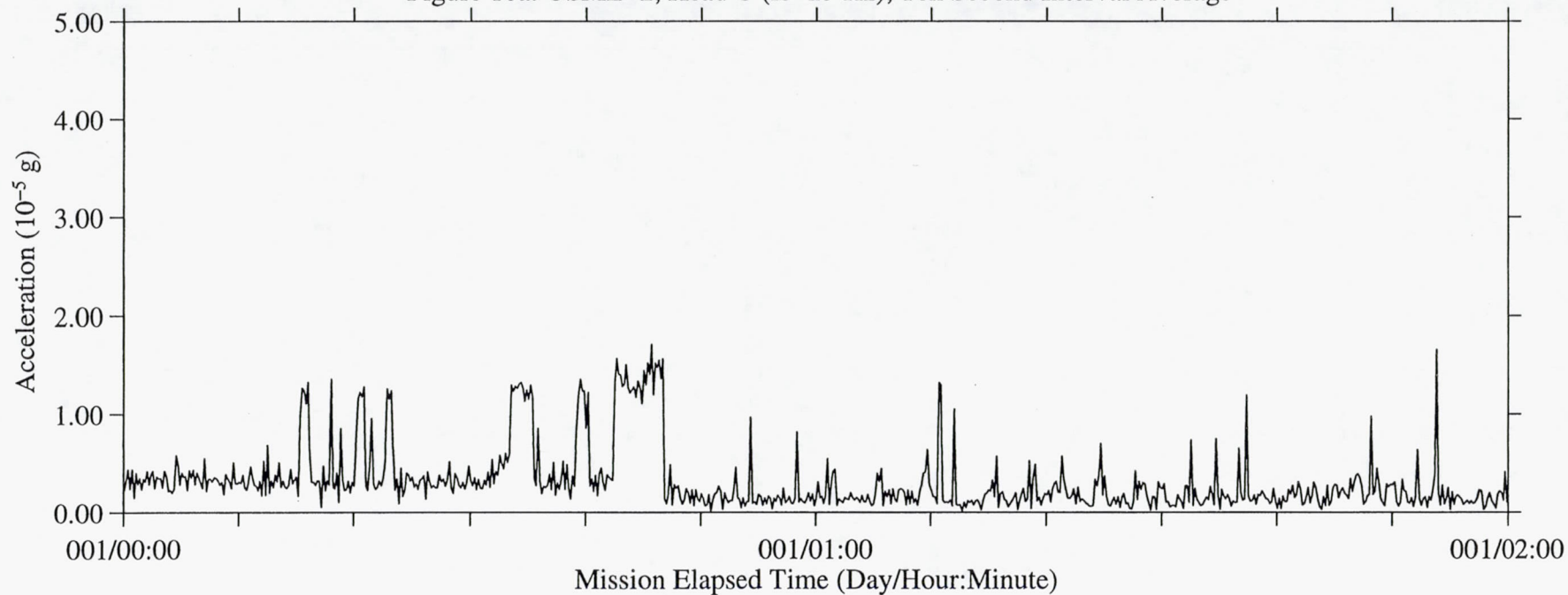


Figure 10b: USML-2, Head C (fc=25 Hz), Ten Second Interval RMS

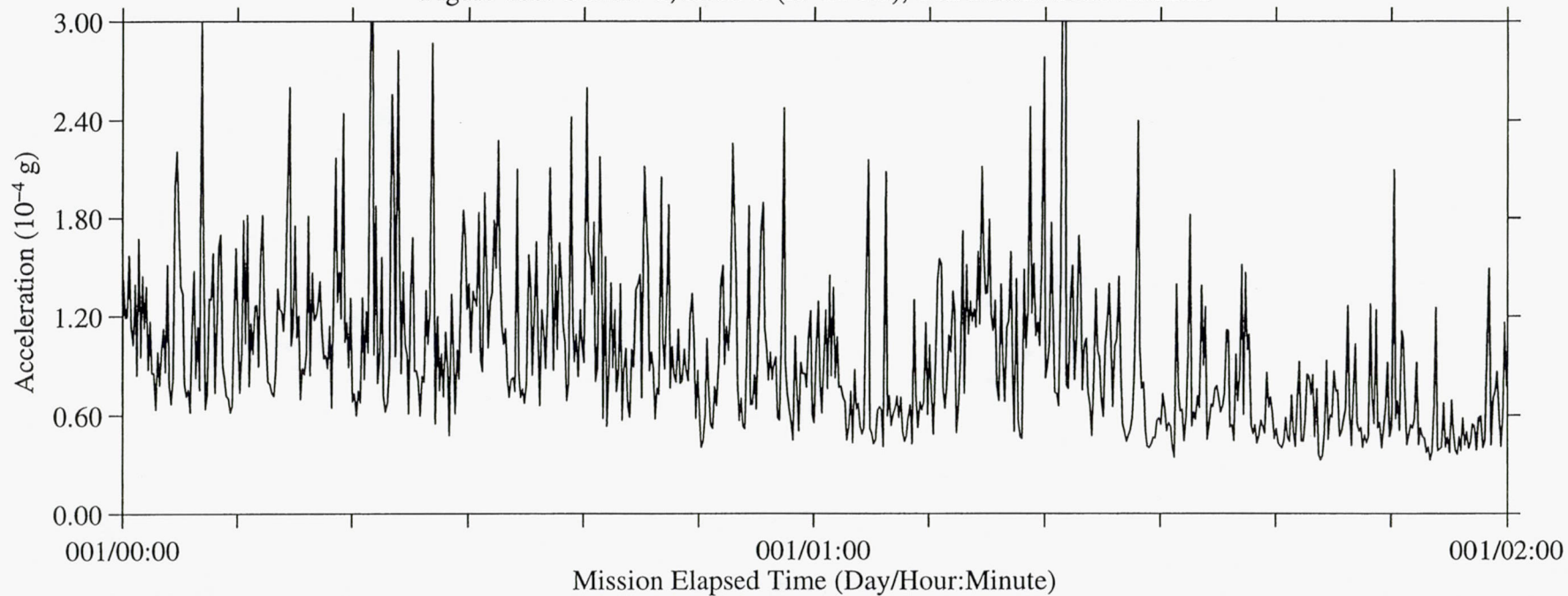




Figure 11a: USML-2, Head C (fc=25 Hz), Ten Second Interval Average

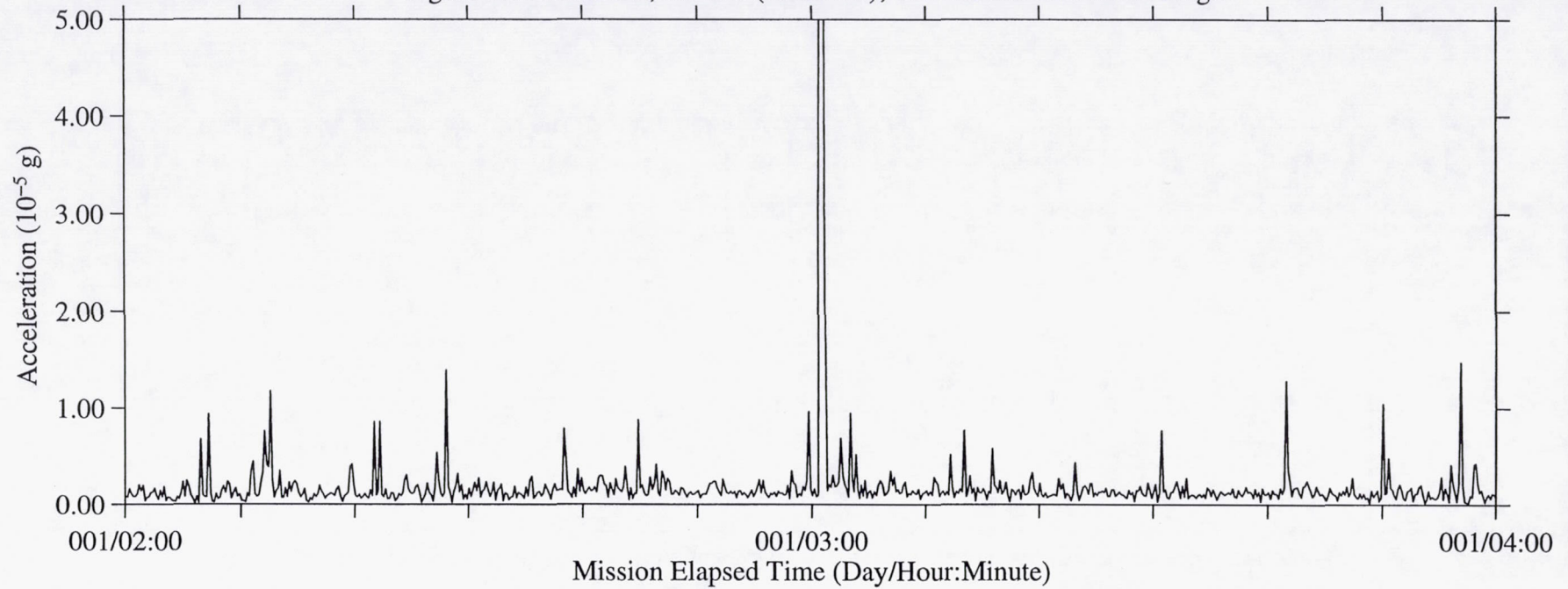


Figure 11b: USML-2, Head C (fc=25 Hz), Ten Second Interval RMS

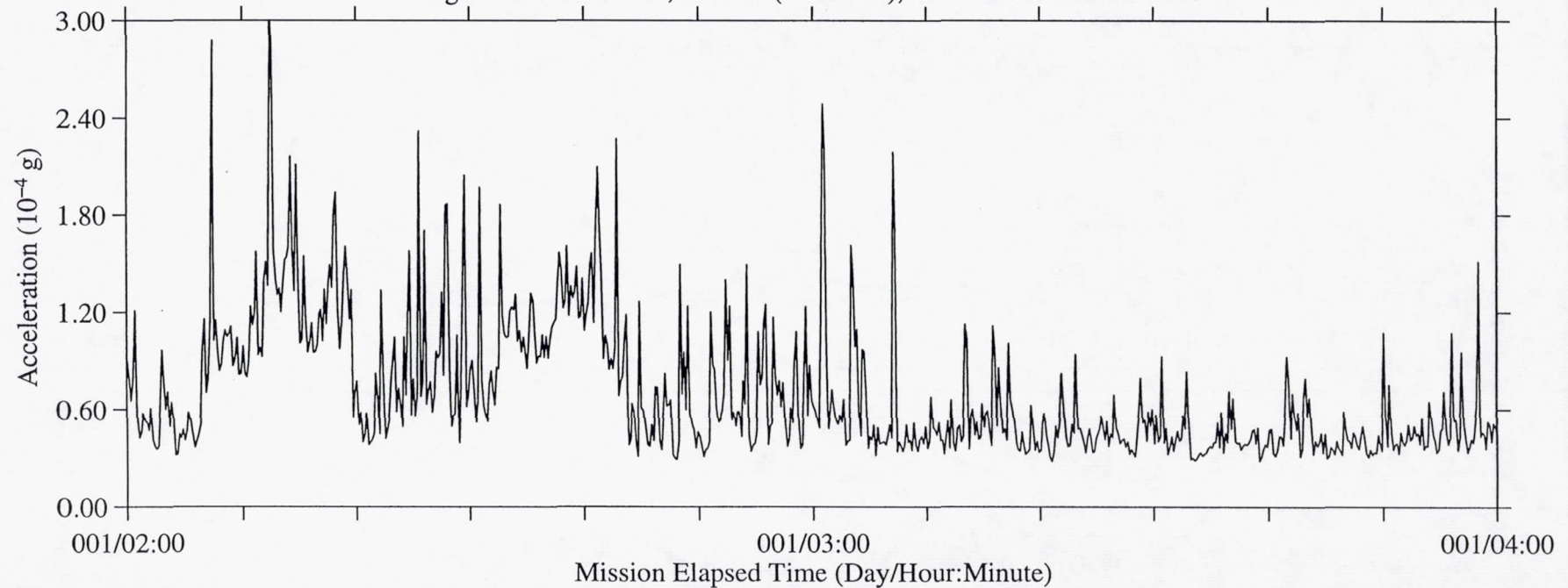


Figure 12a: USML-2, Head C (fc=25 Hz), Ten Second Interval Average

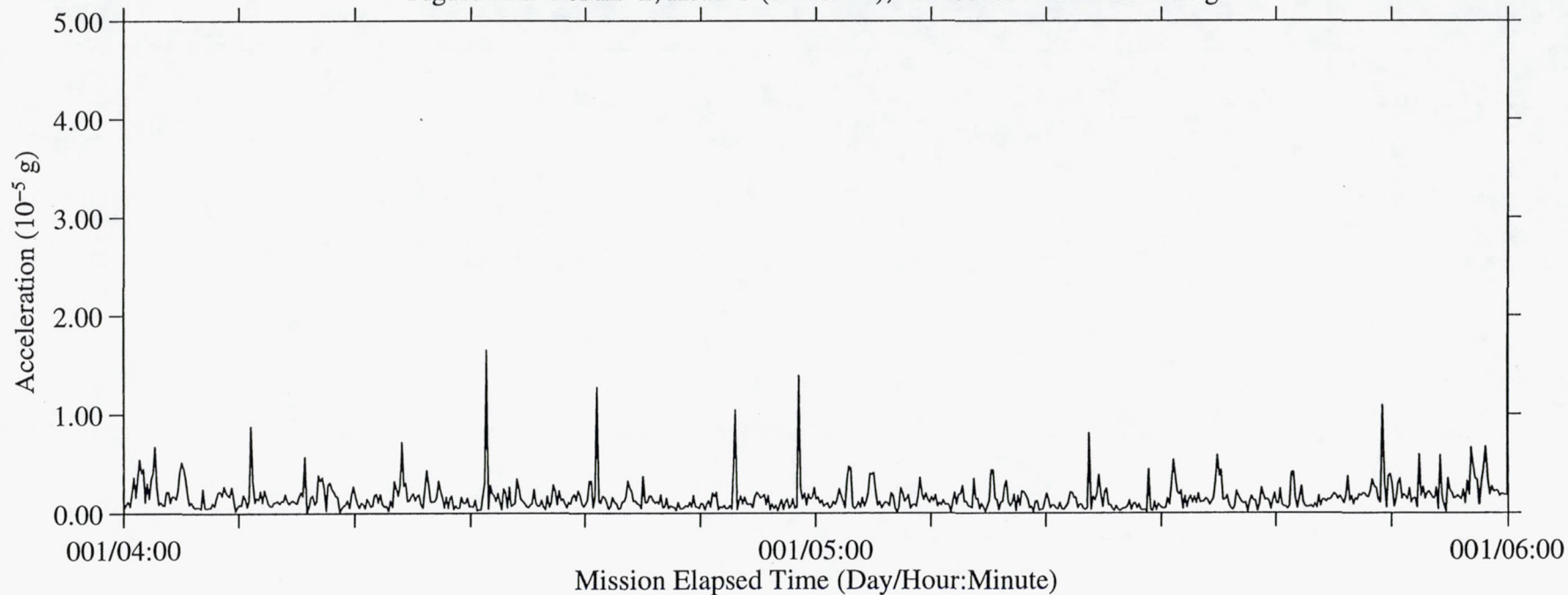


Figure 12b: USML-2, Head C (fc=25 Hz), Ten Second Interval RMS

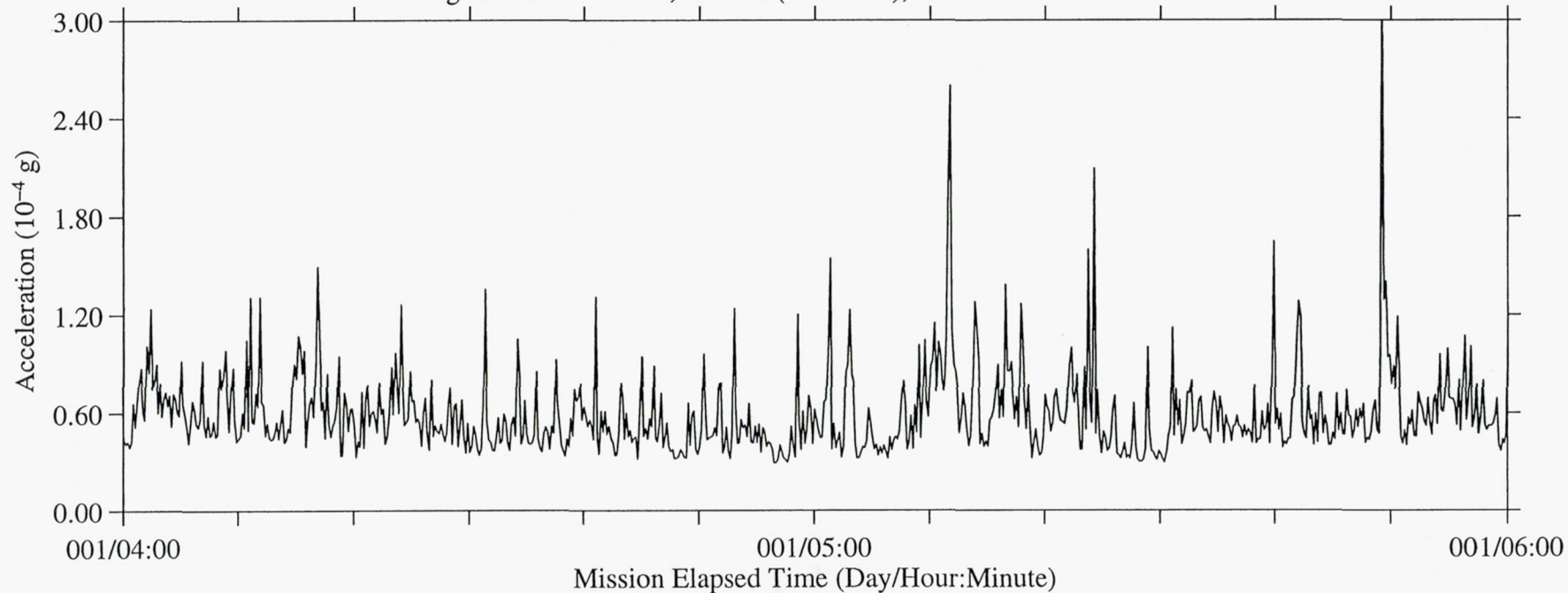




Figure 13a: USML-2, Head C (fc=25 Hz), Ten Second Interval Average

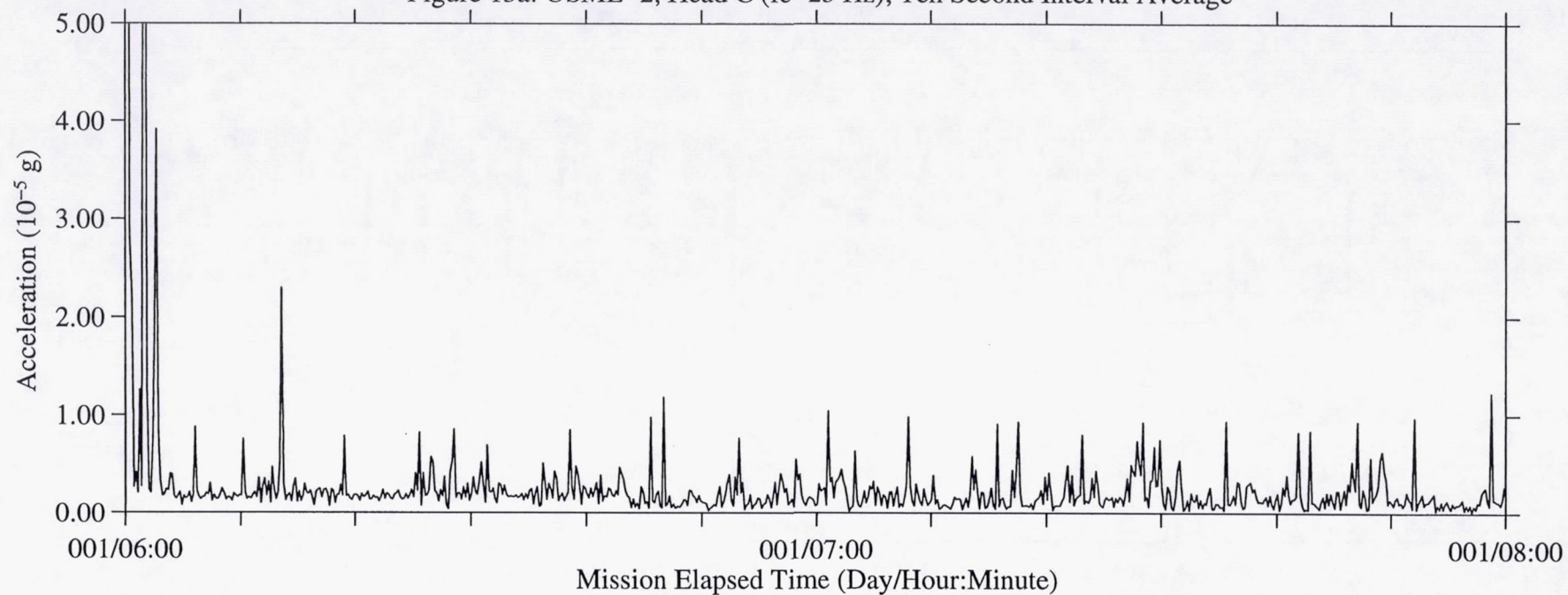
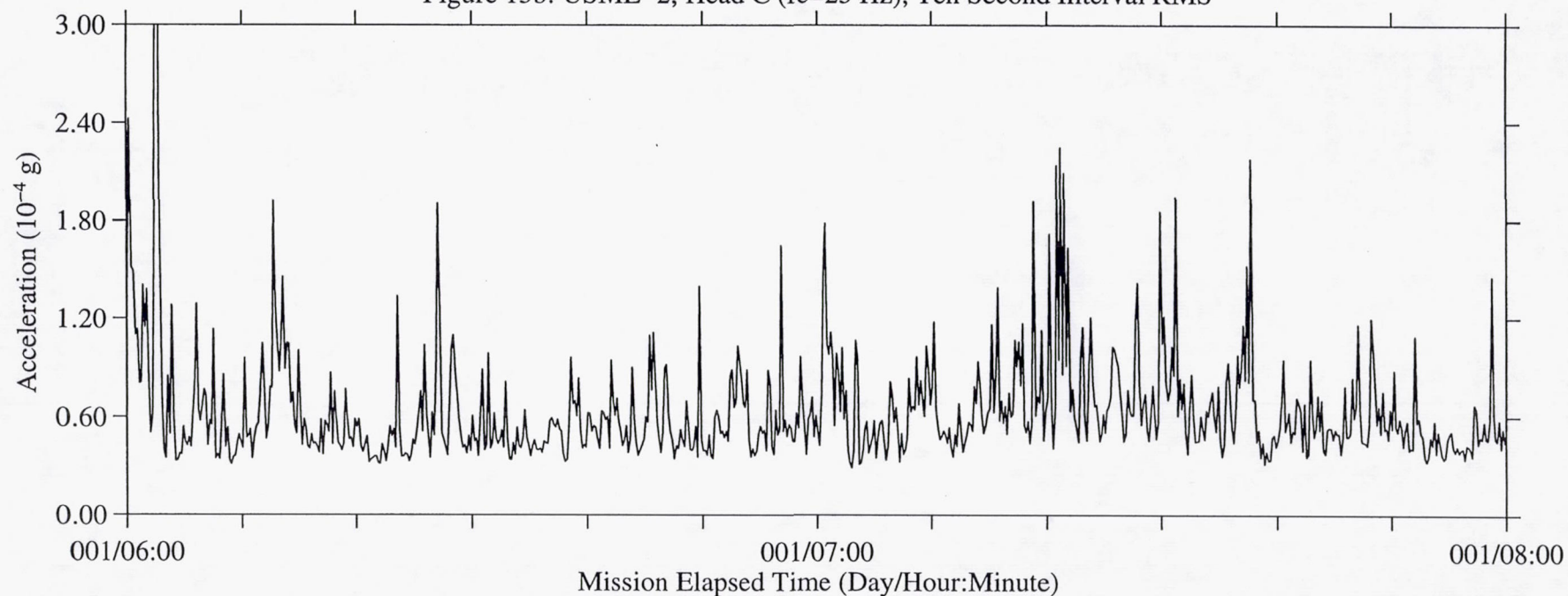


Figure 13b: USML-2, Head C (fc=25 Hz), Ten Second Interval RMS



B-16

Figure 14a: USML-2, Head C (fc=25 Hz), Ten Second Interval Average

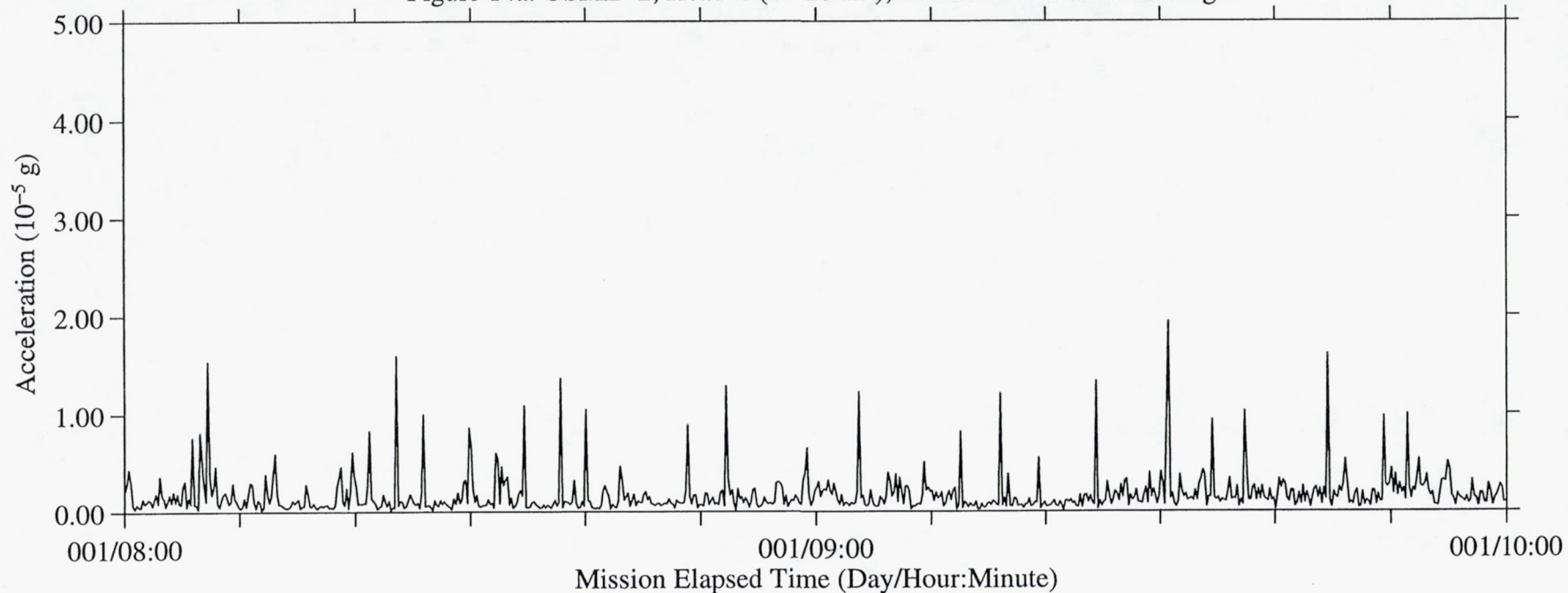


Figure 14b: USML-2, Head C (fc=25 Hz), Ten Second Interval RMS

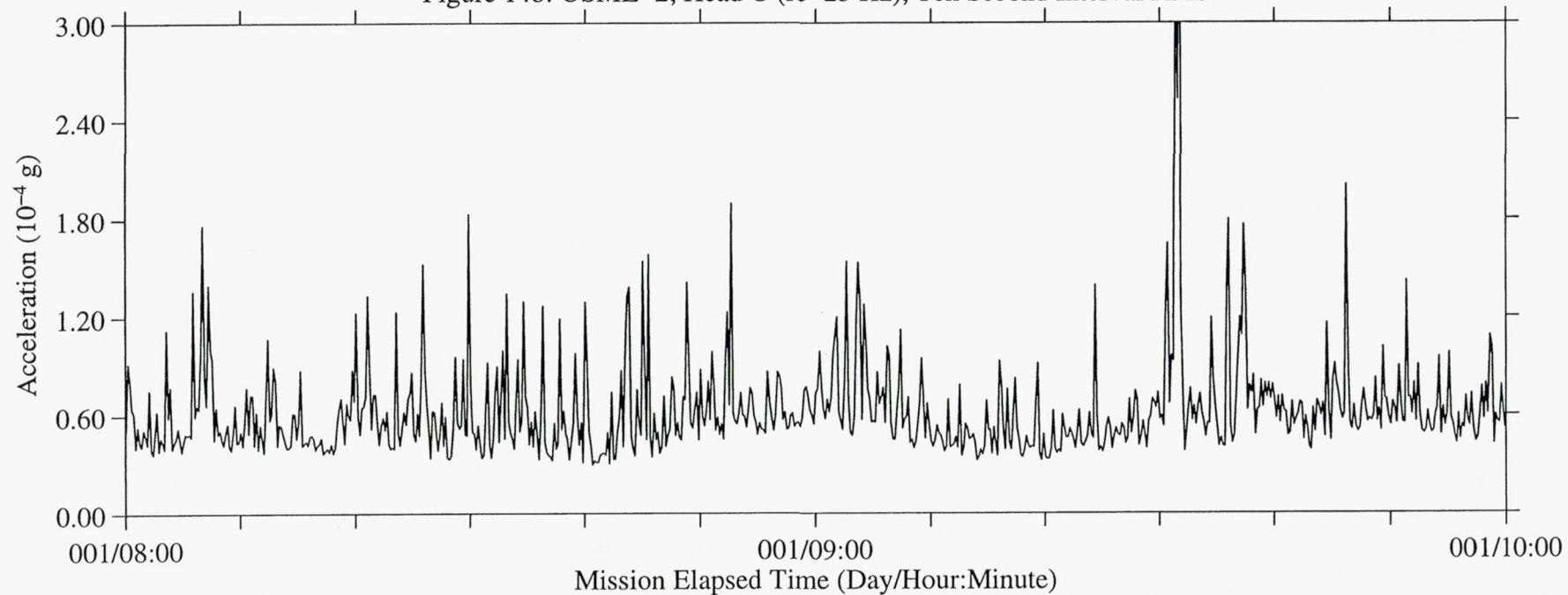




Figure 15a: USML-2, Head C (fc=25 Hz), Ten Second Interval Average

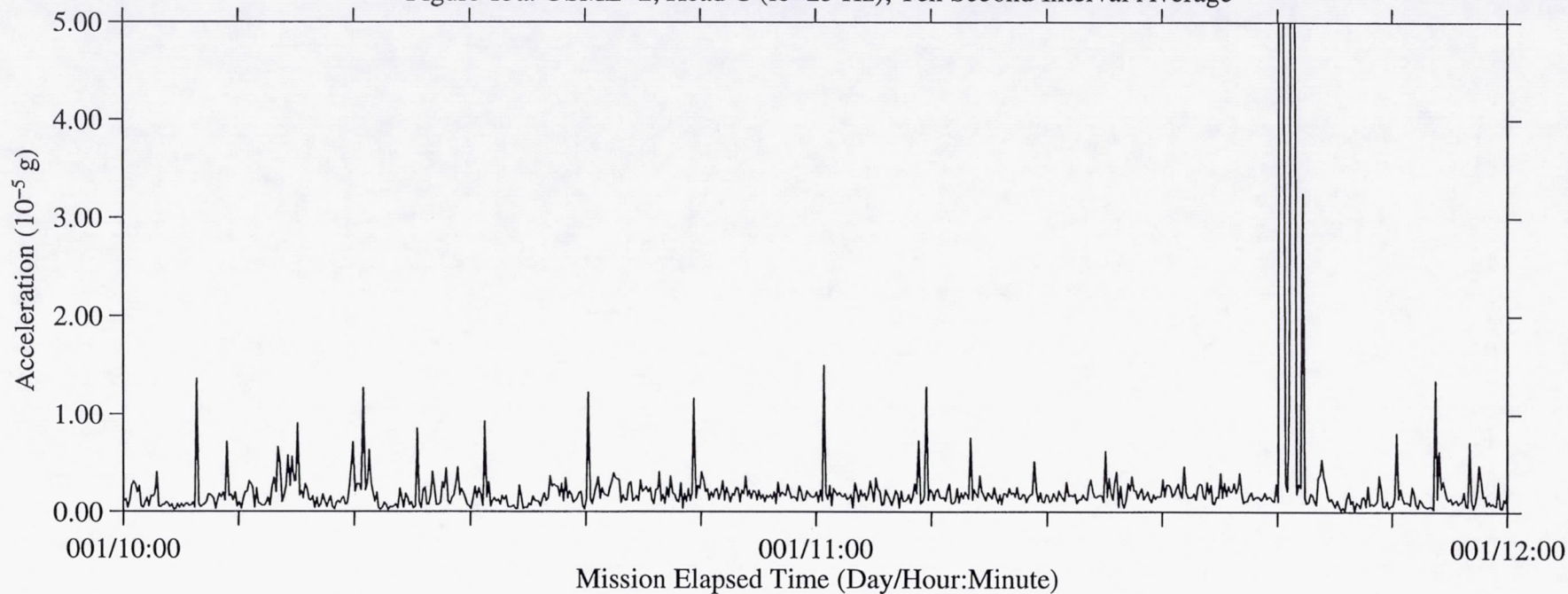


Figure 15b: USML-2, Head C (fc=25 Hz), Ten Second Interval RMS

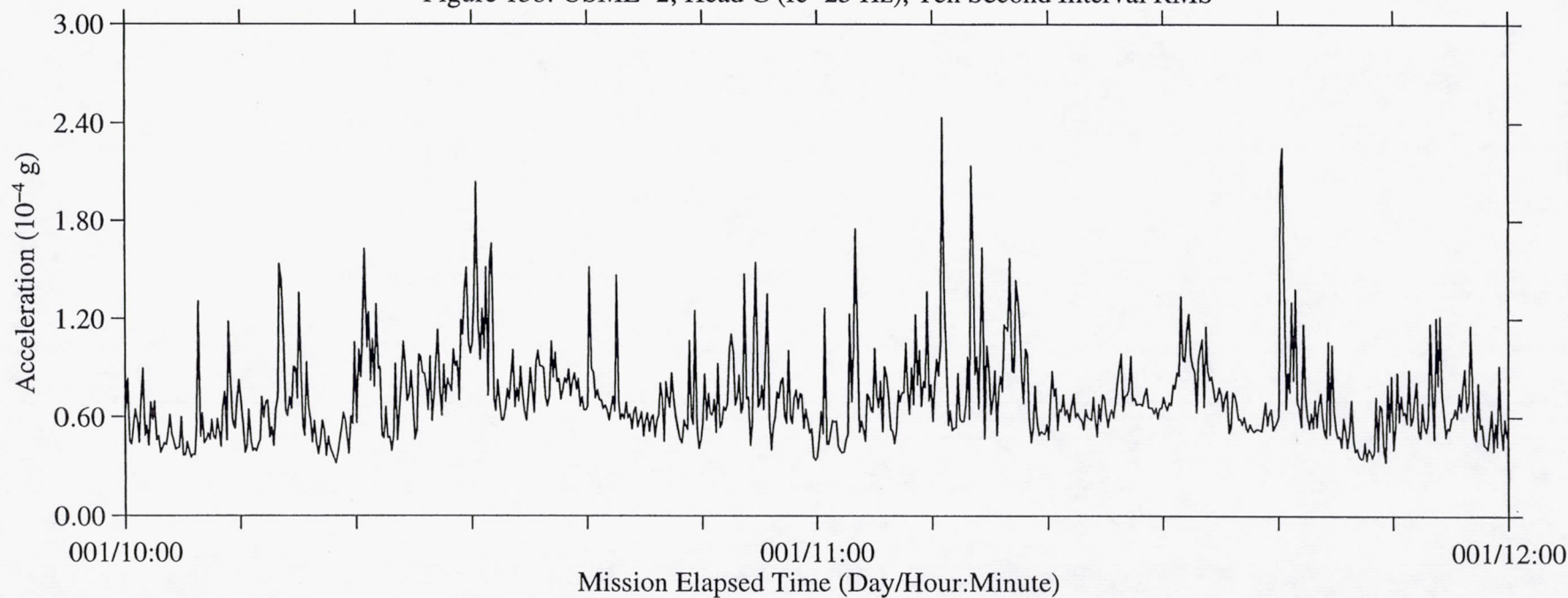


Figure 16a: USML-2, Head C (fc=25 Hz), Ten Second Interval Average

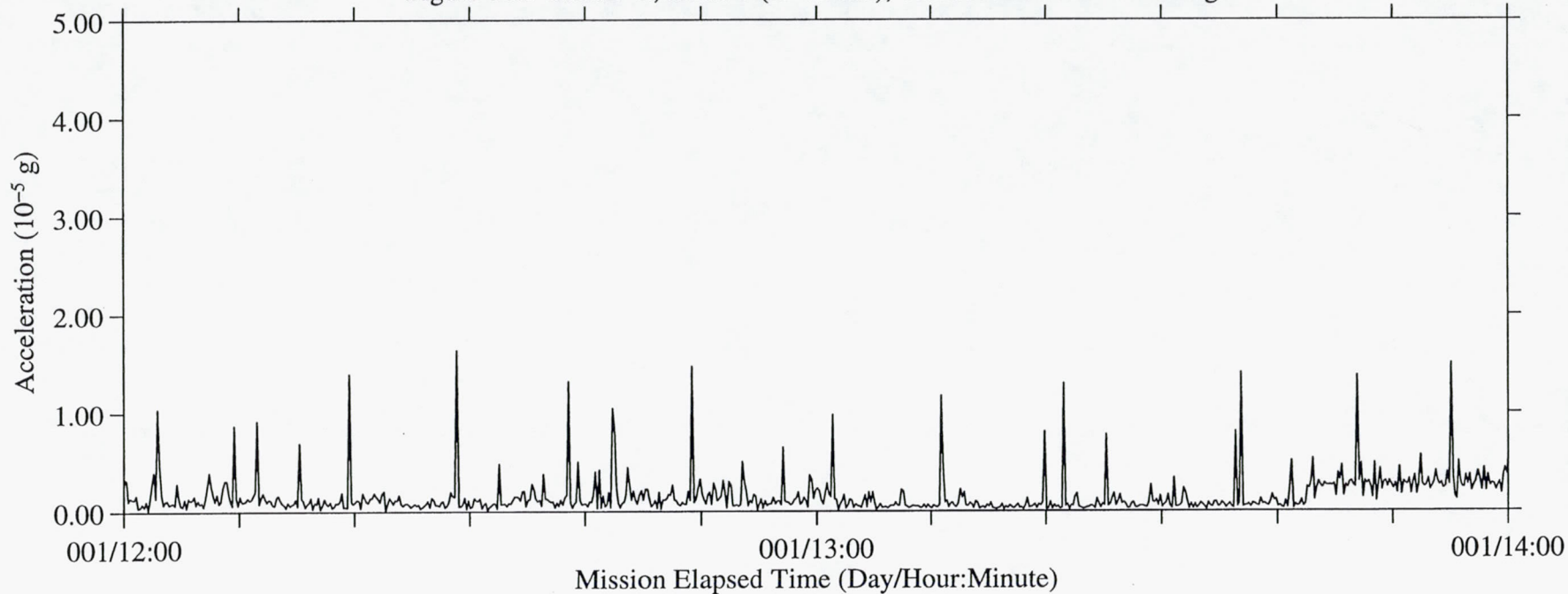
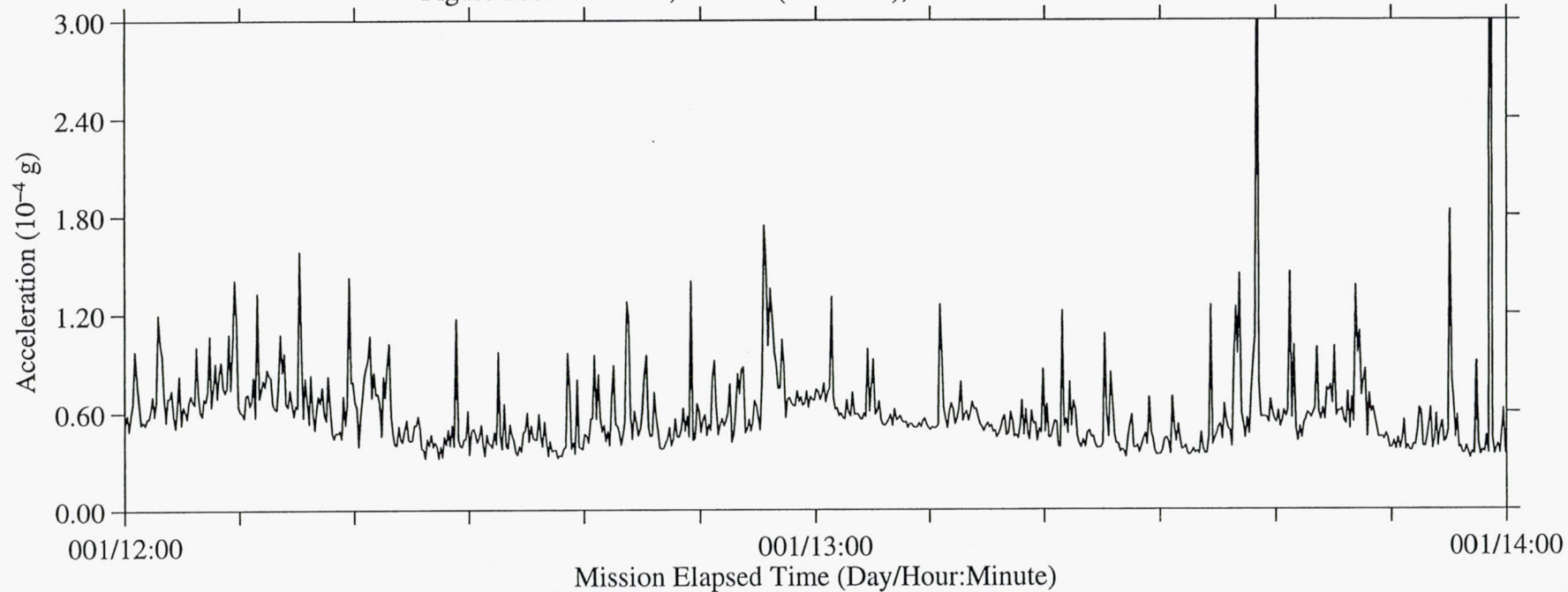


Figure 16b: USML-2, Head C (fc=25 Hz), Ten Second Interval RMS





B-19

Figure 17a: USML-2, Head C (fc=25 Hz), Ten Second Interval Average

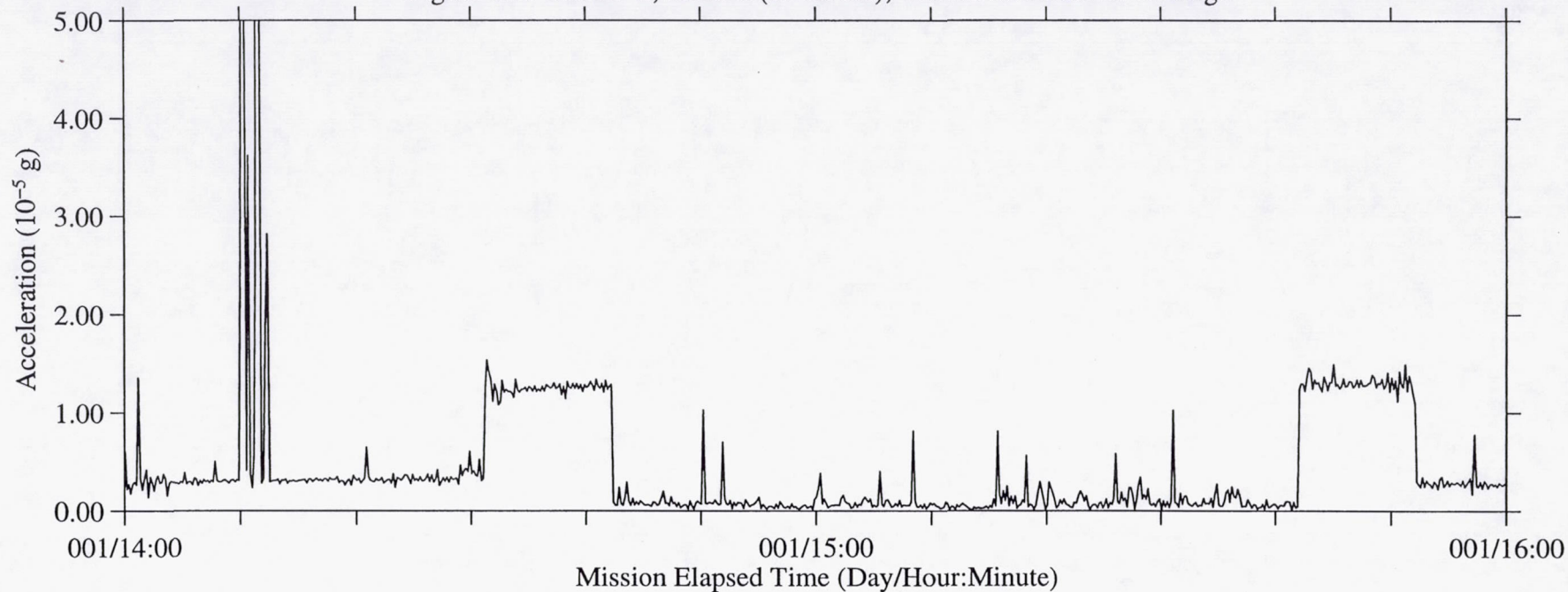


Figure 17b: USML-2, Head C (fc=25 Hz), Ten Second Interval RMS

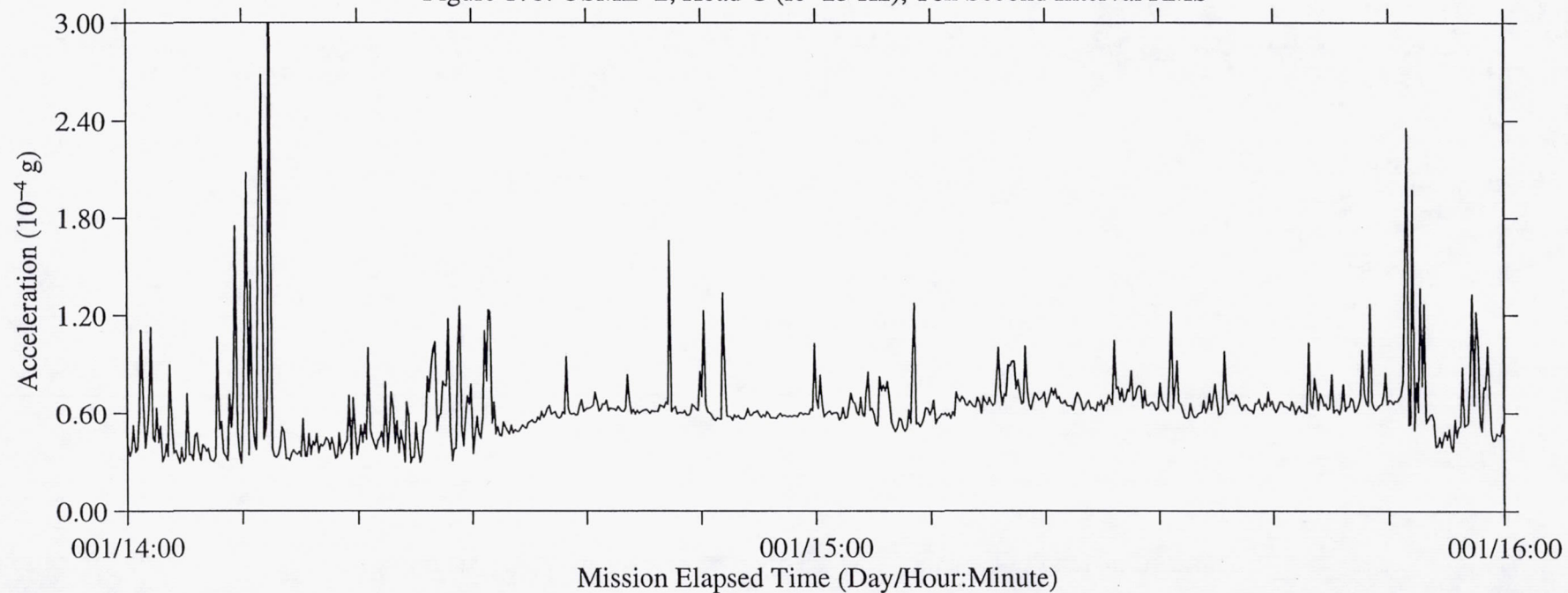


Figure 18a: USML-2, Head C (fc=25 Hz), Ten Second Interval Average

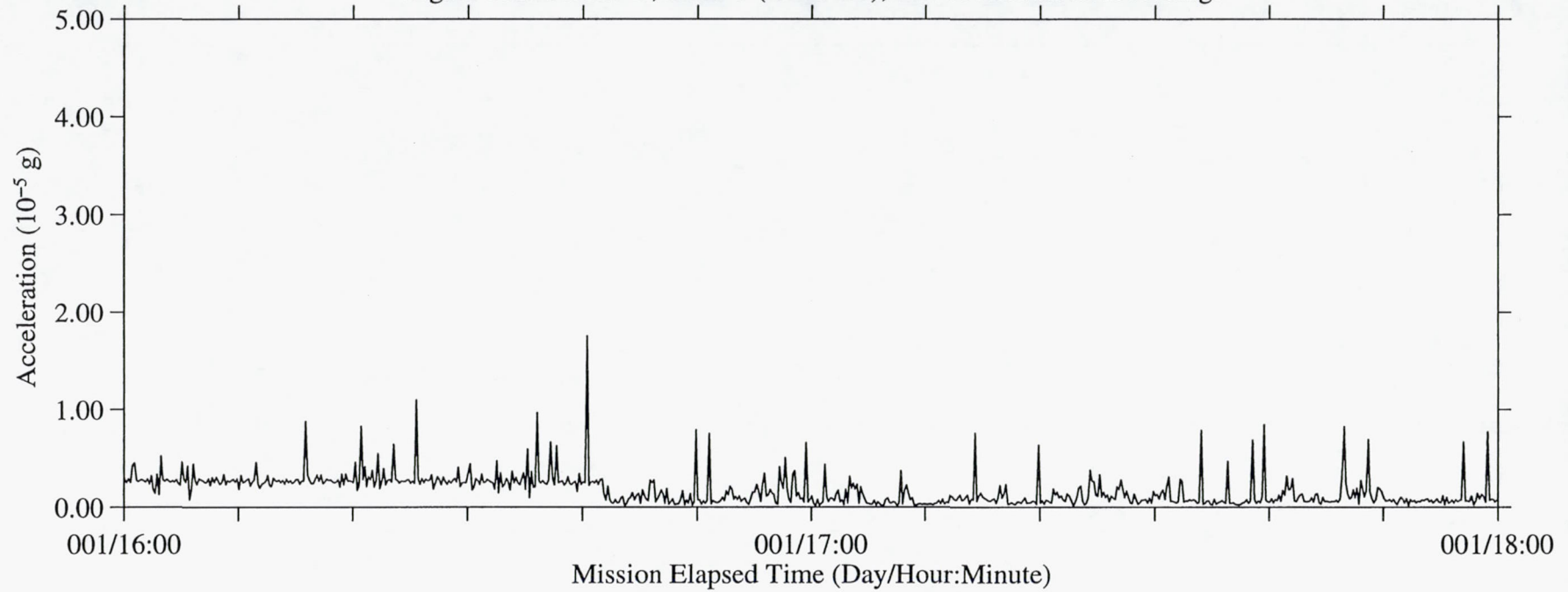


Figure 18b: USML-2, Head C (fc=25 Hz), Ten Second Interval RMS

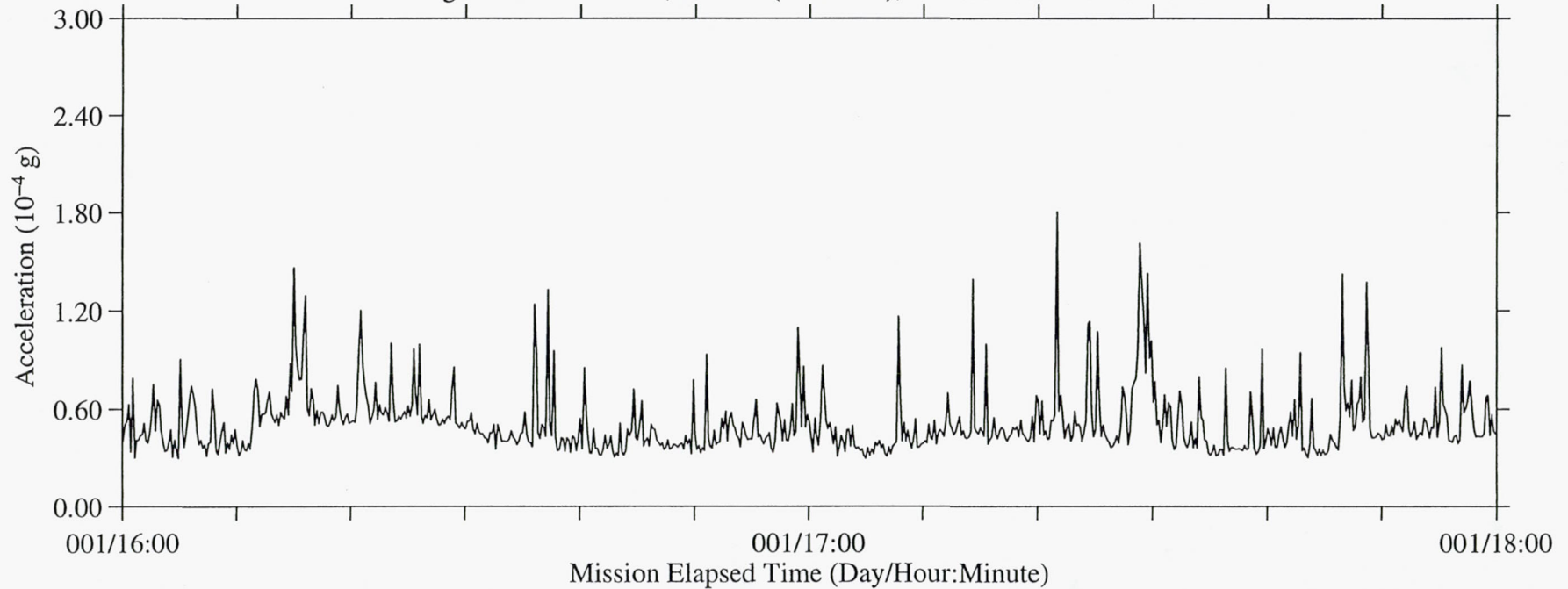




Figure 19a: USML-2, Head C (fc=25 Hz), Ten Second Interval Average

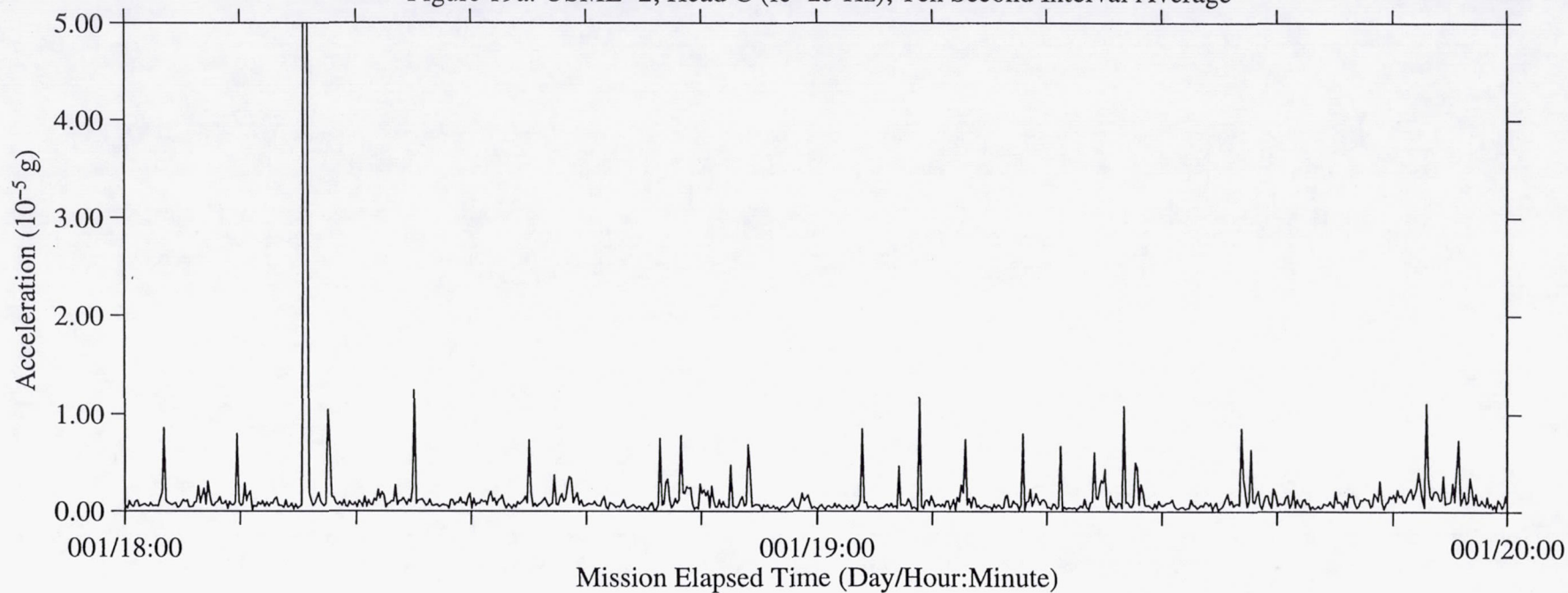


Figure 19b: USML-2, Head C (fc=25 Hz), Ten Second Interval RMS

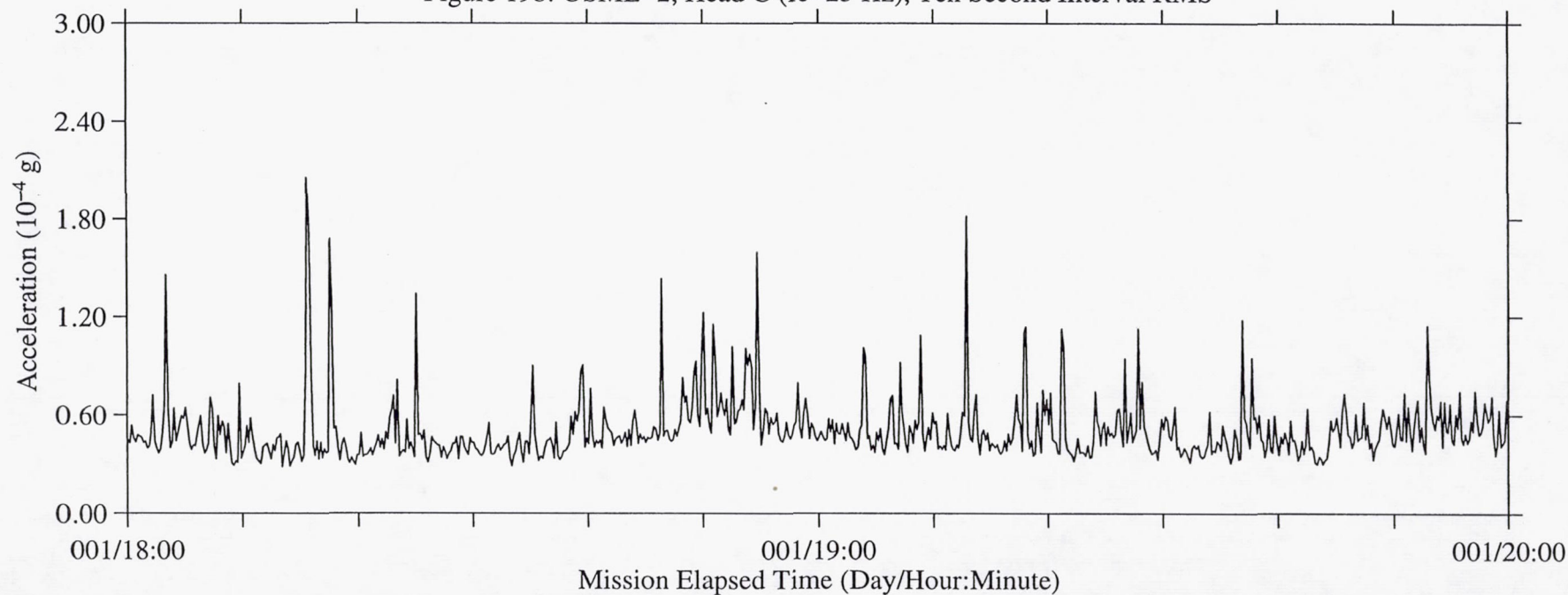


Figure 20a: USML-2, Head C (fc=25 Hz), Ten Second Interval Average

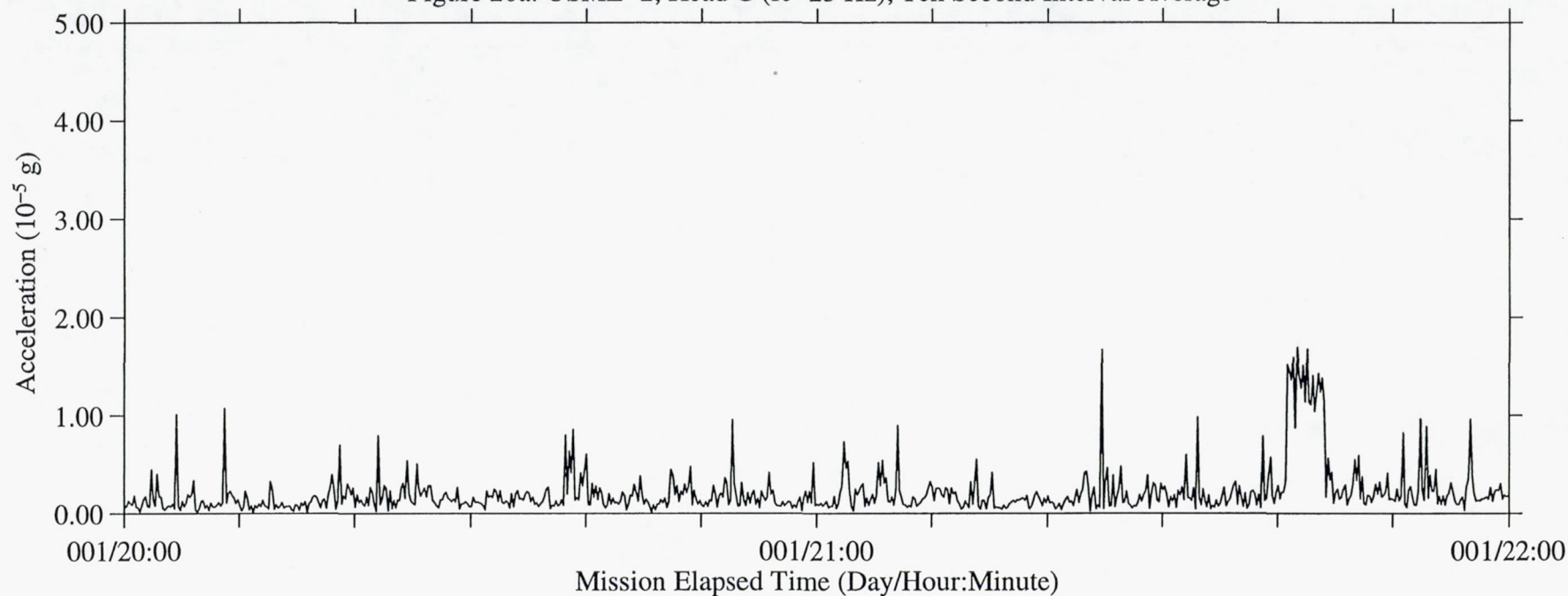


Figure 20b: USML-2, Head C (fc=25 Hz), Ten Second Interval RMS

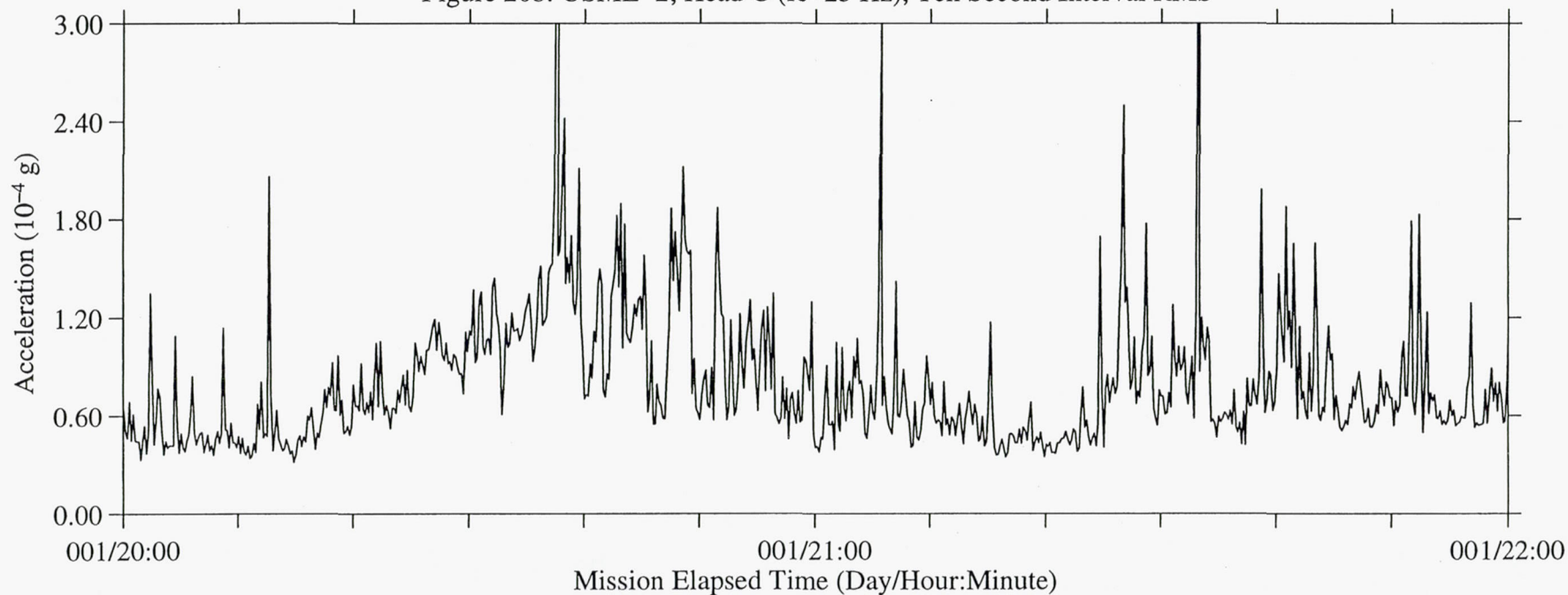




Figure 21a: USML-2, Head C (fc=25 Hz), Ten Second Interval Average

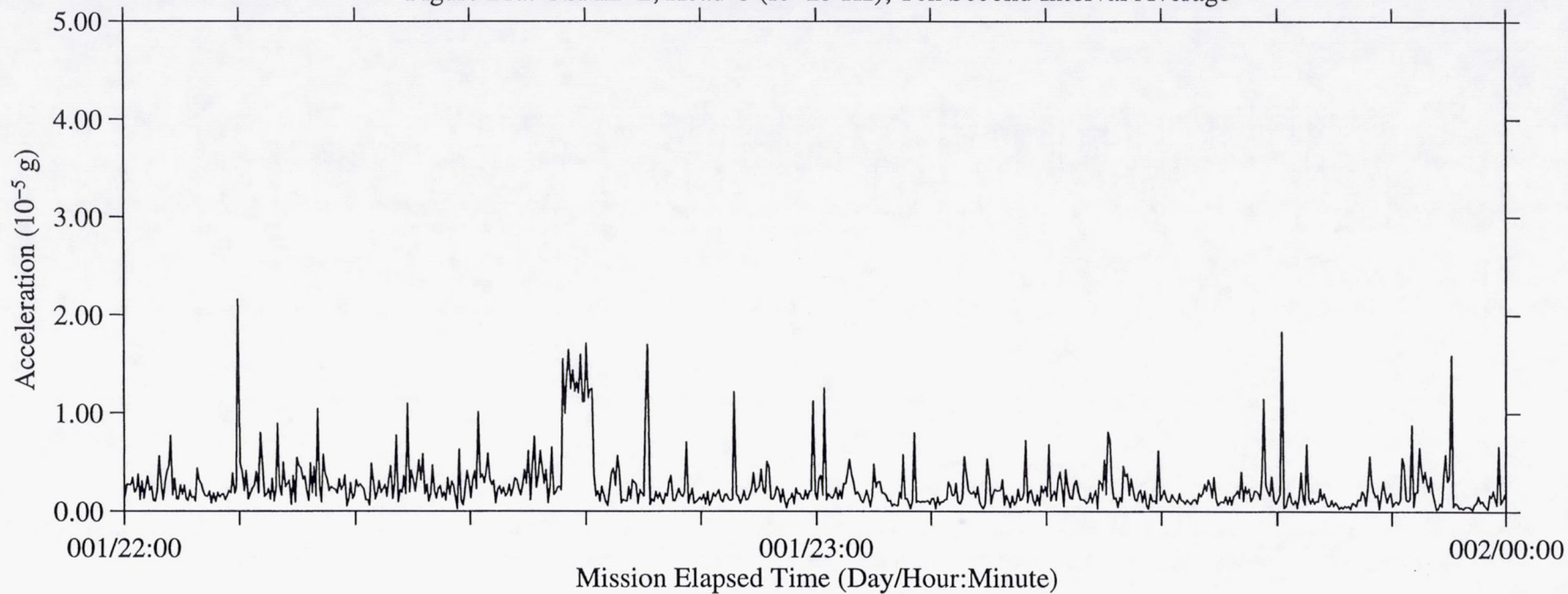


Figure 21b: USML-2, Head C (fc=25 Hz), Ten Second Interval RMS

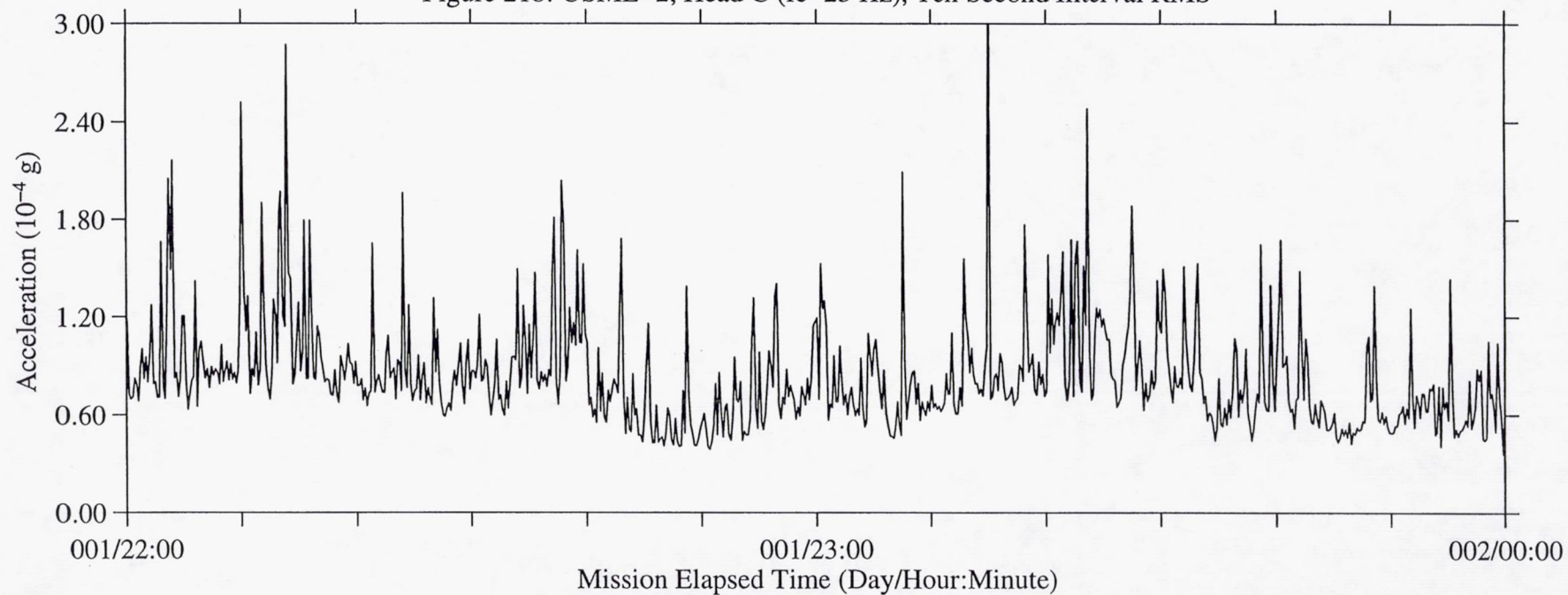


Figure 22a: USML-2, Head C (fc=25 Hz), Ten Second Interval Average

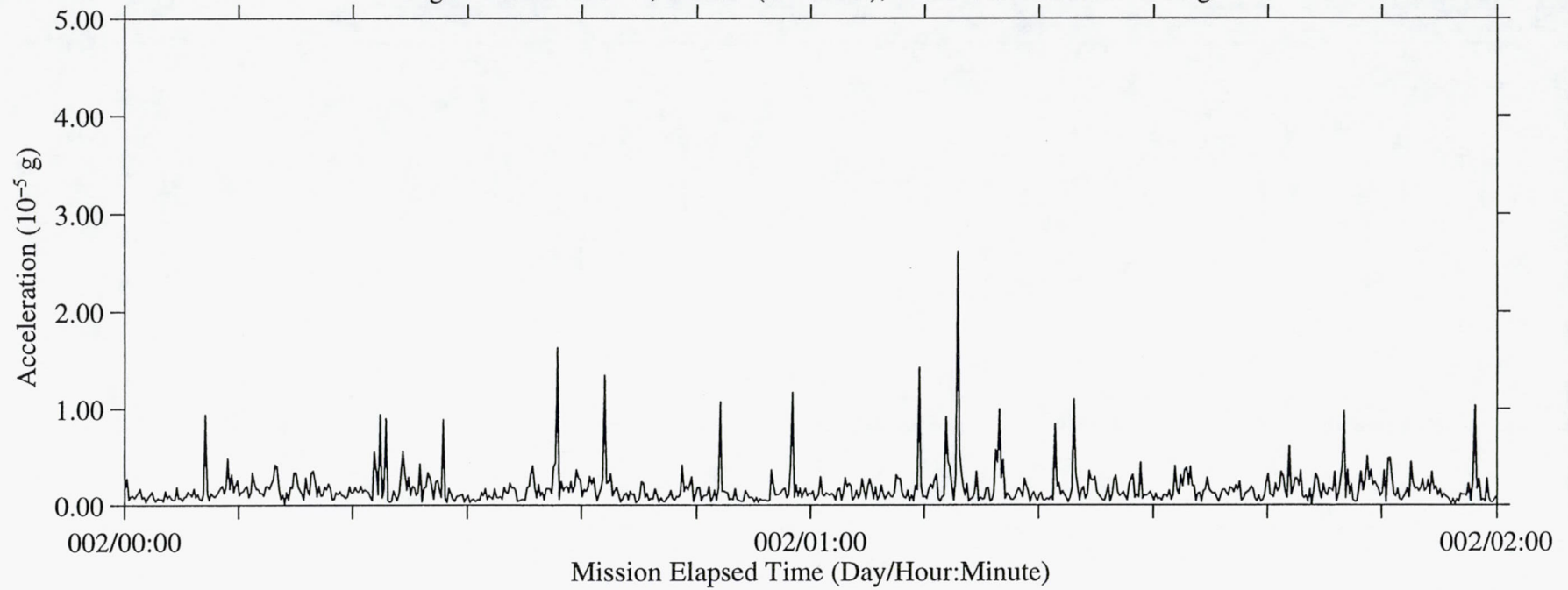


Figure 22b: USML-2, Head C (fc=25 Hz), Ten Second Interval RMS

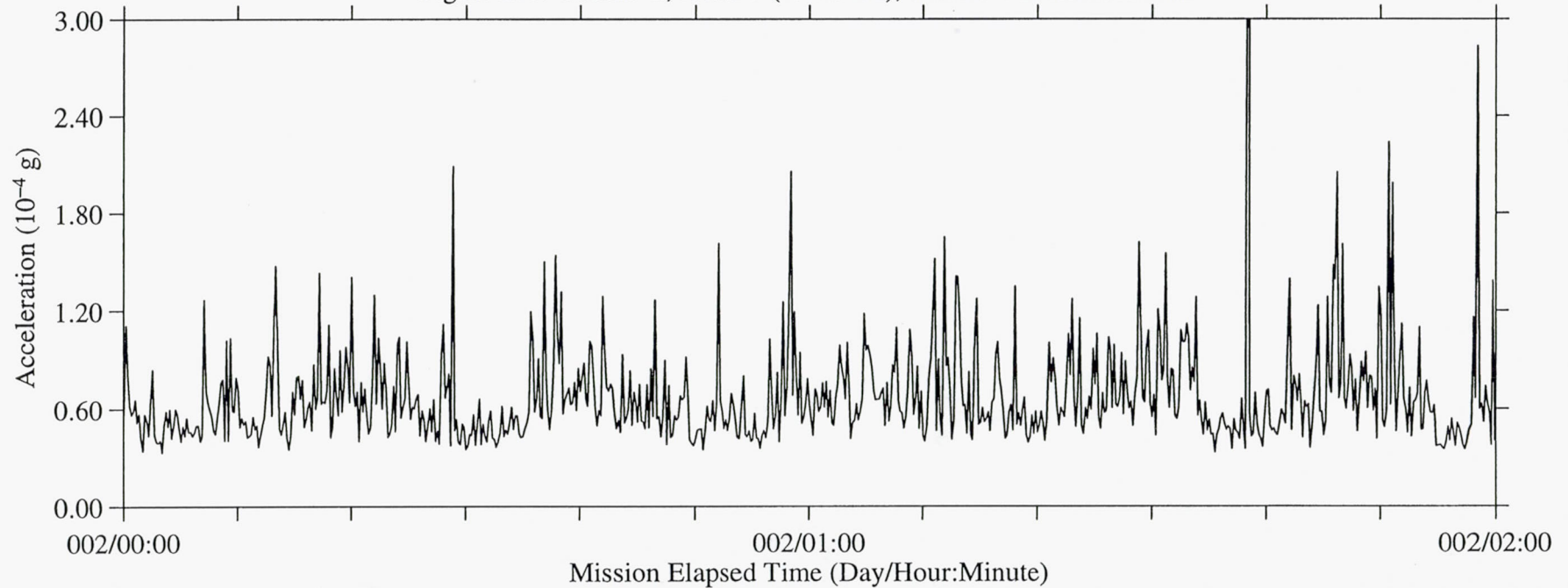




Figure 23a: USML-2, Head C (fc=25 Hz), Ten Second Interval Average

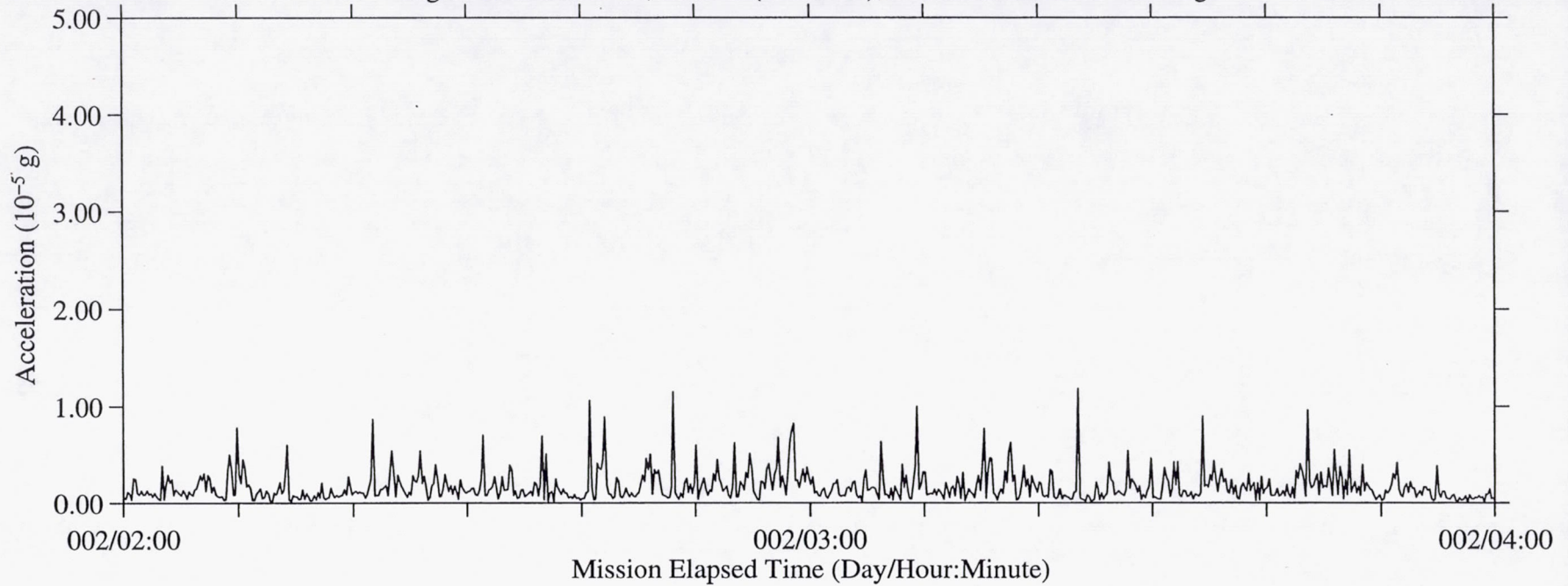


Figure 23b: USML-2, Head C (fc=25 Hz), Ten Second Interval RMS

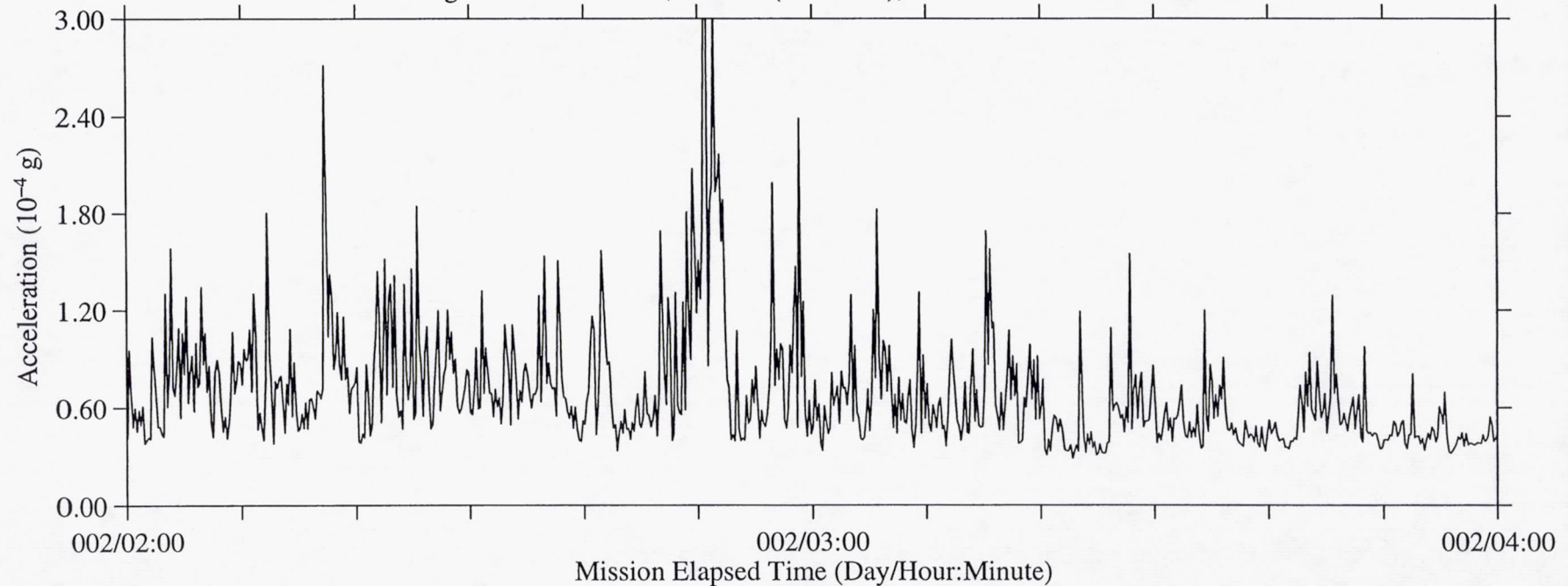


Figure 24a: USML-2, Head C (fc=25 Hz), Ten Second Interval Average

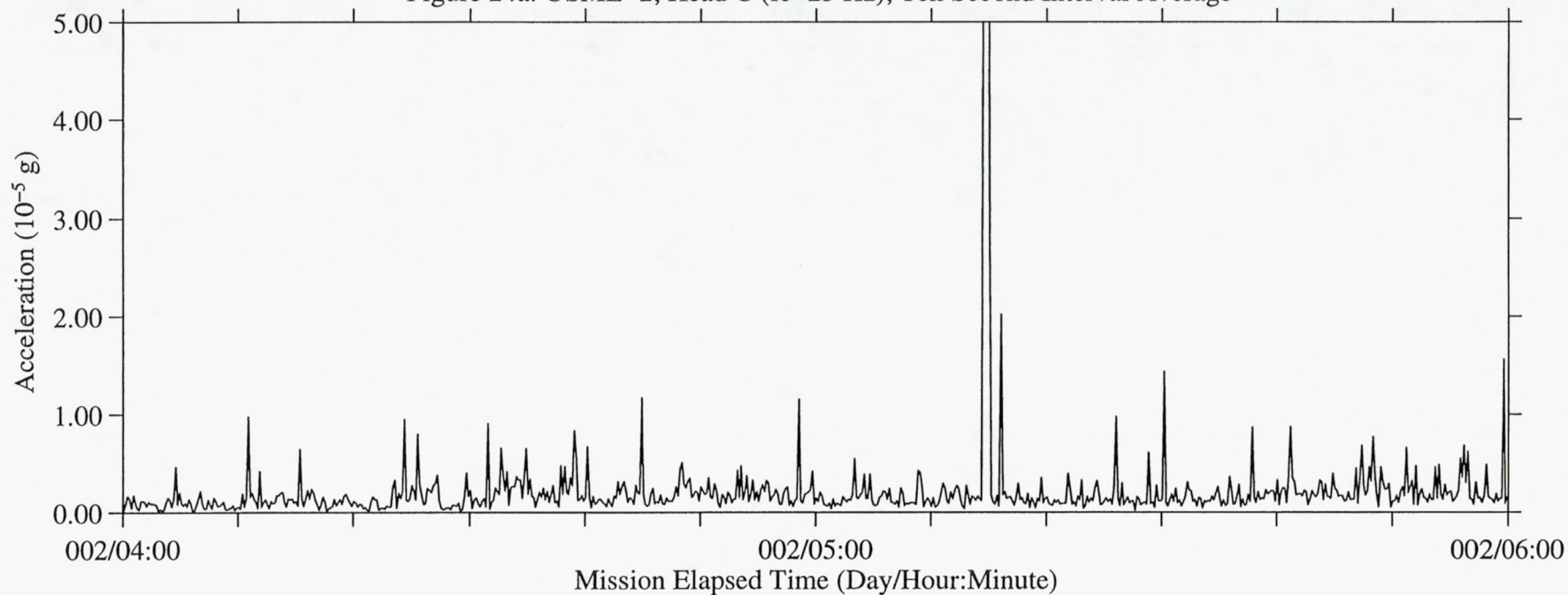


Figure 24b: USML-2, Head C (fc=25 Hz), Ten Second Interval RMS

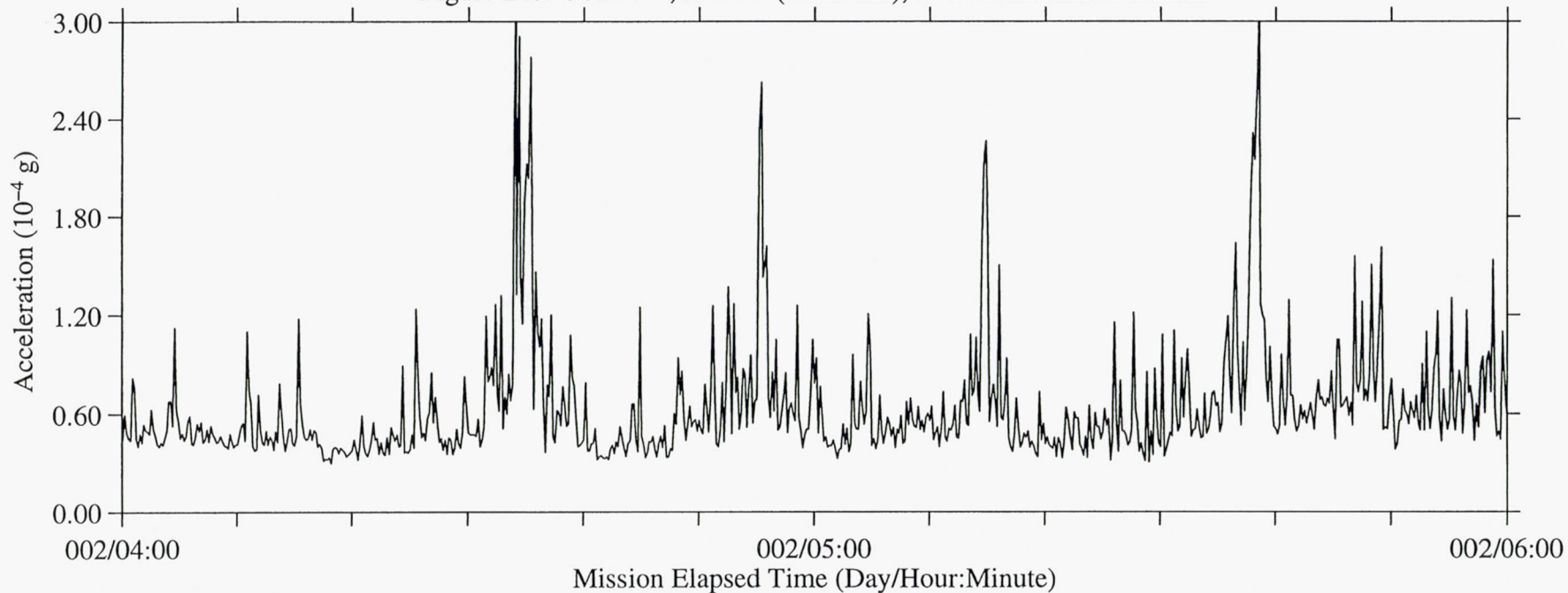




Figure 25a: USML-2, Head C (fc=25 Hz), Ten Second Interval Average

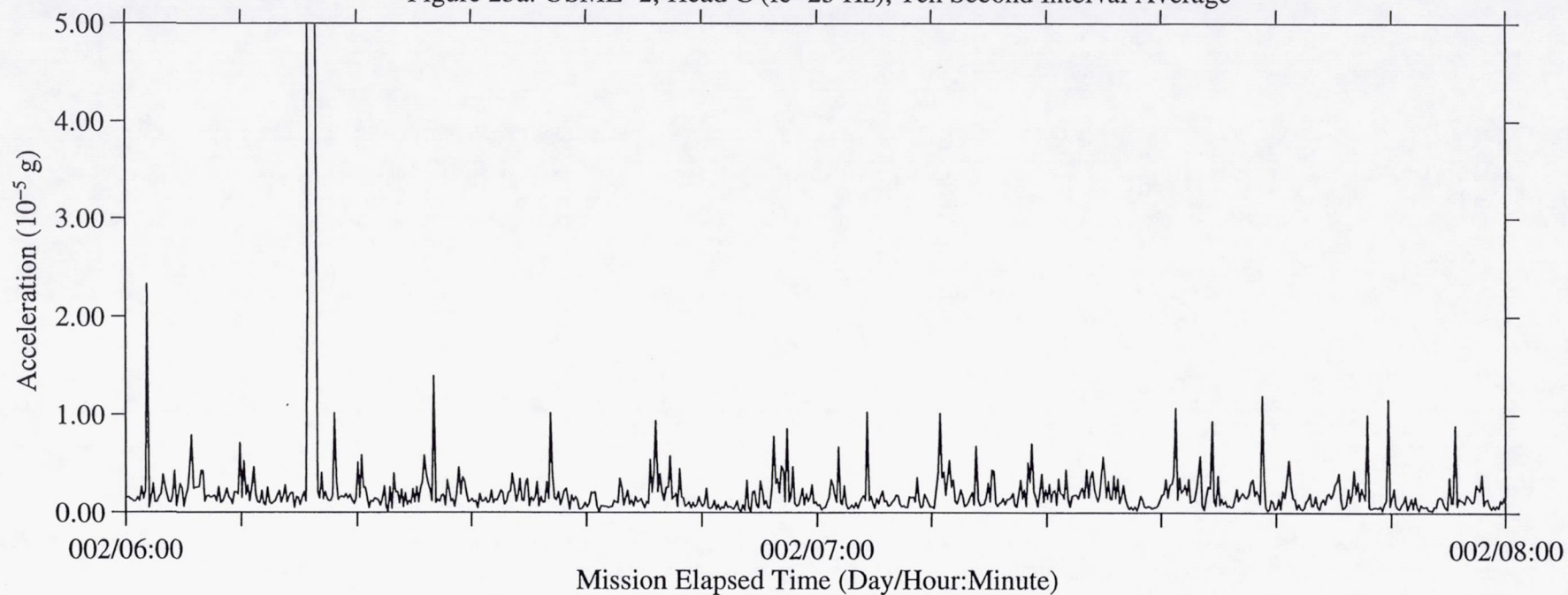


Figure 25b: USML-2, Head C (fc=25 Hz), Ten Second Interval RMS

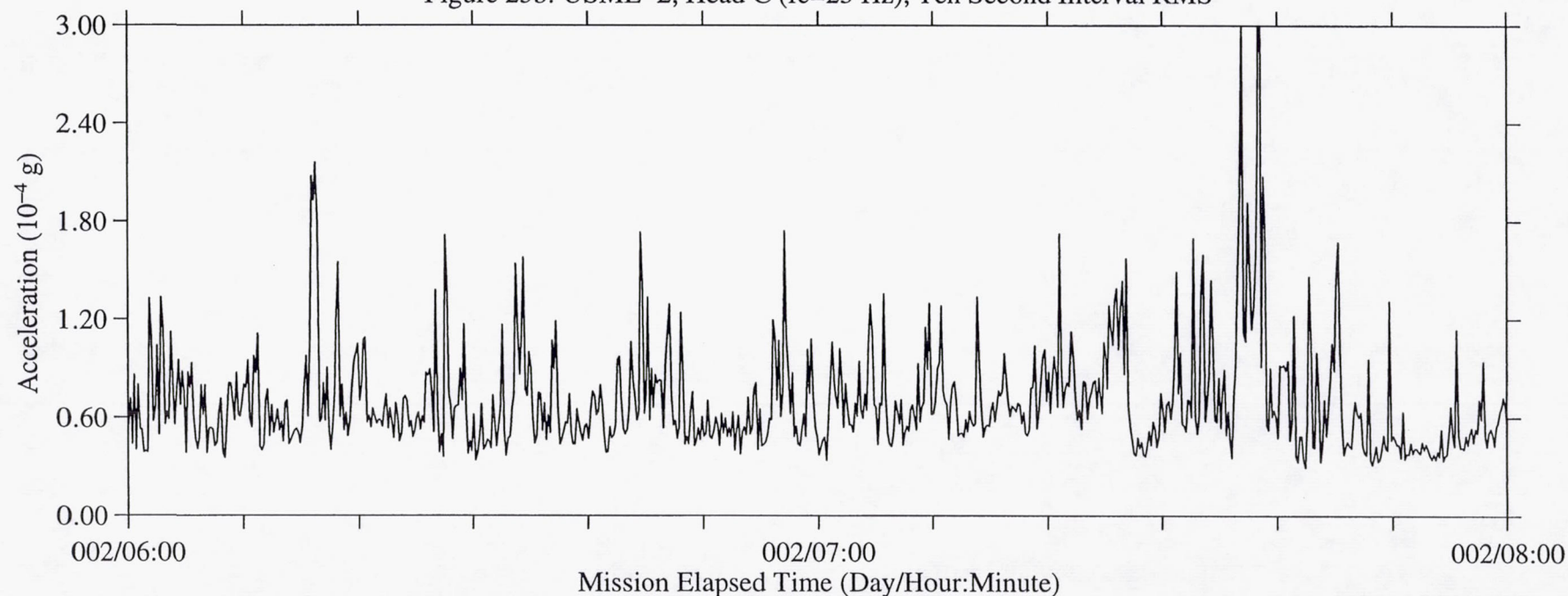


Figure 26a: USML-2, Head C (fc=25 Hz), Ten Second Interval Average

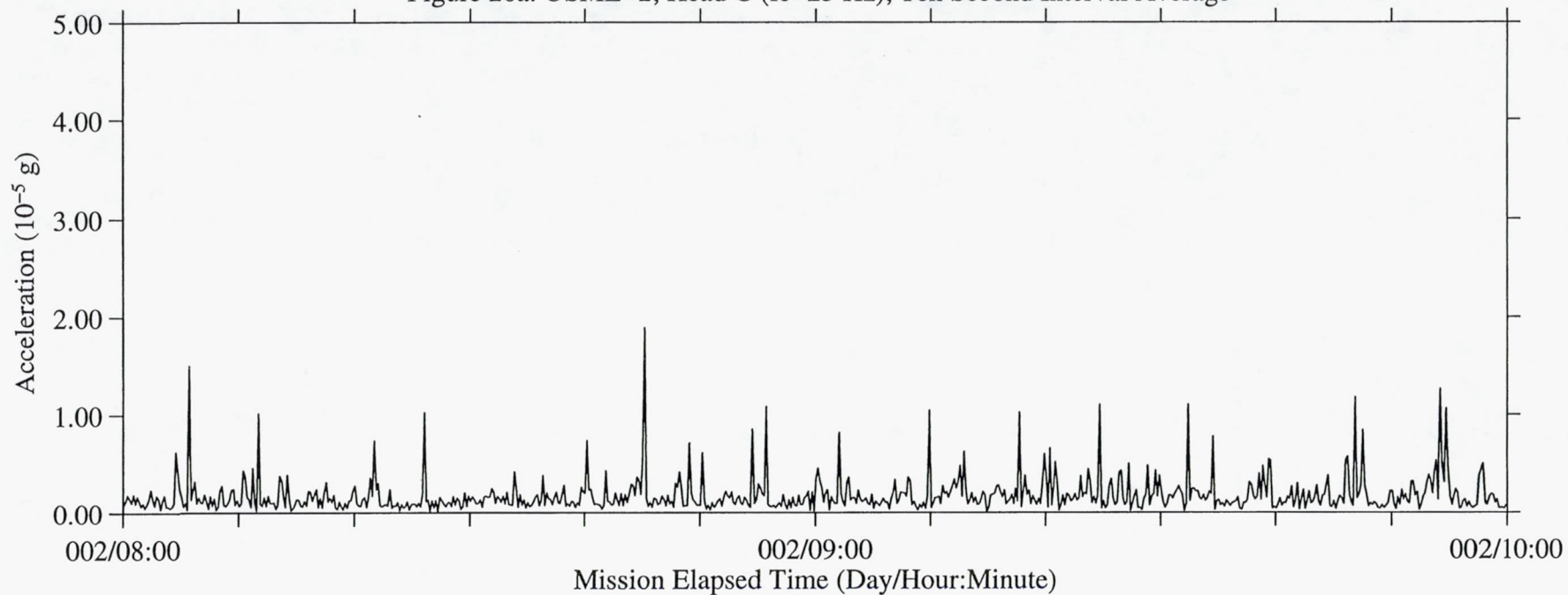


Figure 26b: USML-2, Head C (fc=25 Hz), Ten Second Interval RMS

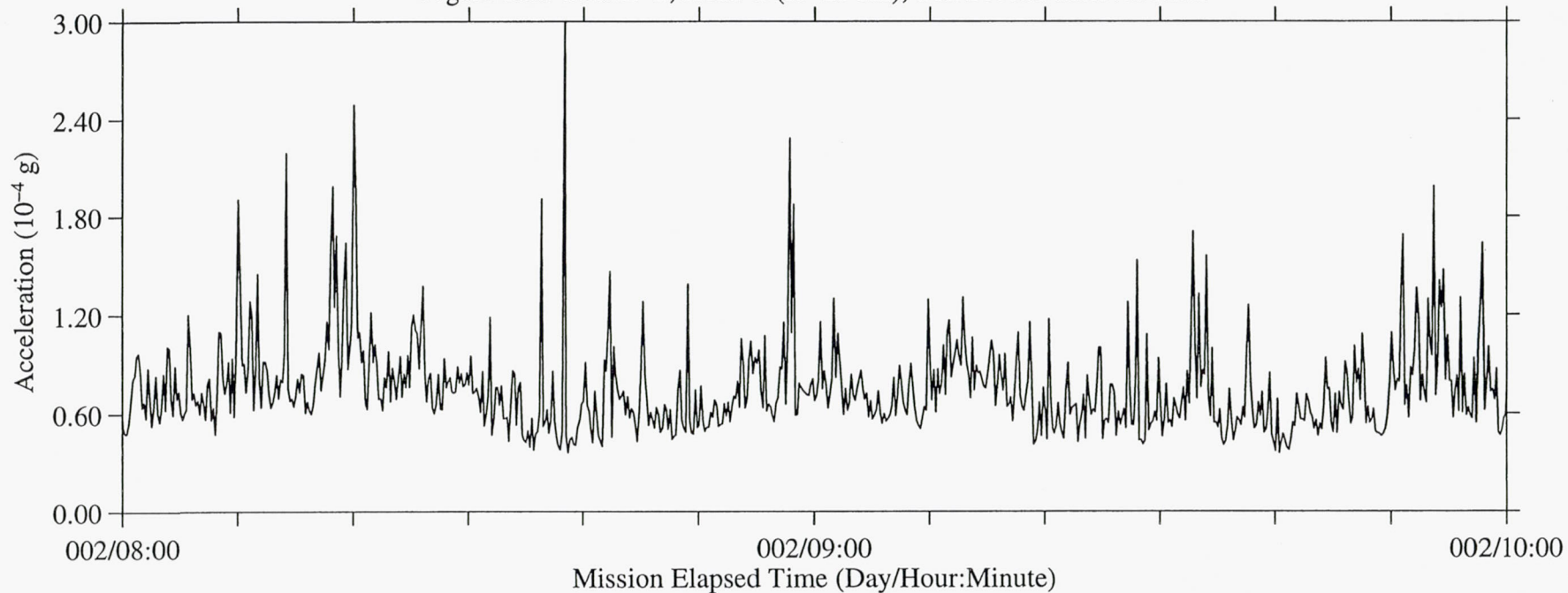




Figure 27a: USML-2, Head C (fc=25 Hz), Ten Second Interval Average

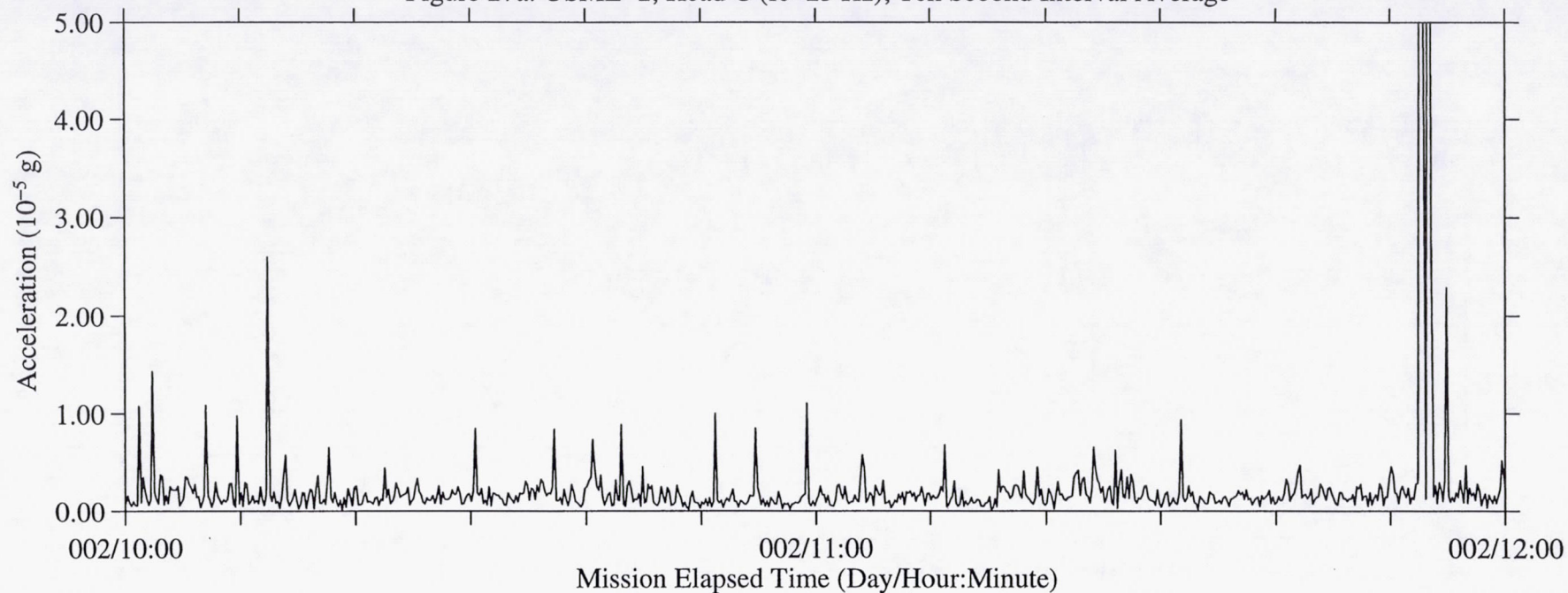
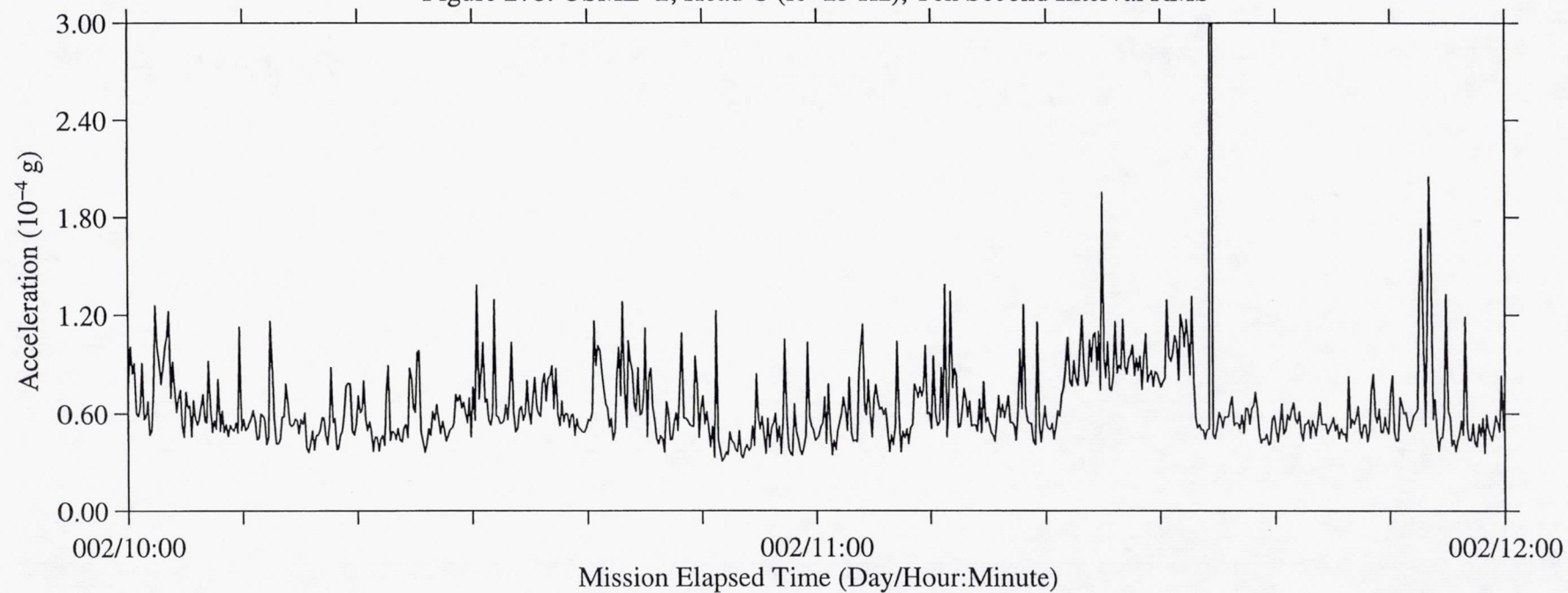


Figure 27b: USML-2, Head C (fc=25 Hz), Ten Second Interval RMS



B-30

Figure 28a: USML-2, Head C (fc=25 Hz), Ten Second Interval Average

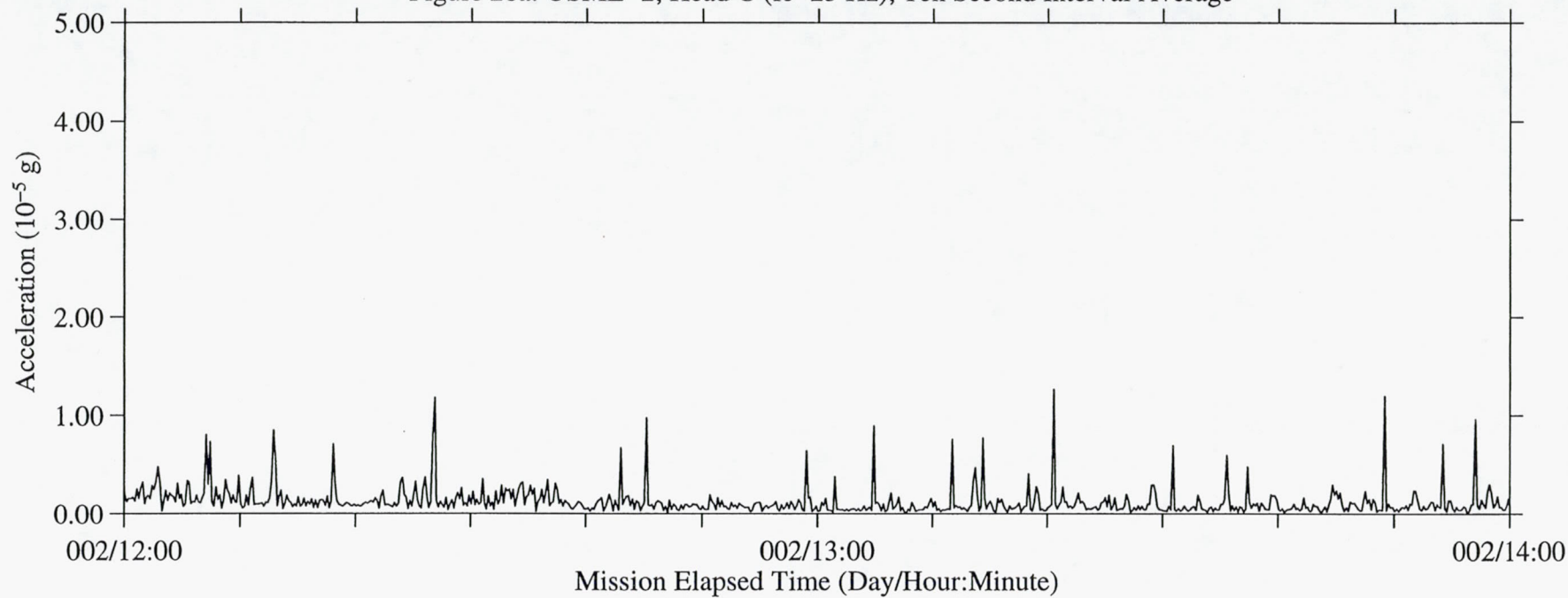


Figure 28b: USML-2, Head C (fc=25 Hz), Ten Second Interval RMS

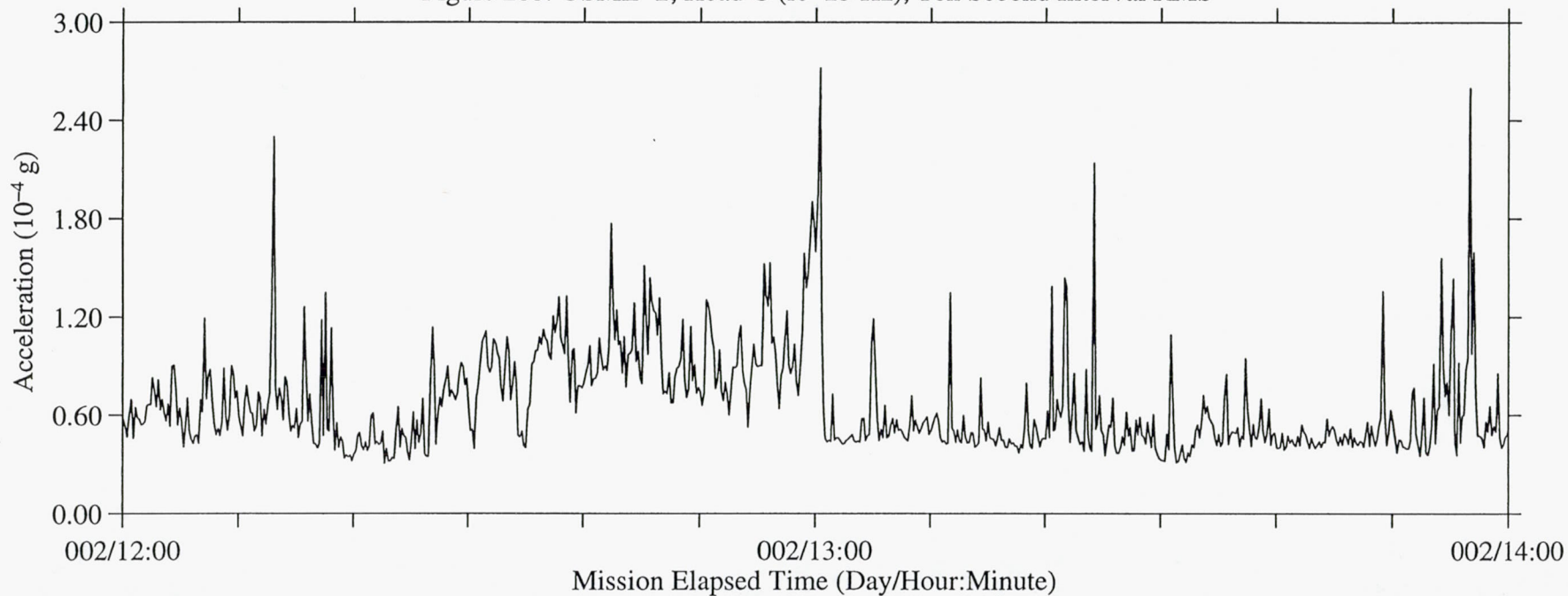




Figure 29a: USML-2, Head C (fc=25 Hz), Ten Second Interval Average

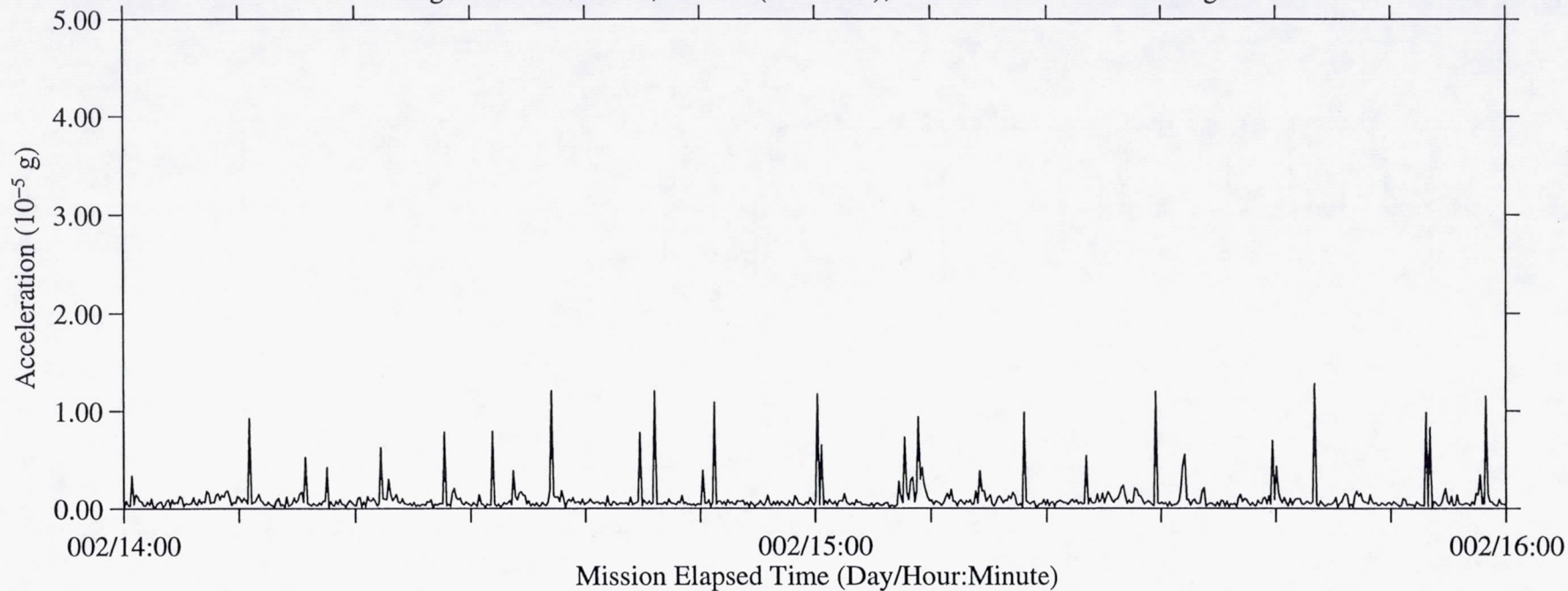


Figure 29b: USML-2, Head C (fc=25 Hz), Ten Second Interval RMS

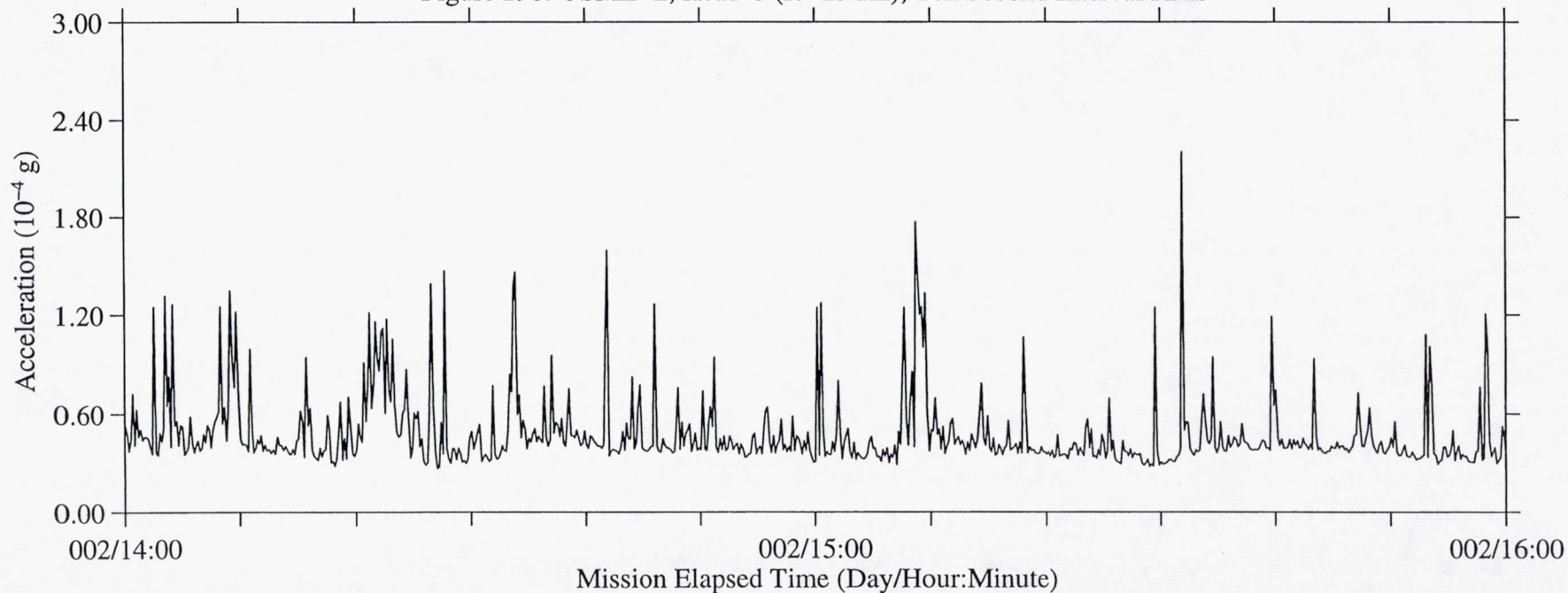


Figure 30a: USML-2, Head C (fc=25 Hz), Ten Second Interval Average

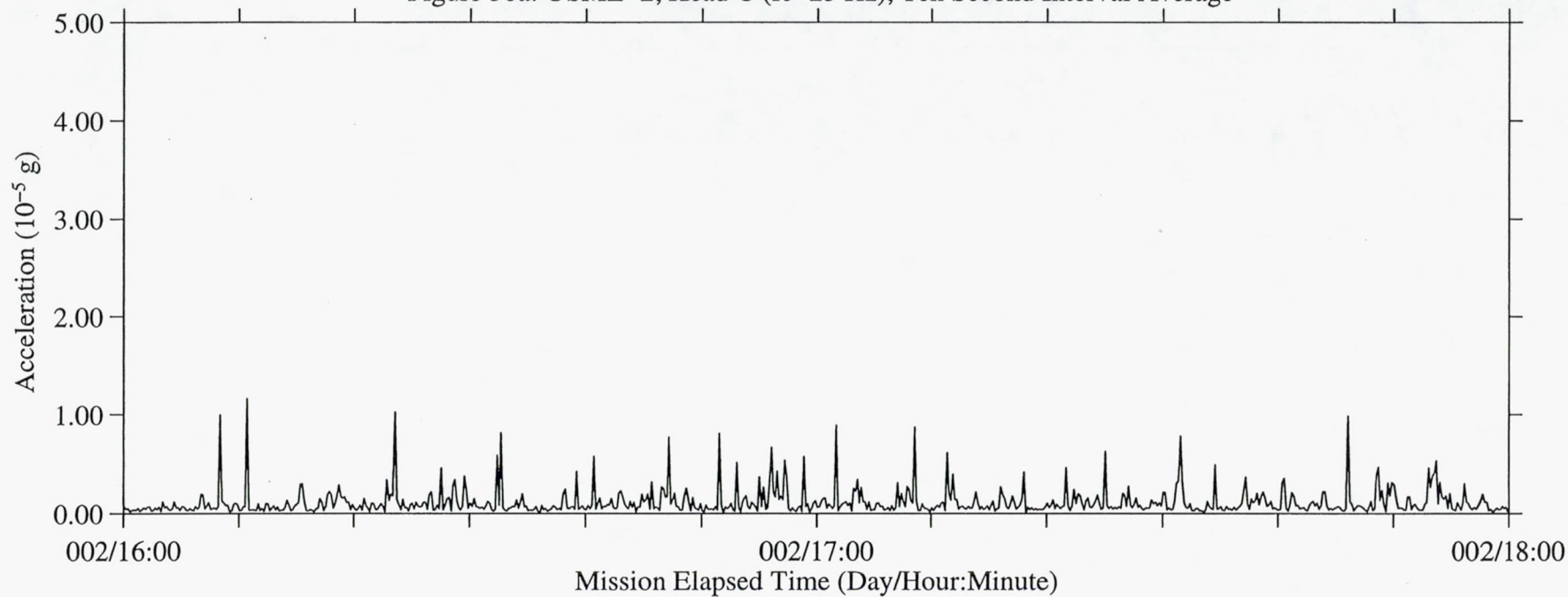


Figure 30b: USML-2, Head C (fc=25 Hz), Ten Second Interval RMS

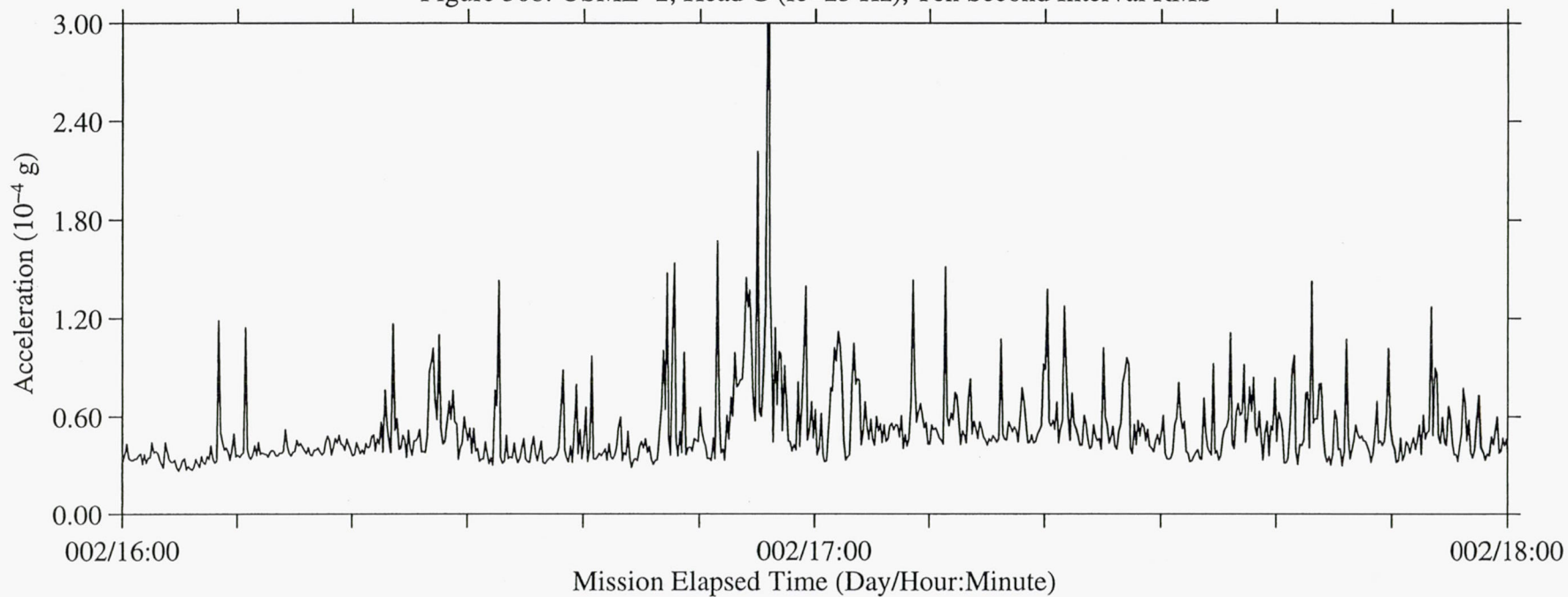




Figure 31a: USML-2, Head C (fc=25 Hz), Ten Second Interval Average

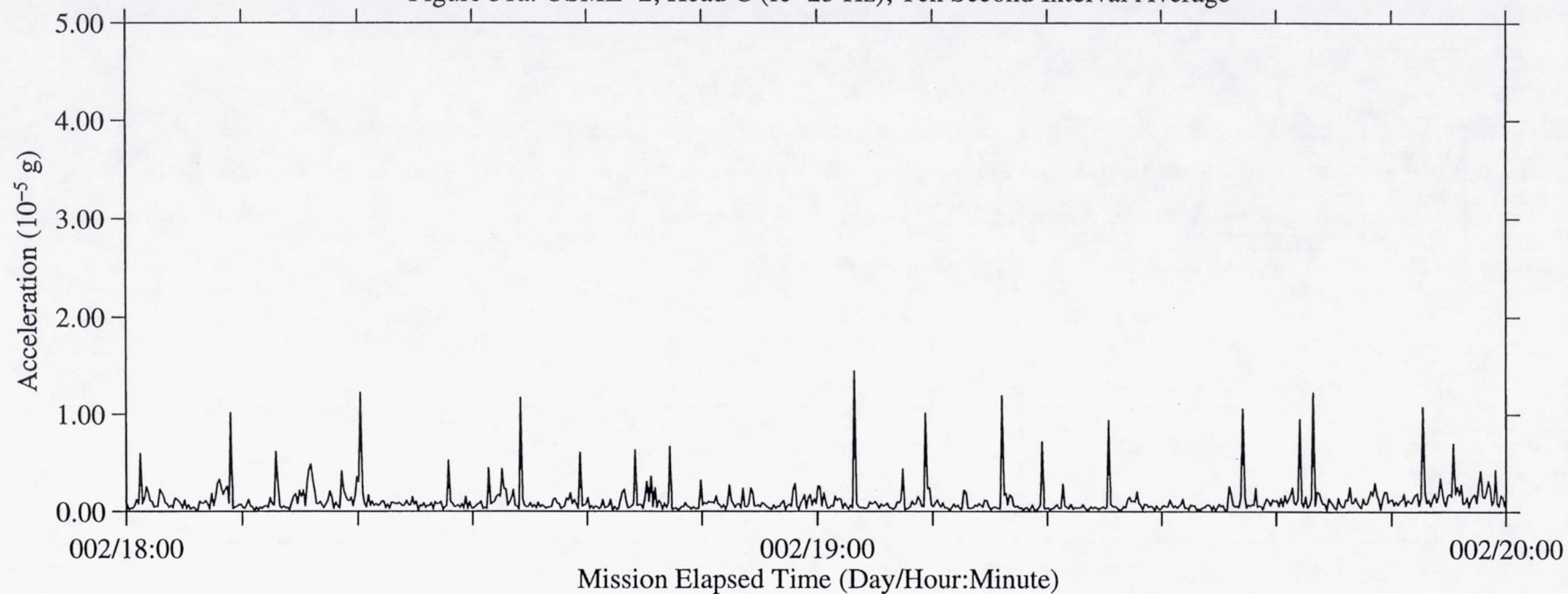


Figure 31b: USML-2, Head C (fc=25 Hz), Ten Second Interval RMS

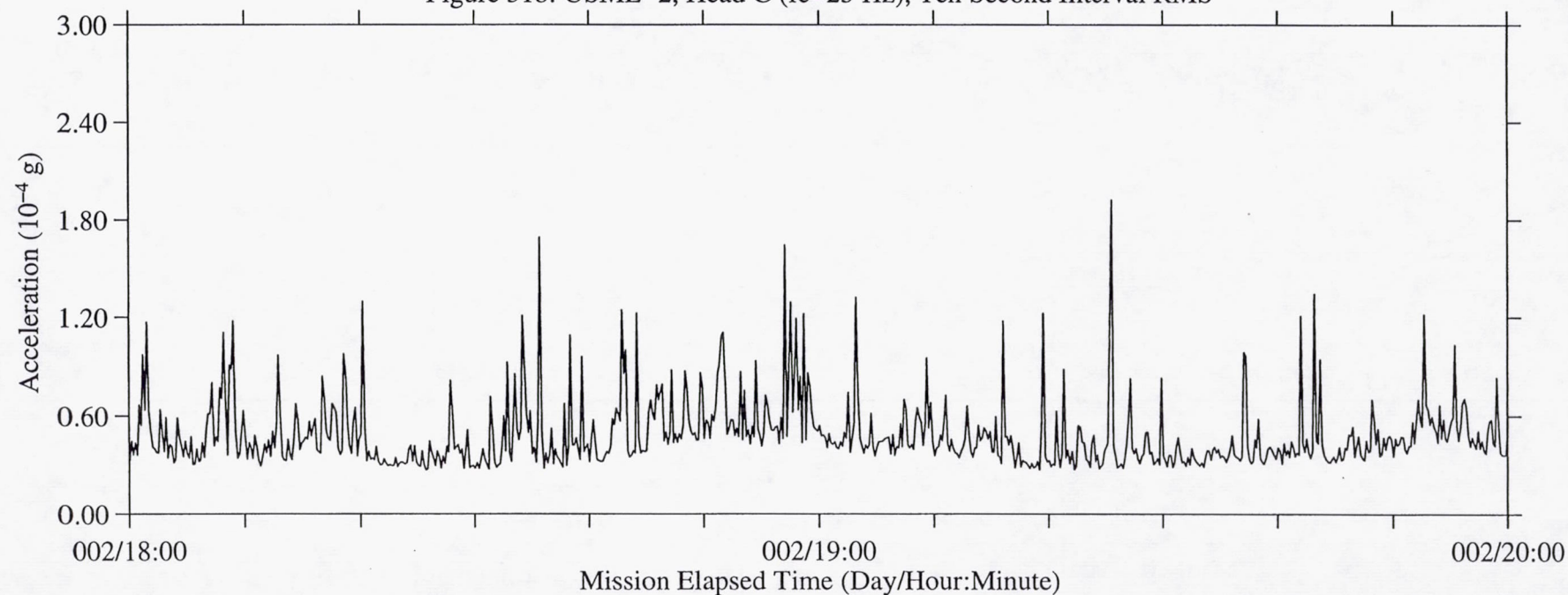


Figure 32a: USML-2, Head C (fc=25 Hz), Ten Second Interval Average

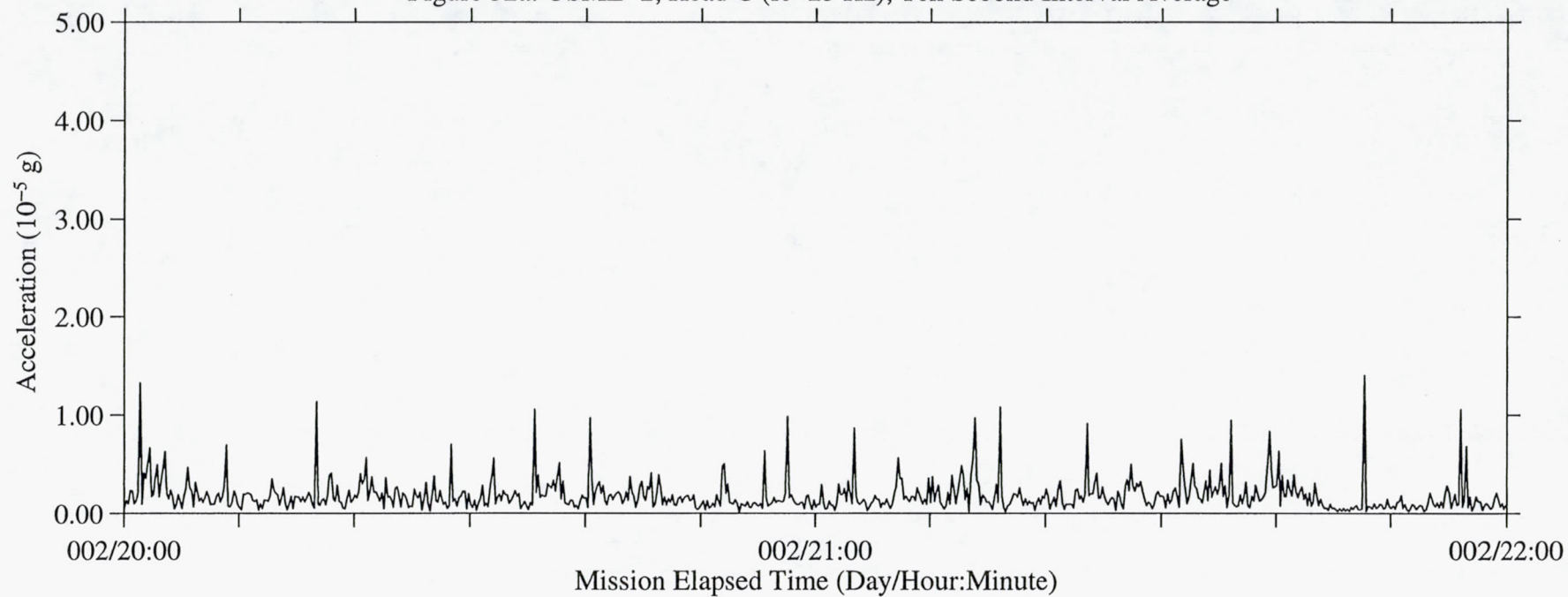


Figure 32b: USML-2, Head C (fc=25 Hz), Ten Second Interval RMS

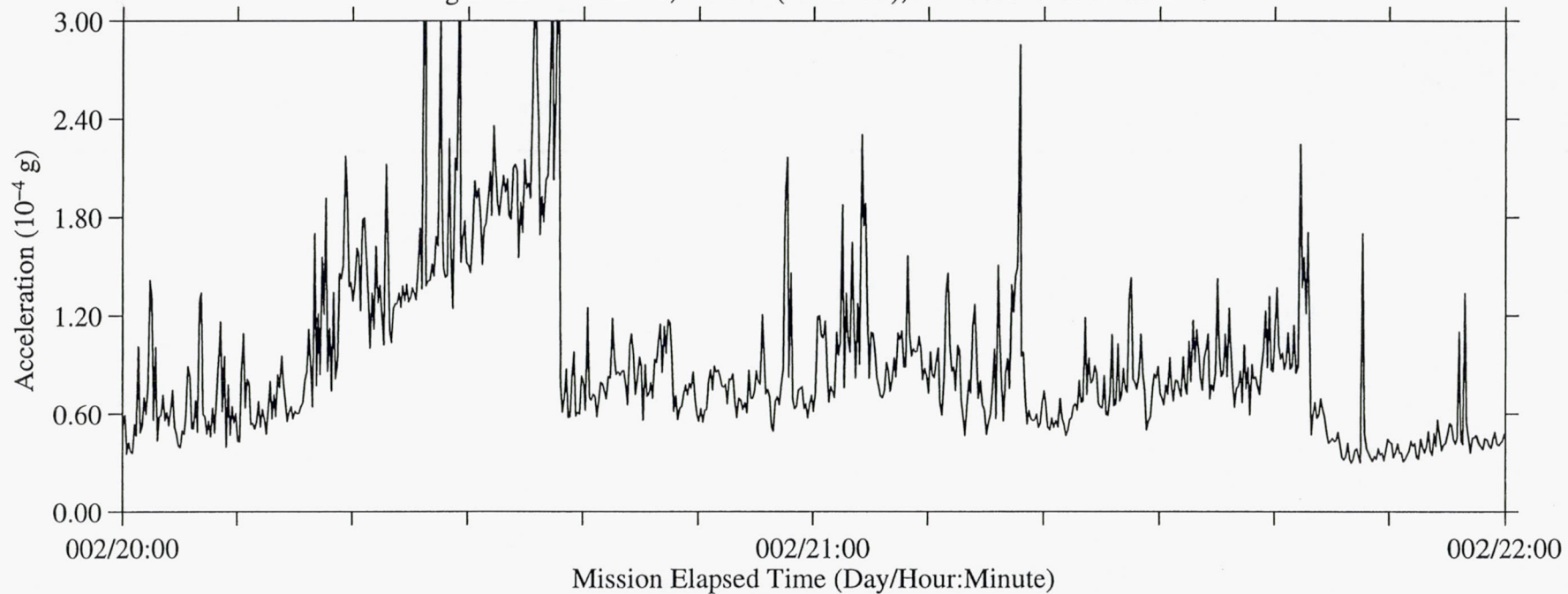




Figure 33a: USML-2, Head C (fc=25 Hz), Ten Second Interval Average

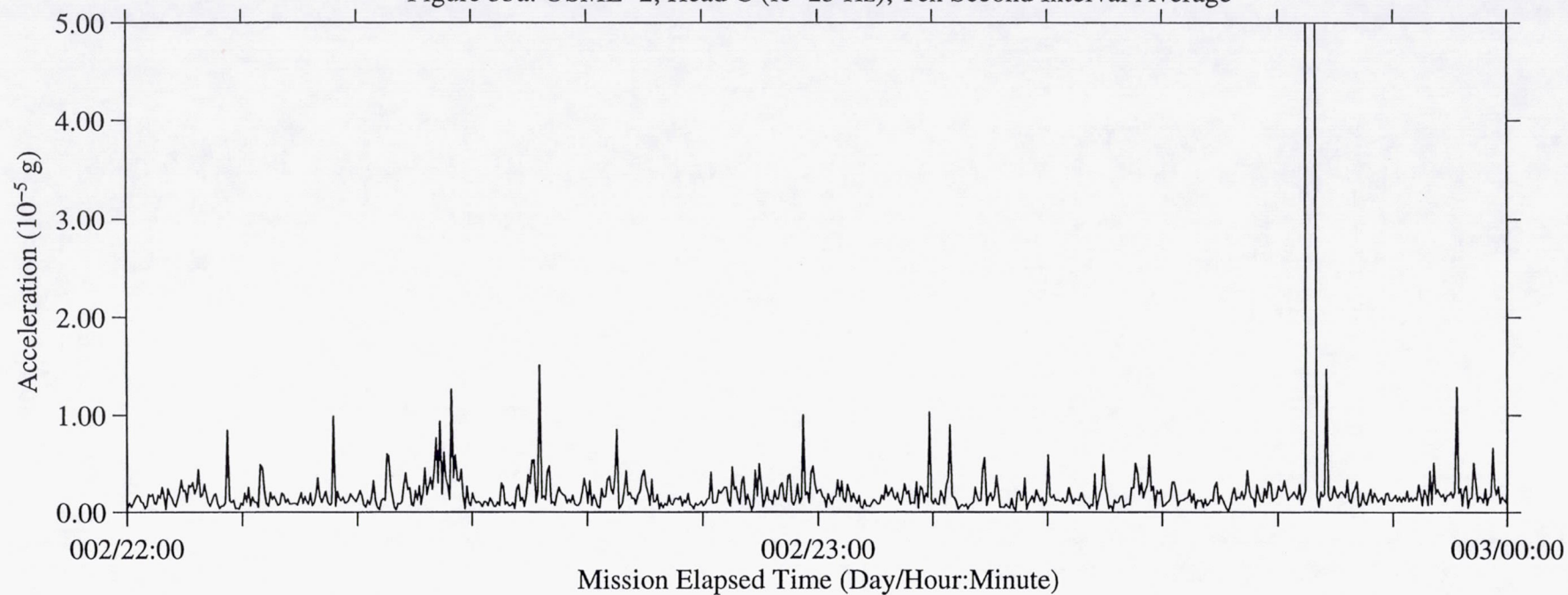


Figure 33b: USML-2, Head C (fc=25 Hz), Ten Second Interval RMS

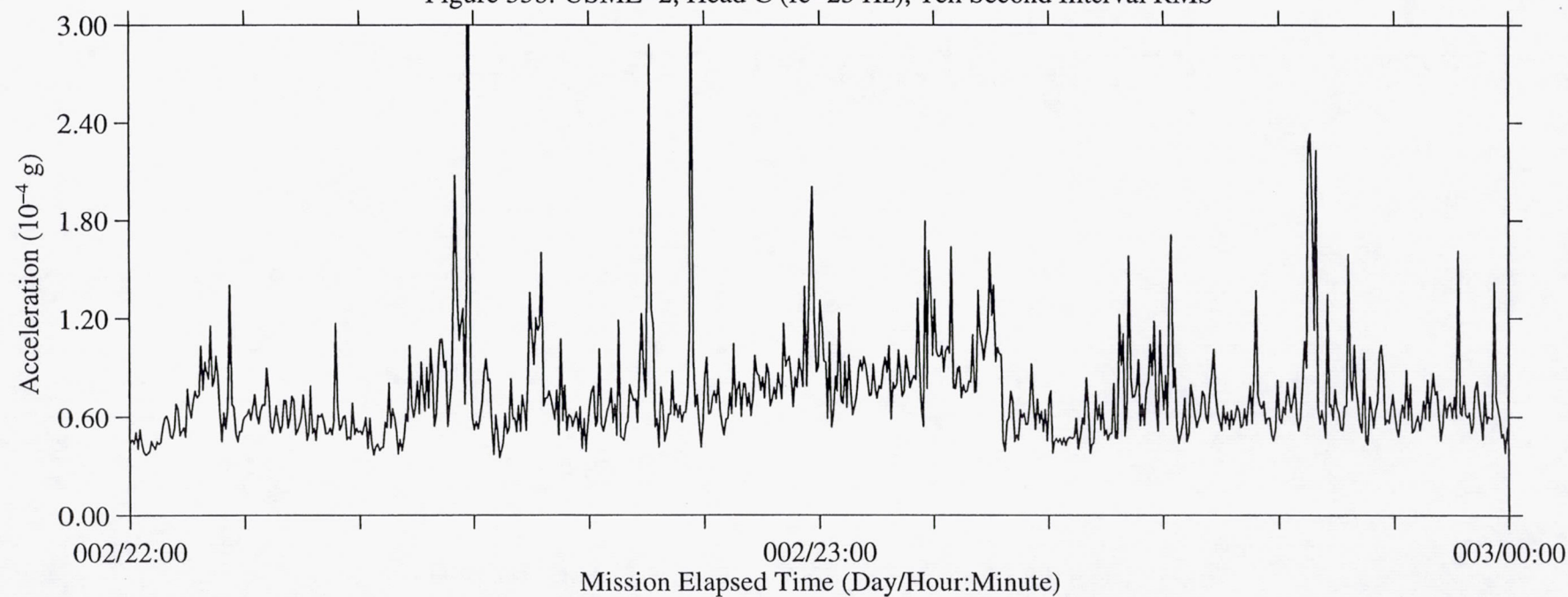


Figure 34a: USML-2, Head C (fc=25 Hz), Ten Second Interval Average

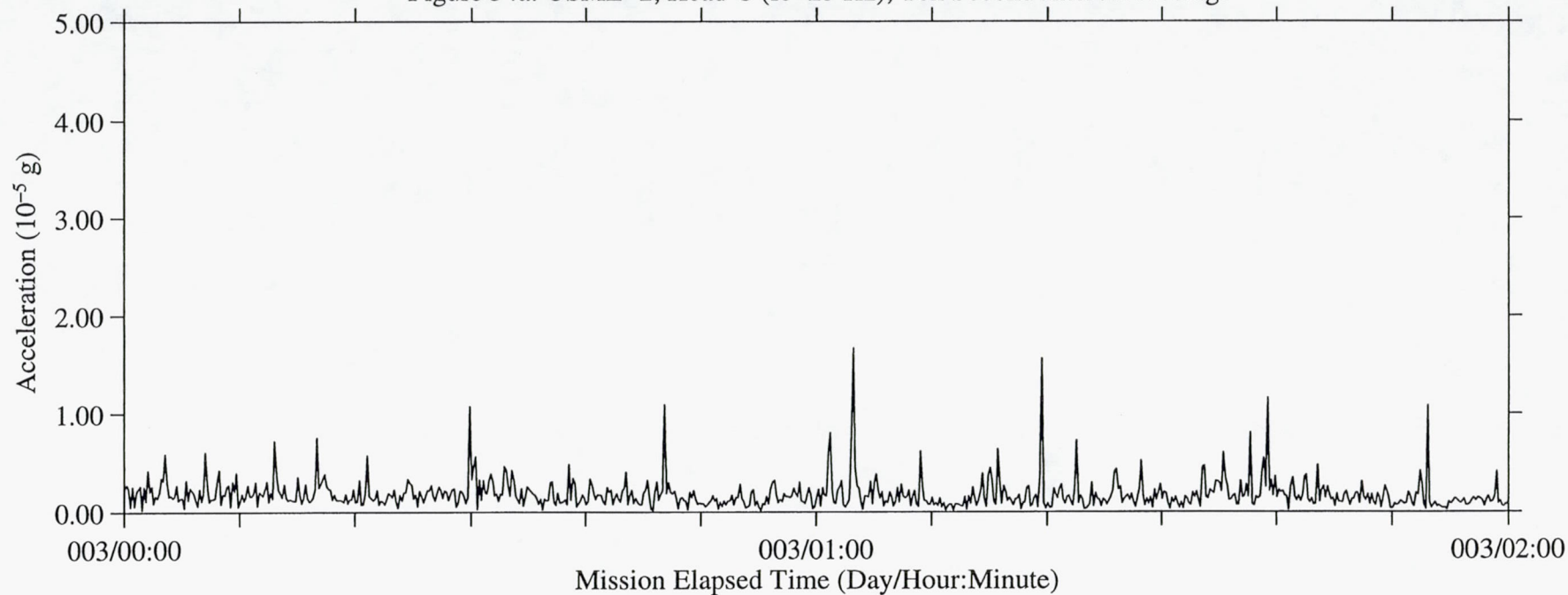


Figure 34b: USML-2, Head C (fc=25 Hz), Ten Second Interval RMS

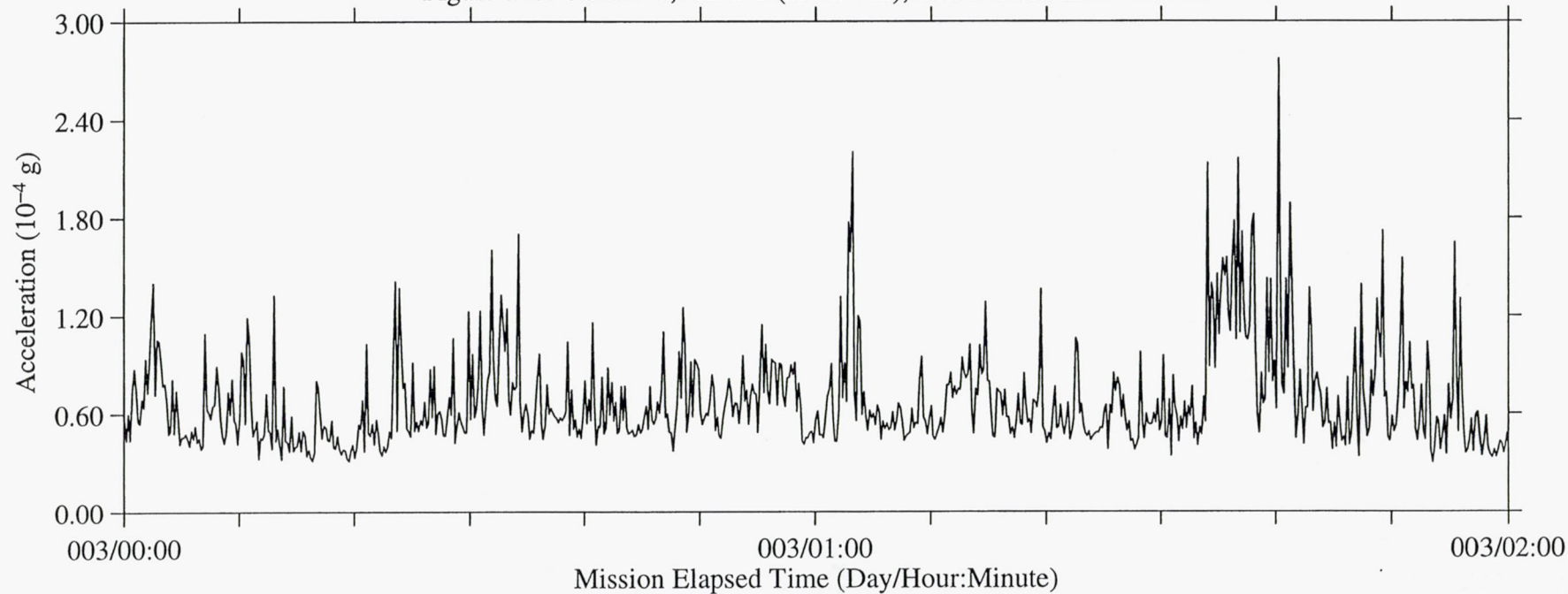




Figure 35a: USML-2, Head C (fc=25 Hz), Ten Second Interval Average

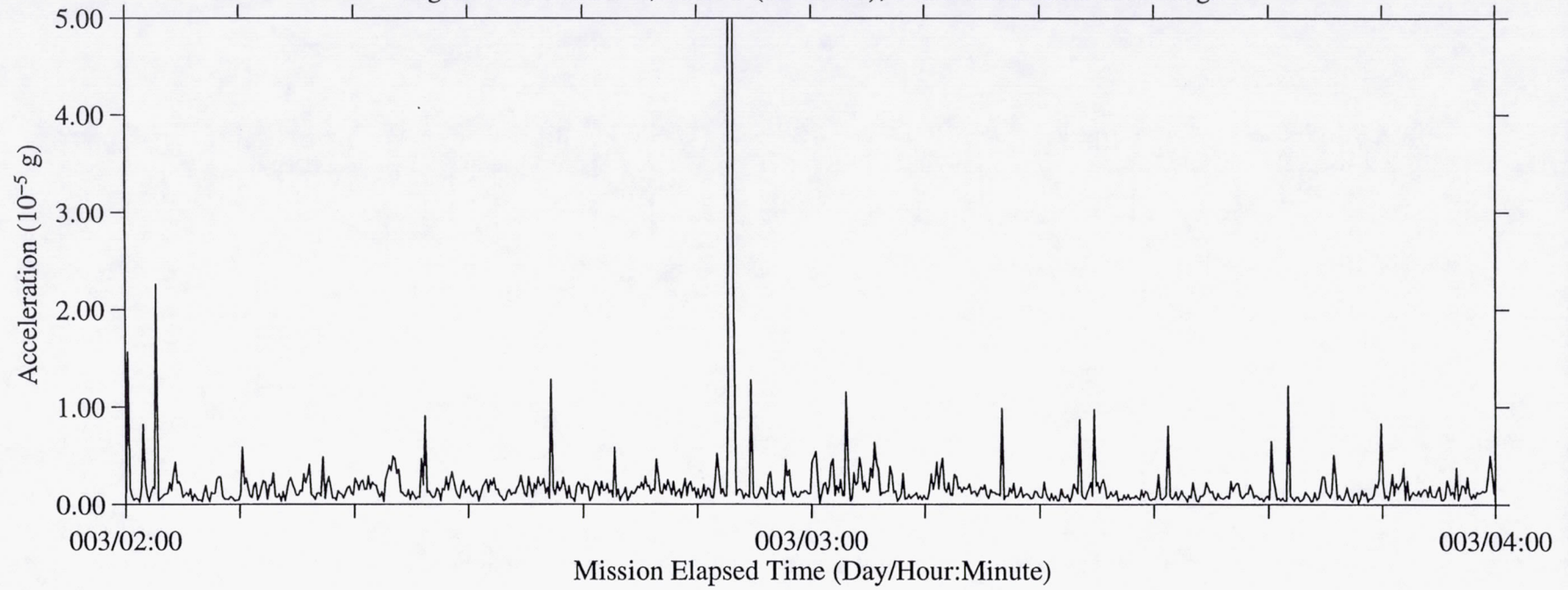


Figure 35b: USML-2, Head C (fc=25 Hz), Ten Second Interval RMS

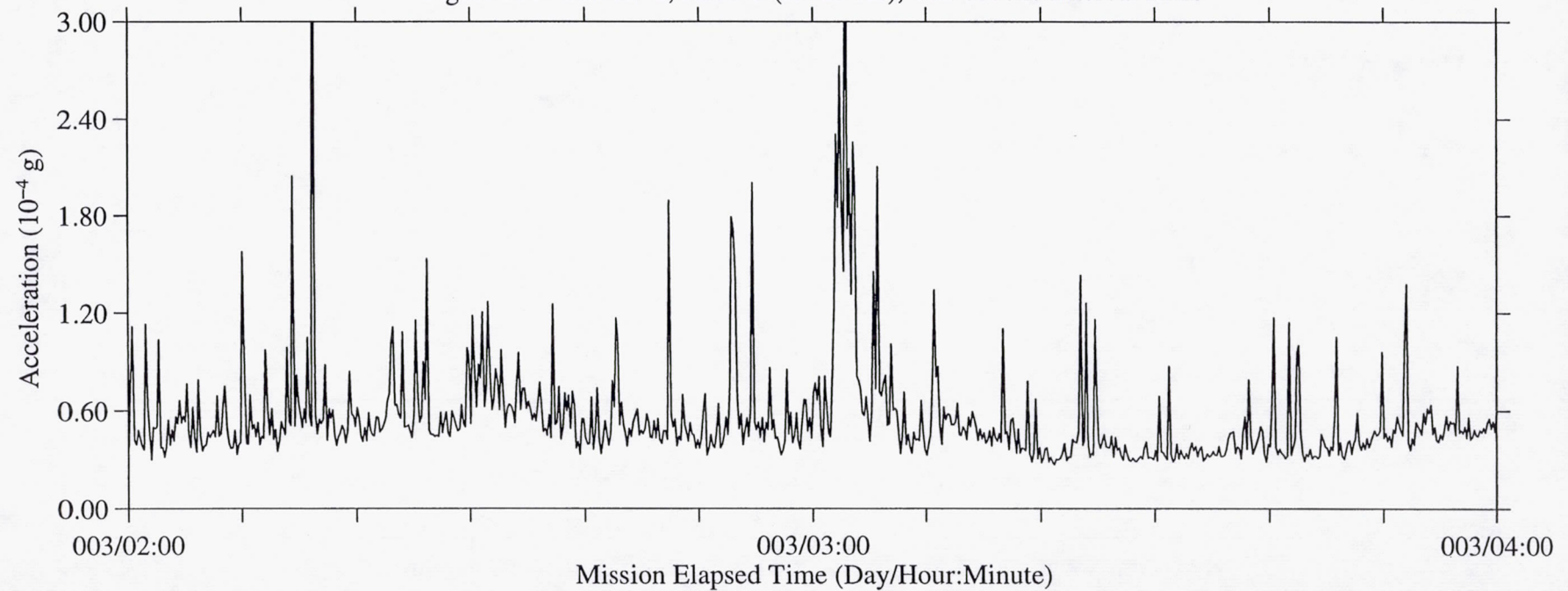


Figure 36a: USML-2, Head C (fc=25 Hz), Ten Second Interval Average

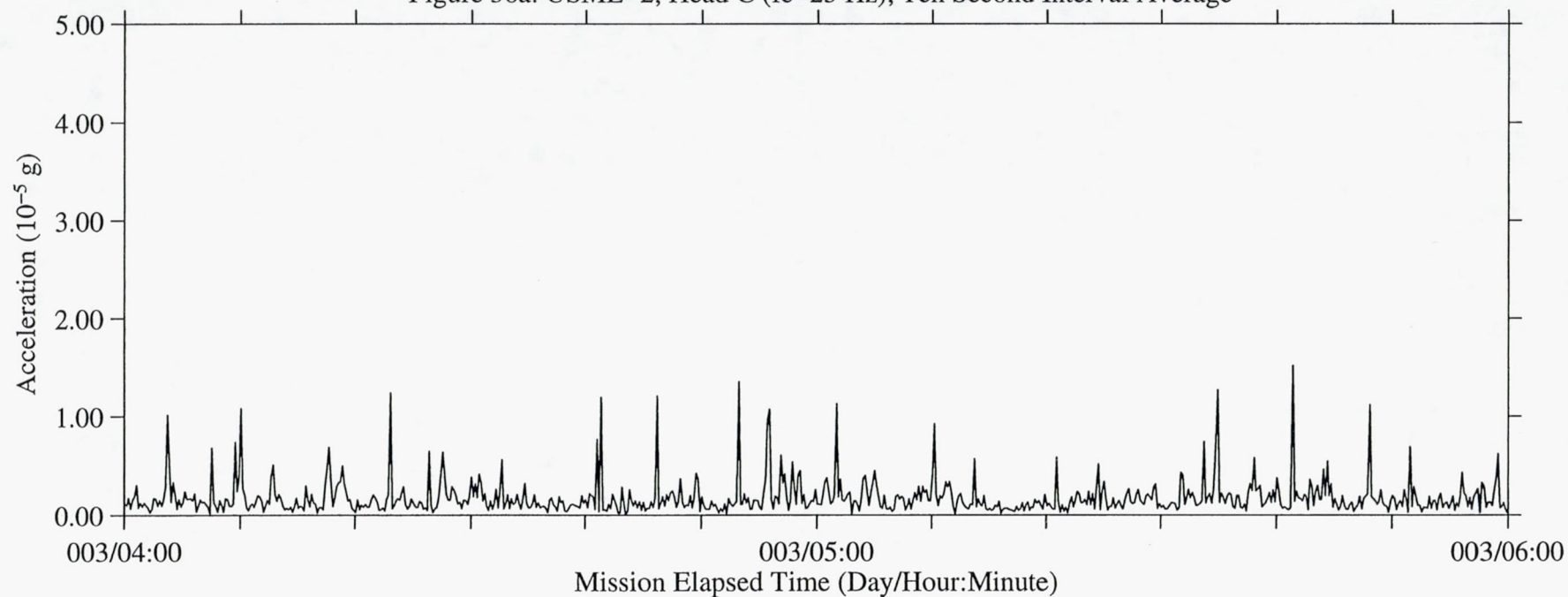


Figure 36b: USML-2, Head C (fc=25 Hz), Ten Second Interval RMS

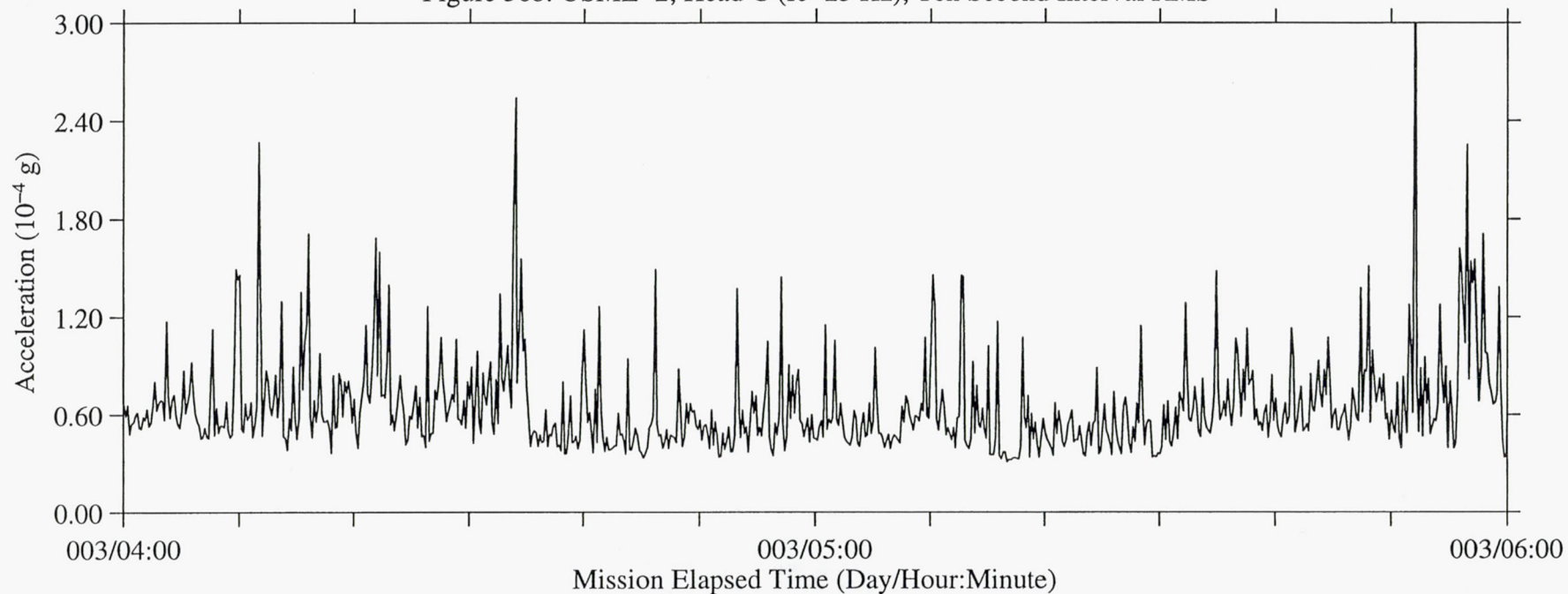




Figure 37a: USML-2, Head C (fc=25 Hz), Ten Second Interval Average

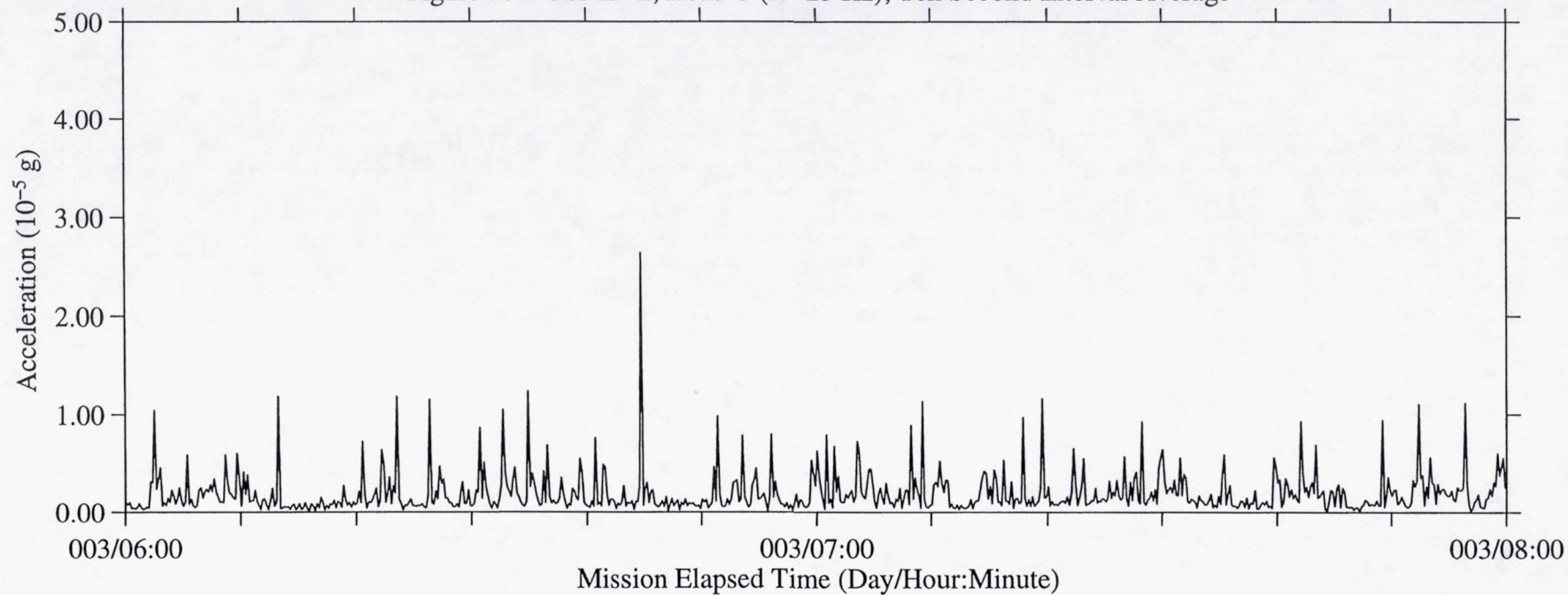


Figure 37b: USML-2, Head C (fc=25 Hz), Ten Second Interval RMS

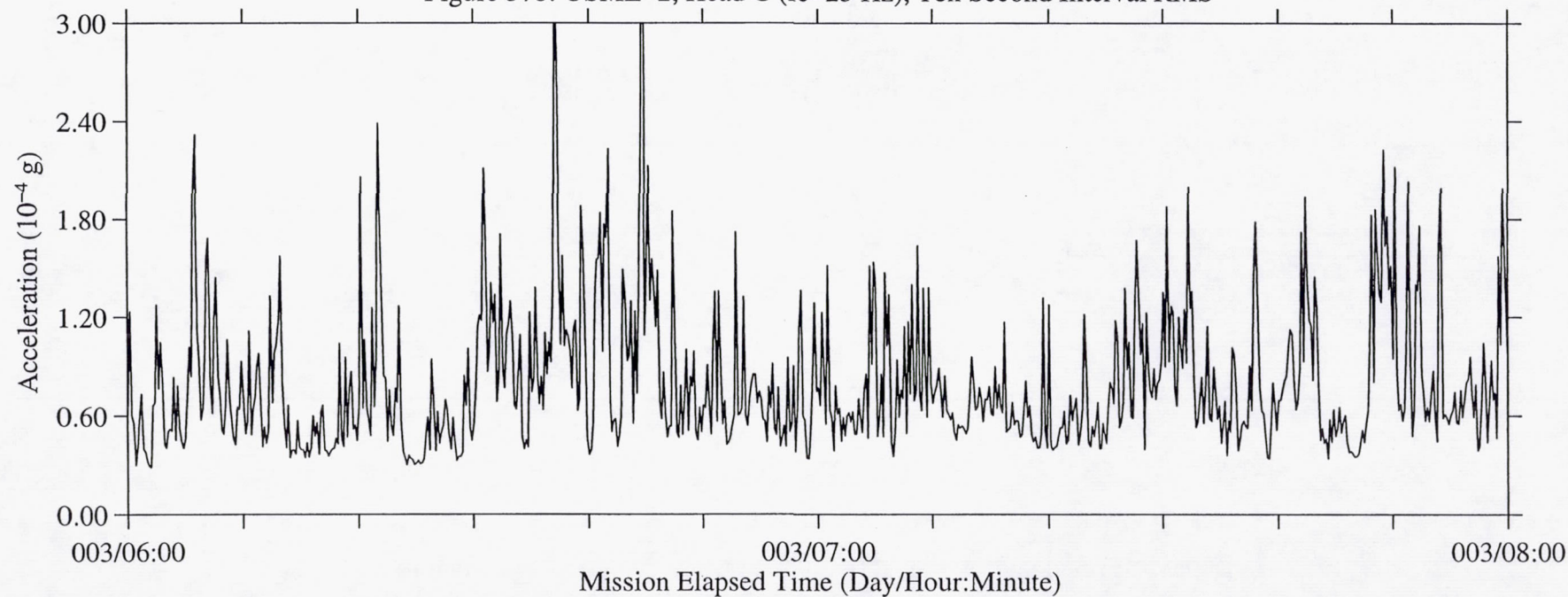


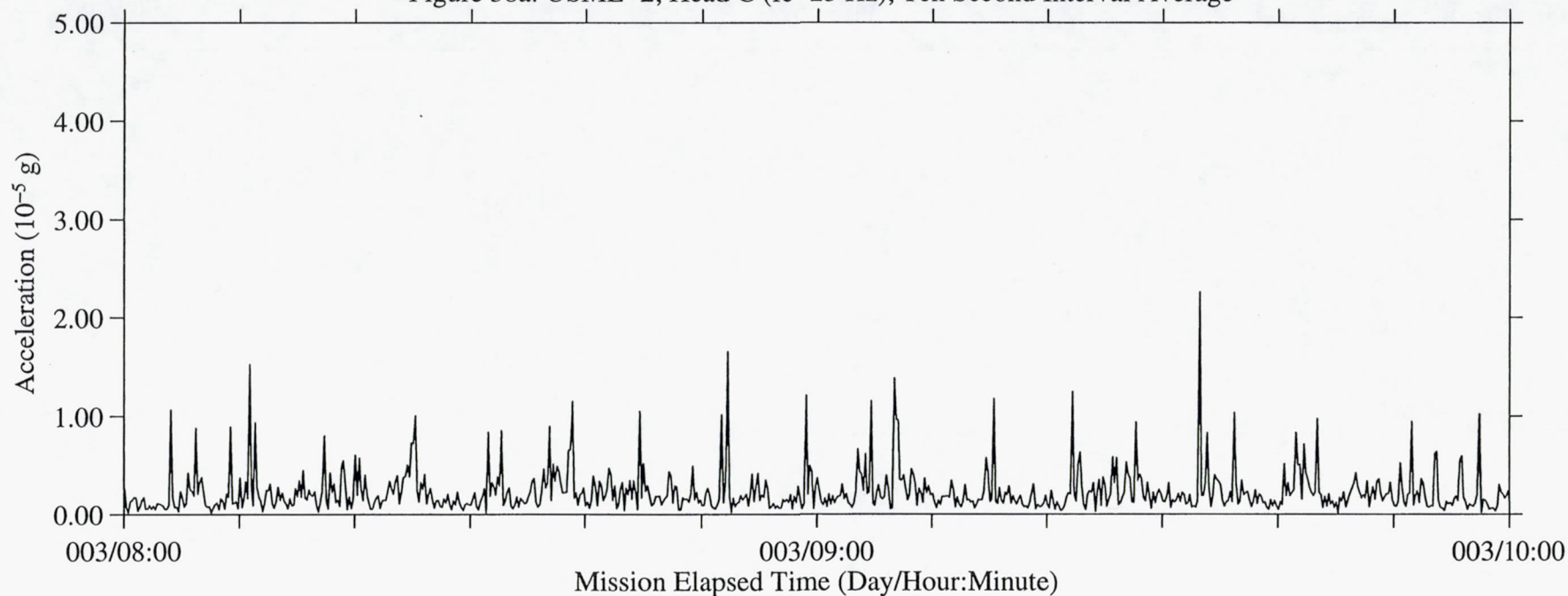
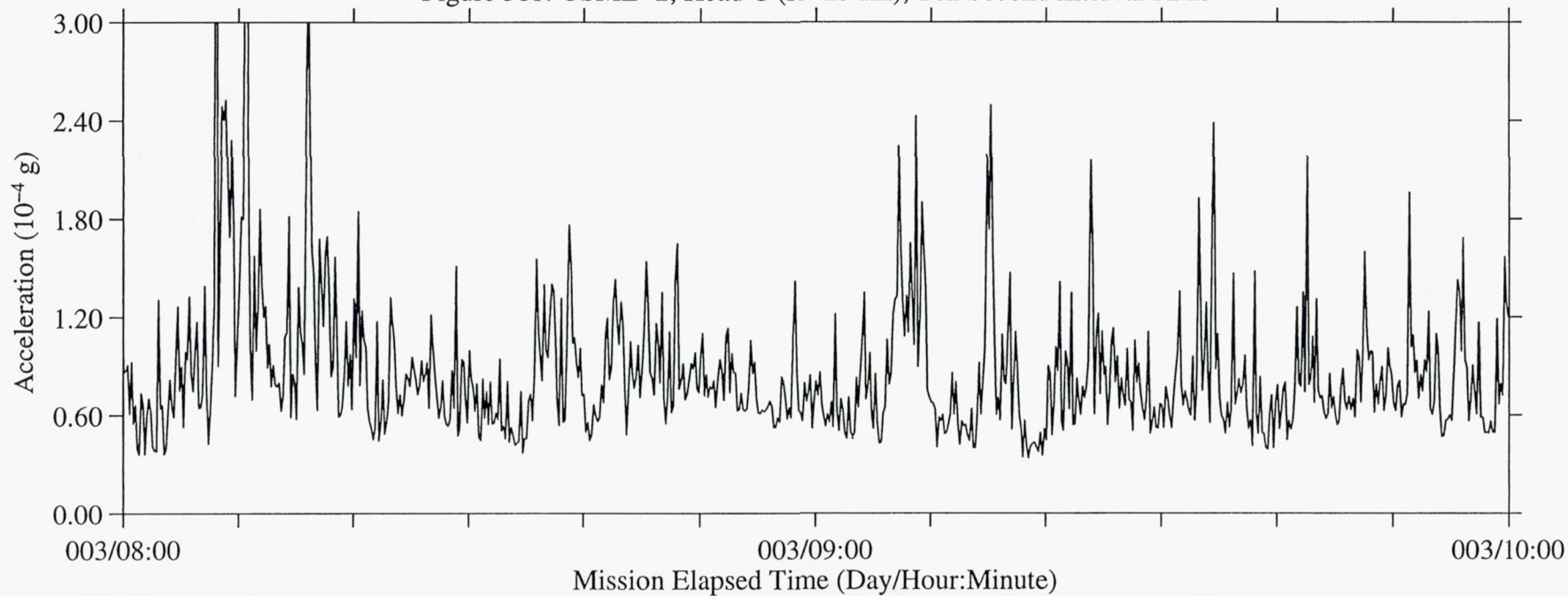
Figure 38a: USML-2, Head C ( $f_c=25$  Hz), Ten Second Interval AverageFigure 38b: USML-2, Head C ( $f_c=25$  Hz), Ten Second Interval RMS



Figure 39a: USML-2, Head C (fc=25 Hz), Ten Second Interval Average

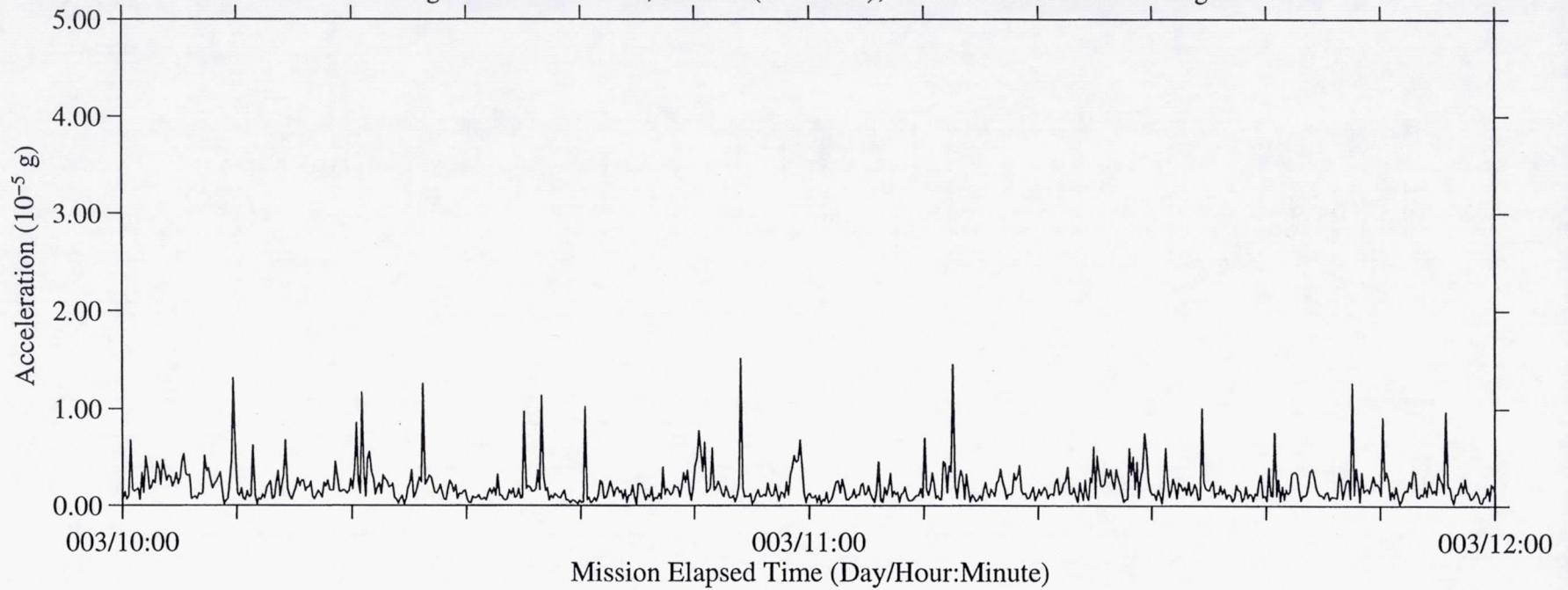


Figure 39b: USML-2, Head C (fc=25 Hz), Ten Second Interval RMS

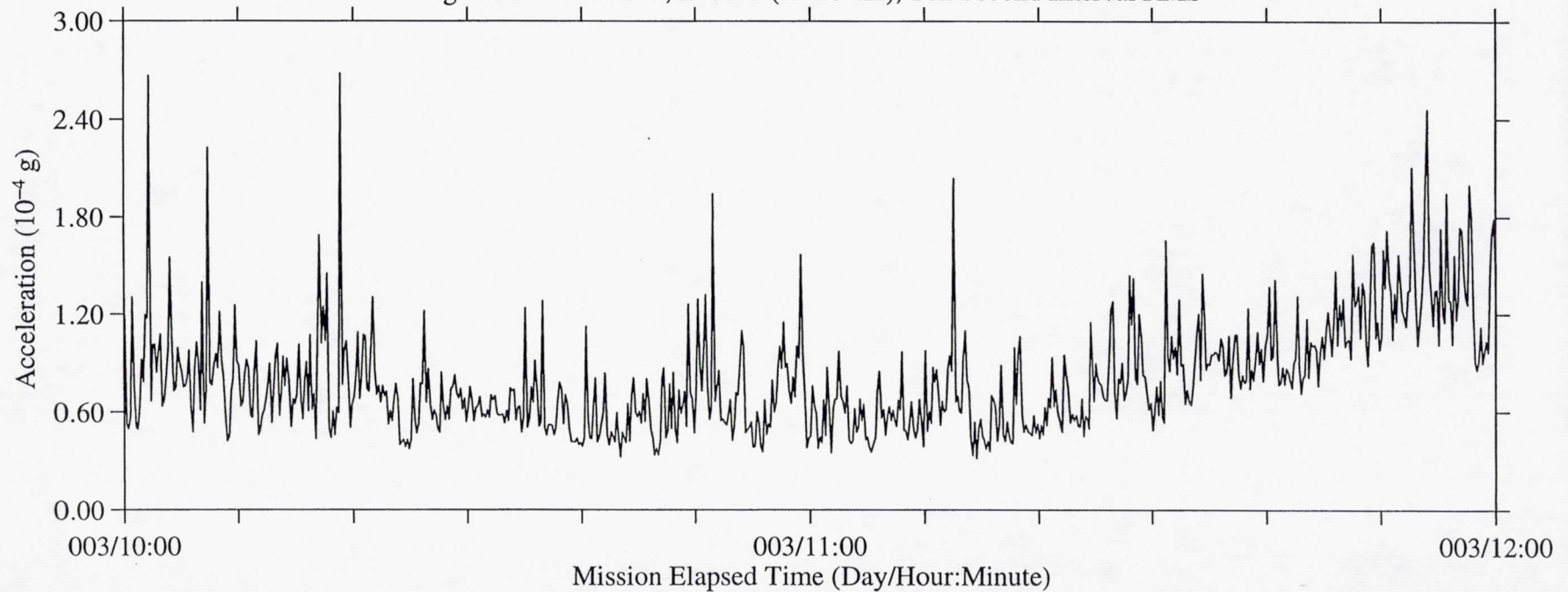


Figure 40a: USML-2, Head C (fc=25 Hz), Ten Second Interval Average

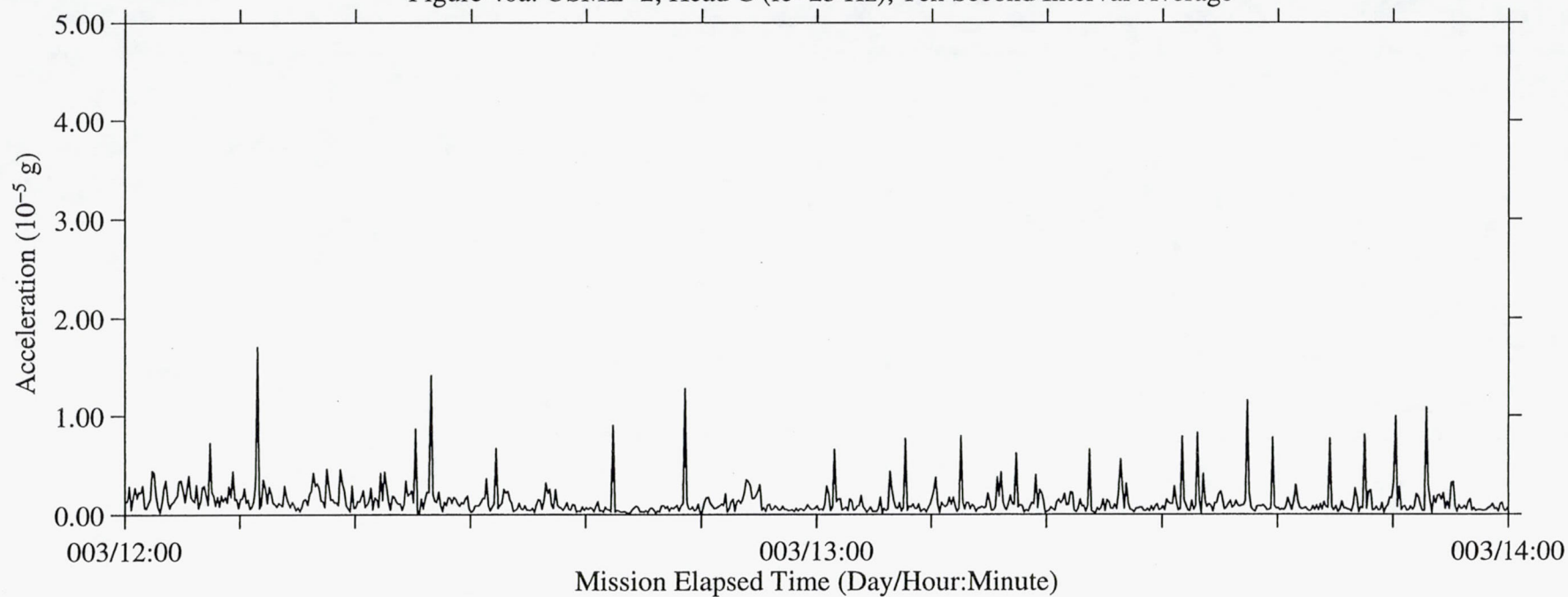


Figure 40b: USML-2, Head C (fc=25 Hz), Ten Second Interval RMS

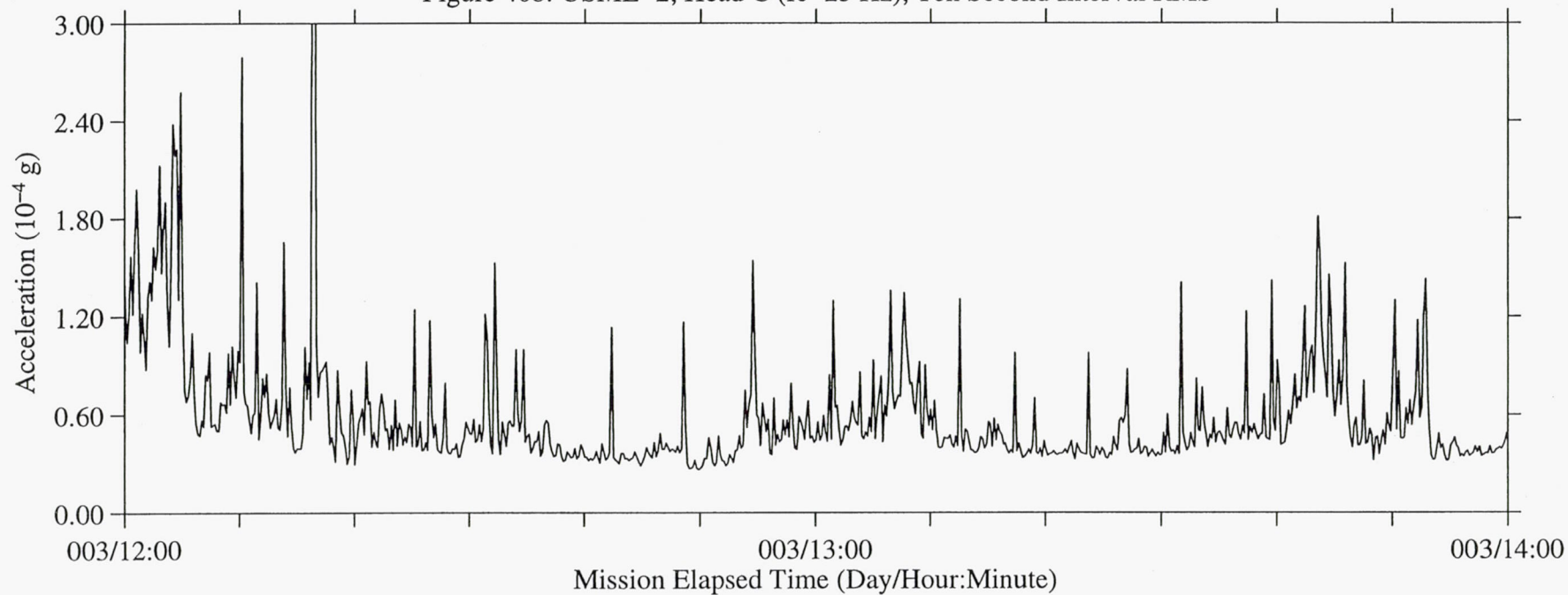




Figure 41a: USML-2, Head C (fc=25 Hz), Ten Second Interval Average

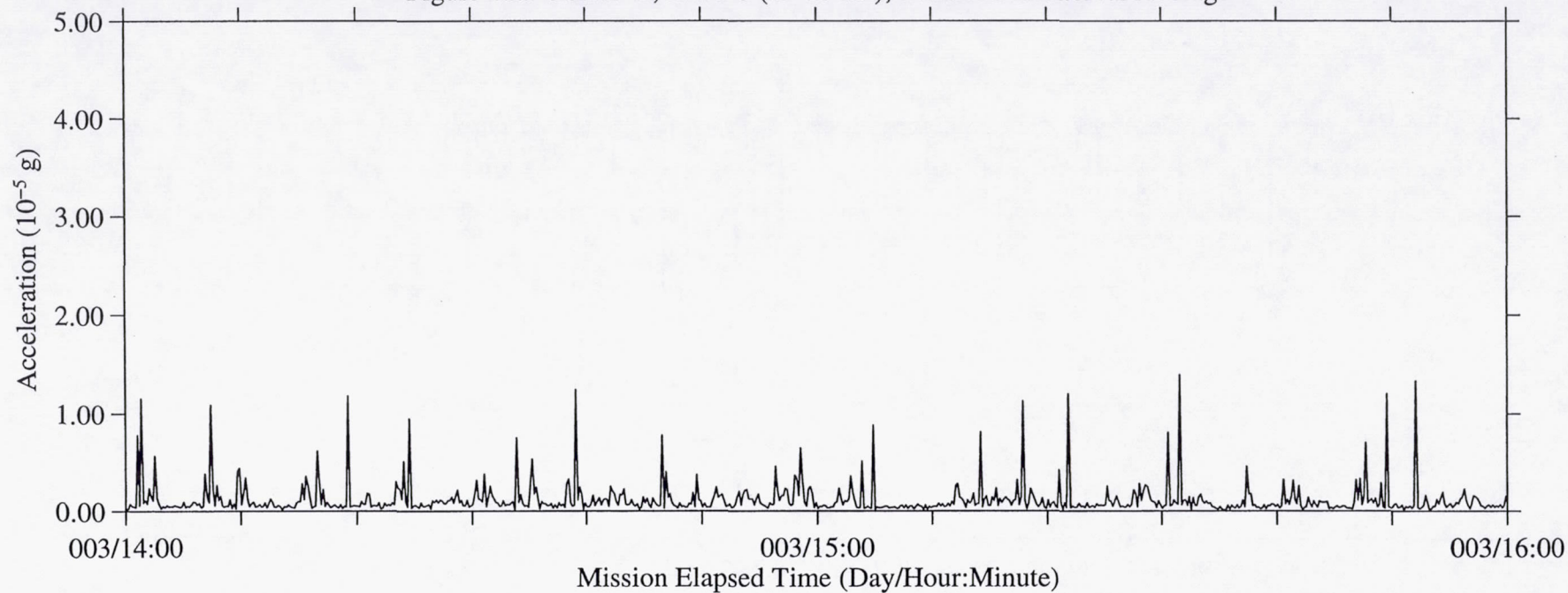


Figure 41b: USML-2, Head C (fc=25 Hz), Ten Second Interval RMS

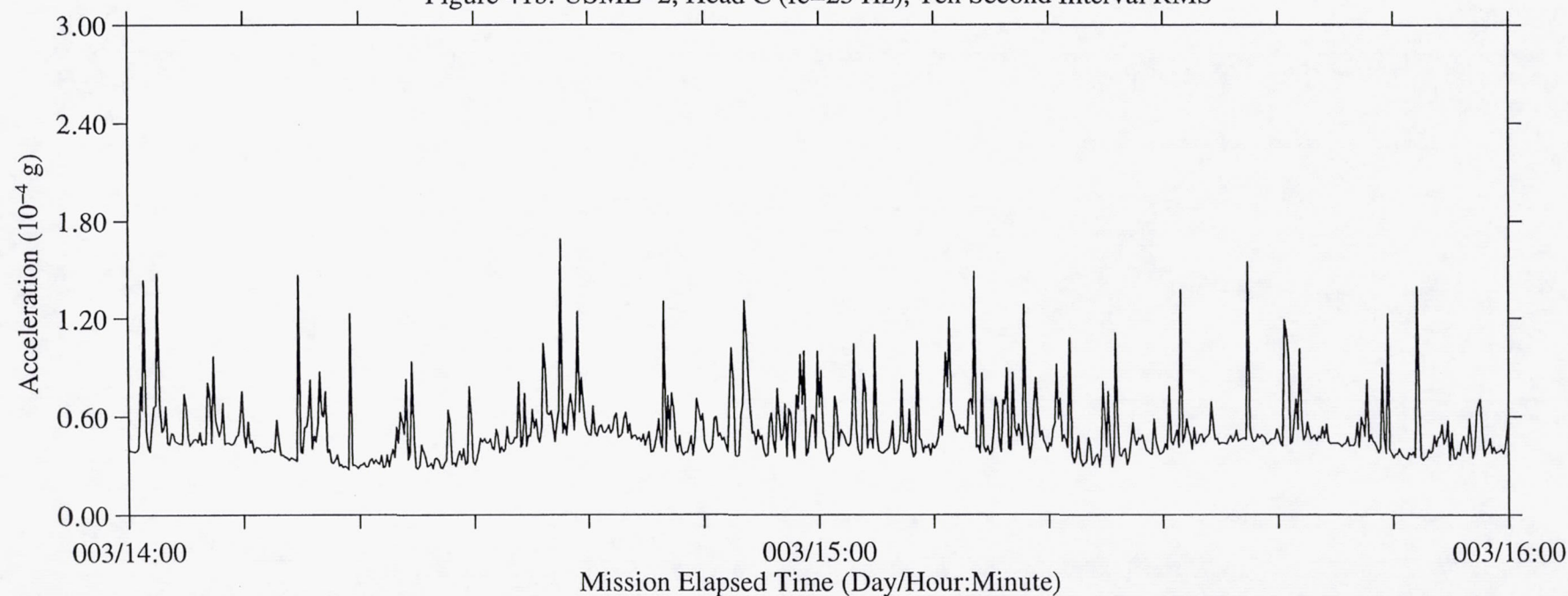


Figure 42a: USML-2, Head C (fc=25 Hz), Ten Second Interval Average

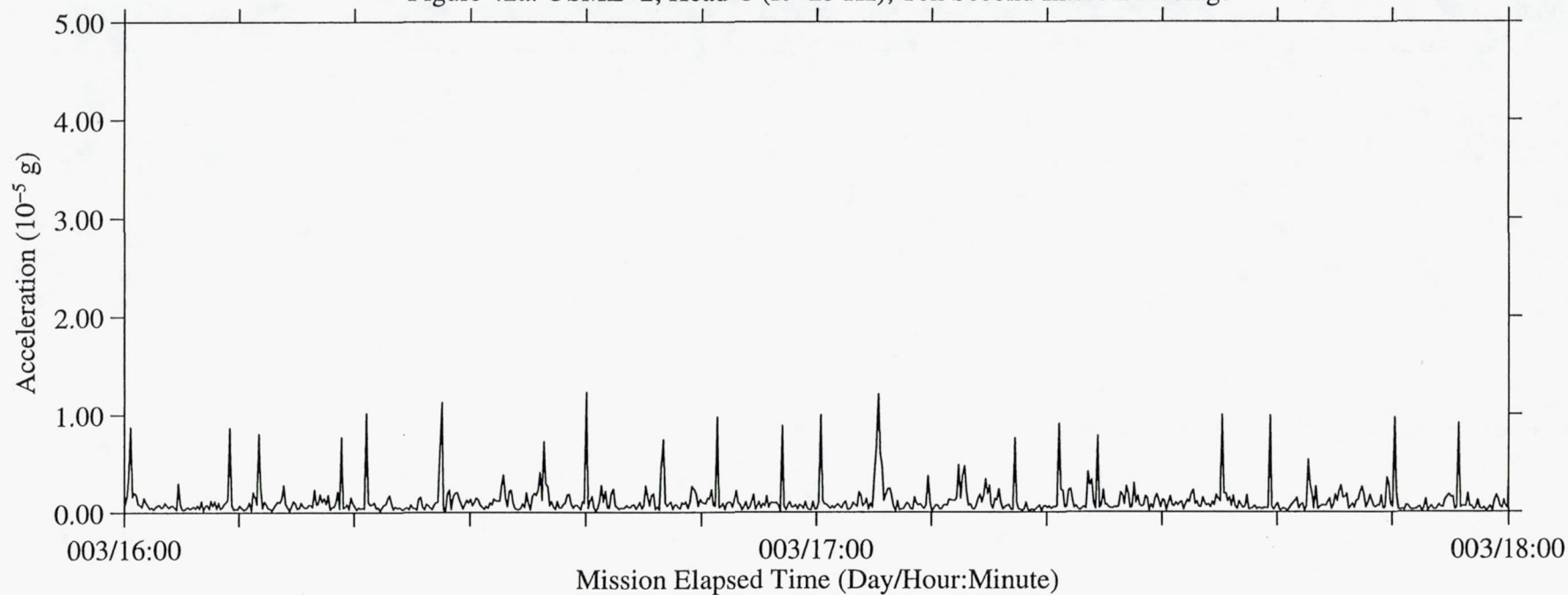


Figure 42b: USML-2, Head C (fc=25 Hz), Ten Second Interval RMS

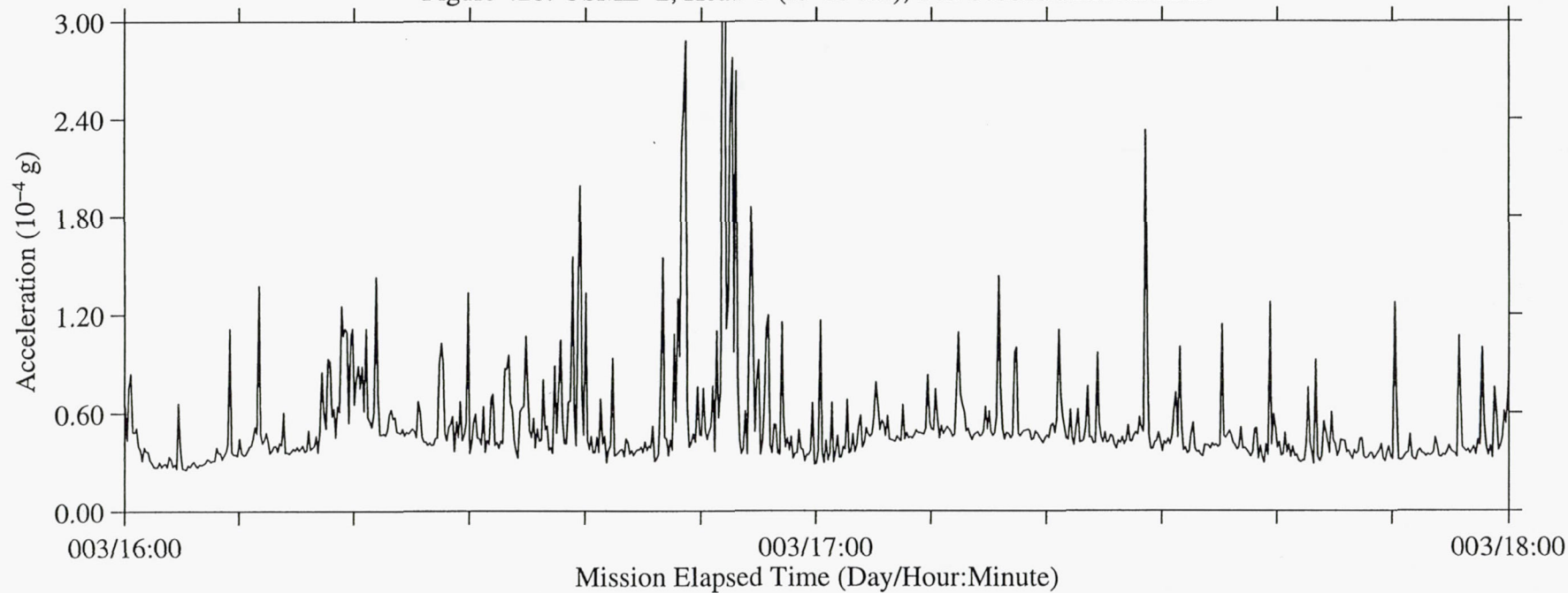




Figure 43a: USML-2, Head C (fc=25 Hz), Ten Second Interval Average

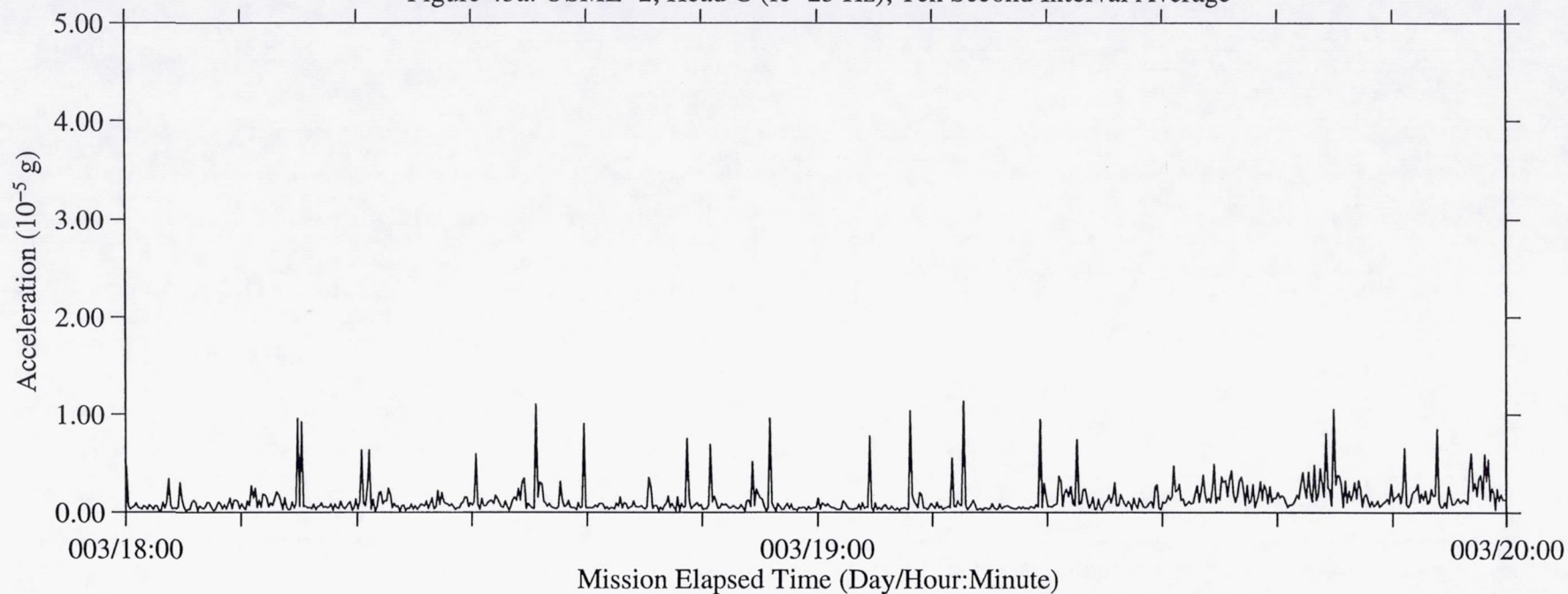


Figure 43b: USML-2, Head C (fc=25 Hz), Ten Second Interval RMS

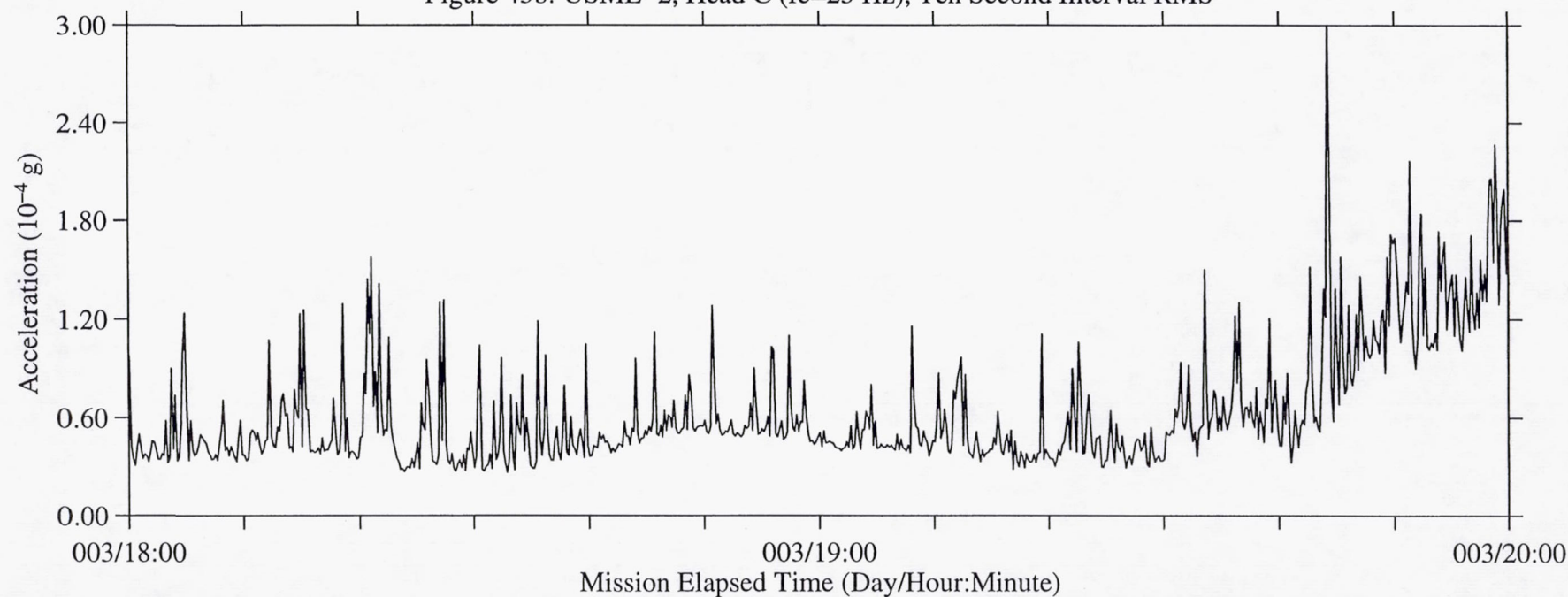


Figure 44a: USML-2, Head C (fc=25 Hz), Ten Second Interval Average

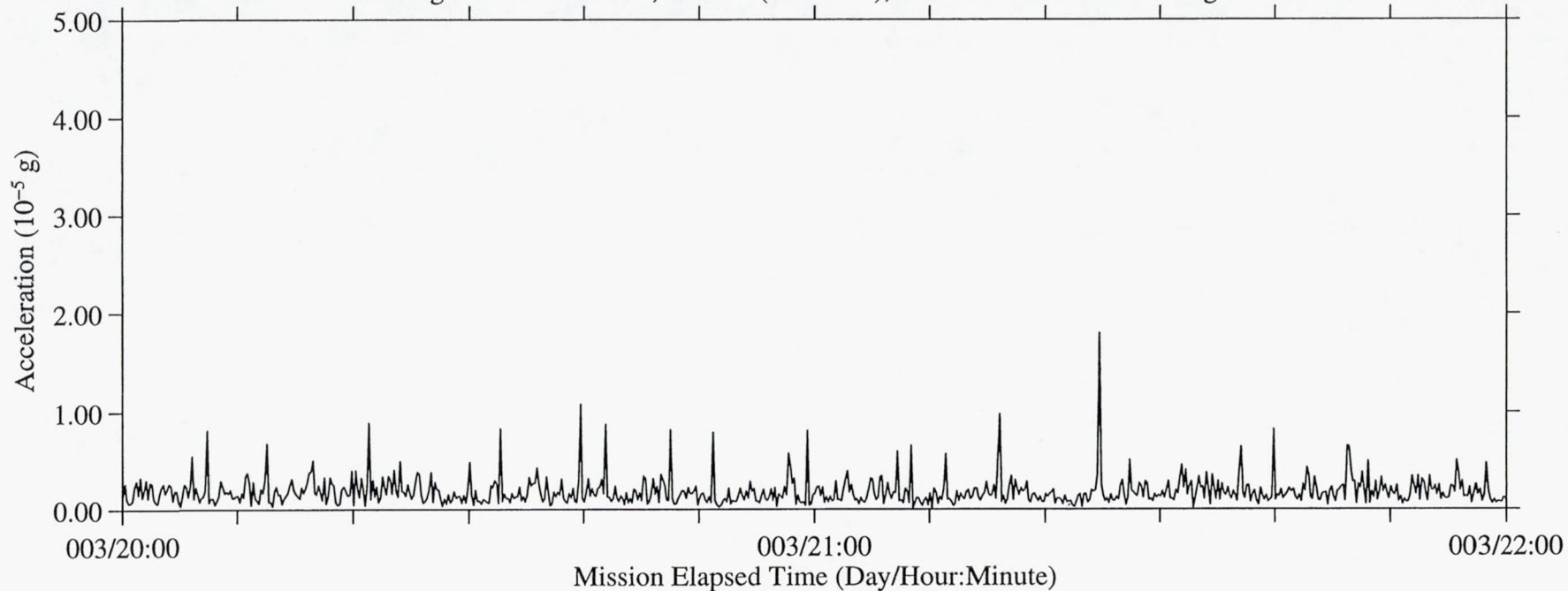


Figure 44b: USML-2, Head C (fc=25 Hz), Ten Second Interval RMS

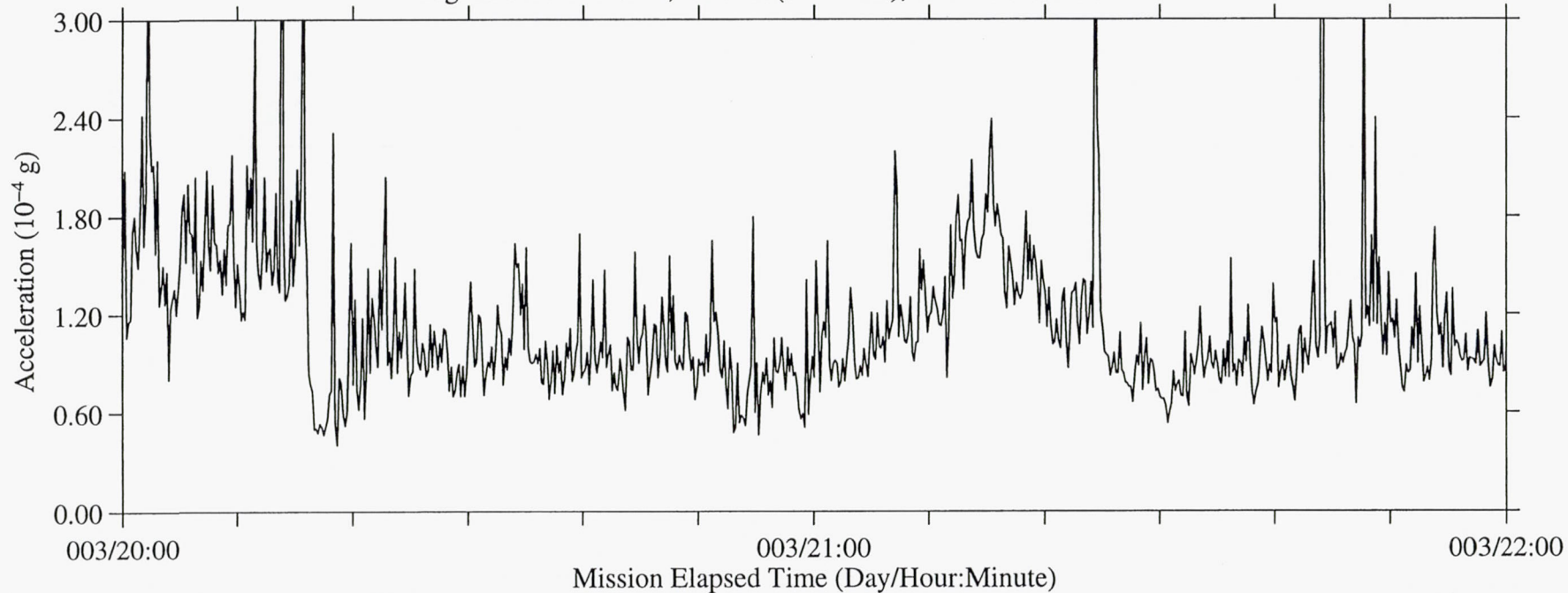




Figure 45a: USML-2, Head C (fc=25 Hz), Ten Second Interval Average

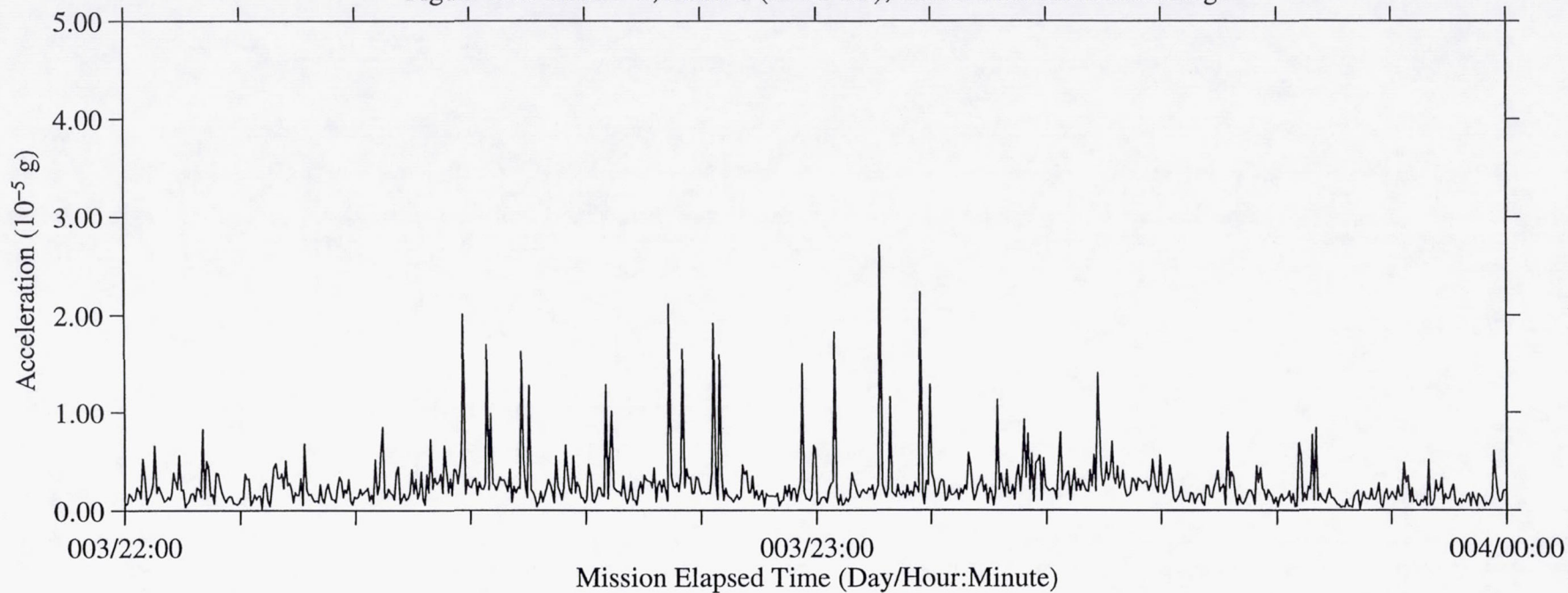


Figure 45b: USML-2, Head C (fc=25 Hz), Ten Second Interval RMS

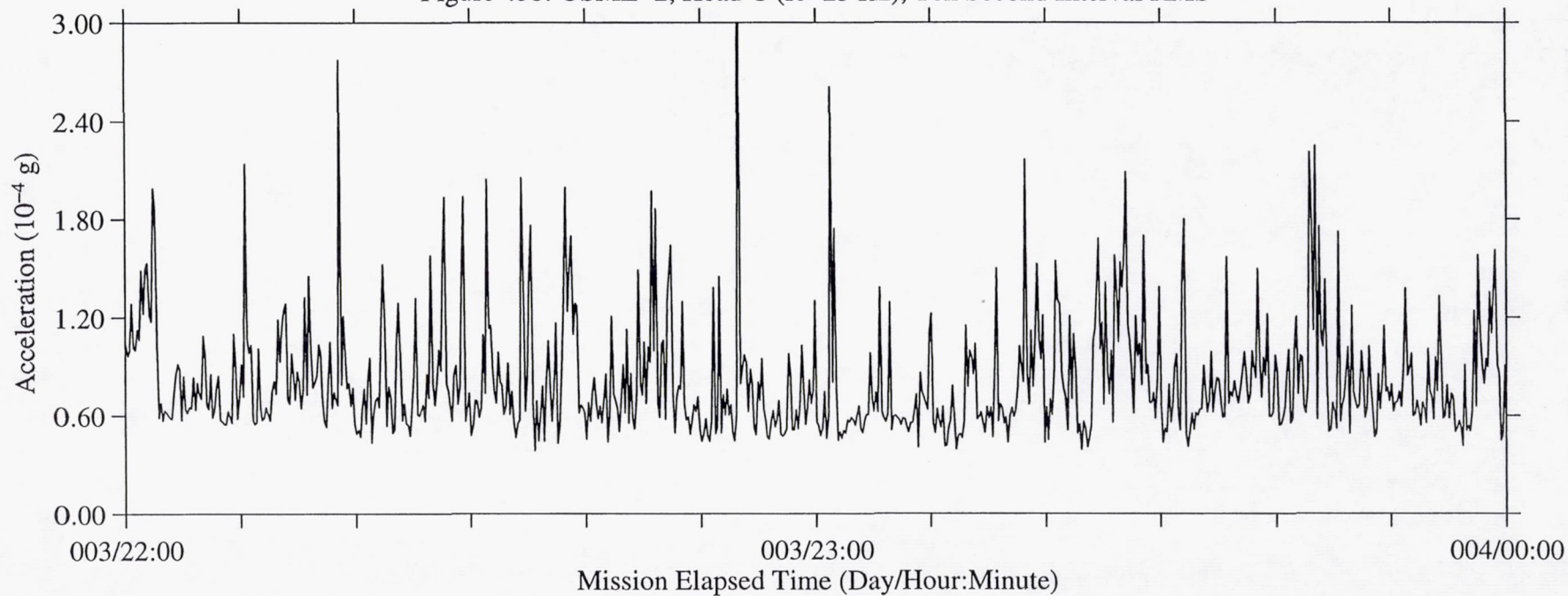


Figure 46a: USML-2, Head C (fc=25 Hz), Ten Second Interval Average

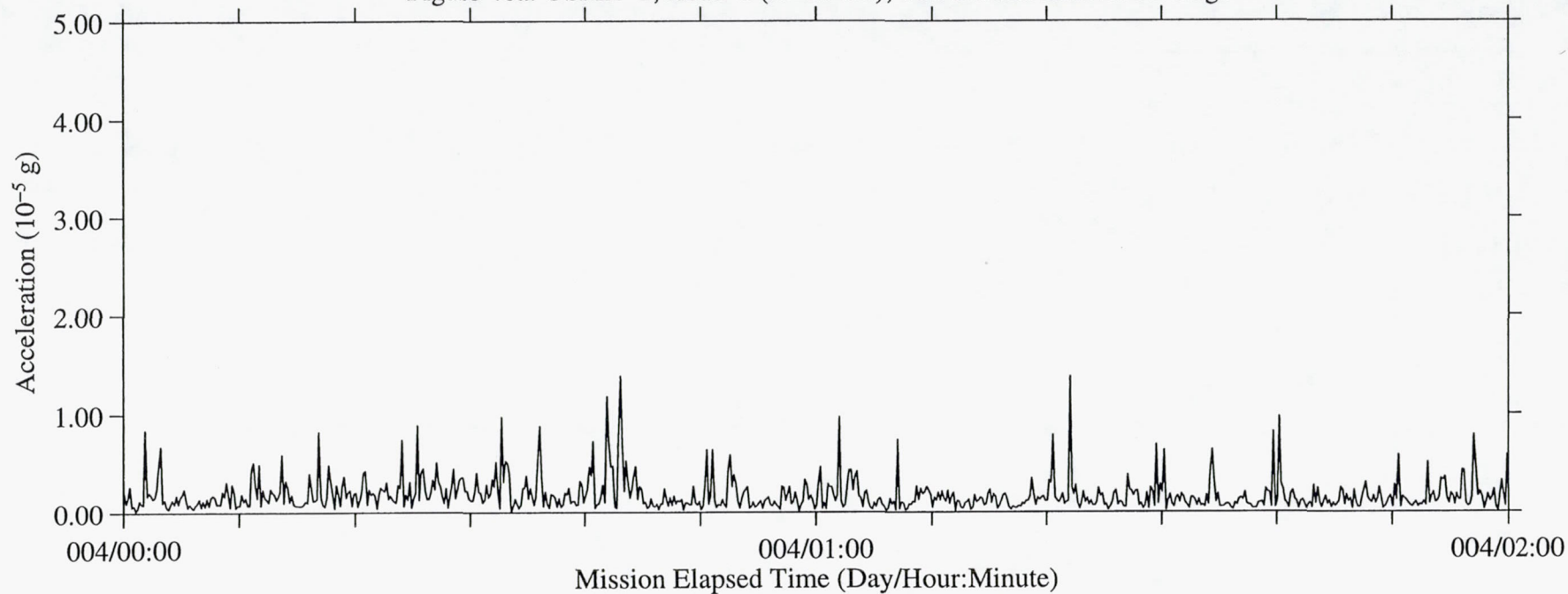


Figure 46b: USML-2, Head C (fc=25 Hz), Ten Second Interval RMS

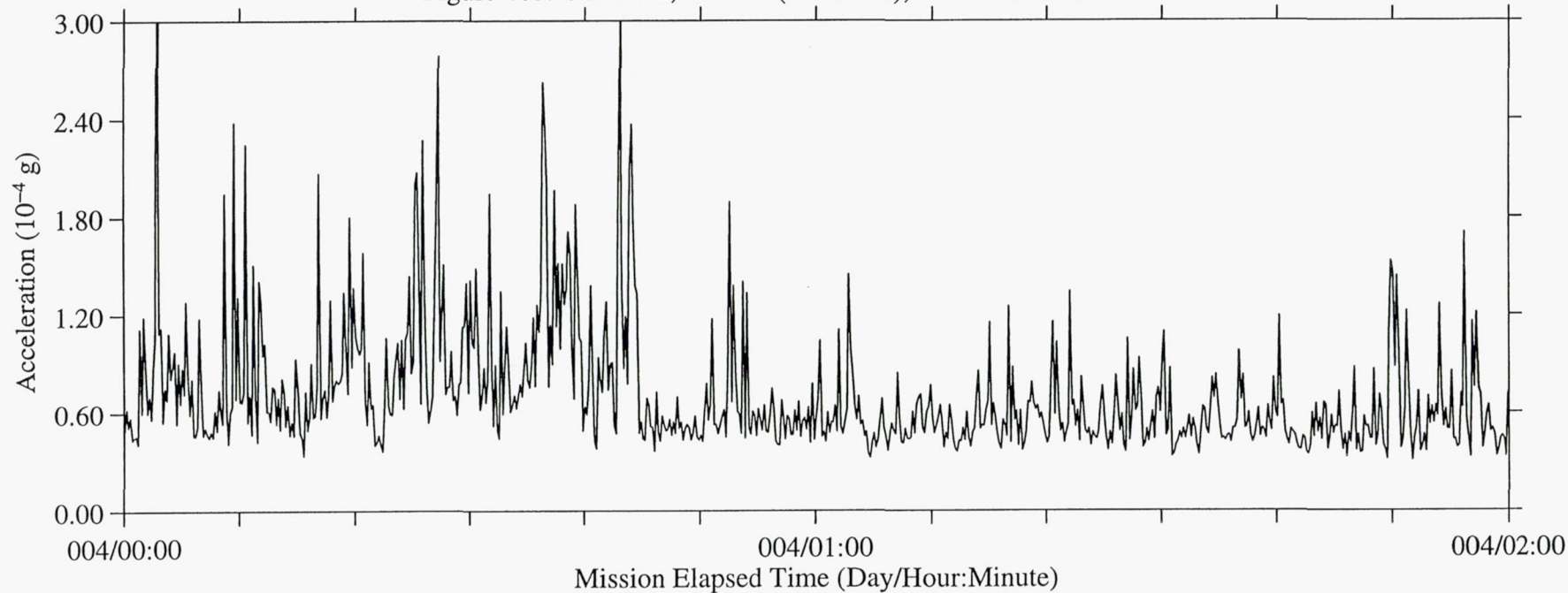




Figure 47a: USML-2, Head C (fc=25 Hz), Ten Second Interval Average

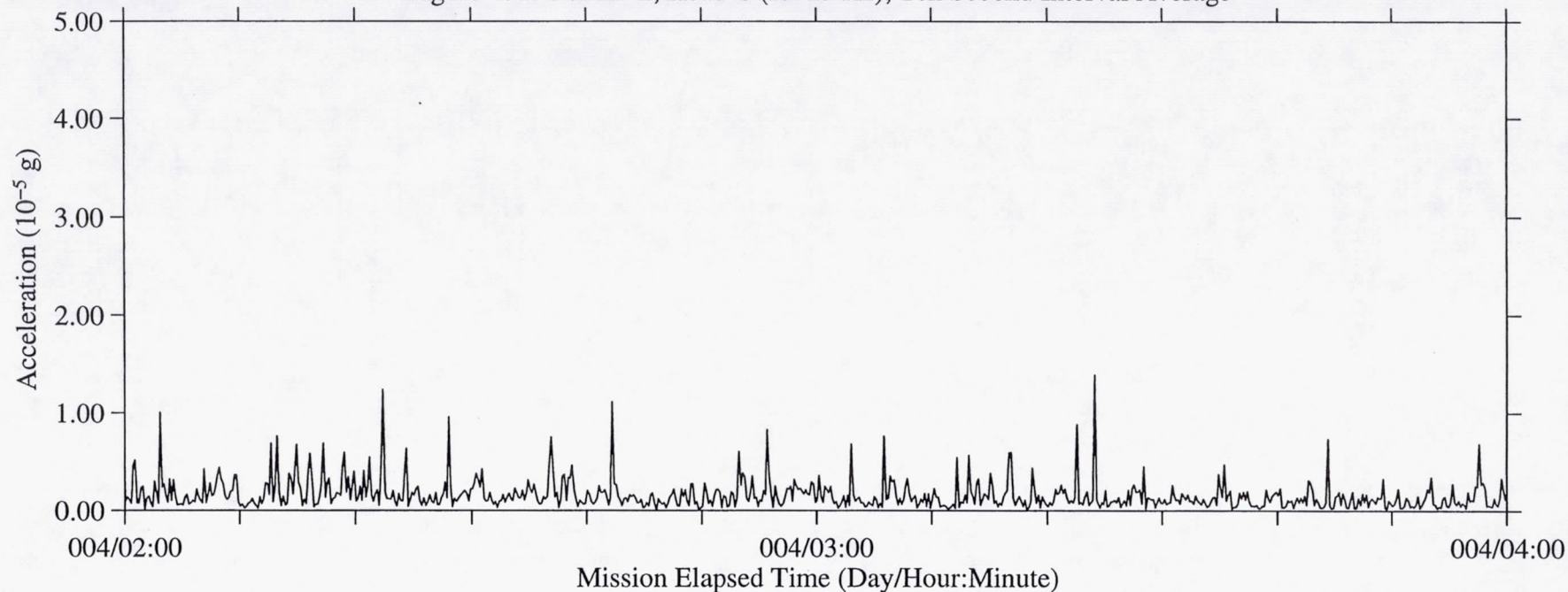


Figure 47b: USML-2, Head C (fc=25 Hz), Ten Second Interval RMS

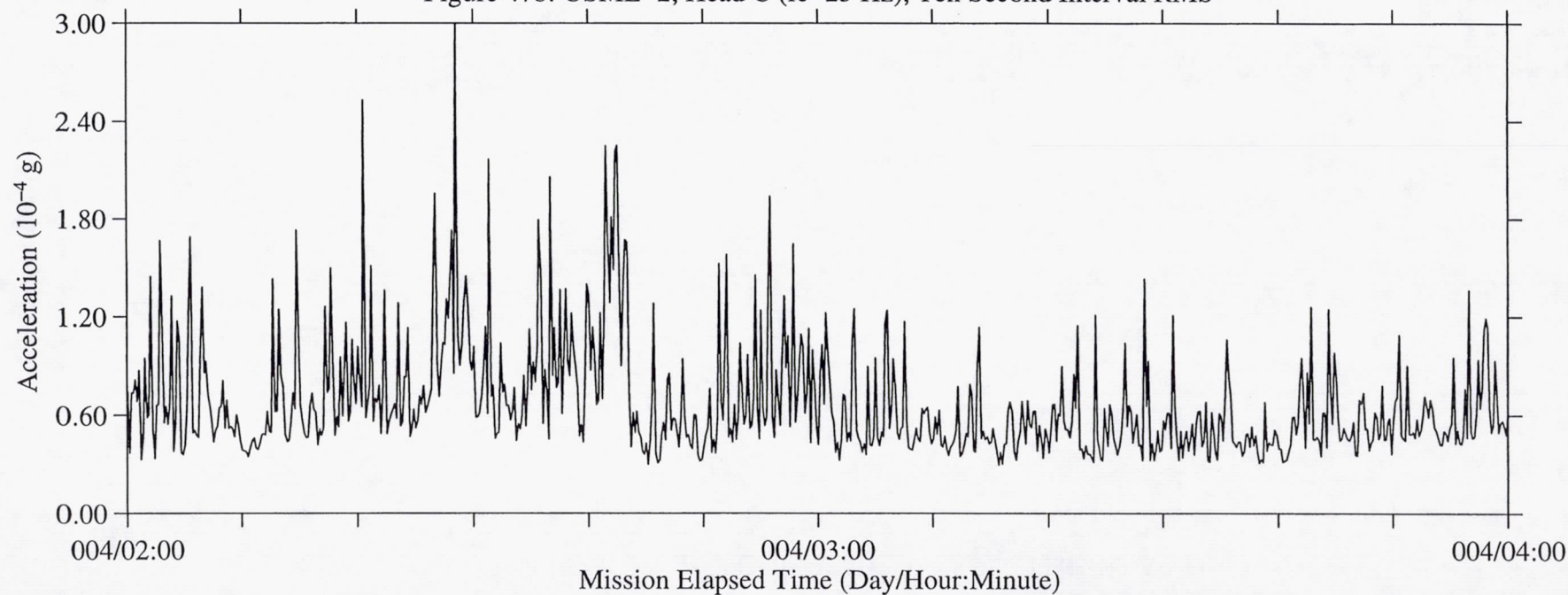


Figure 48a: USML-2, Head C (fc=25 Hz), Ten Second Interval Average

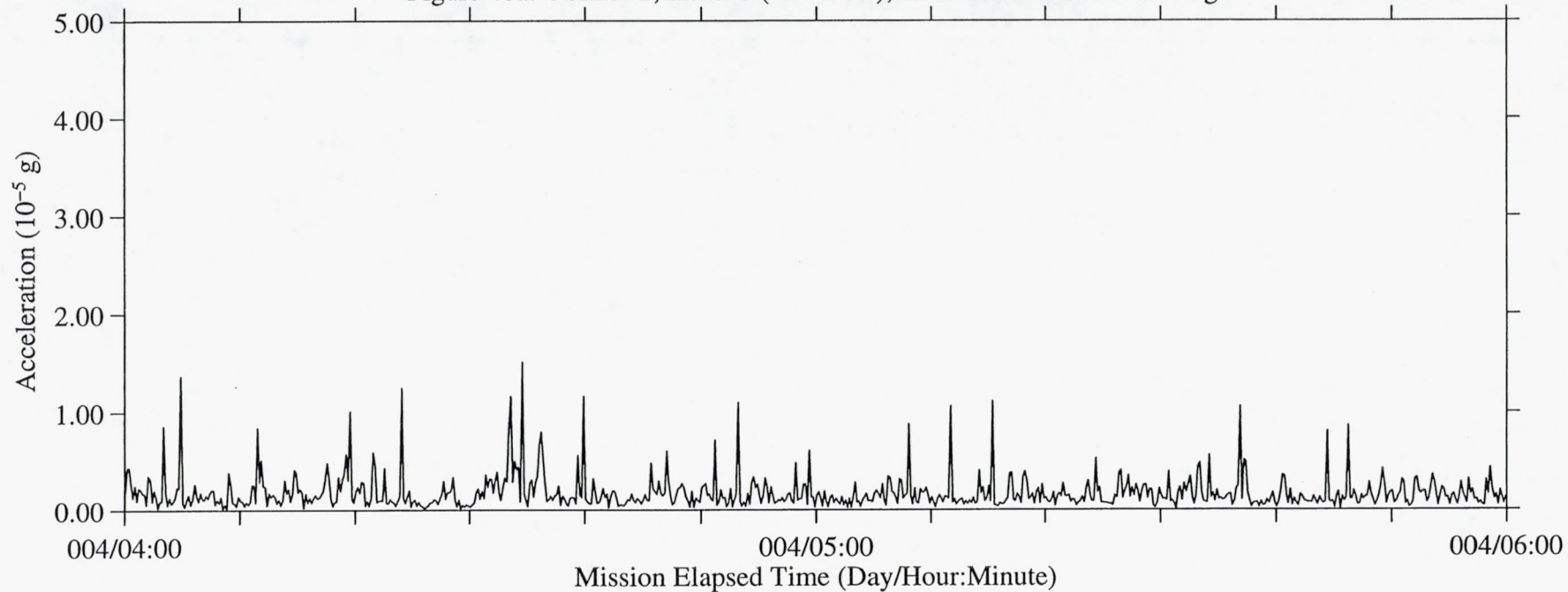
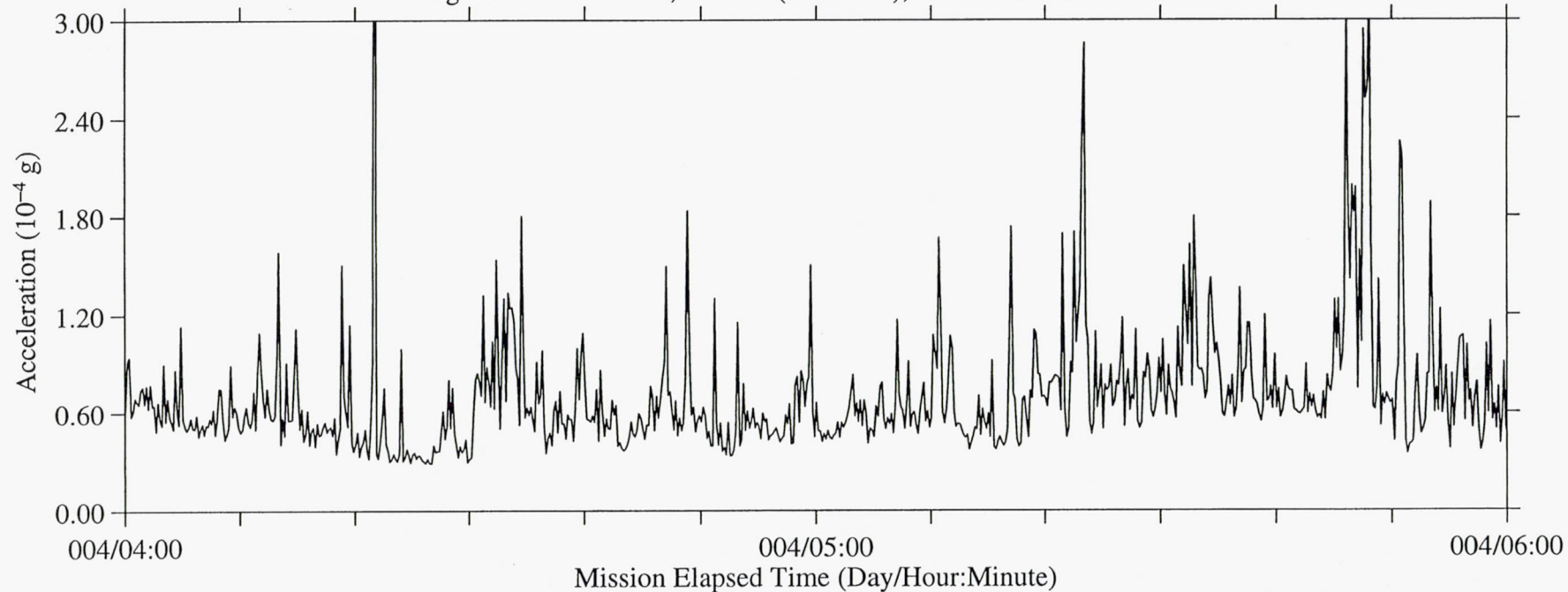


Figure 48b: USML-2, Head C (fc=25 Hz), Ten Second Interval RMS





B-51

Figure 49a: USML-2, Head C (fc=25 Hz), Ten Second Interval Average

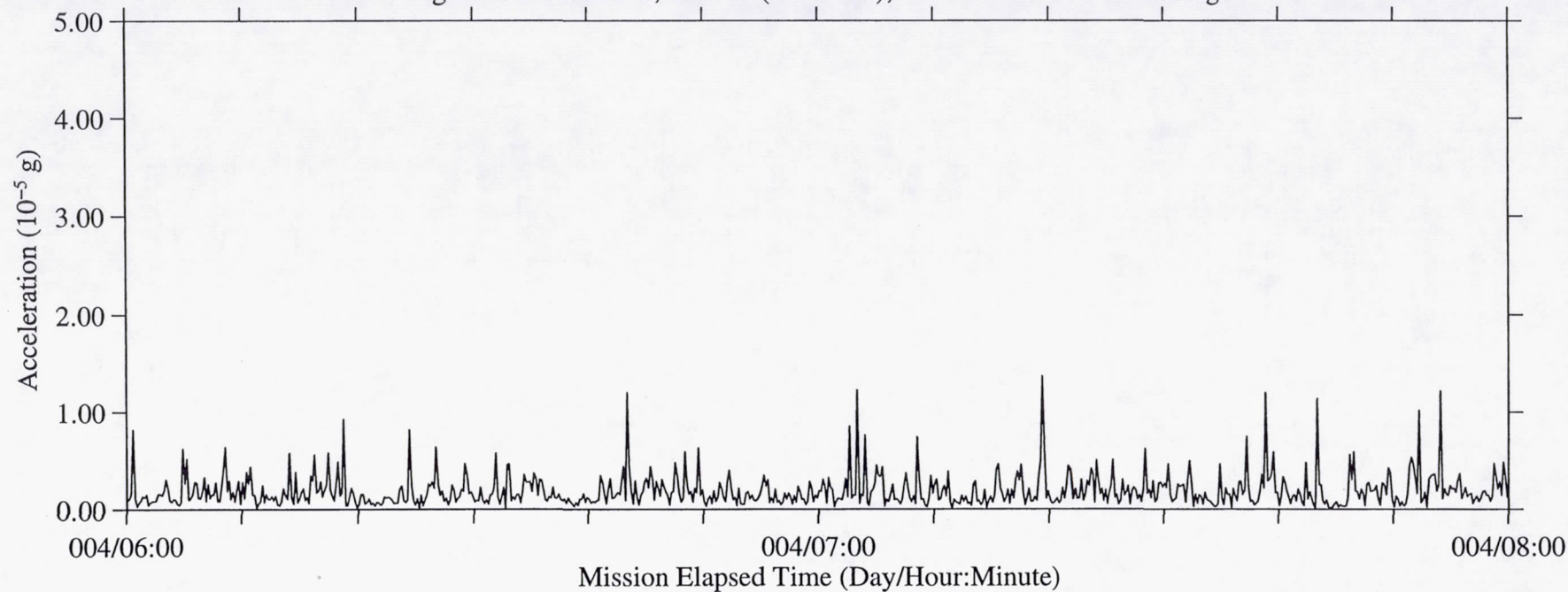


Figure 49b: USML-2, Head C (fc=25 Hz), Ten Second Interval RMS

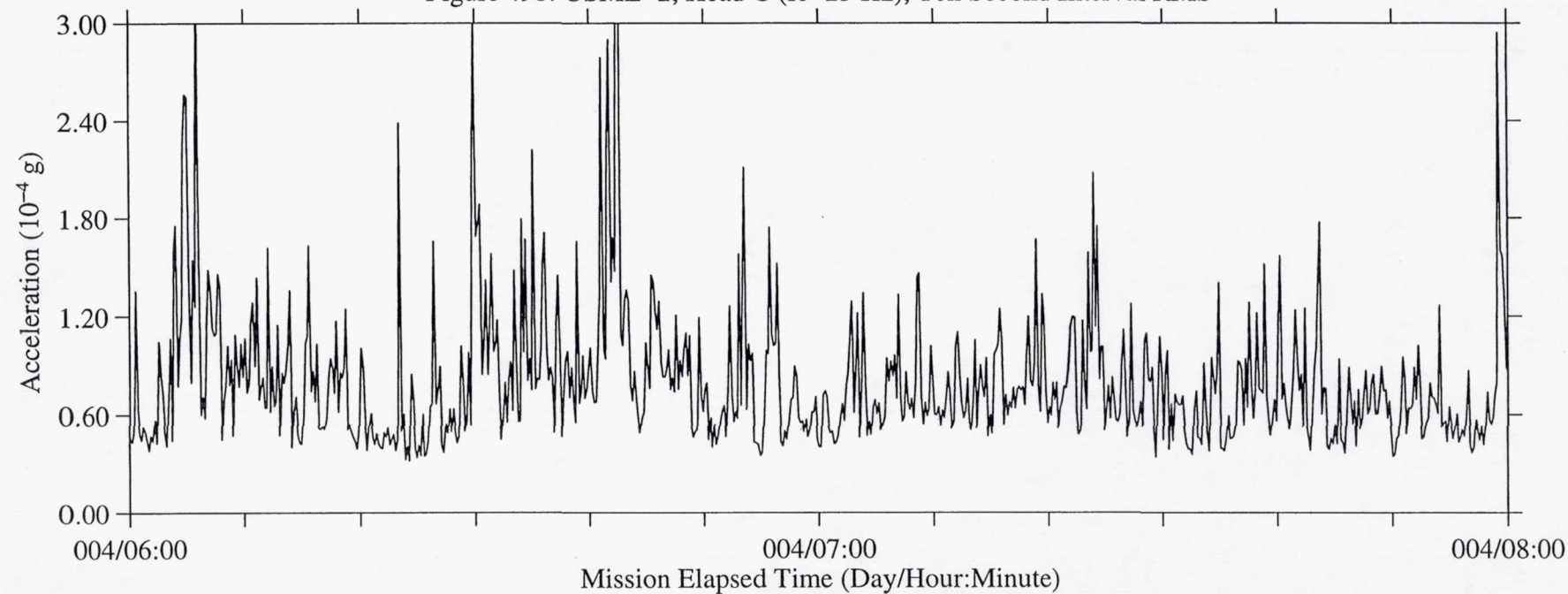


Figure 50a: USML-2, Head C (fc=25 Hz), Ten Second Interval Average

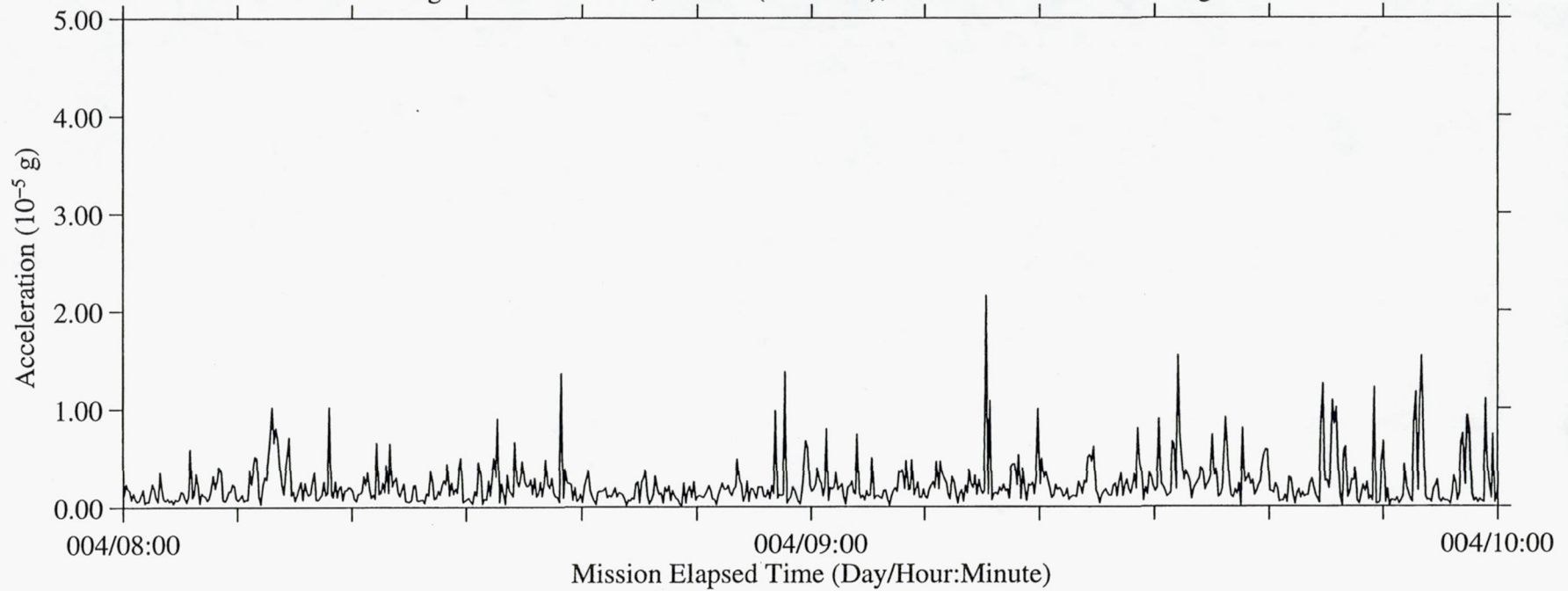


Figure 50b: USML-2, Head C (fc=25 Hz), Ten Second Interval RMS

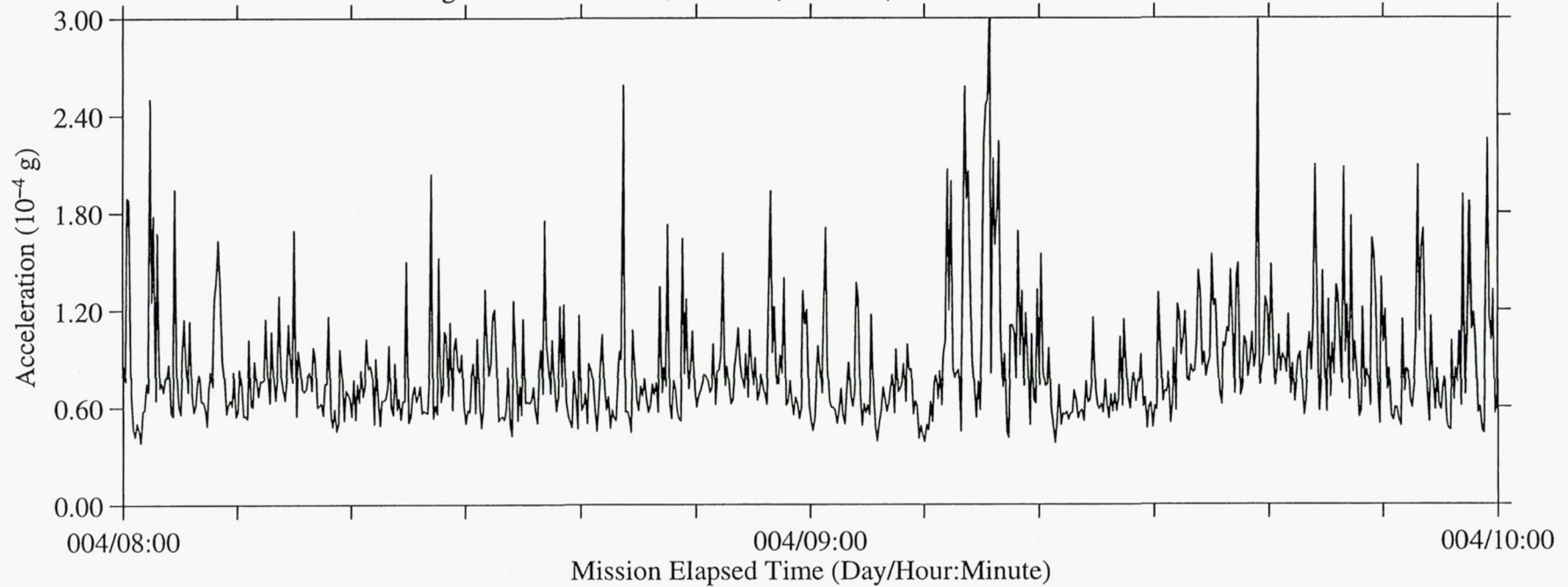




Figure 51a: USML-2, Head C (fc=25 Hz), Ten Second Interval Average

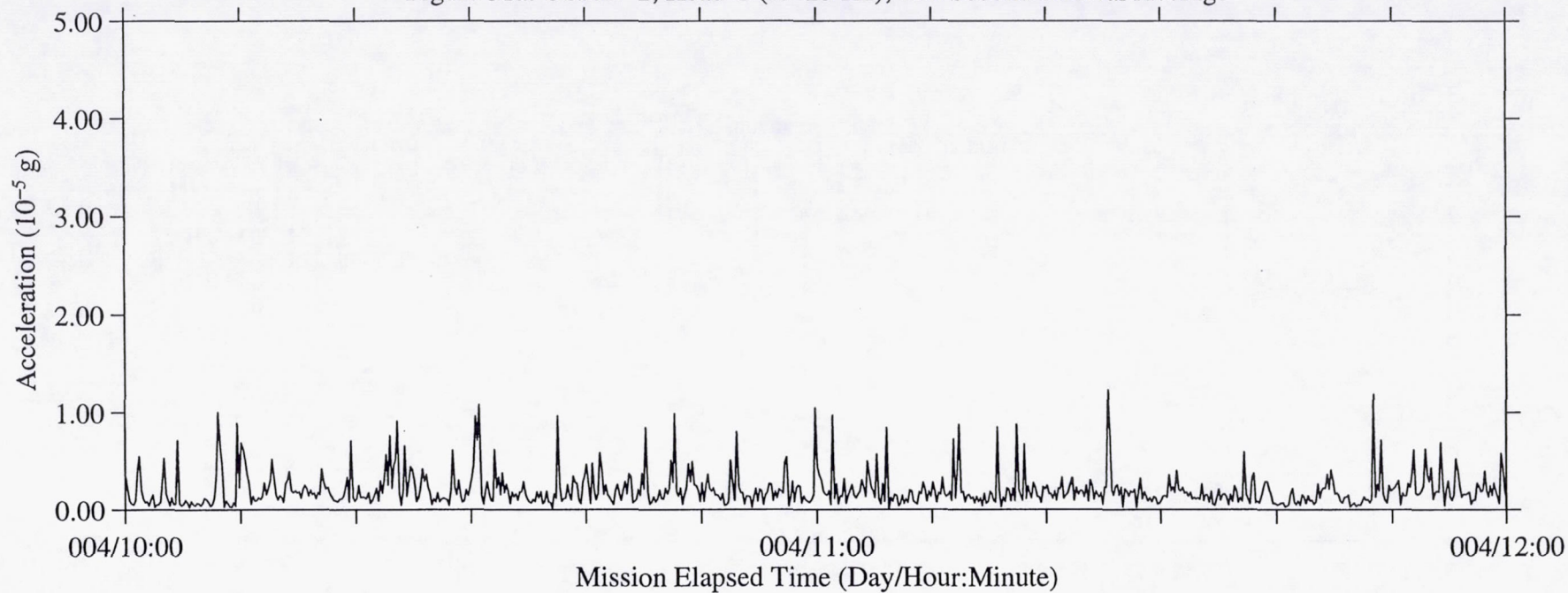


Figure 51b: USML-2, Head C (fc=25 Hz), Ten Second Interval RMS

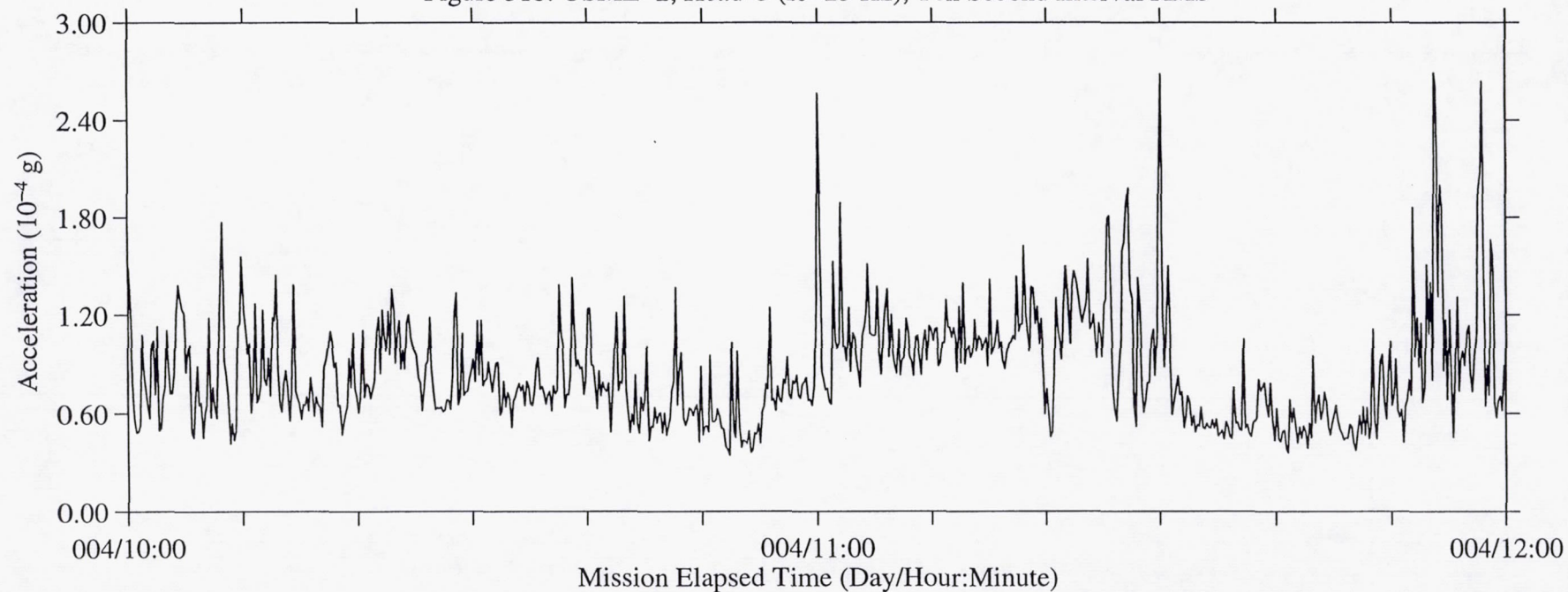


Figure 52a: USML-2, Head C (fc=25 Hz), Ten Second Interval Average

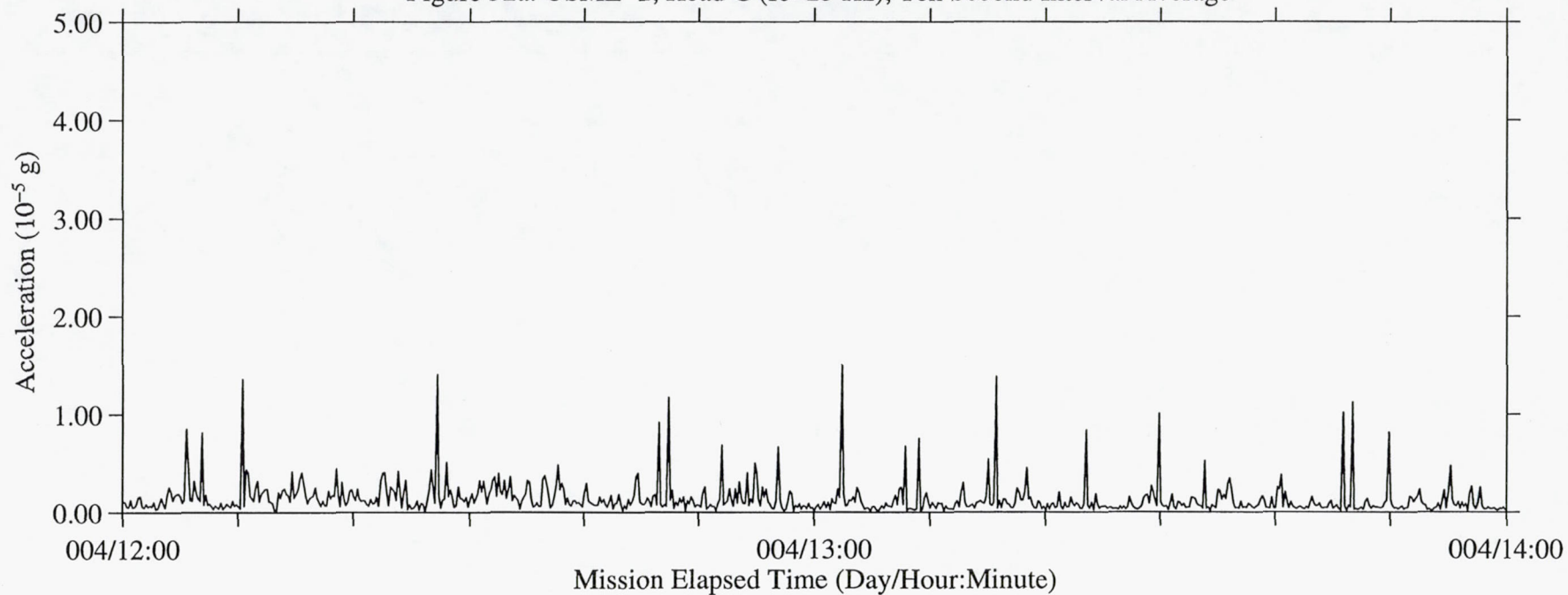


Figure 52b: USML-2, Head C (fc=25 Hz), Ten Second Interval RMS

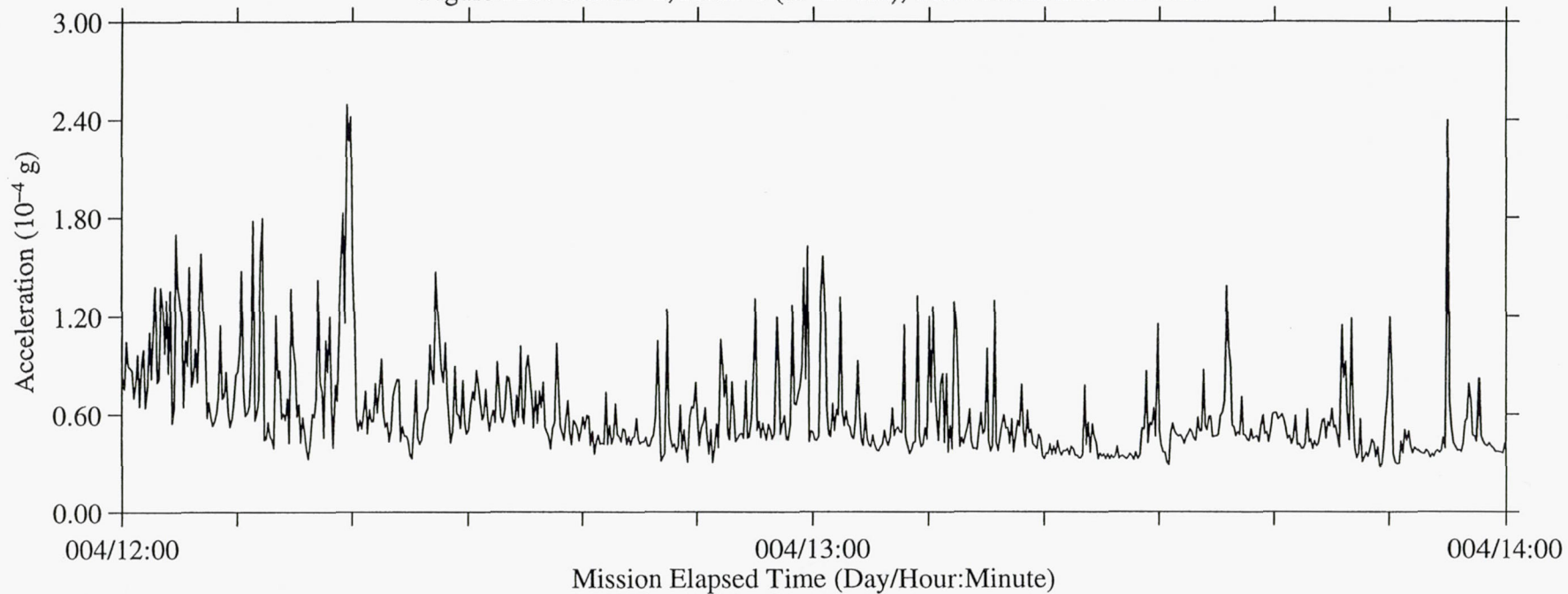




Figure 53a: USML-2, Head C (fc=25 Hz), Ten Second Interval Average

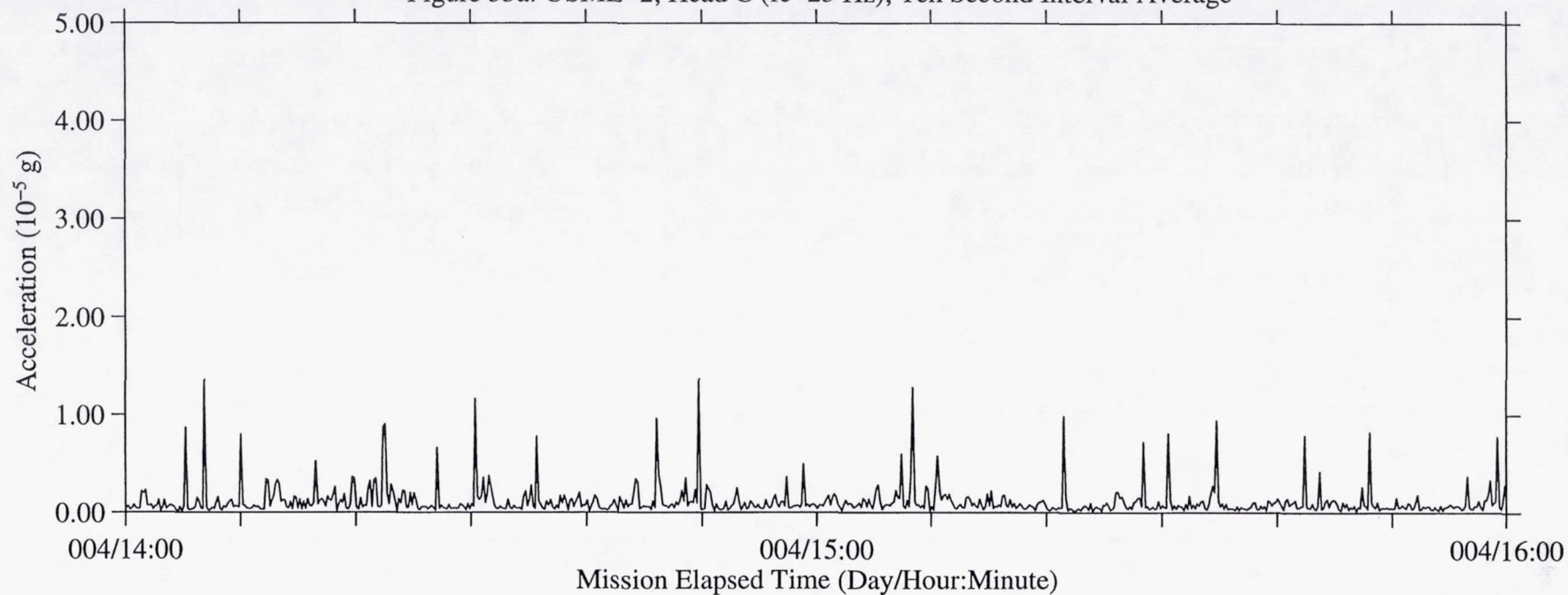


Figure 53b: USML-2, Head C (fc=25 Hz), Ten Second Interval RMS

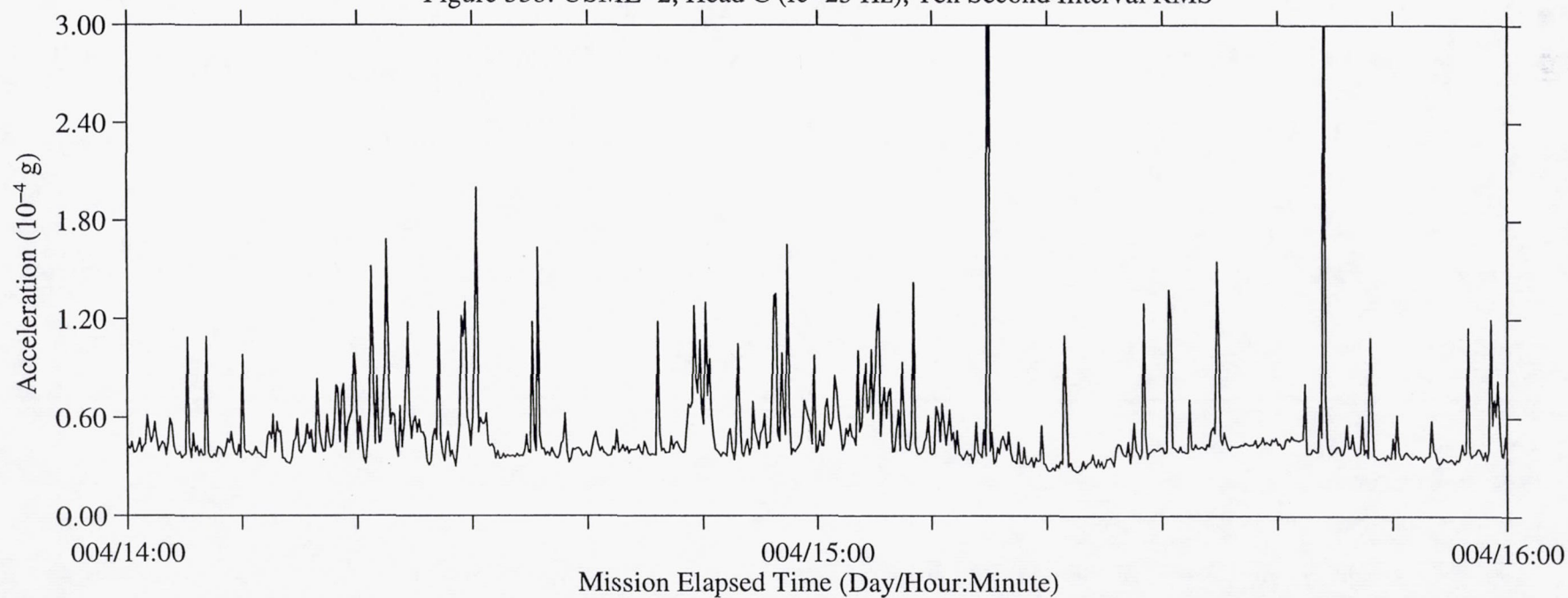


Figure 54a: USML-2, Head C (fc=25 Hz), Ten Second Interval Average

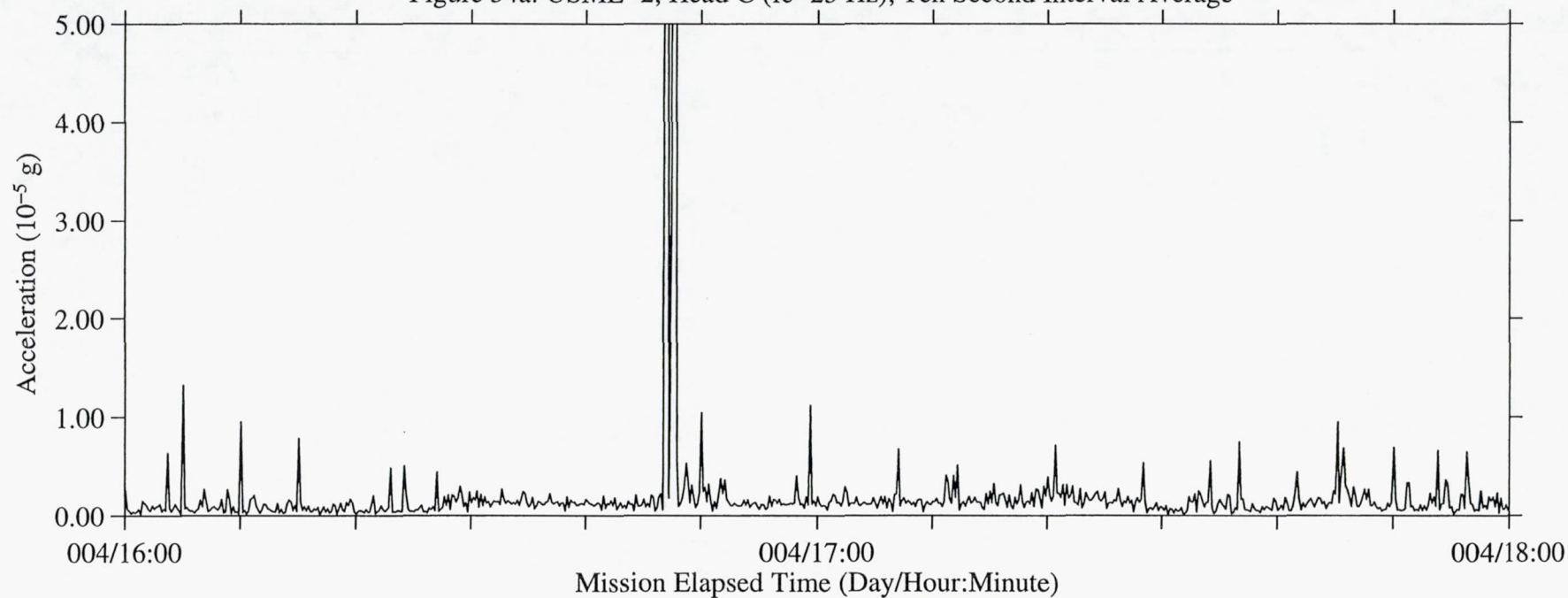


Figure 54b: USML-2, Head C (fc=25 Hz), Ten Second Interval RMS

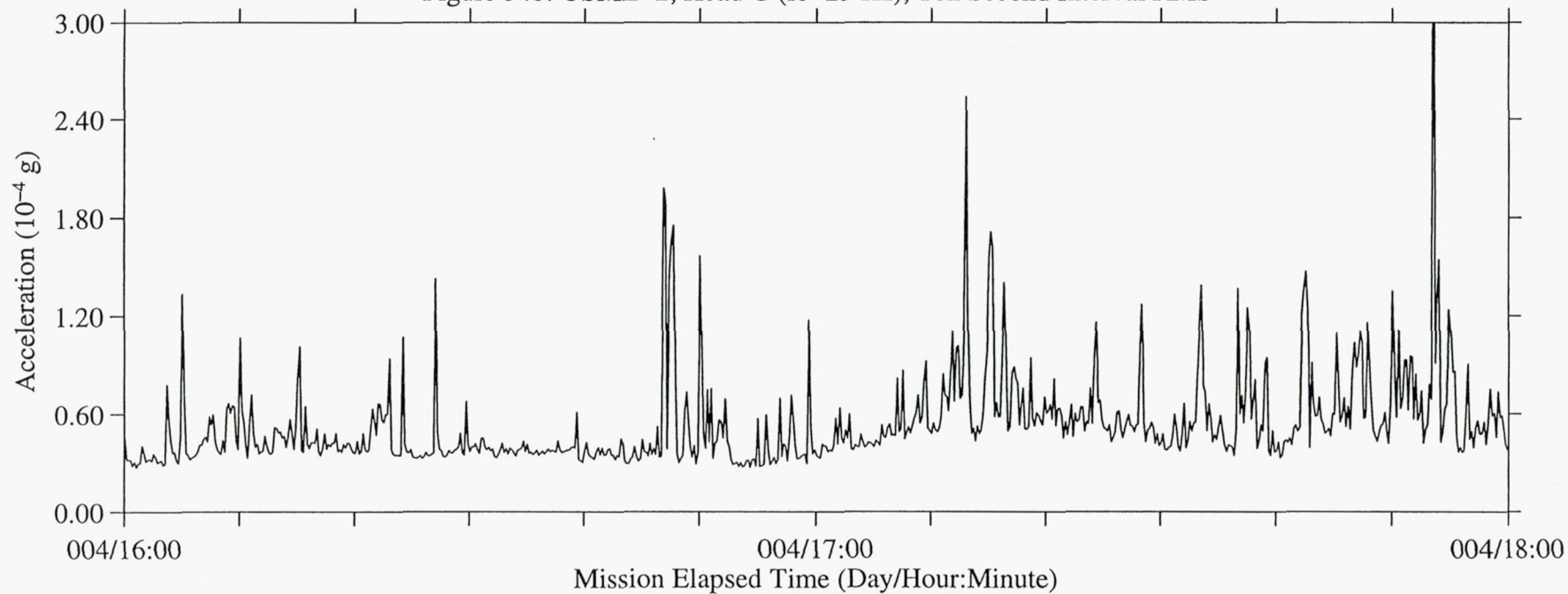




Figure 55a: USML-2, Head C (fc=25 Hz), Ten Second Interval Average

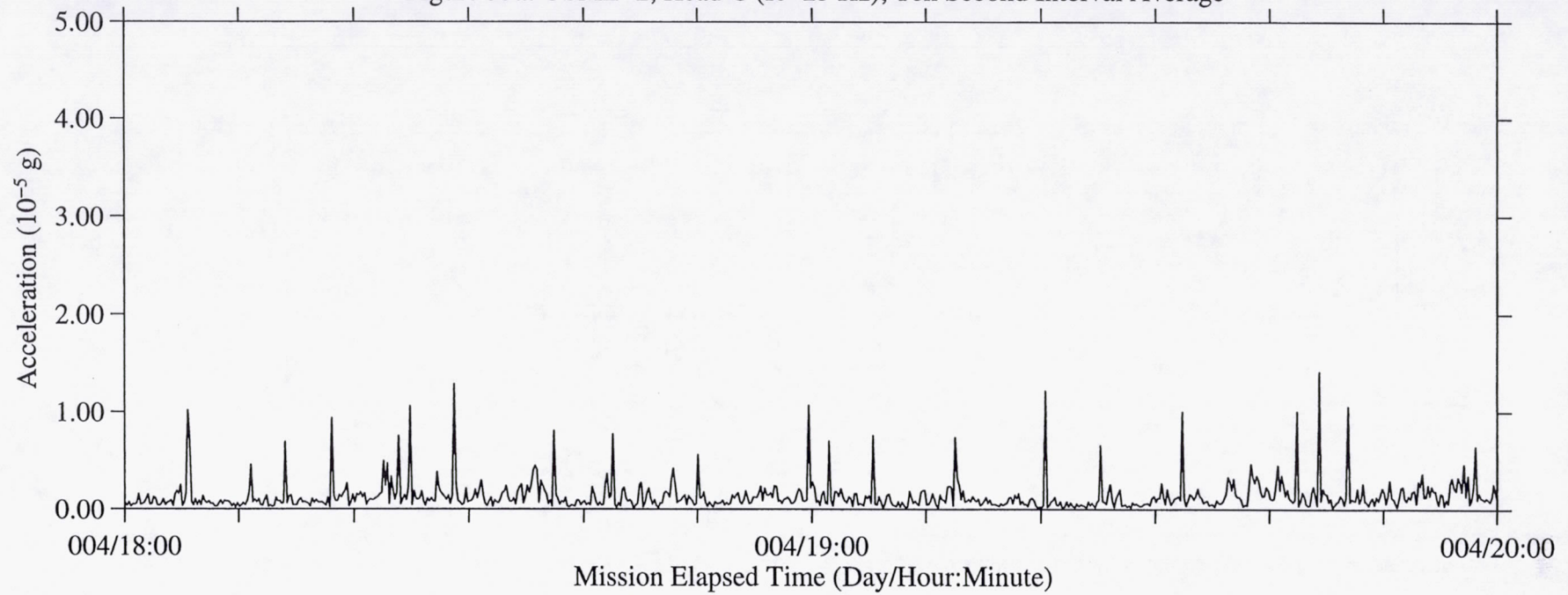


Figure 55b: USML-2, Head C (fc=25 Hz), Ten Second Interval RMS

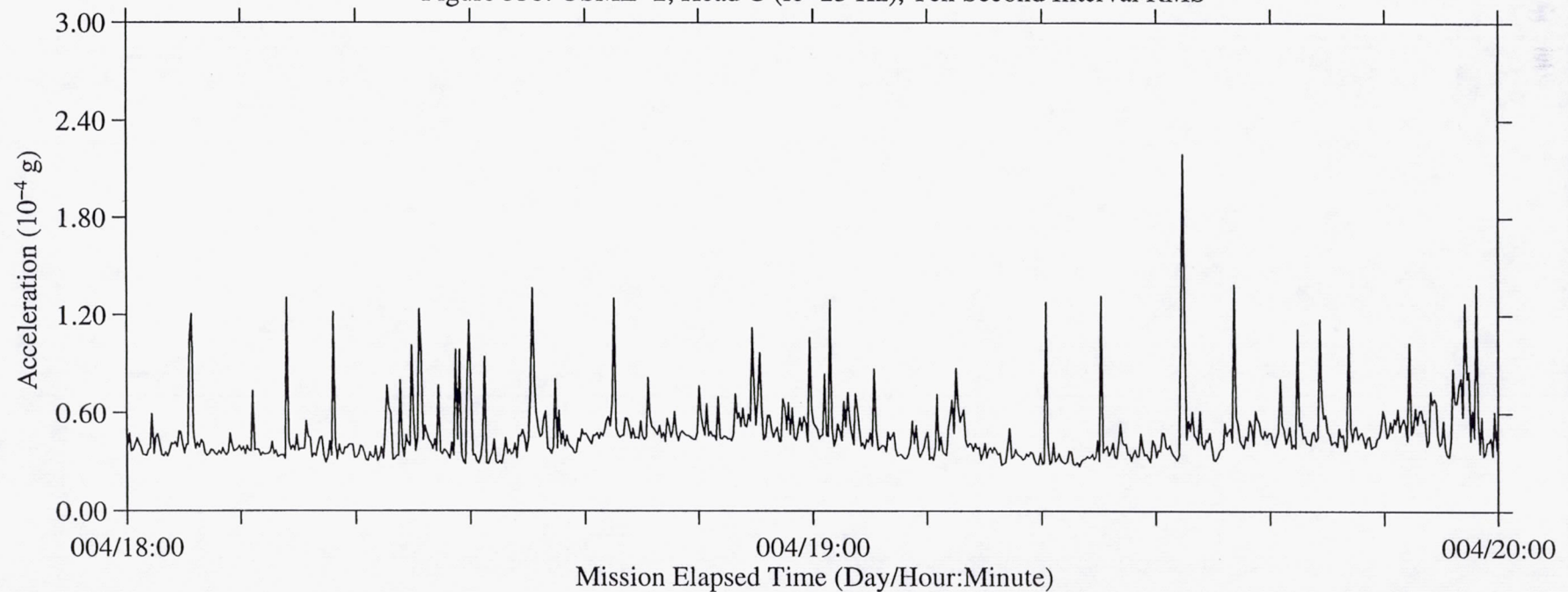


Figure 56a: USML-2, Head C (fc=25 Hz), Ten Second Interval Average

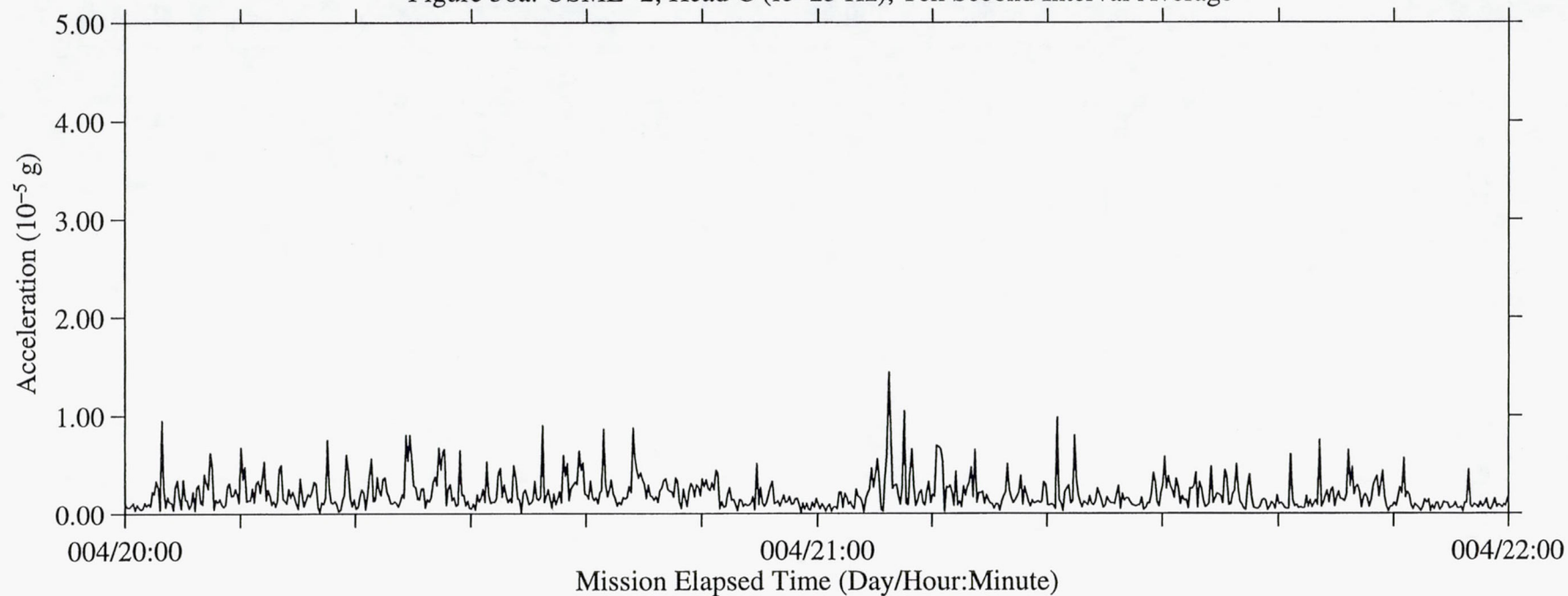


Figure 56b: USML-2, Head C (fc=25 Hz), Ten Second Interval RMS

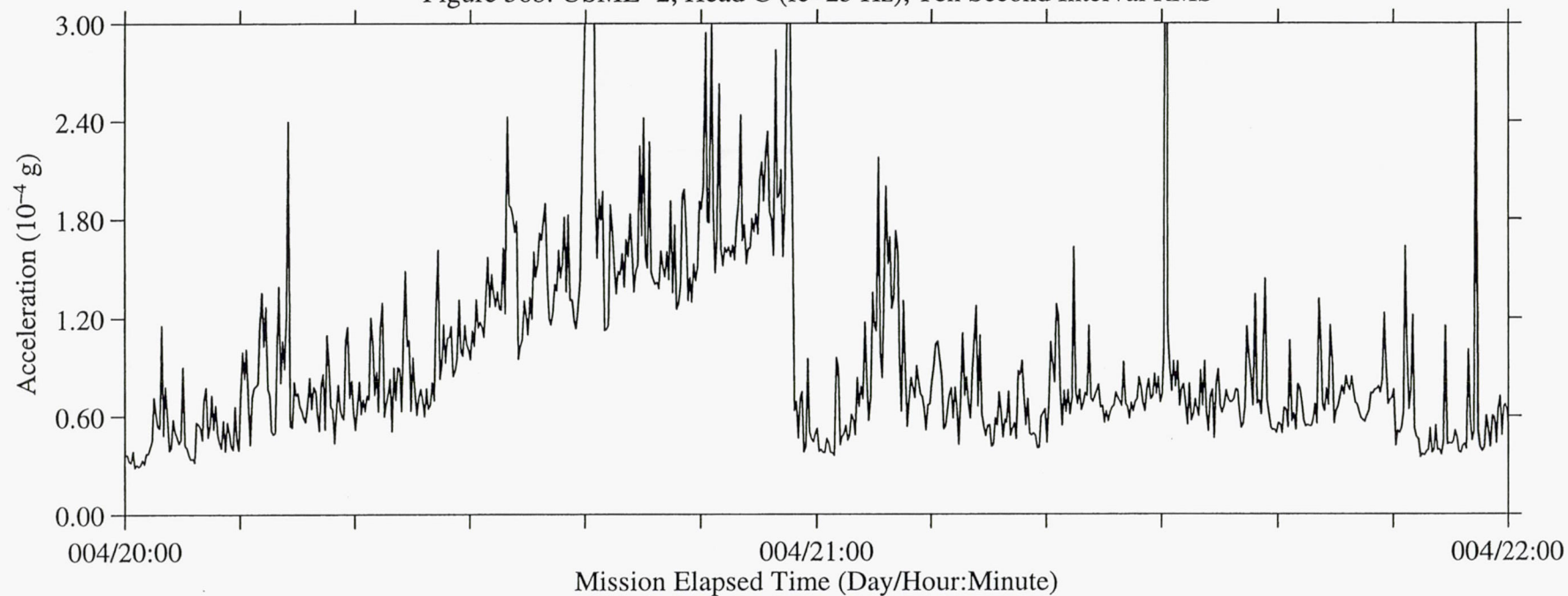




Figure 57a: USML-2, Head C (fc=25 Hz), Ten Second Interval Average

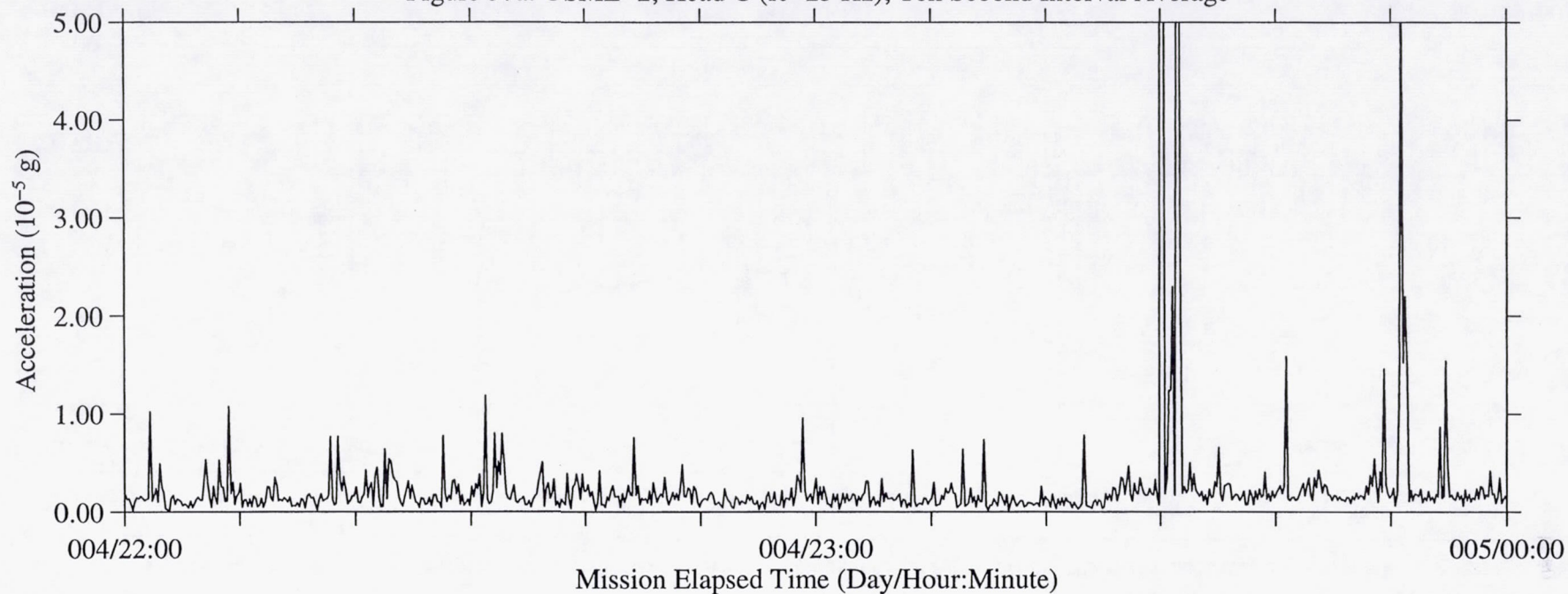


Figure 57b: USML-2, Head C (fc=25 Hz), Ten Second Interval RMS

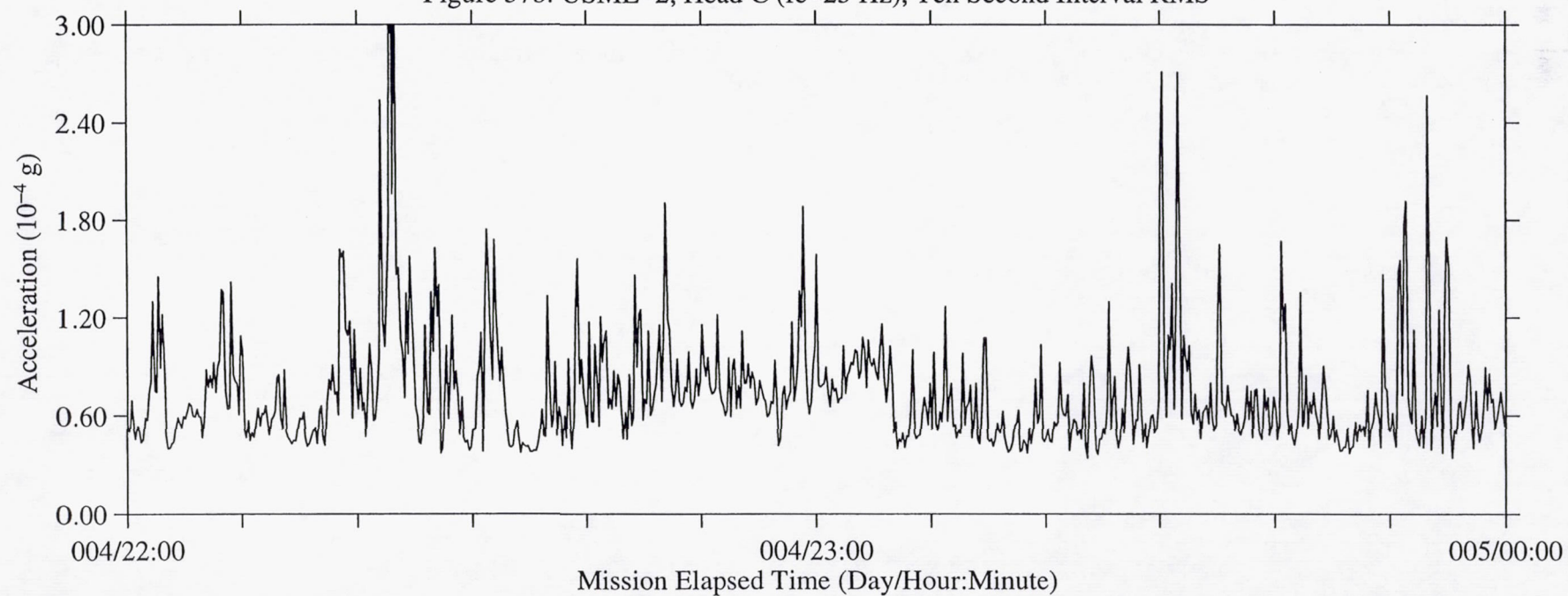


Figure 58a: USML-2, Head C (fc=25 Hz), Ten Second Interval Average

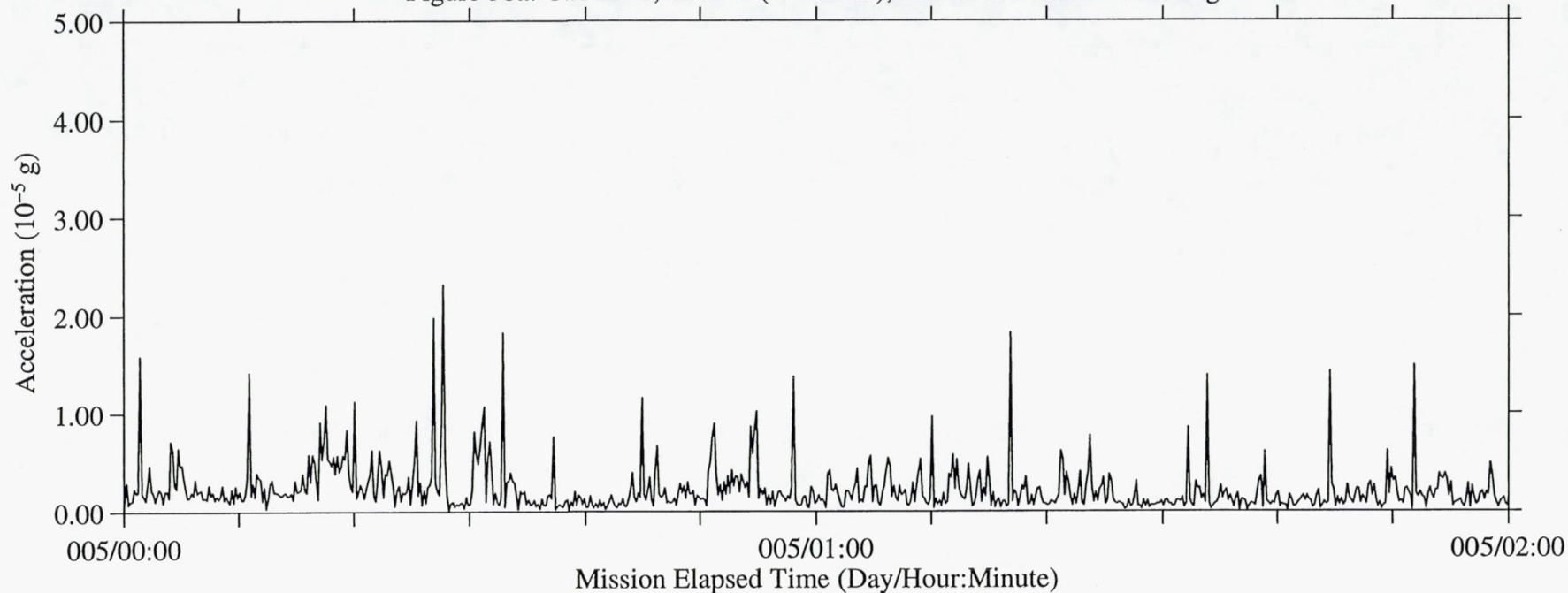
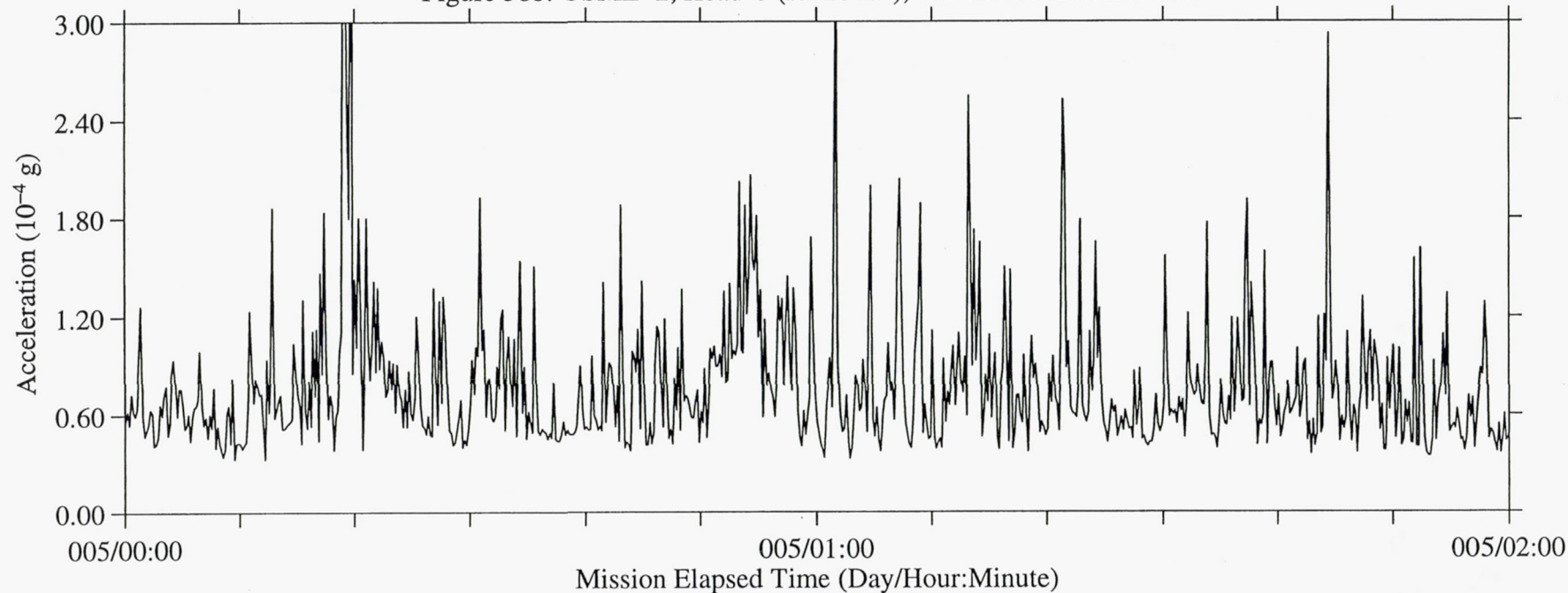


Figure 58b: USML-2, Head C (fc=25 Hz), Ten Second Interval RMS





B-61

Figure 59a: USML-2, Head C (fc=25 Hz), Ten Second Interval Average

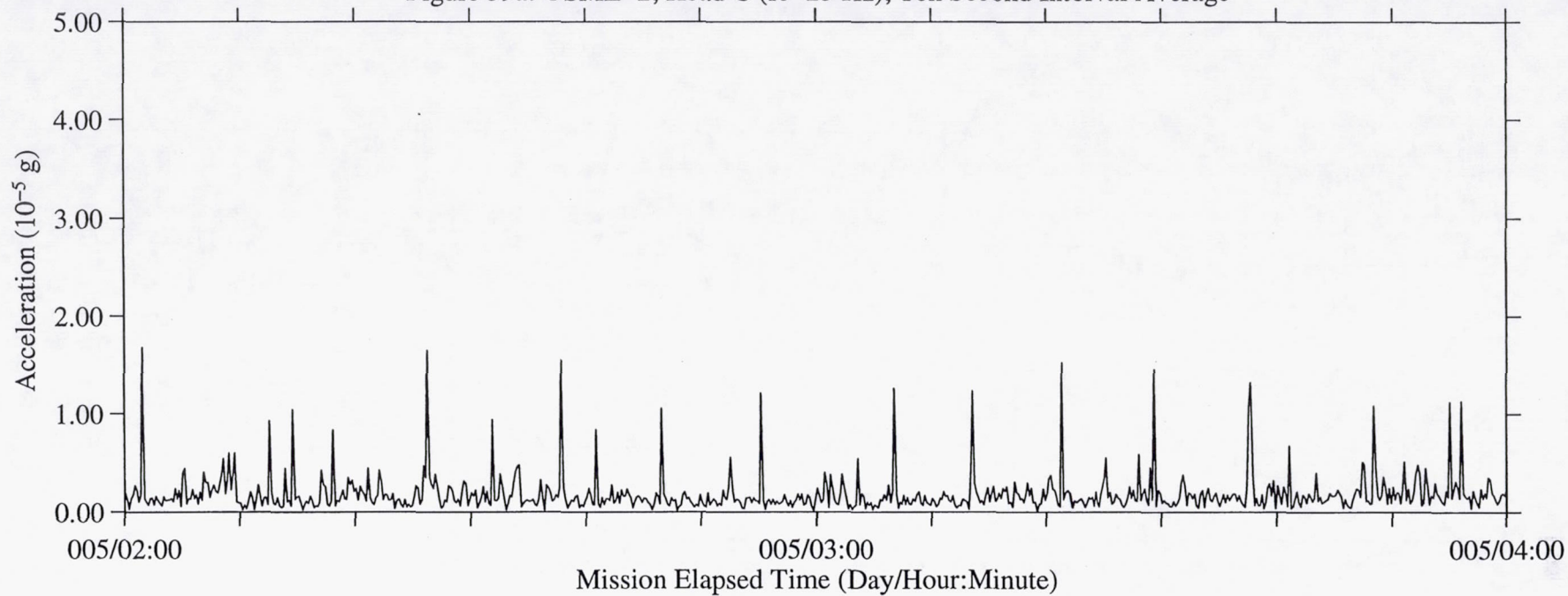


Figure 59b: USML-2, Head C (fc=25 Hz), Ten Second Interval RMS

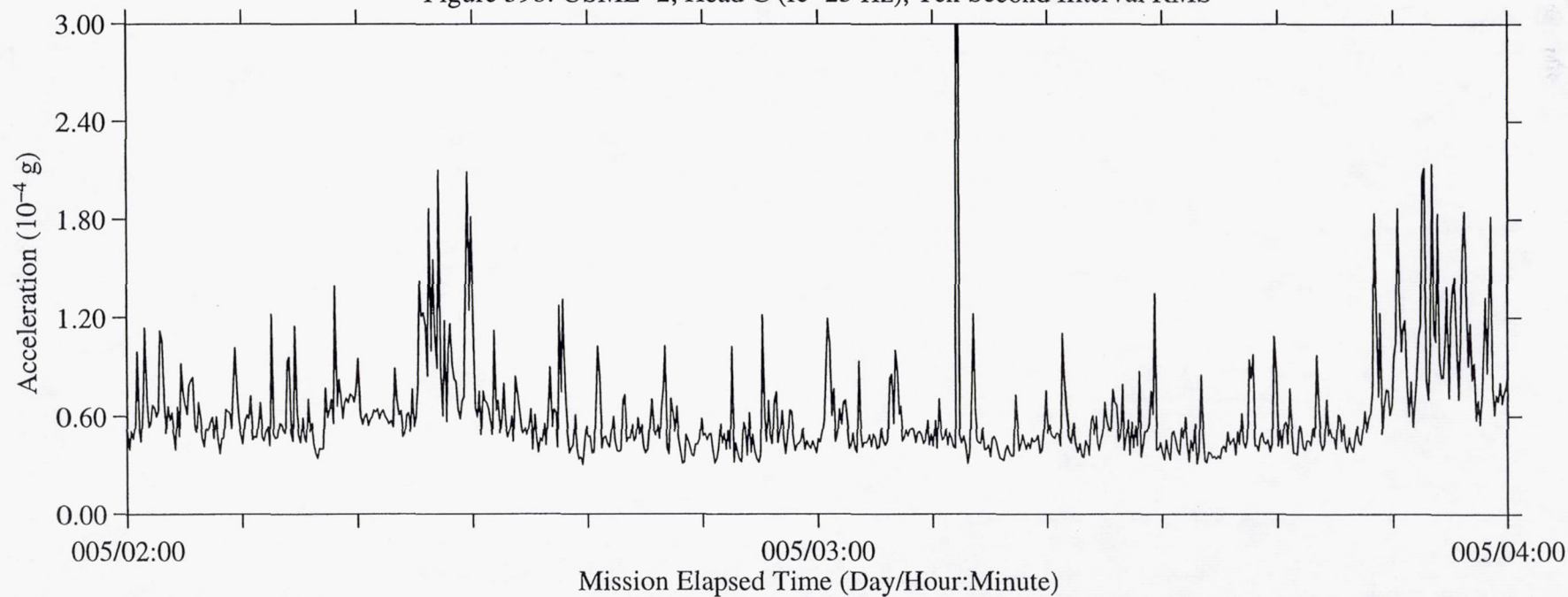


Figure 60a: USML-2, Head C (fc=25 Hz), Ten Second Interval Average

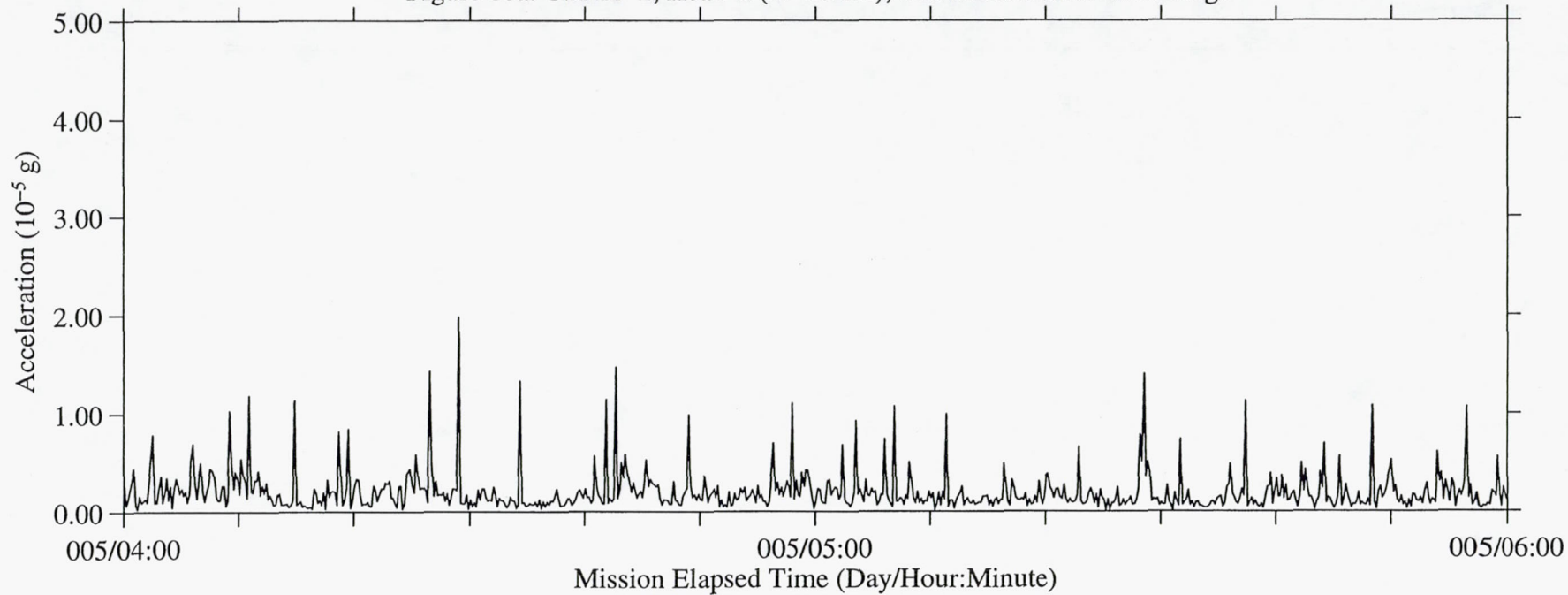


Figure 60b: USML-2, Head C (fc=25 Hz), Ten Second Interval RMS

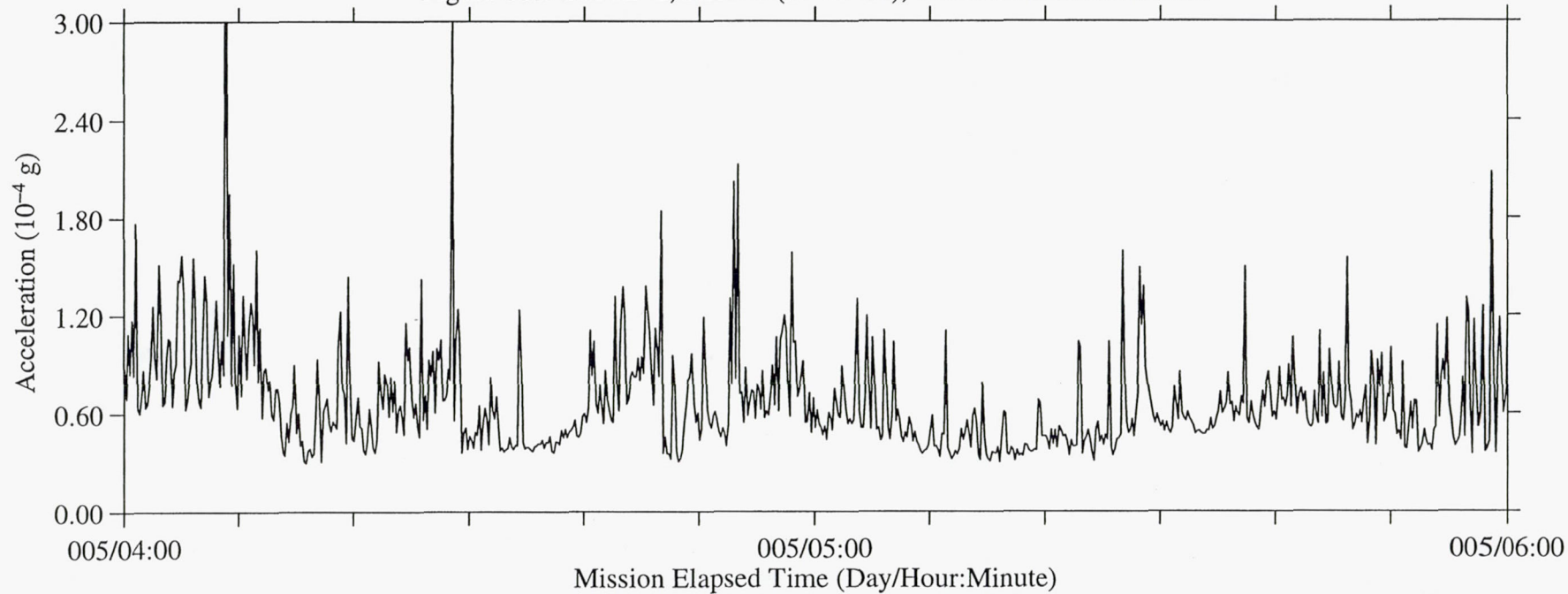




Figure 61a: USML-2, Head C (fc=25 Hz), Ten Second Interval Average

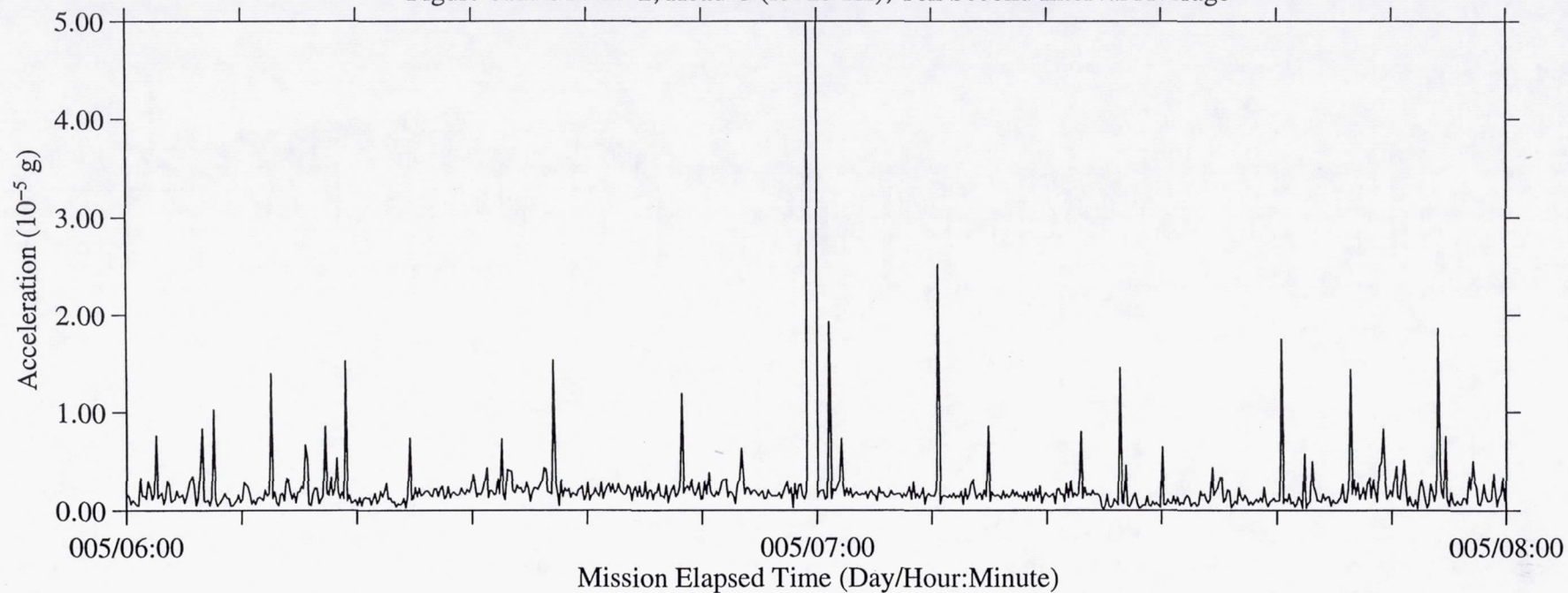


Figure 61b: USML-2, Head C (fc=25 Hz), Ten Second Interval RMS

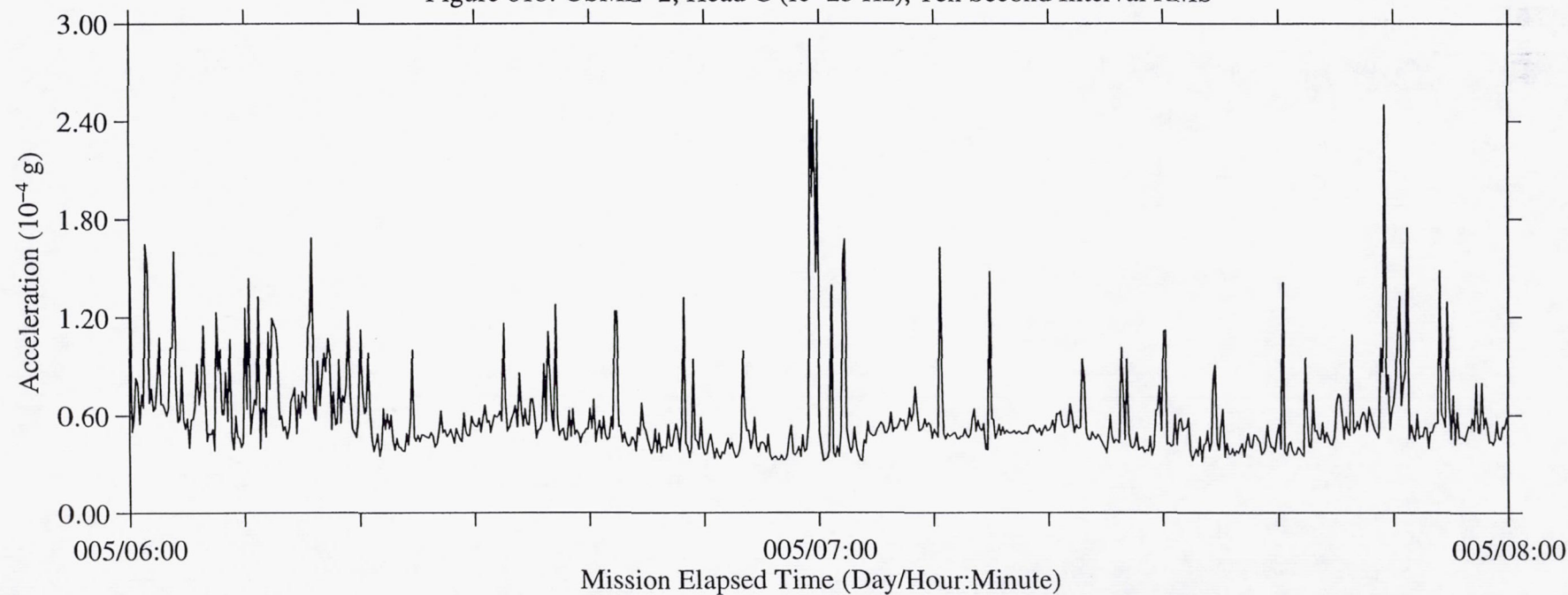


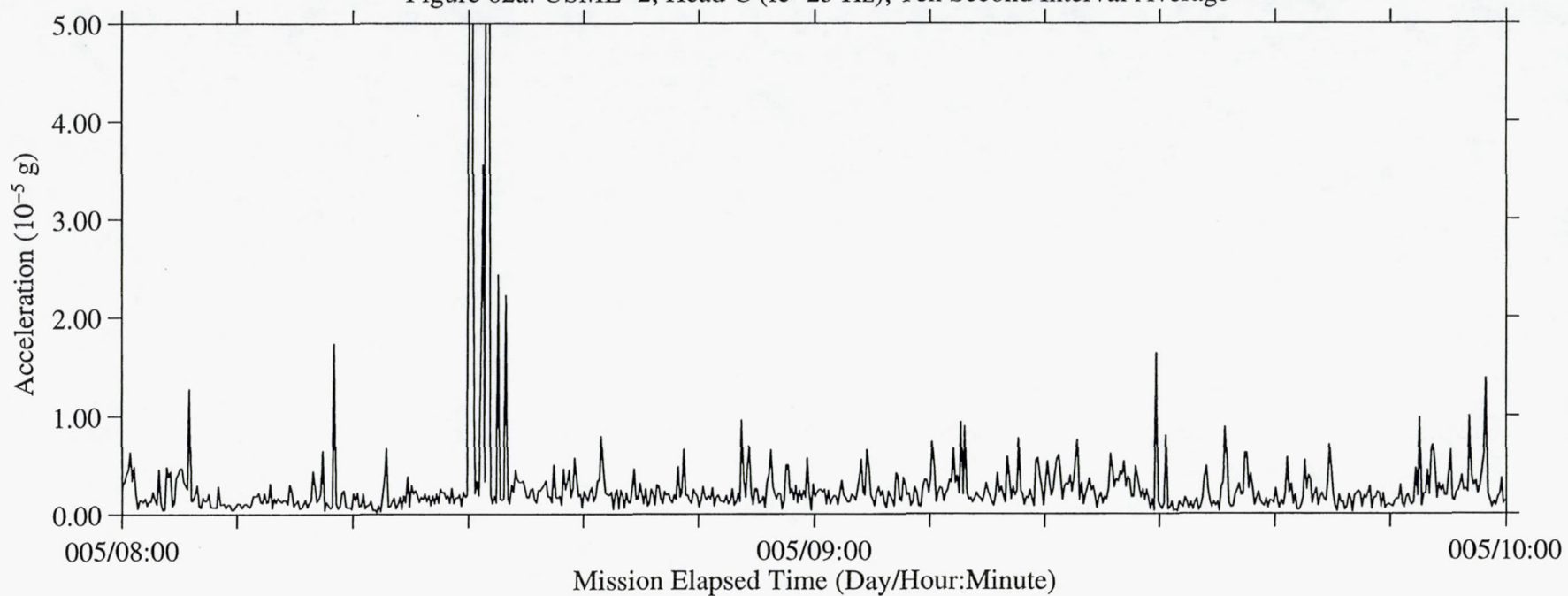
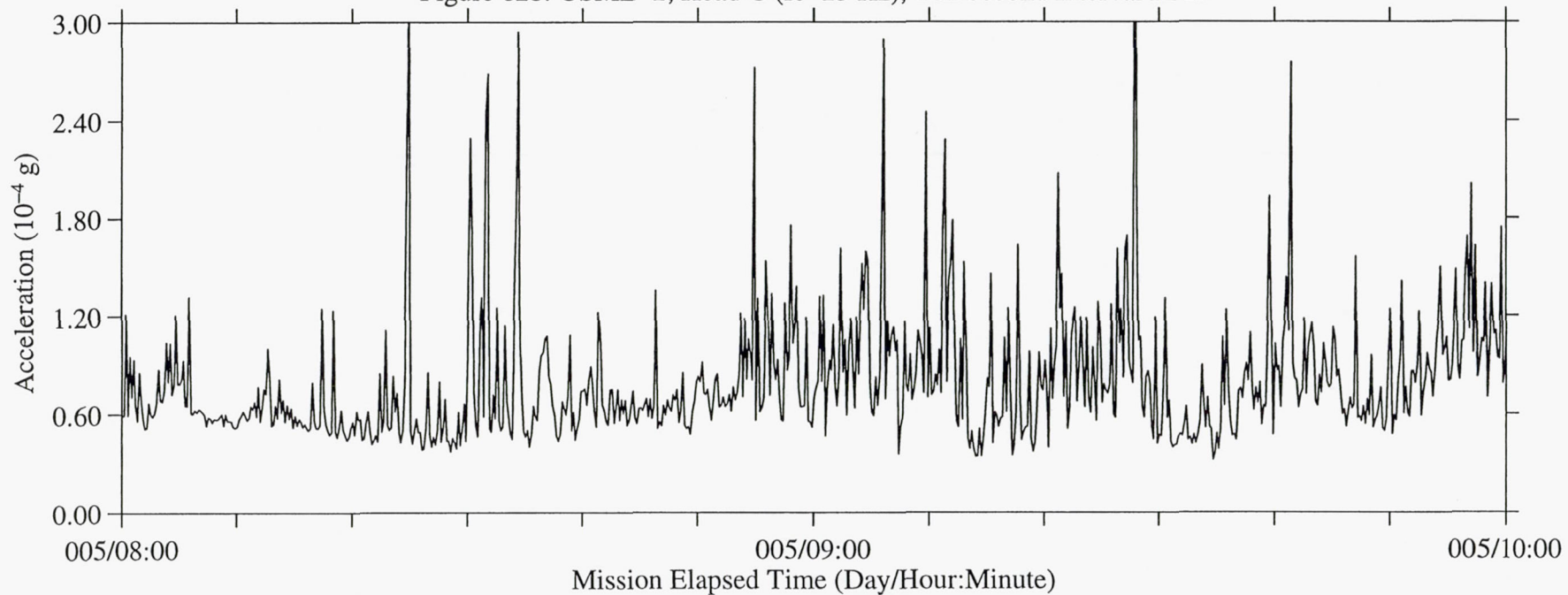
Figure 62a: USML-2, Head C ( $f_c=25$  Hz), Ten Second Interval AverageFigure 62b: USML-2, Head C ( $f_c=25$  Hz), Ten Second Interval RMS



Figure 63a: USML-2, Head C (fc=25 Hz), Ten Second Interval Average

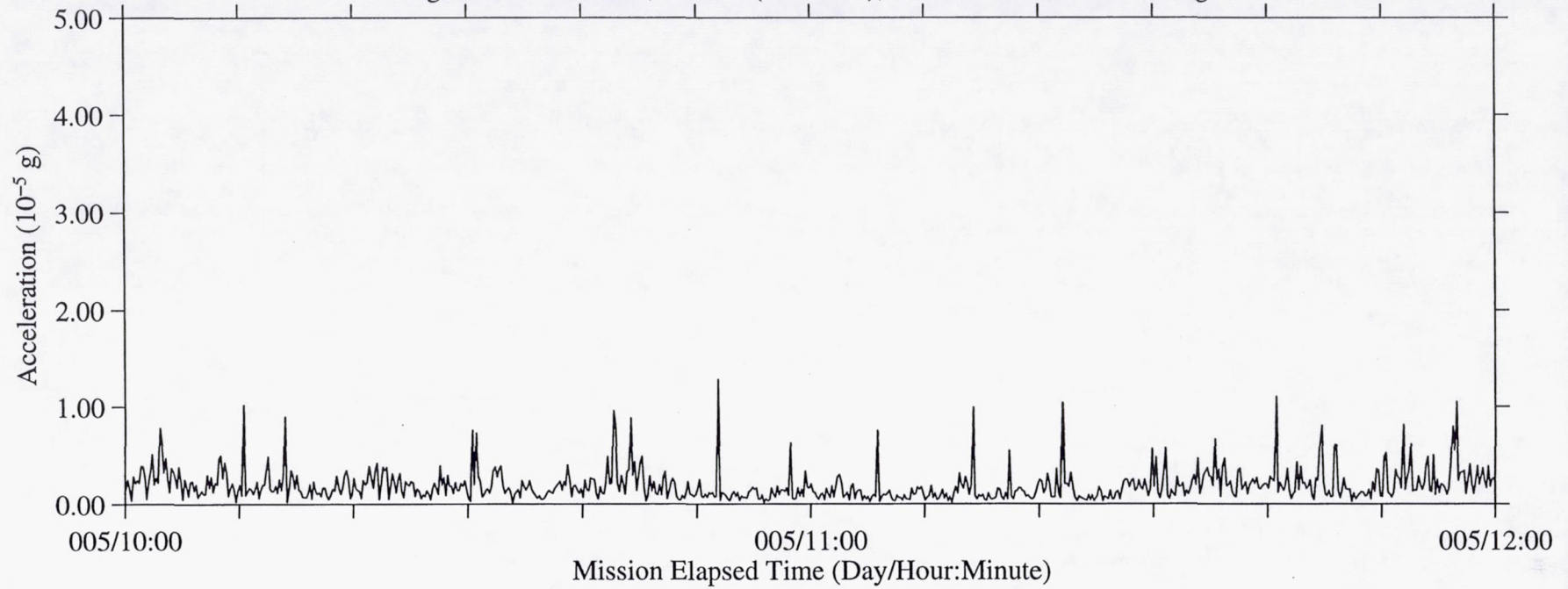


Figure 63b: USML-2, Head C (fc=25 Hz), Ten Second Interval RMS

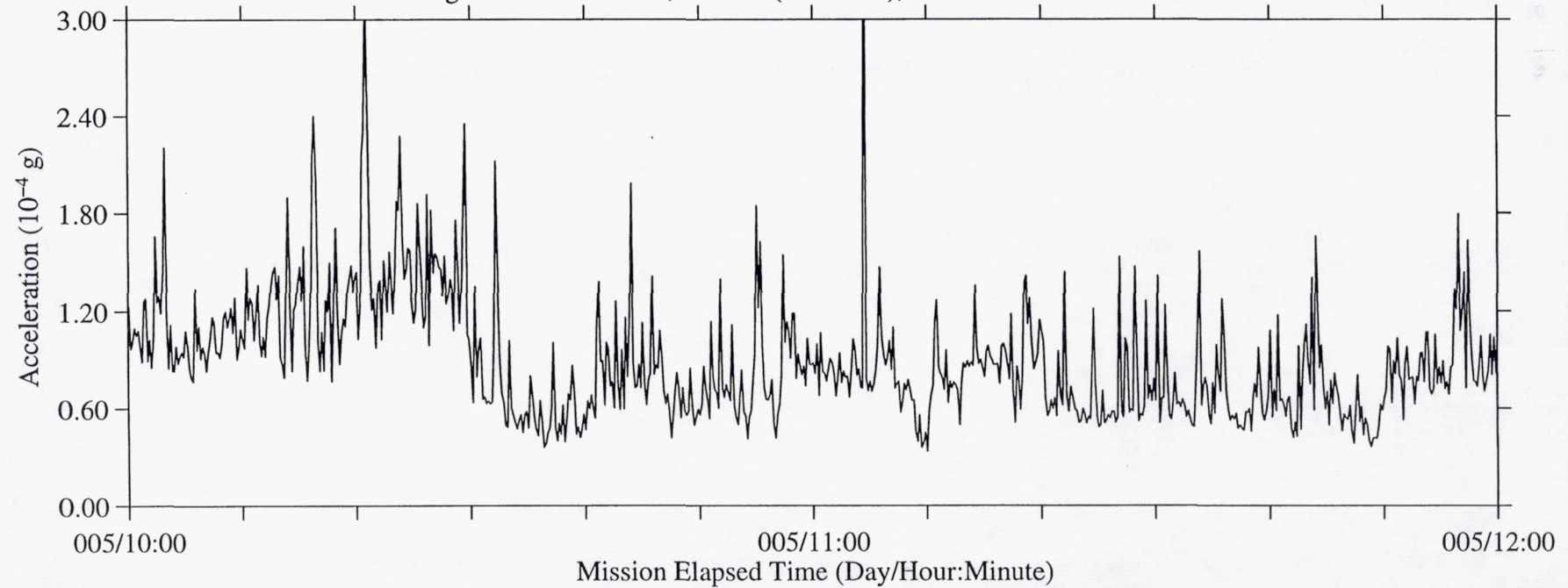


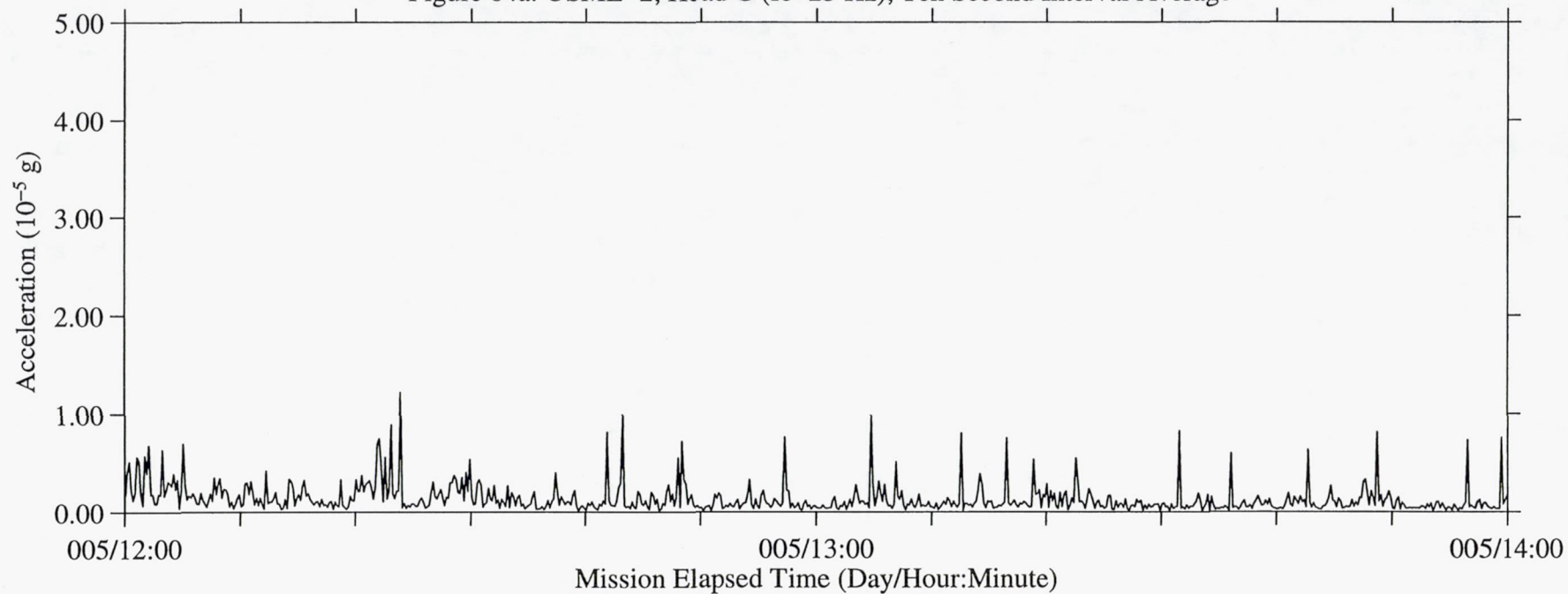
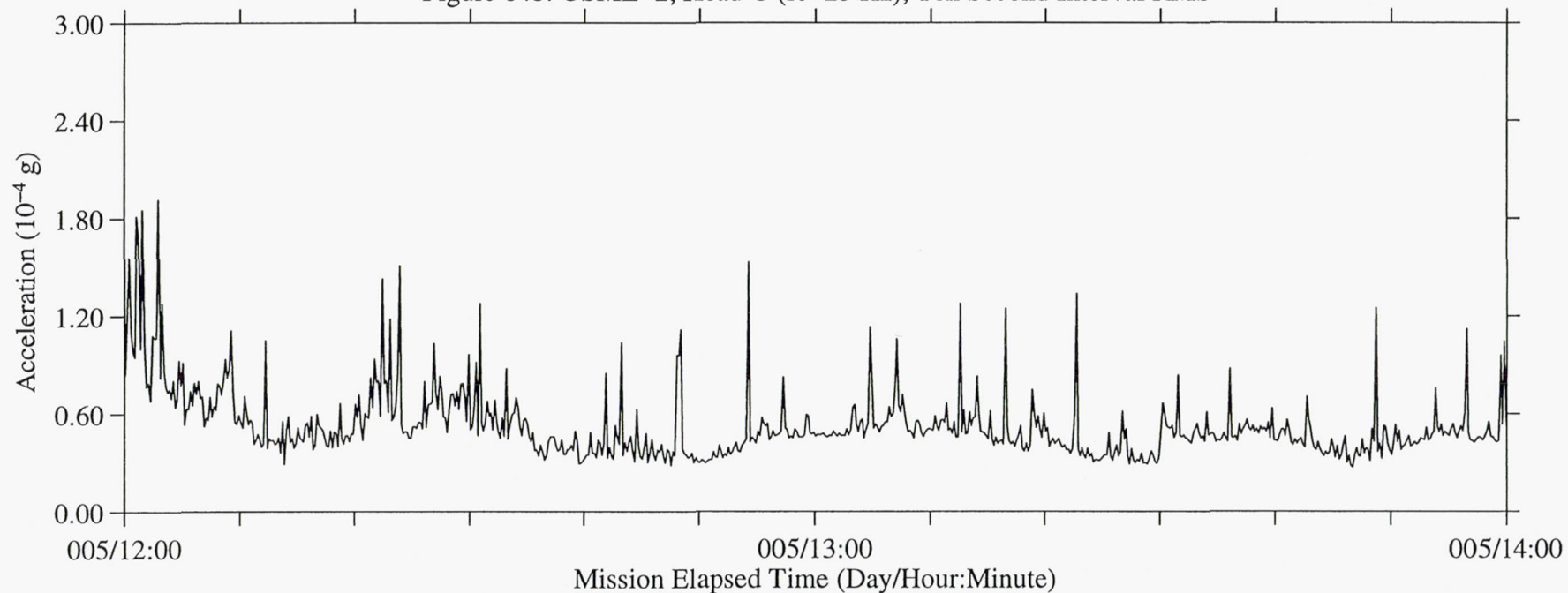
Figure 64a: USML-2, Head C ( $f_c=25$  Hz), Ten Second Interval AverageFigure 64b: USML-2, Head C ( $f_c=25$  Hz), Ten Second Interval RMS



Figure 65a: USML-2, Head C (fc=25 Hz), Ten Second Interval Average

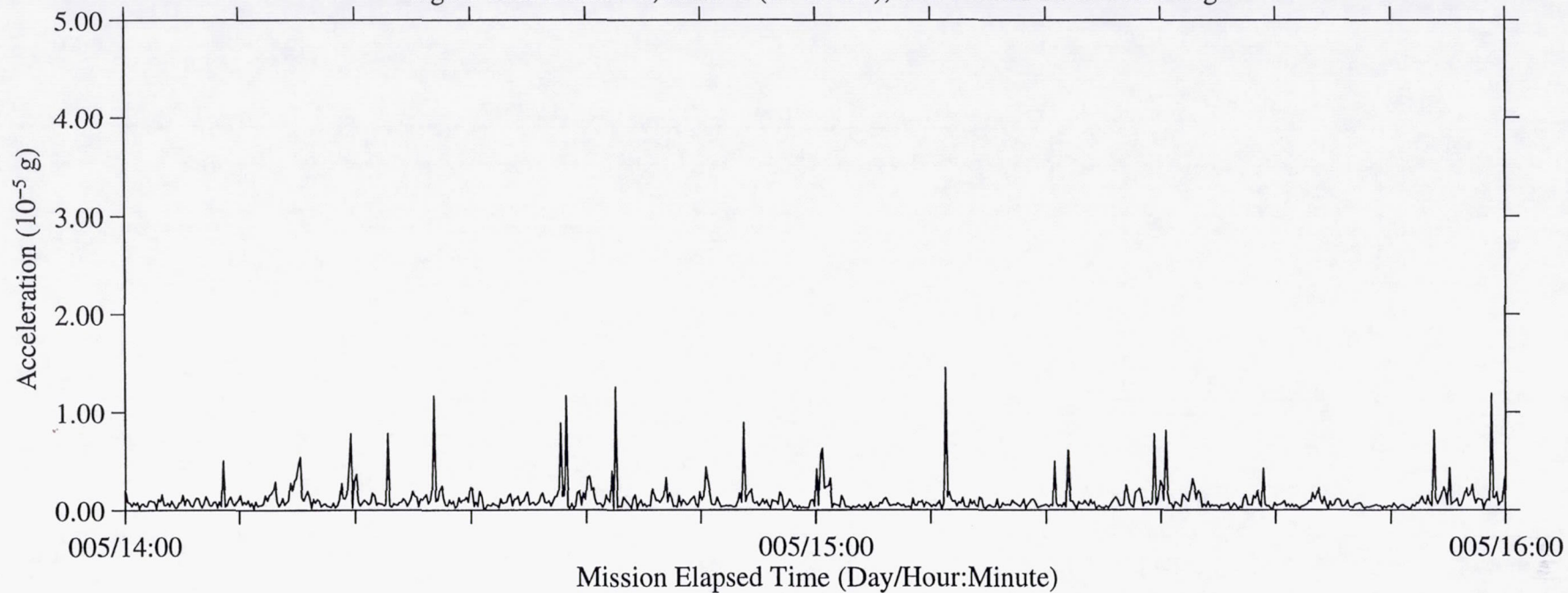


Figure 65b: USML-2, Head C (fc=25 Hz), Ten Second Interval RMS

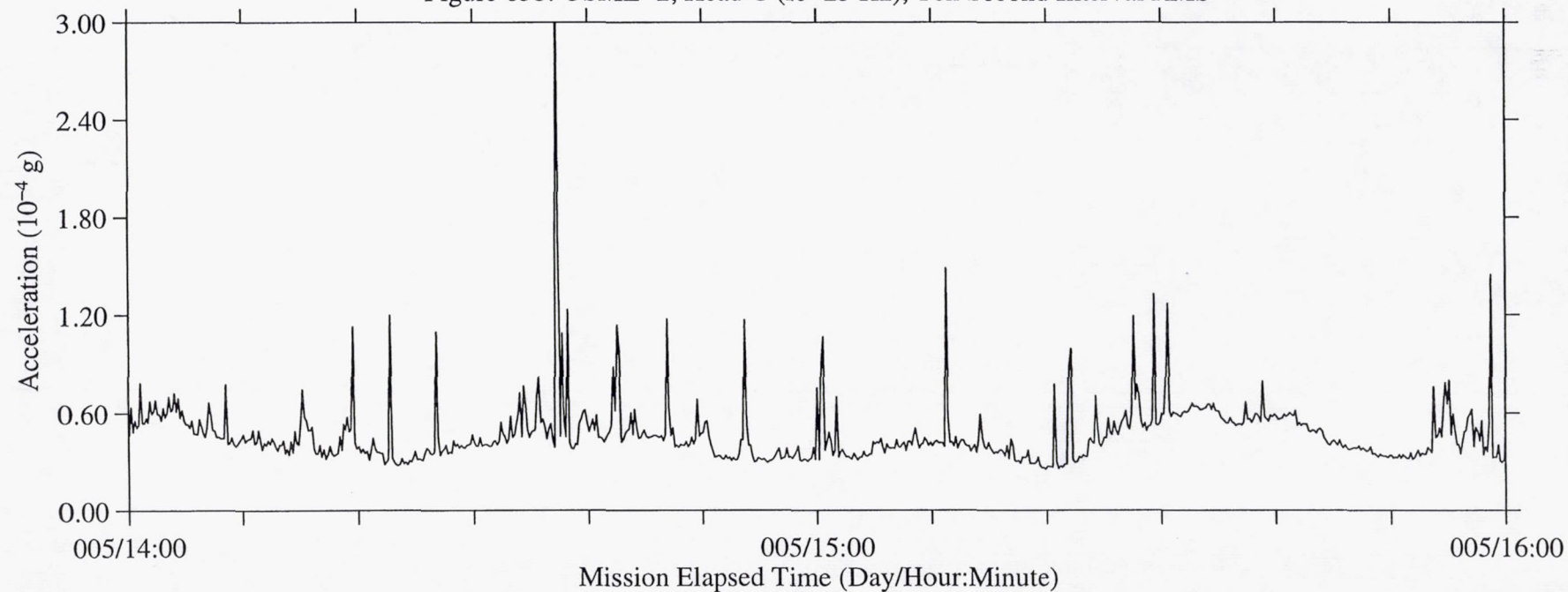
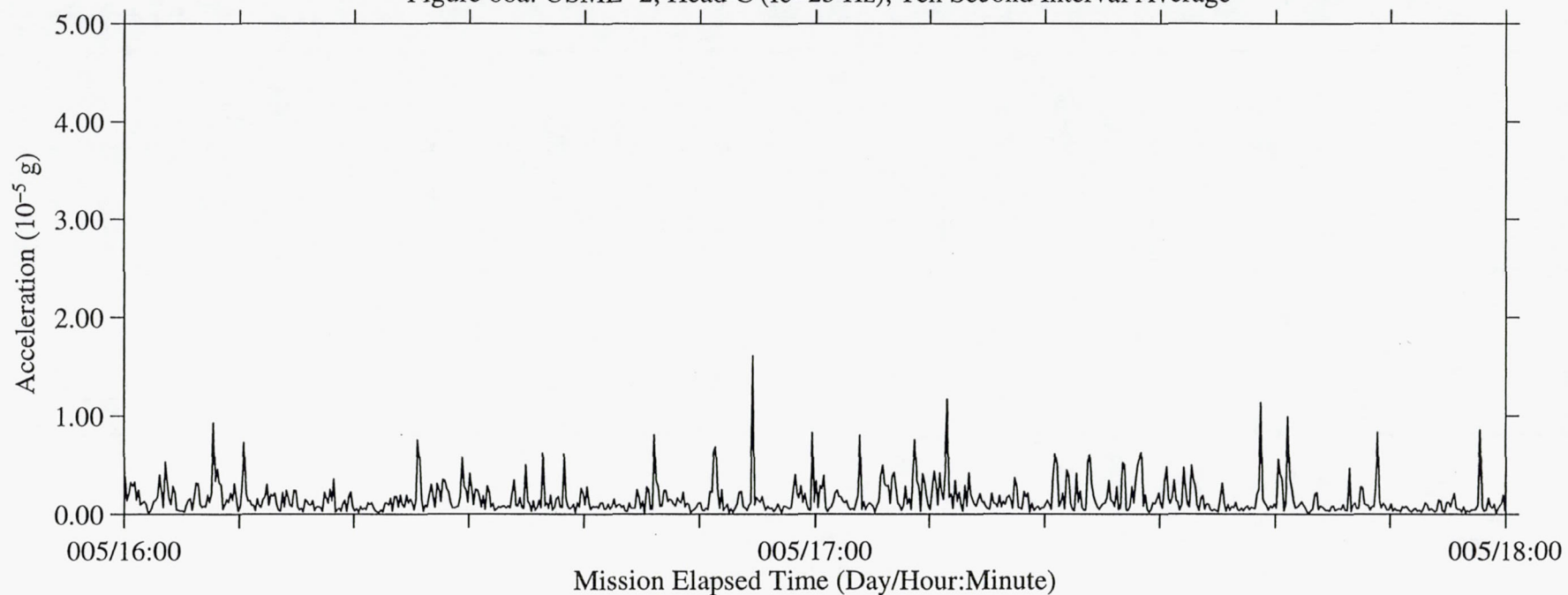
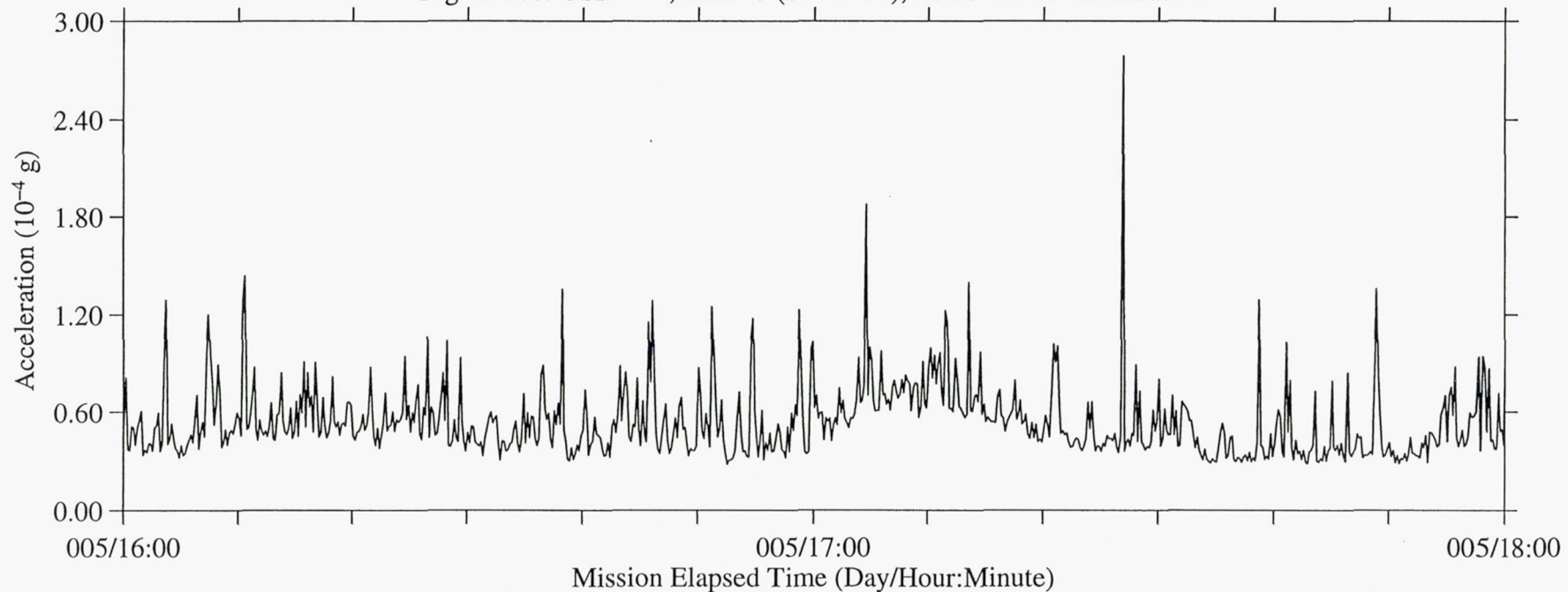


Figure 66a: USML-2, Head C ( $f_c=25$  Hz), Ten Second Interval AverageFigure 66b: USML-2, Head C ( $f_c=25$  Hz), Ten Second Interval RMS



B-69

Figure 67a: USML-2, Head C (fc=25 Hz), Ten Second Interval Average

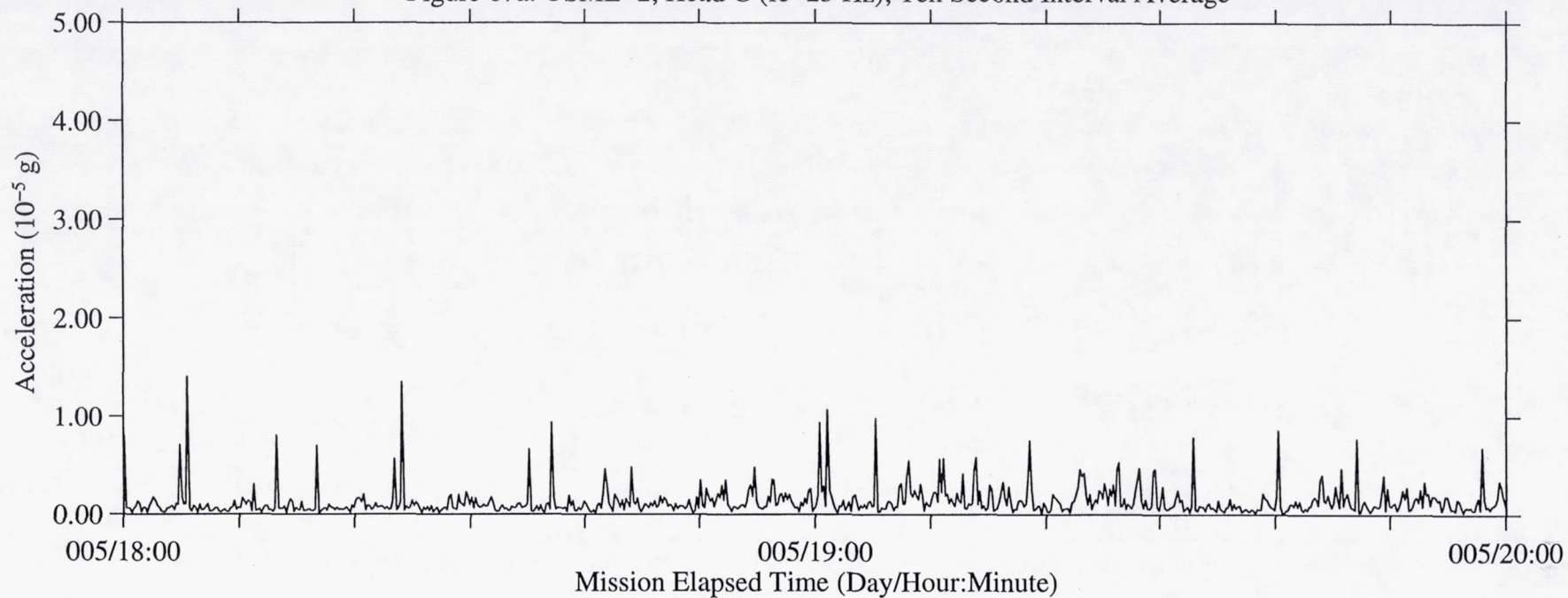


Figure 67b: USML-2, Head C (fc=25 Hz), Ten Second Interval RMS

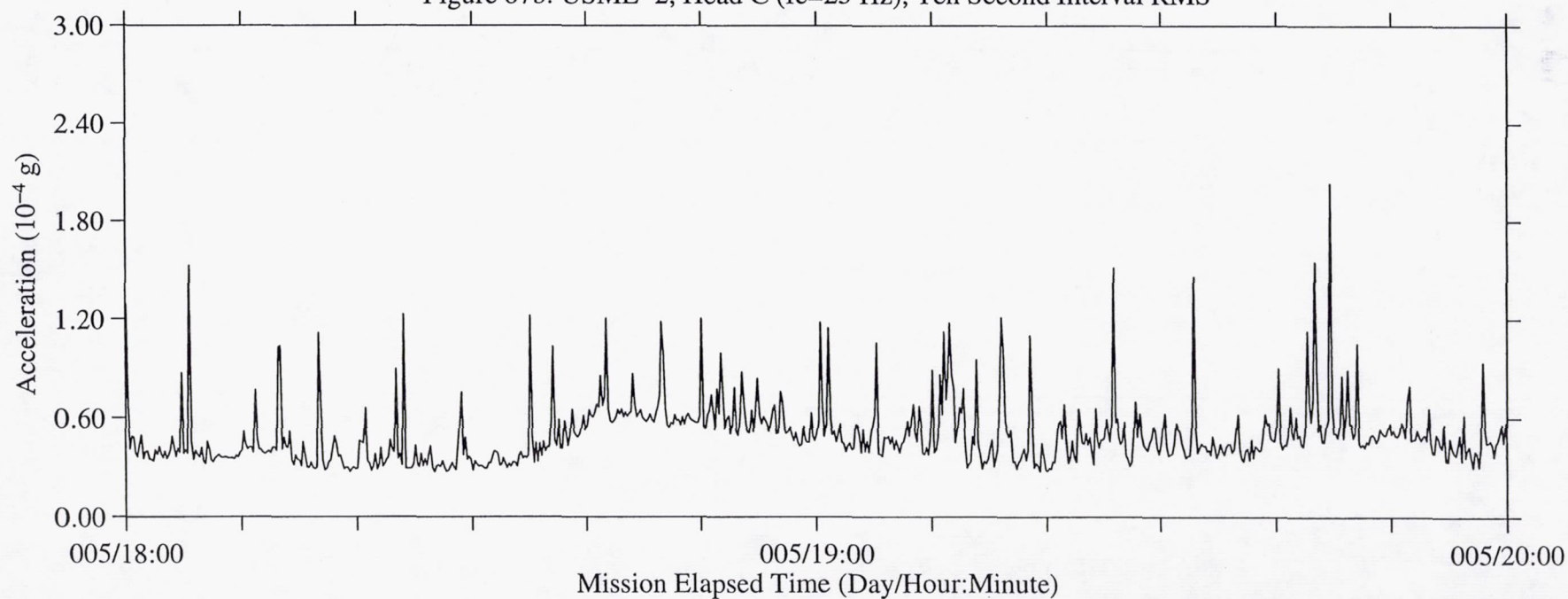


Figure 68a: USML-2, Head C (fc=25 Hz), Ten Second Interval Average

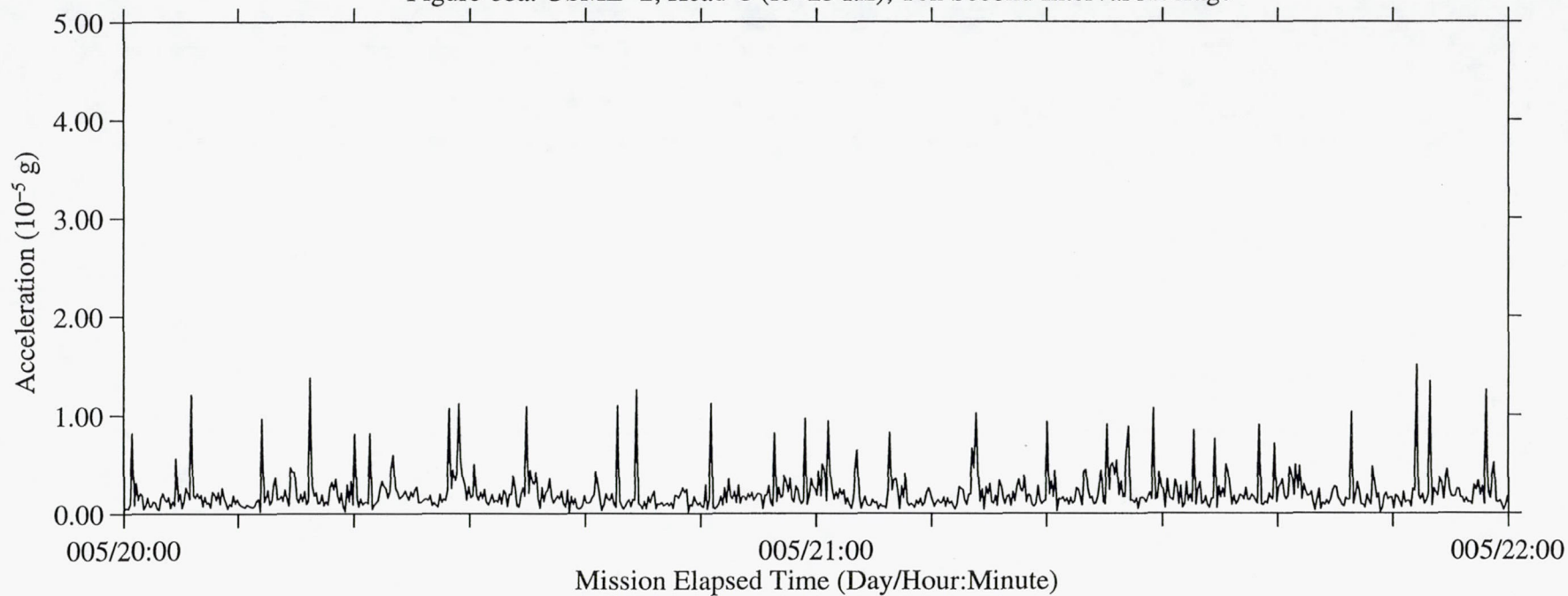


Figure 68b: USML-2, Head C (fc=25 Hz), Ten Second Interval RMS

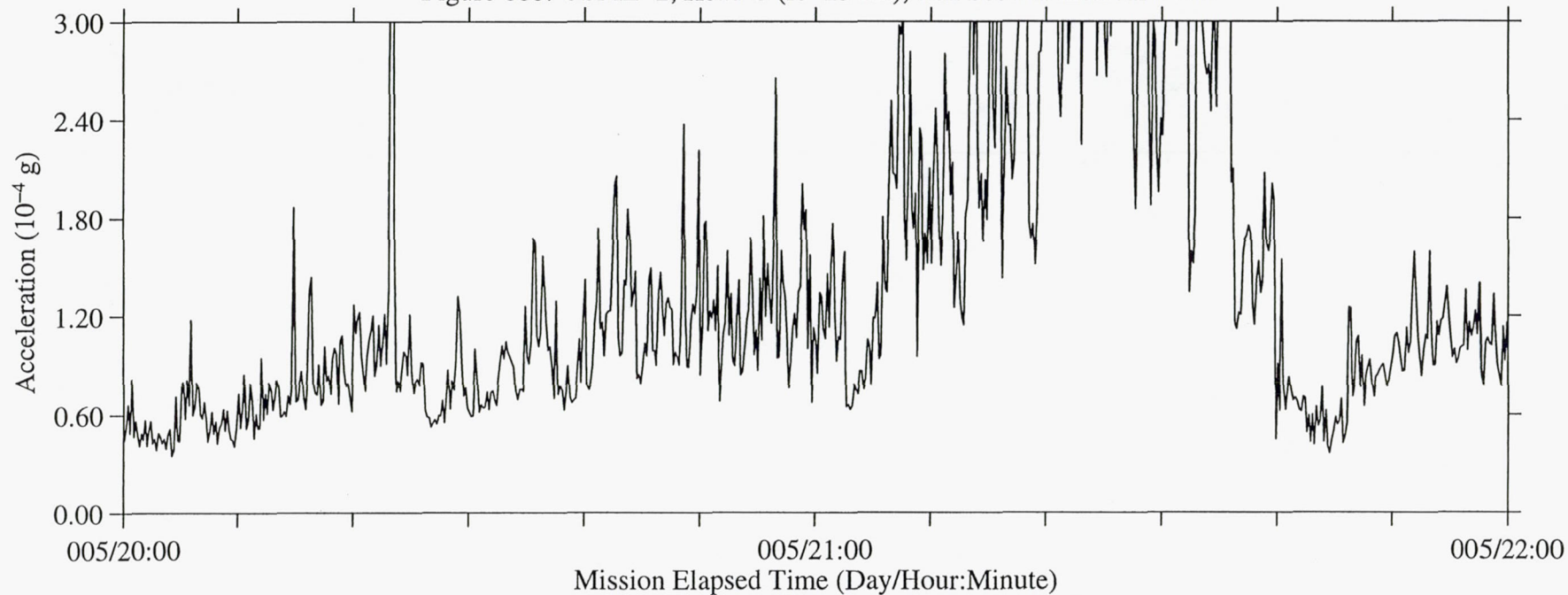




Figure 69a: USML-2, Head C (fc=25 Hz), Ten Second Interval Average

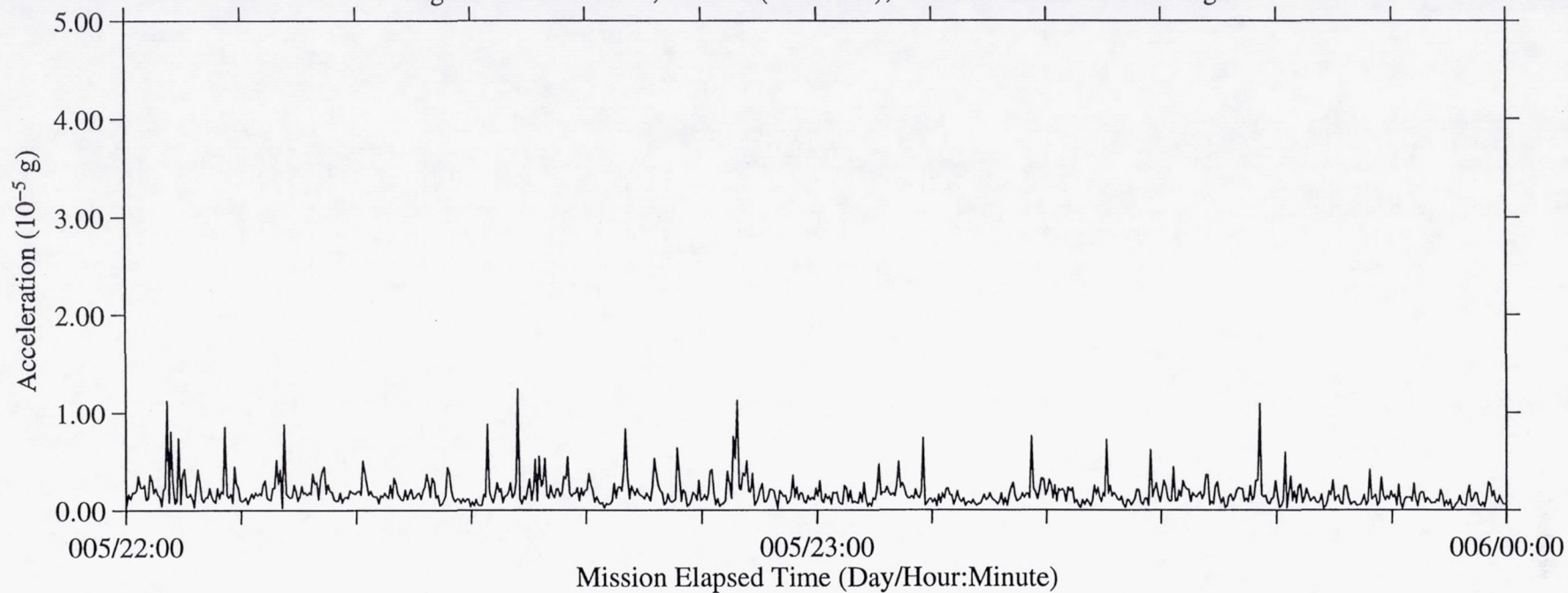


Figure 69b: USML-2, Head C (fc=25 Hz), Ten Second Interval RMS

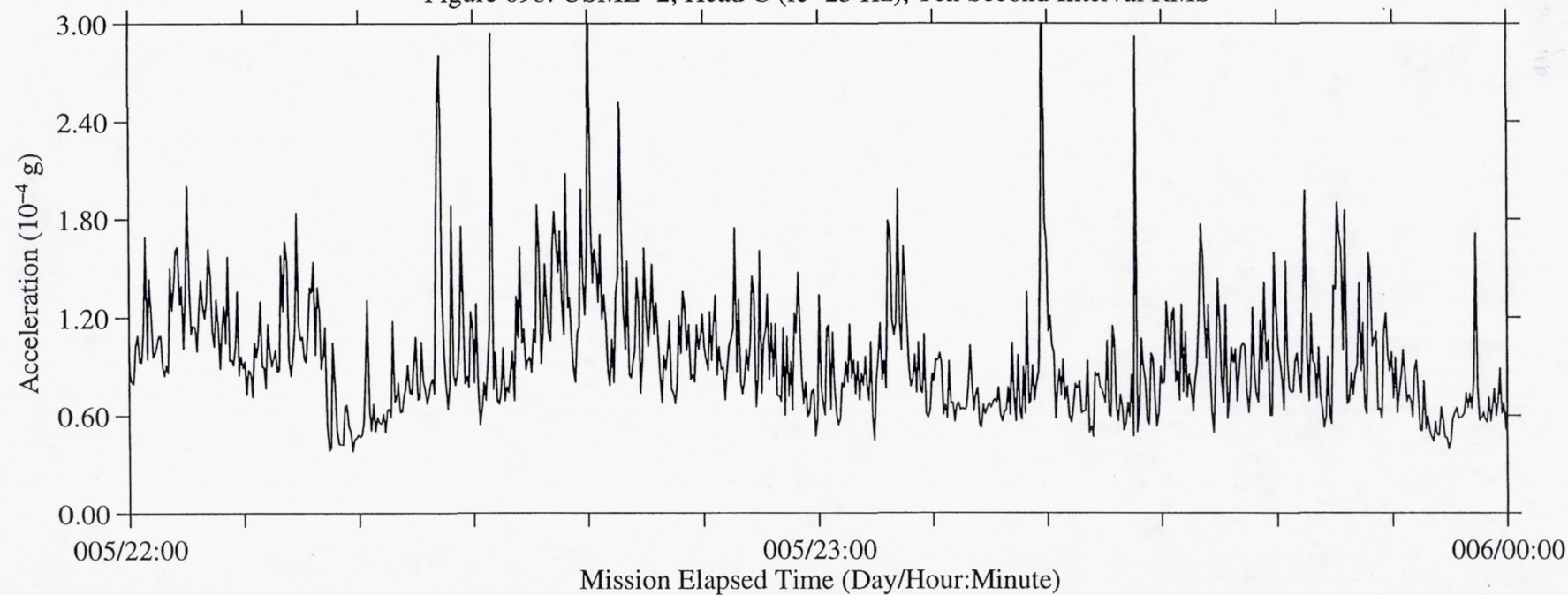


Figure 70a: USML-2, Head C (fc=25 Hz), Ten Second Interval Average

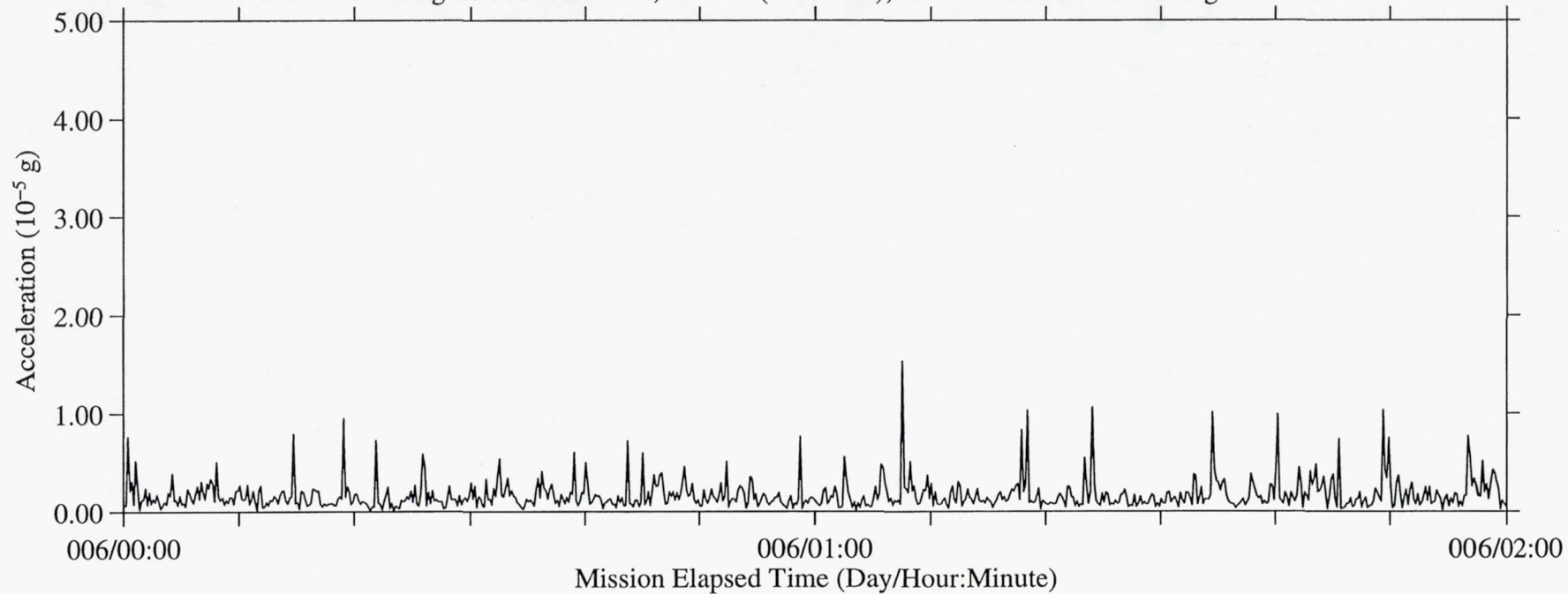


Figure 70b: USML-2, Head C (fc=25 Hz), Ten Second Interval RMS

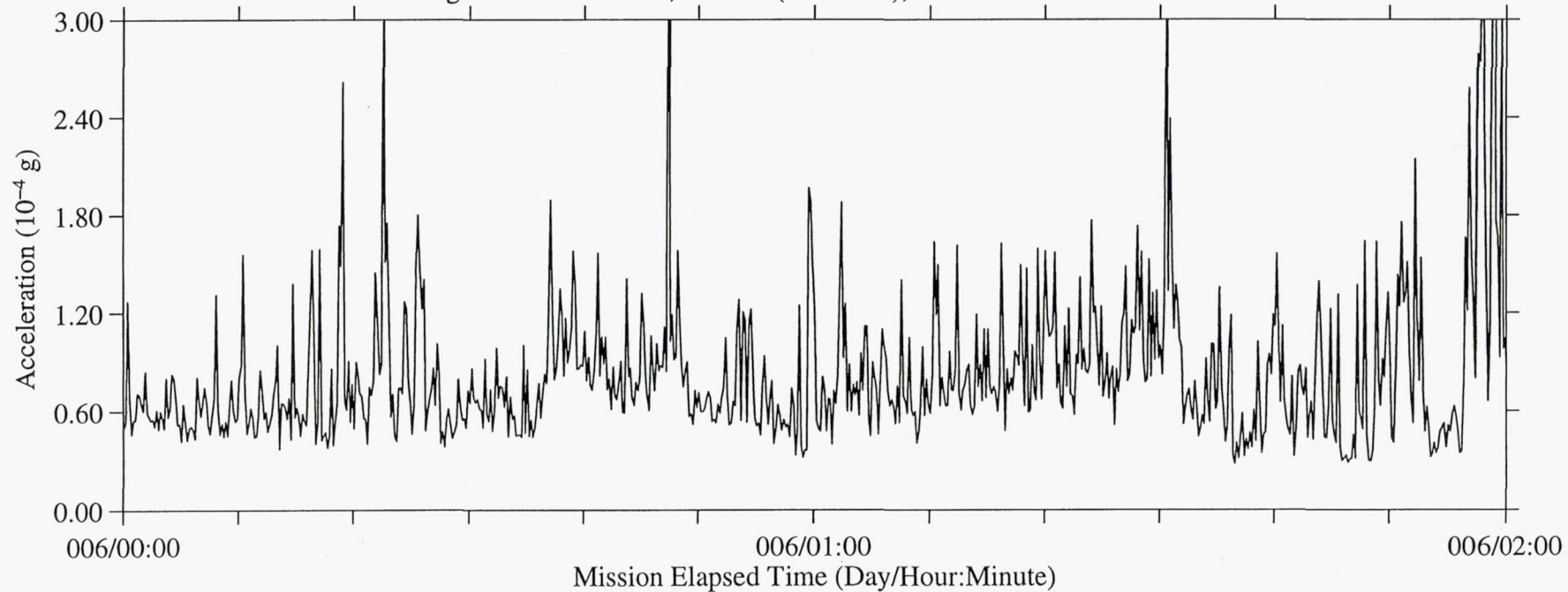




Figure 71a: USML-2, Head C (fc=25 Hz), Ten Second Interval Average

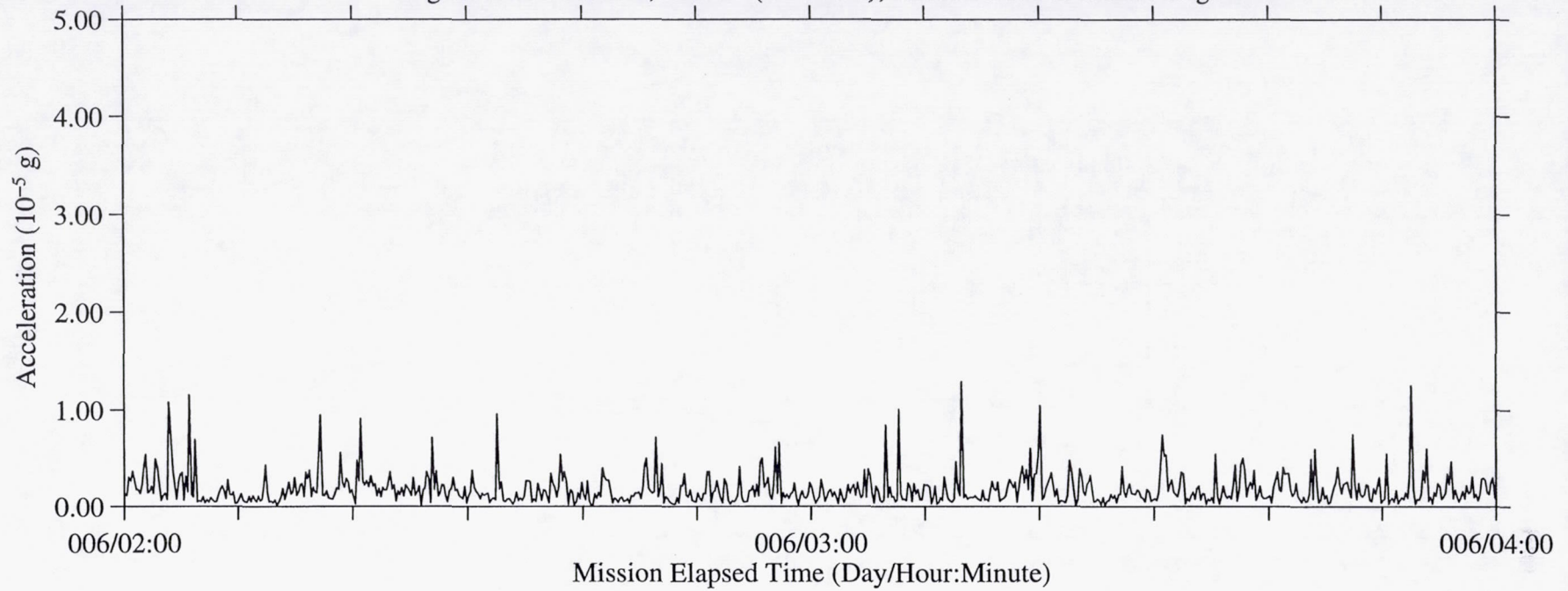


Figure 71b: USML-2, Head C (fc=25 Hz), Ten Second Interval RMS

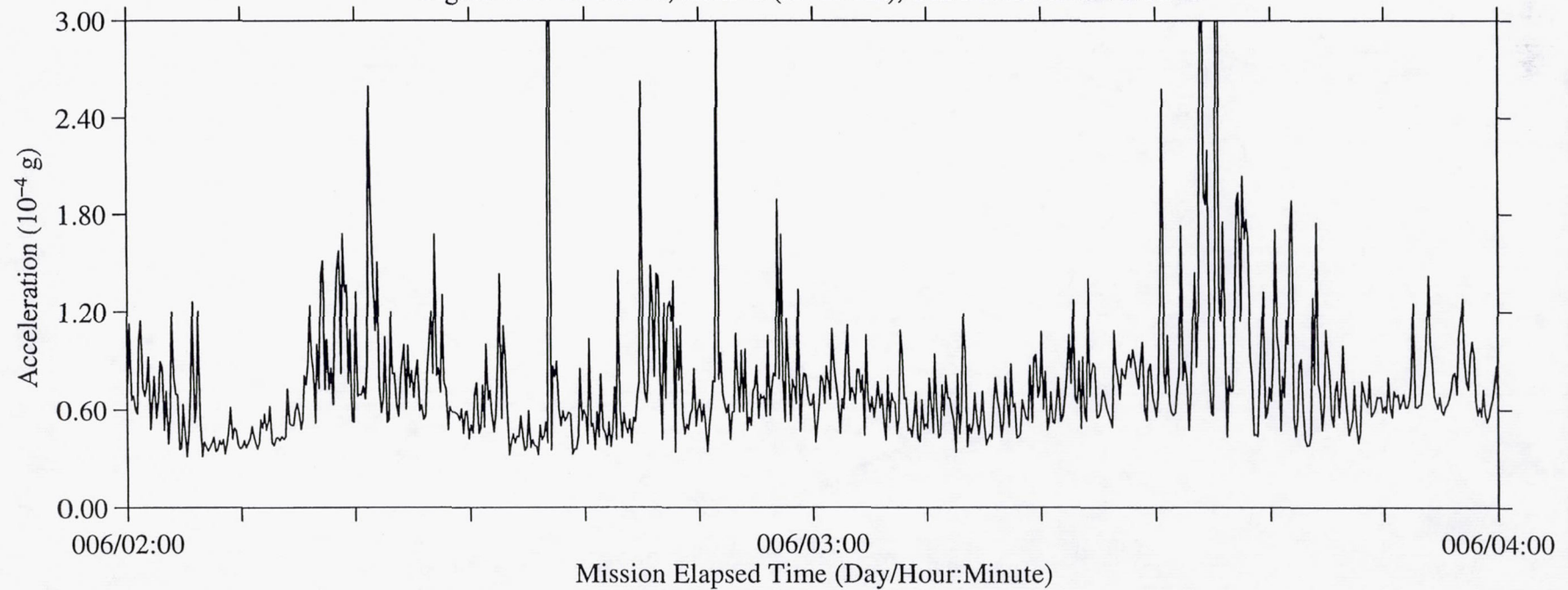


Figure 72a: USML-2, Head C (fc=25 Hz), Ten Second Interval Average

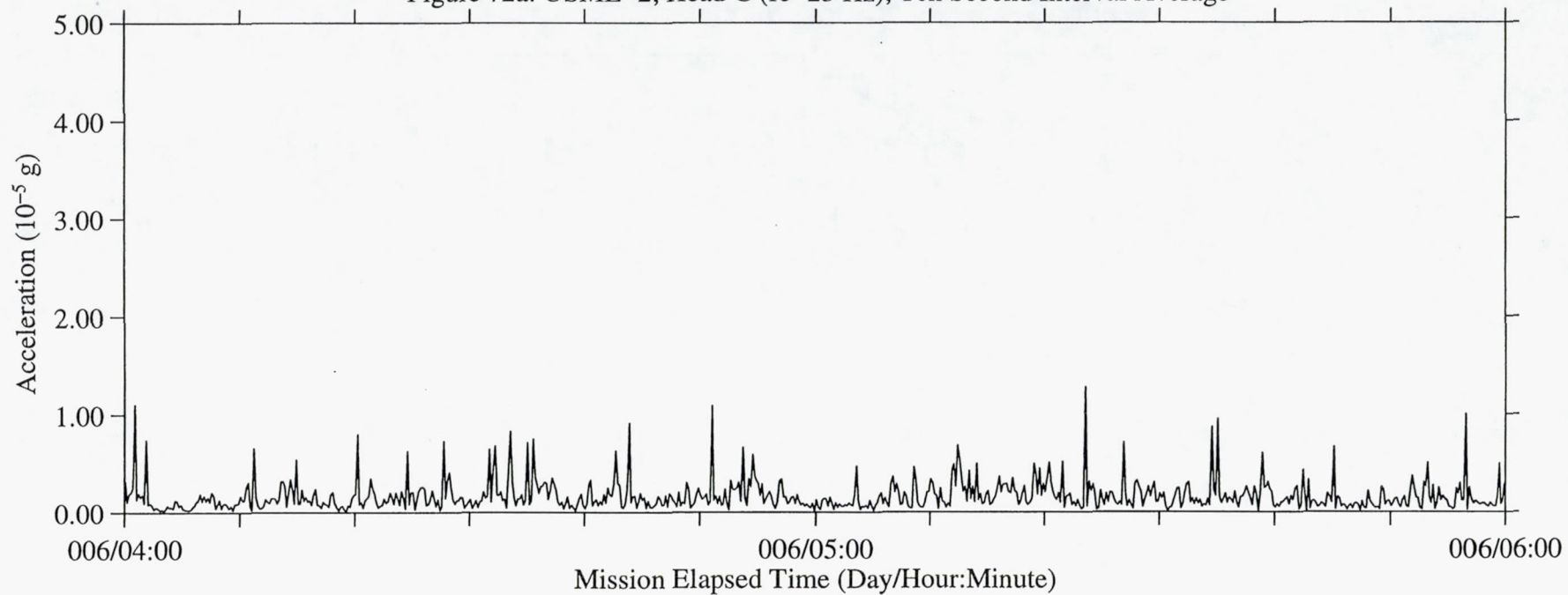


Figure 72b: USML-2, Head C (fc=25 Hz), Ten Second Interval RMS

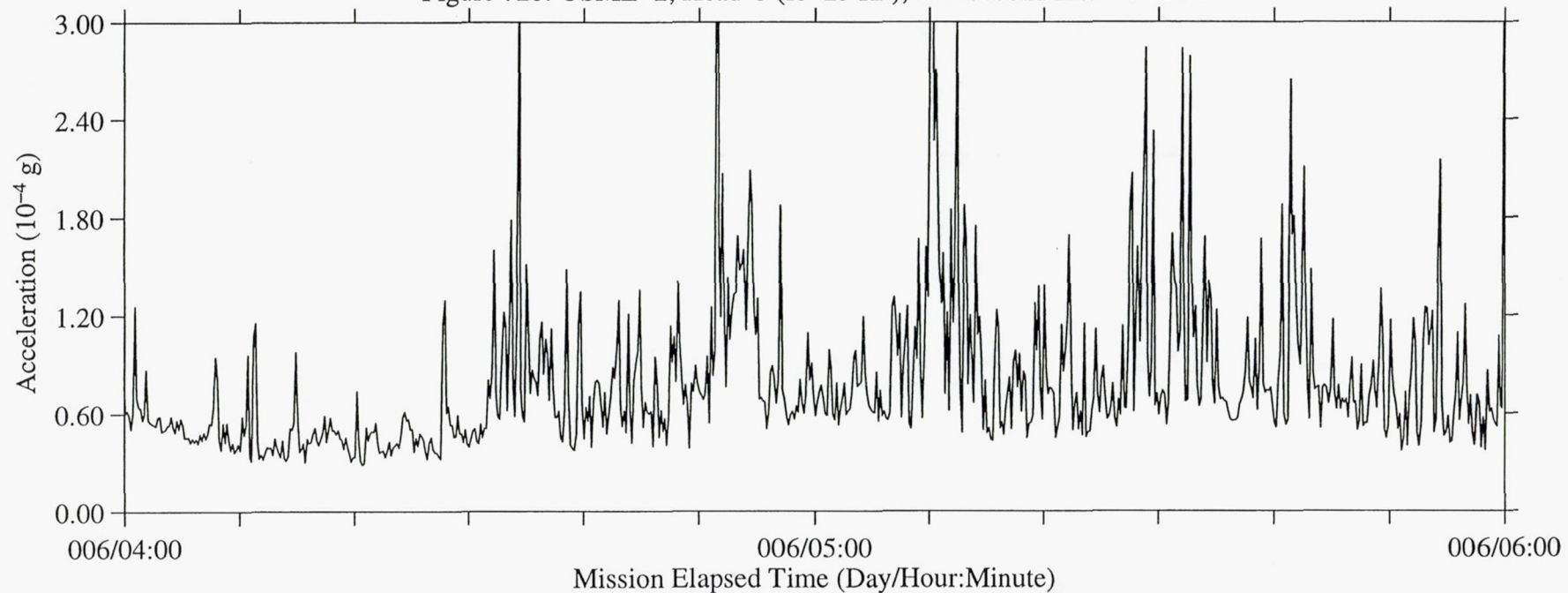




Figure 73a: USML-2, Head C (fc=25 Hz), Ten Second Interval Average

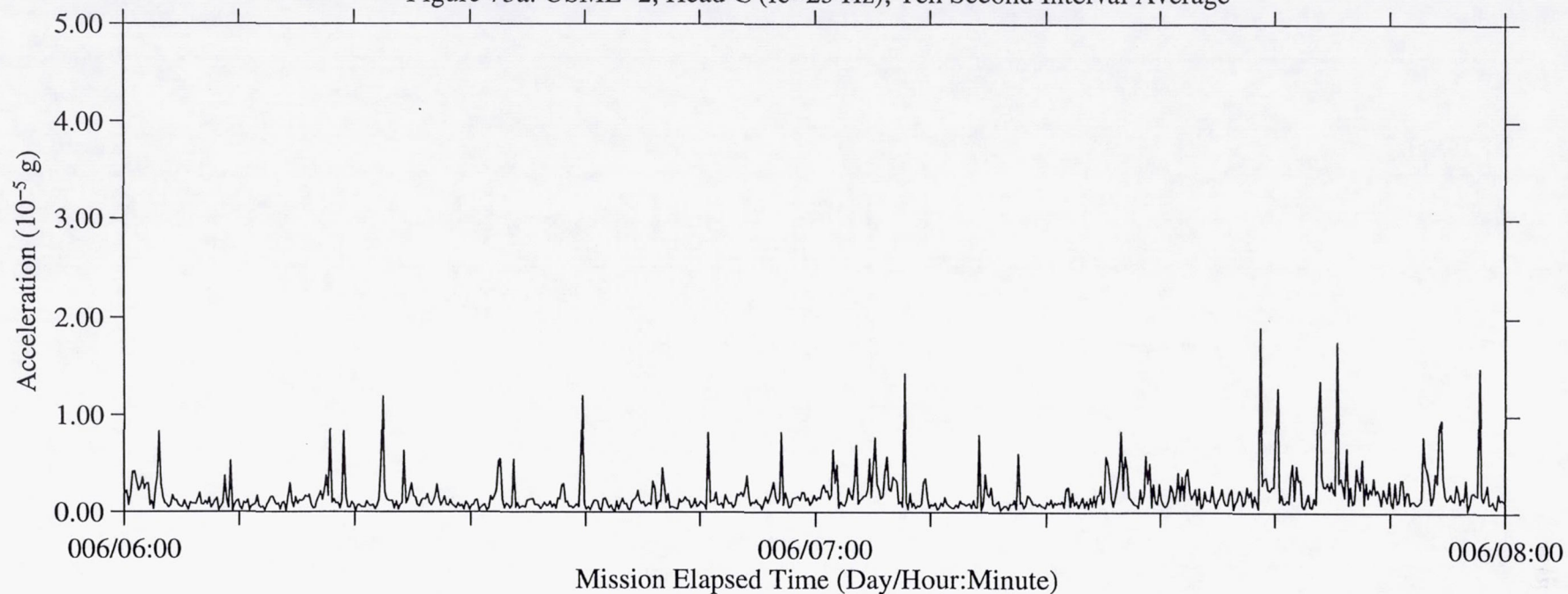


Figure 73b: USML-2, Head C (fc=25 Hz), Ten Second Interval RMS

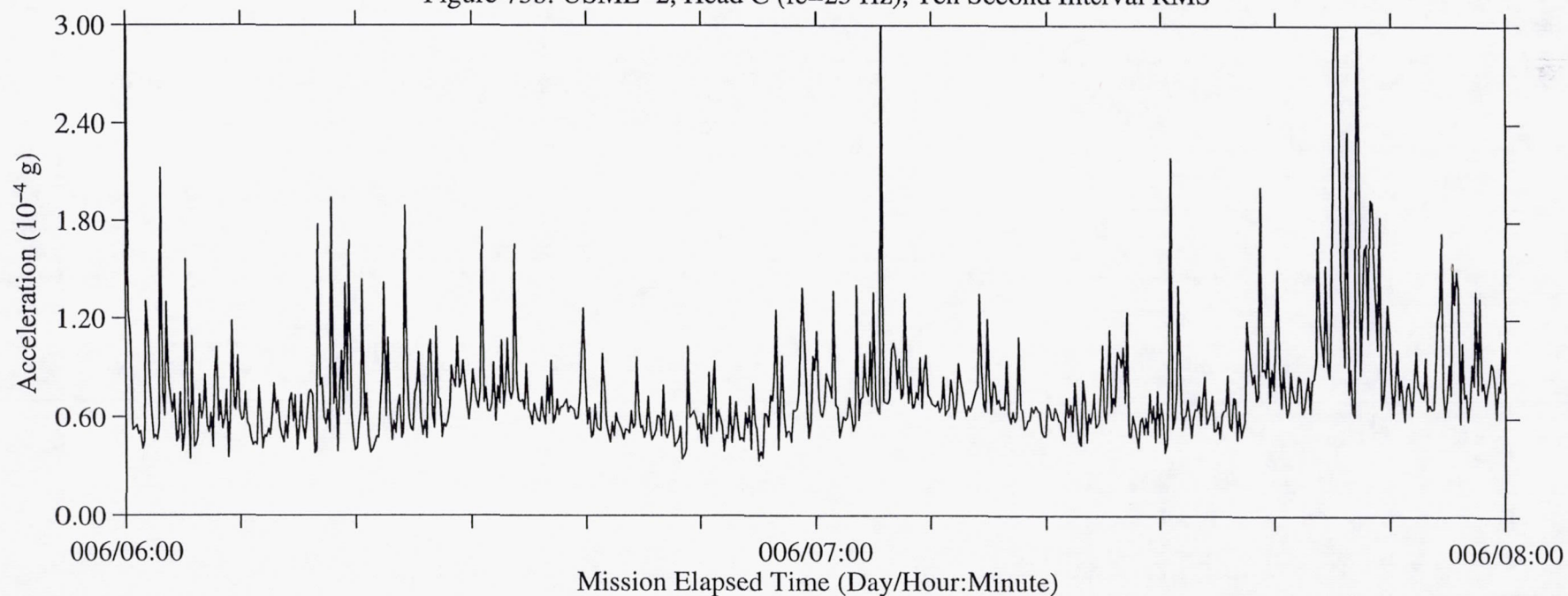


Figure 74a: USML-2, Head C (fc=25 Hz), Ten Second Interval Average

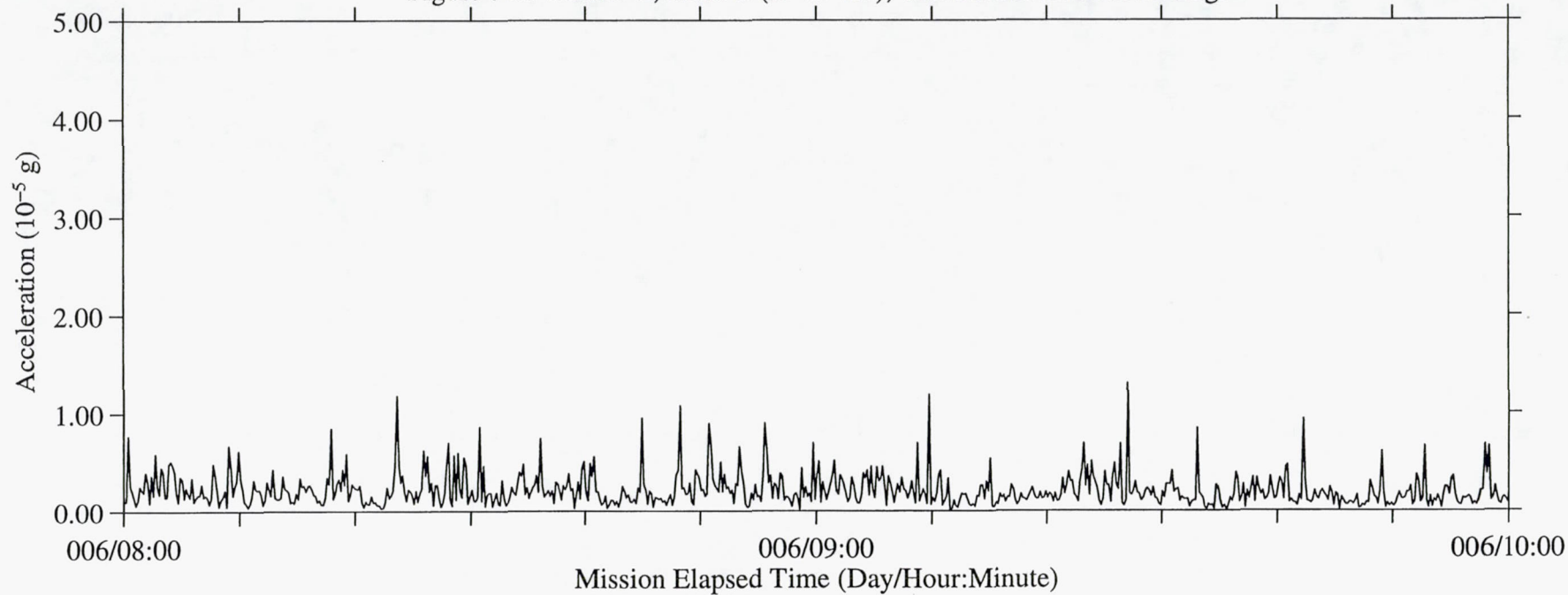


Figure 74b: USML-2, Head C (fc=25 Hz), Ten Second Interval RMS

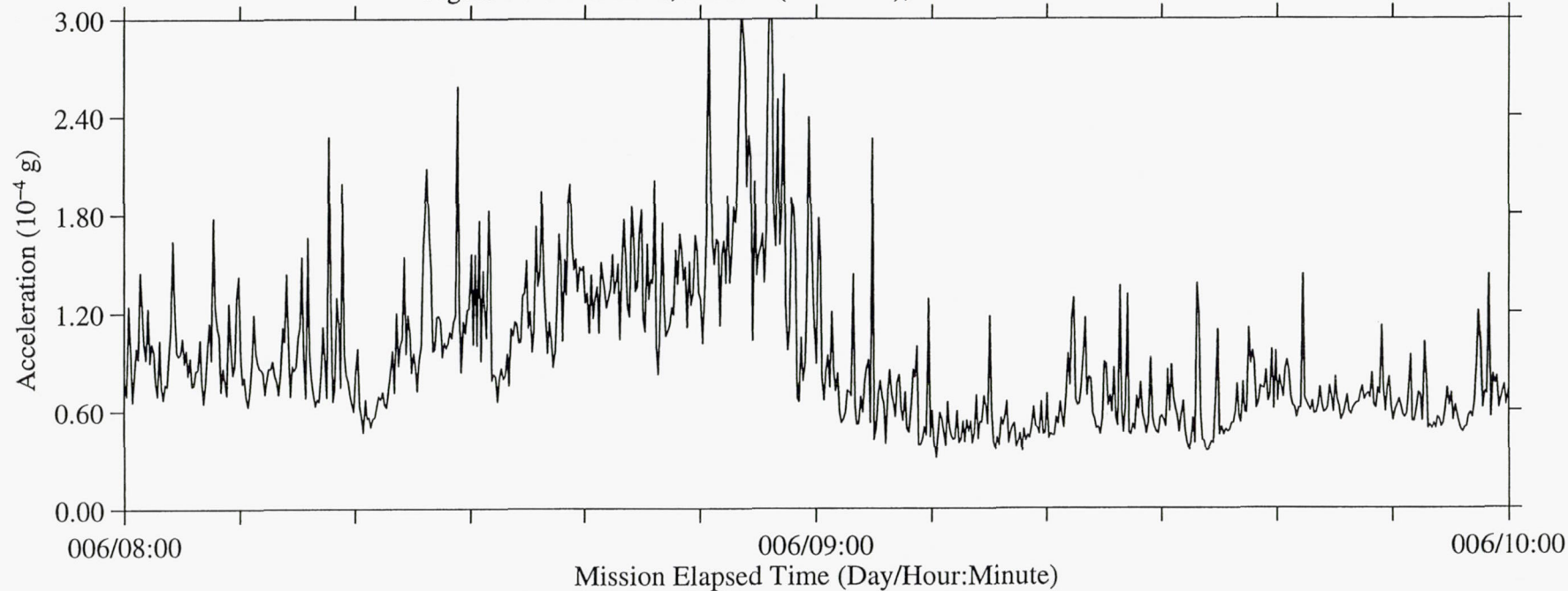




Figure 75a: USML-2, Head C (fc=25 Hz), Ten Second Interval Average

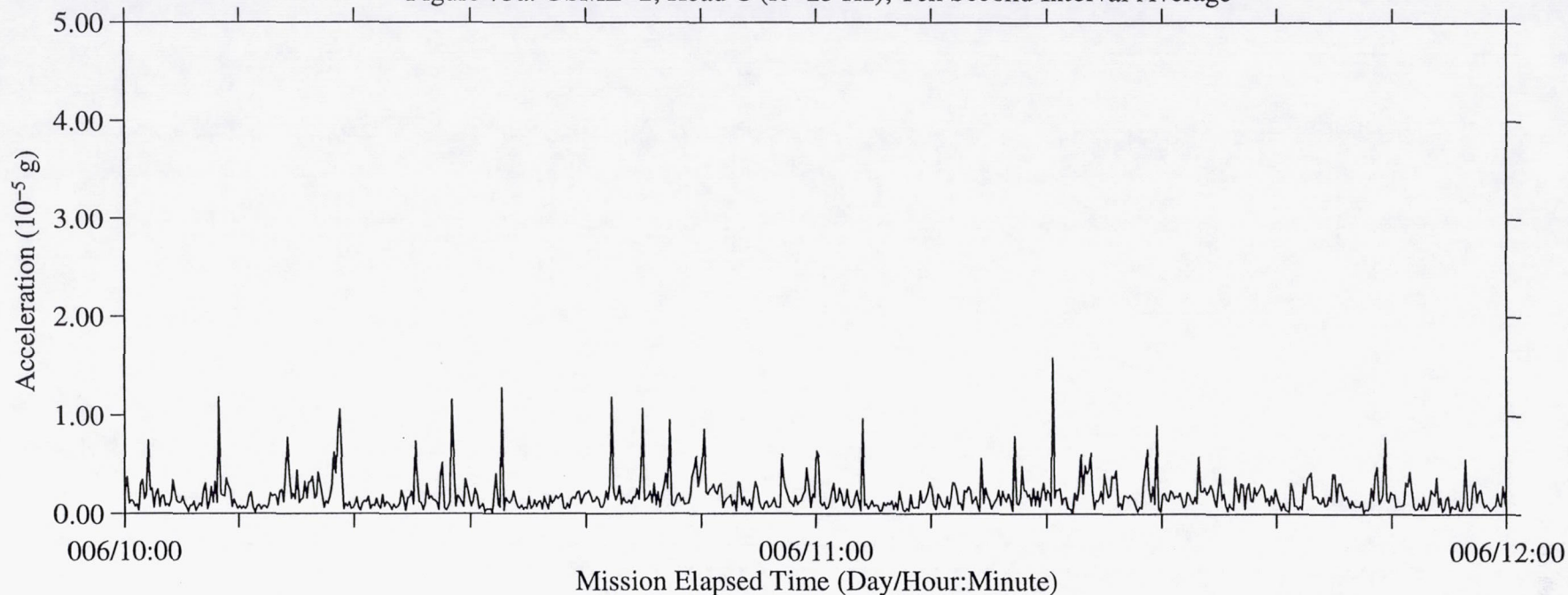


Figure 75b: USML-2, Head C (fc=25 Hz), Ten Second Interval RMS

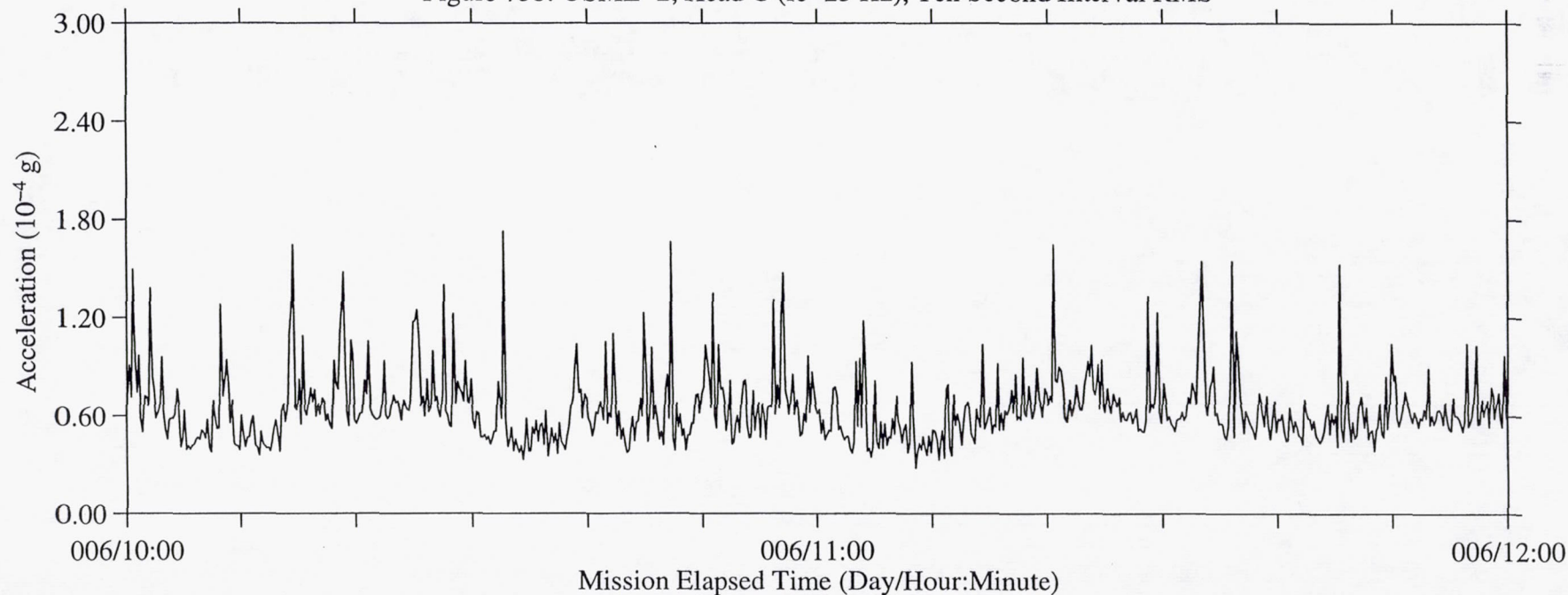


Figure 76a: USML-2, Head C (fc=25 Hz), Ten Second Interval Average

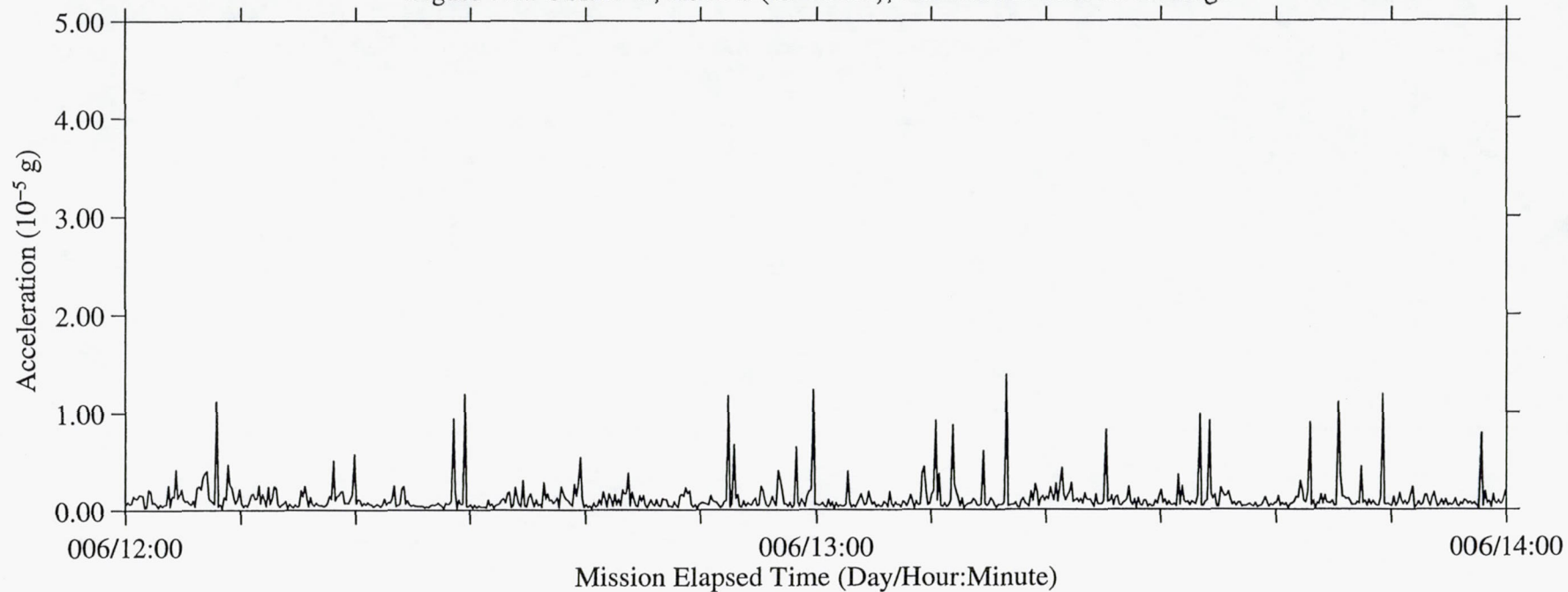


Figure 76b: USML-2, Head C (fc=25 Hz), Ten Second Interval RMS

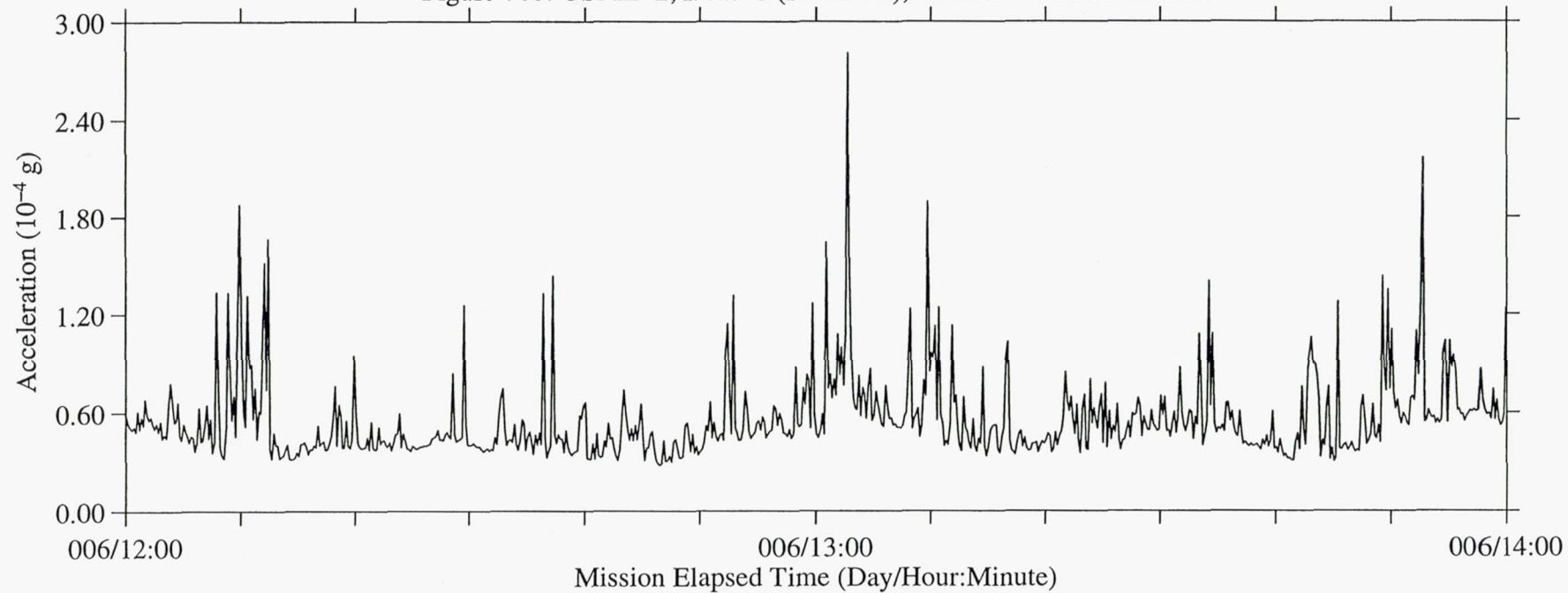




Figure 77a: USML-2, Head C (fc=25 Hz), Ten Second Interval Average

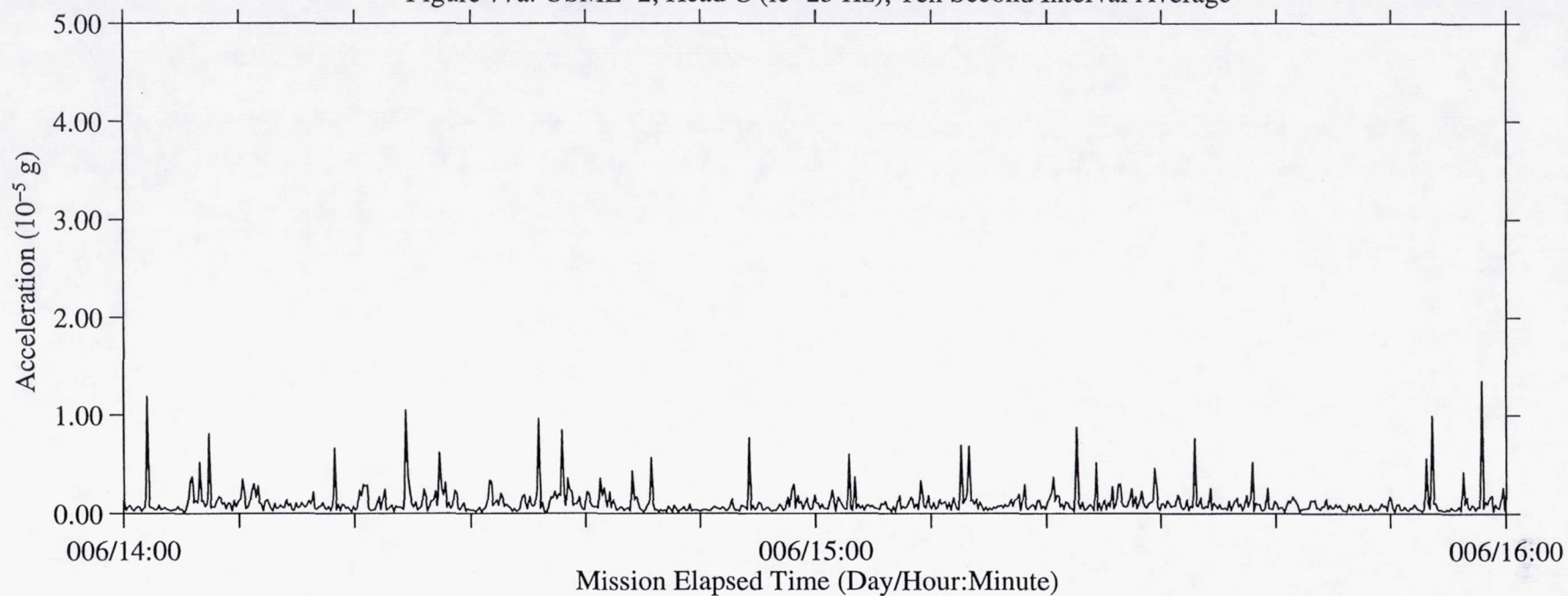


Figure 77b: USML-2, Head C (fc=25 Hz), Ten Second Interval RMS

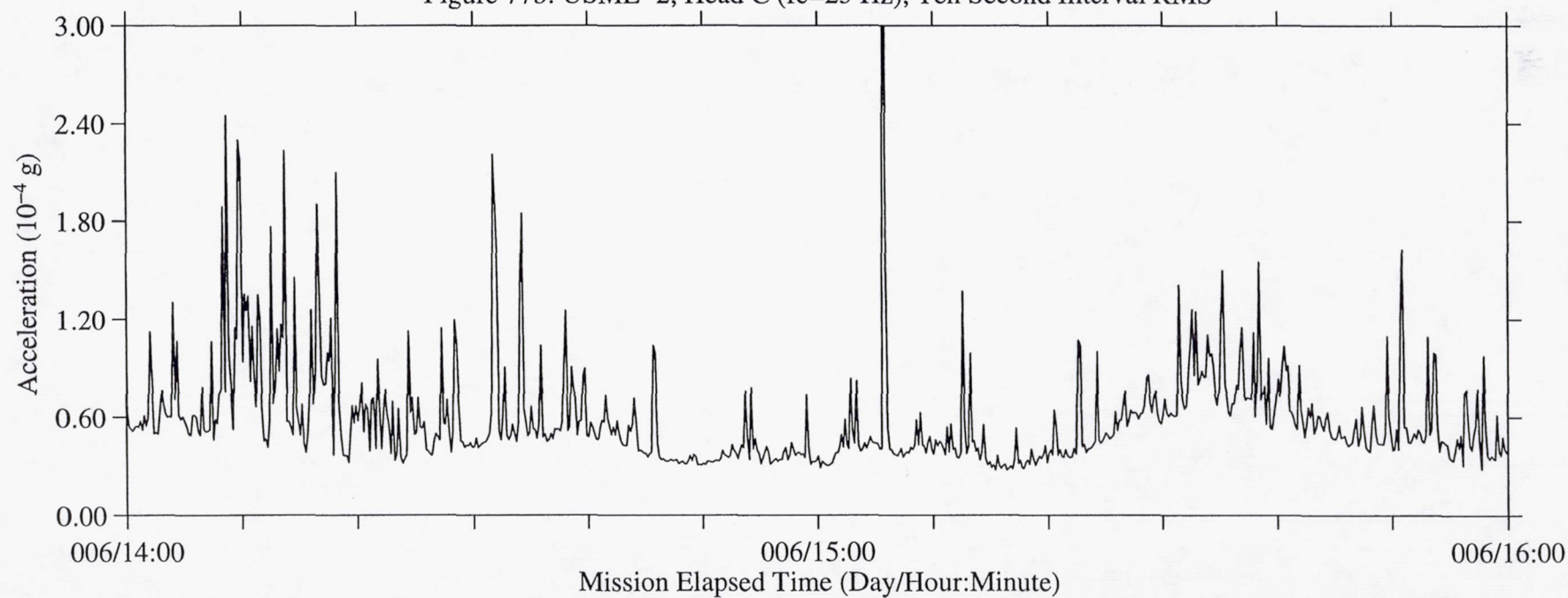


Figure 78a: USML-2, Head C (fc=25 Hz), Ten Second Interval Average

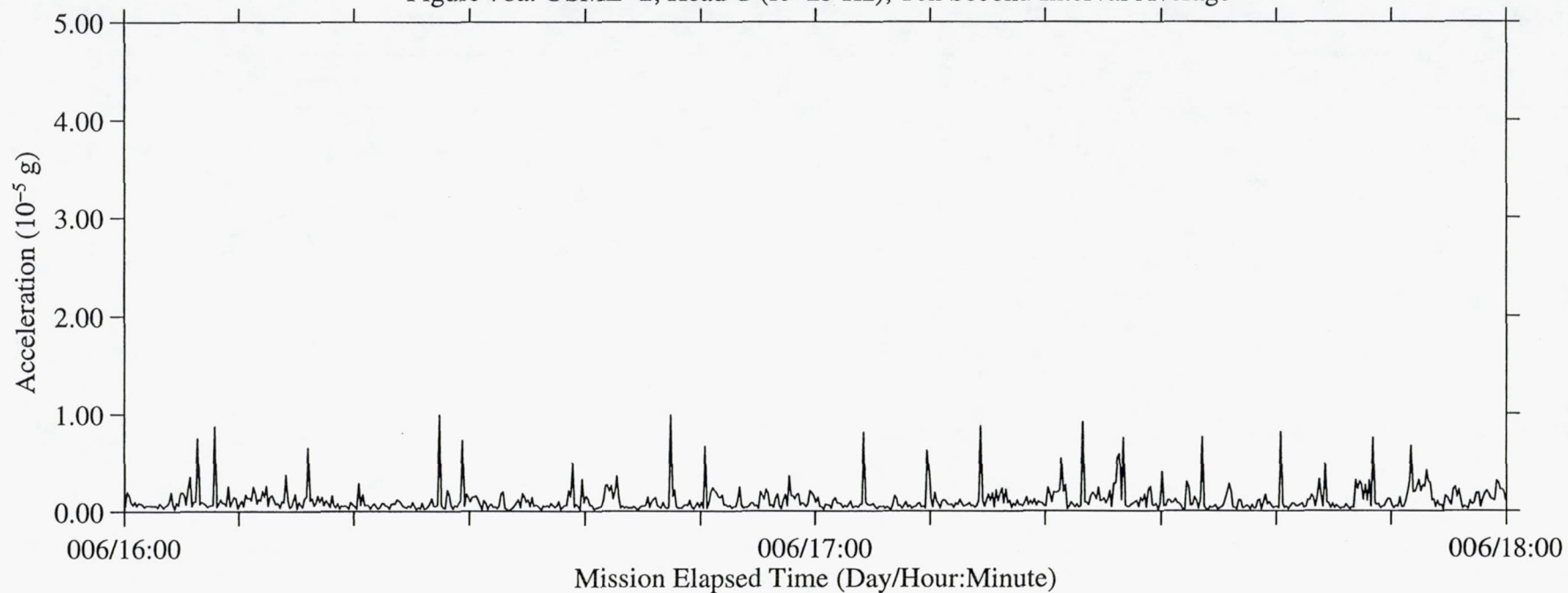


Figure 78b: USML-2, Head C (fc=25 Hz), Ten Second Interval RMS

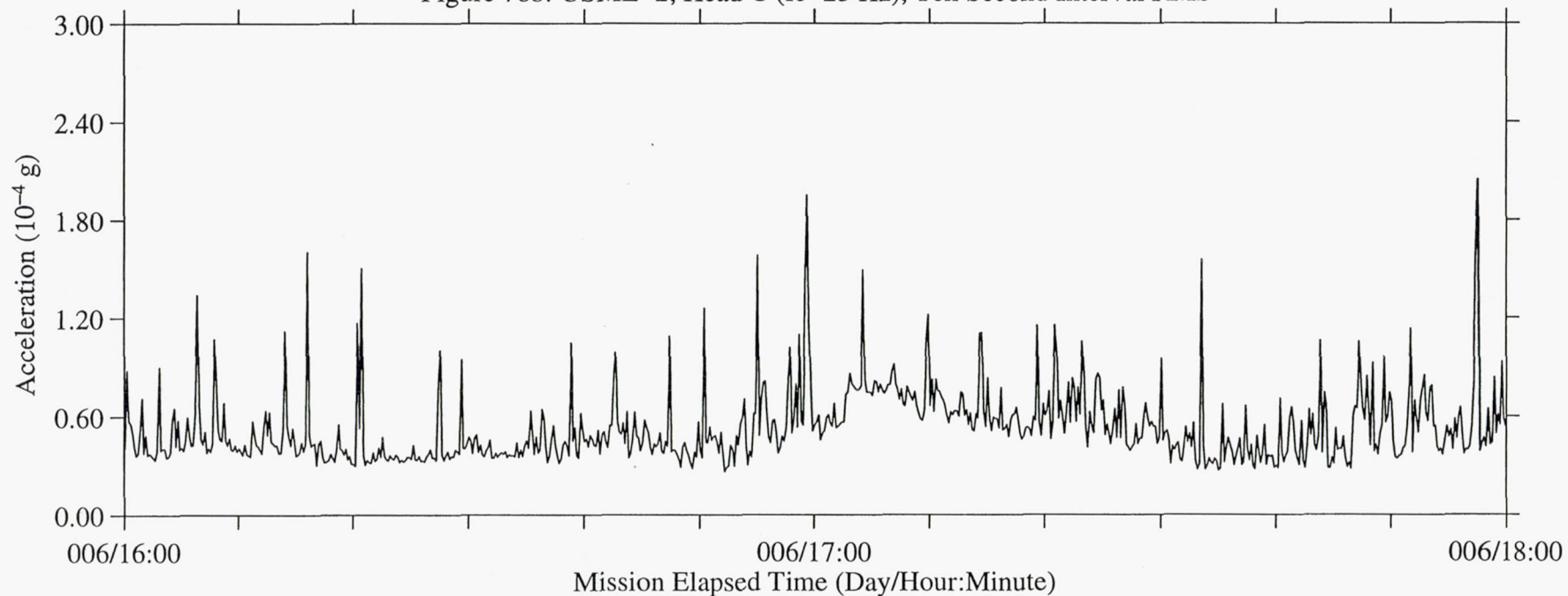




Figure 79a: USML-2, Head C (fc=25 Hz), Ten Second Interval Average

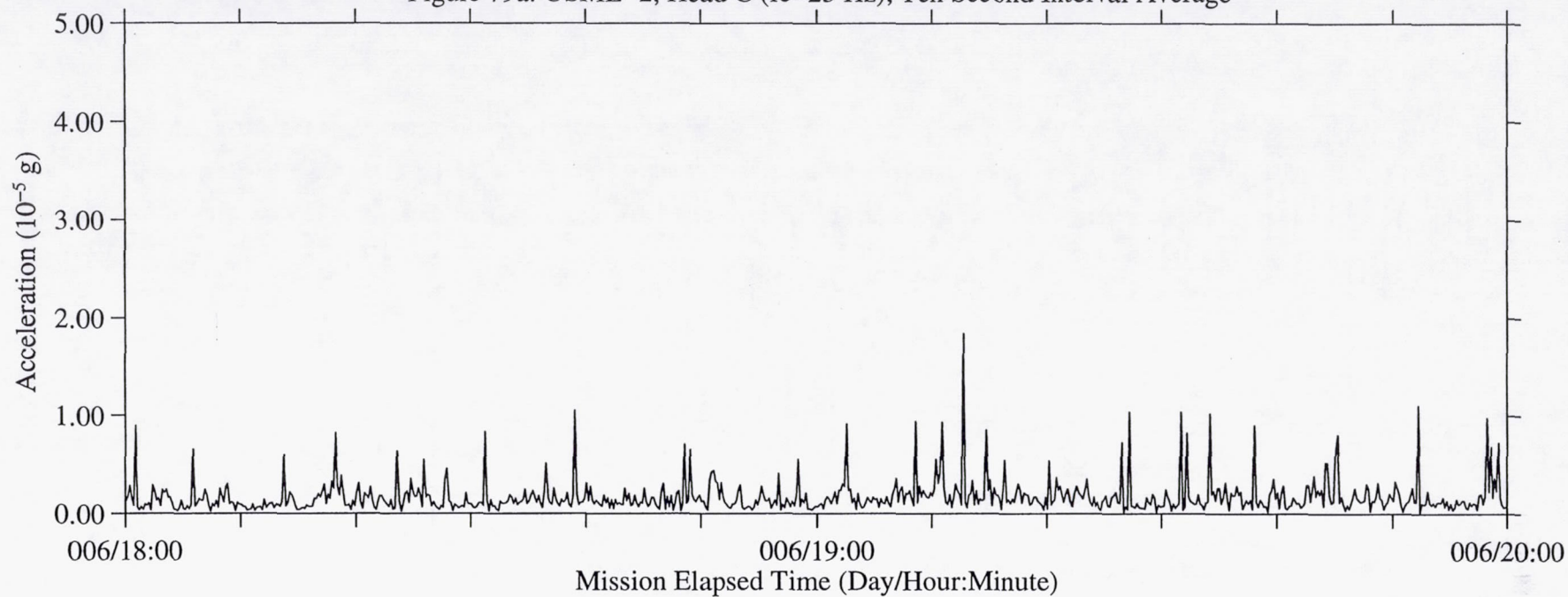


Figure 79b: USML-2, Head C (fc=25 Hz), Ten Second Interval RMS

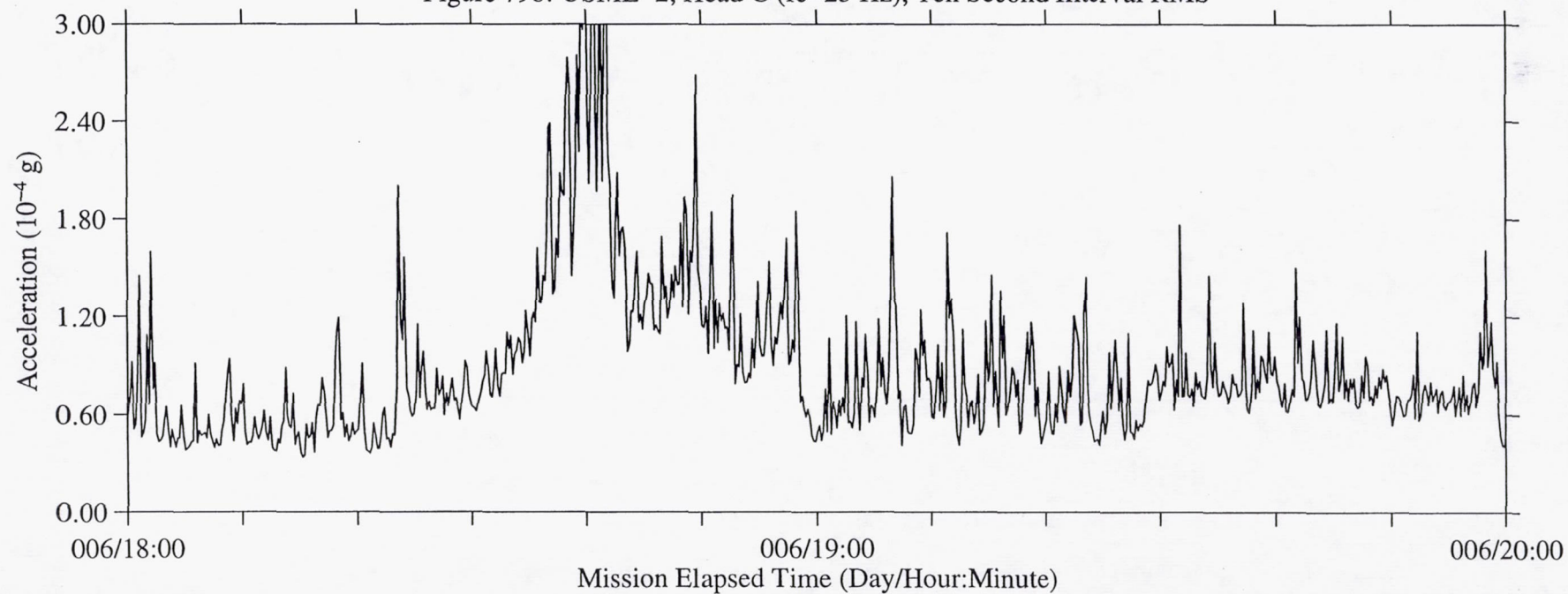


Figure 80a: USML-2, Head C (fc=25 Hz), Ten Second Interval Average

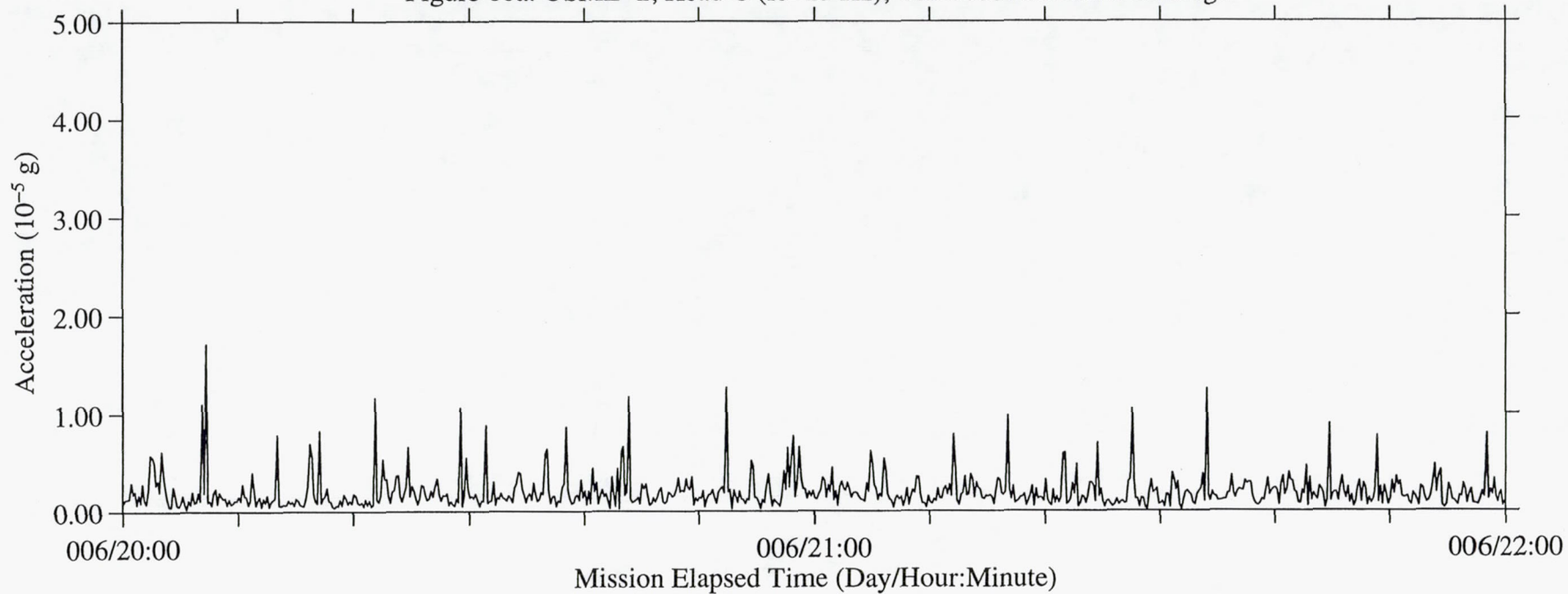


Figure 80b: USML-2, Head C (fc=25 Hz), Ten Second Interval RMS

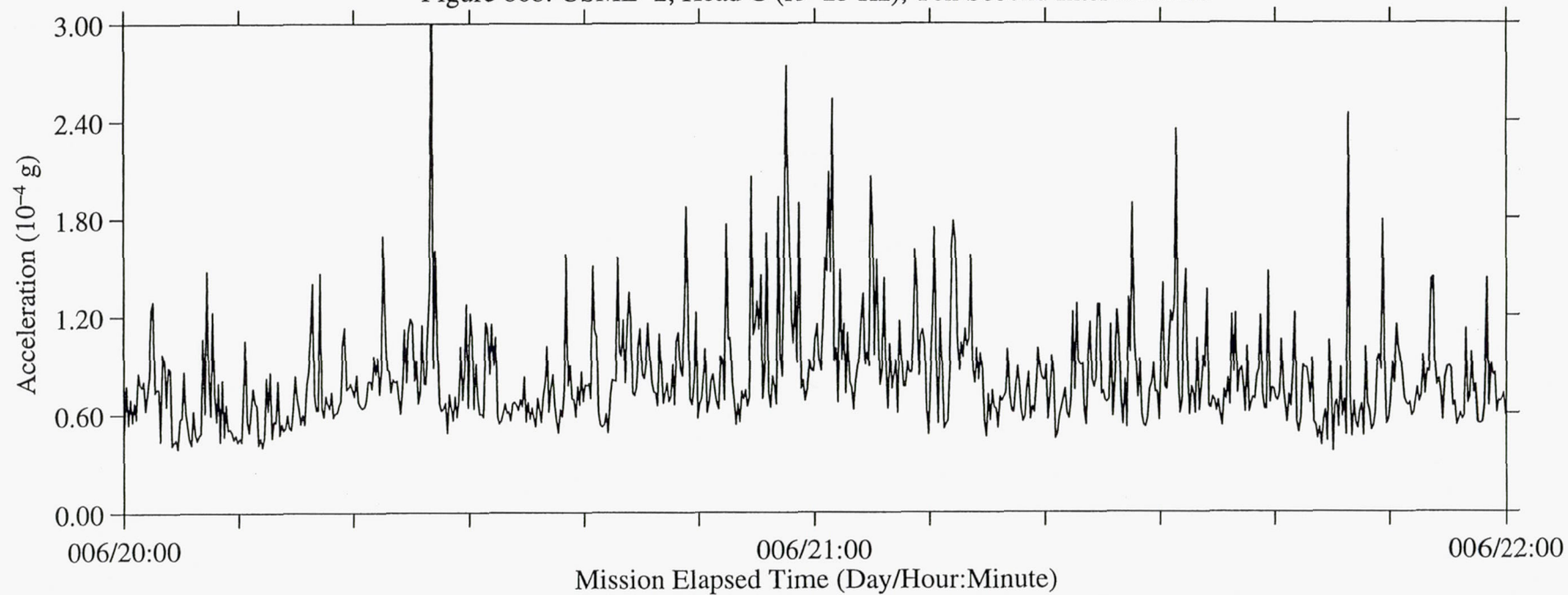




Figure 81a: USML-2, Head C (fc=25 Hz), Ten Second Interval Average

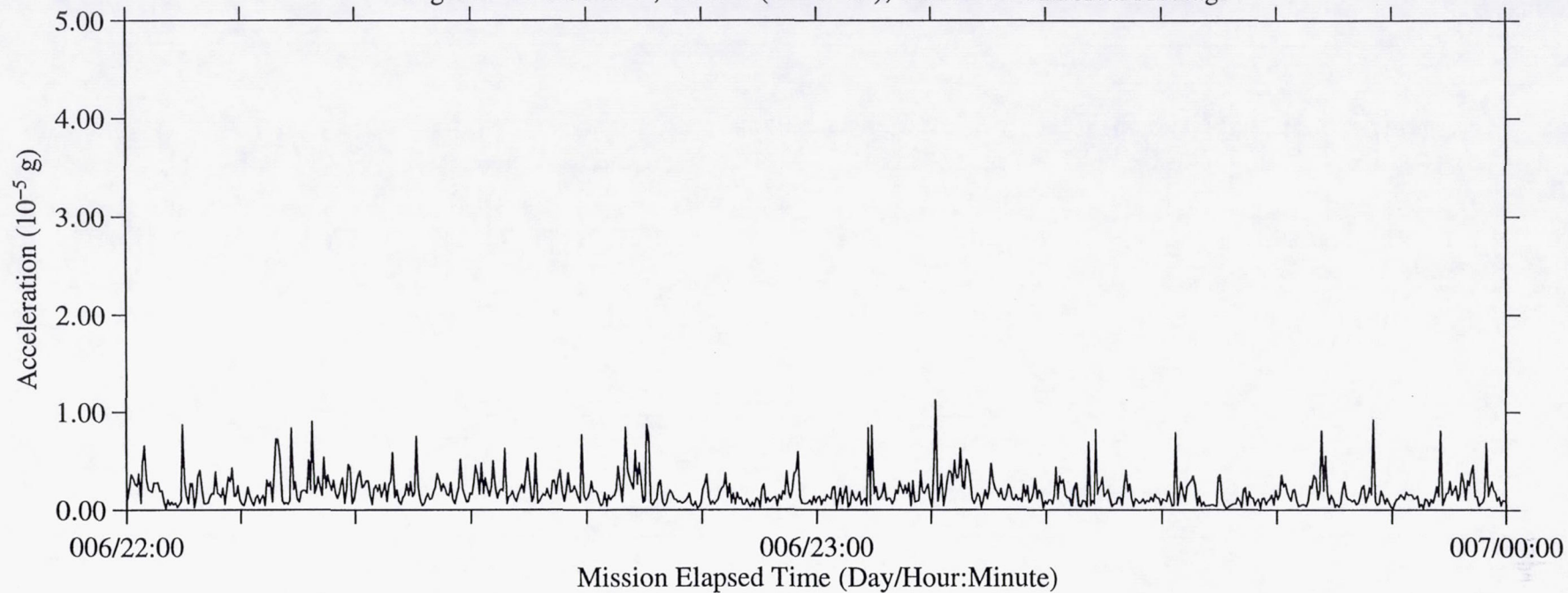


Figure 81b: USML-2, Head C (fc=25 Hz), Ten Second Interval RMS

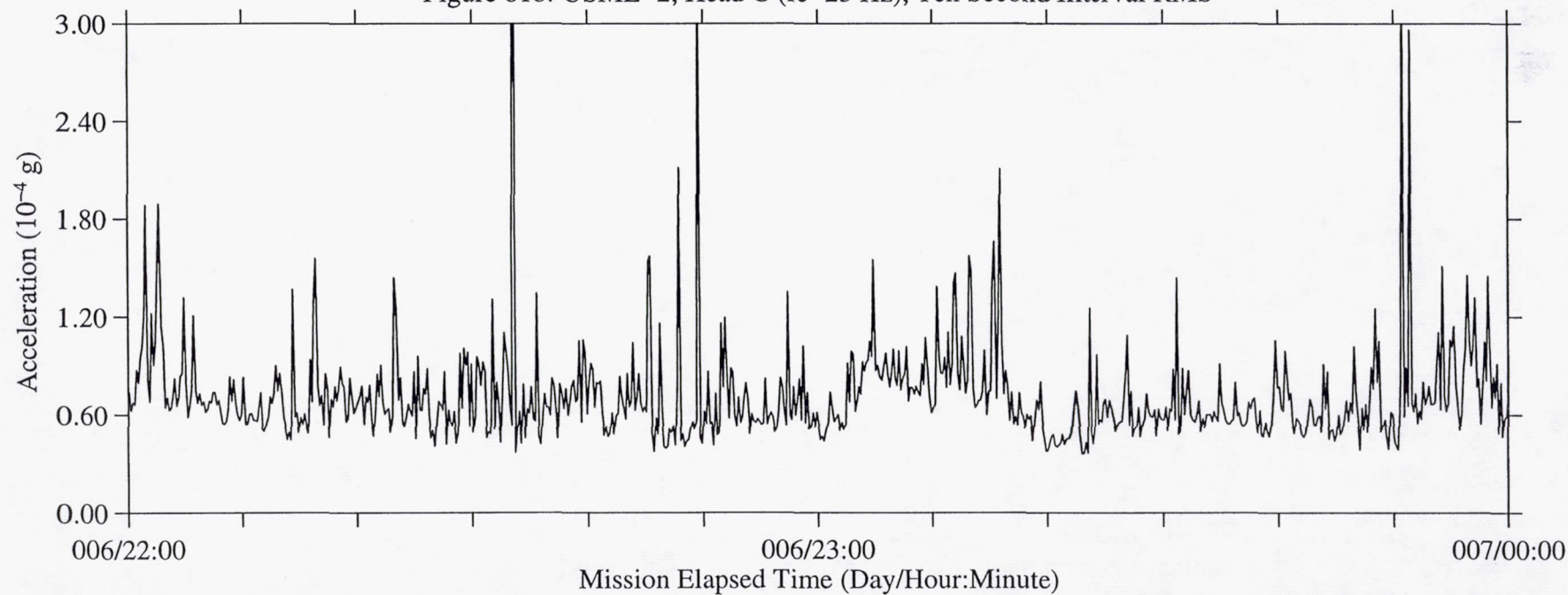


Figure 82a: USML-2, Head C (fc=25 Hz), Ten Second Interval Average

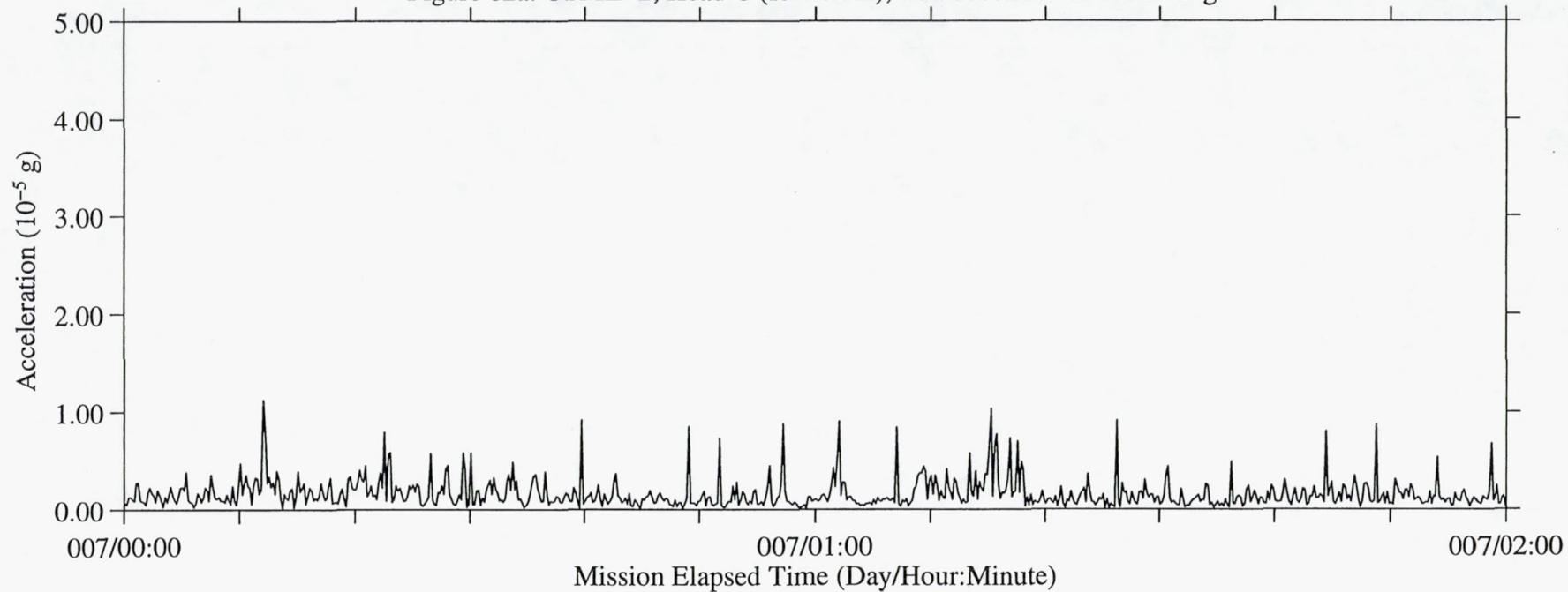


Figure 82b: USML-2, Head C (fc=25 Hz), Ten Second Interval RMS

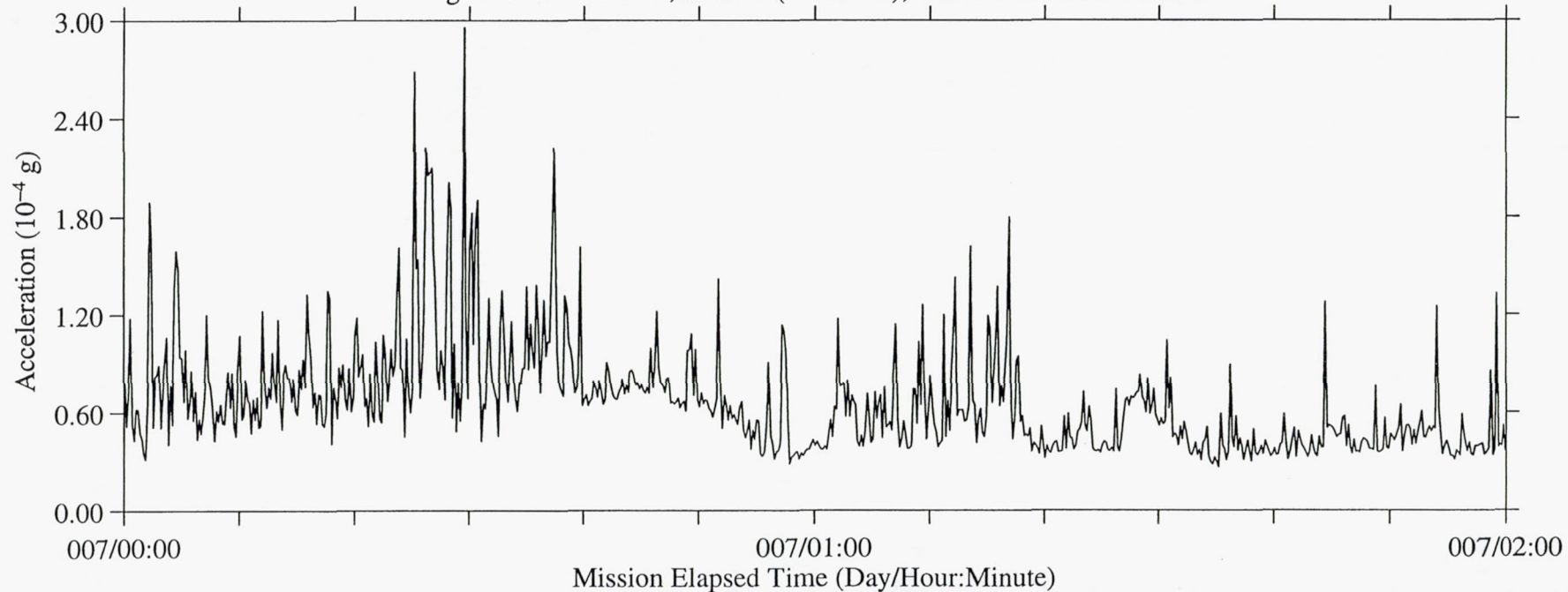




Figure 83a: USML-2, Head C (fc=25 Hz), Ten Second Interval Average

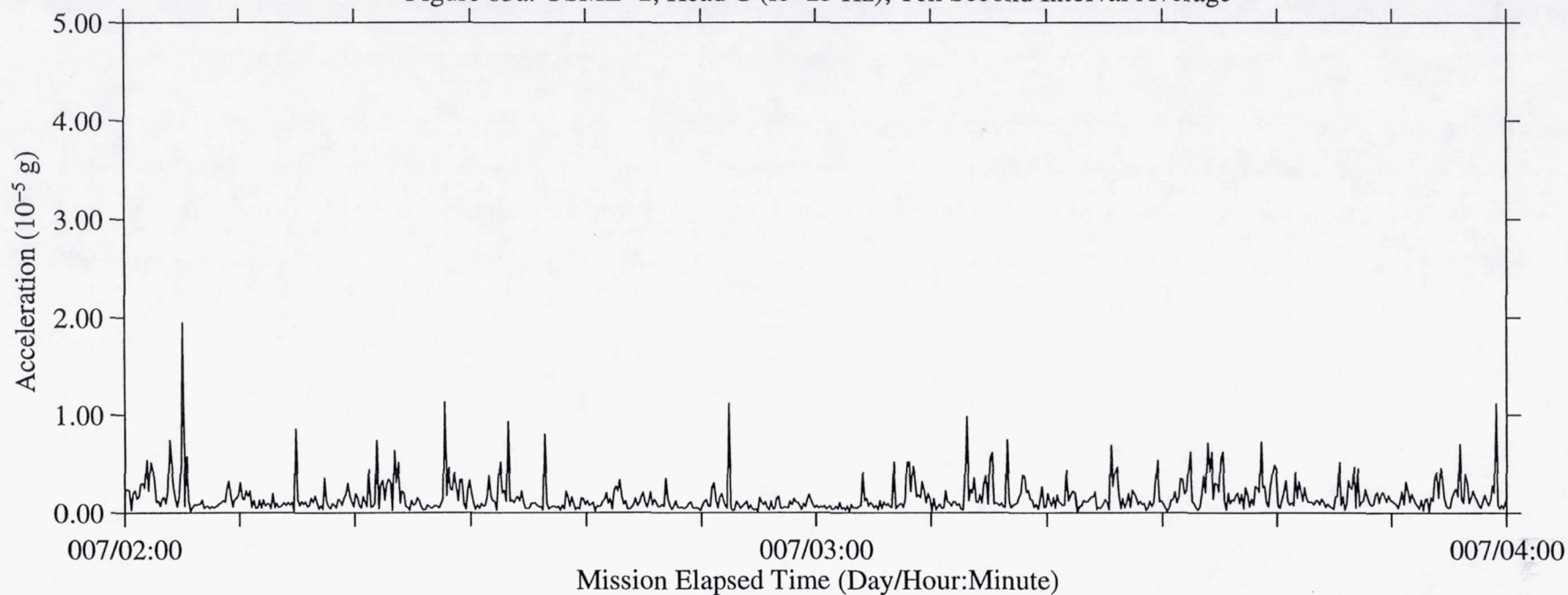


Figure 83b: USML-2, Head C (fc=25 Hz), Ten Second Interval RMS

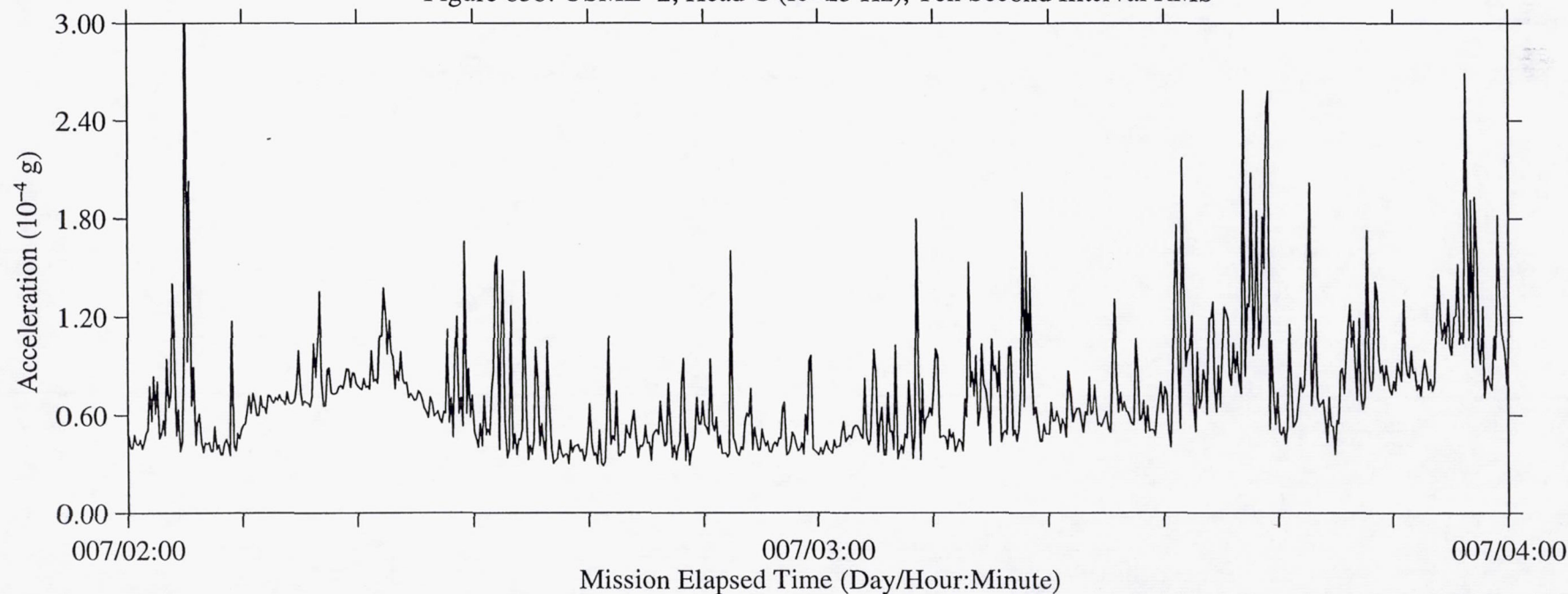


Figure 84a: USML-2, Head C (fc=25 Hz), Ten Second Interval Average

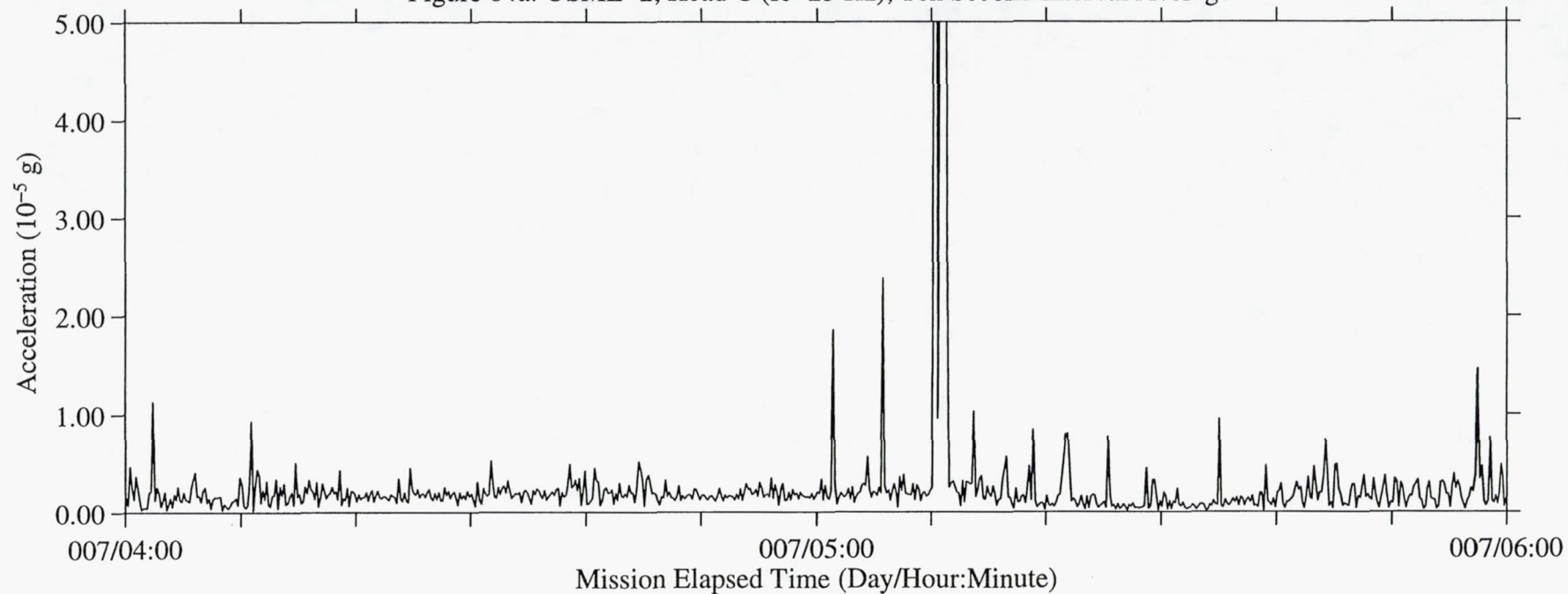


Figure 84b: USML-2, Head C (fc=25 Hz), Ten Second Interval RMS

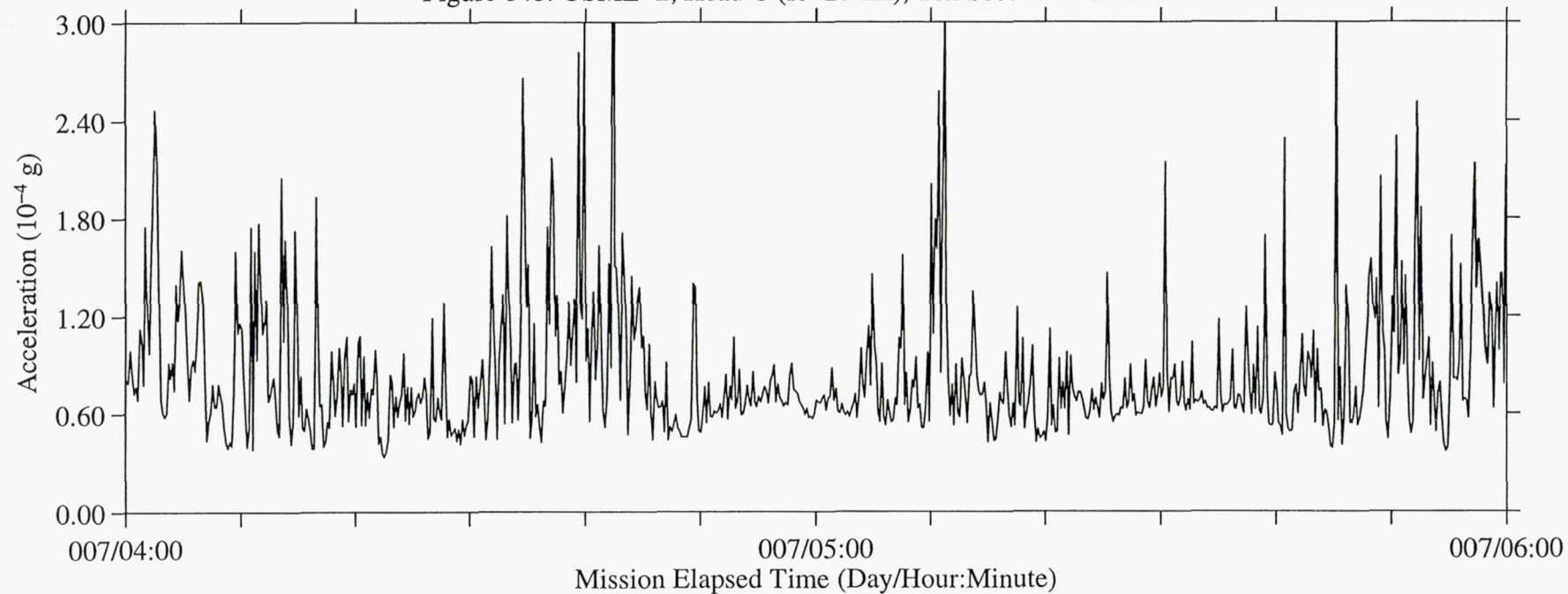




Figure 85a: USML-2, Head C (fc=25 Hz), Ten Second Interval Average

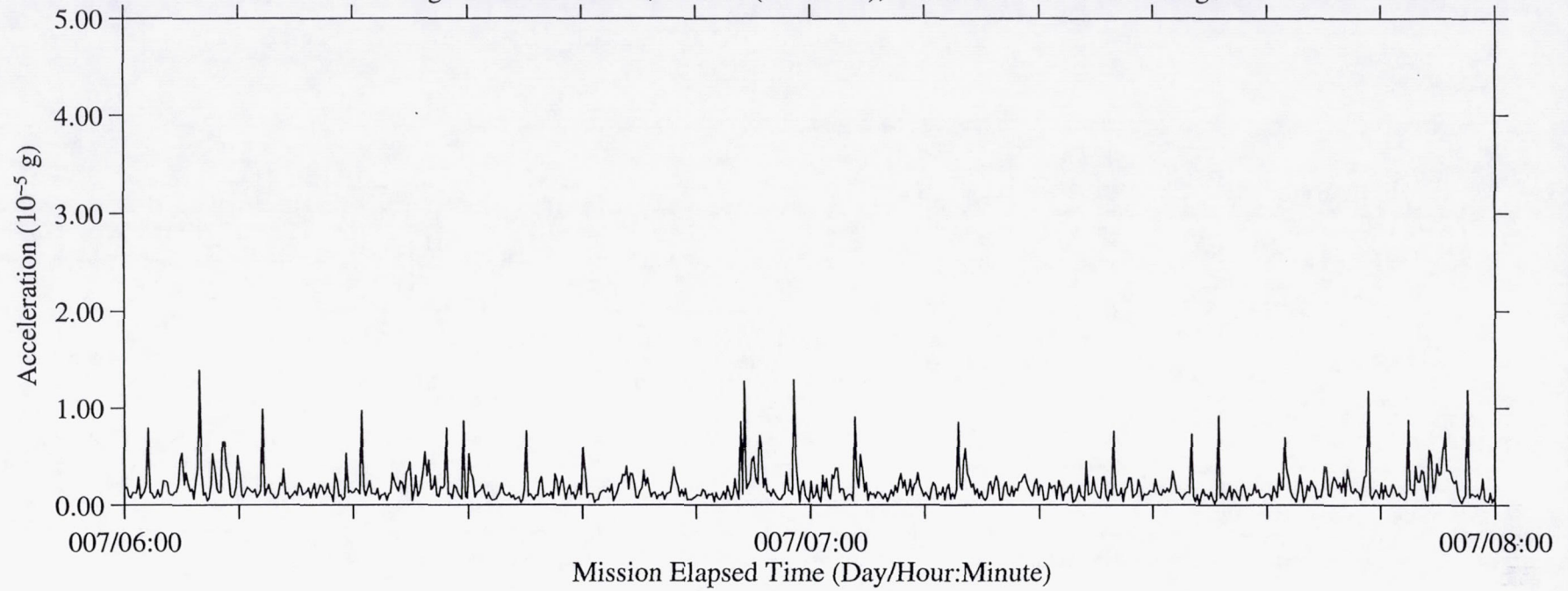


Figure 85b: USML-2, Head C (fc=25 Hz), Ten Second Interval RMS

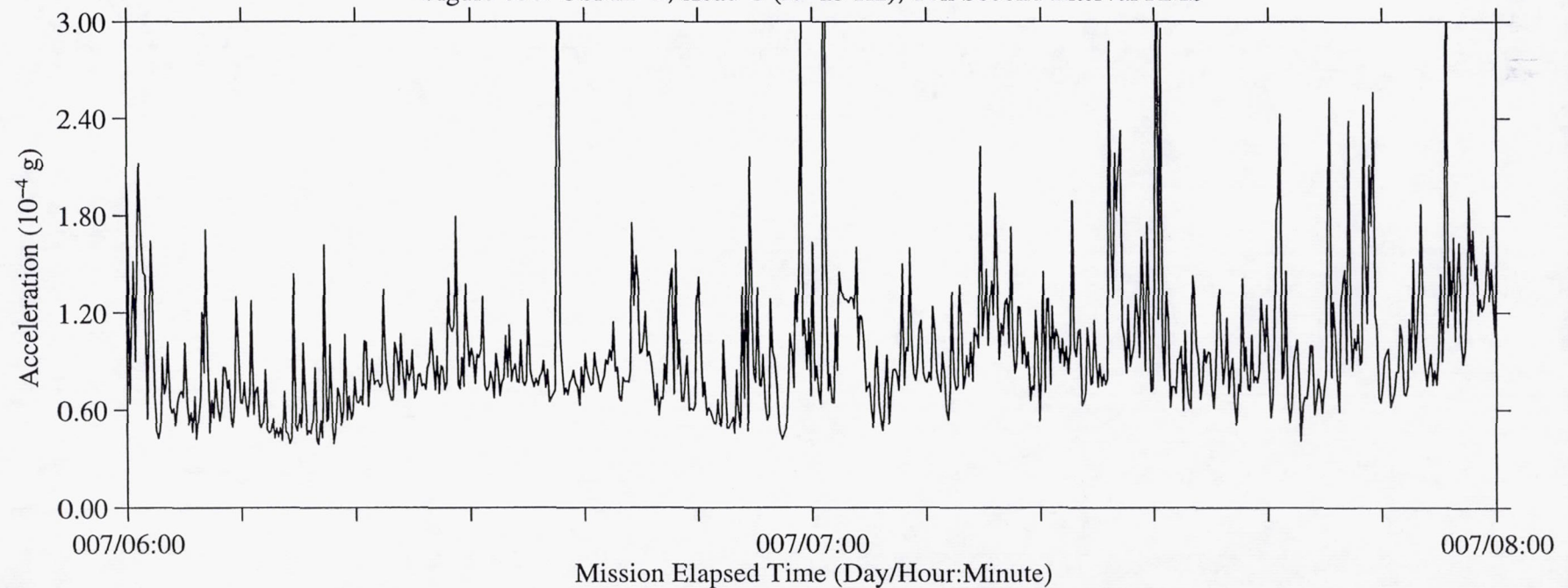


Figure 86a: USML-2, Head C (fc=25 Hz), Ten Second Interval Average

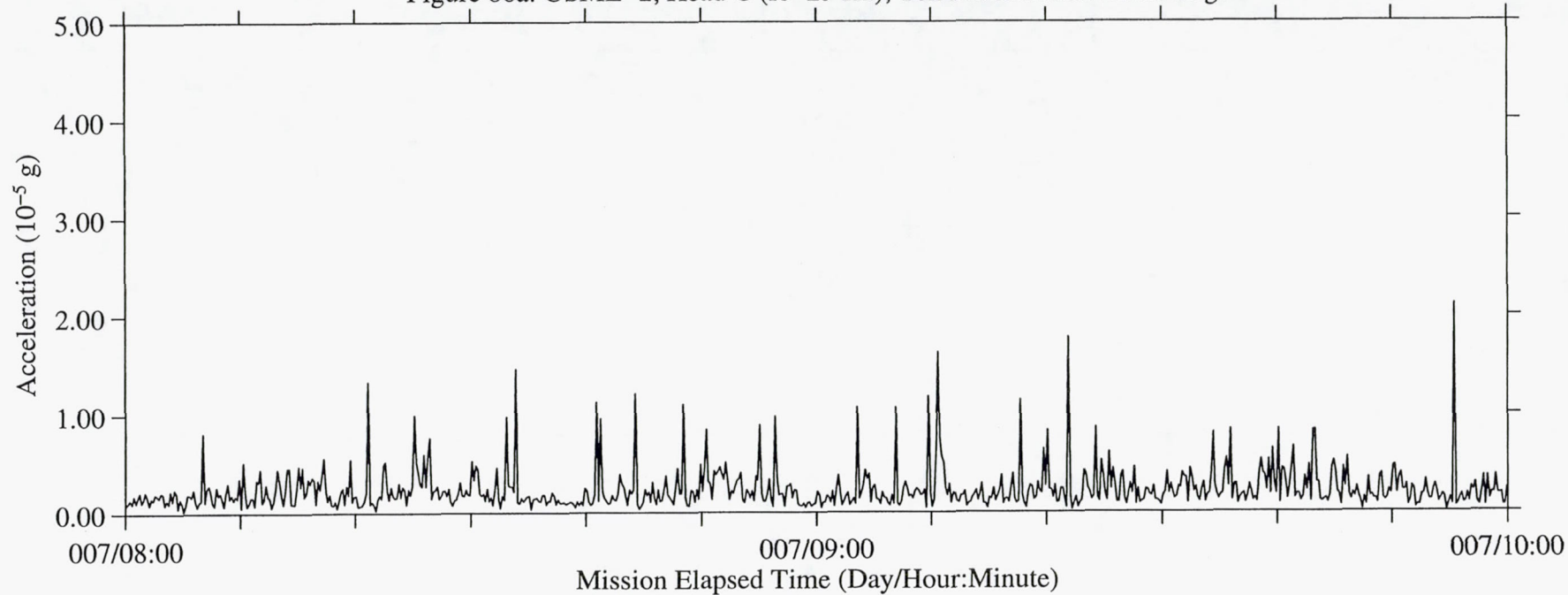
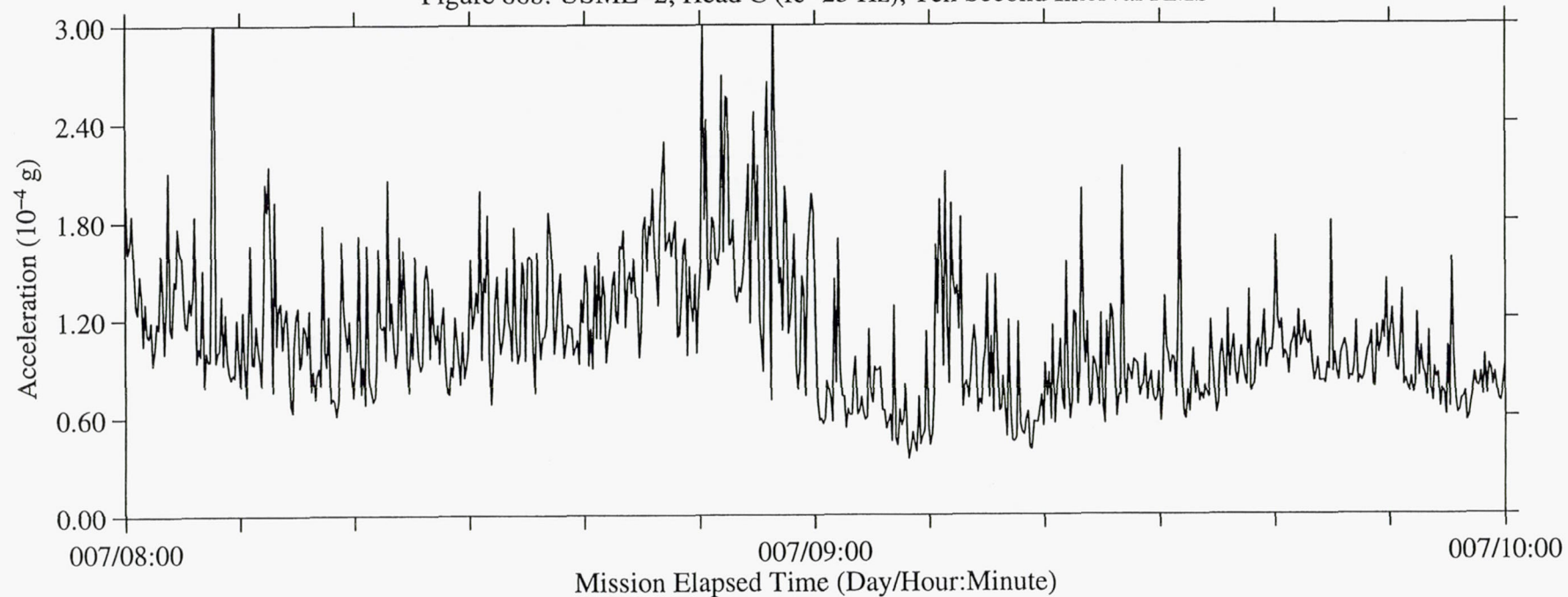


Figure 86b: USML-2, Head C (fc=25 Hz), Ten Second Interval RMS





B-89

Figure 87a: USML-2, Head C (fc=25 Hz), Ten Second Interval Average

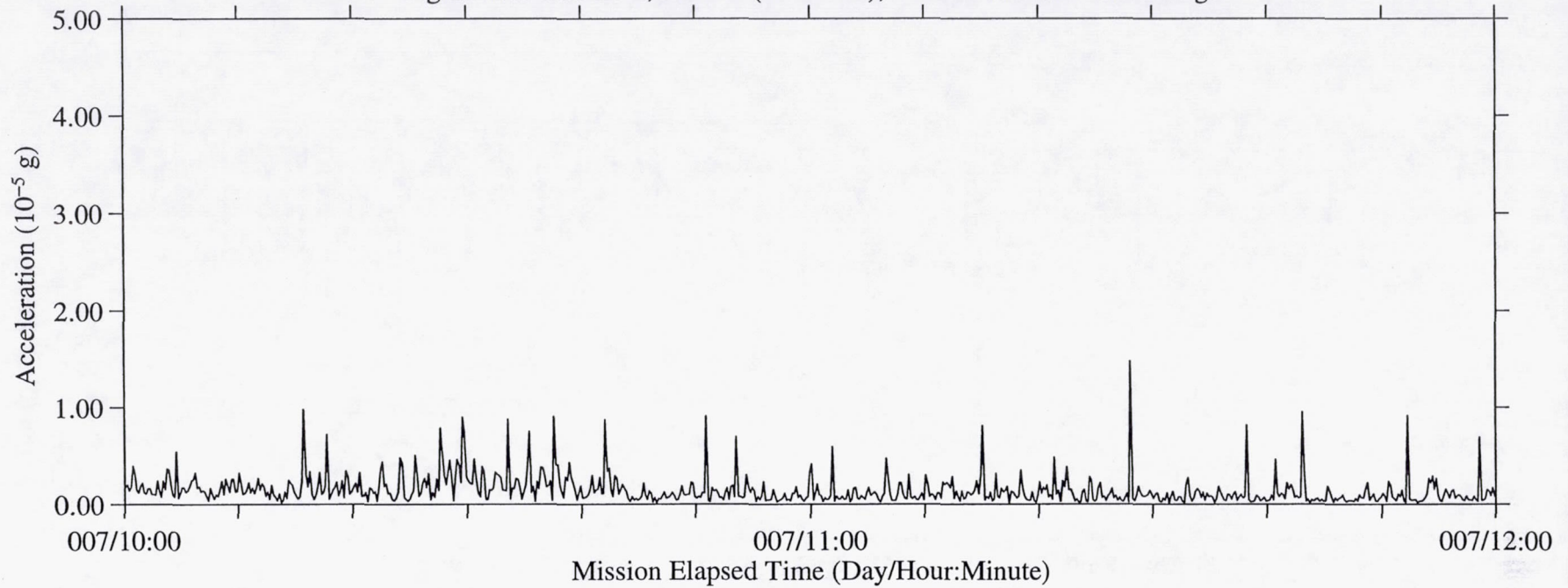


Figure 87b: USML-2, Head C (fc=25 Hz), Ten Second Interval RMS

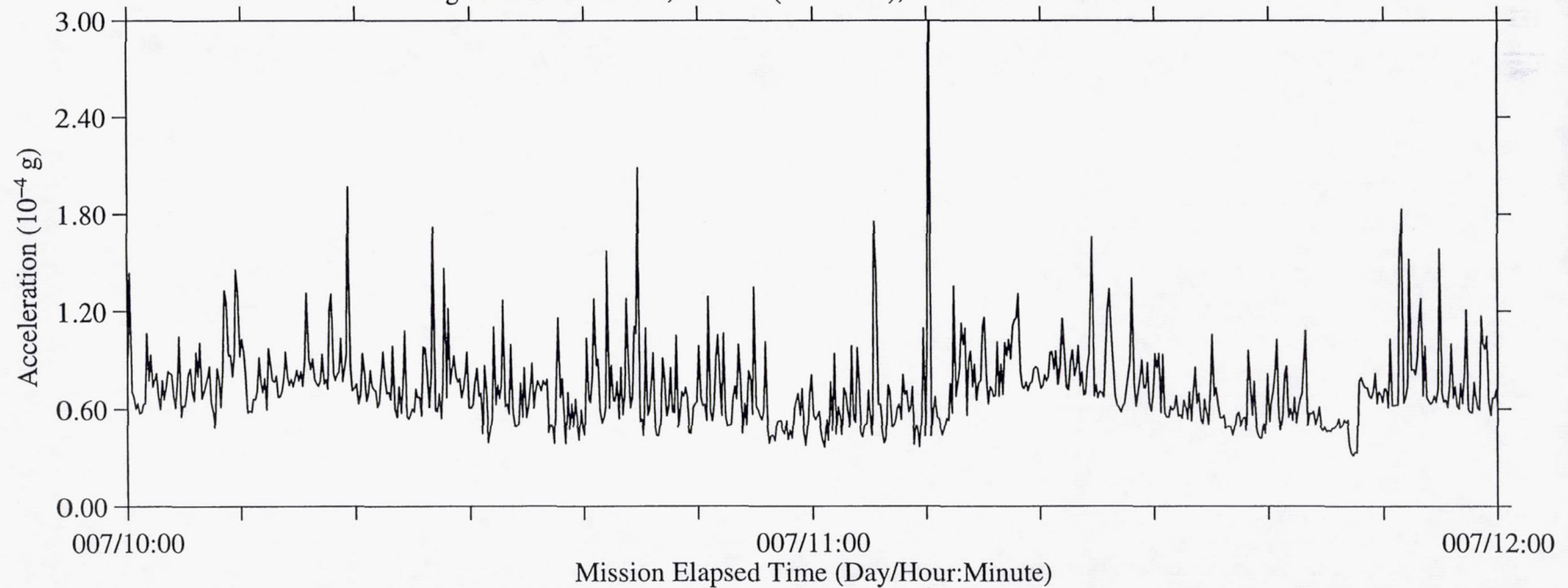


Figure 88a: USML-2, Head C (fc=25 Hz), Ten Second Interval Average

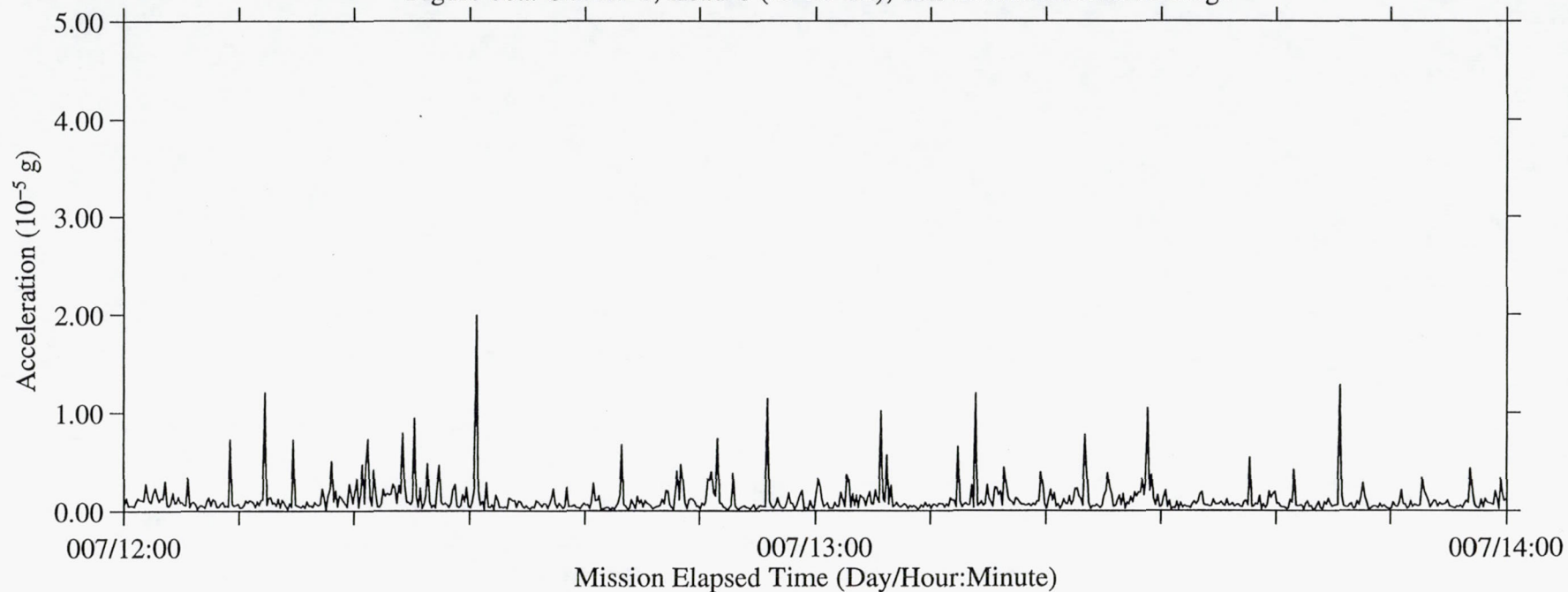
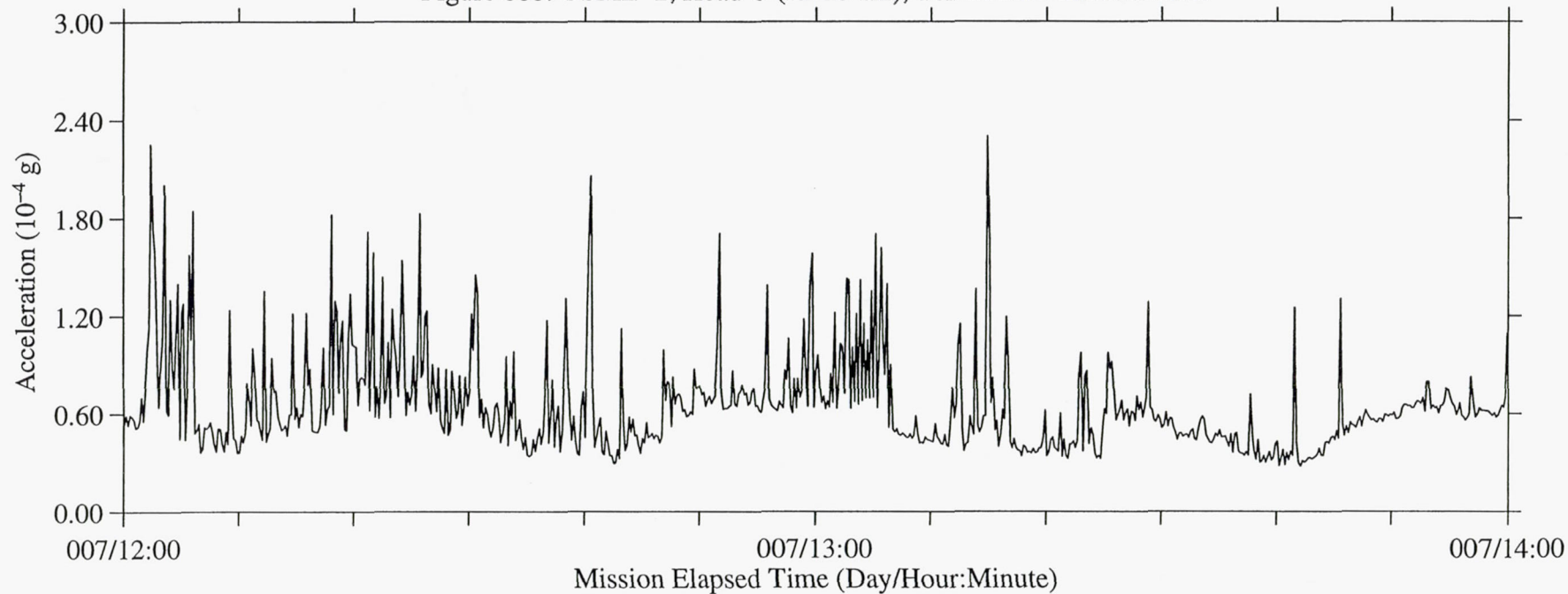


Figure 88b: USML-2, Head C (fc=25 Hz), Ten Second Interval RMS





16-B

Figure 89a: USML-2, Head C (fc=25 Hz), Ten Second Interval Average

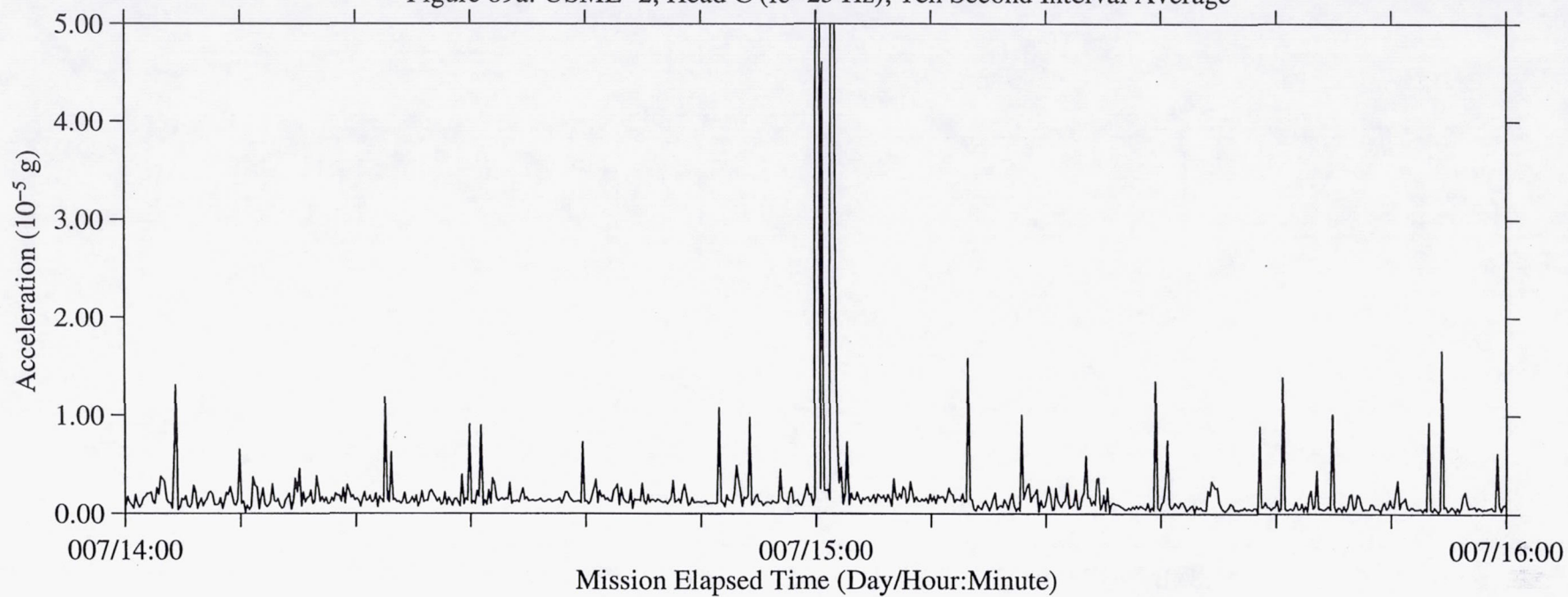


Figure 89b: USML-2, Head C (fc=25 Hz), Ten Second Interval RMS

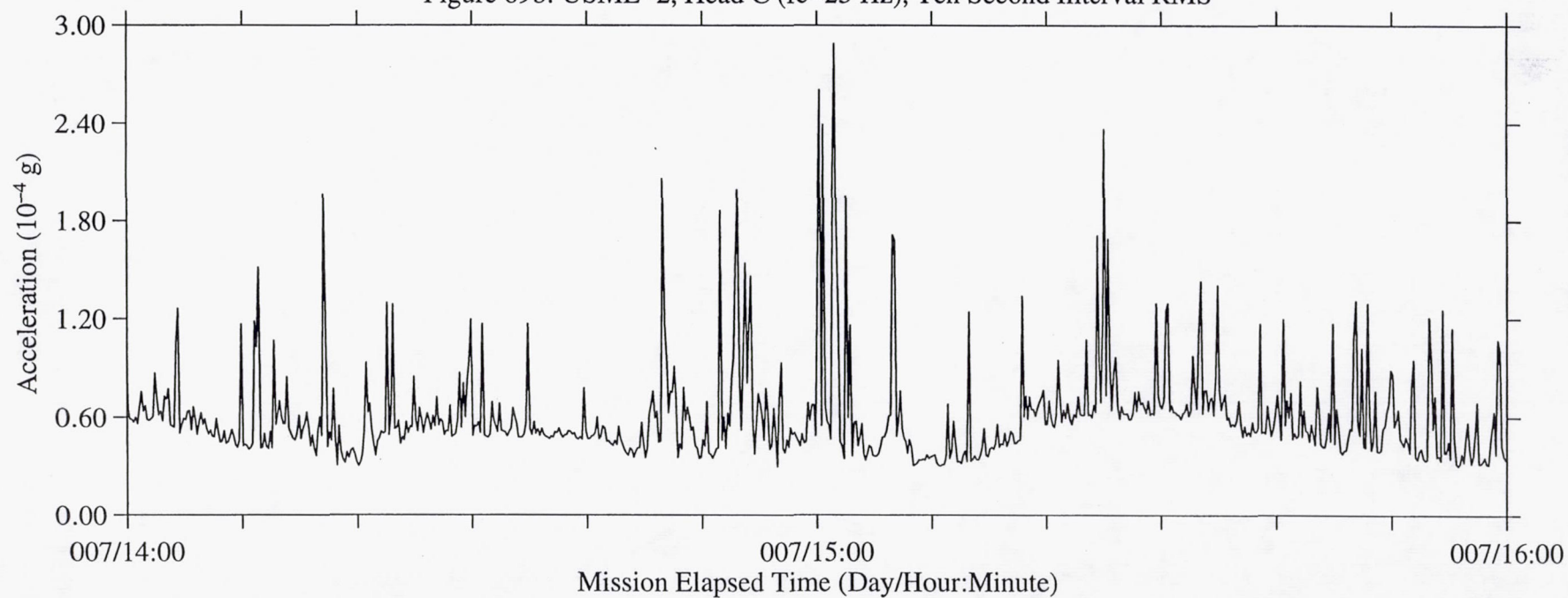


Figure 90a: USML-2, Head C (fc=25 Hz), Ten Second Interval Average

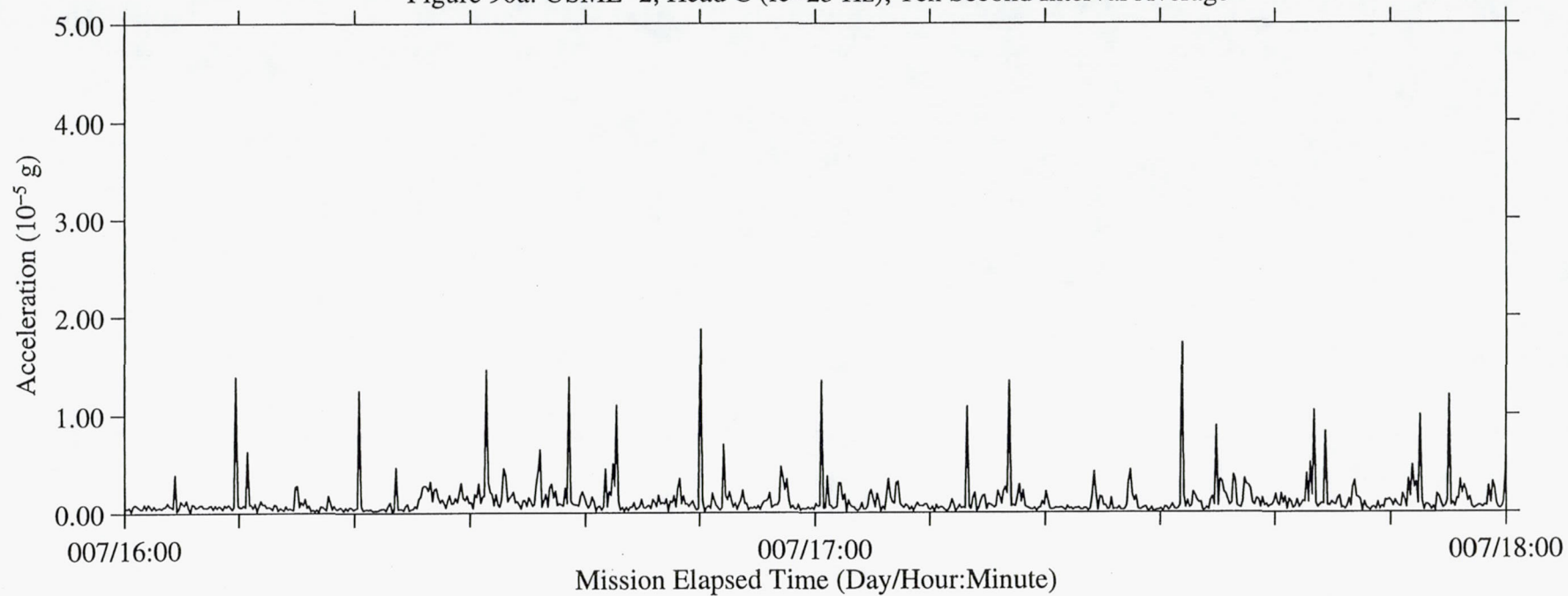


Figure 90b: USML-2, Head C (fc=25 Hz), Ten Second Interval RMS

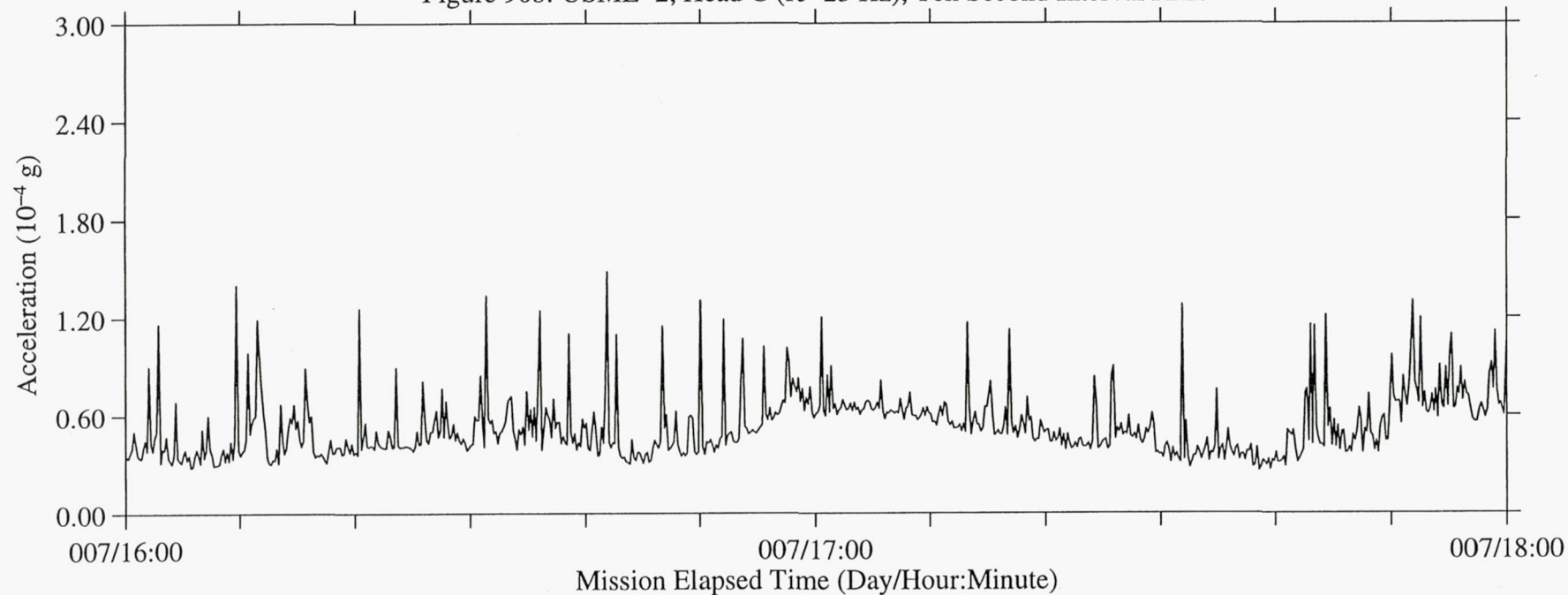




Figure 91a: USML-2, Head C (fc=25 Hz), Ten Second Interval Average

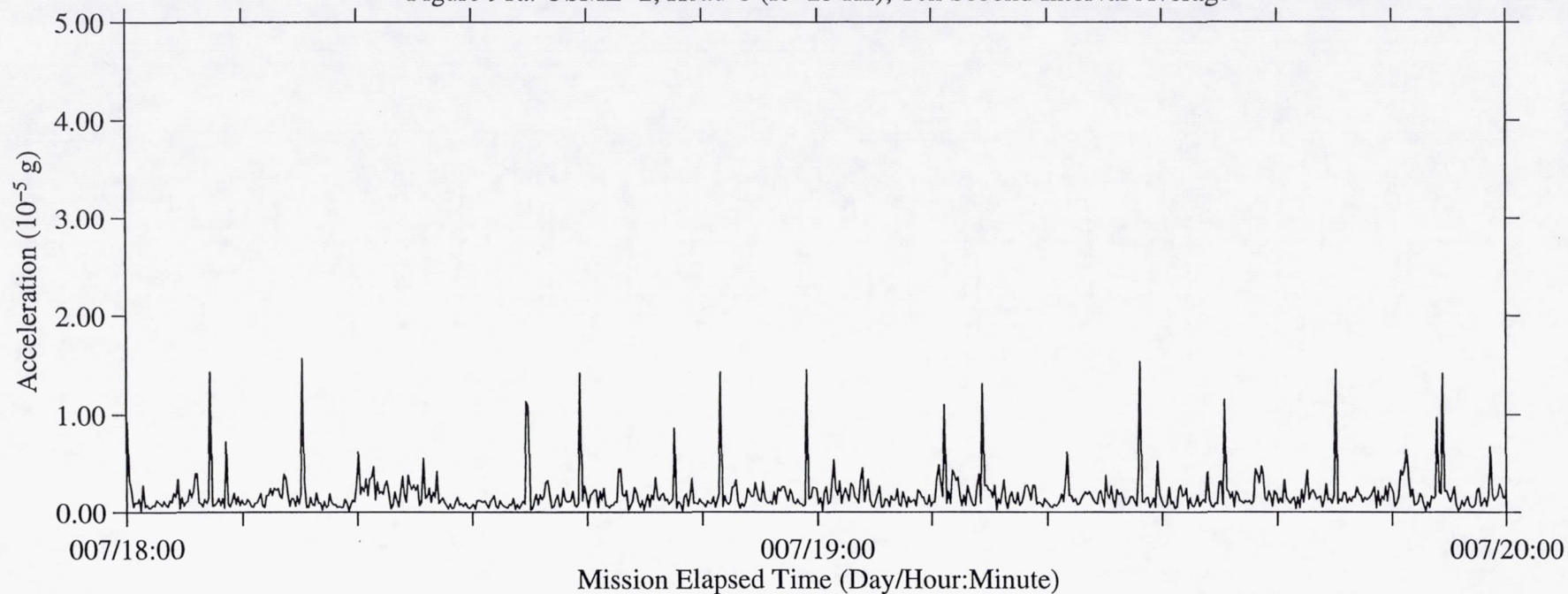


Figure 91b: USML-2, Head C (fc=25 Hz), Ten Second Interval RMS

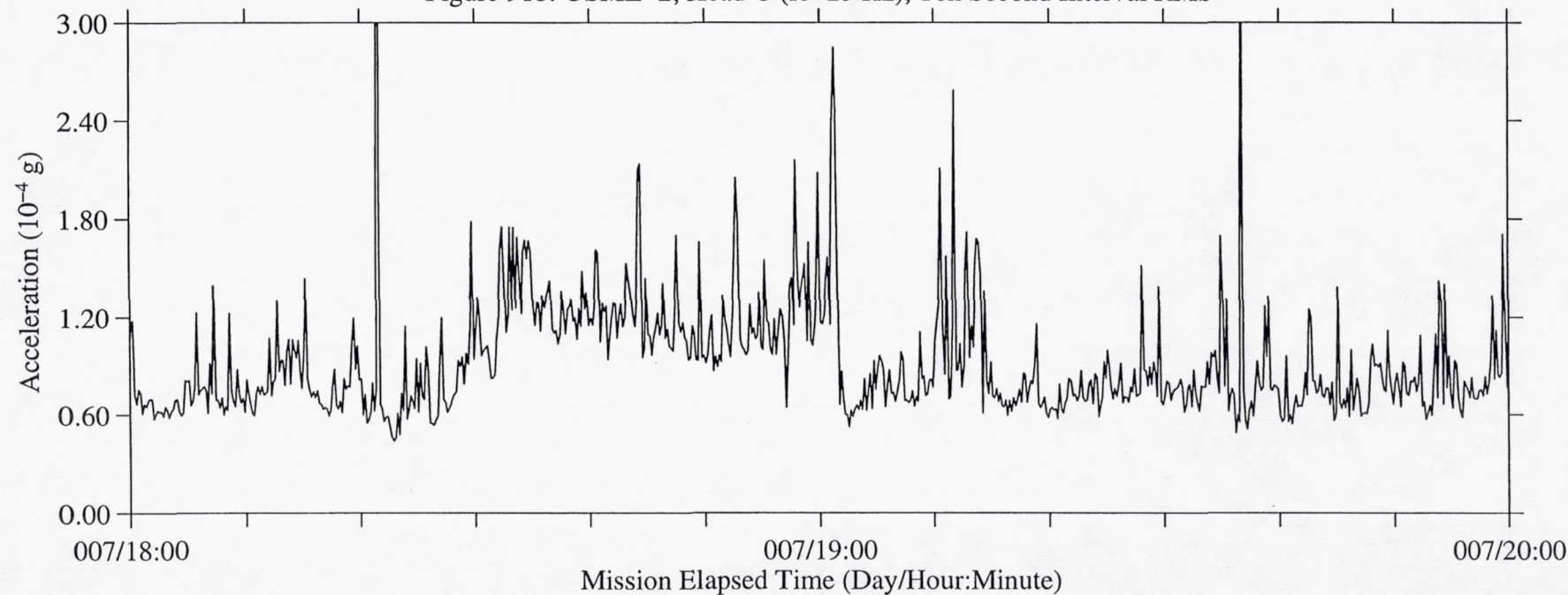


Figure 92a: USML-2, Head C (fc=25 Hz), Ten Second Interval Average

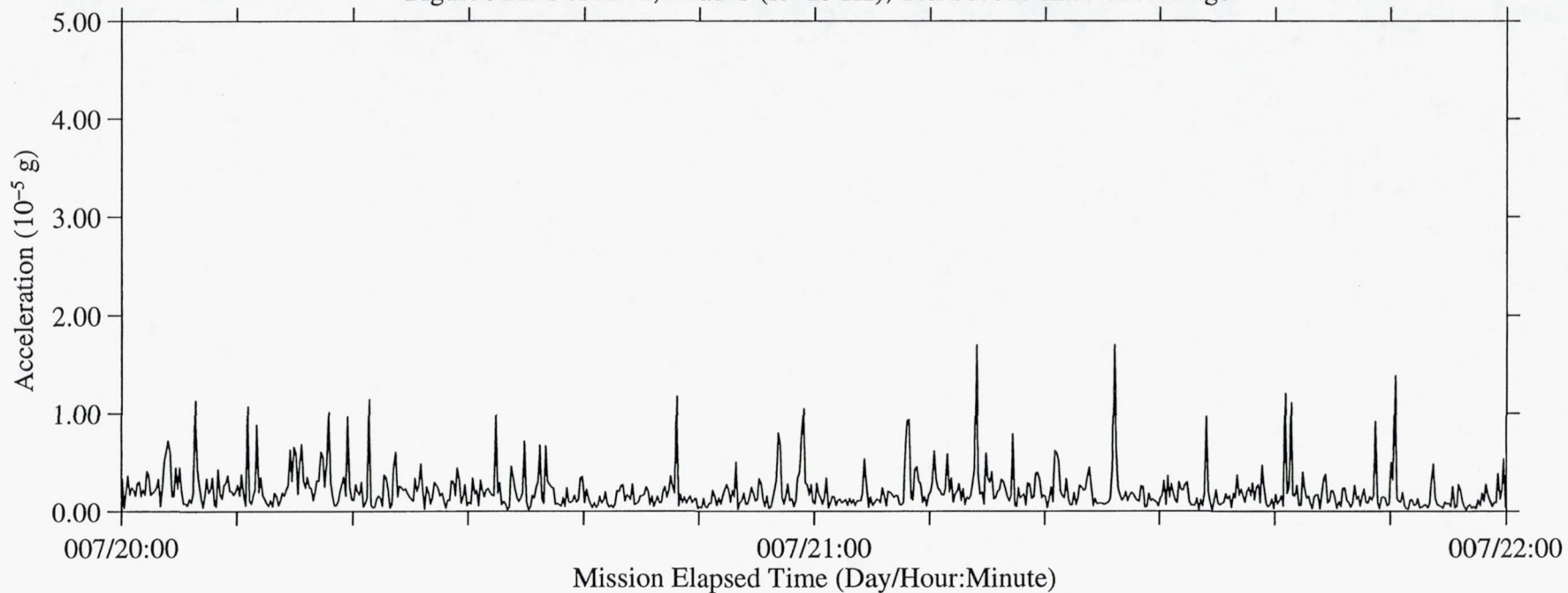


Figure 92b: USML-2, Head C (fc=25 Hz), Ten Second Interval RMS

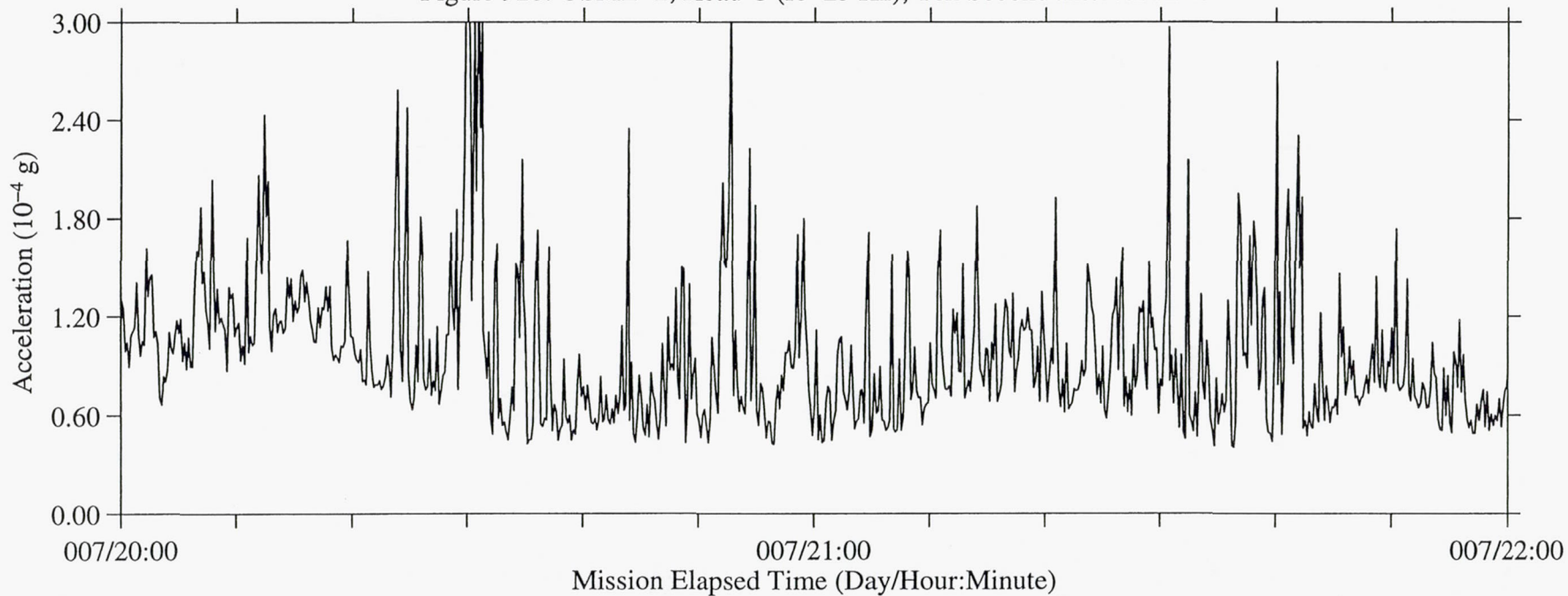




Figure 93a: USML-2, Head C (fc=25 Hz), Ten Second Interval Average

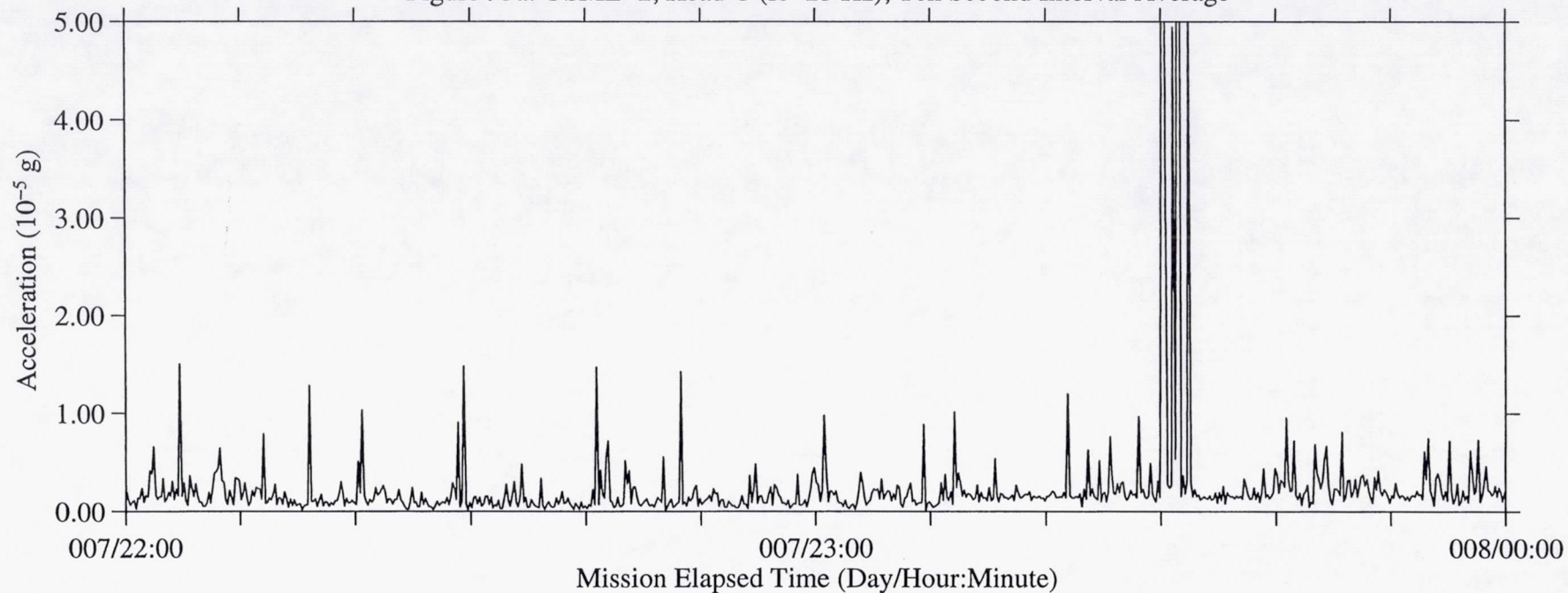


Figure 93b: USML-2, Head C (fc=25 Hz), Ten Second Interval RMS

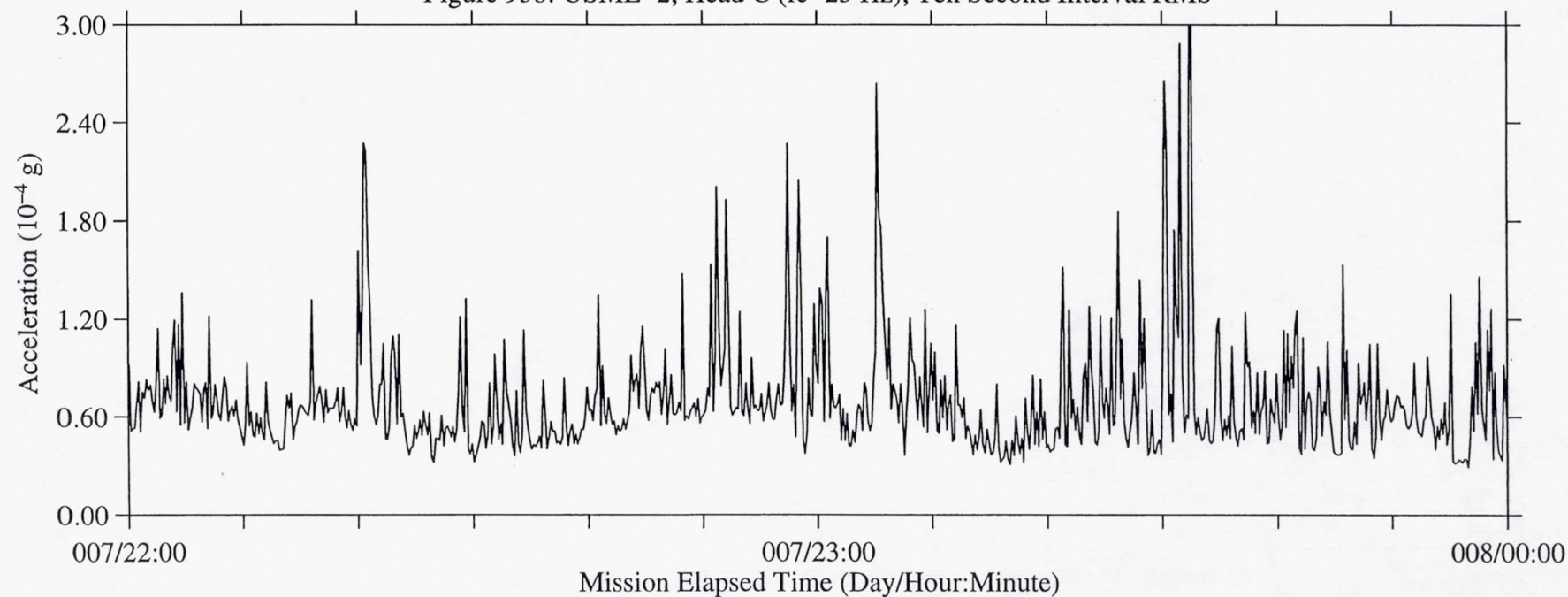


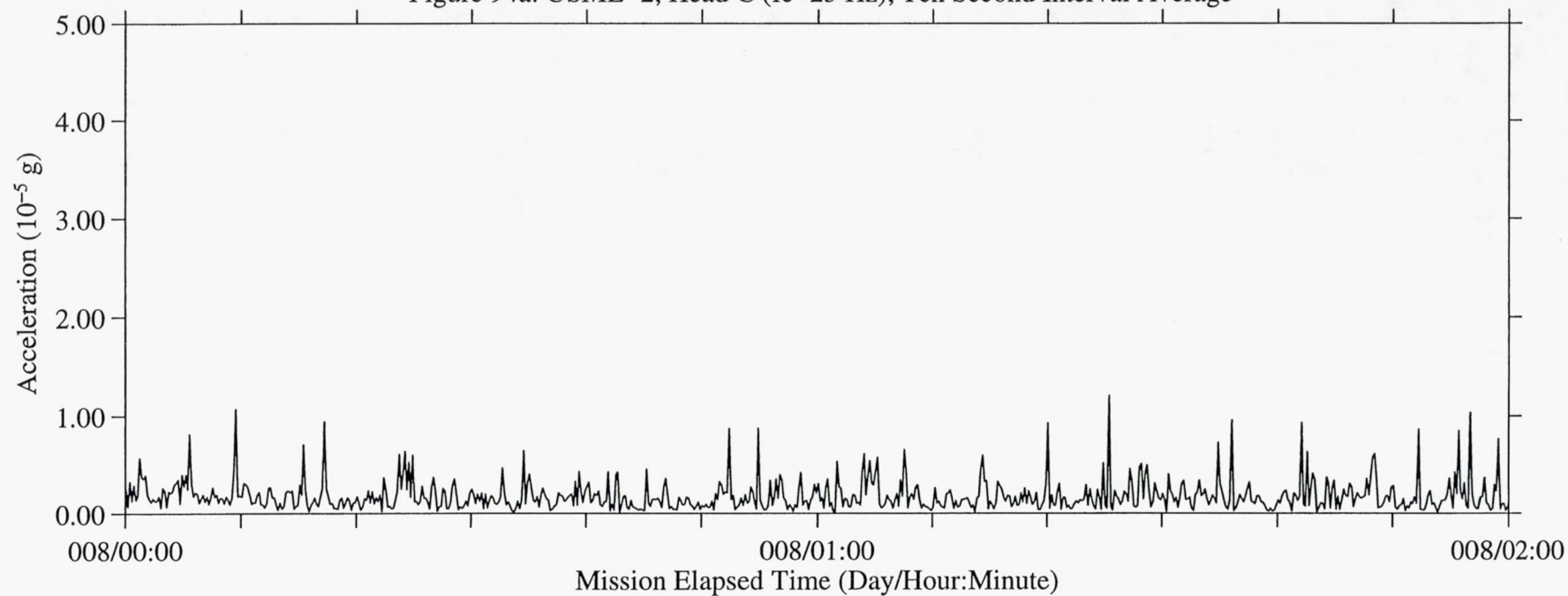
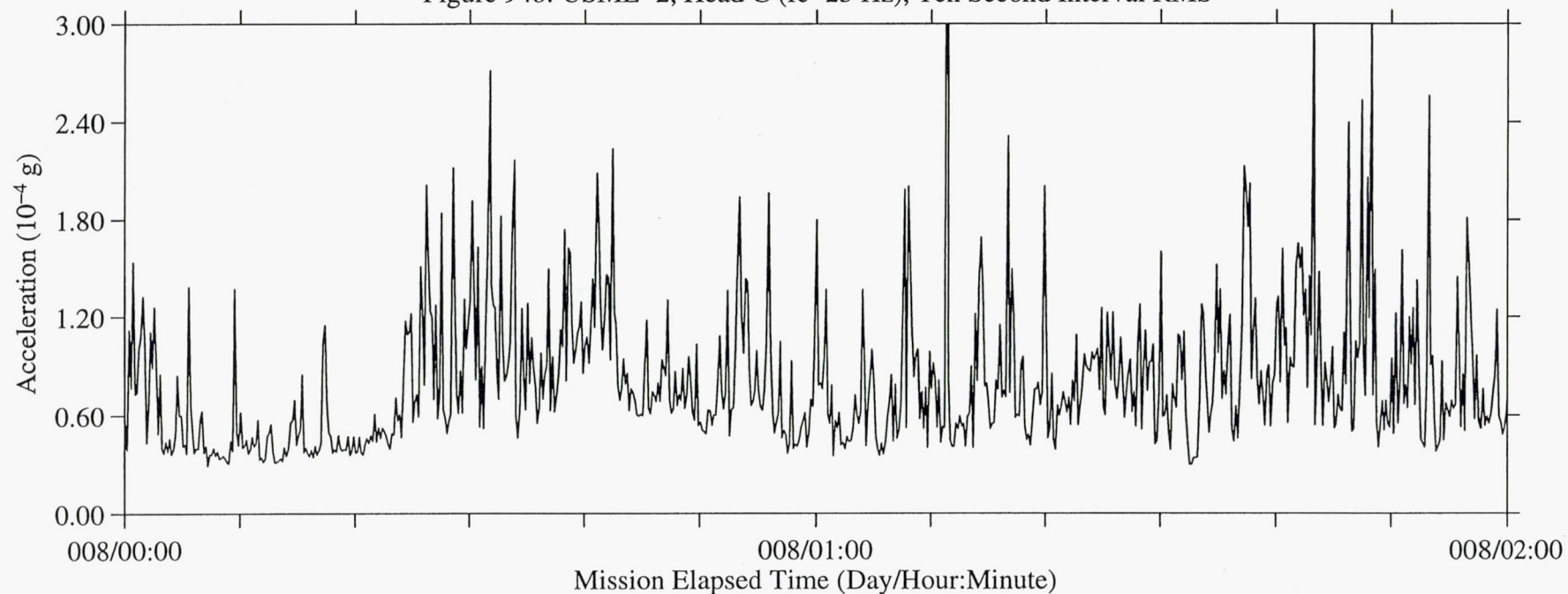
Figure 94a: USML-2, Head C ( $f_c=25$  Hz), Ten Second Interval AverageFigure 94b: USML-2, Head C ( $f_c=25$  Hz), Ten Second Interval RMS



Figure 95a: USML-2, Head C (fc=25 Hz), Ten Second Interval Average

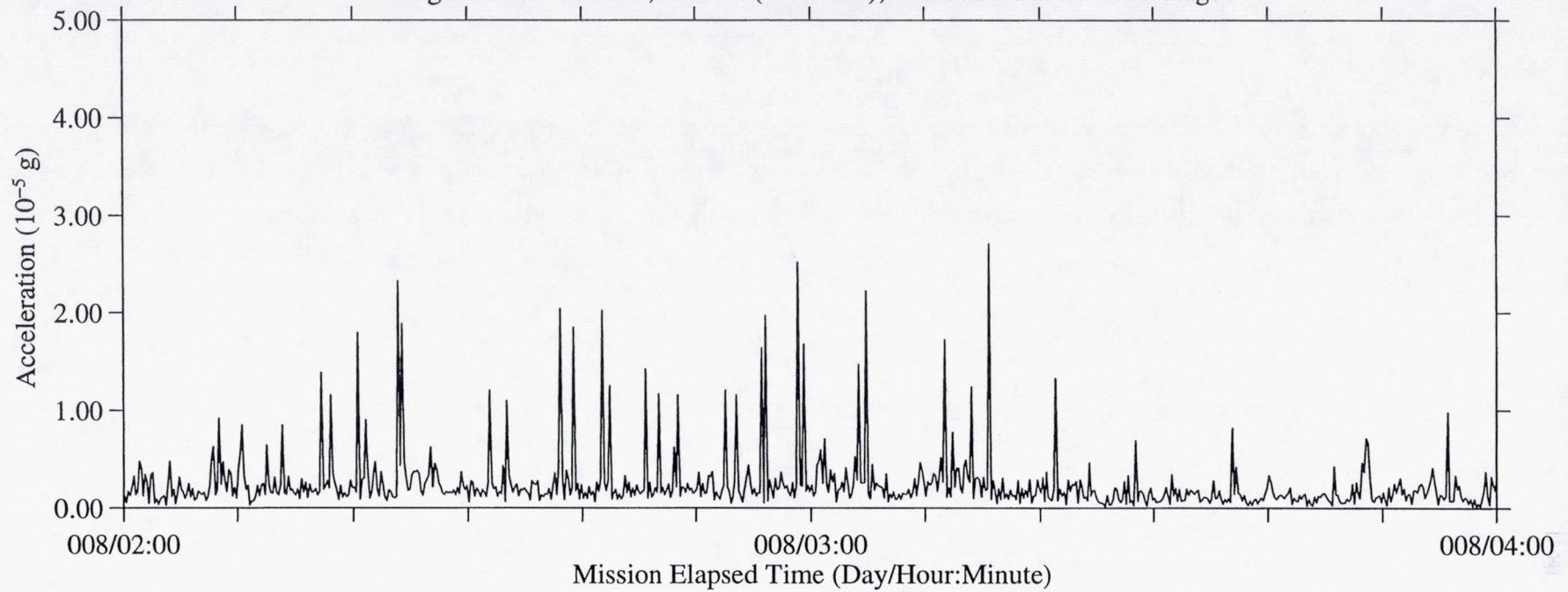


Figure 95b: USML-2, Head C (fc=25 Hz), Ten Second Interval RMS

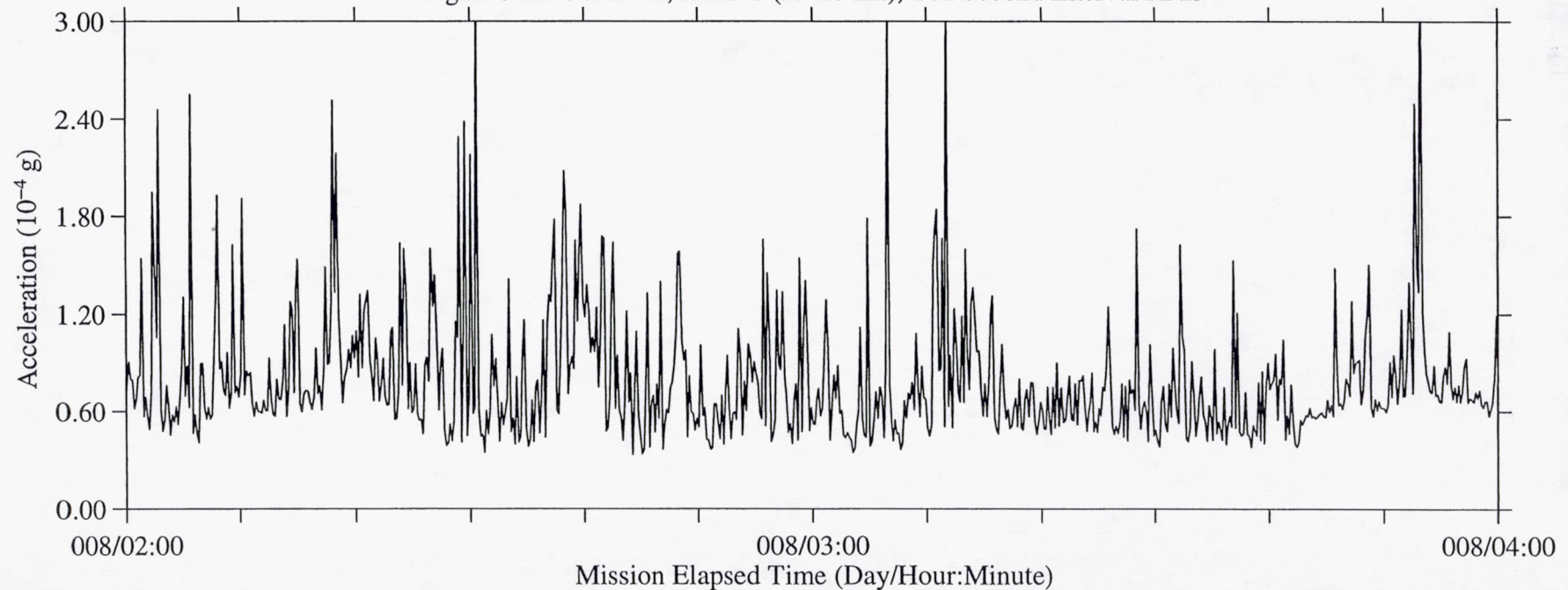


Figure 96a: USML-2, Head C (fc=25 Hz), Ten Second Interval Average

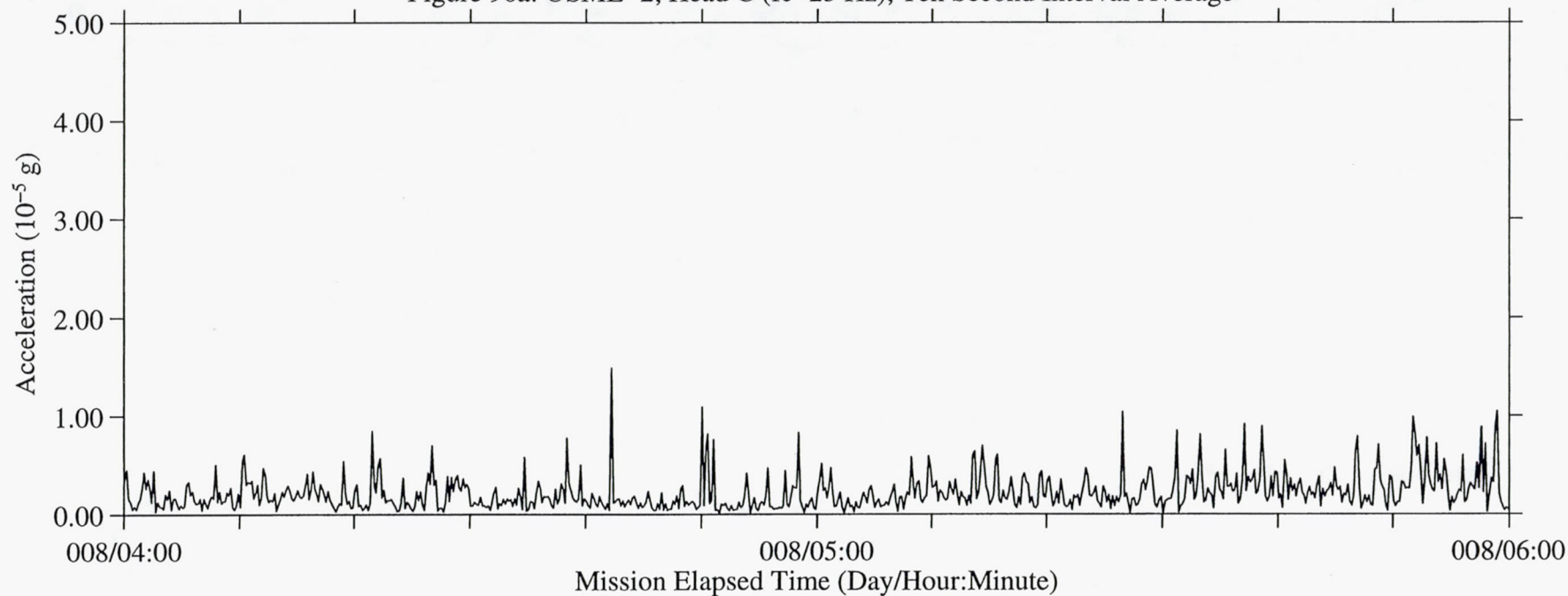


Figure 96b: USML-2, Head C (fc=25 Hz), Ten Second Interval RMS

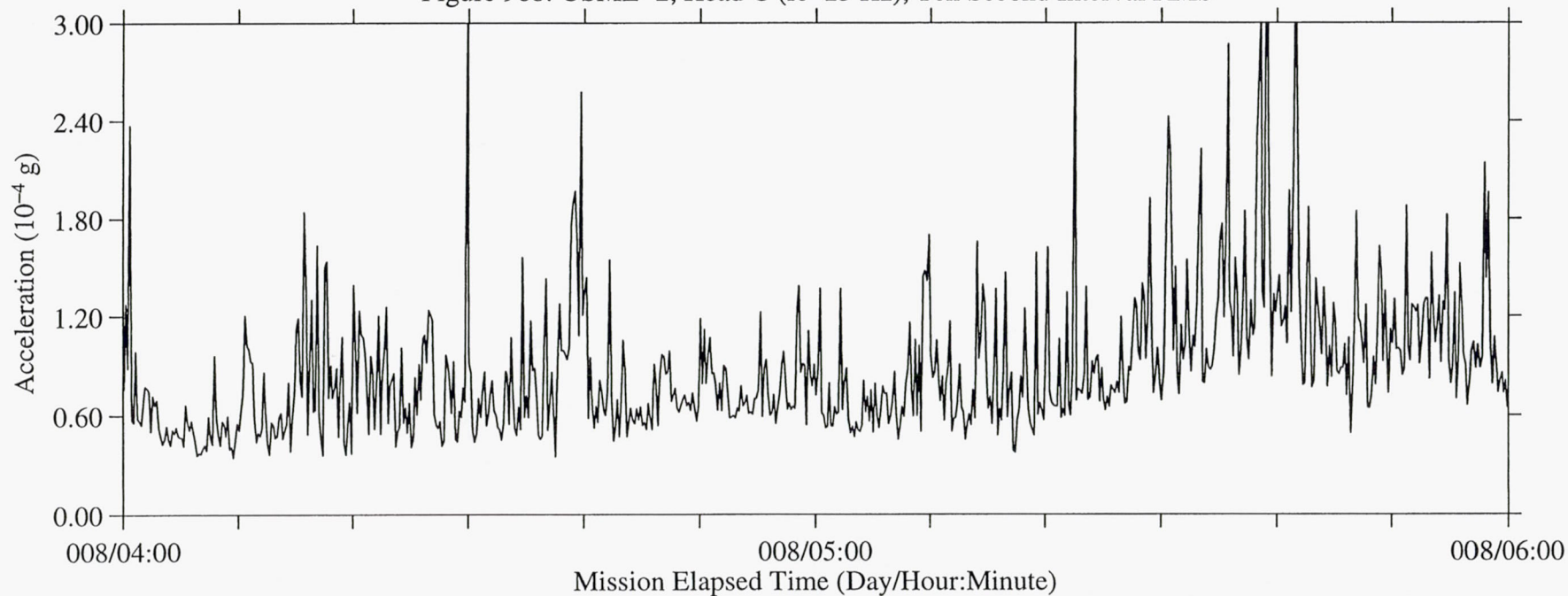




Figure 97a: USML-2, Head C (fc=25 Hz), Ten Second Interval Average

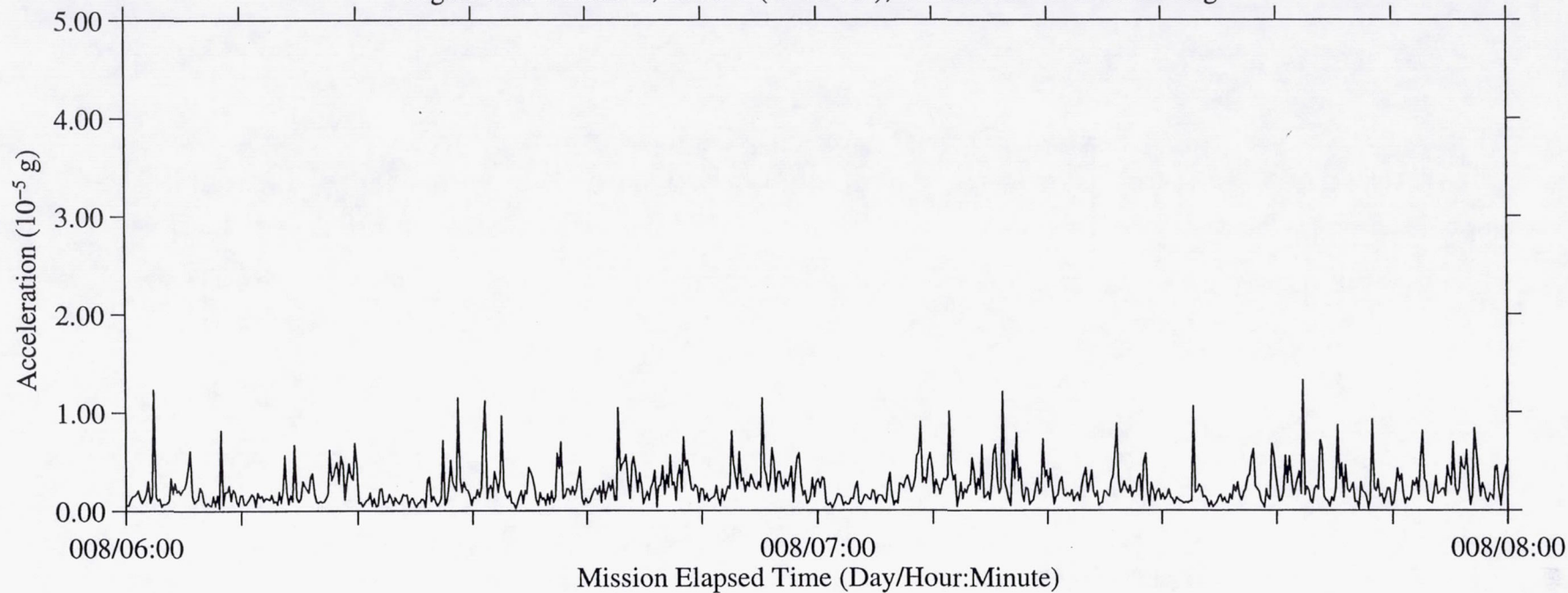


Figure 97b: USML-2, Head C (fc=25 Hz), Ten Second Interval RMS

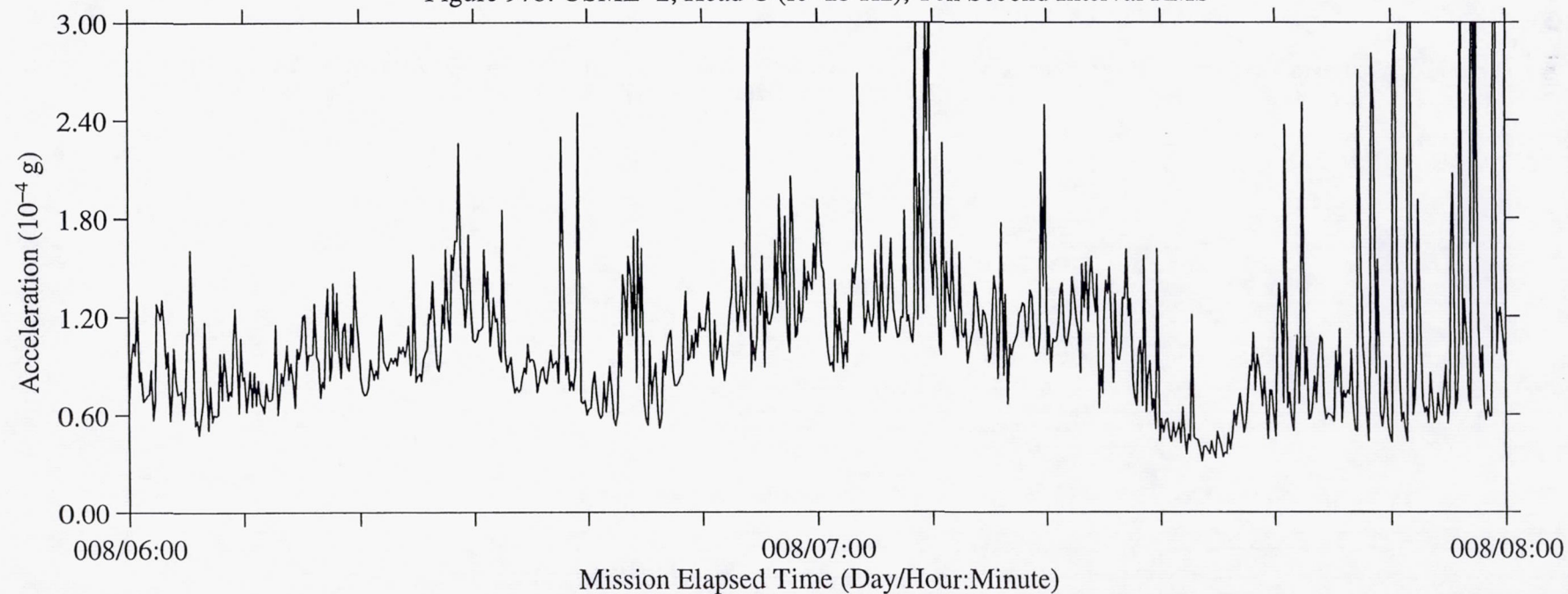


Figure 98a: USML-2, Head C (fc=25 Hz), Ten Second Interval Average

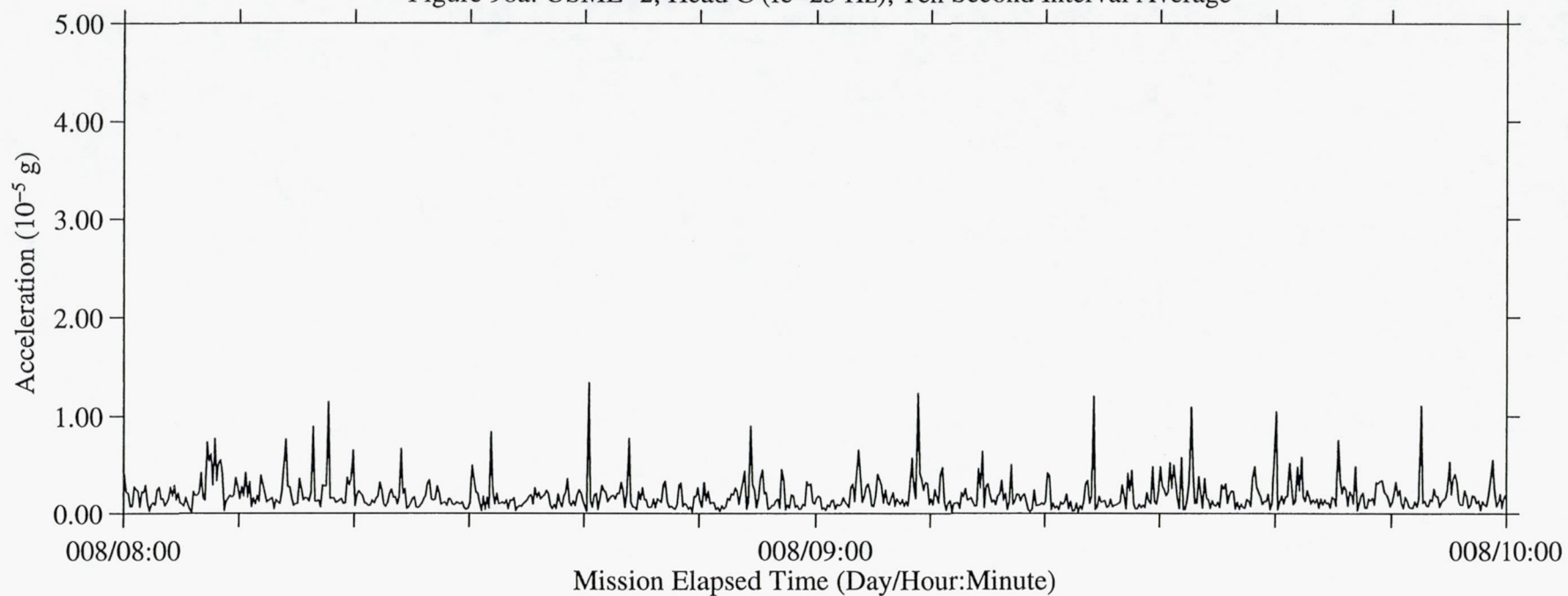


Figure 98b: USML-2, Head C (fc=25 Hz), Ten Second Interval RMS

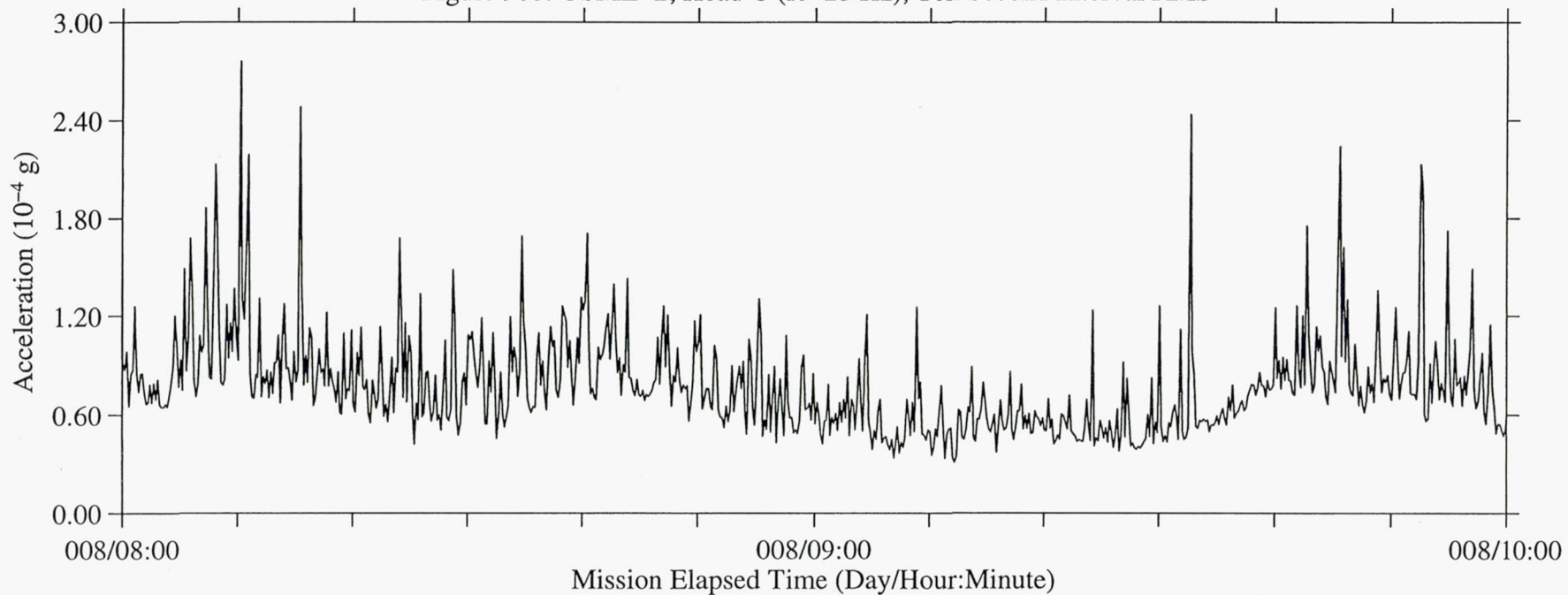




Figure 99a: USML-2, Head C (fc=25 Hz), Ten Second Interval Average

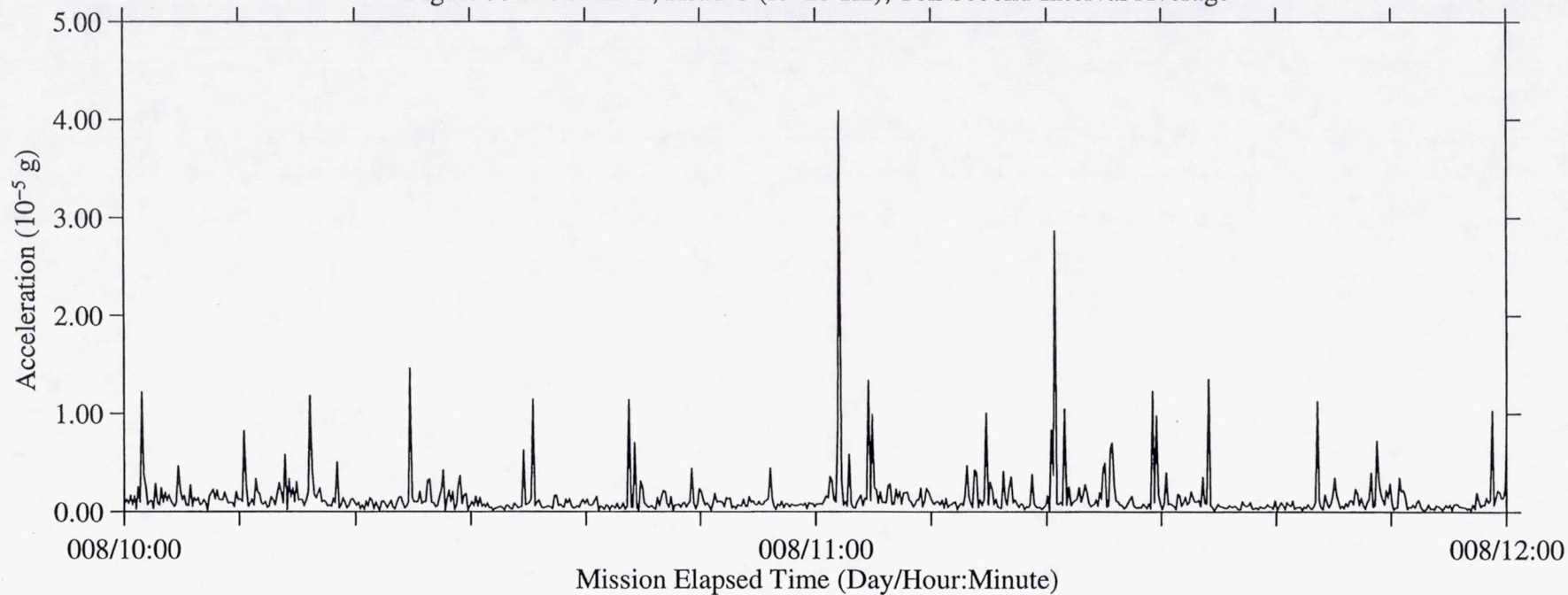


Figure 99b: USML-2, Head C (fc=25 Hz), Ten Second Interval RMS

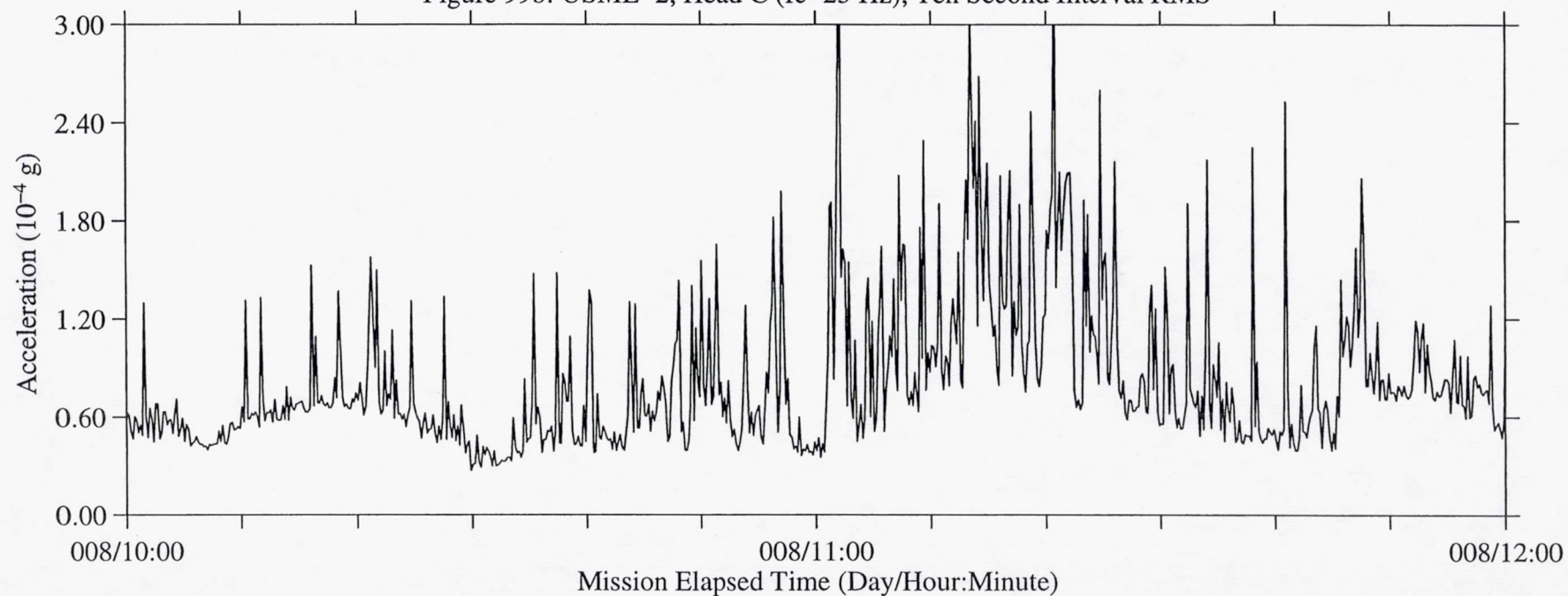


Figure 100a: USML-2, Head C (fc=25 Hz), Ten Second Interval Average

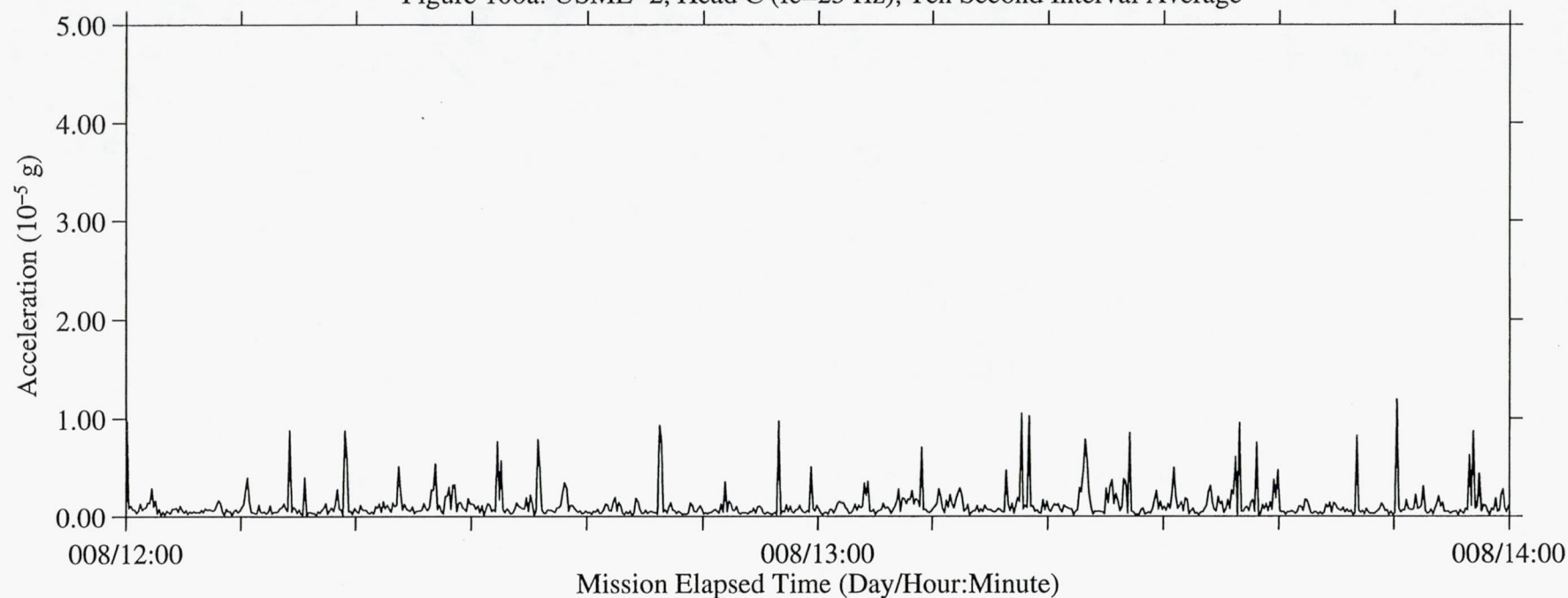


Figure 100b: USML-2, Head C (fc=25 Hz), Ten Second Interval RMS

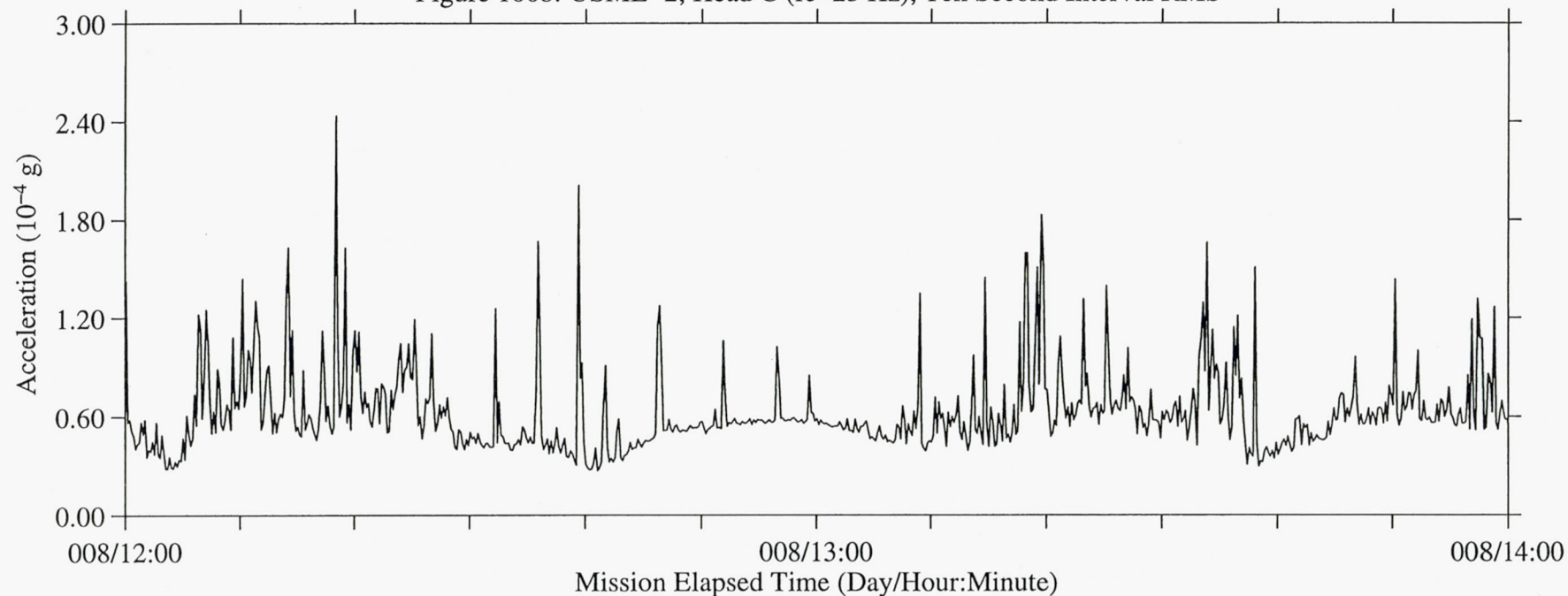




Figure 101a: USML-2, Head C (fc=25 Hz), Ten Second Interval Average

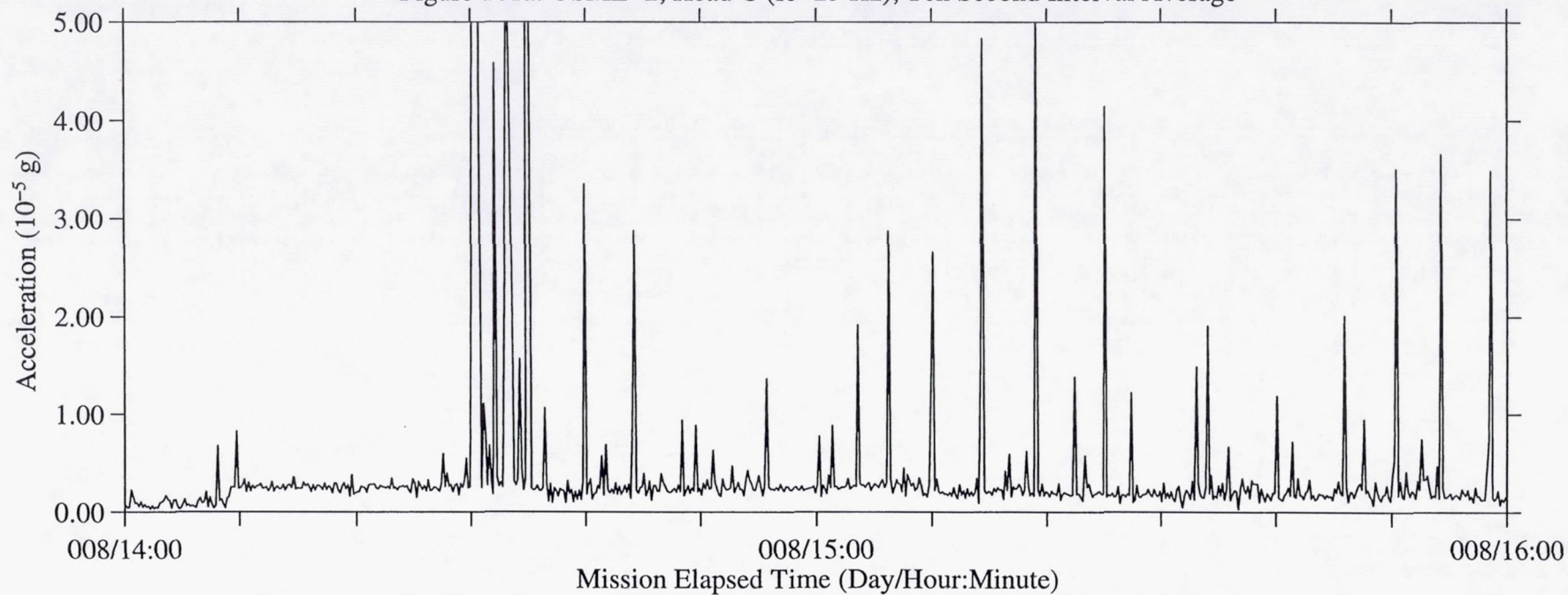


Figure 101b: USML-2, Head C (fc=25 Hz), Ten Second Interval RMS

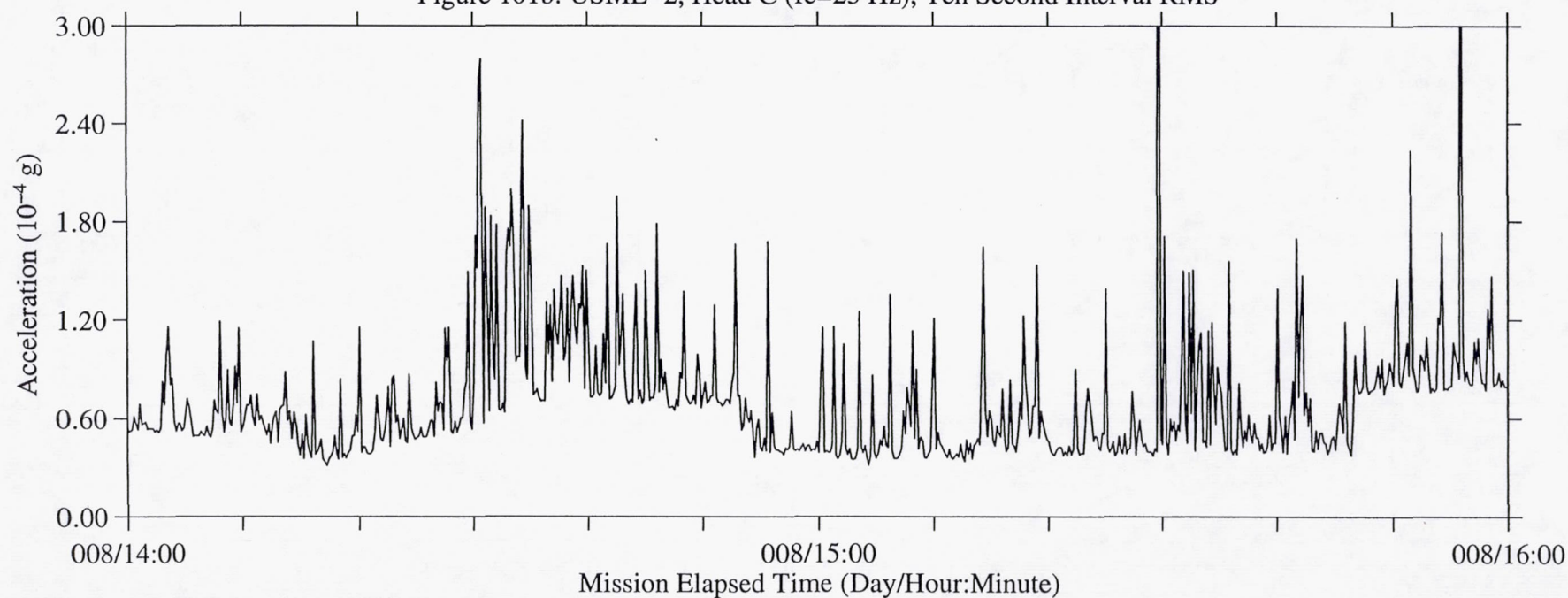


Figure 102a: USML-2, Head C (fc=25 Hz), Ten Second Interval Average

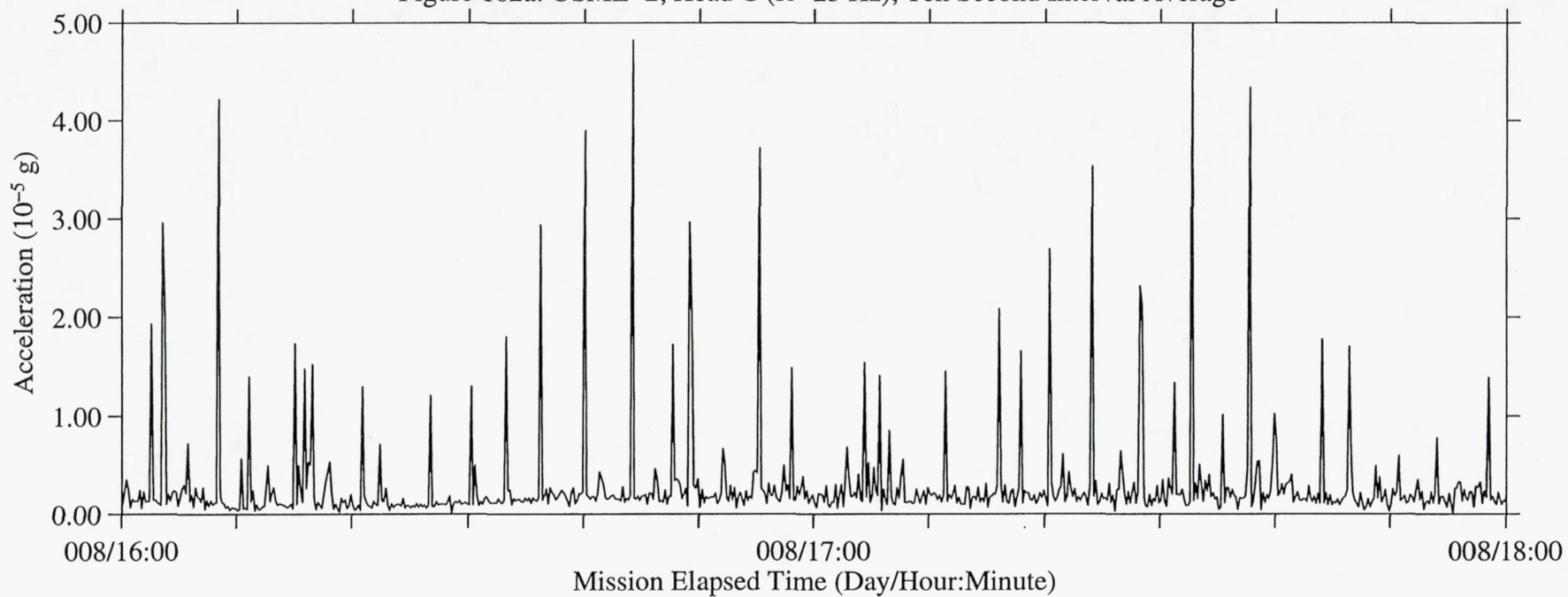


Figure 102b: USML-2, Head C (fc=25 Hz), Ten Second Interval RMS

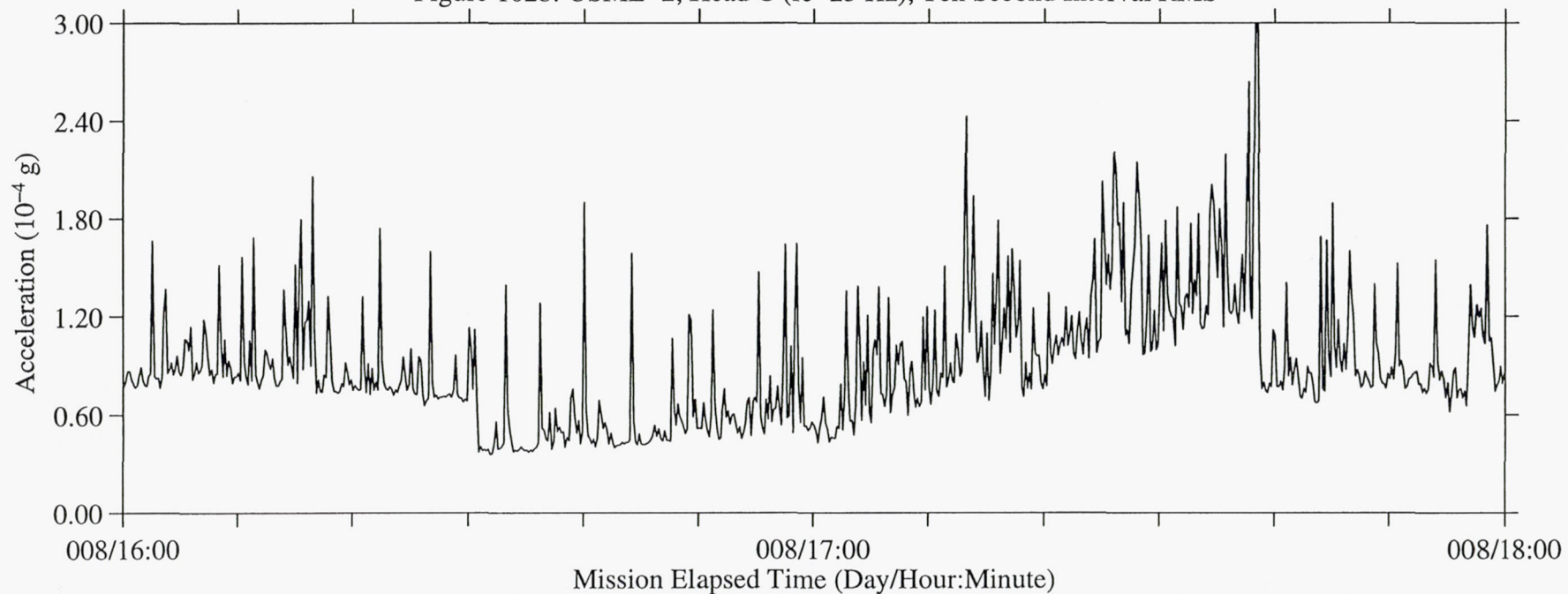




Figure 103a: USML-2, Head C (fc=25 Hz), Ten Second Interval Average

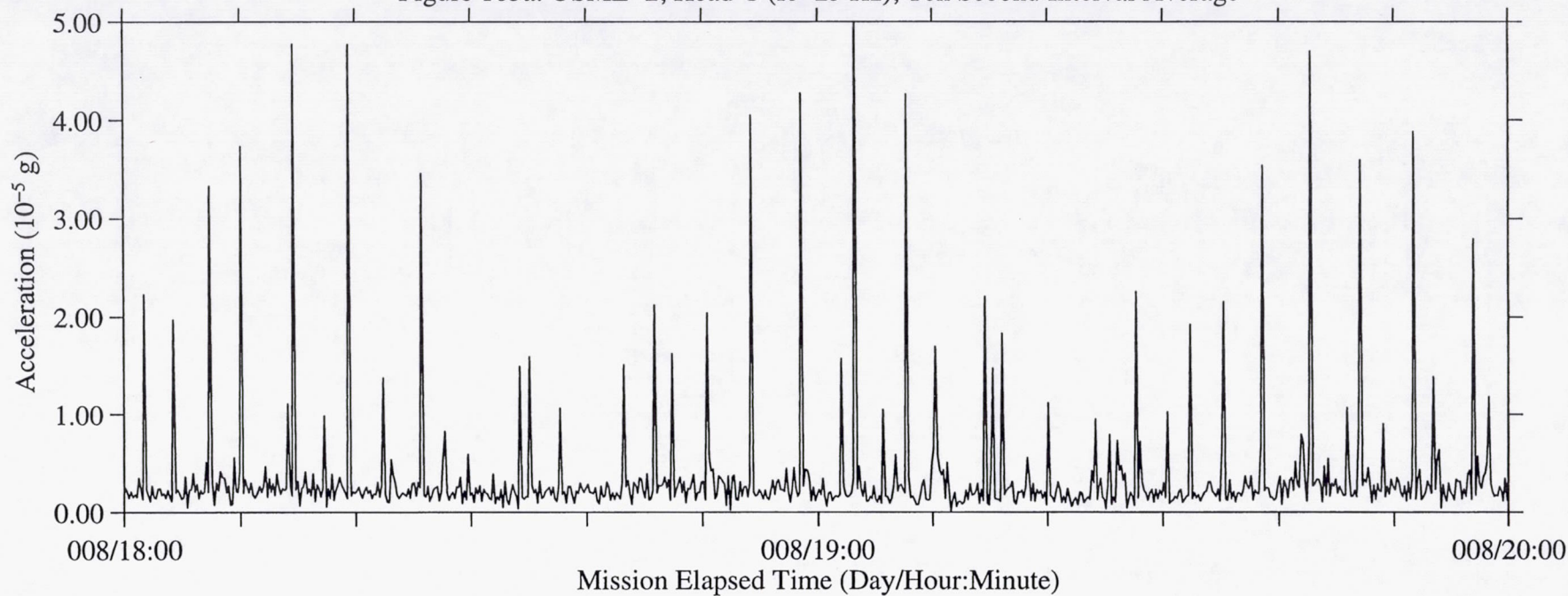


Figure 103b: USML-2, Head C (fc=25 Hz), Ten Second Interval RMS

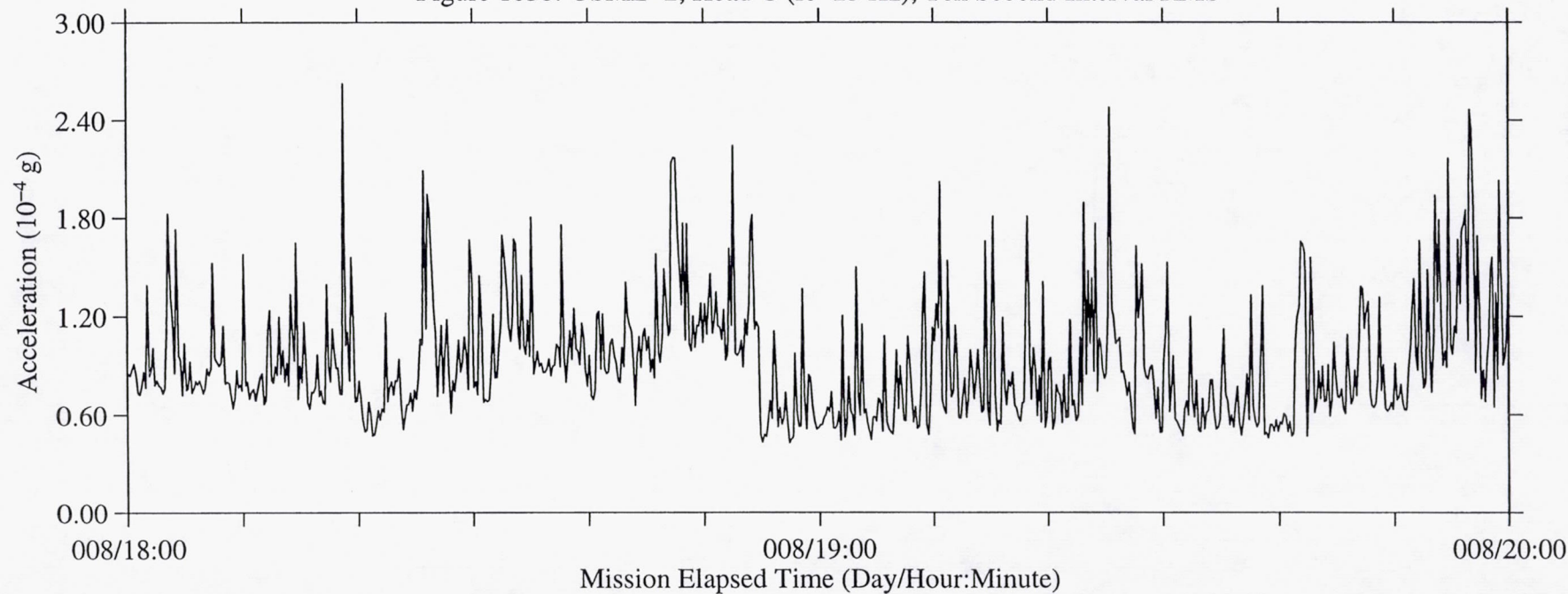


Figure 104a: USML-2, Head C (fc=25 Hz), Ten Second Interval Average

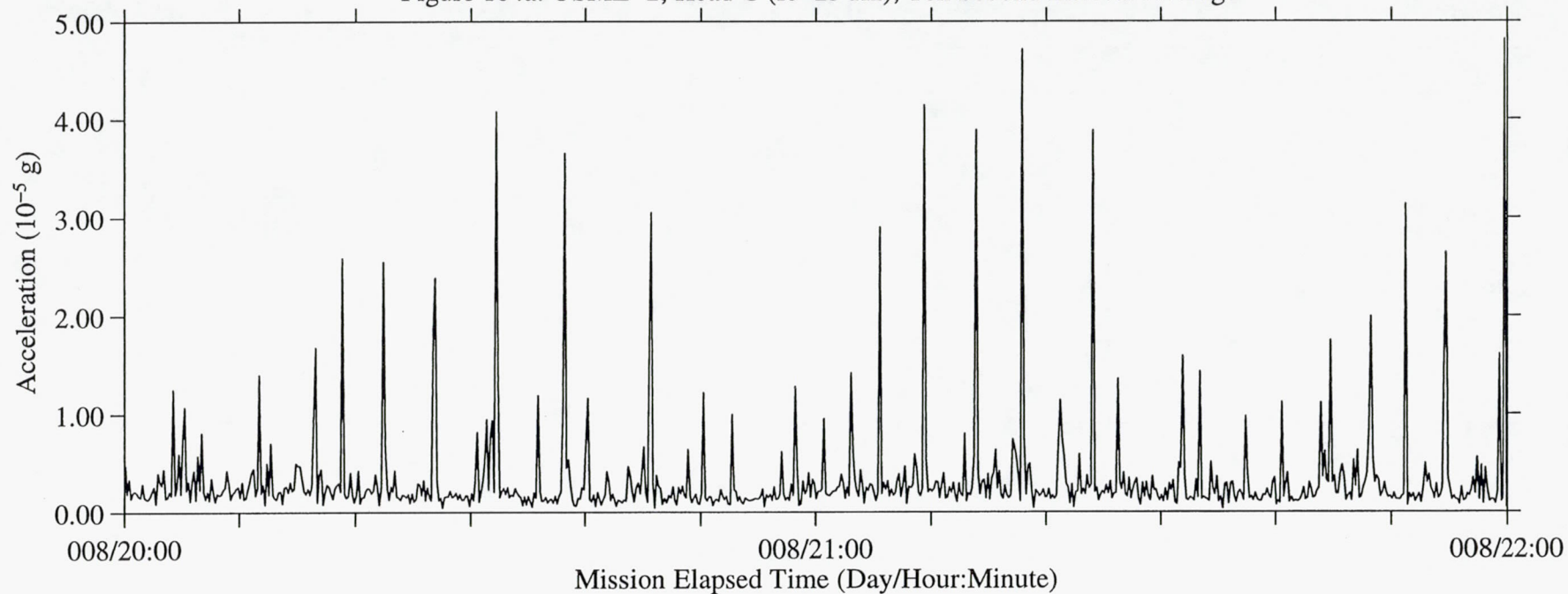
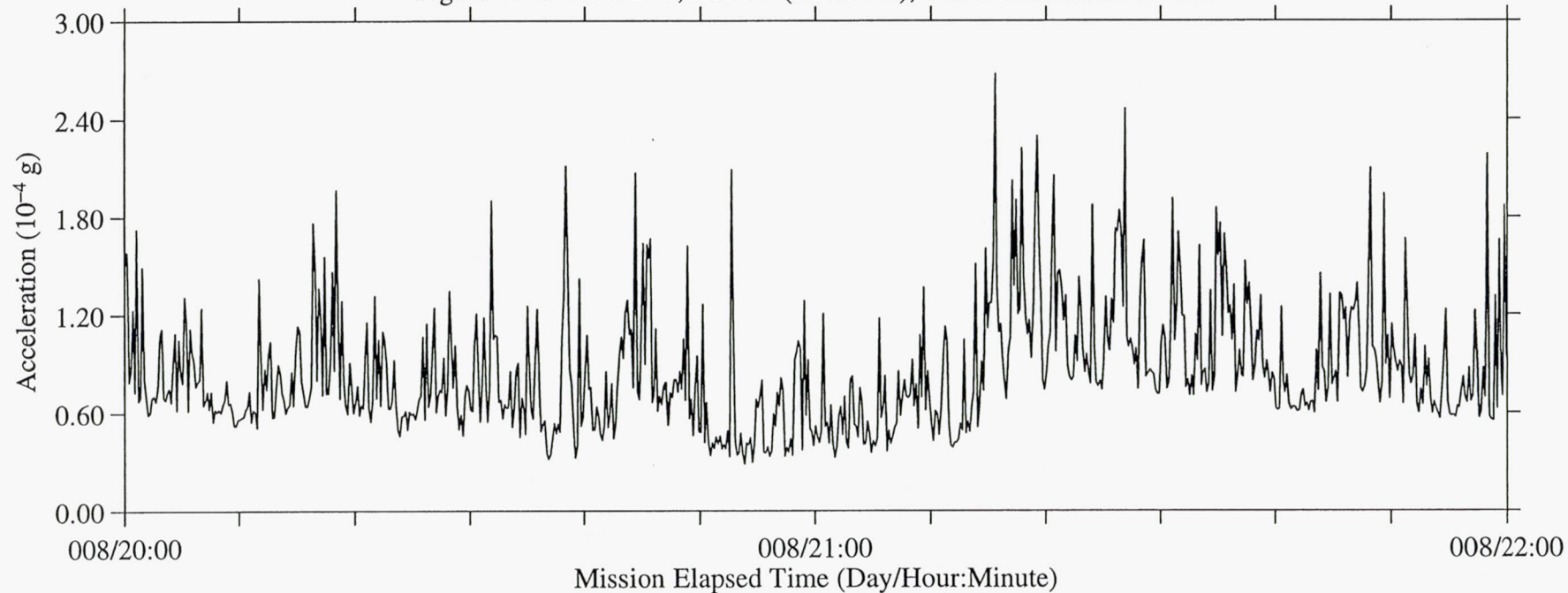


Figure 104b: USML-2, Head C (fc=25 Hz), Ten Second Interval RMS





B-107

Figure 105a: USML-2, Head C (fc=25 Hz), Ten Second Interval Average

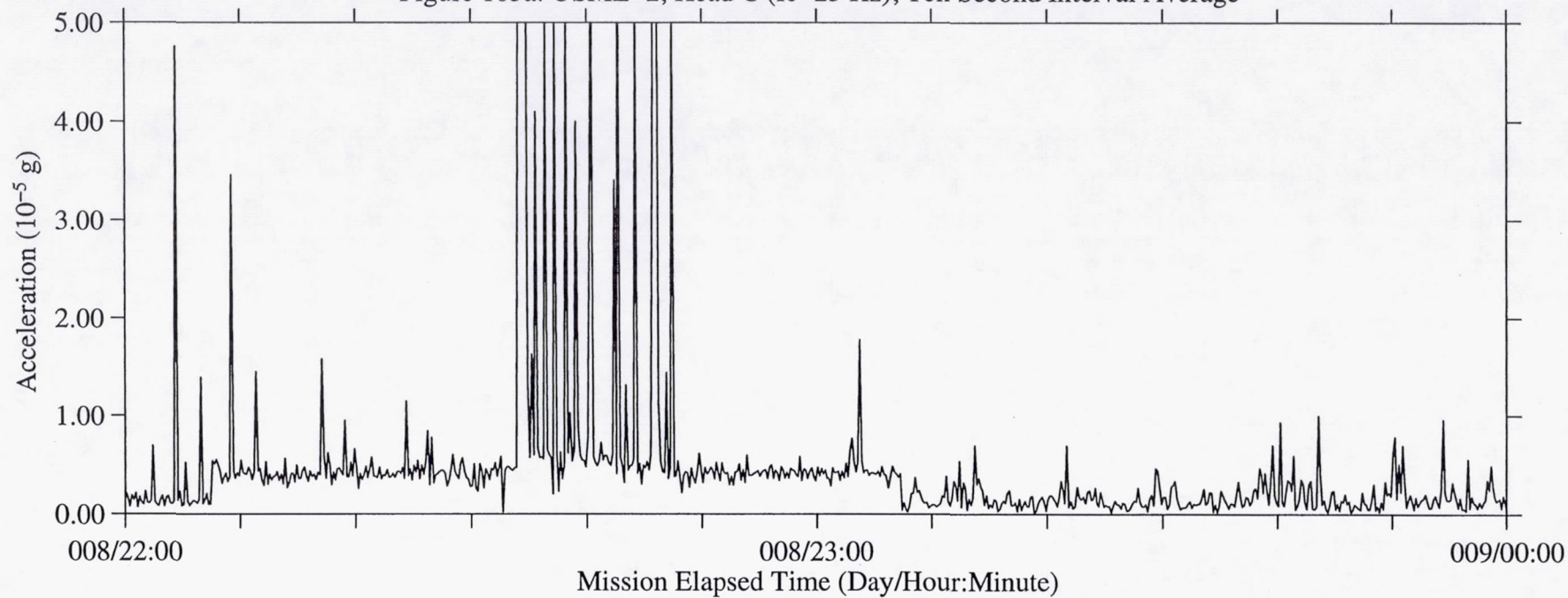


Figure 105b: USML-2, Head C (fc=25 Hz), Ten Second Interval RMS

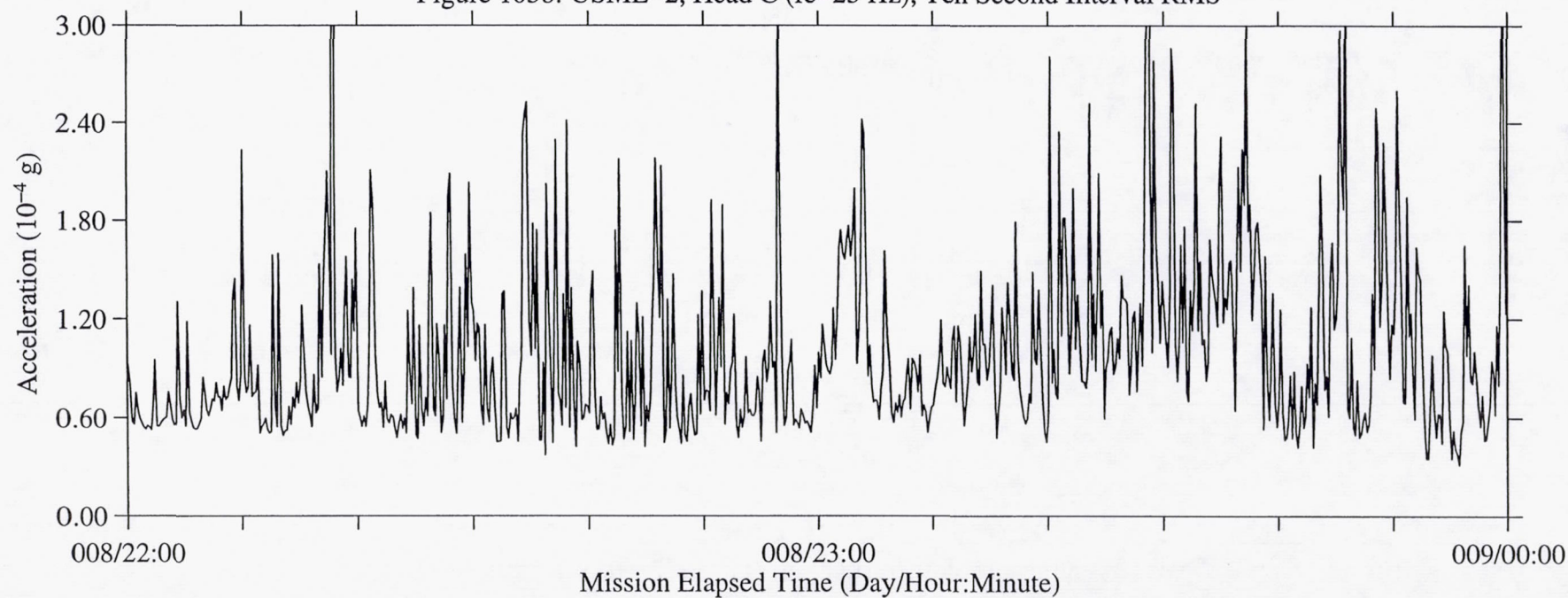


Figure 106a: USML-2, Head C (fc=25 Hz), Ten Second Interval Average

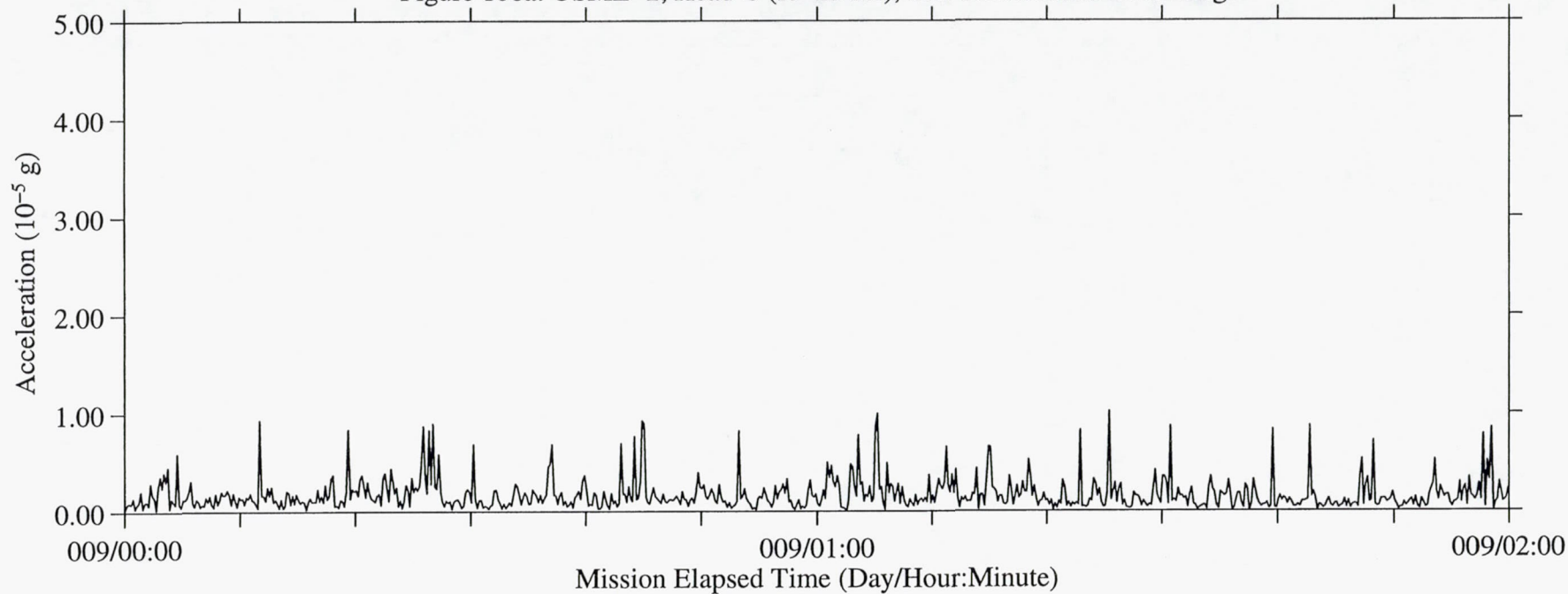


Figure 106b: USML-2, Head C (fc=25 Hz), Ten Second Interval RMS

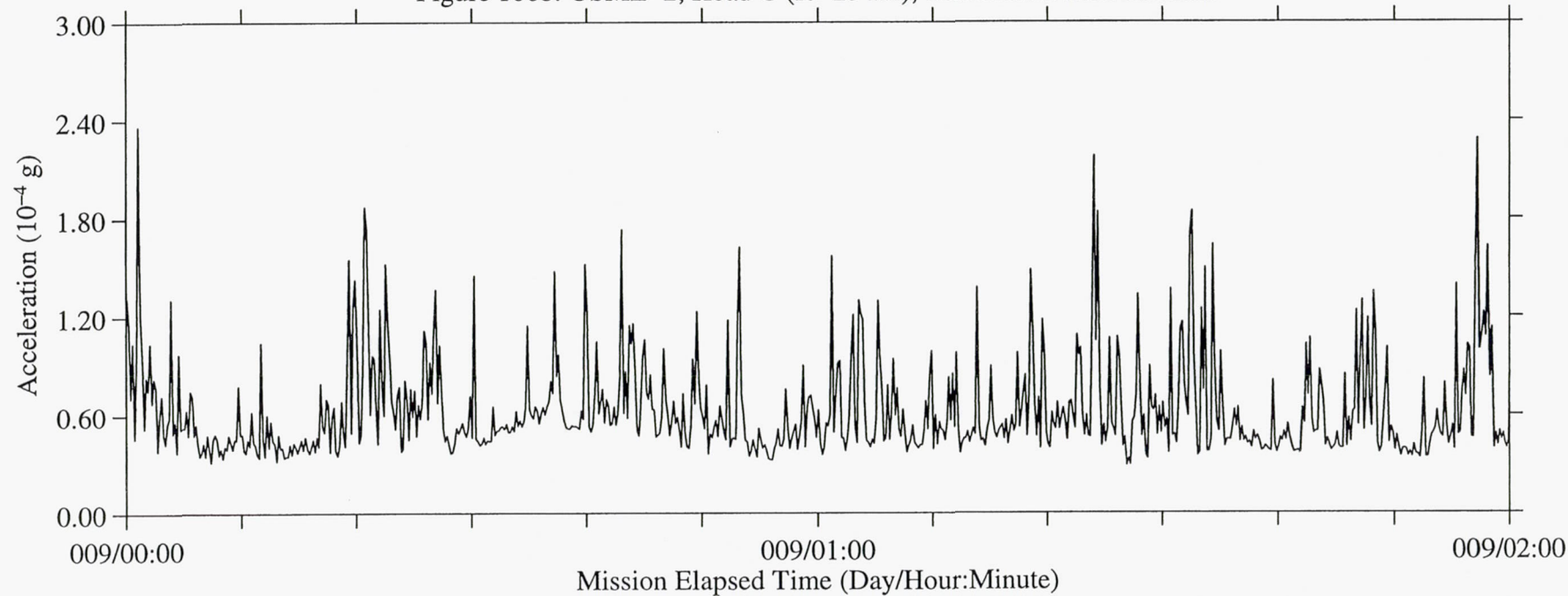




Figure 107a: USML-2, Head C (fc=25 Hz), Ten Second Interval Average

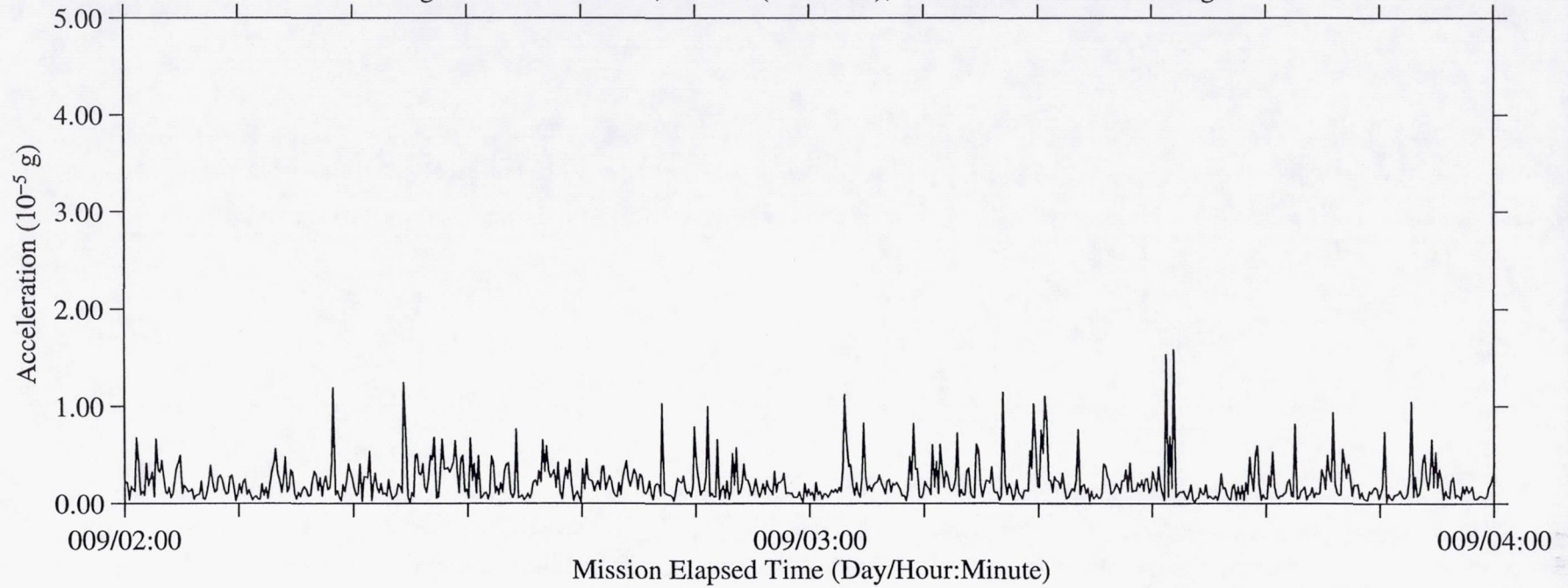


Figure 107b: USML-2, Head C (fc=25 Hz), Ten Second Interval RMS

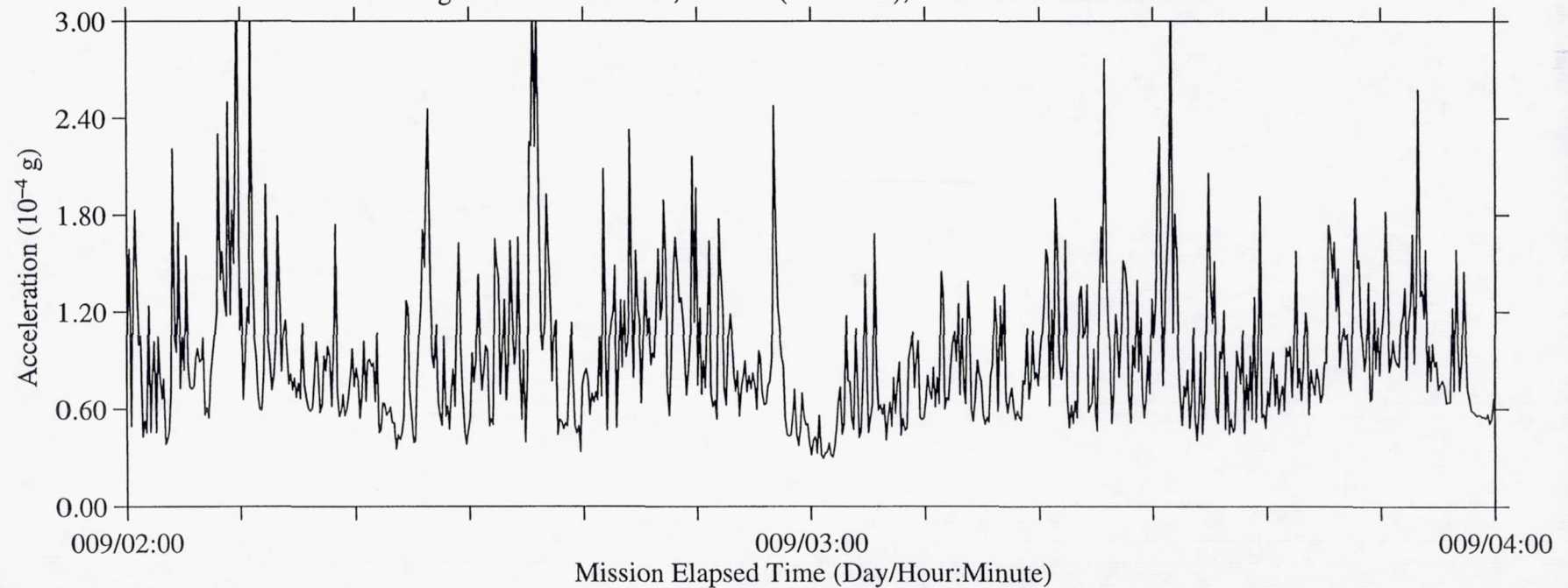


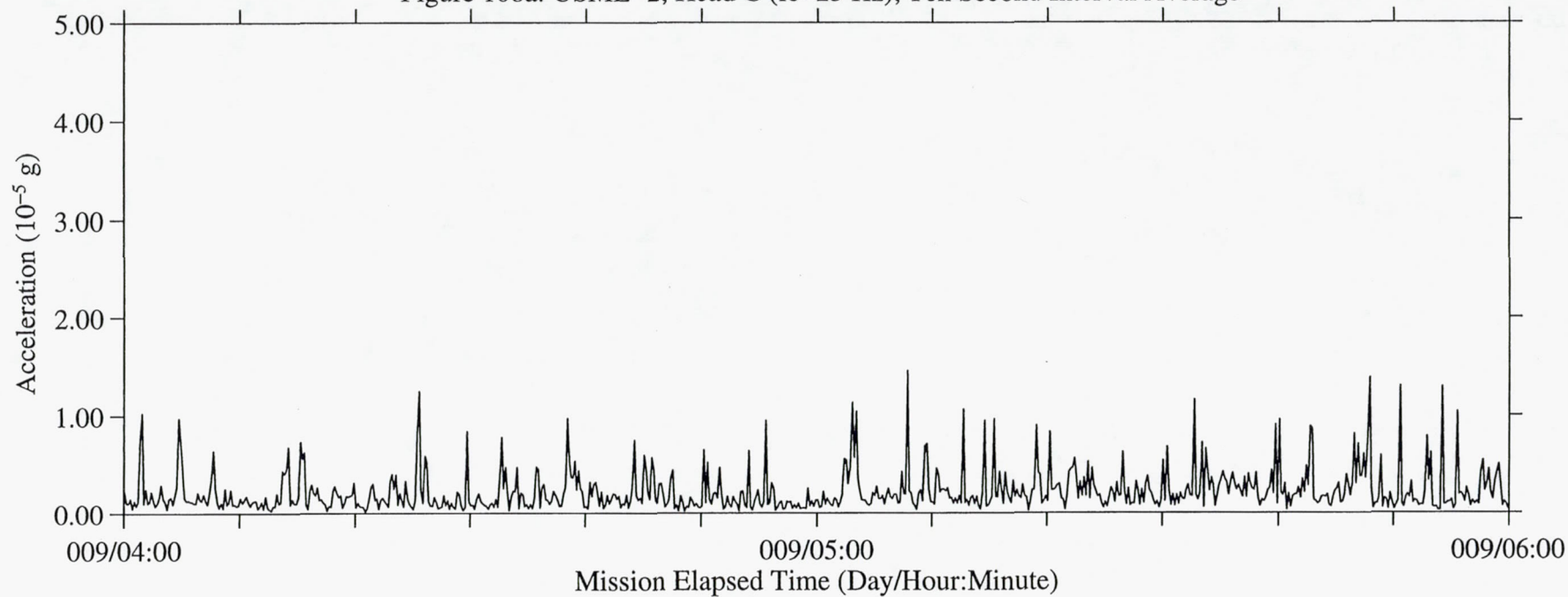
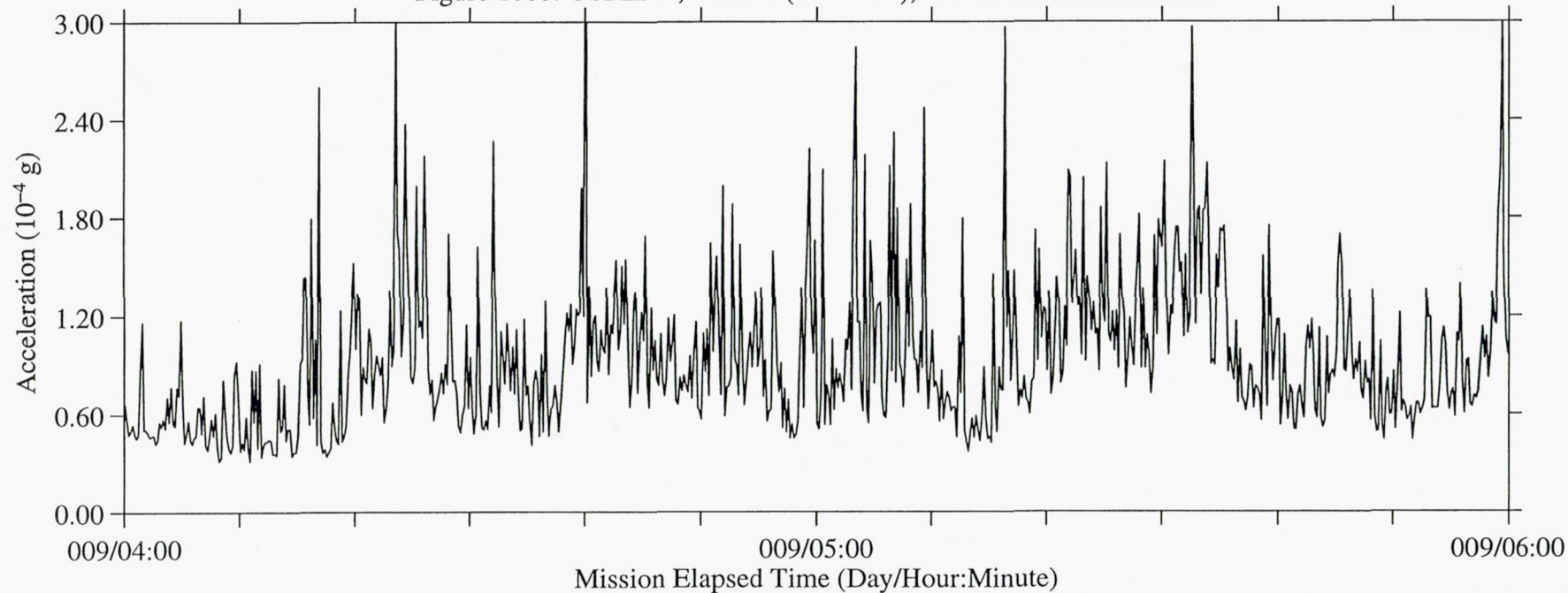
Figure 108a: USML-2, Head C ( $f_c=25$  Hz), Ten Second Interval AverageFigure 108b: USML-2, Head C ( $f_c=25$  Hz), Ten Second Interval RMS



Figure 109a: USML-2, Head C (fc=25 Hz), Ten Second Interval Average

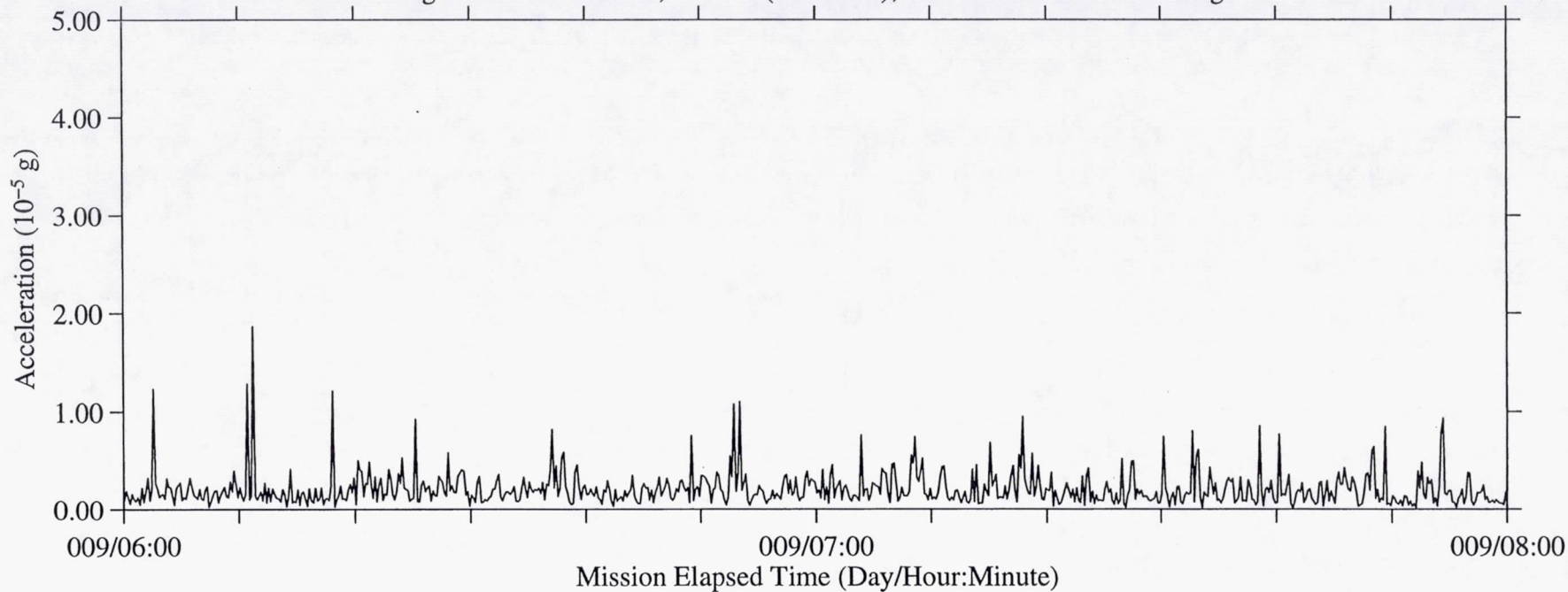


Figure 109b: USML-2, Head C (fc=25 Hz), Ten Second Interval RMS

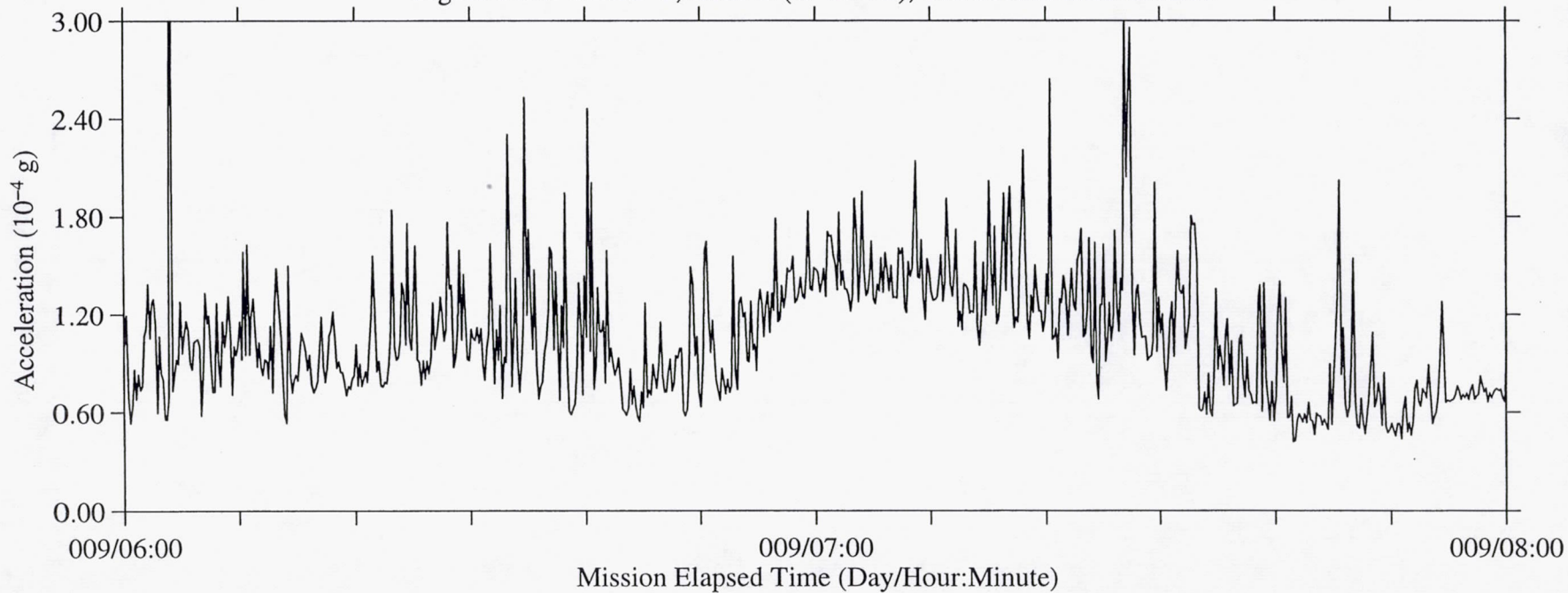


Figure 110a: USML-2, Head C (fc=25 Hz), Ten Second Interval Average

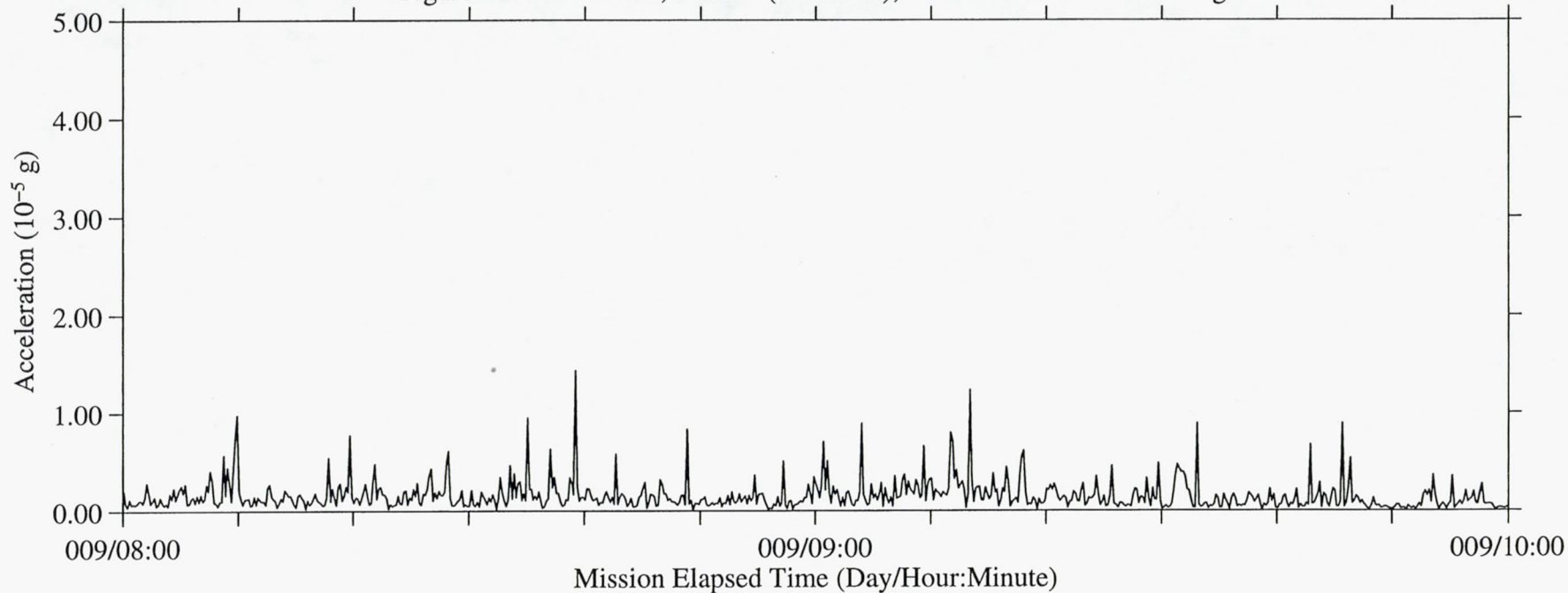


Figure 110b: USML-2, Head C (fc=25 Hz), Ten Second Interval RMS

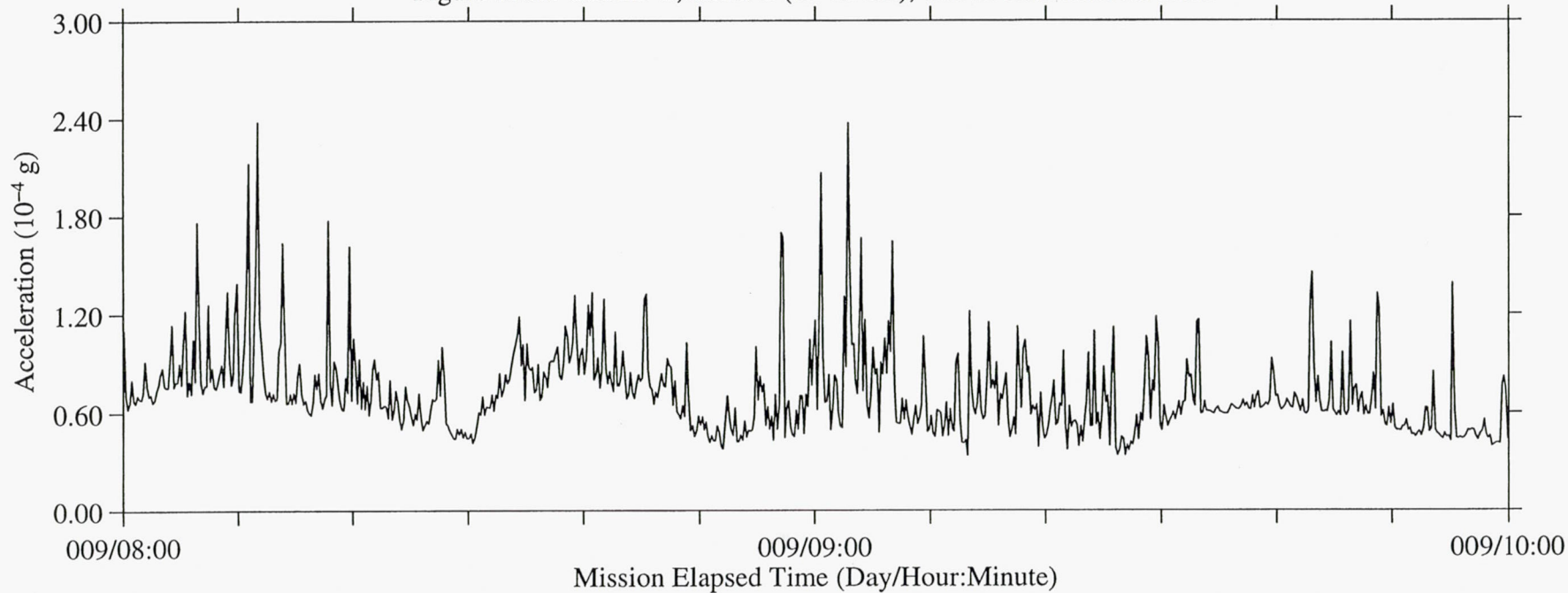




Figure 111a: USML-2, Head C (fc=25 Hz), Ten Second Interval Average

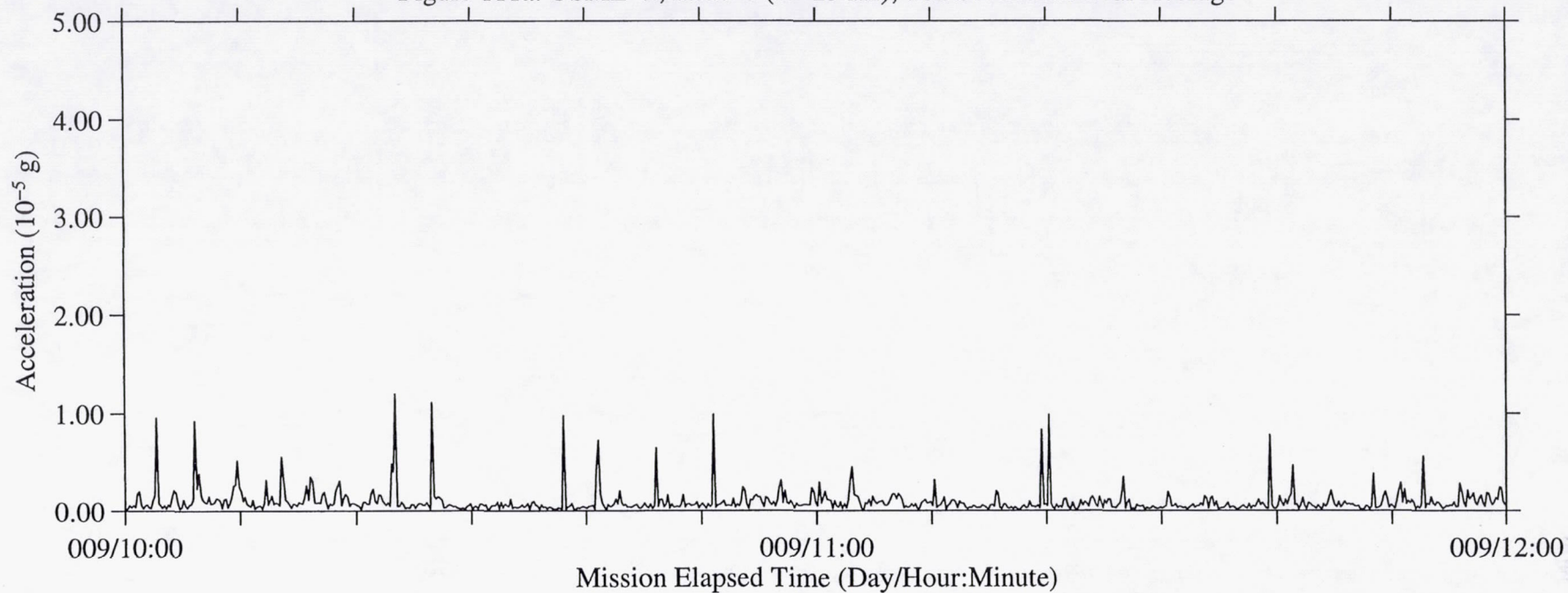


Figure 111b: USML-2, Head C (fc=25 Hz), Ten Second Interval RMS

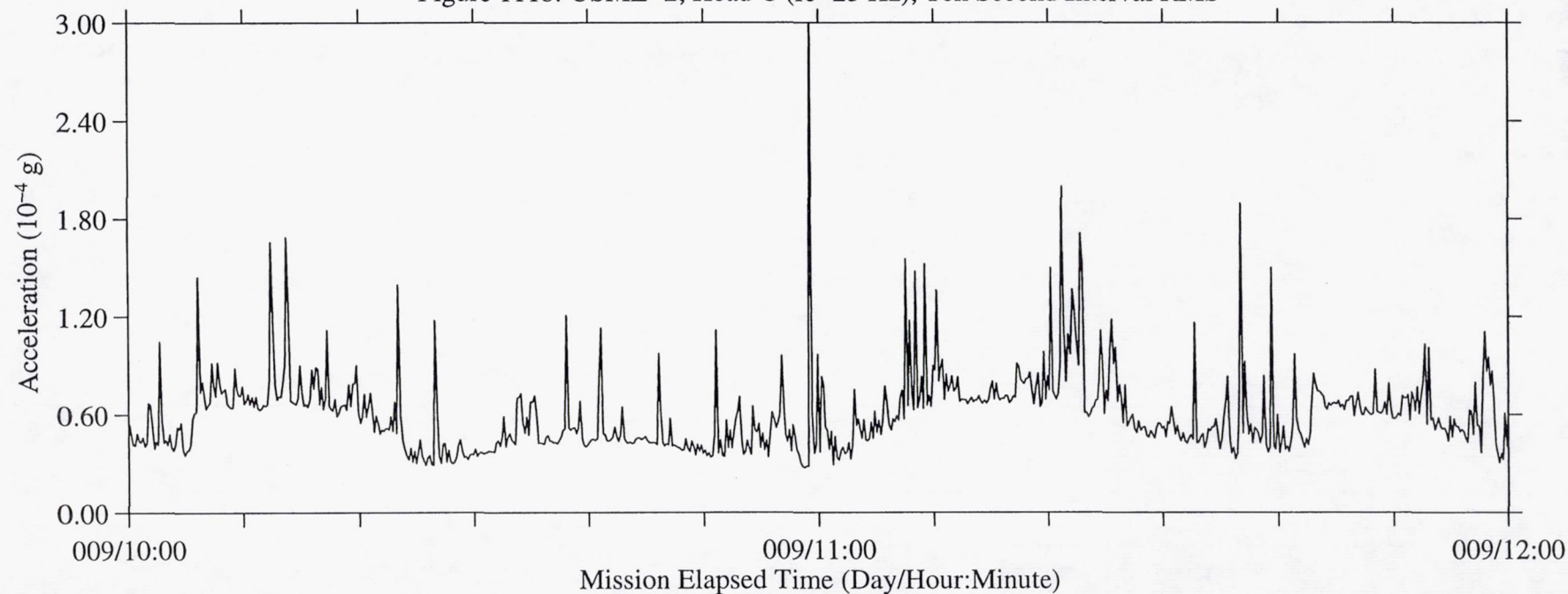


Figure 112a: USML-2, Head C (fc=25 Hz), Ten Second Interval Average

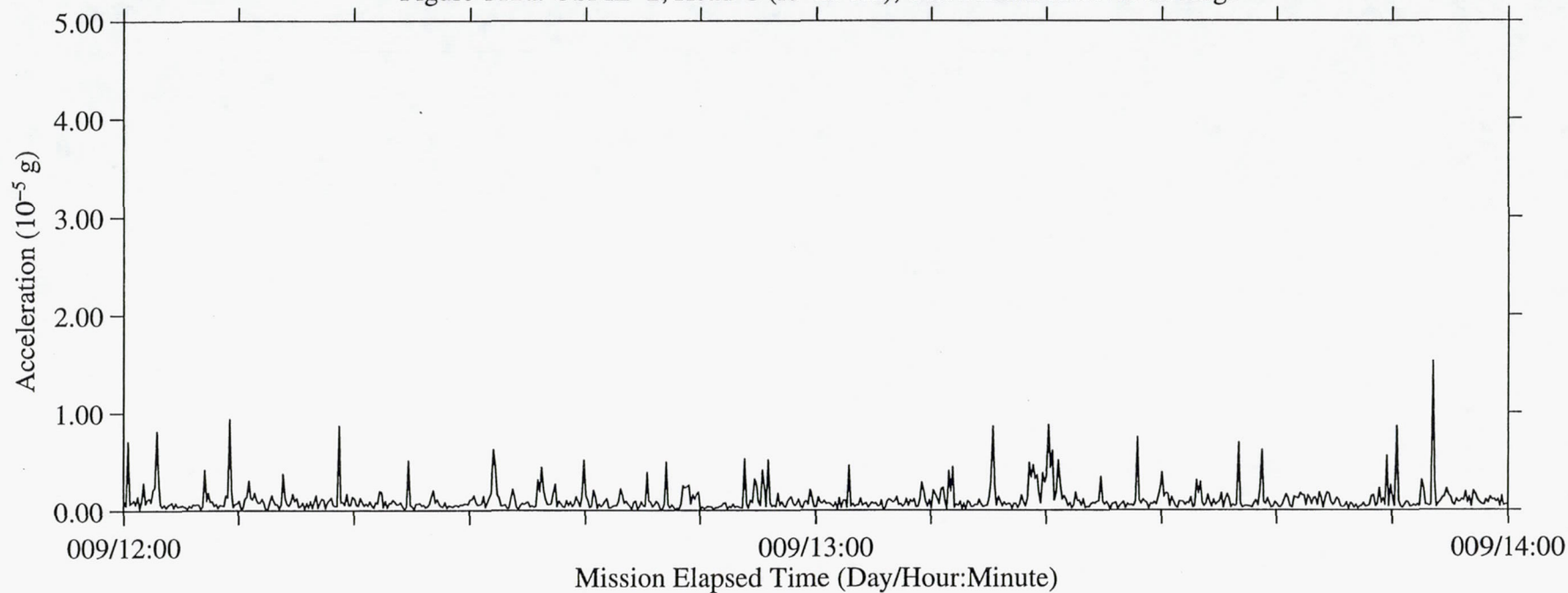
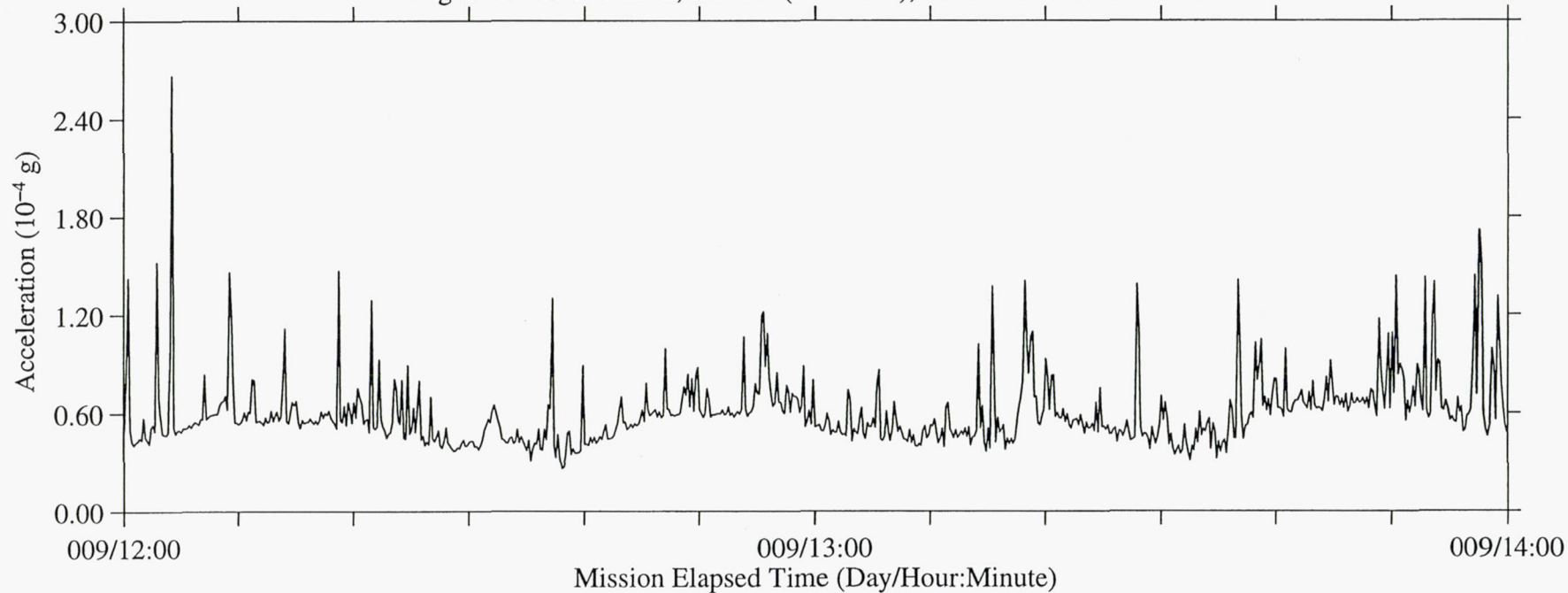


Figure 112b: USML-2, Head C (fc=25 Hz), Ten Second Interval RMS





B-115

Figure 113a: USML-2, Head C (fc=25 Hz), Ten Second Interval Average

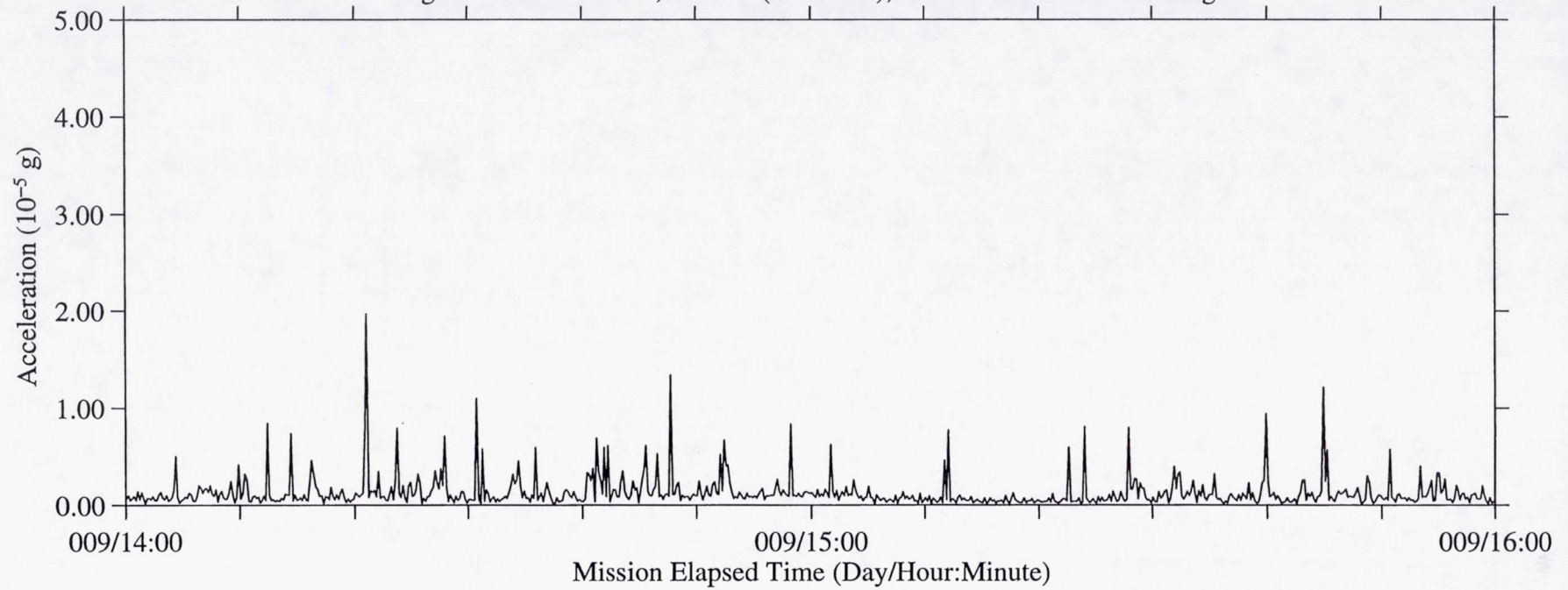


Figure 113b: USML-2, Head C (fc=25 Hz), Ten Second Interval RMS

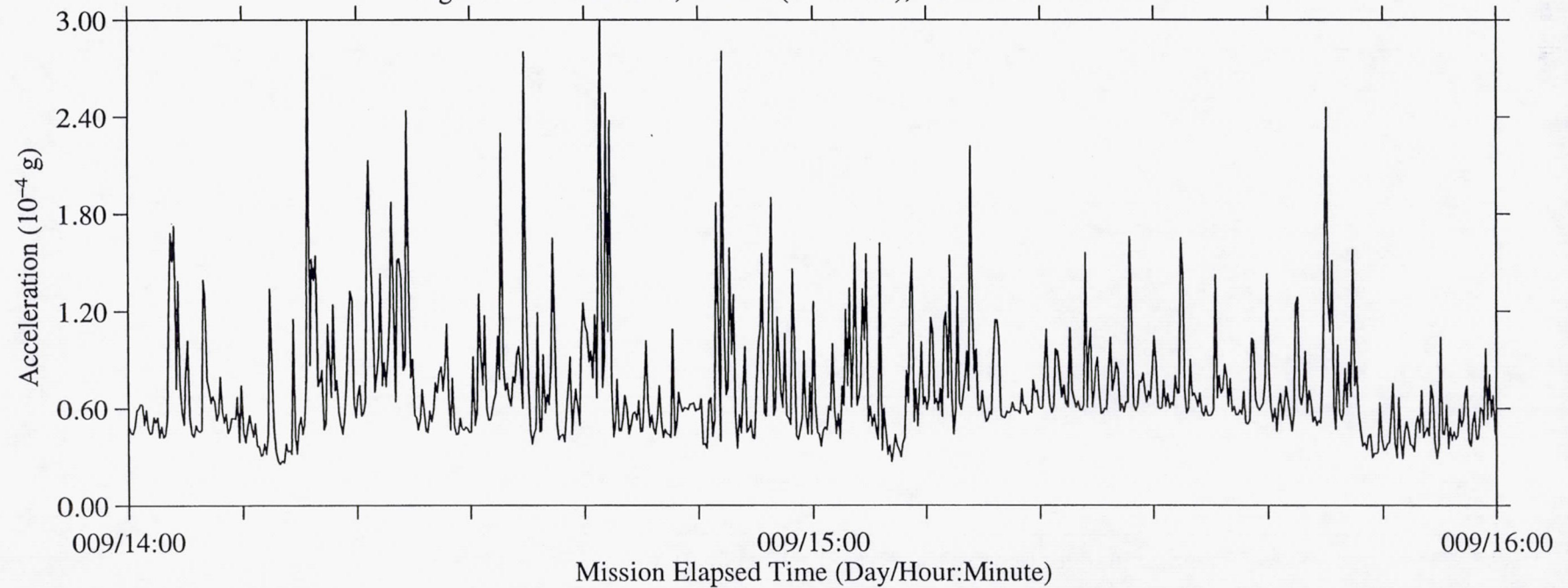


Figure 114a: USML-2, Head C (fc=25 Hz), Ten Second Interval Average

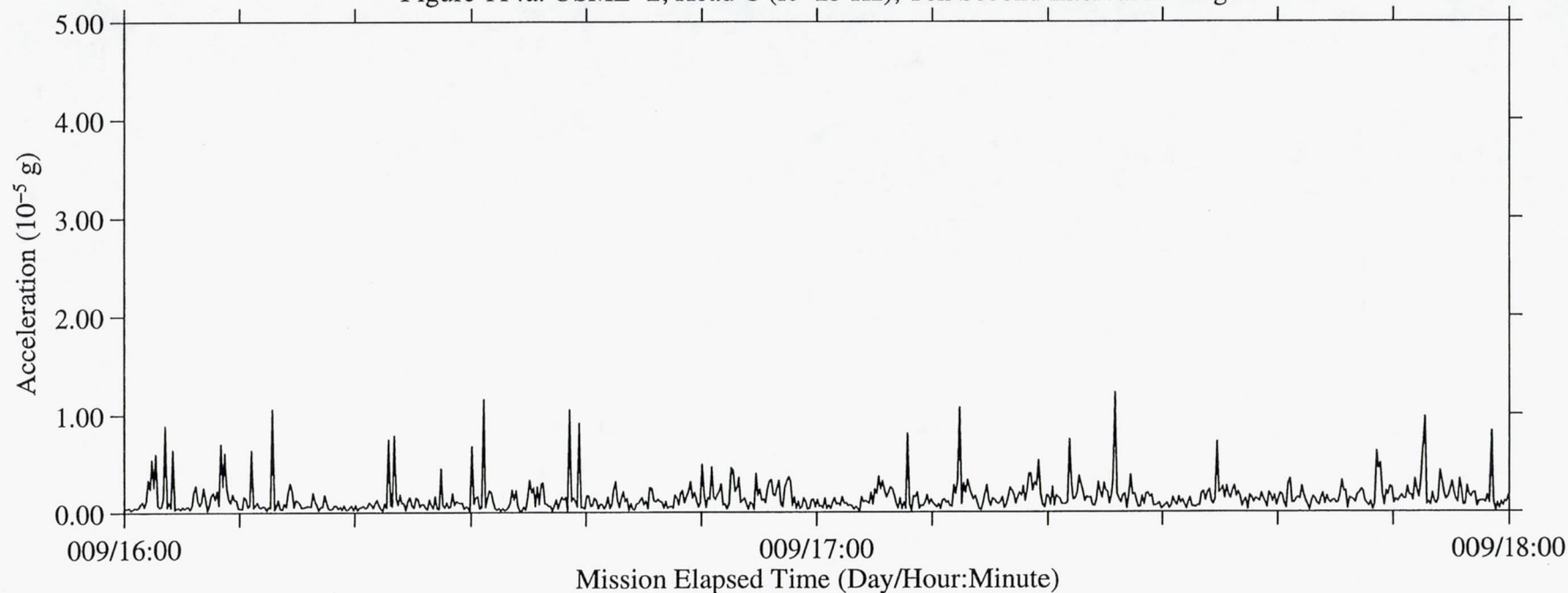


Figure 114b: USML-2, Head C (fc=25 Hz), Ten Second Interval RMS

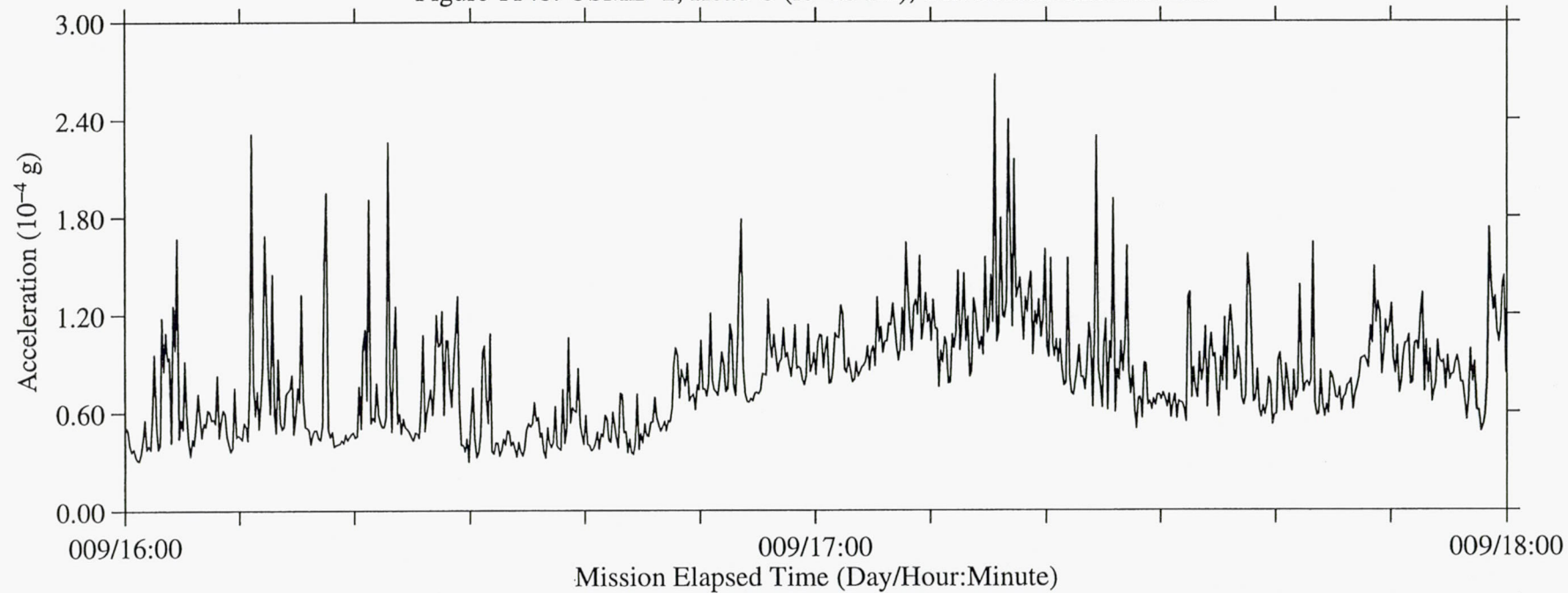




Figure 115a: USML-2, Head C (fc=25 Hz), Ten Second Interval Average

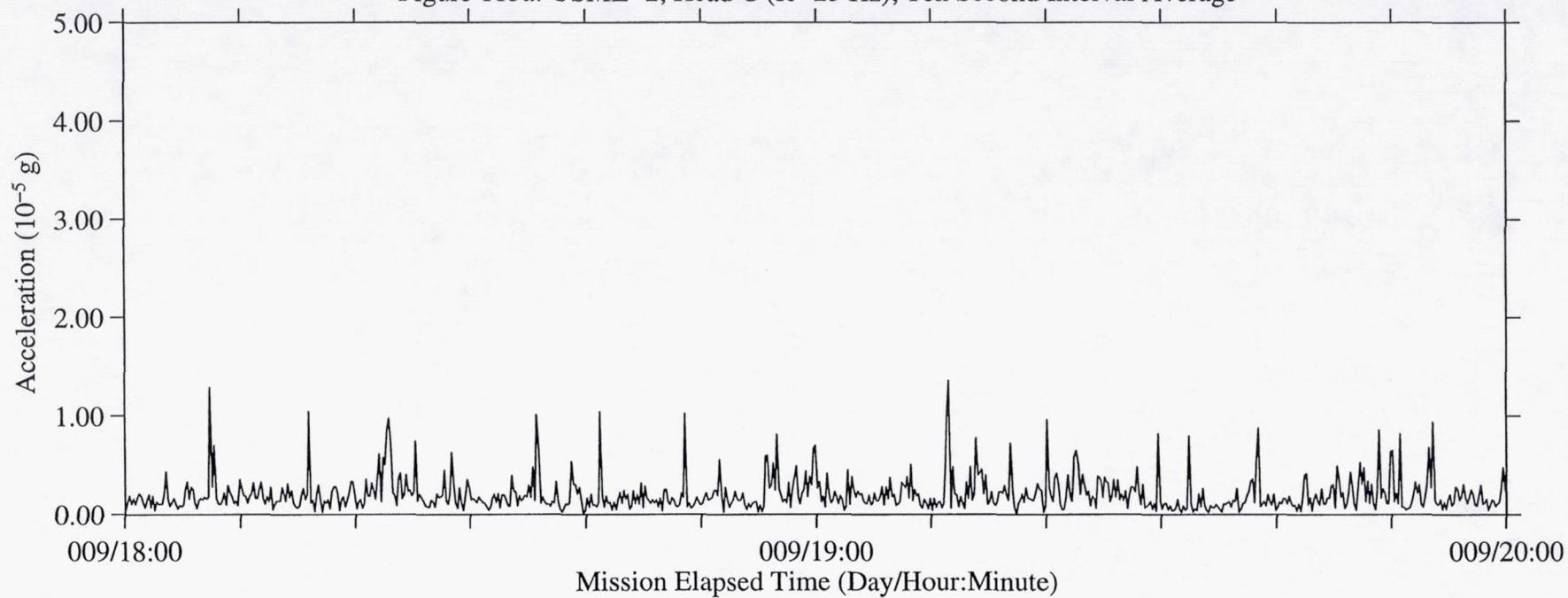


Figure 115b: USML-2, Head C (fc=25 Hz), Ten Second Interval RMS

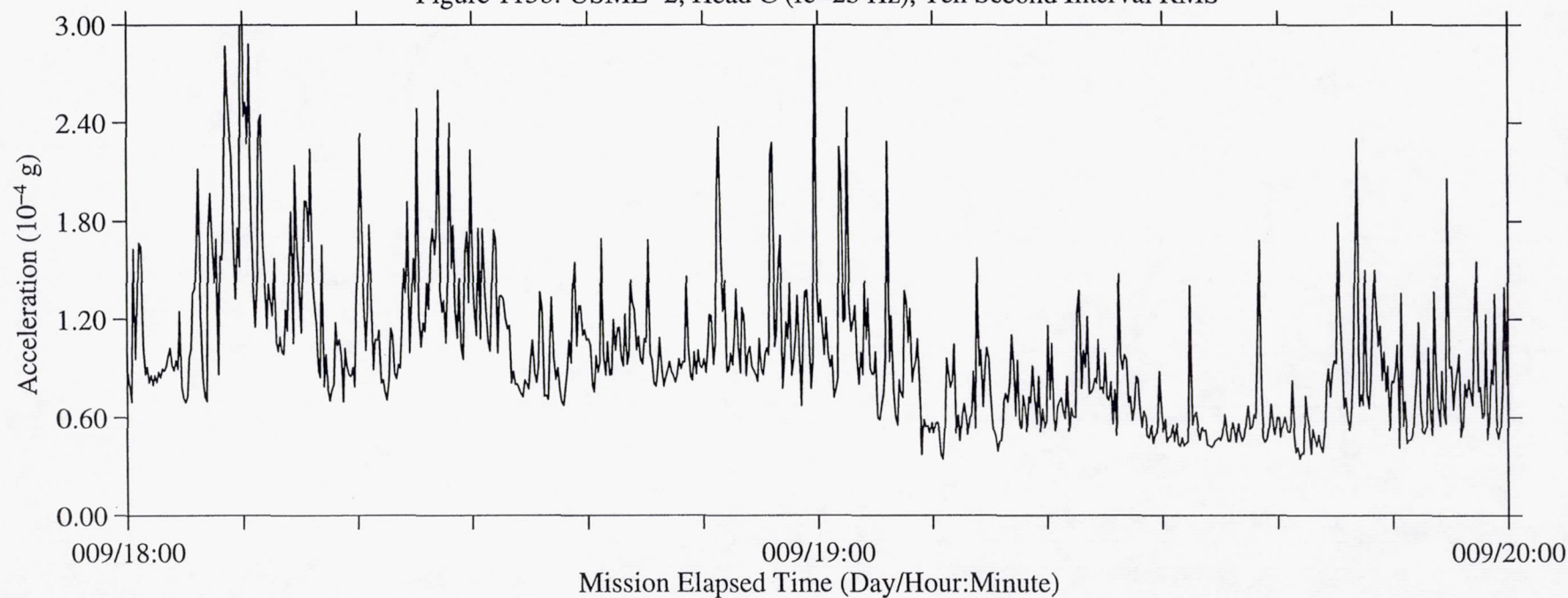


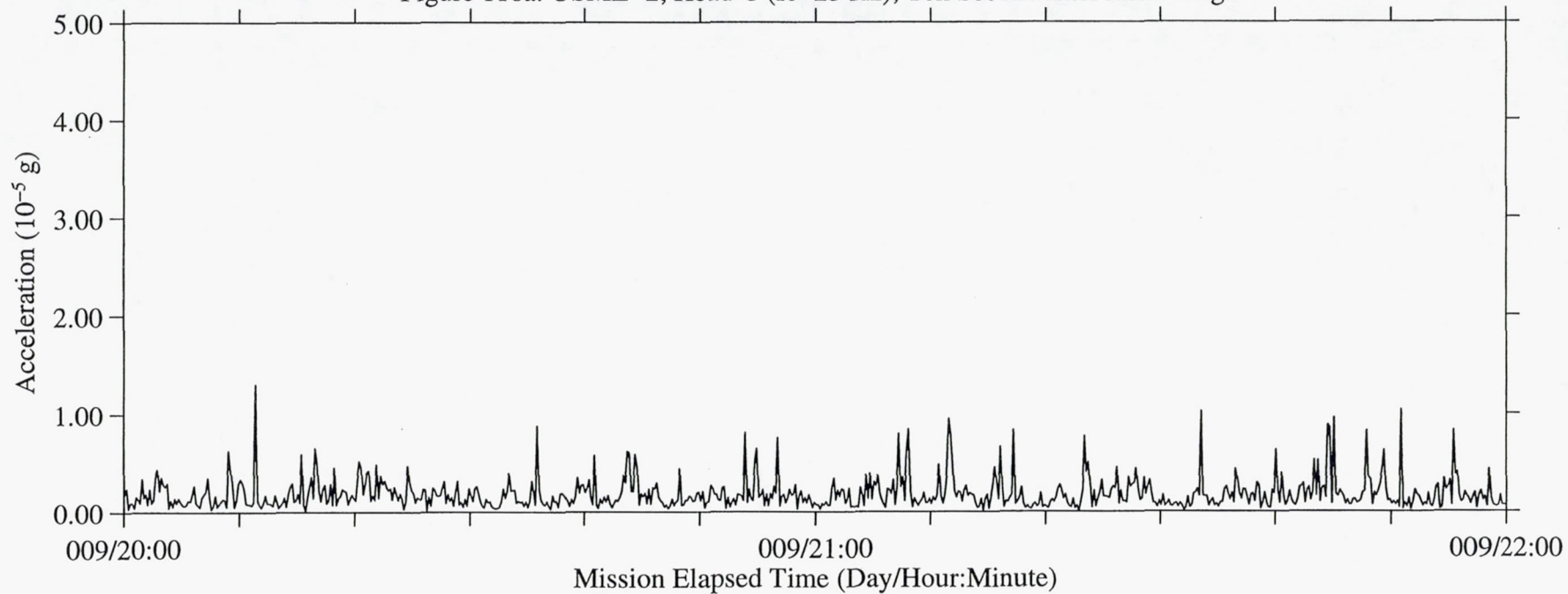
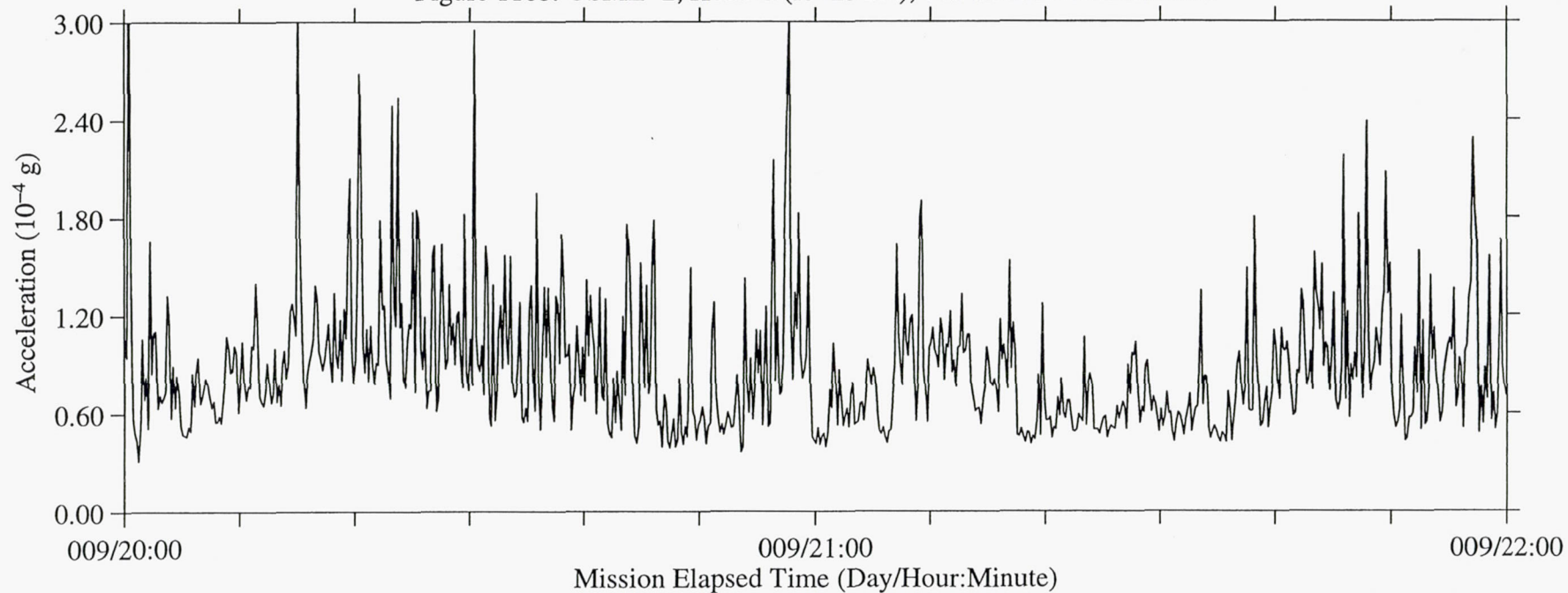
Figure 116a: USML-2, Head C ( $f_c=25$  Hz), Ten Second Interval AverageFigure 116b: USML-2, Head C ( $f_c=25$  Hz), Ten Second Interval RMS



Figure 117a: USML-2, Head C (fc=25 Hz), Ten Second Interval Average

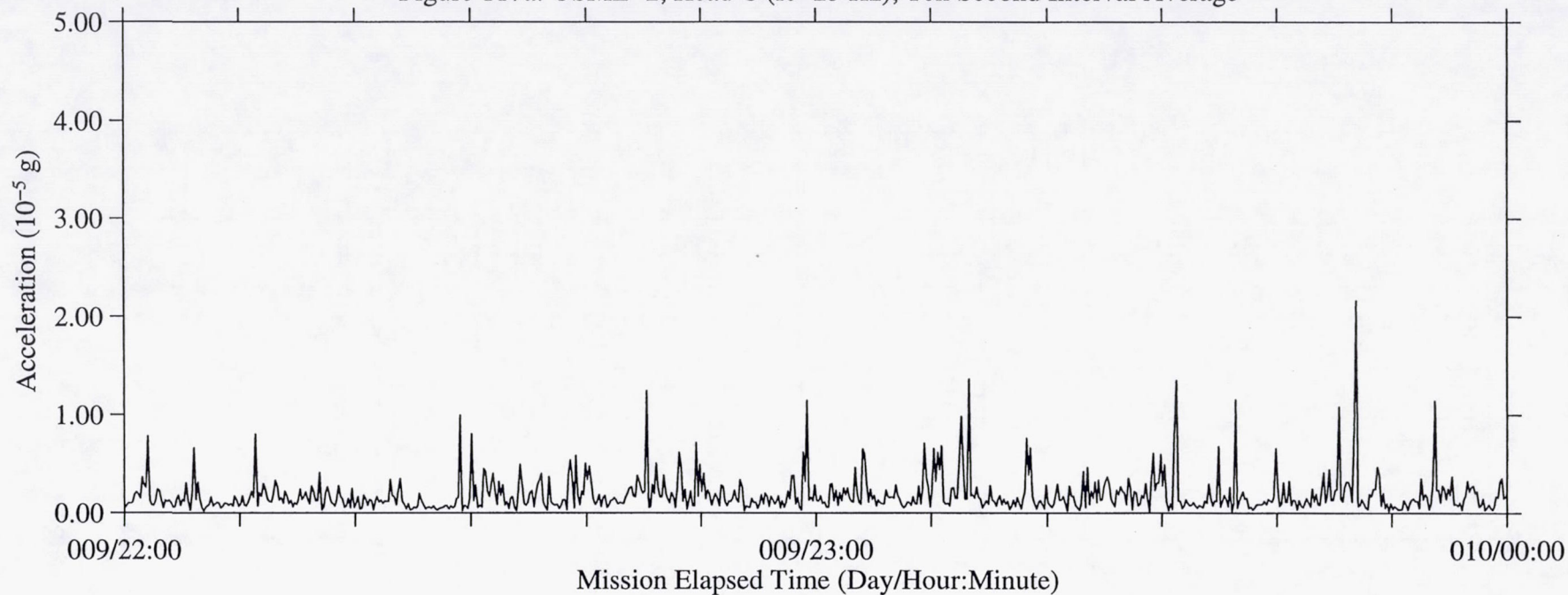


Figure 117b: USML-2, Head C (fc=25 Hz), Ten Second Interval RMS

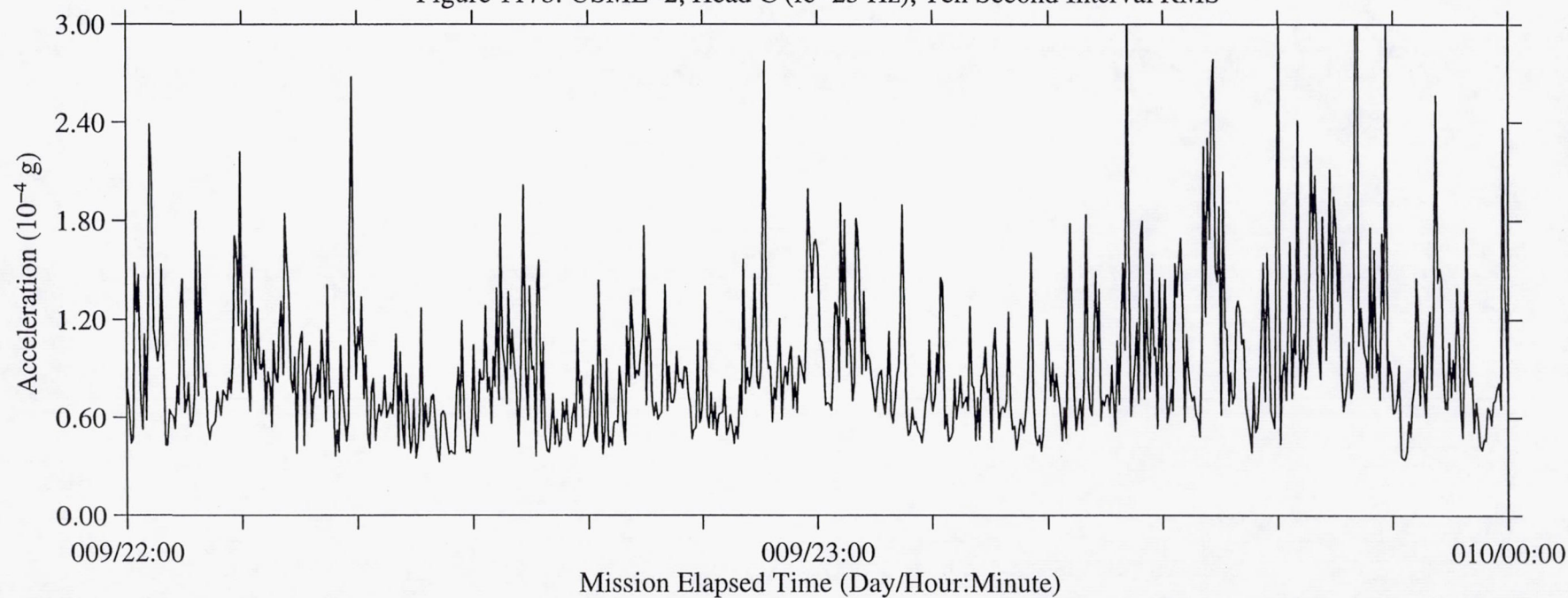


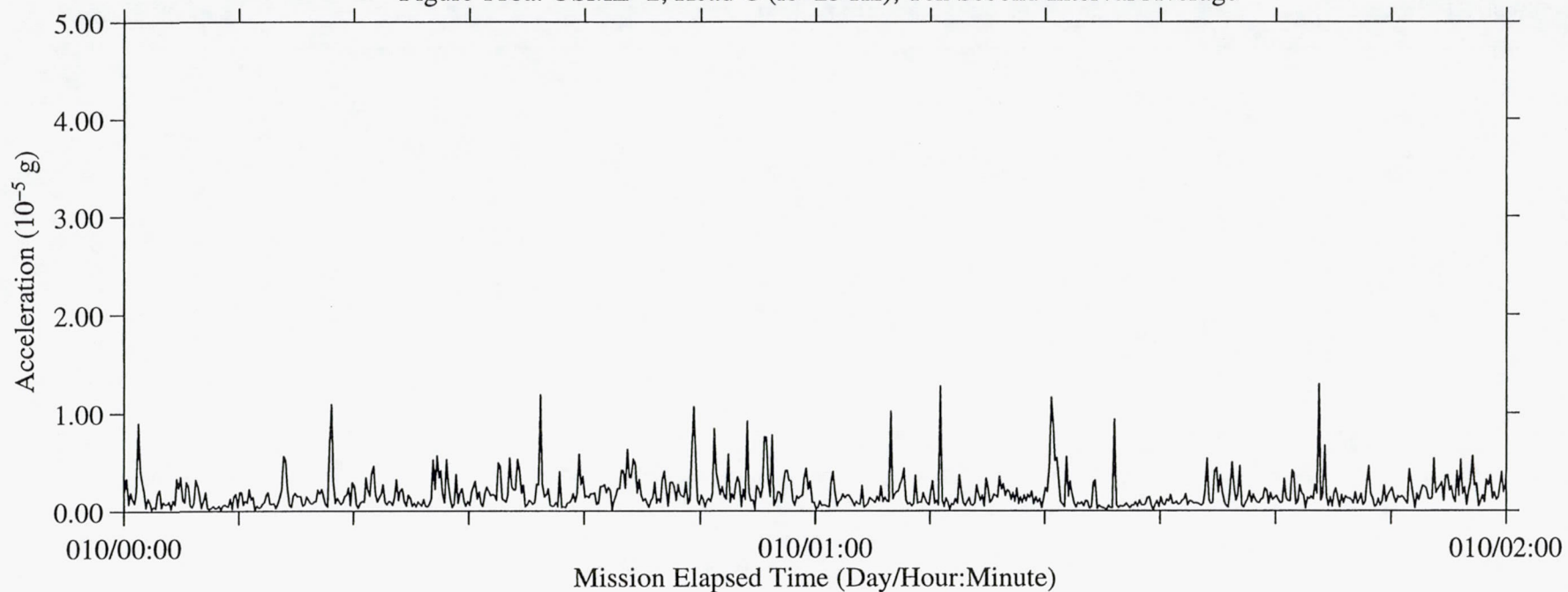
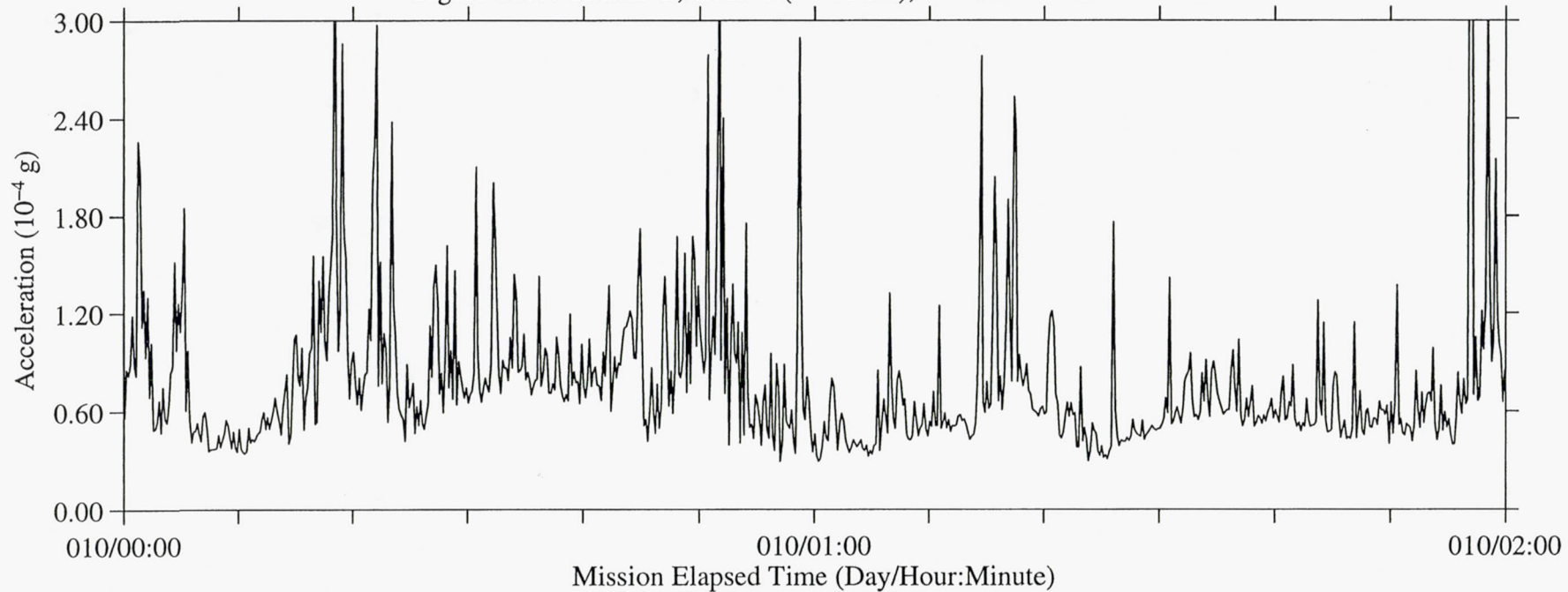
Figure 118a: USML-2, Head C ( $f_c=25$  Hz), Ten Second Interval AverageFigure 118b: USML-2, Head C ( $f_c=25$  Hz), Ten Second Interval RMS



Figure 119a: USML-2, Head C (fc=25 Hz), Ten Second Interval Average

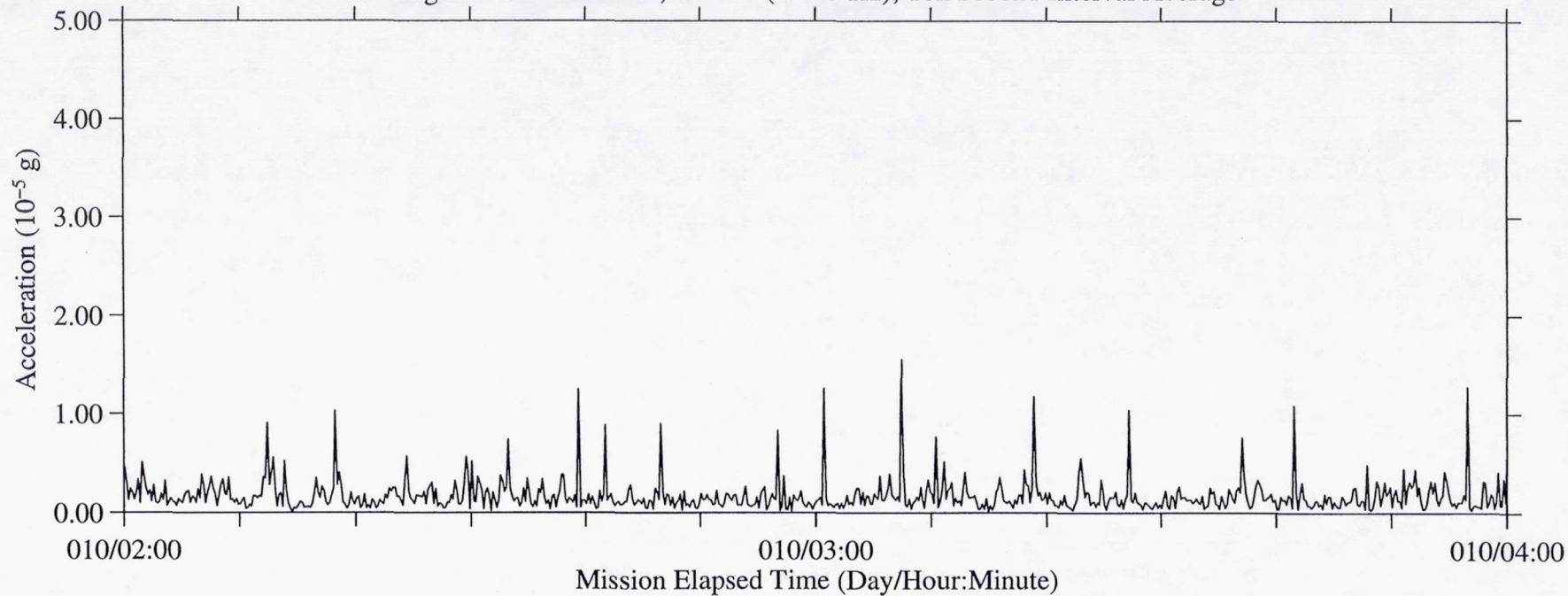


Figure 119b: USML-2, Head C (fc=25 Hz), Ten Second Interval RMS

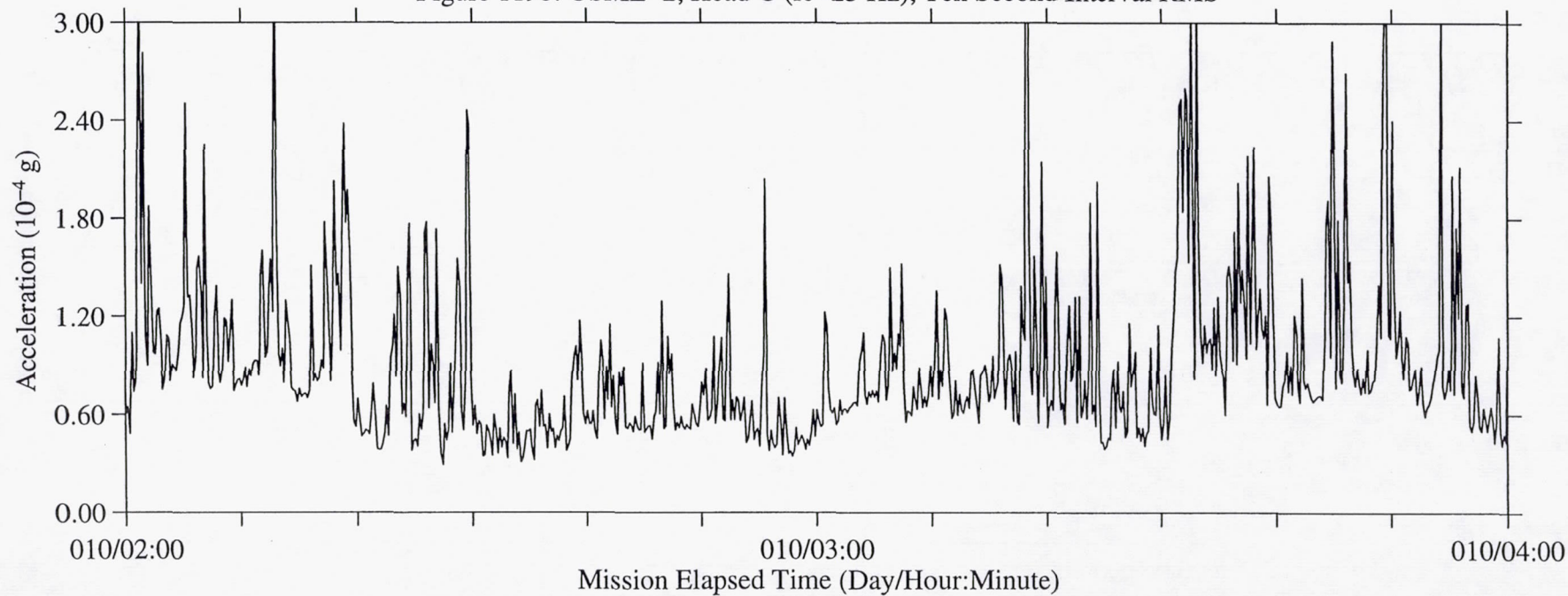


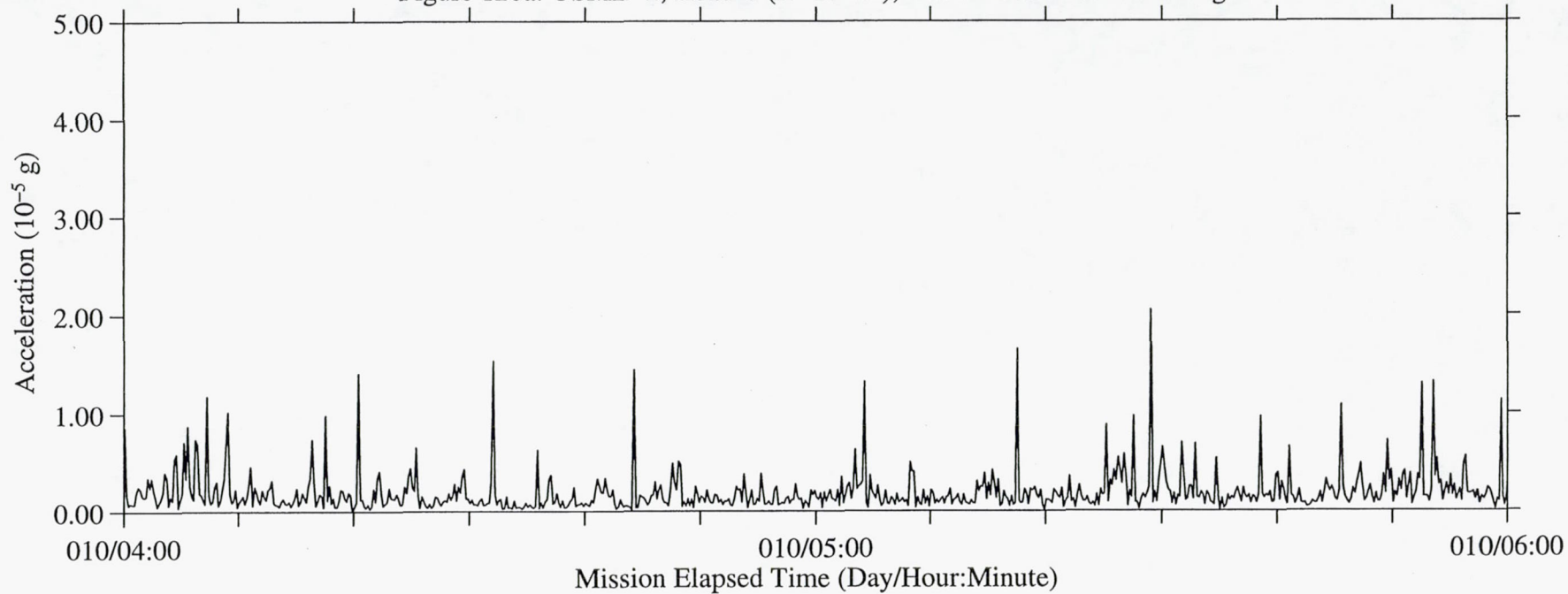
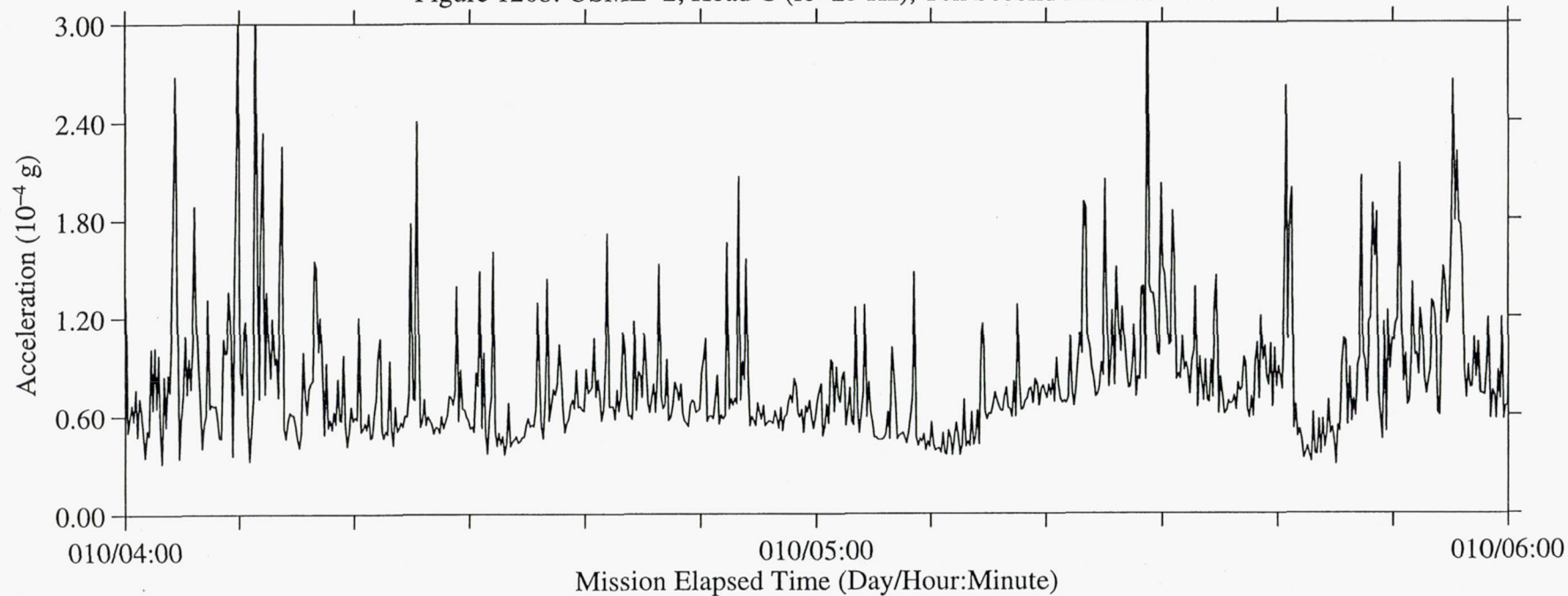
Figure 120a: USML-2, Head C ( $f_c=25$  Hz), Ten Second Interval AverageFigure 120b: USML-2, Head C ( $f_c=25$  Hz), Ten Second Interval RMS



Figure 121a: USML-2, Head C (fc=25 Hz), Ten Second Interval Average

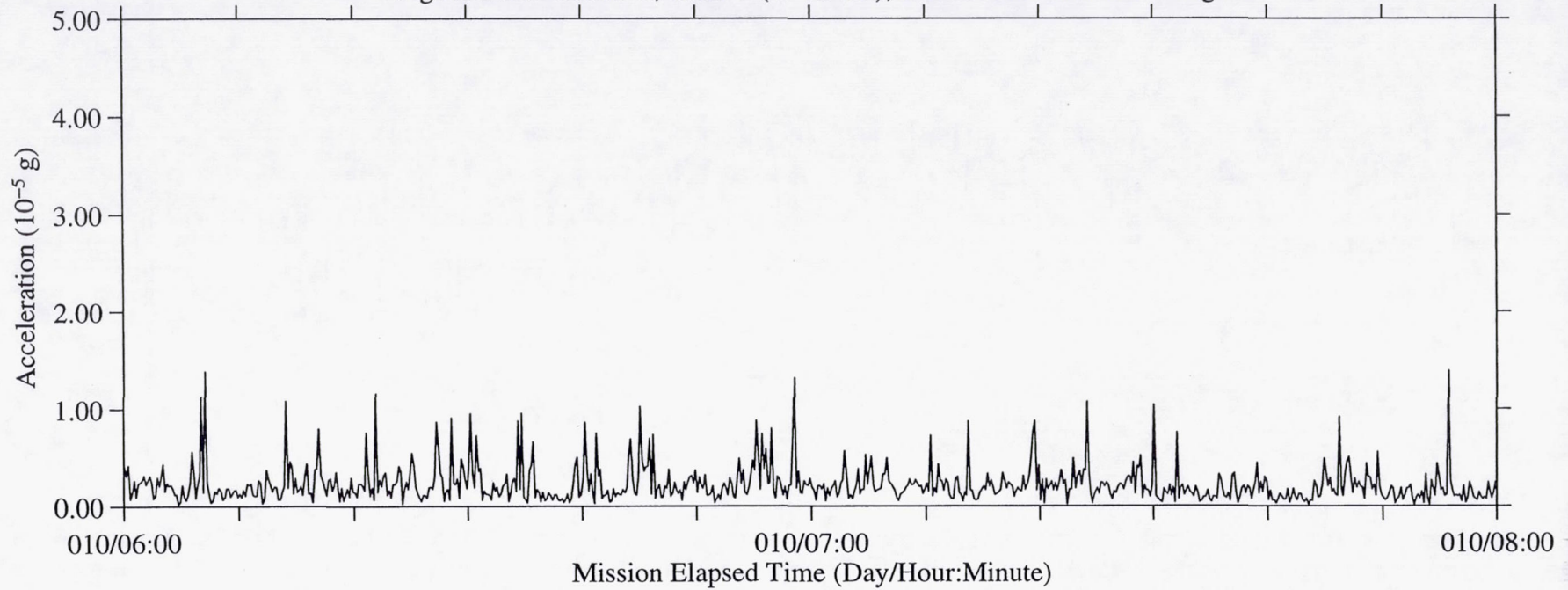


Figure 121b: USML-2, Head C (fc=25 Hz), Ten Second Interval RMS

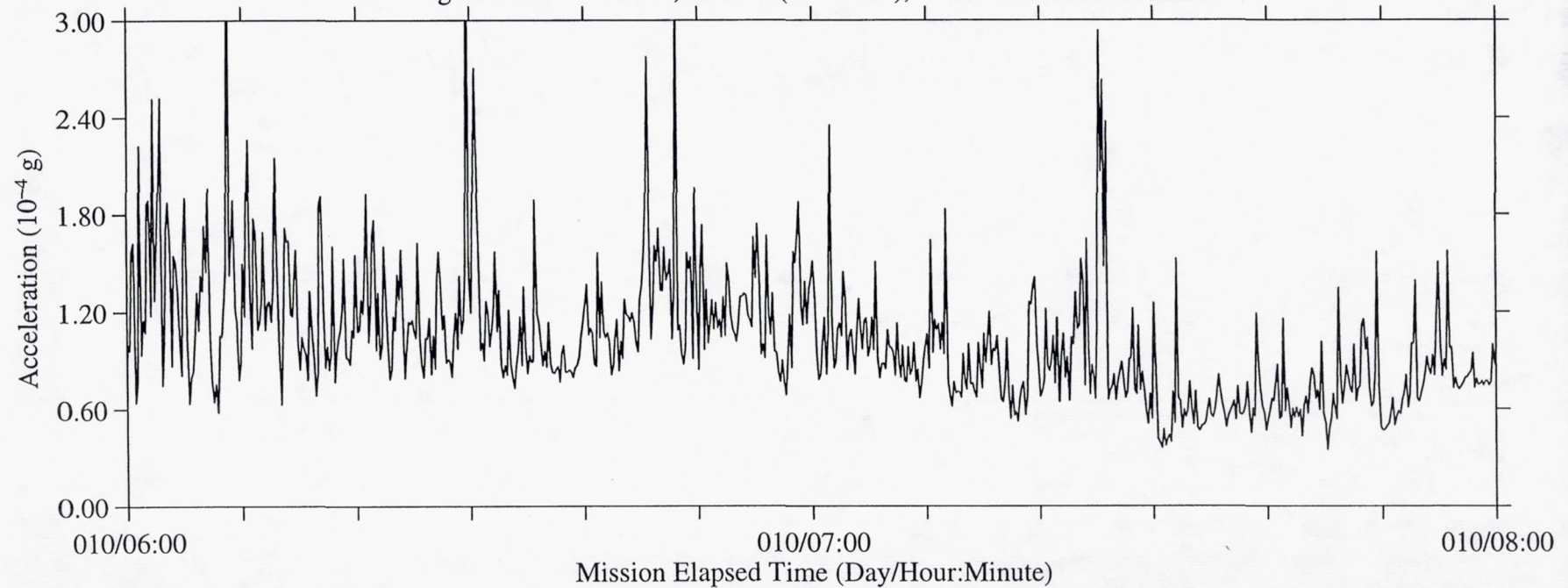


Figure 122a: USML-2, Head C (fc=25 Hz), Ten Second Interval Average

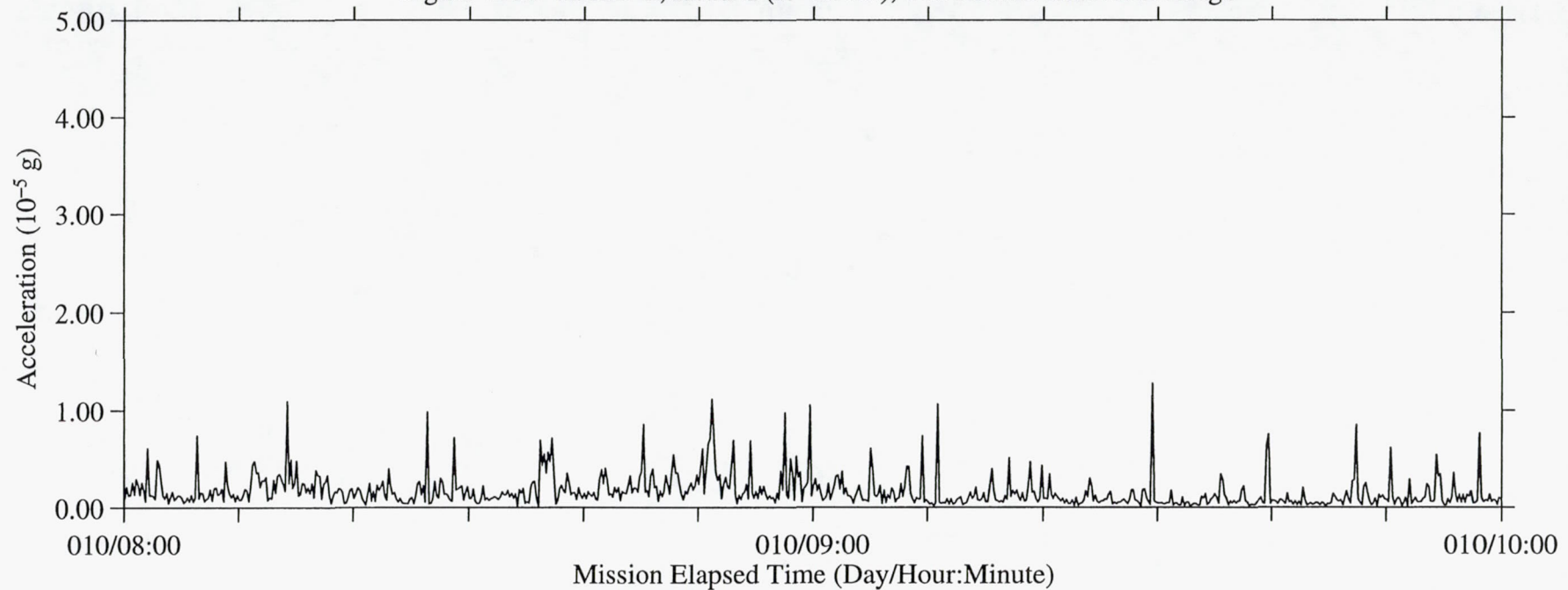


Figure 122b: USML-2, Head C (fc=25 Hz), Ten Second Interval RMS

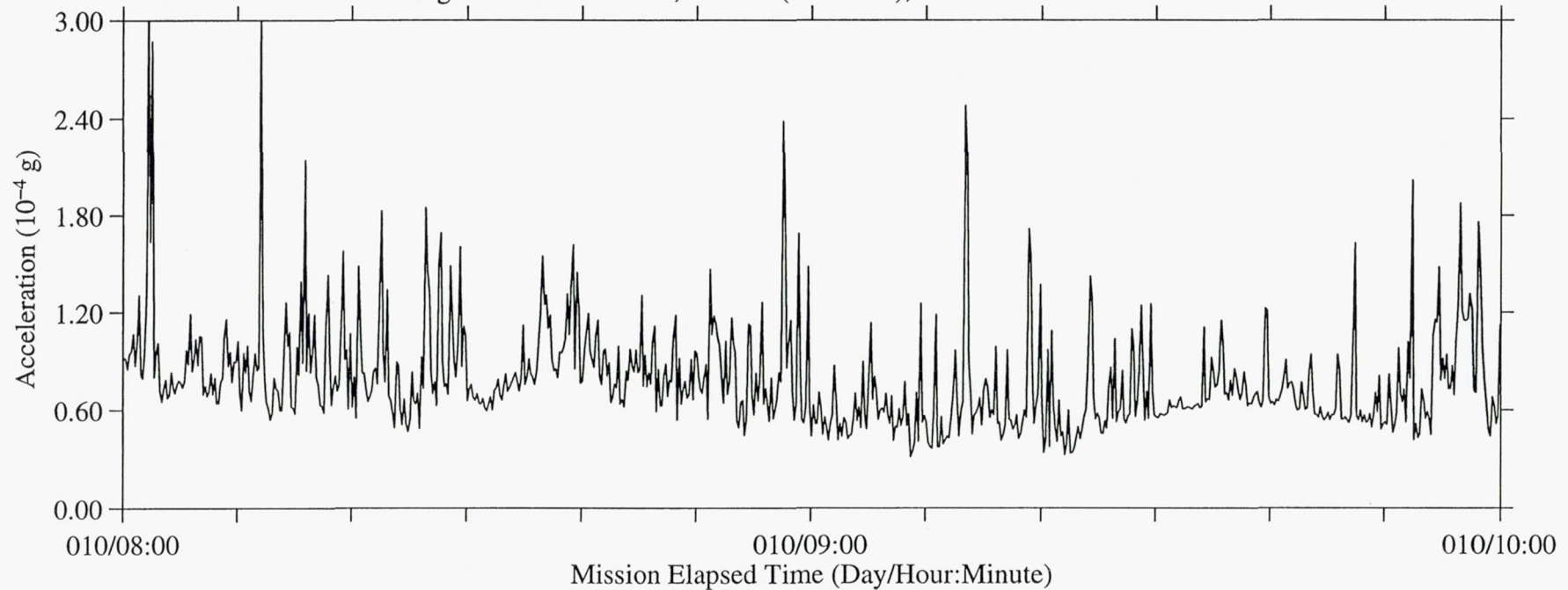




Figure 123a: USML-2, Head C (fc=25 Hz), Ten Second Interval Average

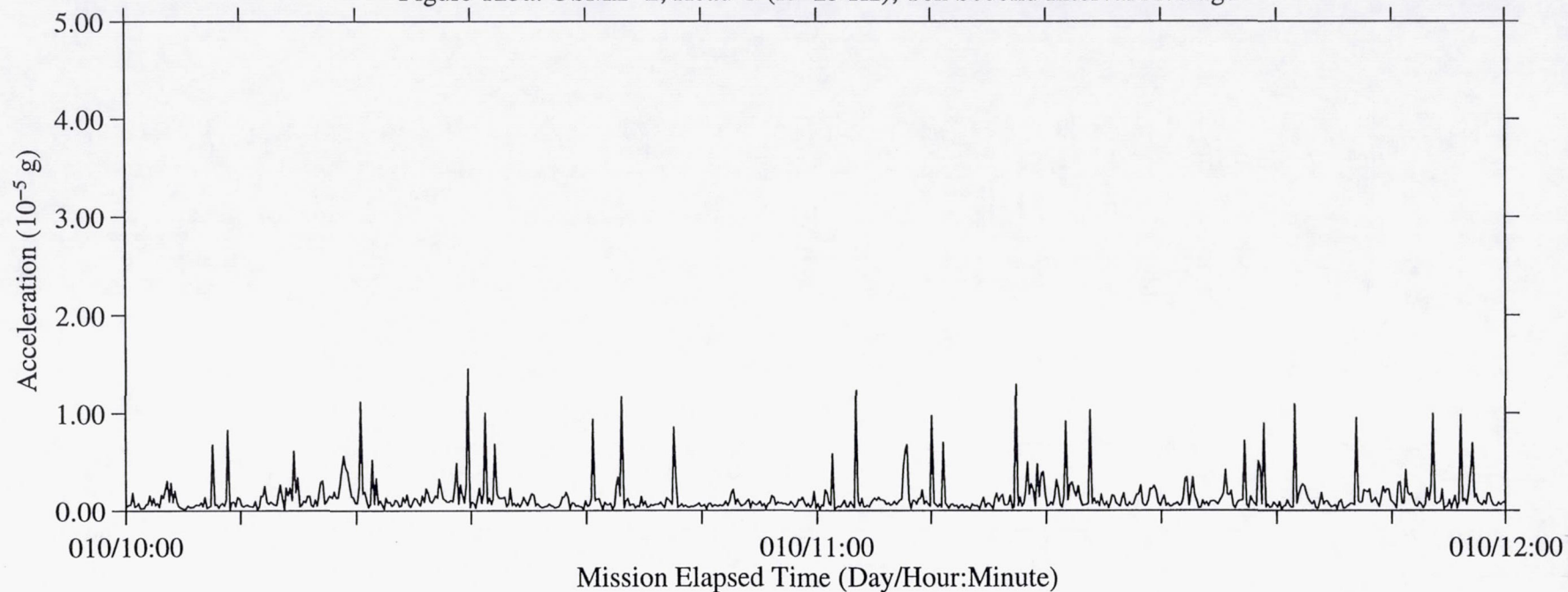


Figure 123b: USML-2, Head C (fc=25 Hz), Ten Second Interval RMS

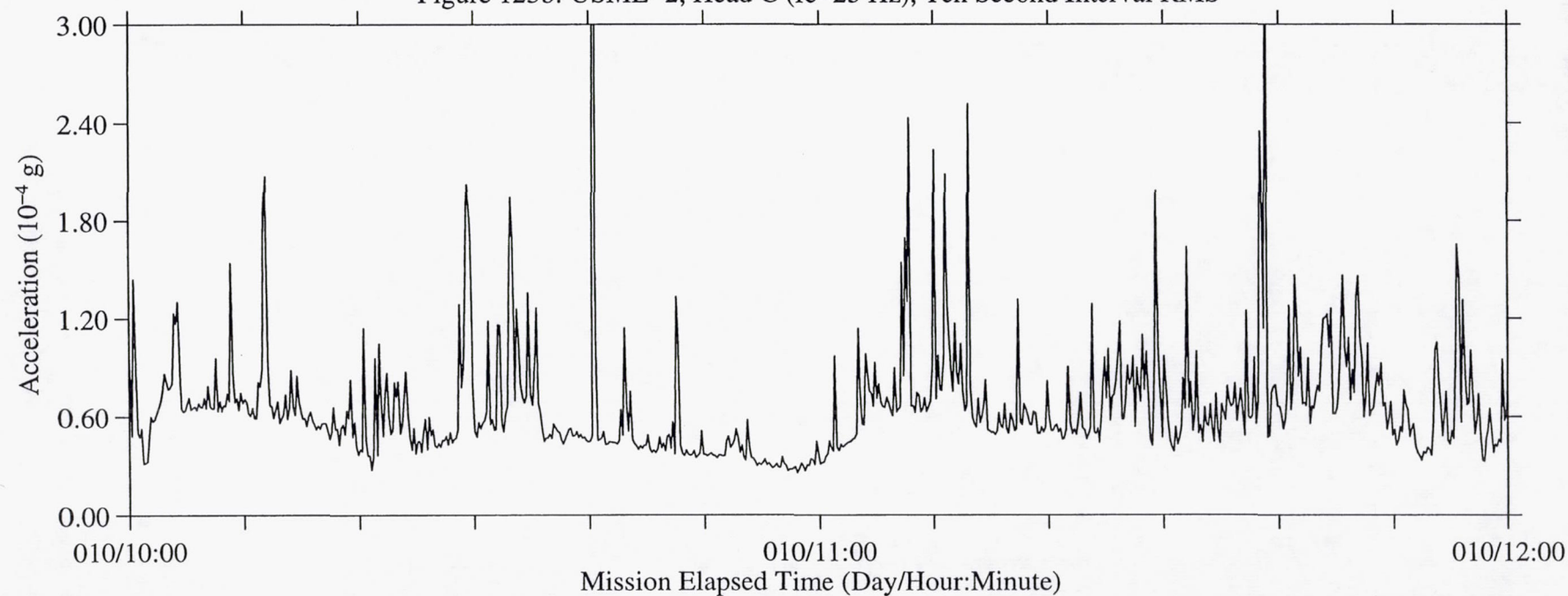


Figure 124a: USML-2, Head C (fc=25 Hz), Ten Second Interval Average

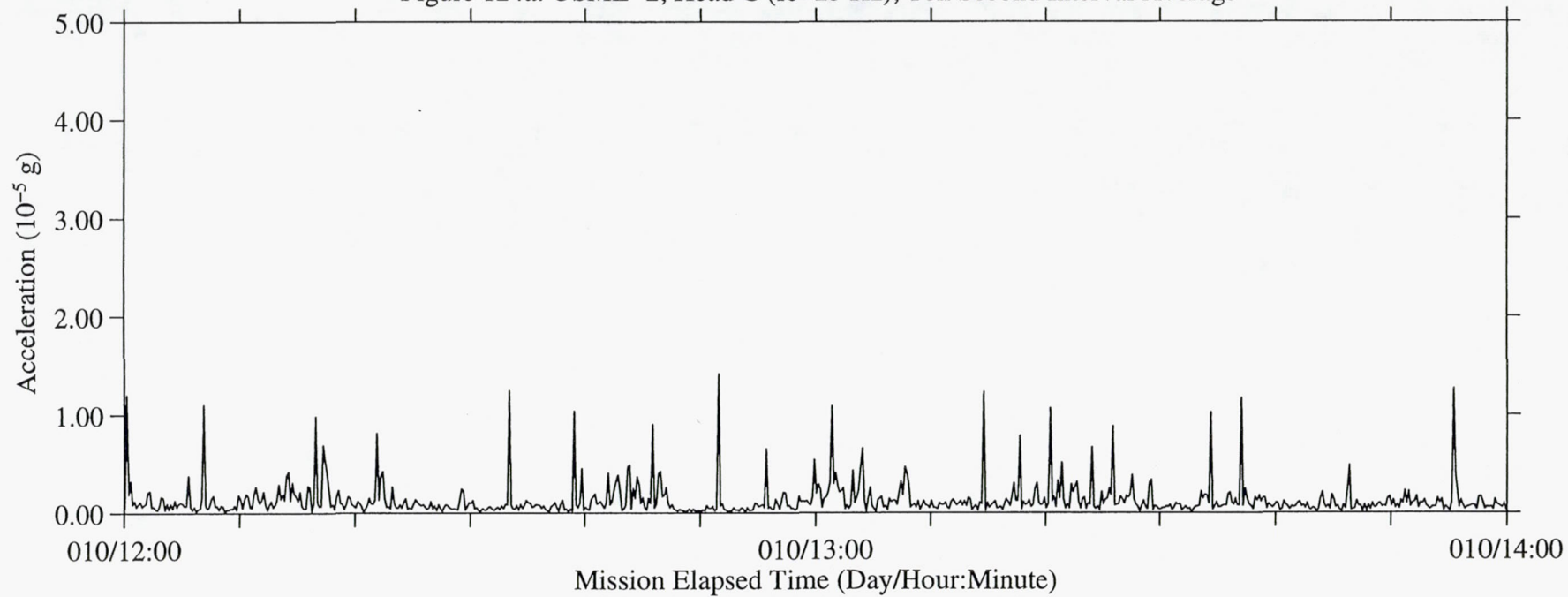


Figure 124b: USML-2, Head C (fc=25 Hz), Ten Second Interval RMS

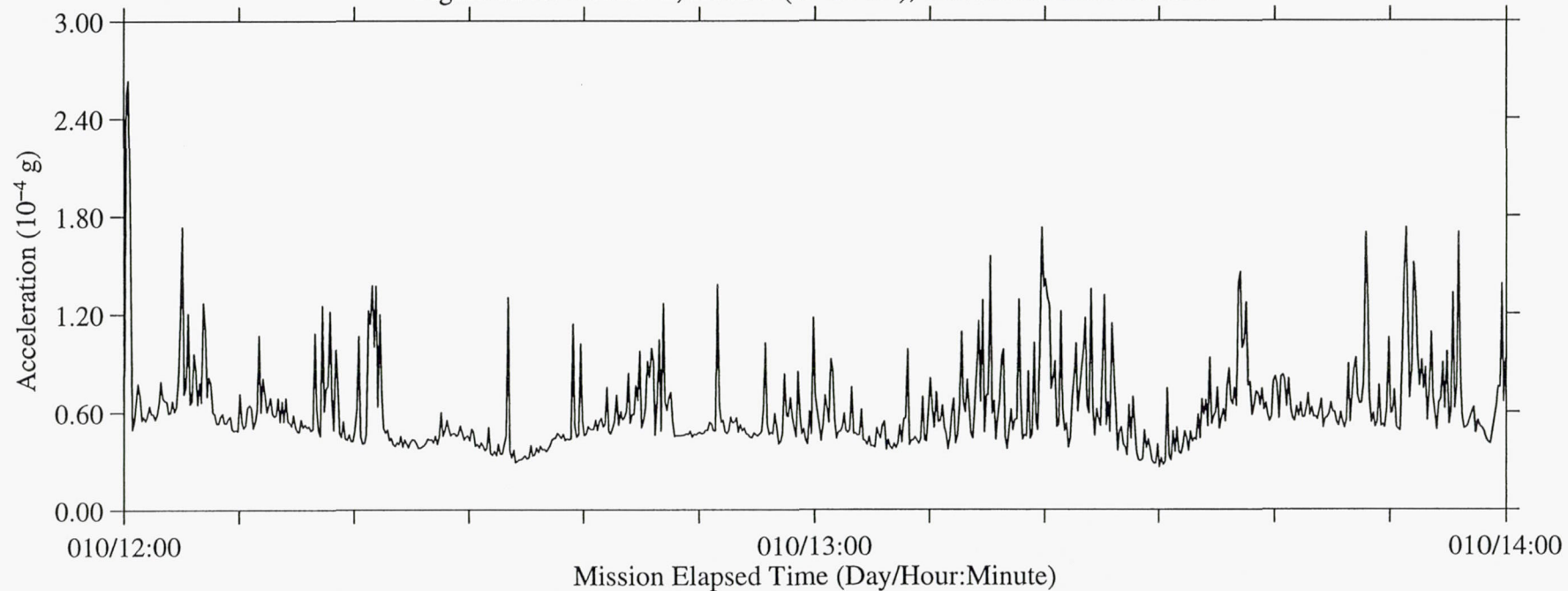




Figure 125a: USML-2, Head C (fc=25 Hz), Ten Second Interval Average

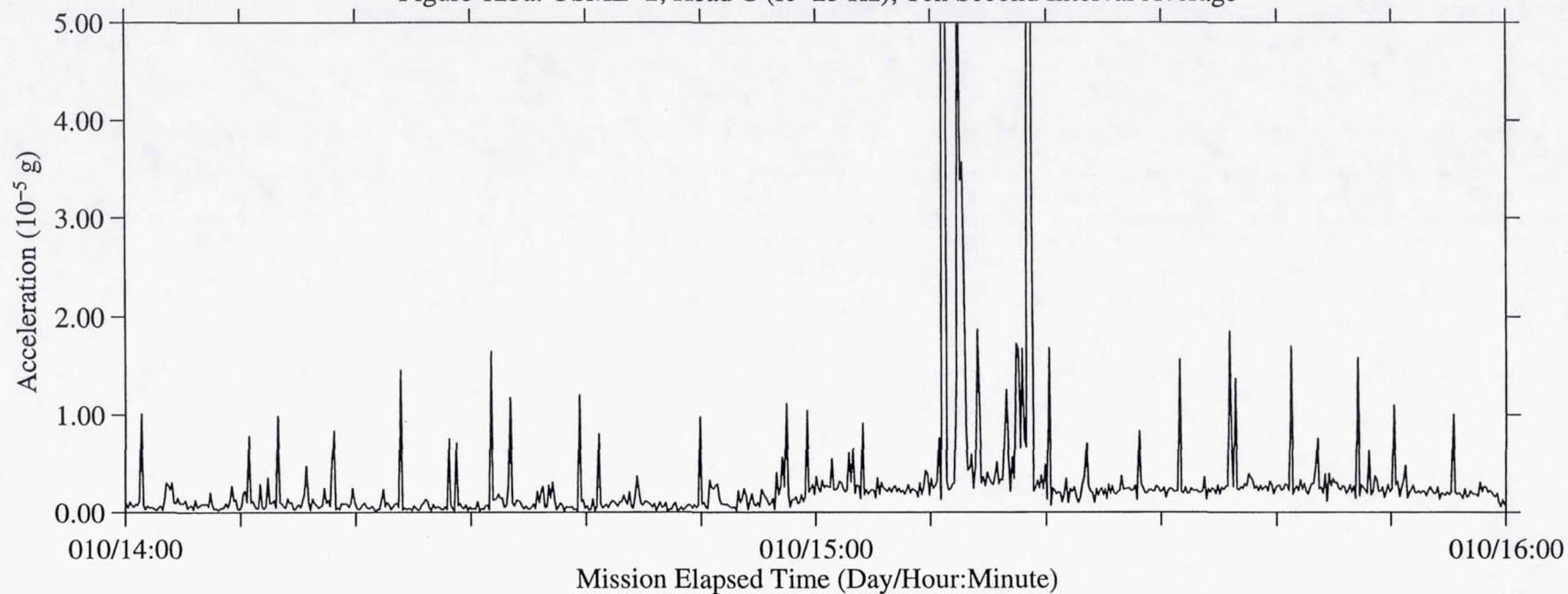


Figure 125b: USML-2, Head C (fc=25 Hz), Ten Second Interval RMS

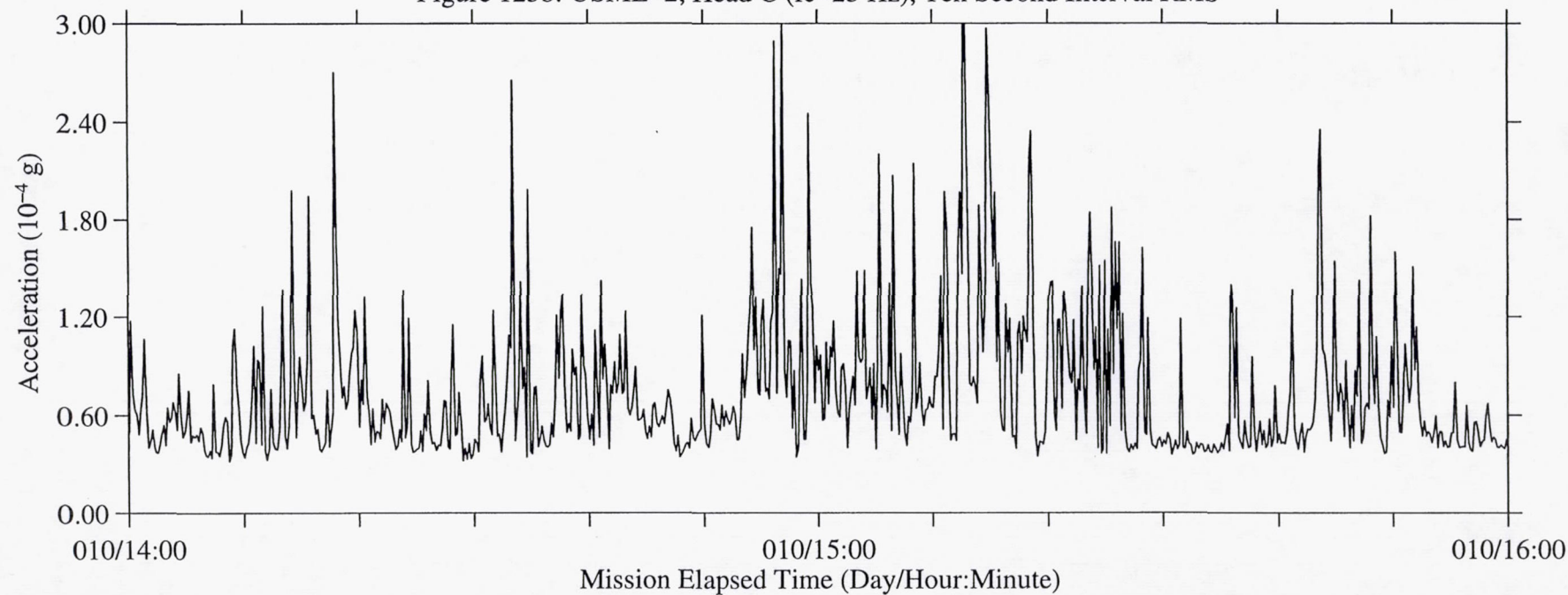


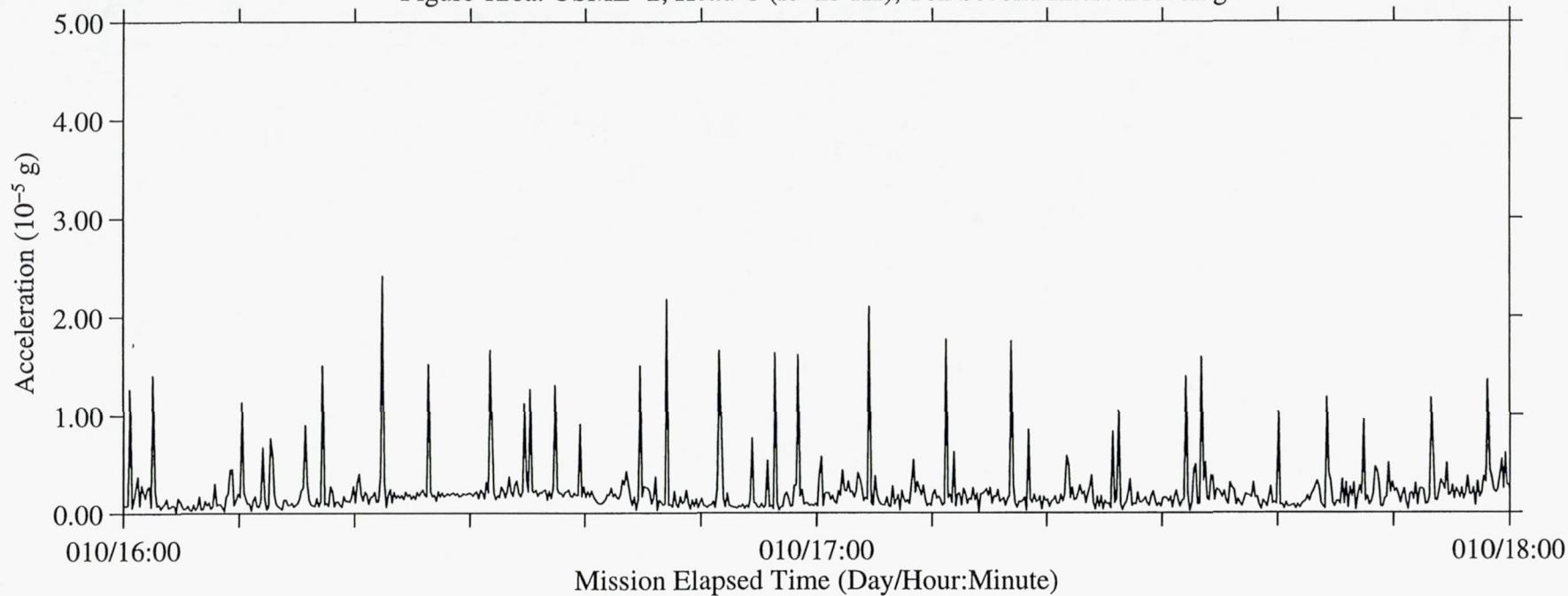
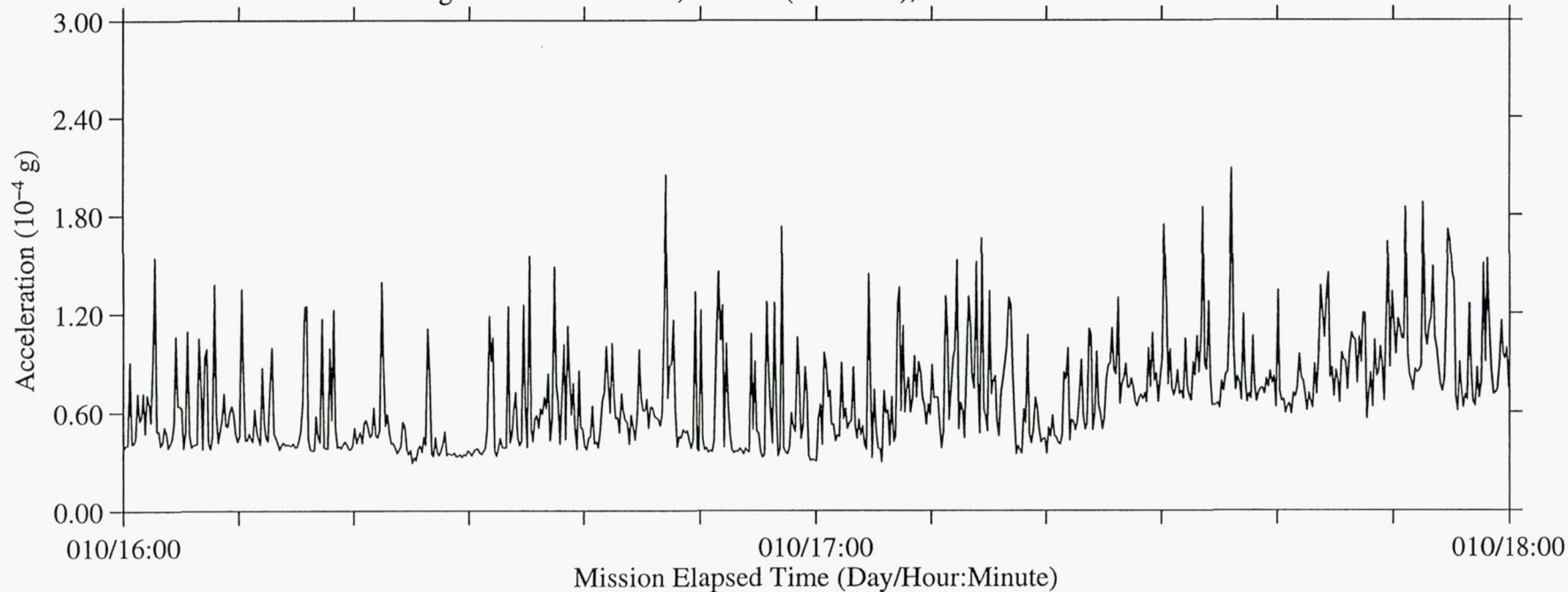
Figure 126a: USML-2, Head C ( $f_c=25$  Hz), Ten Second Interval AverageFigure 126b: USML-2, Head C ( $f_c=25$  Hz), Ten Second Interval RMS



Figure 127a: USML-2, Head C (fc=25 Hz), Ten Second Interval Average

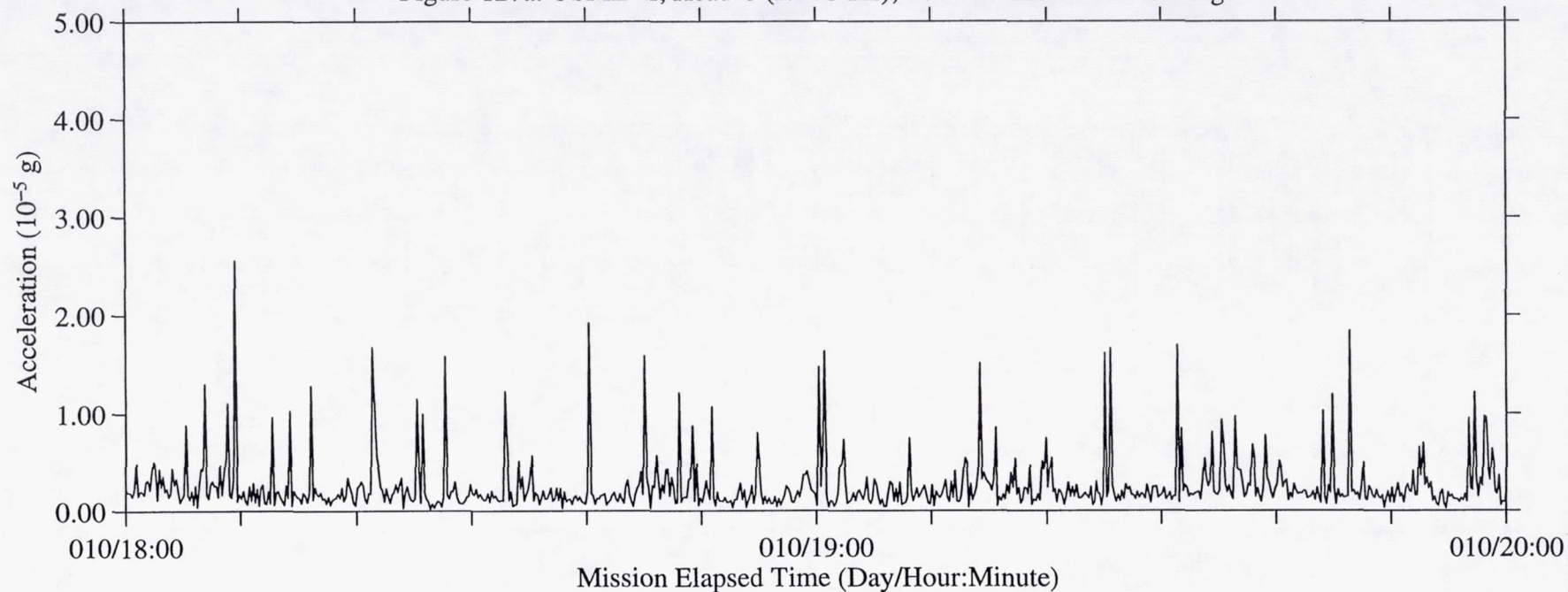


Figure 127b: USML-2, Head C (fc=25 Hz), Ten Second Interval RMS

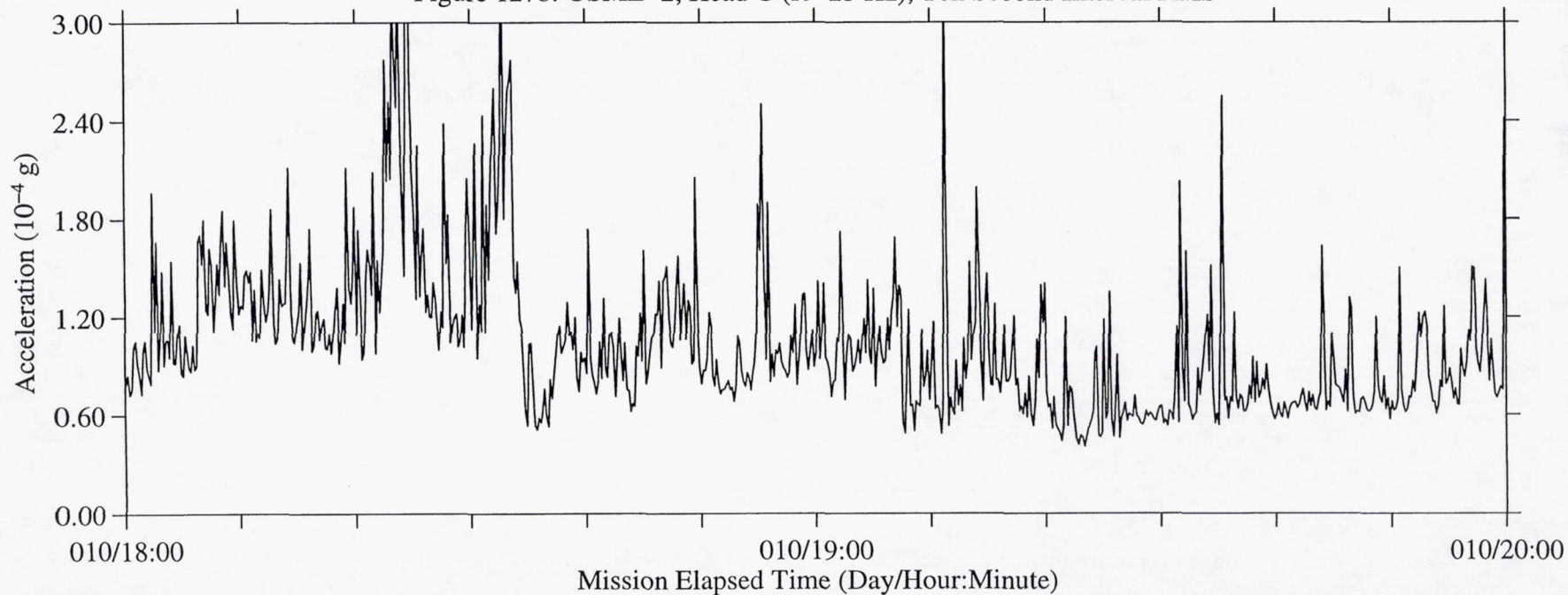


Figure 128a: USML-2, Head C (fc=25 Hz), Ten Second Interval Average

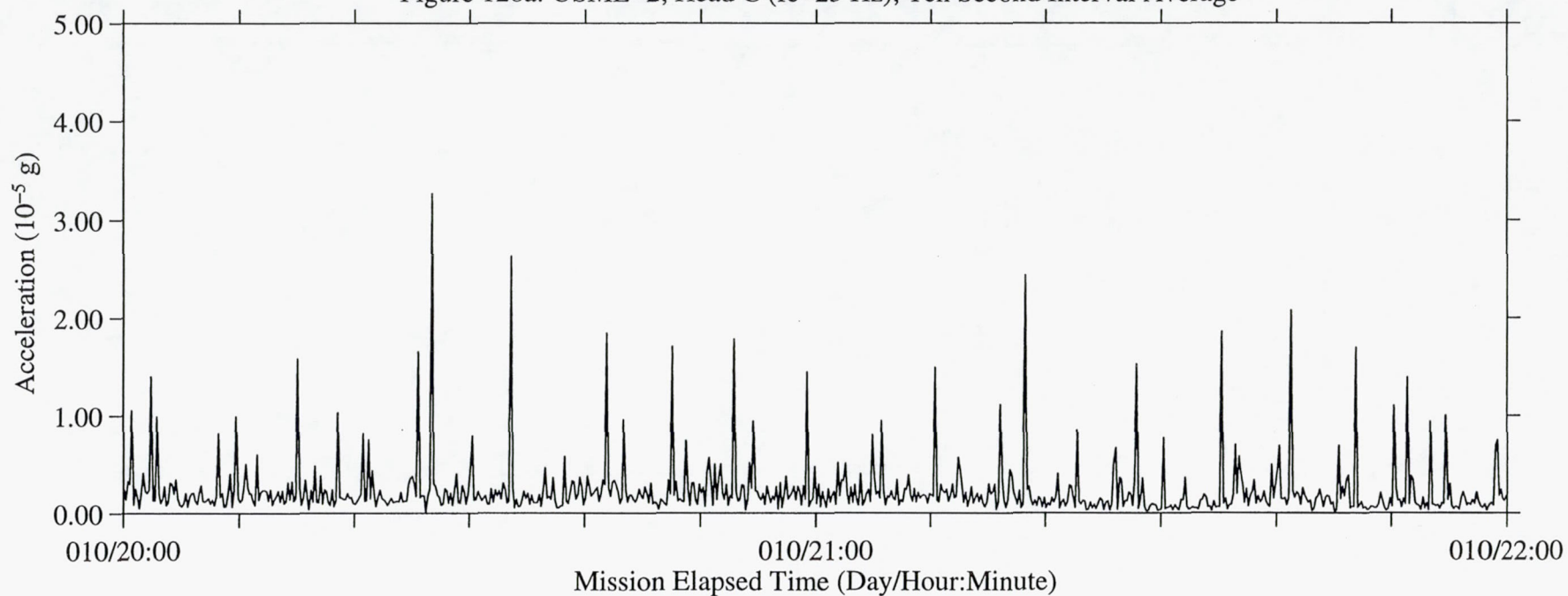


Figure 128b: USML-2, Head C (fc=25 Hz), Ten Second Interval RMS

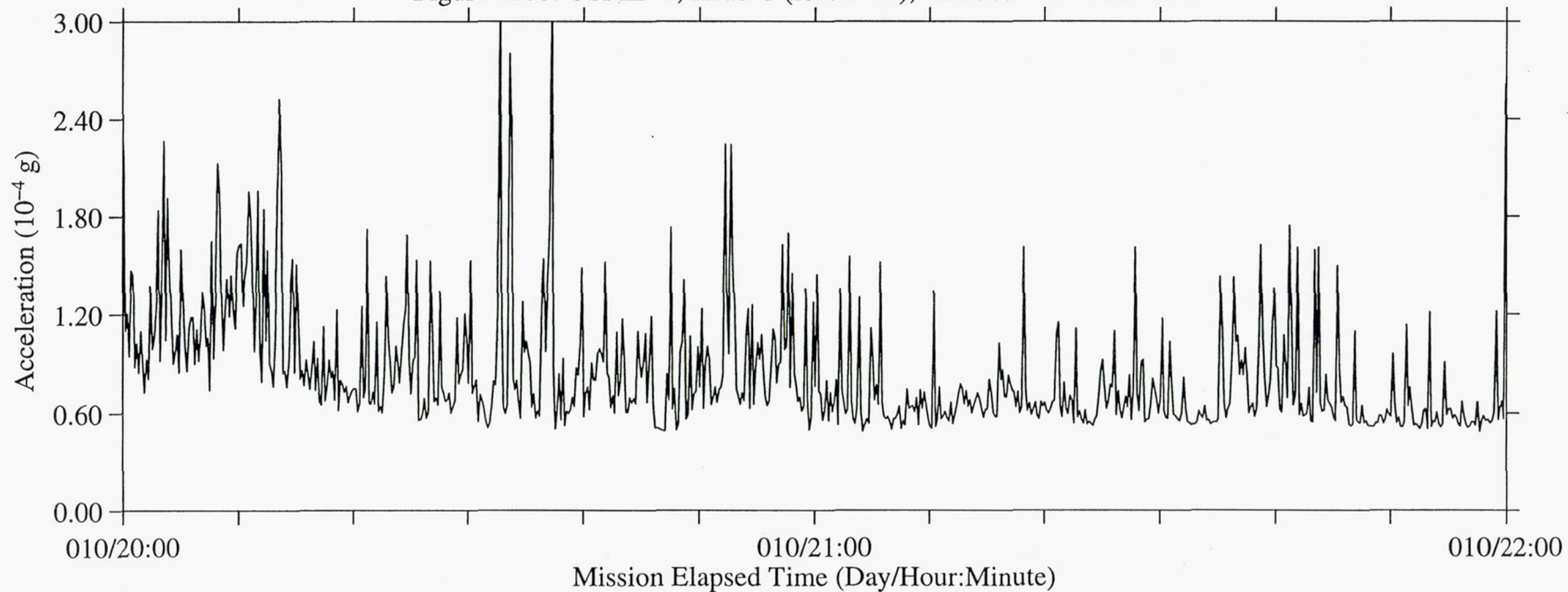




Figure 129a: USML-2, Head C (fc=25 Hz), Ten Second Interval Average

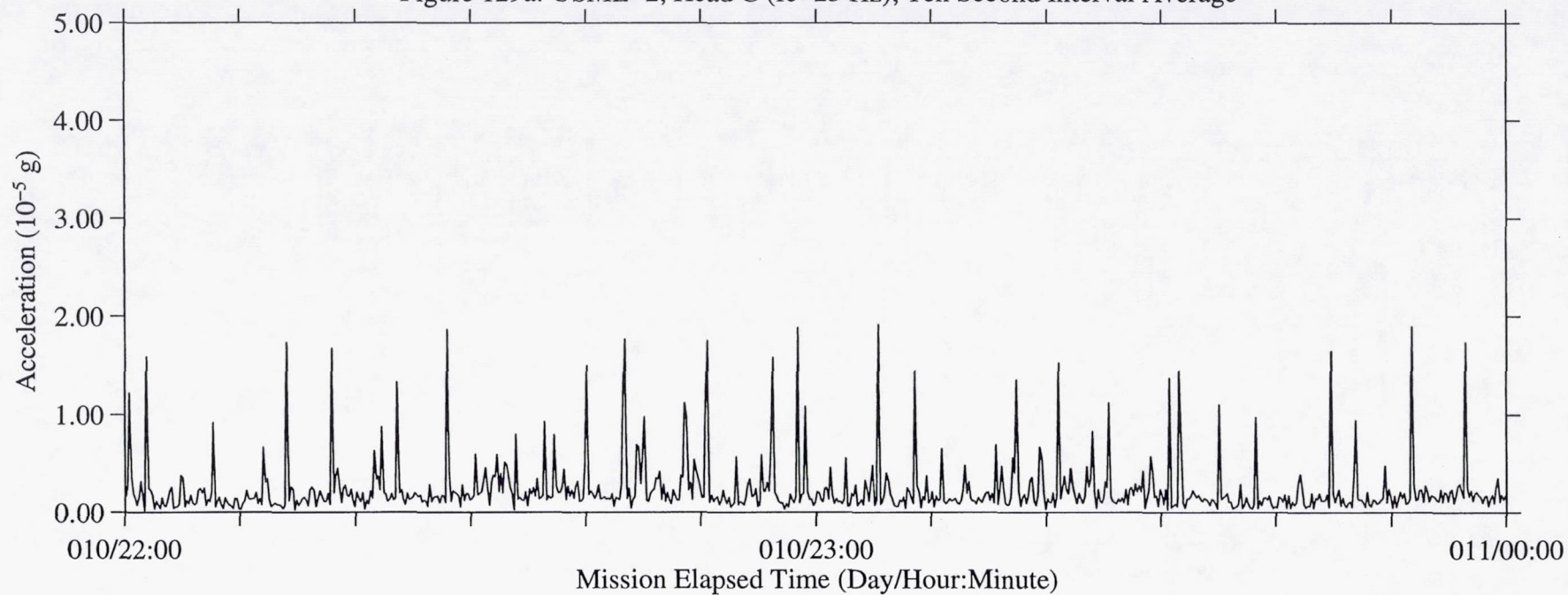


Figure 129b: USML-2, Head C (fc=25 Hz), Ten Second Interval RMS

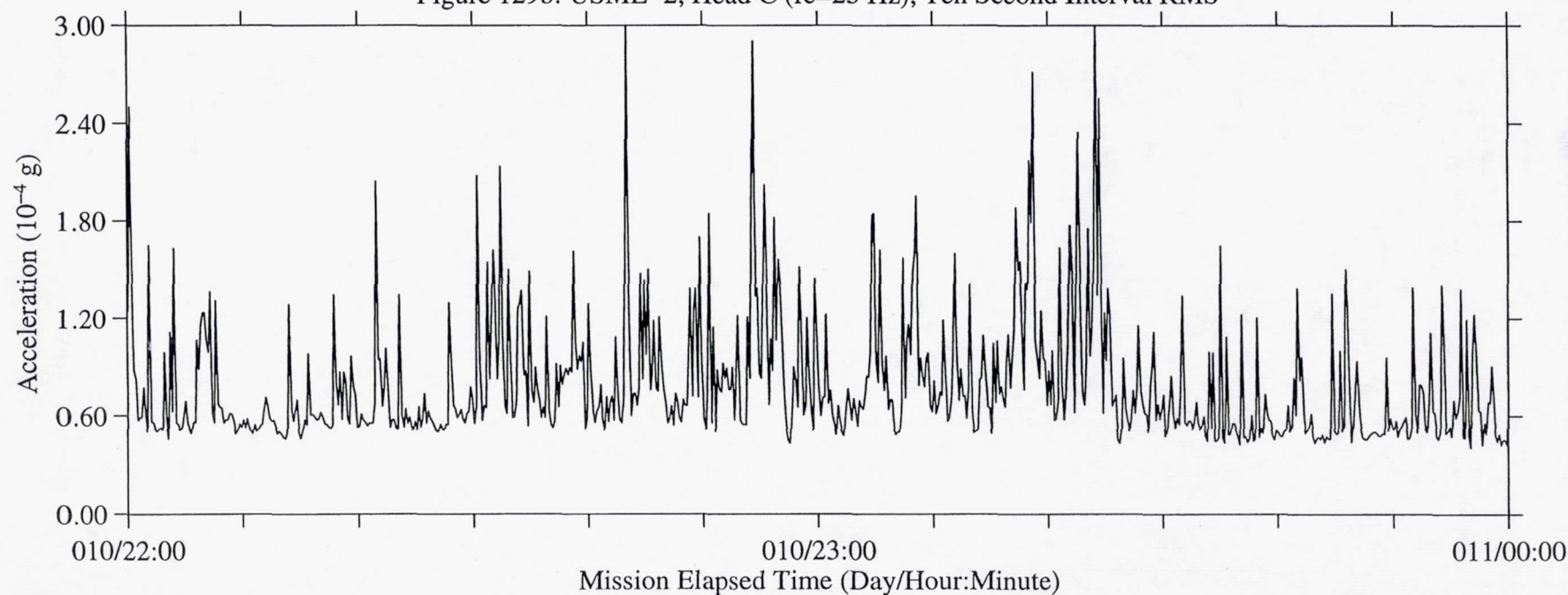


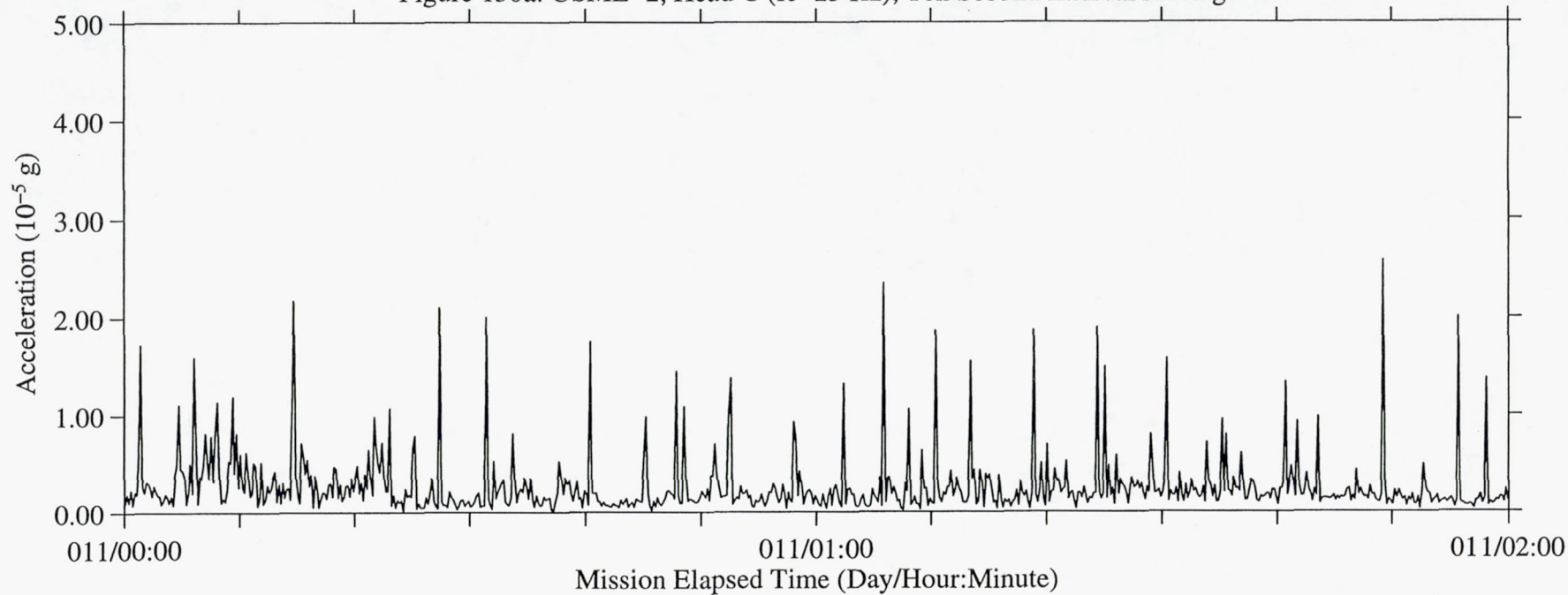
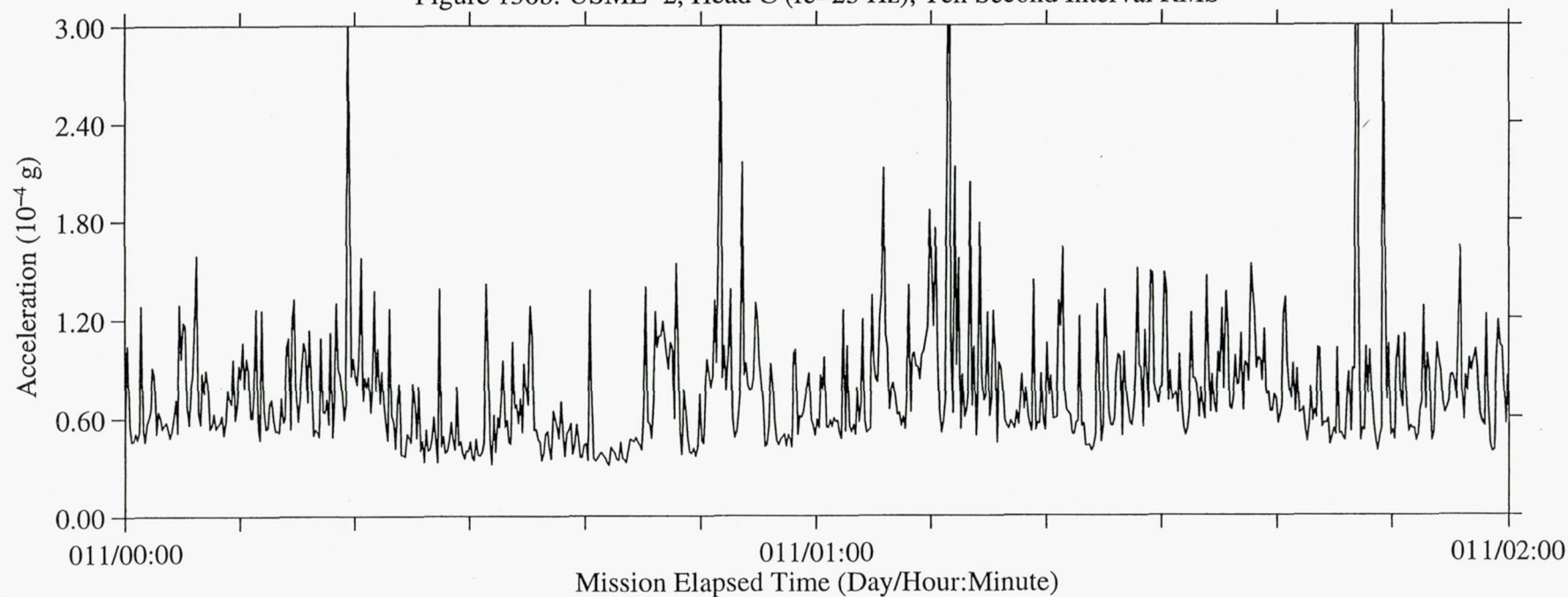
Figure 130a: USML-2, Head C ( $f_c=25$  Hz), Ten Second Interval AverageFigure 130b: USML-2, Head C ( $f_c=25$  Hz), Ten Second Interval RMS



Figure 131a: USML-2, Head C (fc=25 Hz), Ten Second Interval Average

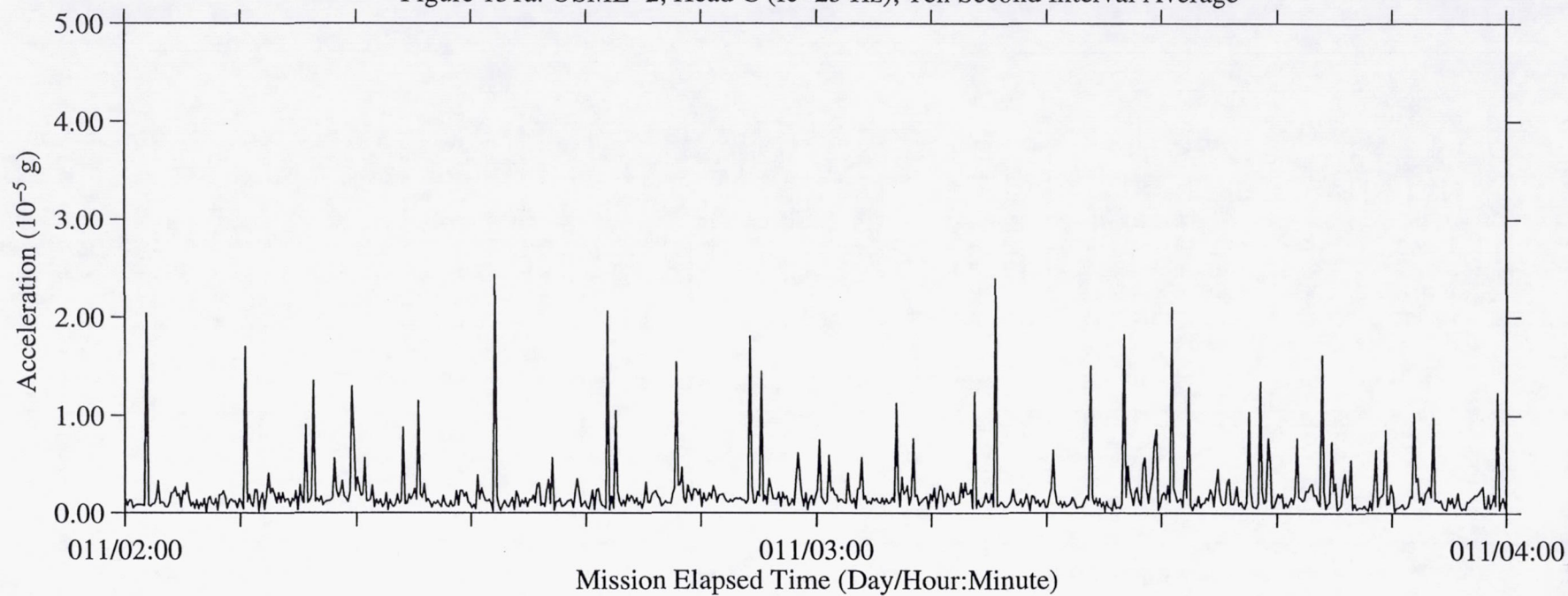


Figure 131b: USML-2, Head C (fc=25 Hz), Ten Second Interval RMS

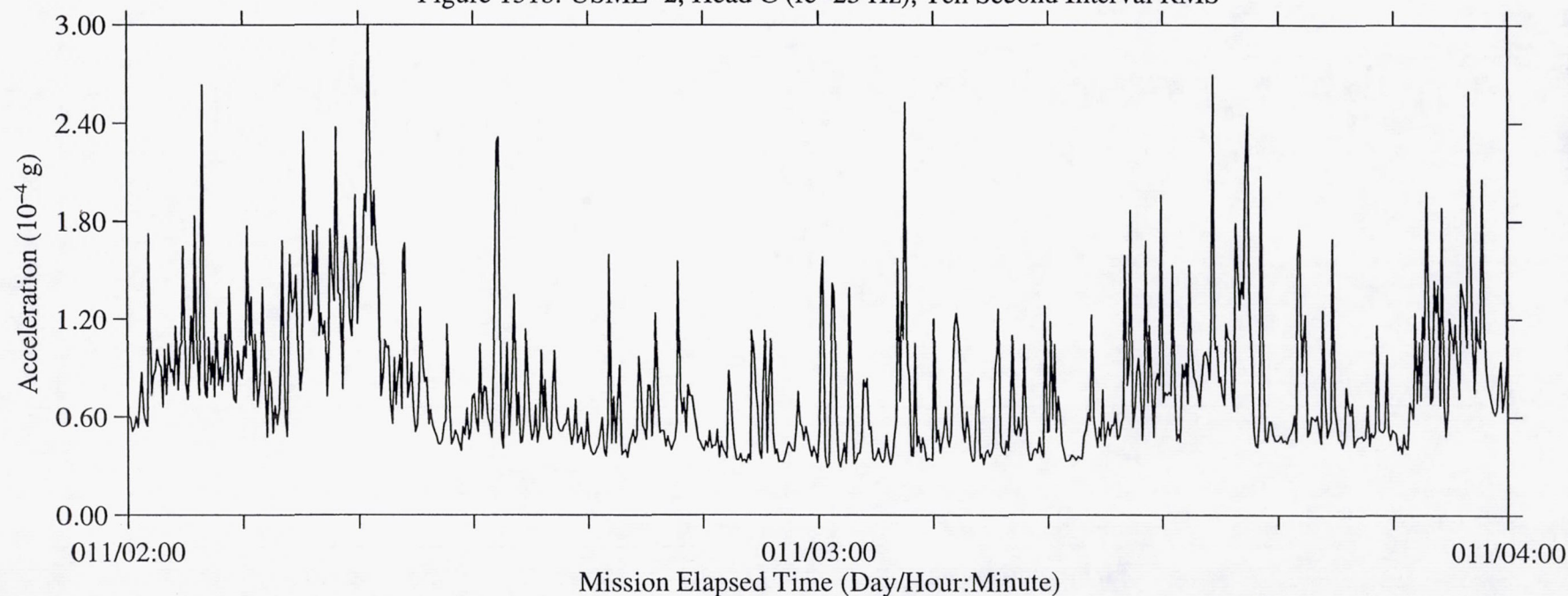


Figure 132a: USML-2, Head C (fc=25 Hz), Ten Second Interval Average

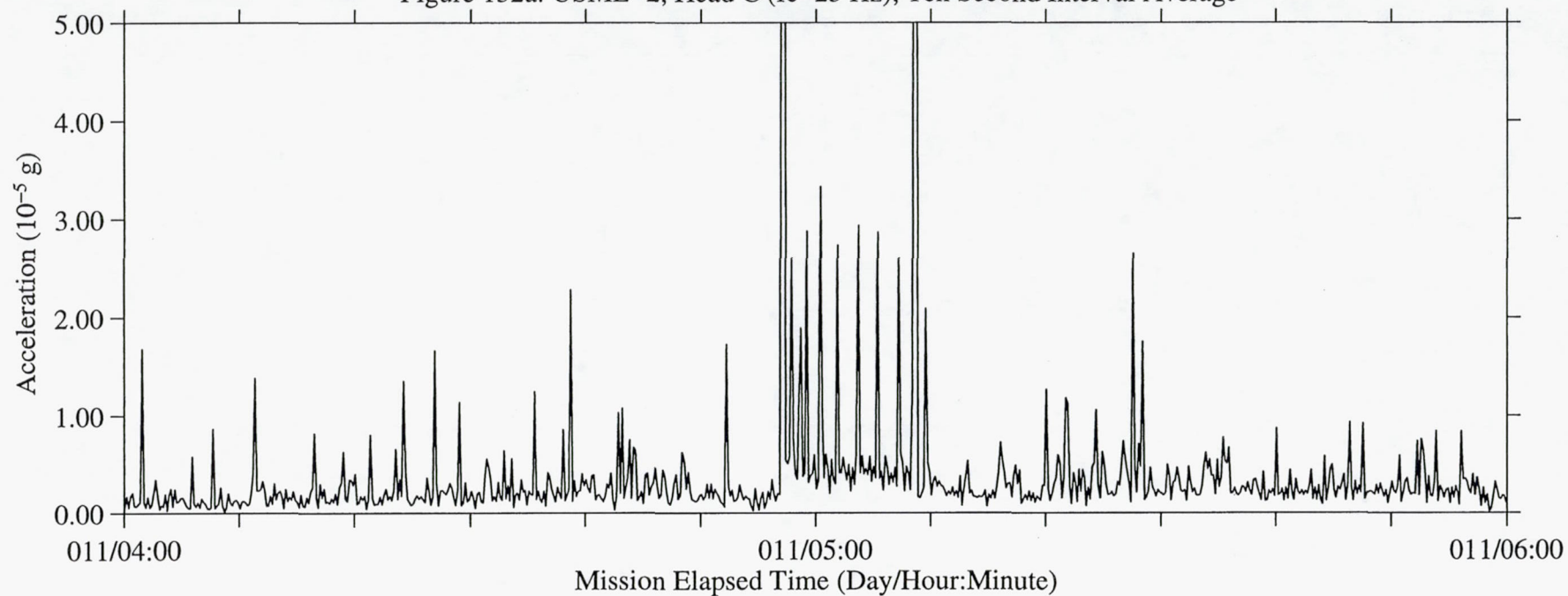


Figure 132b: USML-2, Head C (fc=25 Hz), Ten Second Interval RMS

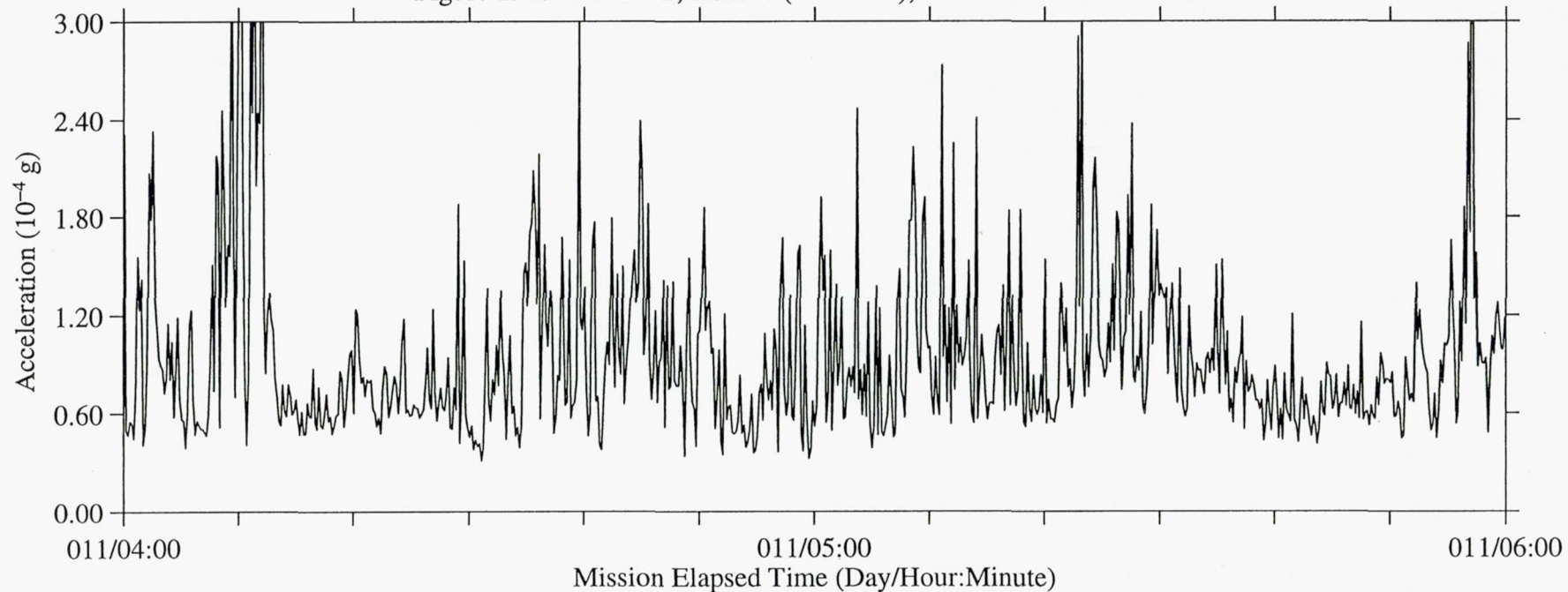




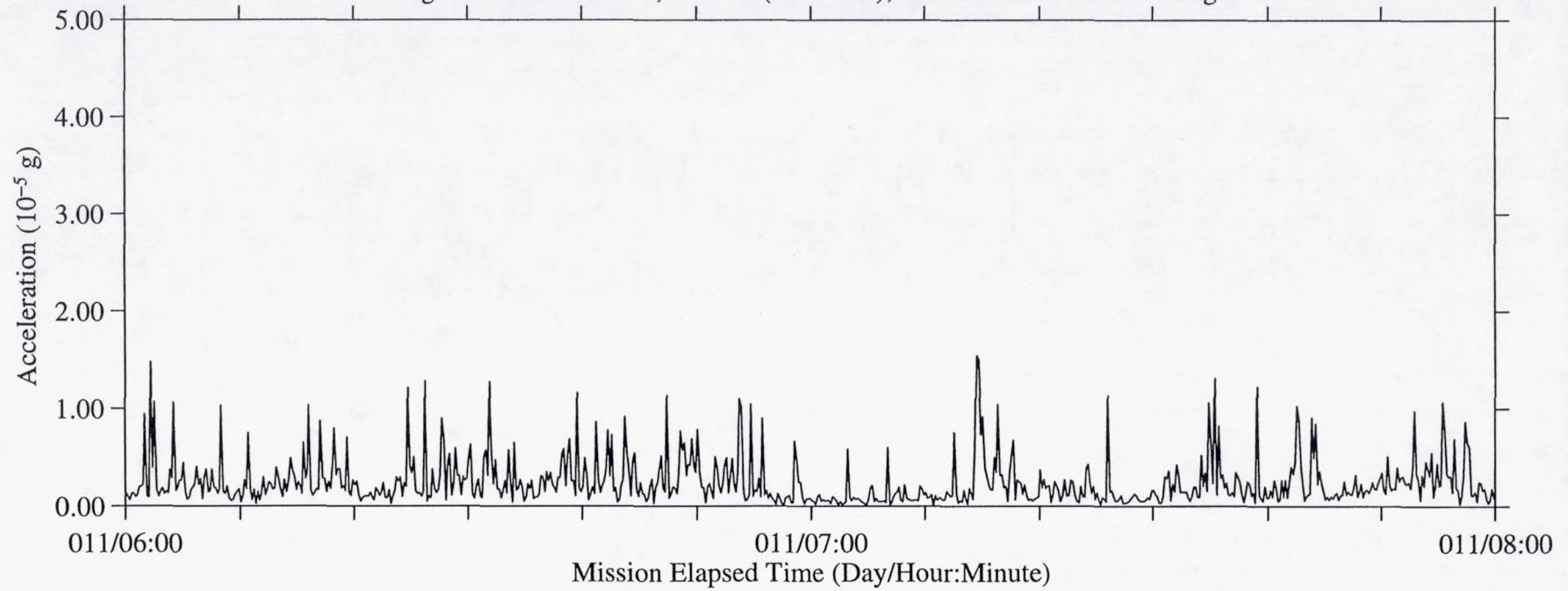
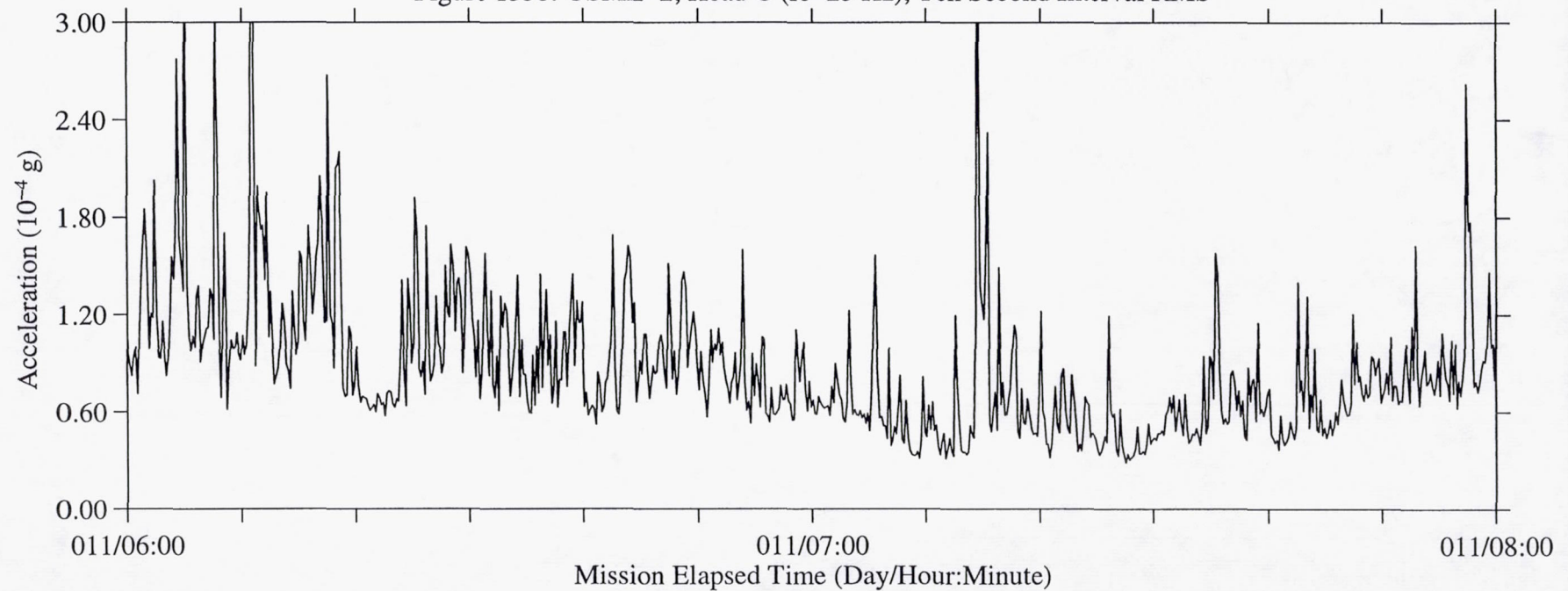
Figure 133a: USML-2, Head C ( $f_c=25$  Hz), Ten Second Interval AverageFigure 133b: USML-2, Head C ( $f_c=25$  Hz), Ten Second Interval RMS

Figure 134a: USML-2, Head C (fc=25 Hz), Ten Second Interval Average

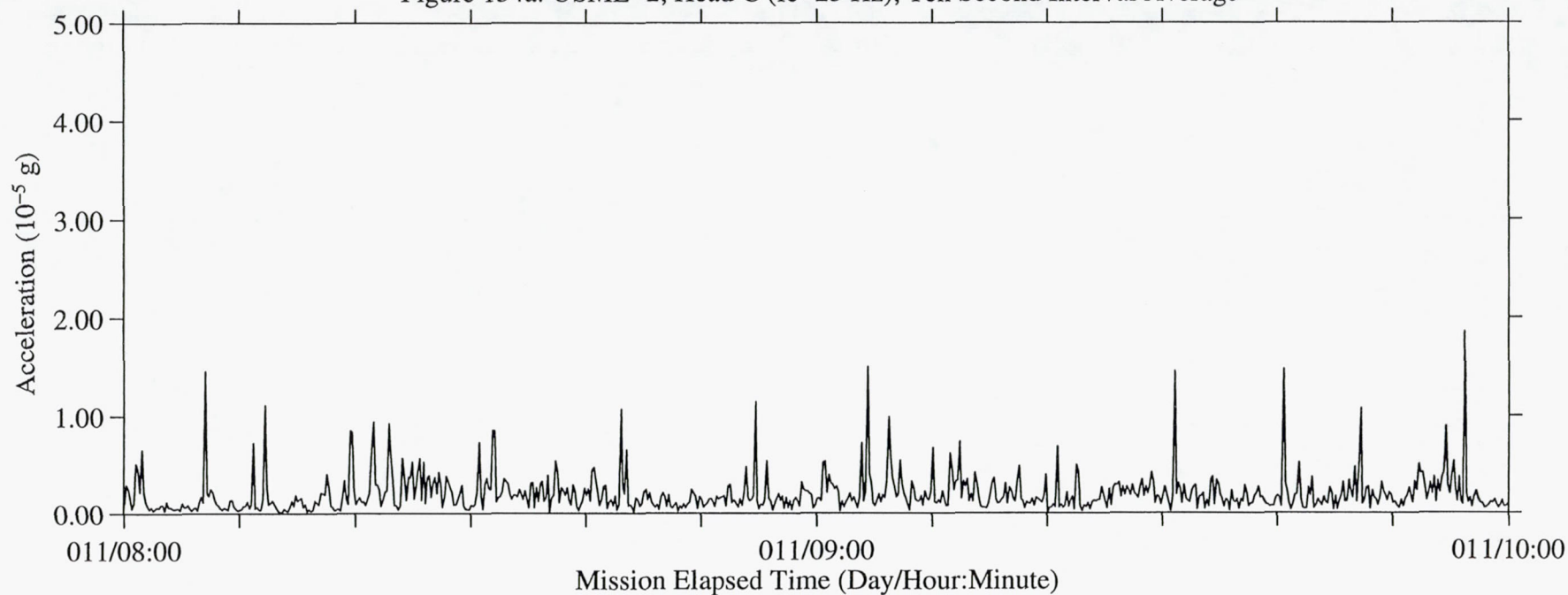


Figure 134b: USML-2, Head C (fc=25 Hz), Ten Second Interval RMS

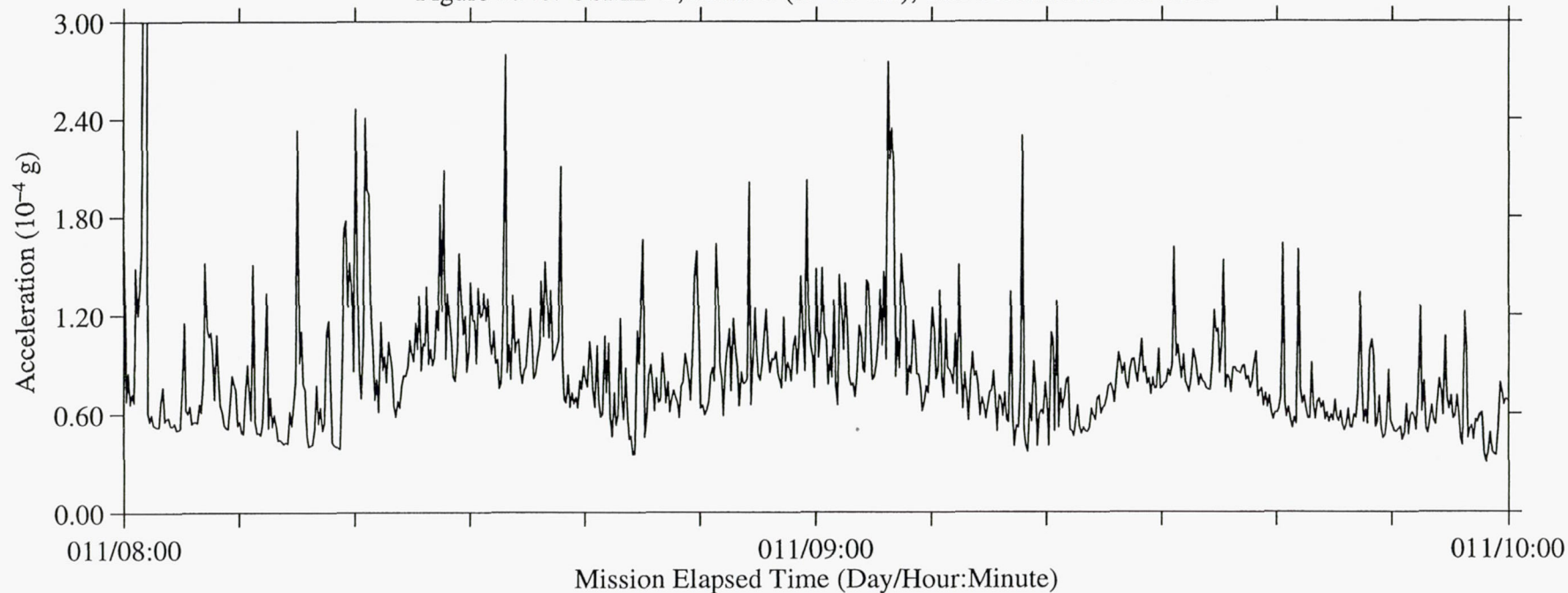




Figure 135a: USML-2, Head C (fc=25 Hz), Ten Second Interval Average

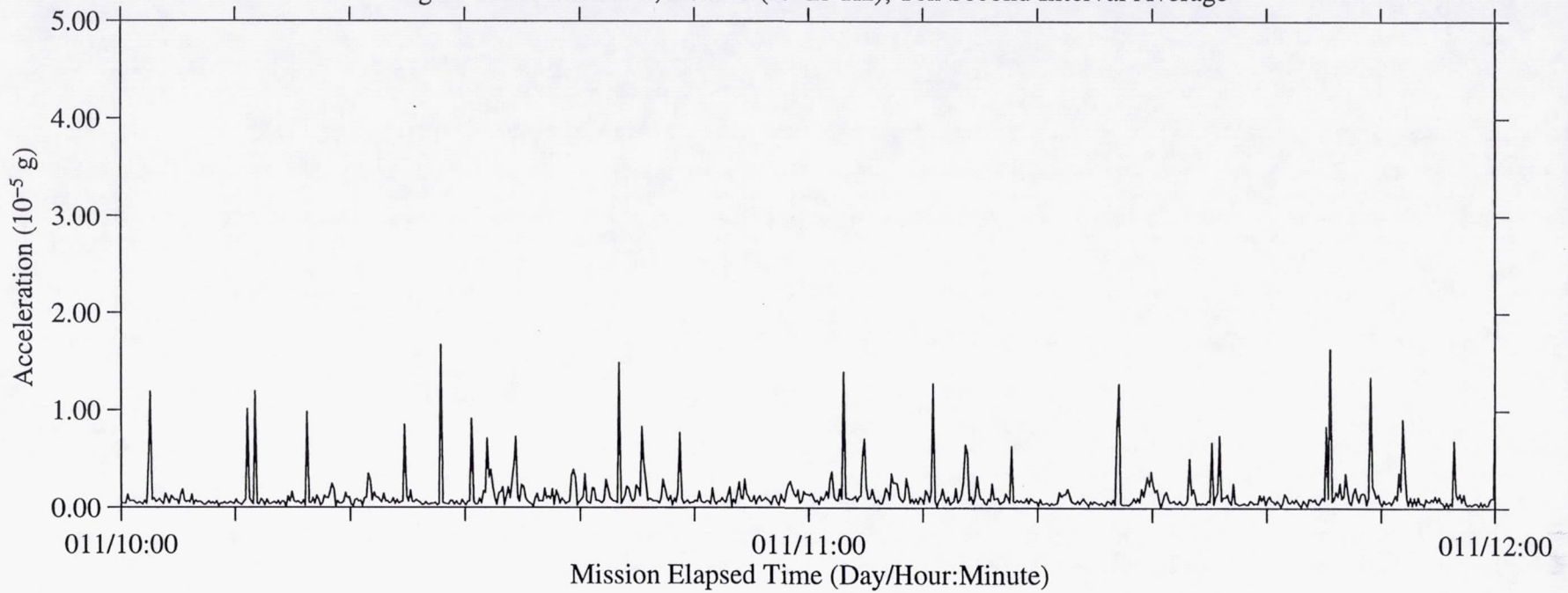


Figure 135b: USML-2, Head C (fc=25 Hz), Ten Second Interval RMS

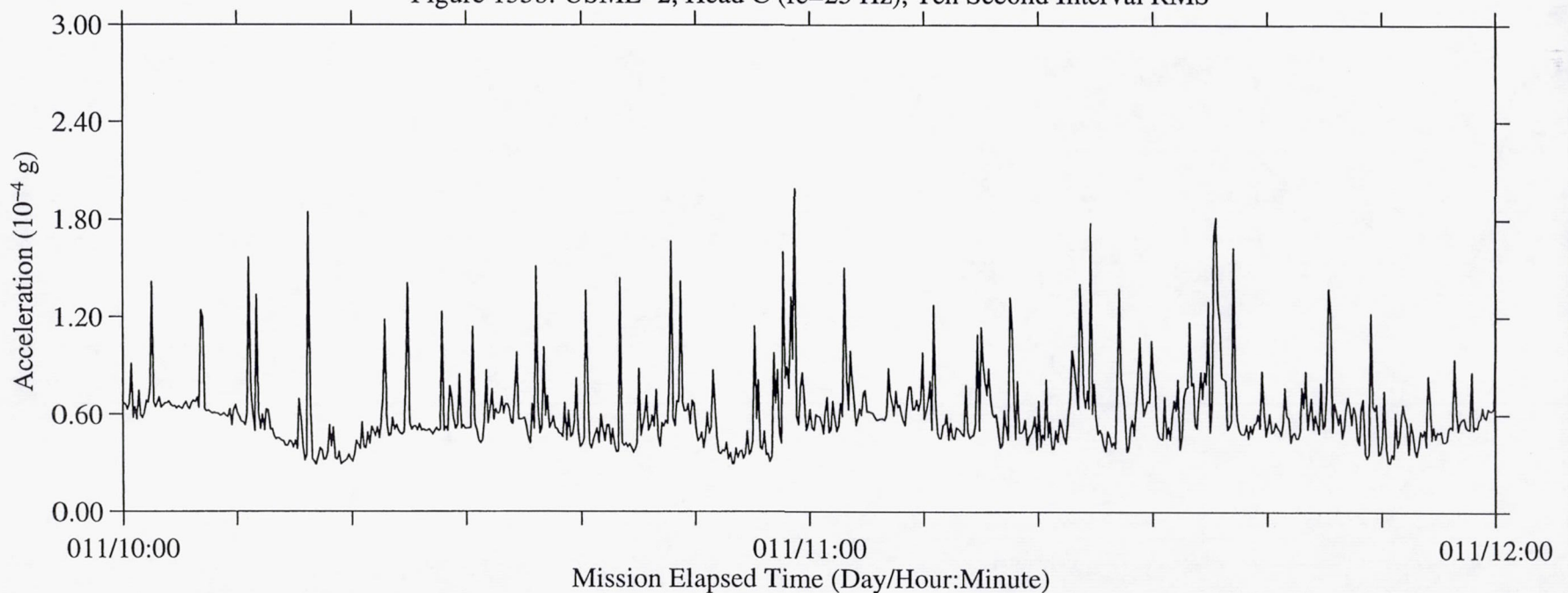


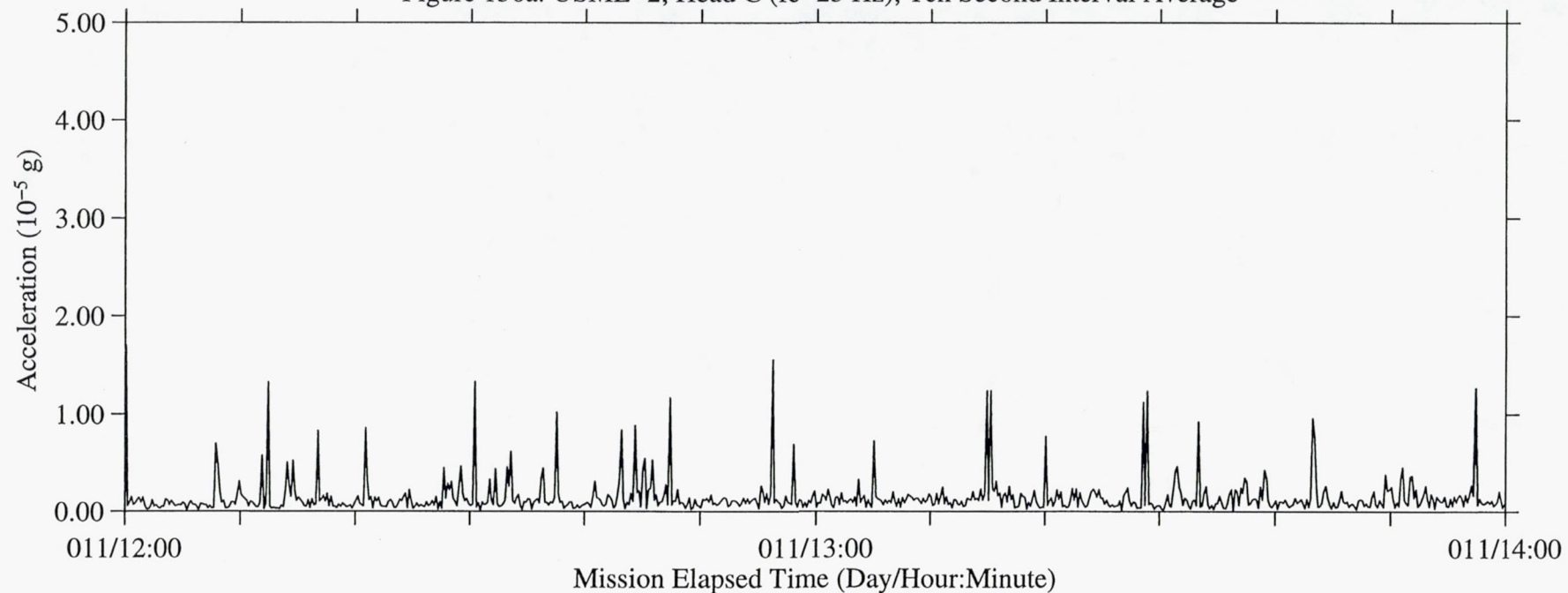
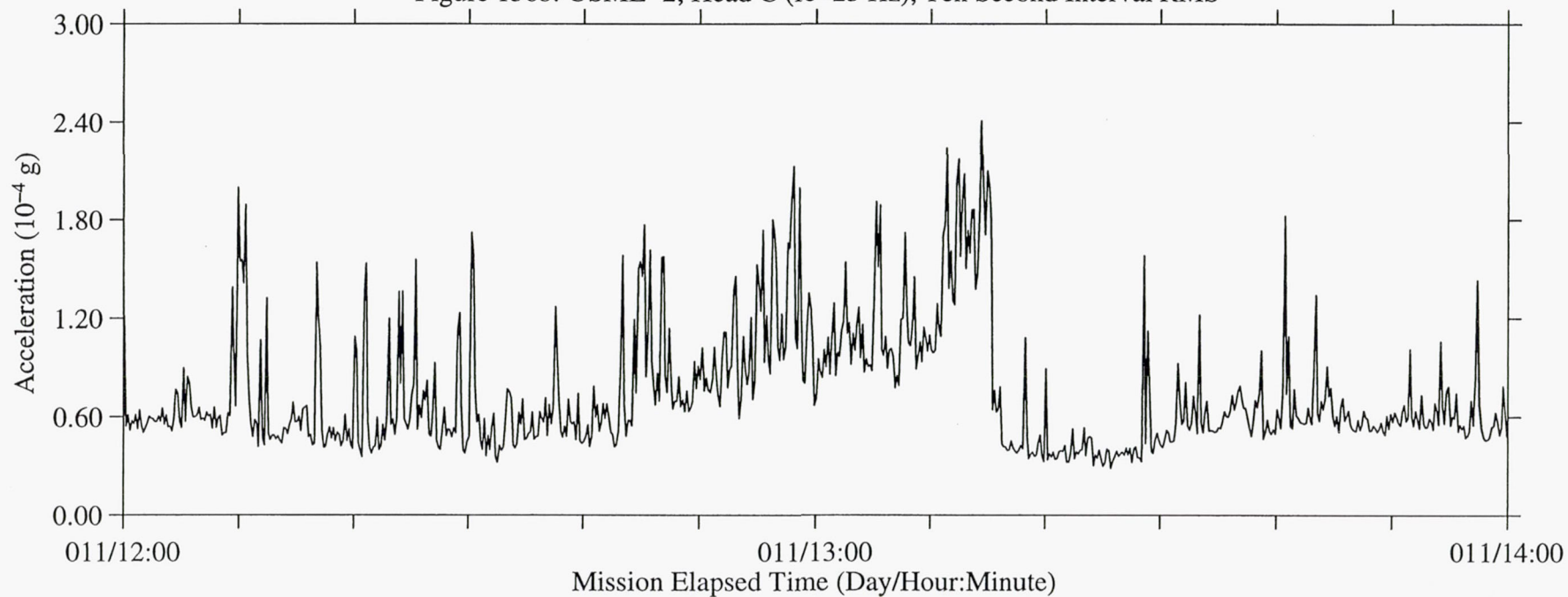
Figure 136a: USML-2, Head C ( $f_c=25$  Hz), Ten Second Interval AverageFigure 136b: USML-2, Head C ( $f_c=25$  Hz), Ten Second Interval RMS



Figure 137a: USML-2, Head C (fc=25 Hz), Ten Second Interval Average

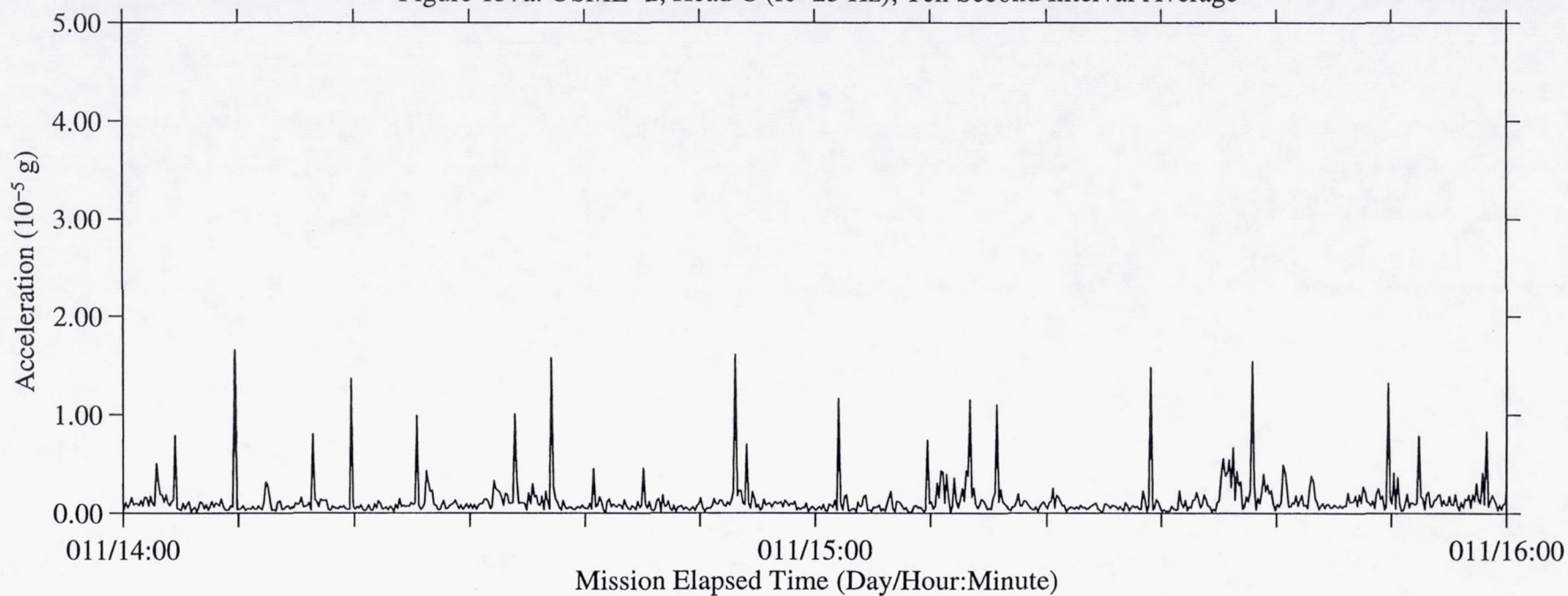


Figure 137b: USML-2, Head C (fc=25 Hz), Ten Second Interval RMS

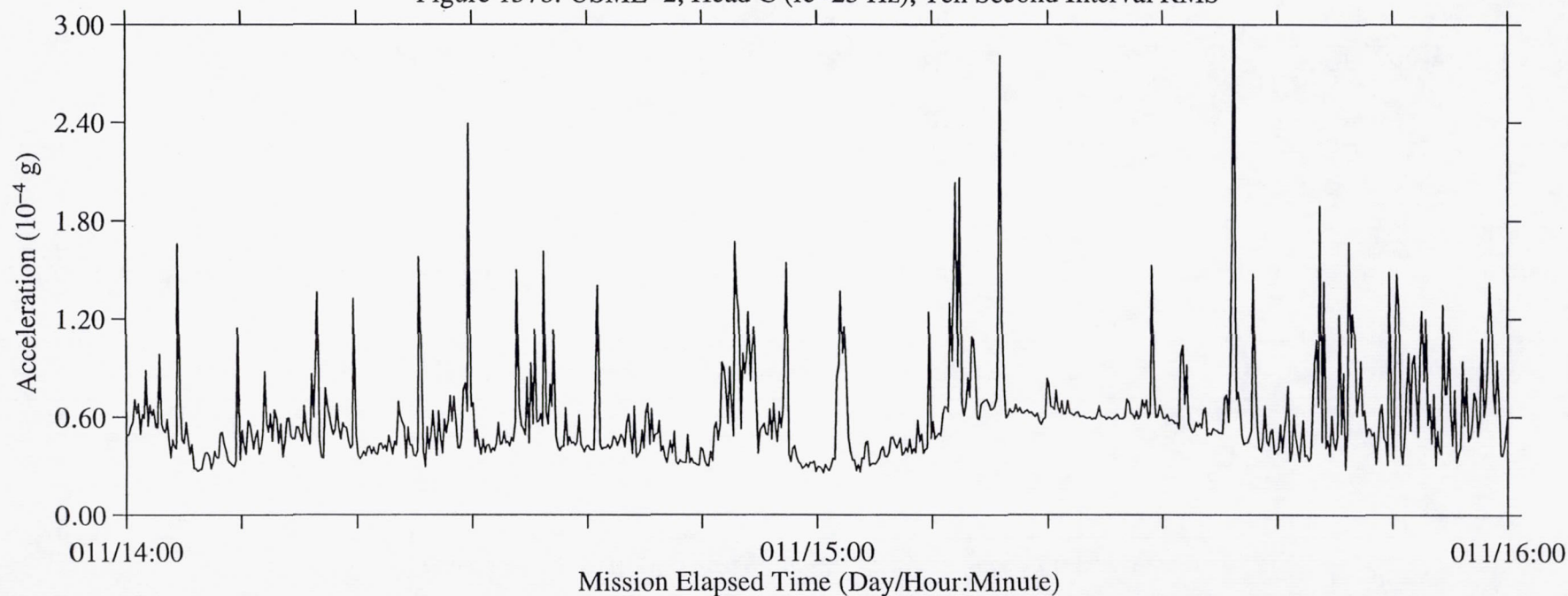


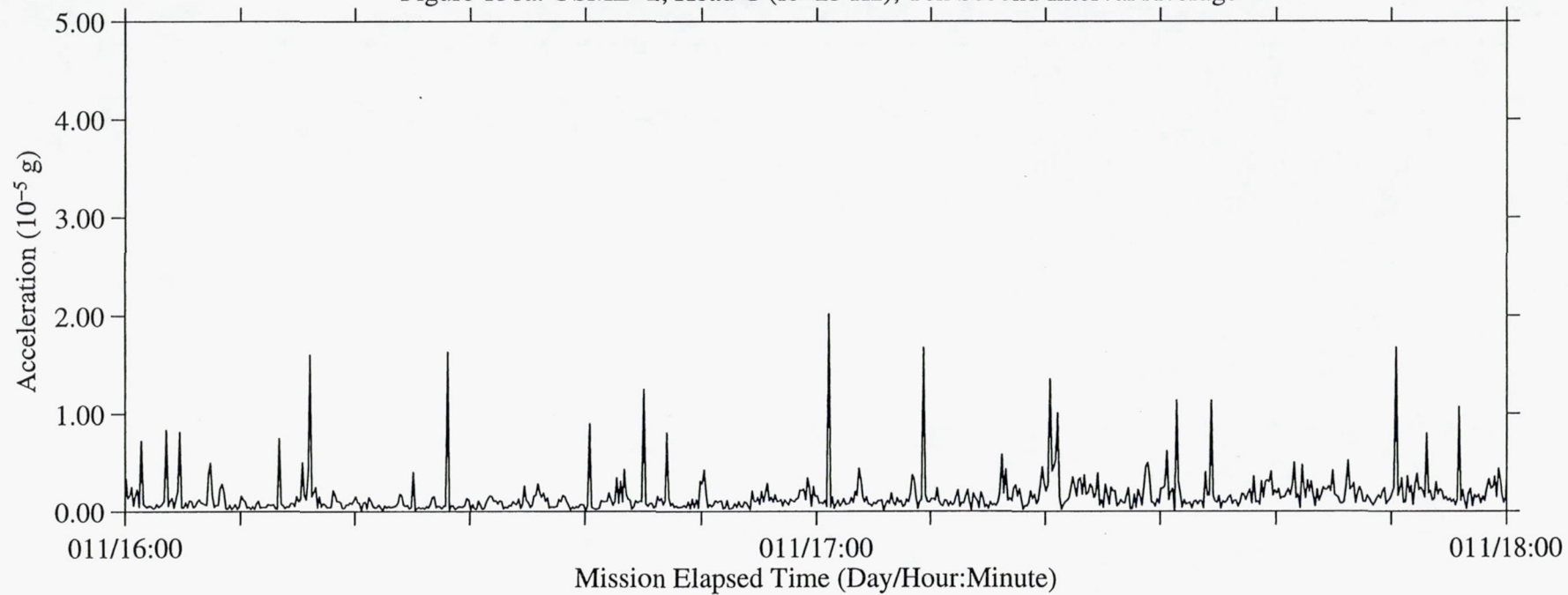
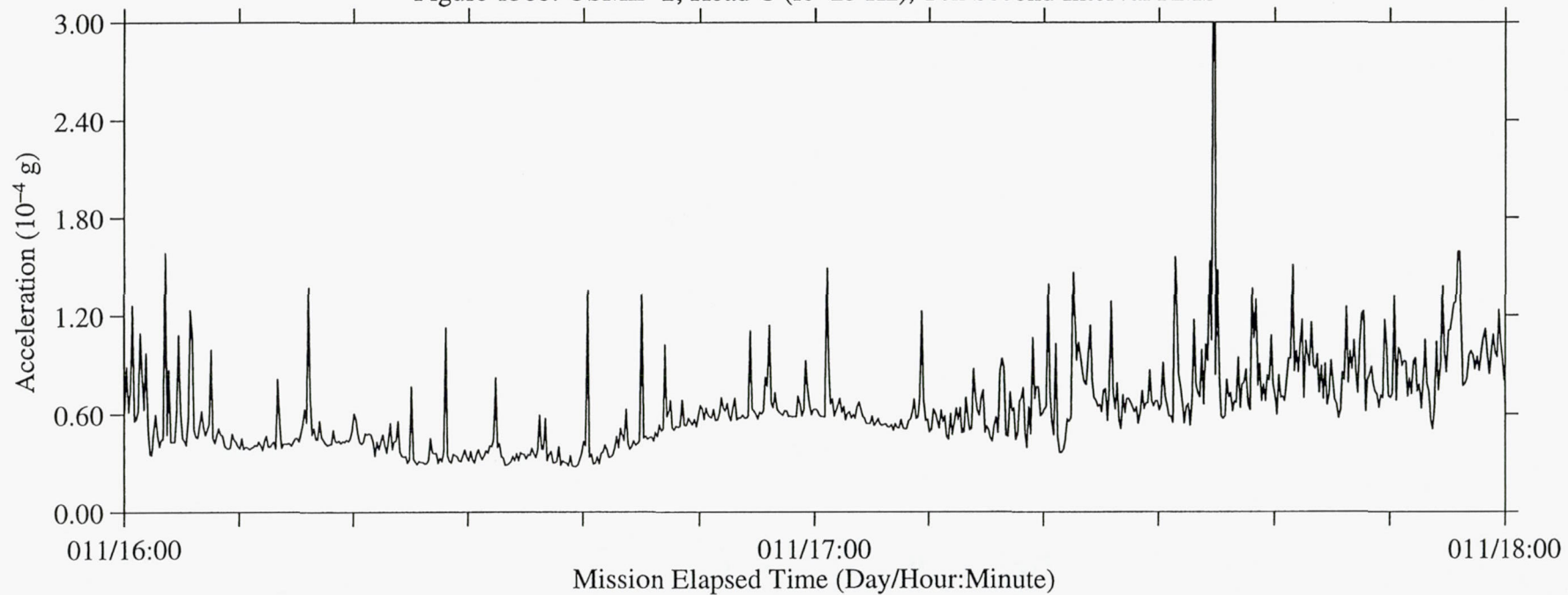
Figure 138a: USML-2, Head C ( $f_c=25$  Hz), Ten Second Interval AverageFigure 138b: USML-2, Head C ( $f_c=25$  Hz), Ten Second Interval RMS



Figure 139a: USML-2, Head C (fc=25 Hz), Ten Second Interval Average

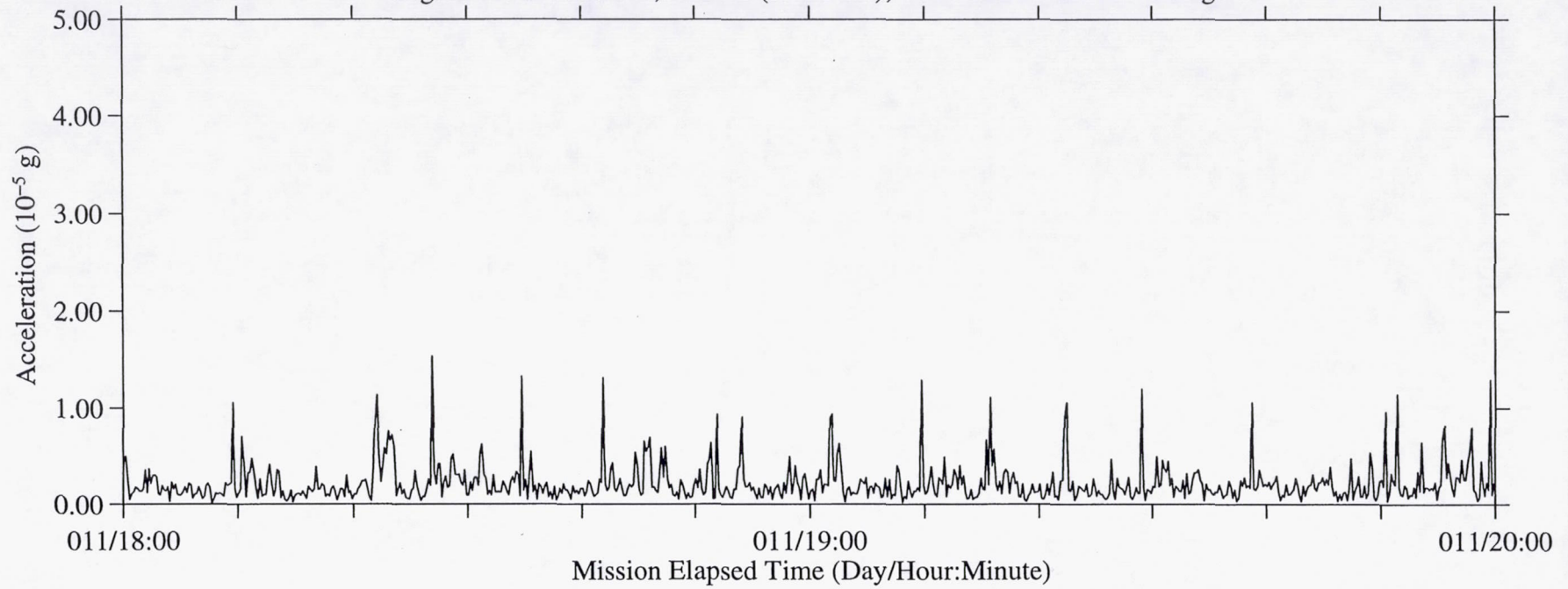


Figure 139b: USML-2, Head C (fc=25 Hz), Ten Second Interval RMS

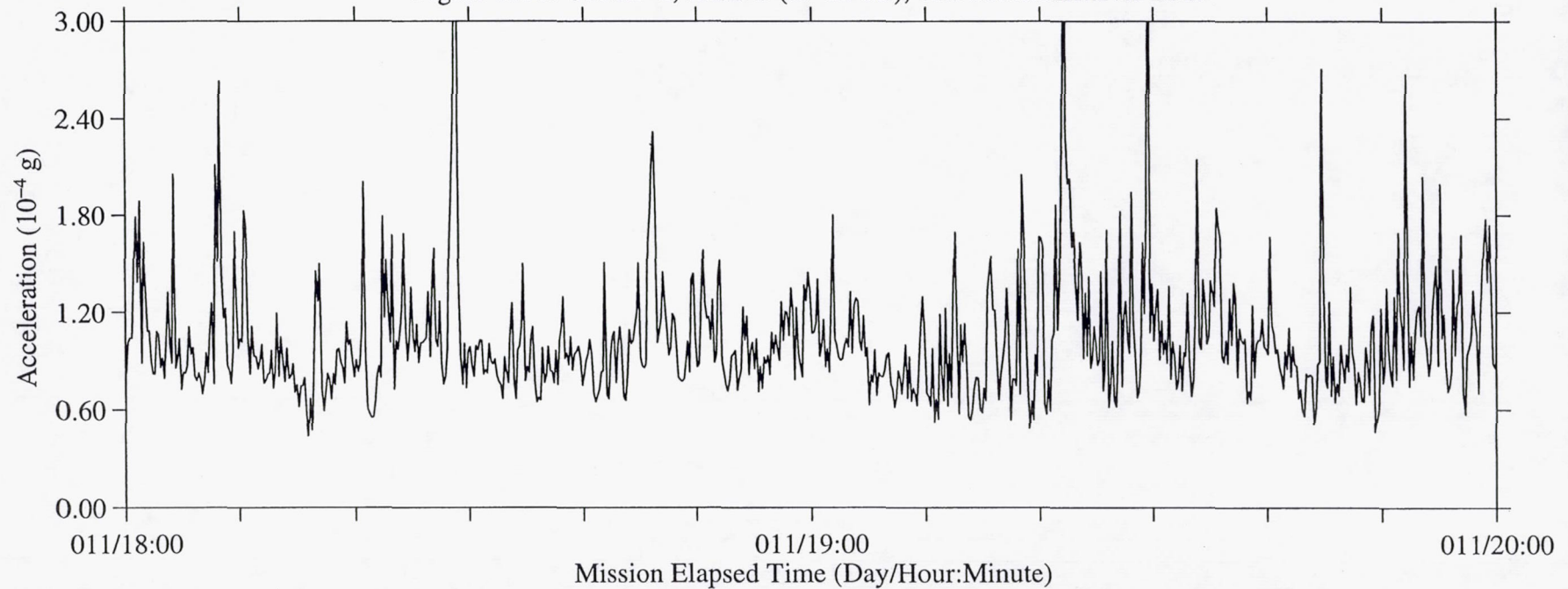


Figure 140a: USML-2, Head C (fc=25 Hz), Ten Second Interval Average

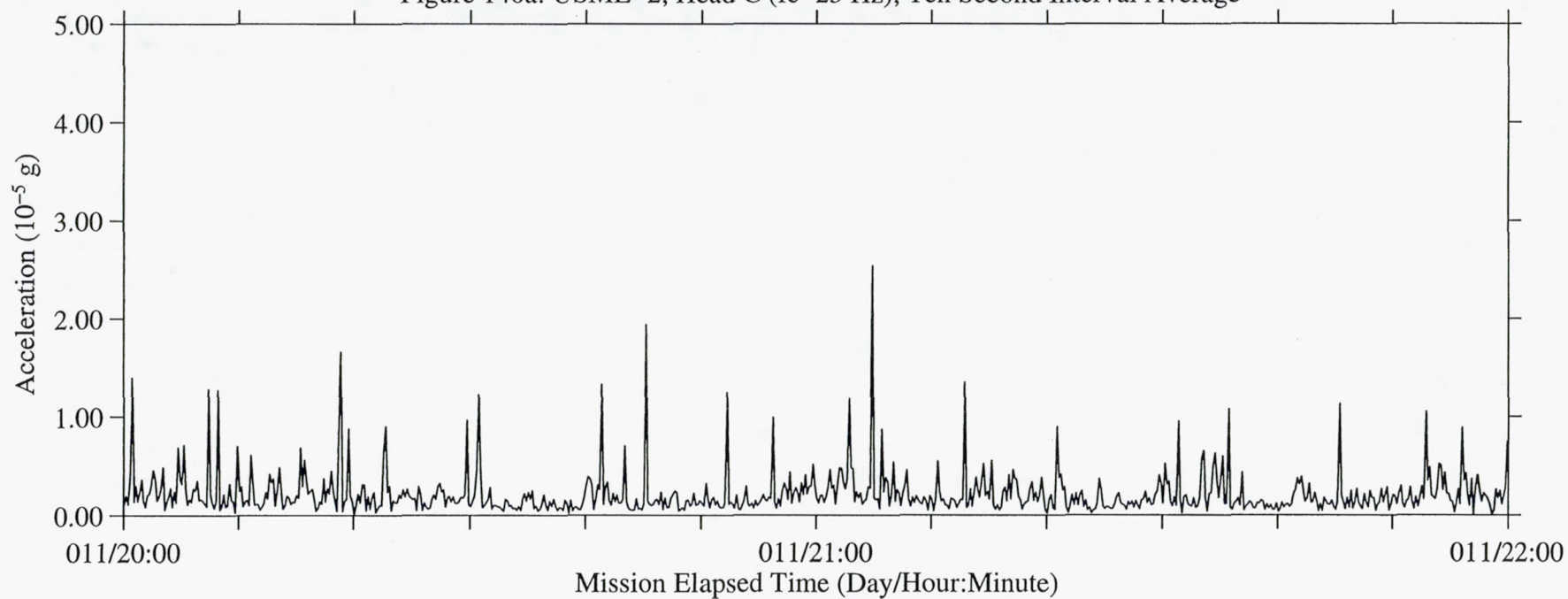


Figure 140b: USML-2, Head C (fc=25 Hz), Ten Second Interval RMS

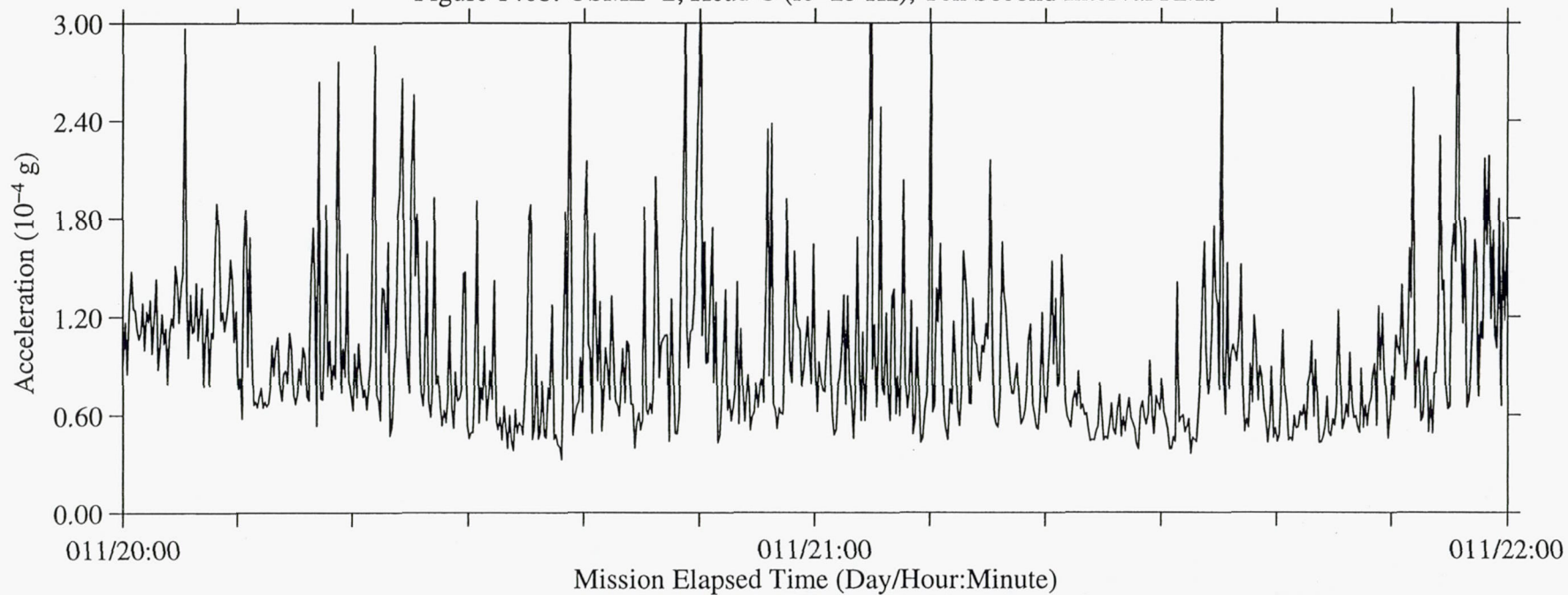




Figure 141a: USML-2, Head C (fc=25 Hz), Ten Second Interval Average

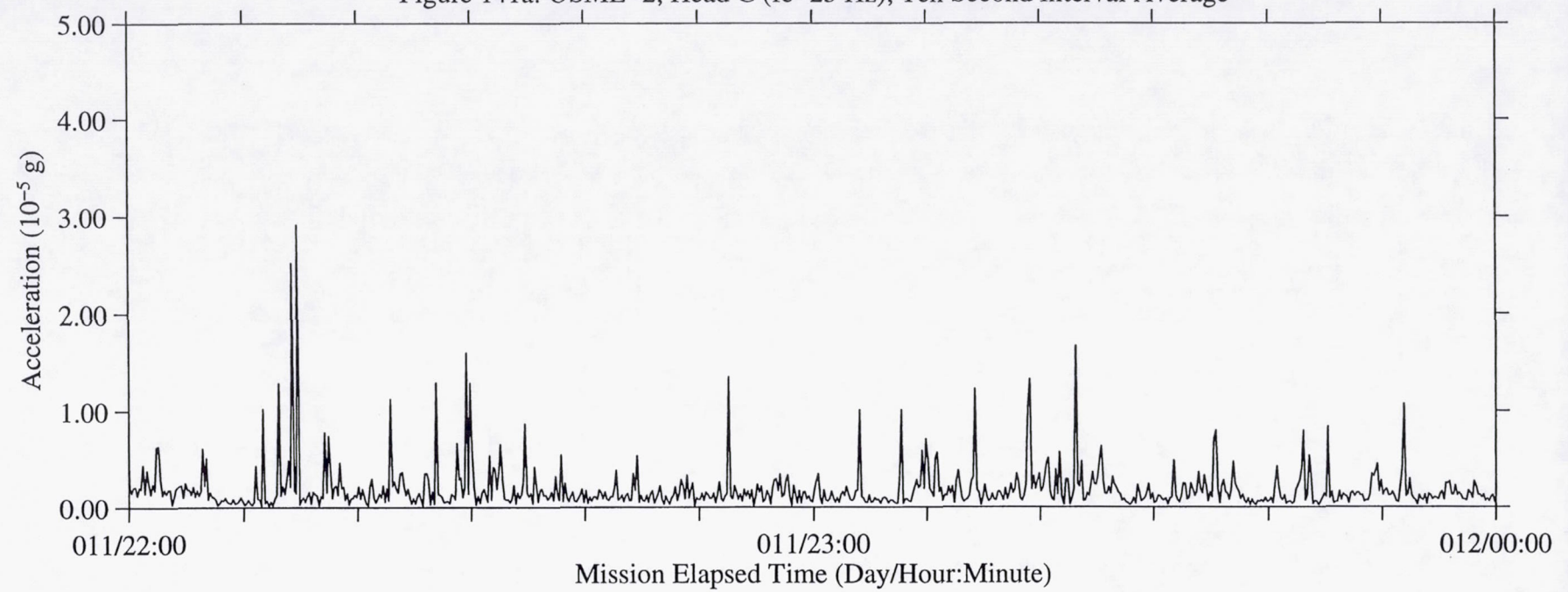


Figure 141b: USML-2, Head C (fc=25 Hz), Ten Second Interval RMS

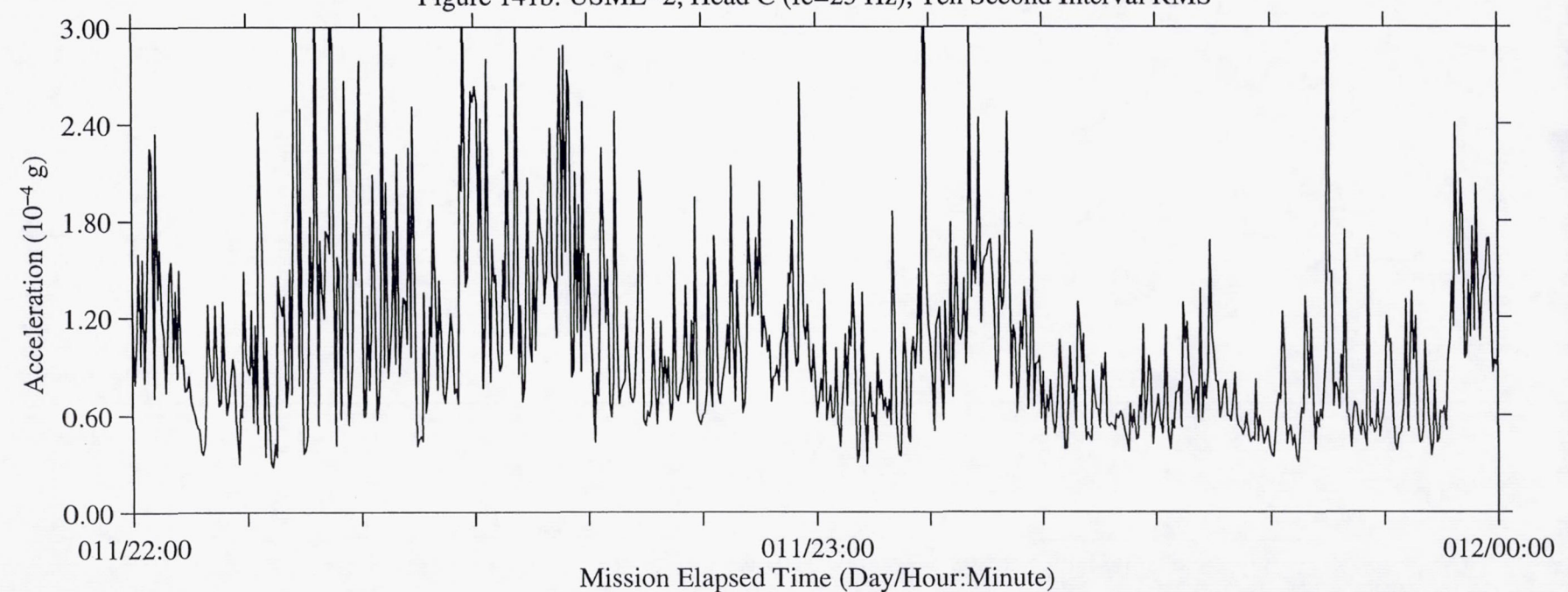


Figure 142a: USML-2, Head C (fc=25 Hz), Ten Second Interval Average

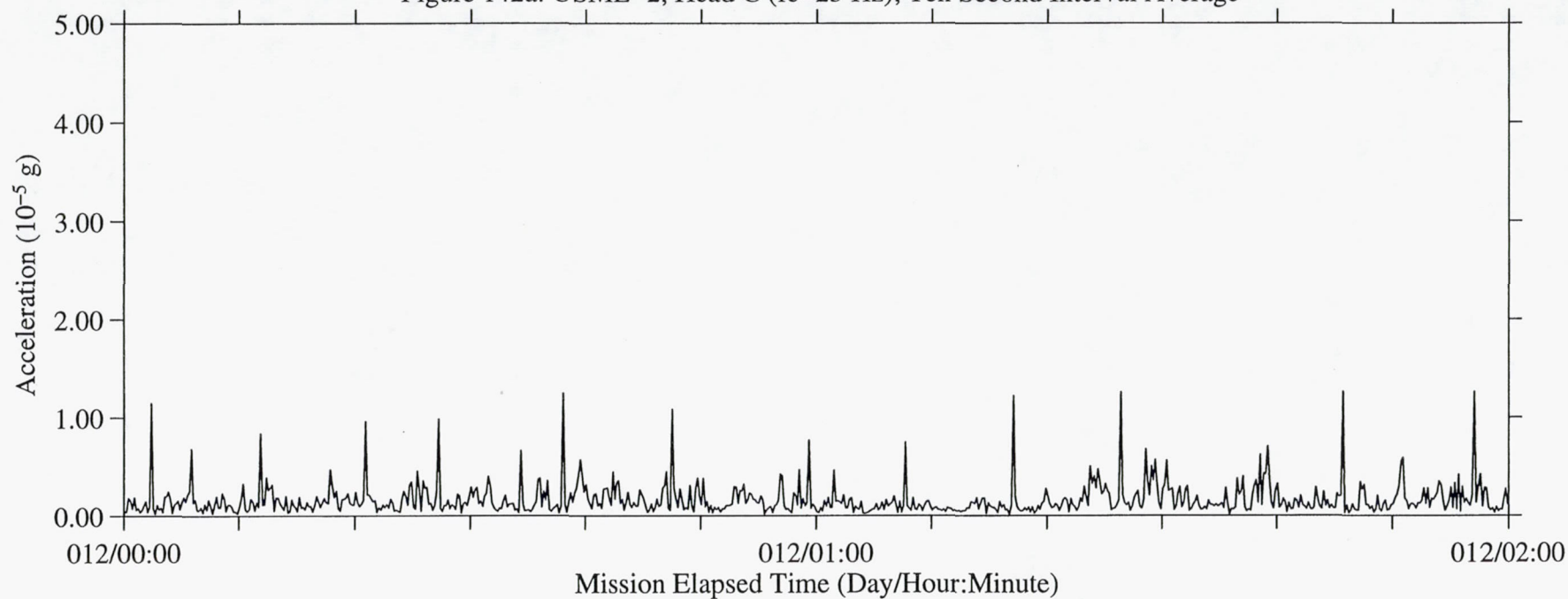


Figure 142b: USML-2, Head C (fc=25 Hz), Ten Second Interval RMS

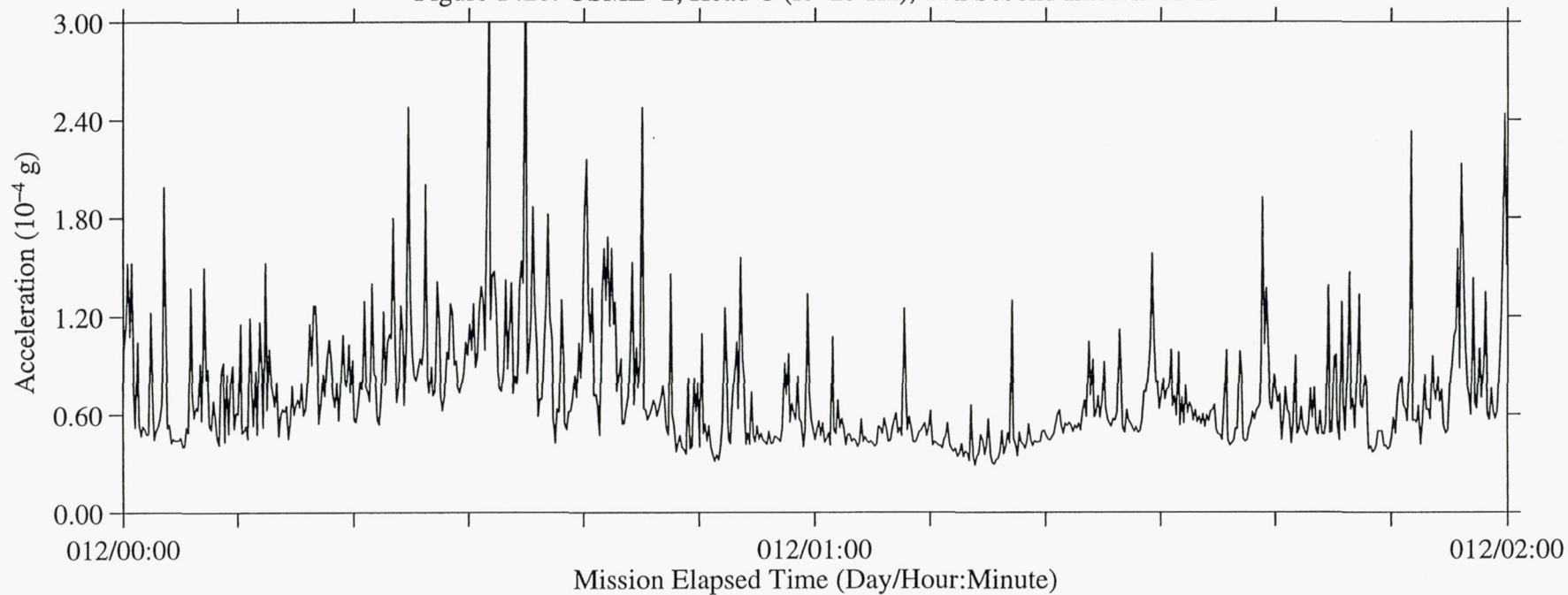




Figure 143a: USML-2, Head C (fc=25 Hz), Ten Second Interval Average

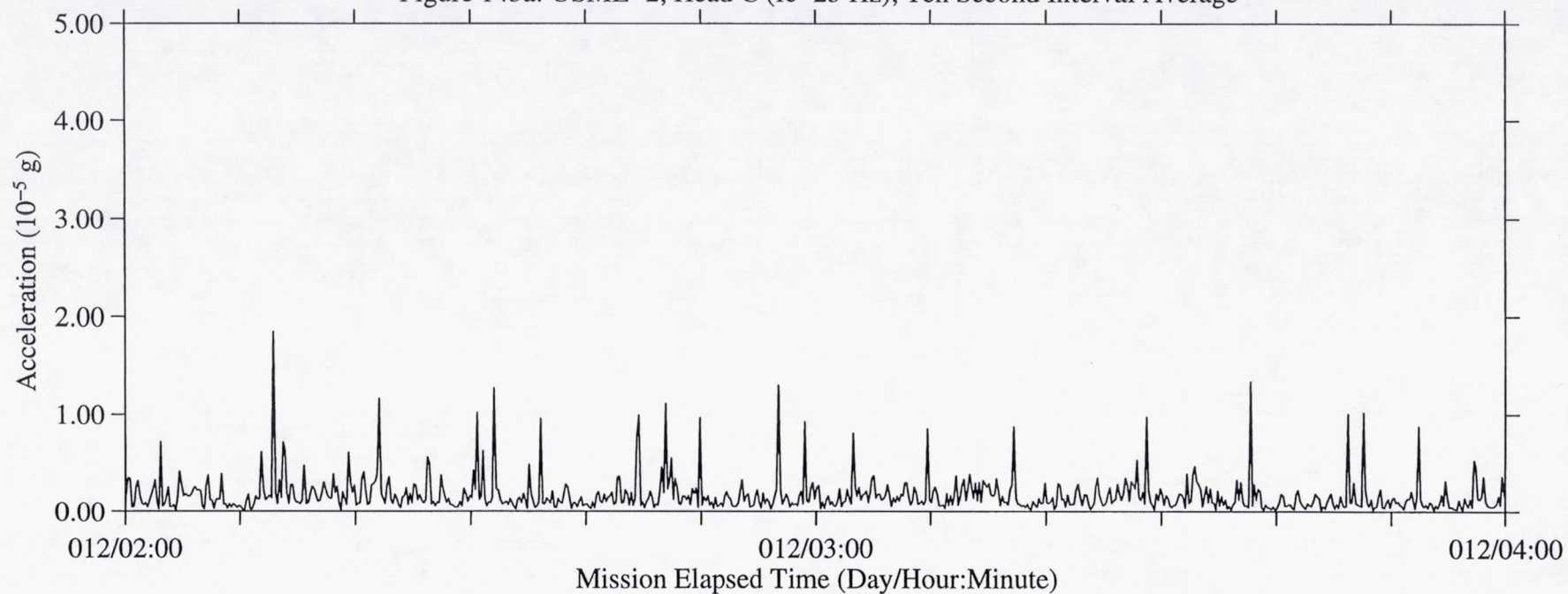


Figure 143b: USML-2, Head C (fc=25 Hz), Ten Second Interval RMS

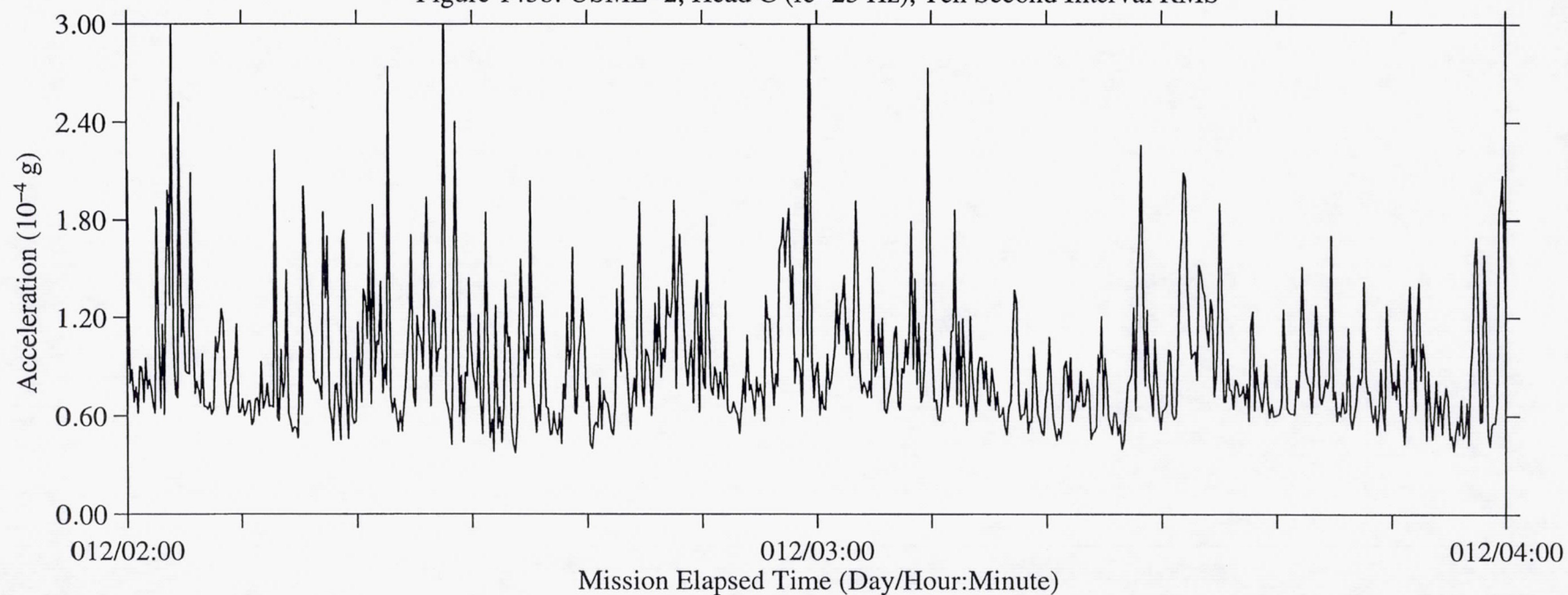


Figure 144a: USML-2, Head C (fc=25 Hz), Ten Second Interval Average

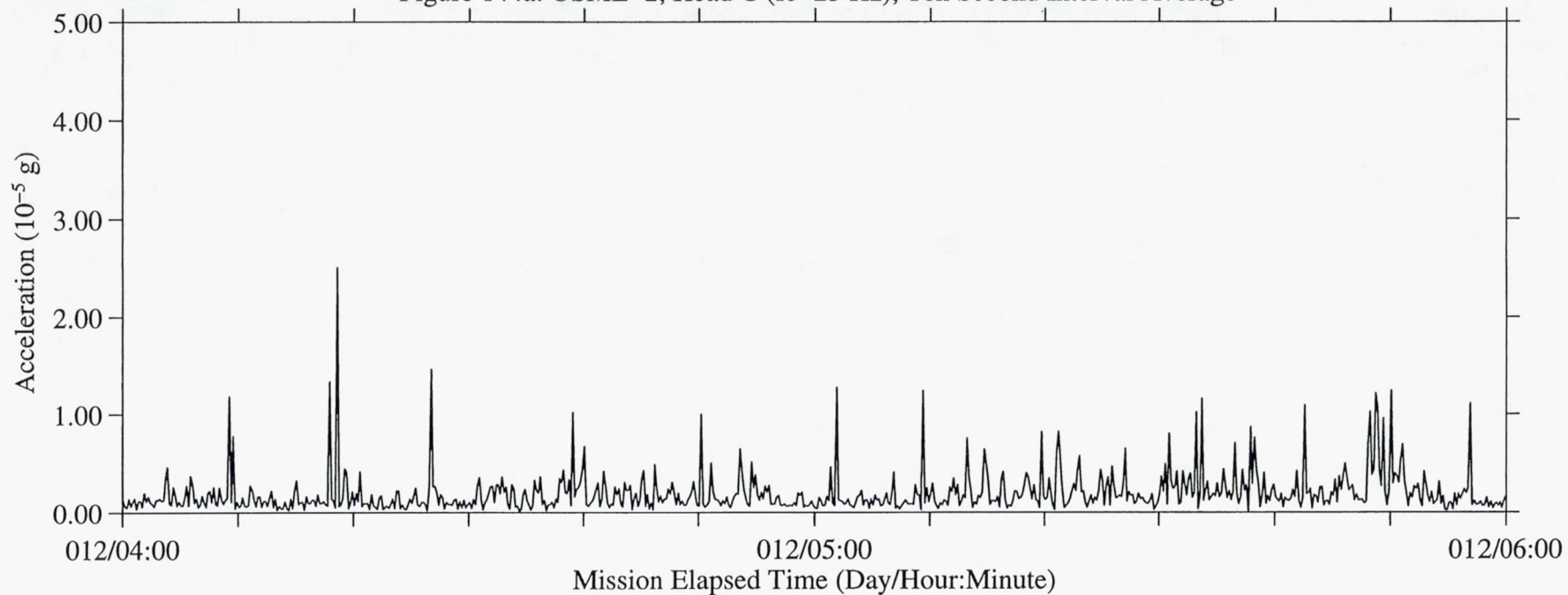


Figure 144b: USML-2, Head C (fc=25 Hz), Ten Second Interval RMS

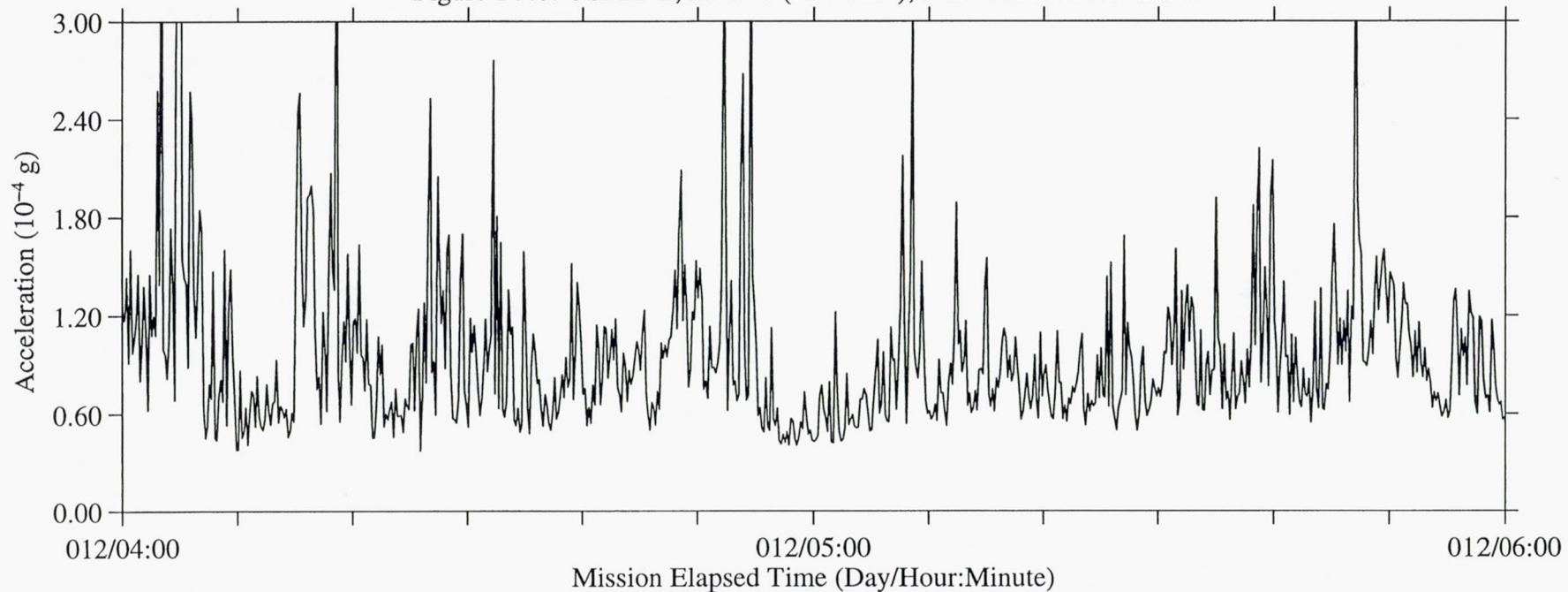




Figure 145a: USML-2, Head C (fc=25 Hz), Ten Second Interval Average

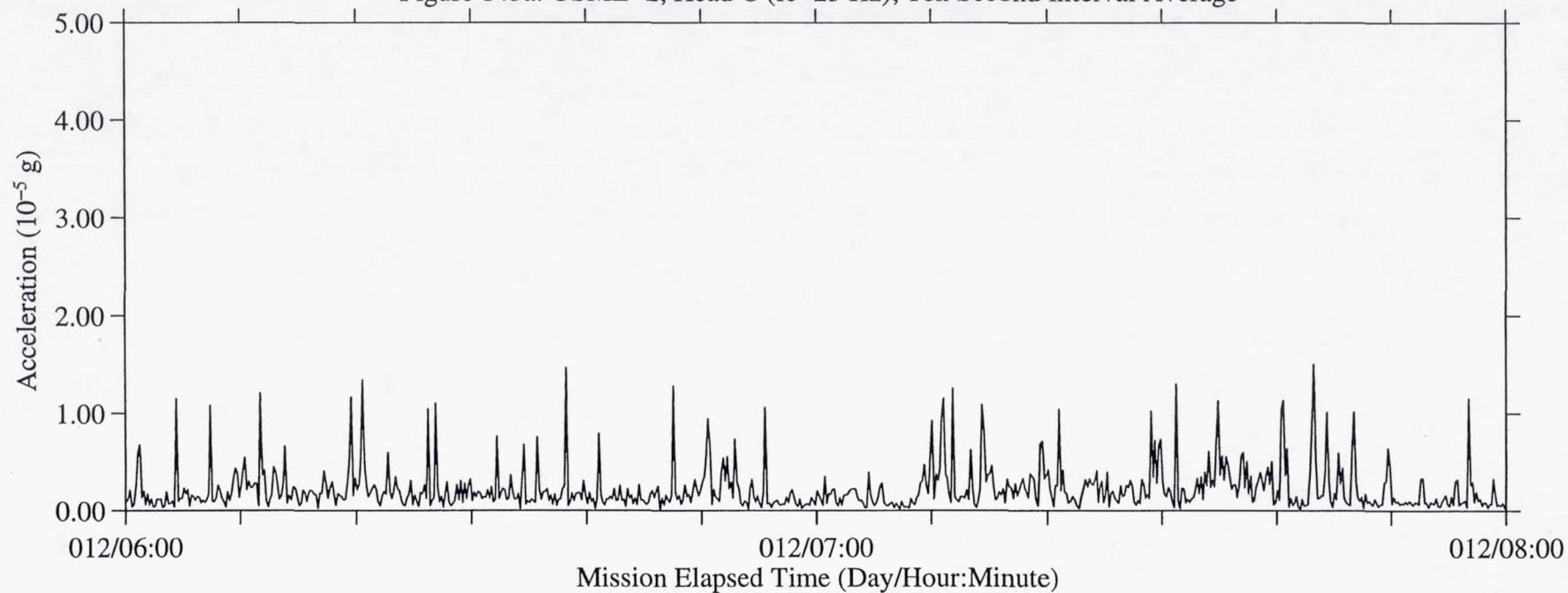


Figure 145b: USML-2, Head C (fc=25 Hz), Ten Second Interval RMS

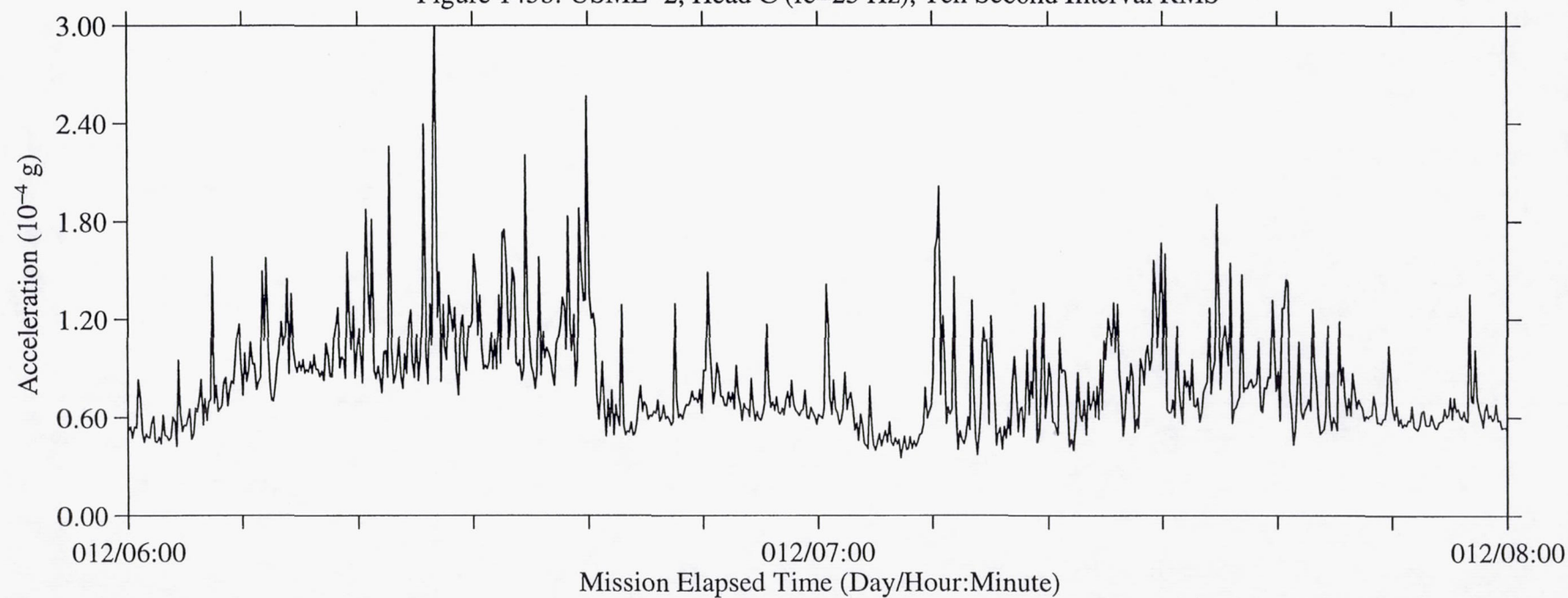


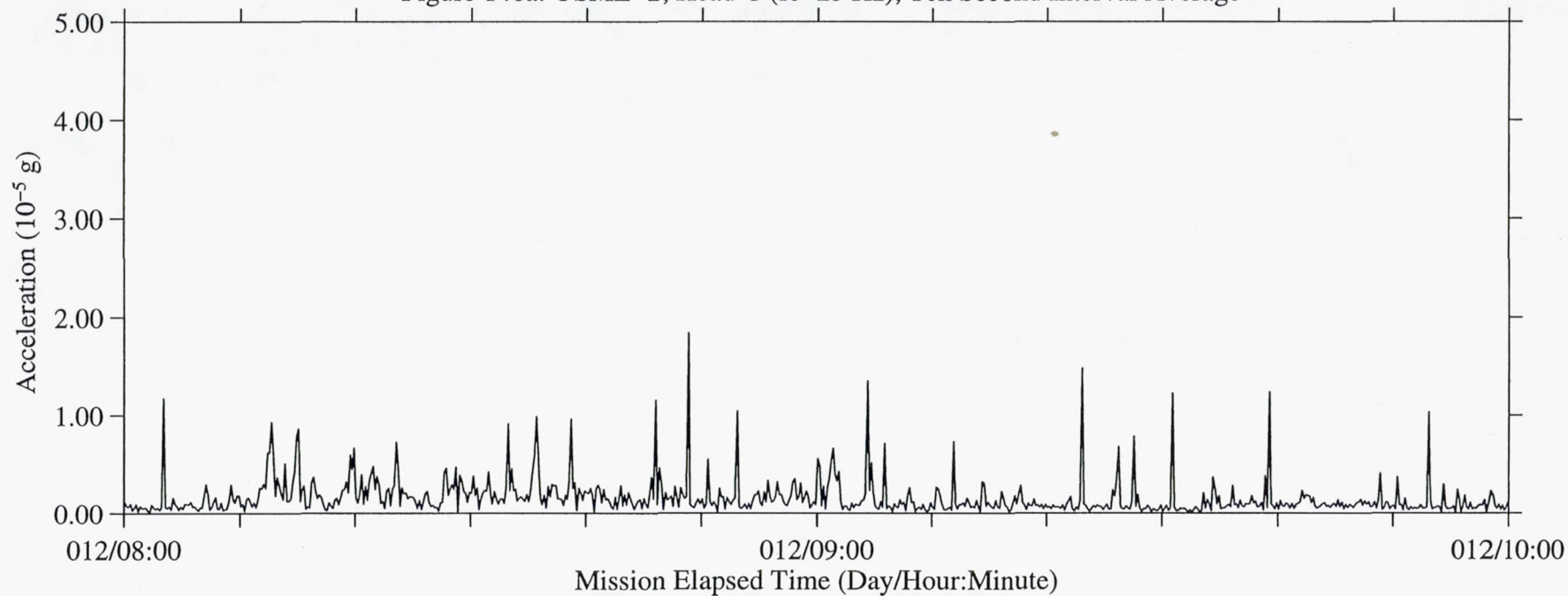
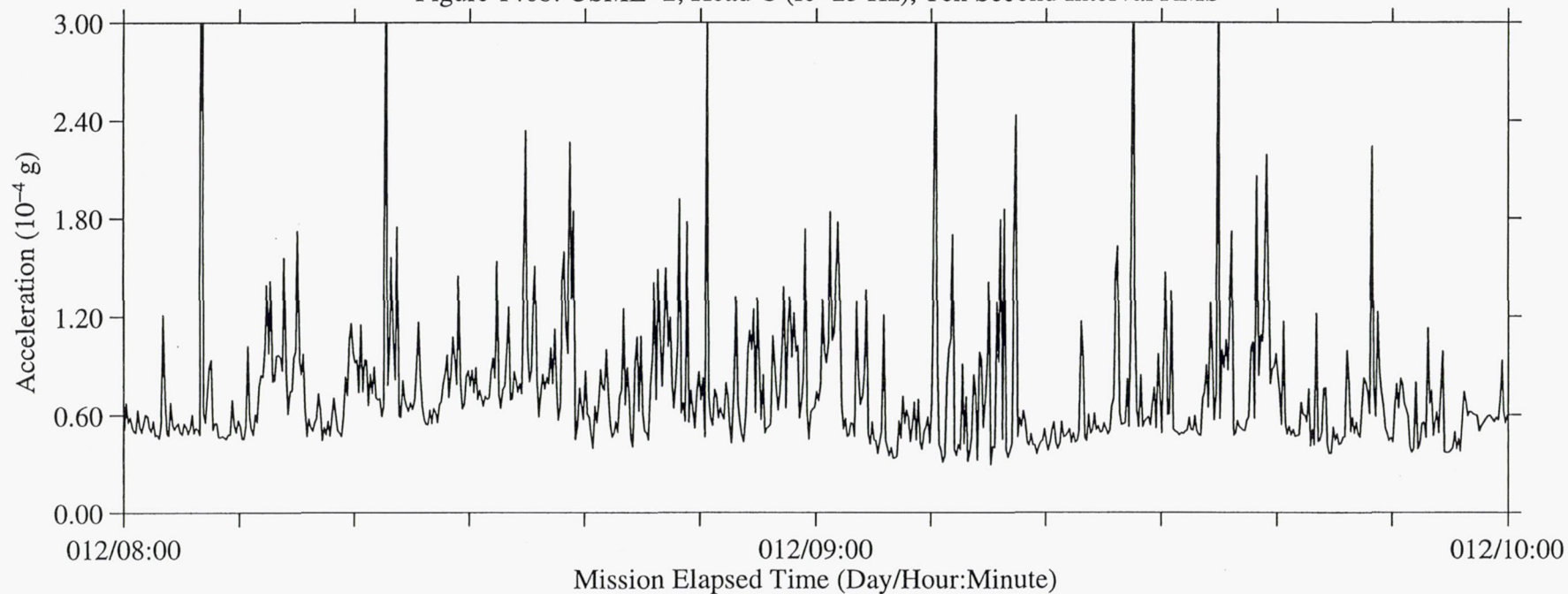
Figure 146a: USML-2, Head C ( $f_c=25$  Hz), Ten Second Interval AverageFigure 146b: USML-2, Head C ( $f_c=25$  Hz), Ten Second Interval RMS



Figure 147a: USML-2, Head C (fc=25 Hz), Ten Second Interval Average

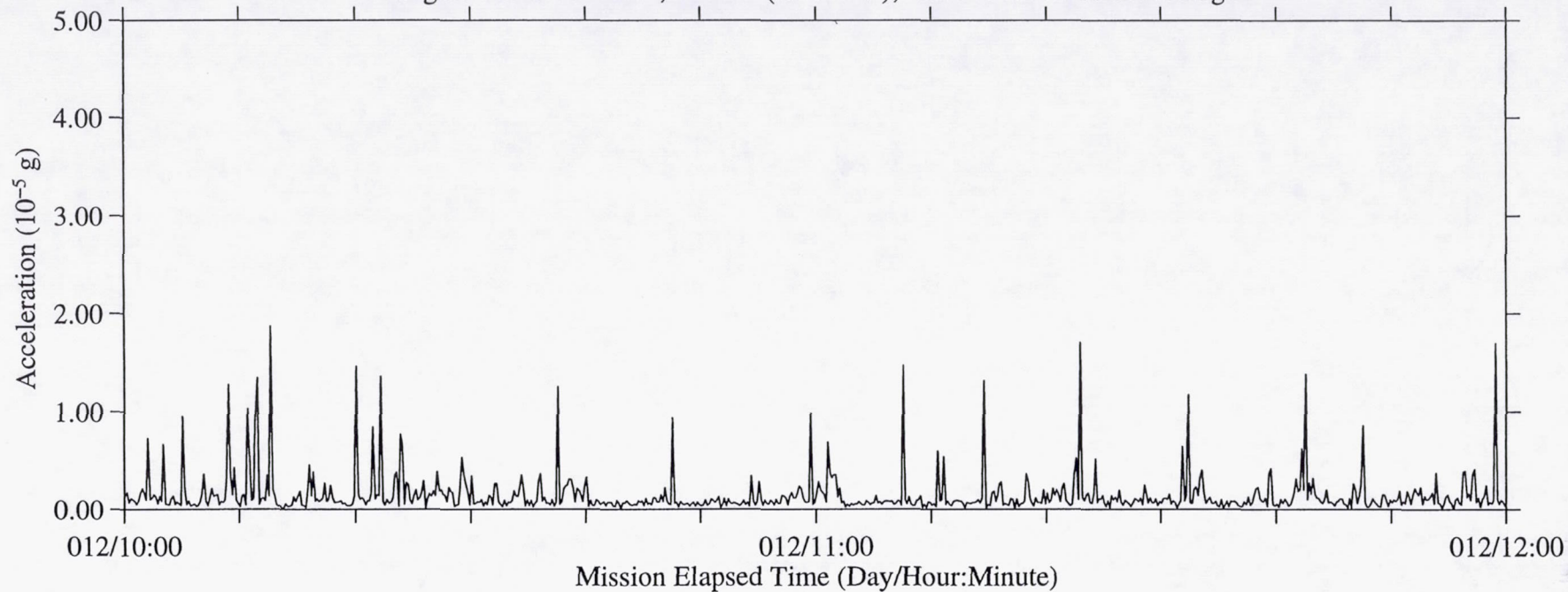
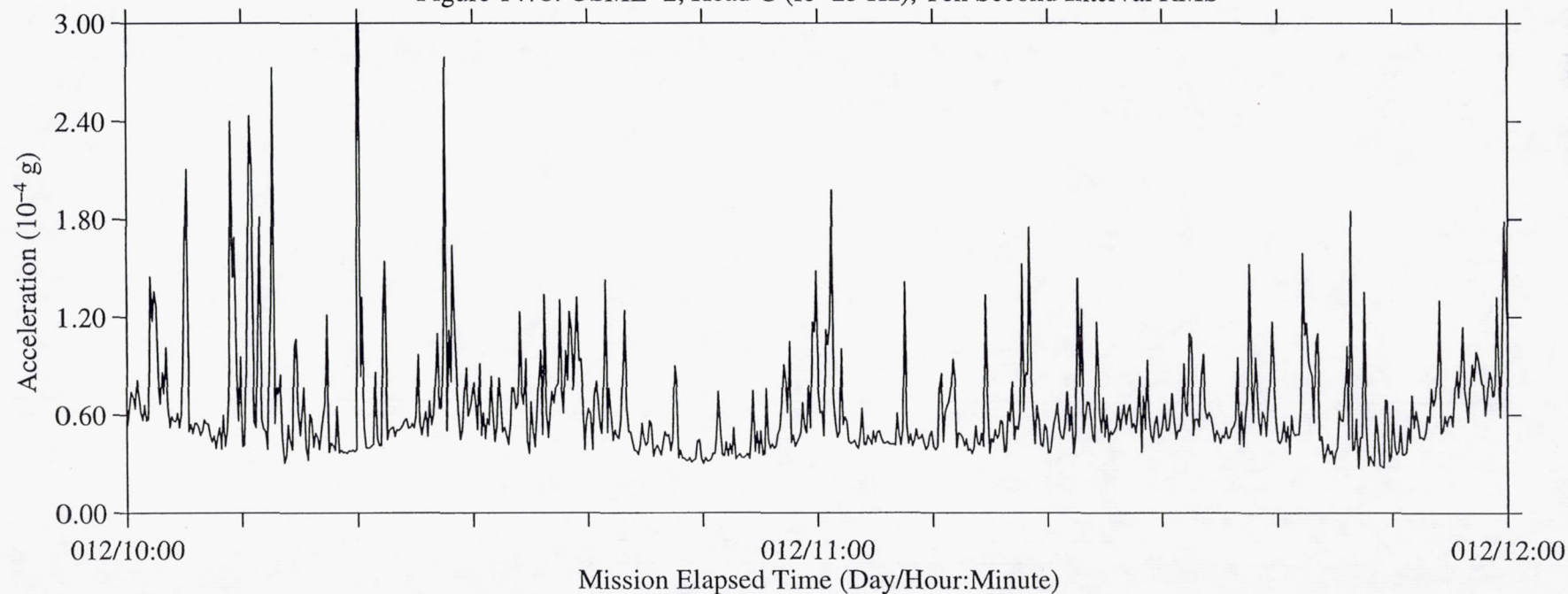


Figure 147b: USML-2, Head C (fc=25 Hz), Ten Second Interval RMS



B-150

Figure 148a: USML-2, Head C (fc=25 Hz), Ten Second Interval Average

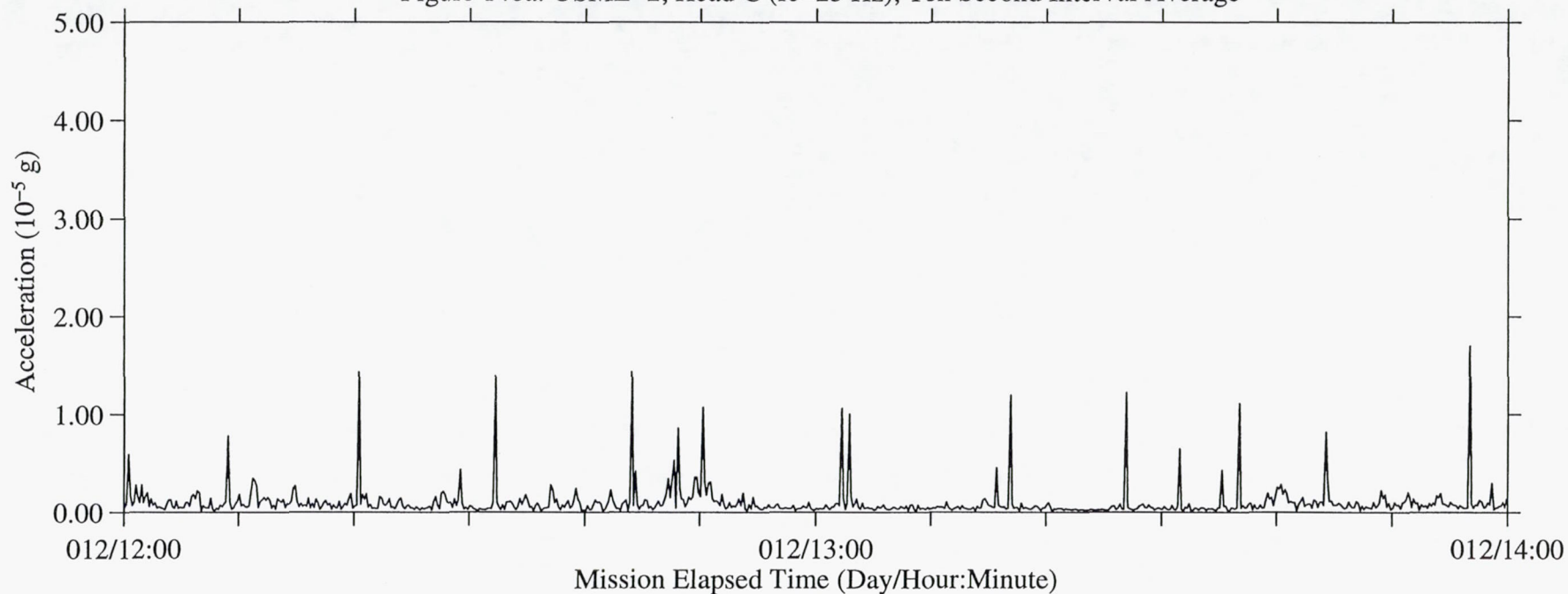


Figure 148b: USML-2, Head C (fc=25 Hz), Ten Second Interval RMS

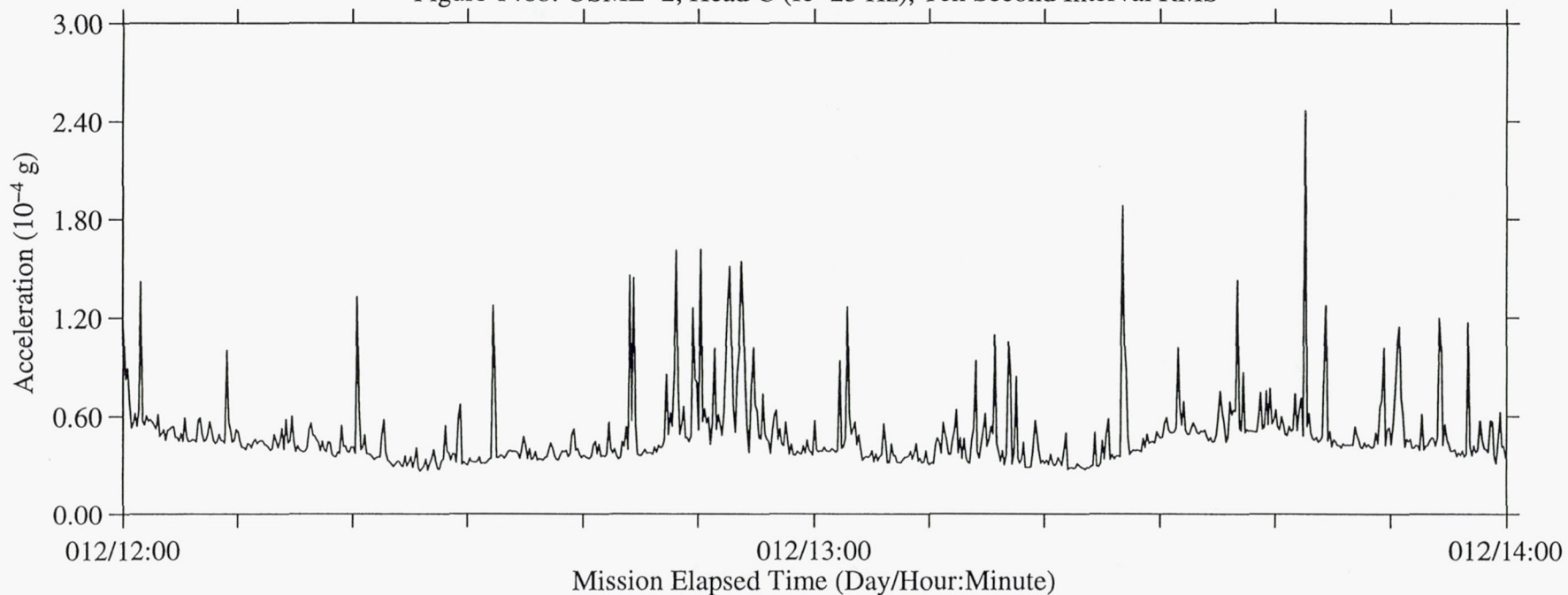




Figure 149a: USML-2, Head C (fc=25 Hz), Ten Second Interval Average

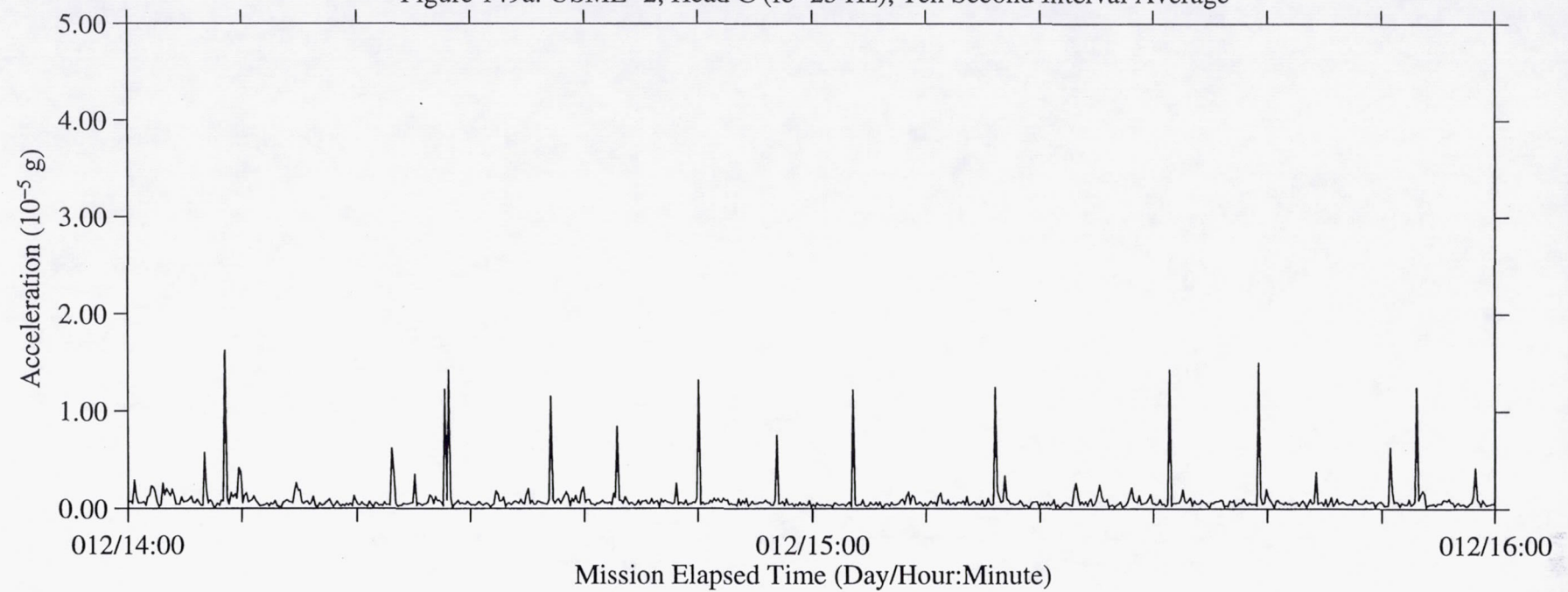
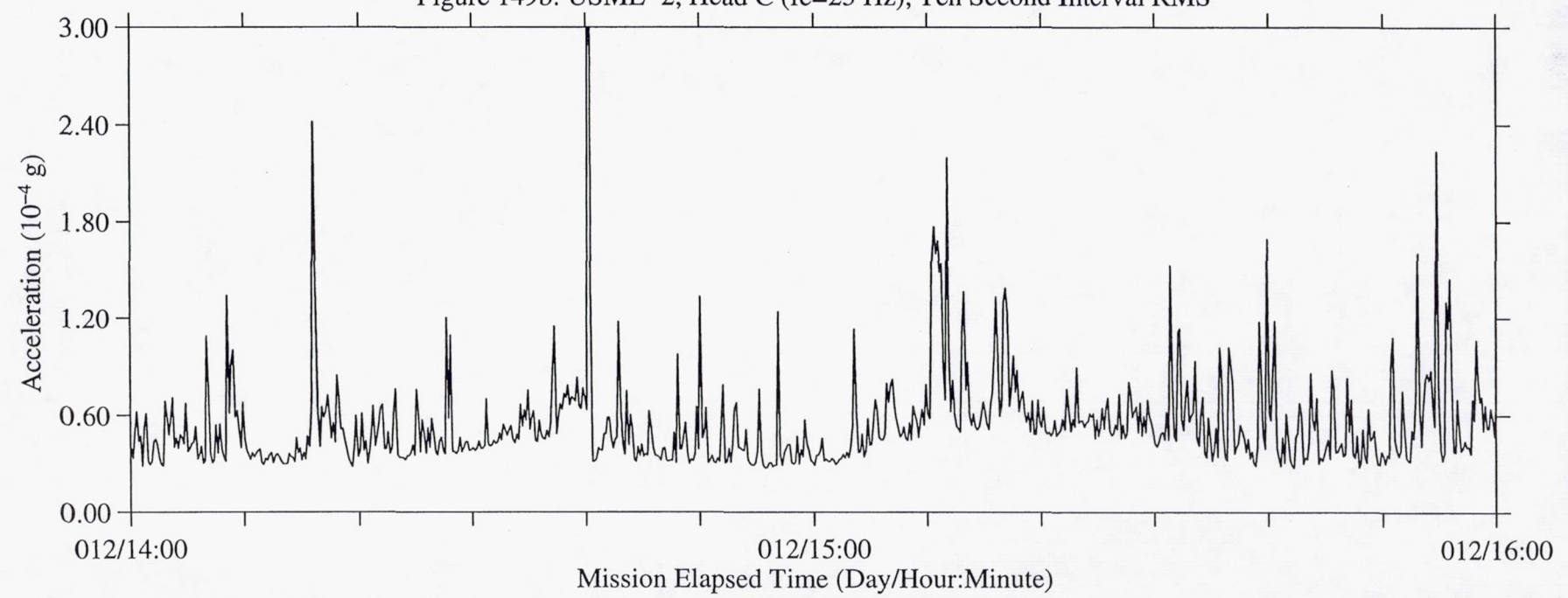


Figure 149b: USML-2, Head C (fc=25 Hz), Ten Second Interval RMS



B-151

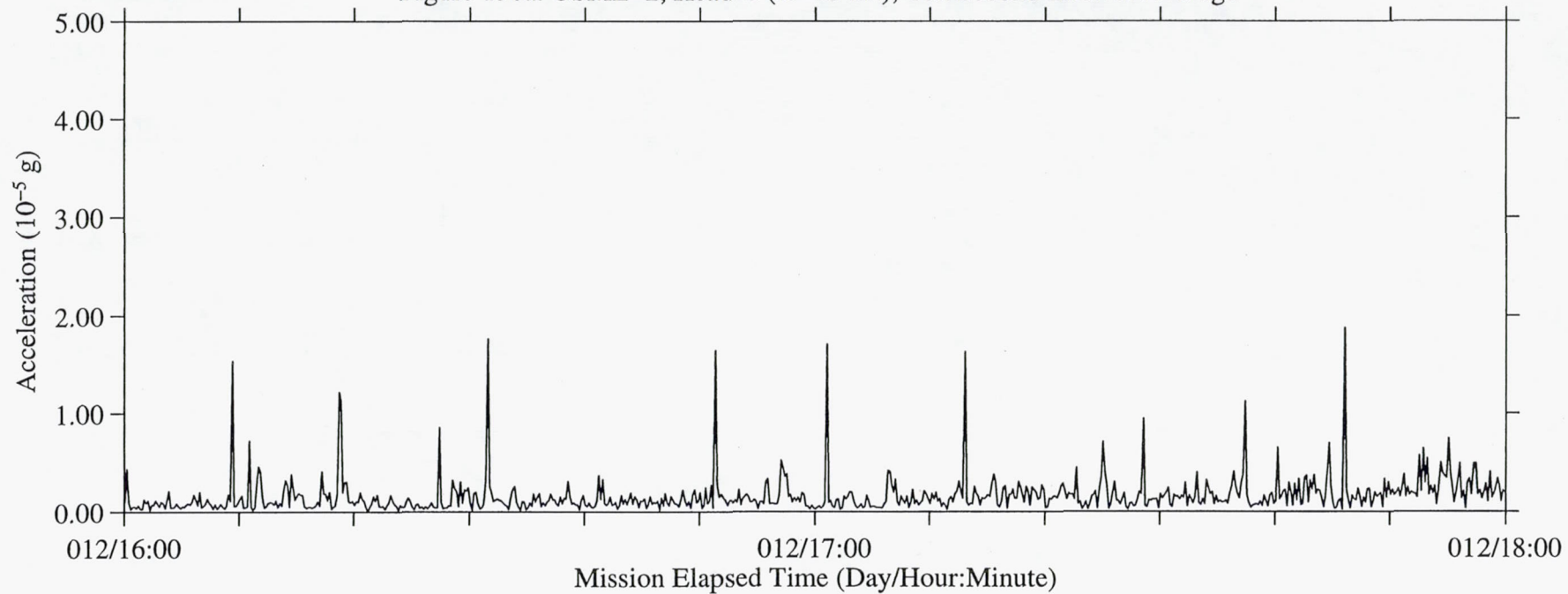
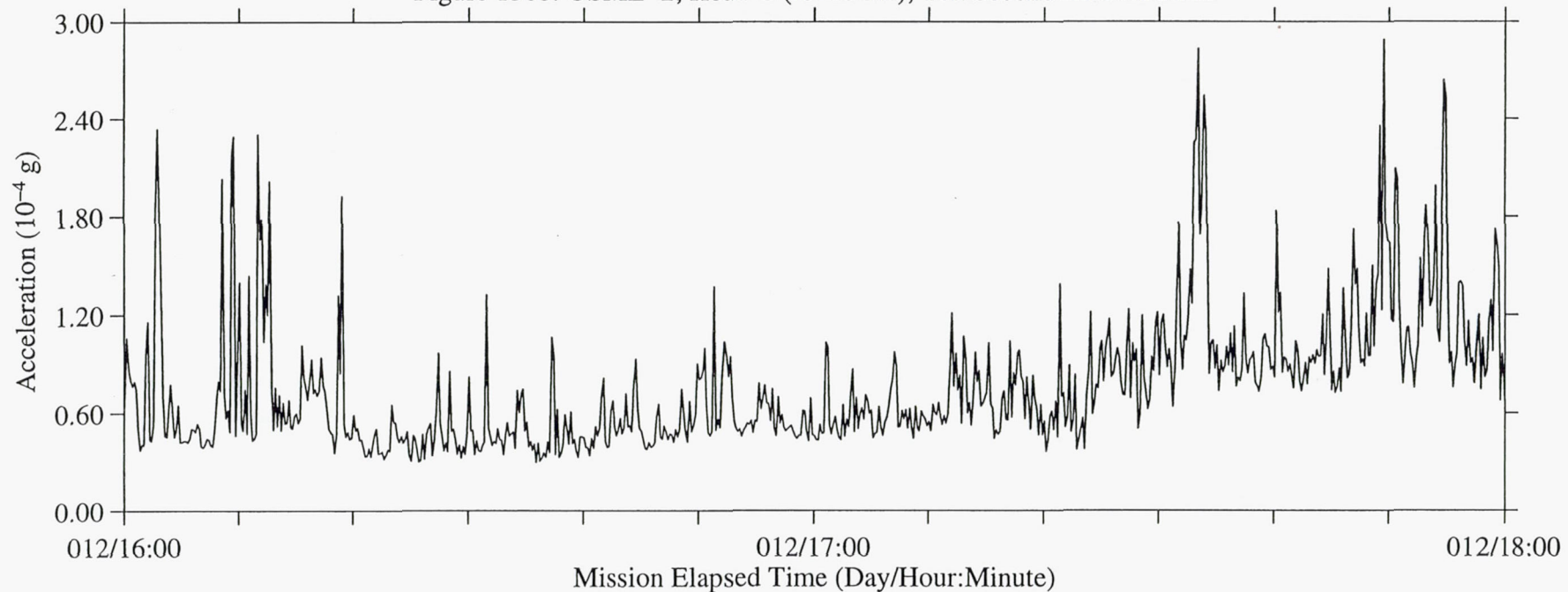
Figure 150a: USML-2, Head C ( $f_c=25$  Hz), Ten Second Interval AverageFigure 150b: USML-2, Head C ( $f_c=25$  Hz), Ten Second Interval RMS



Figure 151a: USML-2, Head C (fc=25 Hz), Ten Second Interval Average

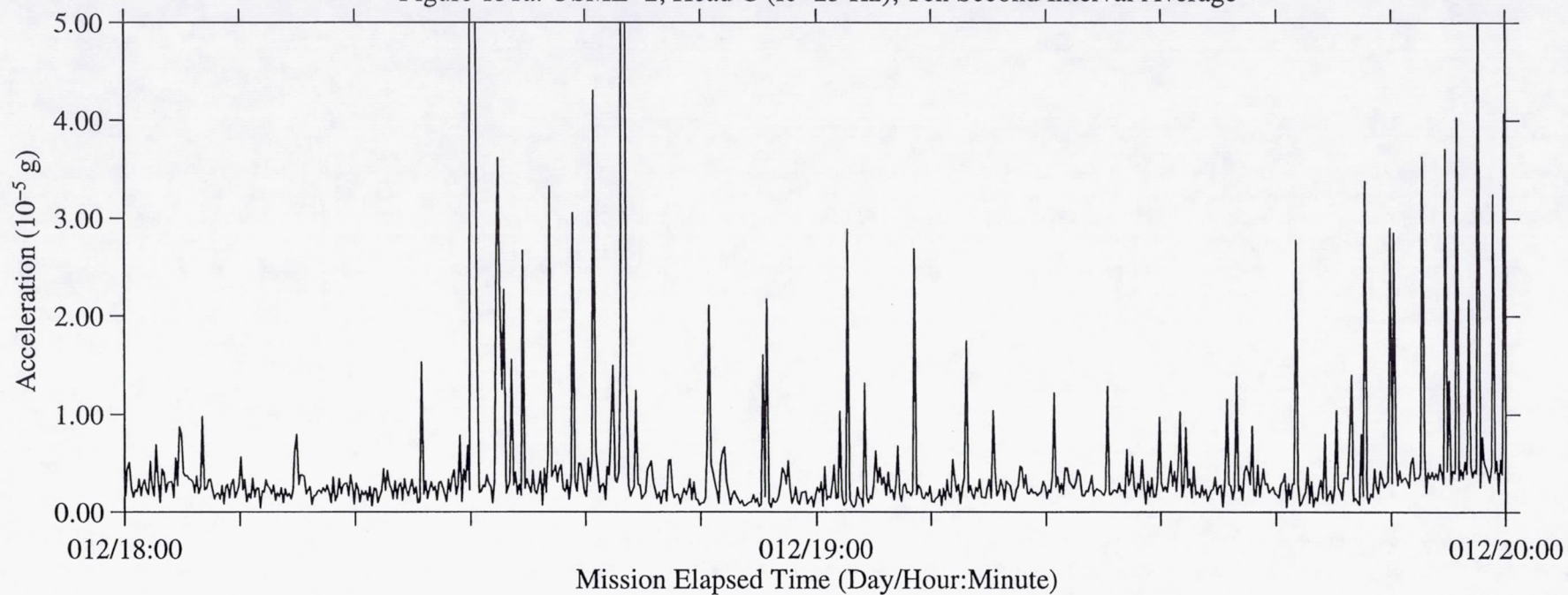


Figure 151b: USML-2, Head C (fc=25 Hz), Ten Second Interval RMS

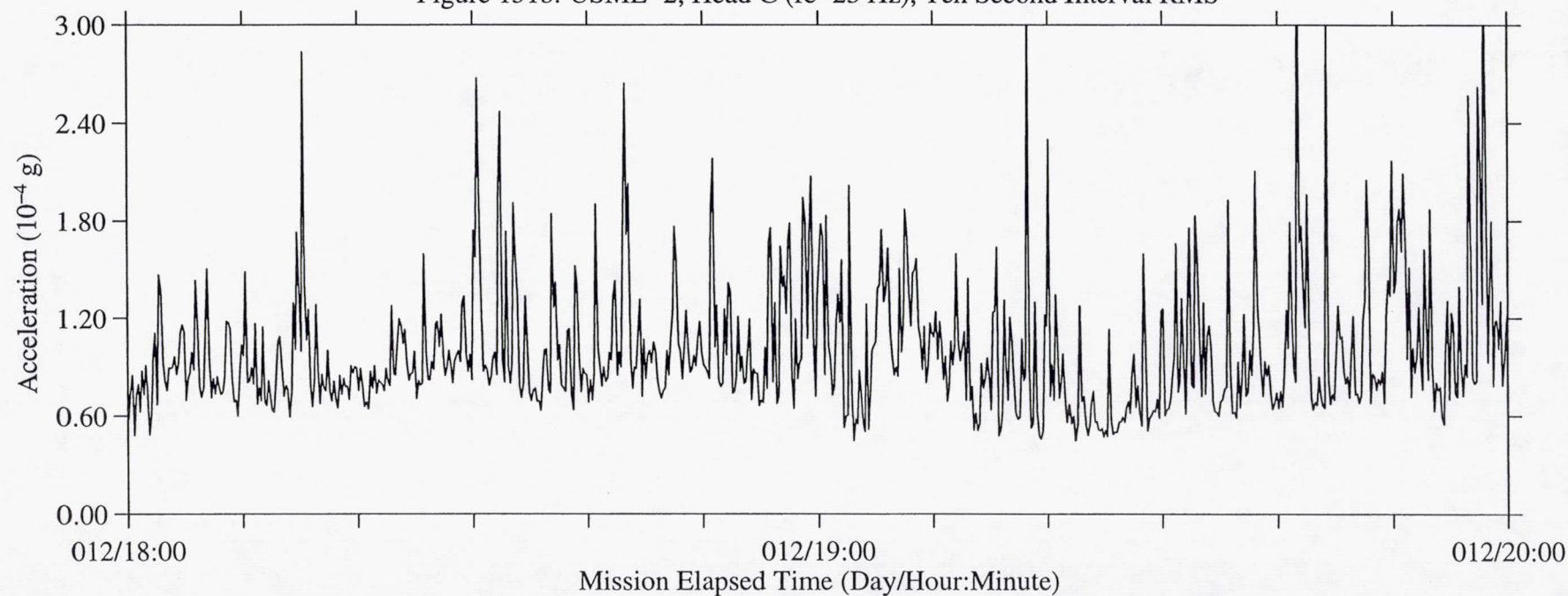


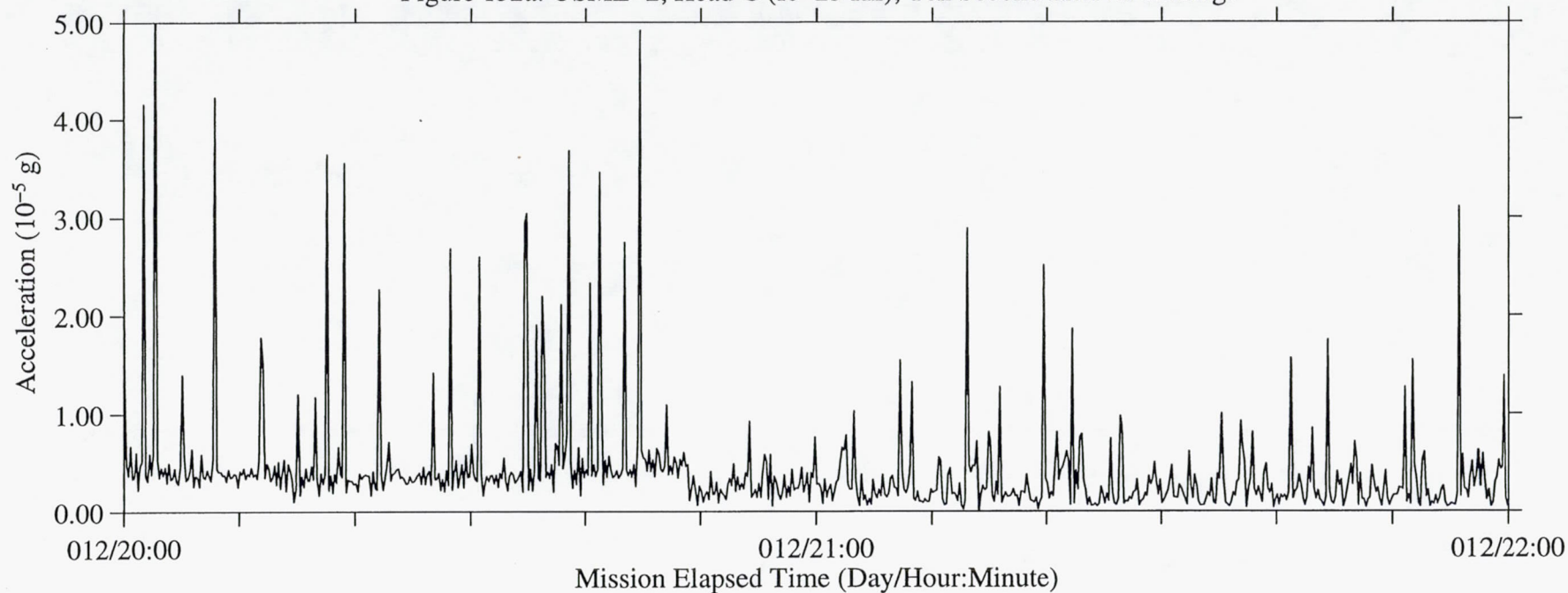
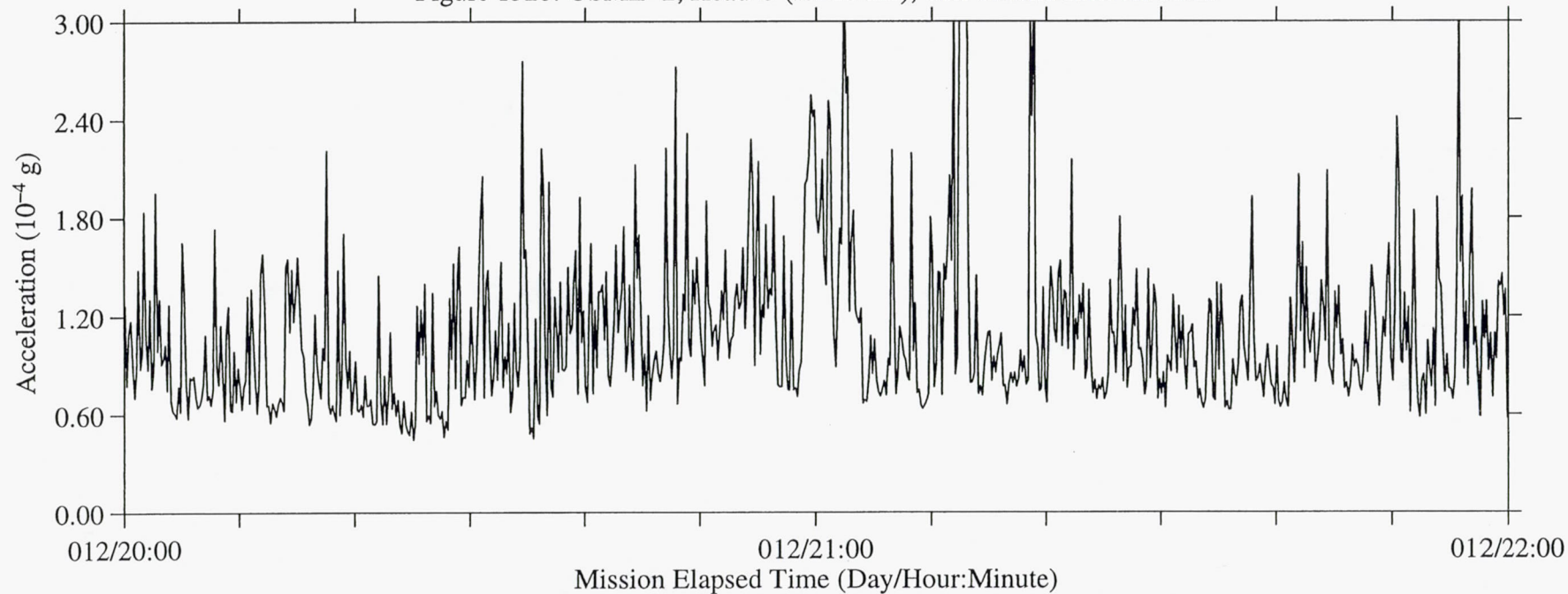
Figure 152a: USML-2, Head C ( $f_c=25$  Hz), Ten Second Interval AverageFigure 152b: USML-2, Head C ( $f_c=25$  Hz), Ten Second Interval RMS



Figure 153a: USML-2, Head C (fc=25 Hz), Ten Second Interval Average

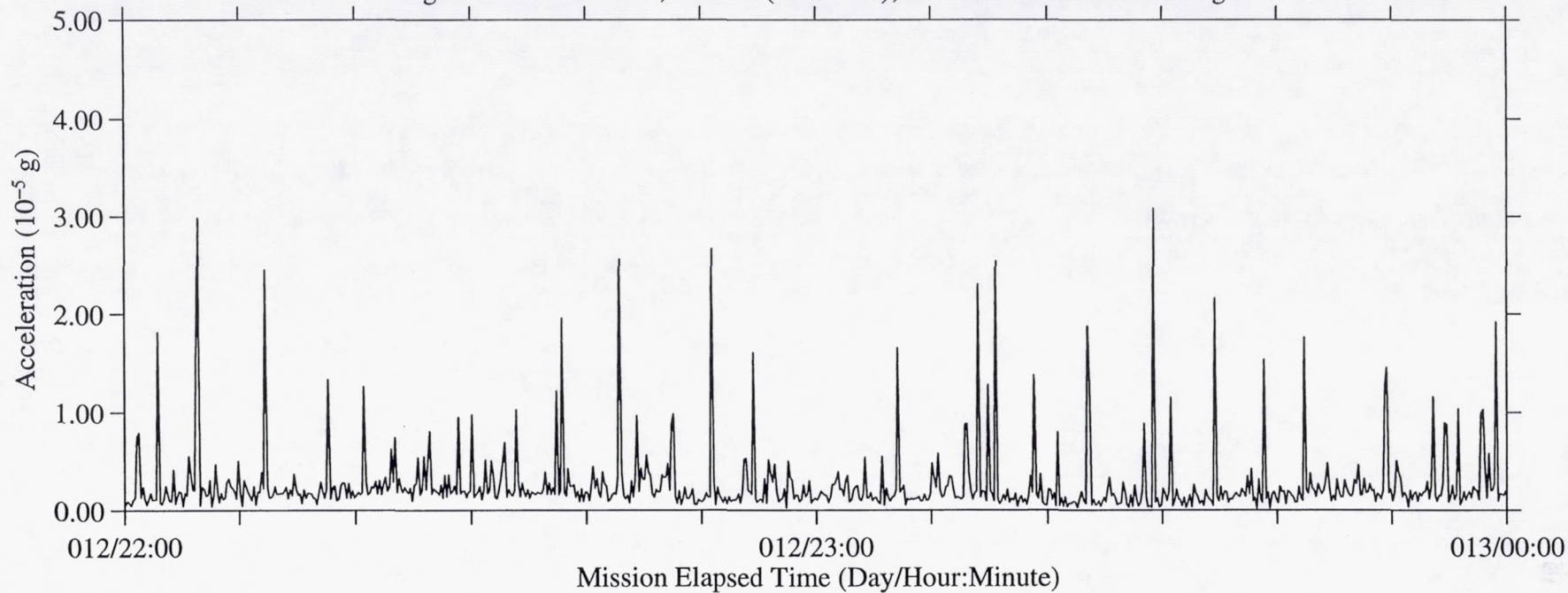


Figure 153b: USML-2, Head C (fc=25 Hz), Ten Second Interval RMS

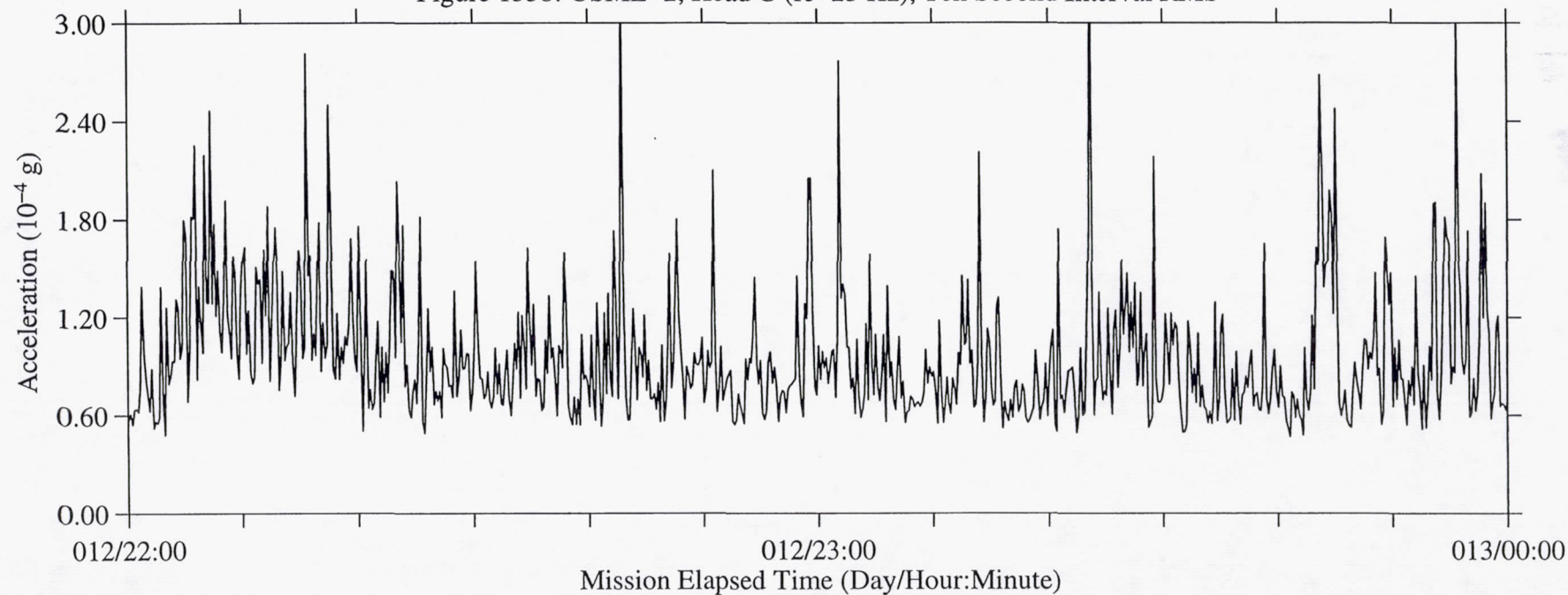


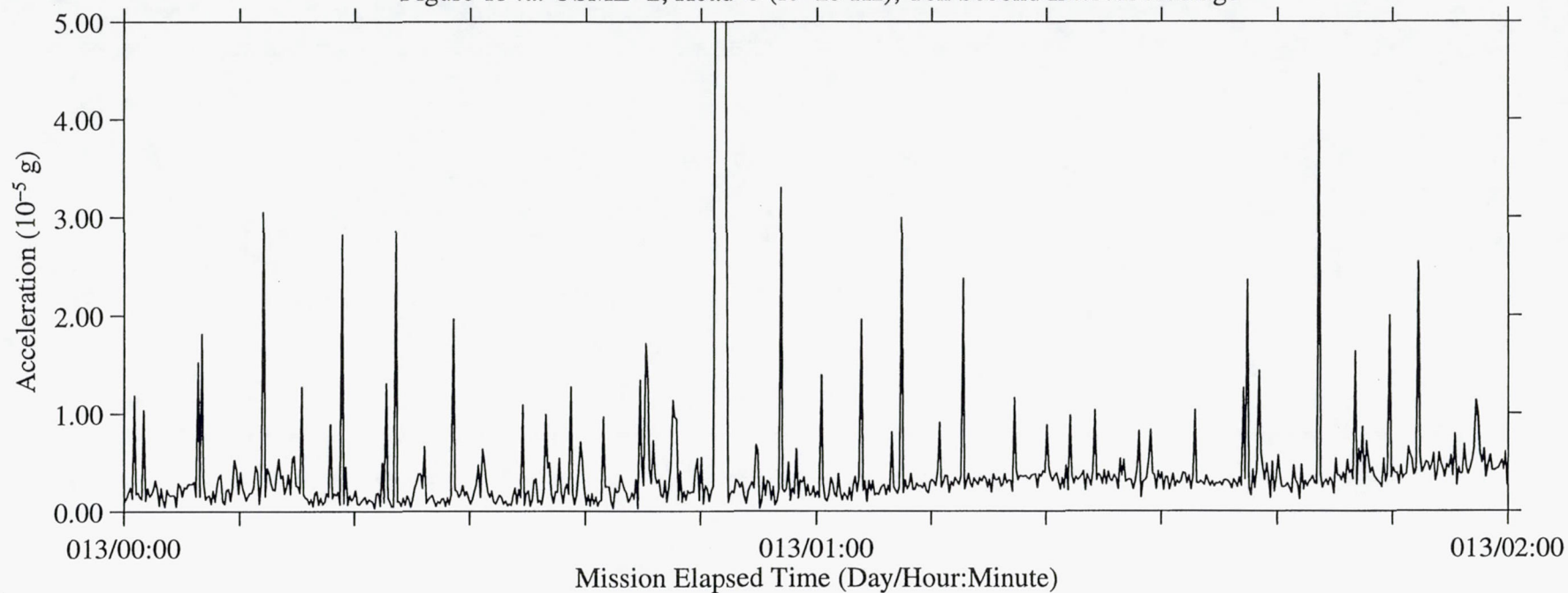
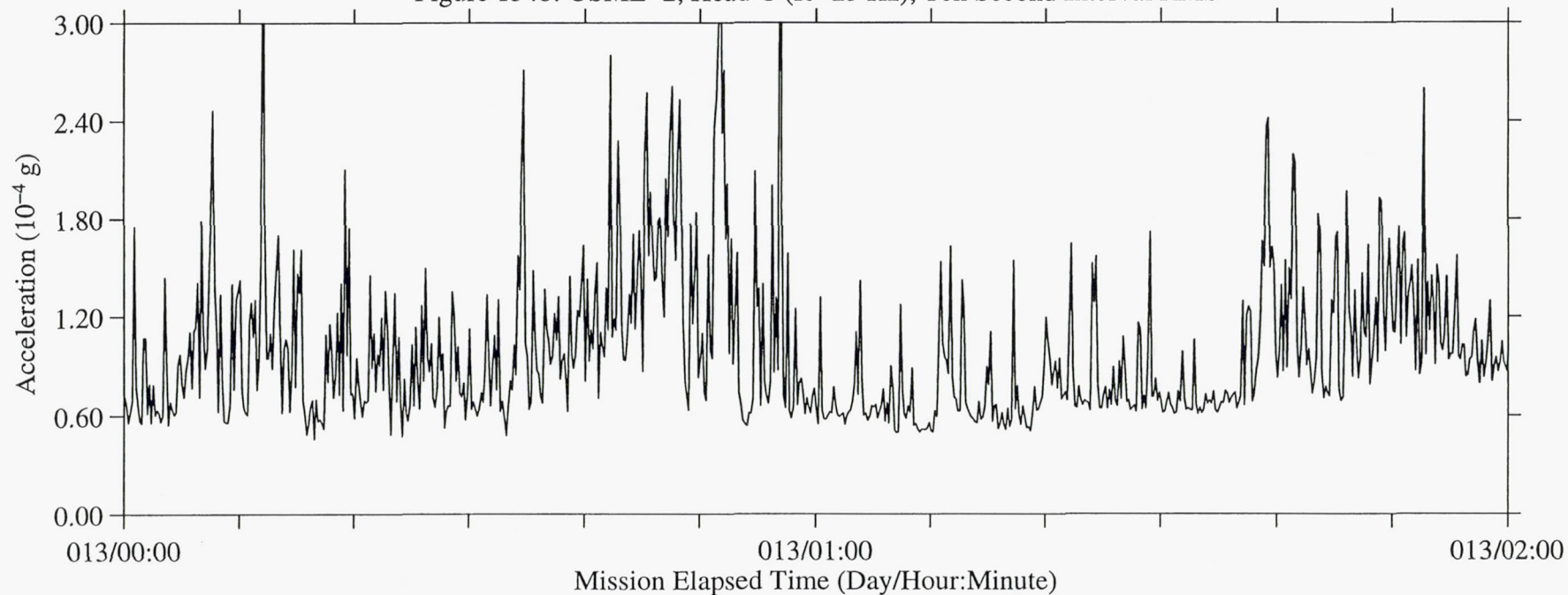
Figure 154a: USML-2, Head C ( $f_c=25$  Hz), Ten Second Interval AverageFigure 154b: USML-2, Head C ( $f_c=25$  Hz), Ten Second Interval RMS



Figure 155a: USML-2, Head C (fc=25 Hz), Ten Second Interval Average

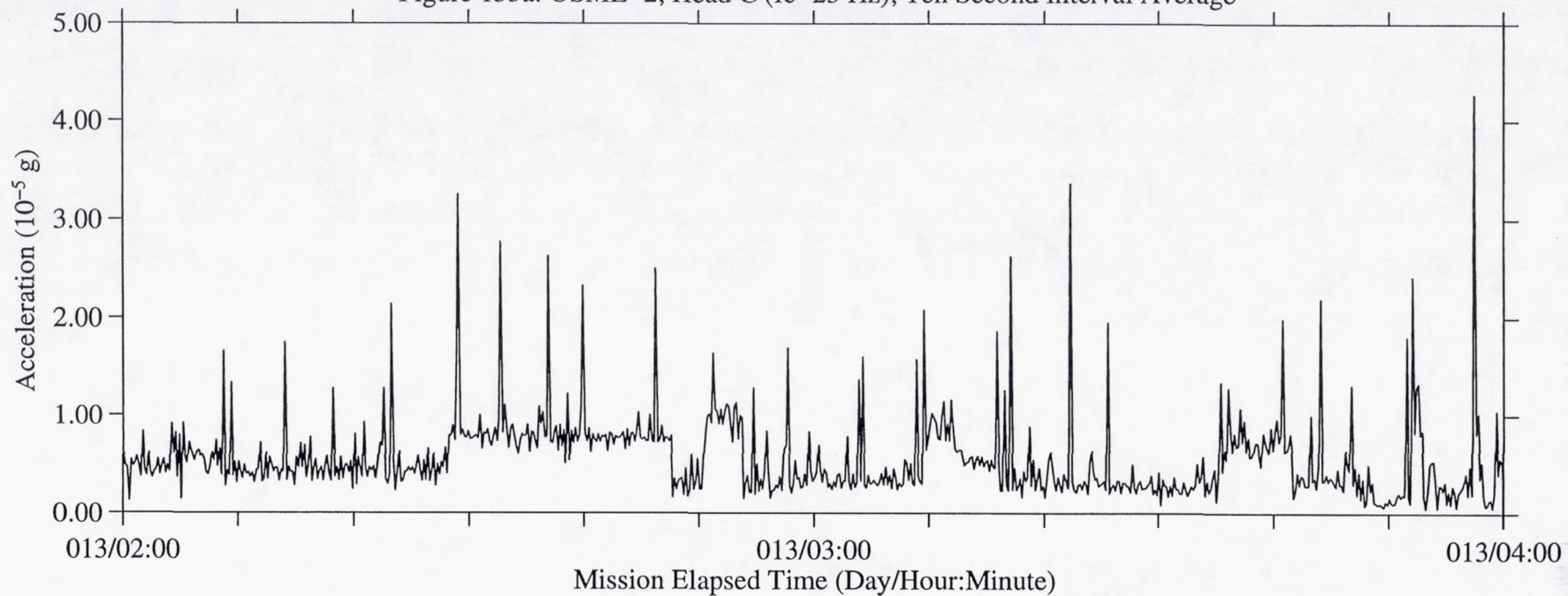


Figure 155b: USML-2, Head C (fc=25 Hz), Ten Second Interval RMS

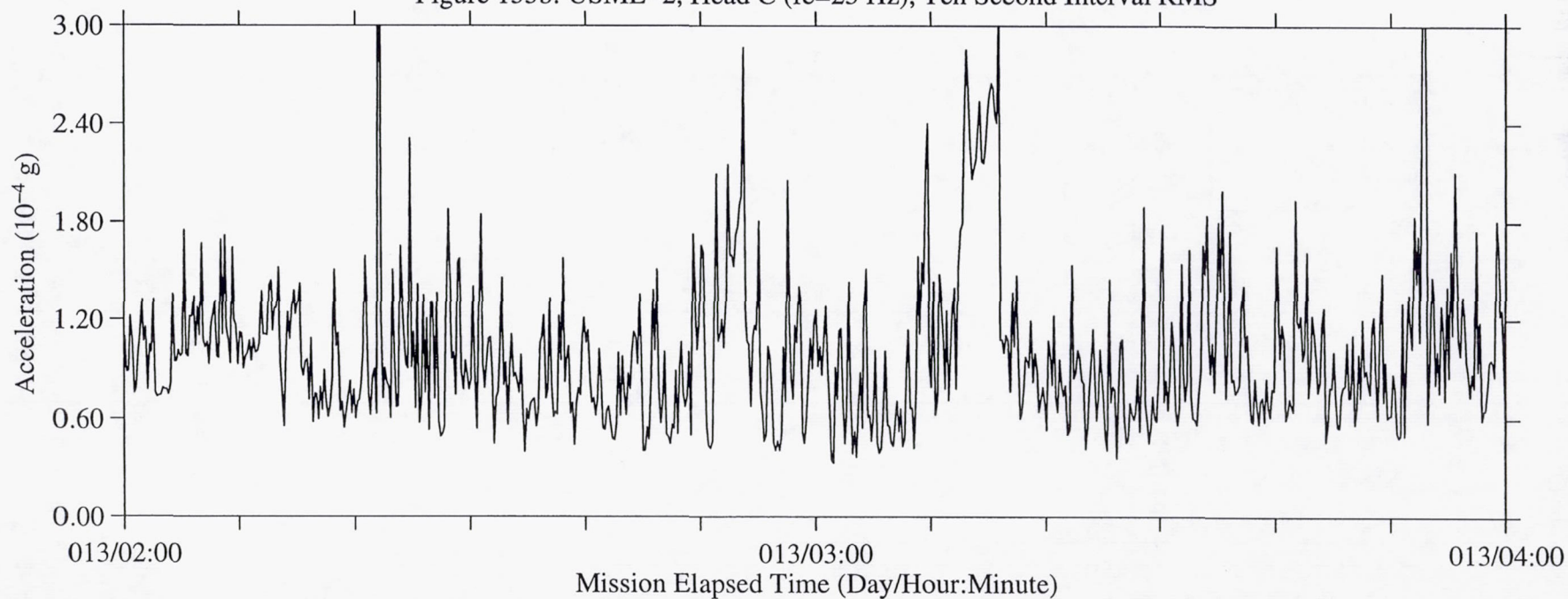


Figure 156a: USML-2, Head C (fc=25 Hz), Ten Second Interval Average

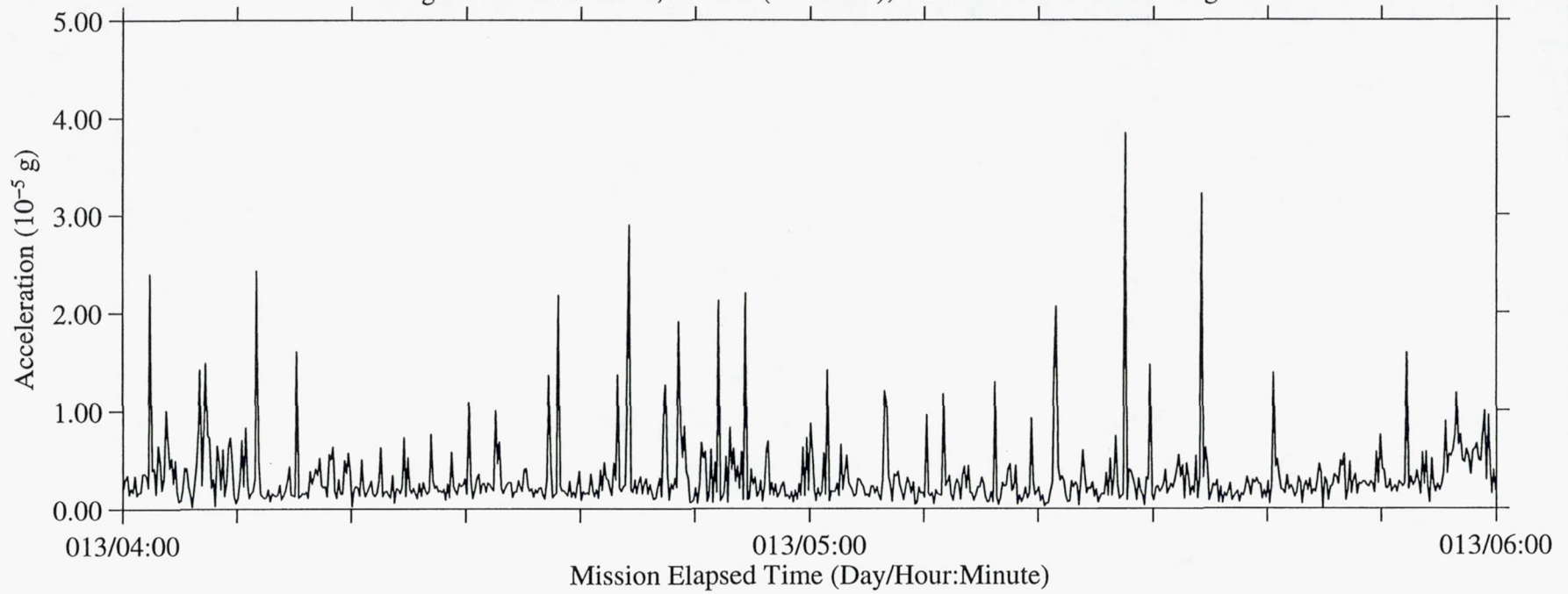


Figure 156b: USML-2, Head C (fc=25 Hz), Ten Second Interval RMS

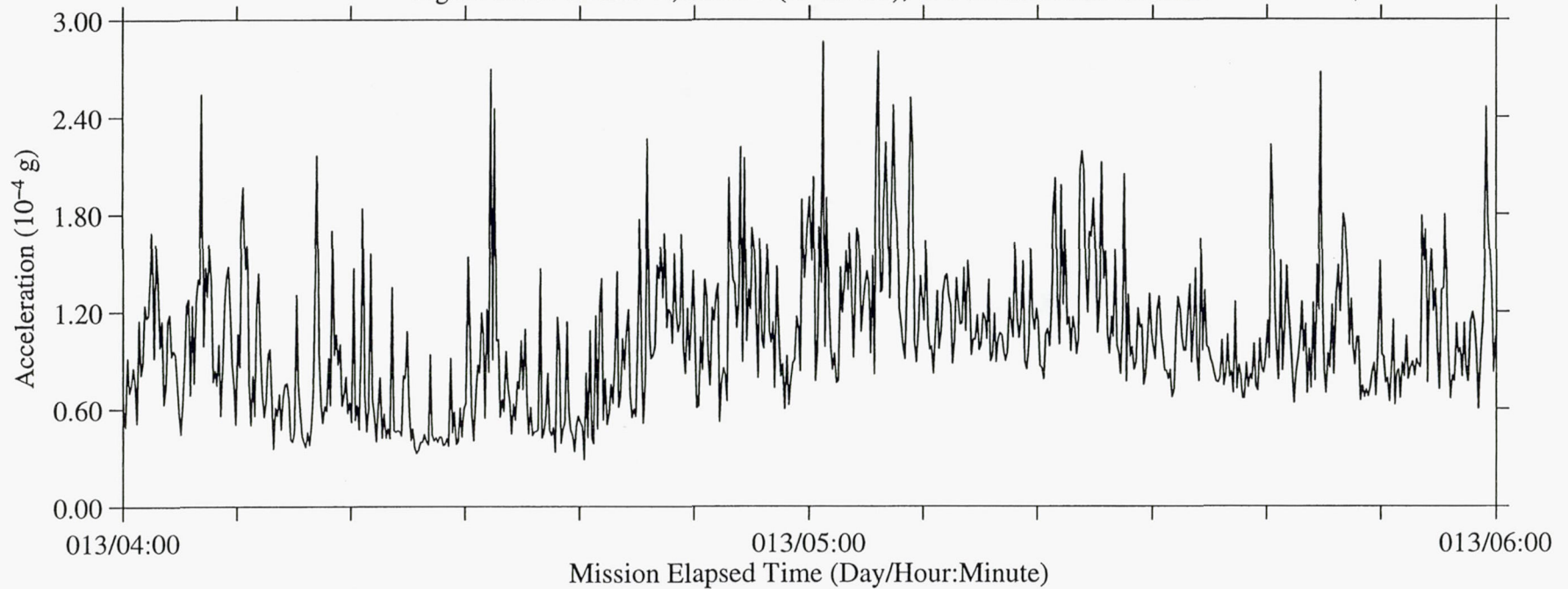




Figure 157a: USML-2, Head C (fc=25 Hz), Ten Second Interval Average

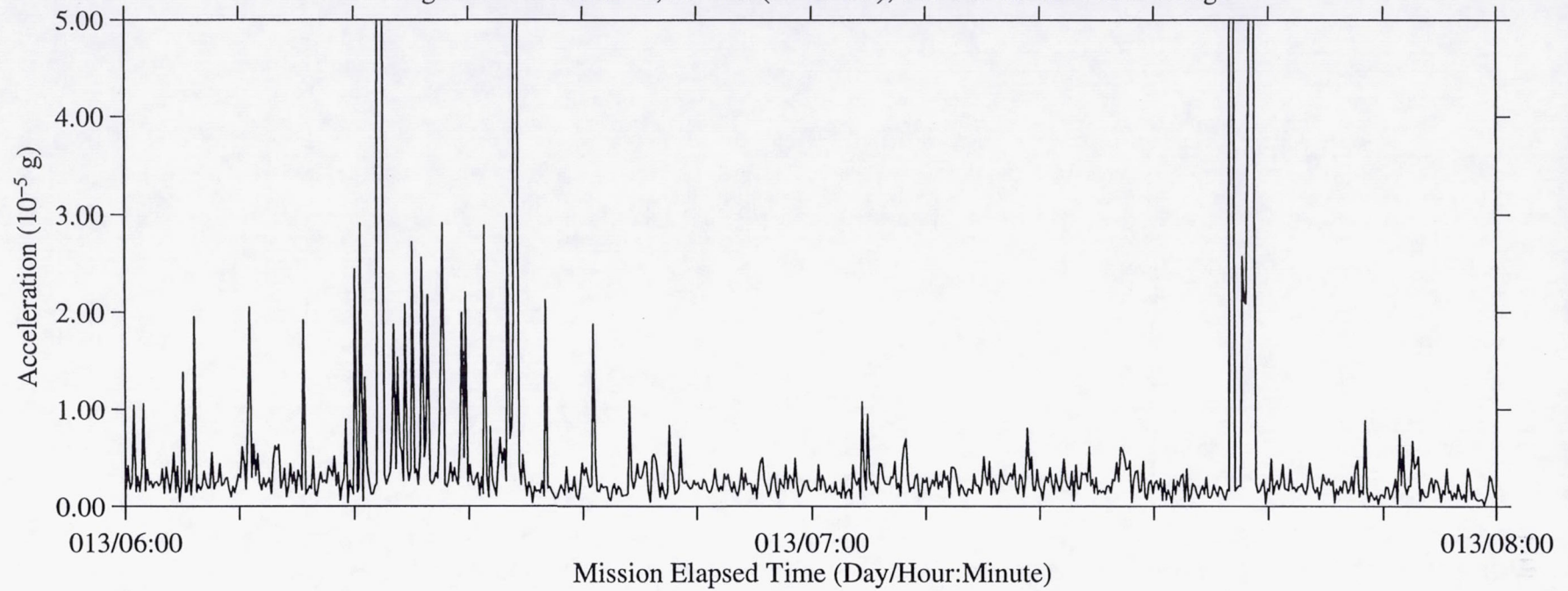


Figure 157b: USML-2, Head C (fc=25 Hz), Ten Second Interval RMS

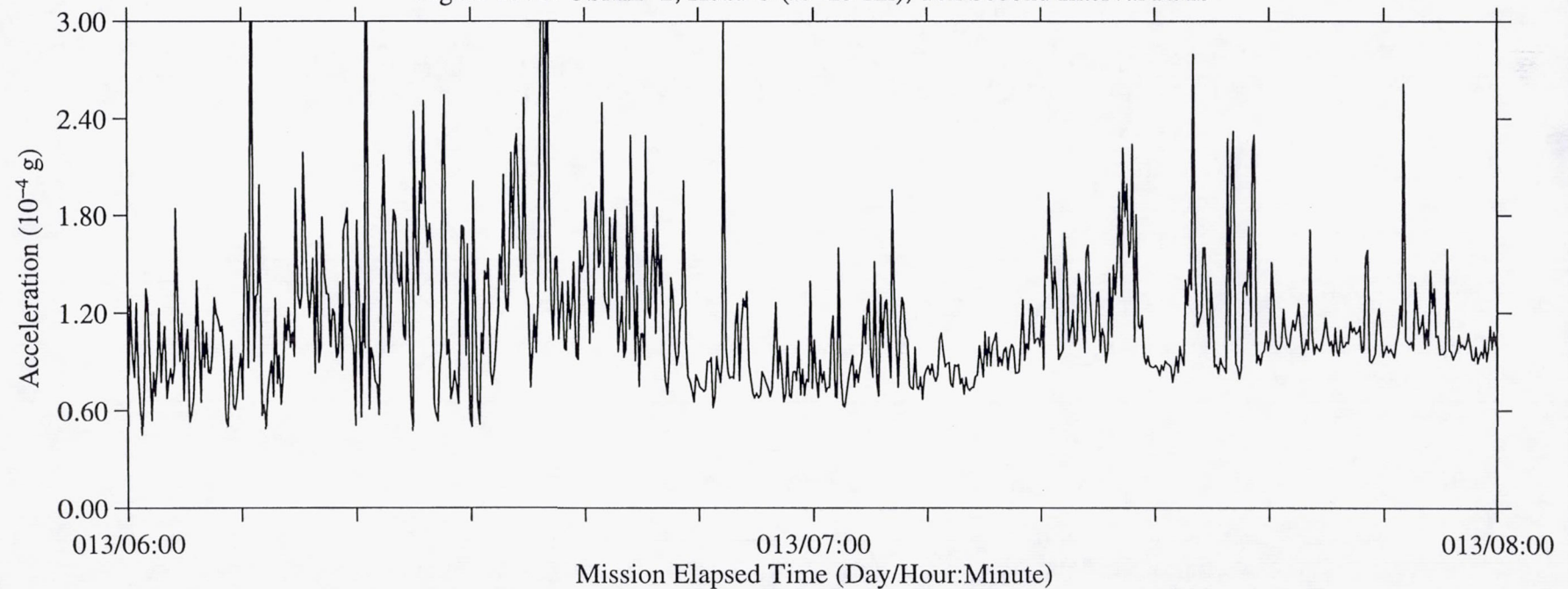


Figure 158a: USML-2, Head C (fc=25 Hz), Ten Second Interval Average

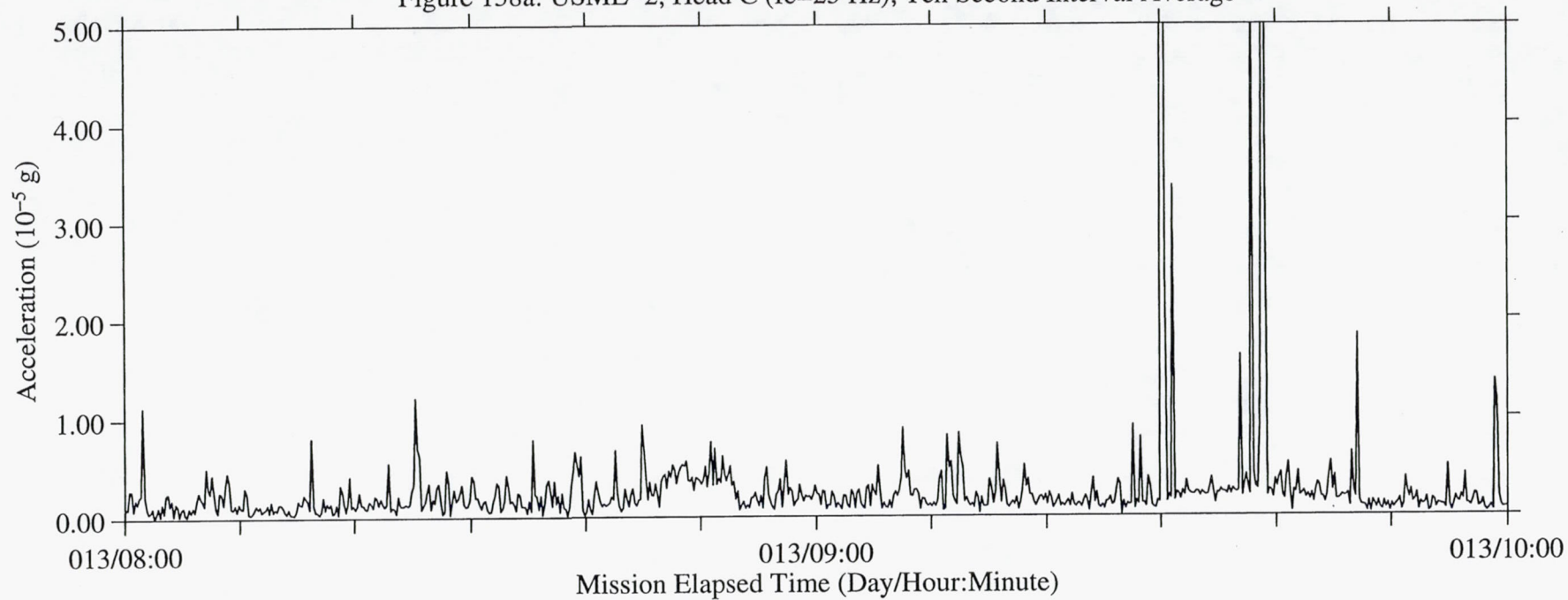


Figure 158b: USML-2, Head C (fc=25 Hz), Ten Second Interval RMS

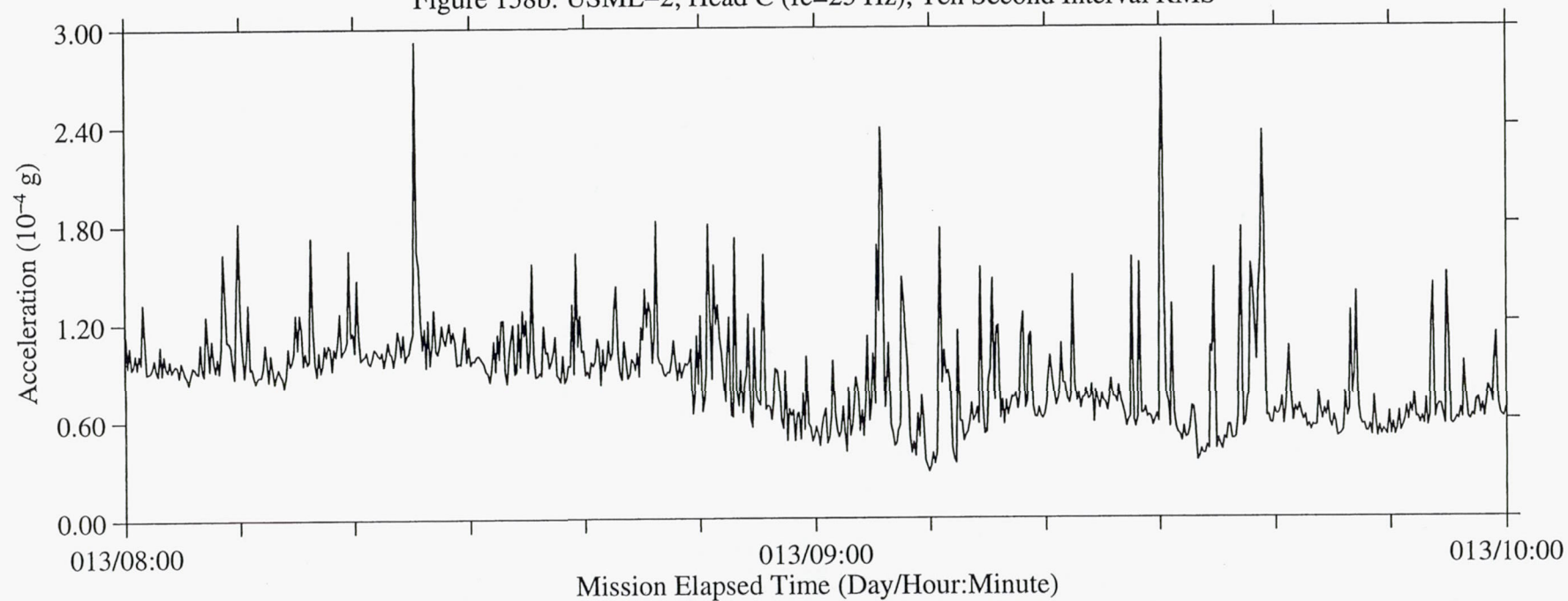




Figure 159a: USML-2, Head C (fc=25 Hz), Ten Second Interval Average

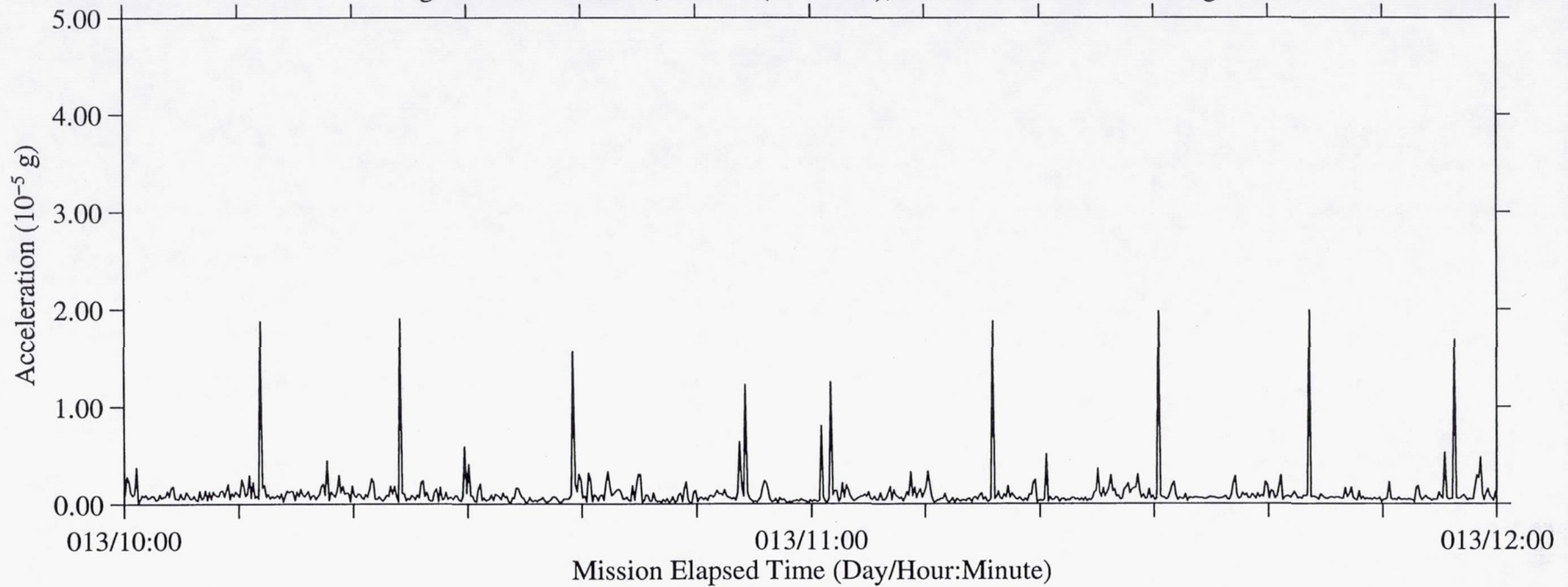


Figure 159b: USML-2, Head C (fc=25 Hz), Ten Second Interval RMS

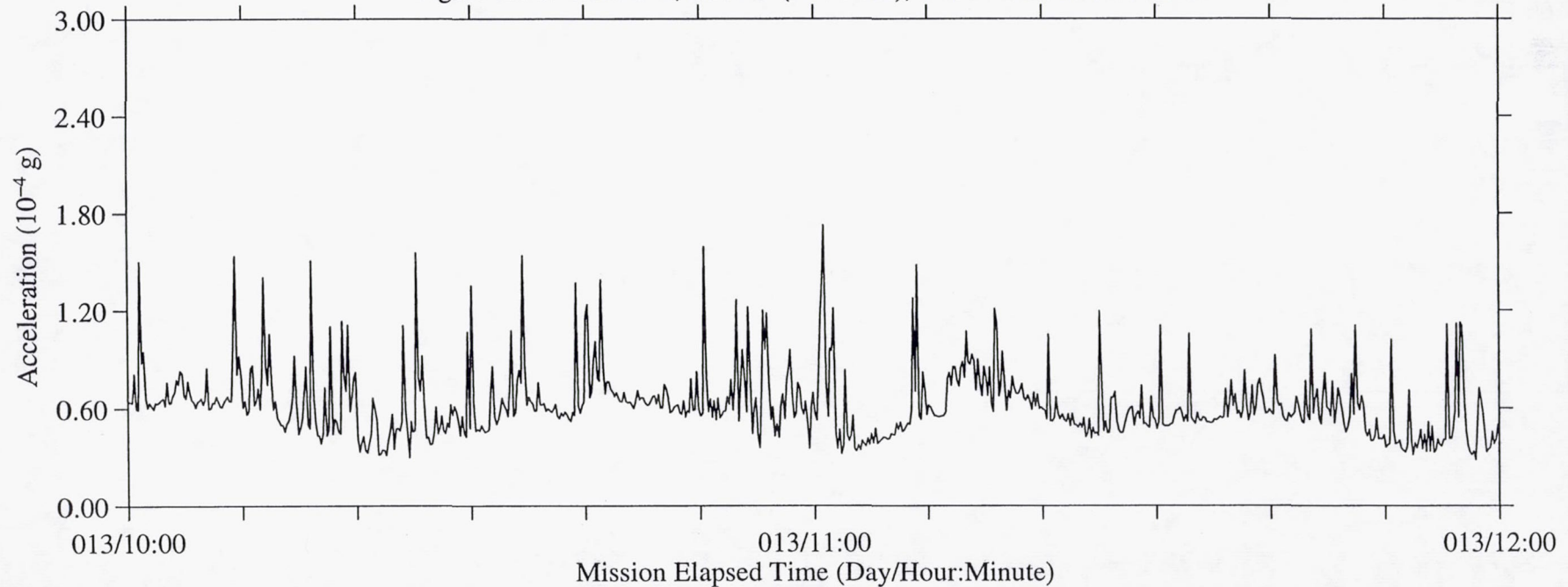
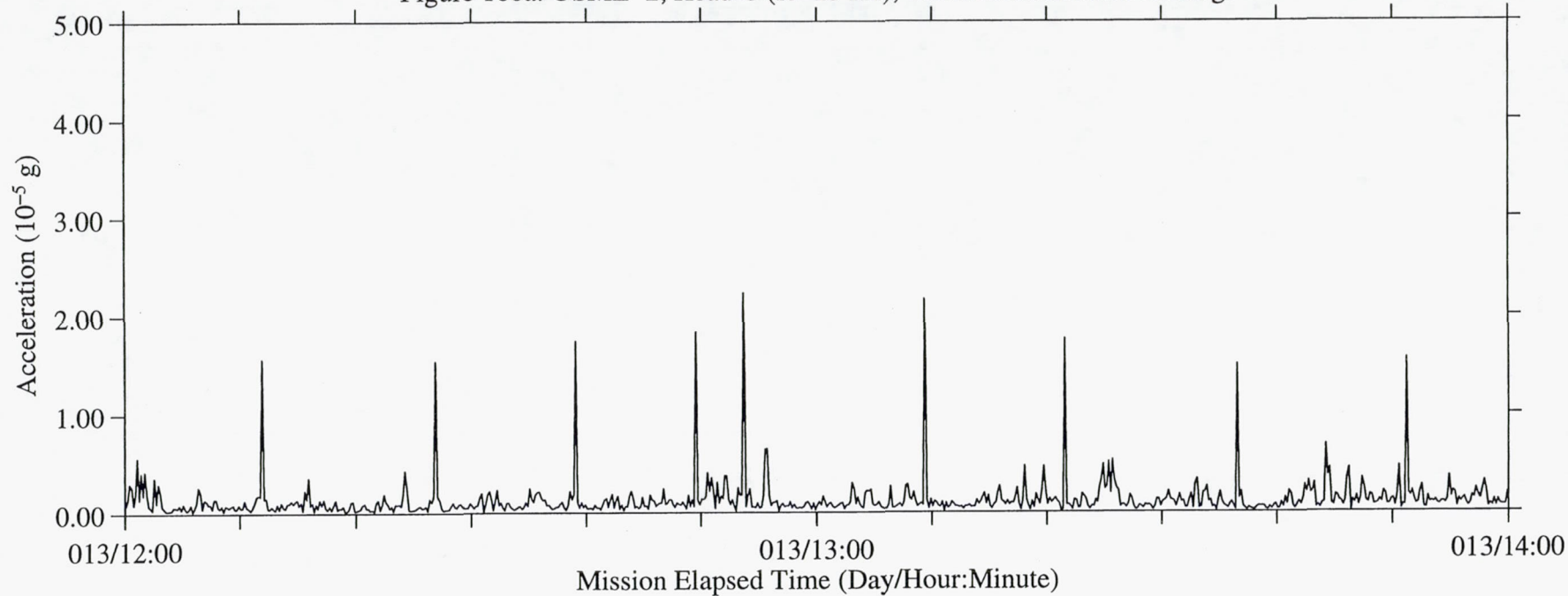
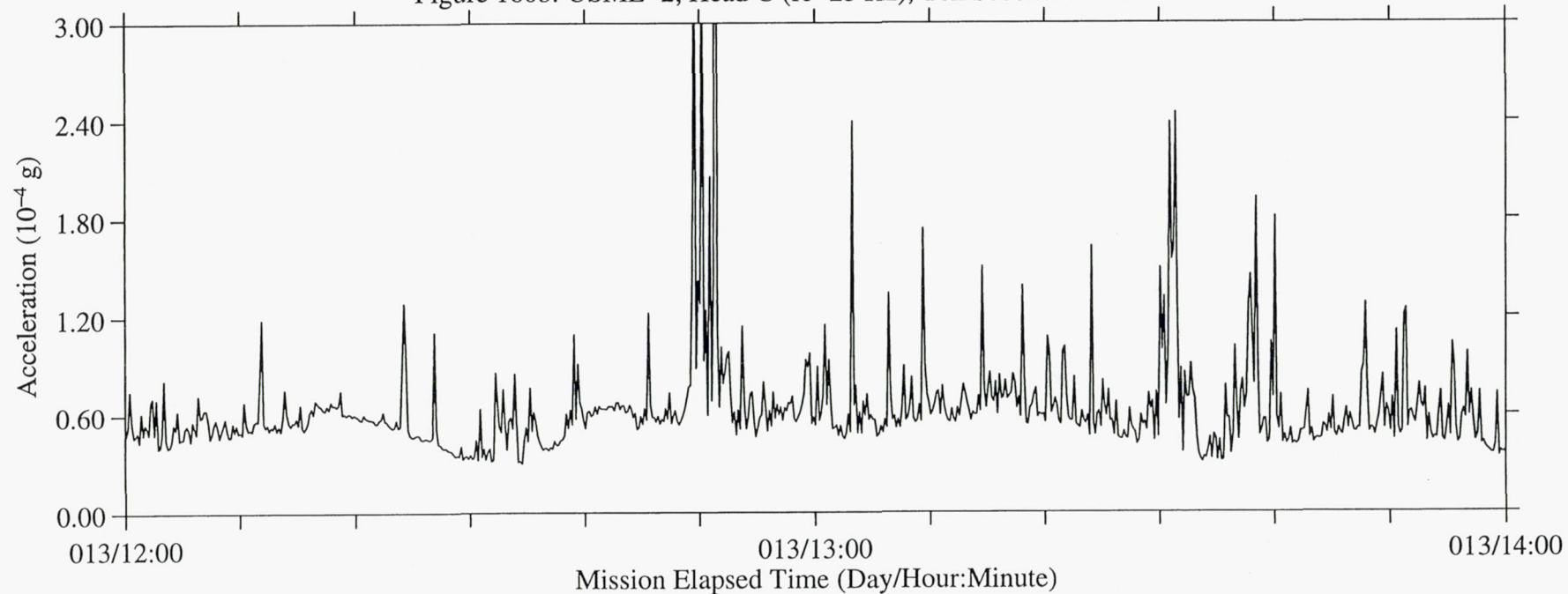


Figure 160a: USML-2, Head C ( $f_c=25$  Hz), Ten Second Interval AverageFigure 160b: USML-2, Head C ( $f_c=25$  Hz), Ten Second Interval RMS



B-163

Figure 161a: USML-2, Head C (fc=25 Hz), Ten Second Interval Average

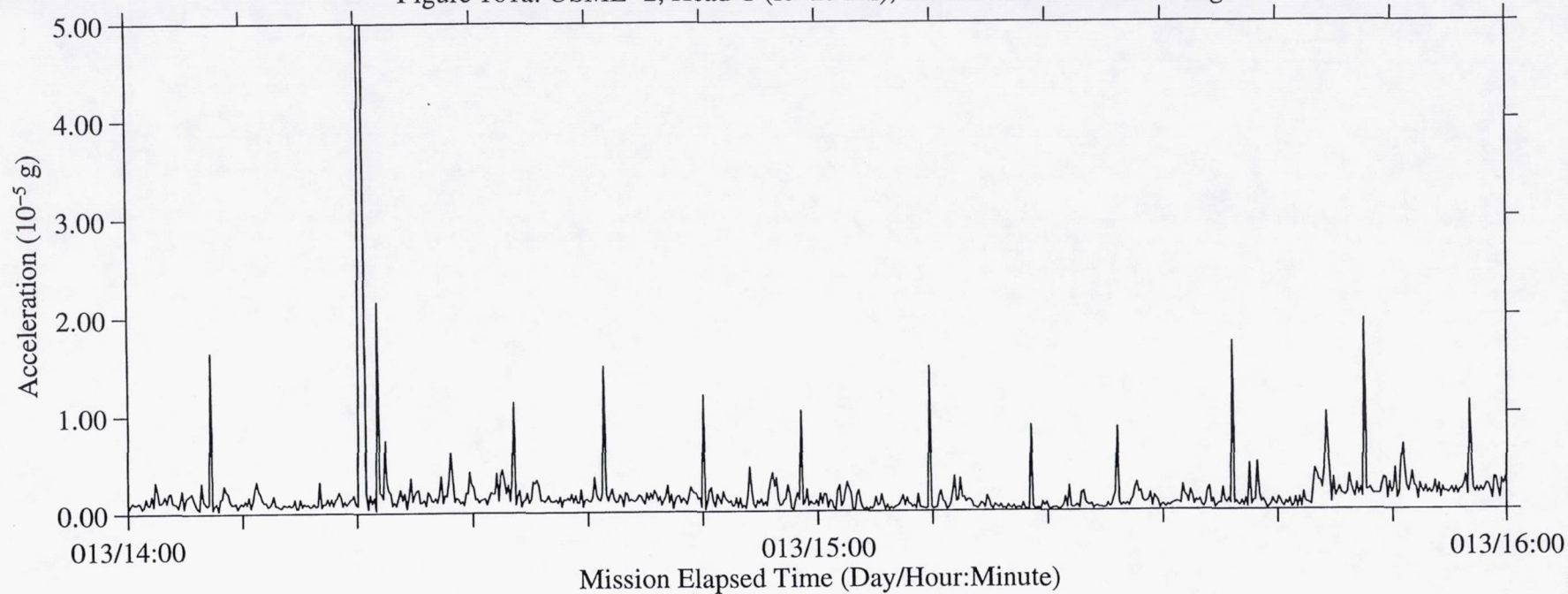
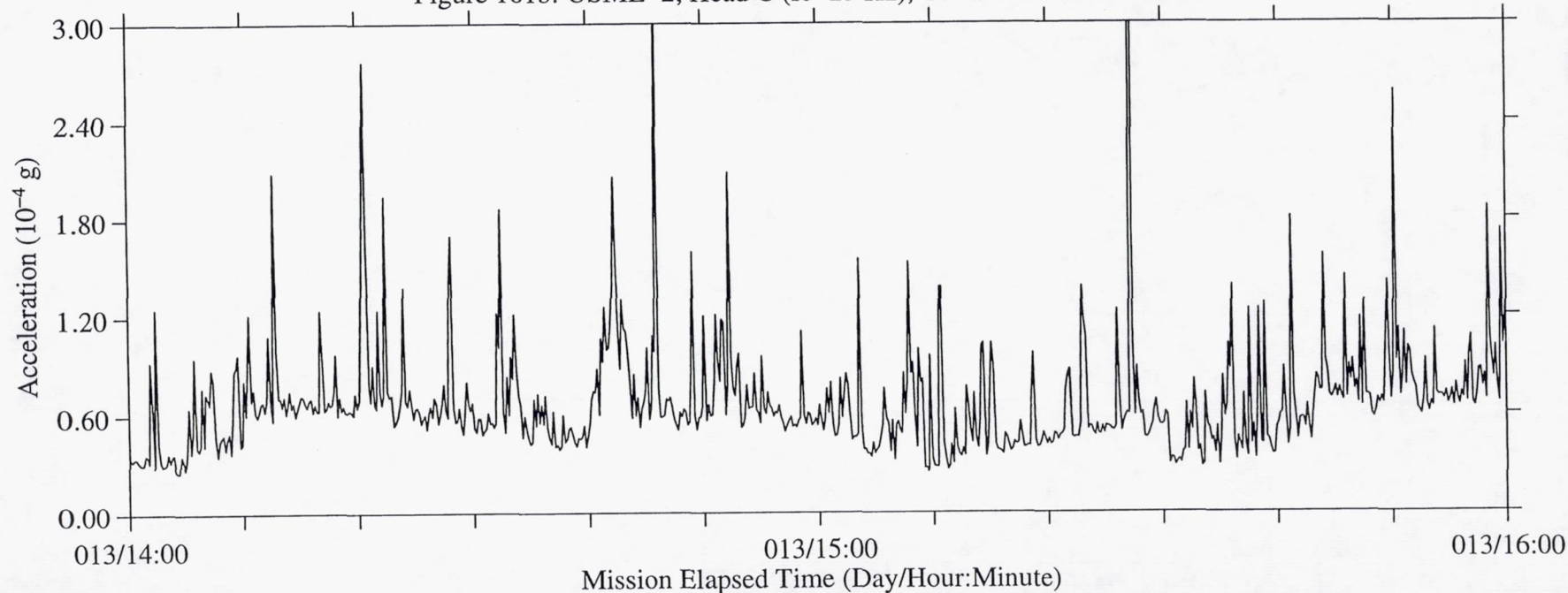


Figure 161b: USML-2, Head C (fc=25 Hz), Ten Second Interval RMS



B-164

Figure 162a: USML-2, Head C (fc=25 Hz), Ten Second Interval Average

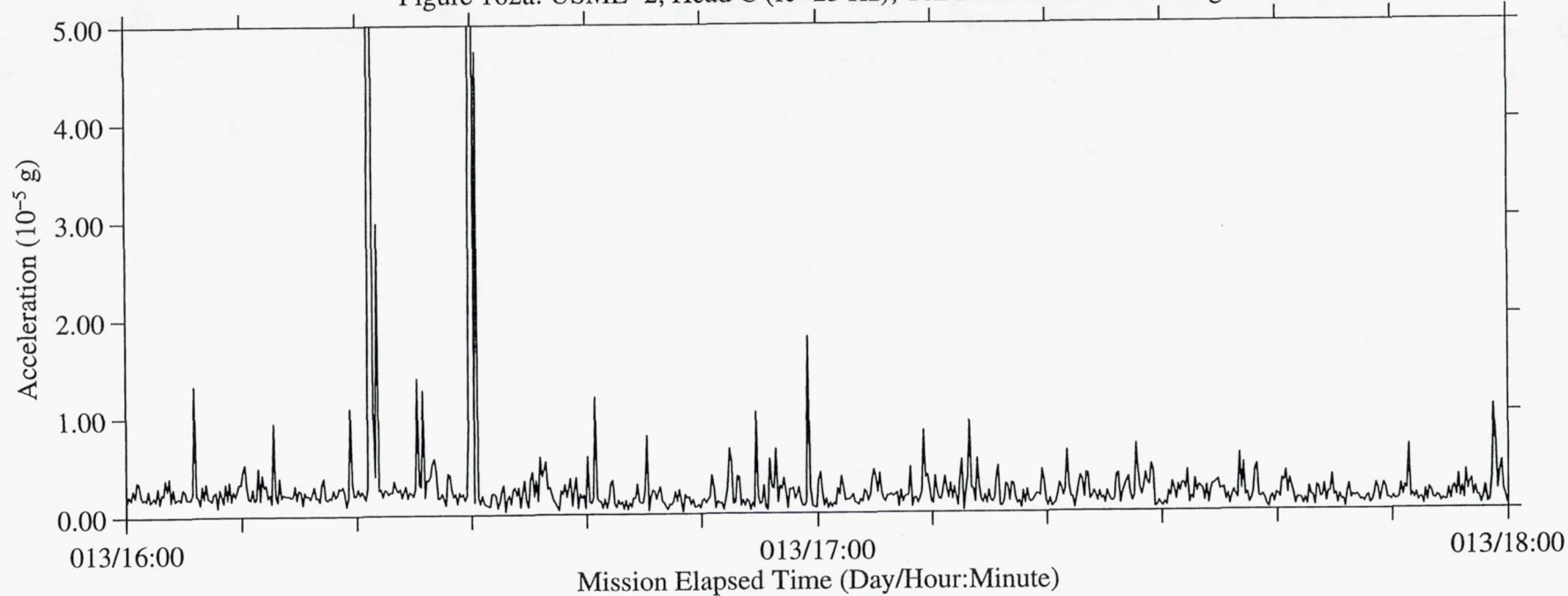
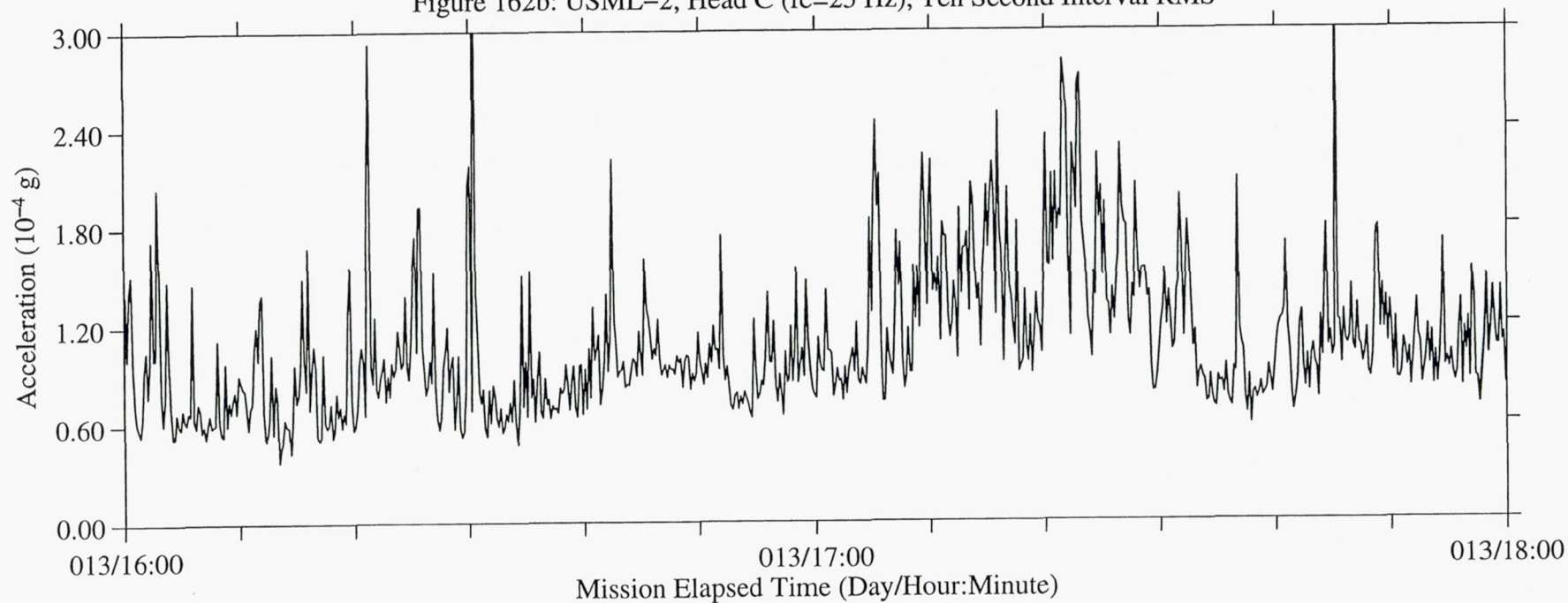


Figure 162b: USML-2, Head C (fc=25 Hz), Ten Second Interval RMS





B-165

Figure 163a: USML-2, Head C (fc=25 Hz), Ten Second Interval Average

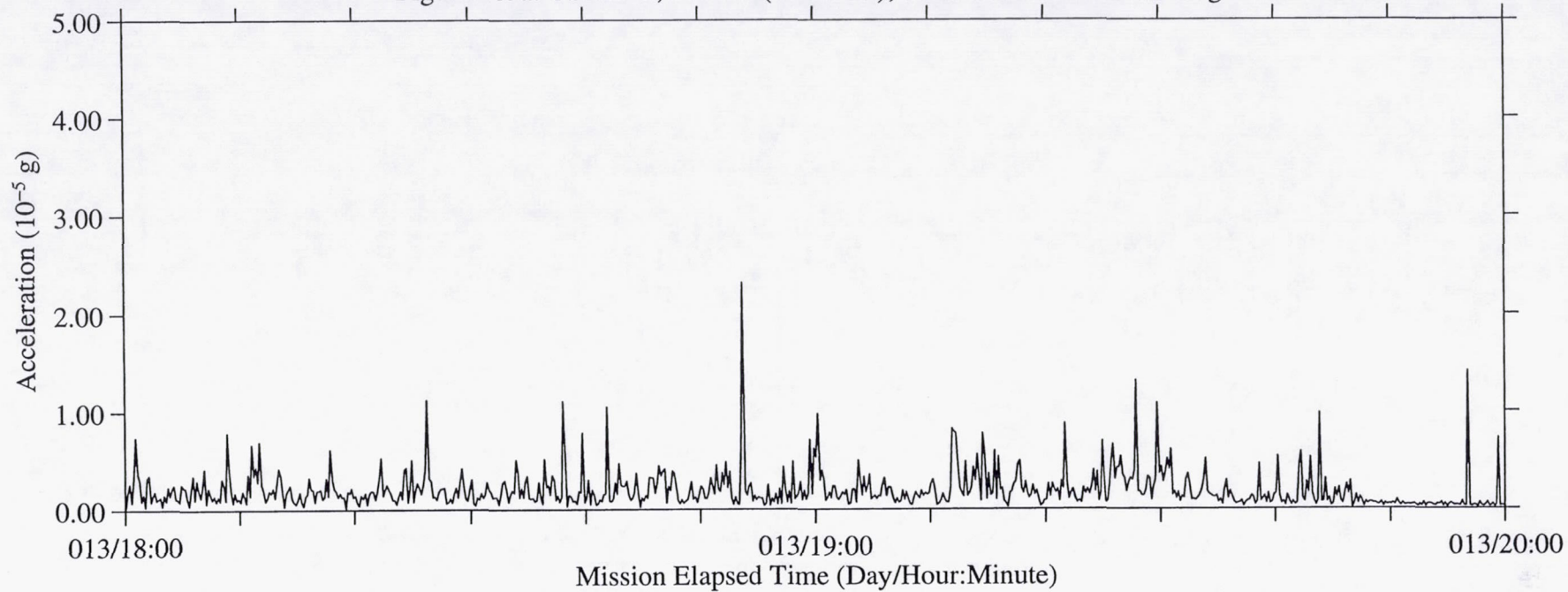


Figure 163b: USML-2, Head C (fc=25 Hz), Ten Second Interval RMS

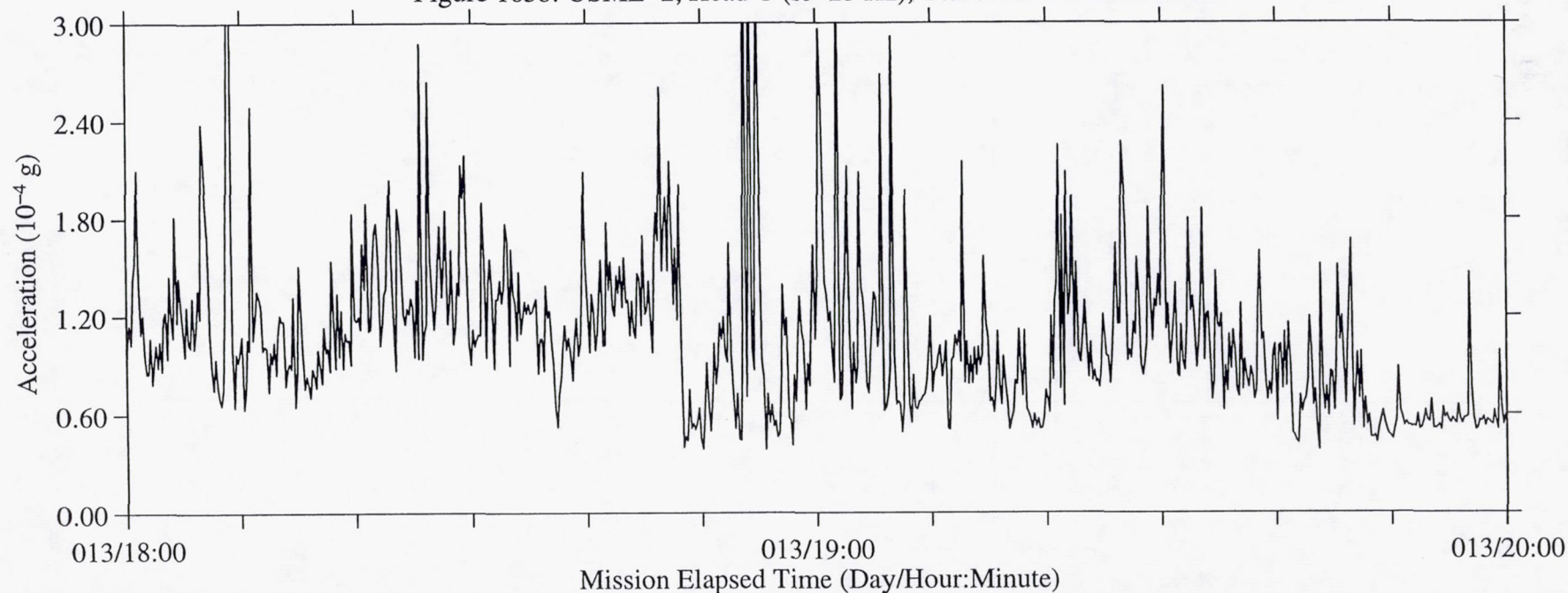


Figure 164a: USML-2, Head C (fc=25 Hz), Ten Second Interval Average

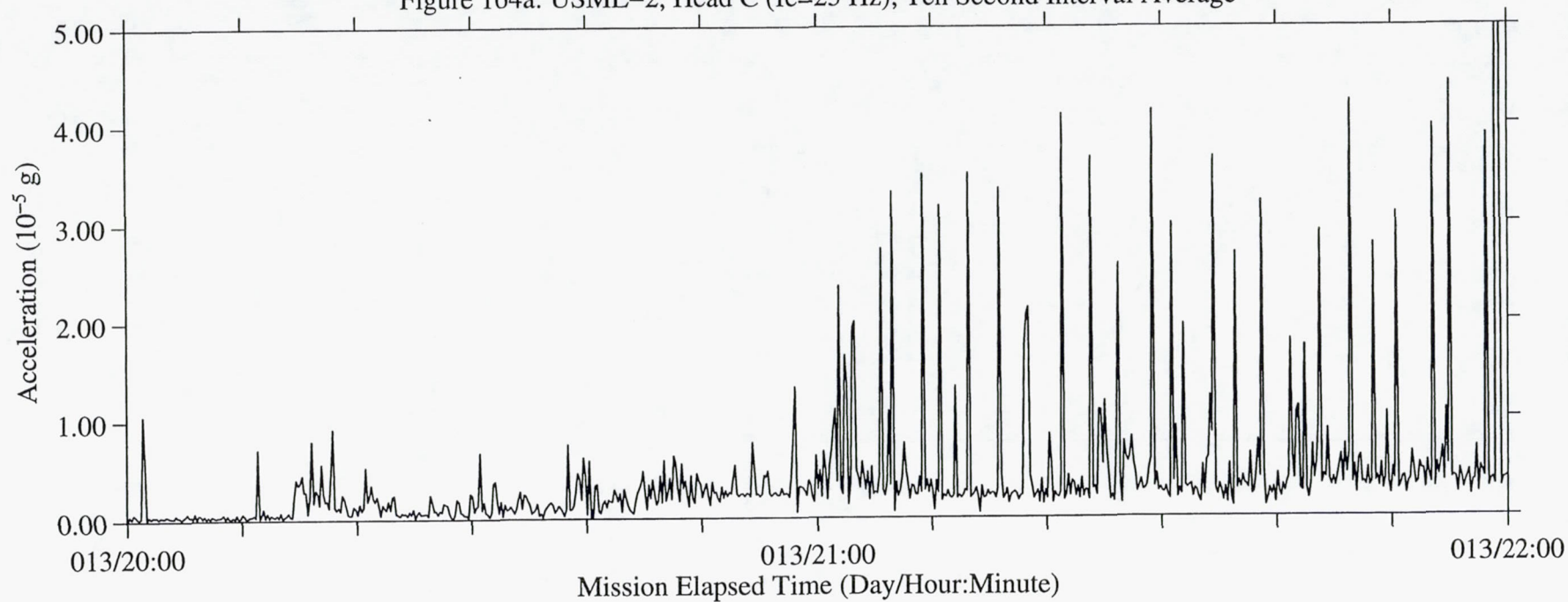


Figure 164b: USML-2, Head C (fc=25 Hz), Ten Second Interval RMS

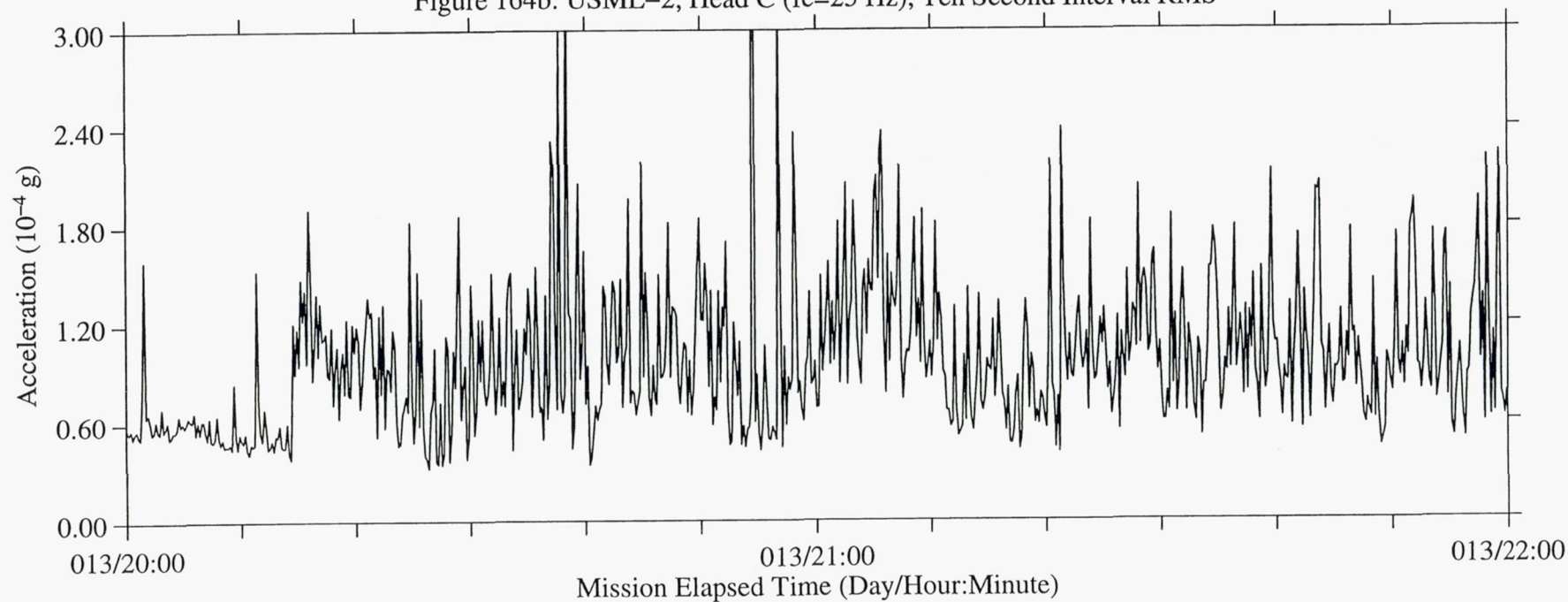




Figure 165a: USML-2, Head C (fc=25 Hz), Ten Second Interval Average

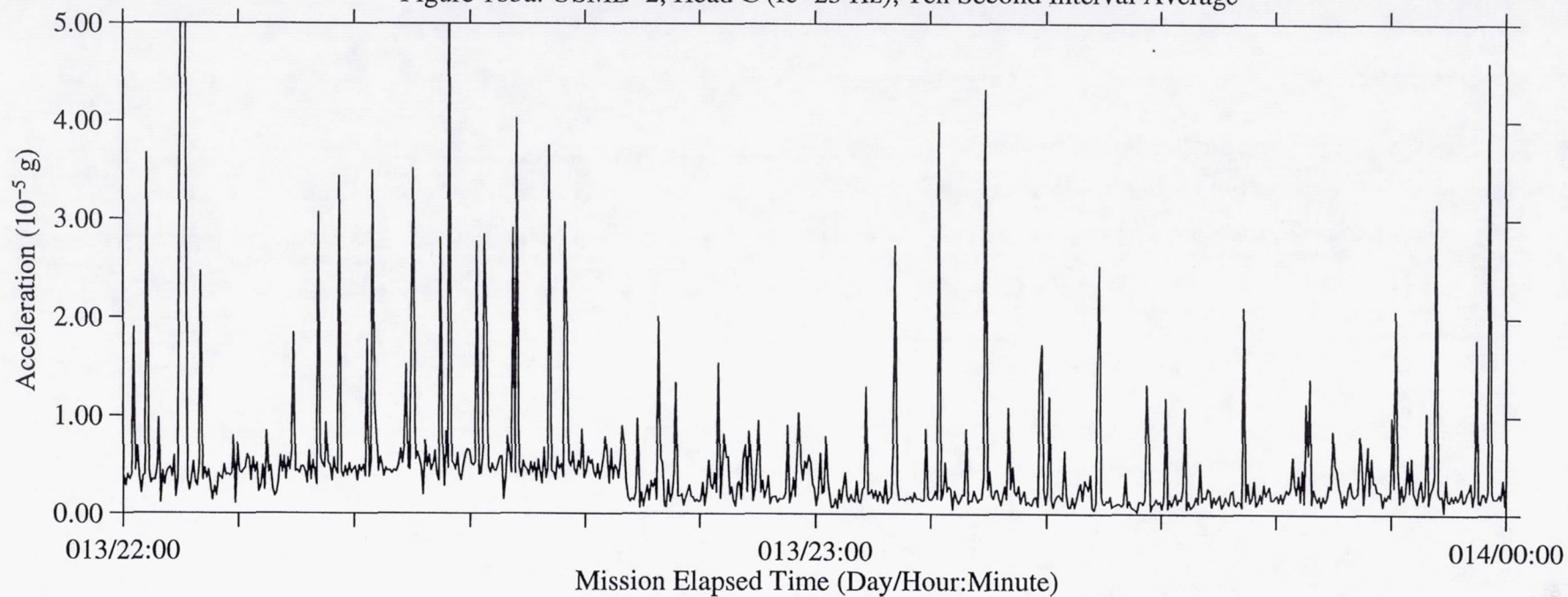


Figure 165b: USML-2, Head C (fc=25 Hz), Ten Second Interval RMS

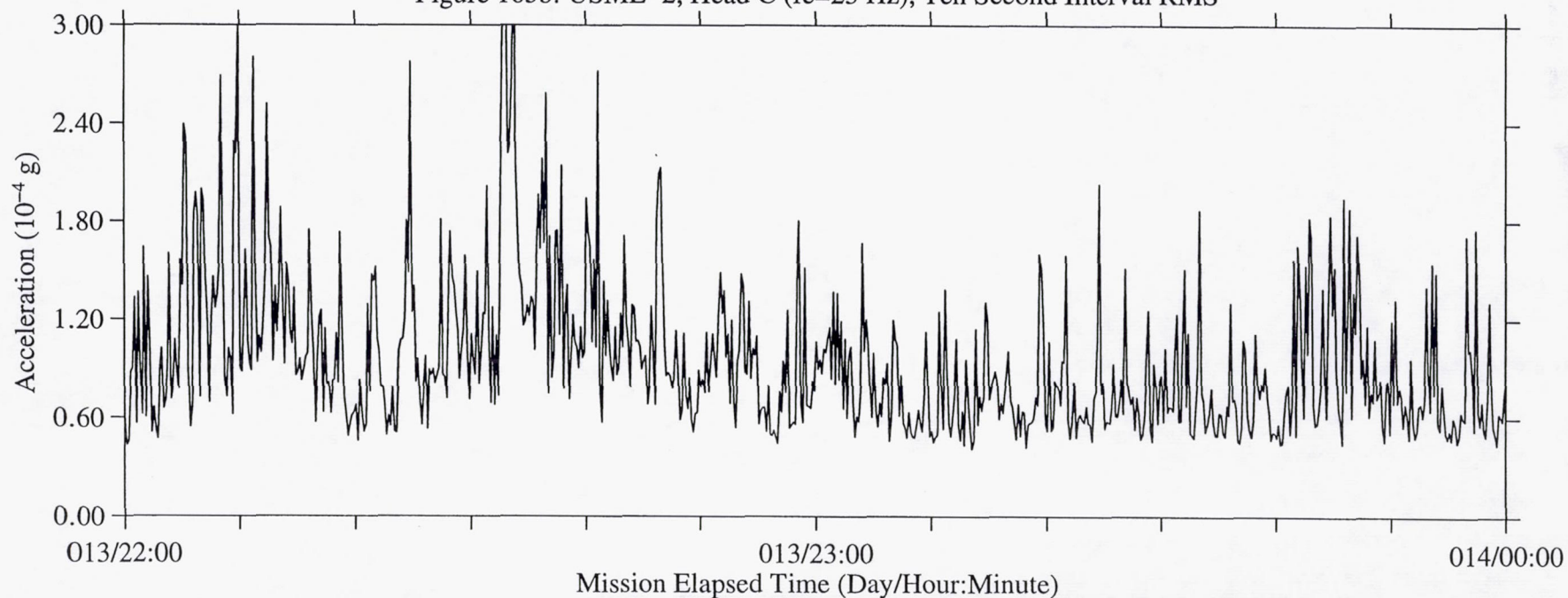


Figure 166a: USML-2, Head C (fc=25 Hz), Ten Second Interval Average

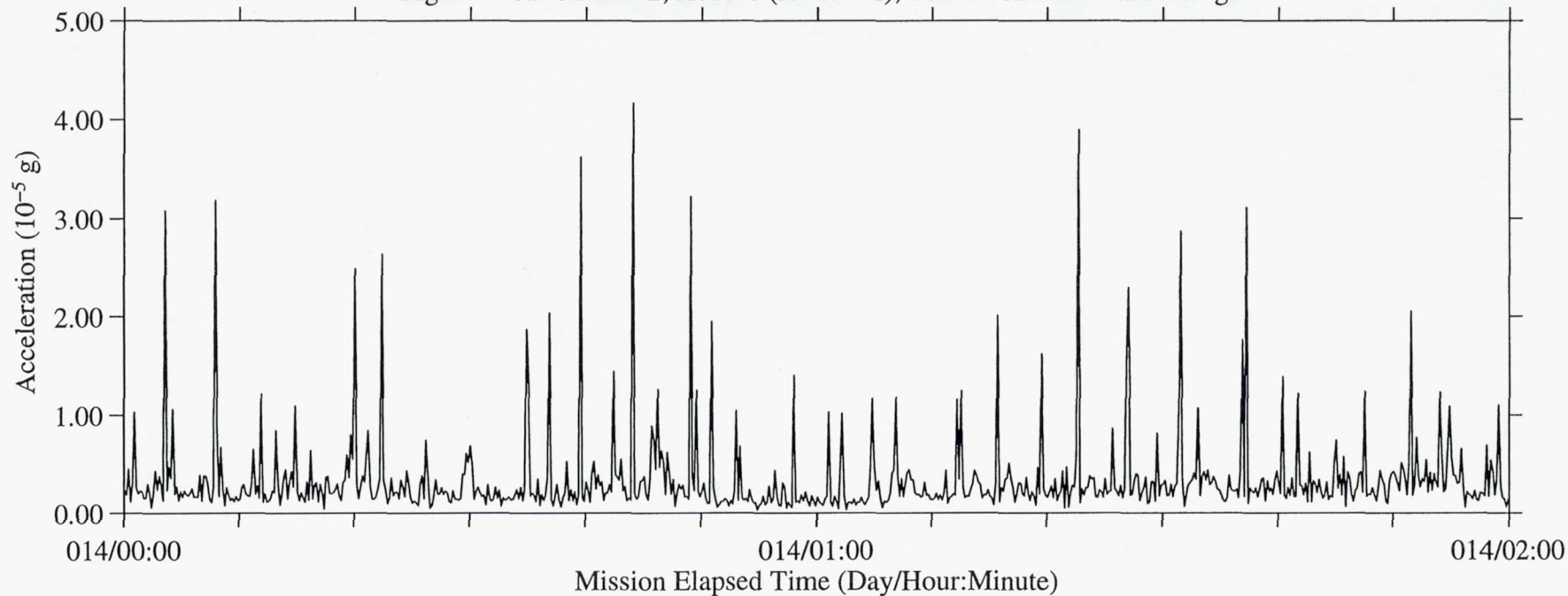
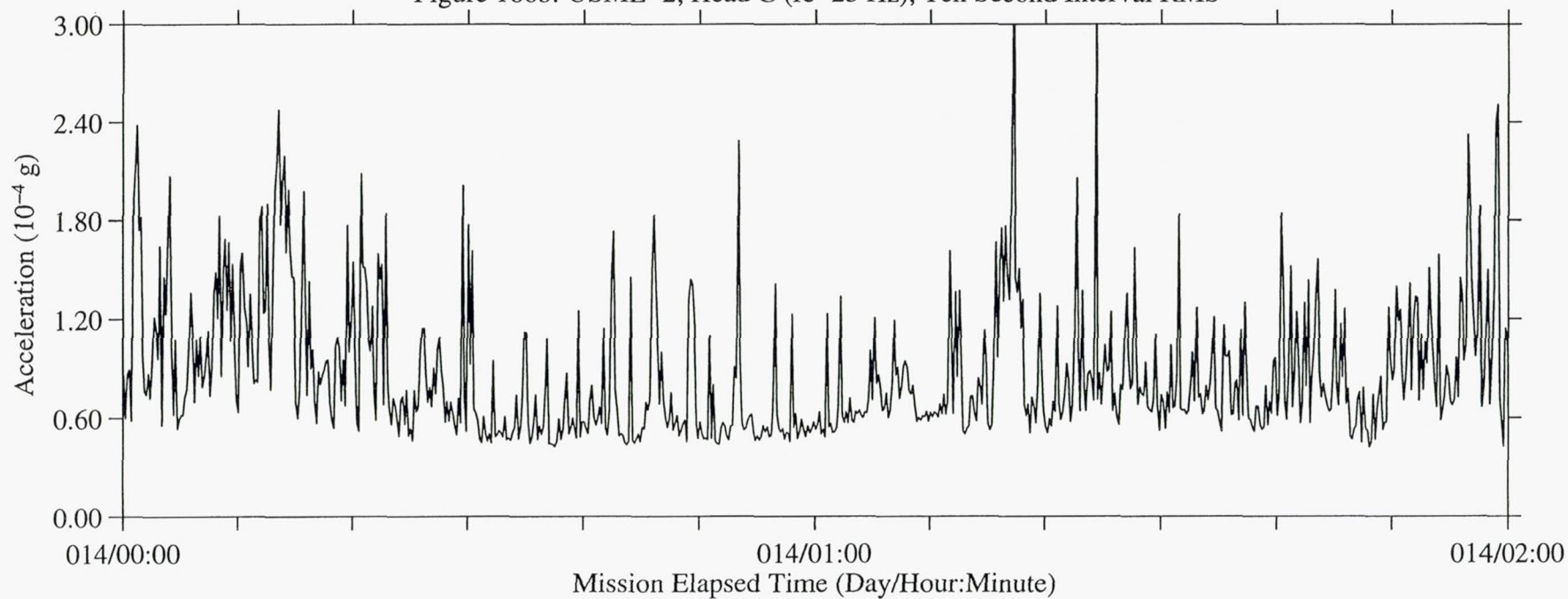


Figure 166b: USML-2, Head C (fc=25 Hz), Ten Second Interval RMS





B-169

Figure 167a: USML-2, Head C (fc=25 Hz), Ten Second Interval Average

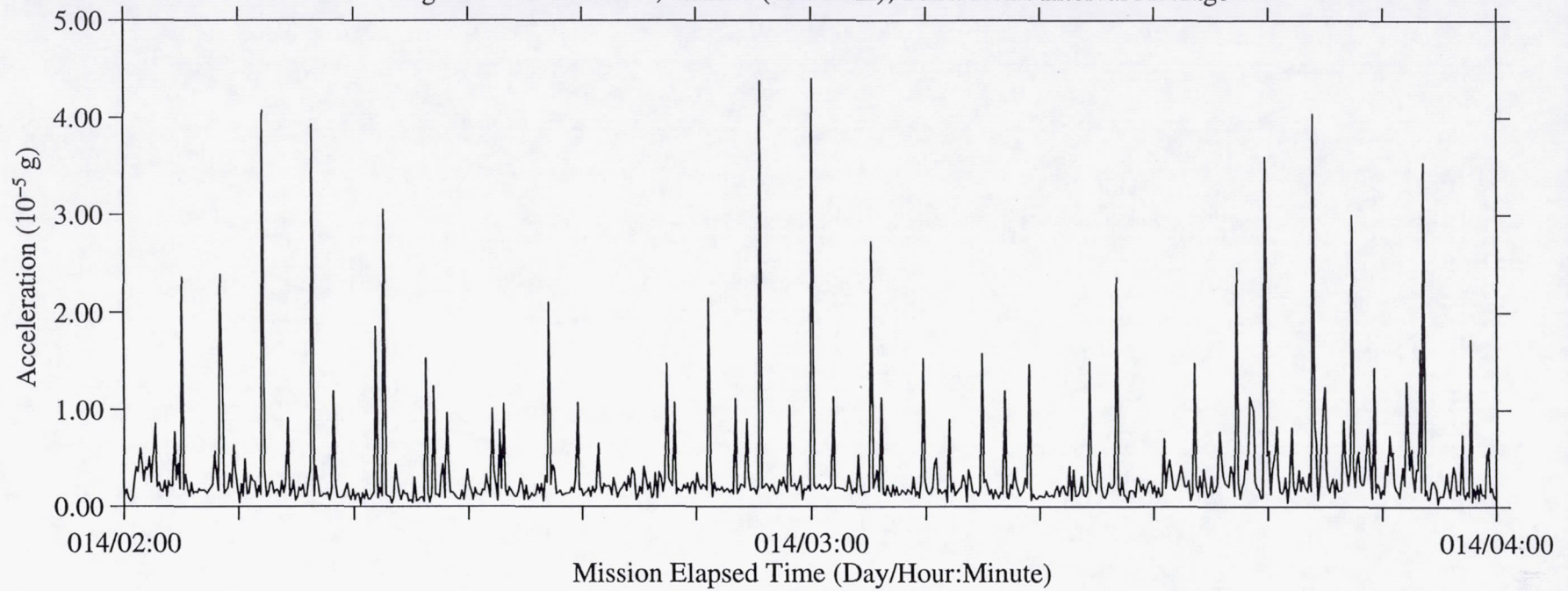


Figure 167b: USML-2, Head C (fc=25 Hz), Ten Second Interval RMS

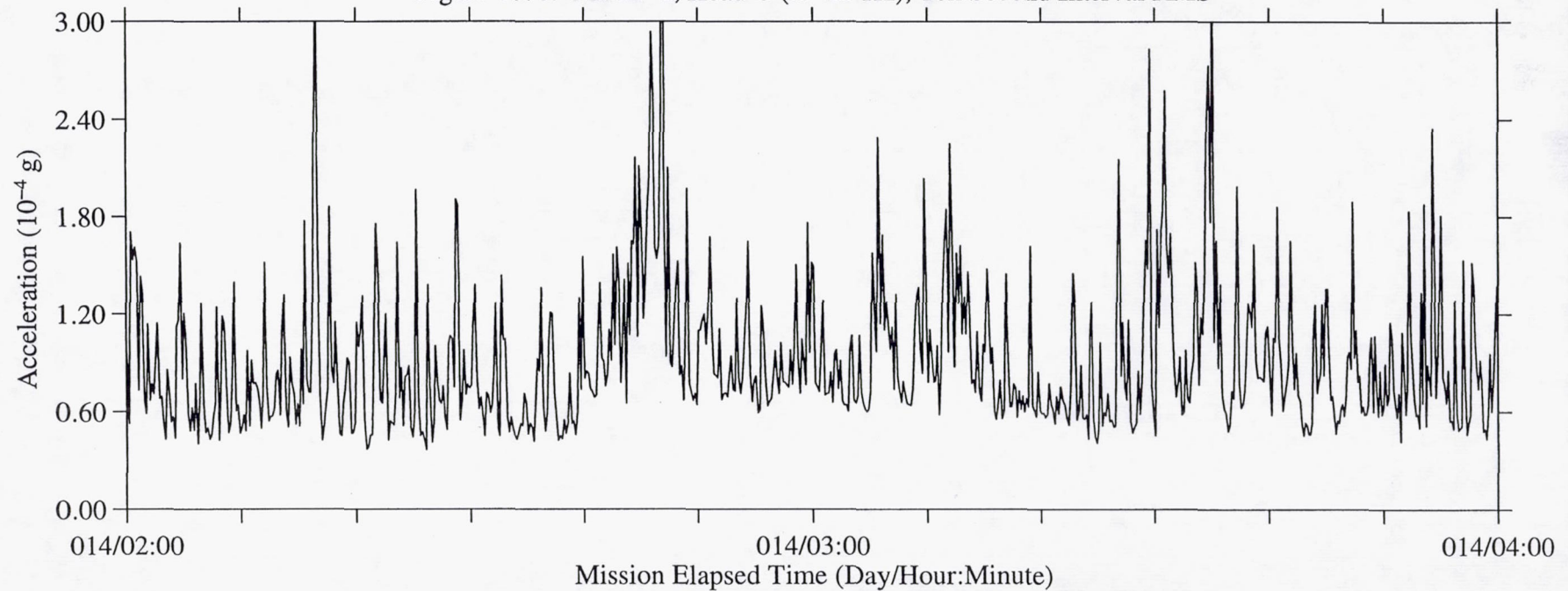


Figure 168a: USML-2, Head C (fc=25 Hz), Ten Second Interval Average

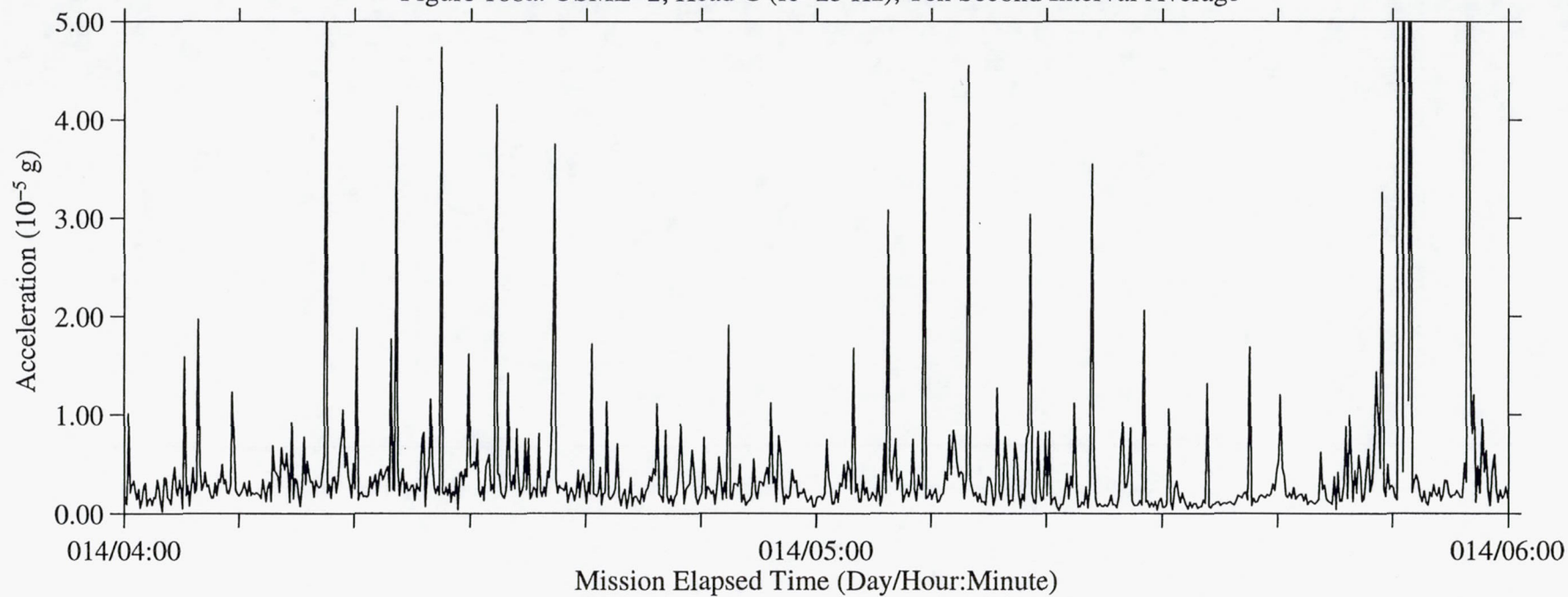


Figure 168b: USML-2, Head C (fc=25 Hz), Ten Second Interval RMS

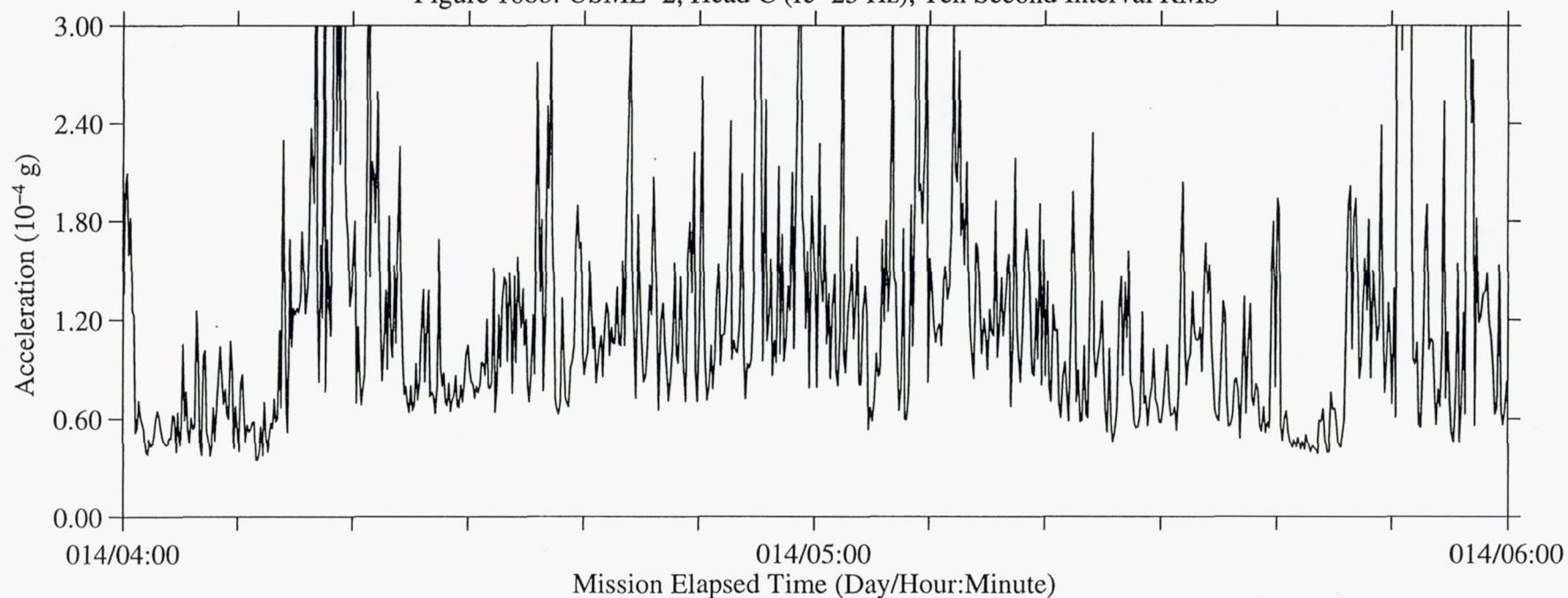




Figure 169a: USML-2, Head C (fc=25 Hz), Ten Second Interval Average

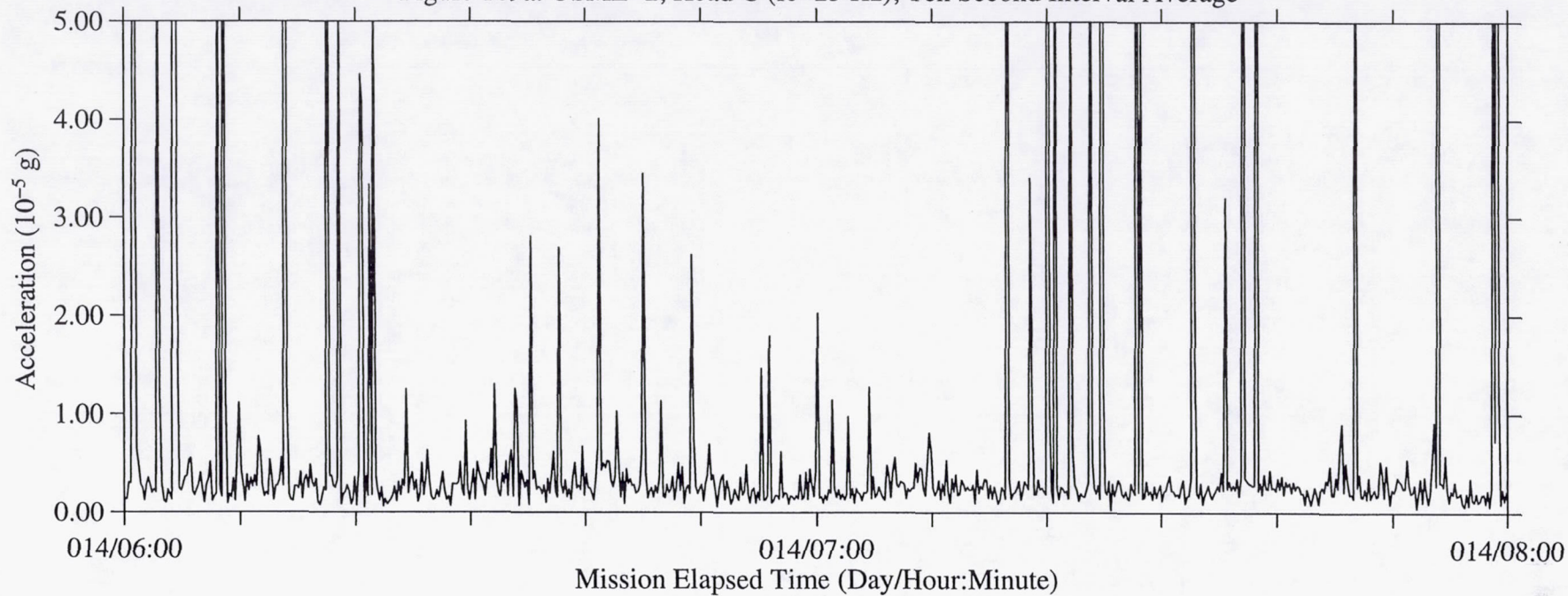


Figure 169b: USML-2, Head C (fc=25 Hz), Ten Second Interval RMS

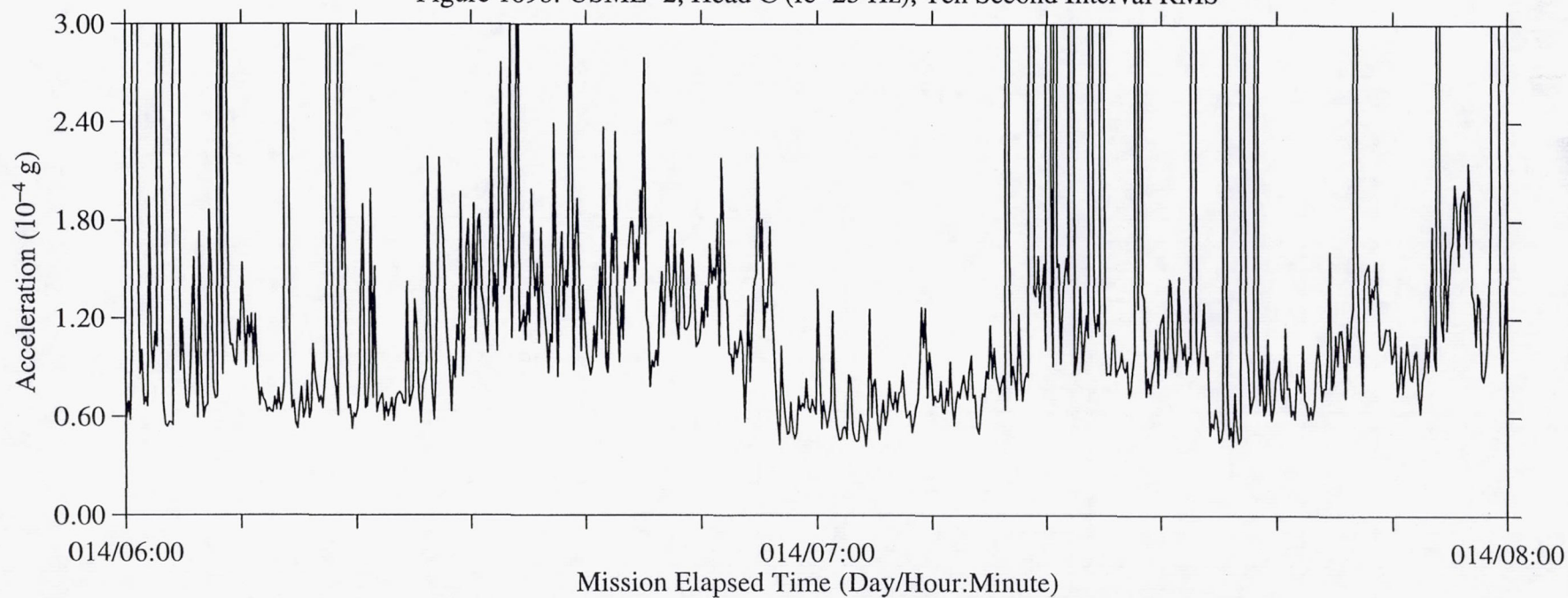


Figure 170a: USML-2, Head C (fc=25 Hz), Ten Second Interval Average

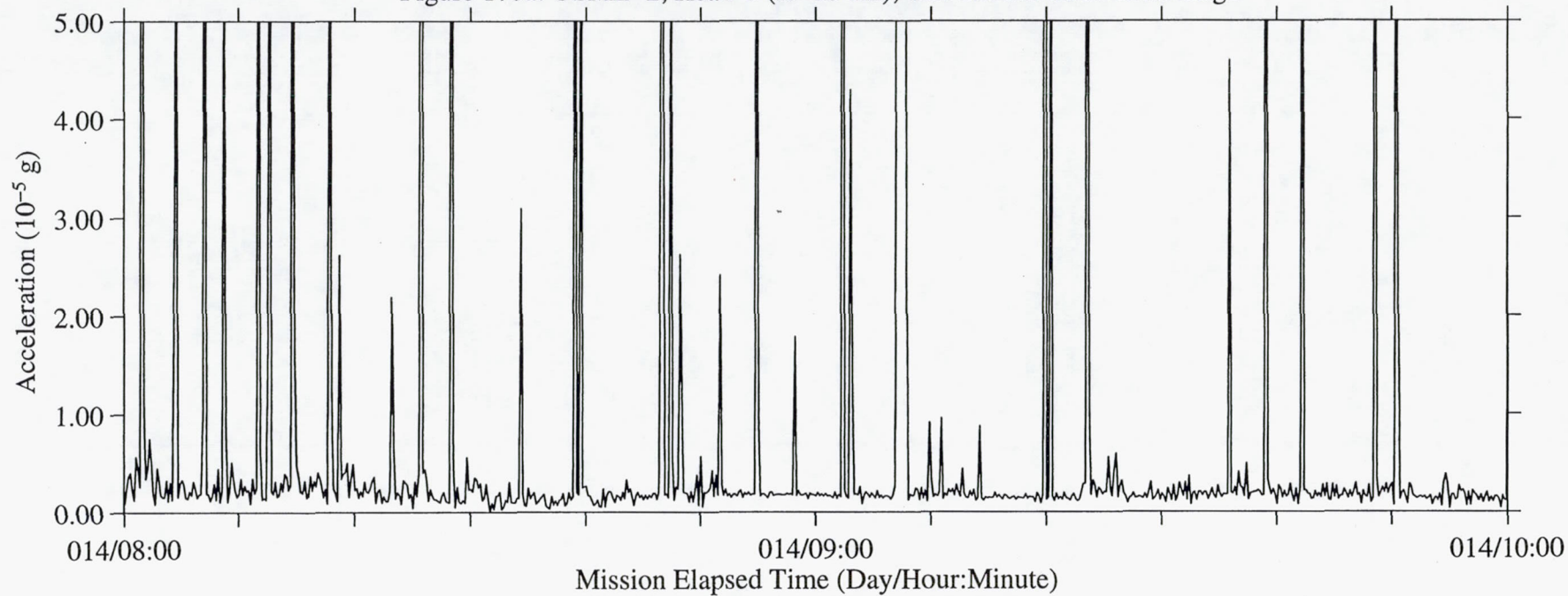


Figure 170b: USML-2, Head C (fc=25 Hz), Ten Second Interval RMS

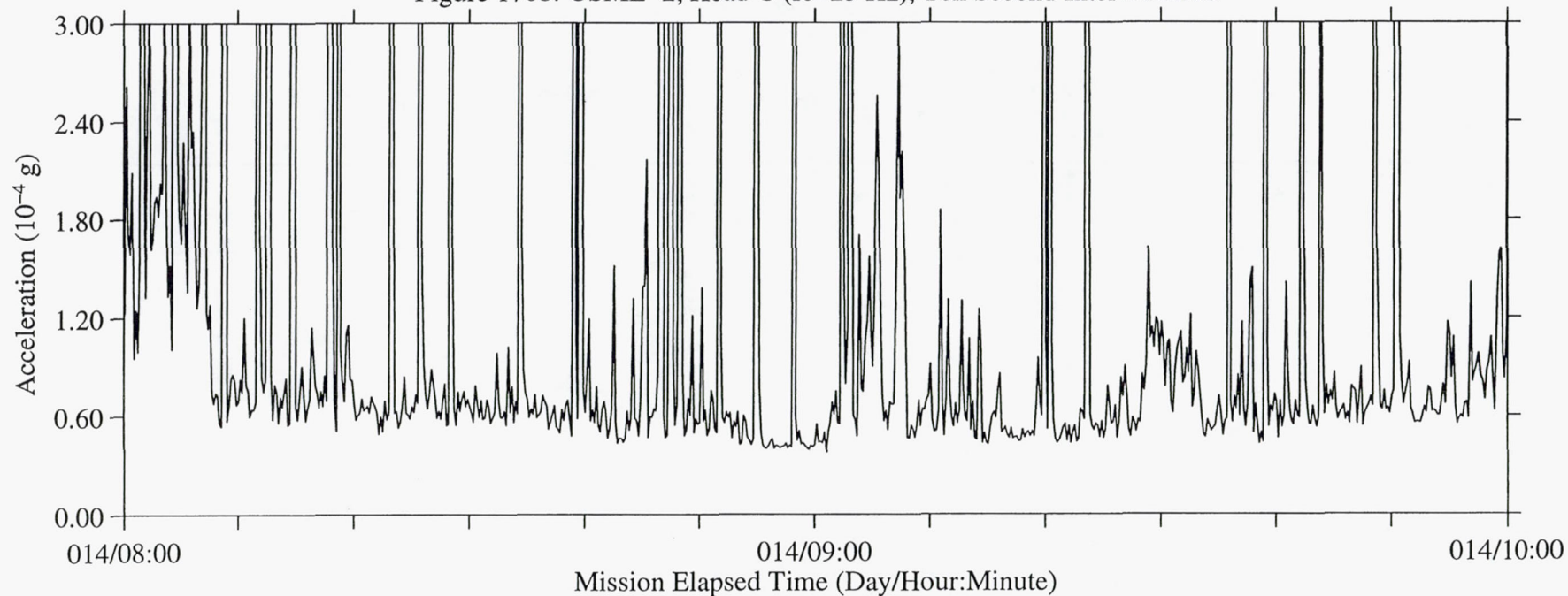




Figure 171a: USML-2, Head C (fc=25 Hz), Ten Second Interval Average

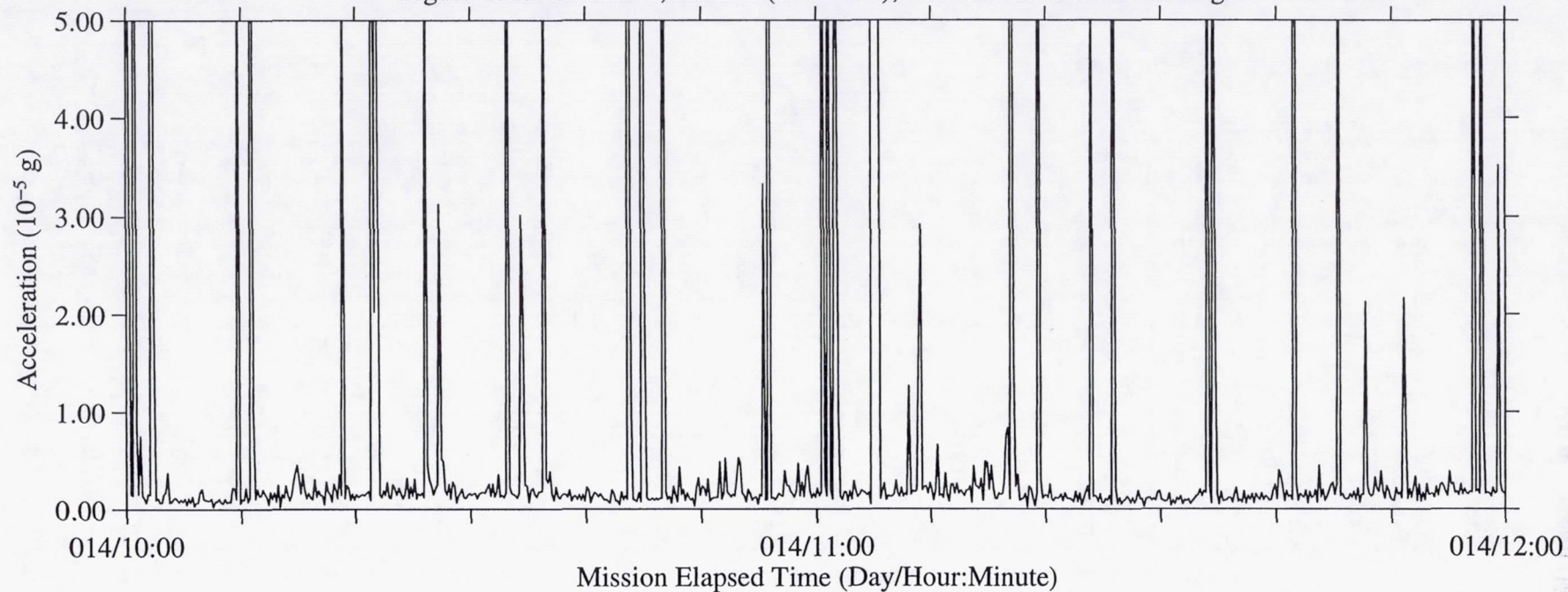


Figure 171b: USML-2, Head C (fc=25 Hz), Ten Second Interval RMS

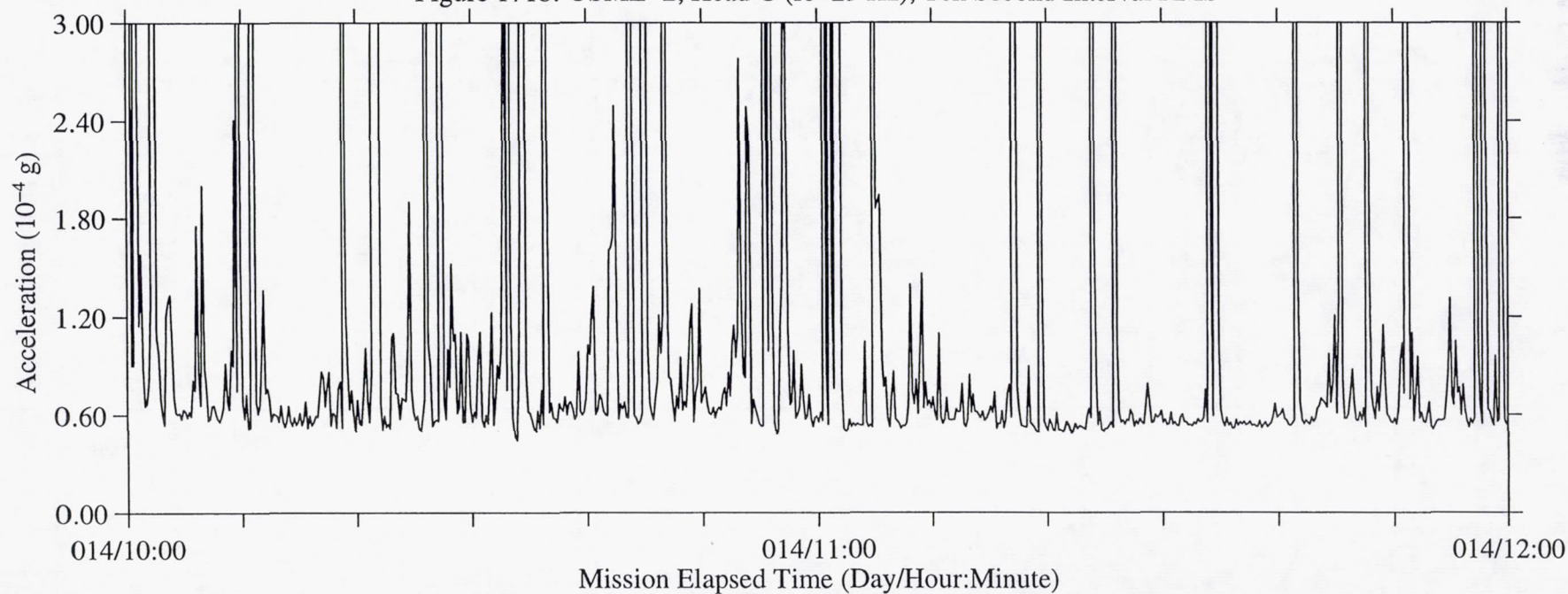


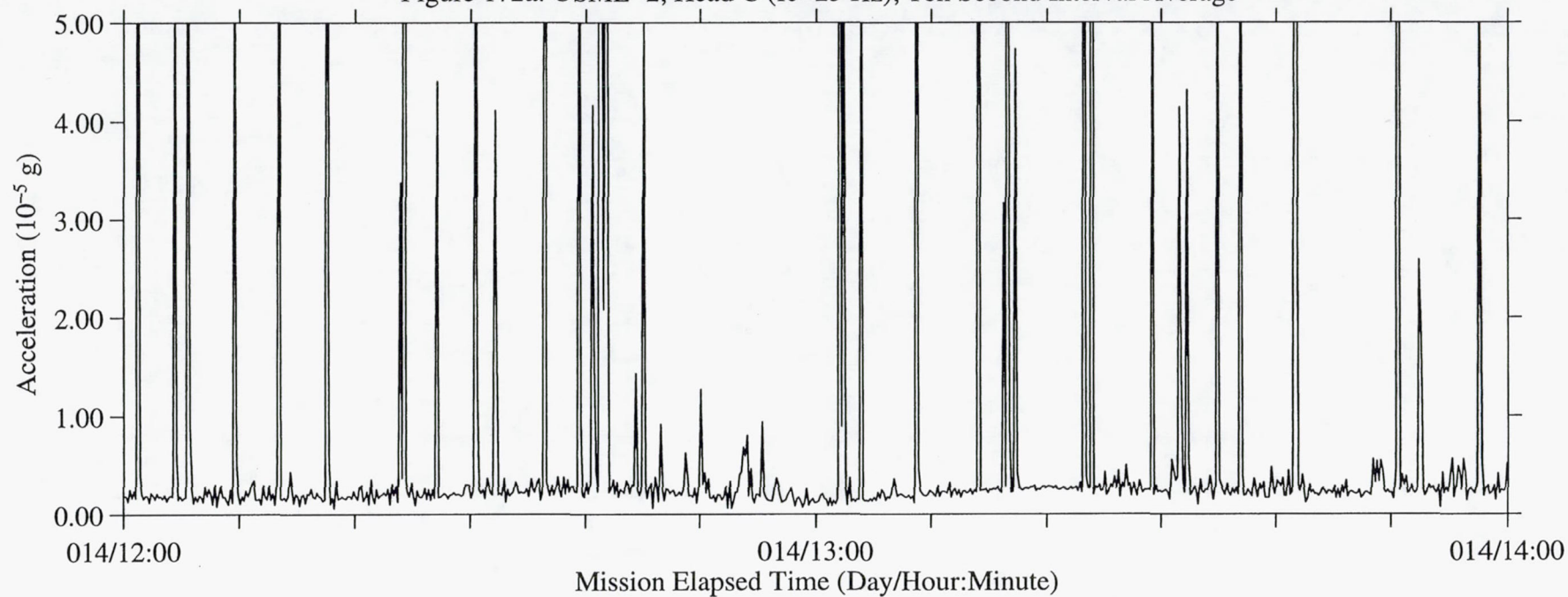
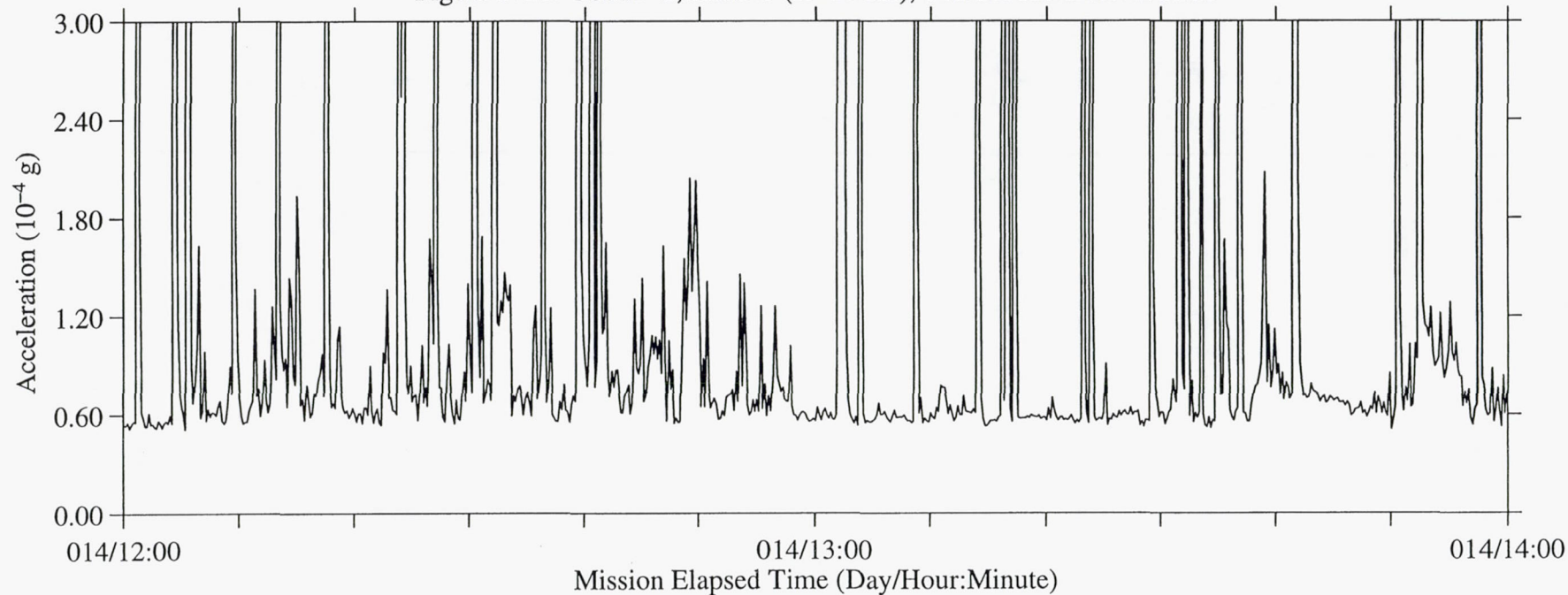
Figure 172a: USML-2, Head C ( $f_c=25$  Hz), Ten Second Interval AverageFigure 172b: USML-2, Head C ( $f_c=25$  Hz), Ten Second Interval RMS



Figure 173a: USML-2, Head C (fc=25 Hz), Ten Second Interval Average

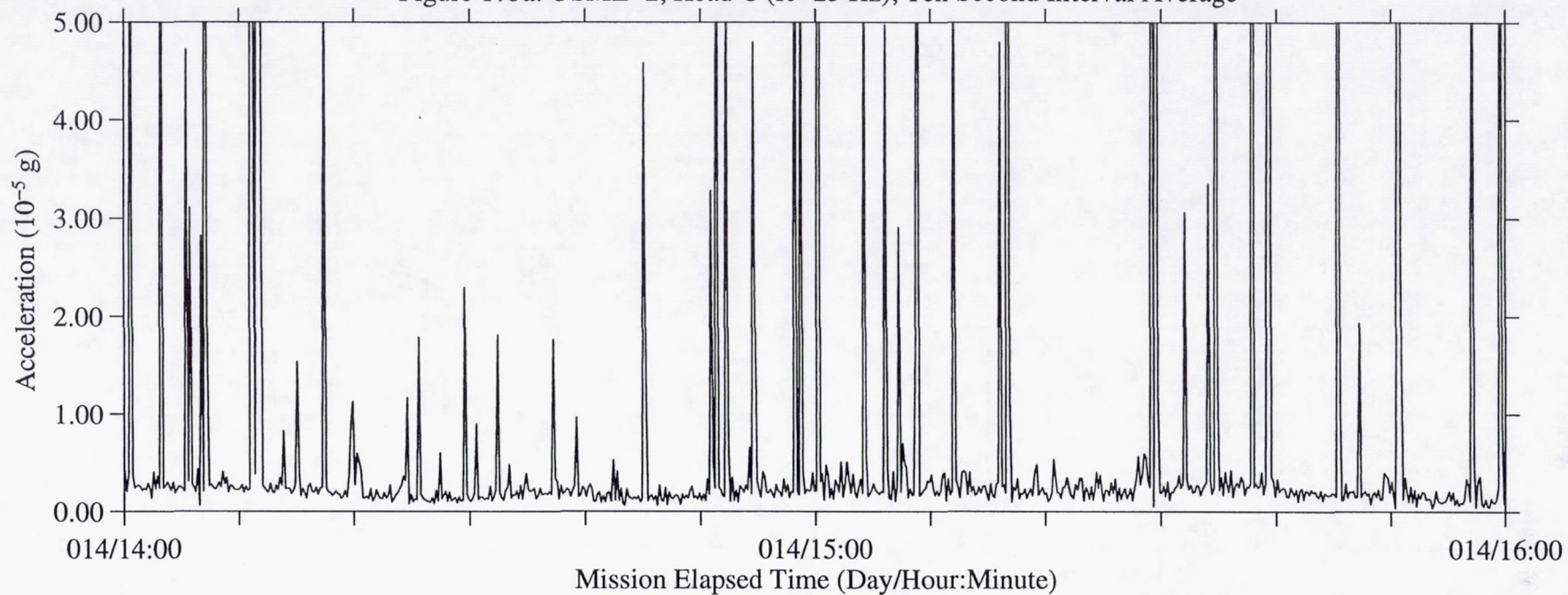


Figure 173b: USML-2, Head C (fc=25 Hz), Ten Second Interval RMS

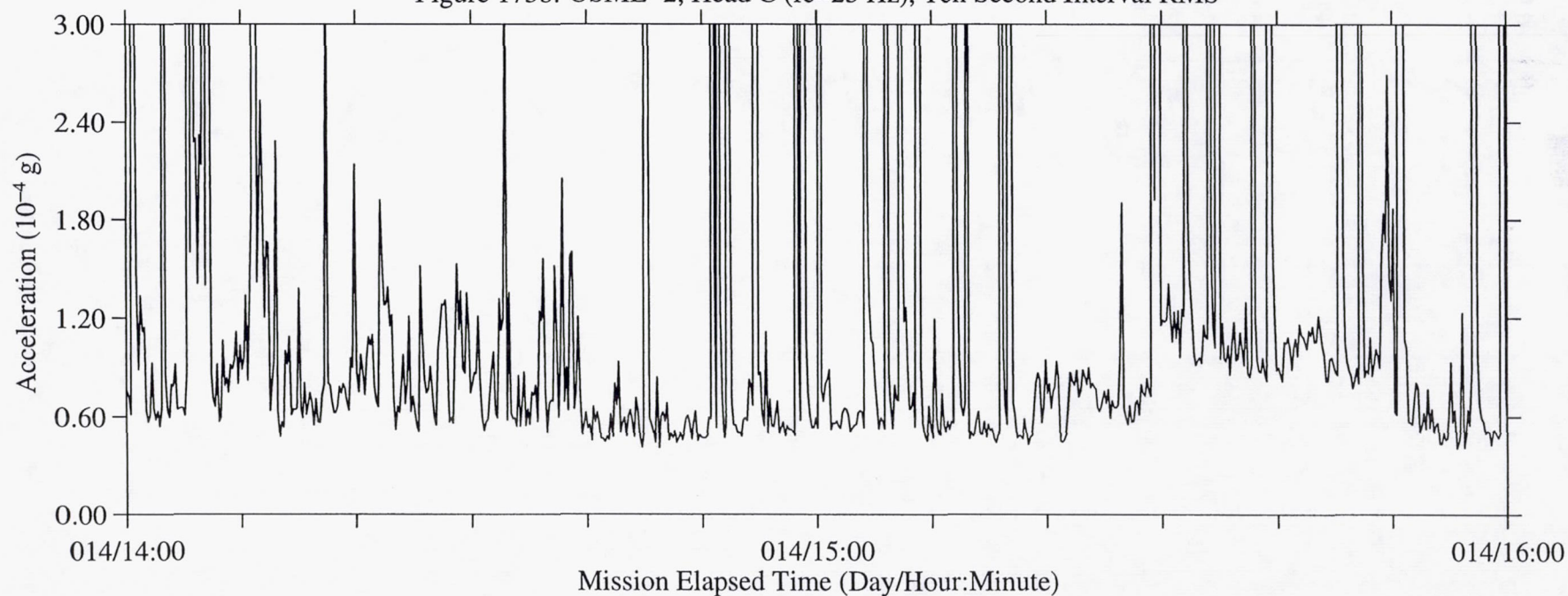


Figure 174a: USML-2, Head C (fc=25 Hz), Ten Second Interval Average

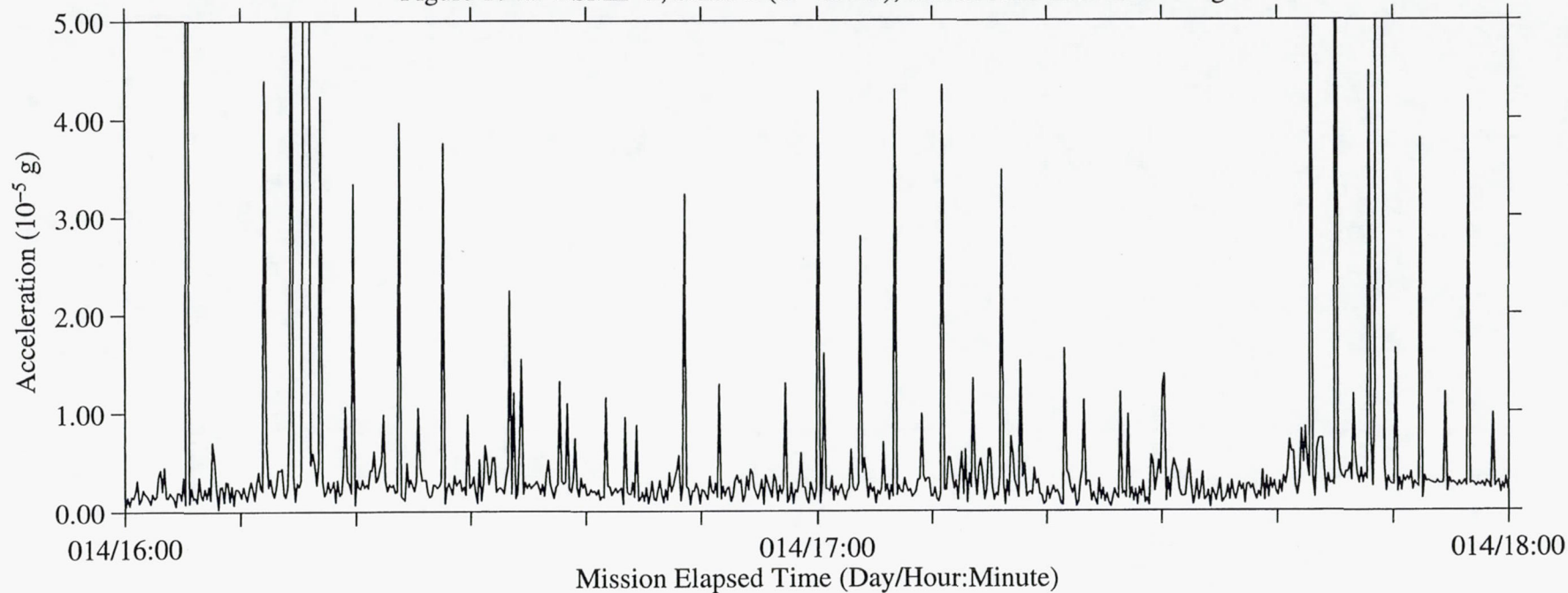


Figure 174b: USML-2, Head C (fc=25 Hz), Ten Second Interval RMS

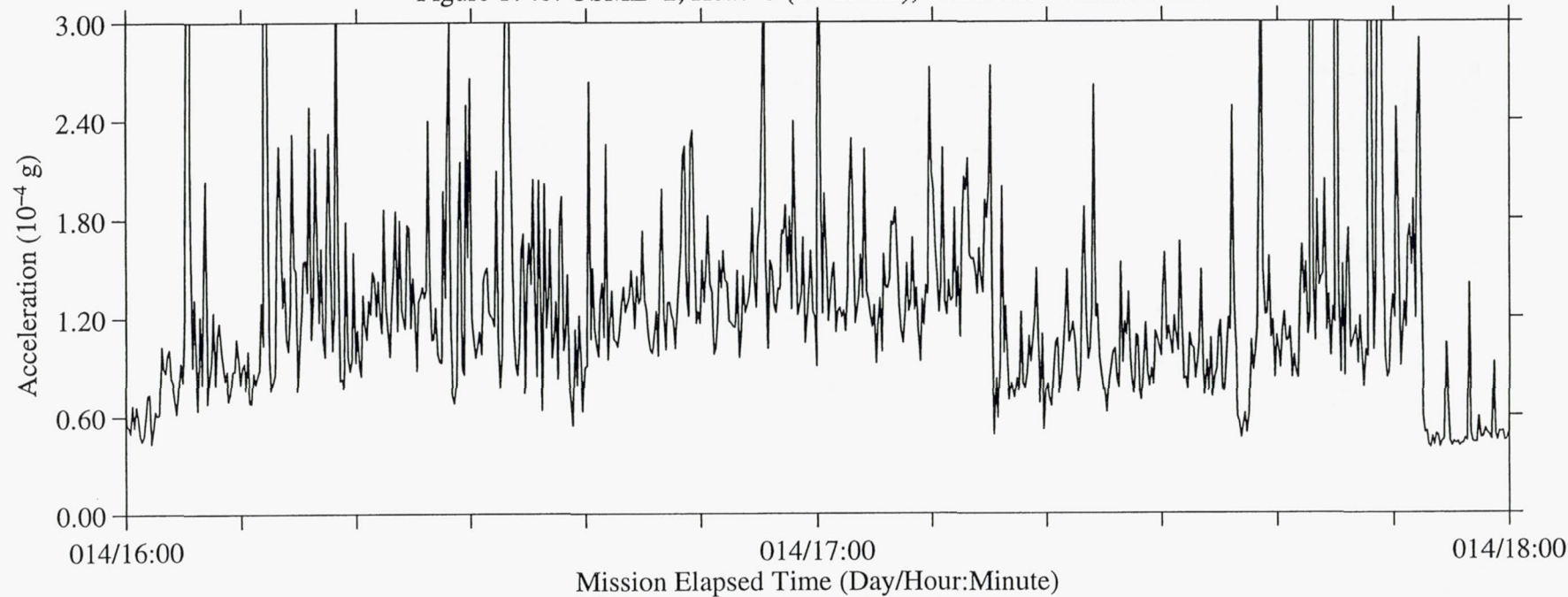




Figure 175a: USML-2, Head C (fc=25 Hz), Ten Second Interval Average

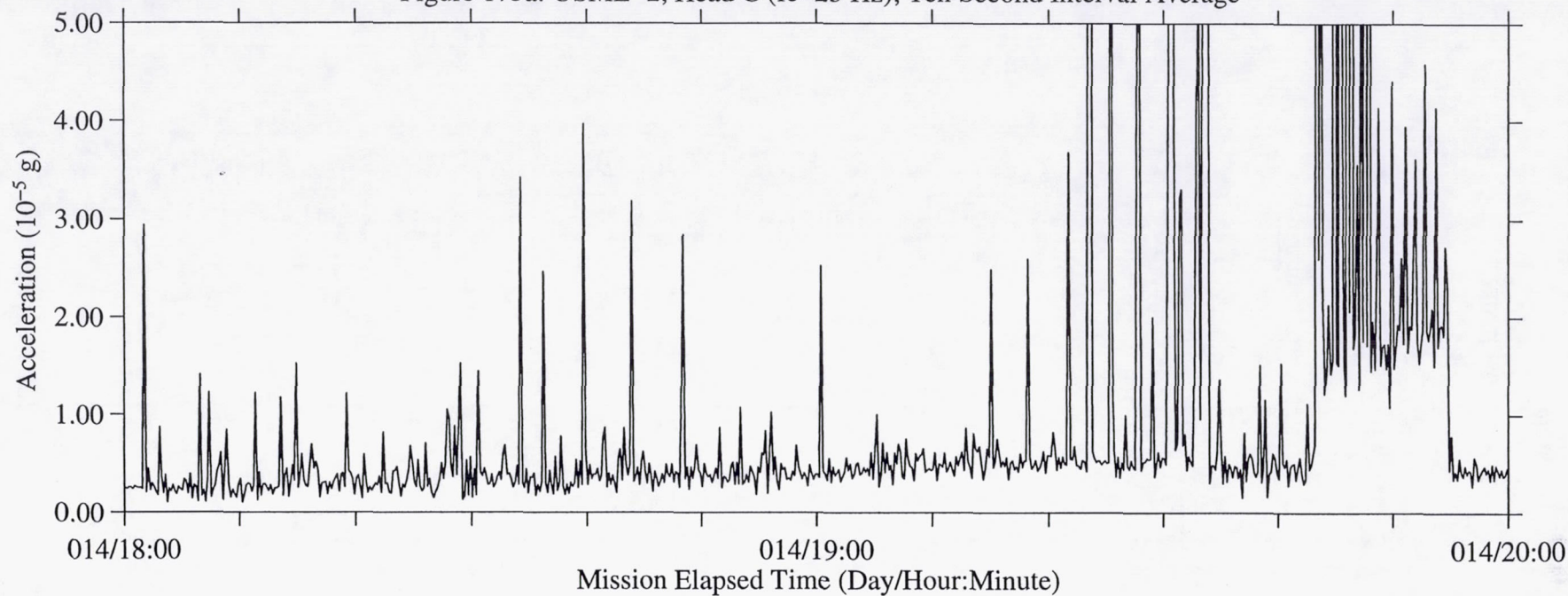


Figure 175b: USML-2, Head C (fc=25 Hz), Ten Second Interval RMS

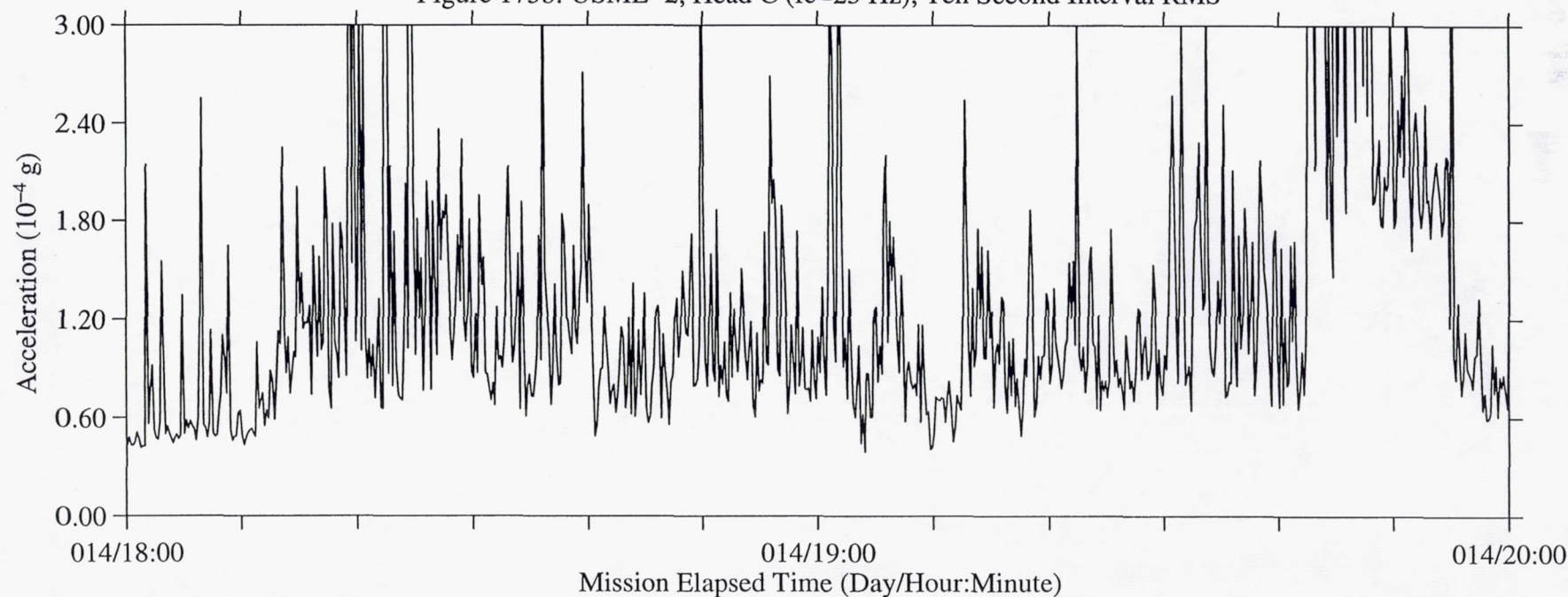


Figure 176a: USML-2, Head C (fc=25 Hz), Ten Second Interval Average

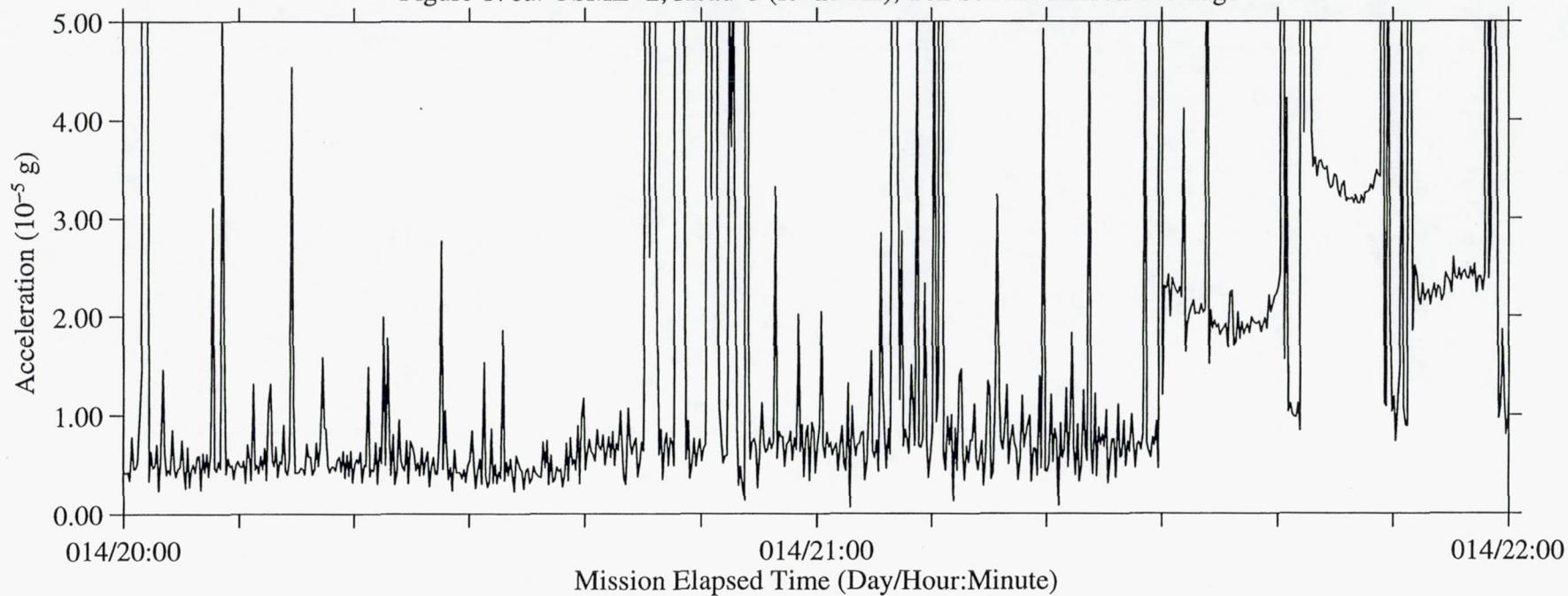


Figure 176b: USML-2, Head C (fc=25 Hz), Ten Second Interval RMS

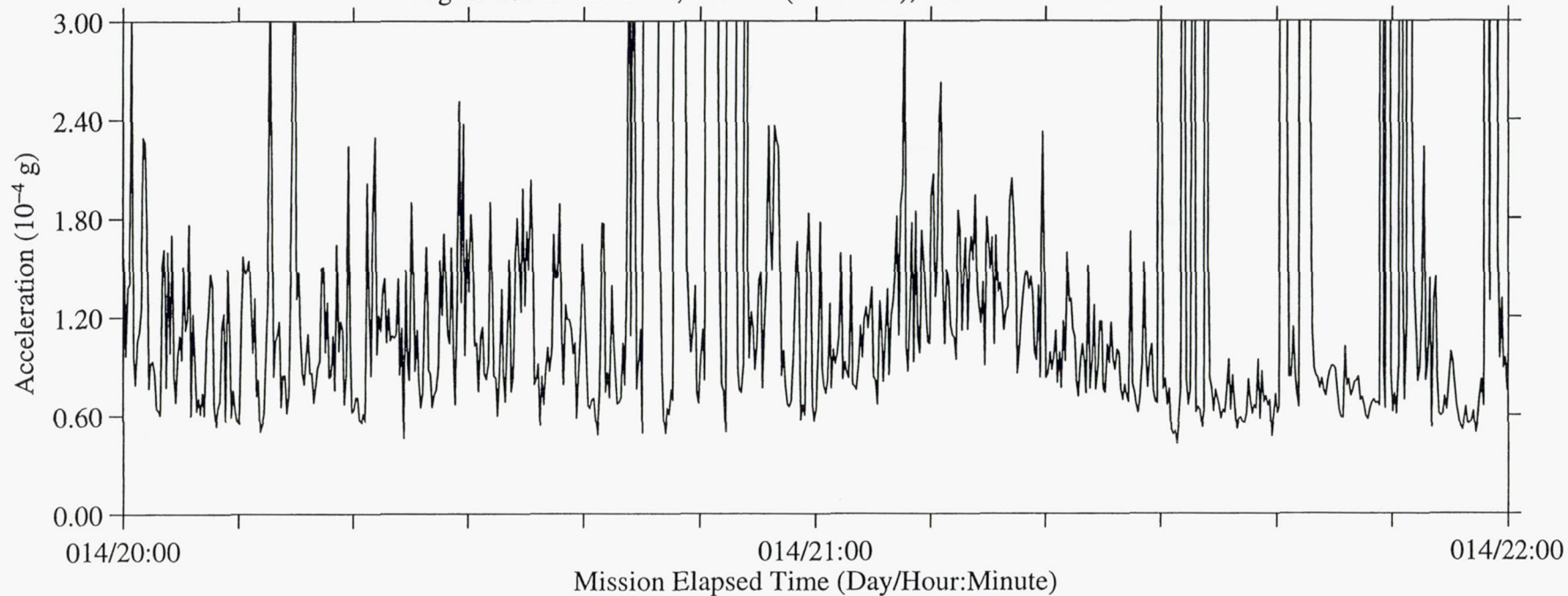




Figure 177a: USML-2, Head C (fc=25 Hz), Ten Second Interval Average

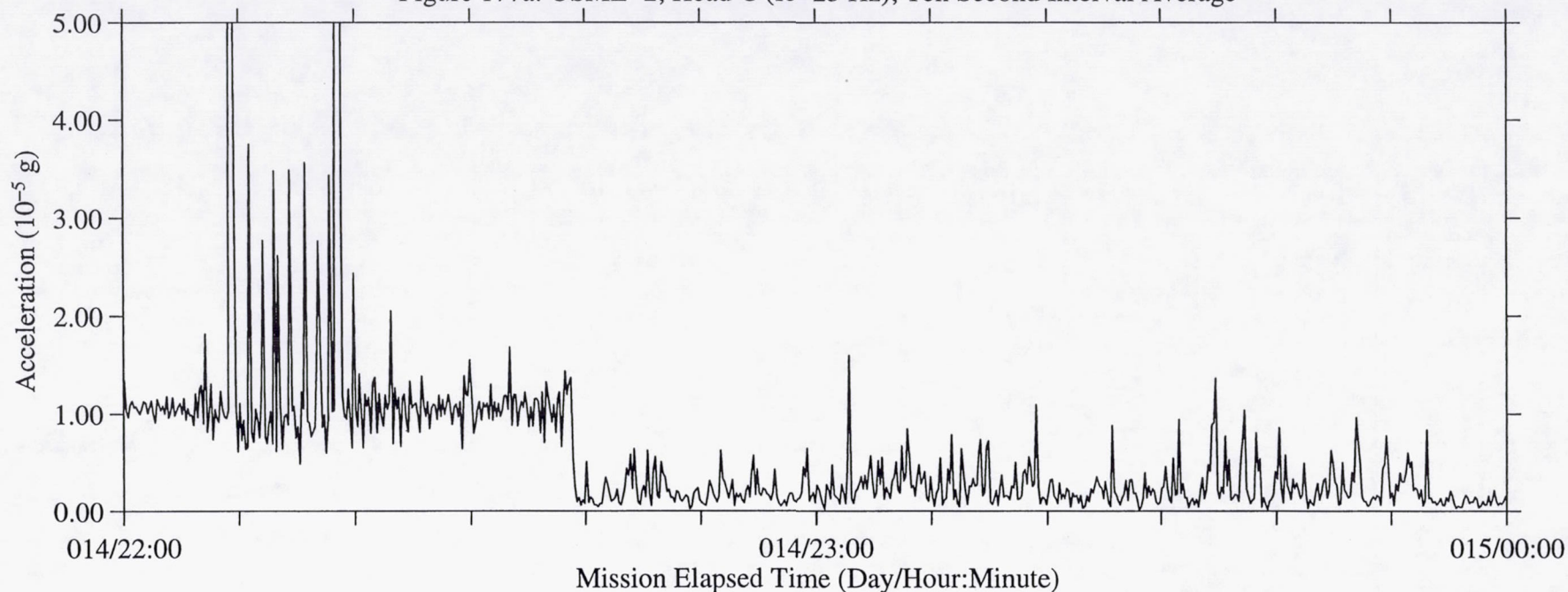


Figure 177b: USML-2, Head C (fc=25 Hz), Ten Second Interval RMS

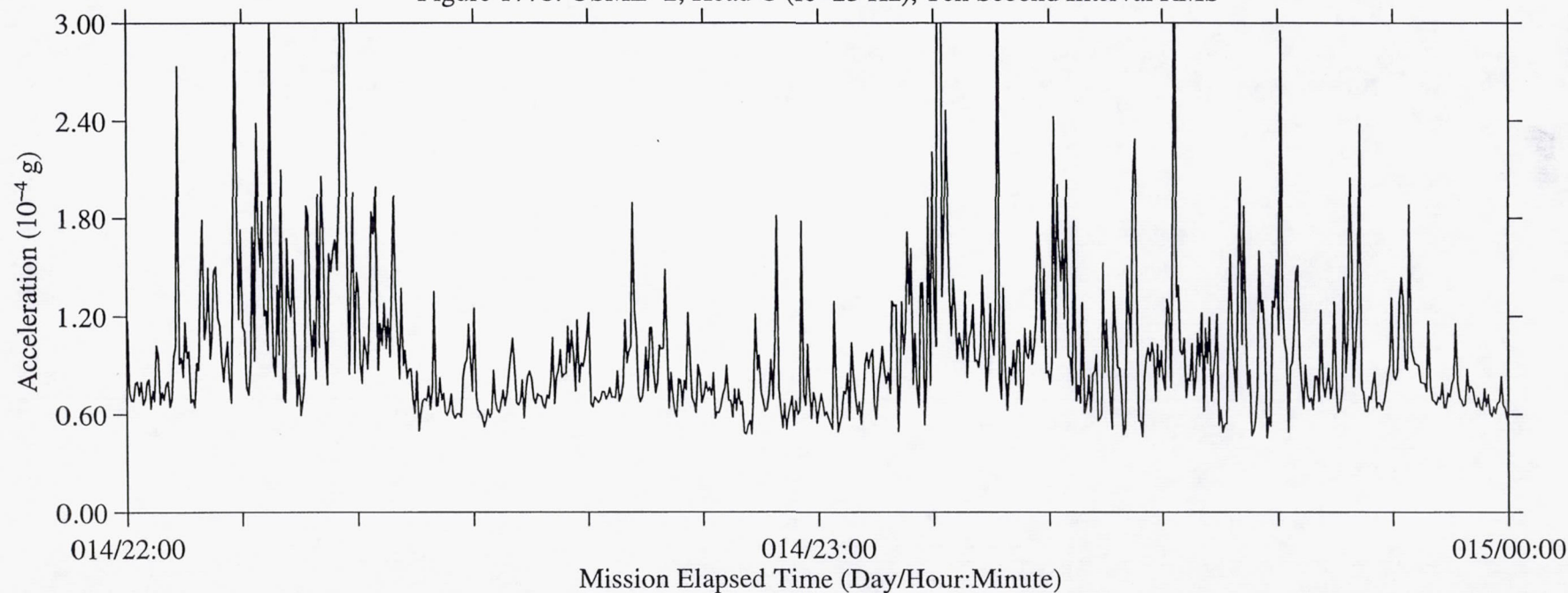


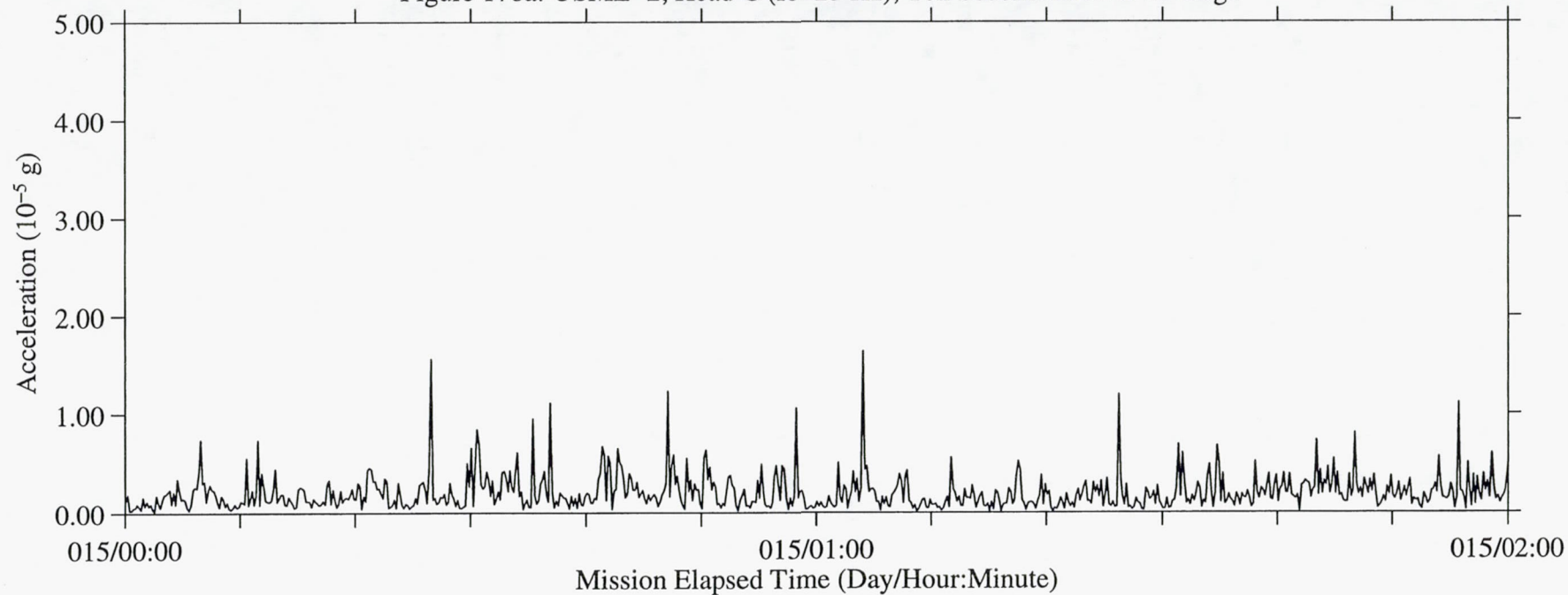
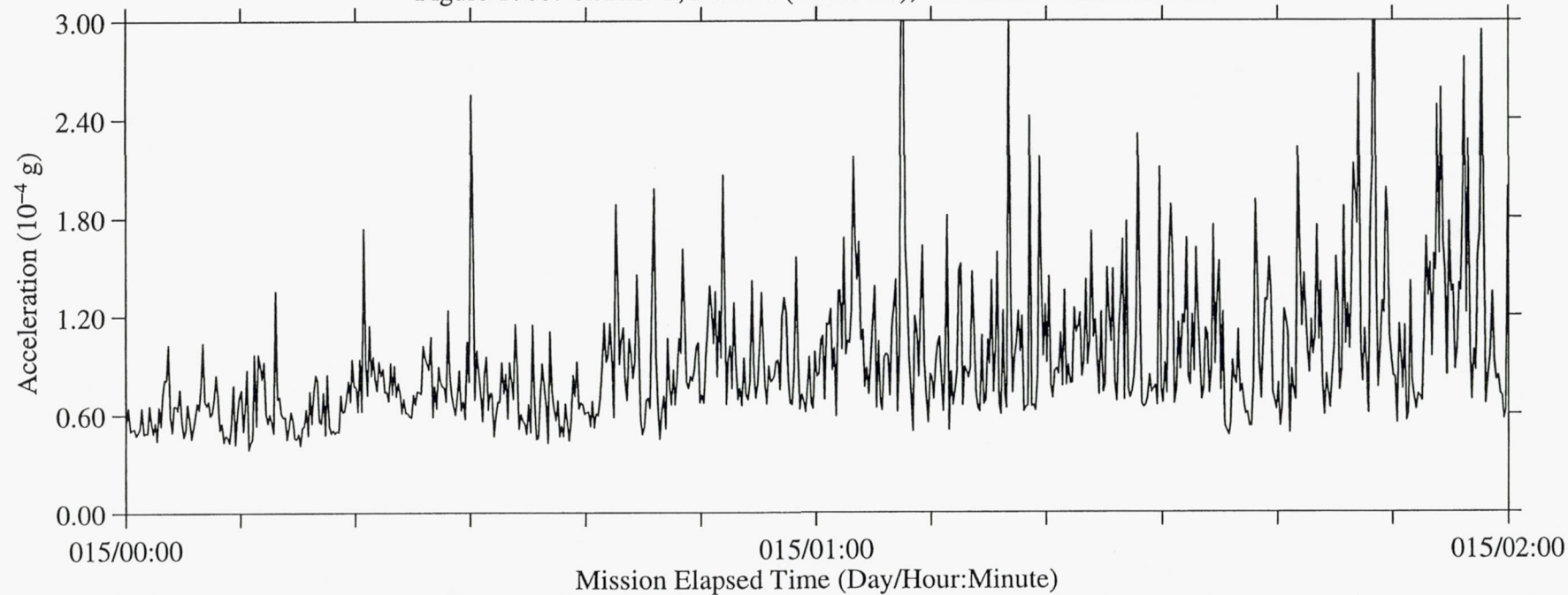
Figure 178a: USML-2, Head C ( $f_c=25$  Hz), Ten Second Interval AverageFigure 178b: USML-2, Head C ( $f_c=25$  Hz), Ten Second Interval RMS



Figure 179a: USML-2, Head C (fc=25 Hz), Ten Second Interval Average

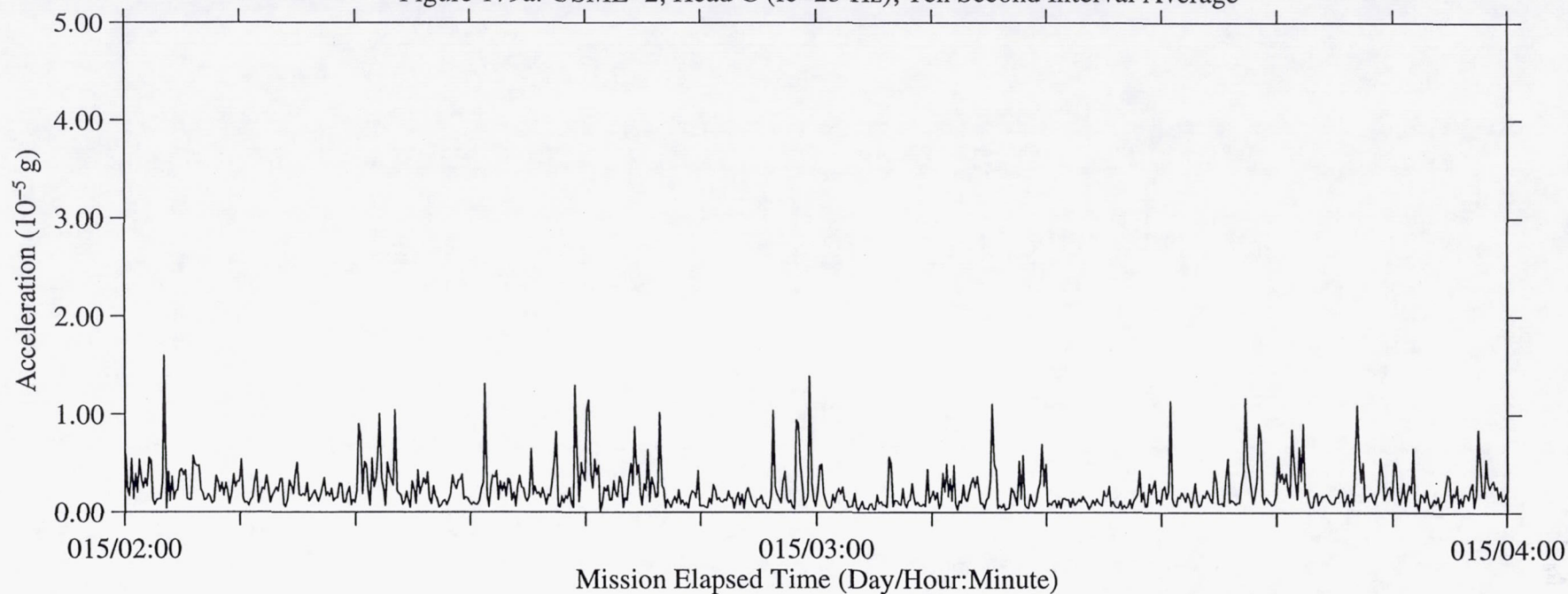


Figure 179b: USML-2, Head C (fc=25 Hz), Ten Second Interval RMS

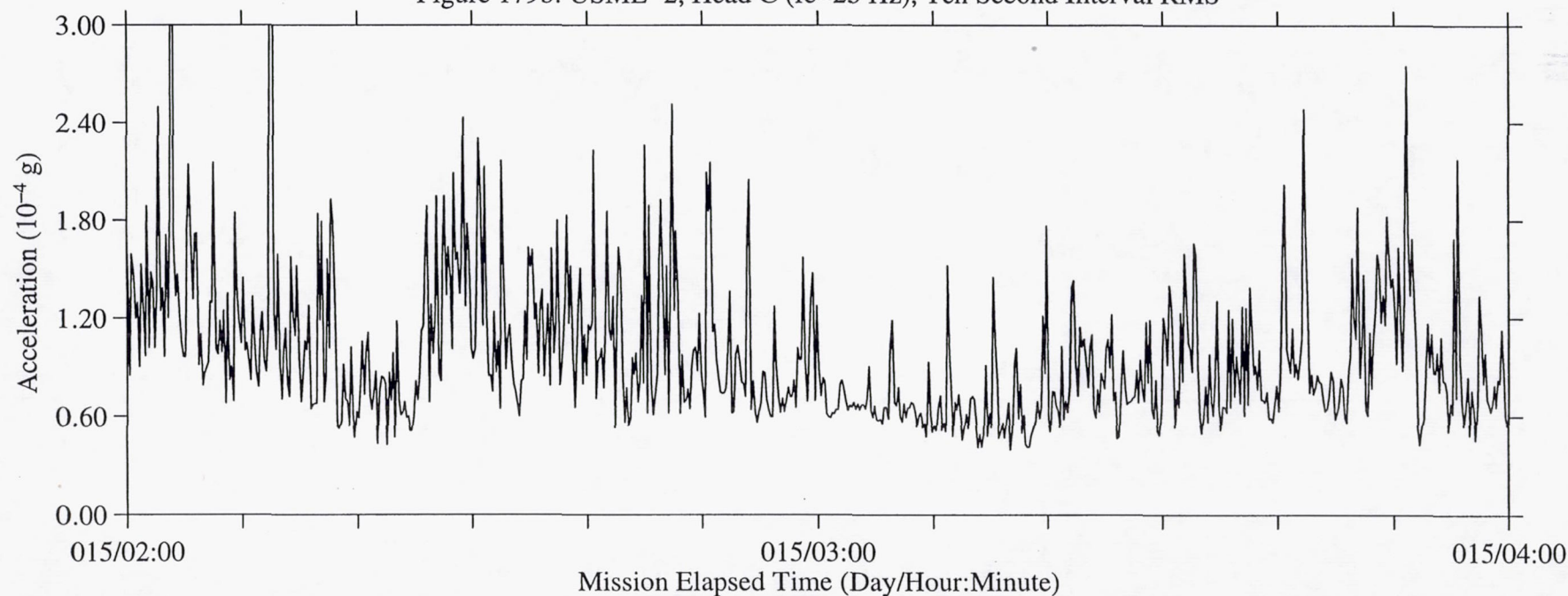


Figure 180a: USML-2, Head C (fc=25 Hz), Ten Second Interval Average

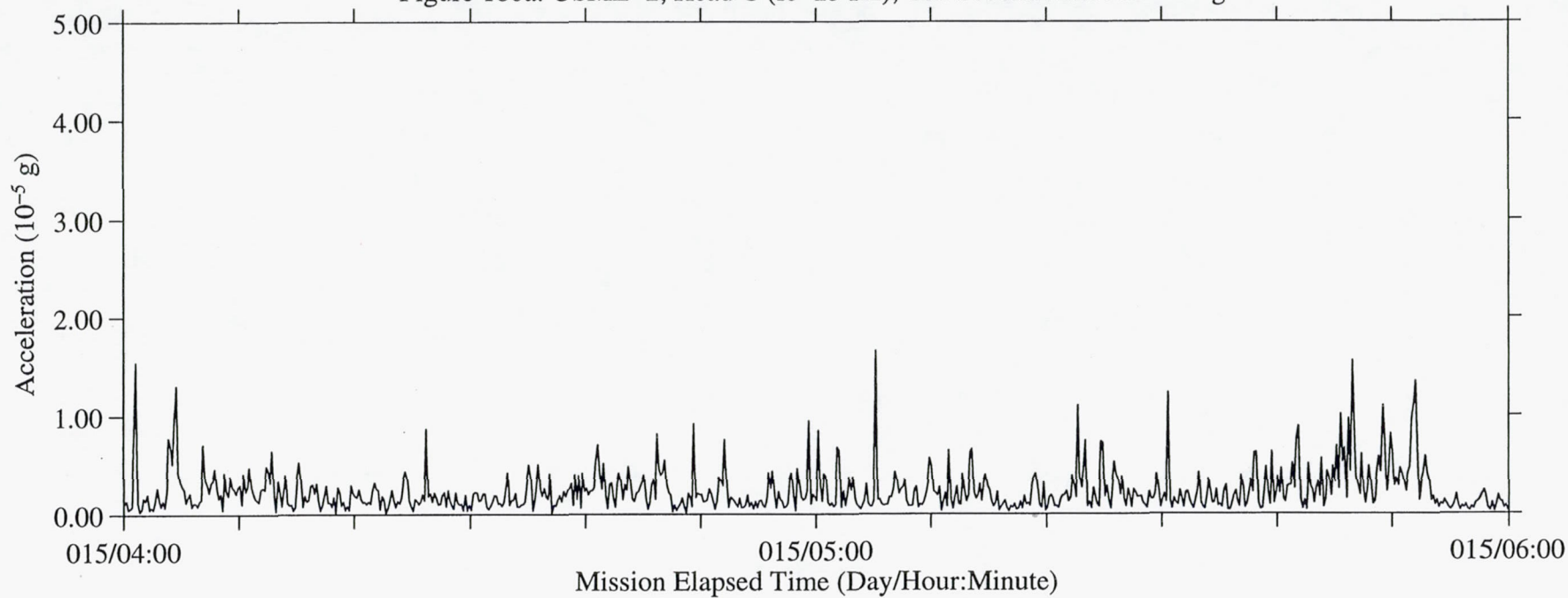


Figure 180b: USML-2, Head C (fc=25 Hz), Ten Second Interval RMS

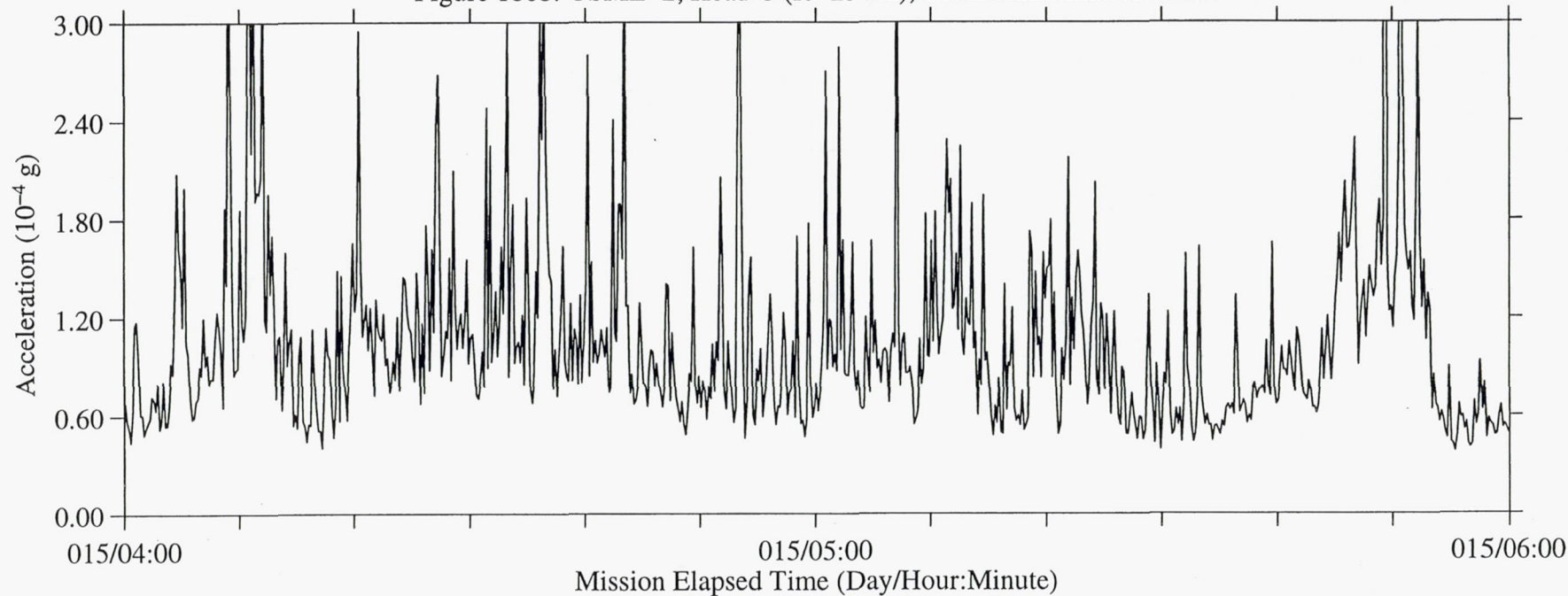




Figure 181a: USML-2, Head C (fc=25 Hz), Ten Second Interval Average

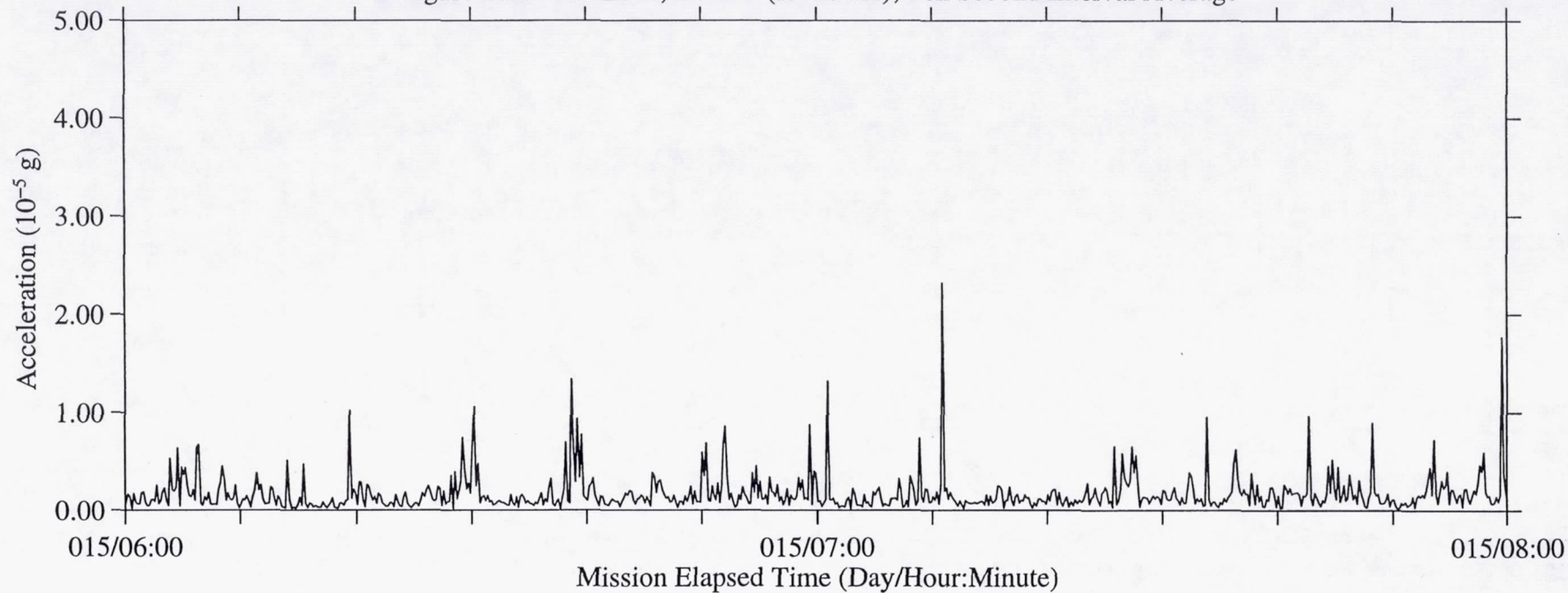


Figure 181b: USML-2, Head C (fc=25 Hz), Ten Second Interval RMS

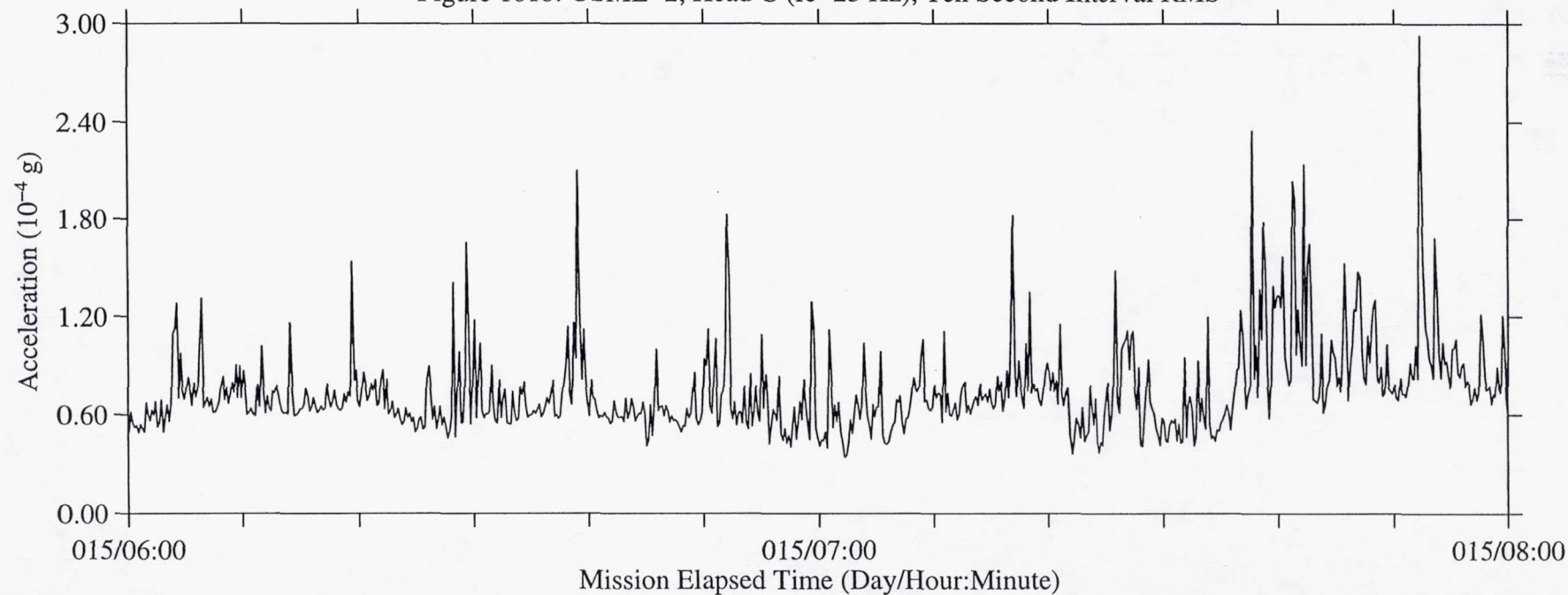


Figure 182a: USML-2, Head C (fc=25 Hz), Ten Second Interval Average

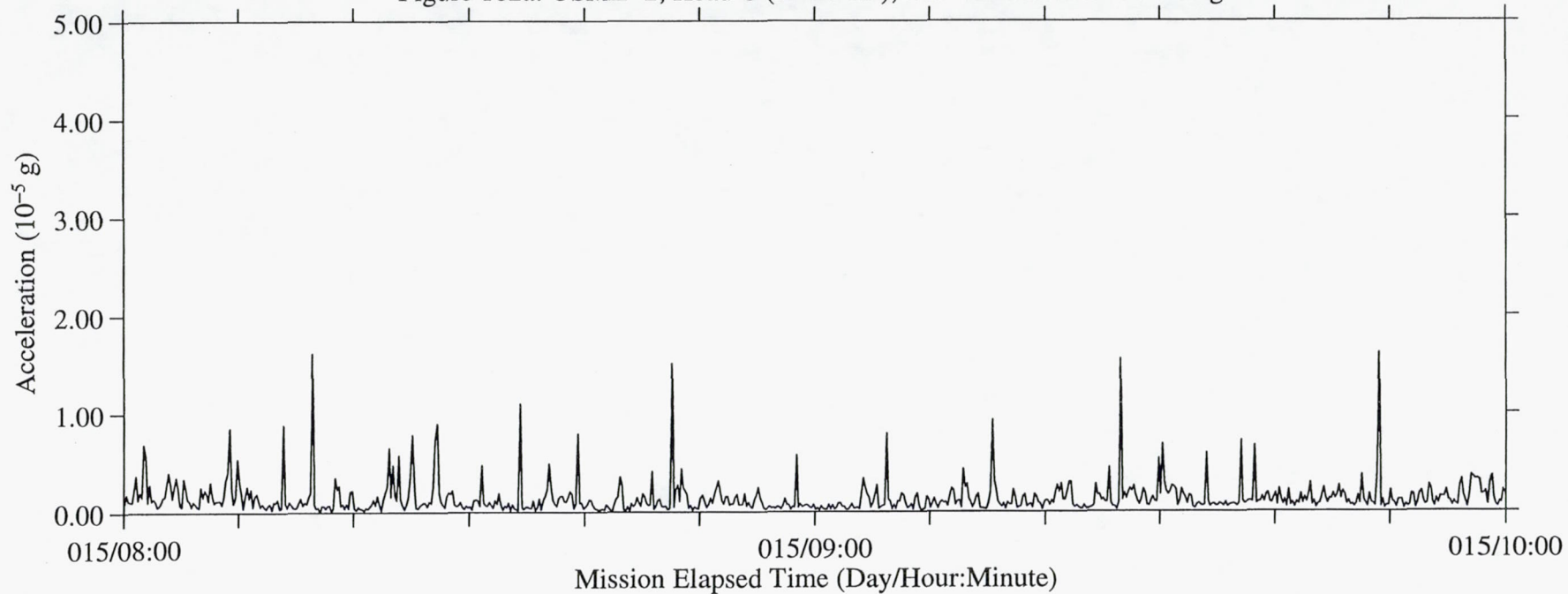


Figure 182b: USML-2, Head C (fc=25 Hz), Ten Second Interval RMS

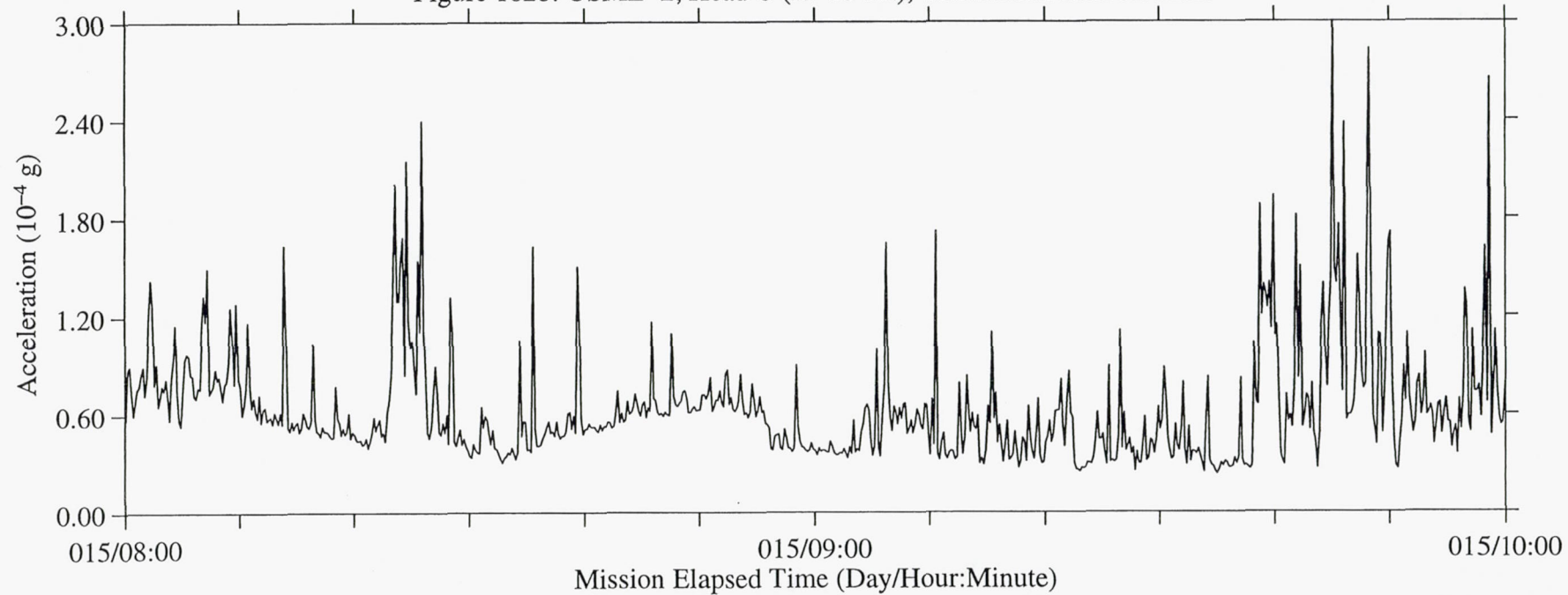




Figure 183a: USML-2, Head C (fc=25 Hz), Ten Second Interval Average

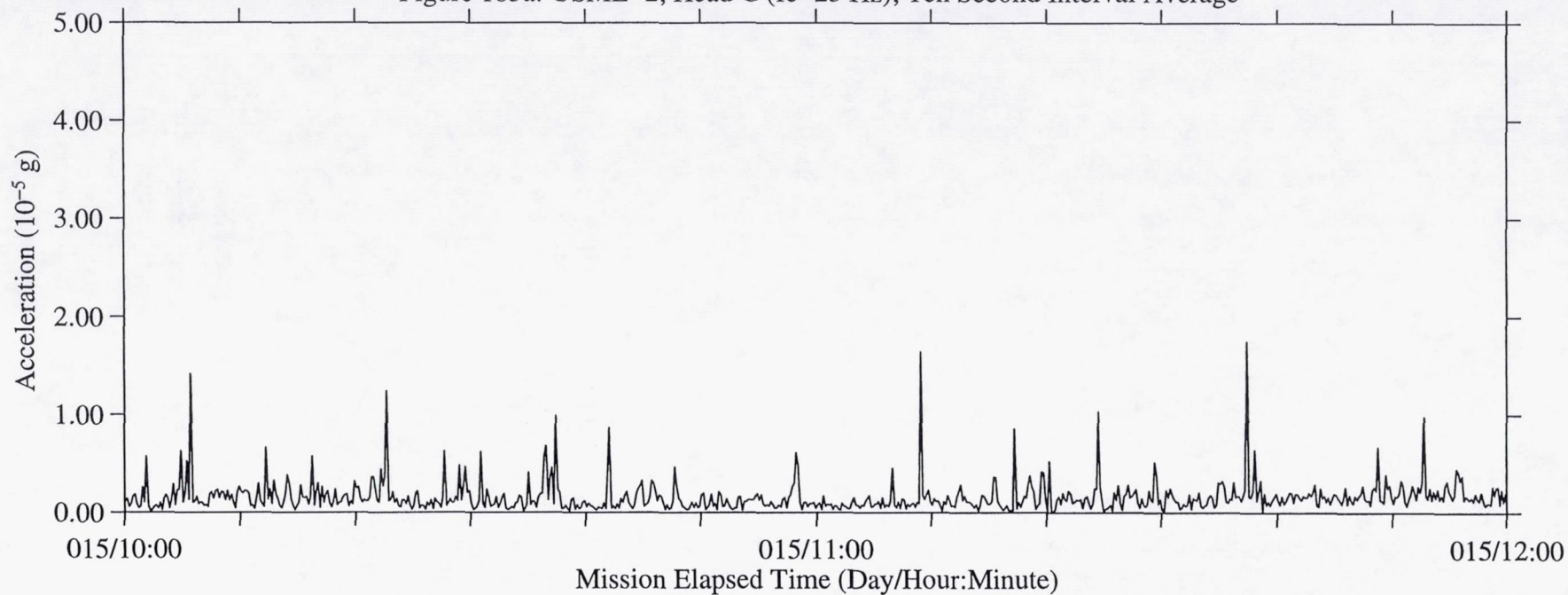


Figure 183b: USML-2, Head C (fc=25 Hz), Ten Second Interval RMS

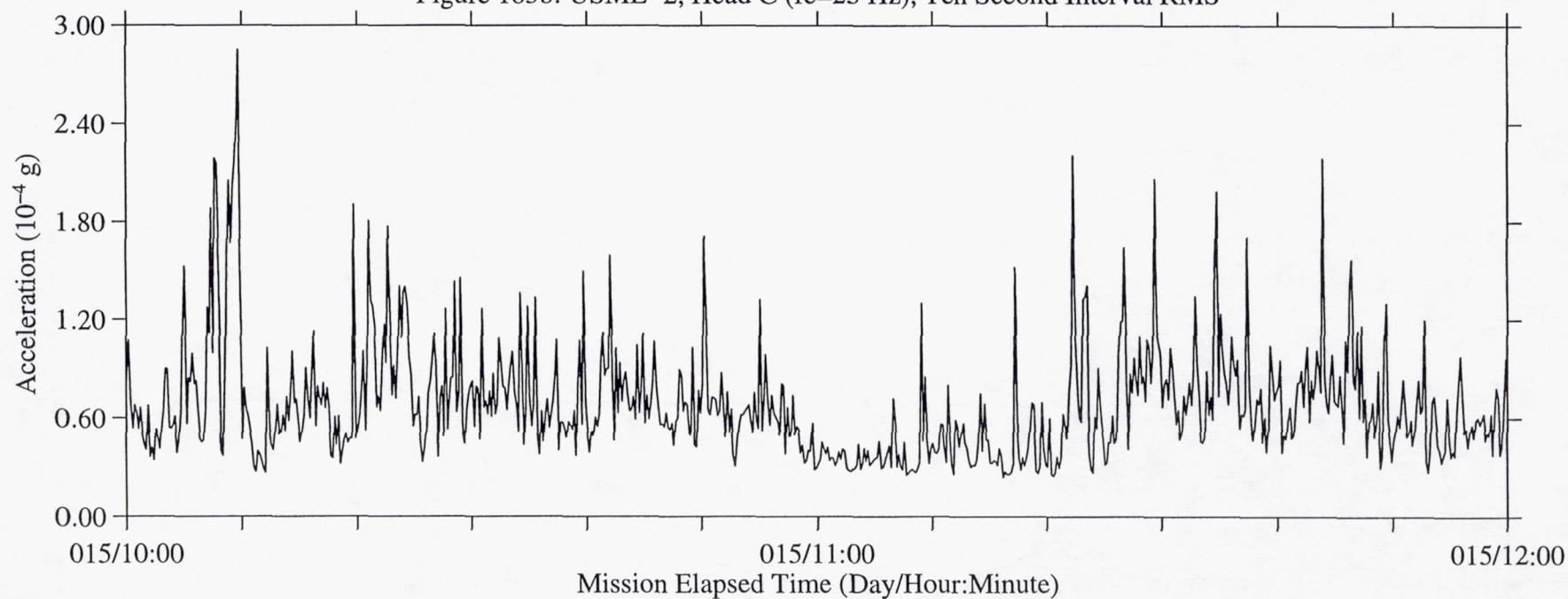


Figure 184a: USML-2, Head C (fc=25 Hz), Ten Second Interval Average

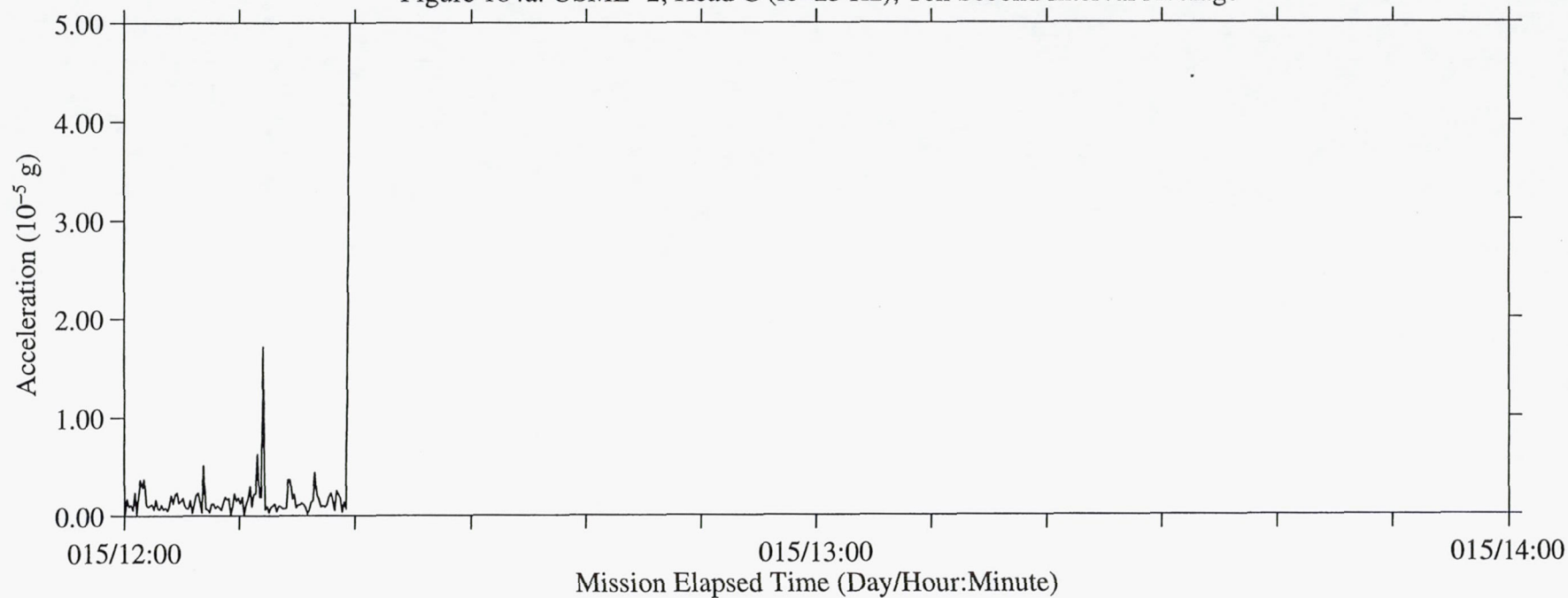
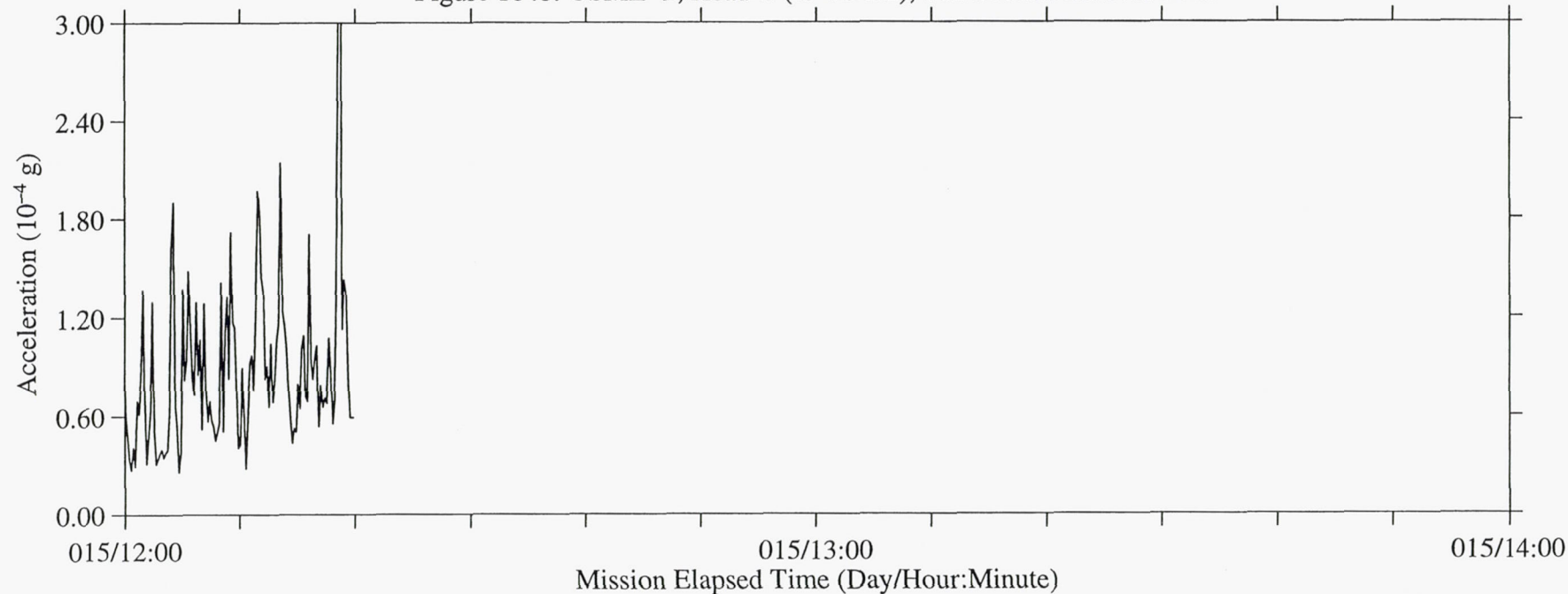


Figure 184b: USML-2, Head C (fc=25 Hz), Ten Second Interval RMS





## Appendix C SAMS Color Spectrograms

The SAMS data have been further processed to produce the plots shown here. Color spectrograms are used to show how the microgravity environment varies in intensity with respect to both the time and frequency domains. These spectrograms are provided as an overview of the frequency characteristics of the SAMS data during the mission. Each spectrogram is a composite of two-hour's worth of data. The time resolution used to compute the spectrograms seen here is 16.384 seconds. This corresponds to a frequency resolution of 0.0610 Hz.

The spectrograms contained herein differ from those spectrograms produced for PIMS mission summary reports prior to January 1996. Previous spectrograms utilized a colormap which had 8 colors. The new spectrograms contain 64 colors. Thus, the magnitude resolution (as represented by the color) shows a significant improvement. Care should be taken to not confuse the current colormap system with that used in reports prior to January 1996. For example, in previous spectrograms, yellow represented a higher magnitude than did red. The new colormap system is opposite when it comes to the yellow-red relation. The user is advised to refer to the colormap key located next to each spectrogram plot.

In order to produce the spectrogram image, Power Spectral Densities (PSDs) were computed for successive time intervals (the length of the interval is equal to the time resolution). For the PSD computation, a boxcar window was applied. In order to combine all three axes into a single plot to show an overall level, a Vector-Magnitude (VM) operation was performed.

Stated mathematically:  $VM = \sqrt{PSD_{x_k}^2 + PSD_{y_k}^2 + PSD_{z_k}^2}$ .

By imaging the base 10 logarithm ( $\log_{10}$ ) magnitude as a color and stacking successive PSDs from left to right, variations of acceleration magnitude and frequency are shown as a function of time. Colors are assigned to discrete magnitude ranges, so that there are 64 colors assigned to the entire range of magnitudes shown. Data which fall outside of the maximum and minimum magnitude limits will be imaged as either the highest or lowest magnitude, depending on which side they have saturated. For this report, 0.01% of the total points lie below the lower limit, and 0.25% of the total points lie above the upper limit. If an area of interest seems to be saturated, care should be taken in that the actual values may lie above or below the color mapping shown on the plot.

Plot gaps (if any exist) are shown by either white or dark blue areas on the page. Care should be taken to not mistake a plot gap (represented by a dark blue vertical band) with a quiet period. If a plot gap exists for an entire plot (or series of successive plots), a comment is placed on the page to let the user know there is a gap in the data. These "no data available" comments will not show exact times for which the data are not available, but will only indicate missing plots.

Due to the nature of spectrograms, care should be taken to not merely read a color's numeric value as being the "amount" of acceleration that is present at a given frequency. In order to get this type of information, the PSDs must be integrated between two frequencies. These frequencies (lower and upper) form the "band" of interest

$$g_{\text{RMS}} = \int_{f_1}^{f_2} \text{PSD} \cdot df.$$

The result of this integration is the  $g_{\text{RMS}}$  acceleration level in the  $[f_{\text{lower}}, f_{\text{upper}}]$  band.

The PIMS group is able to provide this type of analysis on a per-request basis. To request this additional analysis, send an e-mail to [pims@lerc.nasa.gov](mailto:pims@lerc.nasa.gov), or FAX a request to (216) 433-8545.



Figure 1: USML-2, Head C (fc=25 Hz)

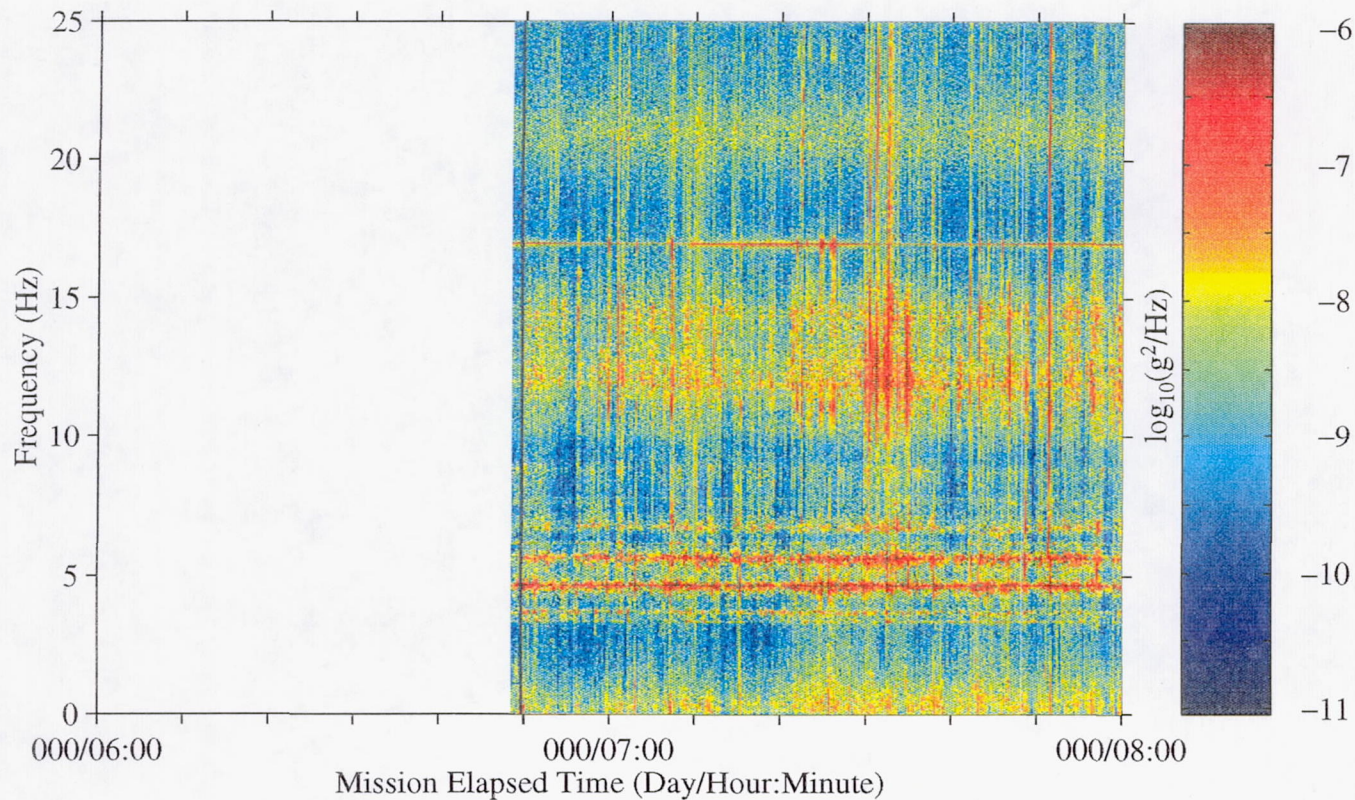


Figure 2: USML-2, Head C (fc=25 Hz)

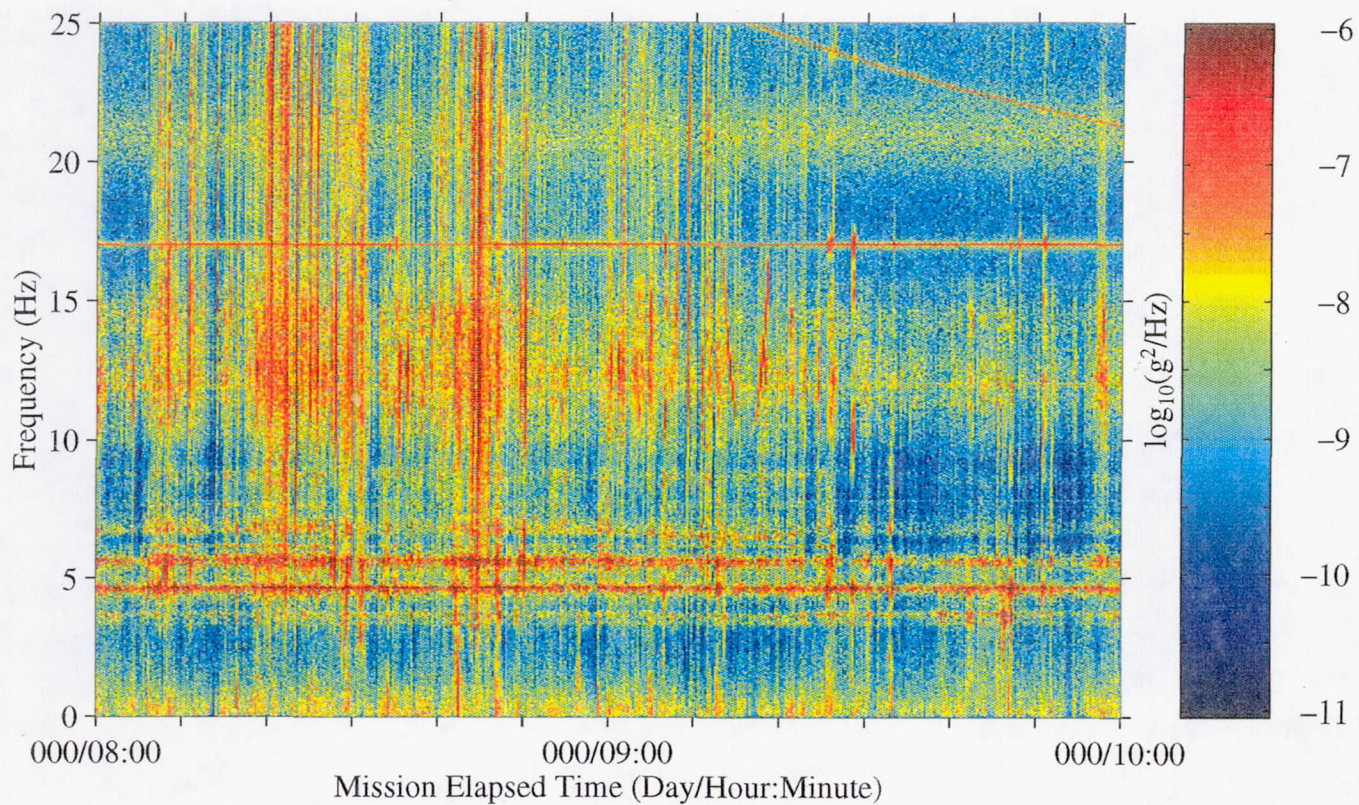




Figure 3: USML-2, Head C (fc=25 Hz)

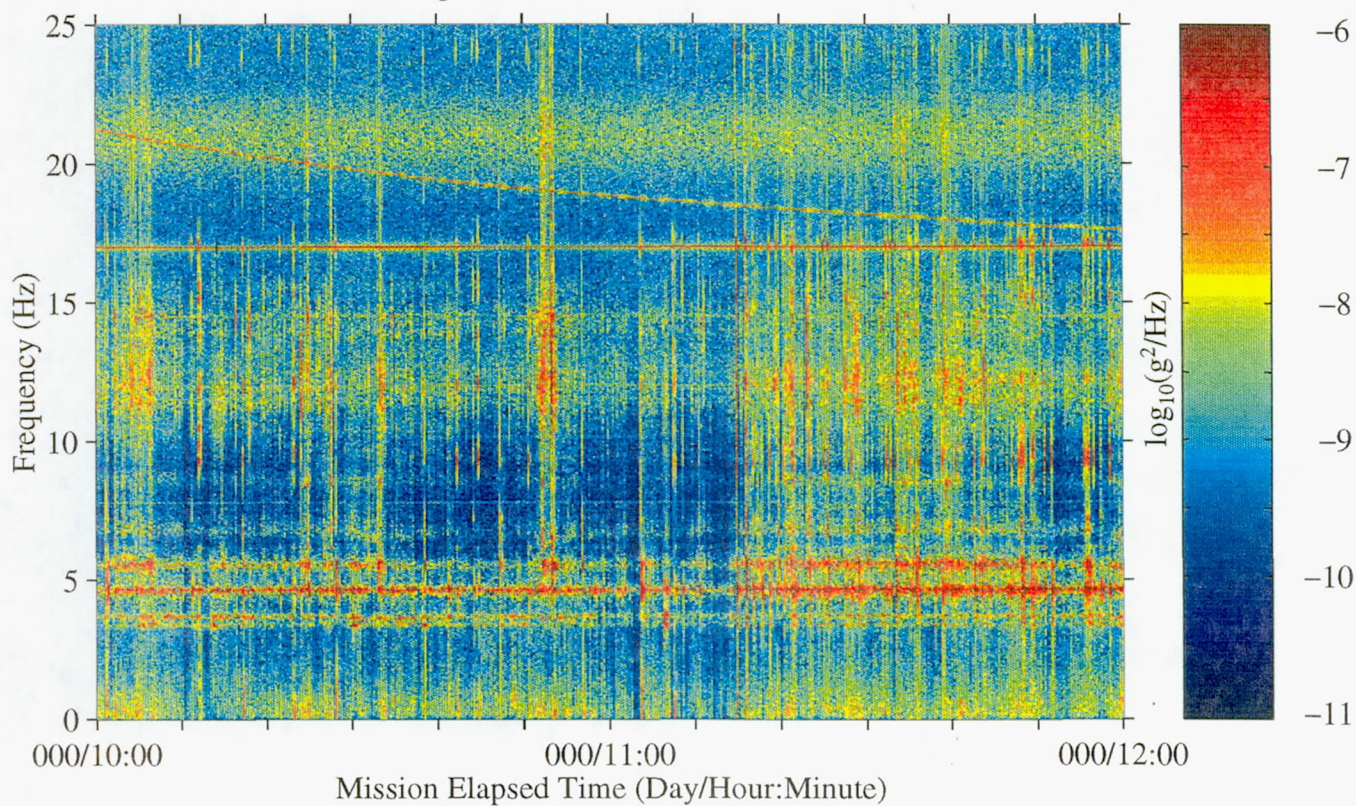


Figure 4: USML-2, Head C (fc=25 Hz)

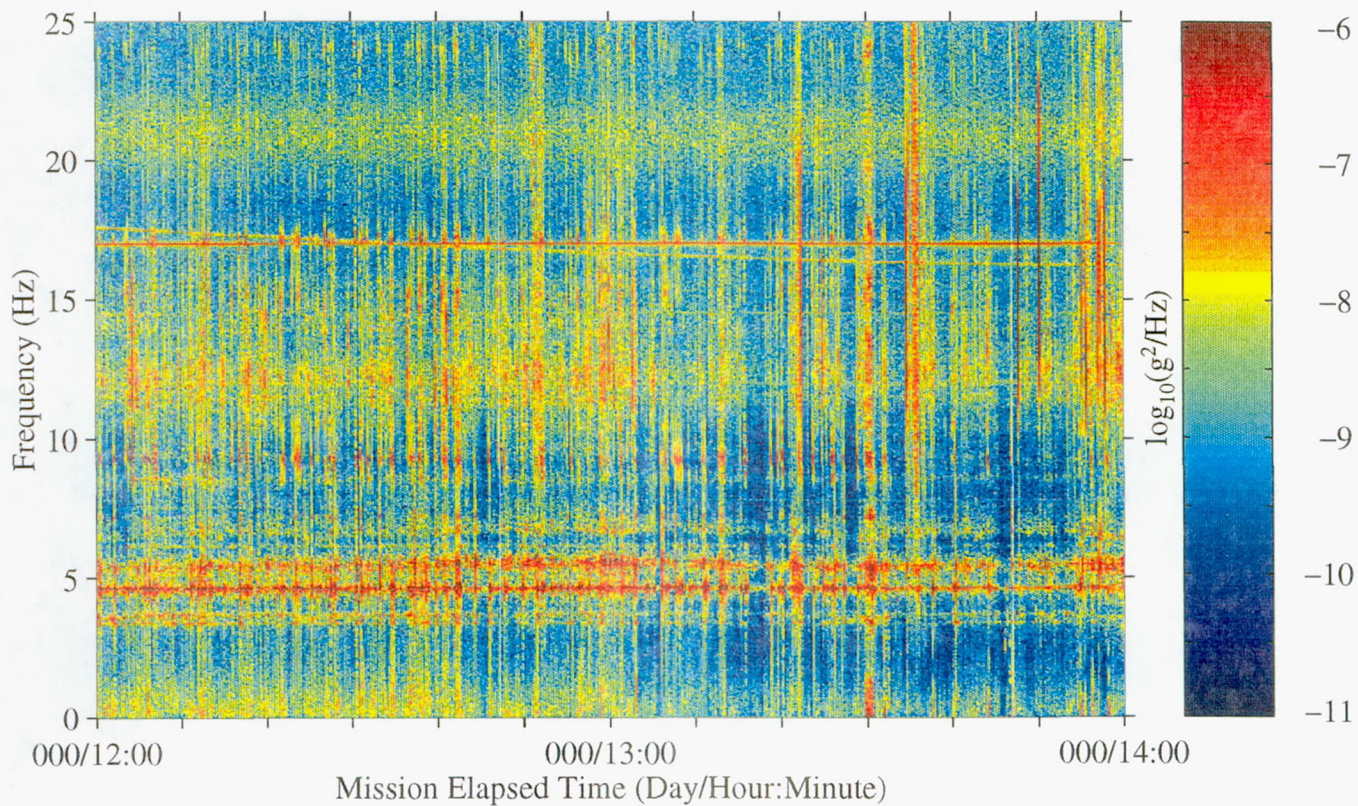




Figure 5: USML-2, Head C (fc=25 Hz)

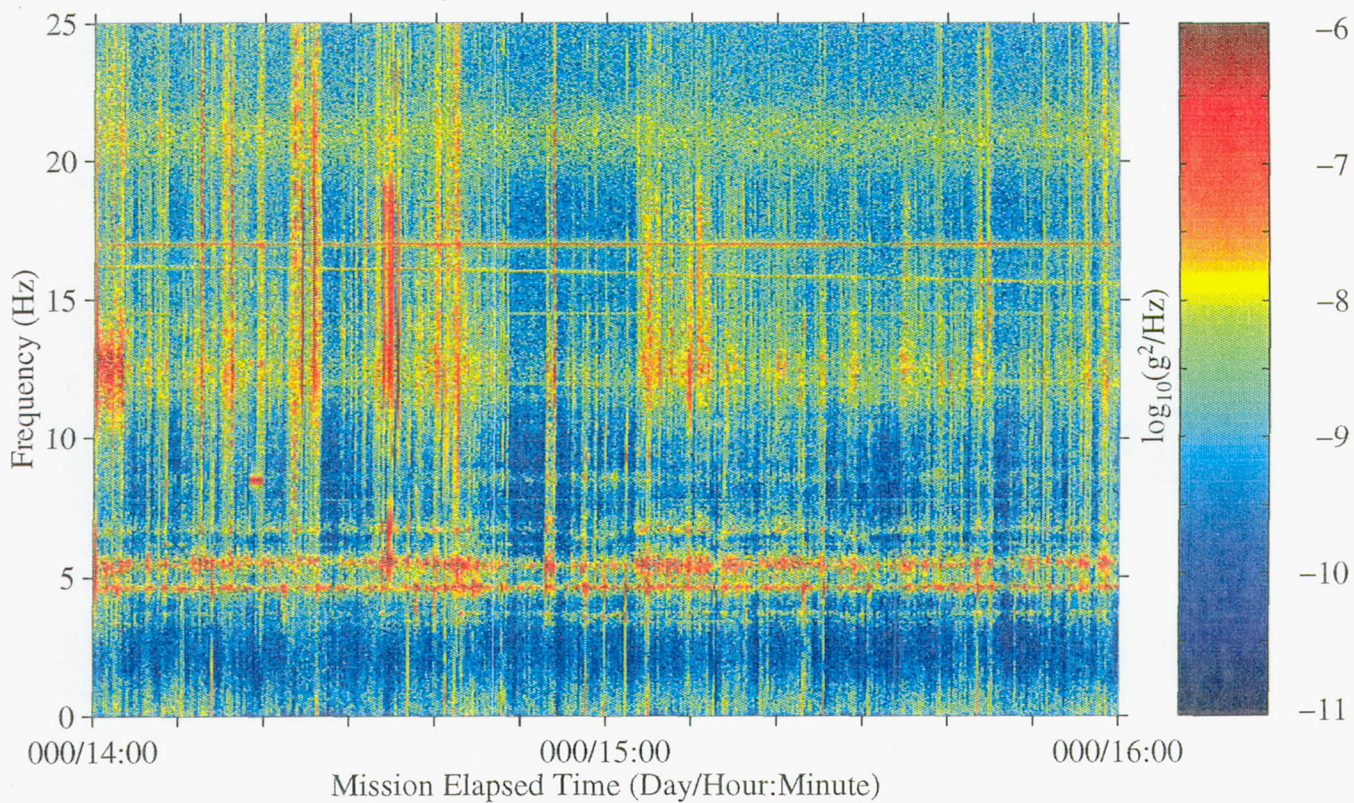


Figure 6: USML-2, Head C (fc=25 Hz)

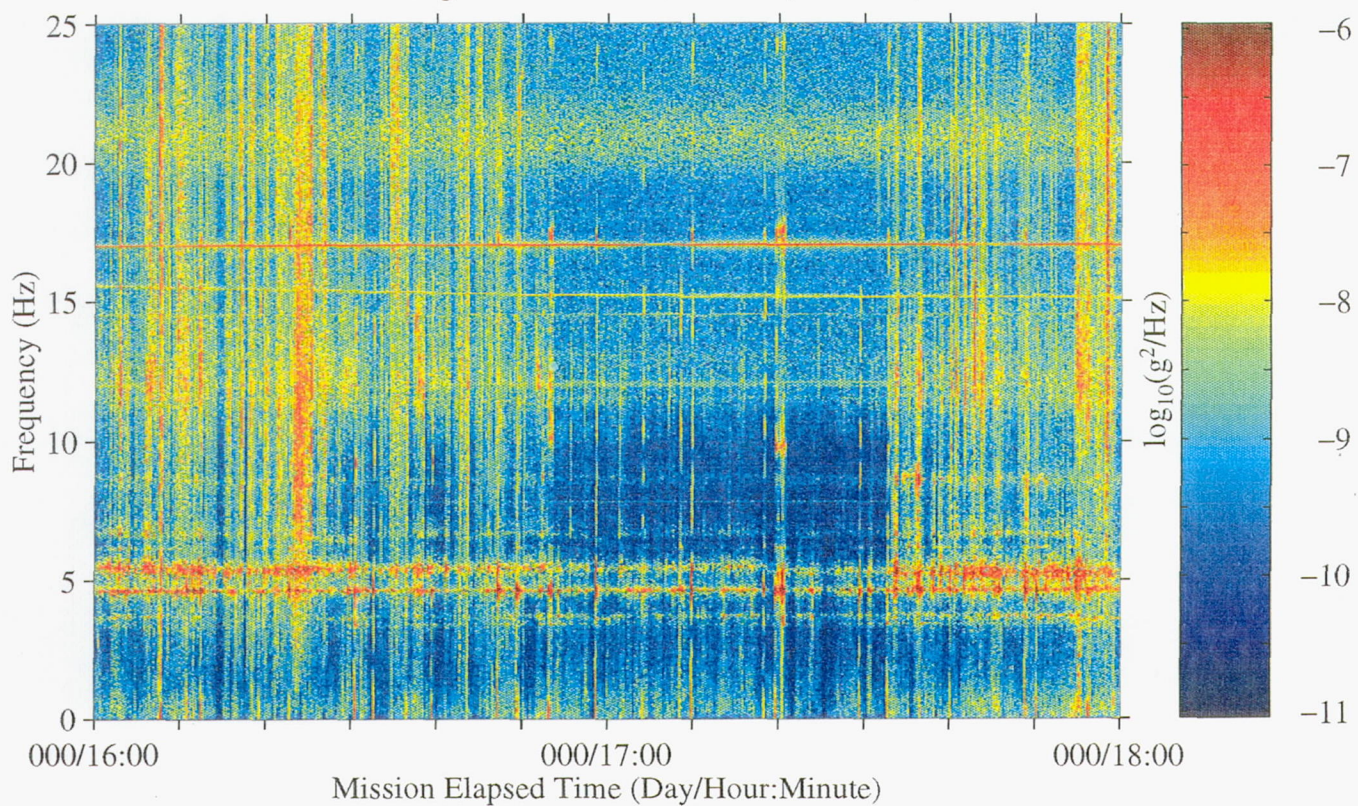




Figure 7: USML-2, Head C (fc=25 Hz)

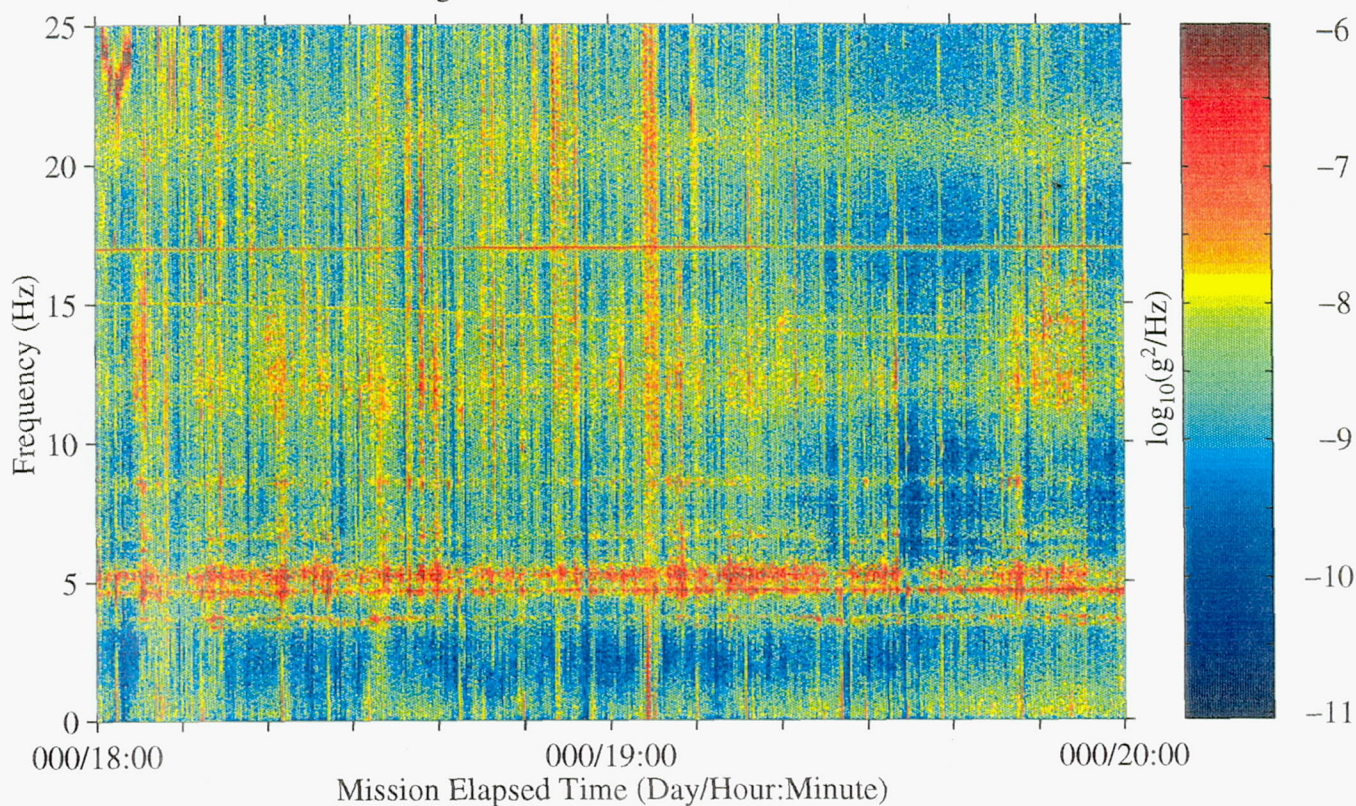


Figure 8: USML-2, Head C (fc=25 Hz)

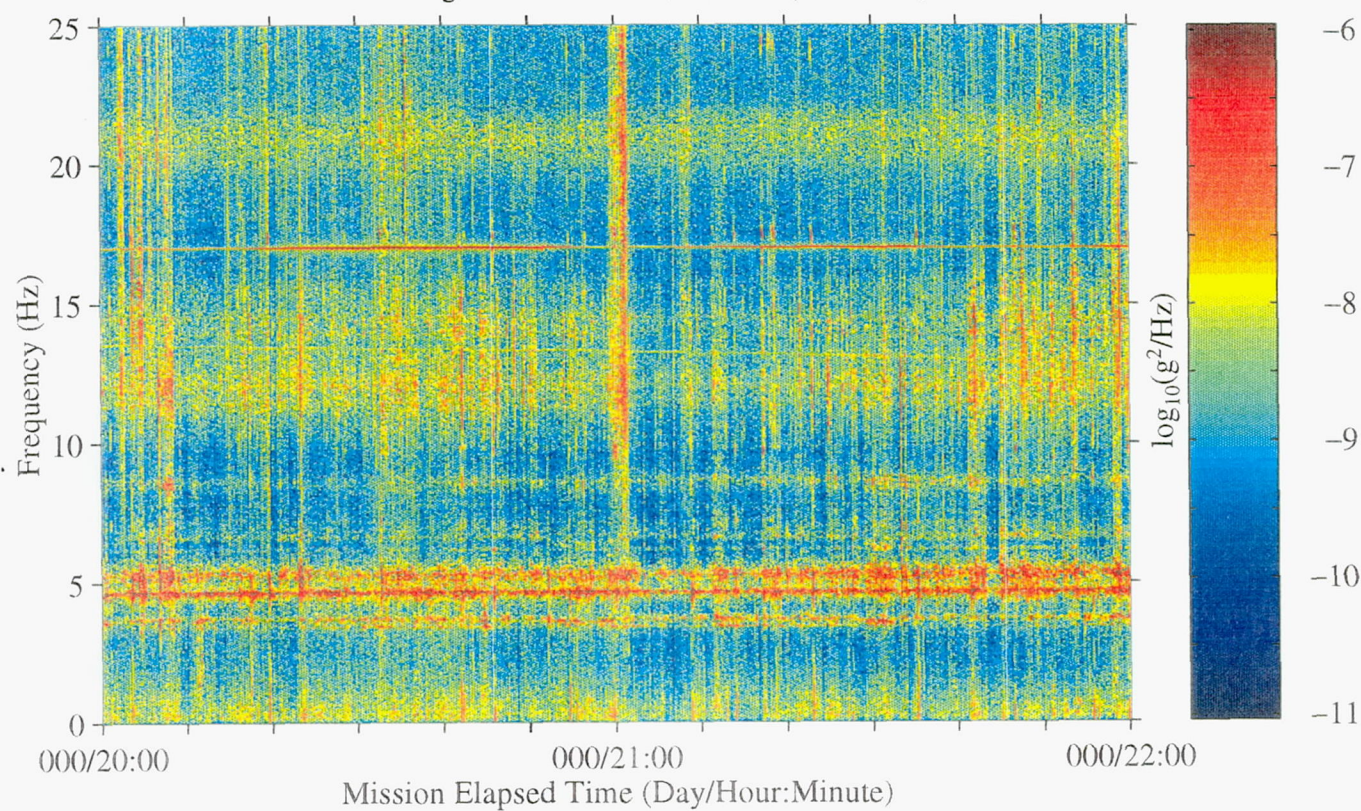




Figure 9: USML-2, Head C (fc=25 Hz)

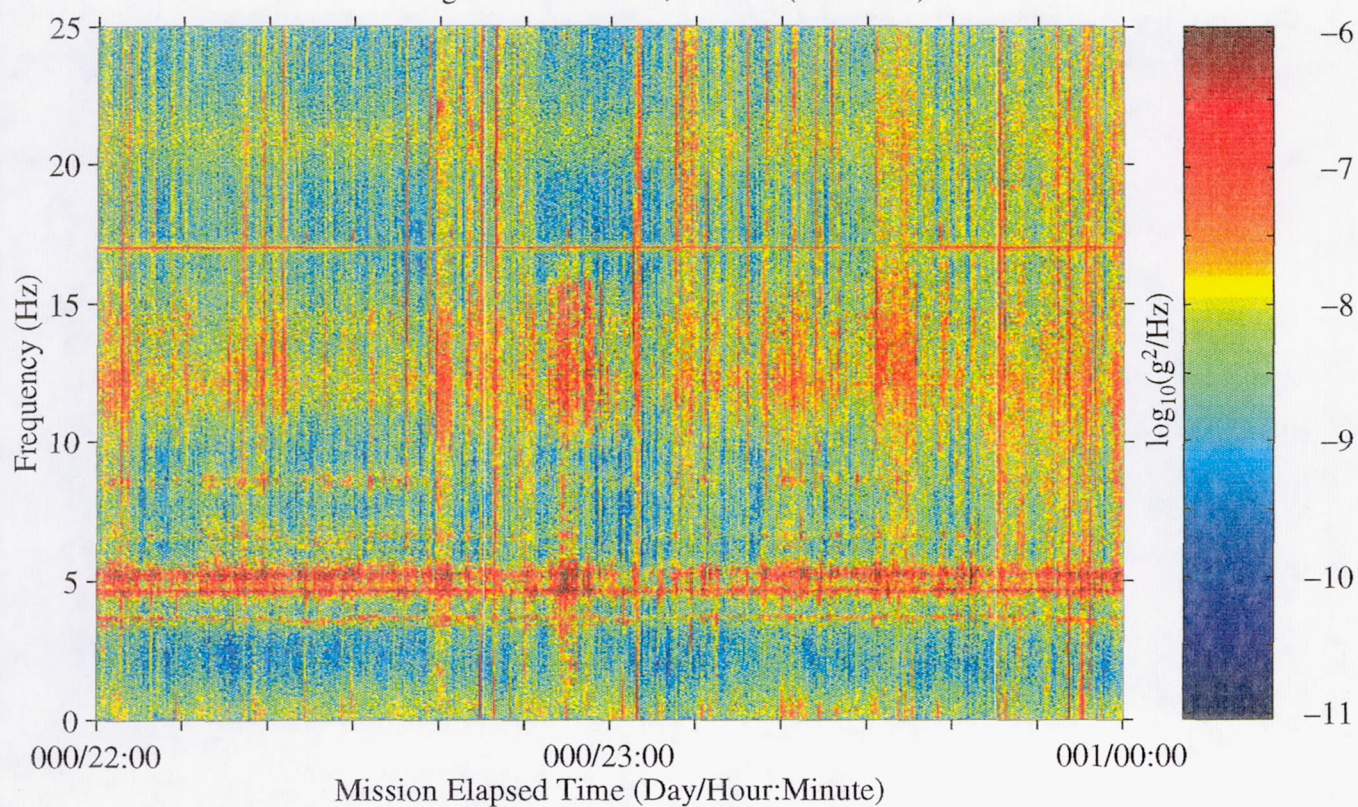


Figure 10: USML-2, Head C (fc=25 Hz)

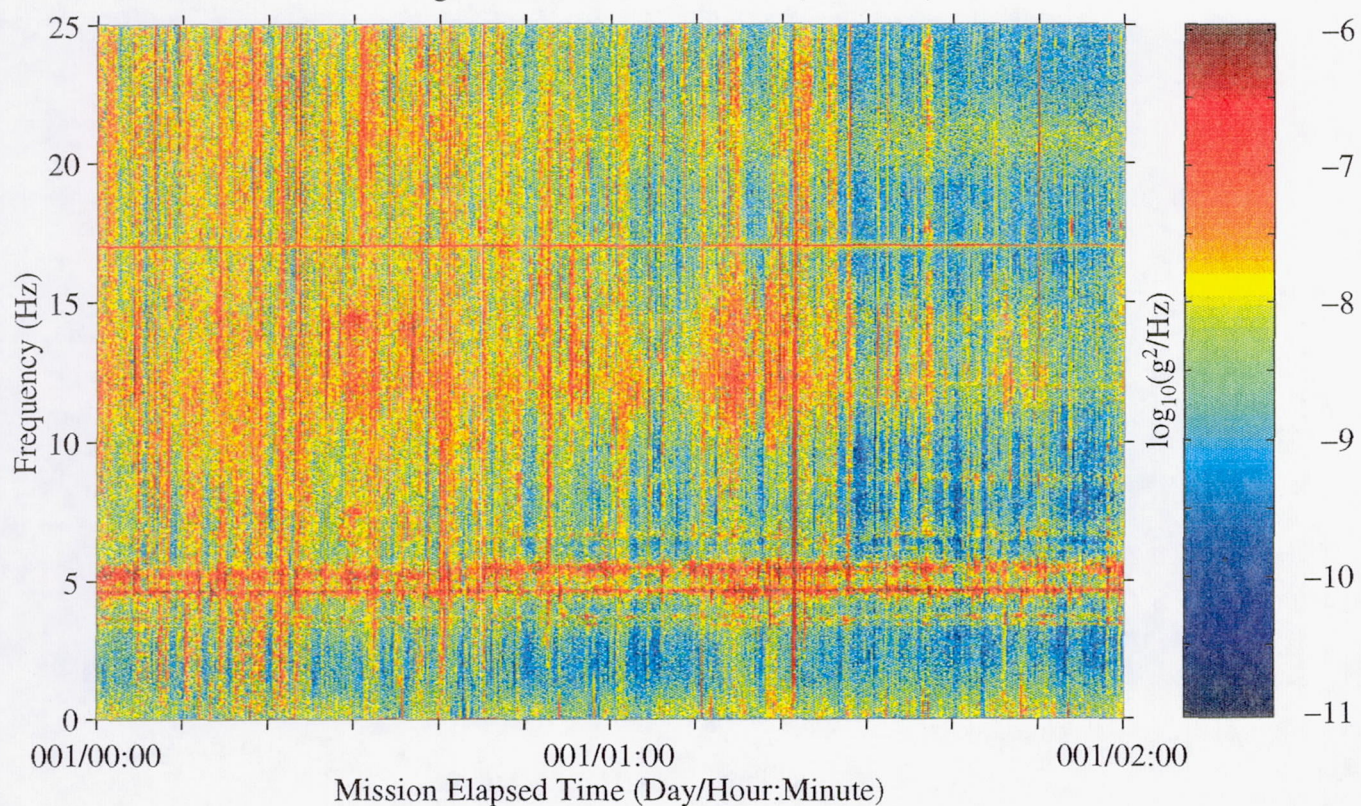




Figure 11: USML-2, Head C (fc=25 Hz)

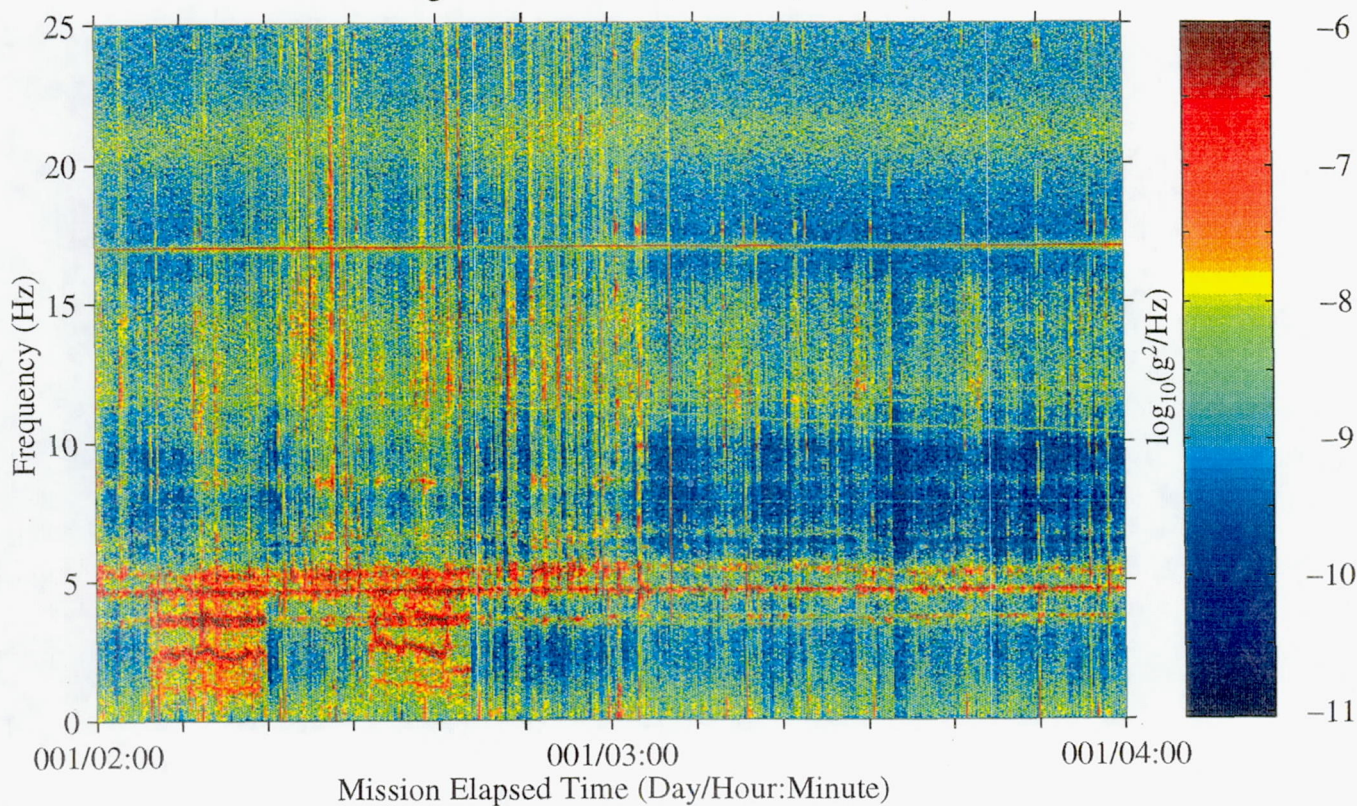


Figure 12: USML-2, Head C (fc=25 Hz)

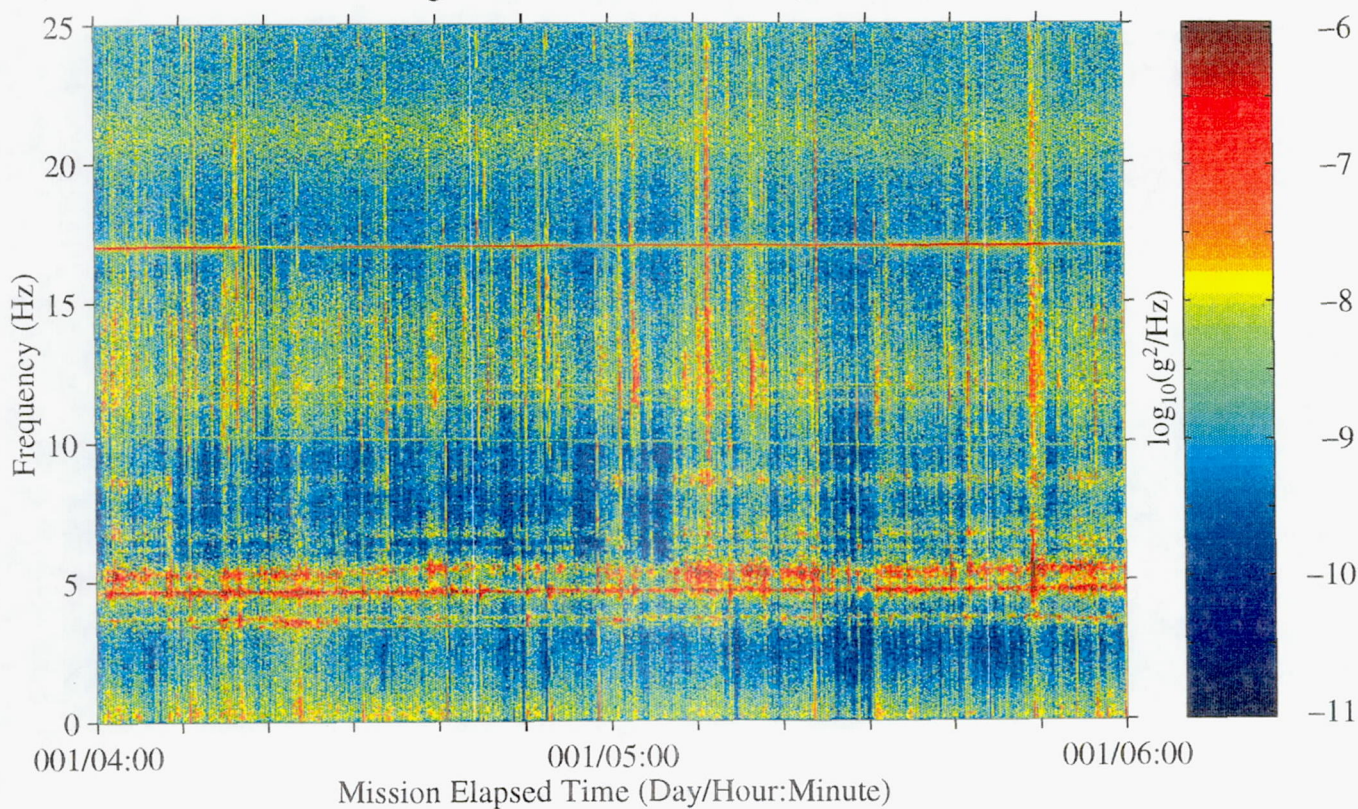




Figure 13: USML-2, Head C (fc=25 Hz)

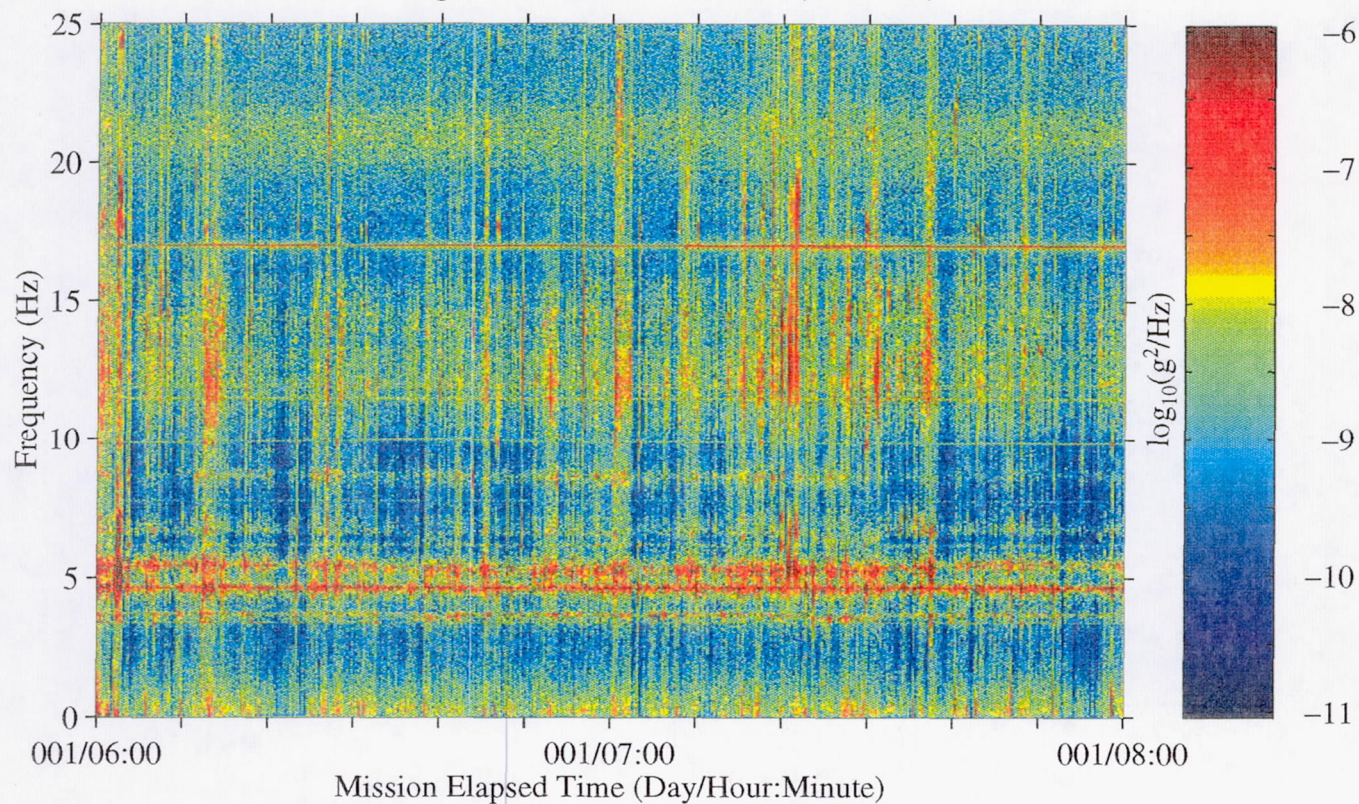


Figure 14: USML-2, Head C (fc=25 Hz)

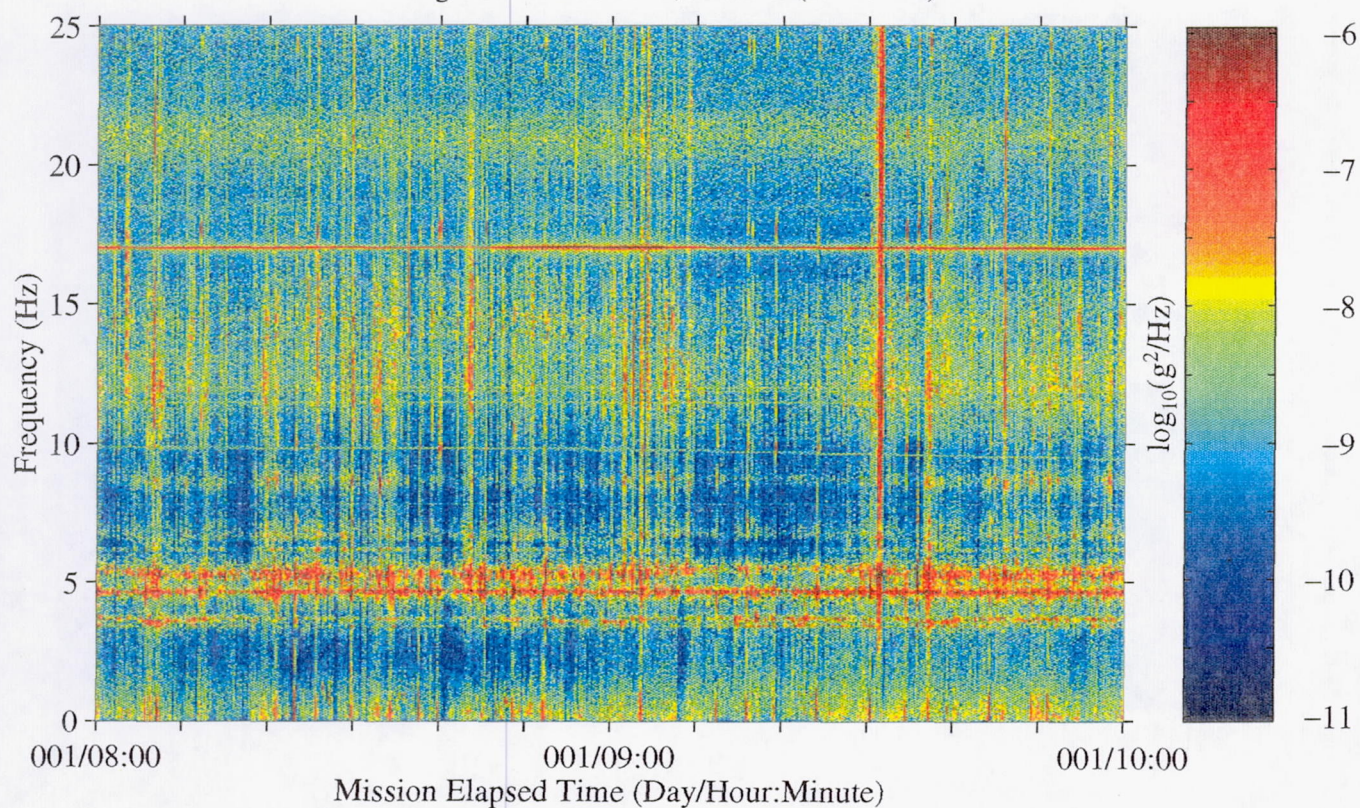




Figure 15: USML-2, Head C (fc=25 Hz)

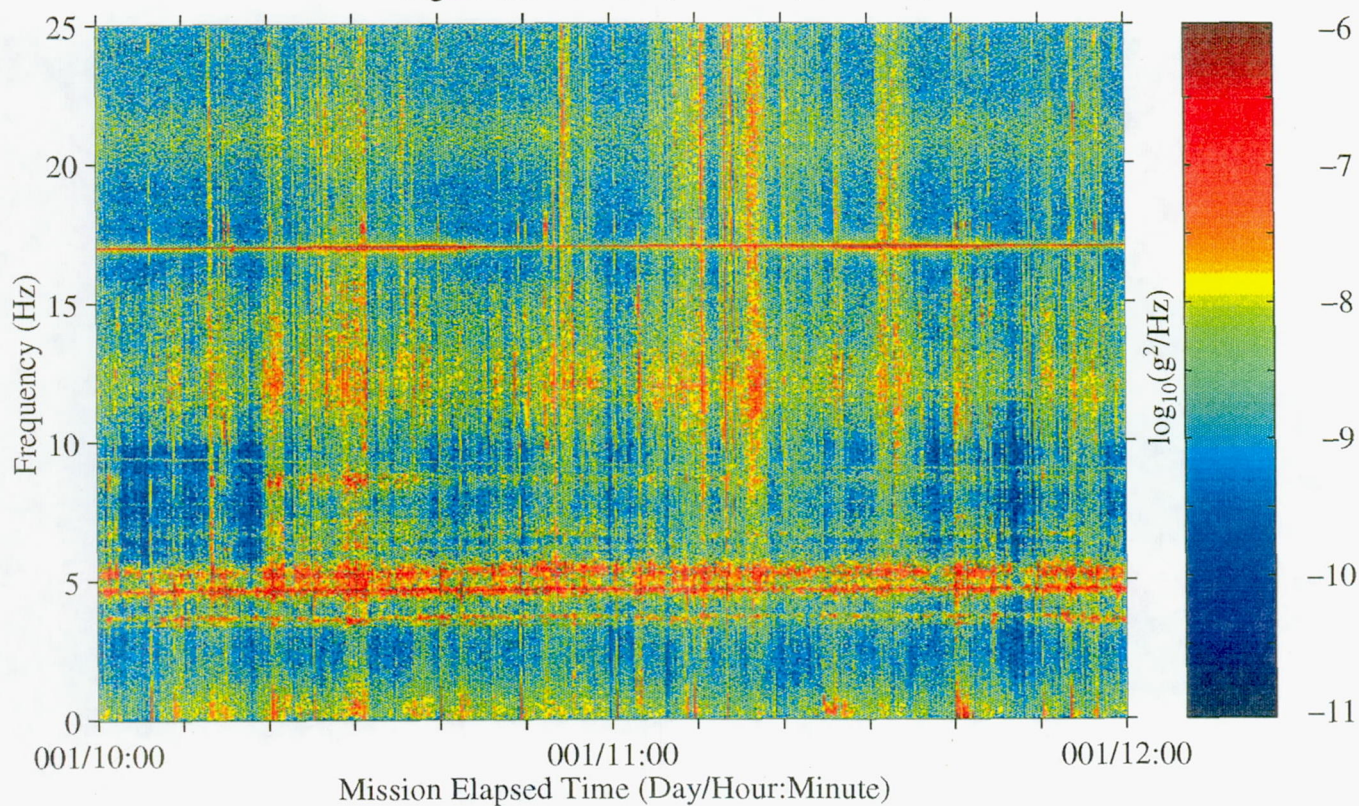


Figure 16: USML-2, Head C (fc=25 Hz)

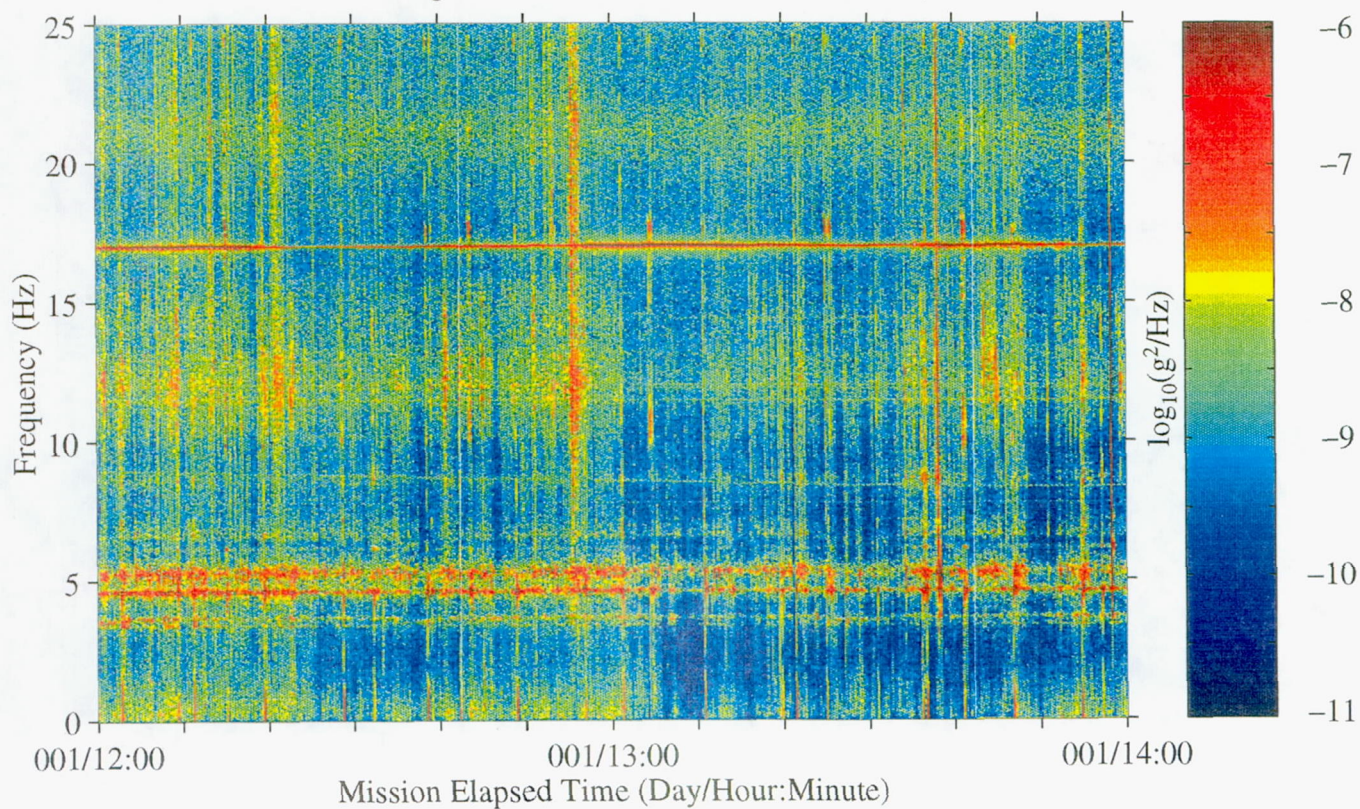




Figure 17: USML-2, Head C (fc=25 Hz)

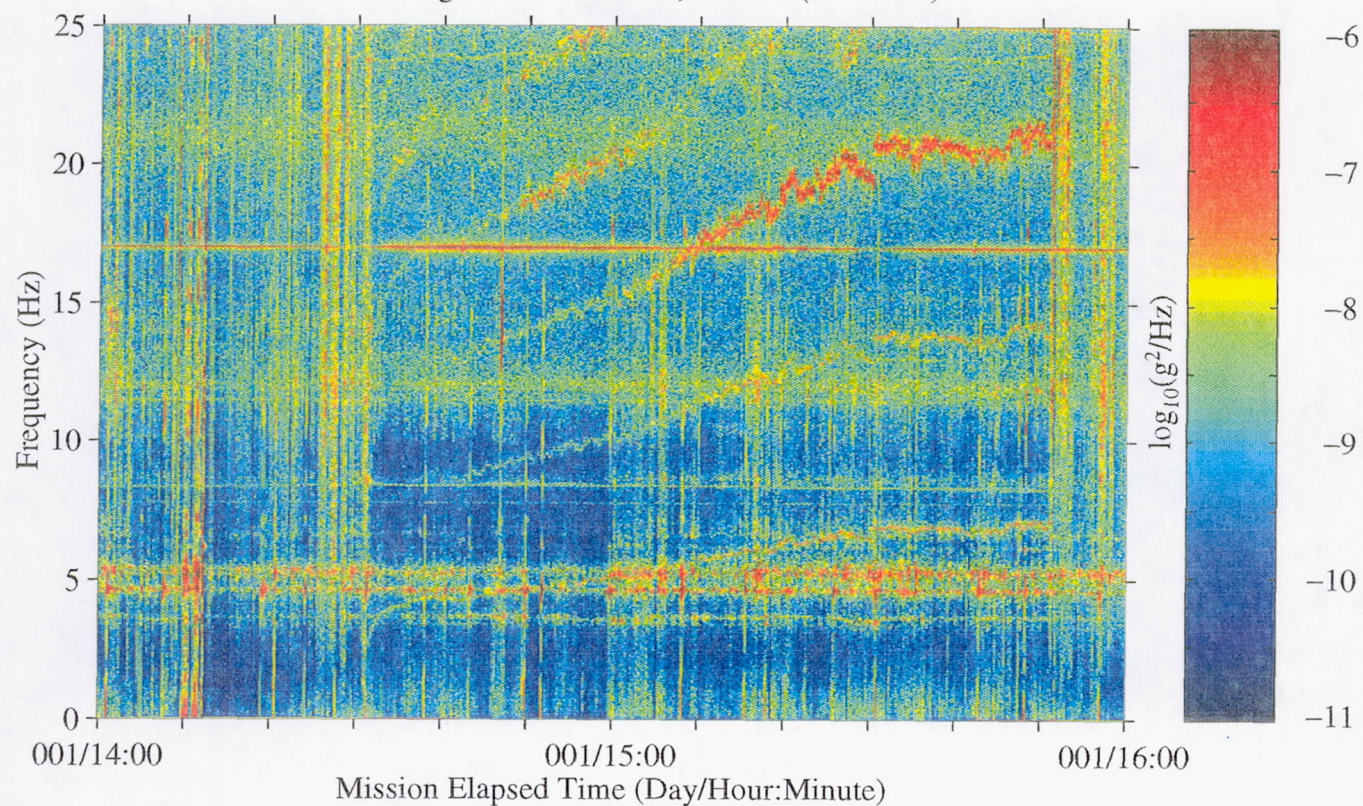


Figure 18: USML-2, Head C (fc=25 Hz)

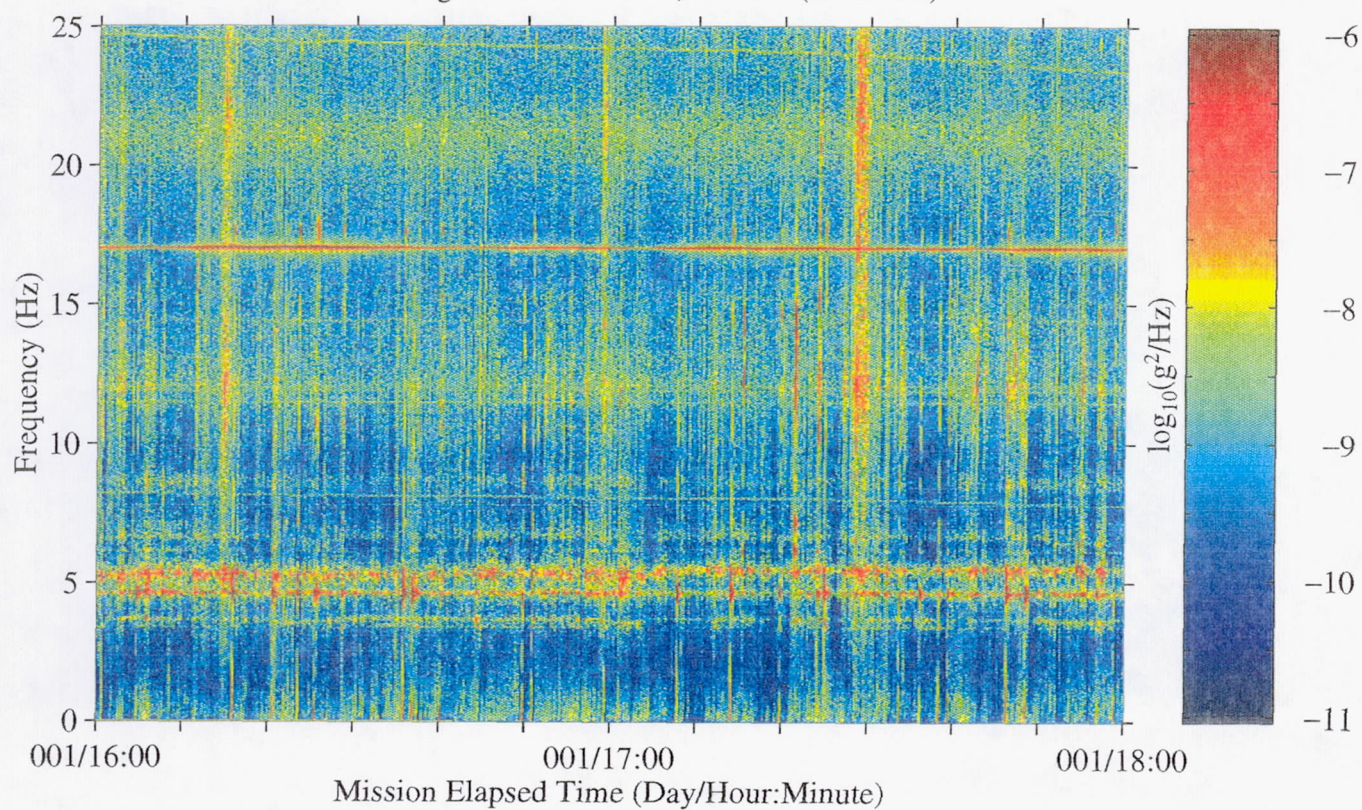




Figure 19: USML-2, Head C (fc=25 Hz)

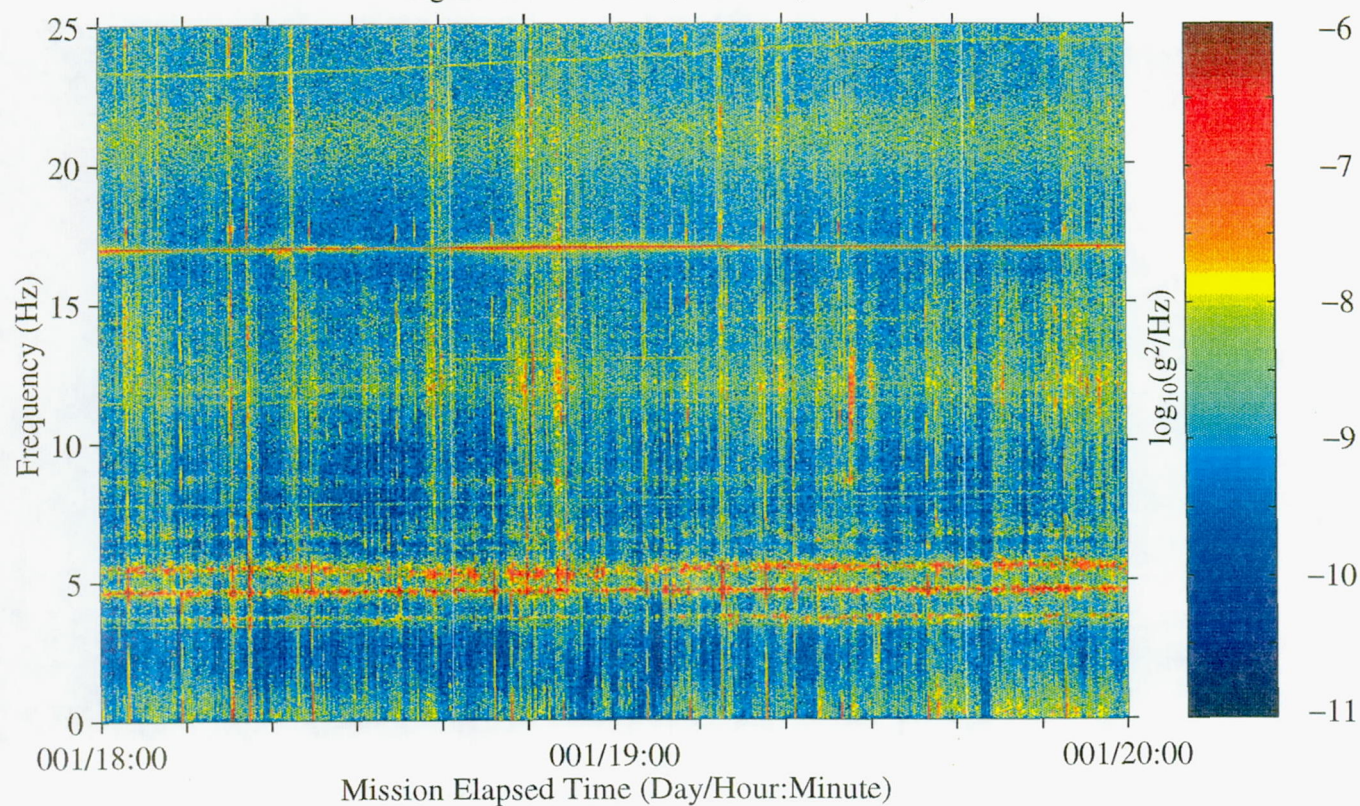


Figure 20: USML-2, Head C (fc=25 Hz)

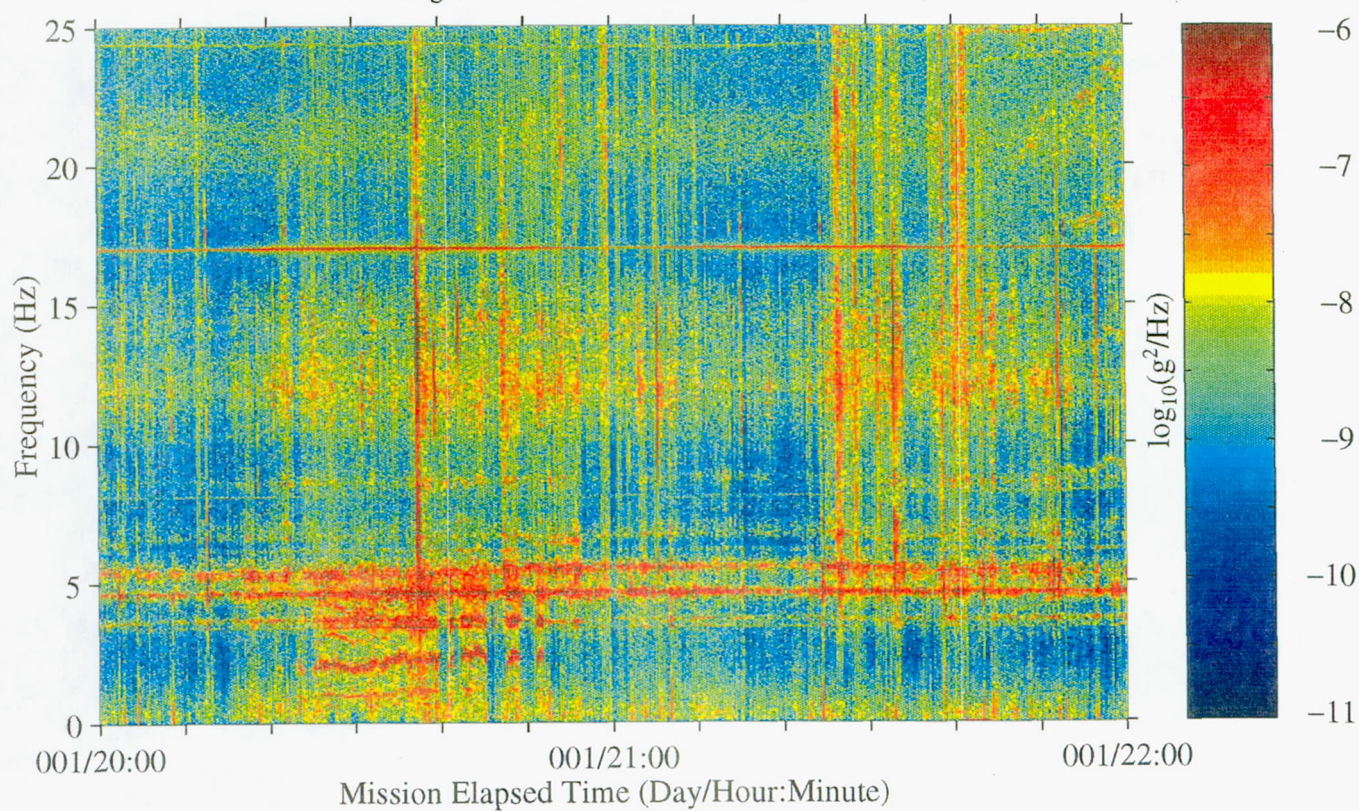




Figure 21: USML-2, Head C (fc=25 Hz)

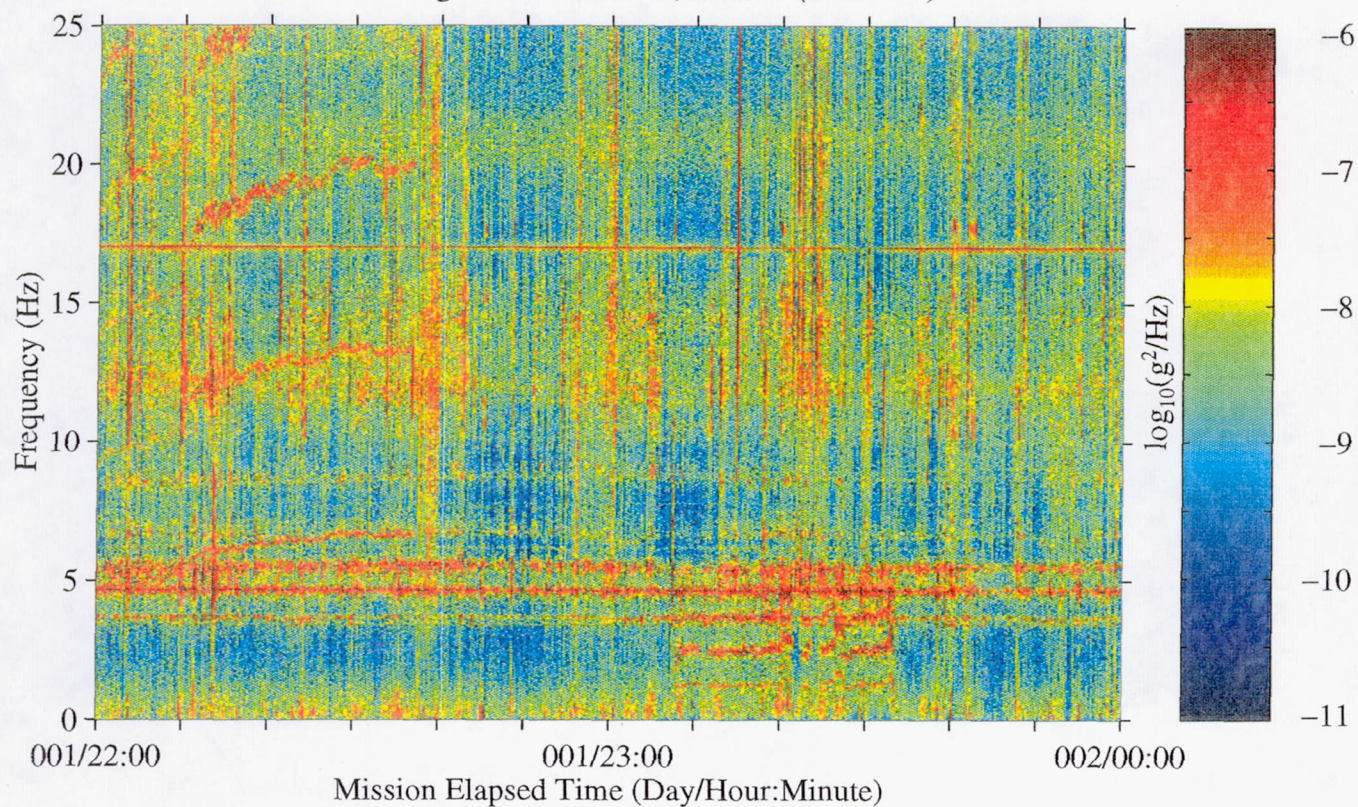


Figure 22: USML-2, Head C (fc=25 Hz)

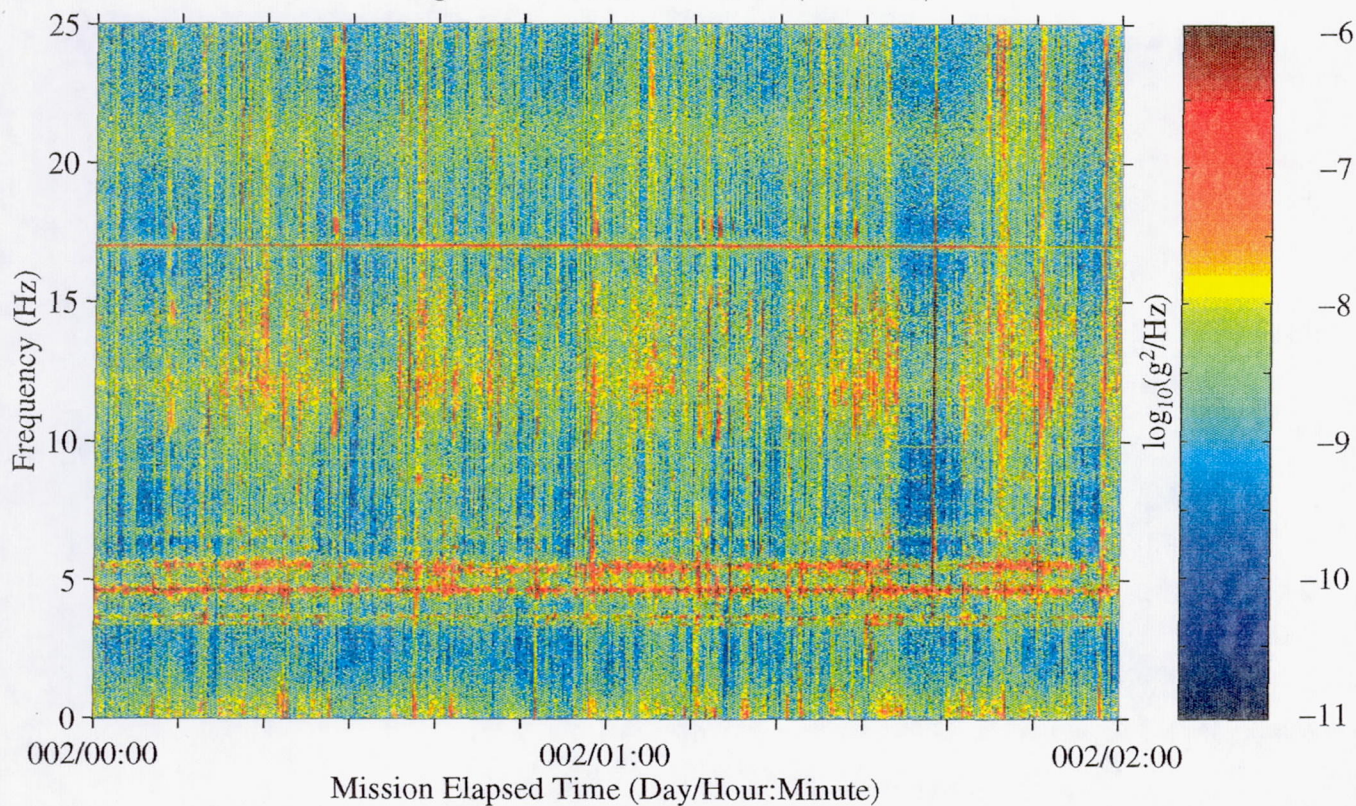




Figure 23: USML-2, Head C (fc=25 Hz)

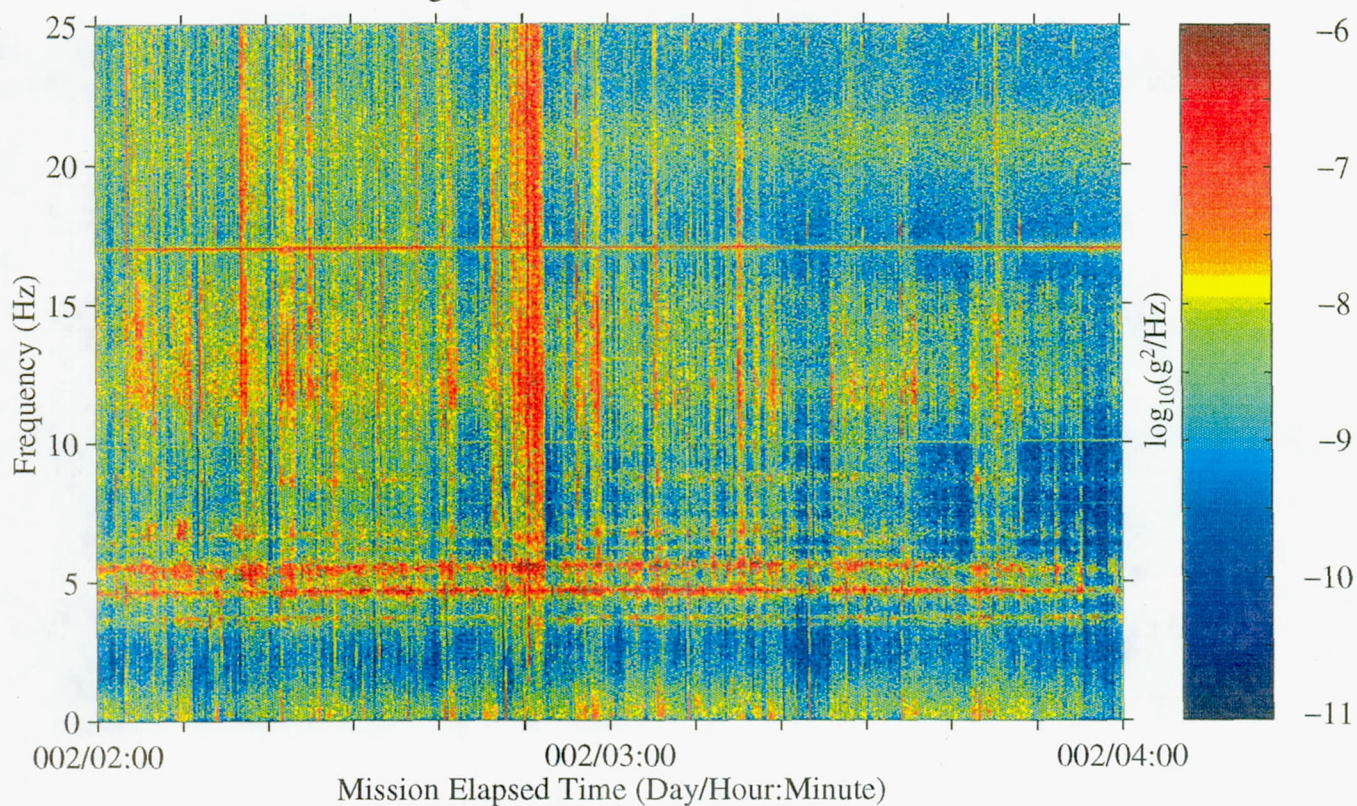


Figure 24: USML-2, Head C (fc=25 Hz)

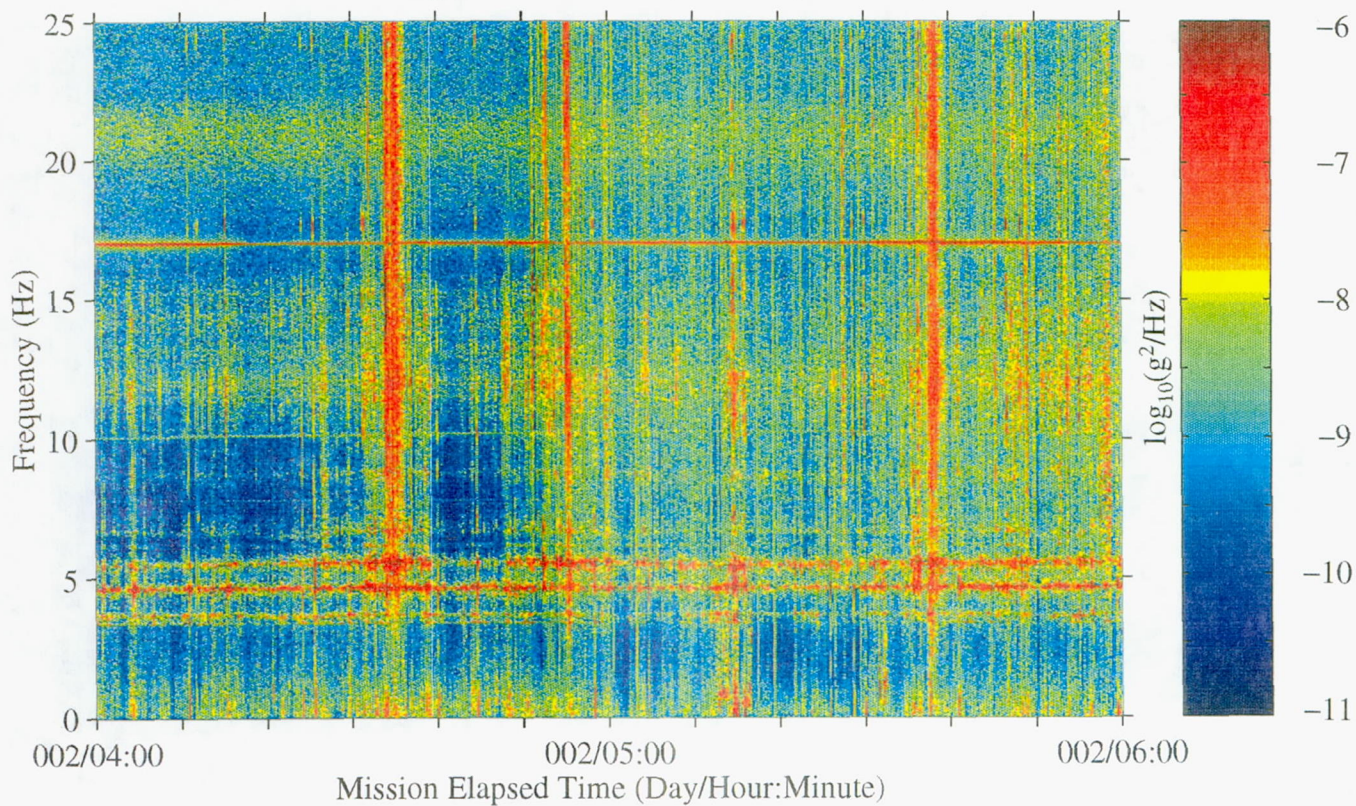




Figure 25: USML-2, Head C (fc=25 Hz)

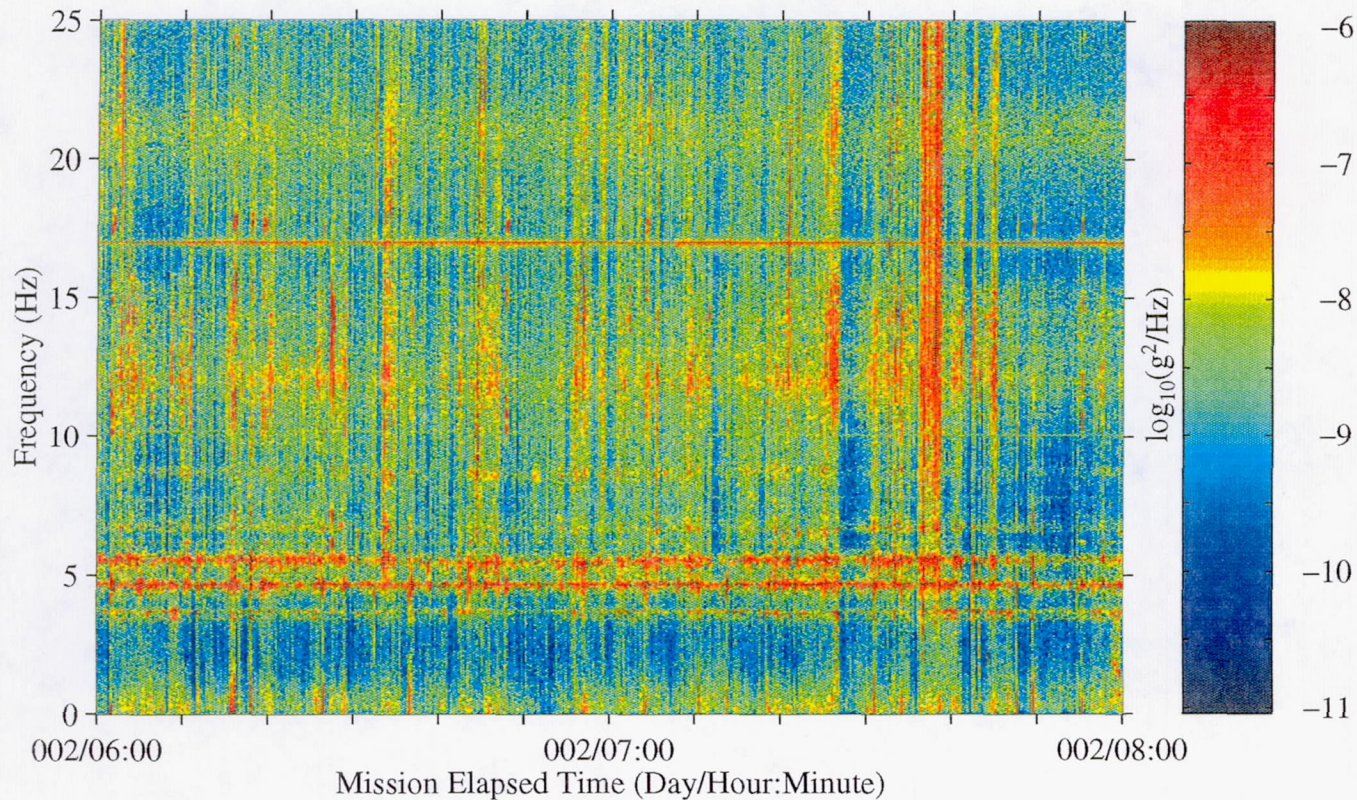


Figure 26: USML-2, Head C (fc=25 Hz)

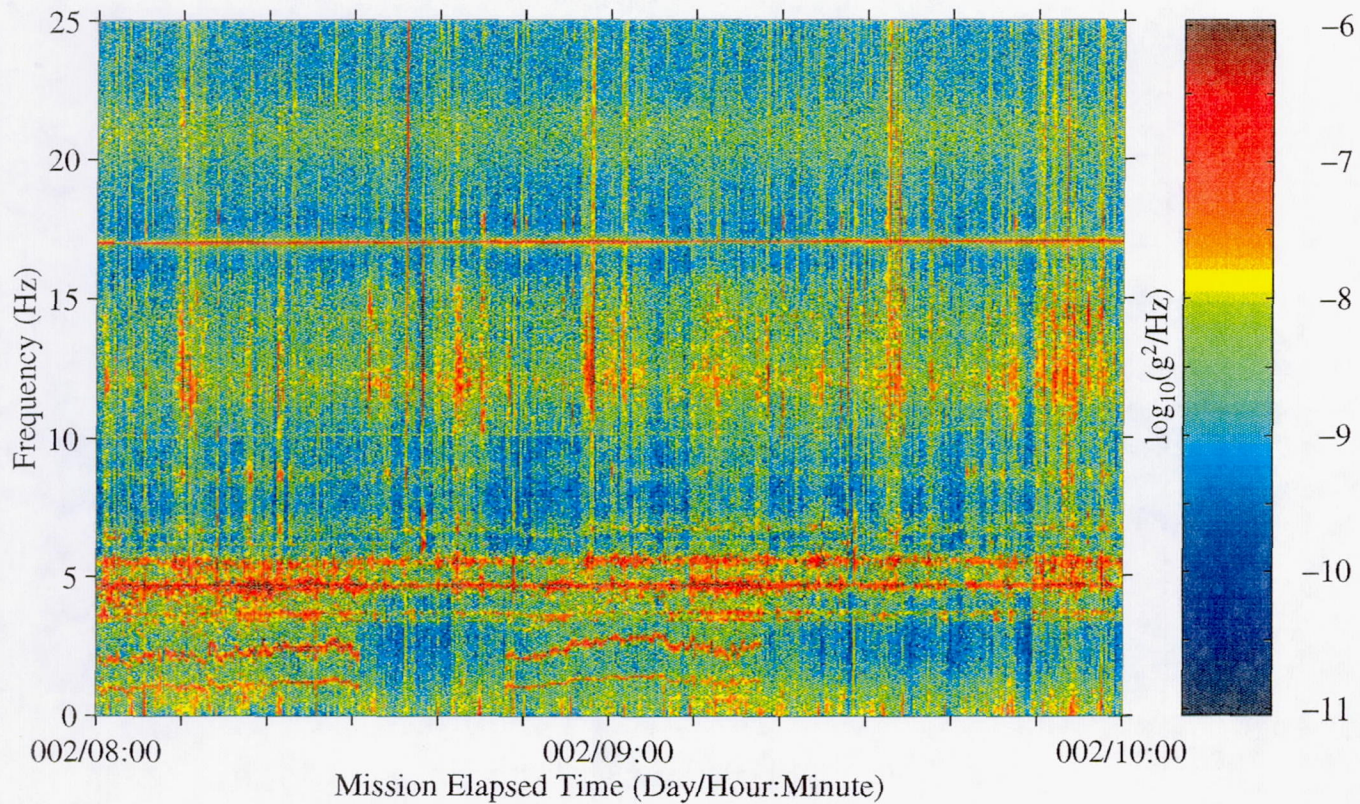




Figure 27: USML-2, Head C (fc=25 Hz)

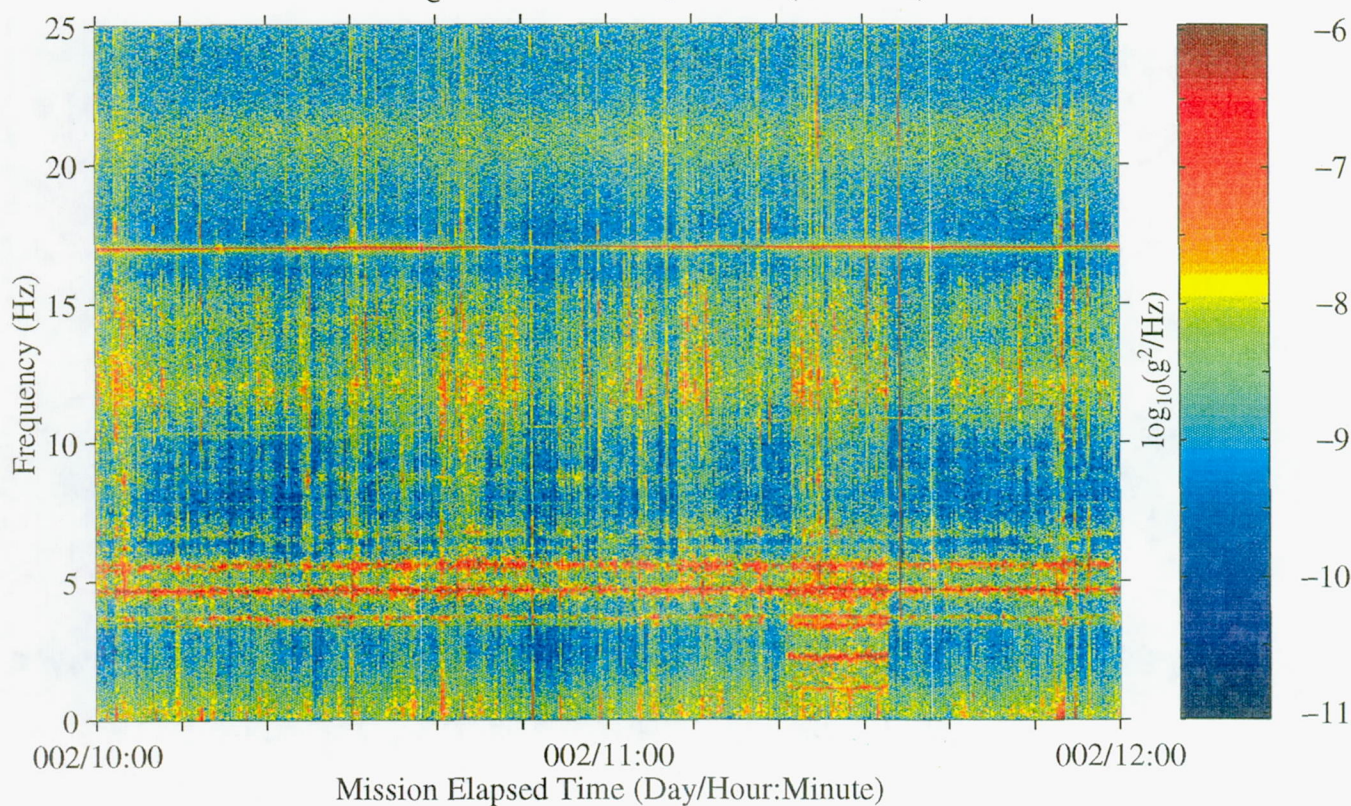


Figure 28: USML-2, Head C (fc=25 Hz)

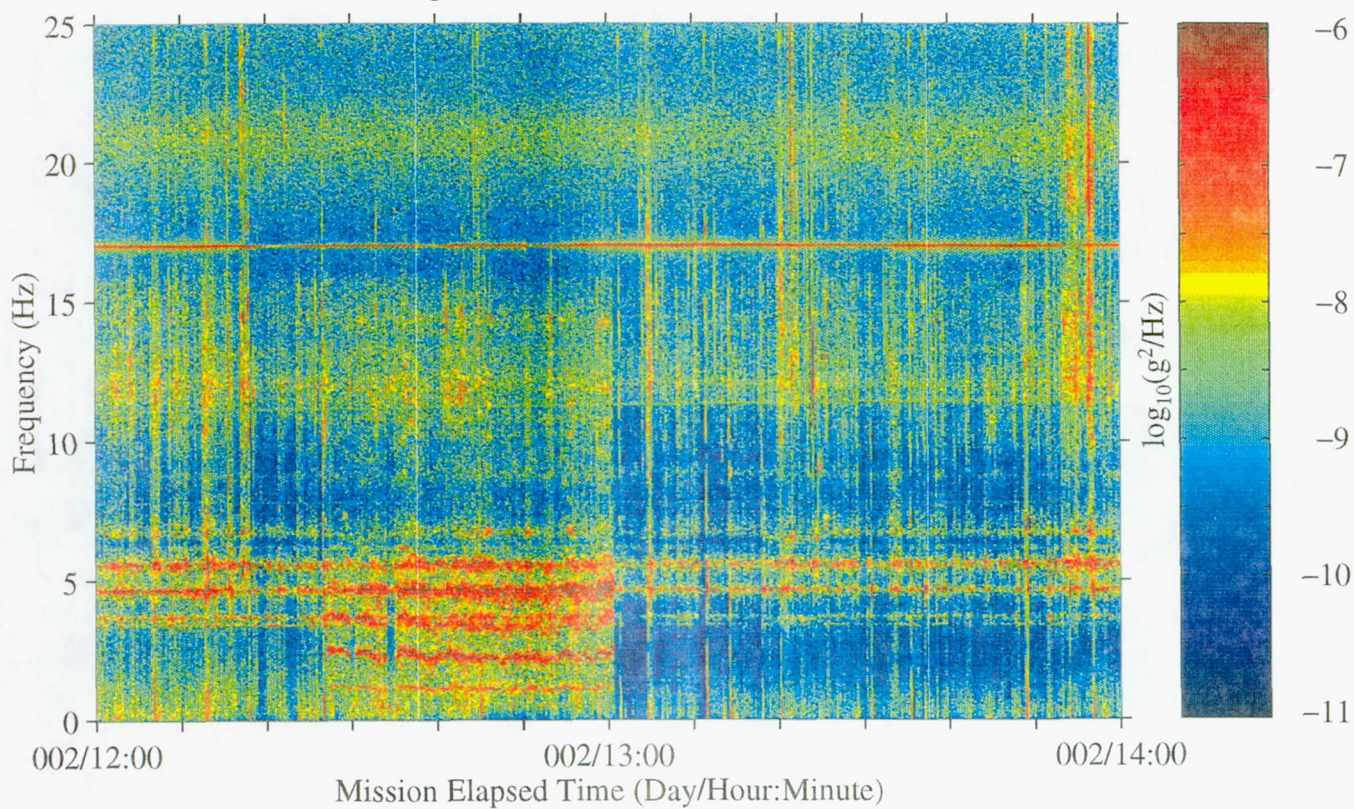




Figure 29: USML-2, Head C (fc=25 Hz)

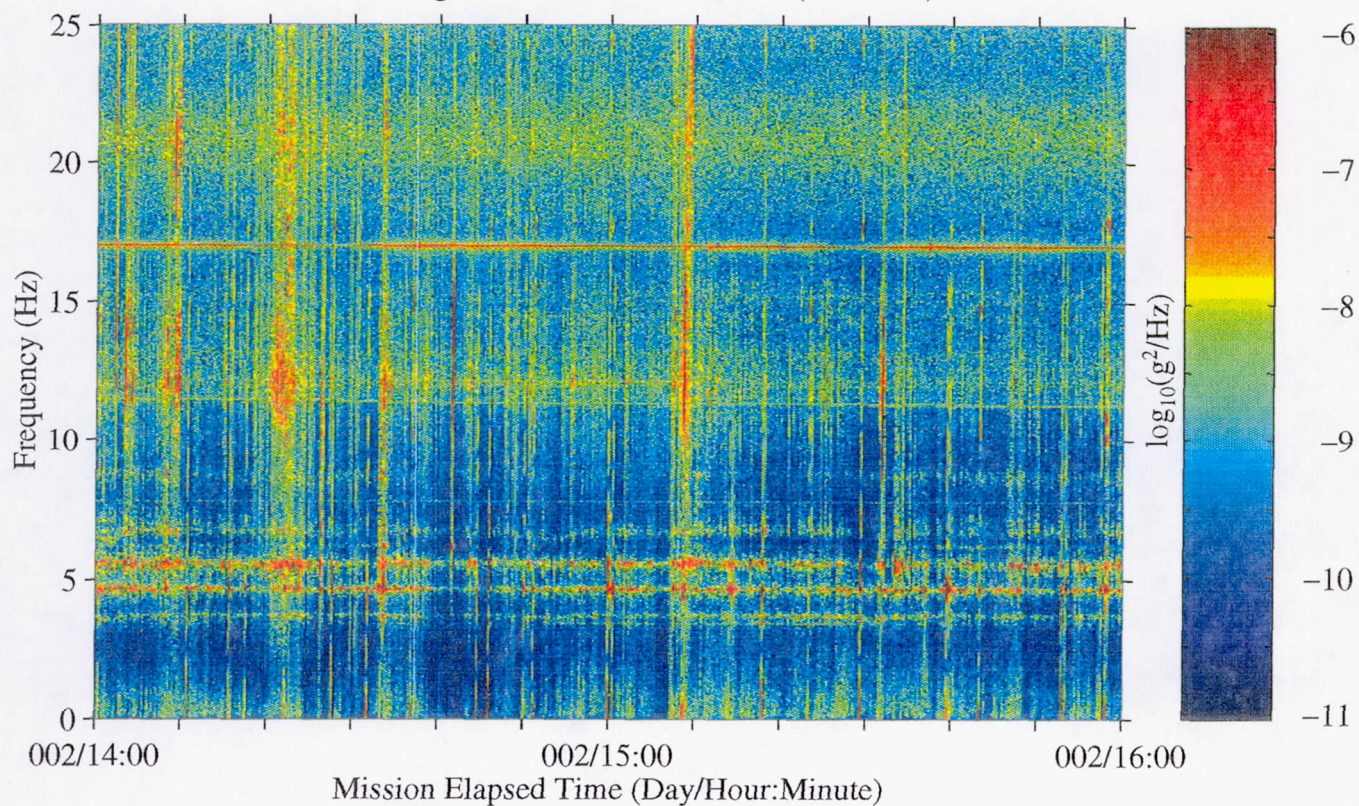


Figure 30: USML-2, Head C (fc=25 Hz)

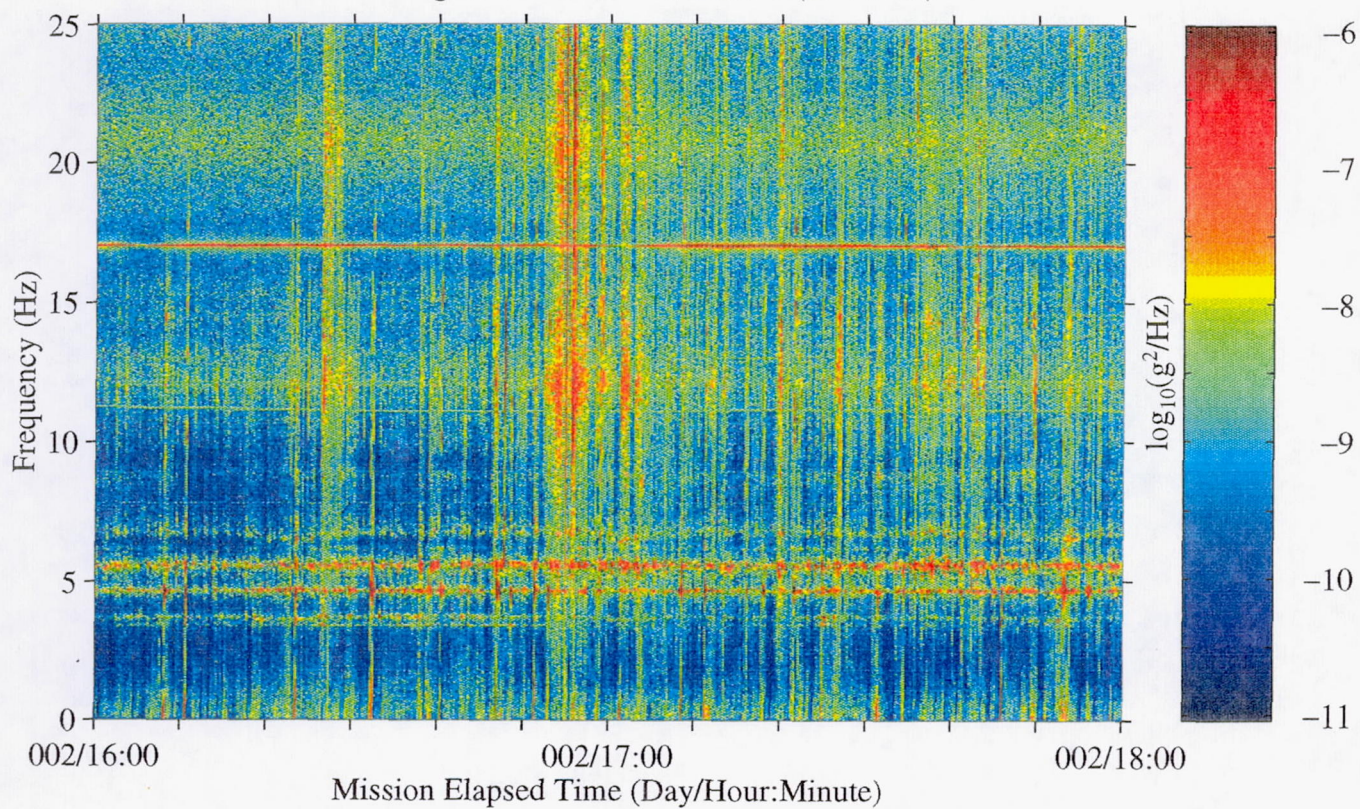




Figure 31: USML-2, Head C (fc=25 Hz)

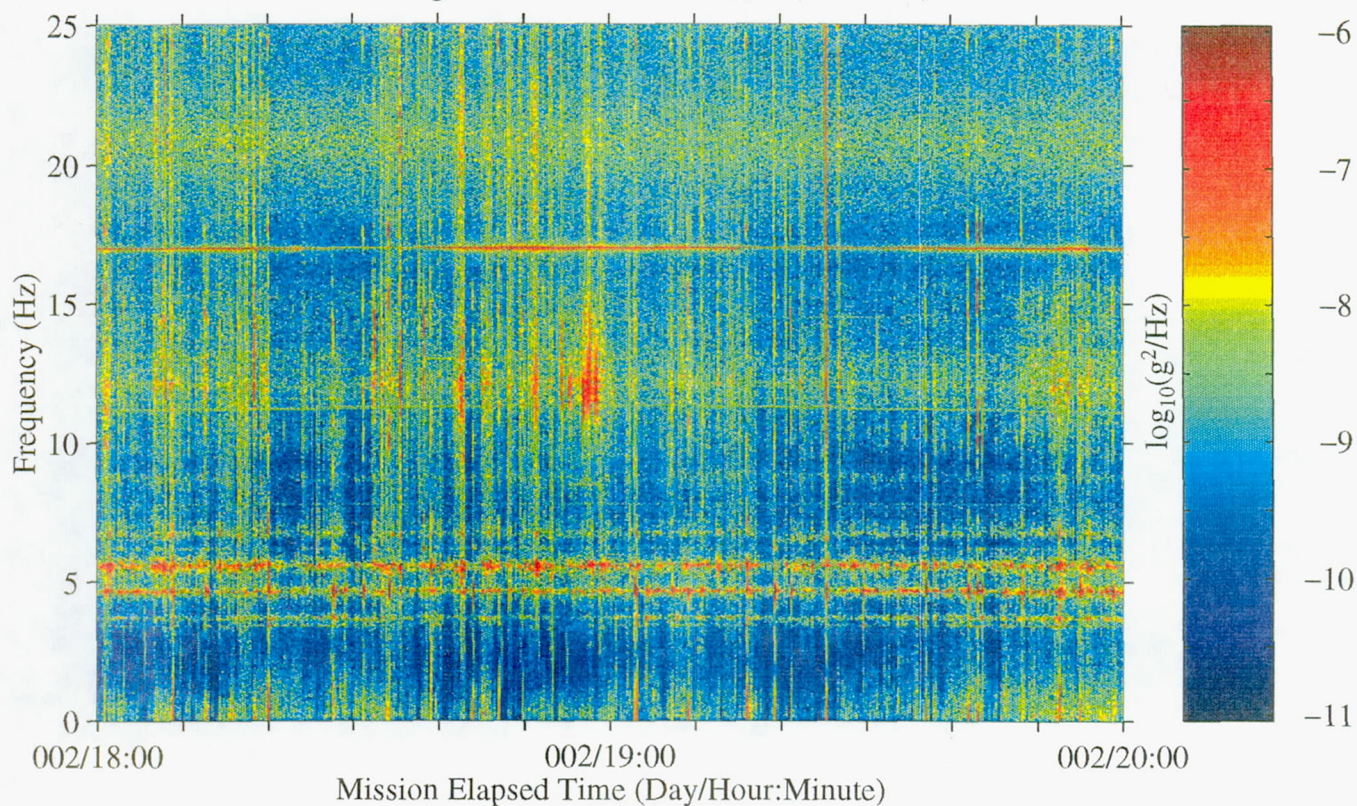


Figure 32: USML-2, Head C (fc=25 Hz)

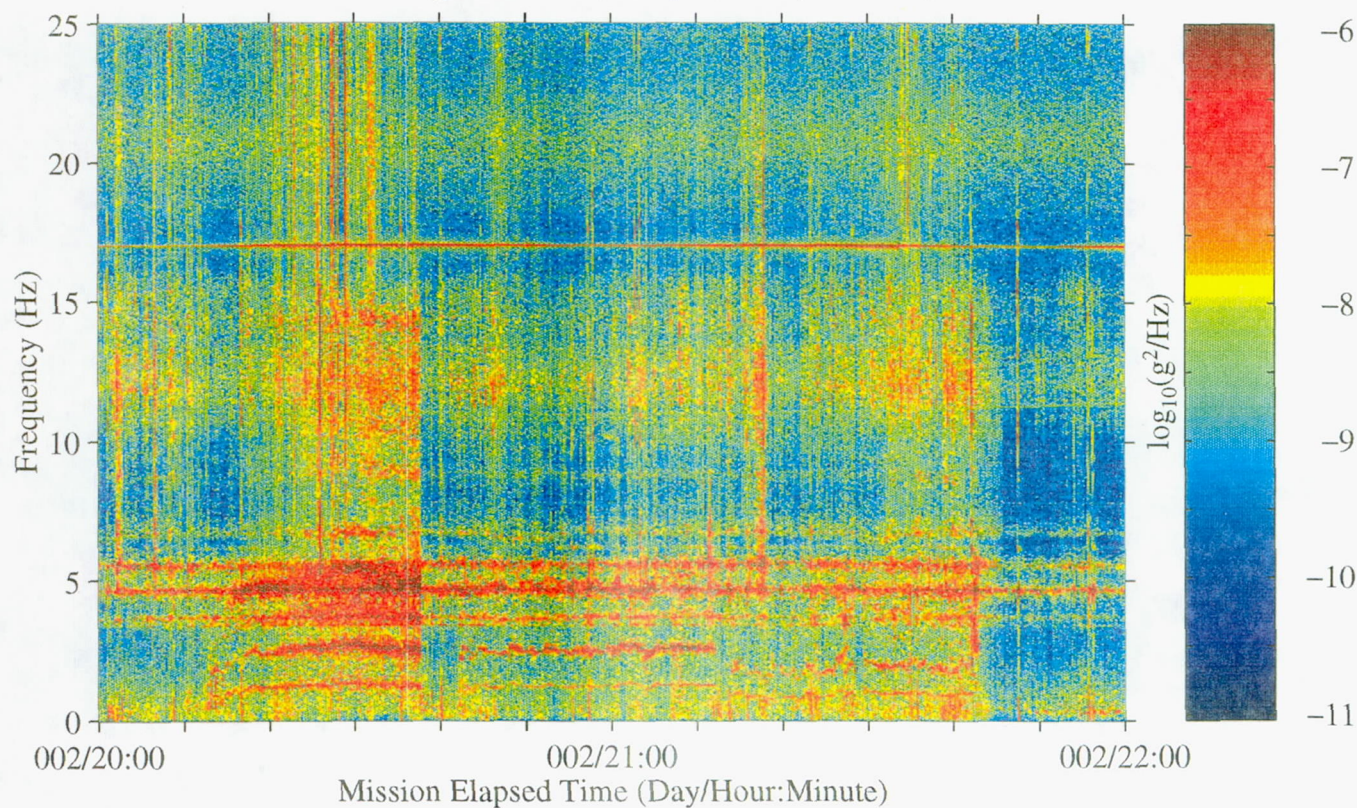




Figure 33: USML-2, Head C (fc=25 Hz)

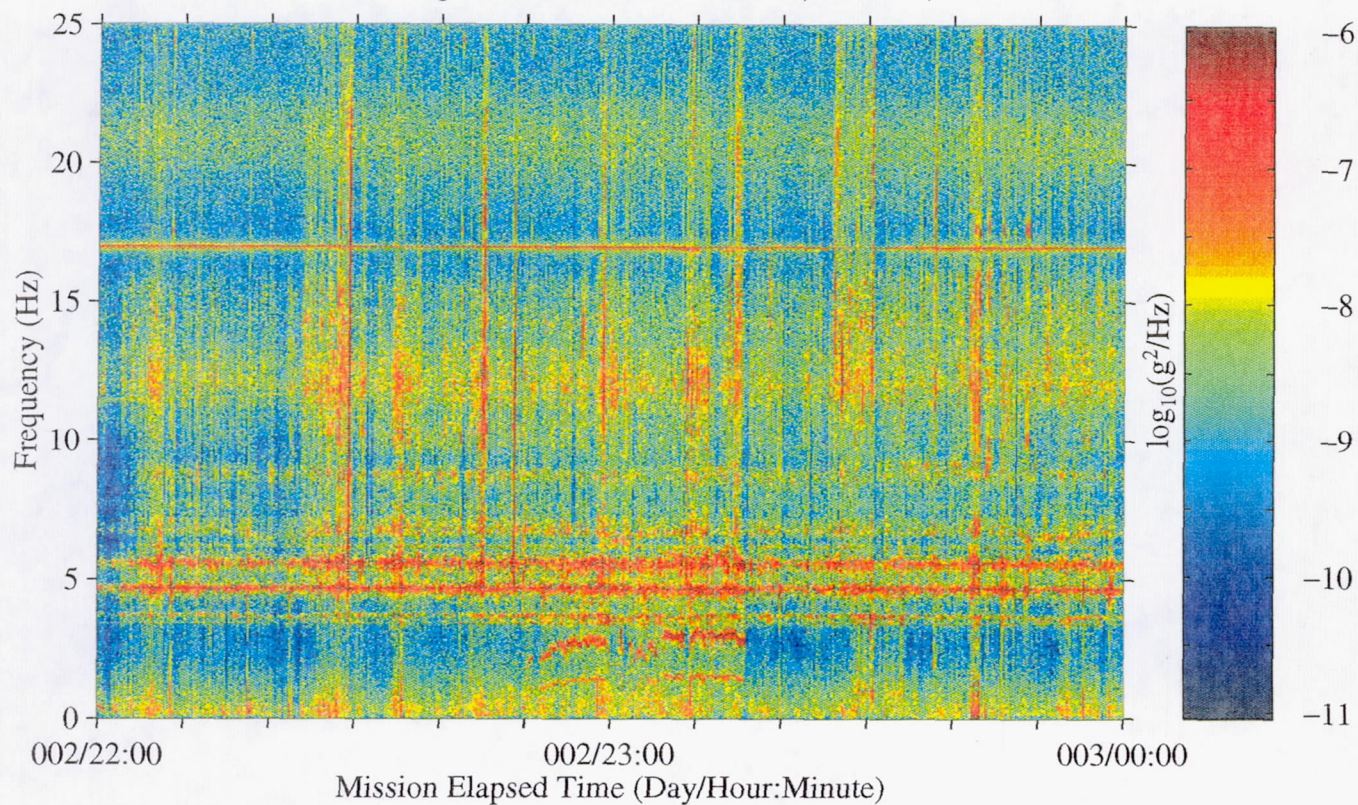


Figure 34: USML-2, Head C (fc=25 Hz)

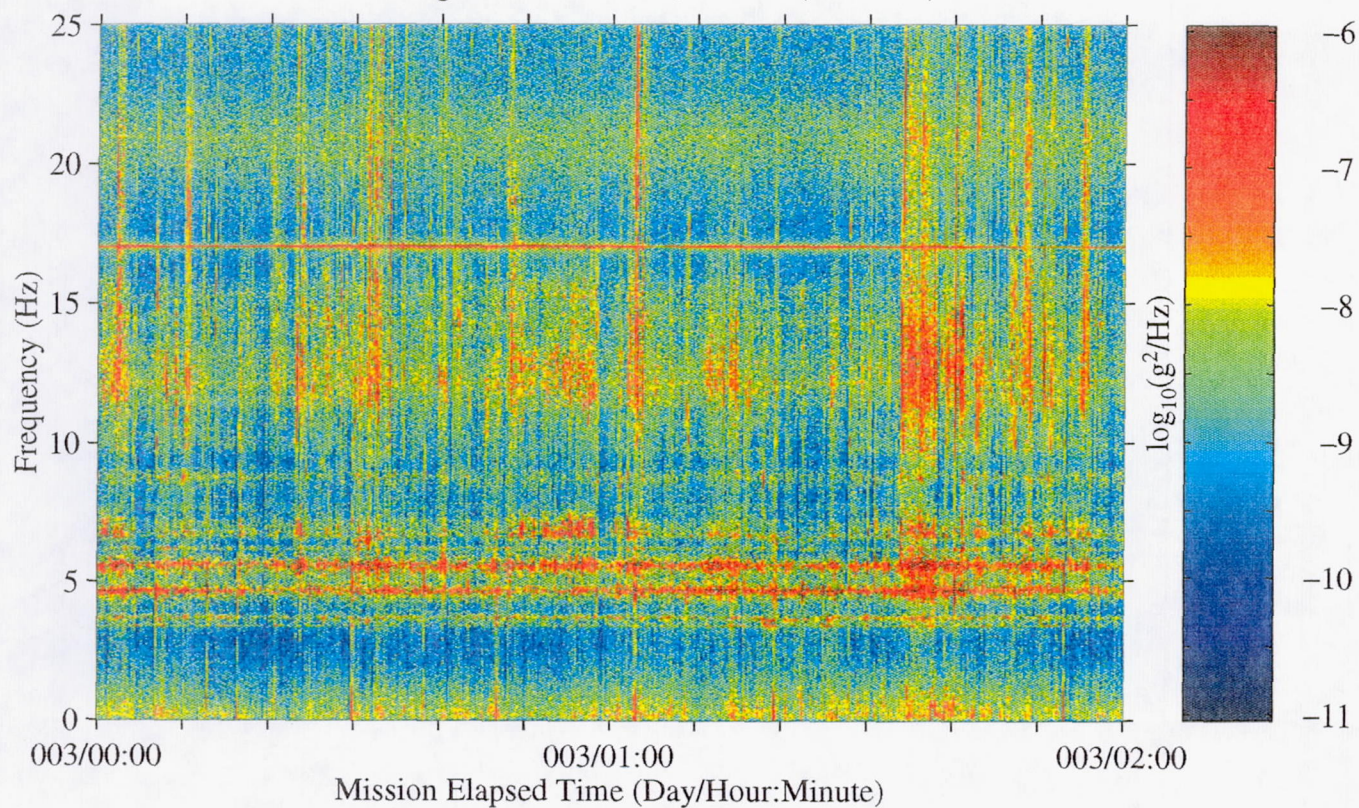




Figure 35: USML-2, Head C (fc=25 Hz)

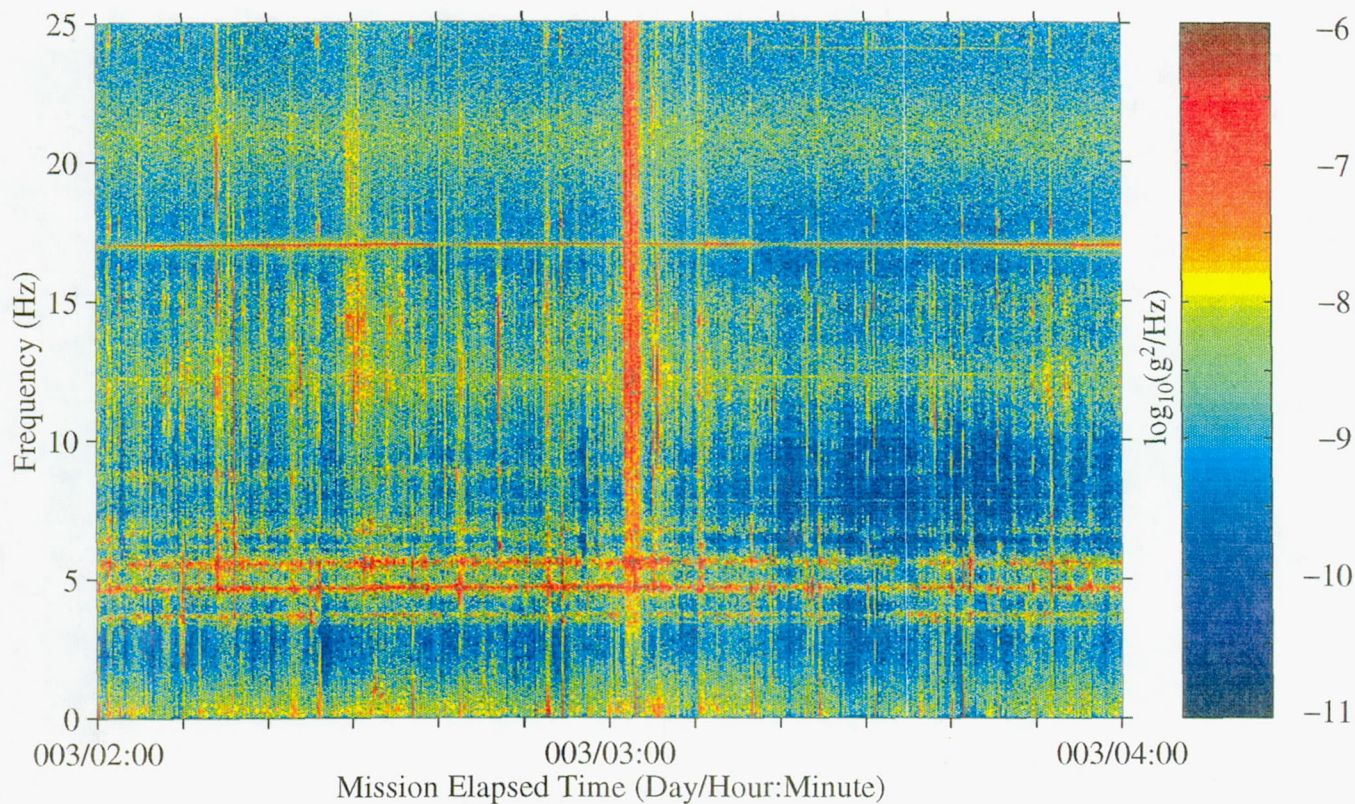


Figure 36: USML-2, Head C (fc=25 Hz)

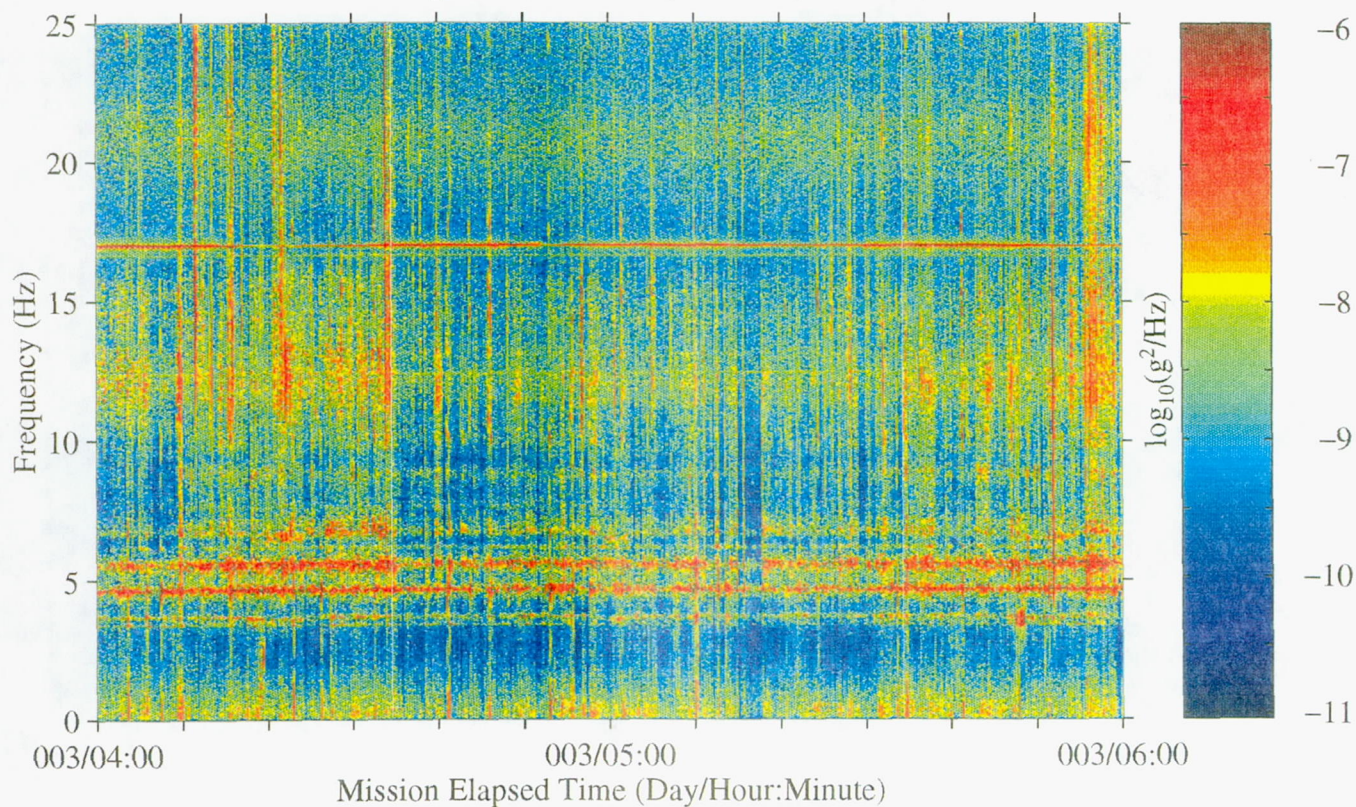




Figure 37: USML-2, Head C (fc=25 Hz)

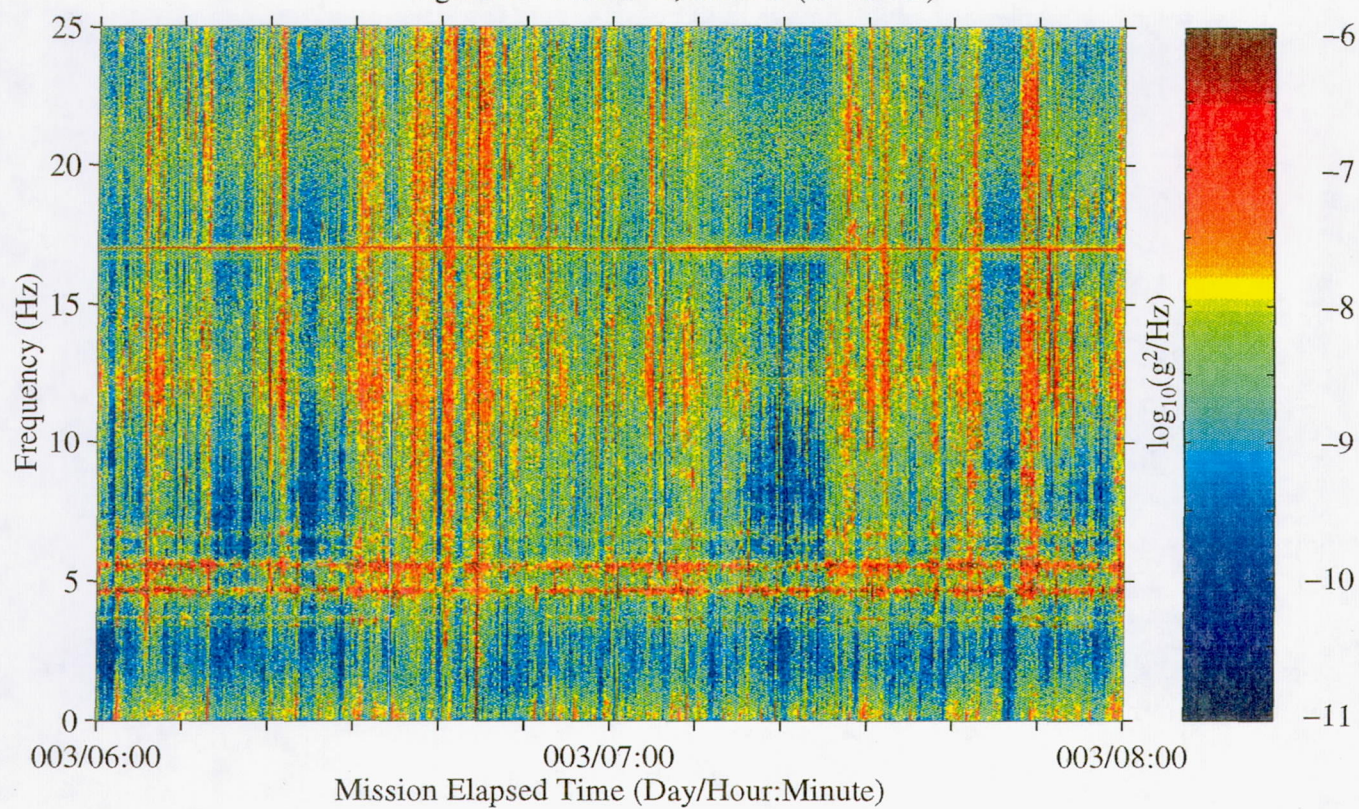


Figure 38: USML-2, Head C (fc=25 Hz)

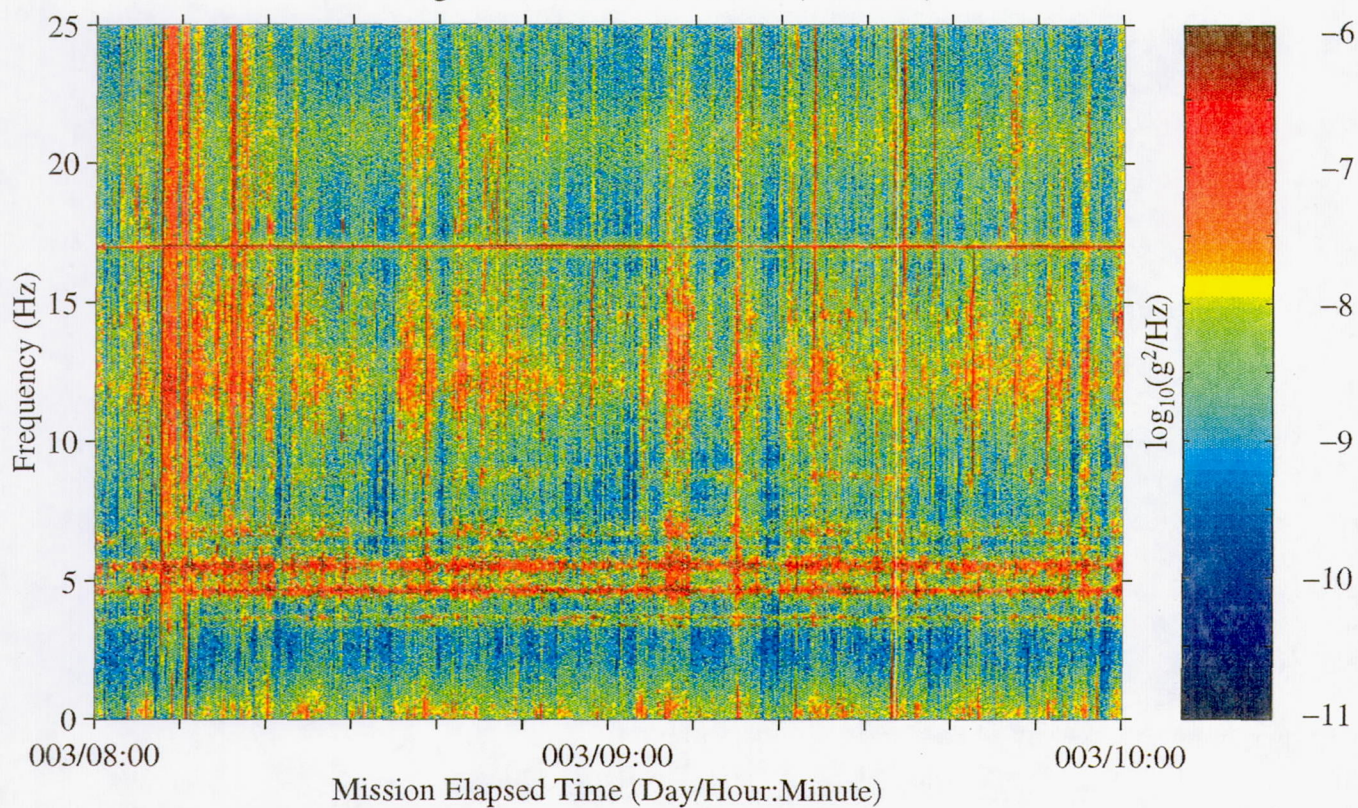




Figure 39: USML-2, Head C (fc=25 Hz)

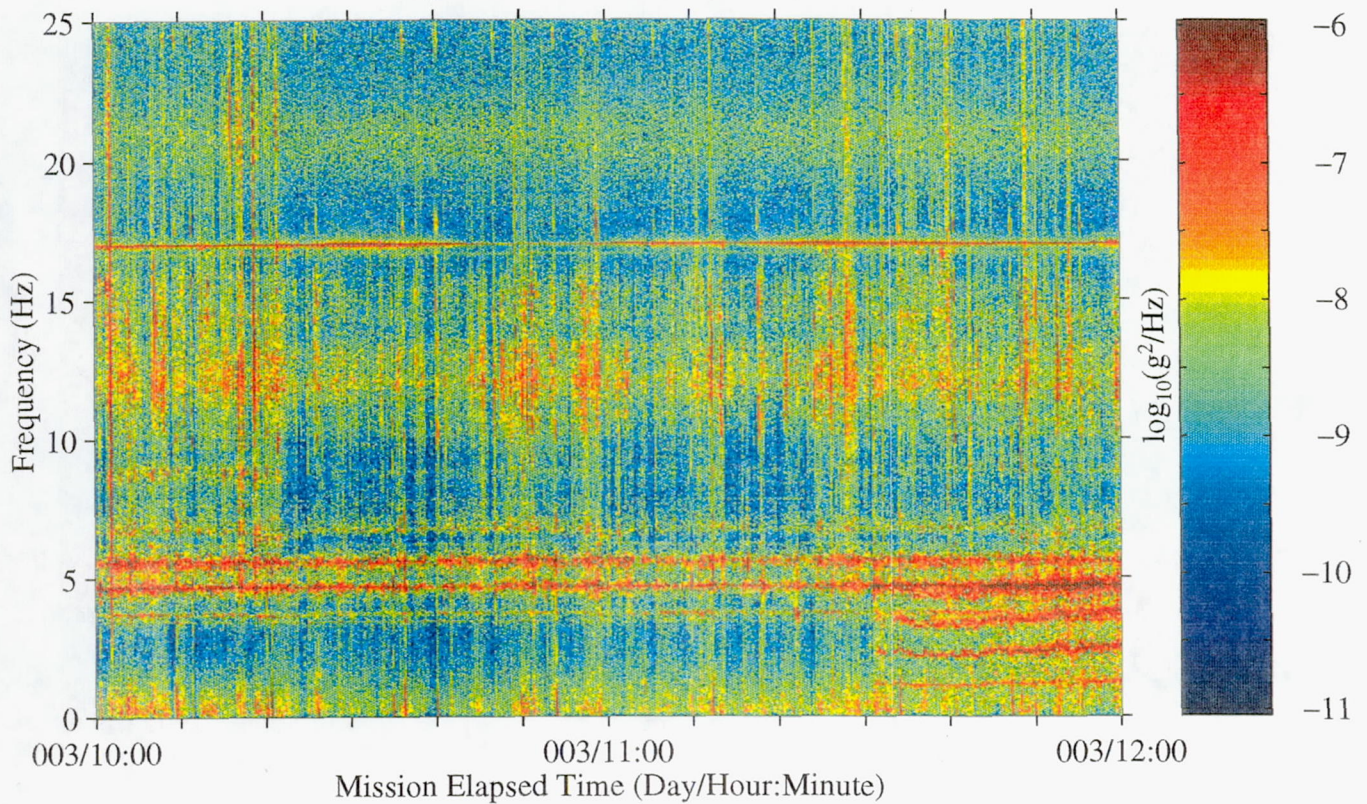


Figure 40: USML-2, Head C (fc=25 Hz)

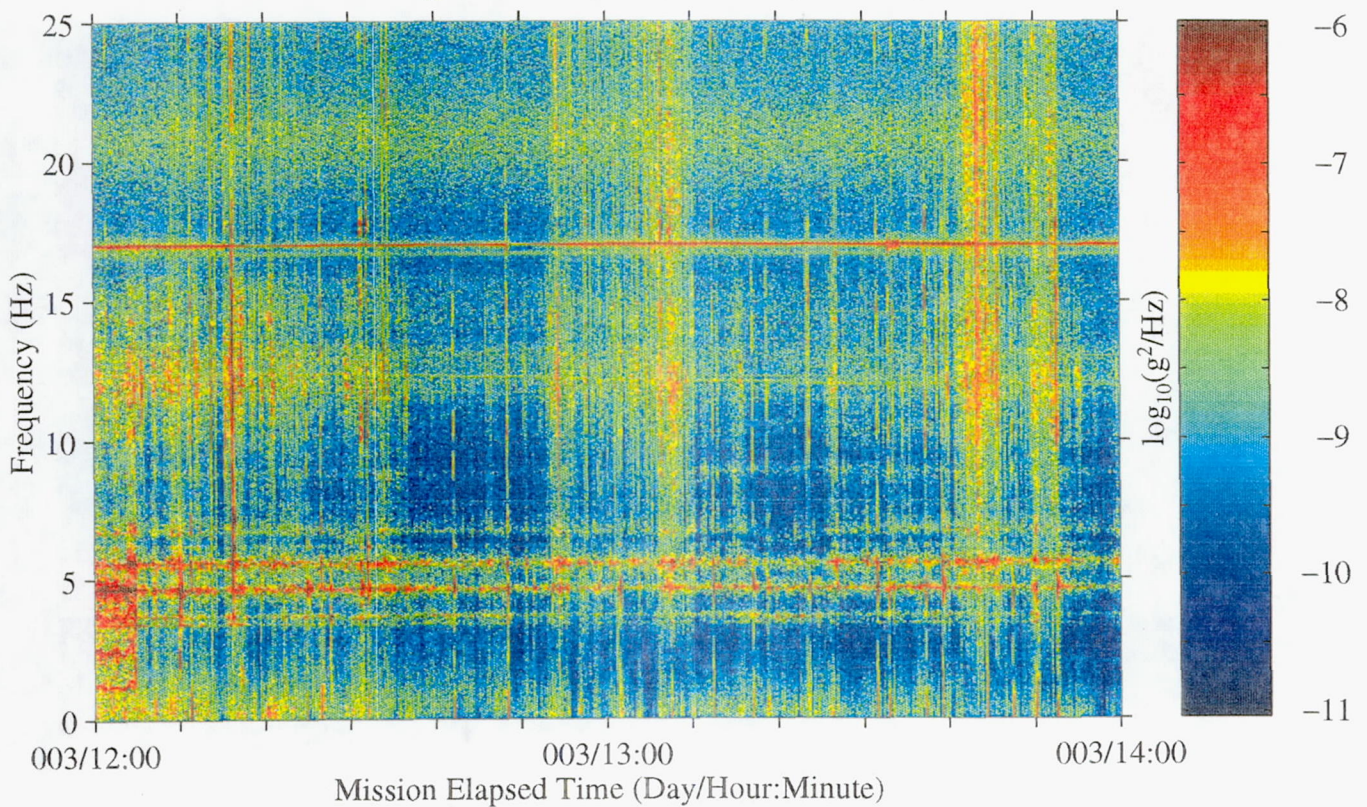




Figure 41: USML-2, Head C (fc=25 Hz)

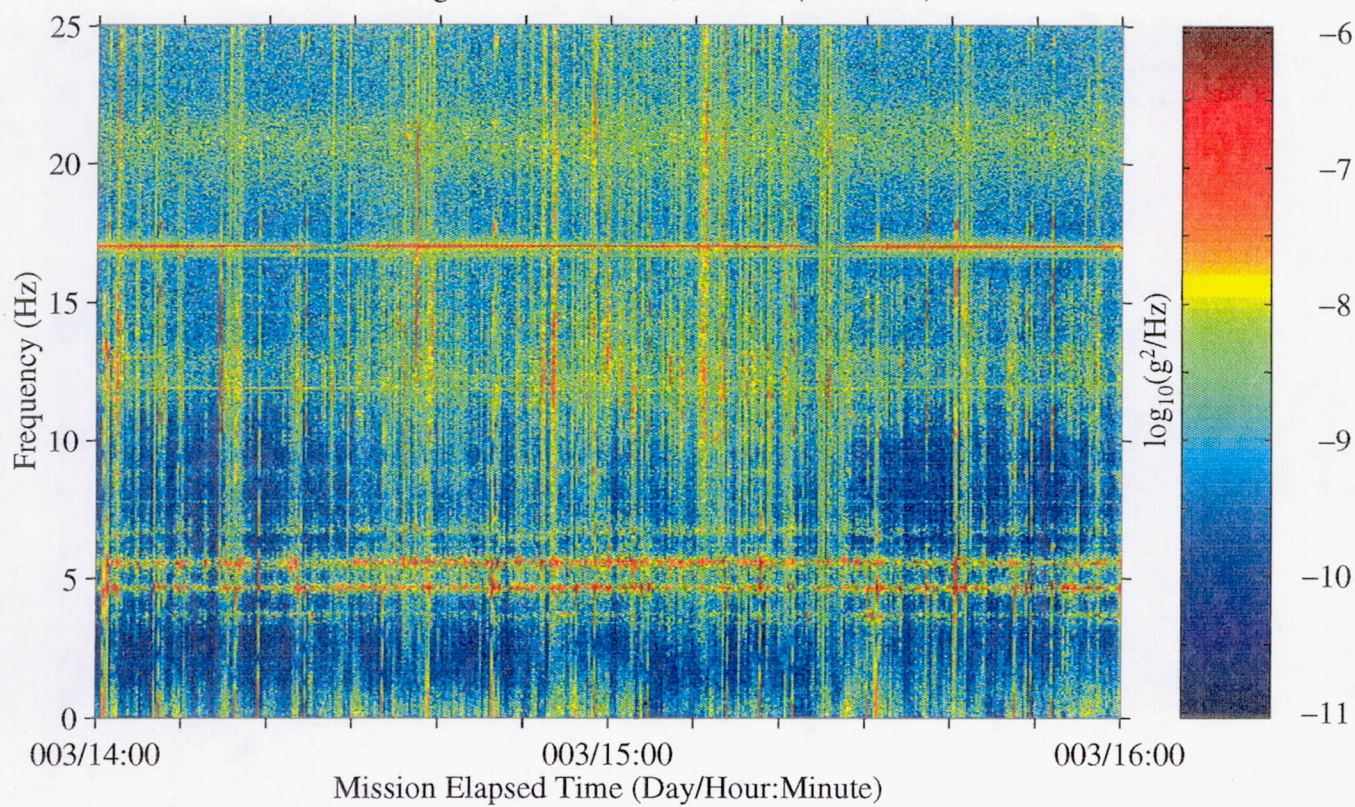


Figure 42: USML-2, Head C (fc=25 Hz)

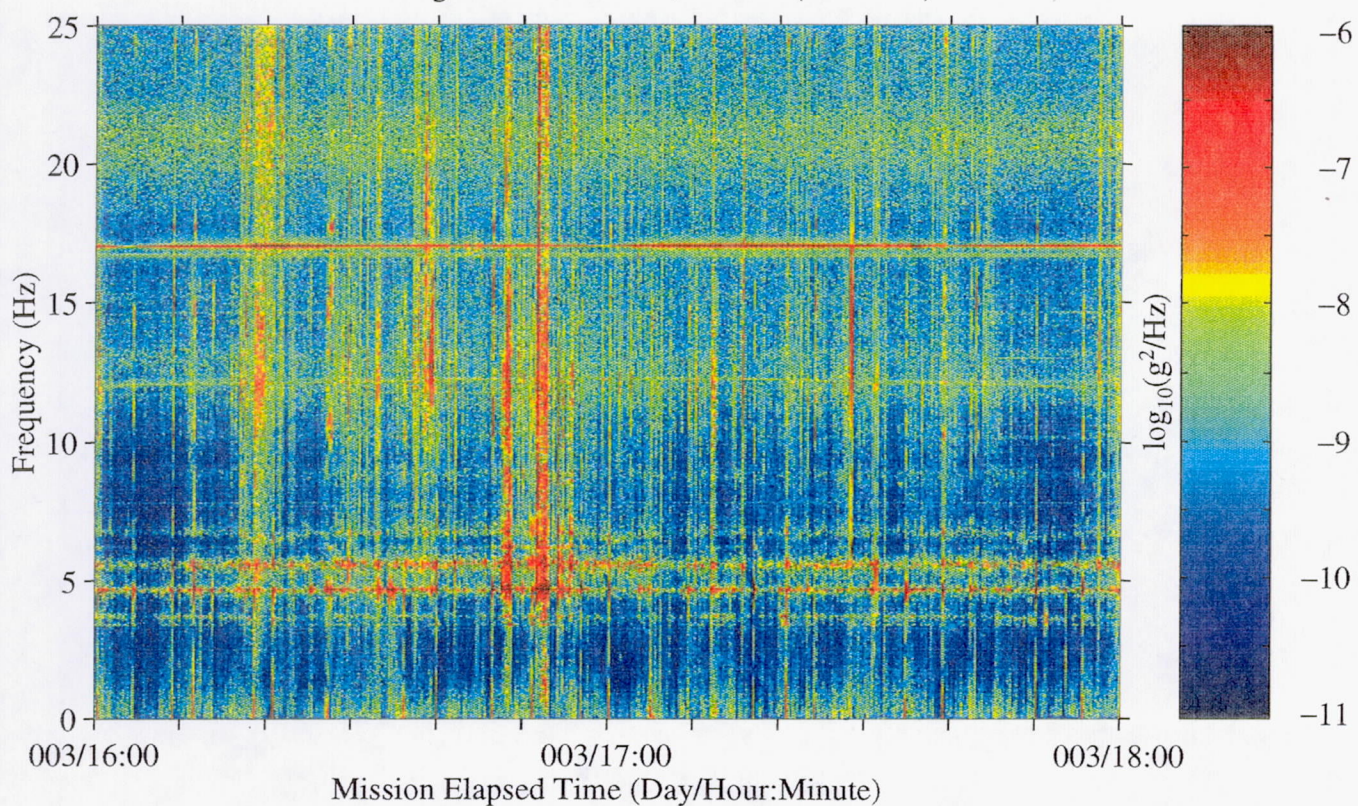




Figure 43: USML-2, Head C (fc=25 Hz)

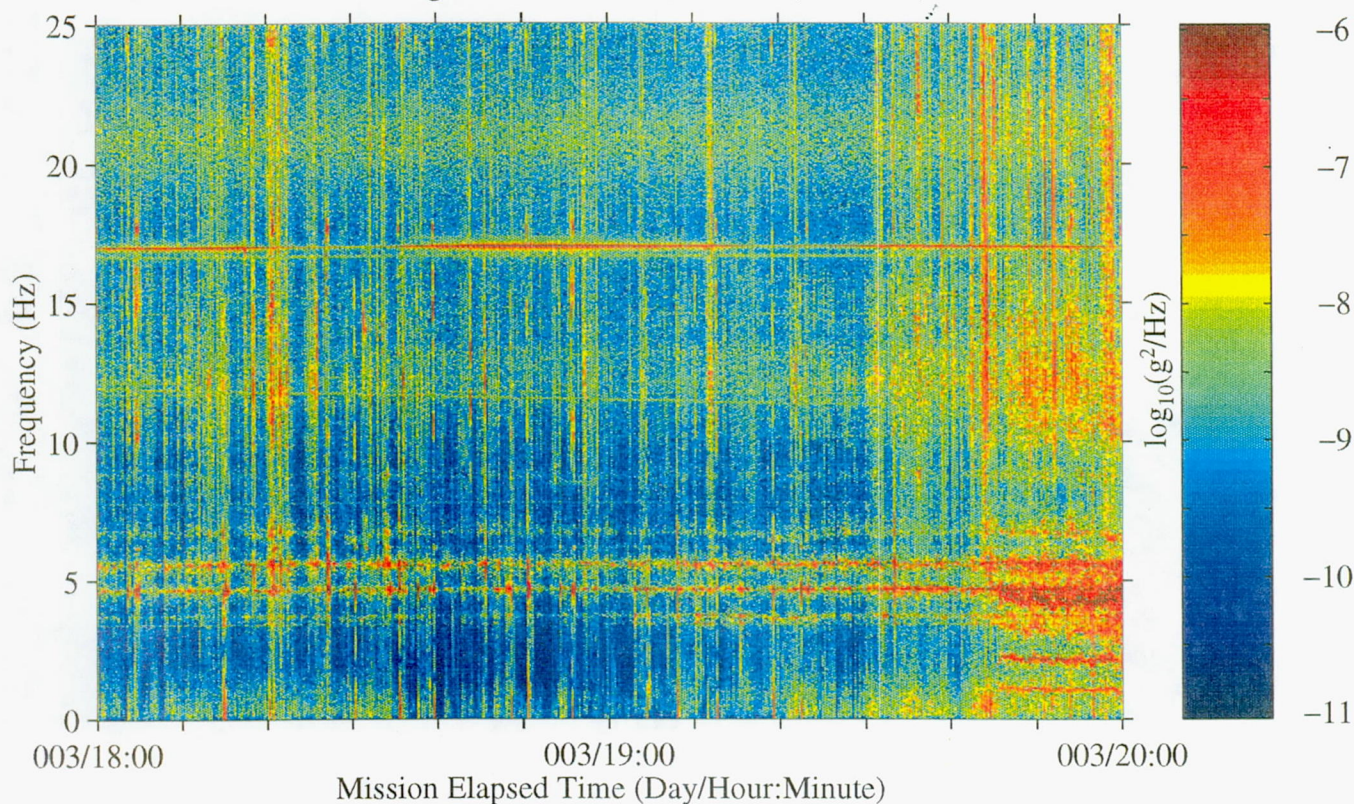


Figure 44: USML-2, Head C (fc=25 Hz)

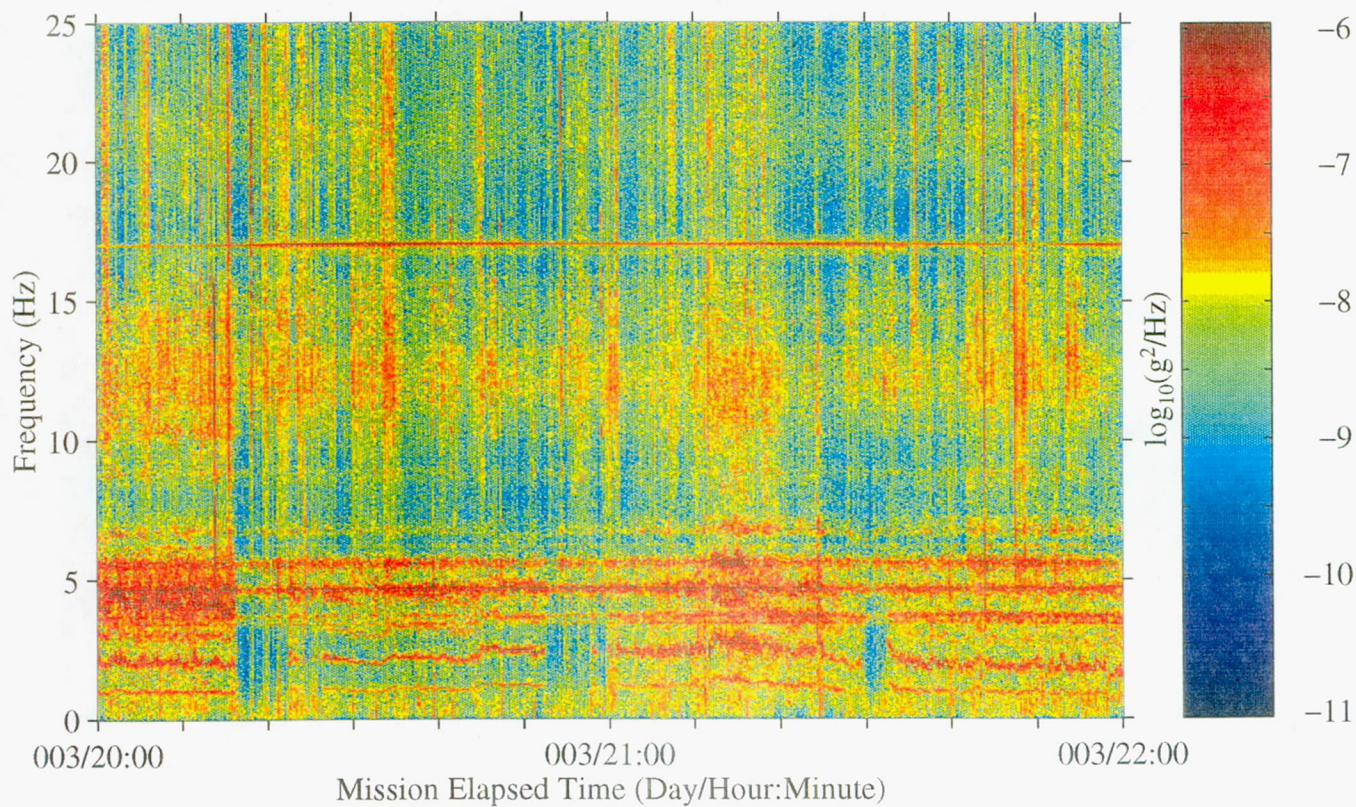




Figure 45: USML-2, Head C (fc=25 Hz)

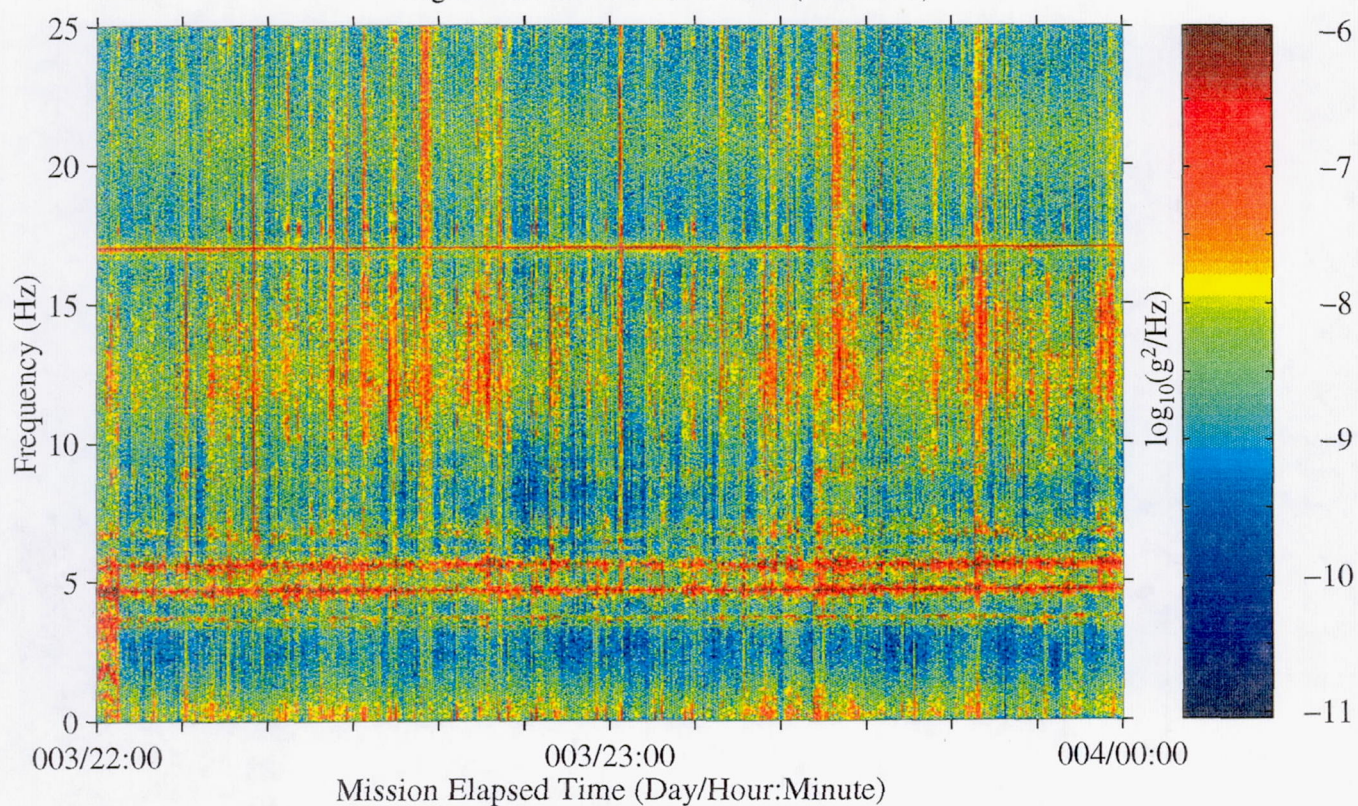


Figure 46: USML-2, Head C (fc=25 Hz)

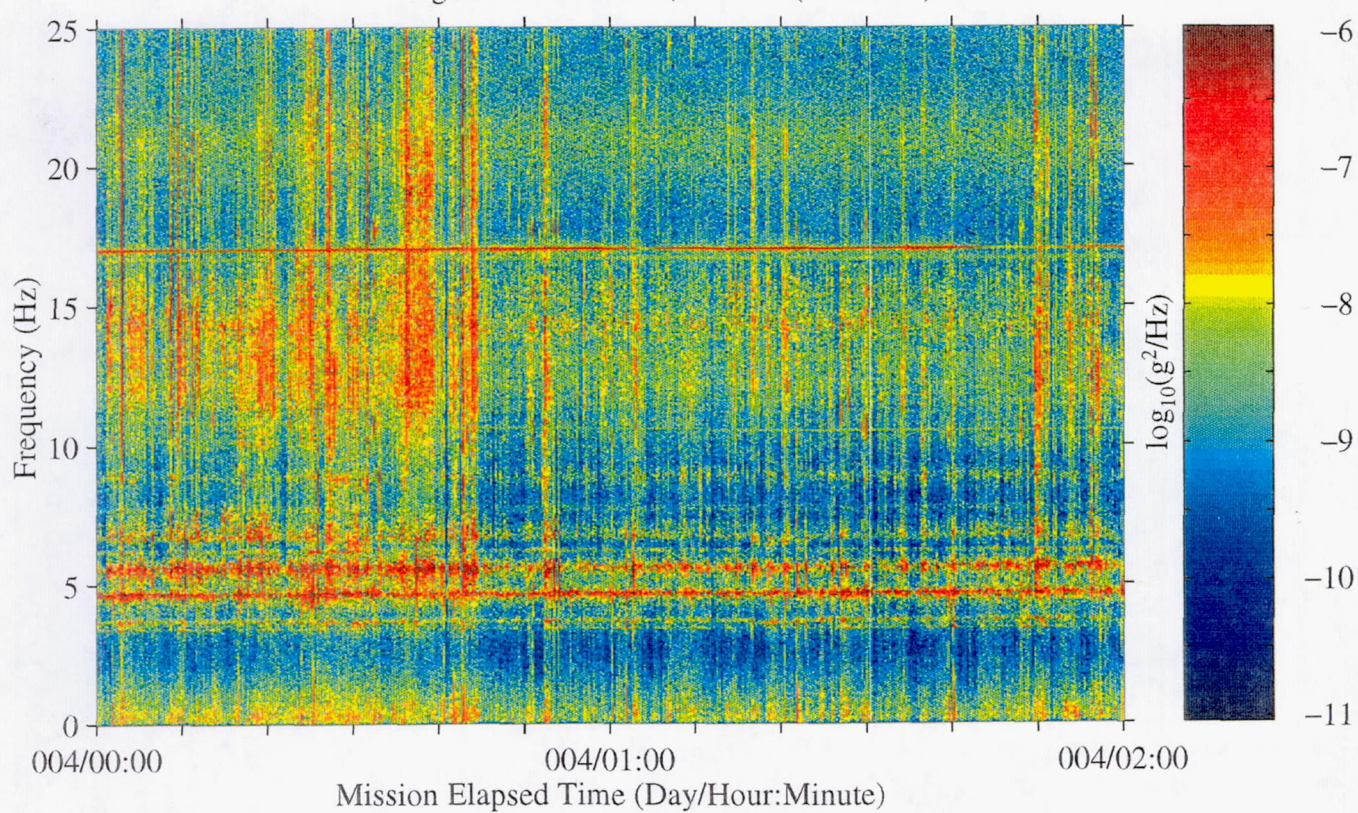




Figure 47: USML-2, Head C (fc=25 Hz)

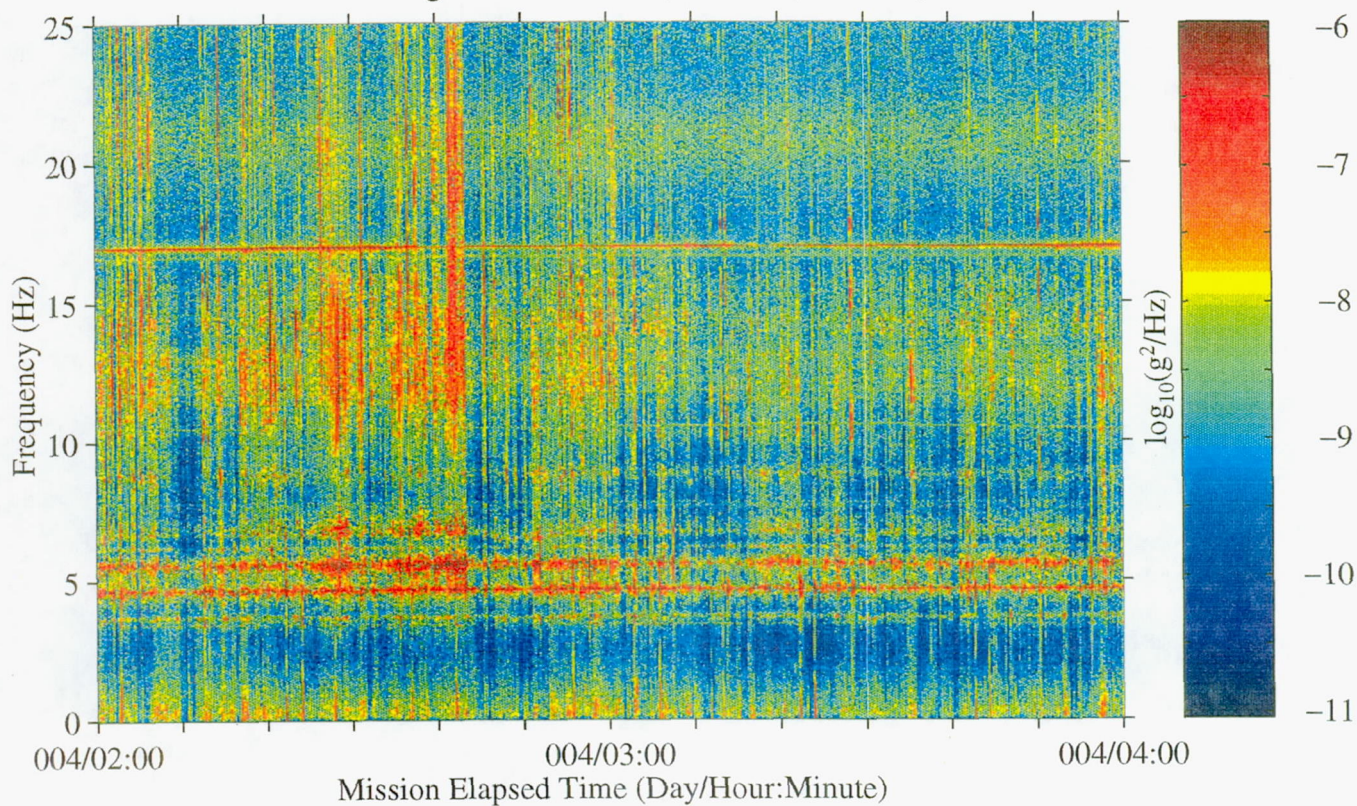


Figure 48: USML-2, Head C (fc=25 Hz)

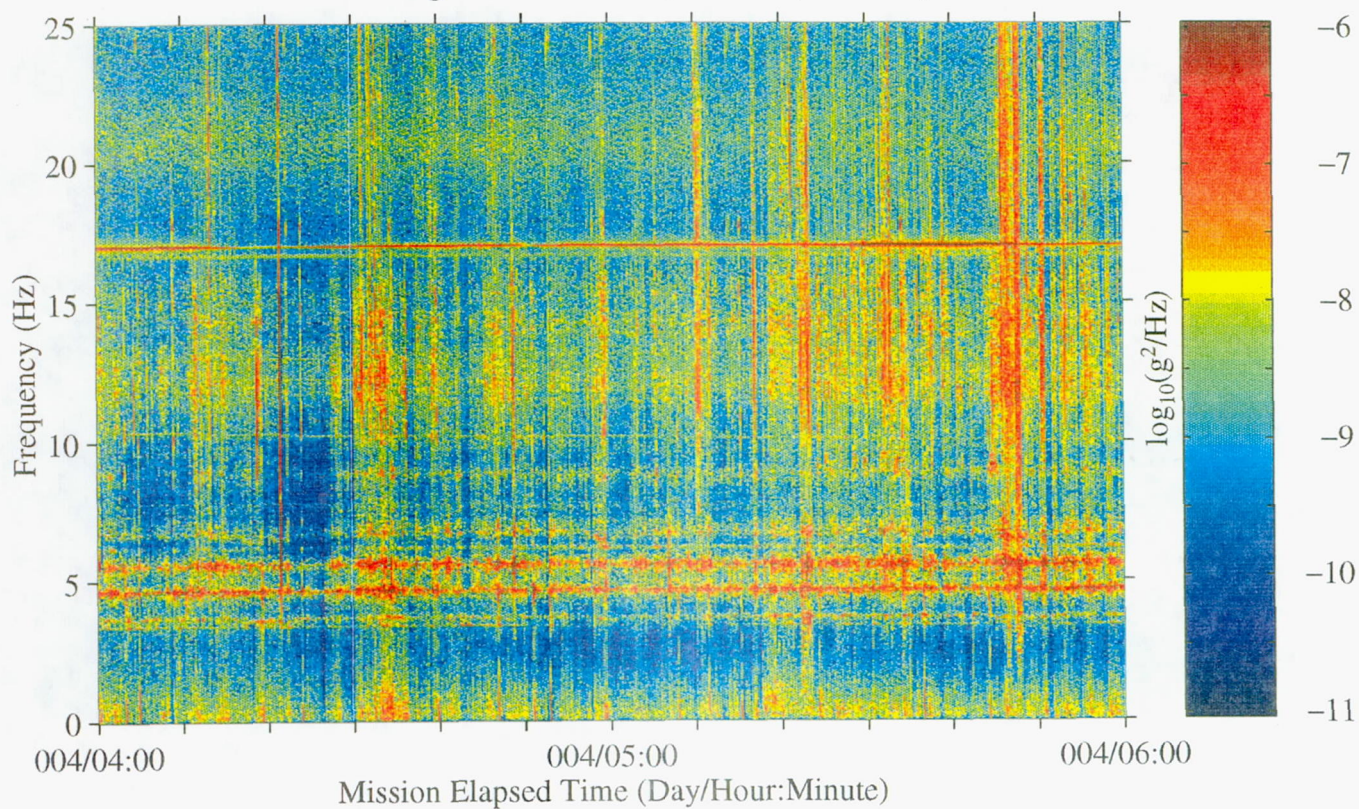




Figure 49: USML-2, Head C (fc=25 Hz)

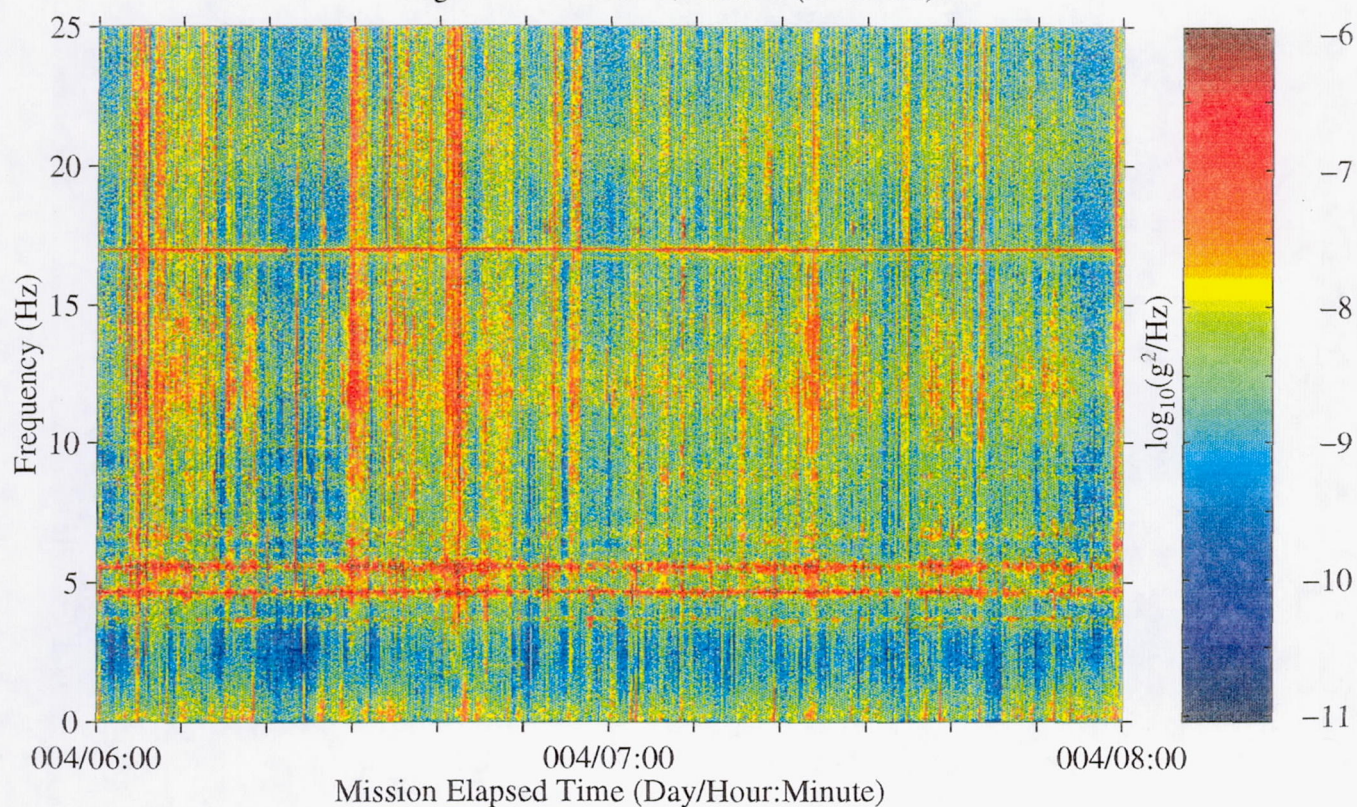


Figure 50: USML-2, Head C (fc=25 Hz)

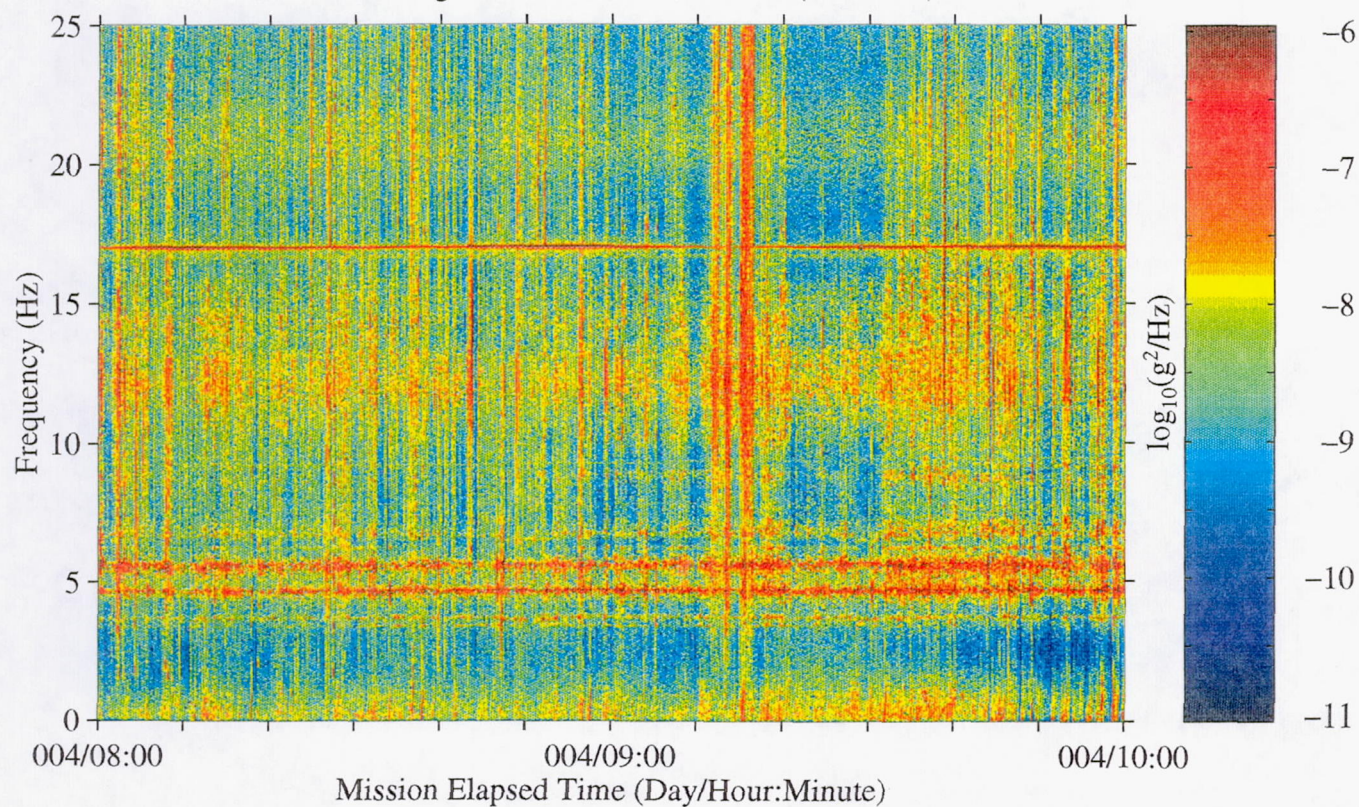




Figure 51: USML-2, Head C (fc=25 Hz)

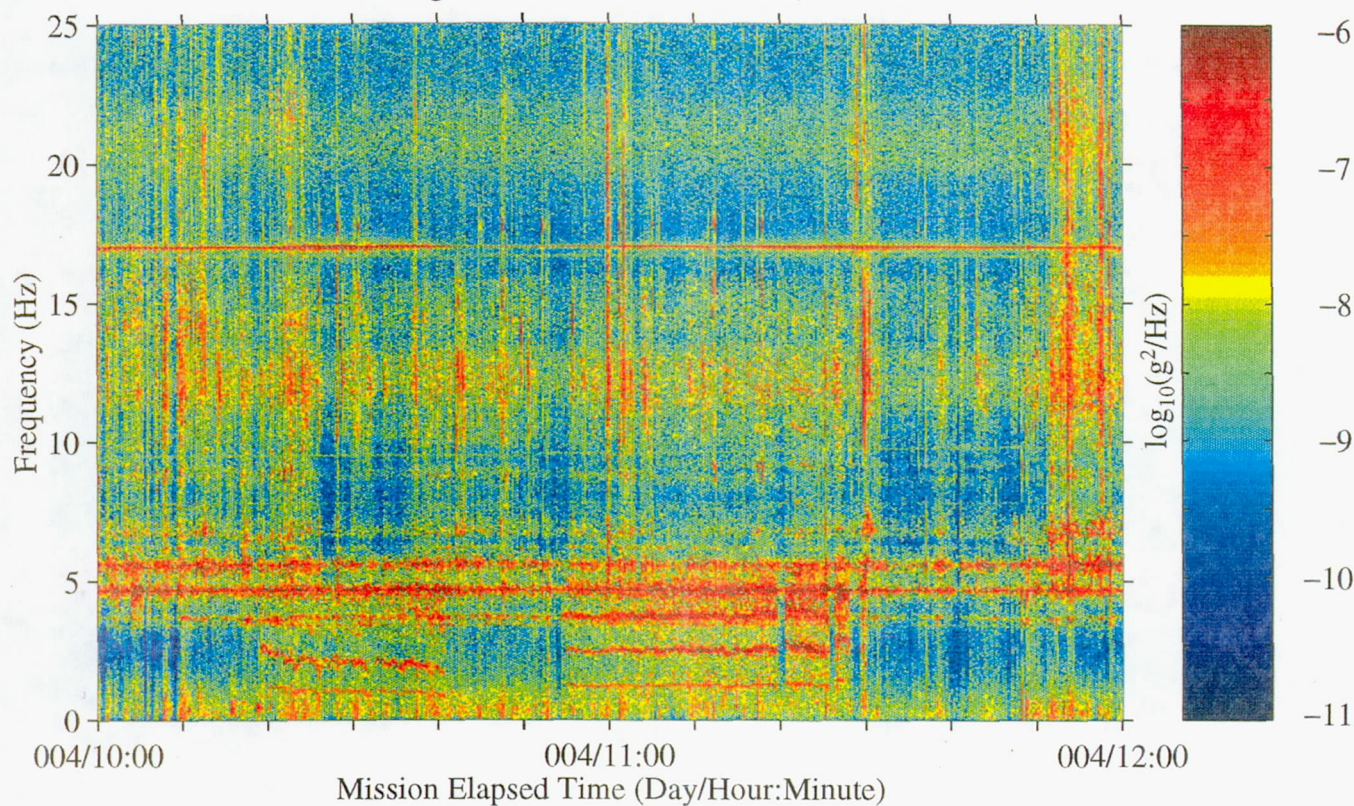


Figure 52: USML-2, Head C (fc=25 Hz)

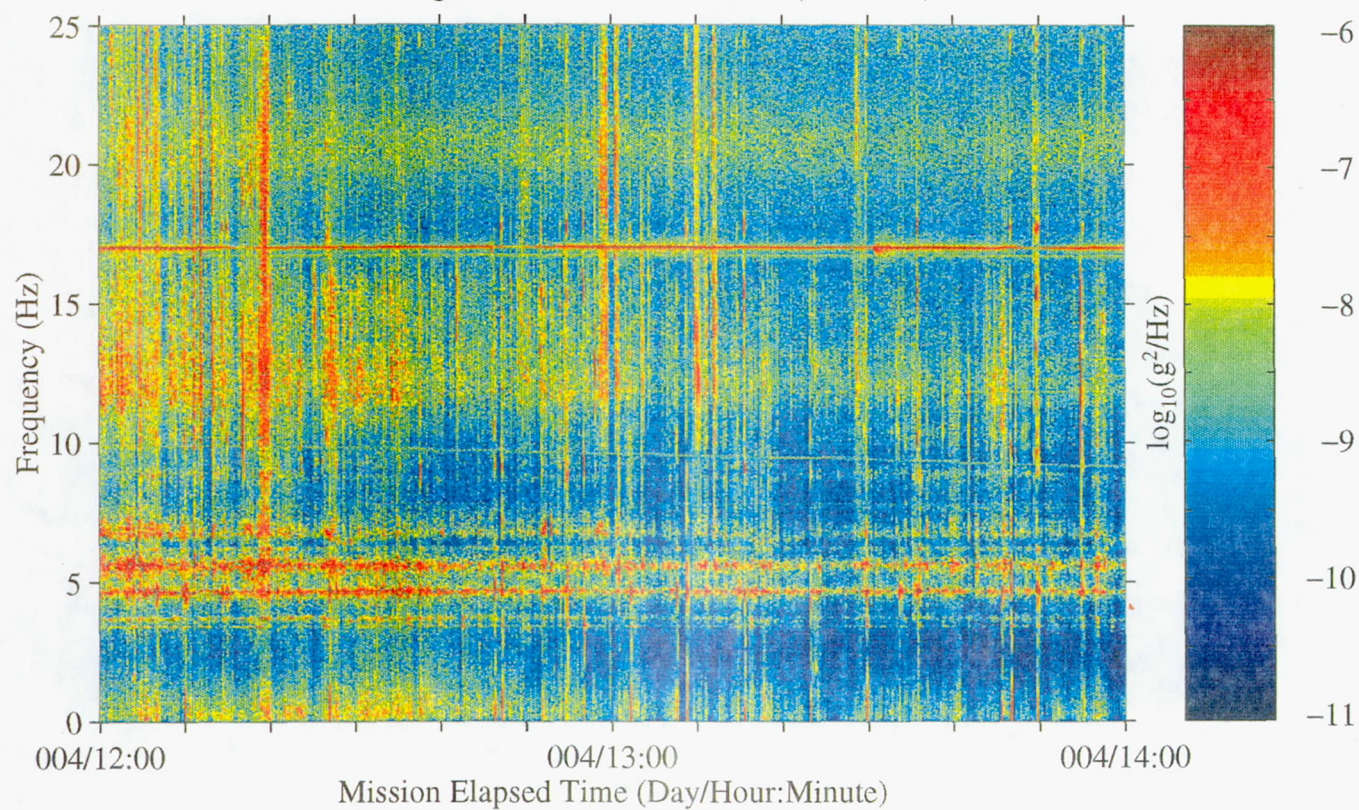




Figure 53: USML-2, Head C (fc=25 Hz)

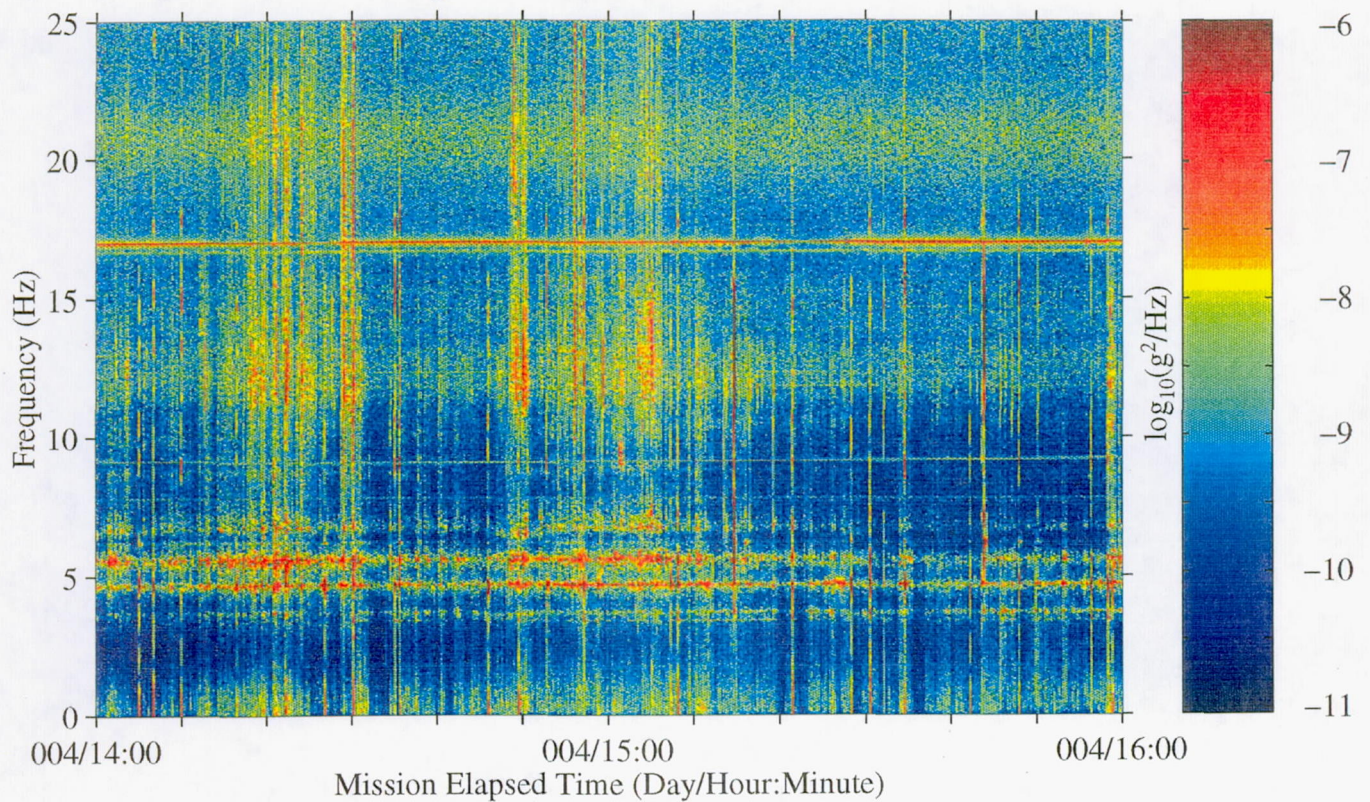


Figure 54: USML-2, Head C (fc=25 Hz)

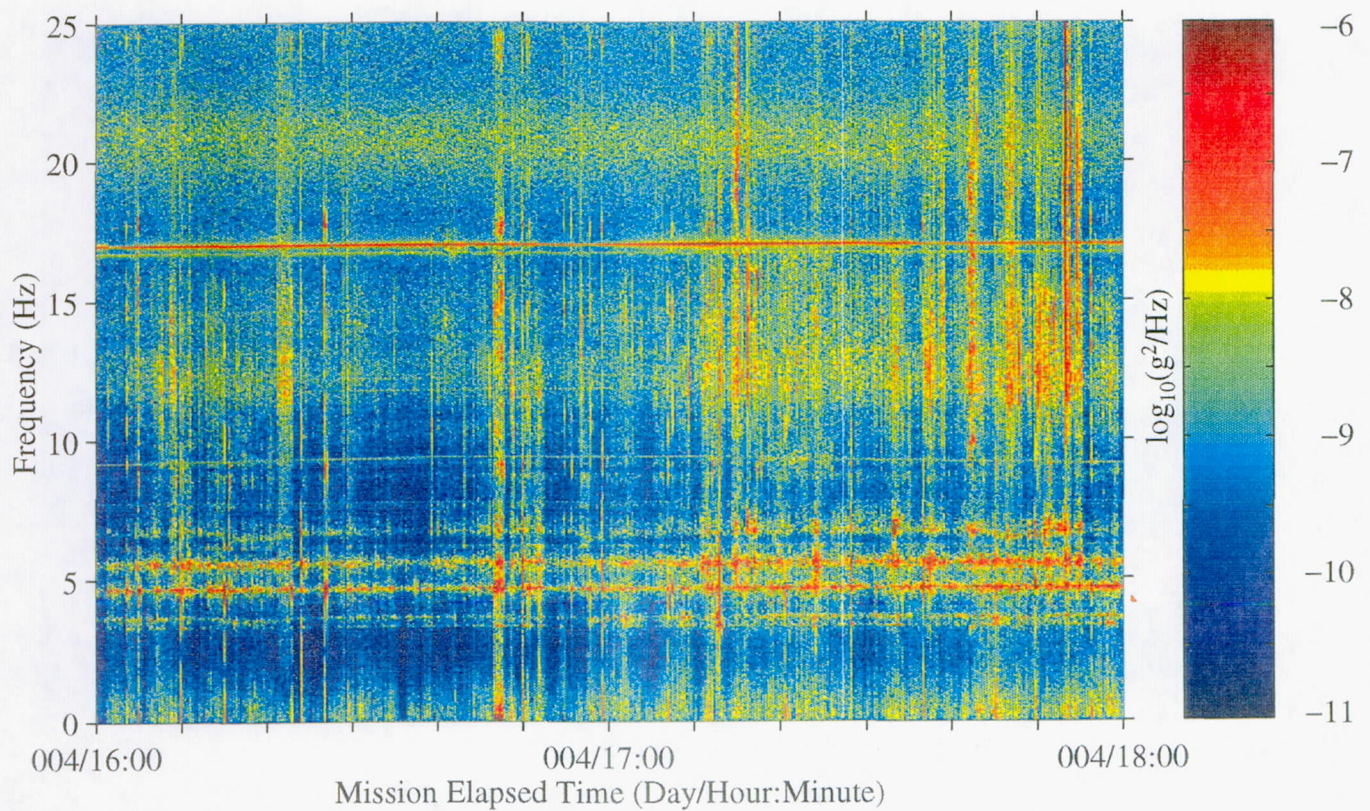




Figure 55: USML-2, Head C (fc=25 Hz)

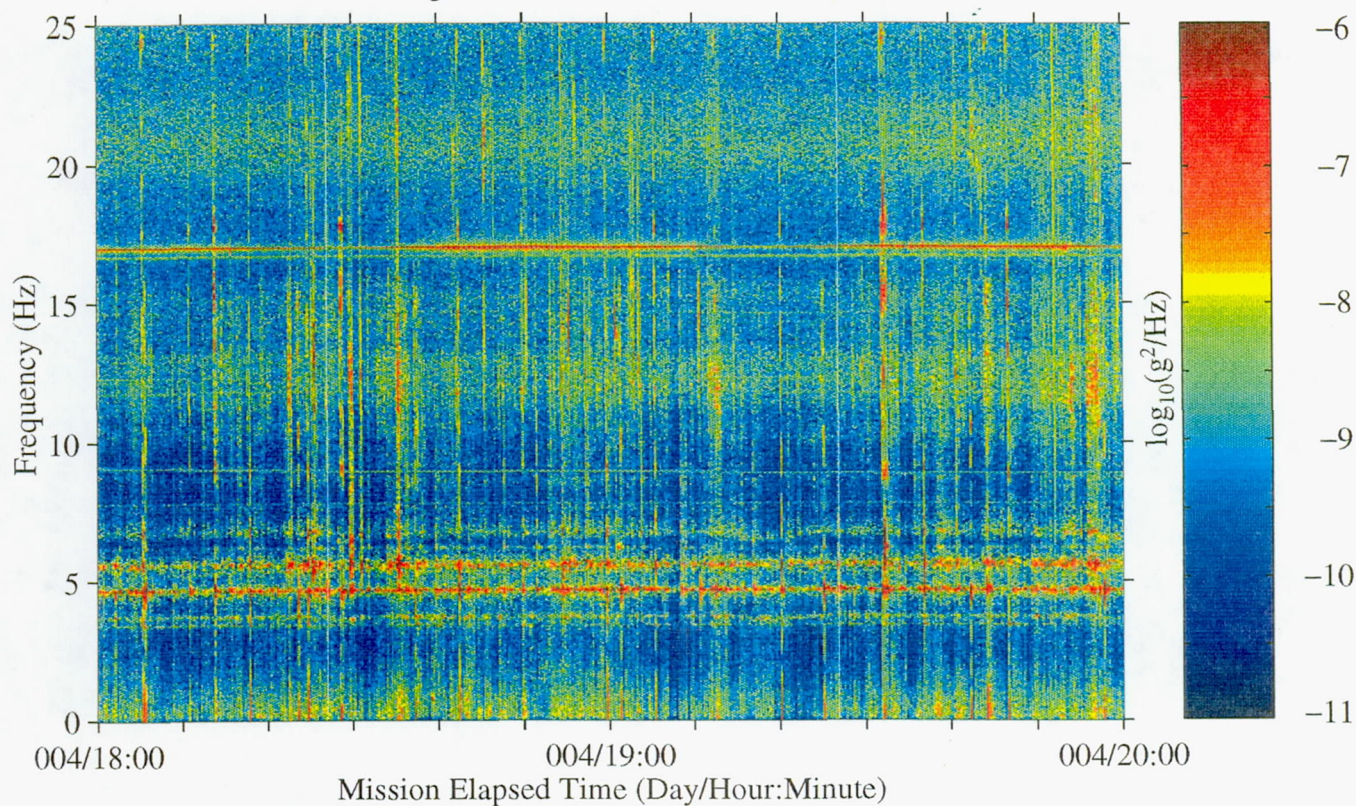


Figure 56: USML-2, Head C (fc=25 Hz)

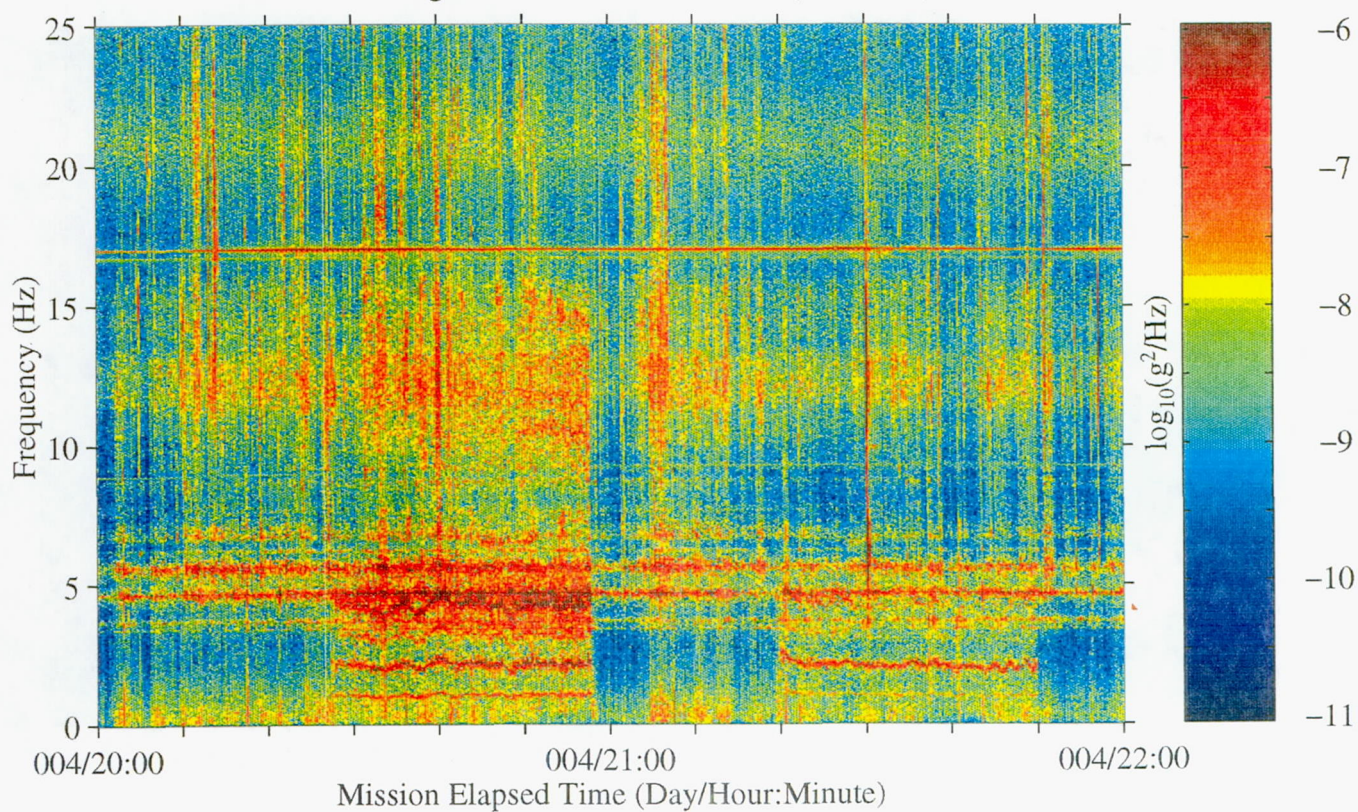




Figure 57: USML-2, Head C (fc=25 Hz)

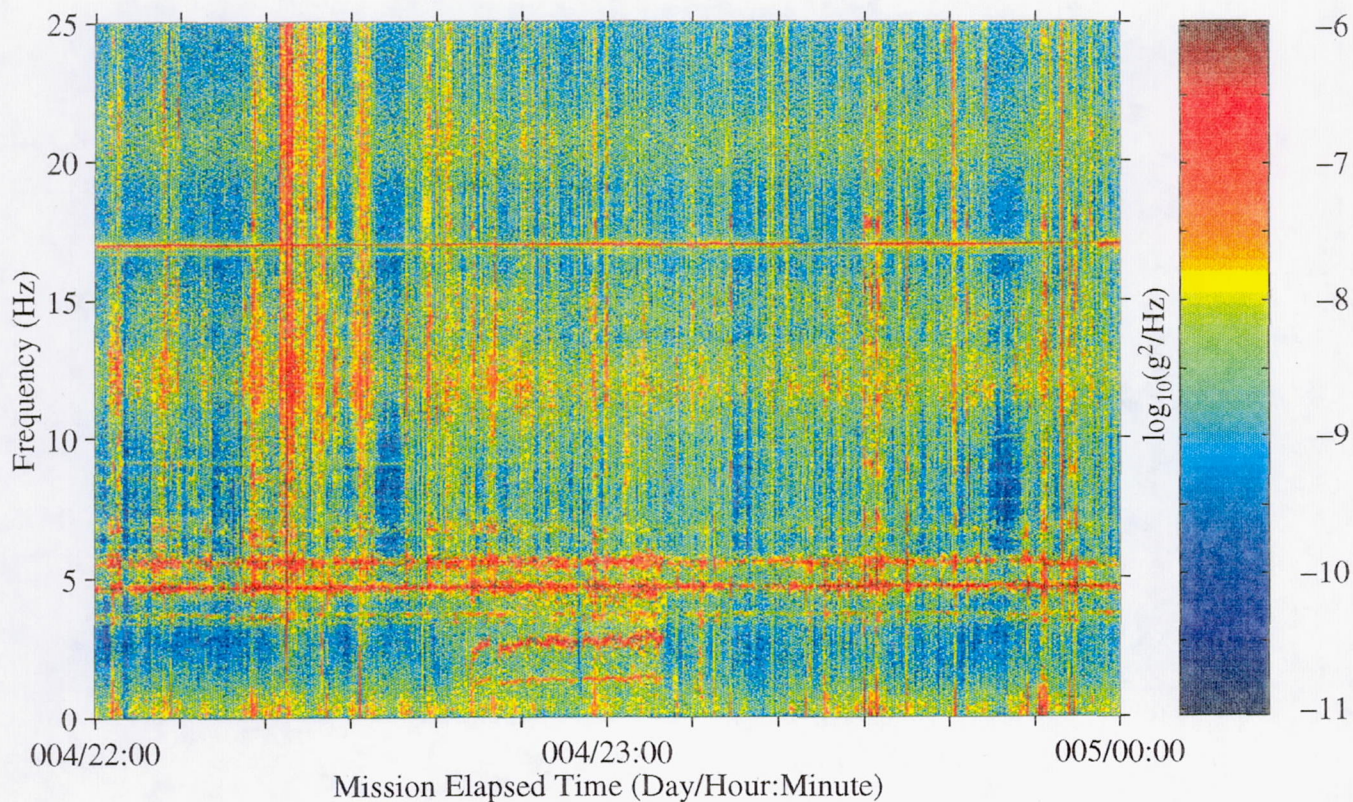


Figure 58: USML-2, Head C (fc=25 Hz)

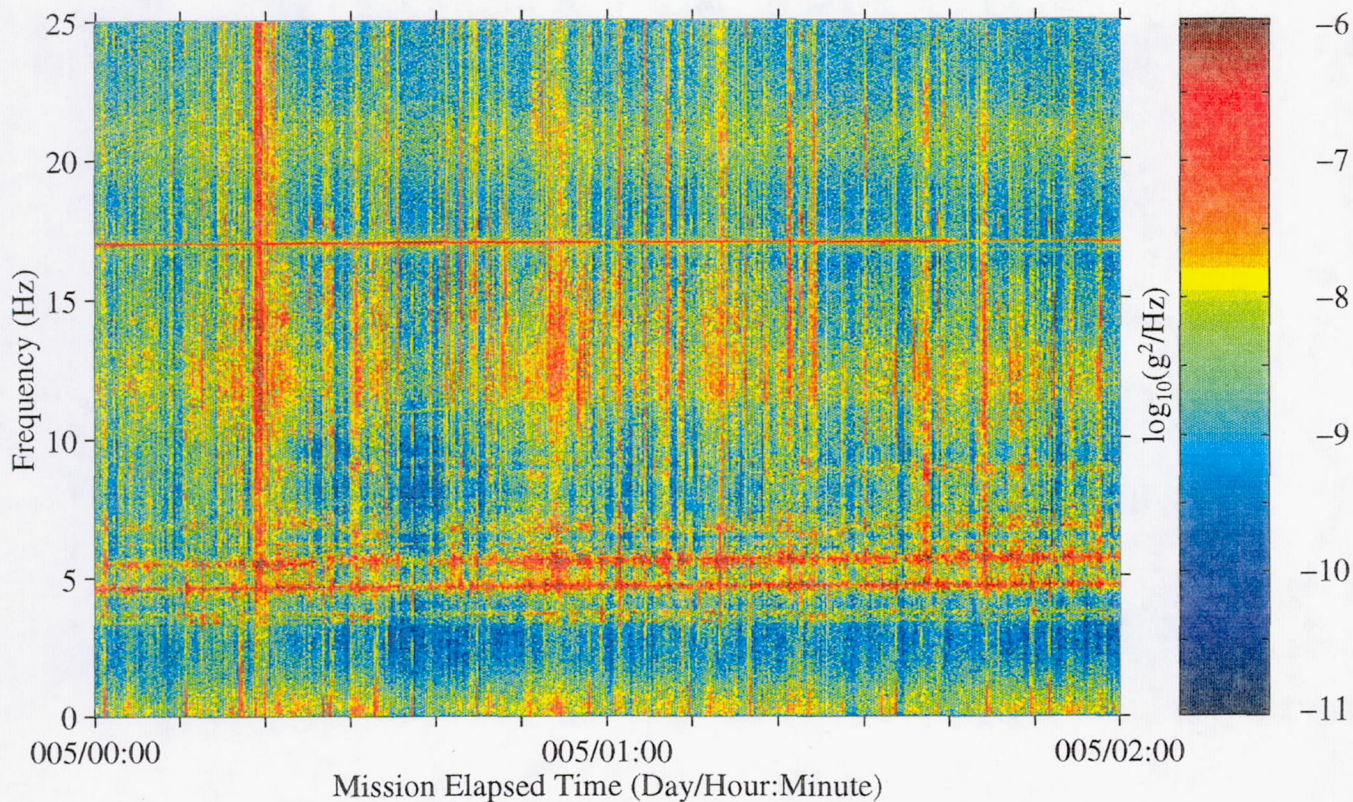




Figure 59: USML-2, Head C (fc=25 Hz)

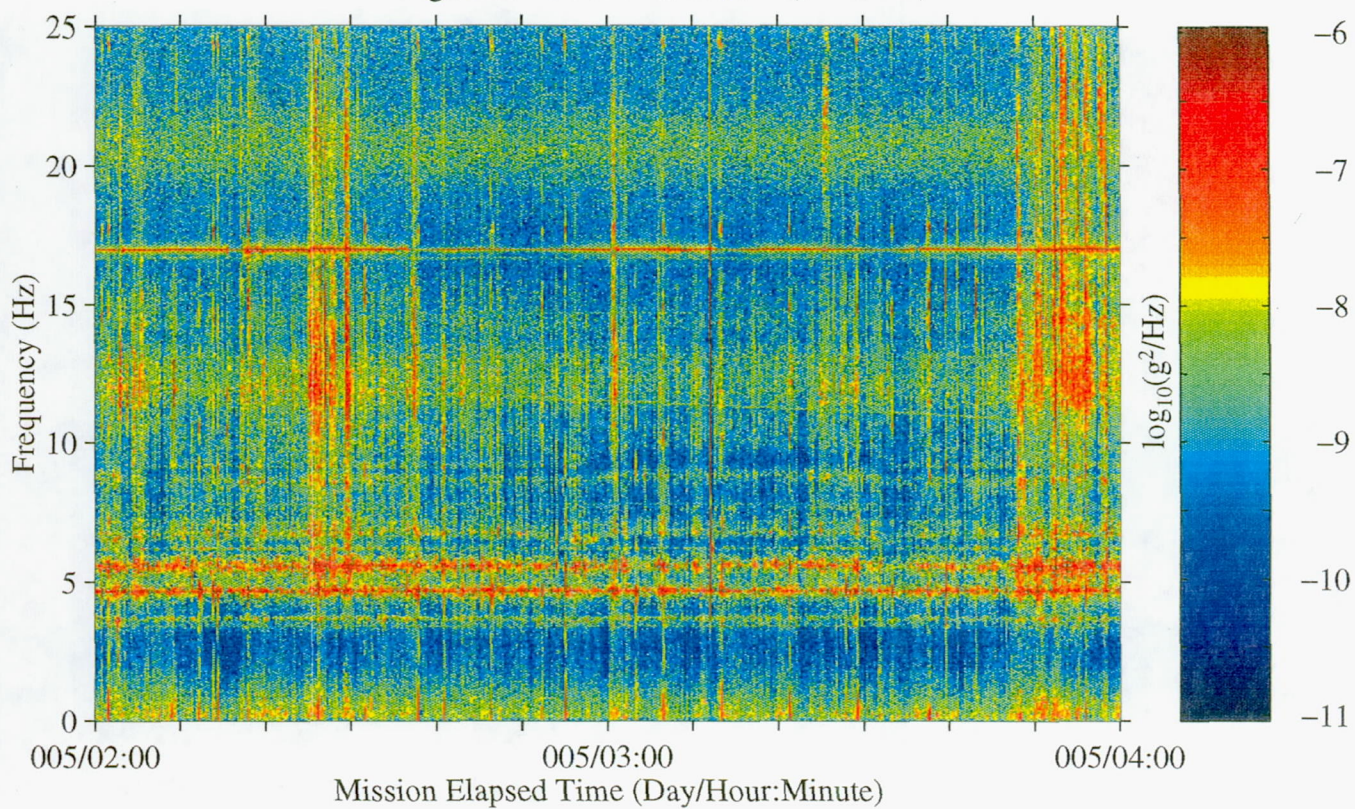


Figure 60: USML-2, Head C (fc=25 Hz)

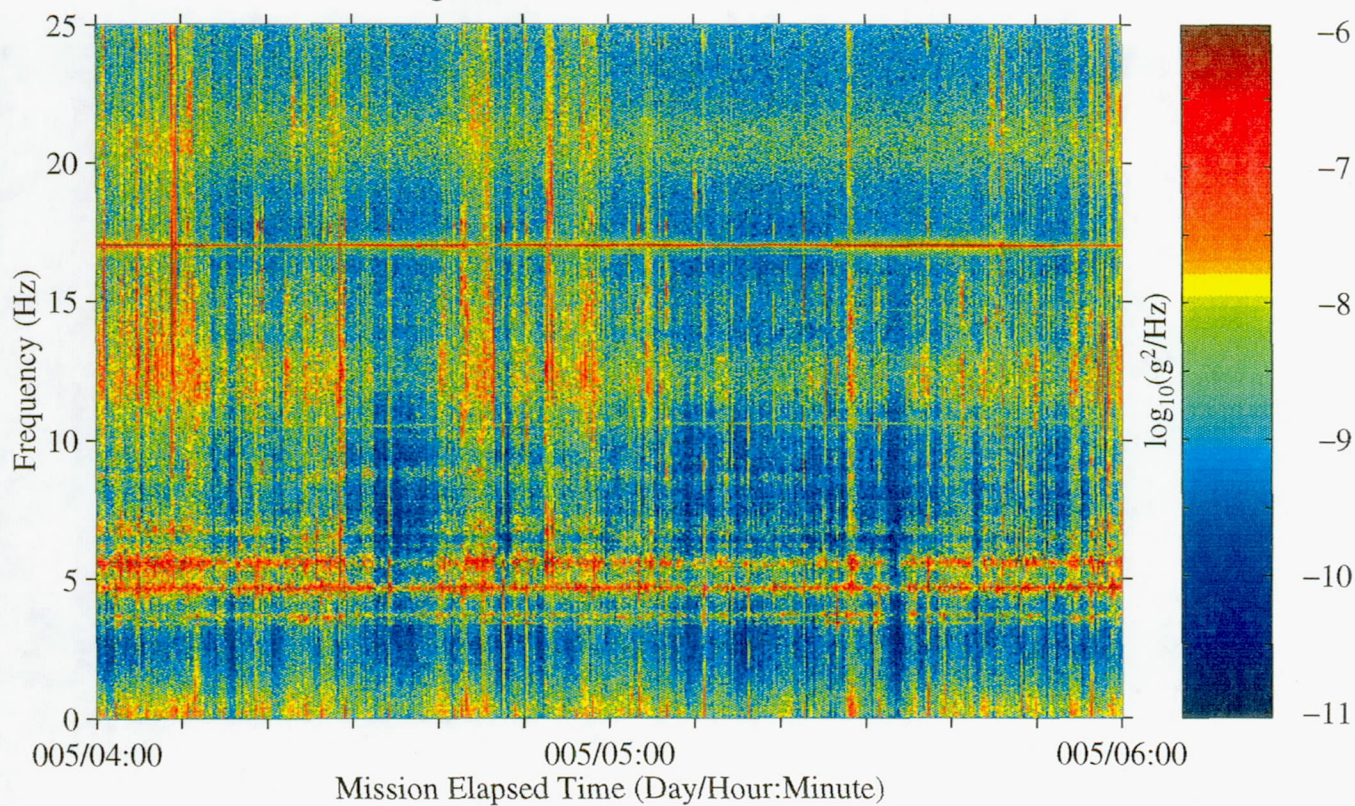




Figure 61: USML-2, Head C (fc=25 Hz)

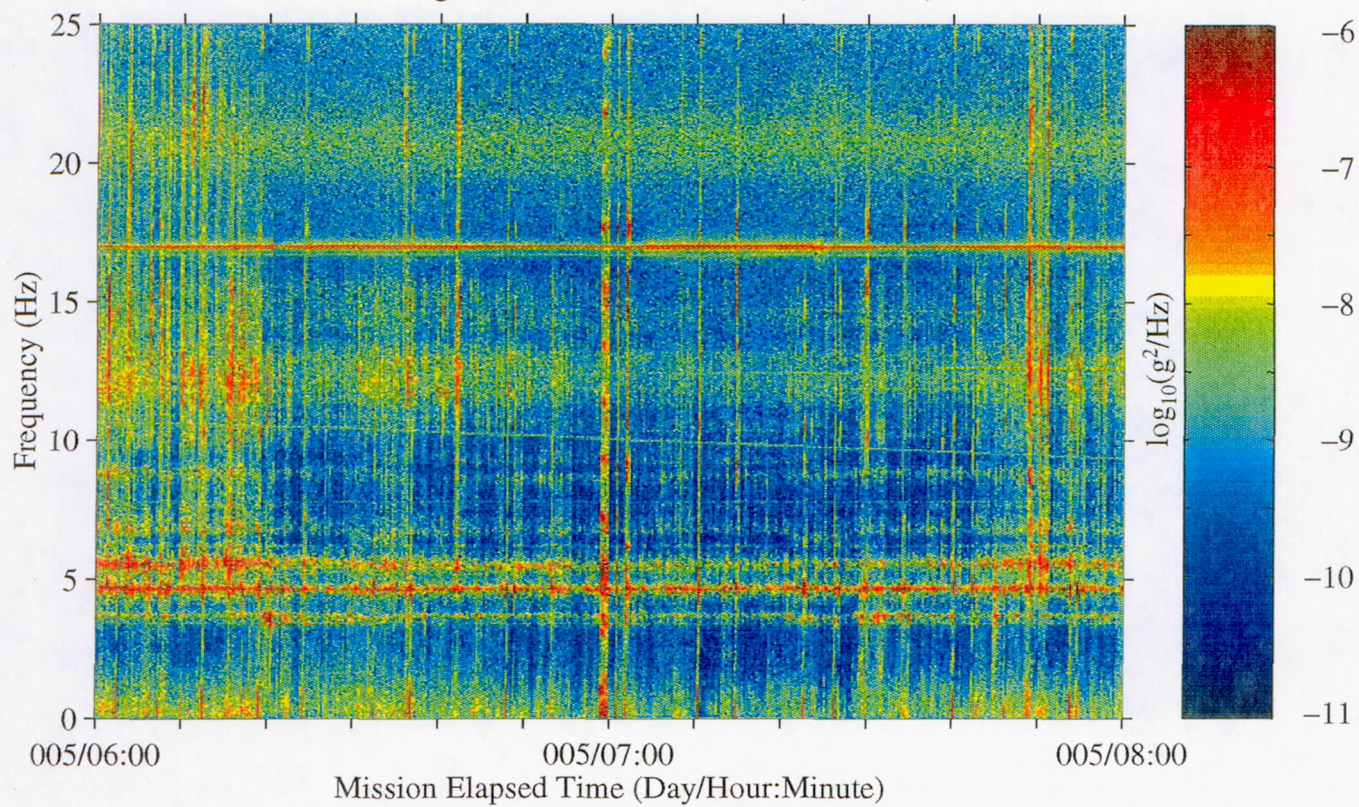


Figure 62: USML-2, Head C (fc=25 Hz)

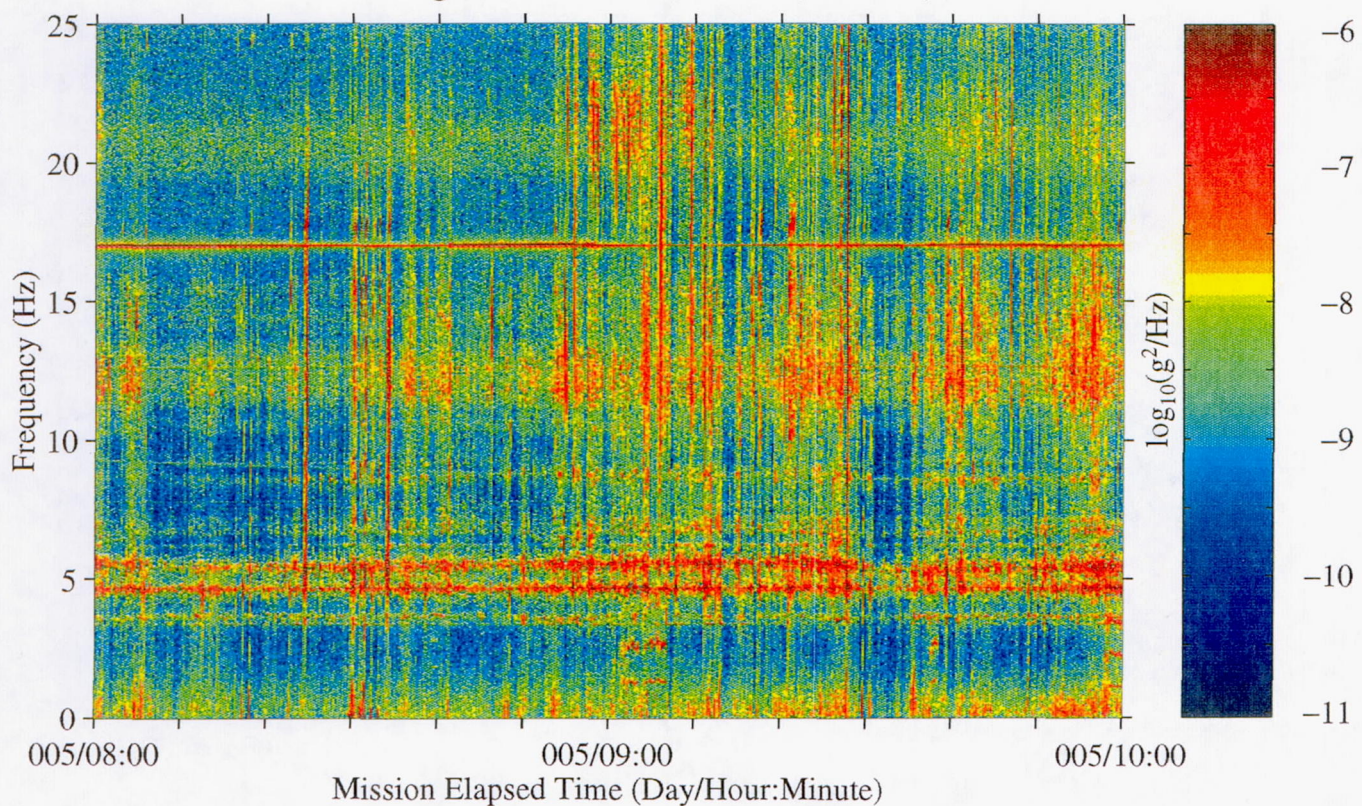




Figure 63: USML-2, Head C (fc=25 Hz)

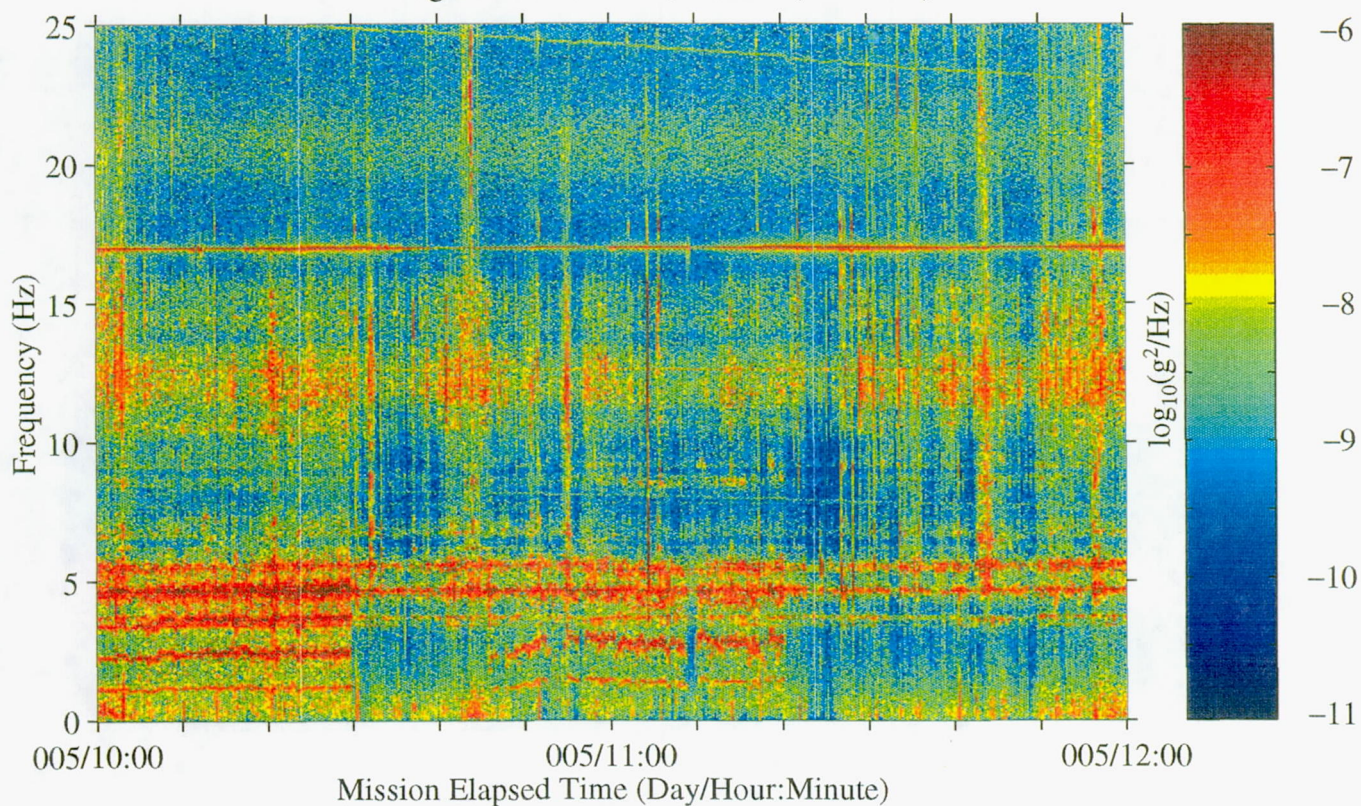


Figure 64: USML-2, Head C (fc=25 Hz)

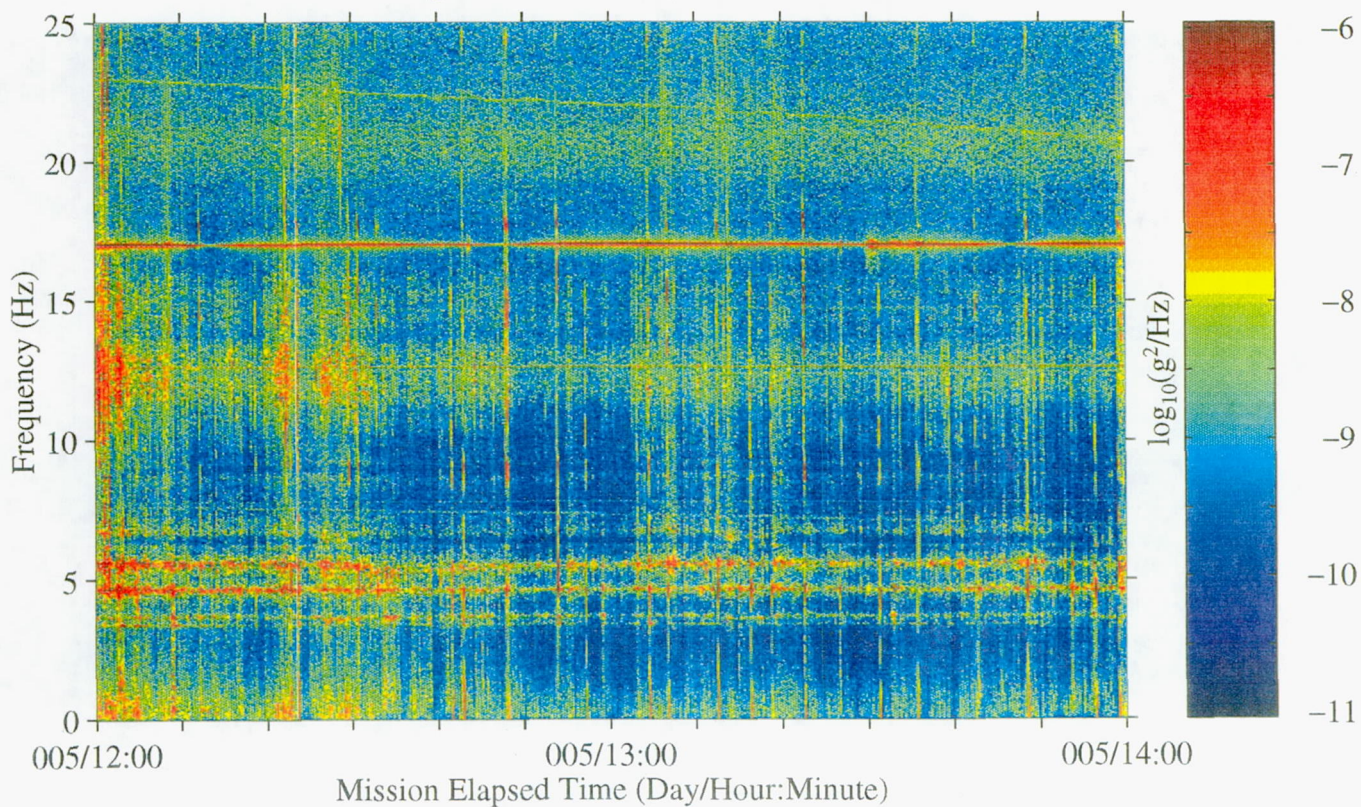




Figure 65: USML-2, Head C (fc=25 Hz)

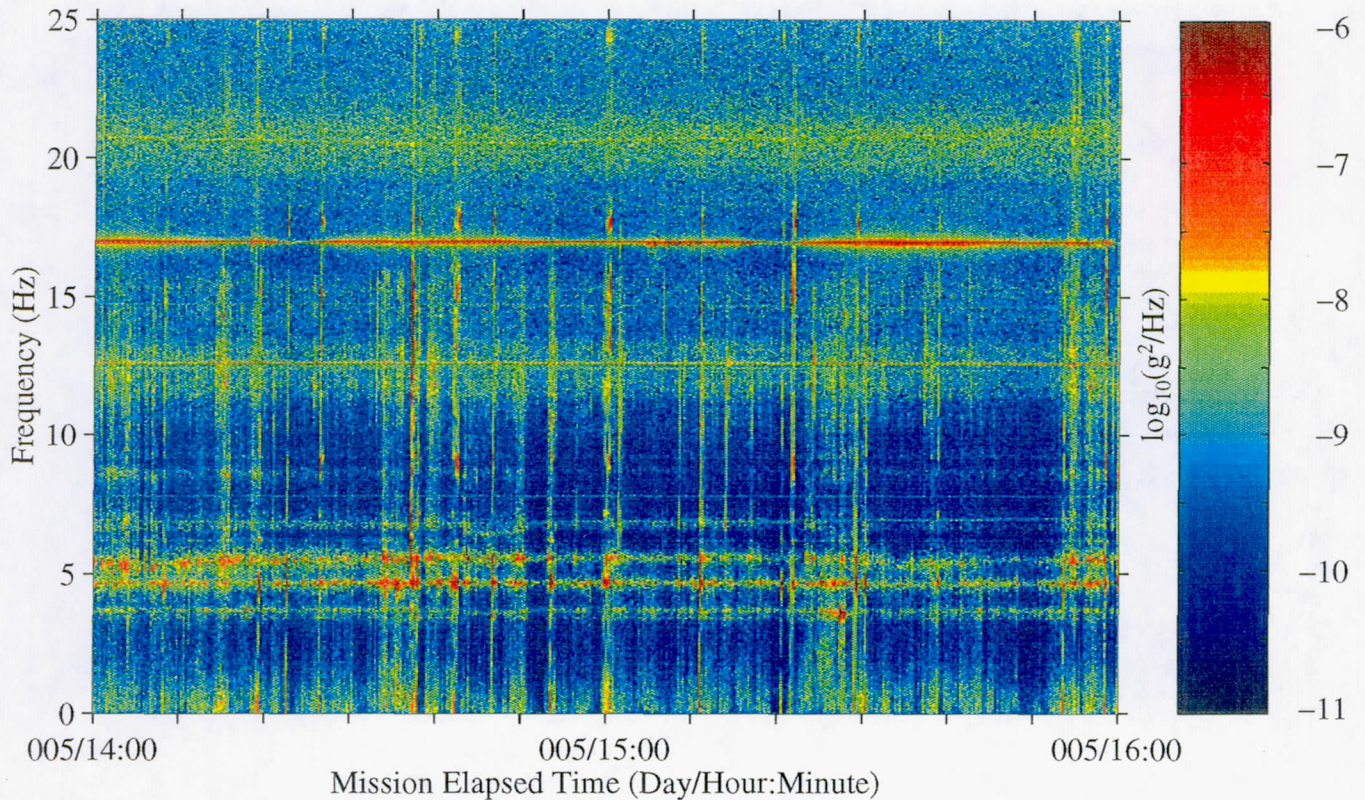


Figure 66: USML-2, Head C (fc=25 Hz)

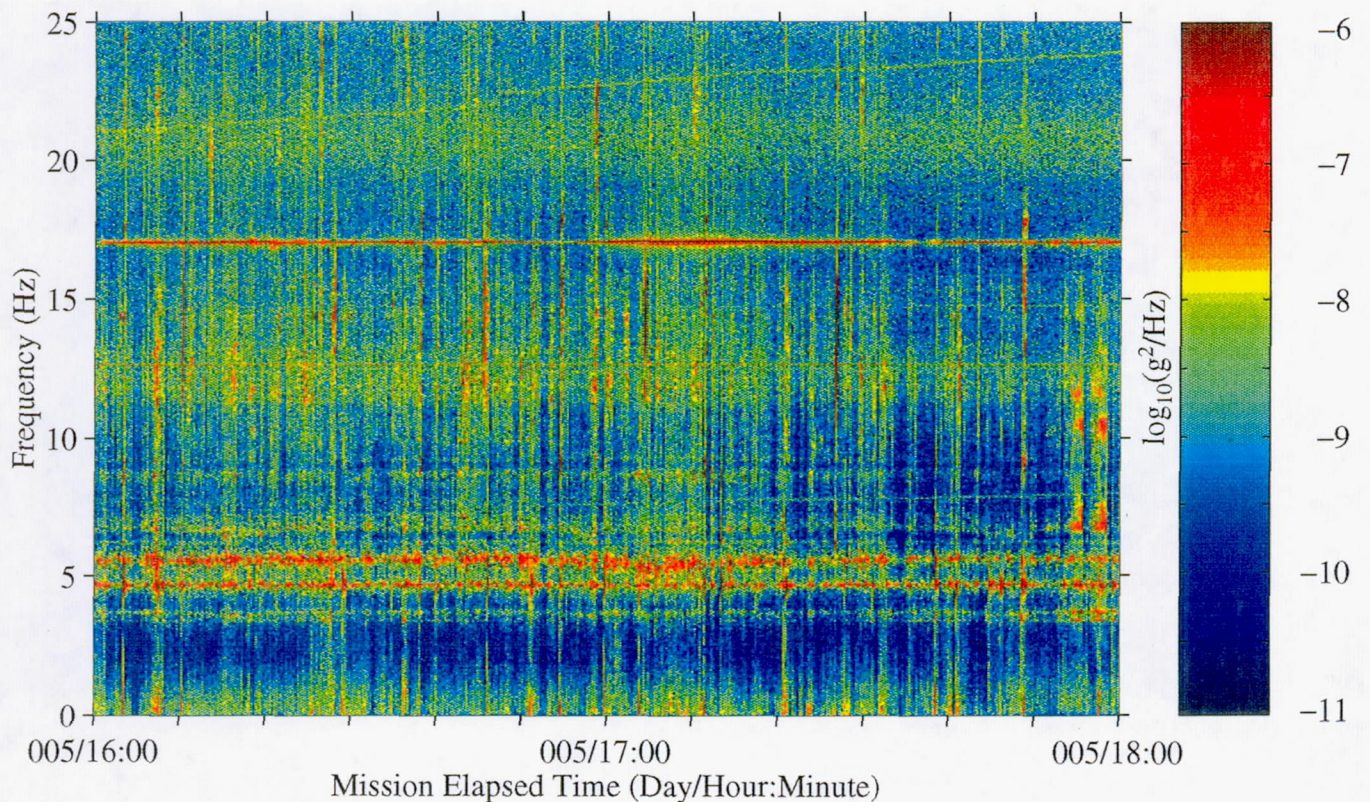




Figure 67: USML-2, Head C (fc=25 Hz)

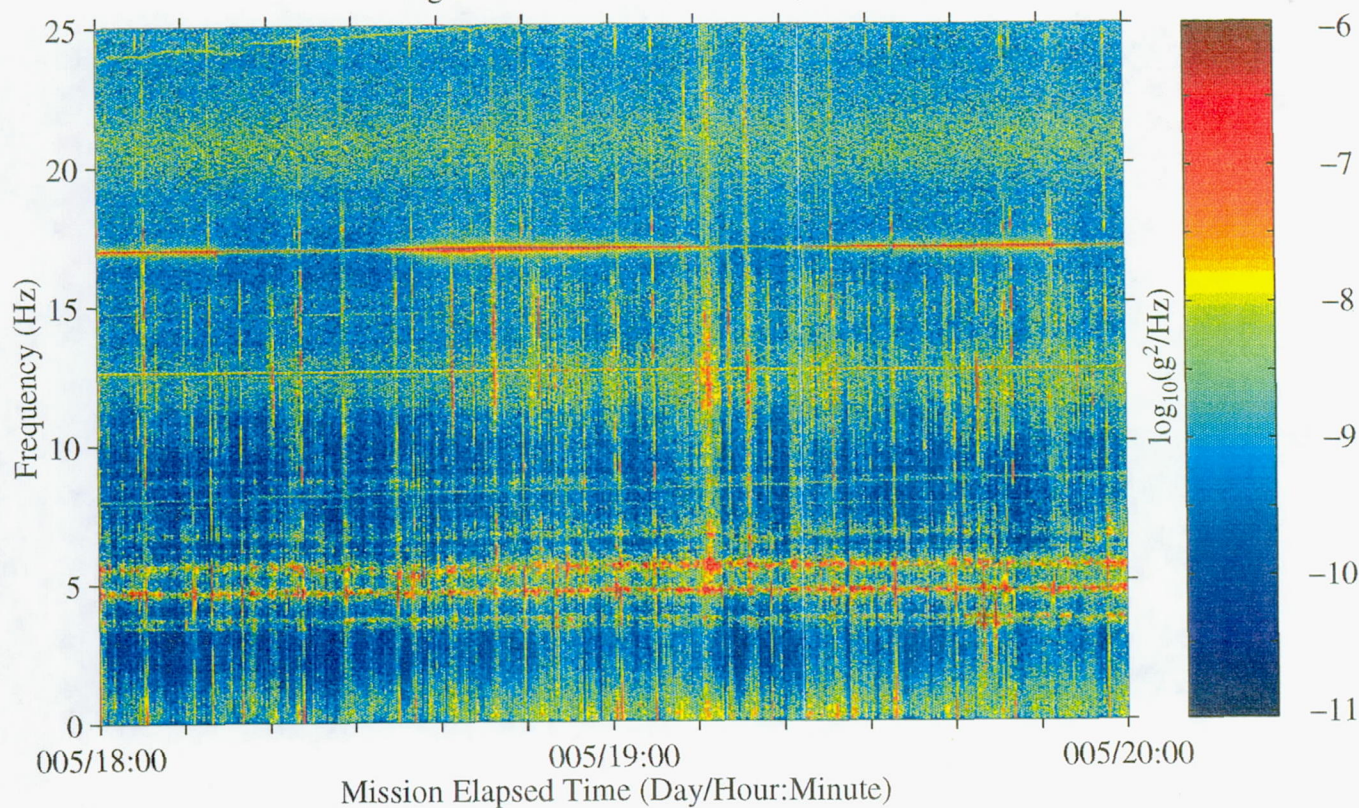


Figure 68: USML-2, Head C (fc=25 Hz)

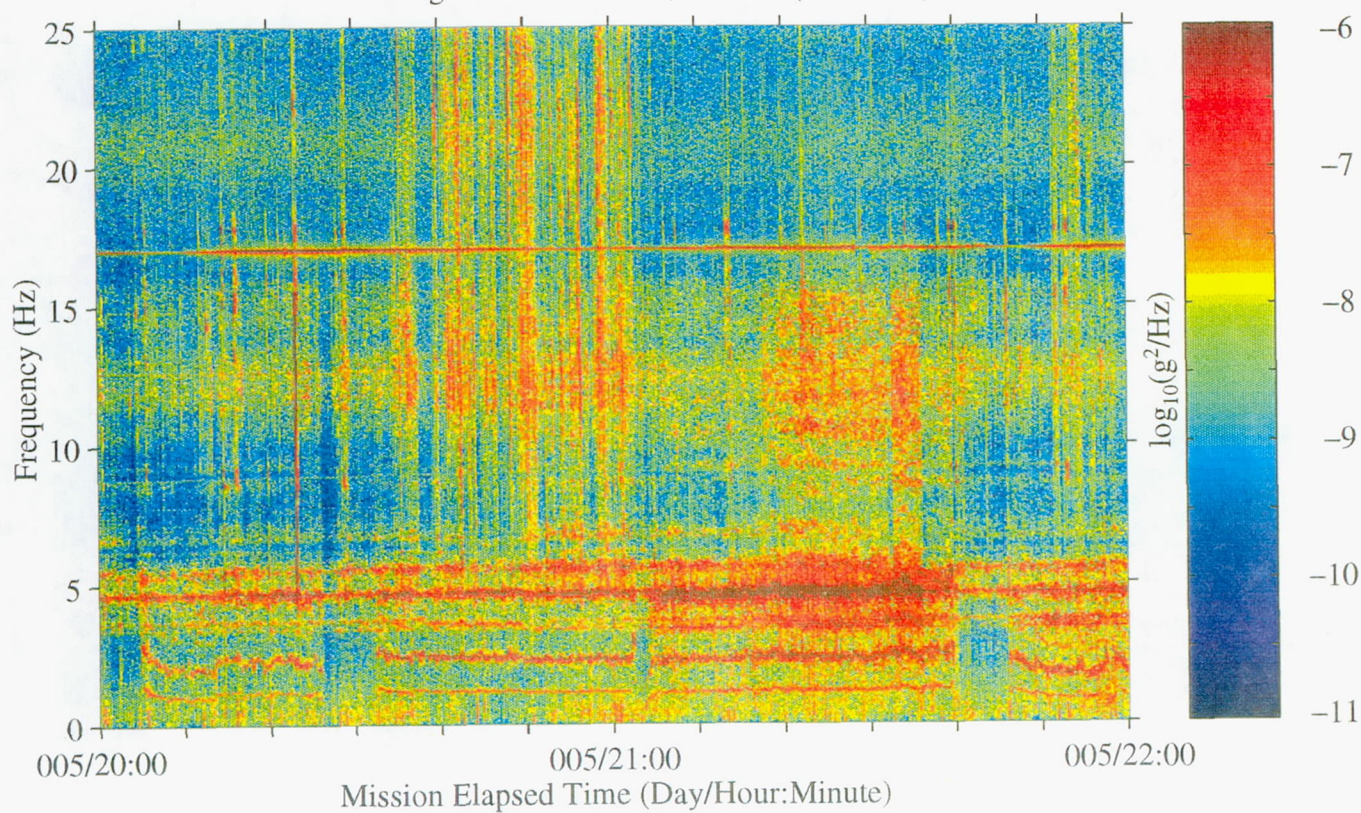




Figure 69: USML-2, Head C (fc=25 Hz)

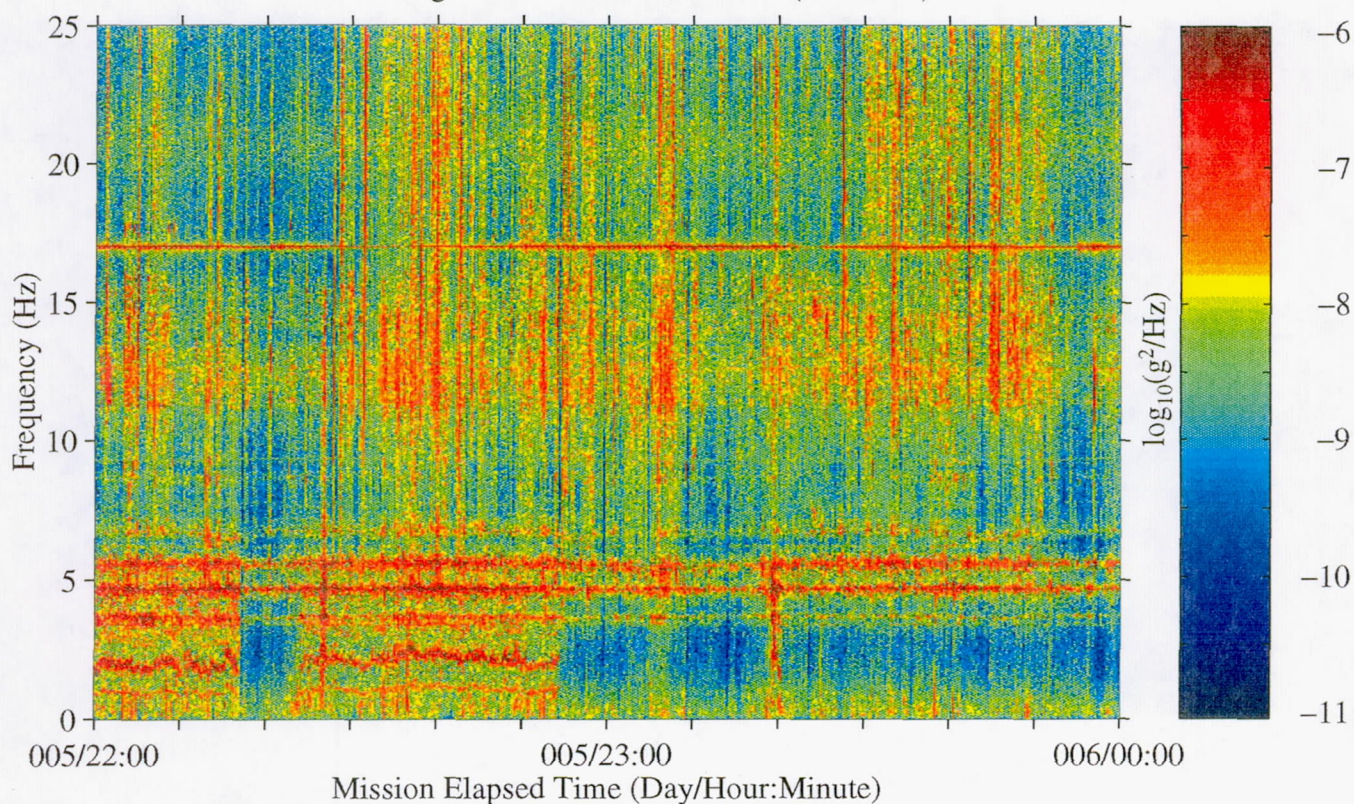


Figure 70: USML-2, Head C (fc=25 Hz)

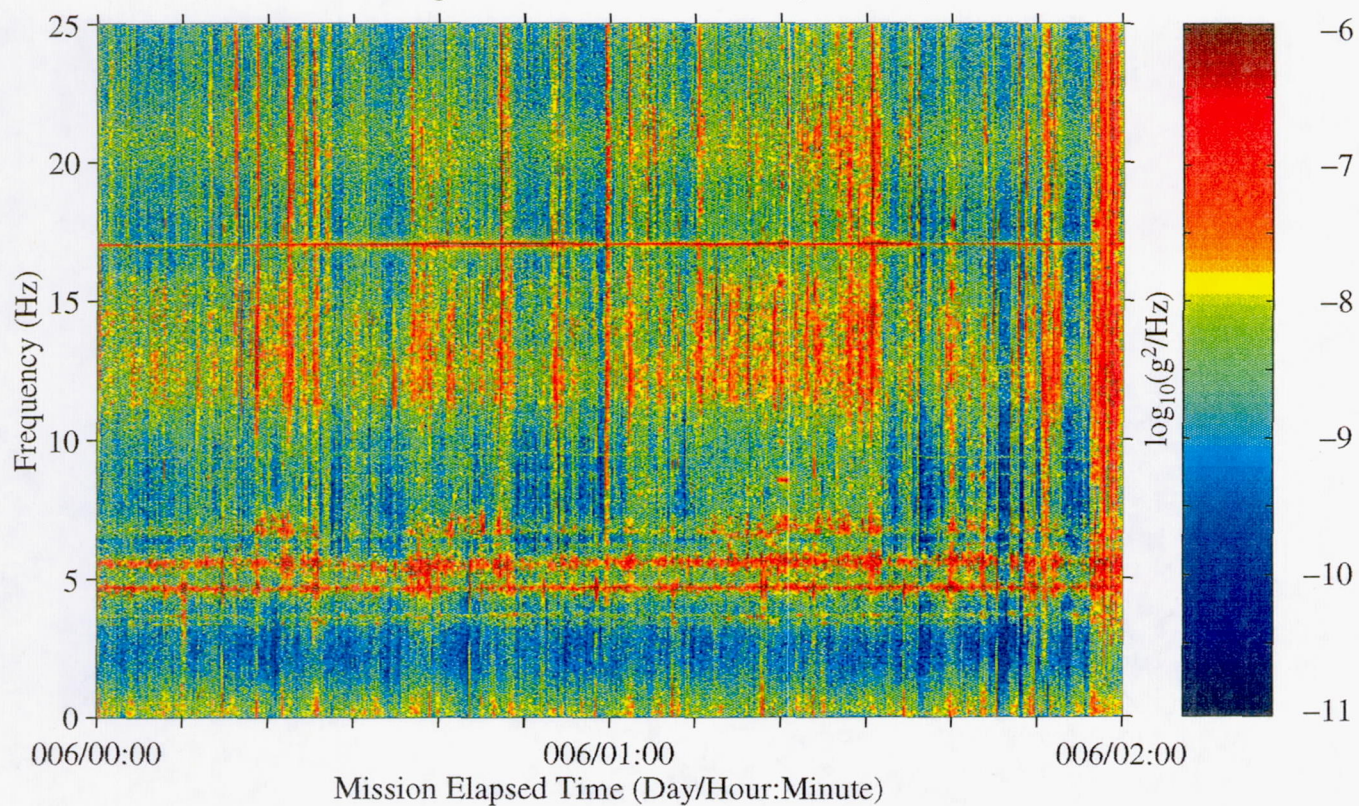




Figure 71: USML-2, Head C (fc=25 Hz)

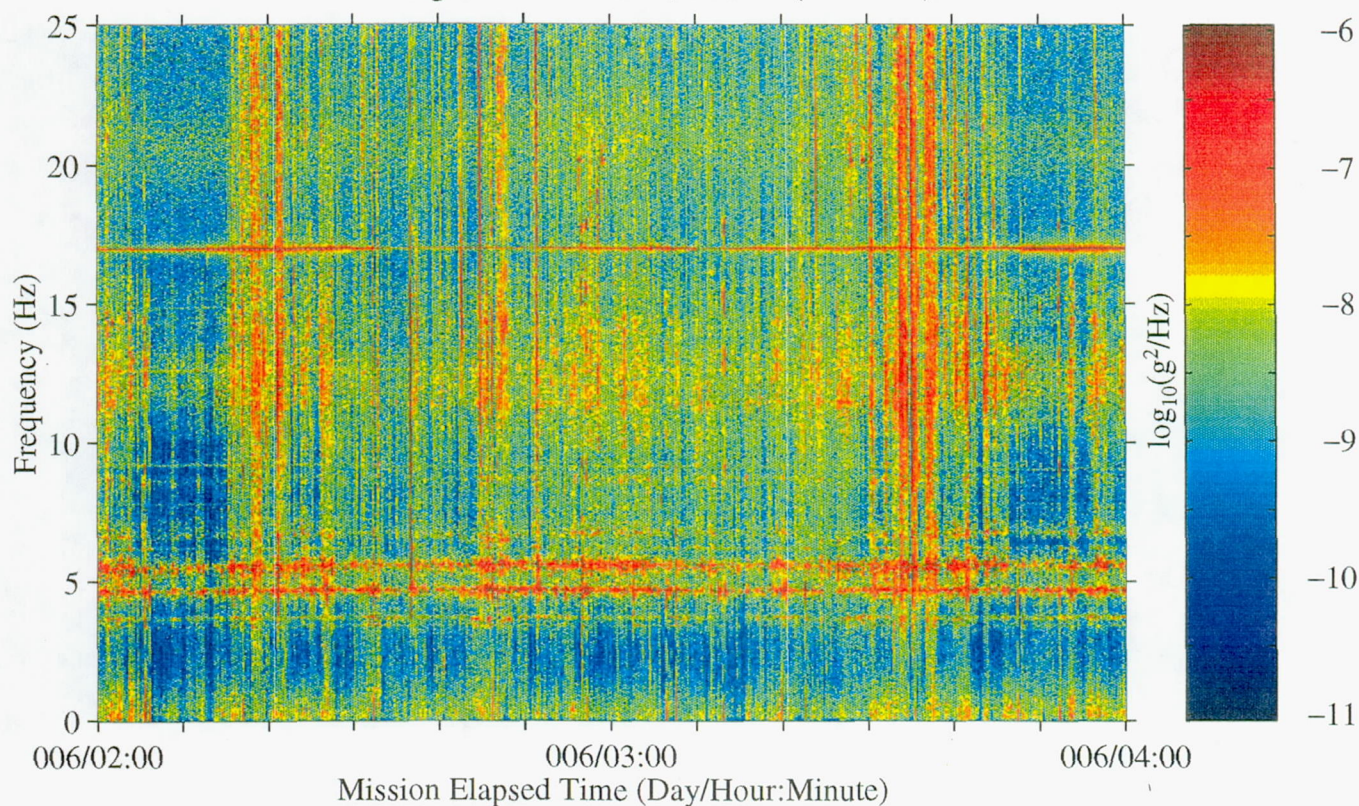


Figure 72: USML-2, Head C (fc=25 Hz)

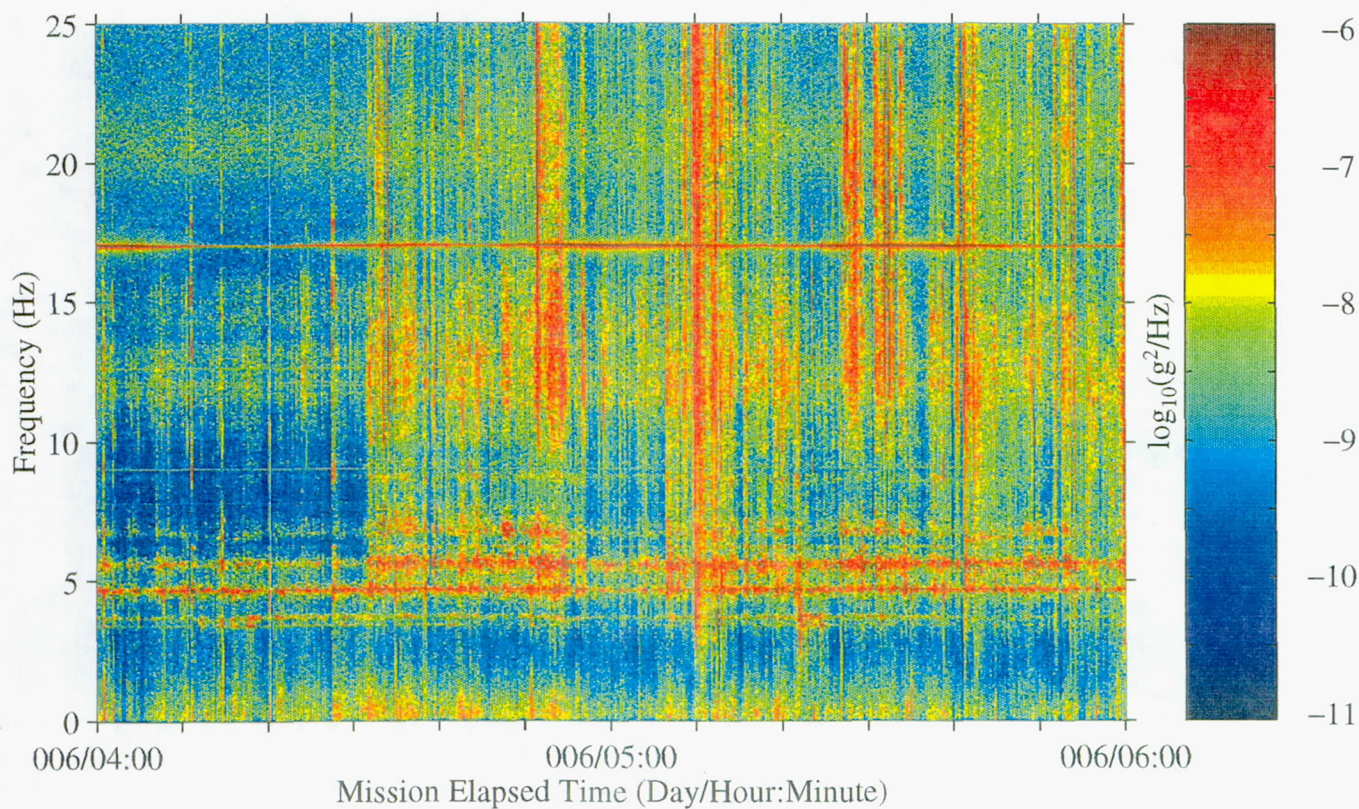




Figure 73: USML-2, Head C (fc=25 Hz)

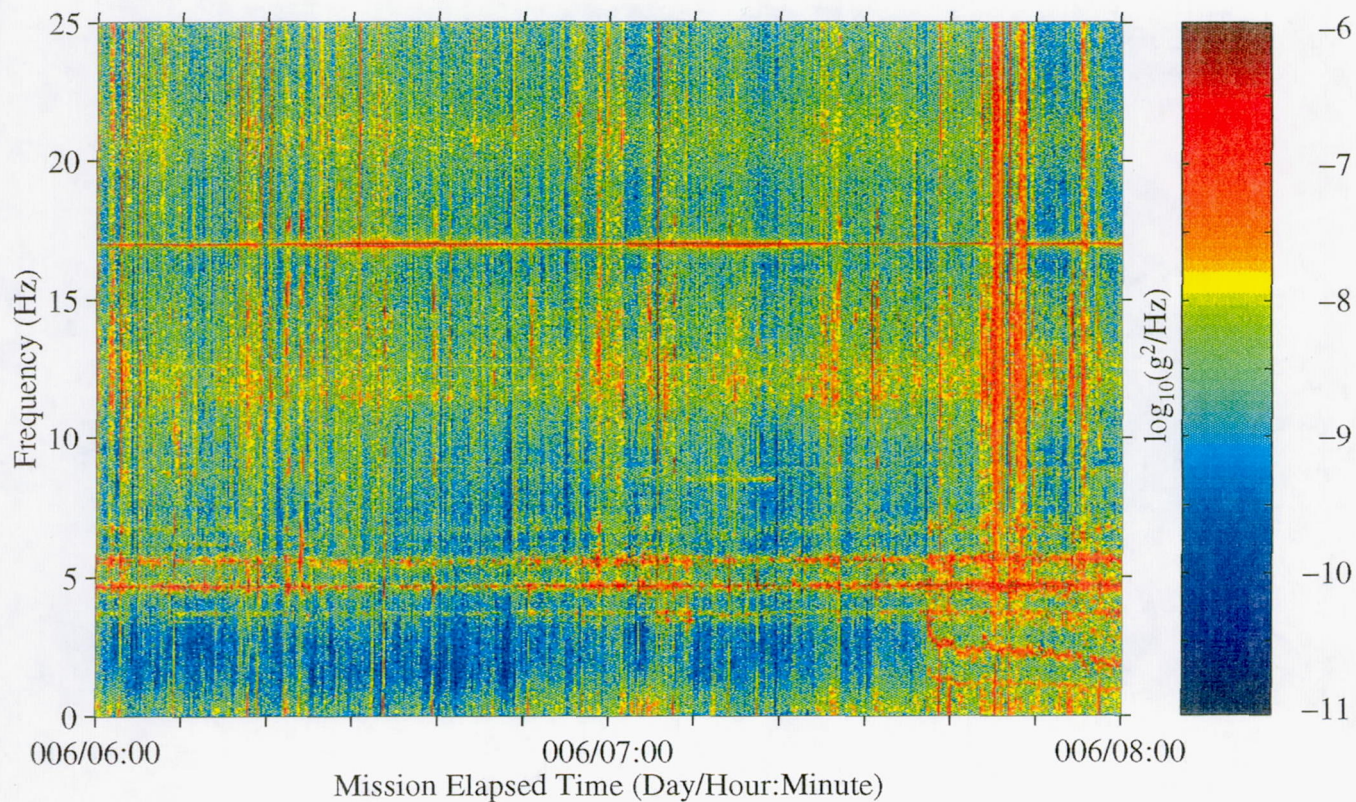


Figure 74: USML-2, Head C (fc=25 Hz)

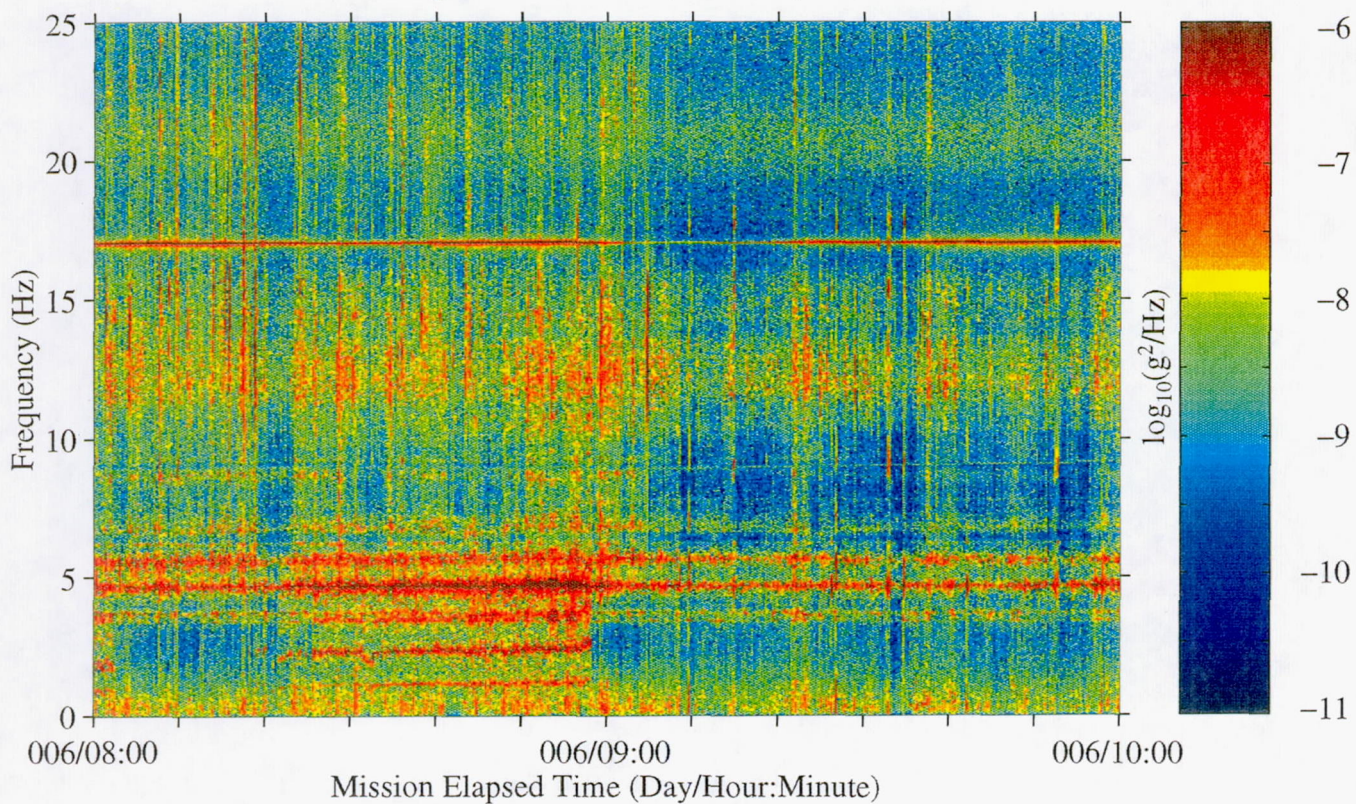




Figure 75: USML-2, Head C (fc=25 Hz)

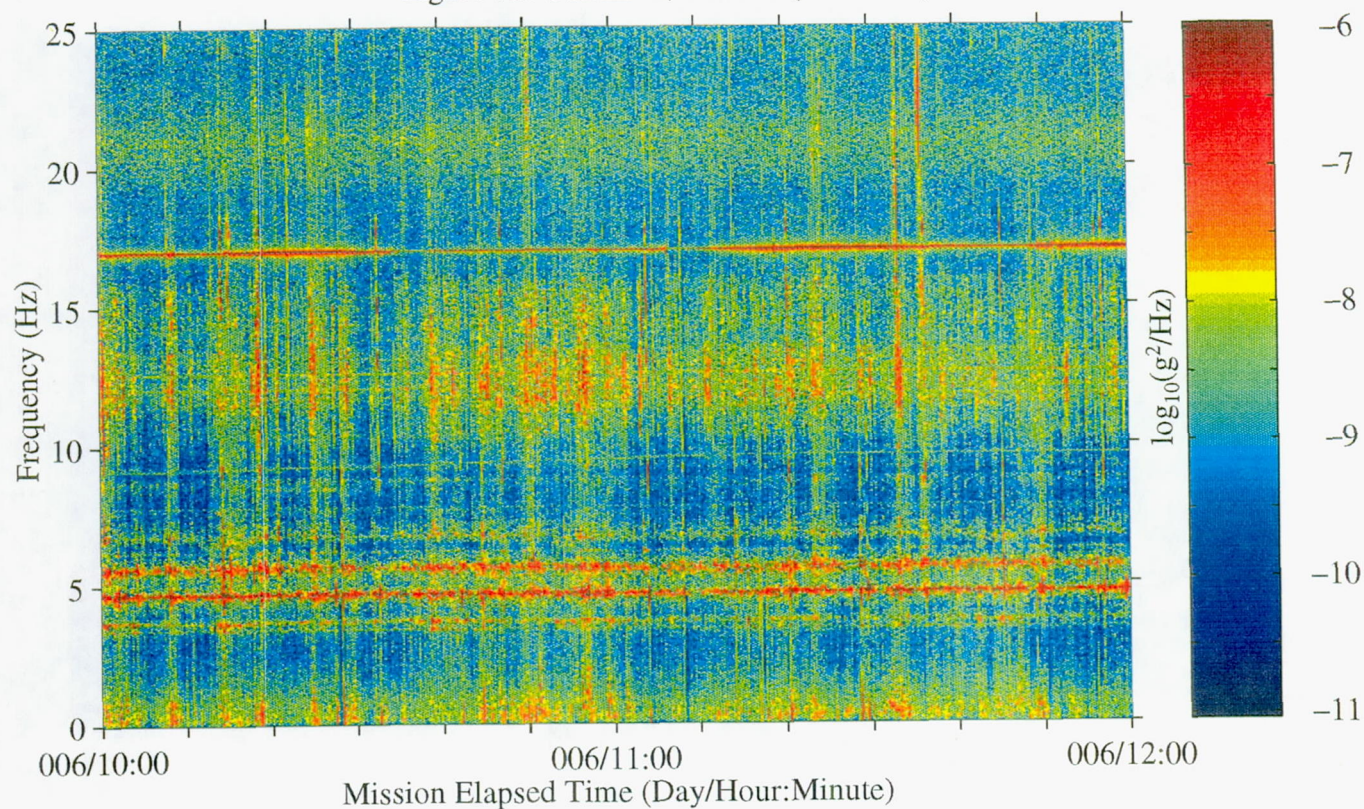


Figure 76: USML-2, Head C (fc=25 Hz)

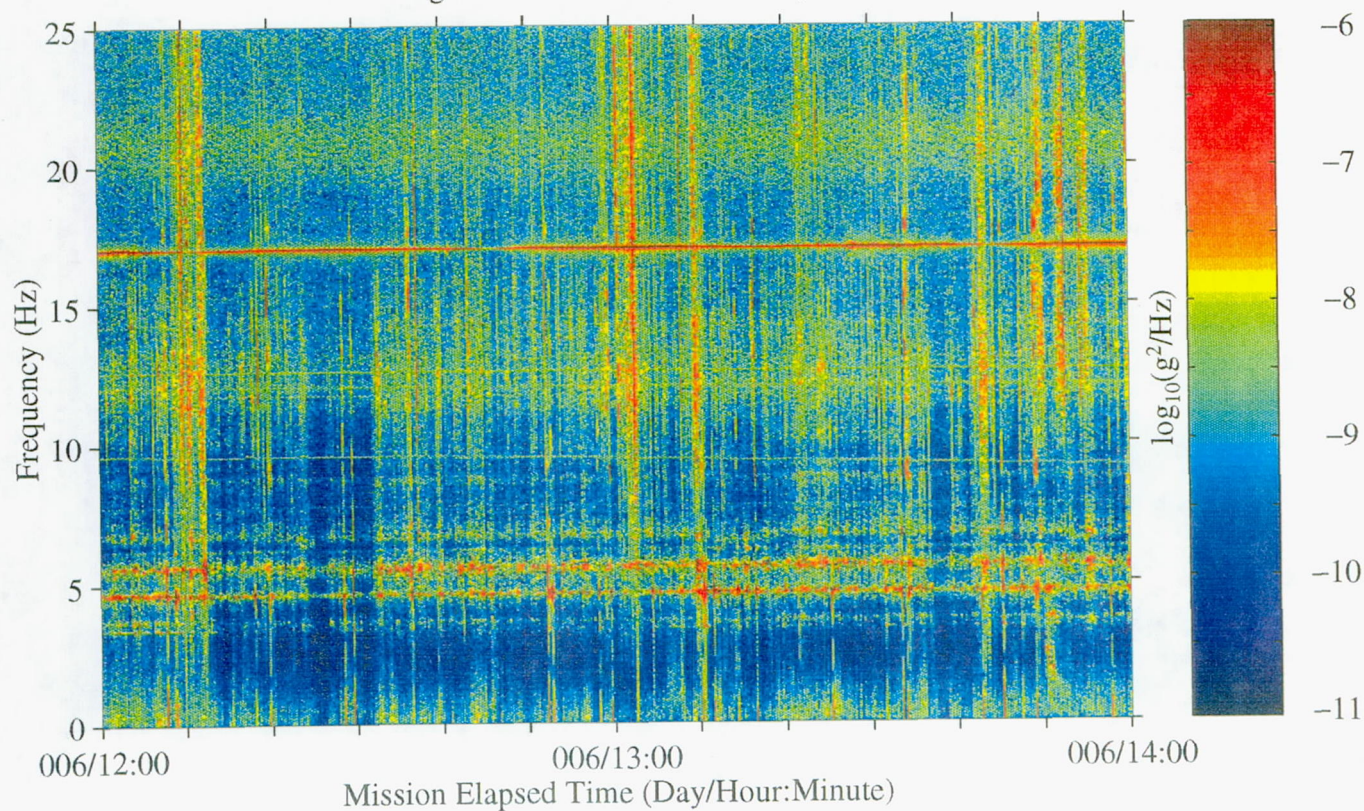




Figure 77: USML-2, Head C (fc=25 Hz)

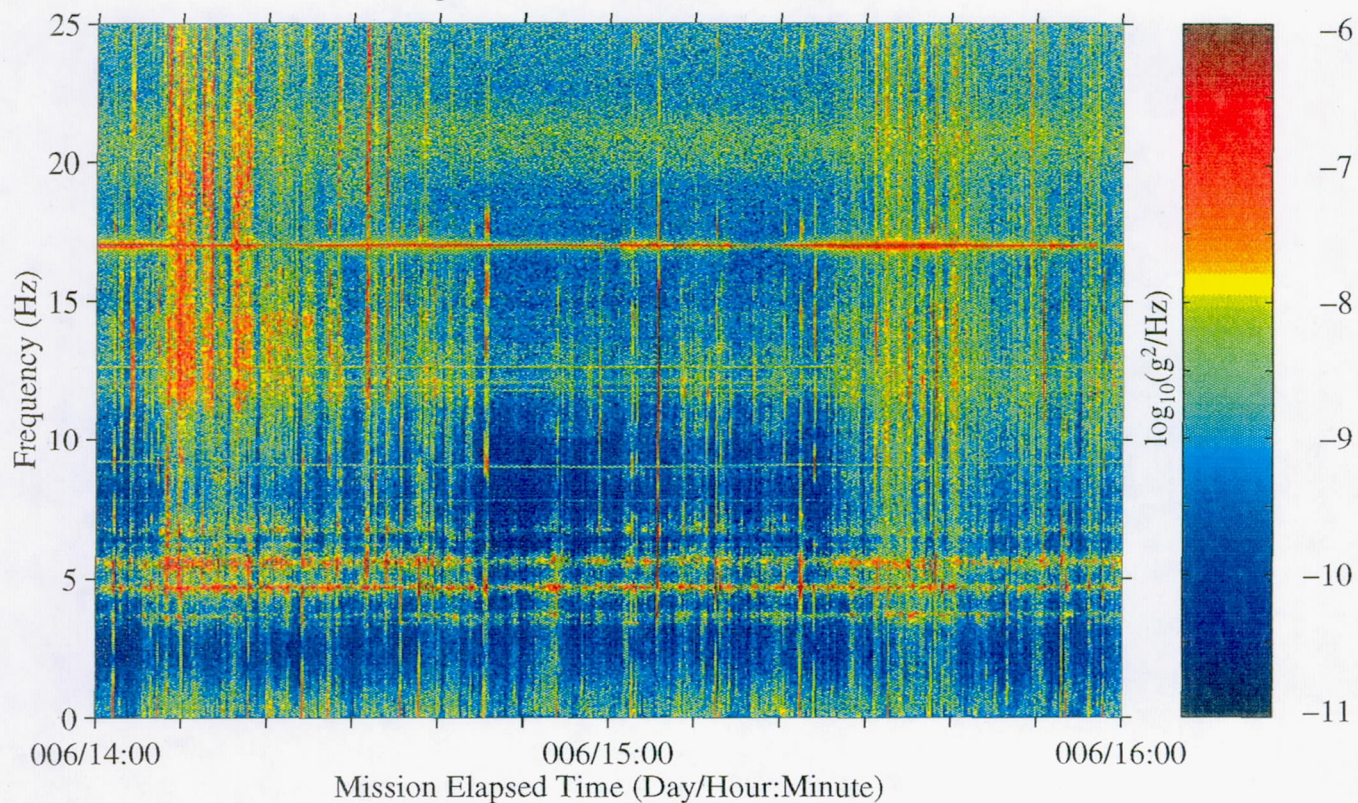


Figure 78: USML-2, Head C (fc=25 Hz)

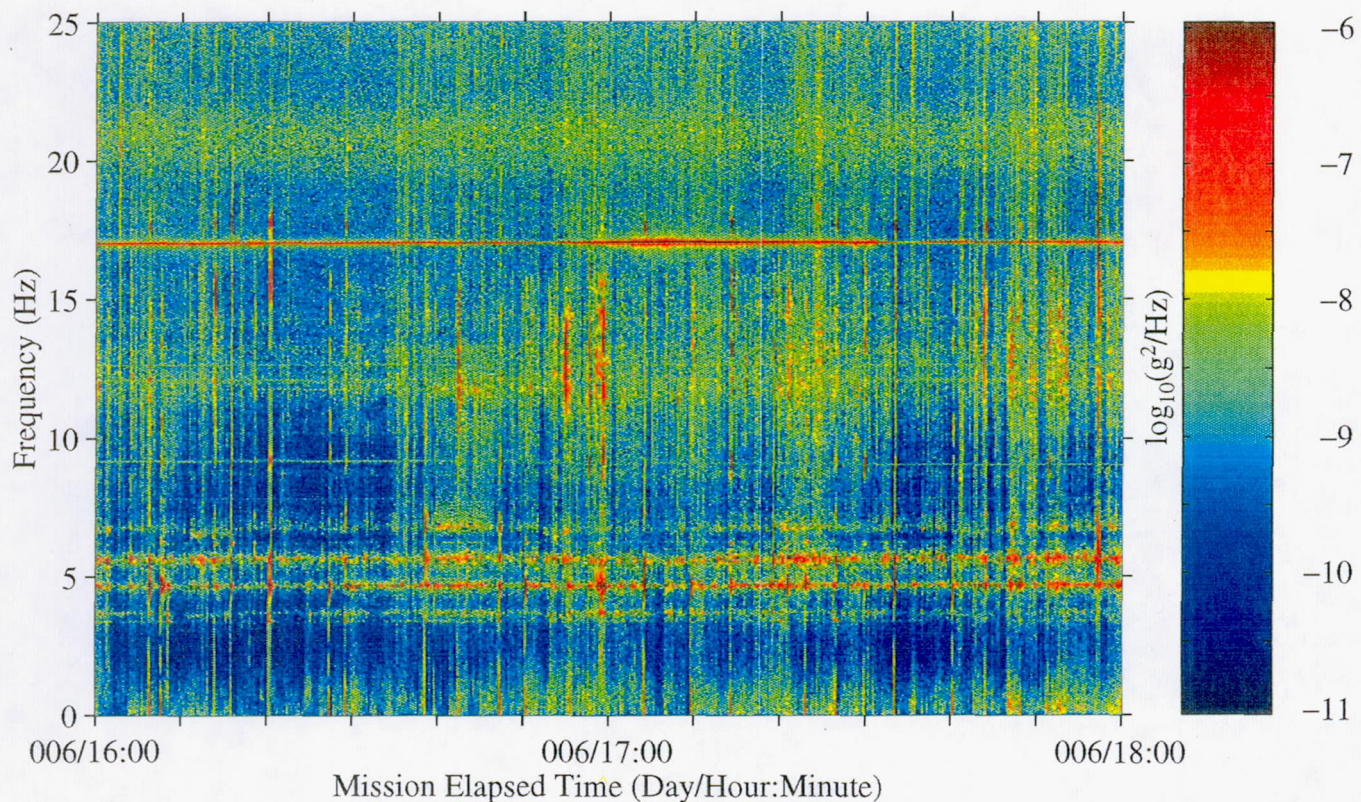




Figure 79: USML-2, Head C (fc=25 Hz)

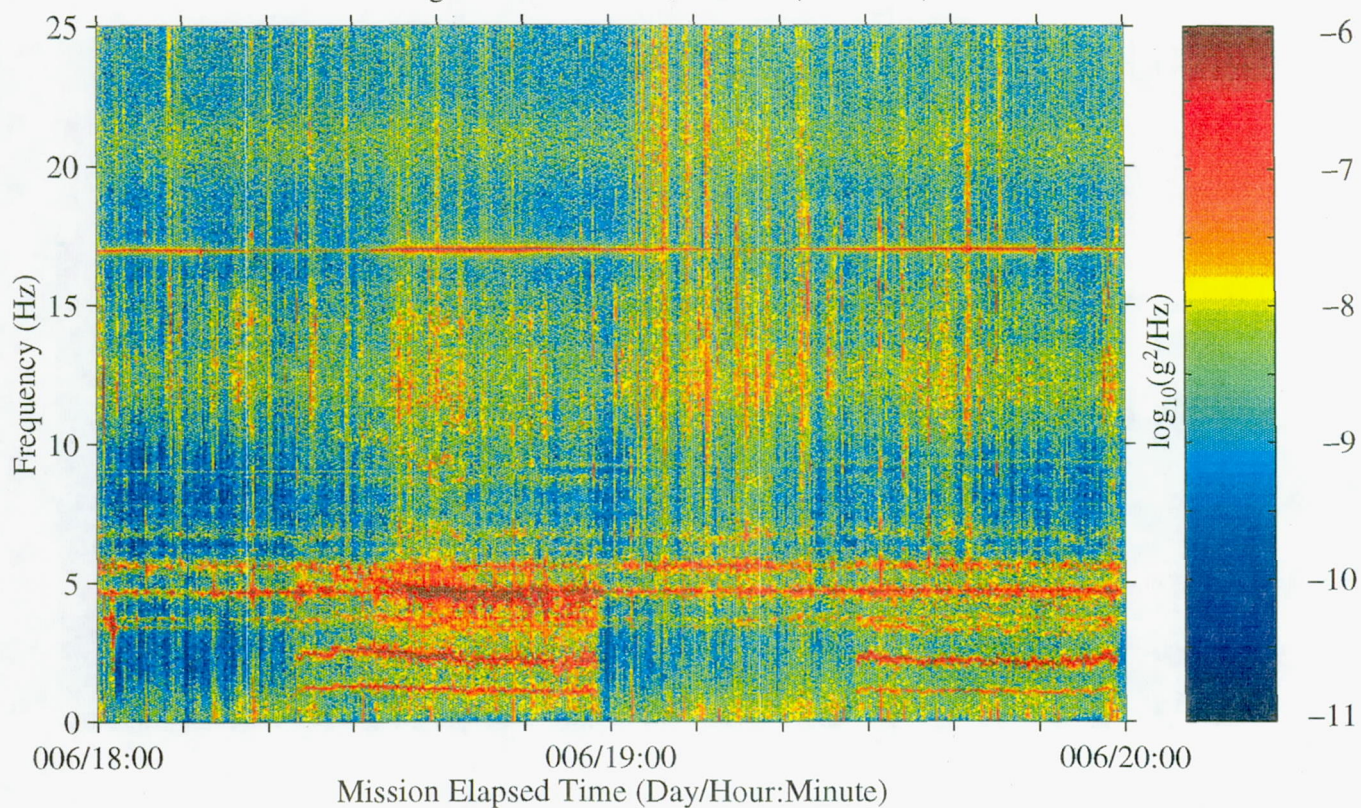


Figure 80: USML-2, Head C (fc=25 Hz)

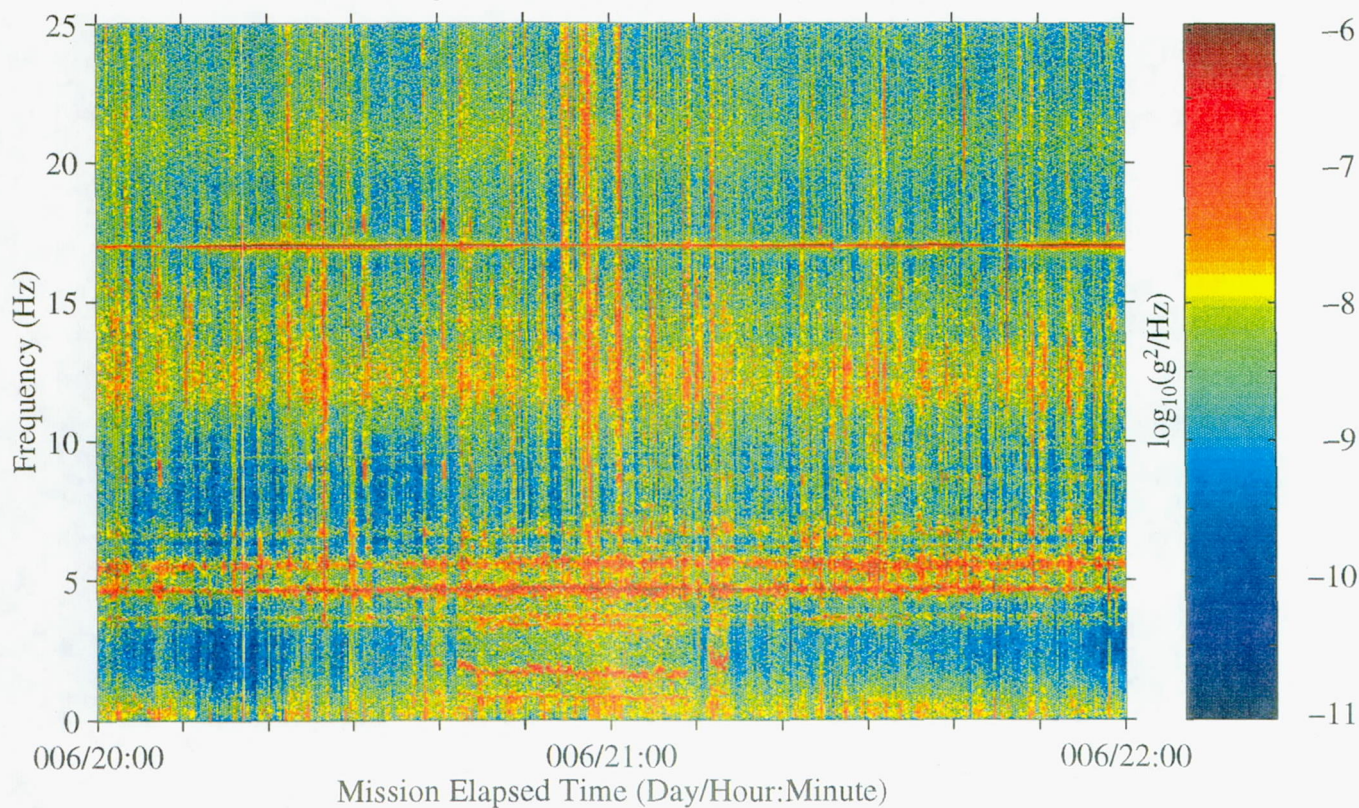




Figure 81: USML-2, Head C (fc=25 Hz)

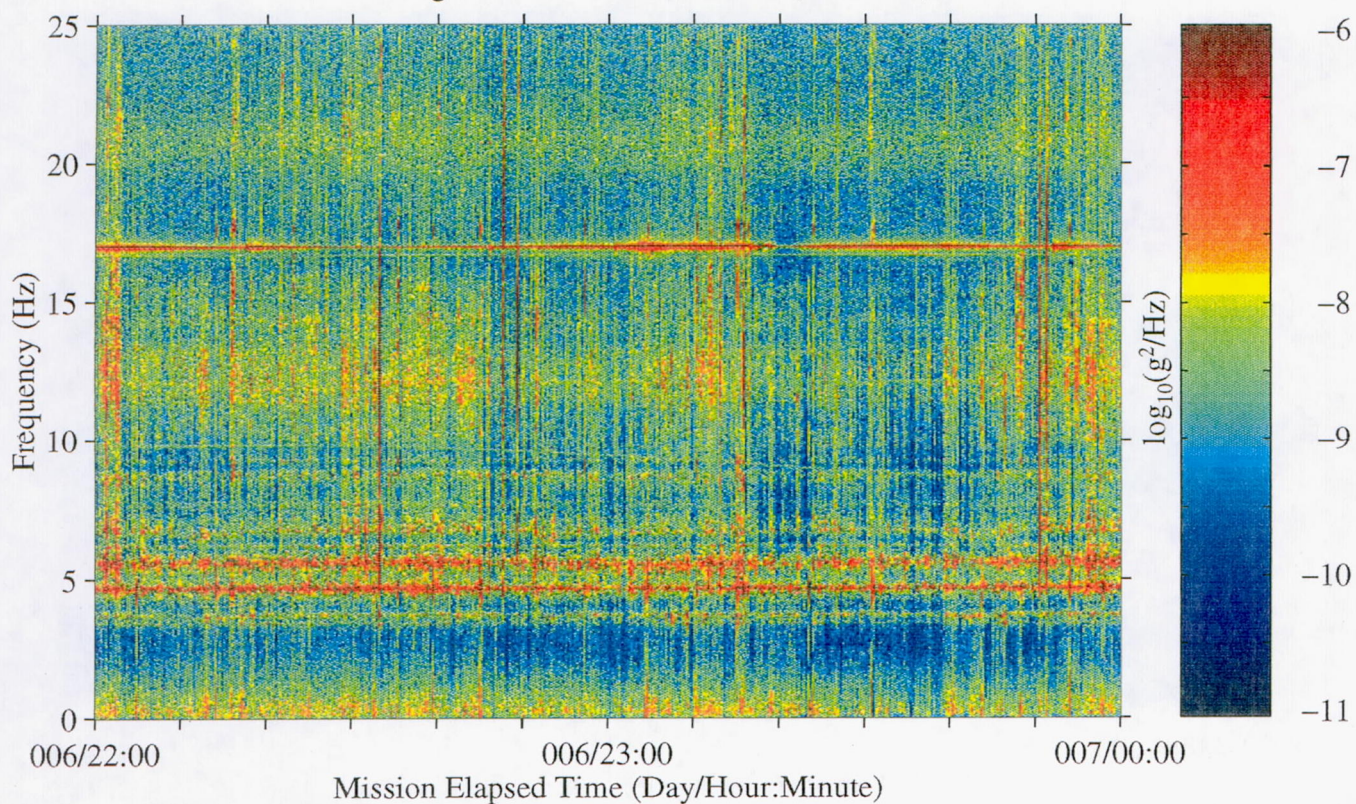


Figure 82: USML-2, Head C (fc=25 Hz)

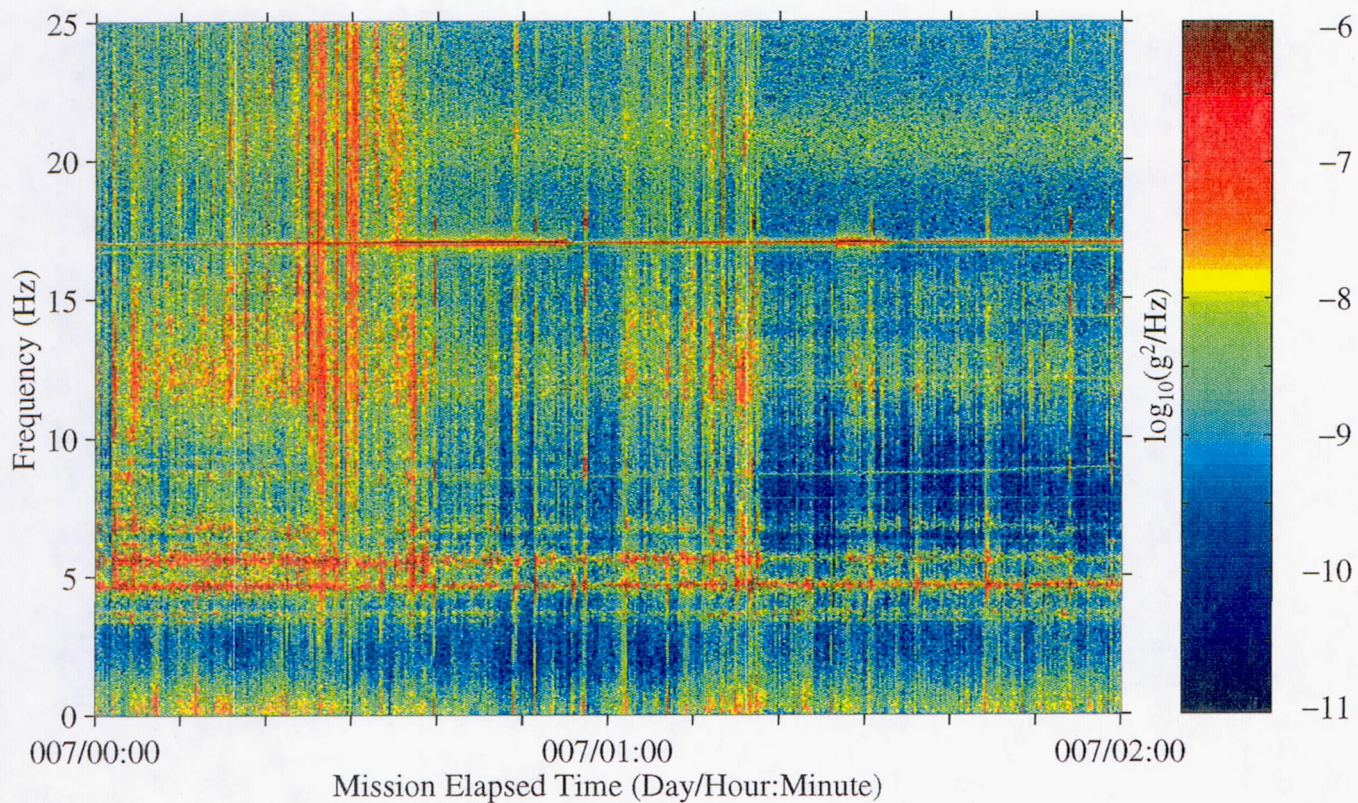




Figure 83: USML-2, Head C (fc=25 Hz)

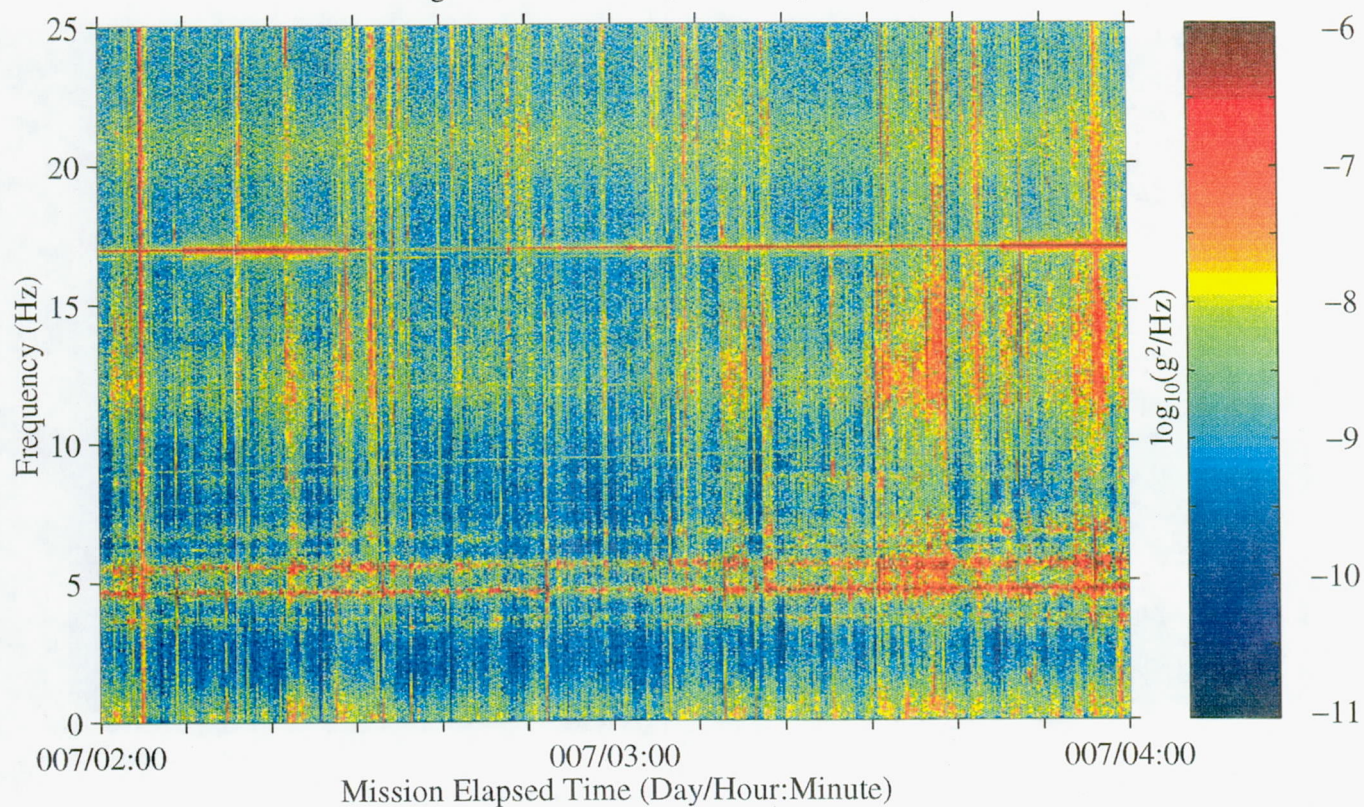


Figure 84: USML-2, Head C (fc=25 Hz)

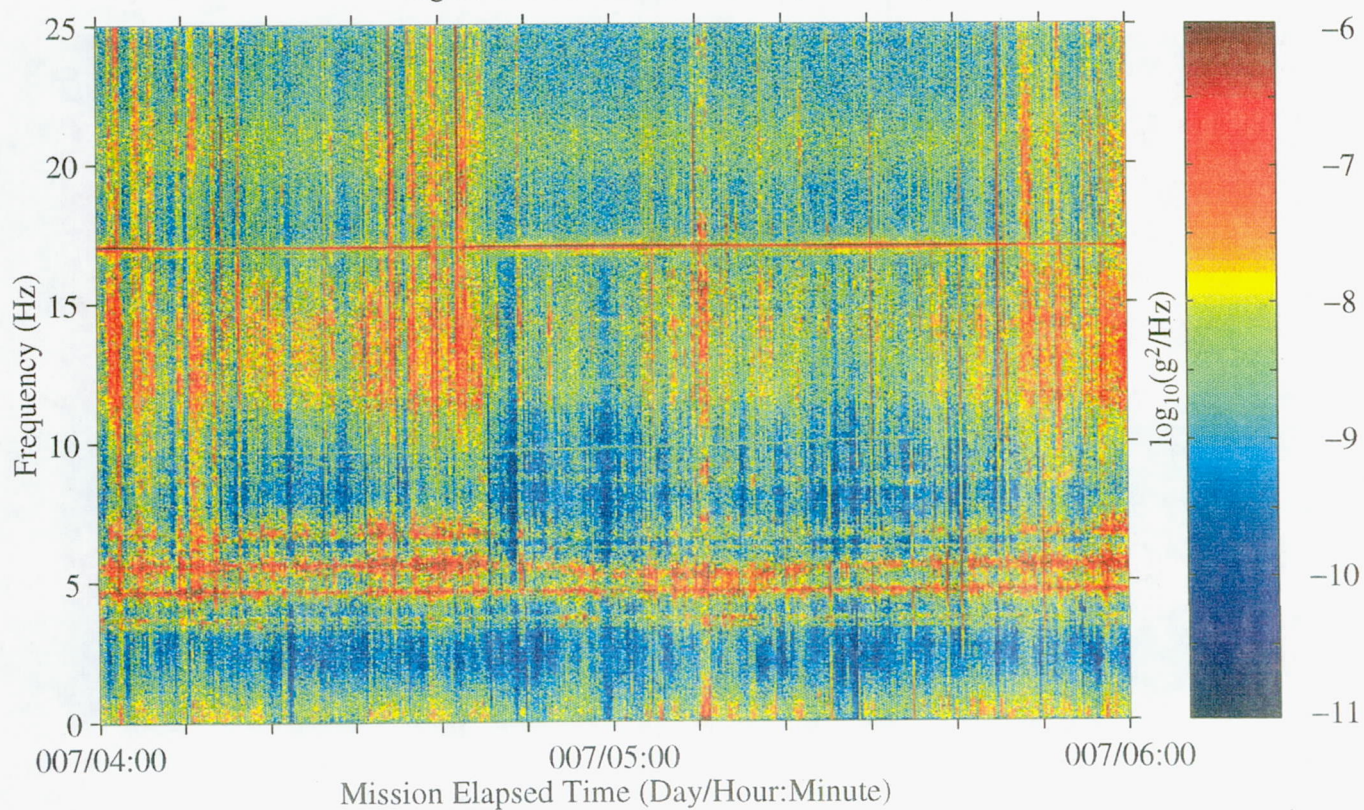




Figure 85: USML-2, Head C (fc=25 Hz)

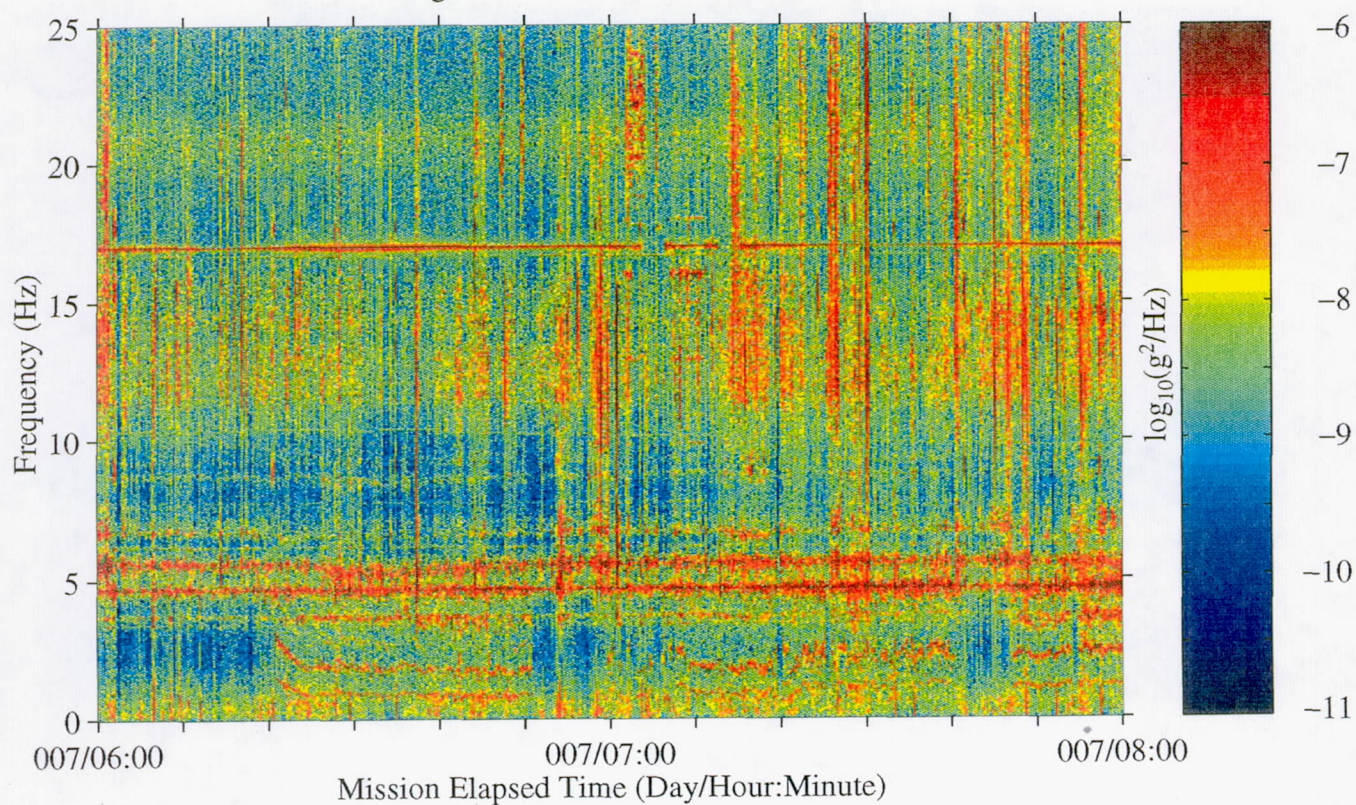


Figure 86: USML-2, Head C (fc=25 Hz)

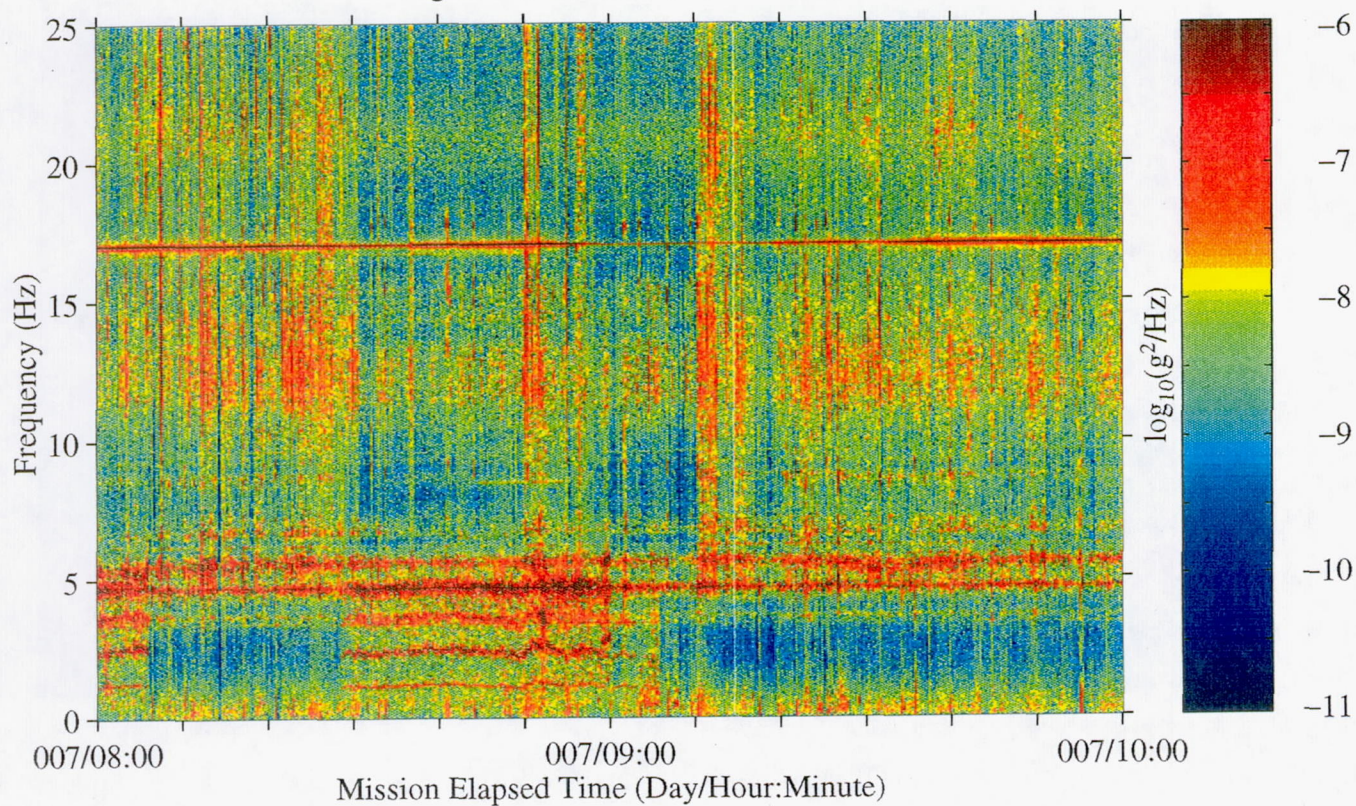




Figure 87: USML-2, Head C (fc=25 Hz)

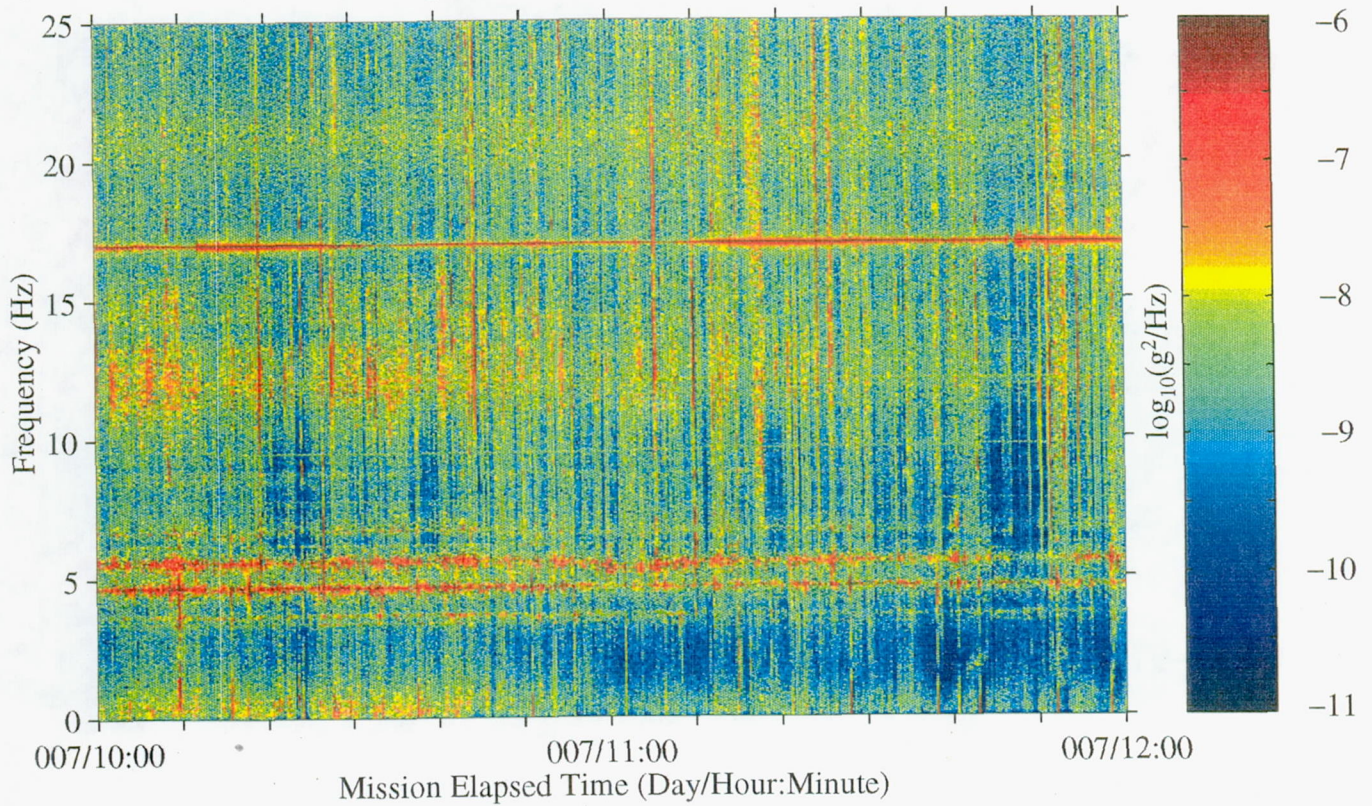


Figure 88: USML-2, Head C (fc=25 Hz)

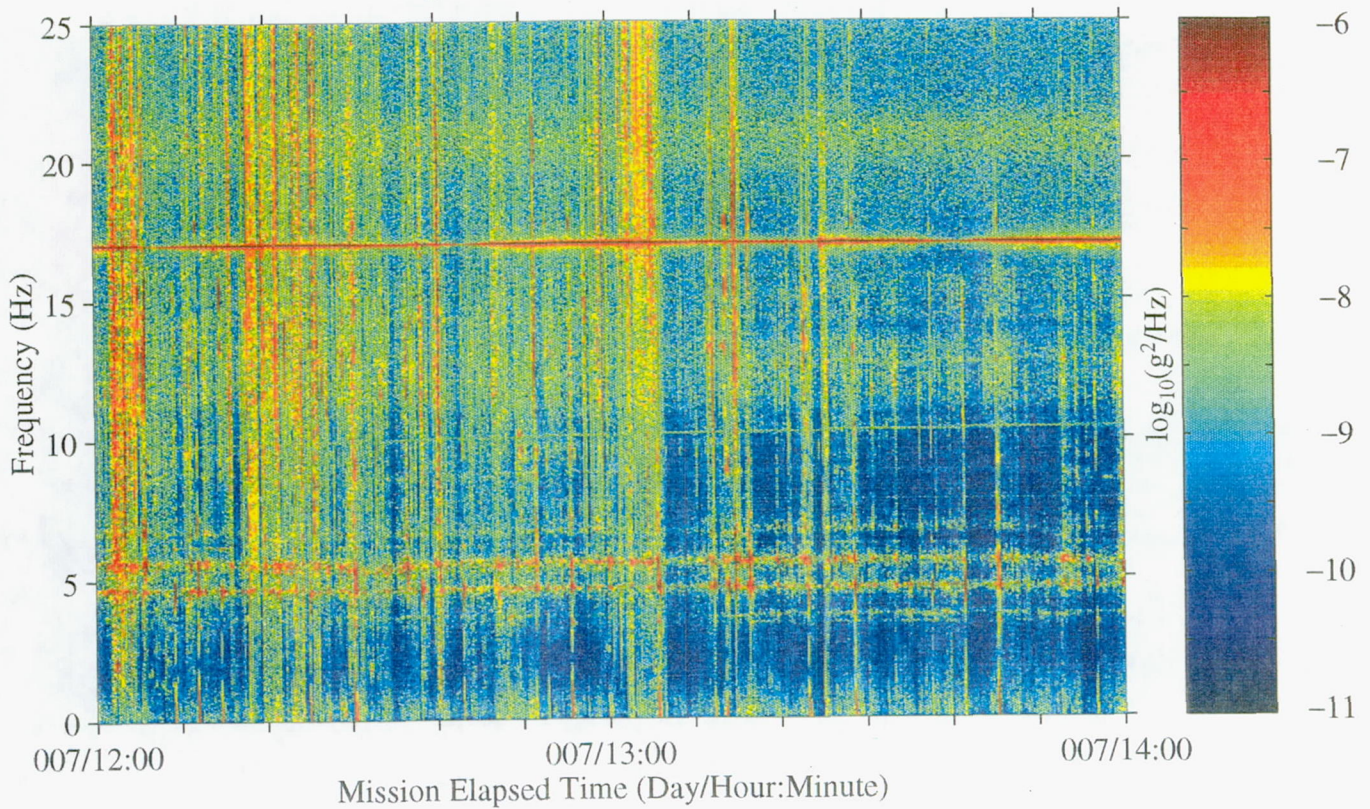




Figure 89: USML-2, Head C (fc=25 Hz)

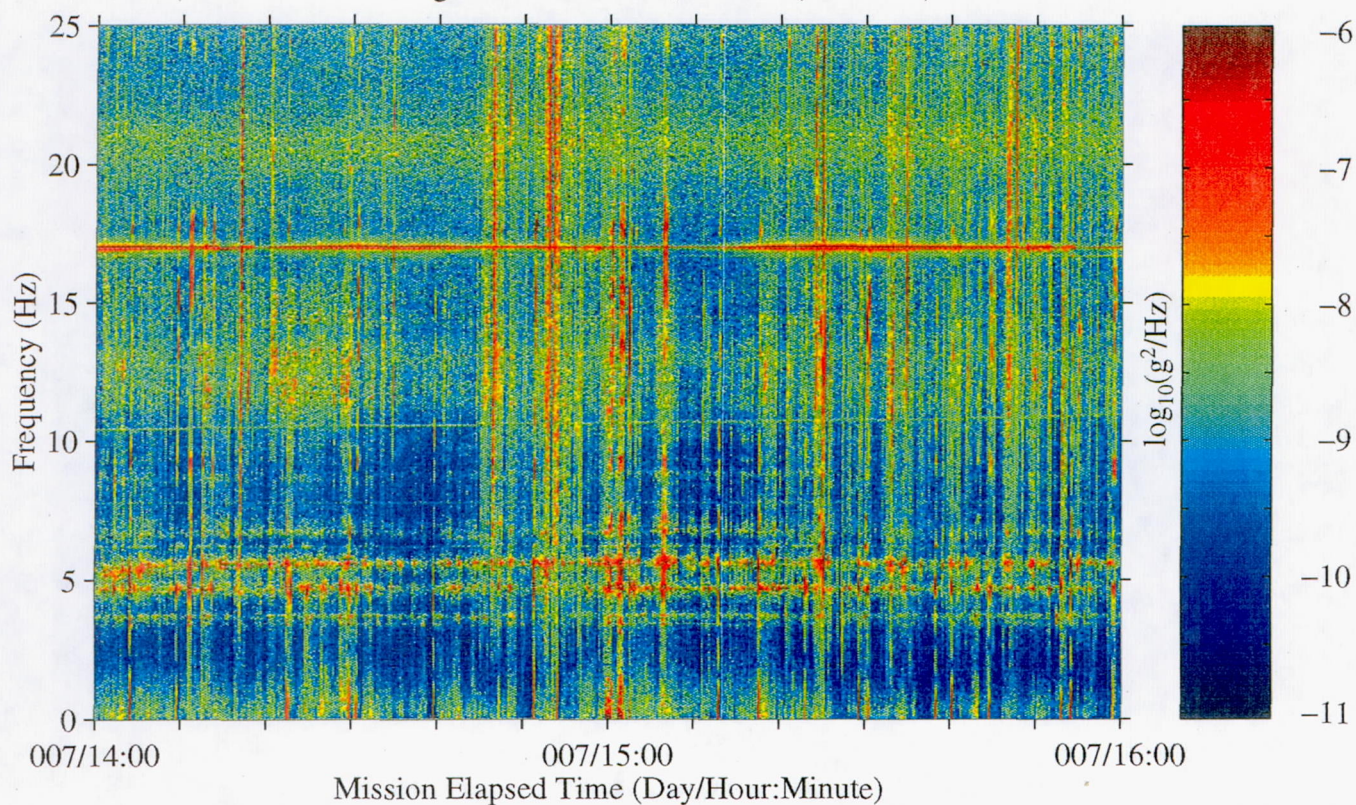


Figure 90: USML-2, Head C (fc=25 Hz)

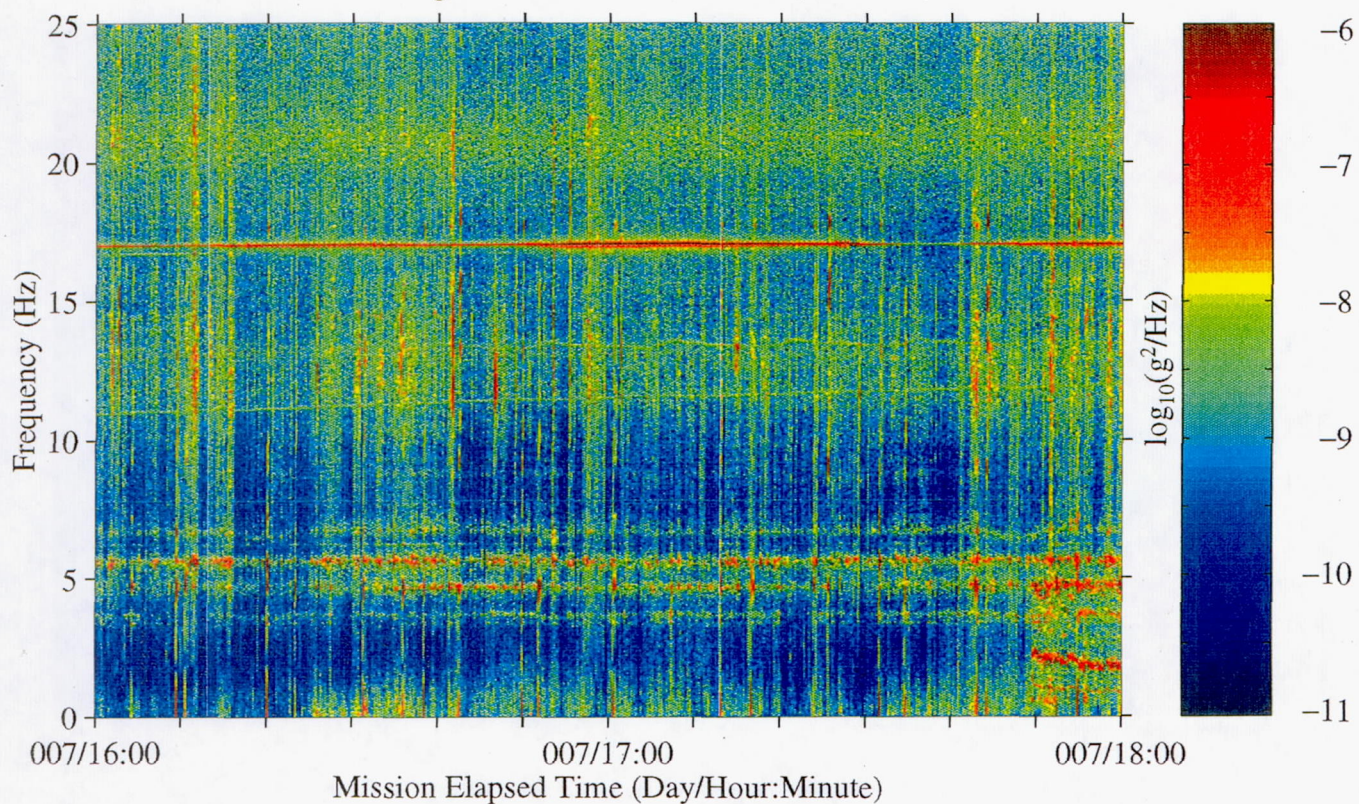




Figure 91: USML-2, Head C (fc=25 Hz)

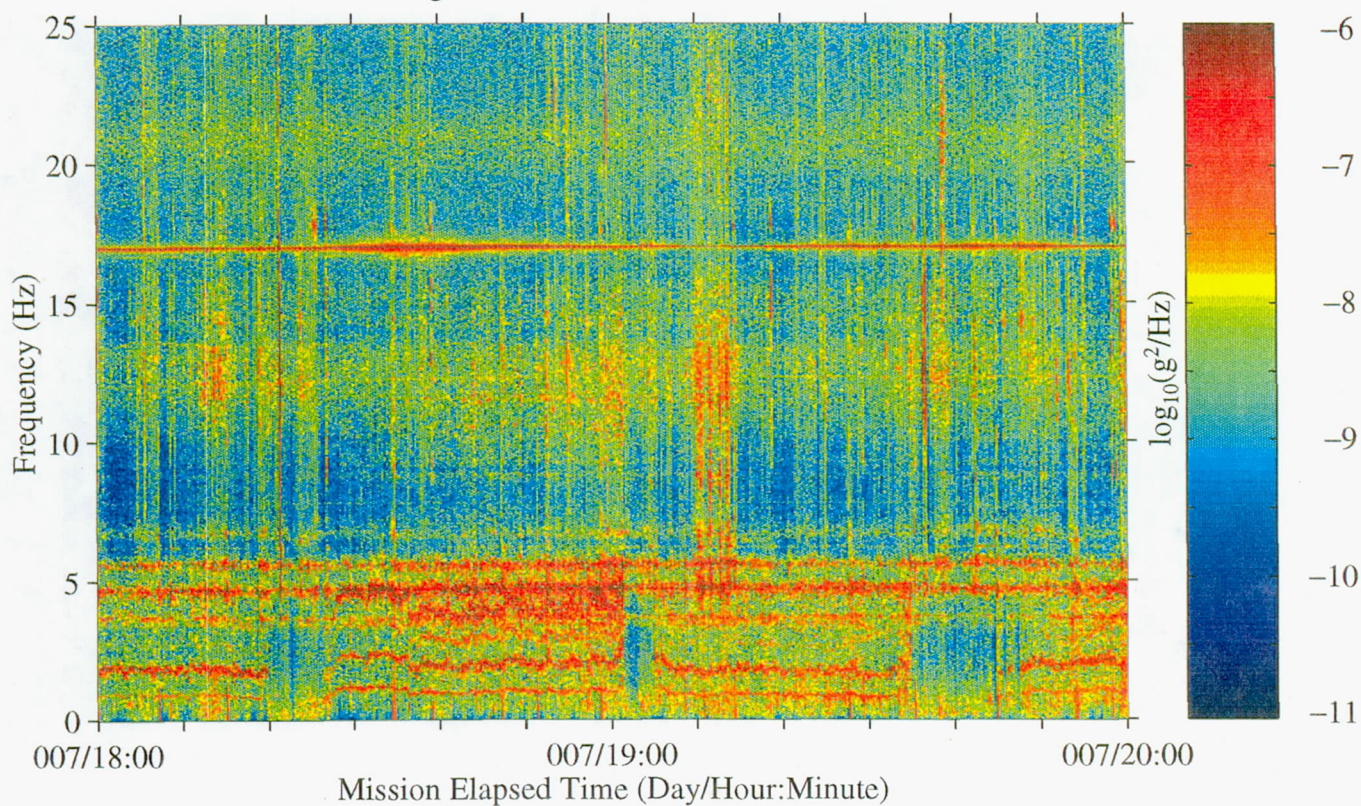


Figure 92: USML-2, Head C (fc=25 Hz)

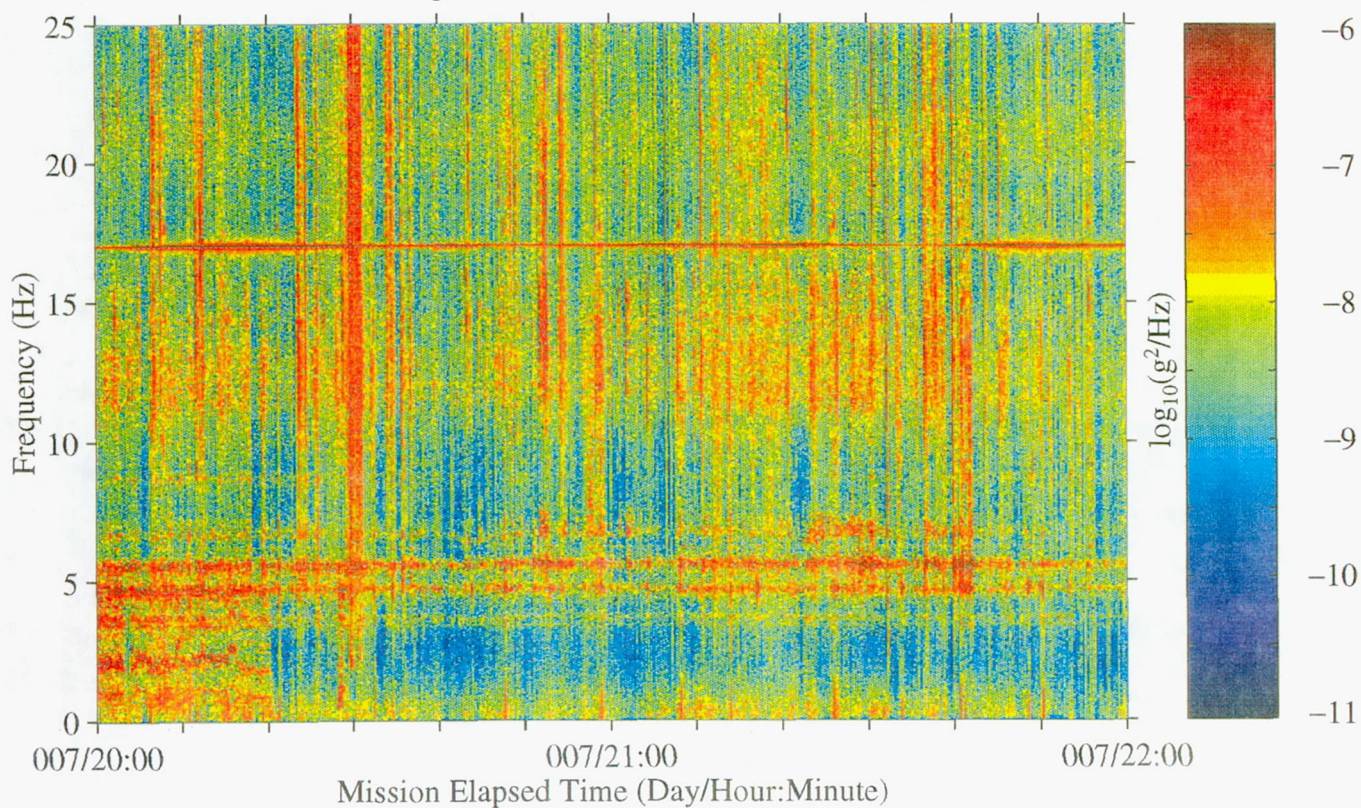




Figure 93: USML-2, Head C (fc=25 Hz)

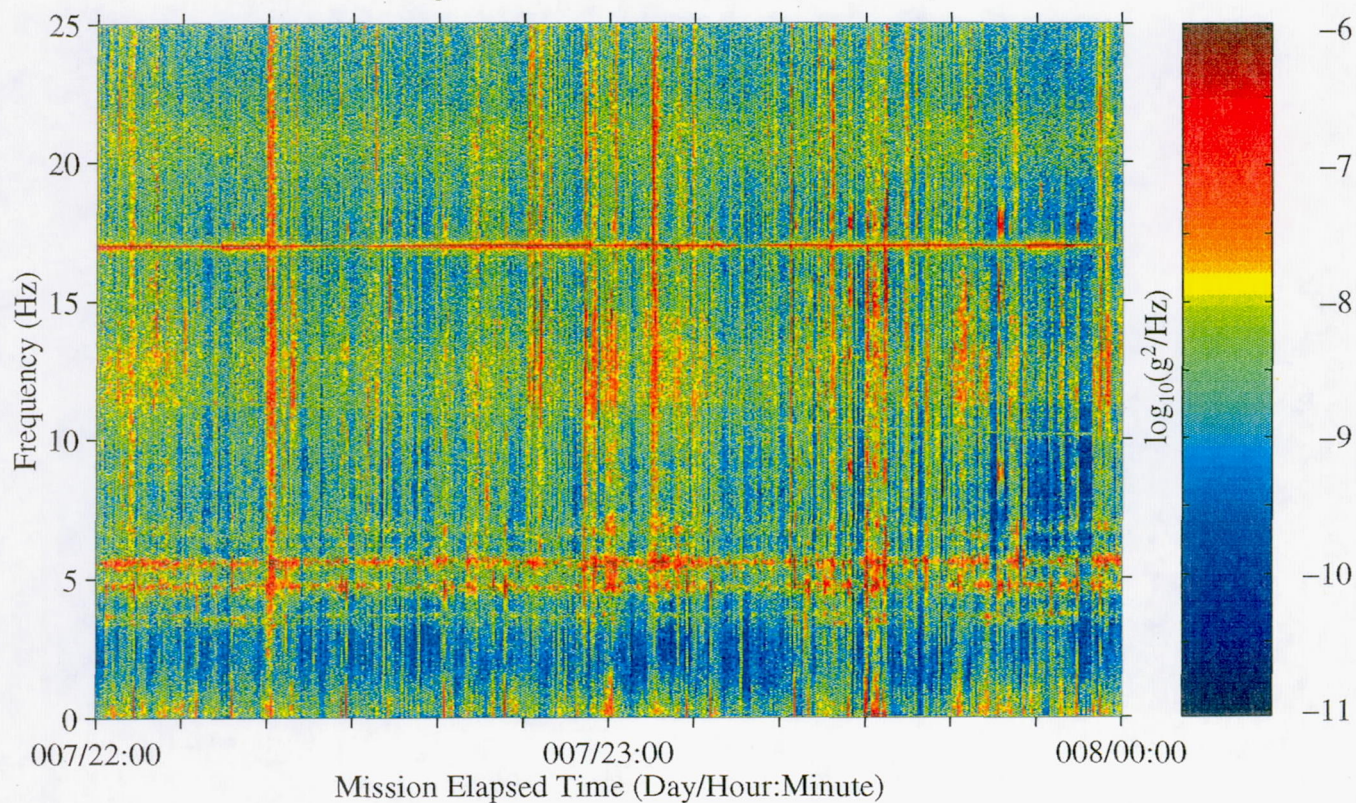


Figure 94: USML-2, Head C (fc=25 Hz)

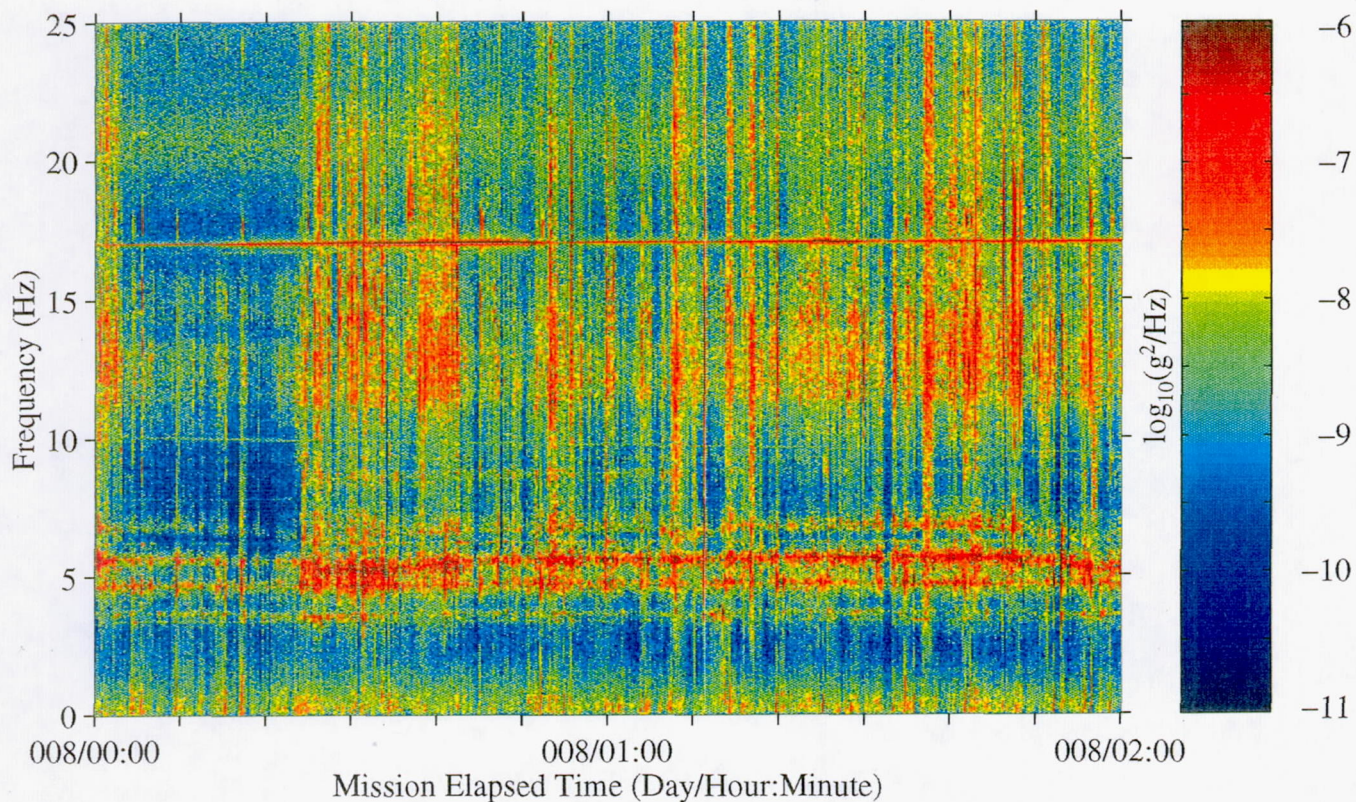




Figure 95: USML-2, Head C (fc=25 Hz)

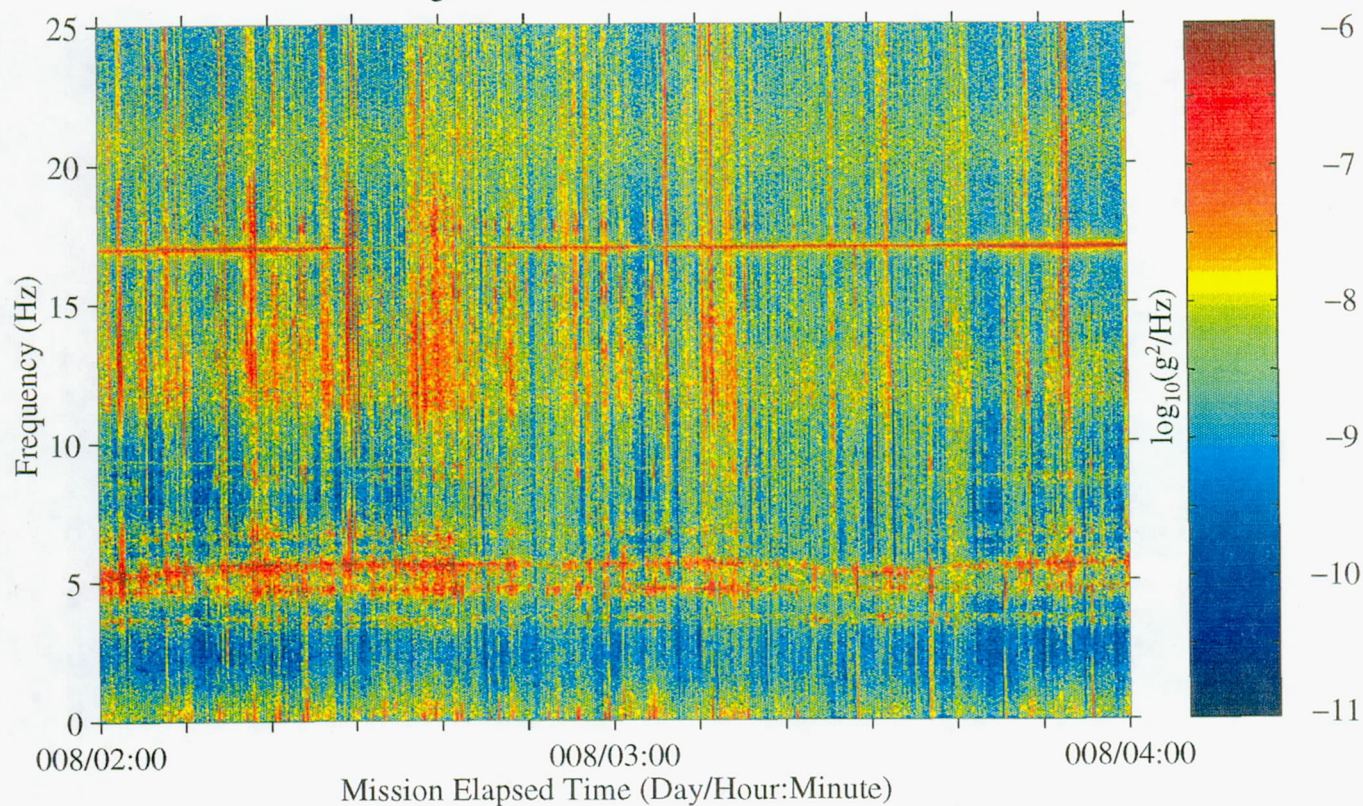


Figure 96: USML-2, Head C (fc=25 Hz)

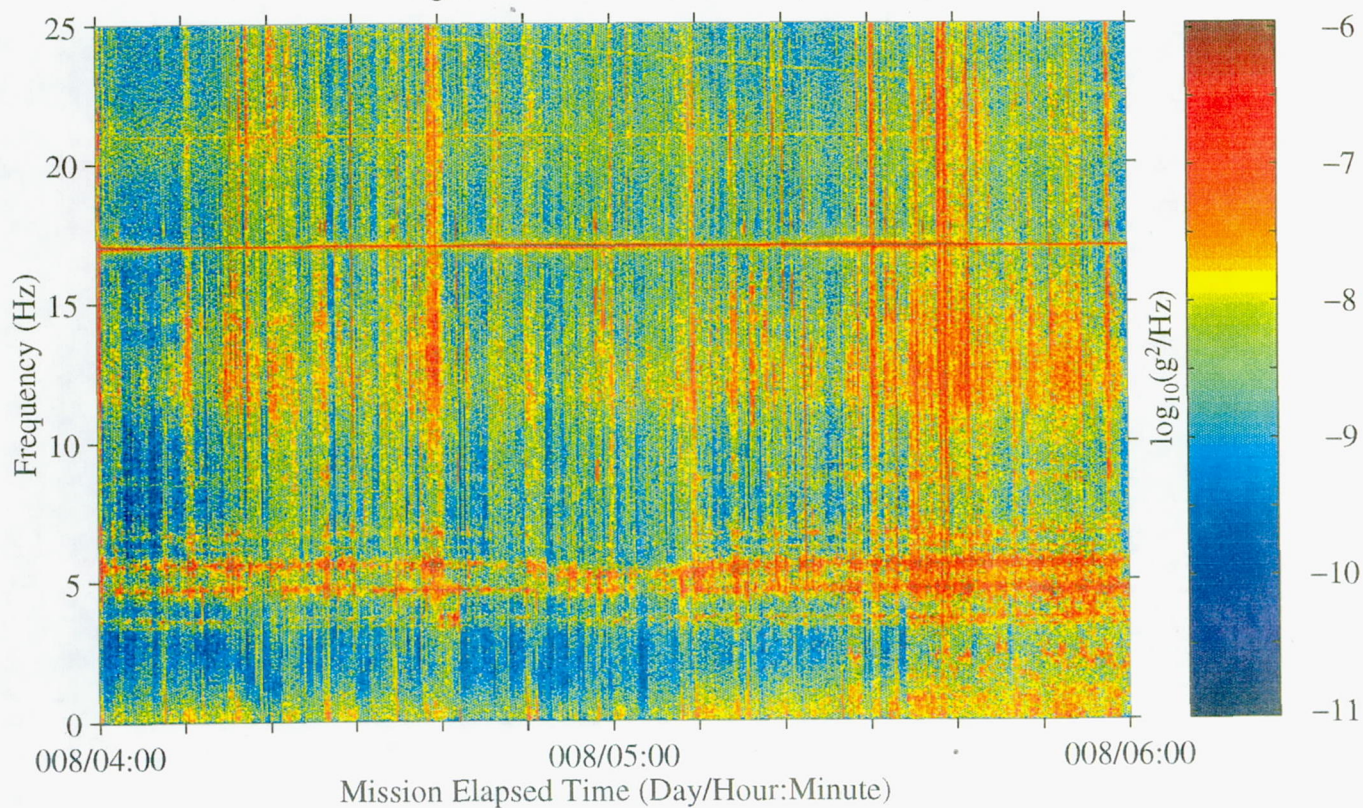




Figure 97: USML-2, Head C (fc=25 Hz)

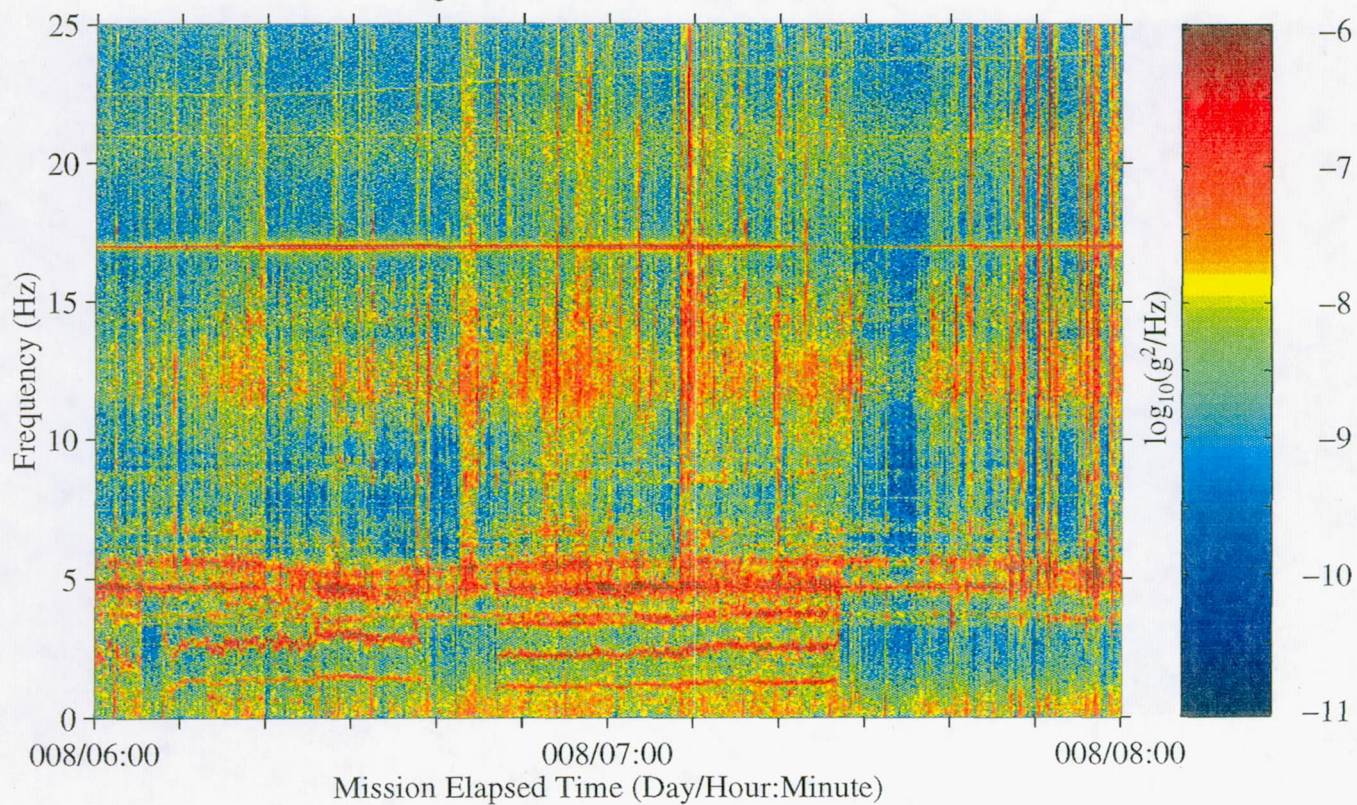


Figure 98: USML-2, Head C (fc=25 Hz)

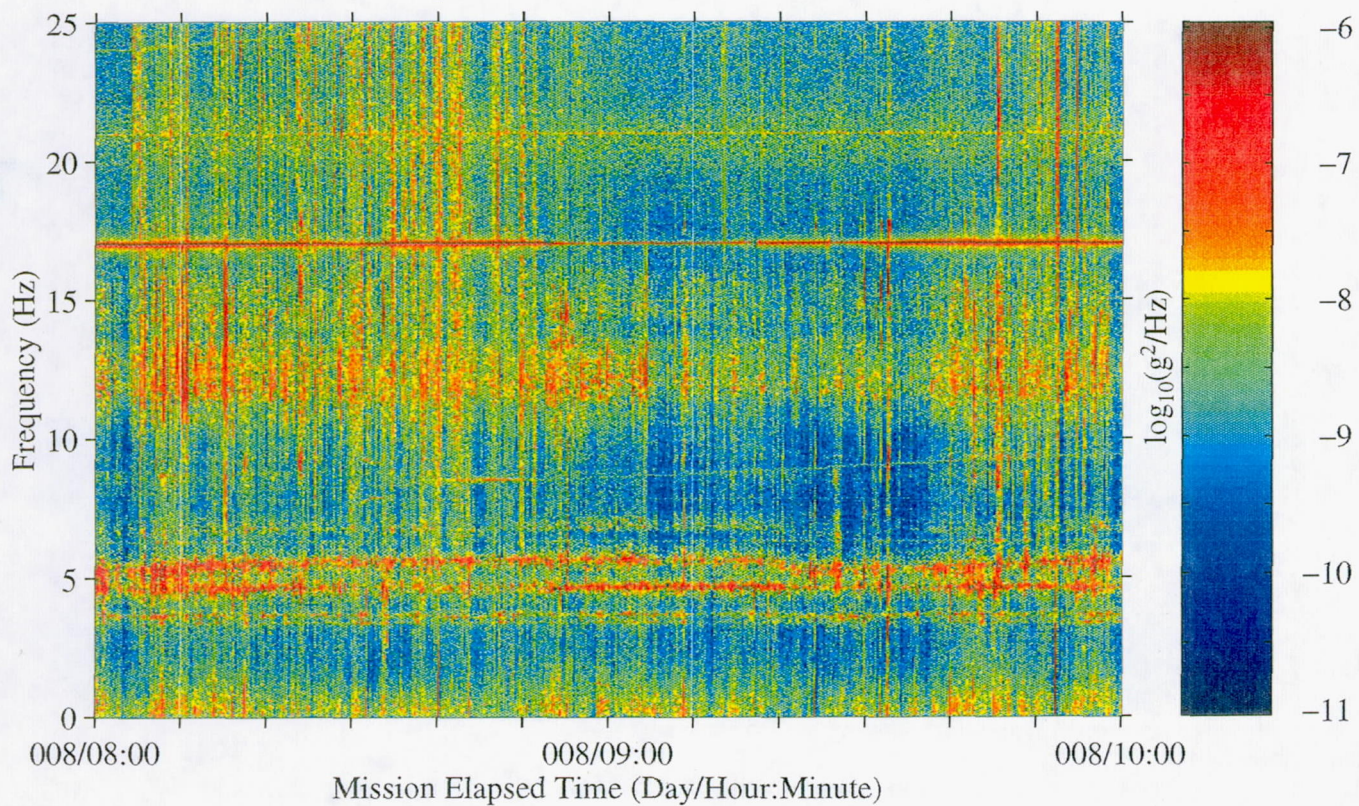




Figure 99: USML-2, Head C (fc=25 Hz)

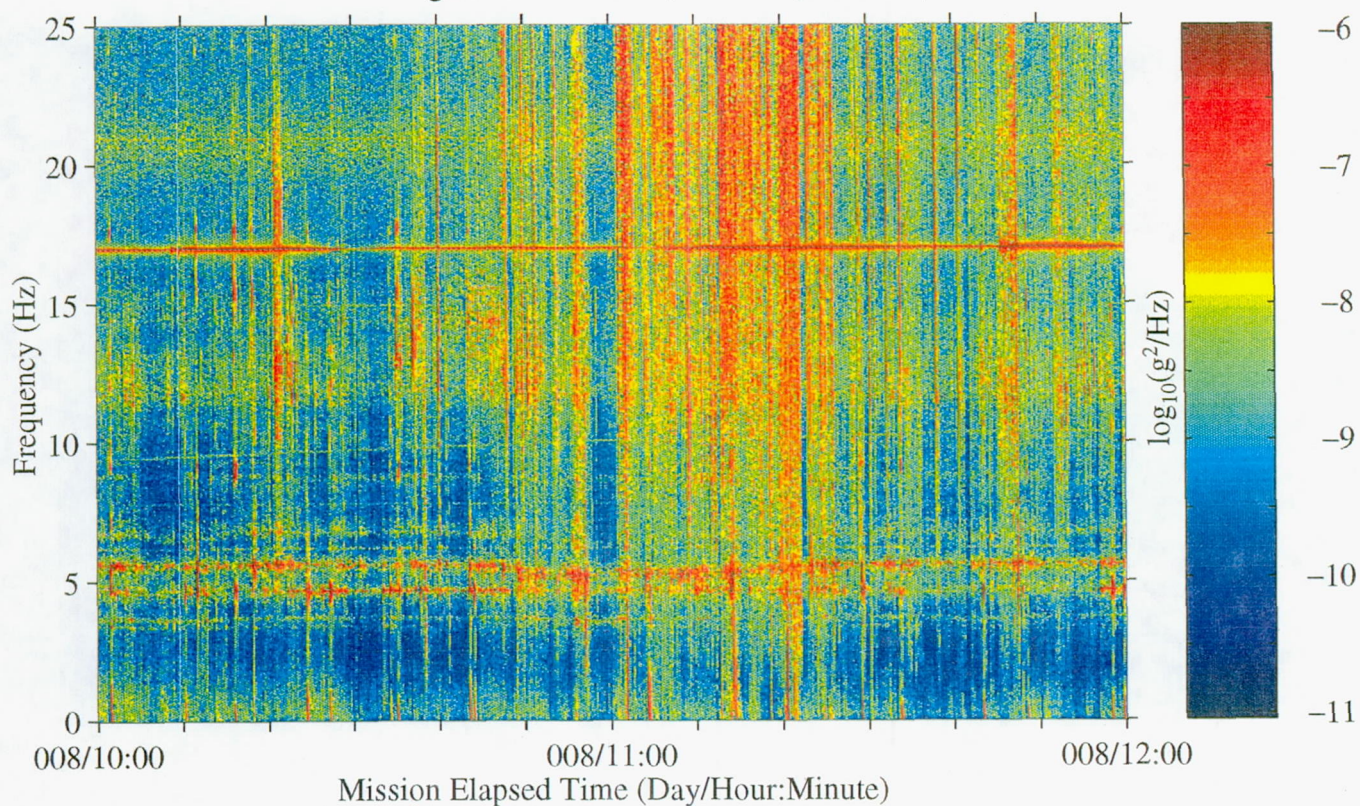


Figure 100: USML-2, Head C (fc=25 Hz)

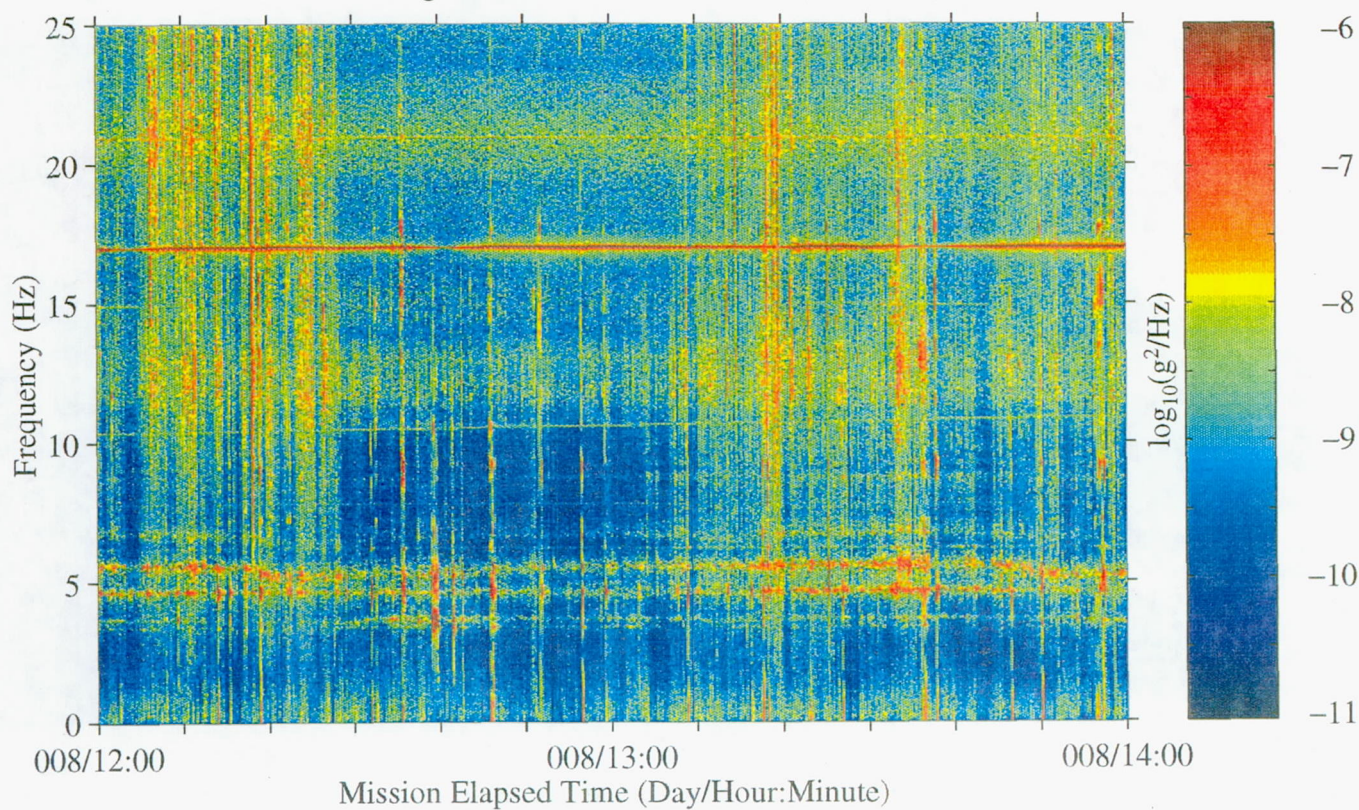




Figure 101: USML-2, Head C (fc=25 Hz)

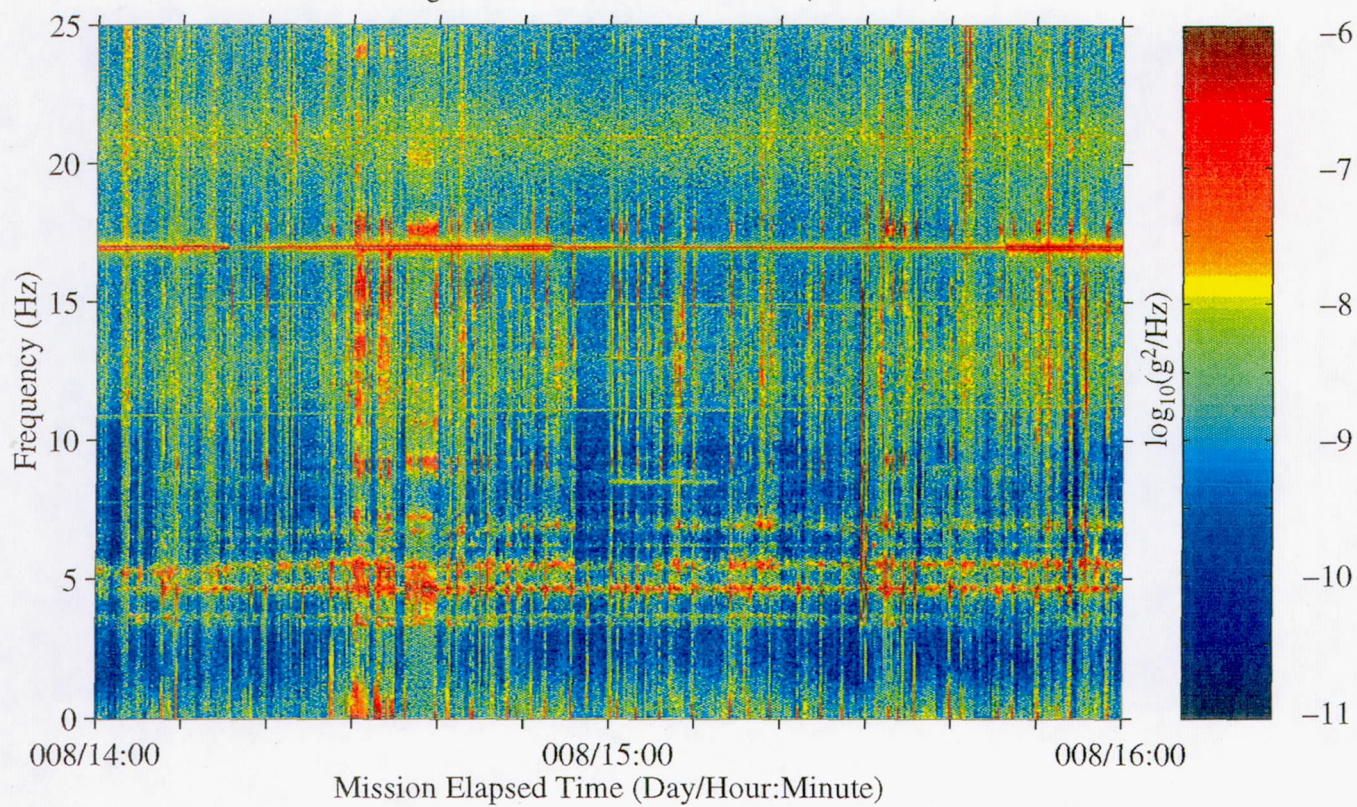


Figure 102: USML-2, Head C (fc=25 Hz)

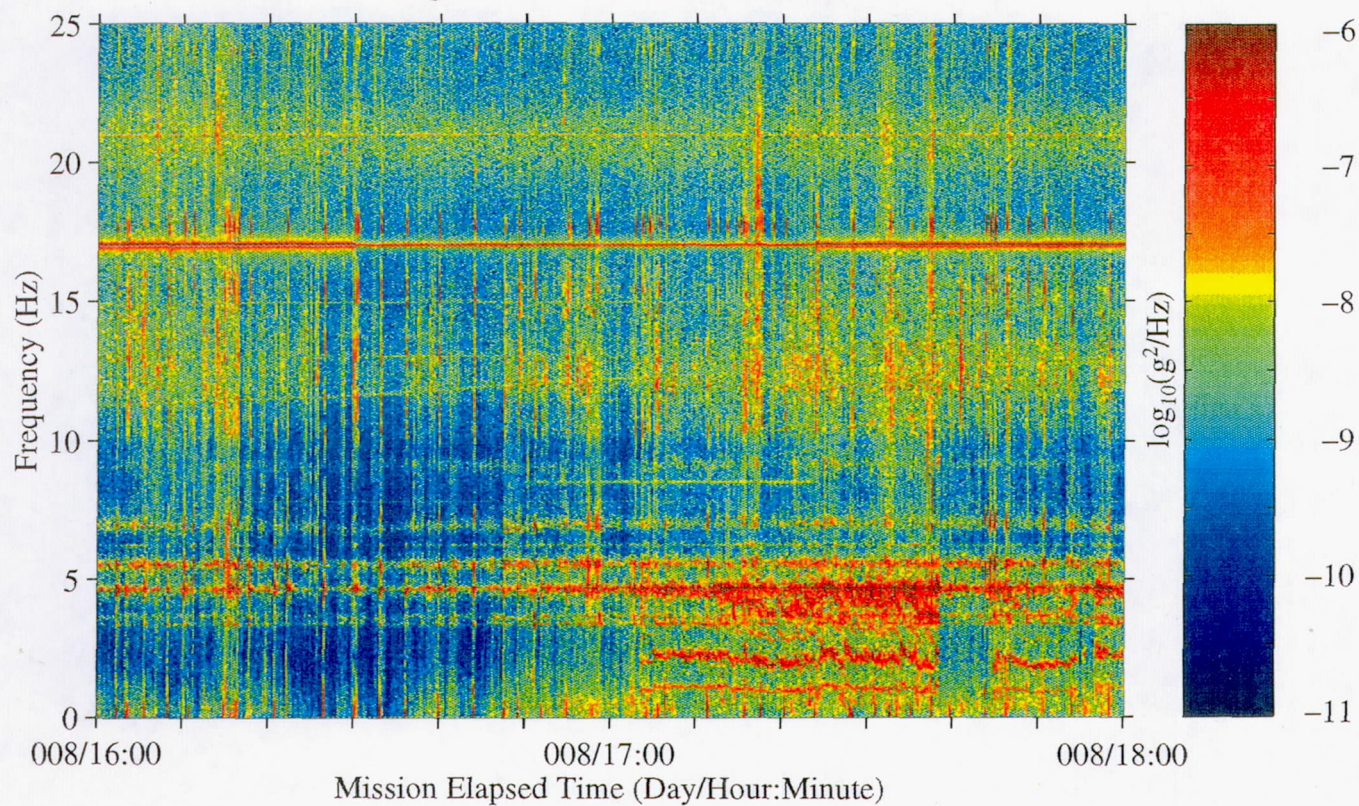




Figure 103: USML-2, Head C (fc=25 Hz)

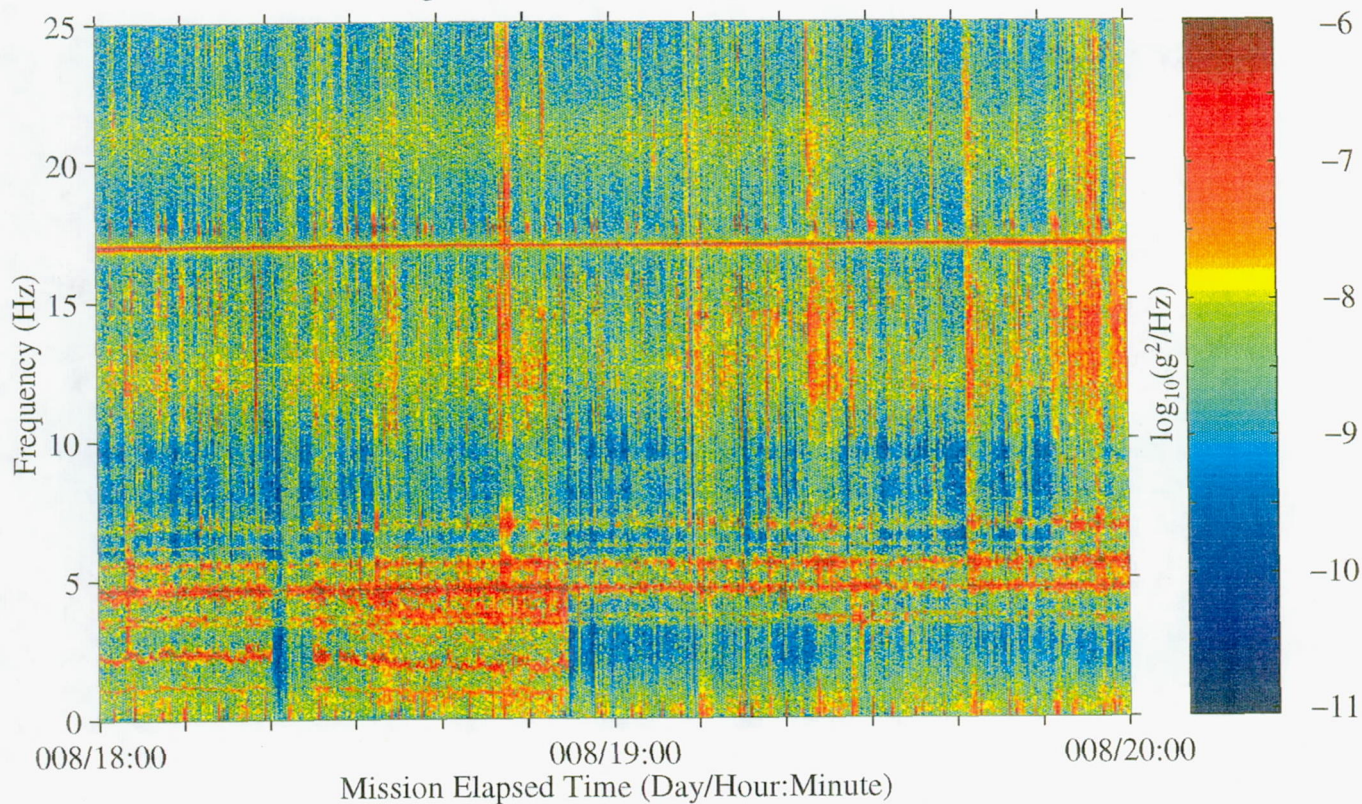


Figure 104: USML-2, Head C (fc=25 Hz)

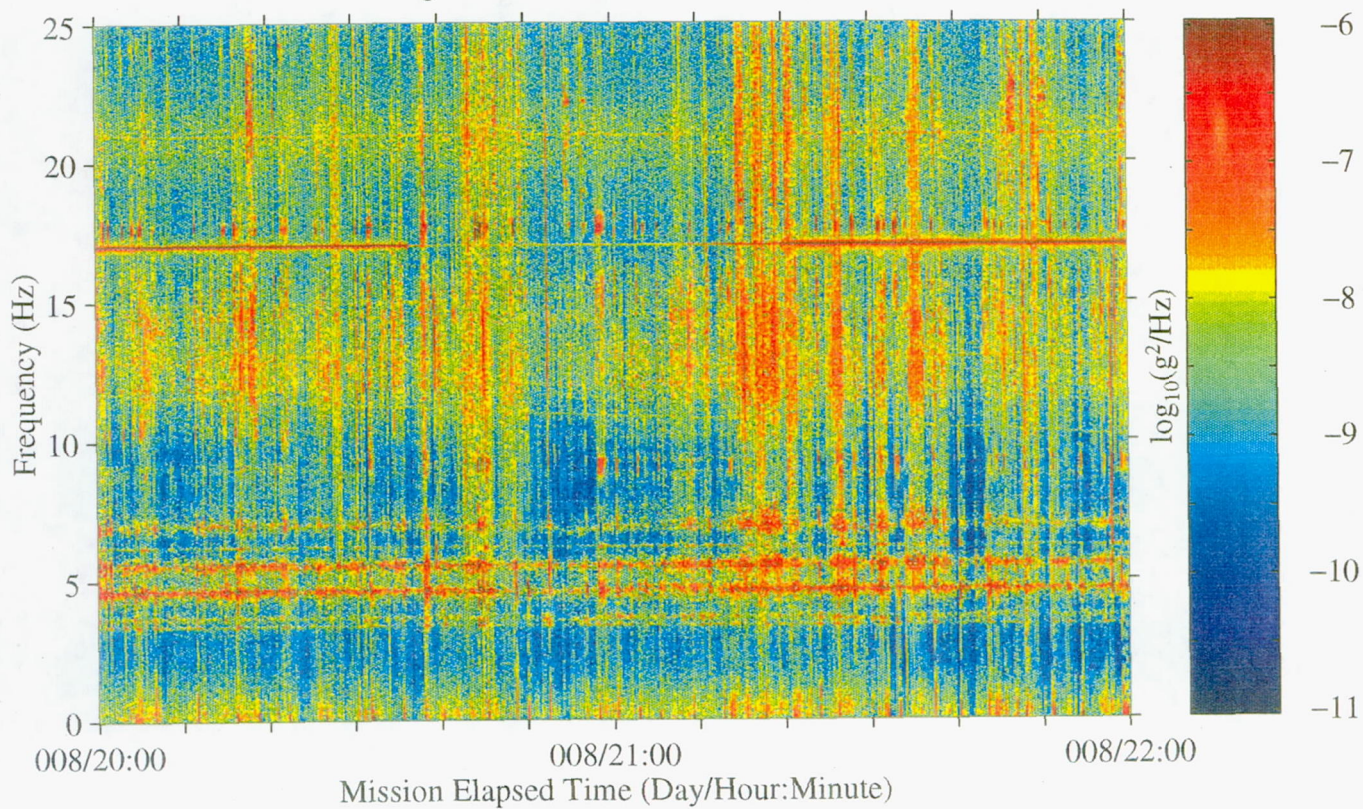




Figure 105: USML-2, Head C (fc=25 Hz)

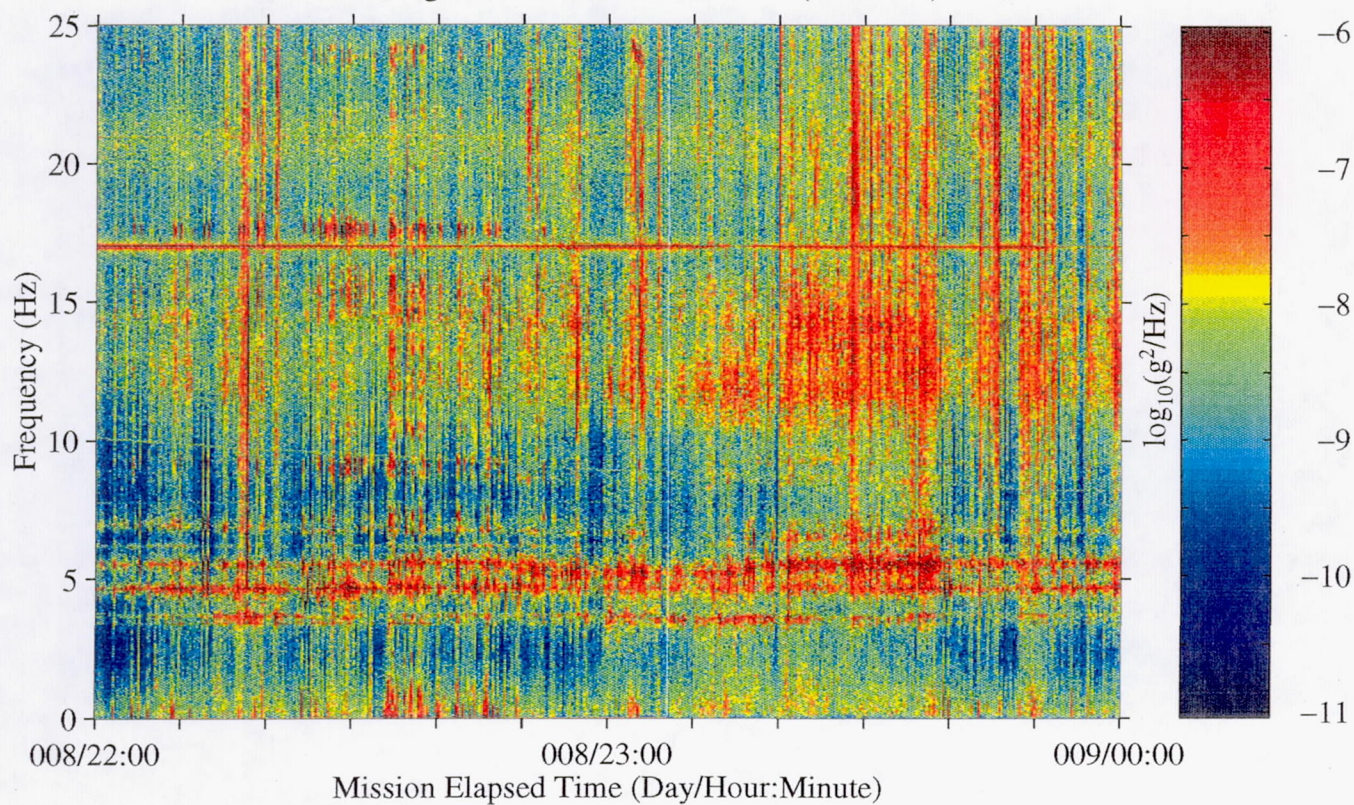


Figure 106: USML-2, Head C (fc=25 Hz)

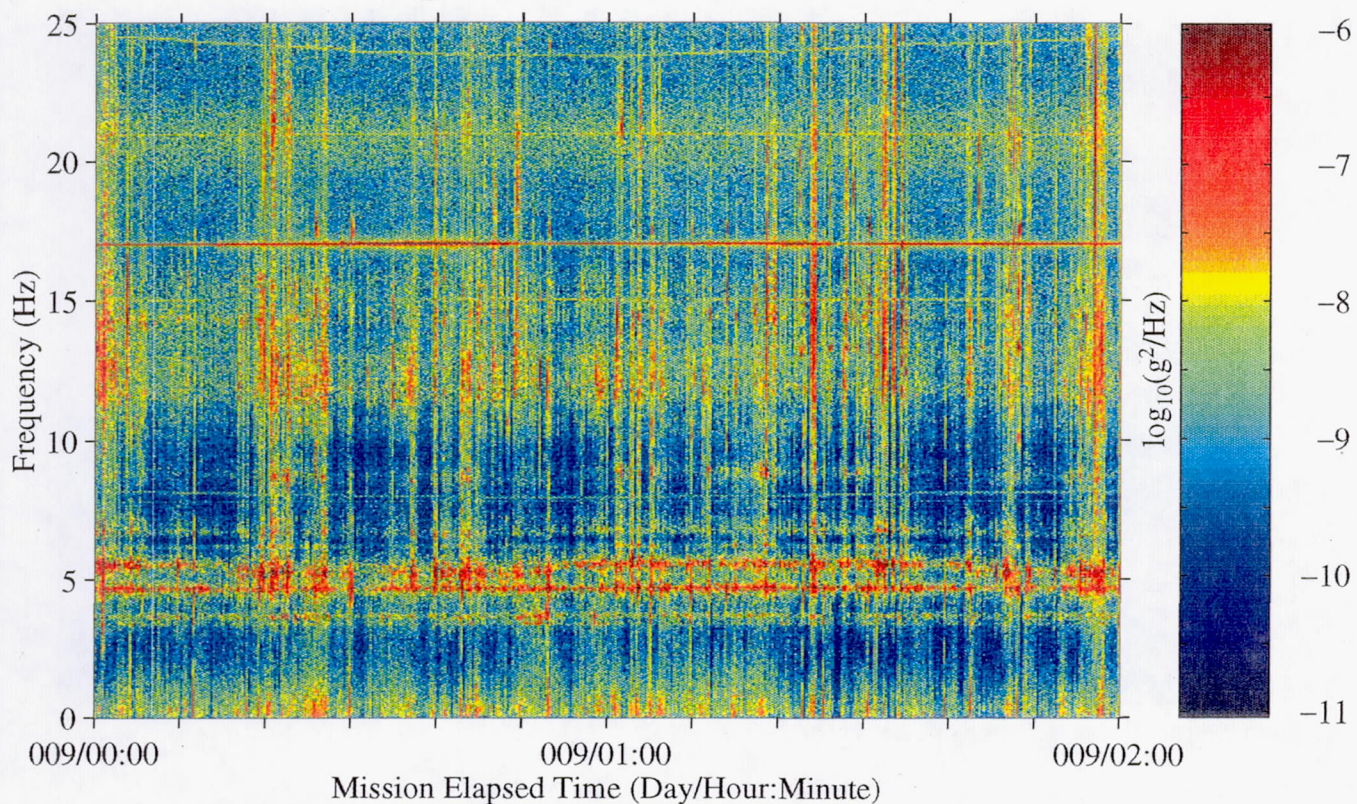




Figure 107: USML-2, Head C (fc=25 Hz)

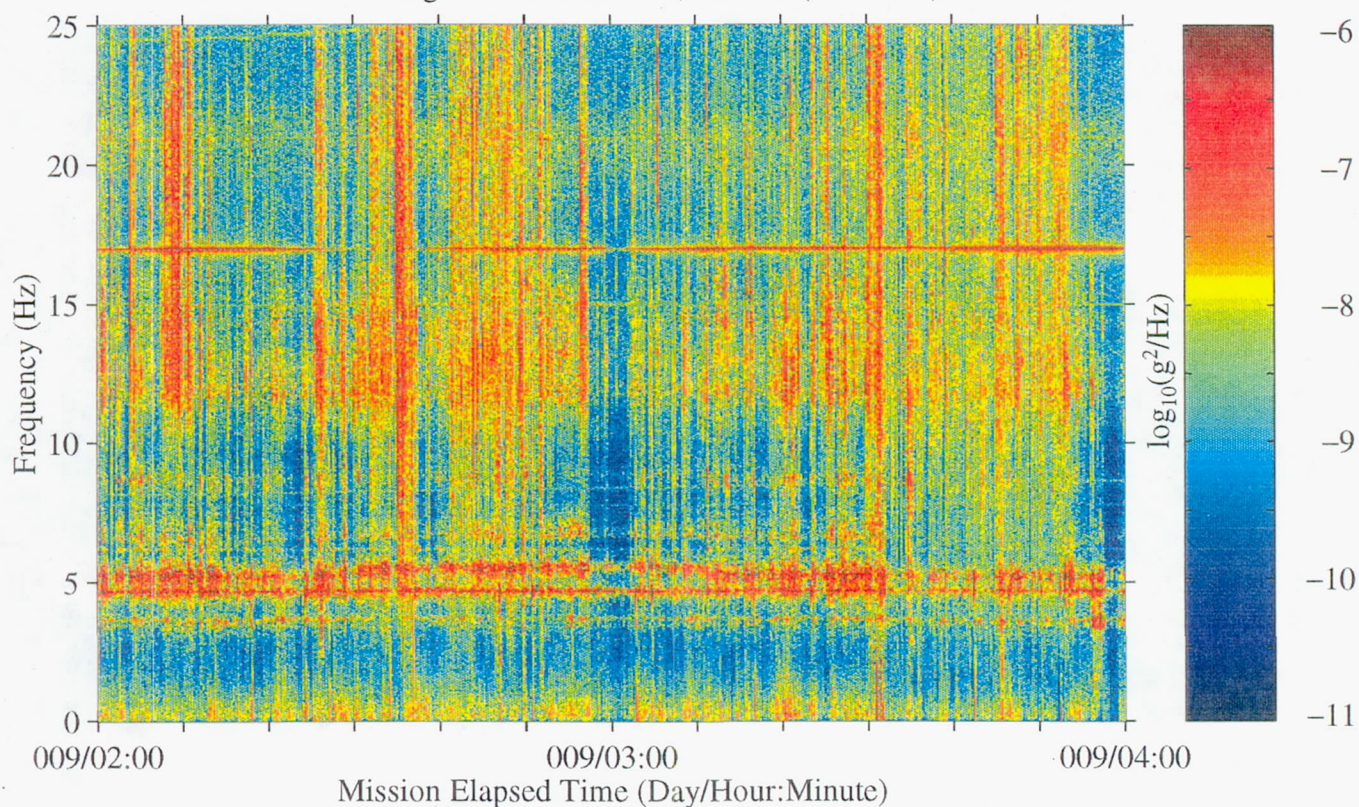


Figure 108: USML-2, Head C (fc=25 Hz)

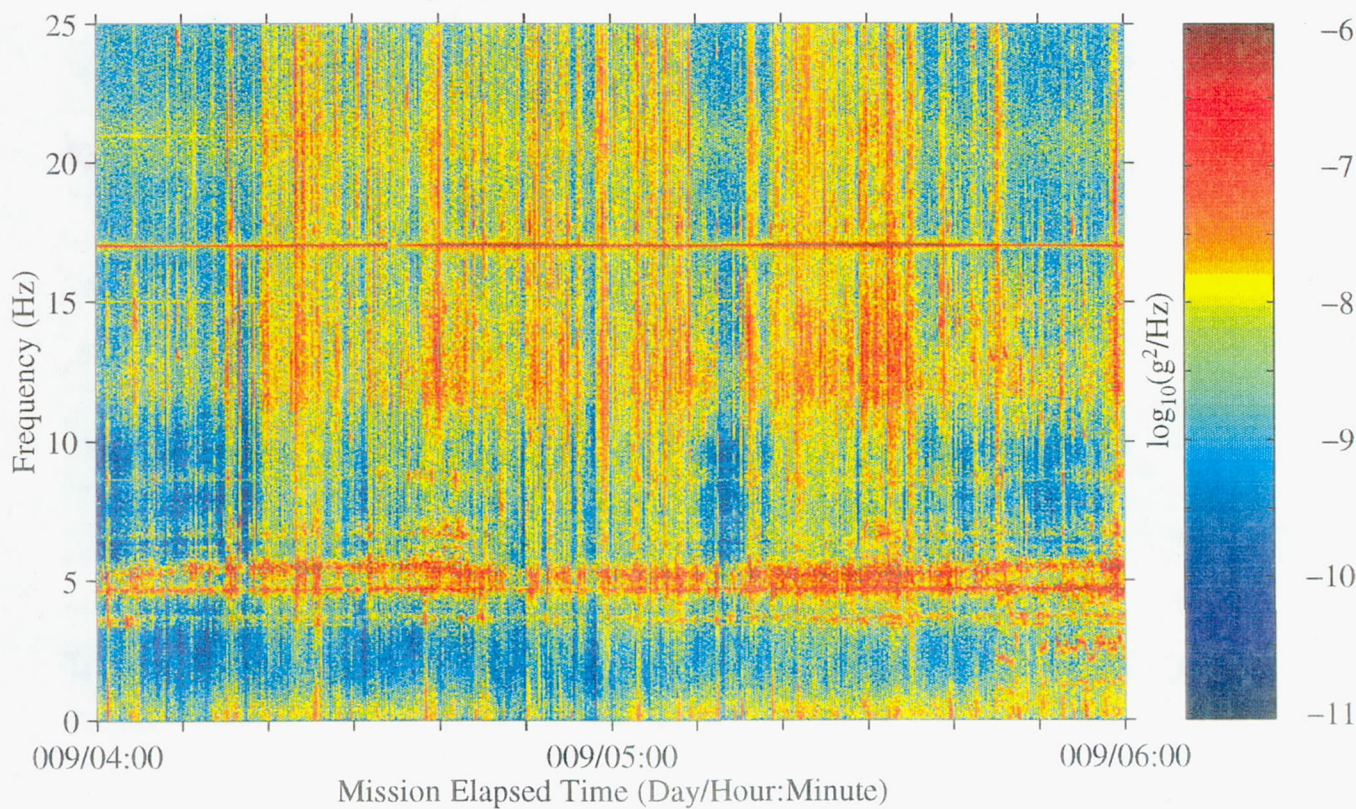




Figure 109: USML-2, Head C (fc=25 Hz)

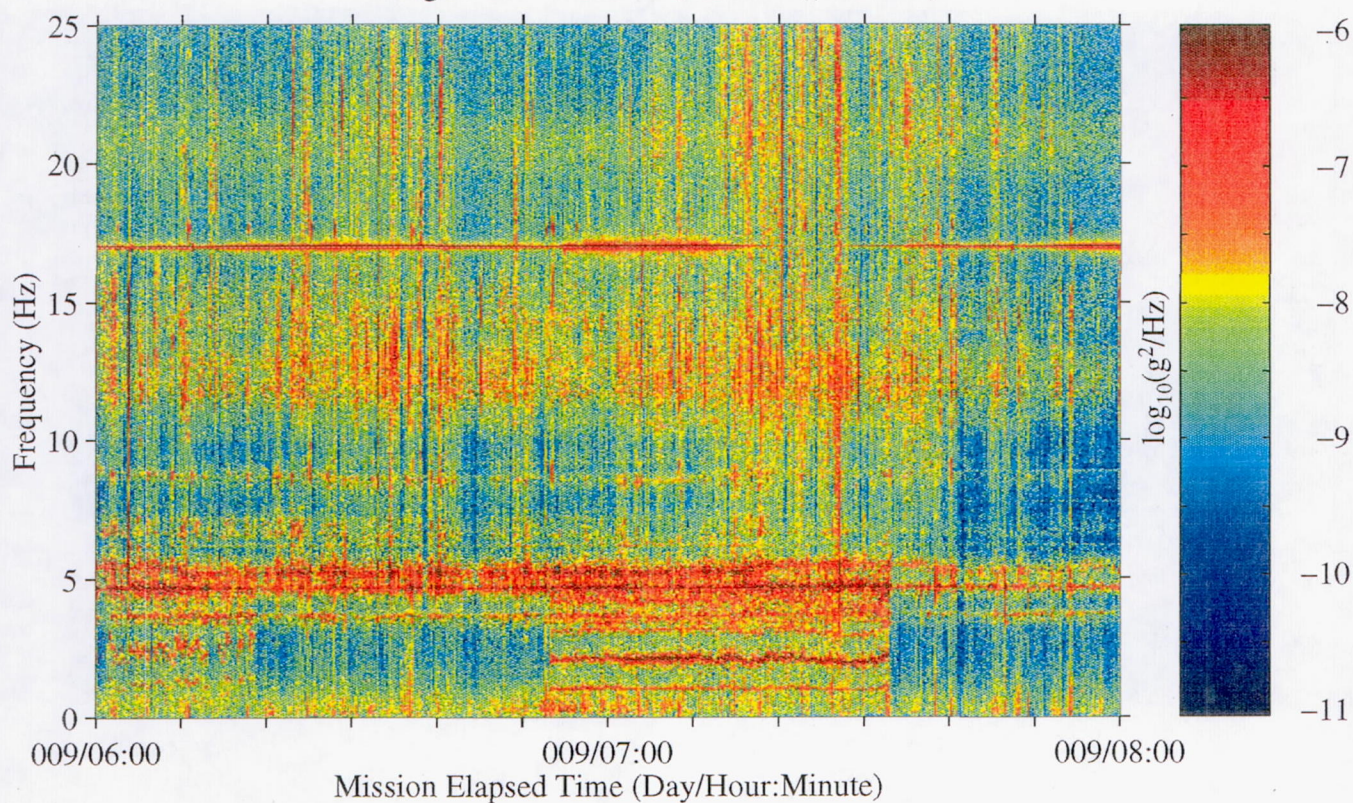


Figure 110: USML-2, Head C (fc=25 Hz)

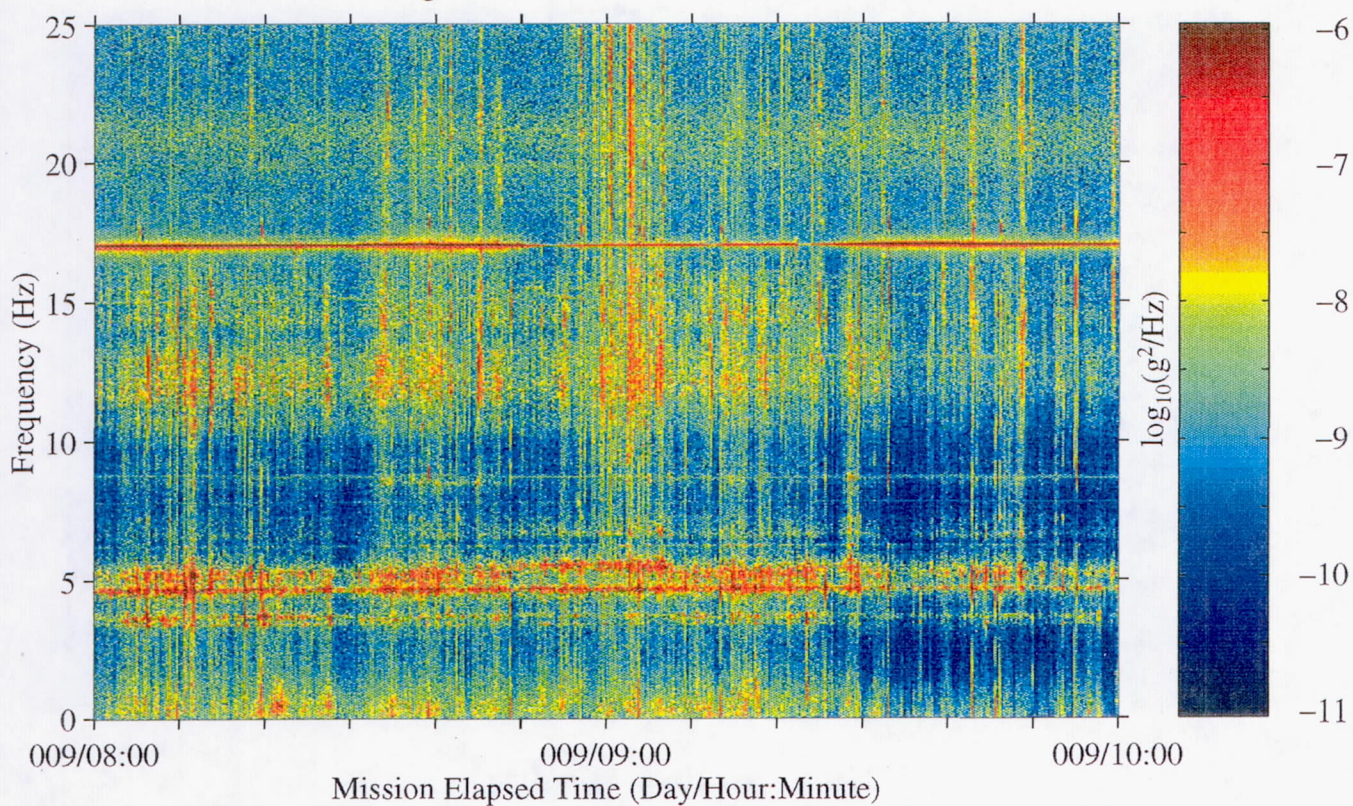




Figure 111: USML-2, Head C (fc=25 Hz)

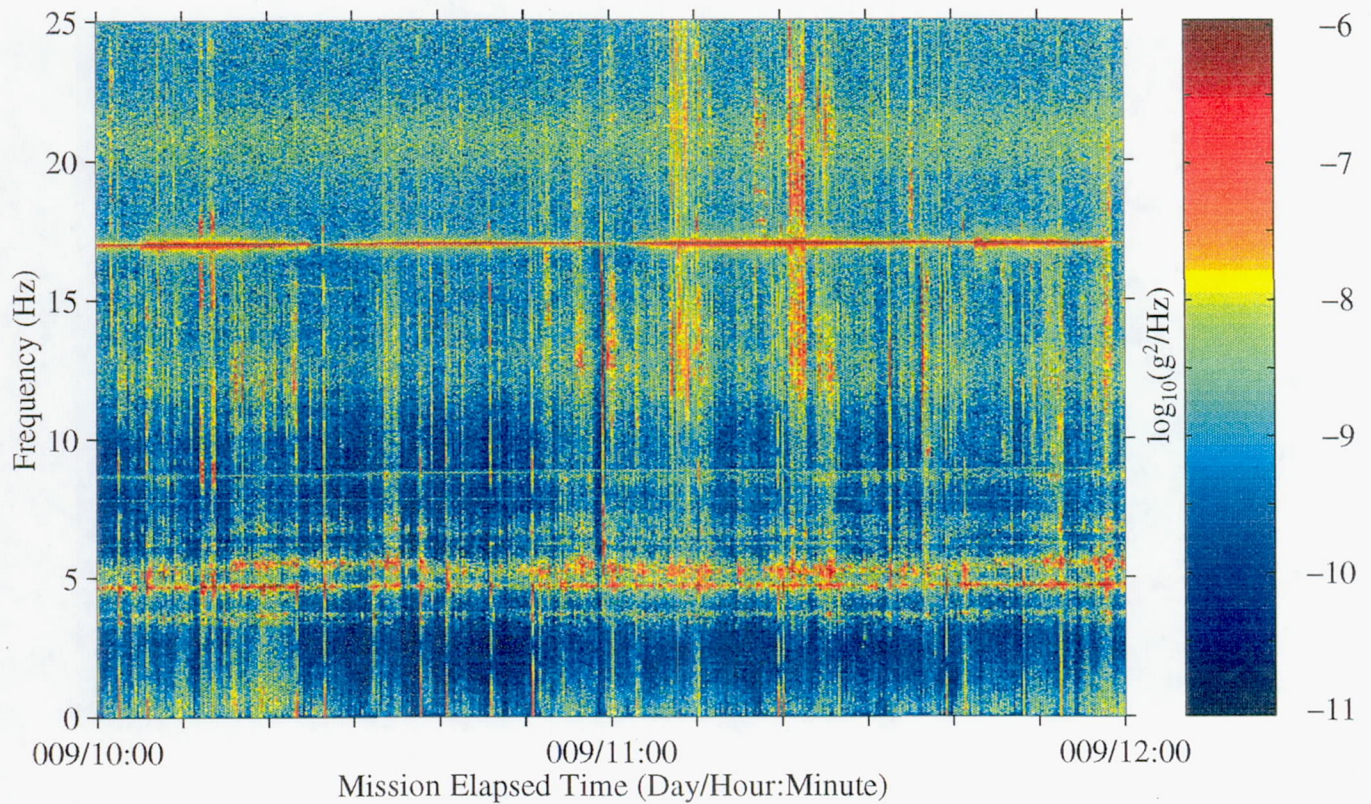


Figure 112: USML-2, Head C (fc=25 Hz)

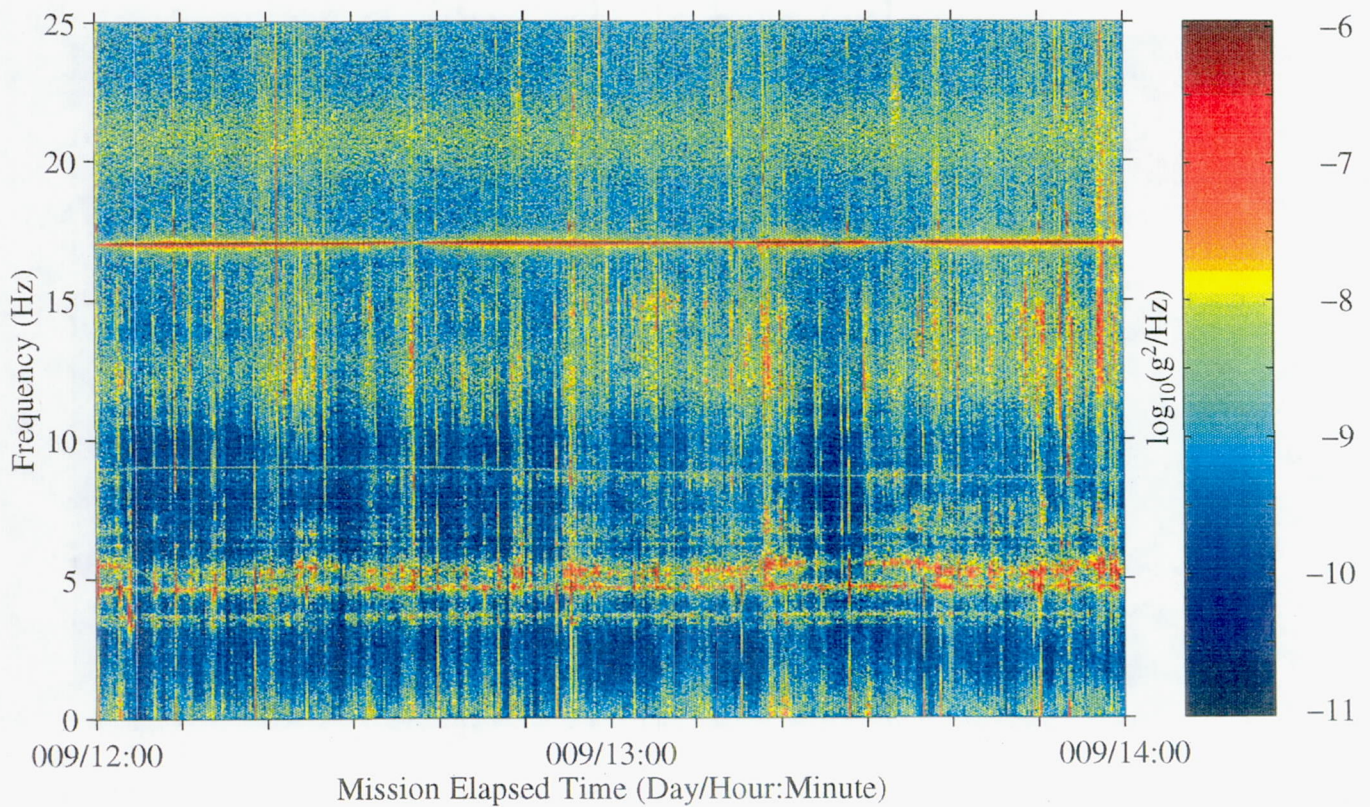




Figure 113: USML-2, Head C (fc=25 Hz)

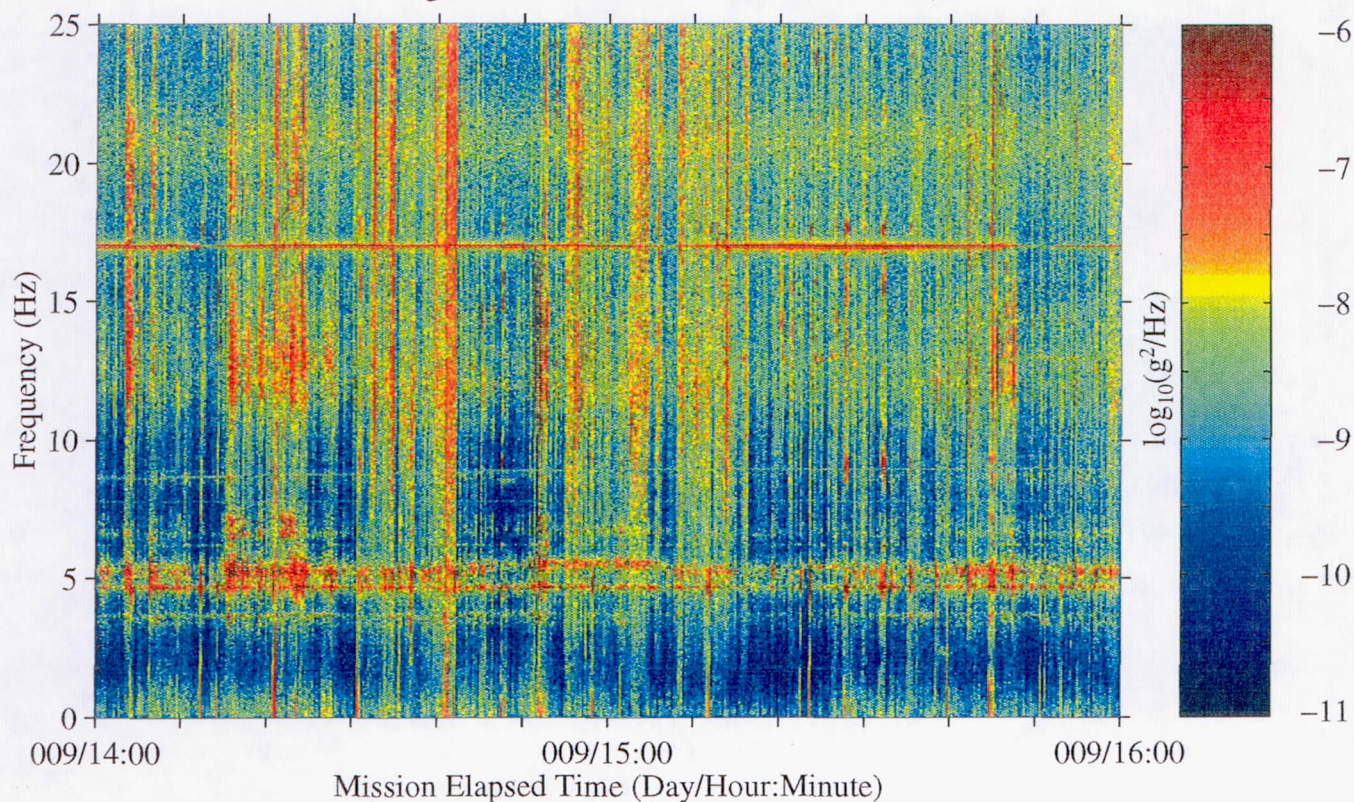


Figure 114: USML-2, Head C (fc=25 Hz)

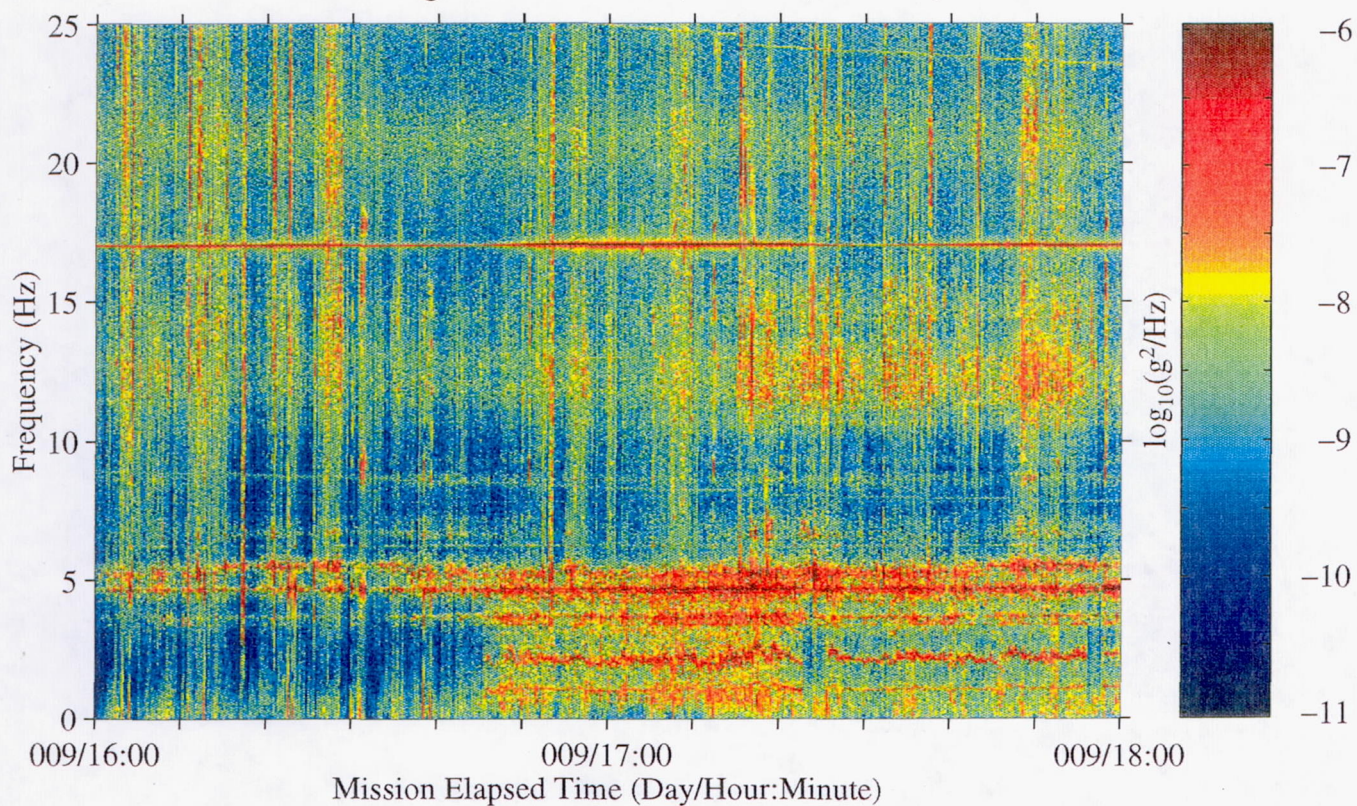




Figure 115: USML-2, Head C (fc=25 Hz)

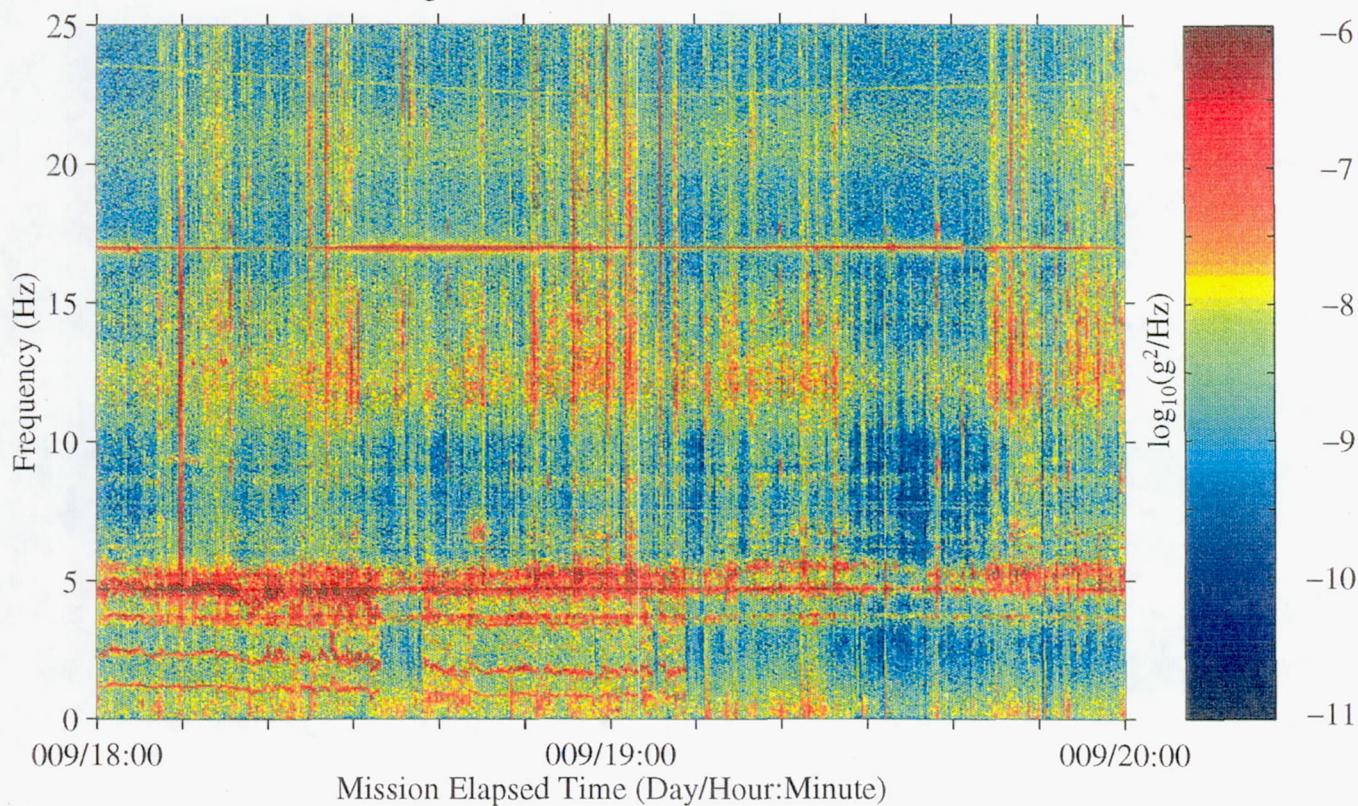


Figure 116: USML-2, Head C (fc=25 Hz)

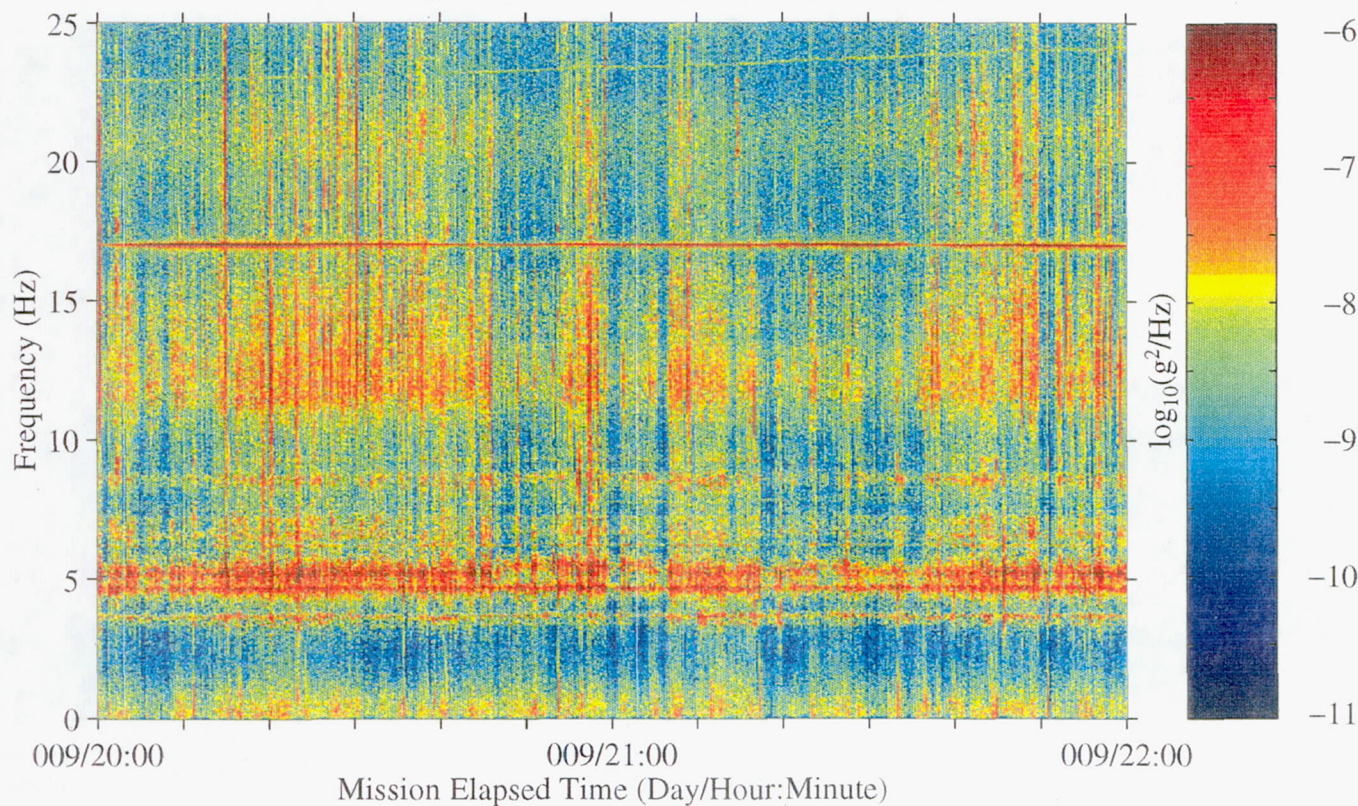




Figure 117: USML-2, Head C (fc=25 Hz)

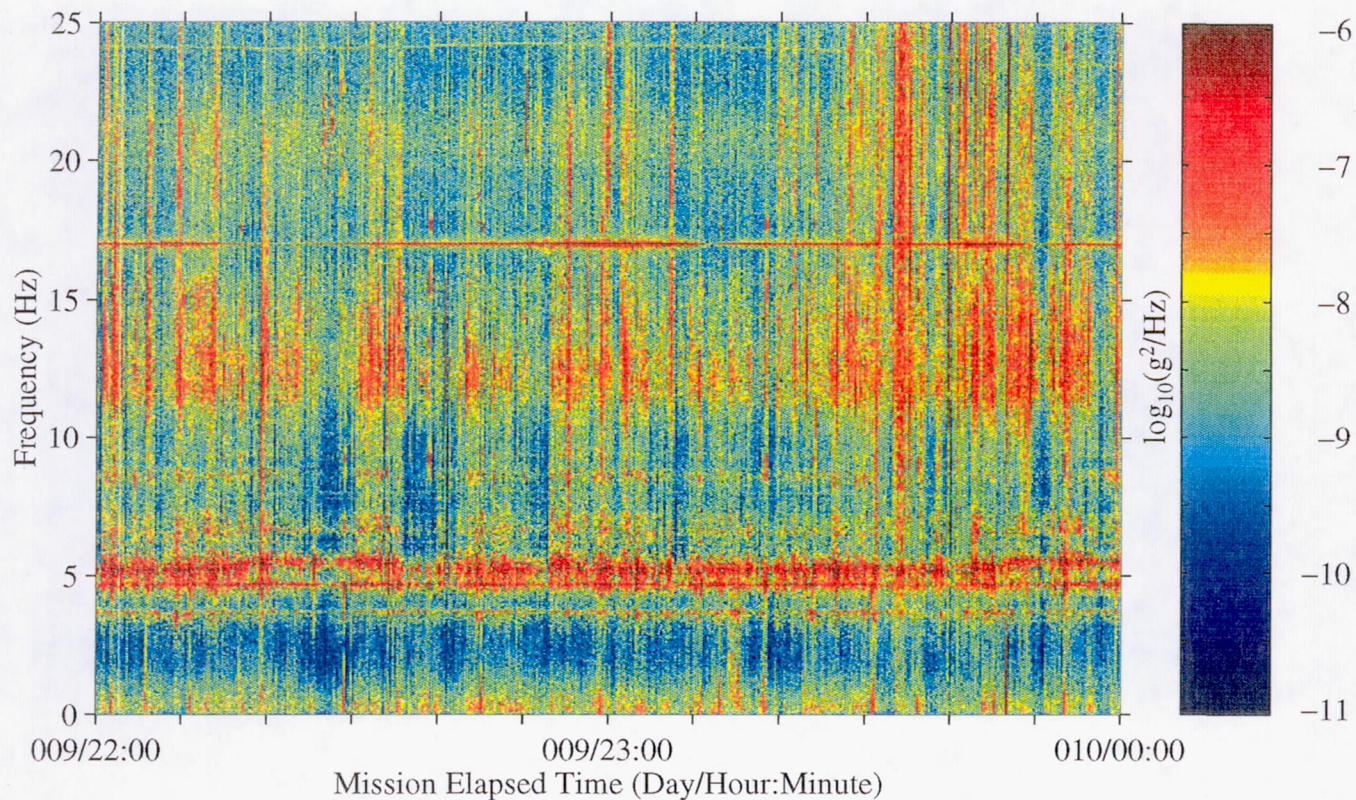


Figure 118: USML-2, Head C (fc=25 Hz)

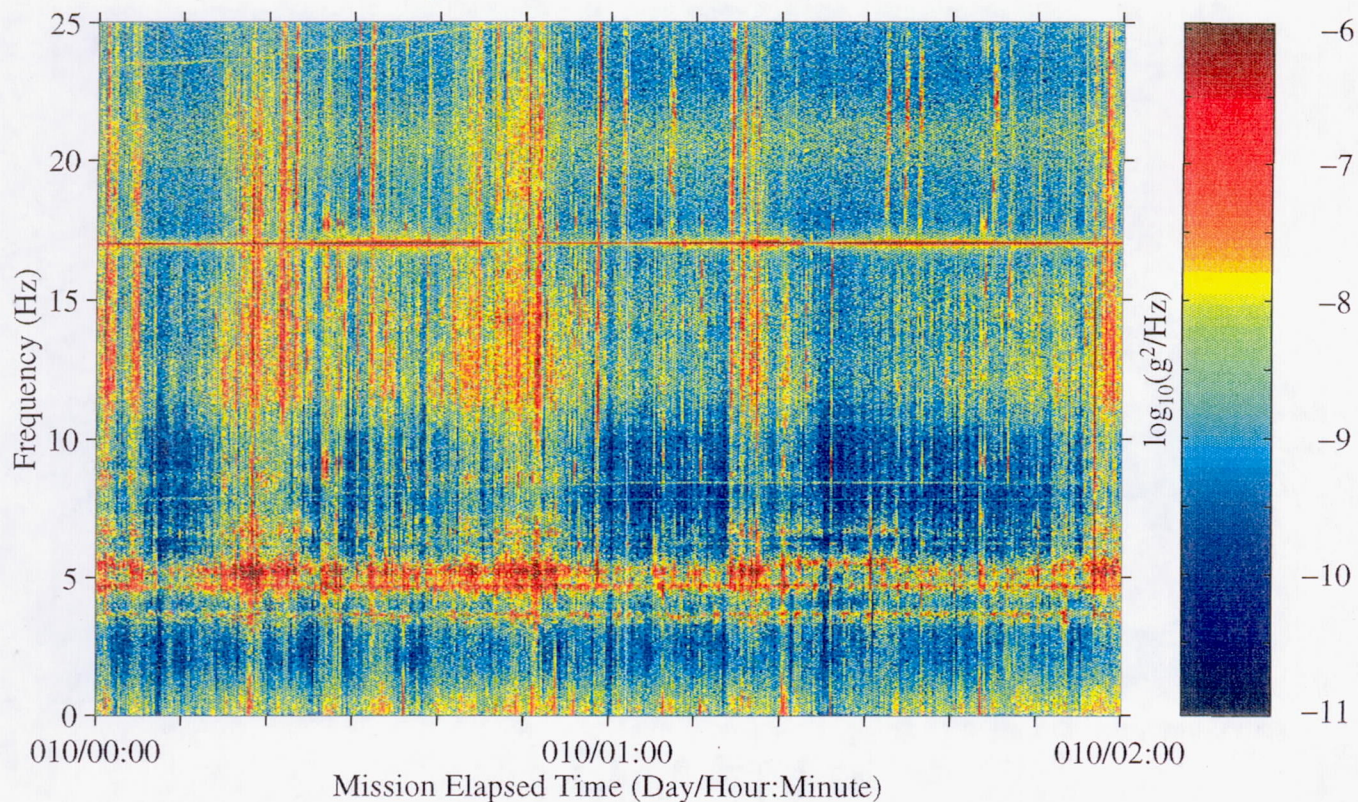




Figure 119: USML-2, Head C (fc=25 Hz)

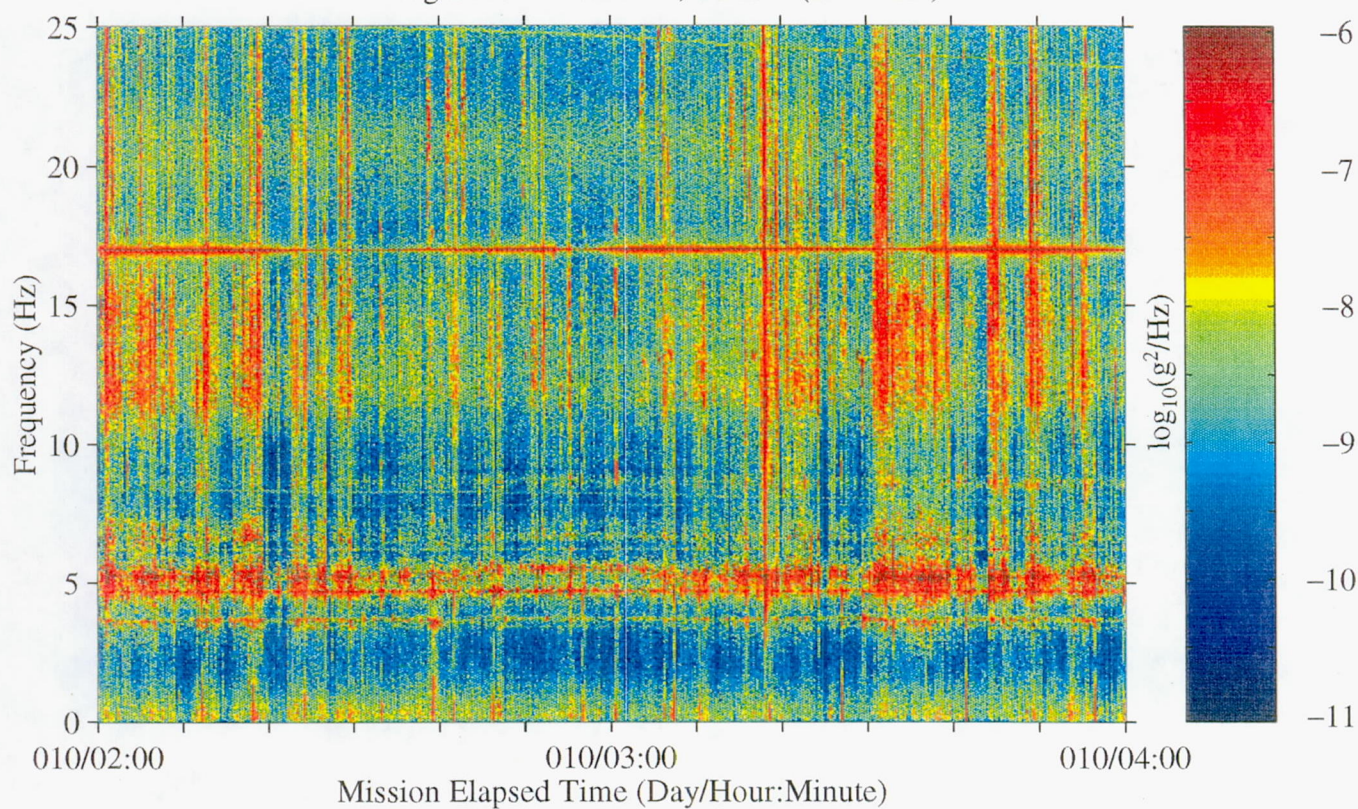


Figure 120: USML-2, Head C (fc=25 Hz)

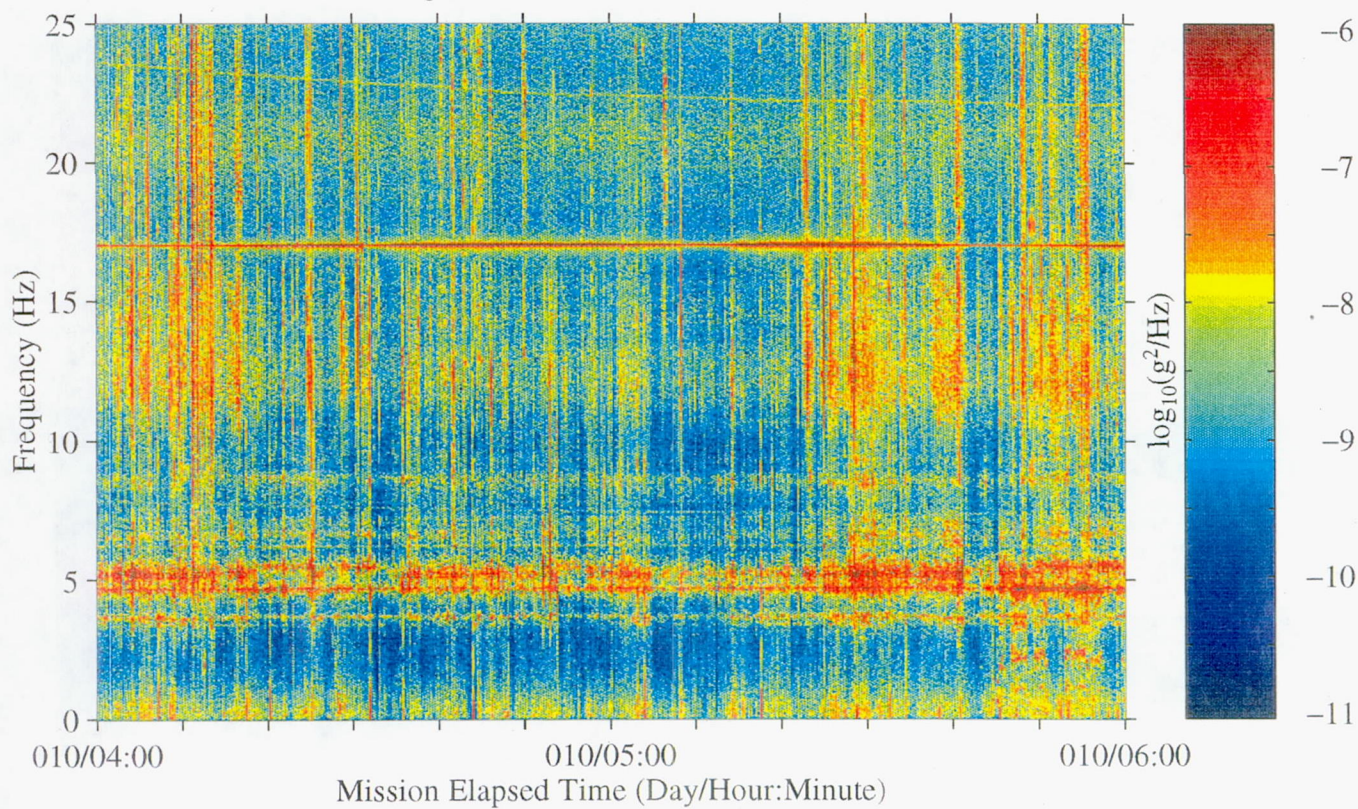




Figure 121: USML-2, Head C (fc=25 Hz)

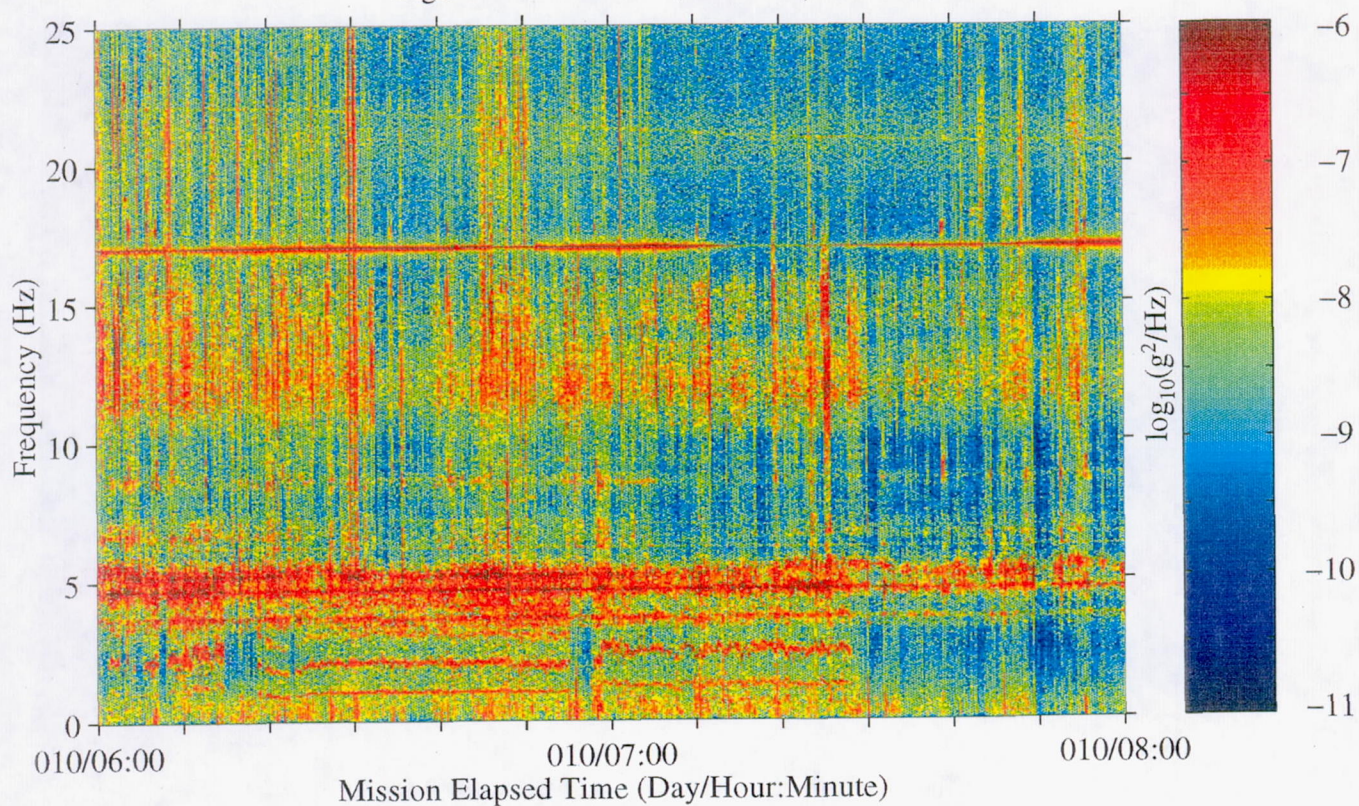


Figure 122: USML-2, Head C (fc=25 Hz)

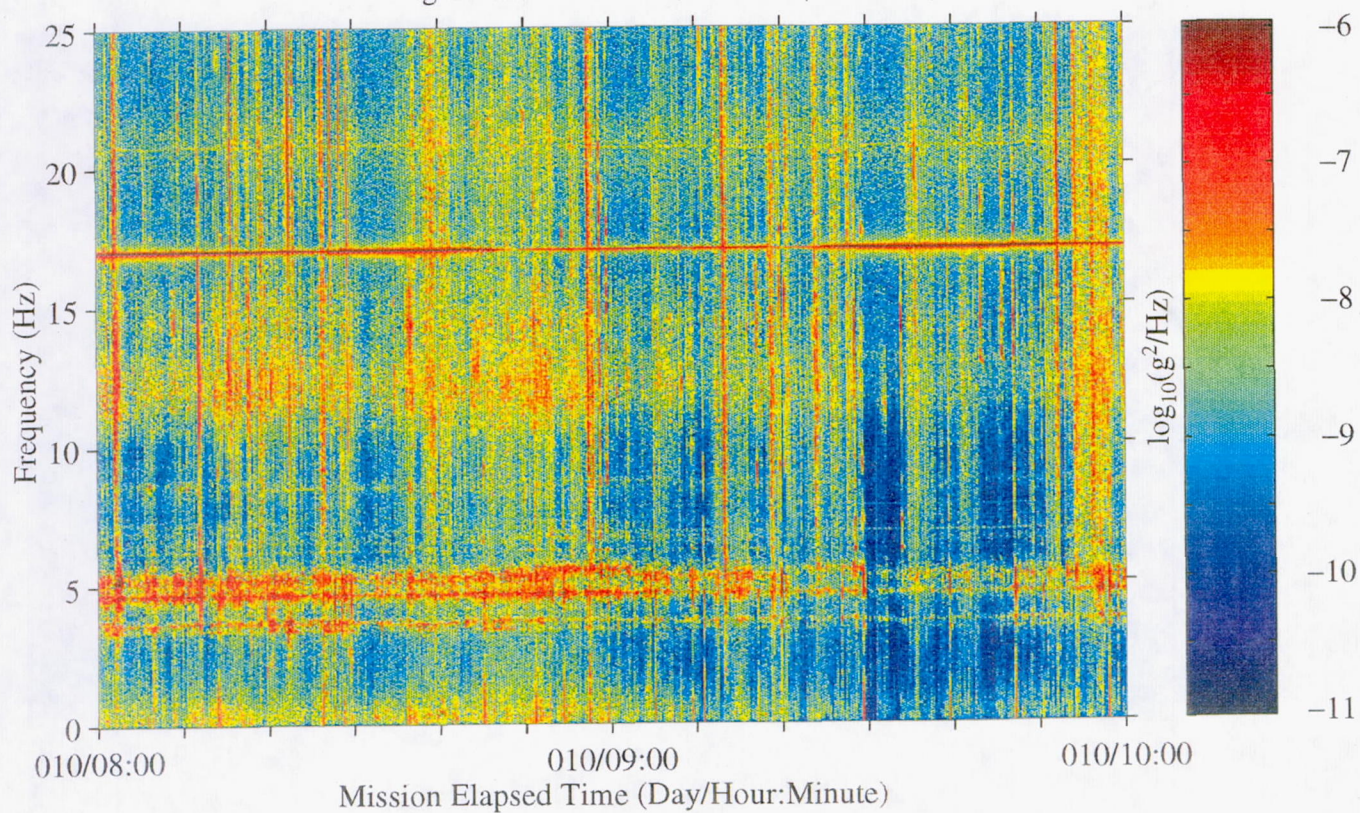




Figure 123: USML-2, Head C (fc=25 Hz)

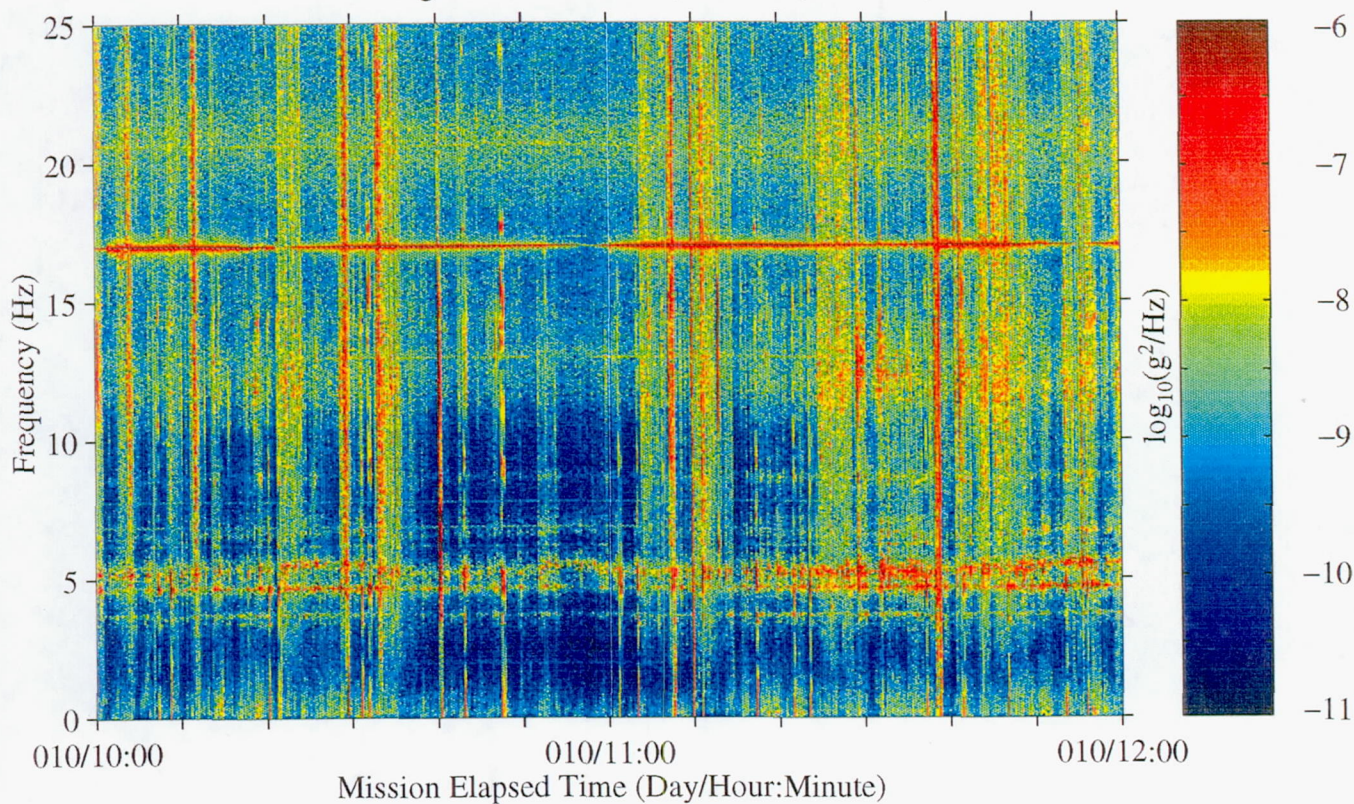


Figure 124: USML-2, Head C (fc=25 Hz)

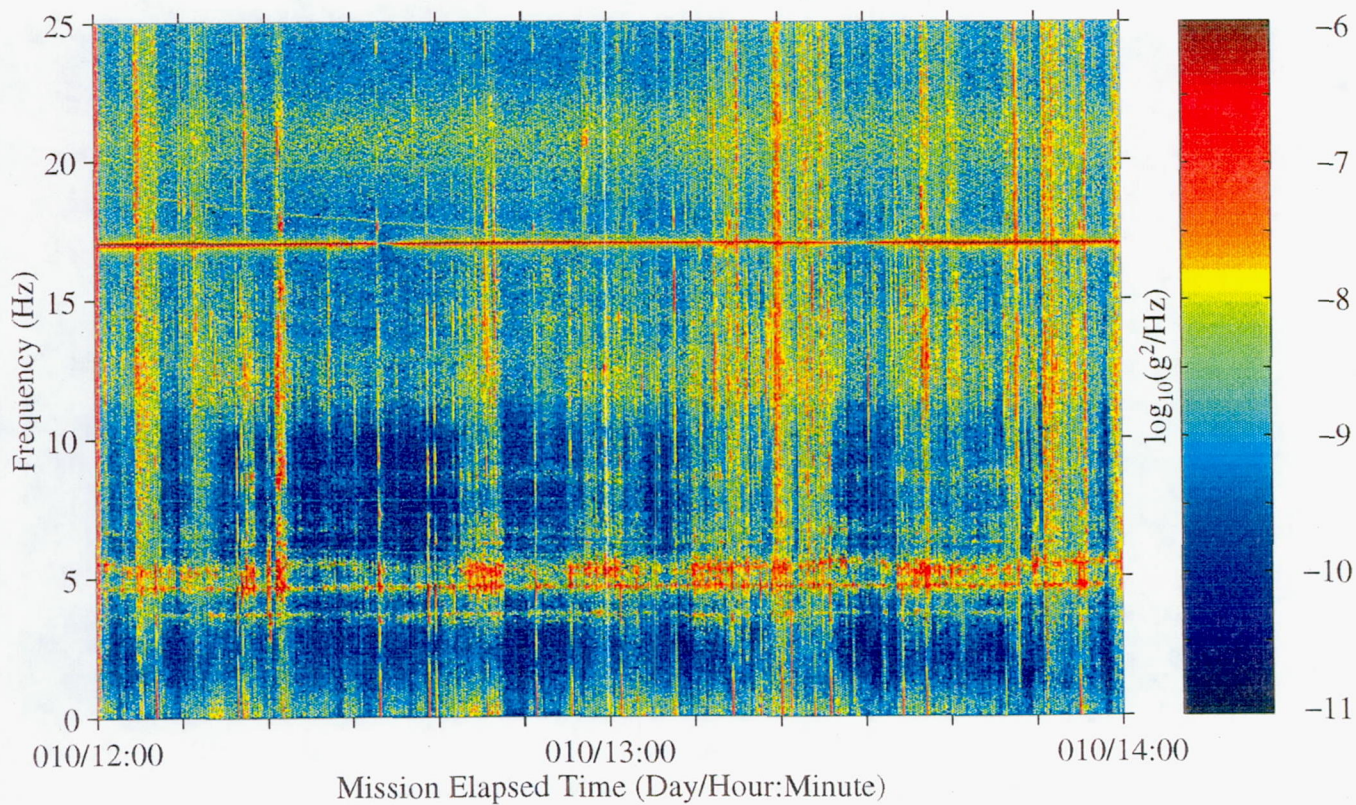




Figure 125: USML-2, Head C (fc=25 Hz)

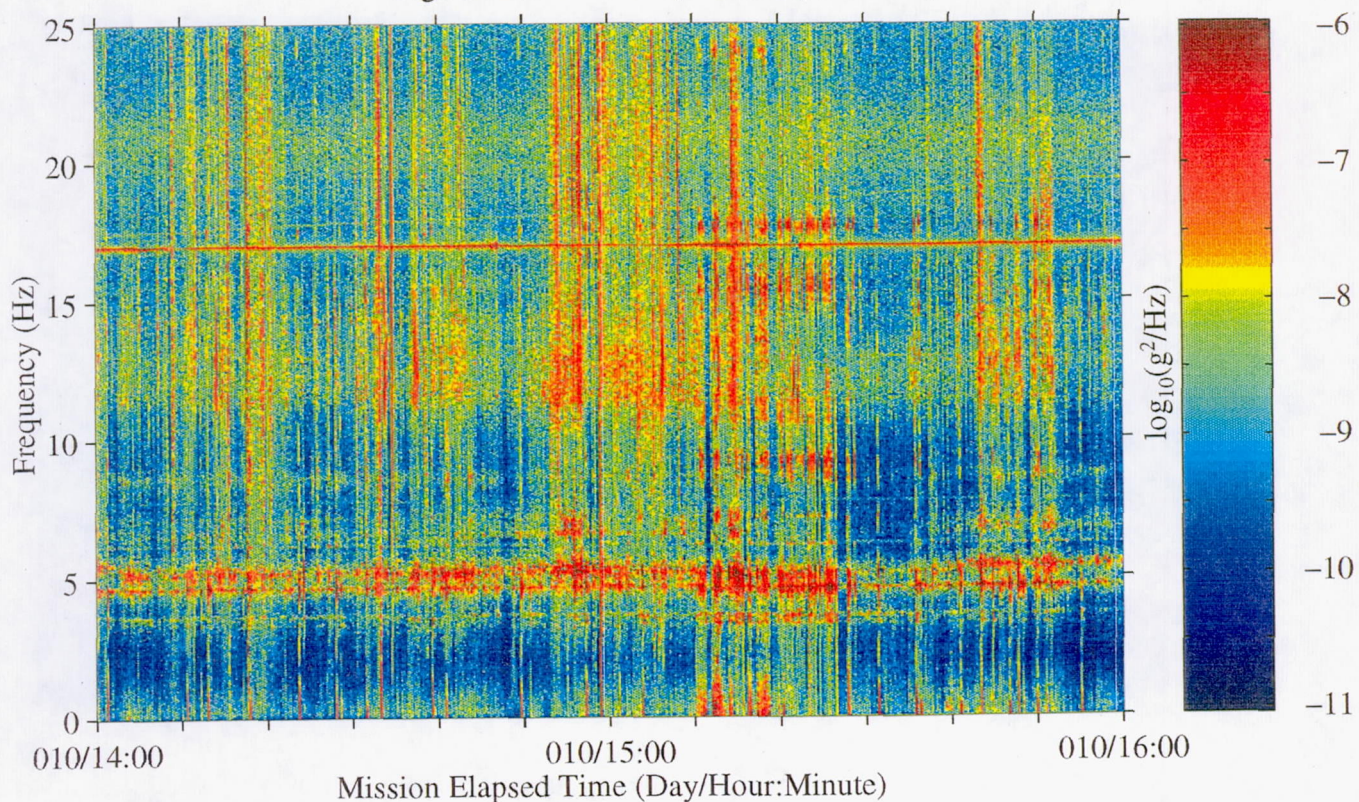


Figure 126: USML-2, Head C (fc=25 Hz)

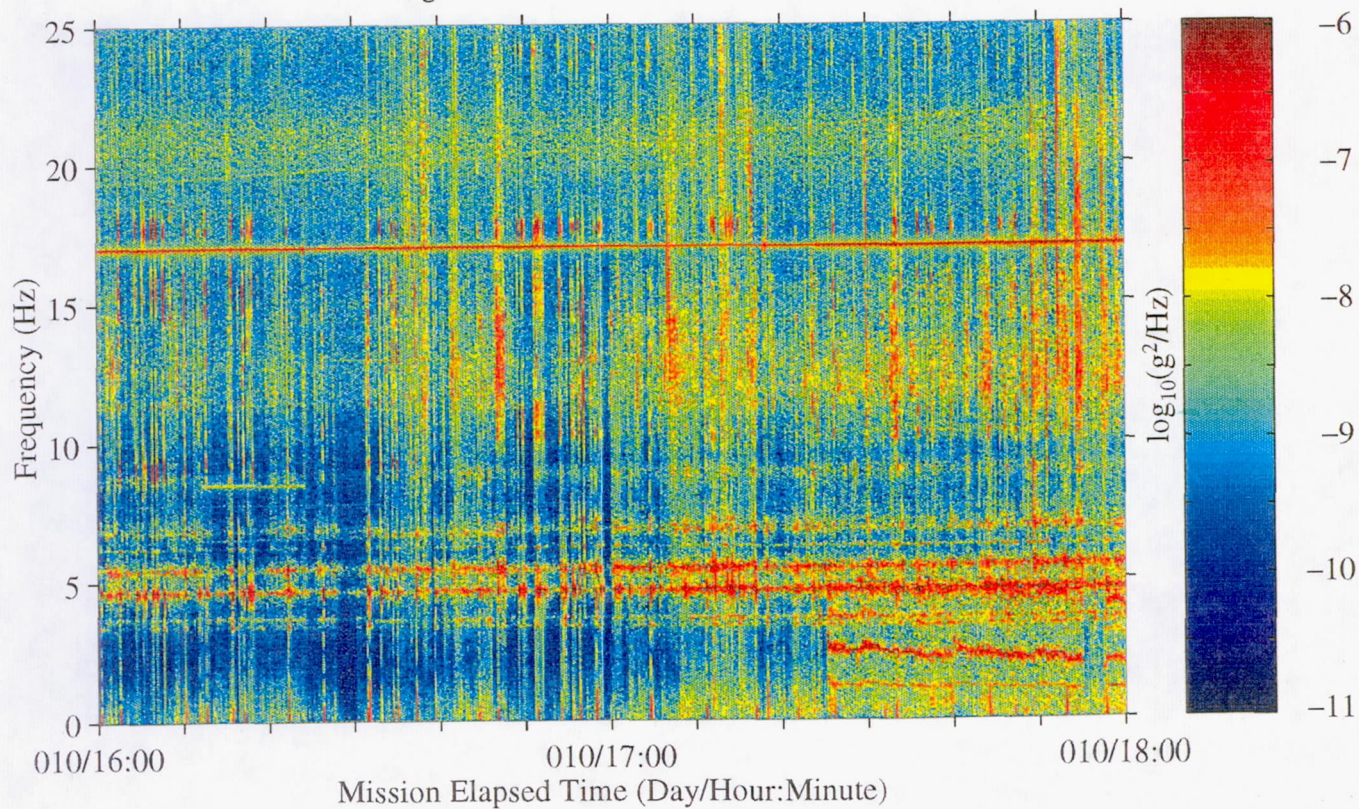




Figure 127: USML-2, Head C (fc=25 Hz)

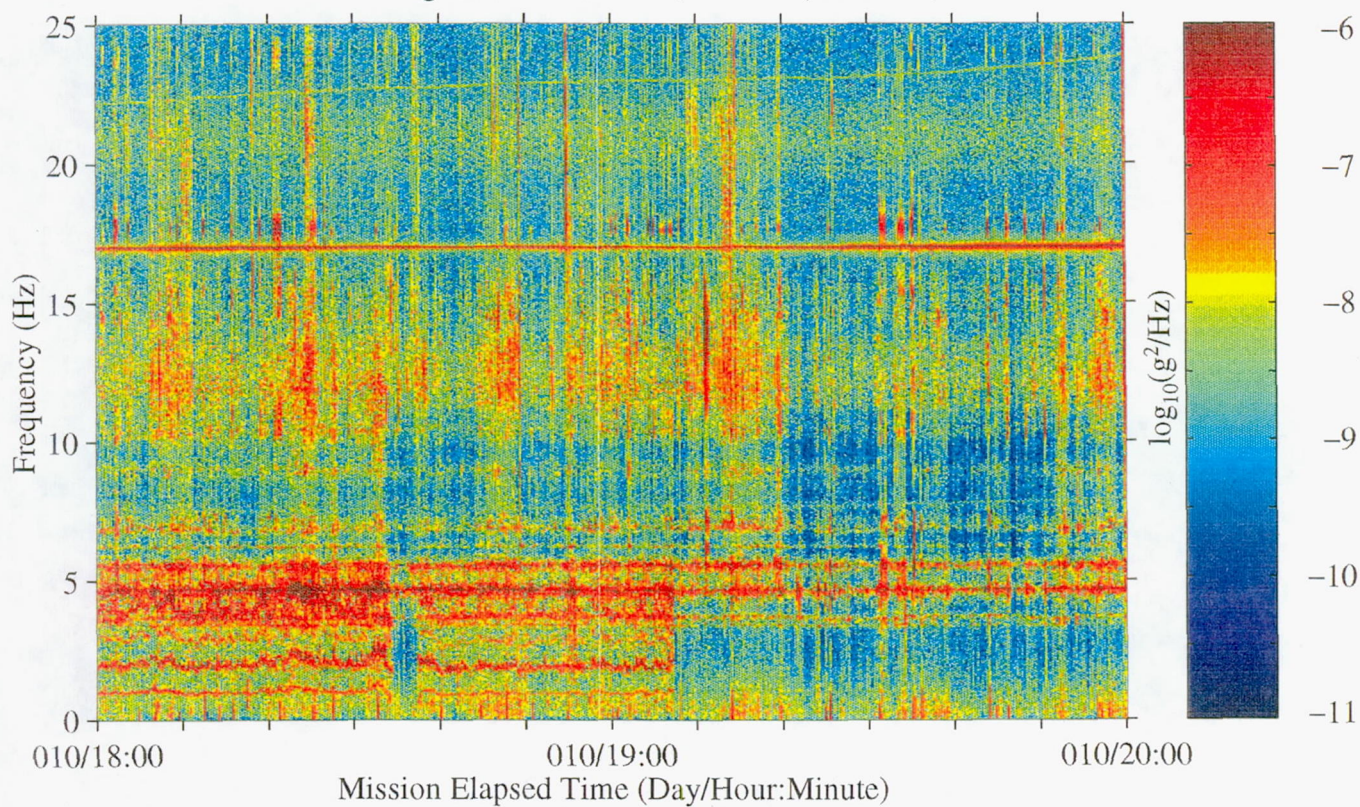


Figure 128: USML-2, Head C (fc=25 Hz)

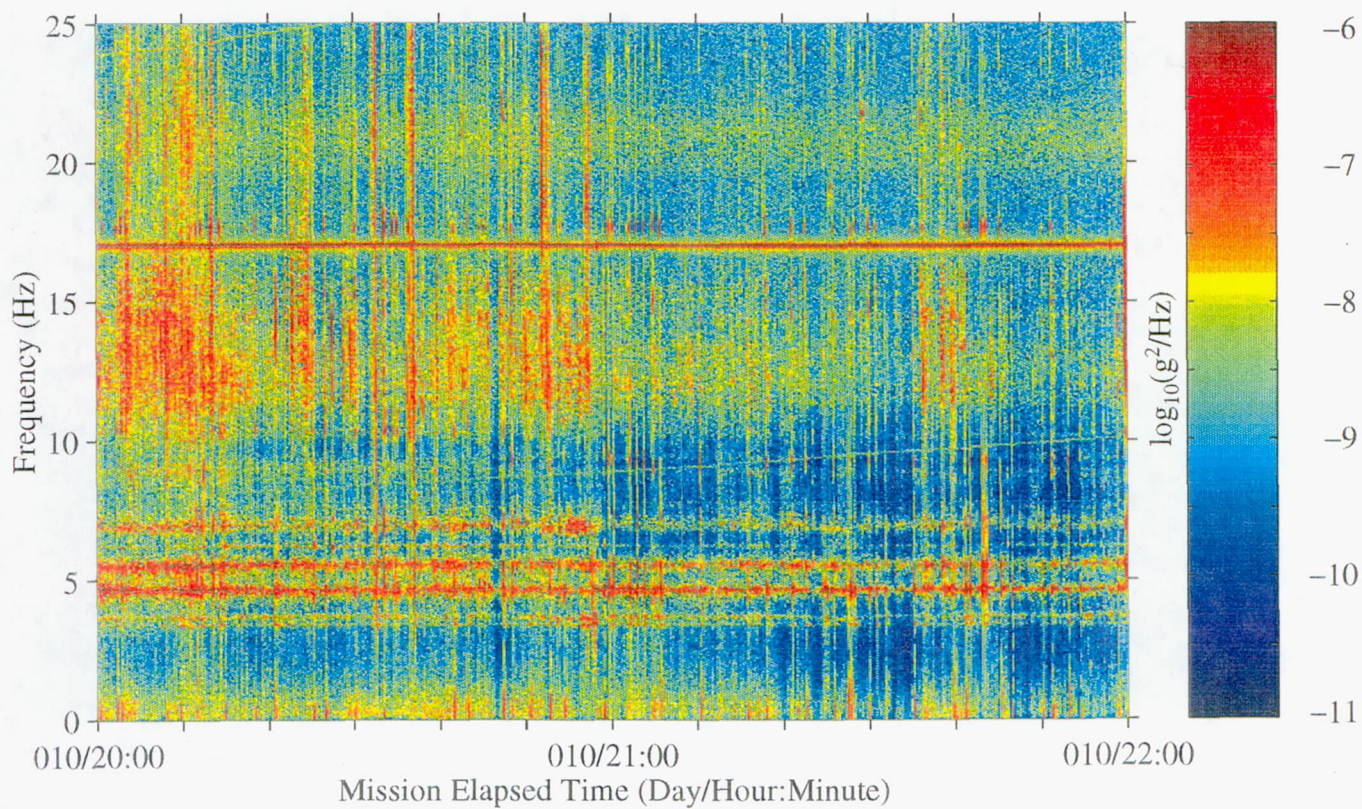




Figure 129: USML-2, Head C (fc=25 Hz)

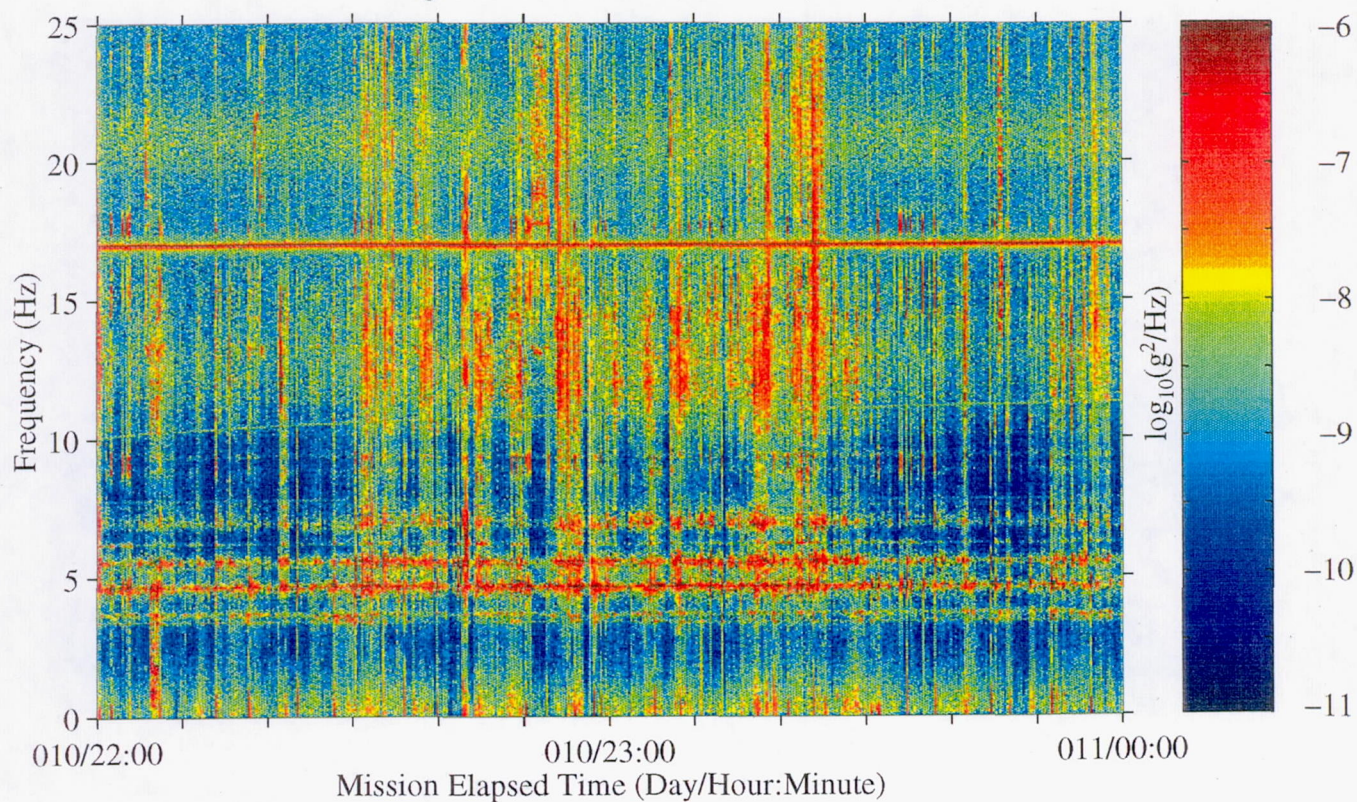


Figure 130: USML-2, Head C (fc=25 Hz)

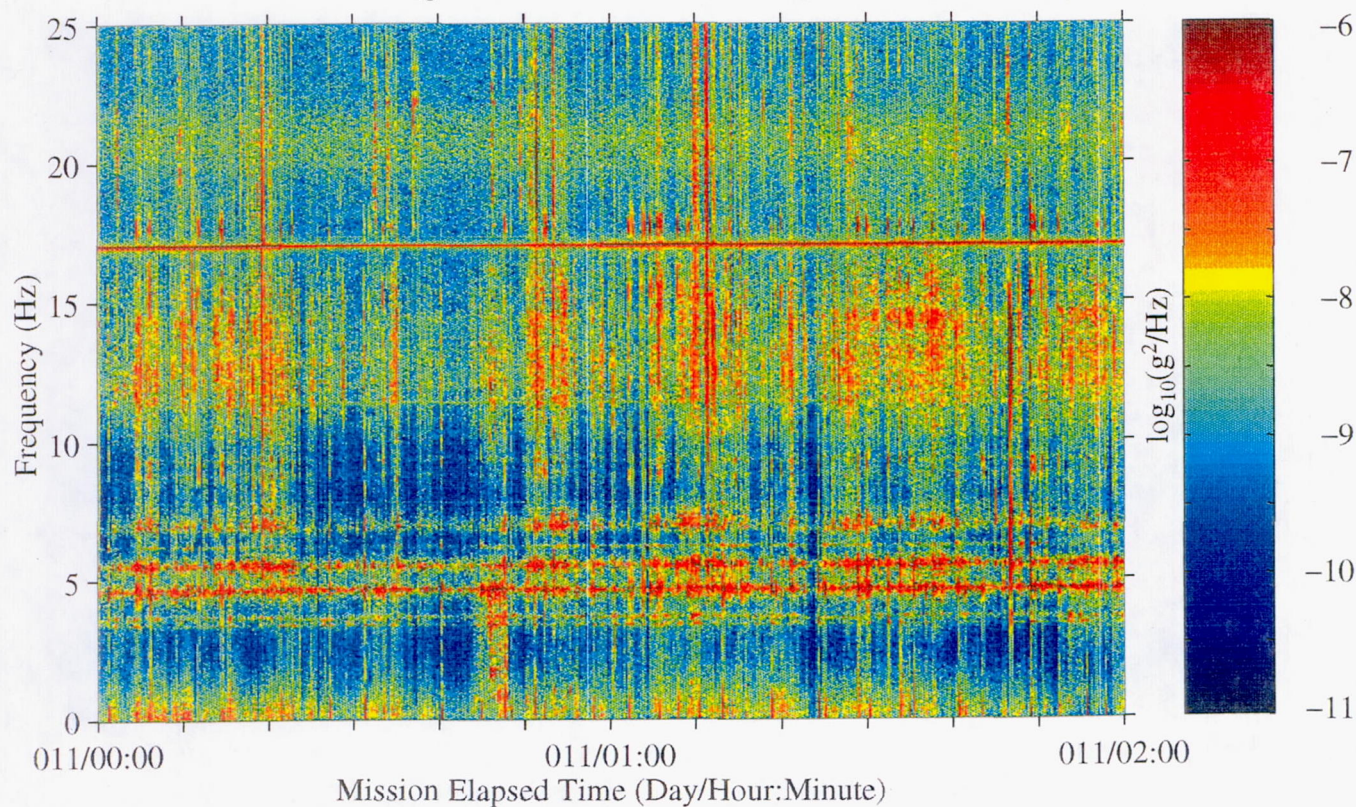




Figure 131: USML-2, Head C (fc=25 Hz)

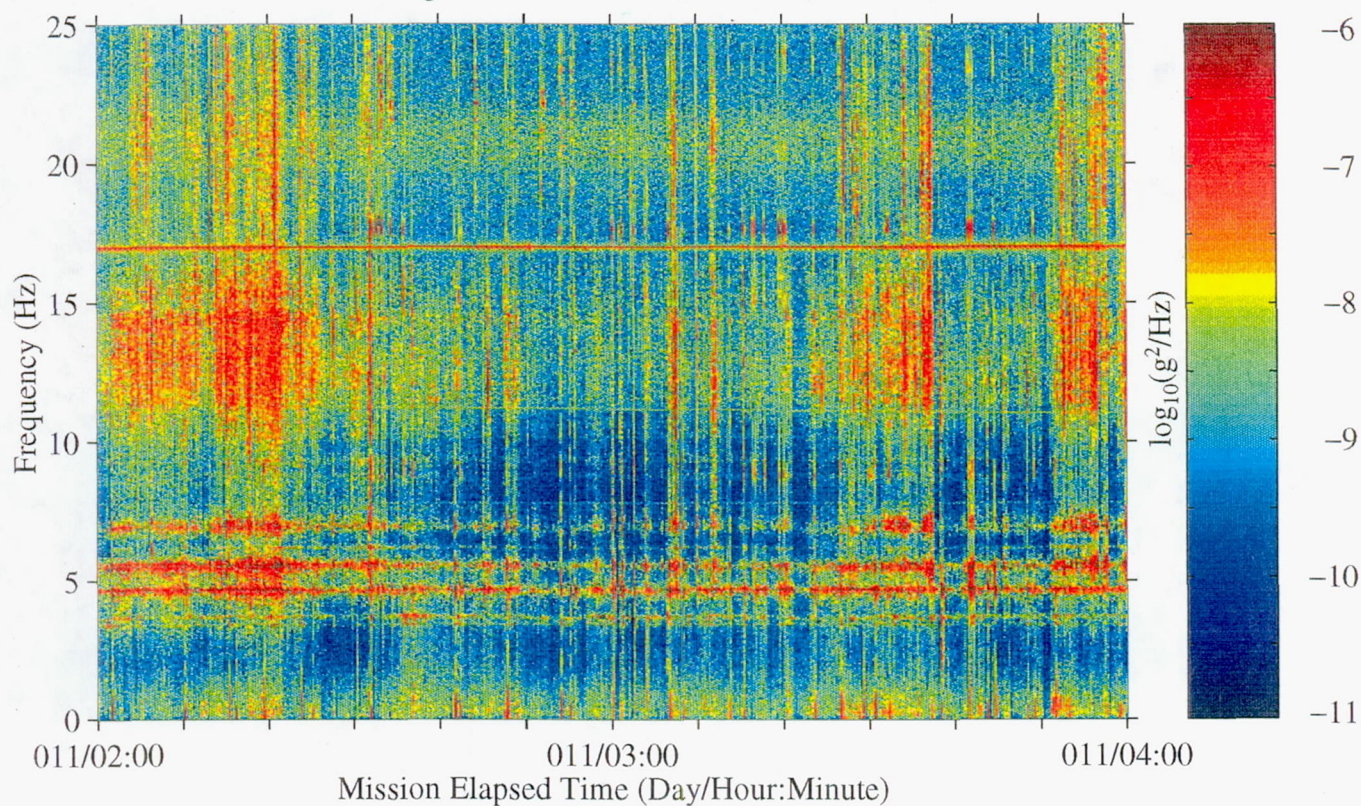


Figure 132: USML-2, Head C (fc=25 Hz)

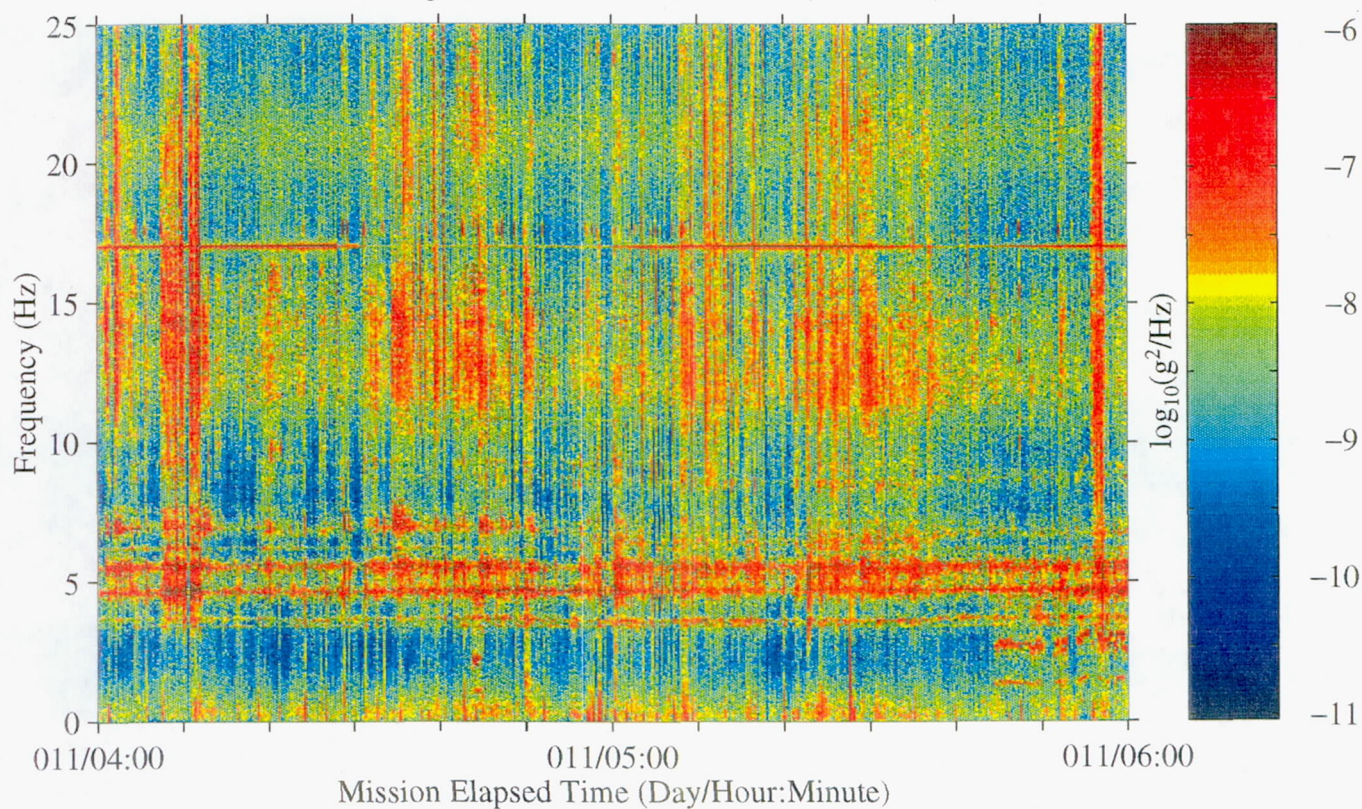




Figure 133: USML-2, Head C (fc=25 Hz)

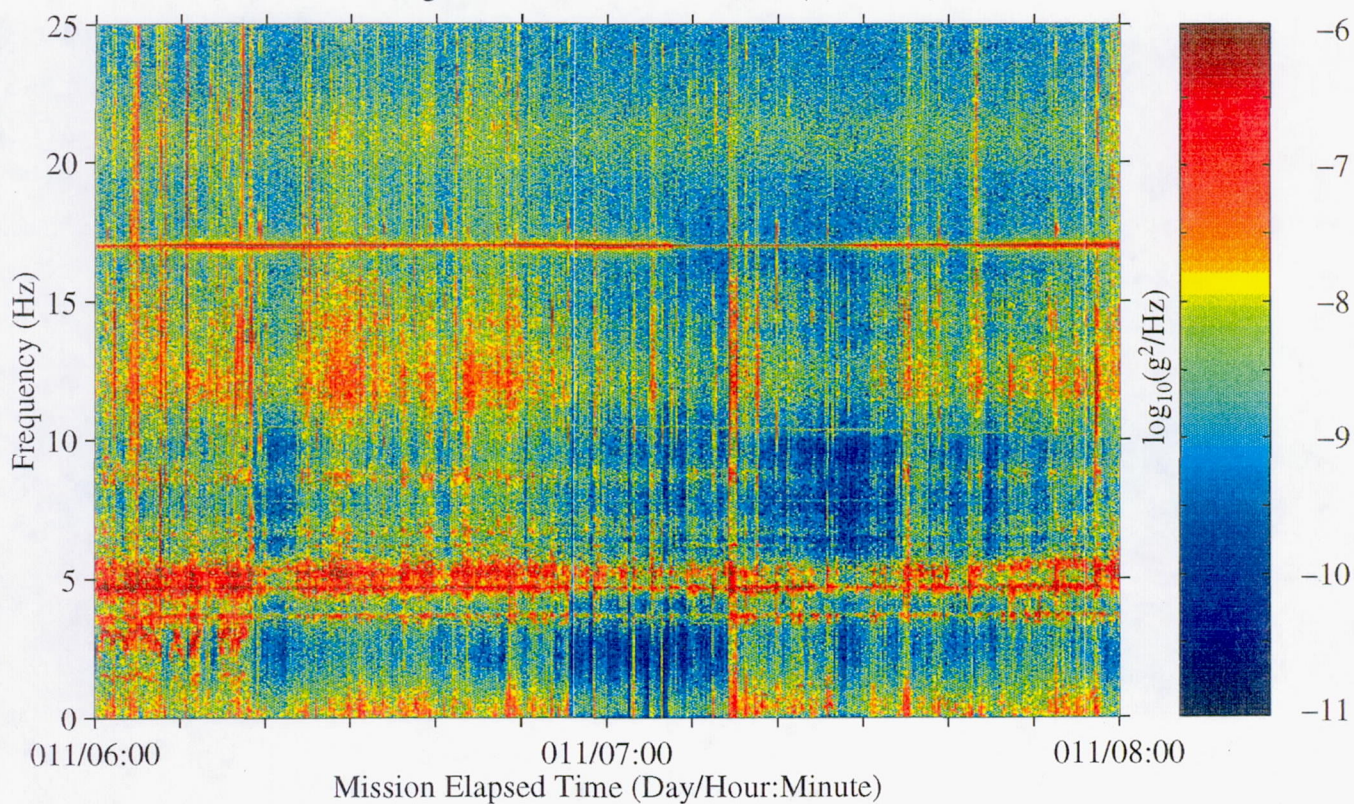


Figure 134: USML-2, Head C (fc=25 Hz)

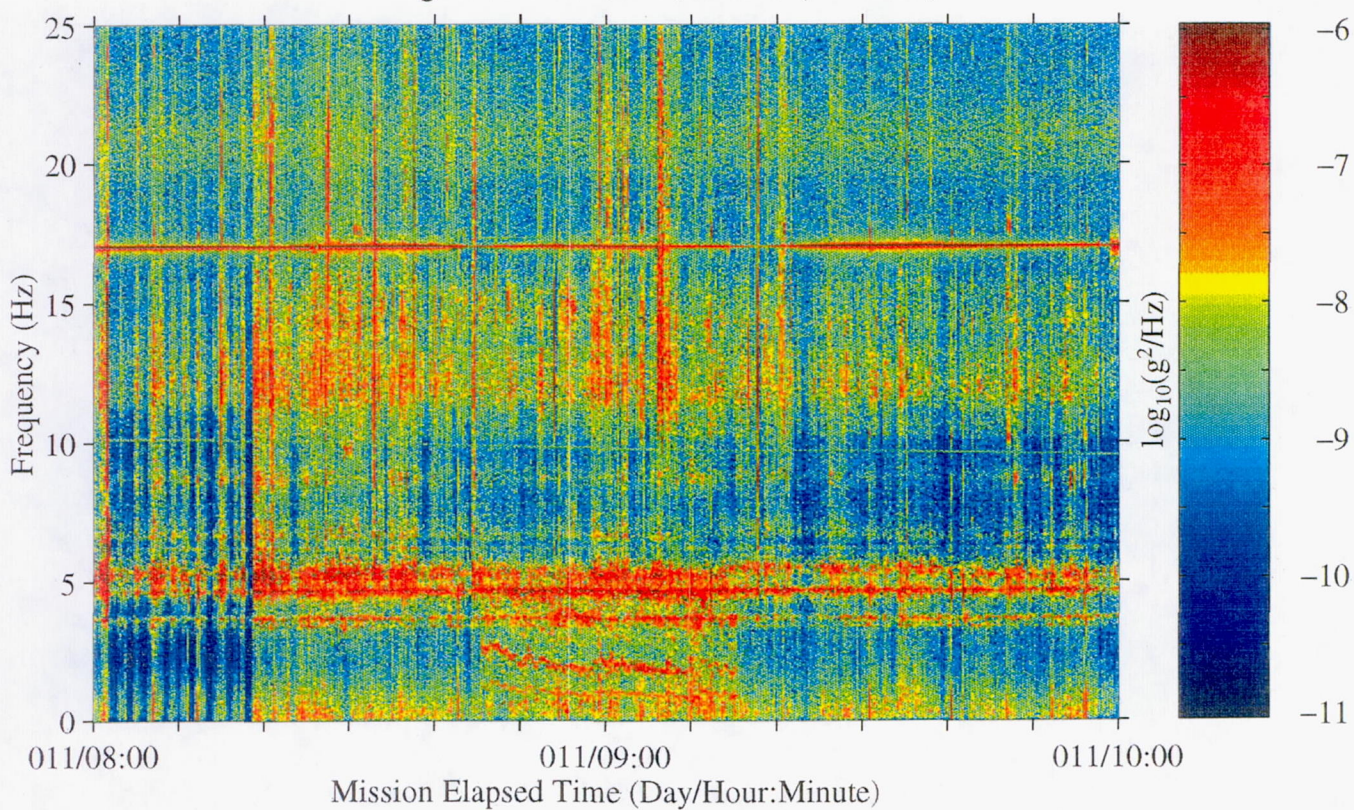




Figure 135: USML-2, Head C (fc=25 Hz)

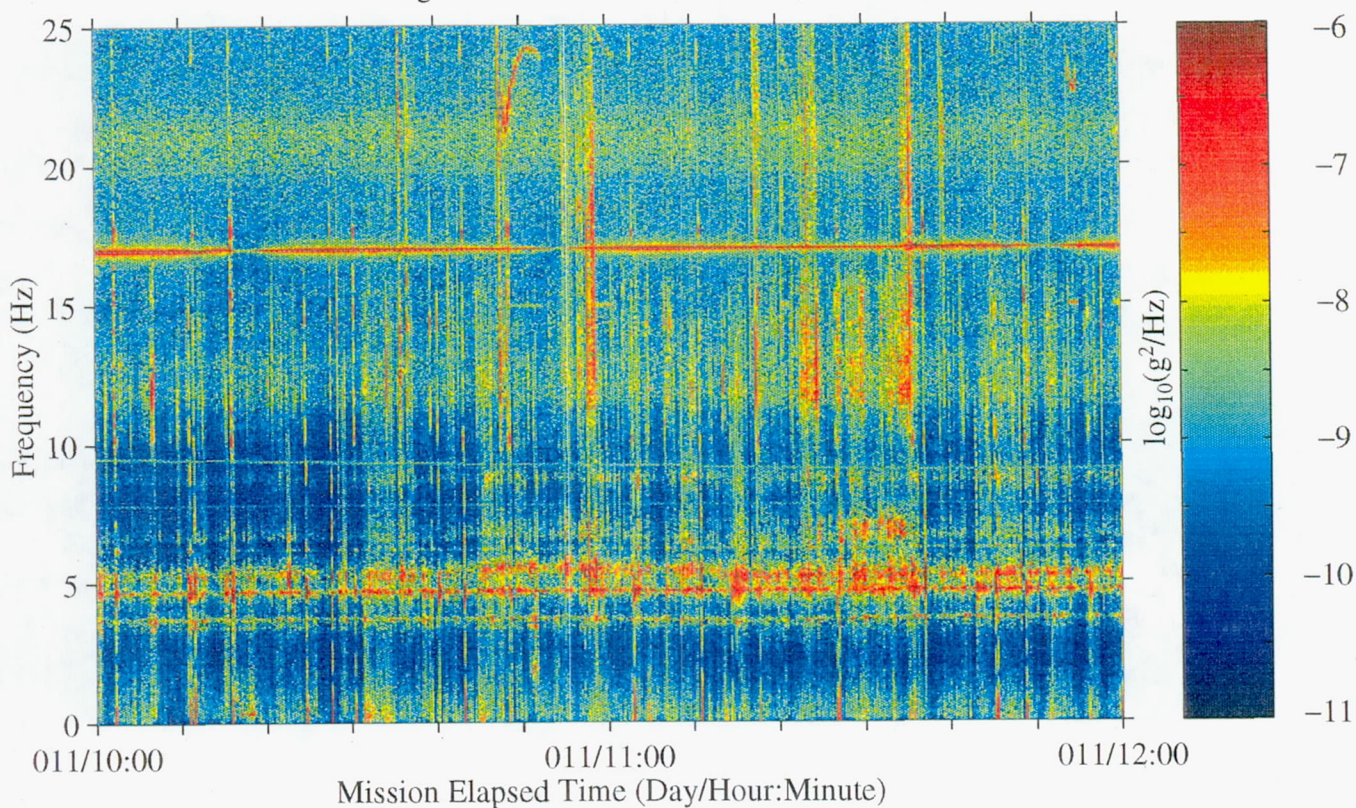


Figure 136: USML-2, Head C (fc=25 Hz)

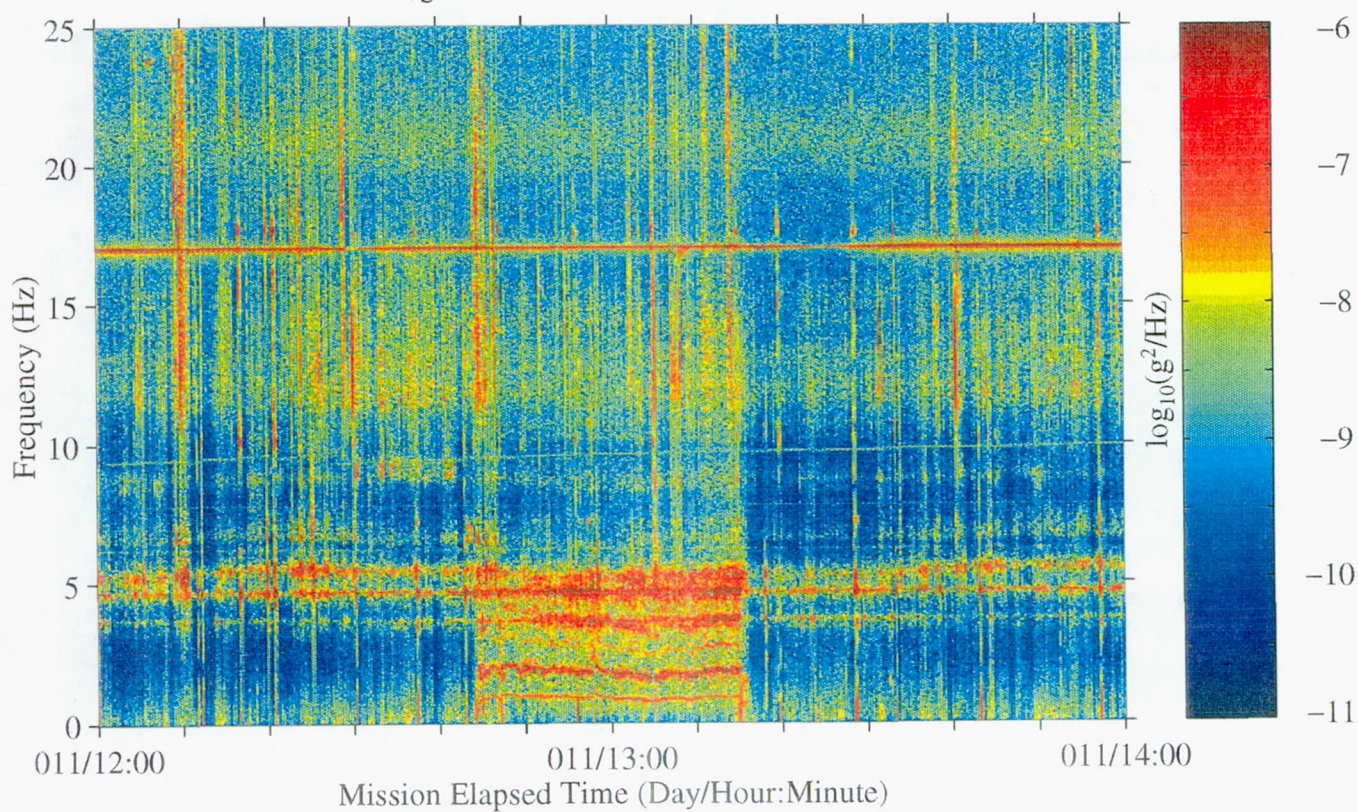




Figure 137: USML-2, Head C (fc=25 Hz)

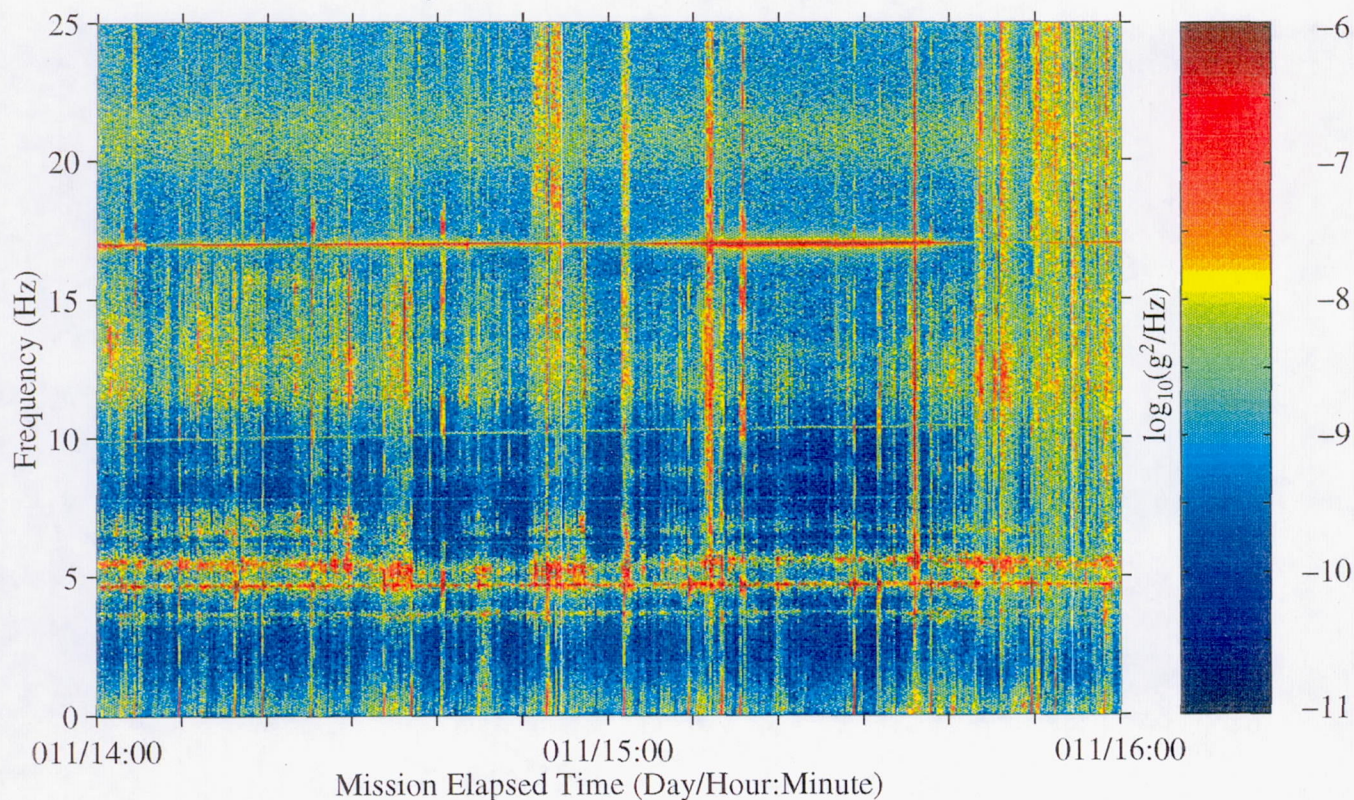


Figure 138: USML-2, Head C (fc=25 Hz)

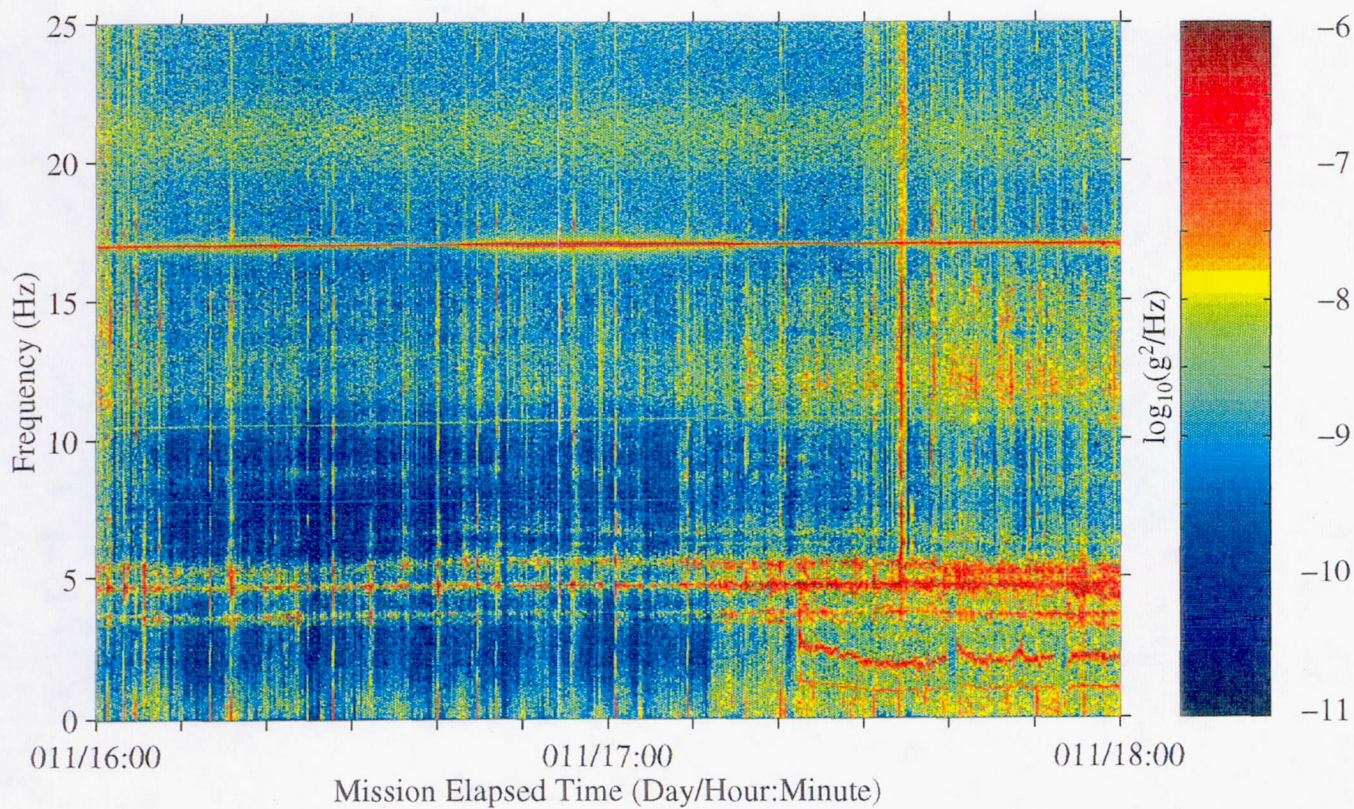




Figure 139: USML-2, Head C (fc=25 Hz)

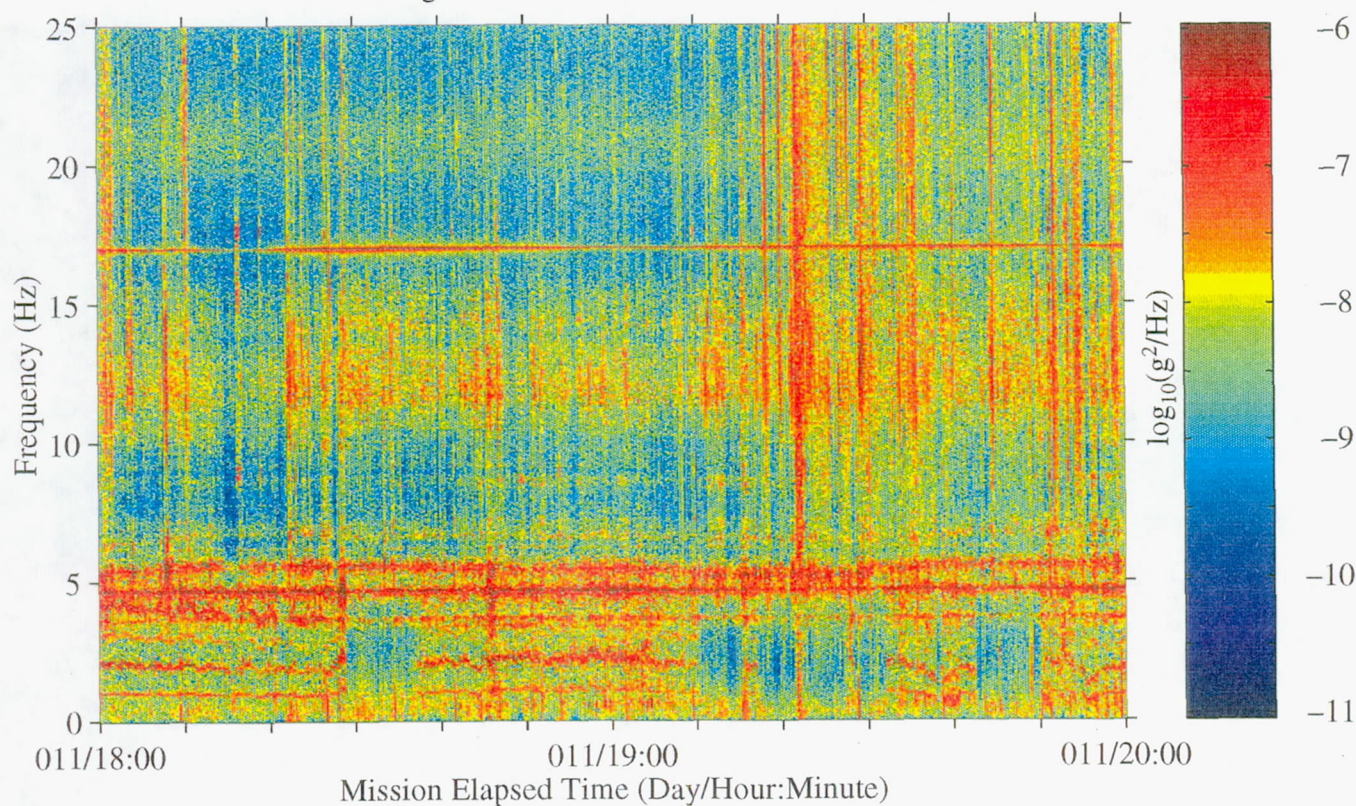


Figure 140: USML-2, Head C (fc=25 Hz)

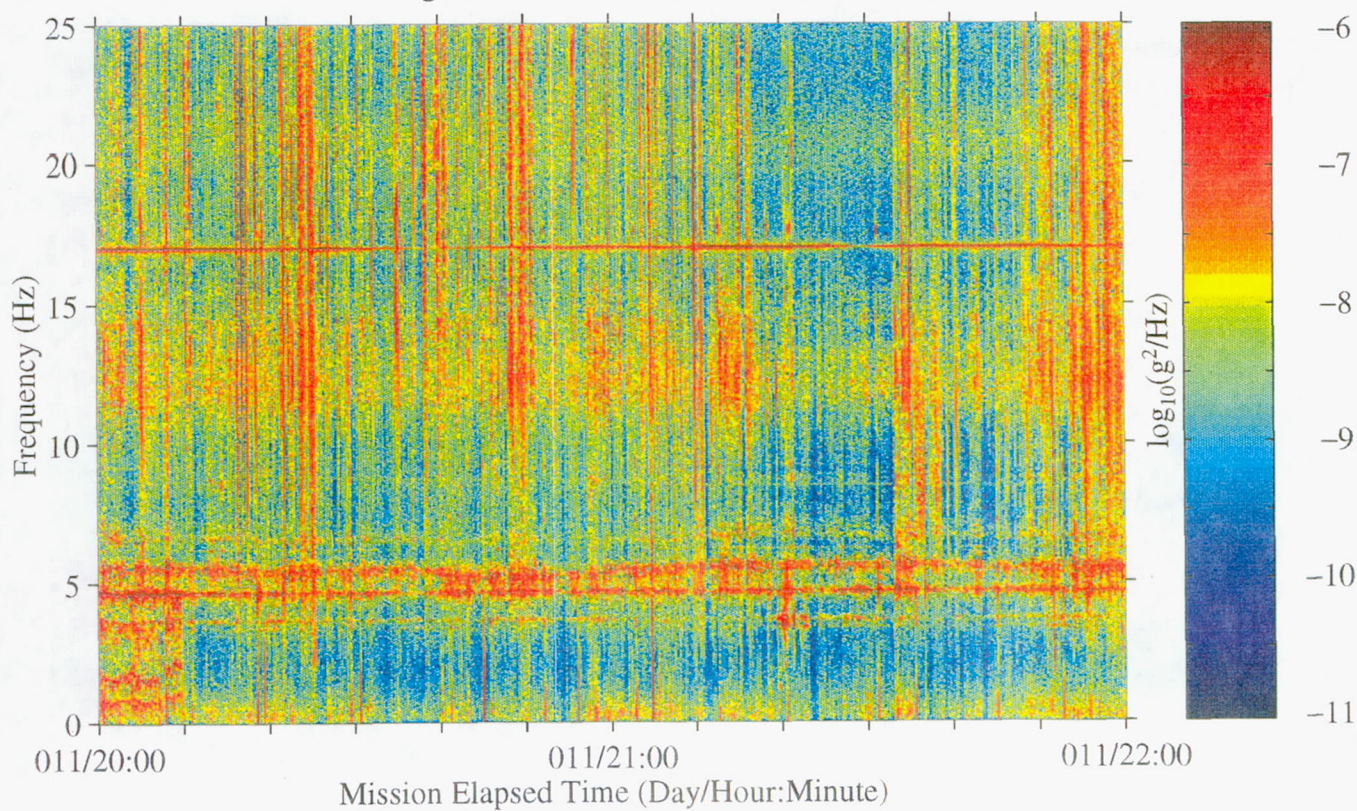




Figure 141: USML-2, Head C (fc=25 Hz)

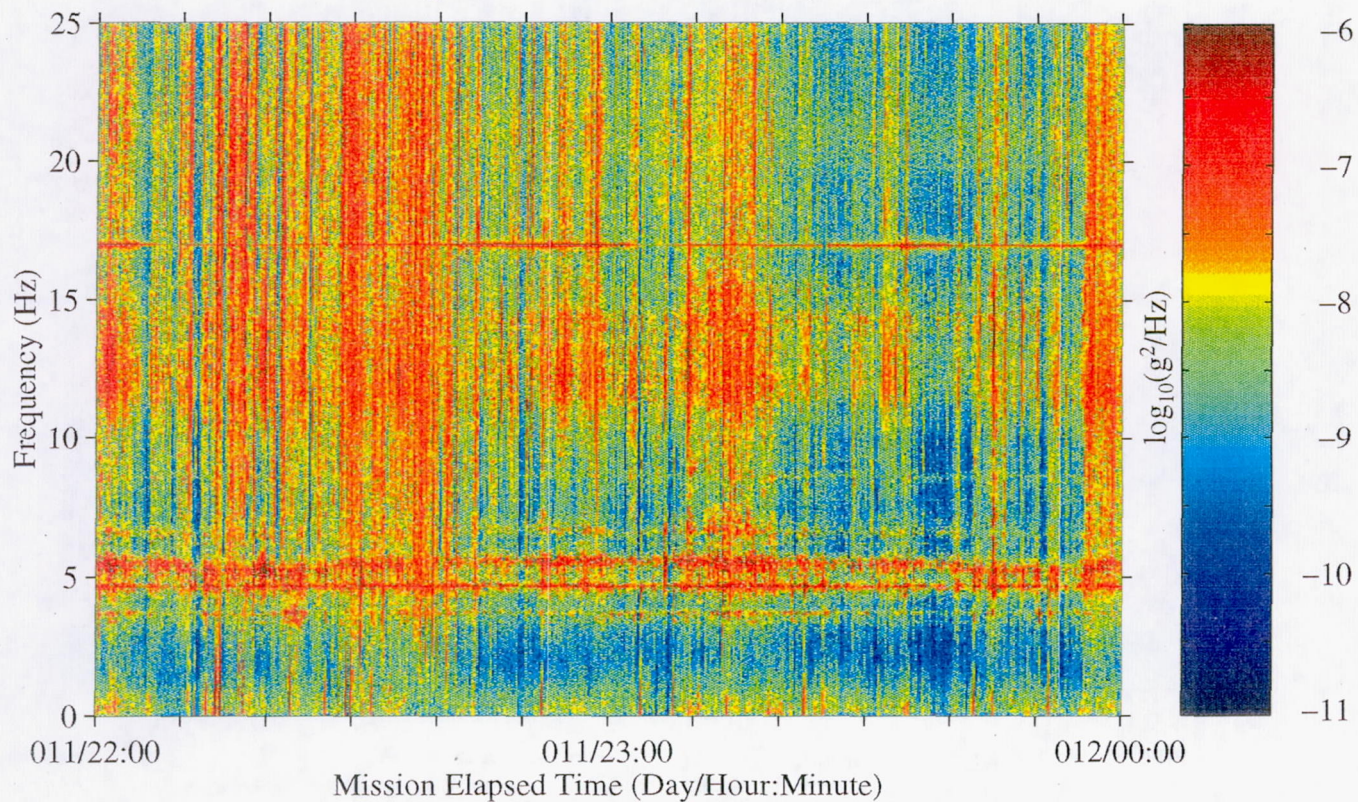


Figure 142: USML-2, Head C (fc=25 Hz)

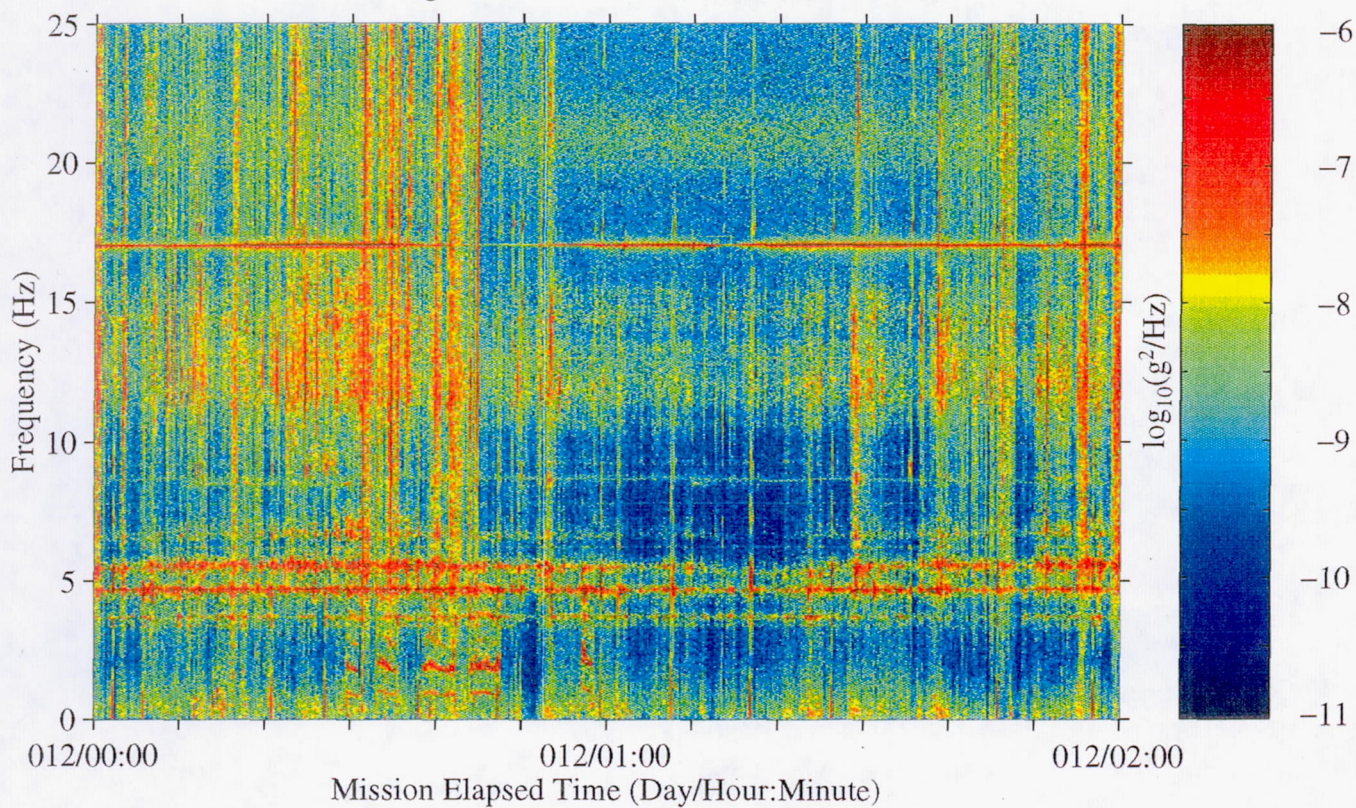




Figure 143: USML-2, Head C (fc=25 Hz)

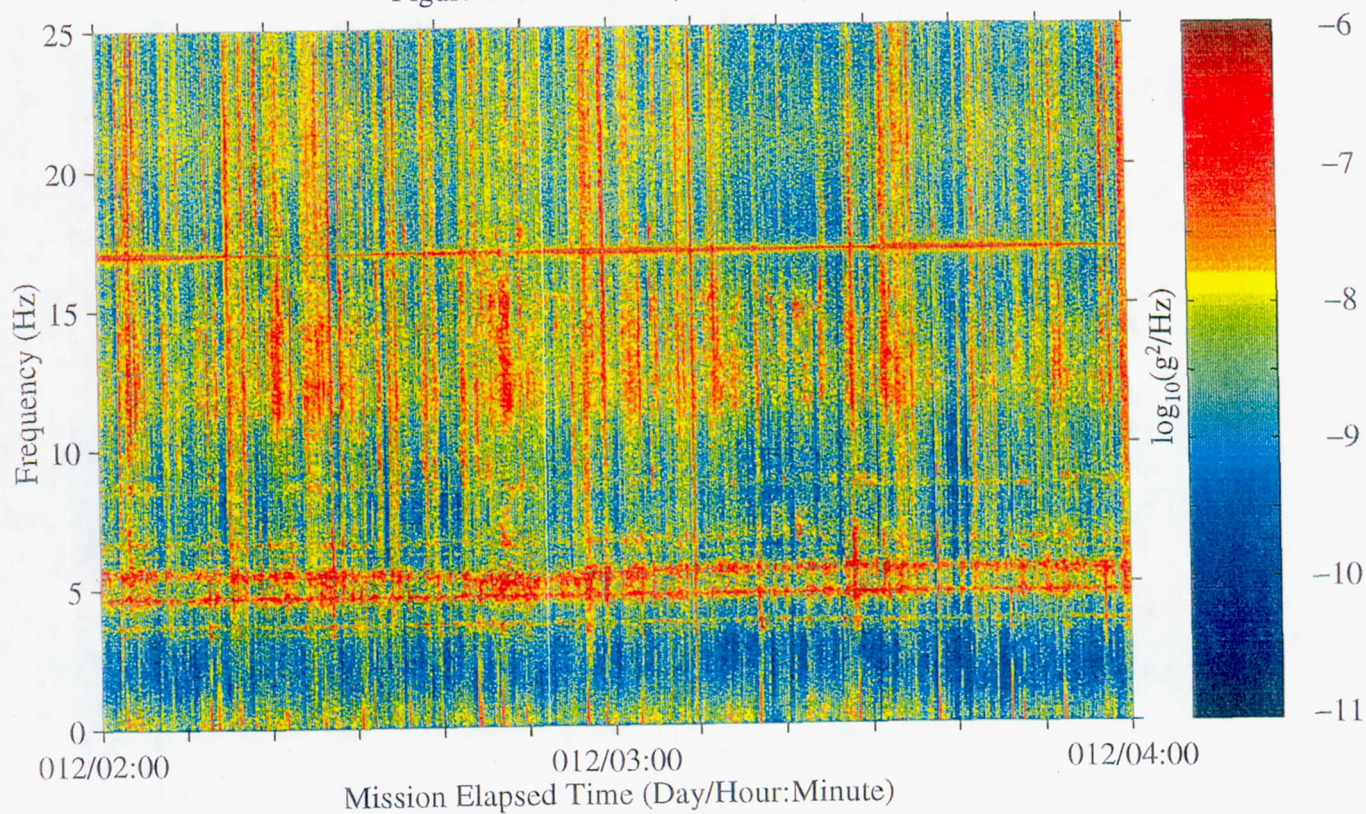


Figure 144: USML-2, Head C (fc=25 Hz)

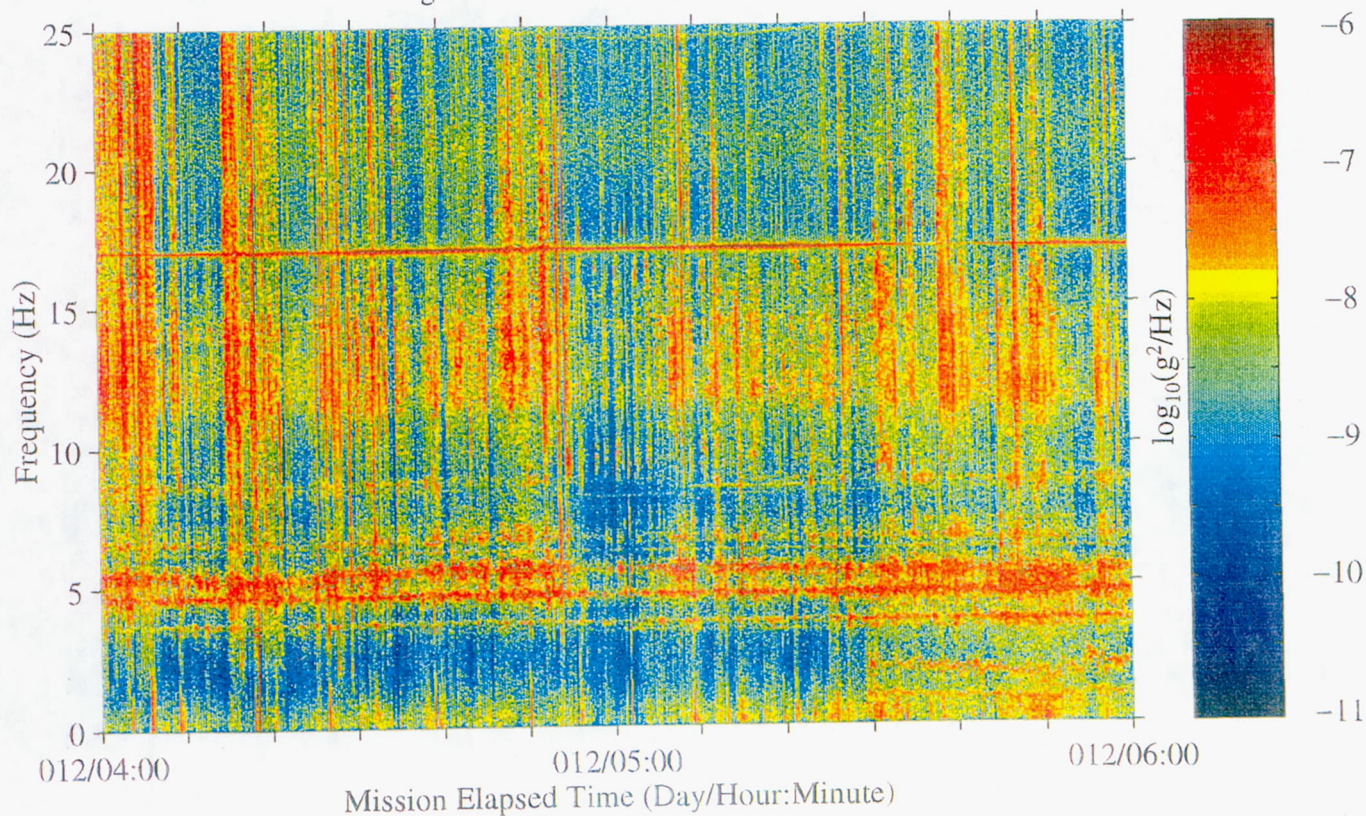




Figure 145: USML-2, Head C (fc=25 Hz)

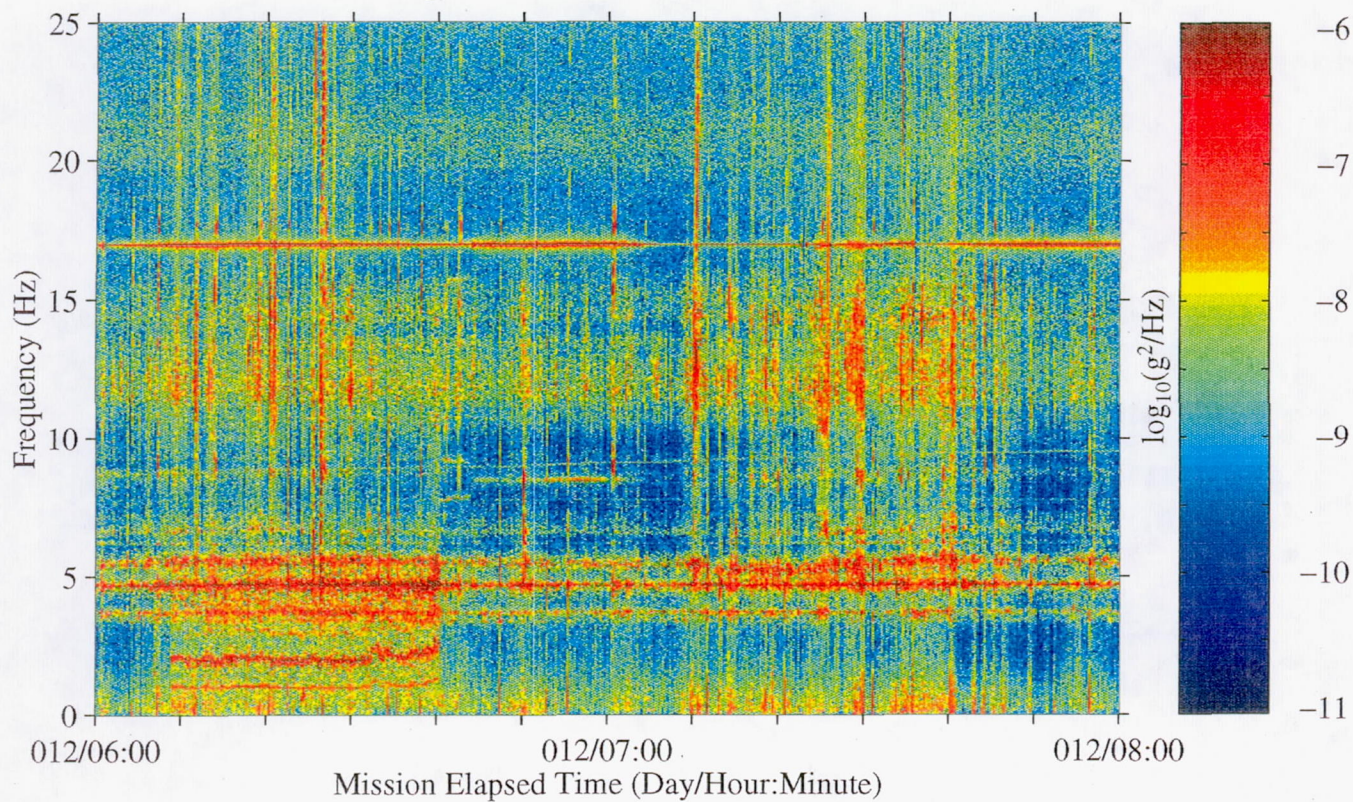


Figure 146: USML-2, Head C (fc=25 Hz)

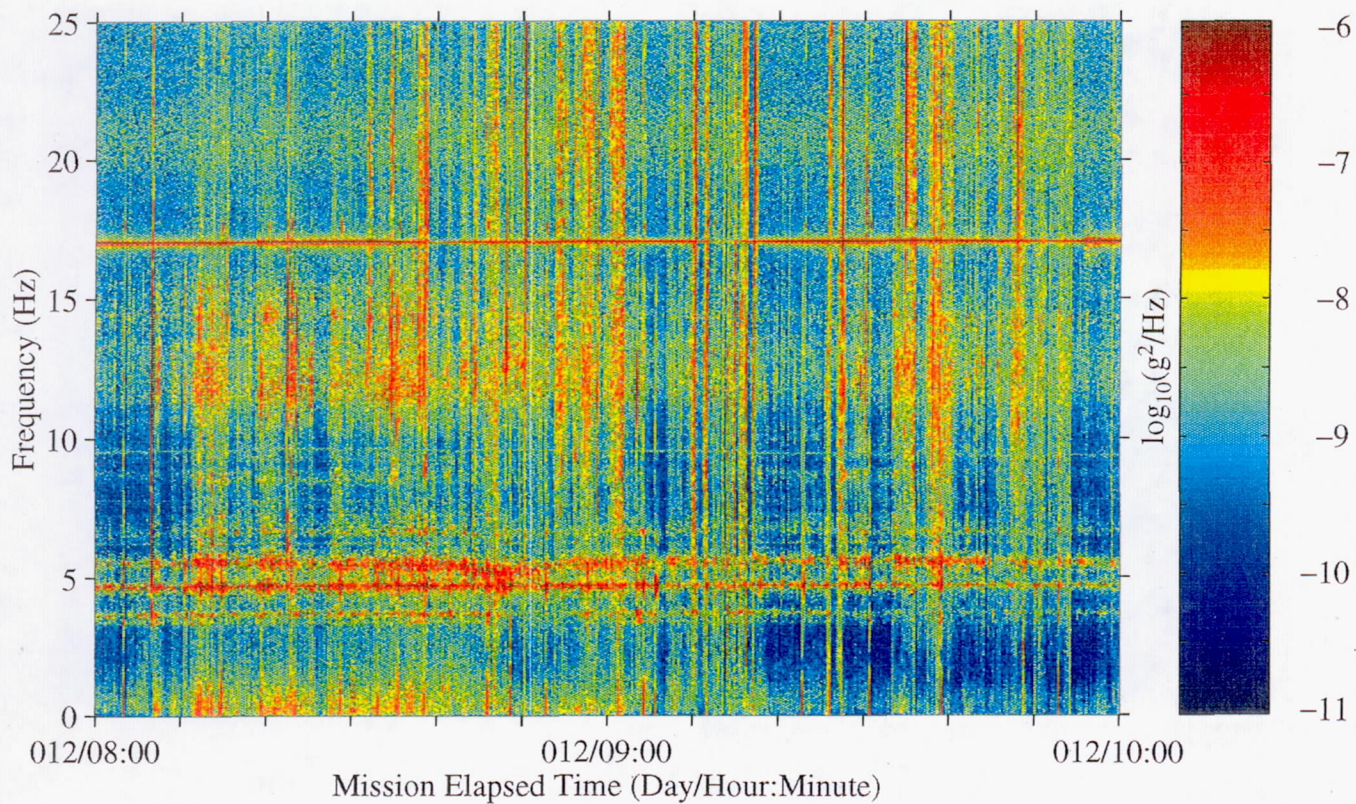




Figure 147: USML-2, Head C (fc=25 Hz)

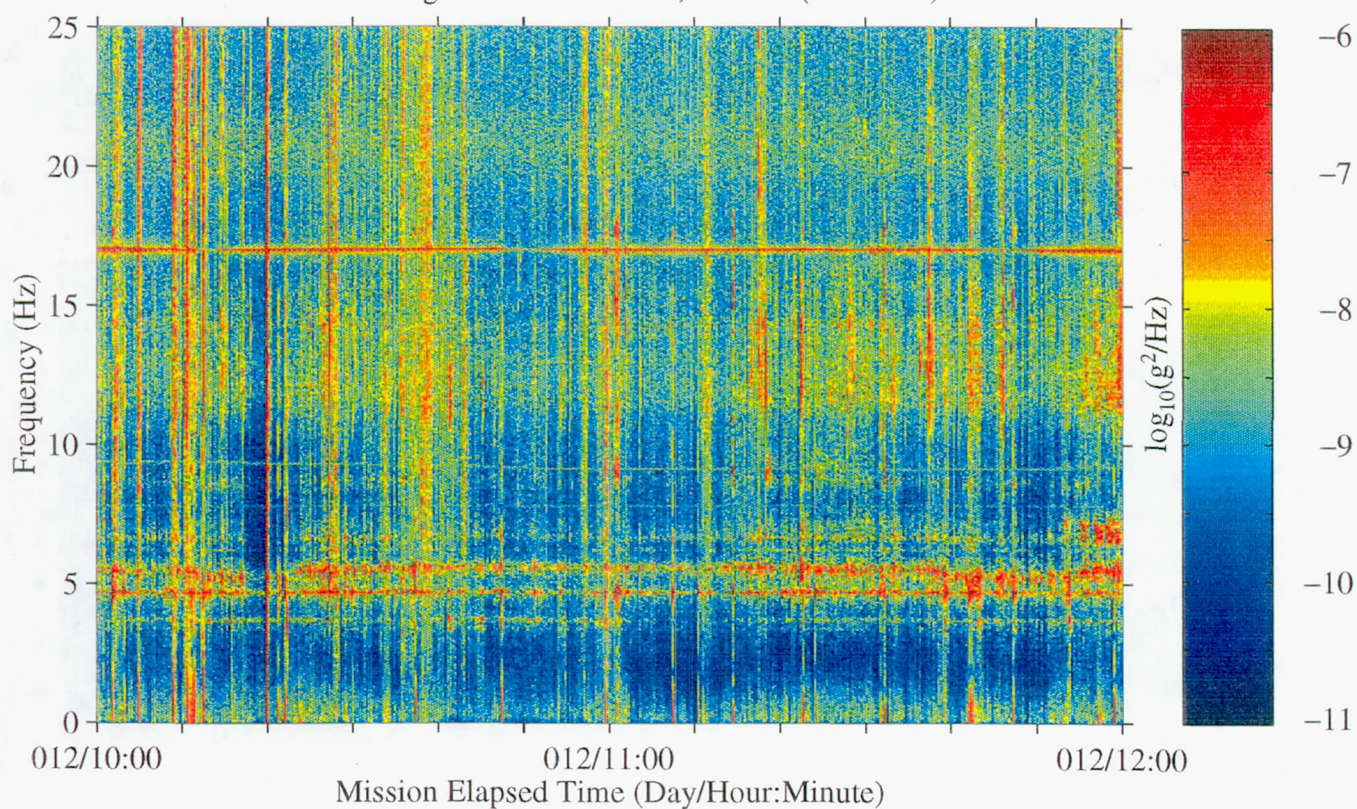


Figure 148: USML-2, Head C (fc=25 Hz)

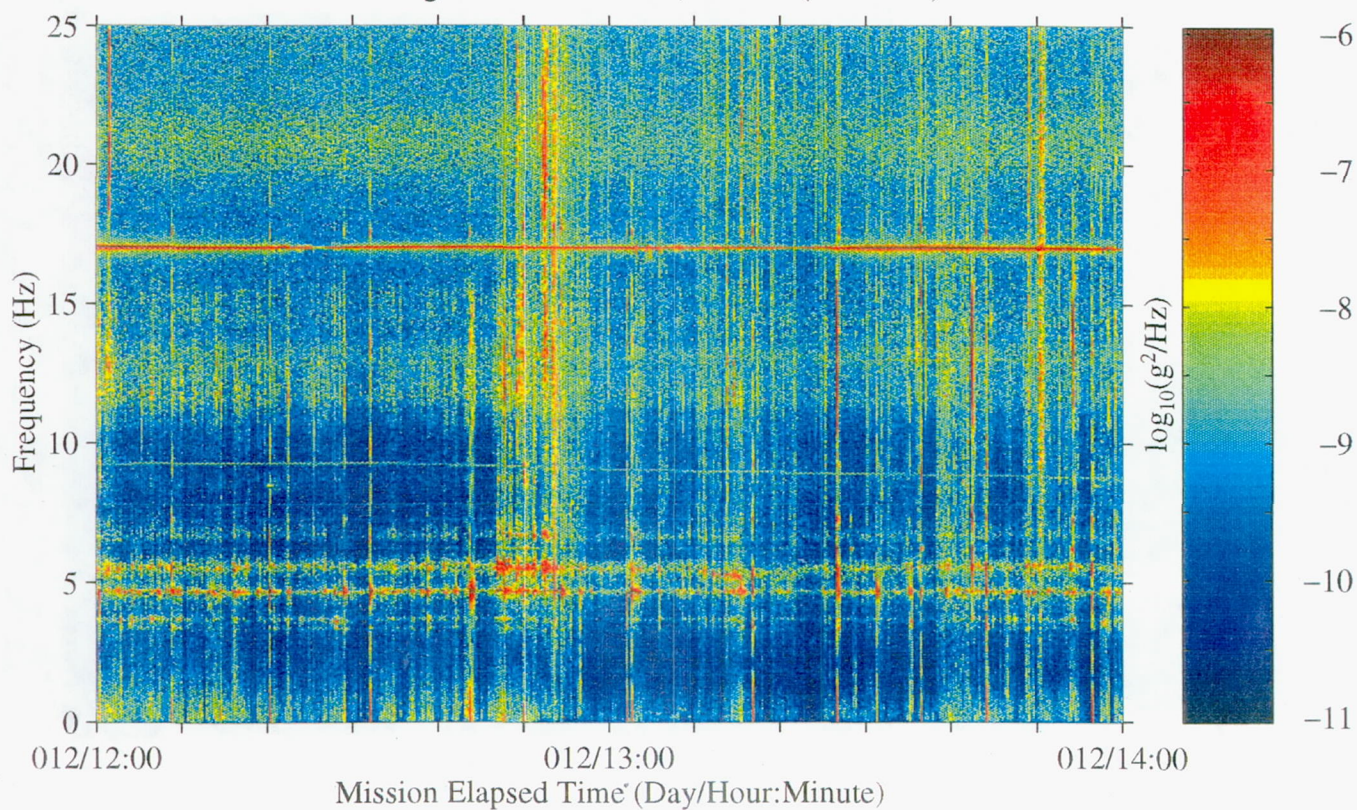




Figure 149: USML-2, Head C (fc=25 Hz)

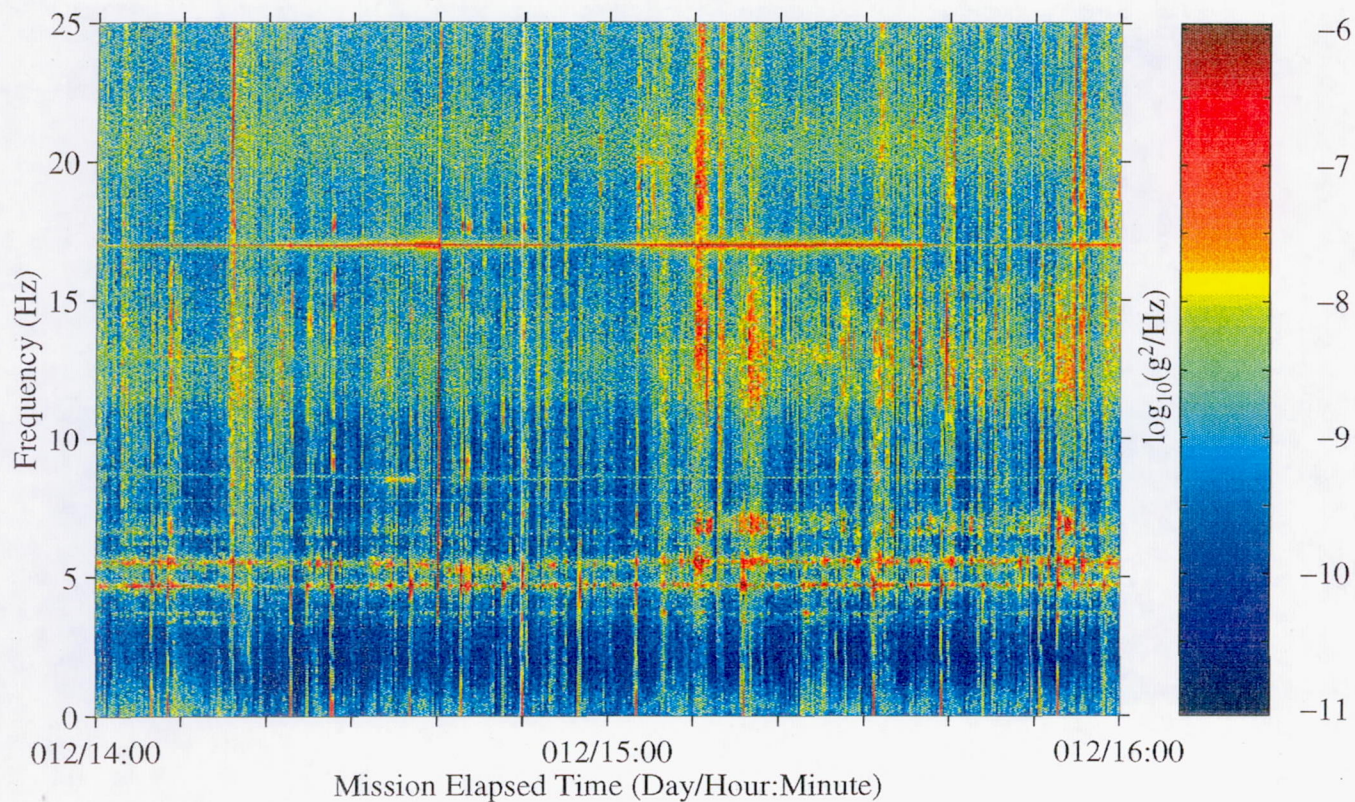


Figure 150: USML-2, Head C (fc=25 Hz)

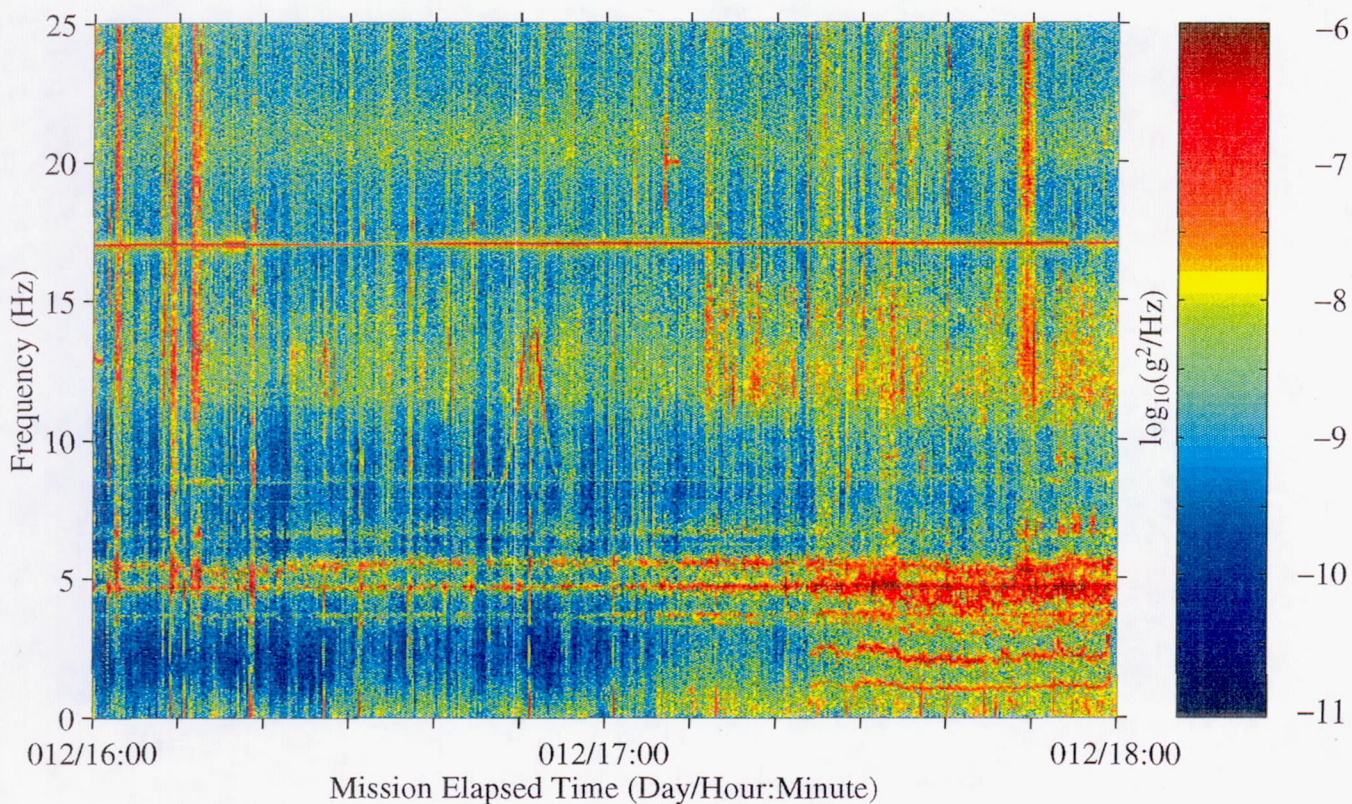




Figure 151: USML-2, Head C (fc=25 Hz)

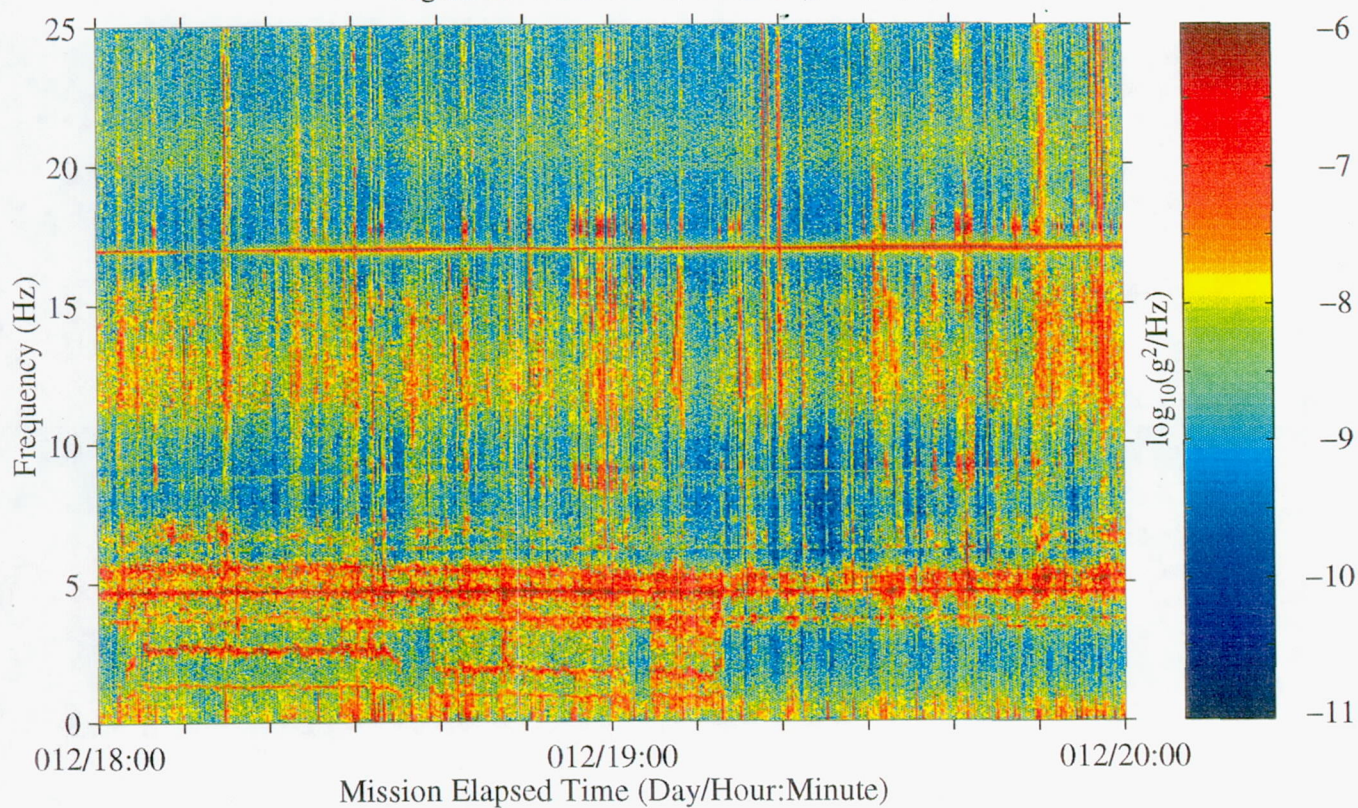


Figure 152: USML-2, Head C (fc=25 Hz)

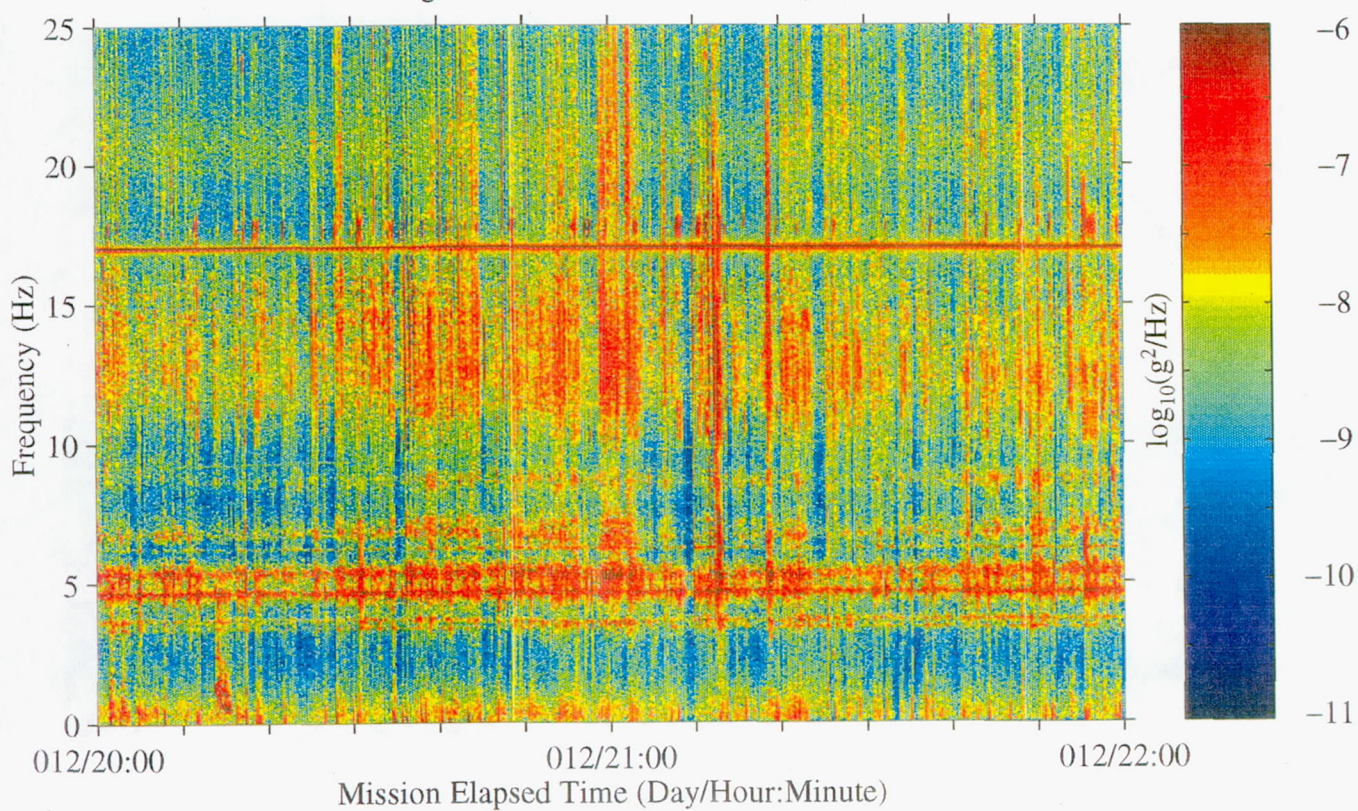




Figure 153: USML-2, Head C (fc=25 Hz)

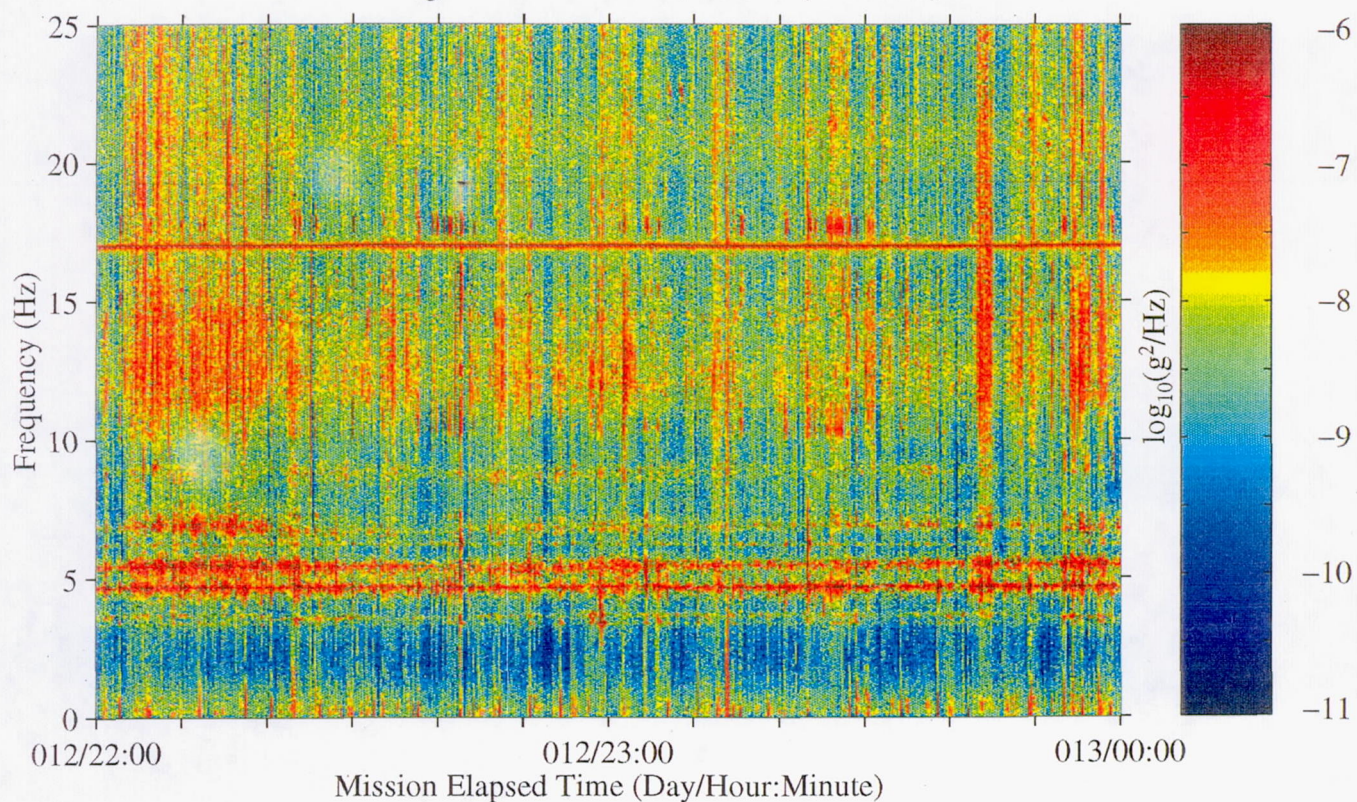


Figure 154: USML-2, Head C (fc=25 Hz)

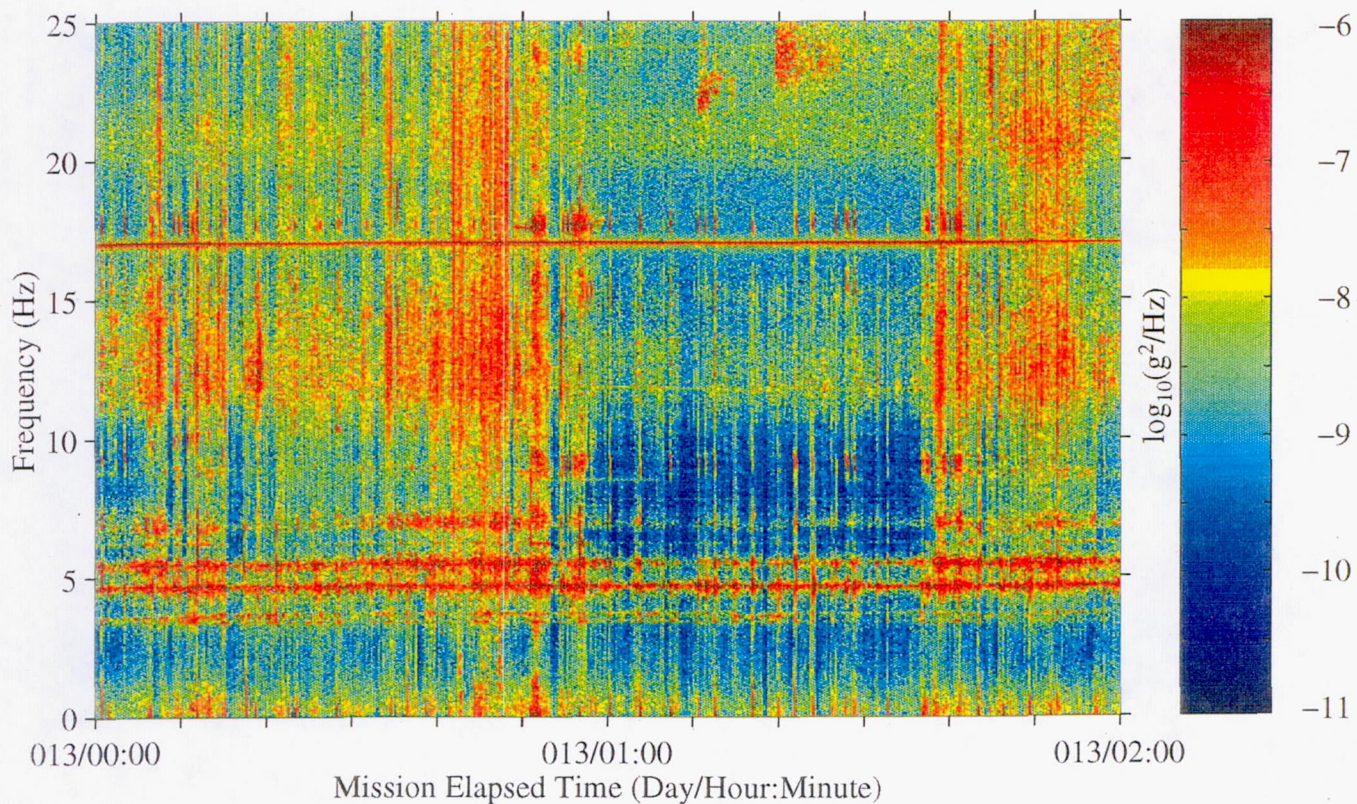




Figure 155: USML-2, Head C (fc=25 Hz)

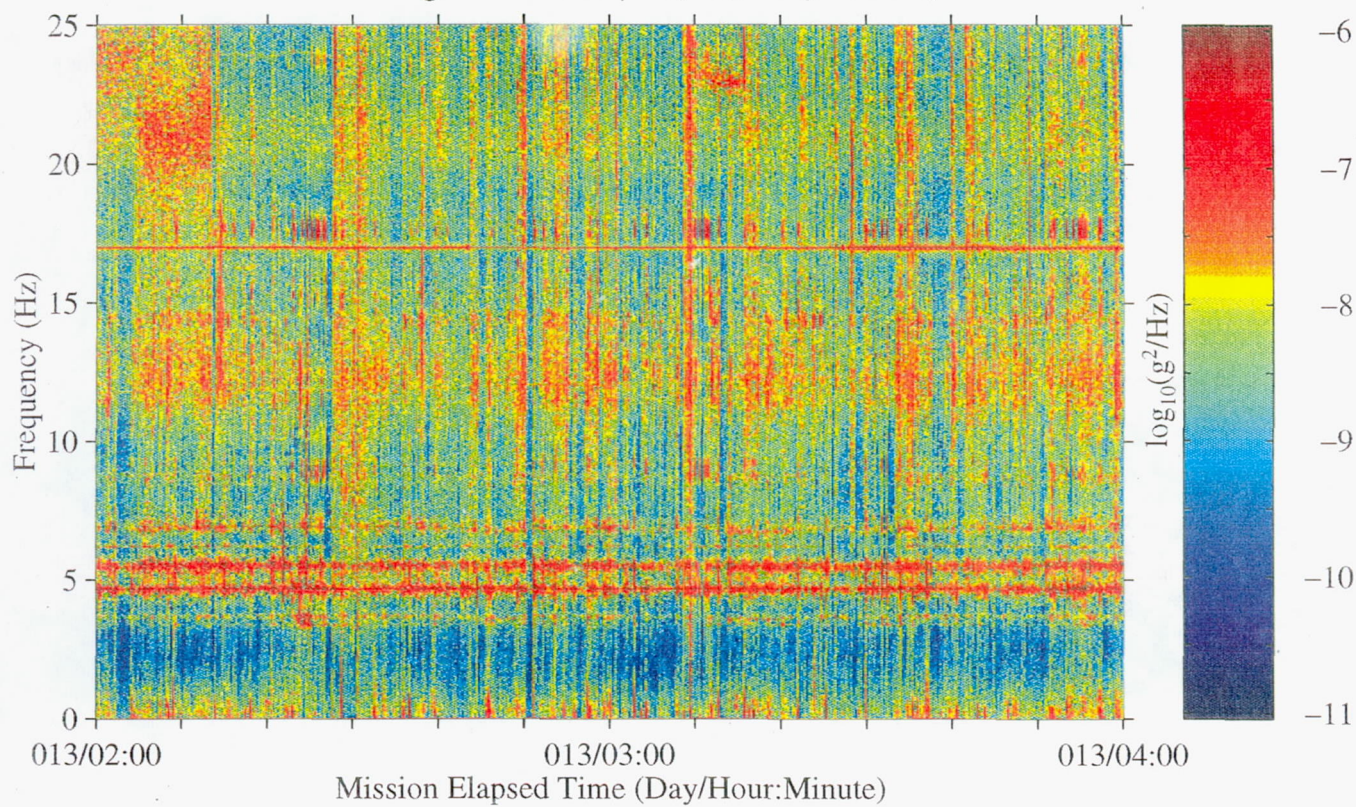


Figure 156: USML-2, Head C (fc=25 Hz)

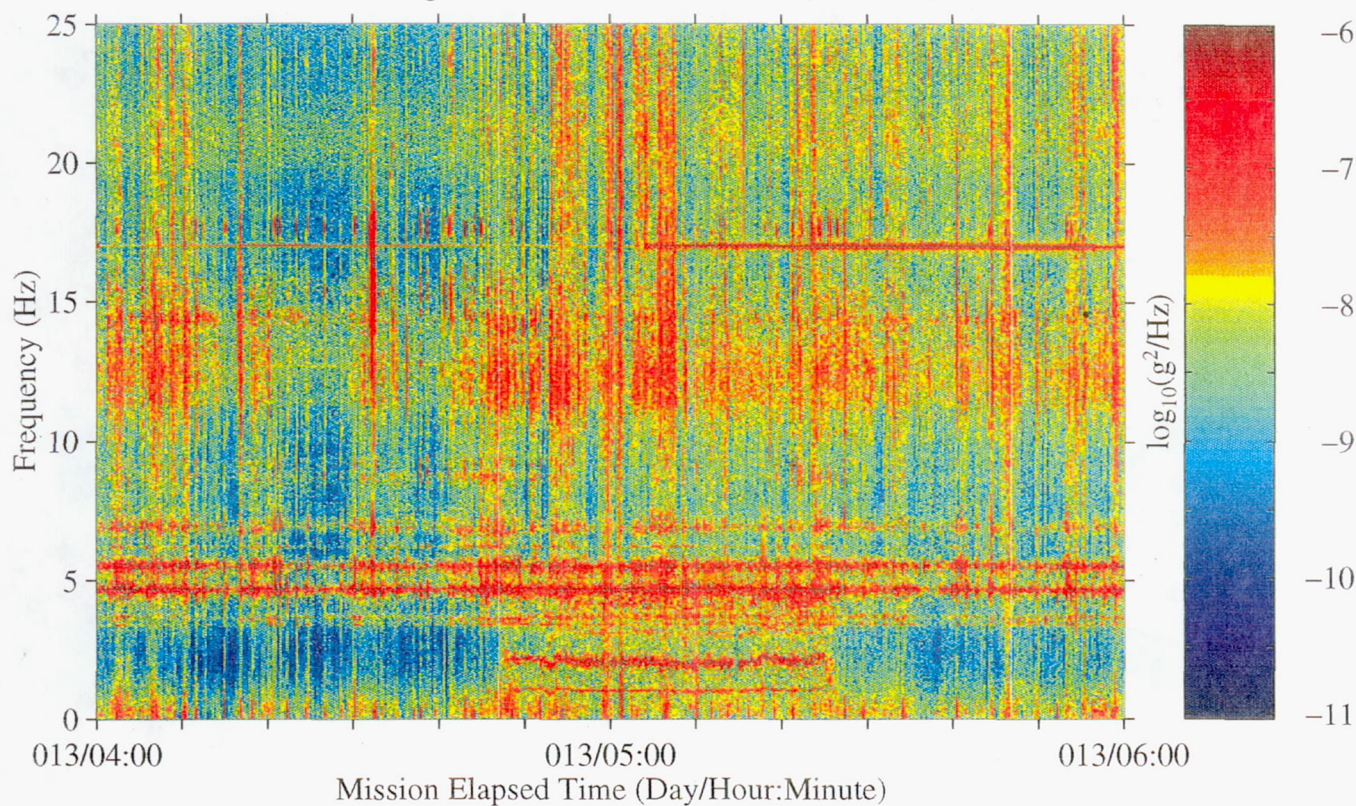




Figure 157: USML-2, Head C (fc=25 Hz)

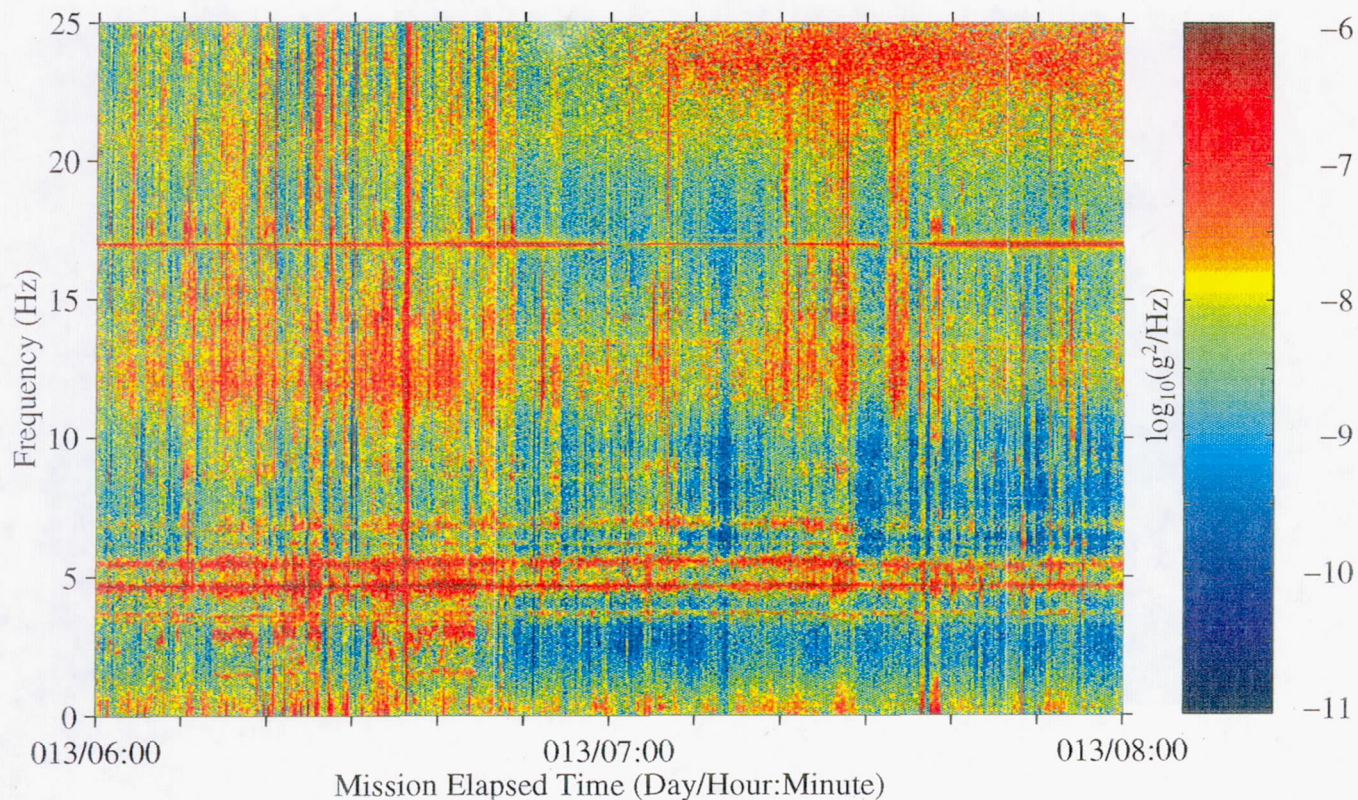


Figure 158: USML-2, Head C (fc=25 Hz)

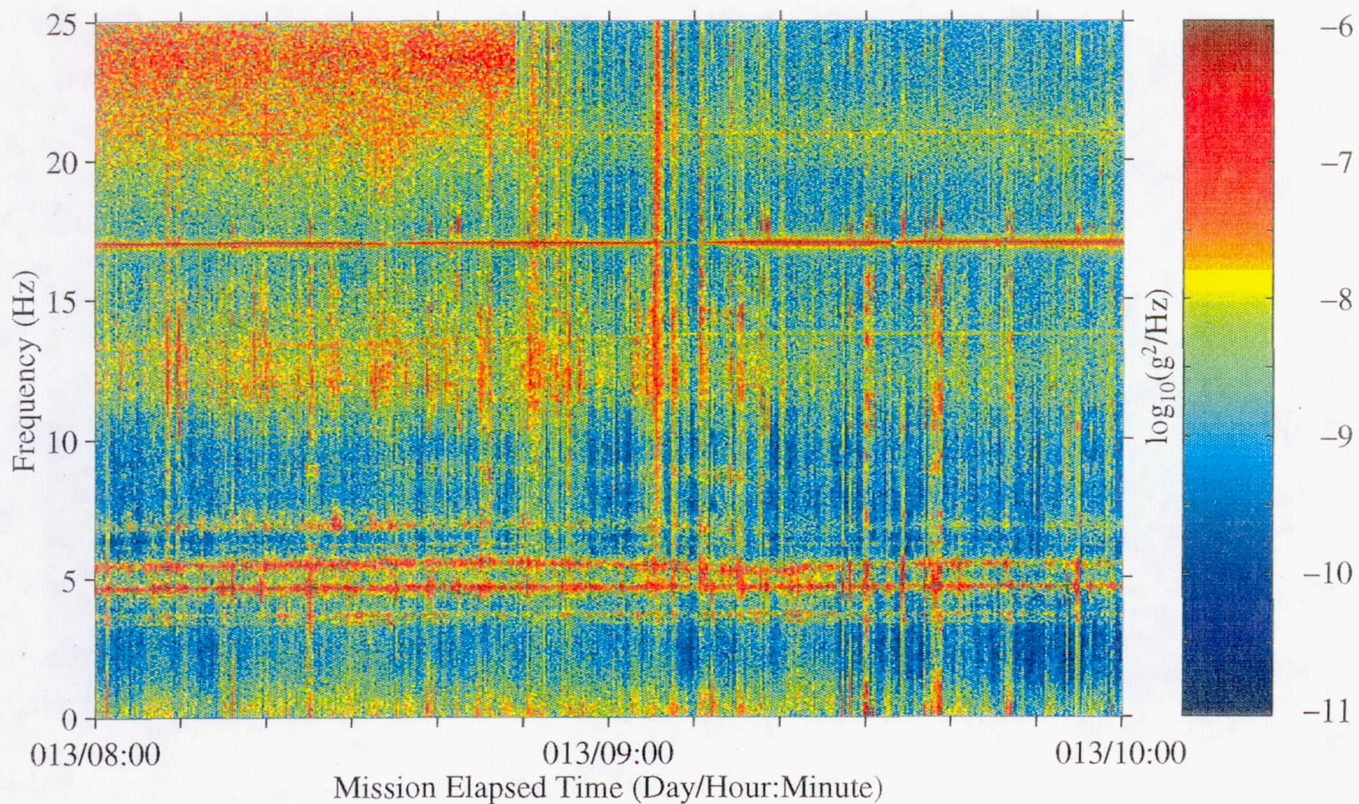




Figure 159: USML-2, Head C (fc=25 Hz)

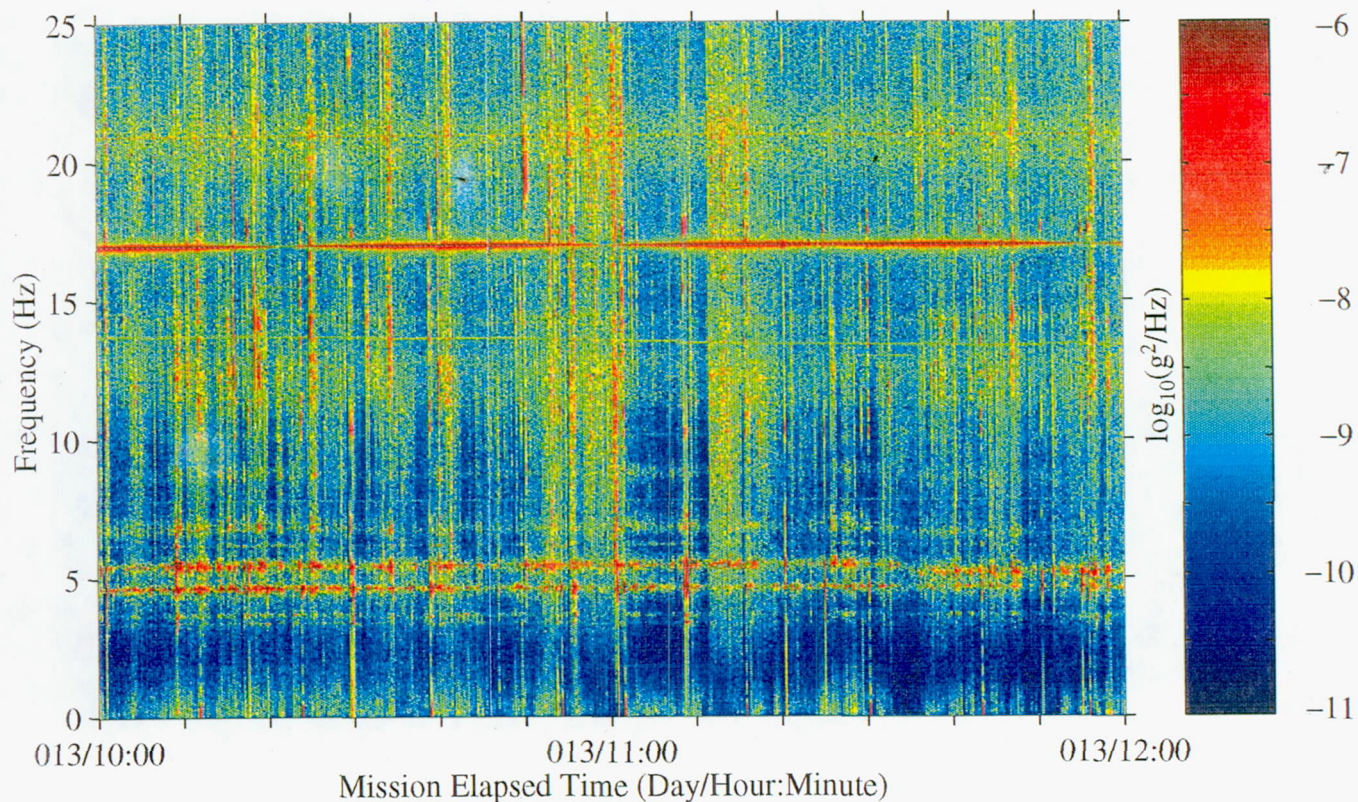


Figure 160: USML-2, Head C (fc=25 Hz)

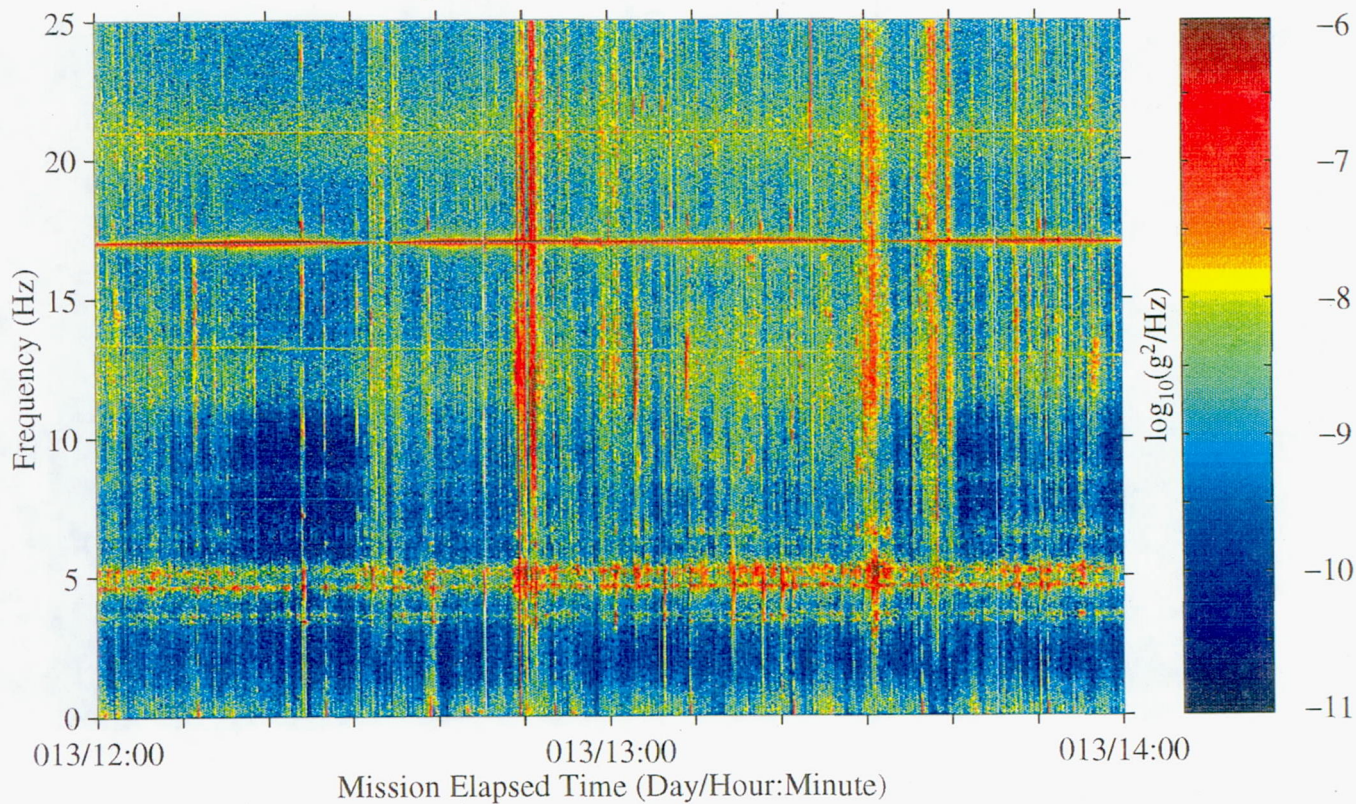




Figure 161: USML-2, Head C (fc=25 Hz)

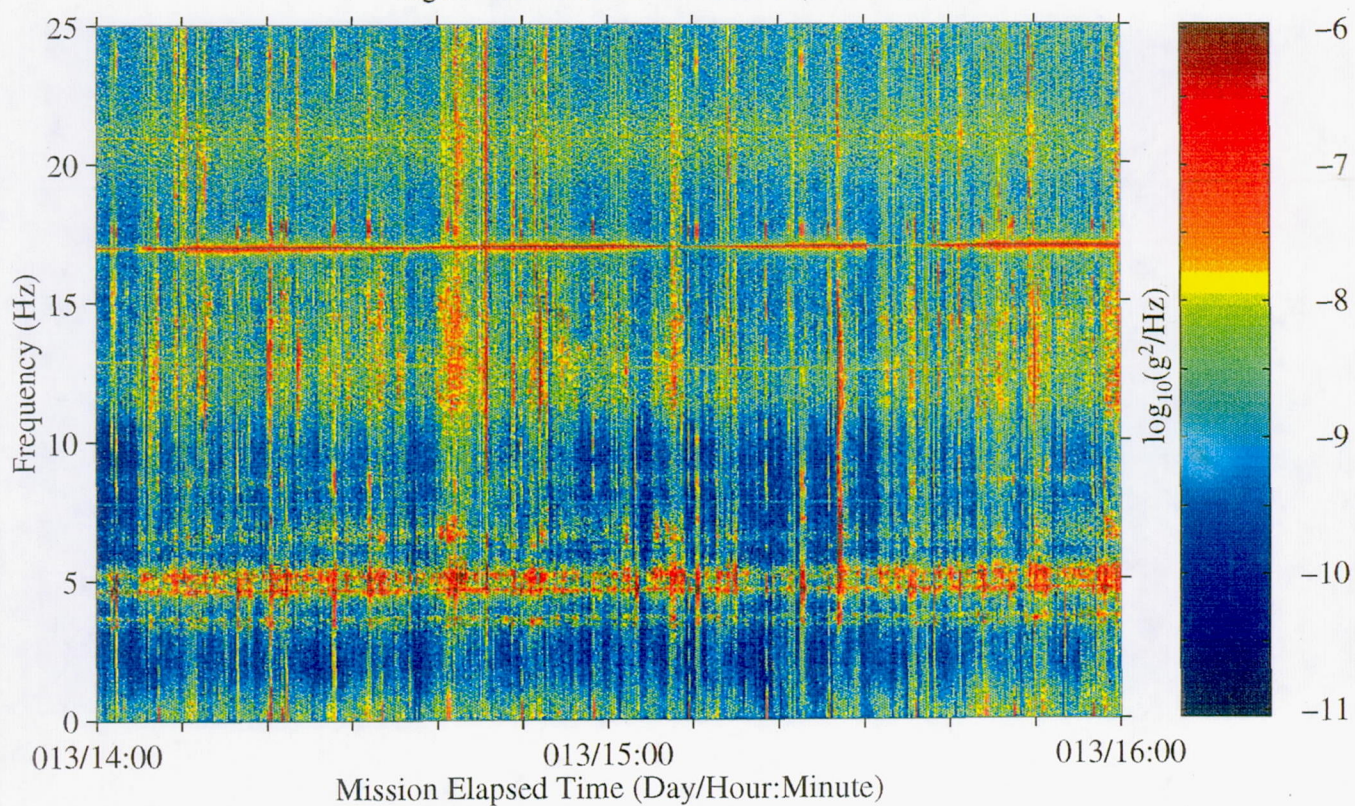


Figure 162: USML-2, Head C (fc=25 Hz)

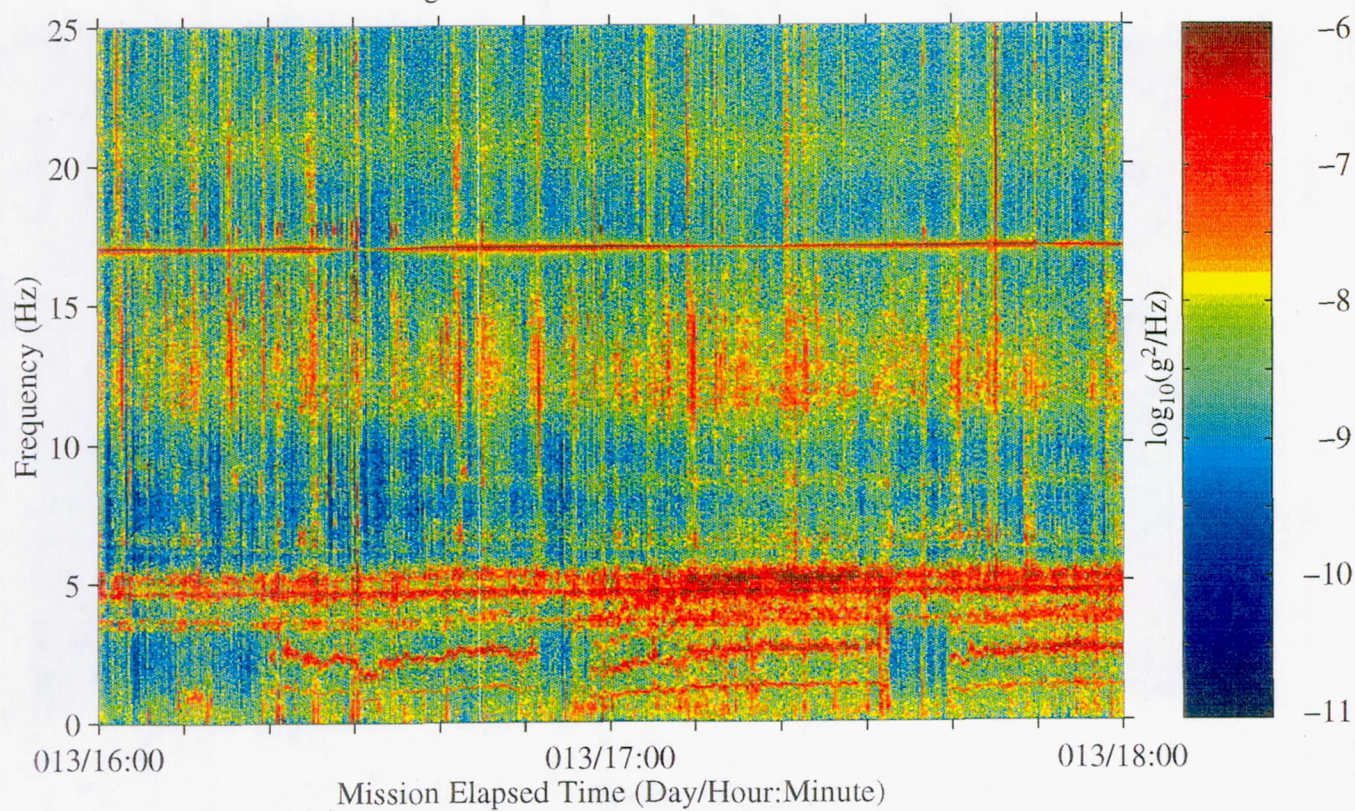




Figure 163: USML-2, Head C (fc=25 Hz)

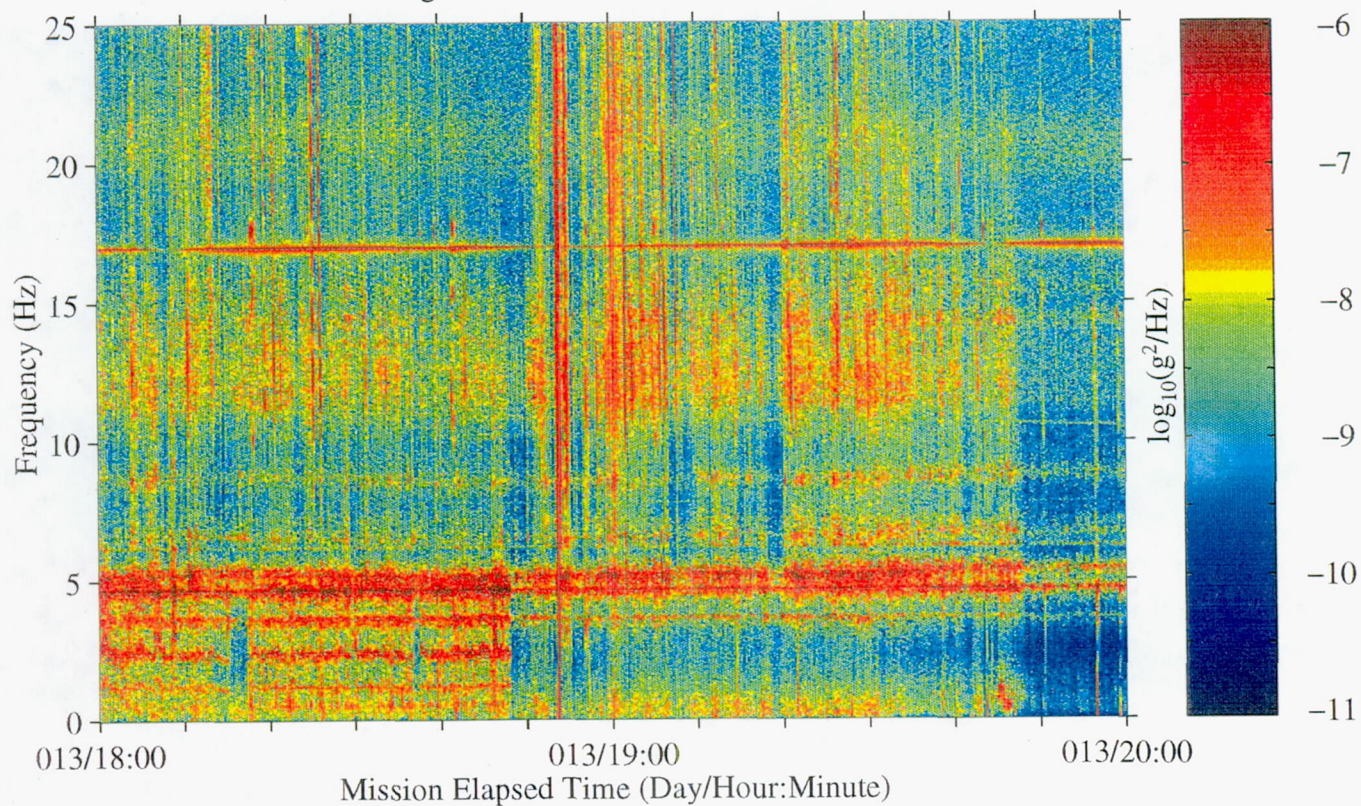


Figure 164: USML-2, Head C (fc=25 Hz)

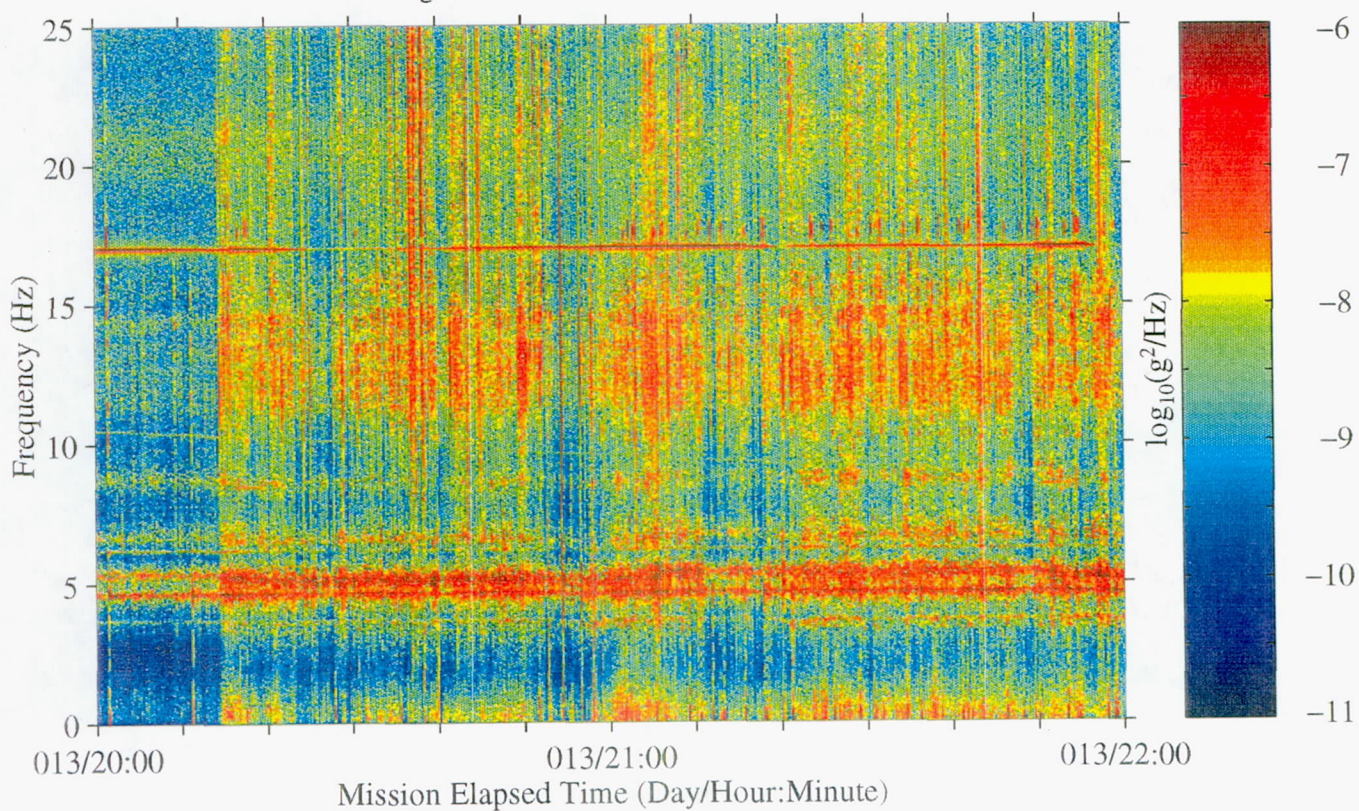




Figure 165: USML-2, Head C (fc=25 Hz)

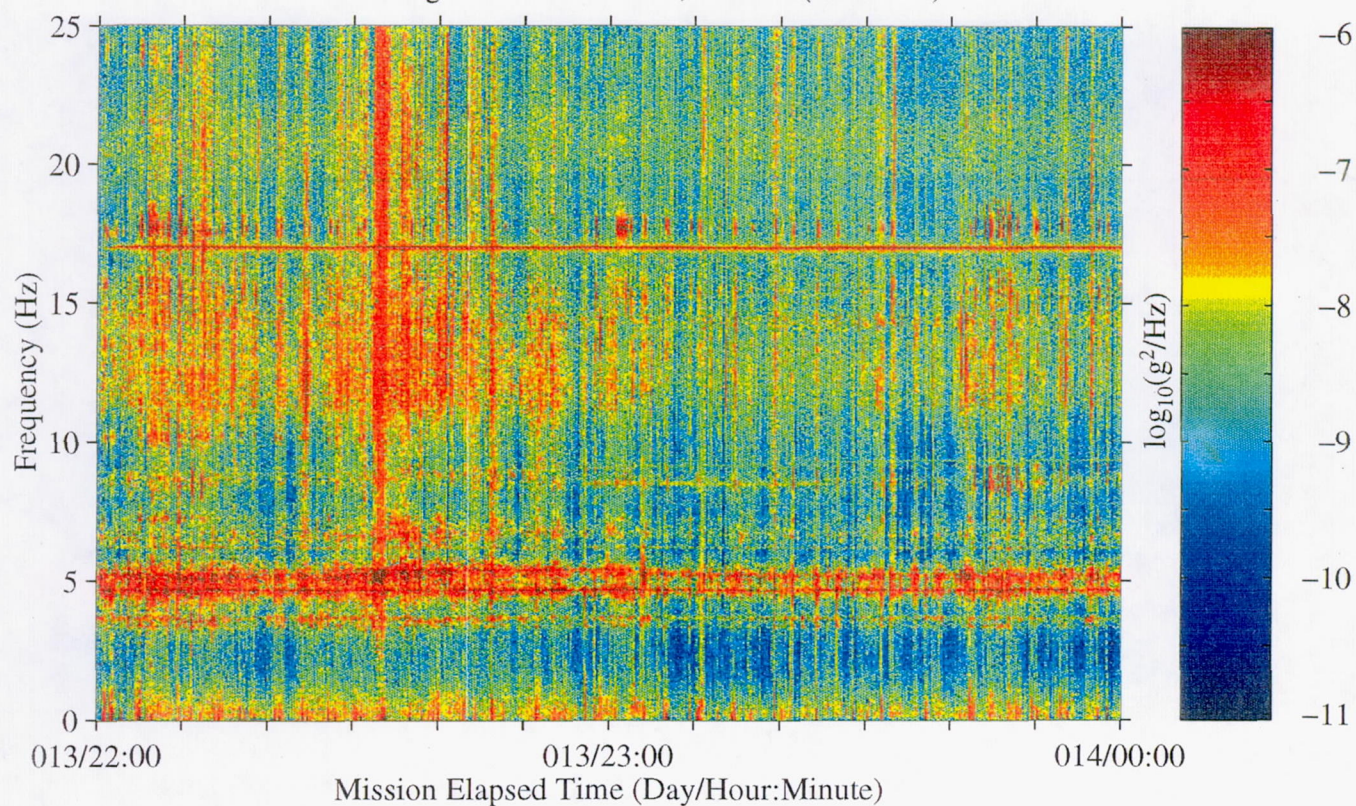


Figure 166: USML-2, Head C (fc=25 Hz)

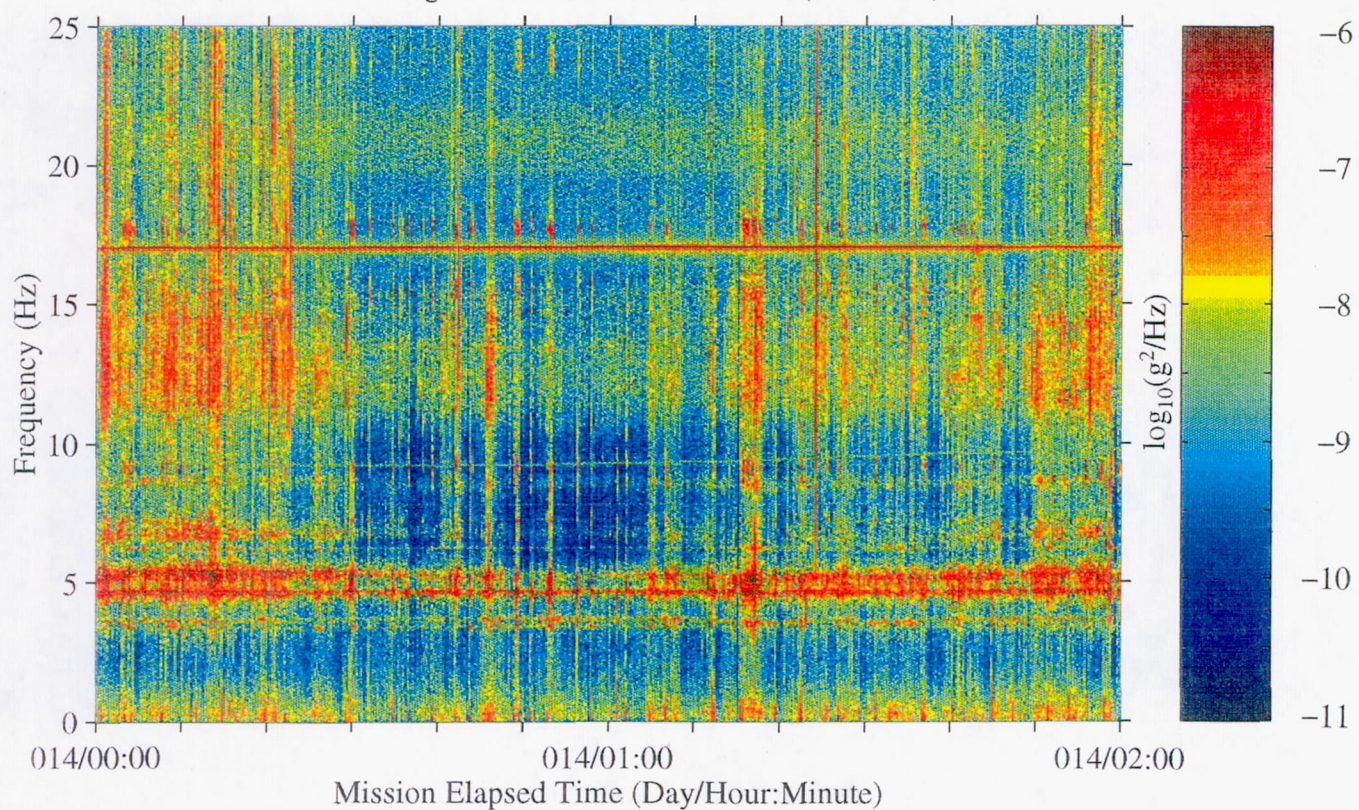




Figure 167: USML-2, Head C (fc=25 Hz)

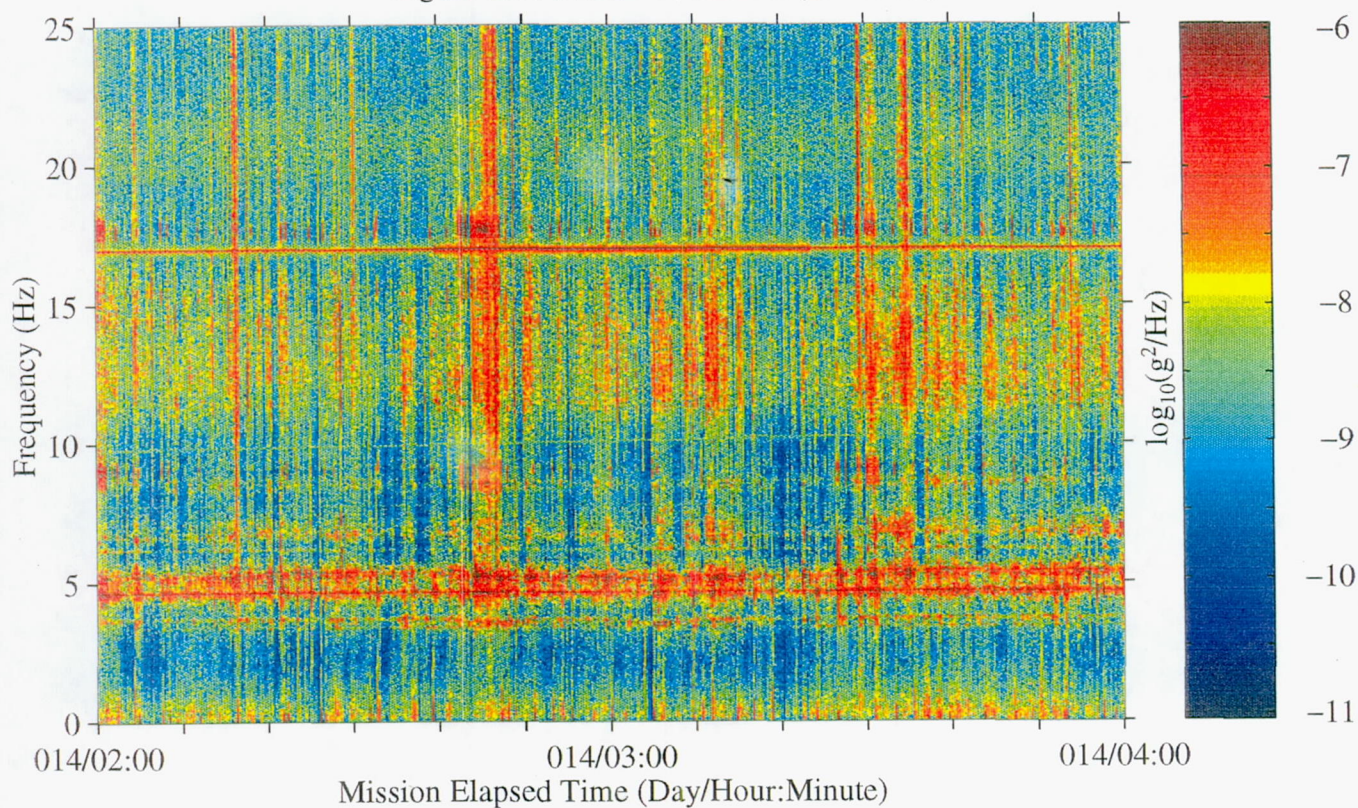


Figure 168: USML-2, Head C (fc=25 Hz)

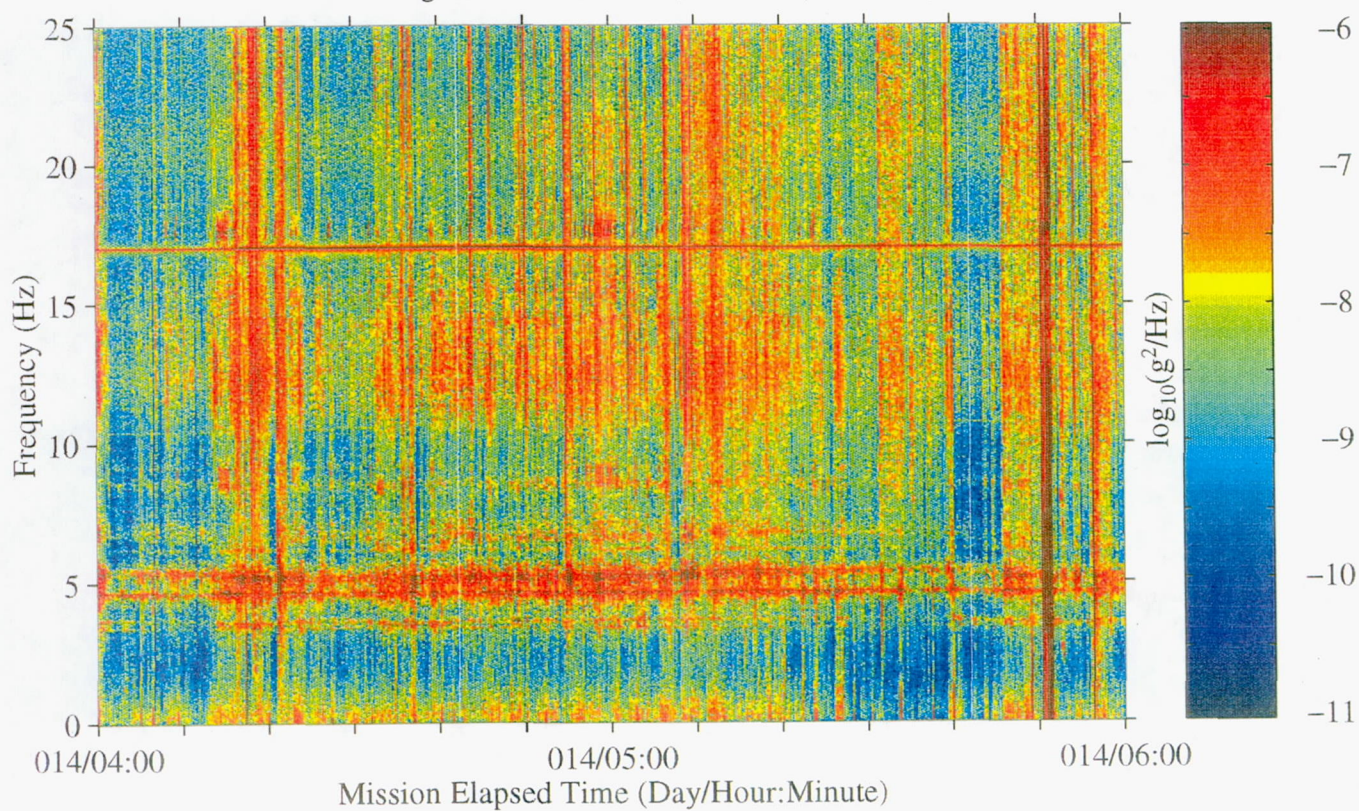




Figure 169: USML-2, Head C (fc=25 Hz)

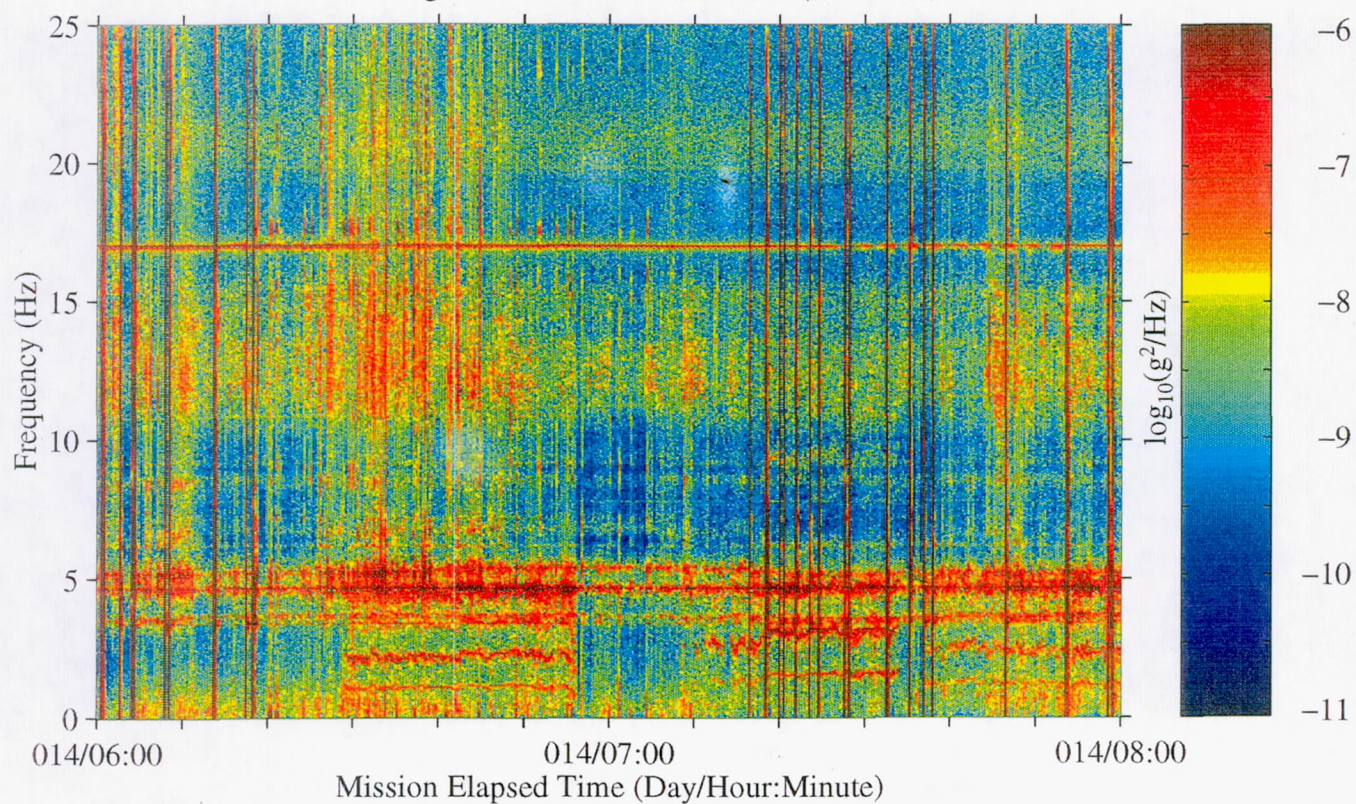


Figure 170: USML-2, Head C (fc=25 Hz)

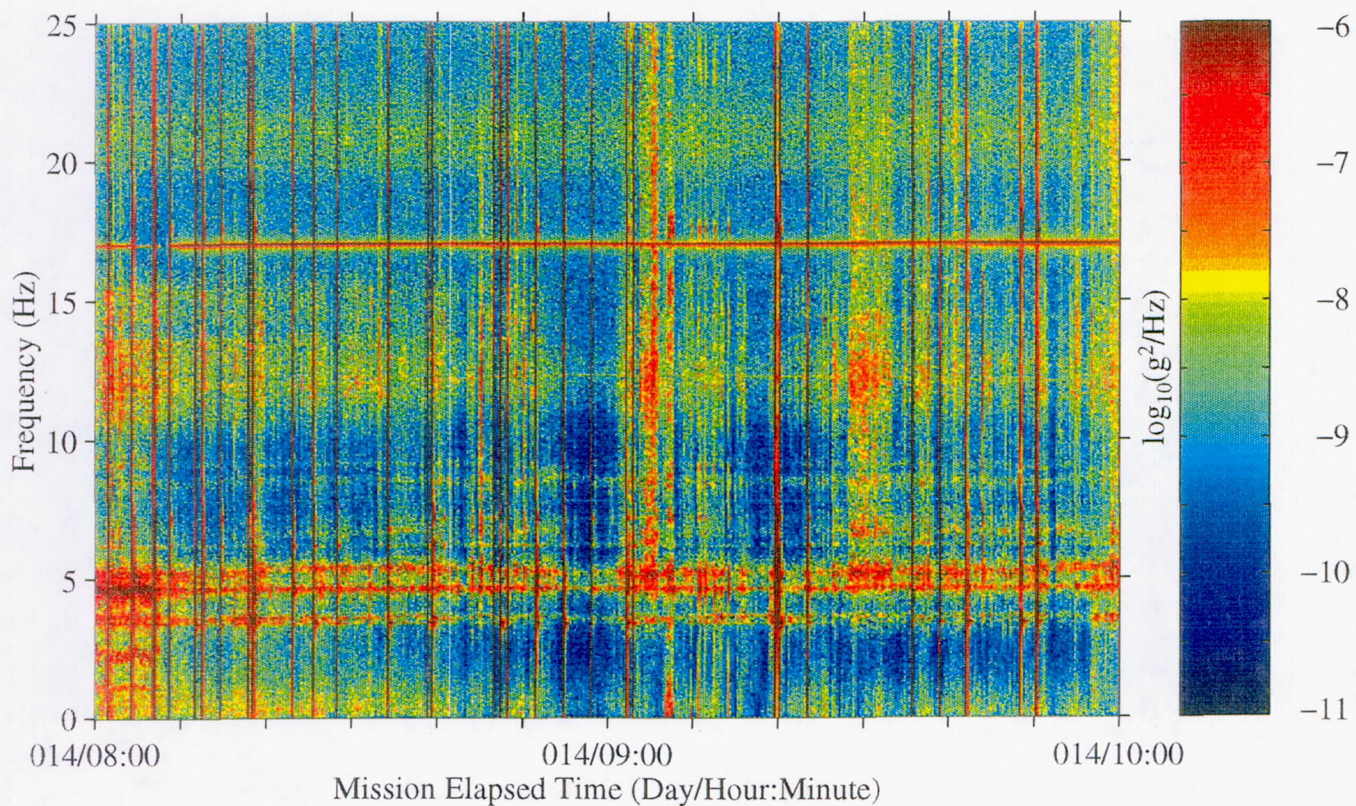




Figure 171: USML-2, Head C (fc=25 Hz)

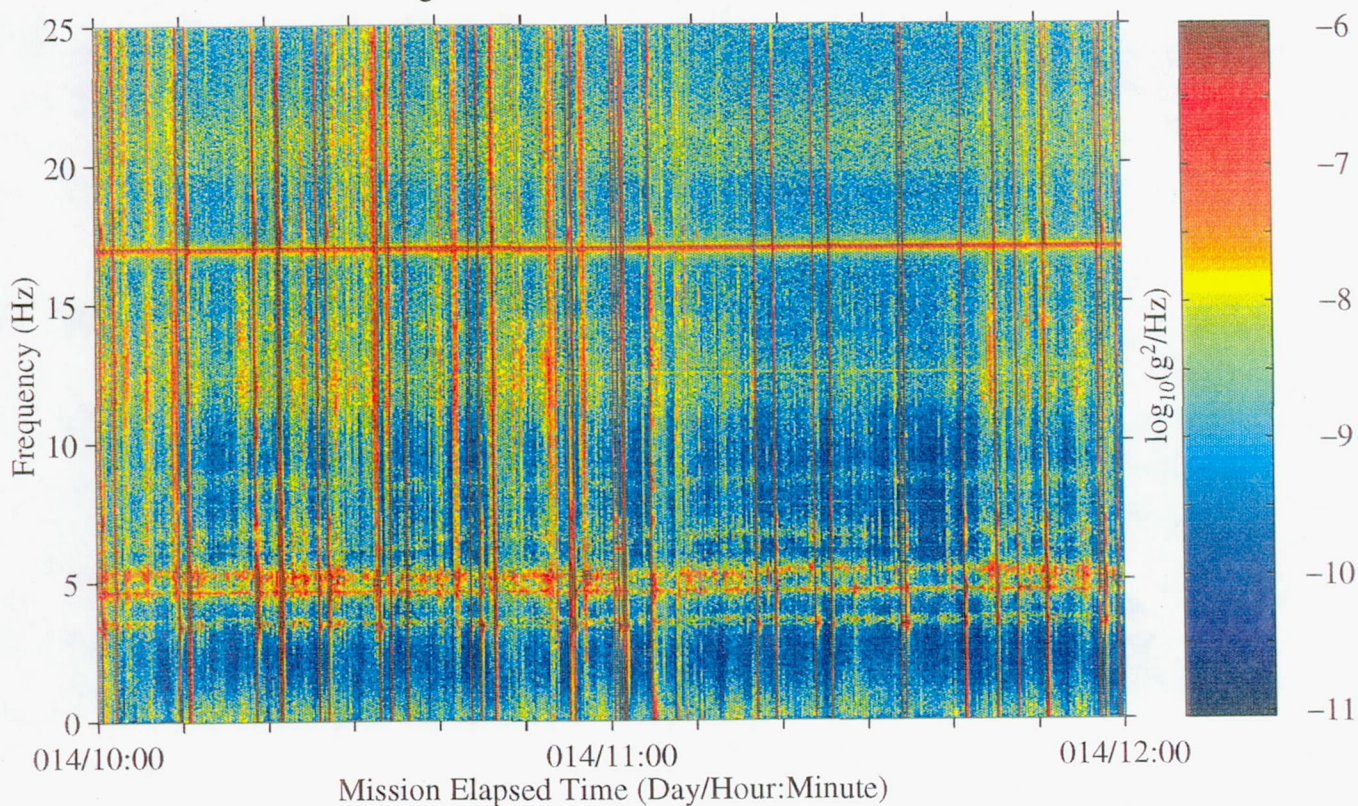


Figure 172: USML-2, Head C (fc=25 Hz)

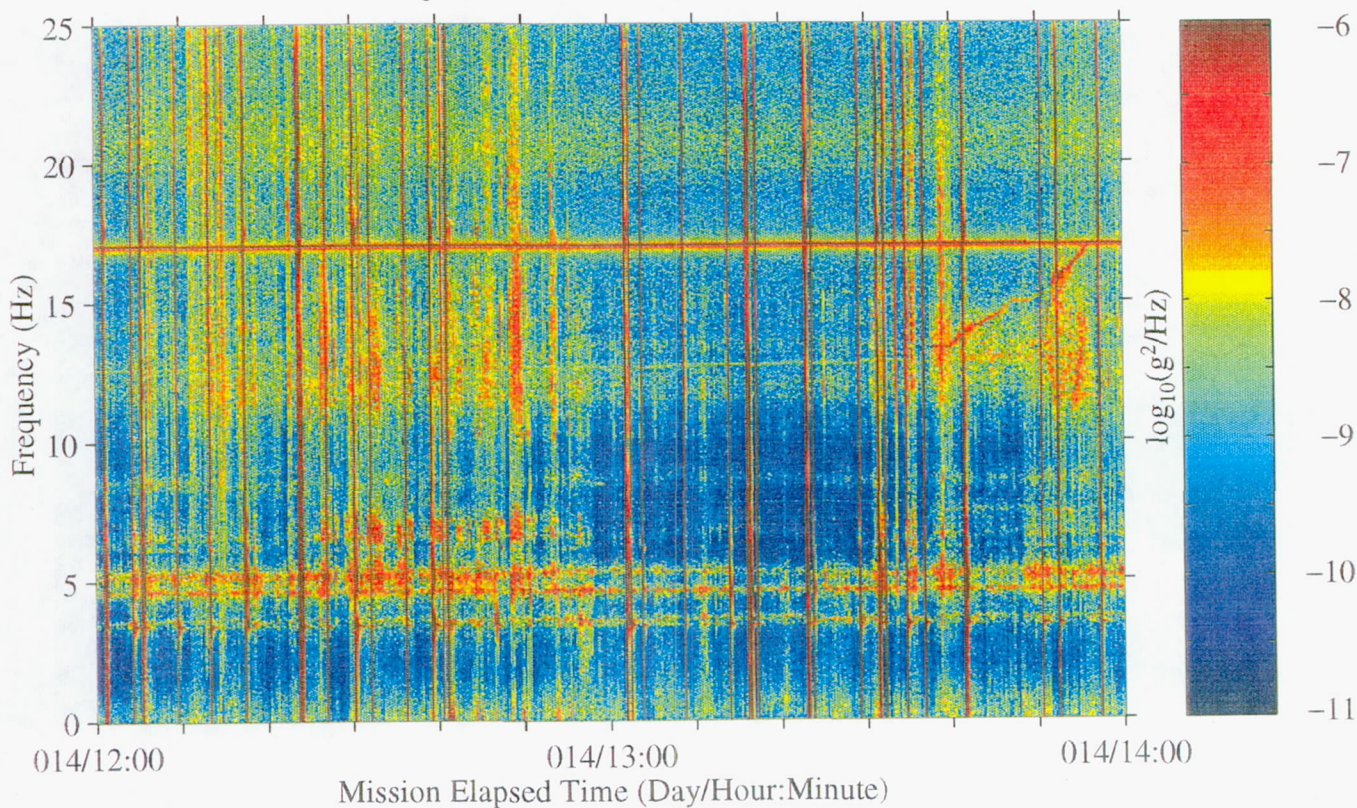




Figure 173: USML-2, Head C (fc=25 Hz)

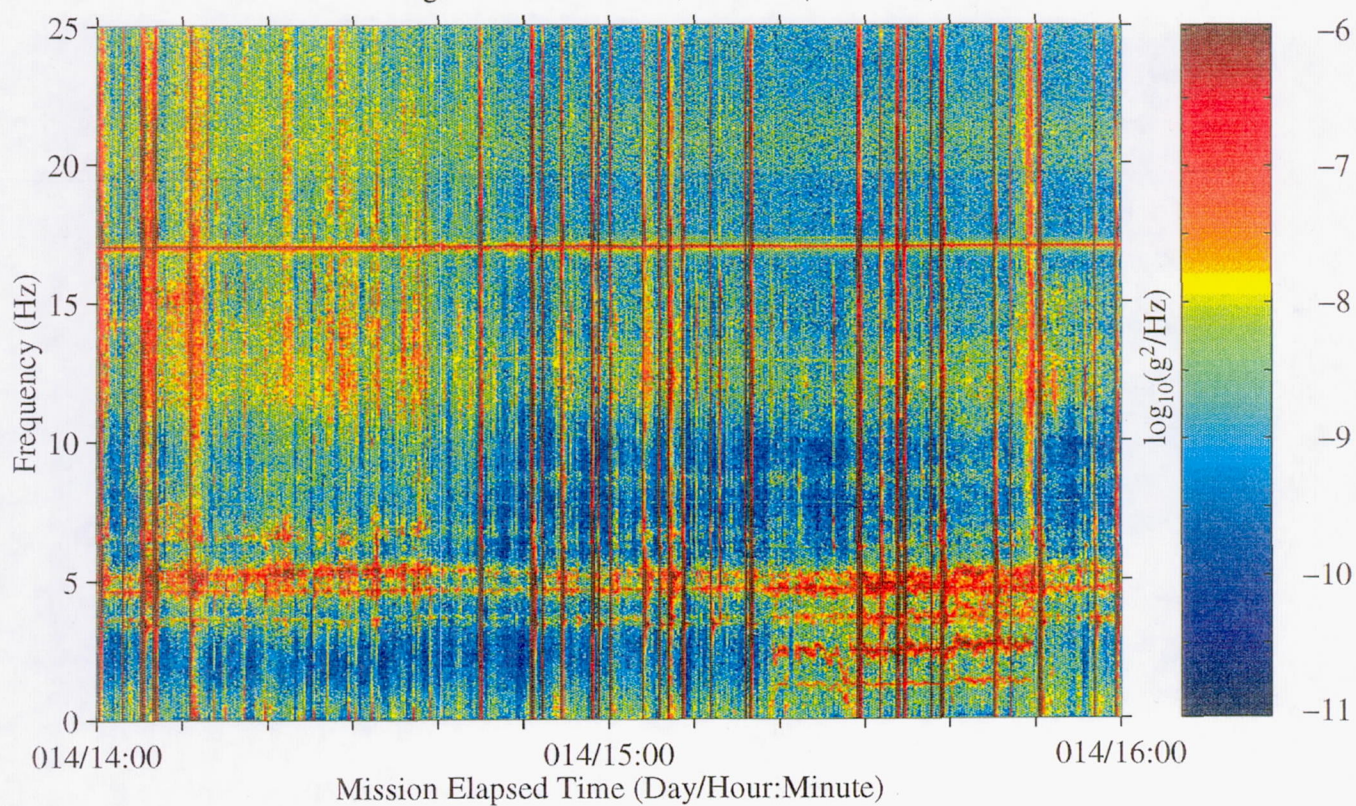


Figure 174: USML-2, Head C (fc=25 Hz)

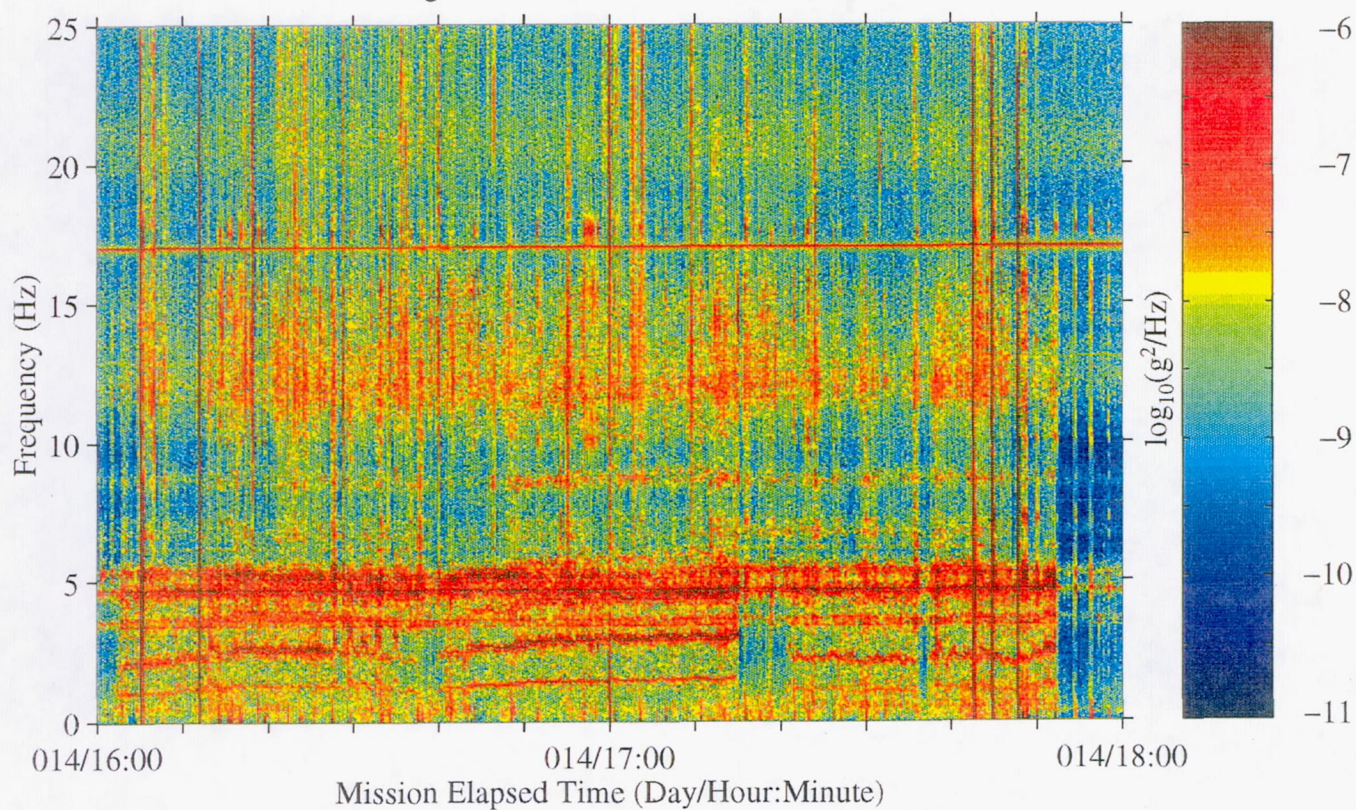




Figure 175: USML-2, Head C (fc=25 Hz)

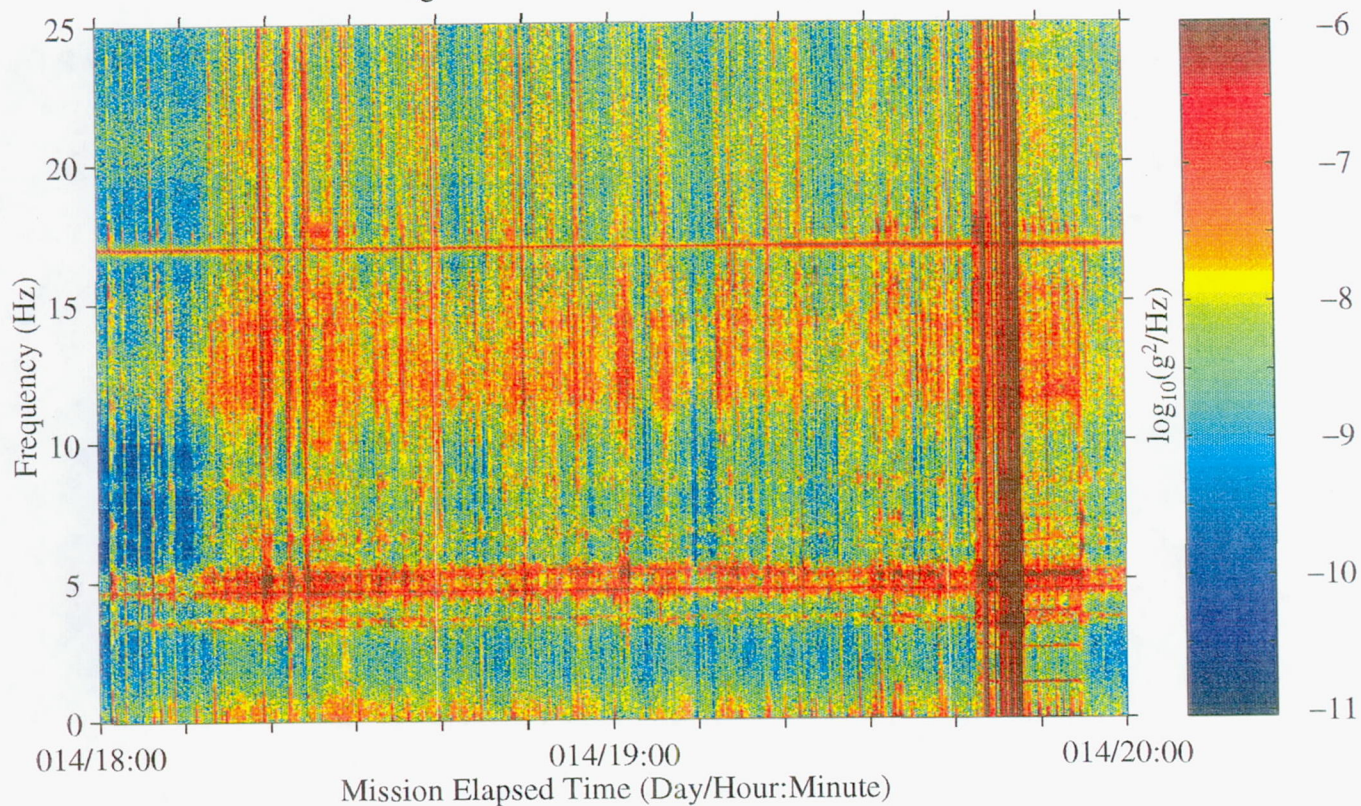


Figure 176: USML-2, Head C (fc=25 Hz)

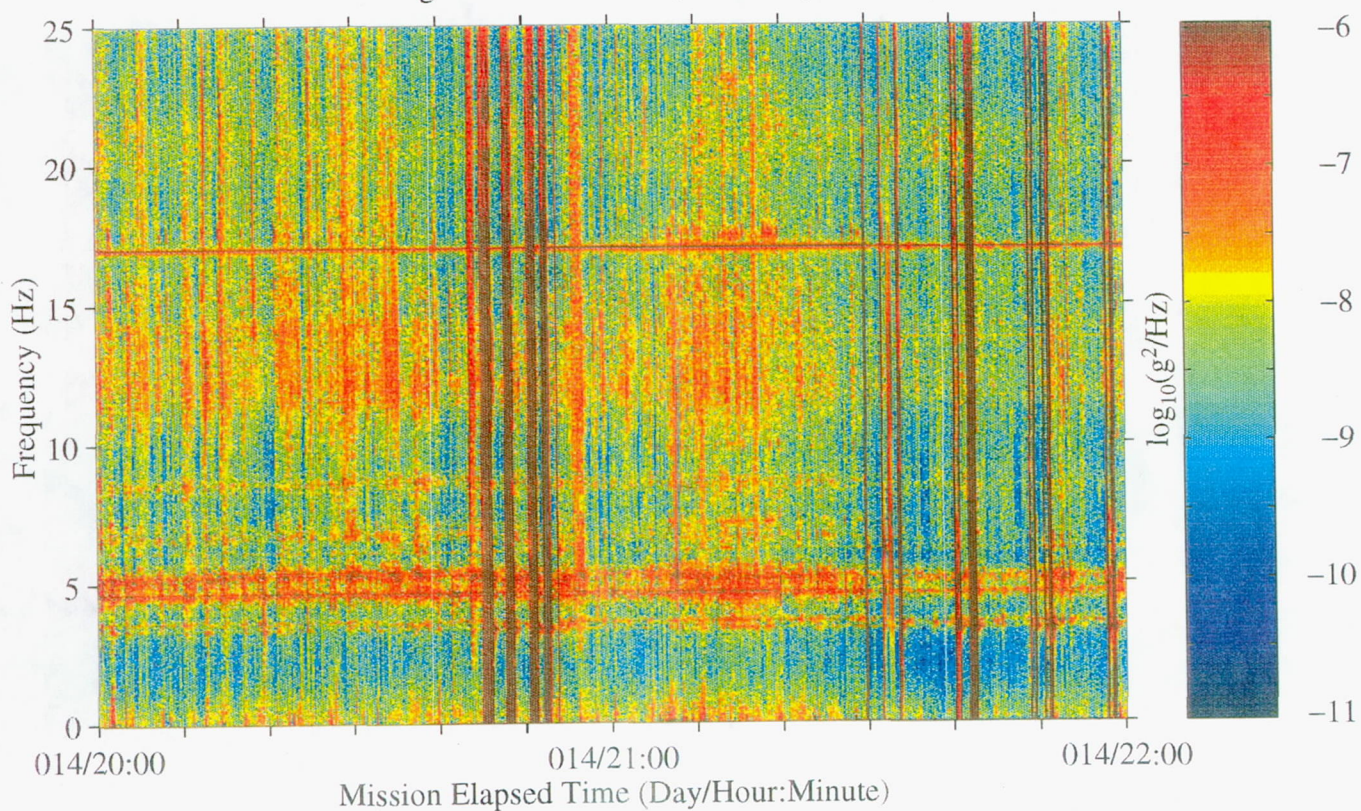




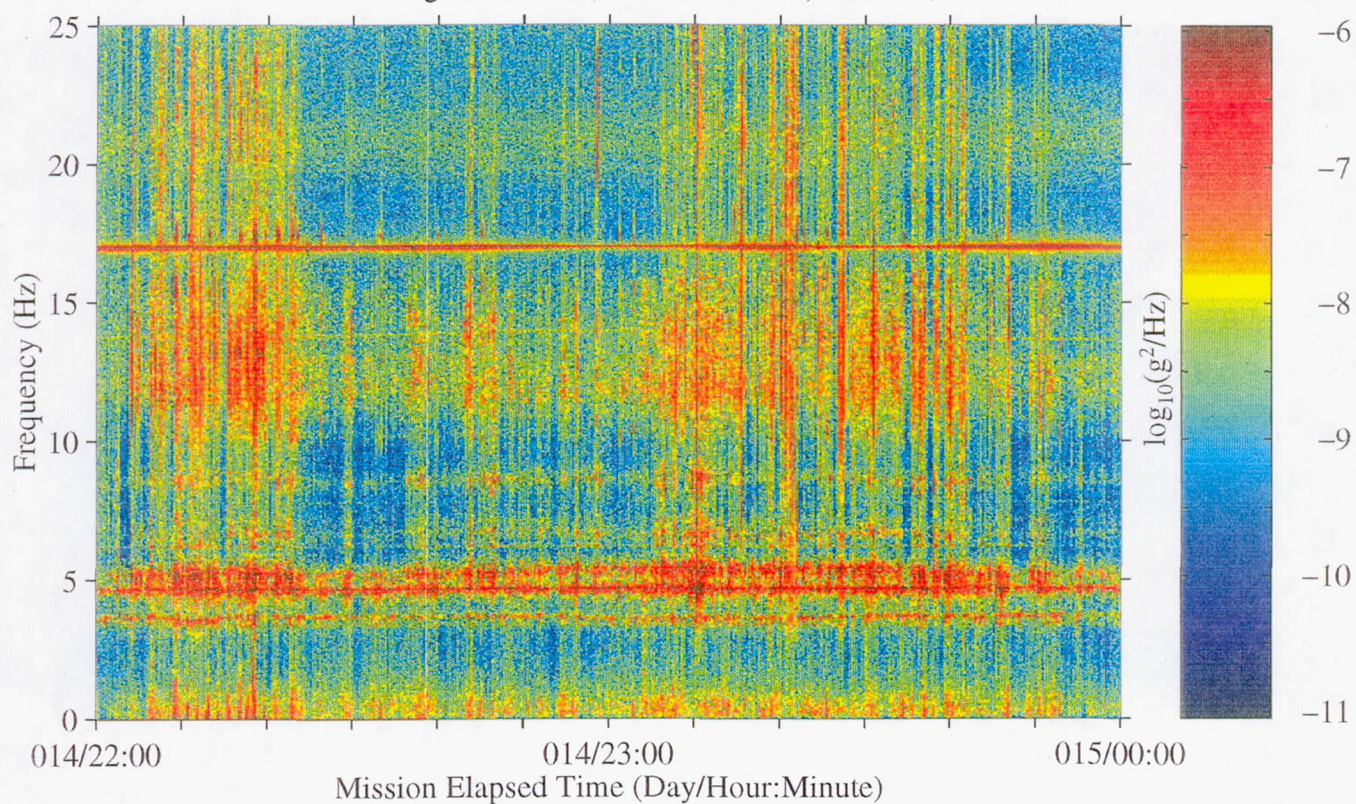
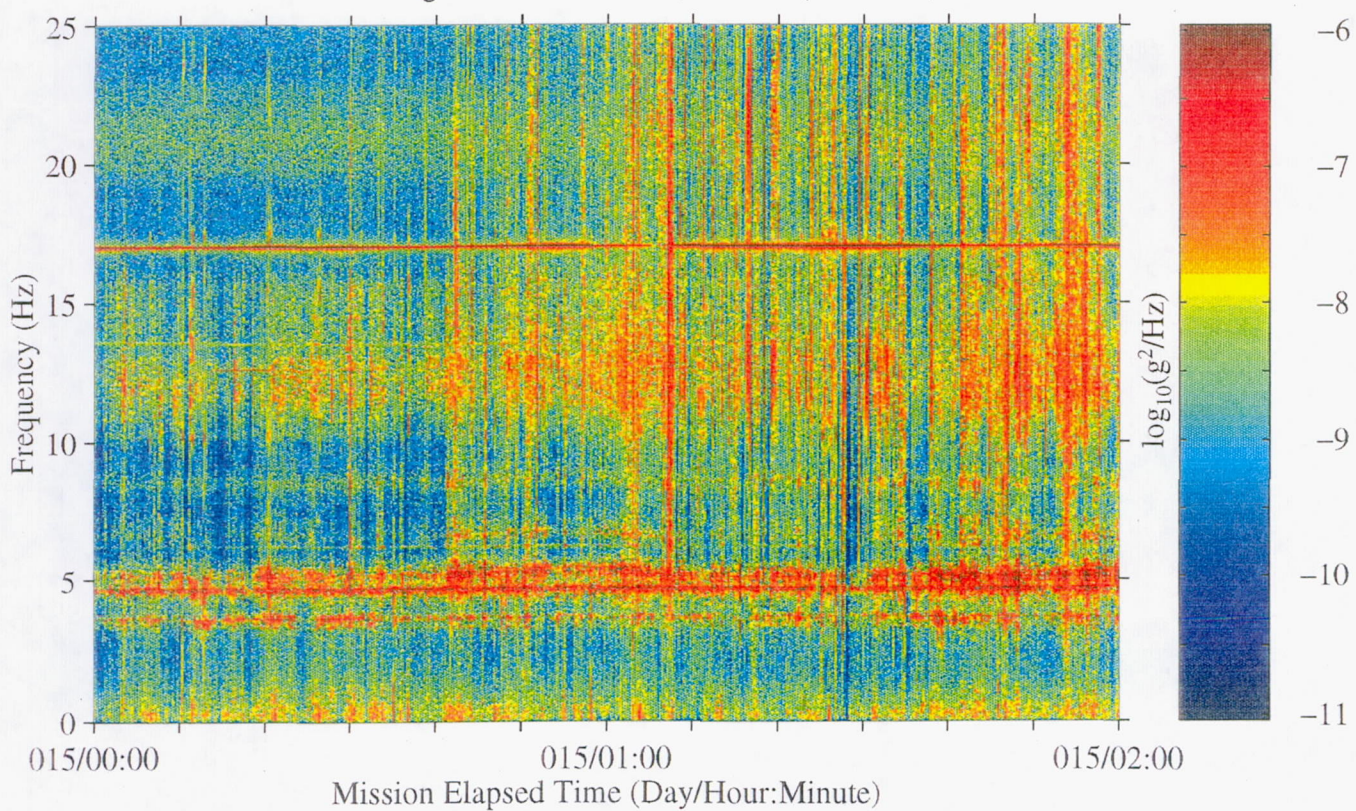
Figure 177: USML-2, Head C ( $f_c=25$  Hz)Figure 178: USML-2, Head C ( $f_c=25$  Hz)



Figure 179: USML-2, Head C (fc=25 Hz)

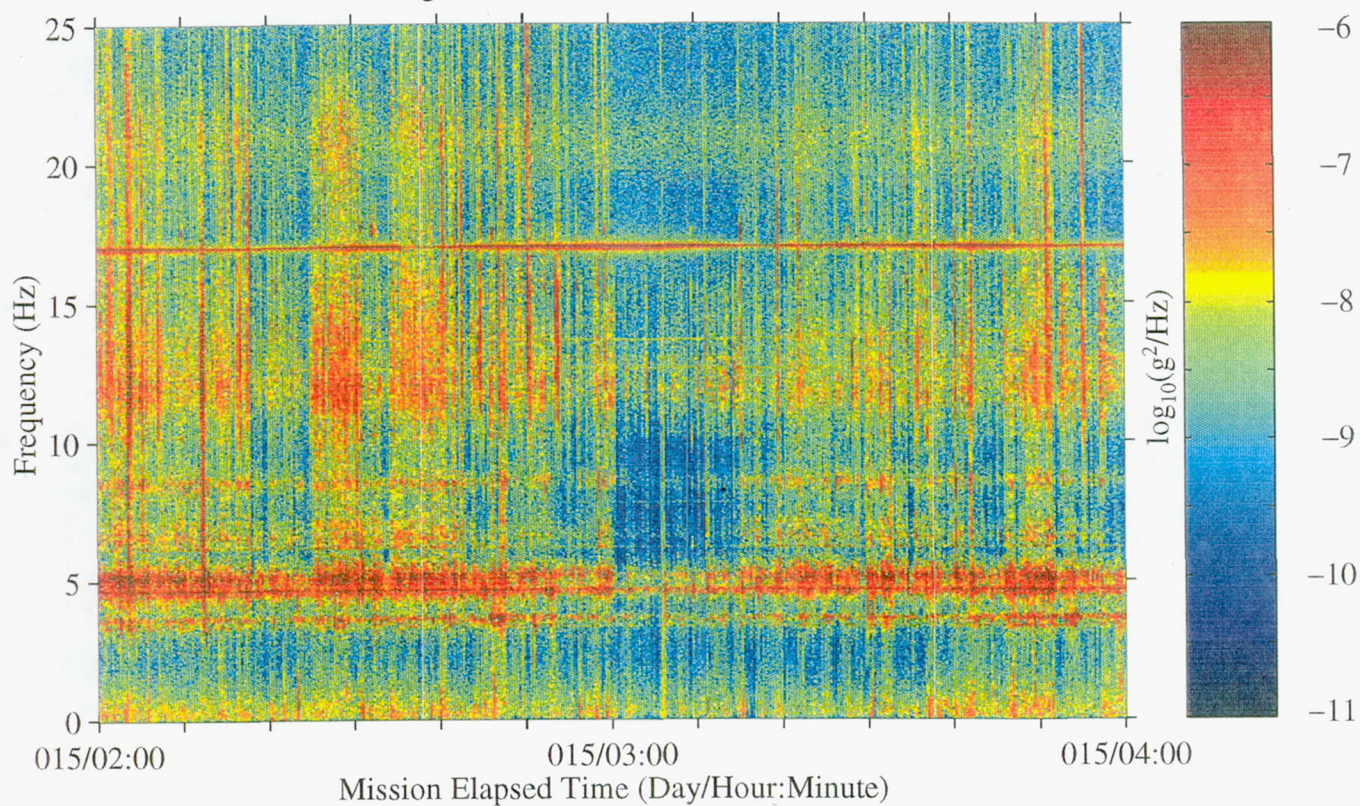


Figure 180: USML-2, Head C (fc=25 Hz)

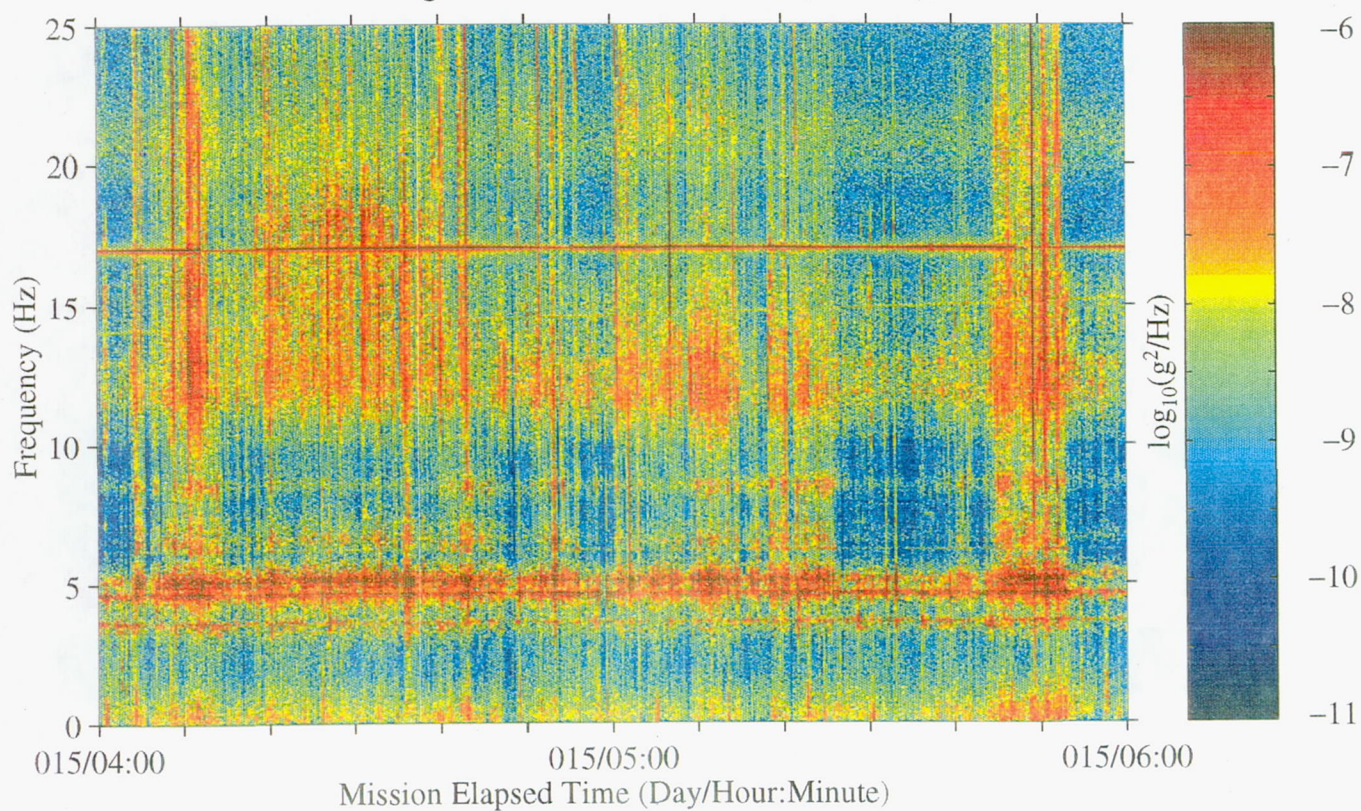




Figure 181: USML-2, Head C (fc=25 Hz)

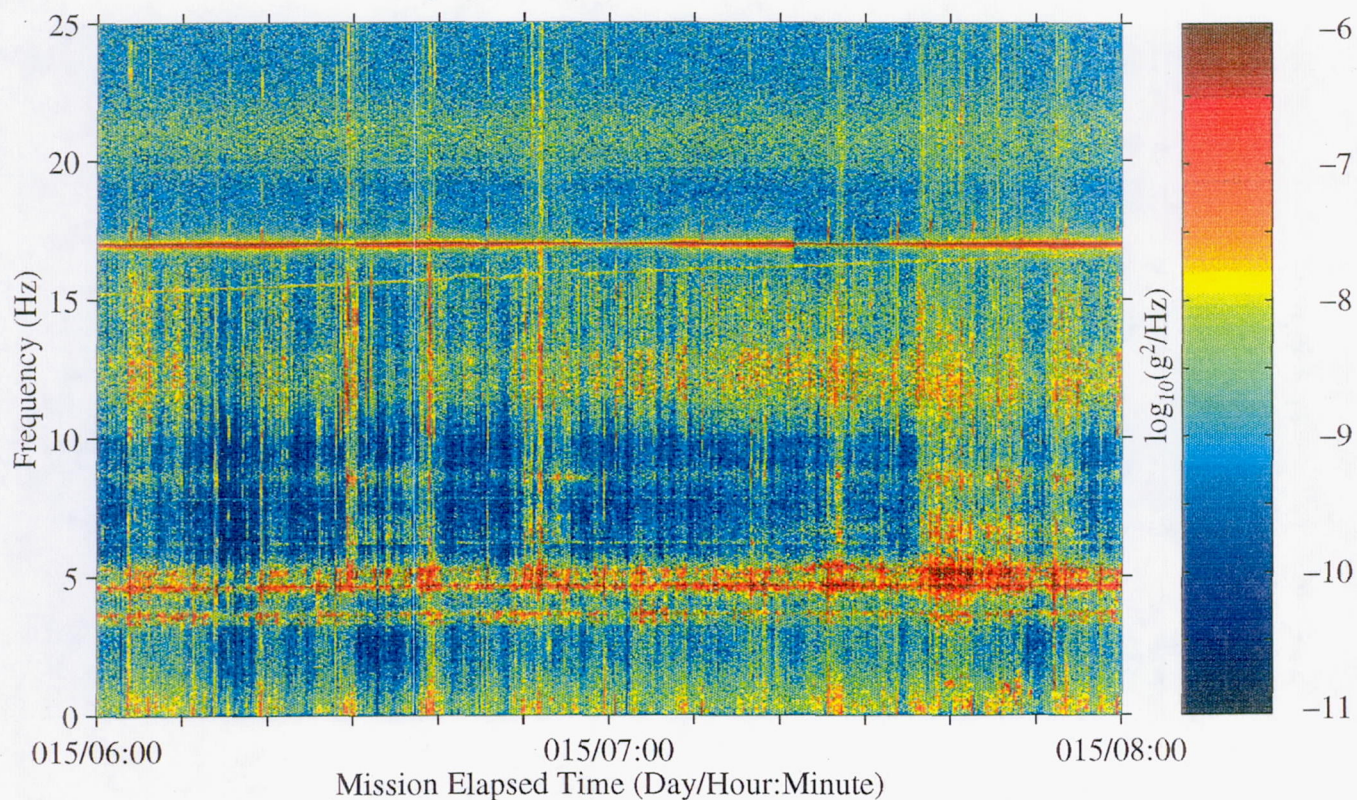


Figure 182: USML-2, Head C (fc=25 Hz)

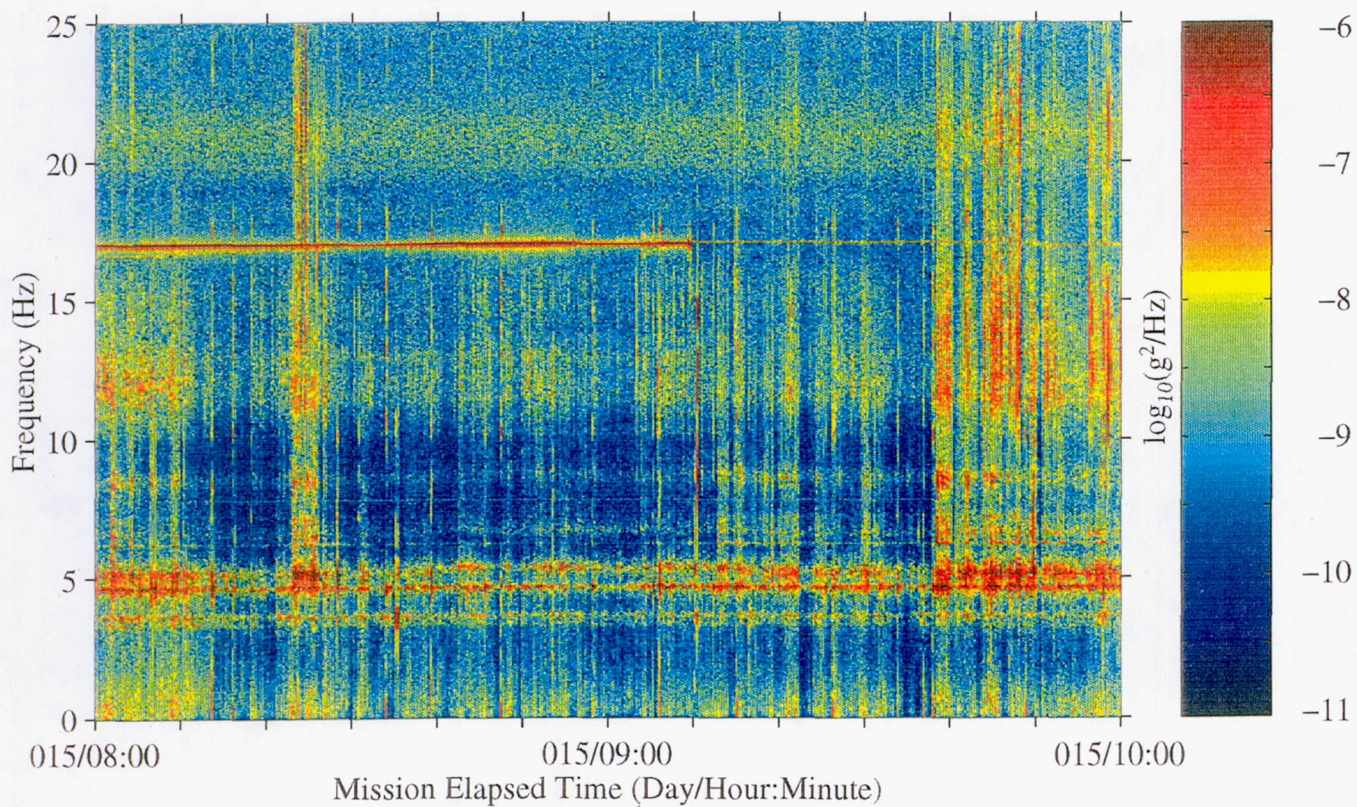




Figure 183: USML-2, Head C (fc=25 Hz)

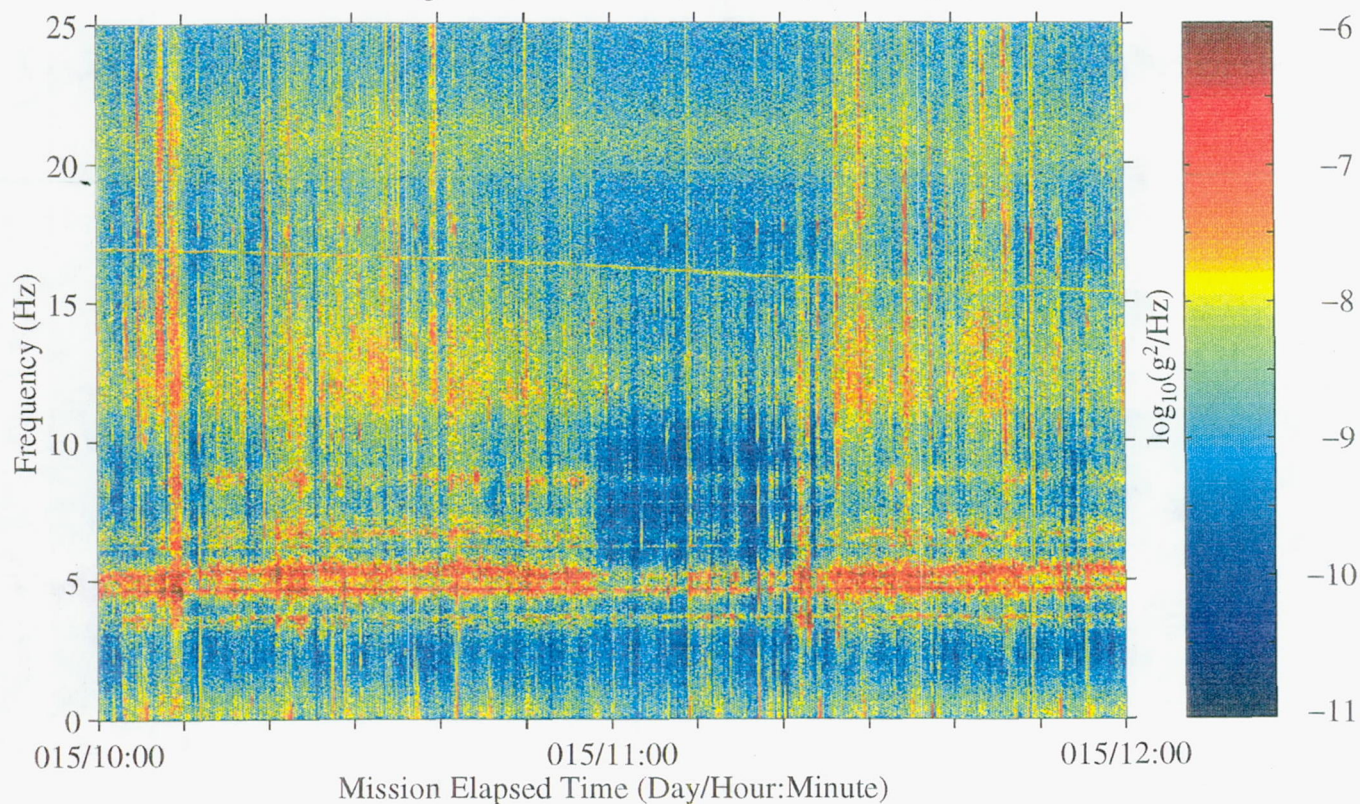
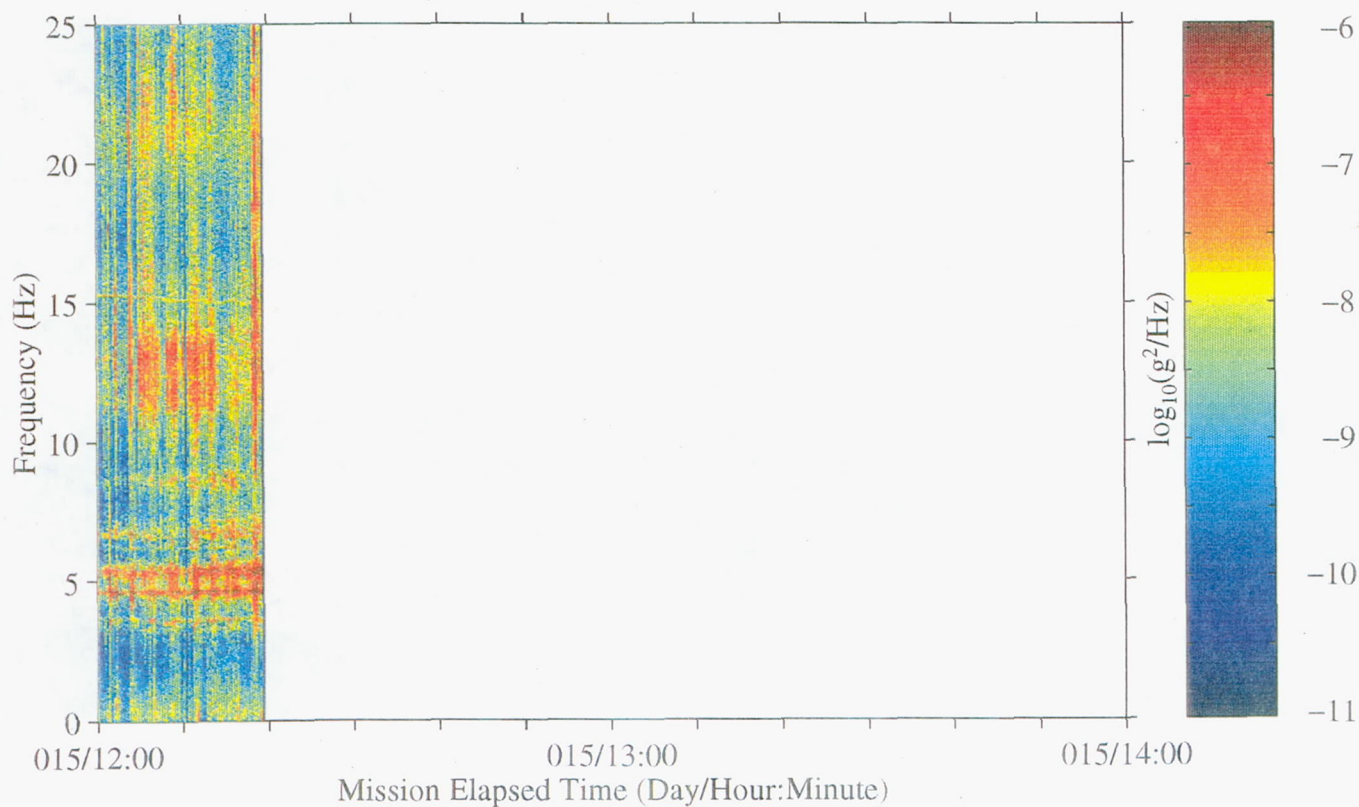


Figure 184: USML-2, Head C (fc=25 Hz)





**Appendix D User Comment Sheet**

We would like you to give us some feedback so that we may improve the Mission Summary Reports. Please answer the following questions and give us your comments.

1. Do the Mission Summary Reports fulfill your requirements for acceleration and mission information? ☐ Yes ☐ No If not why not?

Comments:

---



---

2. Is there additional information which you feel should be included in the Mission Summary Reports? ☐ Yes ☐ No If so what is it?

Comments:

---



---

3. Is there information in these reports which you feel is not necessary or useful?  
☐ Yes ☐ No If so, what is it?

Comments:

---



---

4. Do you have internet access via: ( ☐ )ftp ( ☐ )WWW ( ☐ )gopher ( ☐ )other?  
 Have you already accessed SAMS data or information electronically?

☐ Yes ☐ No

Comments:

---



---

Completed by: Name: \_\_\_\_\_ Telephone \_\_\_\_\_

Address: \_\_\_\_\_ Facsimile \_\_\_\_\_

\_\_\_\_\_ E-mail addr \_\_\_\_\_

**Return this sheet to:**  
**PIMS / M.J.B. Rogers**  
**NASA Lewis Research Center**  
**21000 Brookpark Road MS 500-216**  
**Cleveland, OH 44135**

**or**  
**FAX to PIMS Project: 216-433-8545**  
**e-mail to: melissa@lerc.nasa.gov**



REPORT DOCUMENTATION PAGE			Form Approved OMB No. 0704-0188	
Public reporting burden for this collection of information is estimated to average 1 hour per response, including the time for reviewing instructions, searching existing data sources, gathering and maintaining the data needed, and completing and reviewing the collection of information. Send comments regarding this burden estimate or any other aspect of this collection of information, including suggestions for reducing this burden, to Washington Headquarters Services, Directorate for Information Operations and Reports, 1215 Jefferson Davis Highway, Suite 1204, Arlington, VA 22202-4302, and to the Office of Management and Budget, Paperwork Reduction Project (0704-0188), Washington, DC 20503.				
1. AGENCY USE ONLY (Leave blank)	2. REPORT DATE July 1996	3. REPORT TYPE AND DATES COVERED Technical Memorandum		
4. TITLE AND SUBTITLE Summary Report of Mission Acceleration Measurements for STS-73 Launched October 20, 1995		5. FUNDING NUMBERS  WU-963-60-OD		
6. AUTHOR(S) Melissa J.B. Rogers and Richard DeLombard				
7. PERFORMING ORGANIZATION NAME(S) AND ADDRESS(ES) National Aeronautics and Space Administration Lewis Research Center Cleveland, Ohio 44135-3191		8. PERFORMING ORGANIZATION REPORT NUMBER  E-10336		
9. SPONSORING/MONITORING AGENCY NAME(S) AND ADDRESS(ES) National Aeronautics and Space Administration Washington, D.C. 20546-0001		10. SPONSORING/MONITORING AGENCY REPORT NUMBER  NASA TM-107269		
11. SUPPLEMENTARY NOTES Melissa J.B. Rogers, Tal-Cut Company, 3355 Richmond Road, Suite 251A, Beachwood, Ohio 44122 (work funded by NASA Contract NAS3-27254) and Richard DeLombard, NASA Lewis Research Center. Responsible person, Richard DeLombard, organization code 6743, (216) 433-5285.				
12a. DISTRIBUTION/AVAILABILITY STATEMENT  Unclassified - Unlimited Subject Categories 20, 35, and 18  This publication is available from the NASA Center for Aerospace Information, (301) 621-0390.		12b. DISTRIBUTION CODE		
13. ABSTRACT (Maximum 200 words)  The microgravity environment of the Space Shuttle Columbia was measured during the STS-73 mission using accelerometers from five different instruments: the Orbital Acceleration Research Experiment, the Space Acceleration Measurement System, the Three-dimensional Microgravity Accelerometer, the Microgravity Measuring Device, and Suppression of Transient Accelerations by Levitation Evaluation System. The Microgravity Analysis Workstation quasi-steady environment calculation and comparison of this calculation with Orbital Acceleration Research Experiment data was used to assess how appropriate a planned attitude was expected to be for one Crystal Growth Facility experiment sample. The microgravity environment related to several different Orbiter, crew, and experiment operations is presented and interpreted in this report. Data are examined to show the effects of vernier reaction control system jet firings for Orbiter attitude control. This is compared to examples of data when no thrusters were firing, when the primary reaction control system jets were used for attitude control, and when single vernier jets were fired for test purposes. In general, vernier jets, when used for attitude control, cause accelerations in the $3 \times 10^{-4}$ g to $7 \times 10^{-4}$ g range. Primary jets used in this manner cause accelerations in the 0.01 to 0.025 g range. Other significant disturbance sources characterized are water dump operations, with $Y_b$ axis acceleration deviations of about $1 \times 10^{-6}$ g; payload bay door opening motion, with $Y_o$ and $Z_o$ axis accelerations of frequency 0.4 Hz; and probable Glovebox fan operations with notable frequency components at 20, 38, 43, 48, and 53 Hz. The STS-73 microgravity environment is comparable to the environments measured on earlier microgravity science missions.				
14. SUBJECT TERMS Microgravity environment; USML-2; SAMS; OARE; STS-73; Acceleration measurements		15. NUMBER OF PAGES 339		
		16. PRICE CODE A15		
17. SECURITY CLASSIFICATION OF REPORT Unclassified	18. SECURITY CLASSIFICATION OF THIS PAGE Unclassified	19. SECURITY CLASSIFICATION OF ABSTRACT Unclassified	20. LIMITATION OF ABSTRACT	